SANDIA REPORT
SAND2006-4457
Unlimited Release
Printed August 2006

Characterization of Aluminum Honeycomb and Experimentation for Model Development and Validation

Volume I: Discovery and Characterization Experiments for High-Density Aluminum Honeycomb

Wei-Yang Lu, John S. Korellis, Kenneth L. Lee, Simon Scheffel, Terry D. Hinnerichs, Michael K. Neilsen, and William Scherzinger

Prepared by
Sandia National Laboratories
Albuquerque, New Mexico 87185 and Livermore, California 94550

Sandia is a multiprogram laboratory operated by Sandia Corporation,
a Lockheed Martin Company, for the United States Department of Energy's
National Nuclear Security Administration under Contract DE-AC04-94AL85000.

Issued by Sandia National Laboratories, operated for the United States Department of Energy by Sandia Corporation.

Available to DOE and DOE contractors from
U.S. Department of Energy
Office of Scientific and Technical Information
P.O. Box 62
Oak Ridge, TN 37831

Telephone: (865) 576-8401
Facsimile: (865) 576-5728
E-Mail: reports@adonis.osti.gov
Online ordering: http://www.osti.gov/bridge

Available to the public from
U.S. Department of Commerce
National Technical Information Service
5285 Port Royal Rd.
Springfield, VA 22161

Telephone: (800) 553-6847
Facsimile: (703) 605-6900
E-Mail: orders@ntis.fedworld.gov
Online order: http://www.ntis.gov/help/ordermethods.asp?loc=7-4-0#online

SAND2006-4457
Unlimited Release
Printed August 2006

Characterization of Aluminum Honeycomb and Experimentation for Model Development and Validation

Volume I: Discovery and Characterization Experiments for High-Density Aluminum Honeycomb

Wei-Yang Lu, John S. Korellis, Kenneth L. Lee, and Simon Scheffel[1]
Mechanics of Materials
[1](Currently at W80 System Engineering)
Sandia National Laboratories
P.O. Box 0969
Livermore, California 94551-0969

Terry D. Hinnerichs,[2] Michael K. Neilsen,[3] and William M. Scherzinger[2]
[2]Solid Mechanics
[3]Applied Mechanics Development
Sandia National Laboratories
P.O. Box 5800
Albuquerque, New Mexico 87185

Abstract

Honeycomb is a structure that consists of two-dimensional regular arrays of open cells. High-density aluminum honeycomb has been used in weapon assemblies to mitigate shock and protect payload because of its excellent crush properties. In order to use honeycomb efficiently and to certify the payload is protected by the honeycomb under various loading conditions, a validated honeycomb crush model is required and the mechanical properties of the honeycombs need to be fully characterized.

Volume I of this report documents an experimental study of the crush behavior of high-density honeycombs. Two sets of honeycombs were included in this investigation: commercial grade for initial exploratory experiments, and weapon grade, which satisfied B61 specifications. This investigation also includes developing proper experimental methods for crush characterization, conducting discovery experiments to explore crush behaviors for model improvement, and identifying experimental and material uncertainties.

ACKNOWLEDGMENTS

The authors thank Bonnie Antoun for technical discussions, Steve Brandon for running part of the experiments on the axial-torsional (AT) and two-million-pound (2M) systems, William Langham and Edwin Huestis for video setup and recording, and Wendell Kawahara, Jaime Moya and Kevin Eklund for program support.

CONTENTS

APPENDIX IX: "Summary of Moderate Rate Confined Crush Tests of Alcore & Hexcel honeycombs in the t-direction at Ambient Temperature," Memo Wei-Yang Lu to Distribution, January 10, 2000.

APPENDIX X: "Moderate Rate Confined Crush Tests of Alcore 38 & Hexcel 38 honeycombs in the t-direction at 165^{o}F," Memo Wei-Yang Lu to Distribution, January 18, 2000.

APPENDIX XI: "Moderate Rate Confined Crush Tests of Alcore 35 honeycomb in the t-direction at 165^{o}F," Memo Wei-Yang Lu to Distribution, January 10, 2000.

APPENDIX XII: "Moderate Rate Confined Crush Tests of 38 pcf honeycombs in the t-direction at -65^{o}F," Memo Wei-Yang Lu to Distribution, February, 2000.

APPENDIX XIII: "Moderate Rate Confined Crush Tests of (1)38 pcf honeycombs in the L-direction at ambient, and (2)35 pcf honeycombs in the T-direction at –65^{o}F ," Memo Wei-Yang Lu to Distribution, March 7, 2000.

APPENDIX XIV: "Moderate Rate Confined Crush Tests of 38 pcf honeycombs in the W-direction at ambient," Memo Wei-Yang Lu to Distribution, March 16, 2000.

APPENDIX XV: "In-Plane Biaxial Compressions of High Density Aluminum Honeycombs," (Paper No. 150) Proceedings of the 2002 SEM Annual Conference & Exposition on Experimental and Applied Mechanics, June 10-12, 2002, Milwaukee, Wisconsin.

FIGURES

TABLES

NOMENCLATURE

Ao	cross-sectional area of the gage section of the undeformed specimen
F	force
kips	kilo-pounds
Lo	gage length of the undeformed specimen
MTS	material testing system manufactured by MTS Systems Corporation
pcf	pound per cubic foot
RH	relative humidity
TC	thermal couple
ΔL	change of gage length during loading
σ_c	crush strength

1. INTRODUCTION

Honeycomb is a structure that consists of two-dimensional regular arrays of open cells. Man-made honeycomb can be made of different materials (metal, paper, etc.) and various cell configurations and densities. In many engineering applications, however, honeycomb is treated as a cellular material.

High-density aluminum honeycomb, which usually means its density is greater than 20 pounds per cubic foot (pcf), has been used in weapon assemblies to mitigate shock and protect payload due to its excellent crush properties. As shown schematically in Figure 1-1, the honeycomb has three principal directions due to its composure of corrugated and flat aluminum sheets and is orthotropic. Among these directions, T is the strongest, L has intermediate strength, and W is the weakest.

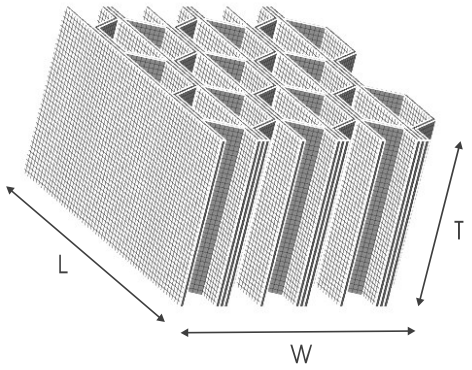

Figure 1-1. Aluminum honeycomb geometry and principal directions.

In order to use honeycomb efficiently and certify that the payload is protected by honeycomb under various loading conditions, a validated honeycomb crush model is required, and the mechanical properties of honeycomb need to be fully characterized. The orthotropic crush model [1] has commonly been used to describe the stress-strain behavior of honeycomb; however, the model does not account for multiaxial coupling, temperature, or strain rate effects and may be inadequate for such application until relevant experiments can be conducted to validate its accuracy [2]. Experimental data in those areas is limited and most is for low-density (less than 20 pcf) aluminum honeycombs. The main area of application is on sandwich structures. Few crush experiments and data exist for high-density honeycomb.

This report documents an experimental study of the crush behavior of high-density honeycomb, which has been considered for weapon applications. In addition to characterizing honeycomb crush properties, this investigation also includes developing proper experimental methods for crush characterization, conducting discovery experiments to explore crush behaviors for model improvement, and identifying experimental and material uncertainties.

Two sets of honeycomb were included in this investigation. The first set was commercial-grade honeycomb for initial exploratory experiments of uniaxial crush; the second set was weapon-grade honeycomb, which satisfied B61 specifications and was mostly for (a) characterizing uniaxial crush properties and uncertainties and (b) exploratory experiments of biaxial crush and temperature and humidity effects.

This page intentionally left blank.

2. EXPLORATORY BARE COMPRESSION AND PUNCH TEST

2.1 Commercial-Grade Honeycomb and Specimen

All honeycomb discussed in this section was commercial grade, and included five different types of hexagonal core and tube-core configurations manufactured by Hexcel.

CR-8-LC-1/8-5052-006 and CR-8-LC-1/8-5052-006-R2 are hexagonal core honeycomb, which is made of 5052-H9 aluminum alloy with a cell size of 1/8 in. and foil thickness of 0.006 in. The difference between these two honeycombs is that every corrugated aluminum ribbon of CR-8-LC-1/8-5052-006-R2 is reinforced by an additional flat aluminum sheet. The density of CR-8-LC-1/8-5052-006 is 22 pcf, and of CR-8-LC-1/8-5052-006-R2 is 38 pcf. For specimens with 3 in. × 3 in. cross-sectional areas, there are about 50 layers of corrugated sheets and more than 1,350 hexagonal cells. The standard specimen size suggested by Hexcel is 3 in. × 3 in. × 0.625 in. However, almost all specimens tested were 3 in. × 3 in. × 3 in. Specimen were cut from honeycomb blocks using a band saw. Samples are shown in Figure 2-1.

Three tube-core honeycombs have outside diameters of D_o = 5 in., 8 in., and 13 in., and inside diameters of D_i = 1.5 in., 0.5 in., and 2 in., respectively. Tube-core is constructed of alternate layers of flat aluminum foil and corrugated aluminum ribbon wrapped around a mandrel and bond with adhesive. These tube-core honeycombs do not have the same thickness of corrugated ribbon; there are two bonded aluminum foils for 5 in. and 13 in. honeycomb, and three bonded foils for 8 in. honeycomb. The 5 in. has 17 corrugated layers across the radius, the 8 in. has 40, and the 13 in. has 56.

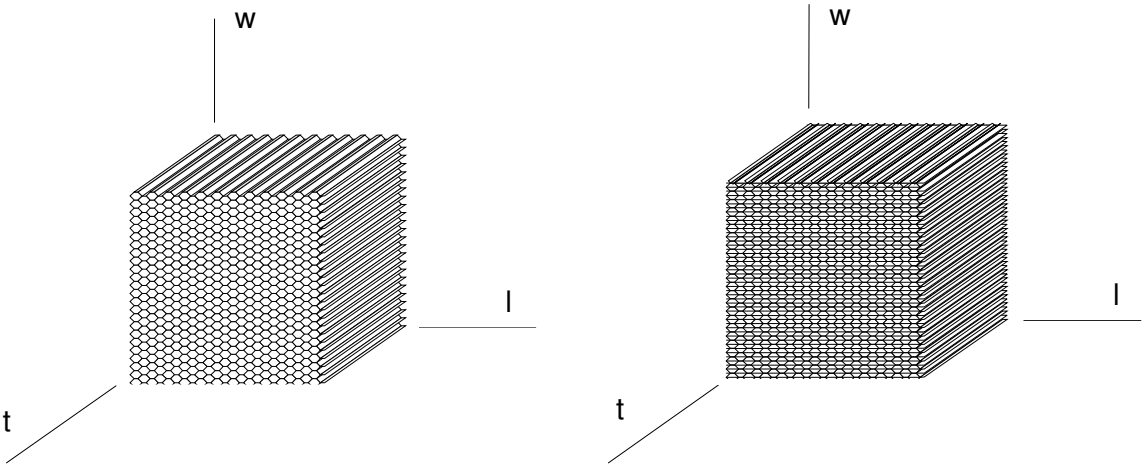

(a) CR-8-LC-1/8-5052-006 (b) CR-8-LC-1/8-5052-006-R2

Figure 2-1. Hexagonal core honeycomb specimen: l represents ribbon (or sheet) direction, w represents ribbon surface, and t represents ribbon width.

2.2 On-Axis Compression Test Matrix

Compression tests were performed along the principle material directions, i.e., the T, W, and L directions of hexagonal core materials and the axial and radial directions of tube-core materials. Punch tests were performed along the T (or axial) direction. Tables 2-1 to 2-3 list the tests performed and conditions. All tests described in this section were conducted at room temperature. The original objectives of the tests were to compare the mechanical properties, such as crush strength and efficiency, directly with the honeycomb vendor tests for a variety of honeycombs and determine a set of tests for purchase and acceptance.

During the punch test, the portion of the honeycomb to be crushed under the punch rod was constrained by the surrounding material. This provided a different condition from the "bare" (or stabilized) compression test, where four faces of the specimen were free and unconstrained. The total force applied can be expressed as

$$F = F_c + F_s + F_f \tag{2-1}$$

where F_c, F_s, and F_f are force components to crush the honeycomb cells, shear the aluminum foils, and overcome the friction between the punch and honeycomb.

Table 2-1. Compression tests of Hexcel CR-8-LC-1/8-5052-006-R2 (38 lb pcf).

Specimen	Size	Loading			Remarks
	T x W x L	Direction	Rate, in/s	System	
h38t_1	3 in. x 3 in. x 3 in.	T	0.001	AT	Extensometers in W and L directions
h38t_2	3 in. x 3 in. x 3 in.	T	0.001	AT	Extensometers
h38t_3	3 in. x 3 in. x 3 in.	T	0.001	AT	End caps, extensometers
h38t_4	1.5 in. x 3 in. x 3 in.	T	0.001	AT	Half height, extensometers
h38t_6	3 in. x 3 in. x 3 in.	T	0.001	220K	
h38t_7	3 in. x 3 in. x 3 in.	T	0.001	220K	
h38l_1	3 in. x 3 in. x 3 in.	L	0.001	AT	Extensometers in T and W directions
h38l_2	3 in. x 3 in. x 3 in.	L	0.001	AT	Extensometers
h38l_3	3 in. x 3 in. x 3 in.	L	0.001	AT	End caps, extensometers
h38l_4	3 in. x 3 in. x 3 in.	L	0.001	220K	
h38w_1	3 in. x 3 in. x 3 in.	W	0.001	AT	Extensometers in T and L directions

Table 2-1. Compression tests of Hexcel CR-8-LC-1/8-5052-006-R2 (38 lb pcf) (continued).

Specimen	Size	Loading			Remarks
	T x W x L	Direction	Rate, in/s	System	
h38w_2	3 in. x 3 in. x 3 in.	W	0.001	2M	
h38w_3	3 in. x 3 in. x 3 in.	W	0.001	2M	
h38p_1	3 in. x 3 in. x 3 in.	T	0.001	880	1 in. diameter punch rod
h38p_2	3 in. x 3 in. x 3 in.	T	0.03	880	1 in. diameter punch rod
h38p_3	3 in. x 3 in. x 3 in.	T	0.03	880	1 in. diameter punch rod
h38p_4	3 in. x 3 in. x 3 in.	T	0.03	880	1 in. diameter punch rod

Table 2-2. Compression tests of Hexcel CR-8-LC-1/8-5052-006 (22.1 lb pcf).

Specimen	Size	Loading			Remarks
	T x W x L	Direction	Rate, in/s	System	
h22t_1	3 in. x 3 in. x 3 in.	T	0.001	AT	Specimen skewed, extensometers
h22t_2	3 in. x 3 in. x 3 in.	T	0.001	AT	Extensometers
h22t_3	3 in. x 3 in. x 3 in.	T	0.001	220K	
h22t_4	3 in. x 3 in. x 3 in.	T	0.001	220K	
h22l_1	3 in. x 3 in. x 3 in.	L	0.001	AT	Extensometers
h22w_1	3 in. x 3 in. x 3 in.	W	0.001	AT	Extensometers
h22p_1	3 in. x 3 in. x 3 in.	T	0.001	880	1 in. diameter punch rod
h22p_2	3 in. x 3 in. x 3 in.	T	0.03	880	1 in. diameter punch rod
h22p_3	3 in. x 3 in. x 3 in.	T	0.03	880	1 in. diameter punch rod

Table 2-3. Tests of Hexcel tube-core samples.

Specimen	Size		Loading			Remarks
	Diameter	Height	Direction	Rate, in./s	system	
a5_t13	5 in.	3 in.	axial	0.02	2M	
a5_t14	5 in.	3 in.	axial	0.02	2M	
a8_t7	8 in.	3 in.	axial	0.02	2M	
a8_t9	8 in.	3 in.	axial	0.02	2M	
a8_t10	8 in.	3 in.	axial	0.02	2M	
p8_t15	8 in.	3 in.	axial	0.02	2M	6 in. punch
p8_t18	8 in.	3 in.	axial	0.02	2M	5 in. punch
s8_t4	8 in.	3 in.	radial	0.02	2M	
s8_t5	8 in.	3 in.	radial	0.02	2M	
s8_t6	8 in.	3 in.	radial	0.02	2M	
s8_t17	8 in.	3 in.	radial	0.02	2M	
a13_t11	13 in.	3 in.	axial	0.02	2M	
a13_t12	13 in.	3 in.	axial	0.02	2M	
a13_t0	13 in.	3 in.	axial	0.02	2M	
p13_t16	13 in.	3 in.	axial	0.02	2M	10.5 in. punch
p13_t19	13 in.	3 in.	axial	0.02	2M	5 in. punch
s13_t1	13 in.	3 in.	radial	0.02	2M	
s13_t2	13 in.	3 in.	radial	0.02	2M	
s13_t3	13 in.	3 in.	radial	0.02	2M	

Most tests were conducted under the bare condition, where the cell edges of a compressive specimen were not stabilized. A stabilized specimen has plates bonded on each loading face. In some tests, end caps were used to constrain the edge displacement, which could be considered "semi-stabilized." In general, bare tests are faster and easier to perform and result in slightly conservative properties.

Depending on the maximum compressive force required, four testing systems were used: 880, AT, 220K, and 2M systems, with capacities of 20 kilo-pounds (kips), 100 kips, 200 kips, and two million pounds, respectively. The 880 and AT systems use TestStar for loading control and data acquisition. The 220K and 2M systems use MTS448.85 controller for test control and a Nicolet 440 for data acquisition. The 880 system was limited to small rod (1 in. diameter) punch tests due to its relatively low capacity.

Loading was quasi-static (10^{-3} in./s) or slow (10^{-2} in./s). The deformation of the honeycomb was measured by the stroke of the loading system. In some tests, extensometers were attached to the specimen to measure the transverse deformations. The rate of data acquisition was at least 10 Hz.

2.3 Crush of CR-8-LC-1/8-5-52-006-R2 (38 pcf)

Experimental results of the honeycomb crush in the T, L, and W directions are shown in Figures 2-2 to 2-5.

Detailed experimental observations and discussions are reported in Lu and Hinnerichs [2001], which is attached as Appendix I and summarized below:

1. The deformation of honeycomb is complex and, usually, nonuniform during crush.
2. Several forms of deformation are possible and can be grouped into normal and abnormal crush modes.
3. In normal crush mode, instability (local buckling) occurs, resulting in the highest possible crush strength and energy absorption rate of the material. (Typically, these are the material data provided by vendors.)
4. Abnormal crush mode, which includes global buckling, delaminating, splitting, etc., yields a lower crush strength and lower energy absorption rate.
5. Both specimen (or component) size and boundary condition influence the crush mode of honeycomb.
6. To ensure honeycomb is deformed under normal crush mode, proper confinement is required.

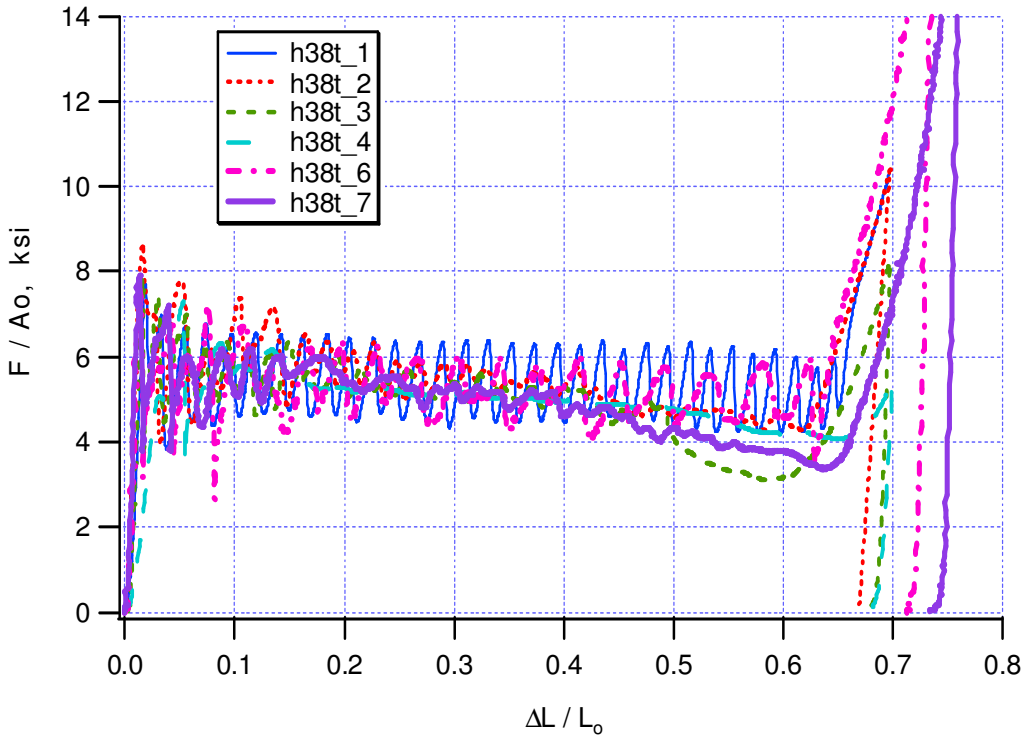

Figure 2-2. Normalized load-displacement curves of Hexcel CR-8-LC-1/8-5052-006-R2 (38 lb) compressed in the T direction.

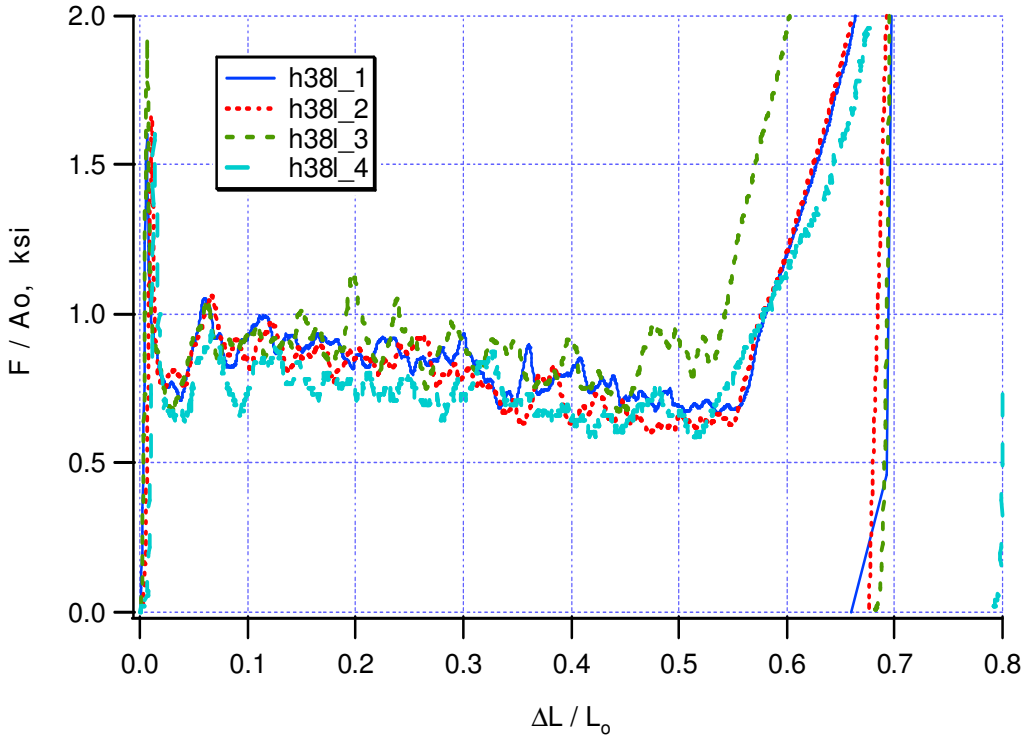

Figure 2-3. Normalized load-displacement curves of Hexcel CR-8-LC-1/8-5052-006-R2 (38 lb) compressed in the L direction.

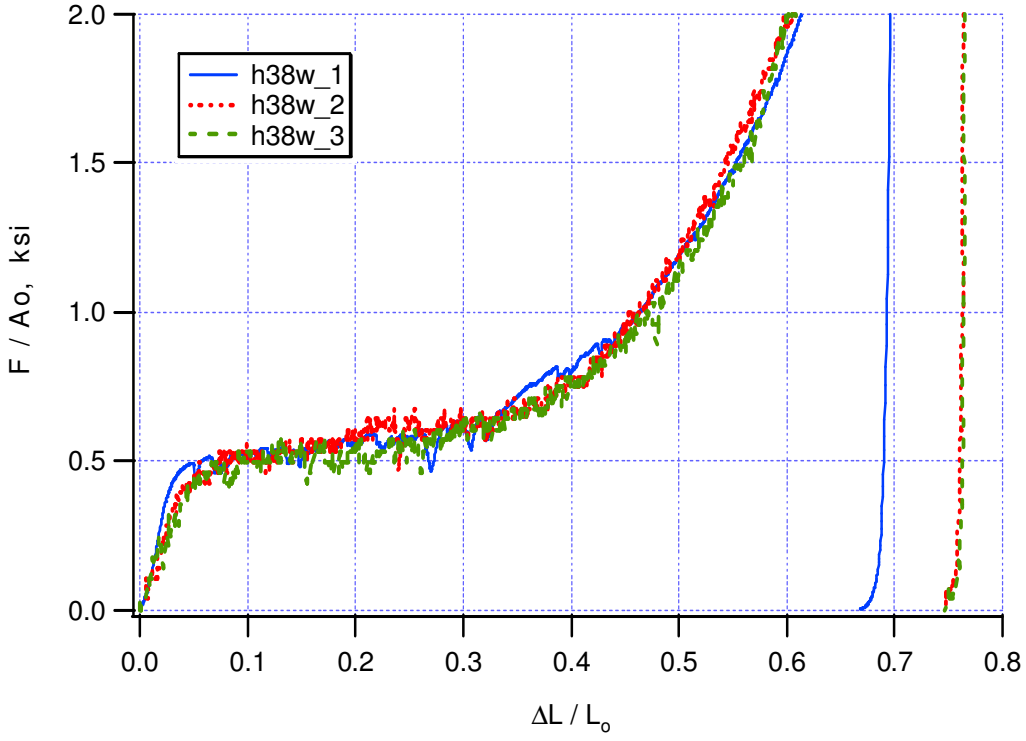

Figure 2-4. Normalized load-displacement curves of Hexcel CR-8-LC-1/8-5052-006-R2 (38 lb) compressed in the W direction.

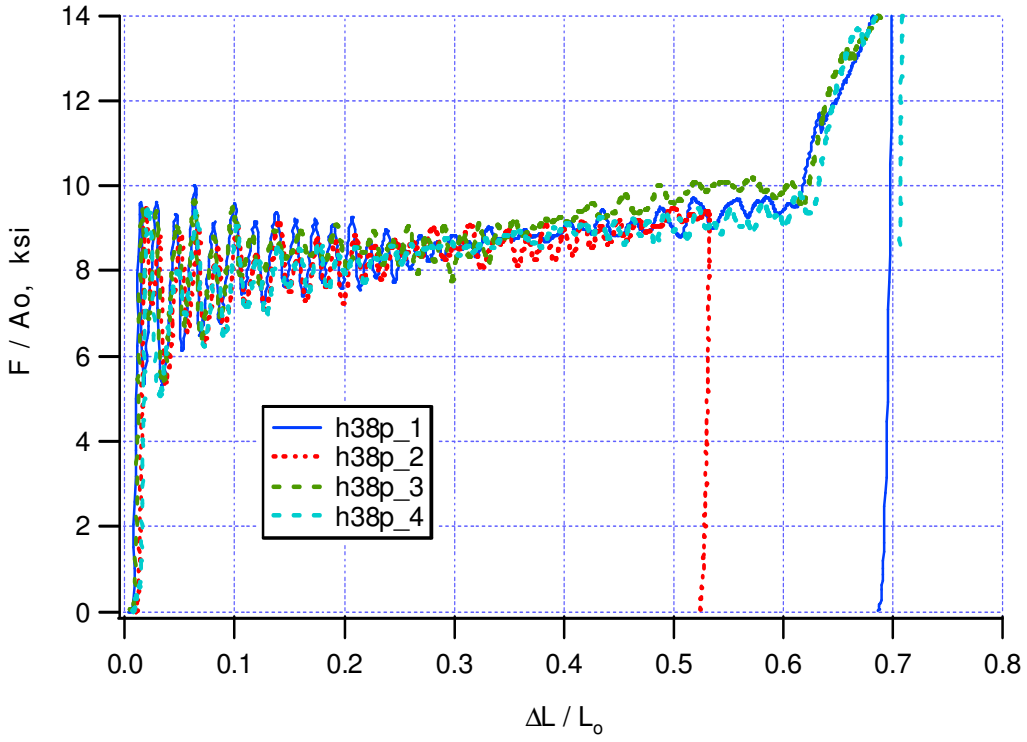

Figure 2-5. Normalized load-displacement curves of Hexcel CR-8-LC-1/8-5052-006-R2 (38 lb) punched in the W direction.

2.4 Punch of CR-8-LC-1/8-5-52-006-R2 (38 pcf) in T direction

The diameter of the punch was 1 in., and specimens were 3-in. cubes. All four tests showed consistent results, which are shown in Figure 2-5.

The normalized load-displacement (or "stress-strain") curves of punch and compression tests are different in several ways. The peak stress was 9.7 ksi, and the initial mean crush stress was 7.8 ksi, which was higher than those of bare compressions, 8.0 ksi and 5.6 ksi, respectively. If one assumes the initial friction was negligible, $F_f \approx 0$, then the shearing force was $F_s \approx 2.3$ ksi, if the rate effect was negligible. Notice that the loading rate of compression specimen was much slower than that of punch specimen (see Table 2-1).

The mean stress in the crush region increased linearly at a slope of 3.3 ksi/strain. The crush stress was 9.8 ksi at the lock-up strain 62 percent. The increase of crush stress may be due to the friction between punch and honeycomb. It is also possible that the stress generated in the transverse direction makes the honeycomb more difficult to crush. More studies on biaxial loadings are needed to validate these assumptions.

The initial peak-to-peak amplitude of stress oscillation was 4.0 ksi. It decreased to 0.8 ksi when the strain reached 30 percent and remained at that level for the rest of the crush region. The period of oscillation was 0.055 in., which was smaller than the period observed from the bare testing condition.

A typical punched specimen is shown in Figure 2-6. Notice the crack at the center of the specimen running along the L direction and the diameter of the punched hole. The crack occurred in the fully compacted state ($\Delta L/Lo > 0.6$).

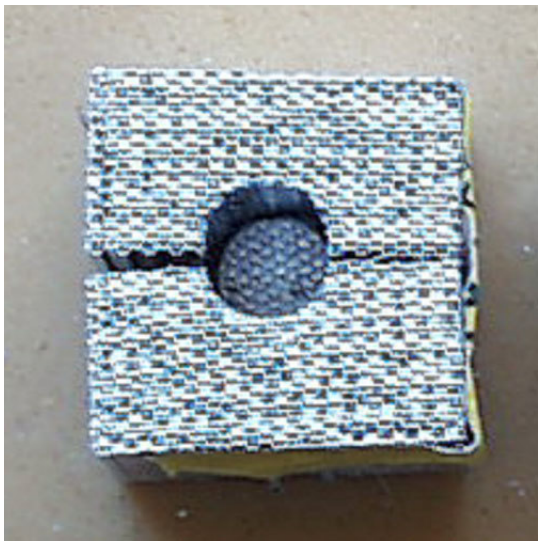

Figure 2-6. A post-experiment punch specimen of CR-8-LC-1/8-5-52-006-R2 (38 pcf).

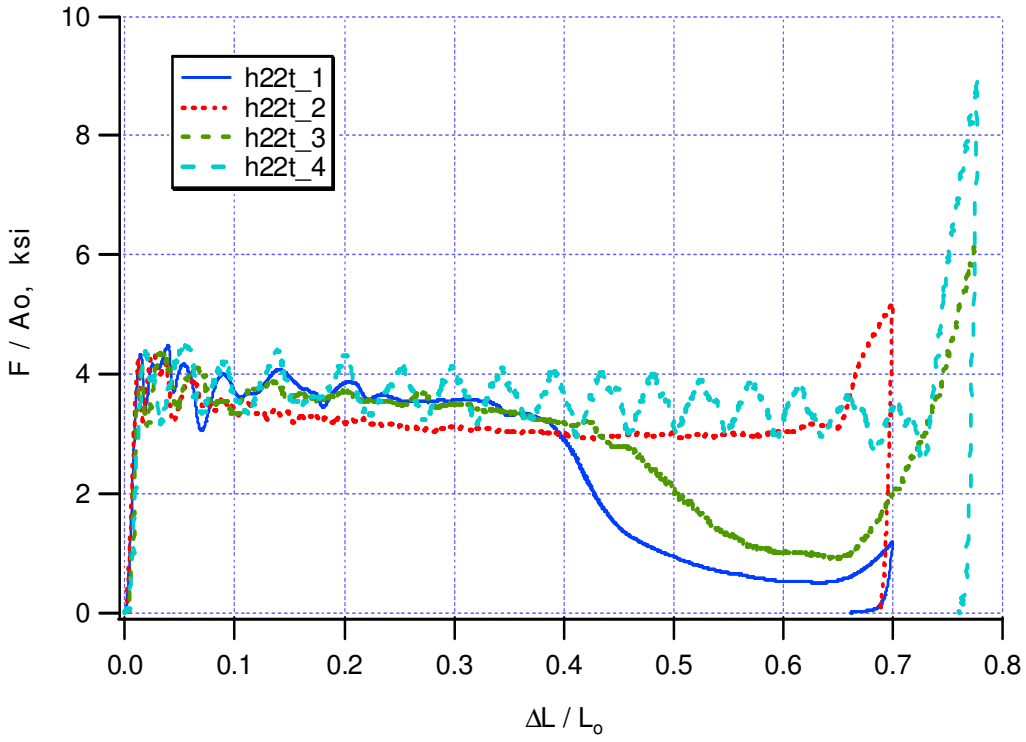

Figure 2-7. Normalized load-displacement curves of Hexcel CR-8-LC-1/8-5052-006 (22 lb) compressed in the T direction.

2.5 Crush of CR-8-LC-1/8-5-52-006 (22 pcf)

Figure 2-7 shows the results of compressing the 22 pcf honeycomb in the T direction. The stress-strain curves of this 22 pcf honeycomb were very similar to that of 38 pcf honeycomb. The peak stress was about 4.4 ksi; mean crush stress was 3.8 ksi; and the lock-up strain was 0.70 ±0.05. The crush stress of specimen h22t_4 oscillated with amplitude 1.0 ksi. As with Group 1 specimens of 38 pcf honeycomb described in Appendix I, the post-experiment specimen shows an orderly crushed pattern (see Figure 2-8). Specimen h22t_2 was similar to h38t_4 (Group 2) in that the crush was not synchronized, but retained its regular energy absorption capability. Specimen h22t_1 and h22t_3 changed from local to global buckling mode (or from regular to low-energy-absorption mode) when the strain was greater than 40 percent, which was typical for Group 3 specimens.

Only one specimen was tested in L direction compression. As shown in Figure 2-9, the peak stress was about 0.24 ksi; mean crush stress was 0.17 ksi; and the lock-up strain was about 65 percent. Without confinement, the sample delaminated and did not have an orderly crushed pattern. The post-experiment specimen shows the W dimension became much larger (see Figure 2-10).

For the compression in the W direction, similar to 38 pcf honeycomb, there was no peak load before crush, and the crush stress increased during crush (see Figure 2-11). The initial crush stress was about 0.19 ksi, and the deformation was uniform, flattening, corrugated ribbons. Without a flat sheet to constrain the expansion in the L direction as the 38 pcf honeycomb, the L dimension of post-experiment specimens was clearly larger than the initial length, as shown in Figure 2-12.

Figure 2-8. Post-experiment specimens, from top to bottom, h22t_1, h22t_2, h22t_3, and h22t_4. All were compressed in the T direction.

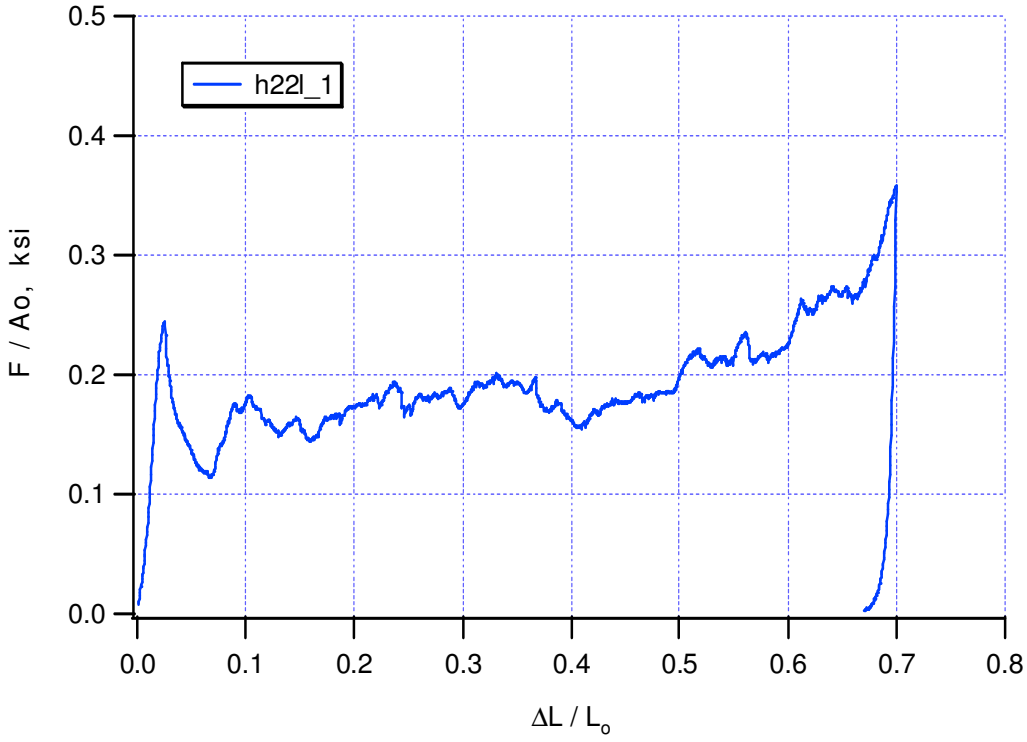

Figure 2-9. Normalized load-displacement curves of Hexcel CR-8-LC-1/8-5052-006 (22 pcf) compressed in the L direction.

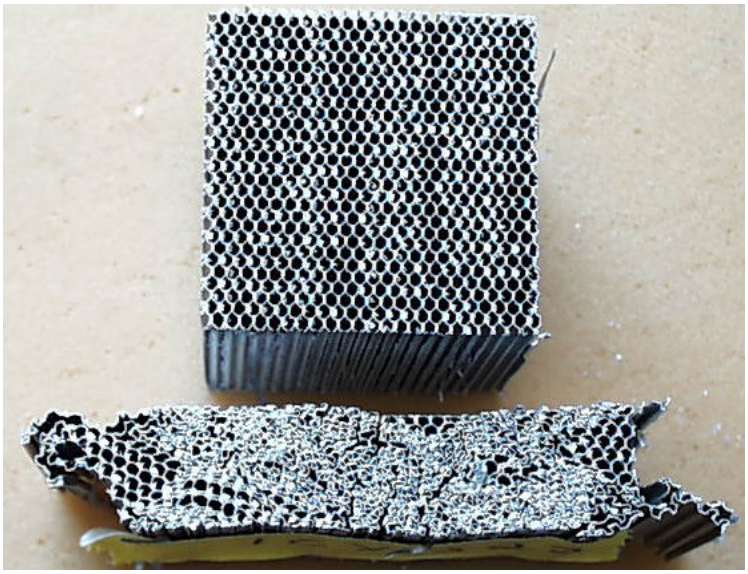

Figure 2-10. Specimen h22l_1 before (top) and after (bottom) experiment.

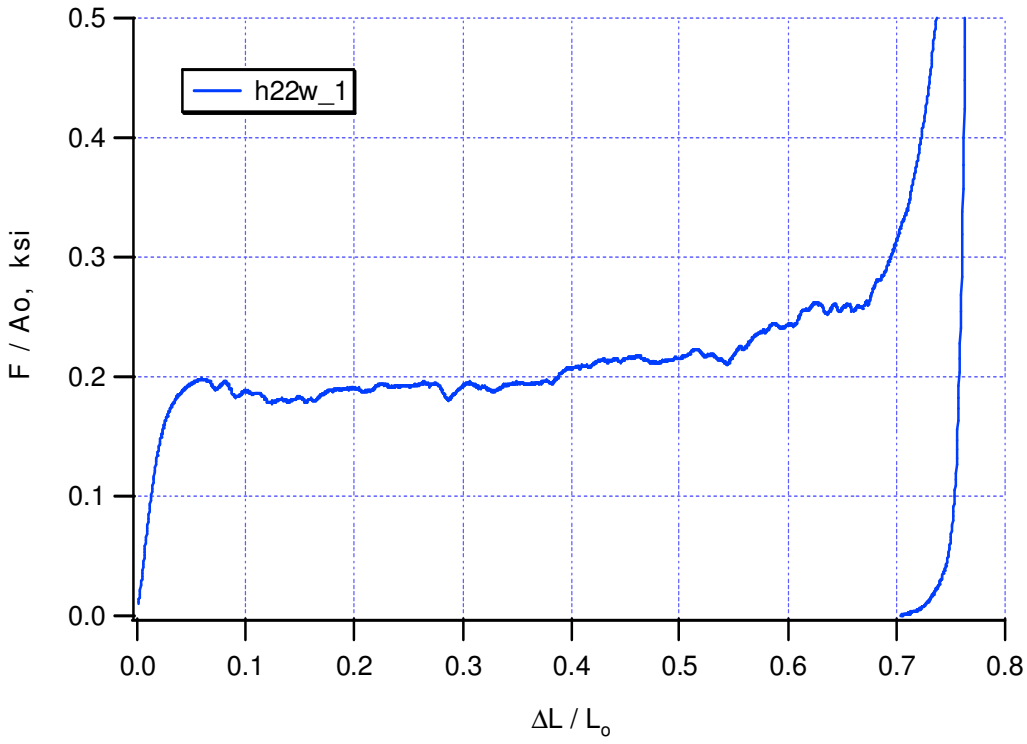

Figure 2-11. Normalized load-displacement curves of Hexcel CR-8-LC-1/8-5052-006 (22 pcf) compressed in the W direction.

Figure 2-12. Specimen h22w_1 before (top) and after (bottom) experiment.

2.6 Punch of CR-8-LC-1/8-5-52-006 (22 pcf) in the T Direction

The sizes of the punch and specimen were 1-in. diameter and 3-in. cube, respectively. The results of the three tests are shown in Figure 2-13. The normalized load-displacement curves of h22p_2 and h22p_33 have higher stress than the h22p_1 curve. Notice that specimen h22p_1

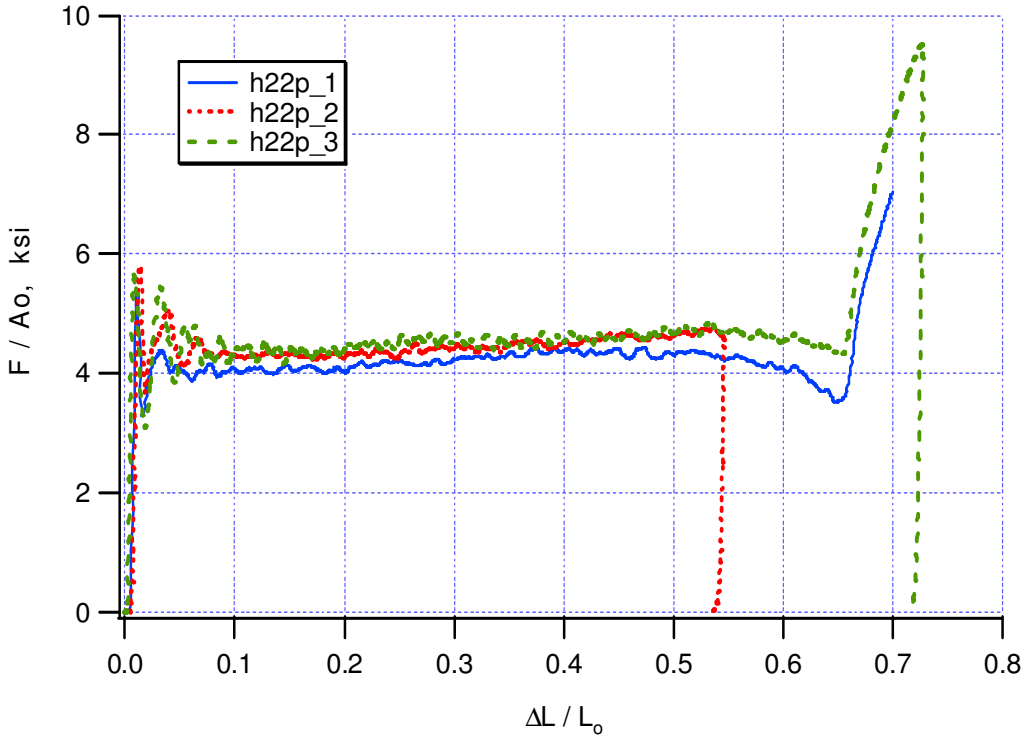

Figure 2-13. Normalized load-displacement curves of Hexcel CR-8-LC-1/8-5052-006 (22pcf) punched in the W direction.

was conducted at a much slower rate. The difference in stress displays the rate effect of the honeycomb. For h22p_1, the initial peak stress was 5.4 ksi. The initial crush stress was 4.2 ksi, which was only 0.4 ksi higher than that of bare compression. Assuming the initial friction was negligible, the shearing force was $F_s \approx 0.4$ ksi.

The crush stress increased slightly during crush, up to $\Delta L/L_o=0.55$. No cracking was observed. A post-experiment specimen is shown in Figure 2-14.

Figure 2-14. A post-experiment punch specimen of Hexcel CR-8-LC-1/8-5052-006 (22pcf).

2.7 Compression of Tube-Core Honeycombs

Tube-core honeycomb is constructed of alternate sheets of flat aluminum foil and corrugated aluminum foil wrapped around a mandrel and bound with adhesive. As shown in Table 2-3, three different sizes of tube core were involved in this set of experiments. For 5 in., 8 in., and 13 in. tube-cores, the inner diameters were 1.5 in., 0.5 in., and 2 in., and had 17, 40, and 56 layers of flat/corrugate sheet, respectively.

Tube-core honeycomb is considered axisymmetric and has two principal directions: axial and radial. Comparing the cell structures of tube-core and hexagonal-core honeycombs, the axial and radial directions resemble the T and W directions, respectively.

The 5 in. tube-core specimens were compressed in the axial direction only. The result is shown in Figure 2-15. The axial crush behavior is similar to that of the T direction of hexagonal-core honeycomb. For 8 in. and 13 in. tube cores, compressions were performed in the axial direction, as well as diametrically. Punch tests were conducted in the axial direction. Results are plotted in Figures 2-16 through 2-21. Post-experimental specimens are displayed in Figures 2-22 through 2-24.

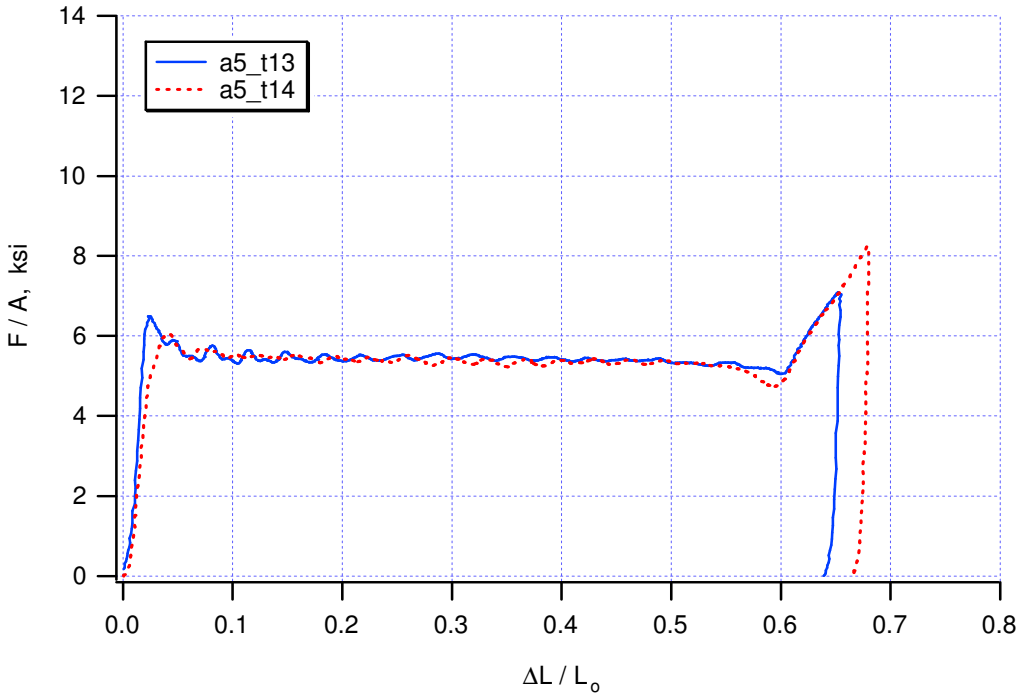

Figure 2-15. Normalized load-displacement curves of Hexcel tube-core (5 in.) compressed in the axial direction.

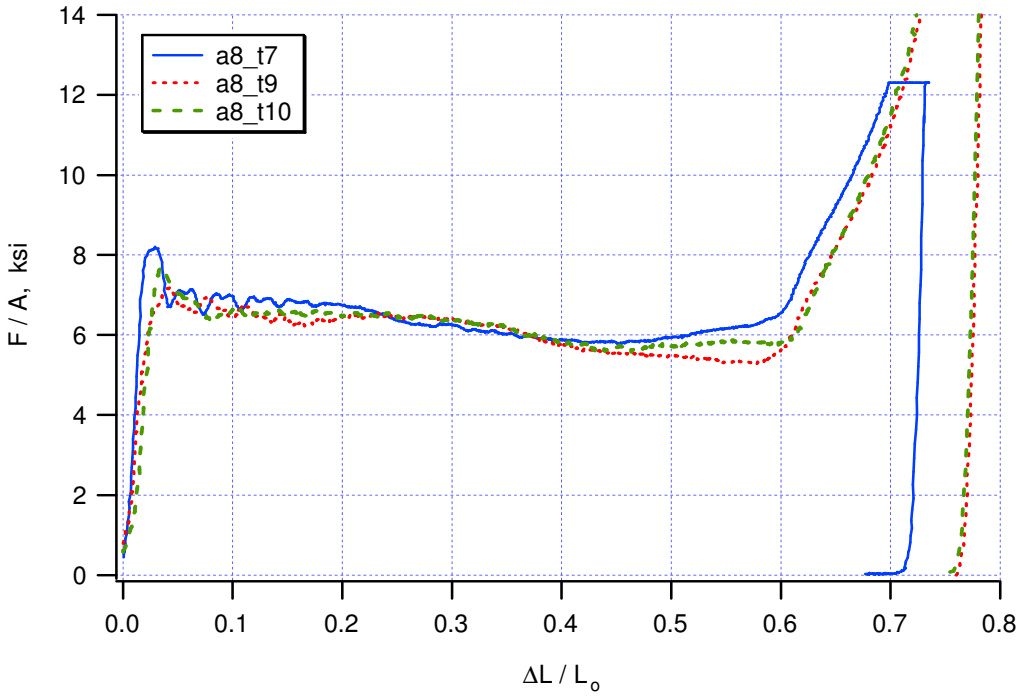

Figure 2-16. Normalized load-displacement curves of Hexcel tube-core (8 in.) compressed in the axial direction.

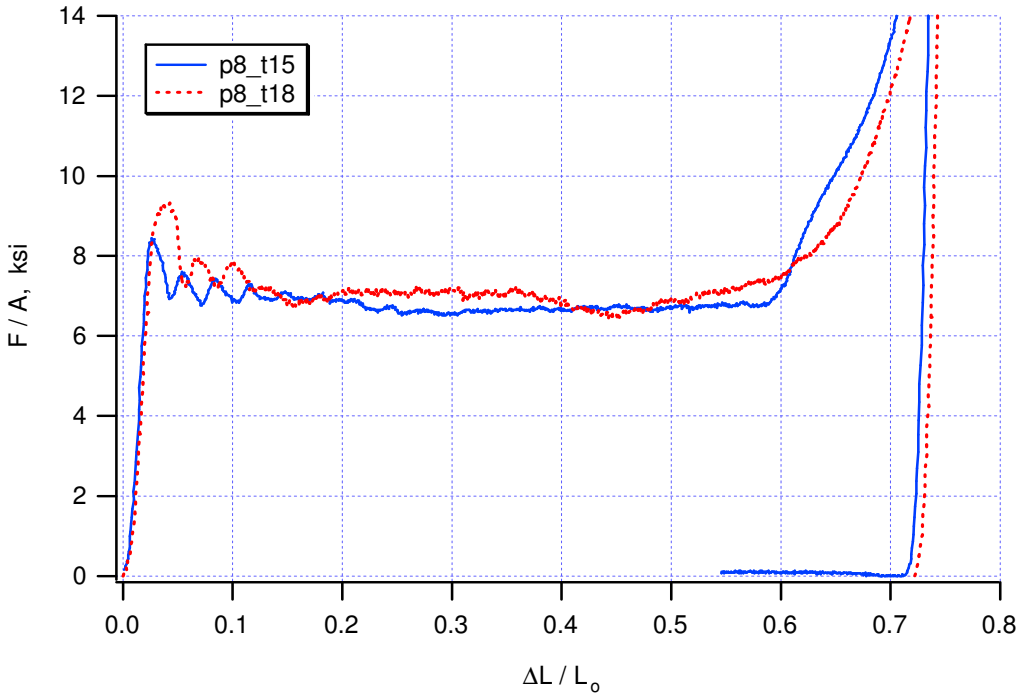

Figure 2-17. Normalized load-displacement curves of Hexcel tube-core (8 in.) punched in the axial direction.

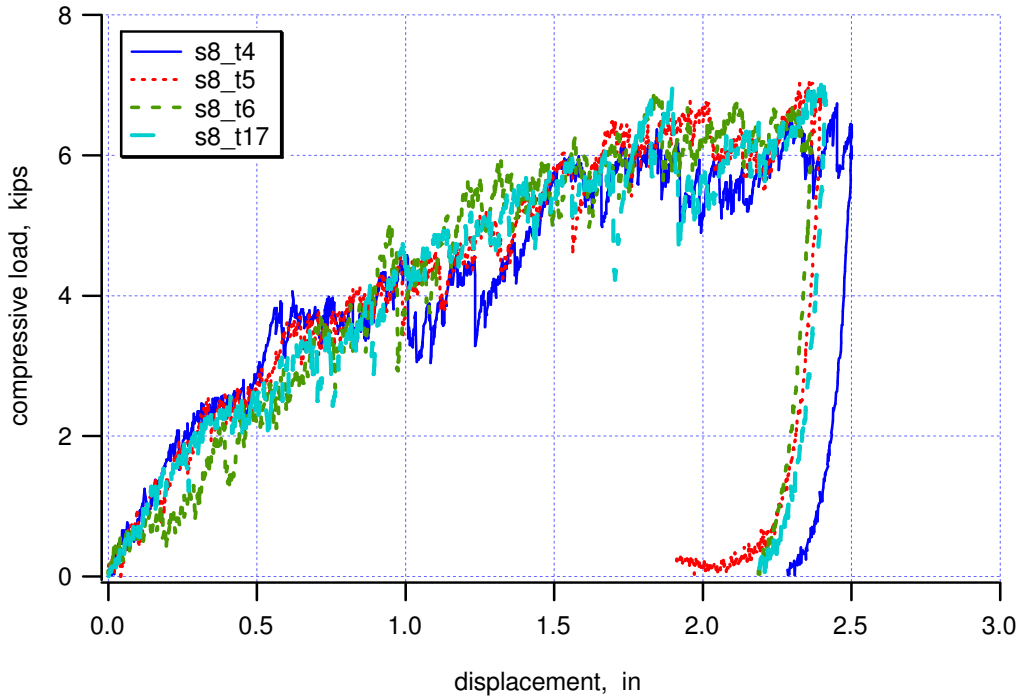

Figure 2-18. Load-displacement curves of Hexcel tube-core (8 in.) compressed diametrically.

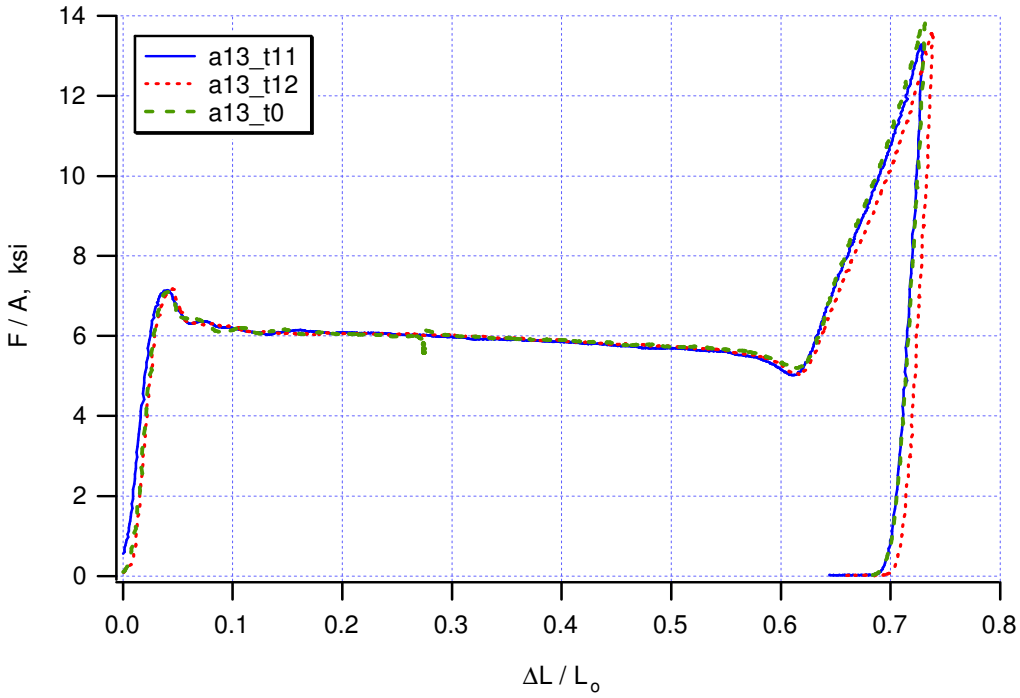

Figure 2-19. Normalized load-displacement curves of Hexcel tube-core (13 in.) compressed in the axial direction.

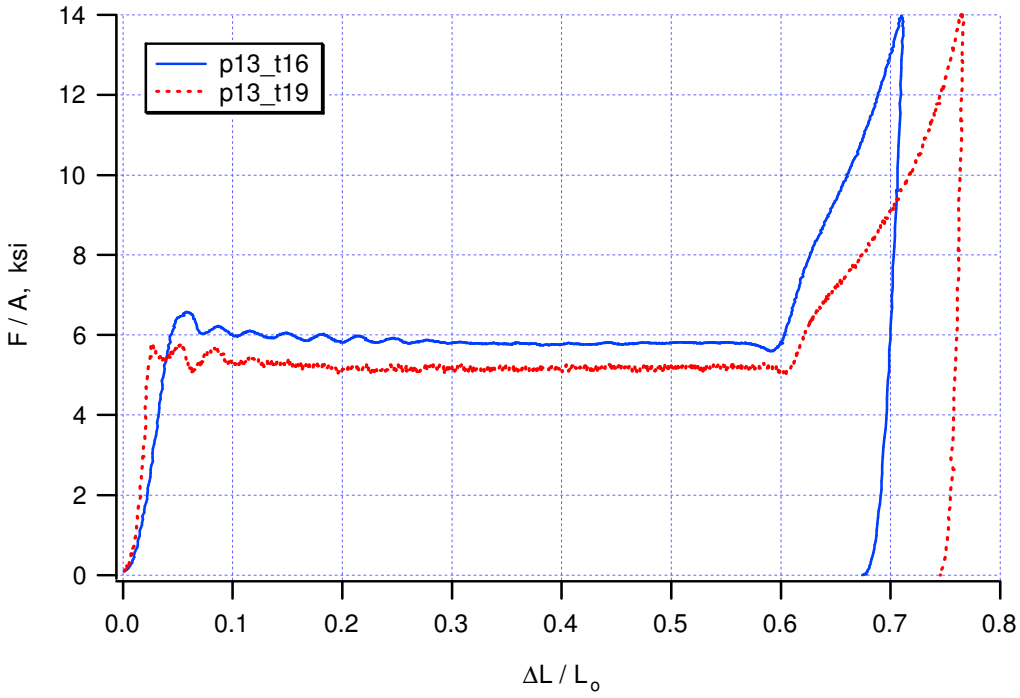

Figure 2-20. Normalized load-displacement curves of Hexcel tube-core (13 in.) punched in the axial direction.

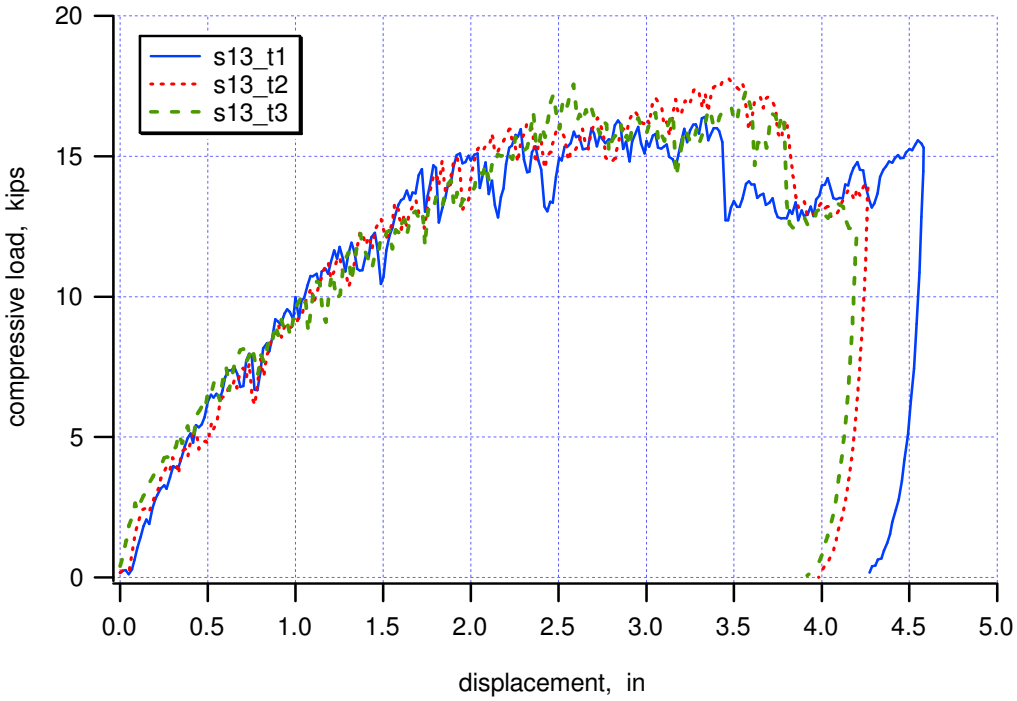

Figure 2-21. Load-displacement curves of Hexcel tube-core (13 in.) compressed diametrically.

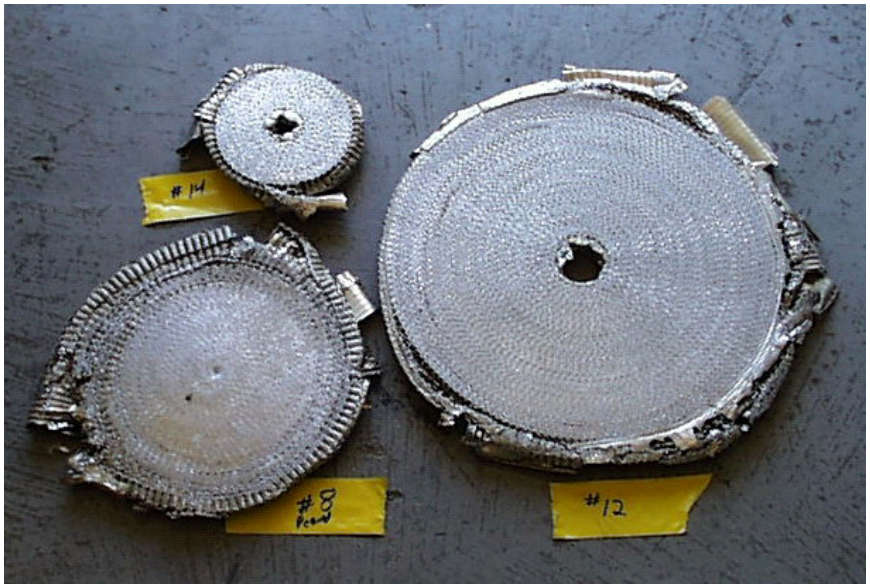

Figure 2-22. Post-experiment tube core compression specimen: 5 in. (top left), 8 in. (lower left), and 13 in. (right).

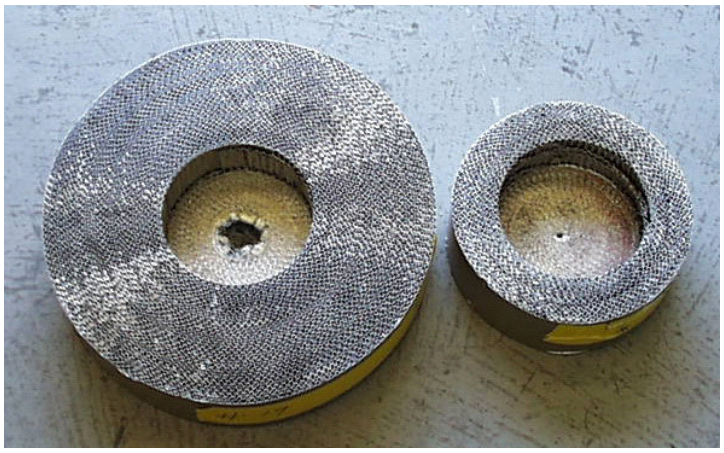

Figure 2-23. Post-experiment tube core punch specimens: 8 in. (right left) and 13 in. (left).

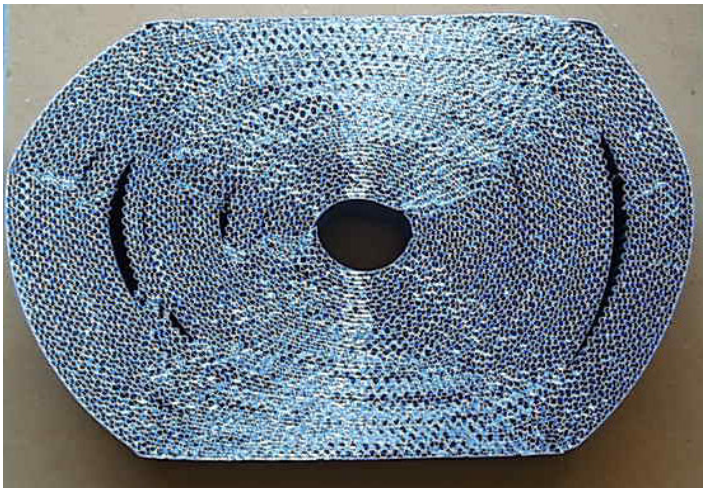

Figure 2-24. Diametrically compressed tube core specimens: 8 in. (top) and 13 in. (bottom).

This page intentionally left blank.

3. TEMPERATURE EFFECT

Similarly to all engineering components during application, honeycomb will experience a wide temperature range, typically from -65°F to 165°F. The material properties of aluminum are well known and their changes are negligible over this temperature span; however, the adhesive that binds aluminum sheets is usually temperature-dependent. The adhesive material and its mechanical and thermal properties are rarely available. Quasi-static experiments were conducted to study the temperature effect of honeycomb.

3.1 Weapons-Grade Honeycombs

Five batches of aluminum honeycomb, which satisfied the weapon specifics, were used in the rest of the honeycomb investigation. They are defined in Table 3-1 based on their nominal density.

Table 3-1. Aluminum honeycomb batches.

Vendor	Density (lb./ft^3)	Density (lb./ft^3)
Alcore	35	38
Hexcel	35	38
Hexcel-C6		38

3.2 Experimental Setup and Matrixes

In the experimental setup, shown in Figure 3-1, a long push rod was used because of the environmental chamber on the loading system. To ensure a good alignment and eliminate the lateral loading on the load cell, a self-aligned compression fixture was designed. Refer to Appendix I for lateral force during crush.

3.3 Experimental Results of Alcore35

Normalized load-displacement curves of Alcore35 are plotted in Figures 3-2 through 3-10, and experimental results are summarized in Table 3-2. In the crush curve of A35_1 (the blue curve) in Figure 3-2, for example, the crush strength is calculated by taking the average of stress data between the first valley on the curve, about 0.06 strain, and the beginning of densification, about 0.63 strain. The crush efficiency is the difference between strains that correspond to the initial peak stress σ_p and the point on the densification curves that has the same value as σ_p. For A35_1, the values are about 4 percent and 64 percent, respectively, and the crush efficiency is about 60 percent. The features of initial peak, first valley, and densification are easily identified from the crush curves of the T and L crushes. Those features, however, are not clear in the W direction crush curves as shown in Figures 3-4, 3-6, or 3-10. The crush strength is calculated as the average of stress for the flat portion of the curve; for example, between 0.1 and 0.3 strain.

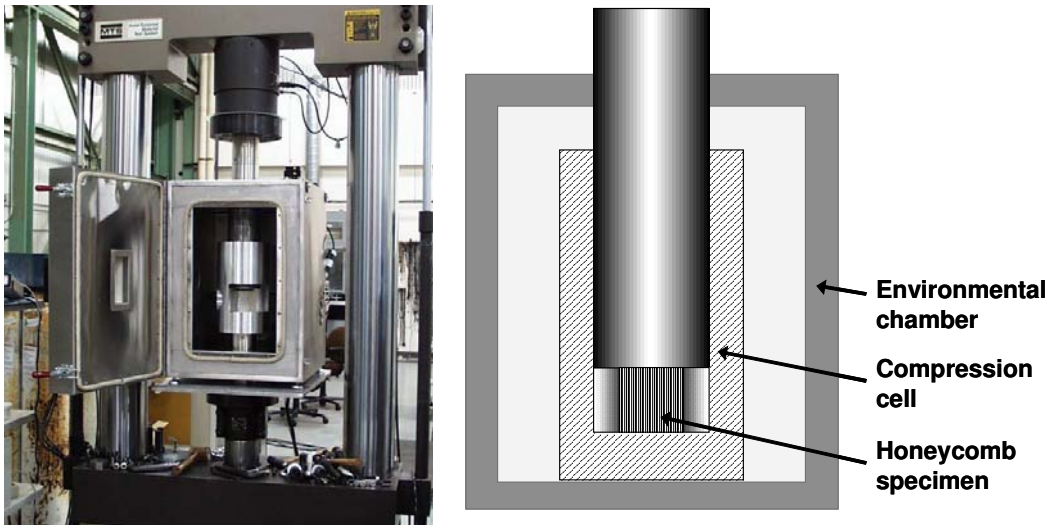

Figure 3-1. Experimental setup for quasi-static bare compression of honeycomb. Test matrixes are listed in Tables 3-2 and 3-3 for Alcore 35 and Hexcel 38, respectively. Bare compression and punch test were considered. A knurled plate was used in some bare compression tests (A35_5, 6, 9 and H38_5, 6, 6a) to see if it improved normal crush mode. In punch test, the punch rod diameter was one inch.

Table 3-2. Quasi-static crush of Alcore35 at various temperatures.

A35_	Loading	Dir	Temp	Size (T x L x W)	System	Rate in/s	Strength ksi	Efficiency %
1	comp	T	Ambient	3 x 3 x 3	220K	0.0002	4.99	59.92
2	comp	T	Ambient	3 x 3 x 3	220K	0.0002	5.05	59.25
3	punch	T	Ambient	3 x 3 x 3	220K	0.0017	6.71	63.83
4	punch	T	Ambient	3 x 3 x 3	220K	0.0025	7.07	61.5
5	comp	T	Ambient	1.5 x 3 x 3	220K	0.0002	5.33	57.07
6	comp	T	Ambient	1.5 x 1.5 x 1.5	220K	0.0002	5.29	57.28
6a	comp	T	Ambient	1.5 x 1.5 x 1.5	220K	0.0002	5.04	57.28
7	comp	L	Ambient	3 x 3 x 3	220K	0.0002	0.821	55.56
8	comp	L	Ambient	3 x 3 x 3	220K	0.0002	0.806	55.83
9	comp	L	Ambient	3 x 1.5 x 3	220K	0.0008	0.765	51.75
10	comp	L	Ambient	3 x 1.5 x 3	220K	0.0008	0.79	55.43
11	comp	W	Ambient	3 x 3 x 1.5	220K	0.0008	0.538	
12	comp	W	Ambient	3 x 3 x 1.5	220K	0.0008	0.523	
13	comp	T	165°F	3 x 3 x 3	AT	0.0167	4.05	
14	comp	T	165°F	3 x 3 x 3	AT	0.0167	4.2	
15	punch	T	165°F	3 x 3 x 3	AT	0.0167	5.84	65.69
16	comp	T	165°F	1.5 x 3 x 3	AT	0.0167	4.65	62.97
17a	comp	T	165°F	1.5 x 1.5 x 1.5	AT	0.0167	4.37	
18	comp	L	165°F	3 x 3 x 3	AT	0.0167	0.746	69.5
19	comp	L	165°F	3 x 3 x 3	AT	0.0167	0.734	65.3

Table 3-2. Quasi-static crush of Alcore35 at various temperatures (continued).

A35_	Loading	Dir	Temp	Size (T x L x W)	System	Rate in/s	Strength ksi	Efficiency %
20	comp	L	165°F	3 x 1.5 x 3	AT	0.0167	0.766	57.1
21a	comp	L	165°F	1.5 x 1.5 x 1.5	AT	0.0167	0.666	
22	comp	W	165°F	3 x 3 x 1.5	AT	0.0167	0.493	
23a	comp	W	165°F	1.5 x 1.5 x 1.5	AT	0.0167	0.42	
24	comp	T	-65°F	3 x 3 x 3	AT	0.0167	5.27	68.2
25	comp	T	-65°F	3 x 3 x 3	AT	0.0167	3.41	73.5
26	punch	T	-65°F	3 x 3 x 3	AT	0.0167	7.6	
27	comp	T	-65°F	1.5 x 3 x 3	AT	0.0167	5.42	62.6
28a	comp	T	-65°F	1.5 x 1.5 x 1.5	AT	0.0167	5.13	68.8
29	comp	L	-65°F	3 x 3 x 3	AT	0.0167	0.559	
30a	comp	L	-65°F	3 x 3 x 3	AT	0.0167	0.62	
31	comp	L	-65°F	3 x 1.5 x 3	AT	0.0167	0.715	60.7
32a	comp	L	-65°F	1.5 x 1.5 x 1.5	AT	0.0167	0.586	70.1
33	comp	W	-65°F	3 x 3 x 1.5	AT	0.0167	0.553	
34a	comp	W	-65°F	1.5 x 1.5 x 1.5	AT	0.0167	0.523	

Table 3-3. Quasi-static crush of Hexcel38 at various temperatures.

H38_	Loading	Dir	Temp	Size (T x L x W)	System	Rate (in./s)	Strength (ksi)	Efficiency (Percent)
1	comp	T	Ambient	3 x 3 x 3	AT	0.0167	5.76	63.68
5	comp	T	Ambient	1.5 x 3 x 3	AT	0.0167	5.98	56.11
6	comp	T	Ambient	1.5 x 1.5 x 1.5	AT	0.0167	4.91	61.28
6a	comp	T	Ambient	1.5 x 1.5 x 1.5	AT	0.0167	5.36	
13	comp	T	165	3 x 3 x 3	AT	0.0167	5.05	65.40
15	punch	T	165	3 x 3 x 3	AT	0.0167	7.42	58.84
24	comp	T	-65	3 x 3 x 3	AT	0.0167	6.33	64.50
26	punch	T	-65	3 x 3 x 3	AT	0.0167	8.99	59.56

For those tests, a knurled plate was used. Part of the honeycomb was squeezed into the knurl plate, so the initial stress peak and the subsequent crush appeared to happen at a larger strain when compared to platen-platen compression. The normalized load-displacement curve did not precisely describe the deformation of those honeycomb specimens; however, the crush strength was not affected and the value was still accurate. (Note that in this series of experiments, the focus was on crush behaviors and large deformation of honeycomb. In general, the measured strain was not accurate enough to characterize the elastic behavior due to uncertainties in dimensions and displacement measurements.)

The crush behavior of Alcore35 at ambient conditions is very similar to the commercial grade honeycomb. The curves for the punch tests show that stress increases at a rate of about 3 ksi/strain during crush (see Figure 3-2).

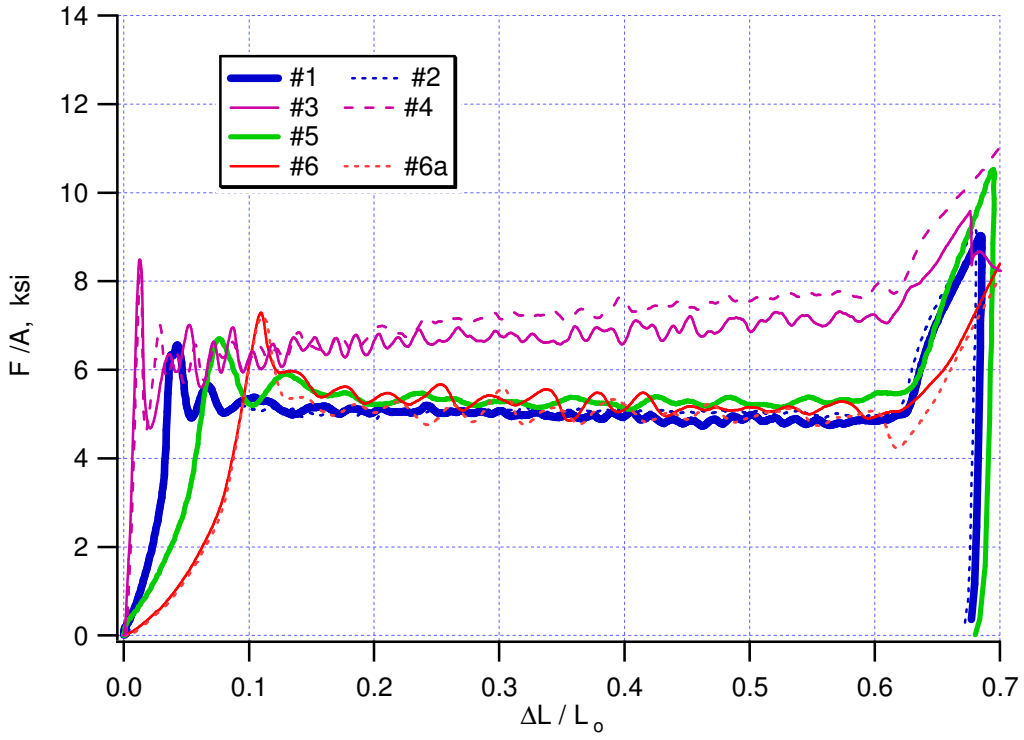

Figure 3-2. Normalized load-displacement curves of Alcore35 crushed in the T direction, quasi-static loading at ambient temperature.

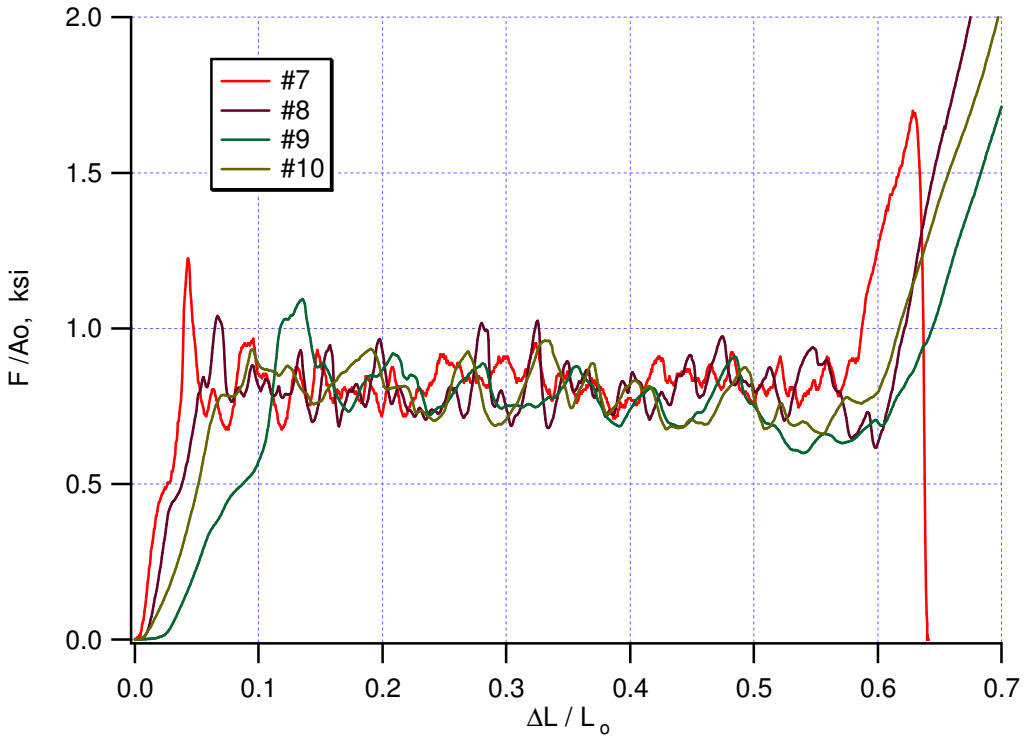

Figure 3-3. Normalized load-displacement curves of Alcore35 crushed in the L direction, quasi-static loading at ambient temperature.

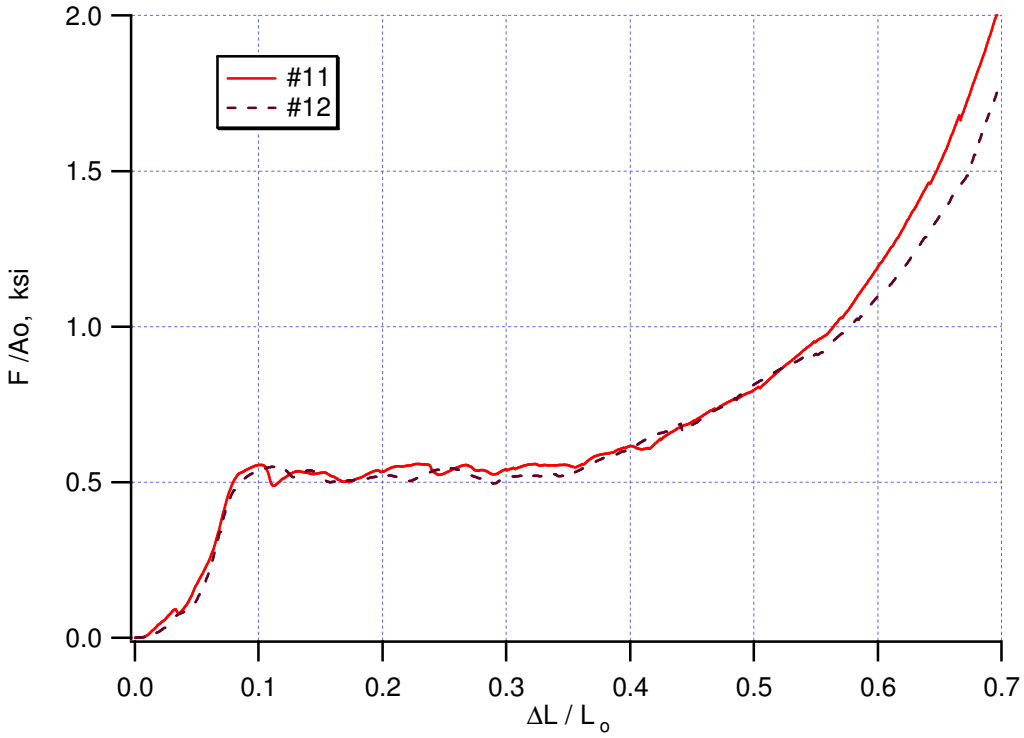

Figure 3-4. Normalized load-displacement curves of Alcore35 crushed in the W direction, quasi-static loading at ambient temperature.

Figures 3-5 to 3-7 show compression results of Alcore35 at 165°F. Almost all specimens that uniformly compressed in the T direction (except #16 [the green curve]) were deformed in low-energy-absorption mode, and the stress dropped below 2 ksi at strain less than 0.15 (shown in Figure 3-5). The punch curve was different from ambient conditions in that it remained level instead of increasing during most of the crush period. The crush of Alcor35 in the L and W directions at 165°F was similar to ambient conditions.

The results of Alcore35 tests at -65°F are shown in Figure 3-8 to 3-10. Again, most of the specimens showed changes from normal to abnormal during crush in the T direction. Specimen A35_25 immediately fell to abnormal mode after the initial peak stress. Specimen A35_24 and 28a changed mode at 0.35 and 0.25, respectively. For the punch test at the cold temperature, the stress slowly increased with strain during the first half of the crush, then decreased at strain = 0.3, which indicated an abnormal crush condition.

The crush strength data, listed in Table 3-2, shows a general trend toward higher temperatures resulting in lower crush strength of Alcore35. The temperature effect was not quantified, since many samples were deformed in the abnormal mode, especially at high and low temperatures. These results show that bare compression of honeycomb is not an ideal experimental method to yield consistent data.

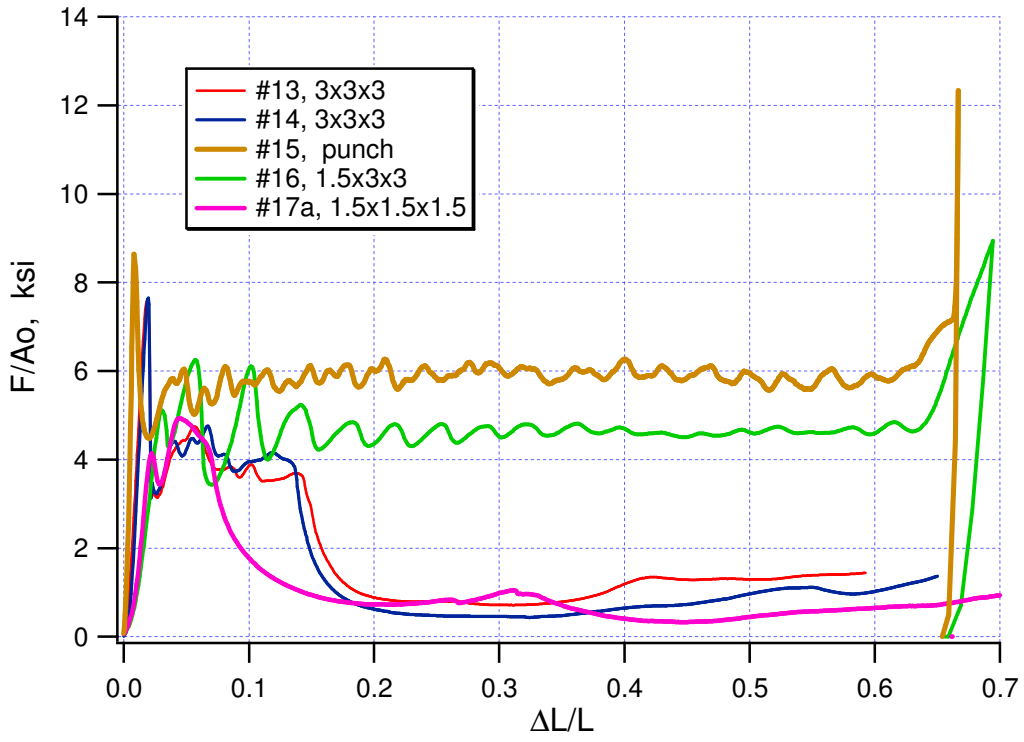

Figure 3-5. Normalized load-displacement curves of Alcore35 crushed in the T direction, quasi-static loading at 165°F.

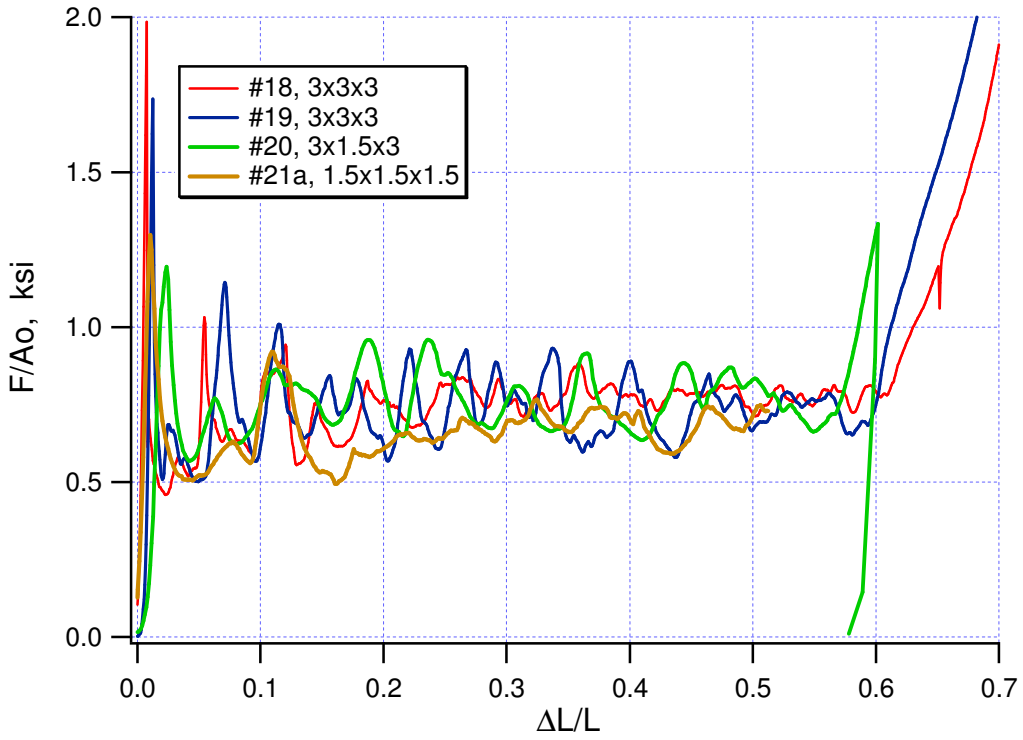

Figure 3-6. Normalized load-displacement curves of Alcore35 crushed in the L direction, quasi-static loading at 165°F.

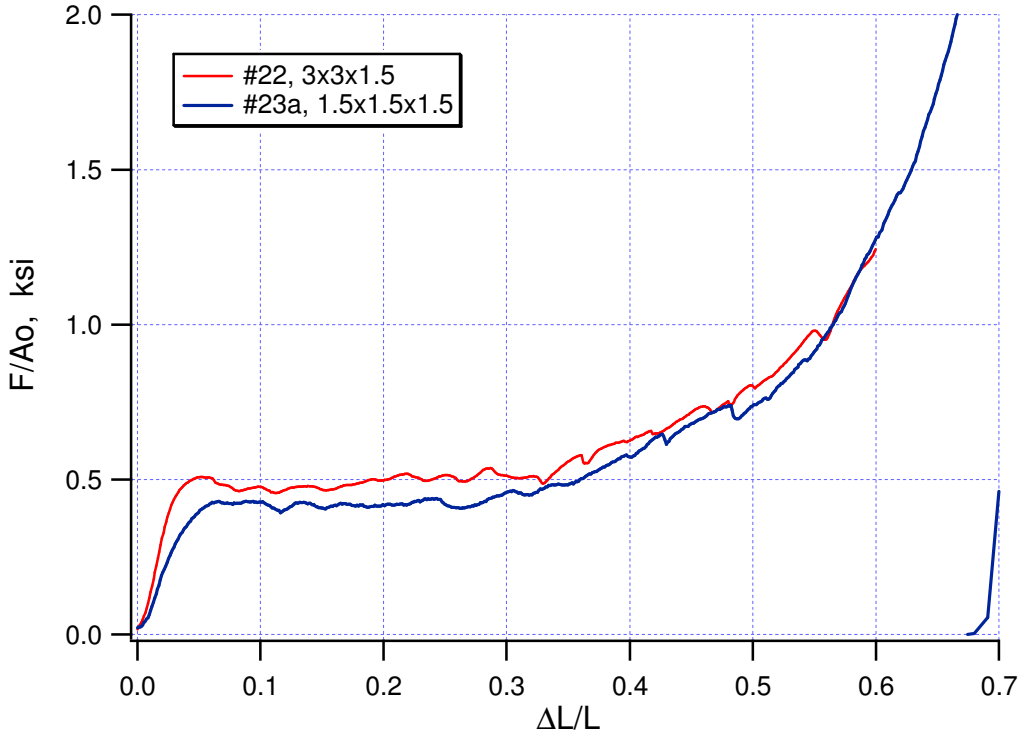

Figure 3-7. Normalized load-displacement curves of Alcore35 crushed in the W direction, quasi-static loading at 165°F.

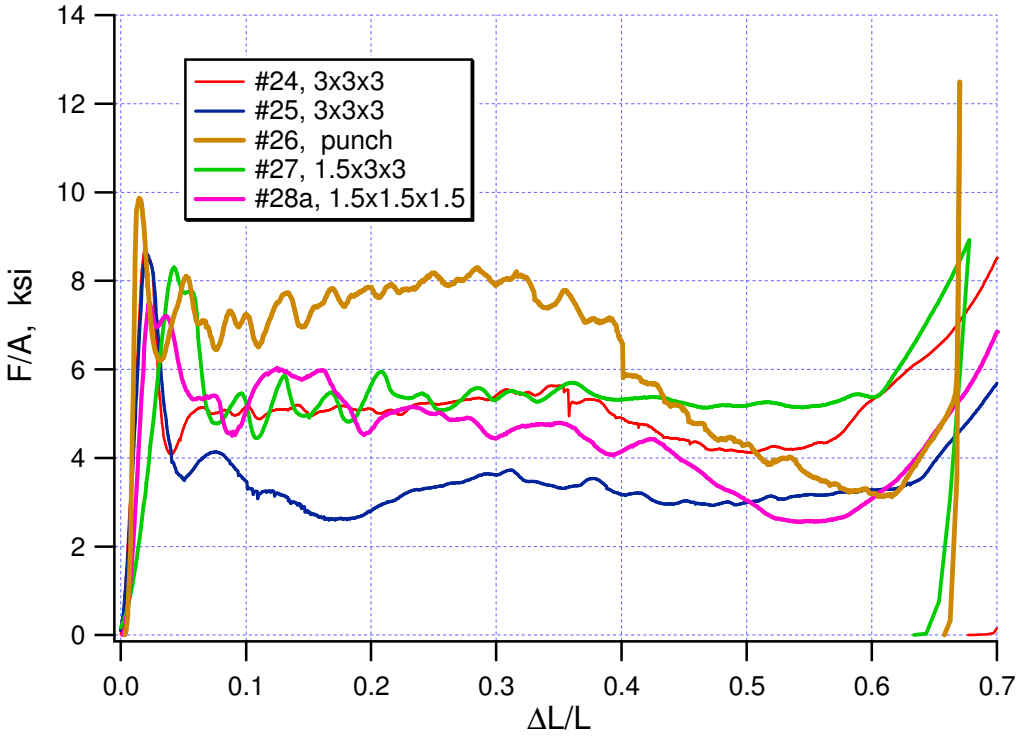

Figure 3-8. Normalized load-displacement curves of Alcore35 crushed in the T direction, quasi-static loading at -65°F.

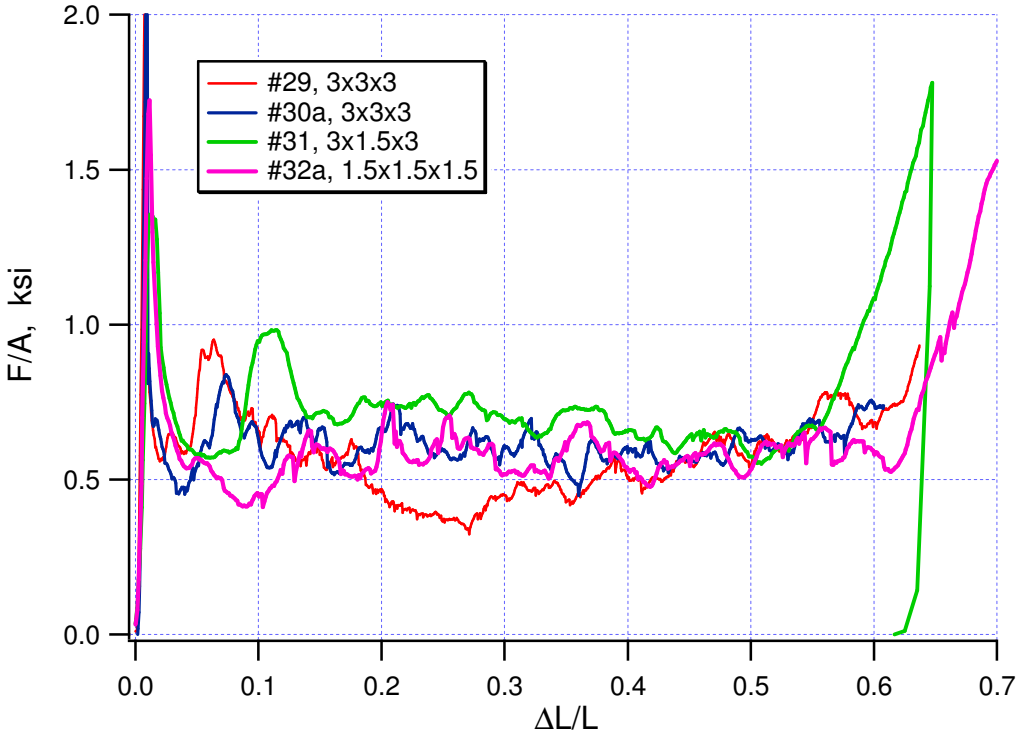

Figure 3-9. Normalized load-displacement curves of Alcore35 crushed in the L direction, quasi-static loading at -65°F.

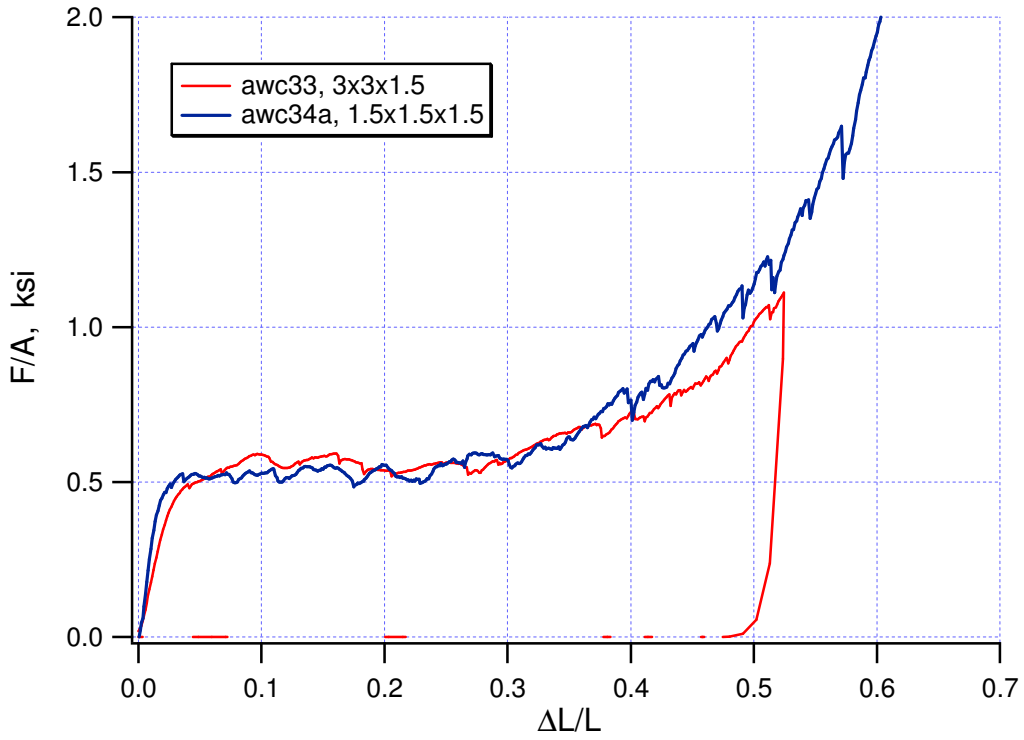

Figure 3-10. Normalized load-displacement curves of Alcore35 crushed in the W direction, quasi-static loading at -65°F.

3.3.1 Normal and Abnormal Crush Modes

Some typical deformation patterns of Alcore35 during bare compression at ambient conditions are shown in Figure 3-11 through 3-13. Specimen A35_16 demonstrates an ideal normal mode of crush in Figure 3-11. The series of pictures show the deformation of the T-W plane. As the lower platen moved upwards, the aluminum sheets buckled locally, layer by layer, and gradually propagated through the whole specimen.

Specimen A35_14 displays a possible abnormal crush mode at 165°F (Figure 3-12). The specimen deformed in global buckling, exhibiting the second buckling mode. Instead of creating numbers of plastic hinges by local buckling, as A35_16, the specimen had only two rows of plastic hinge. As the number of plastic hinges decreased, the honeycomb reduced its energy absorption capability. Note that not all specimens deformed this way at high temperature.

At -65°F, Alcore35 honeycomb tended to split during compression. As shown in Figure 3-13, specimen A35_25 split open at small strain. One part fell flat and did not carry the load. It was hardly deformed and did not absorb much energy. Even though the other half of the specimen nicely crushed, the energy absorption capacity of the honeycomb was not fully utilized and the specimen was considered crushed in an abnormal mode.

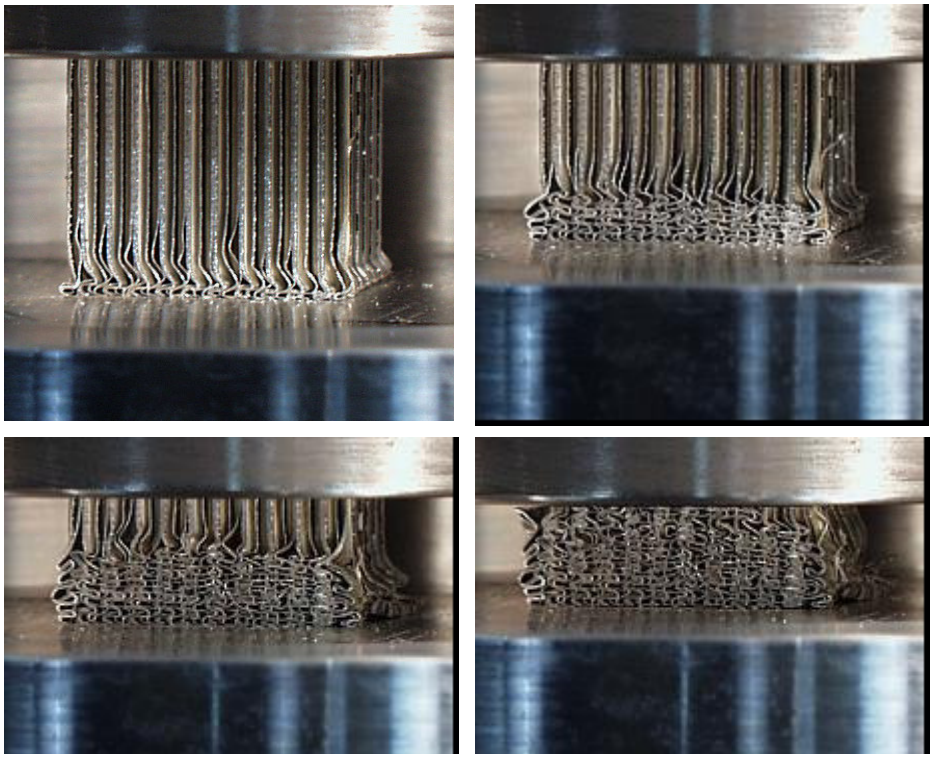

Figure 3-11. Specimen A35_16 showed normal crush mode (local buckling) at ambient temperature.

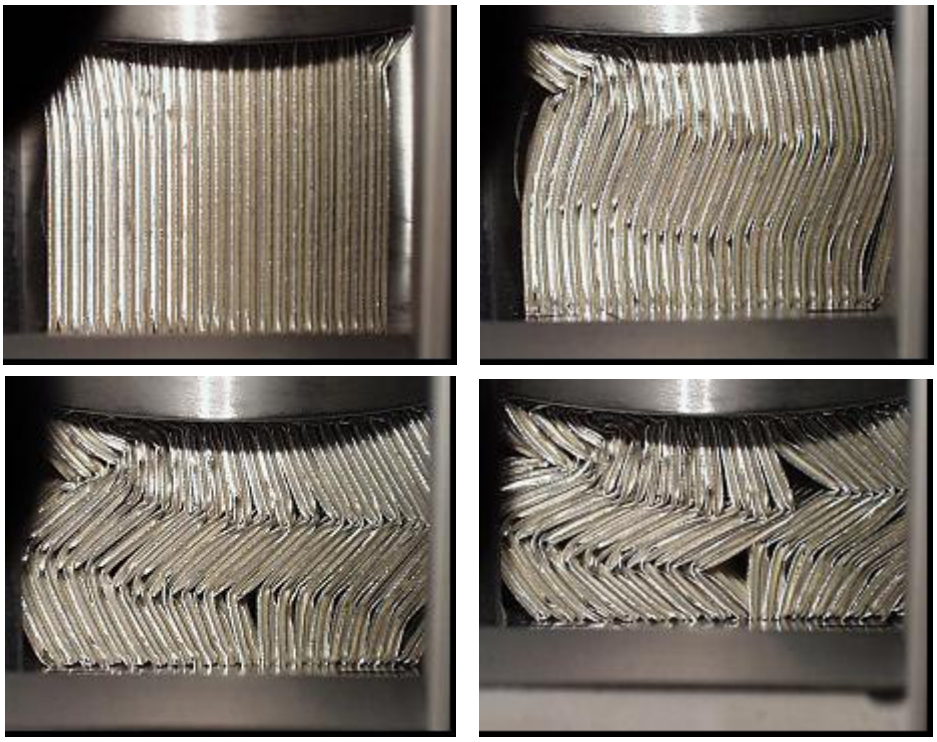

Figure 3-12. Specimen A35_14 deformed in global buckling at 165°F.

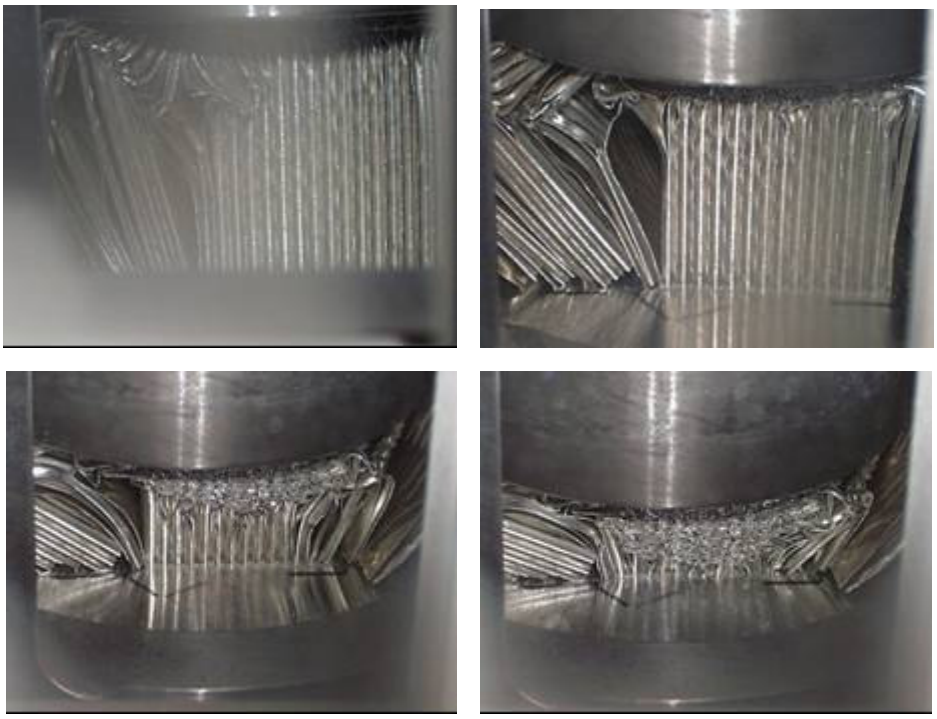

Figure 3-13. Specimen A35_14 deformed in global buckling at -65°F.

3.4 Experimental Results of Hexcel38

The results of crush of Hexcel38 in the T direction, shown in Figures 3-14 through 3-16, indicated a similar temperature effects as Alcore35. Although the number of tests was very limited and specimens were mostly not in the normal mode of crush, the punch results in Figure 3-16 clearly implied that the crush strength of Hexcel38 was higher when tested in a lower temperature. The effect of temperature on crush mode, however, was not quite the same for these two honeycombs. Some post-experiment specimens are displayed in Figure 3-17. For bare compression at ambient conditions, Hexcel38 tended to split open and the normalized load-displacement curve exhibited a slightly negative slope during compression, shown in Figure 3-14. This was rarely observed on Alcore35 specimens tested in the same condition. At 165°F, Hexcel38 crushed in normal mode, while Alcore35 easily got into global buckling mode. This can be seen from the normalized load-displacement curves in Figure 3-15, as well as the post-experiment specimen in Figure 3-17. Depending on the size of the specimen, Alcore35 could buckle in the first mode, Specimen A35_17a, or the second mode, A35_13. At -65°F, there was no difference between these two honeycombs; both were inclined to split open and deform in abnormal mode.

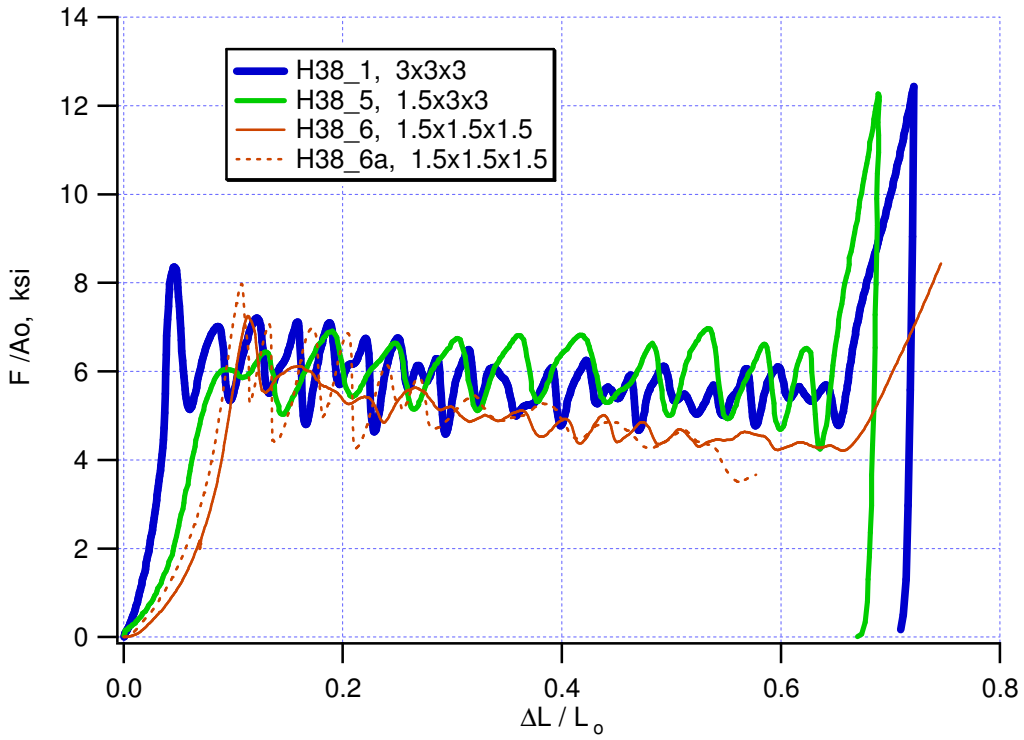

Figure 3-14. Normalized load-displacement curves of Hexcel38 crushed in the T direction at ambient temperature.

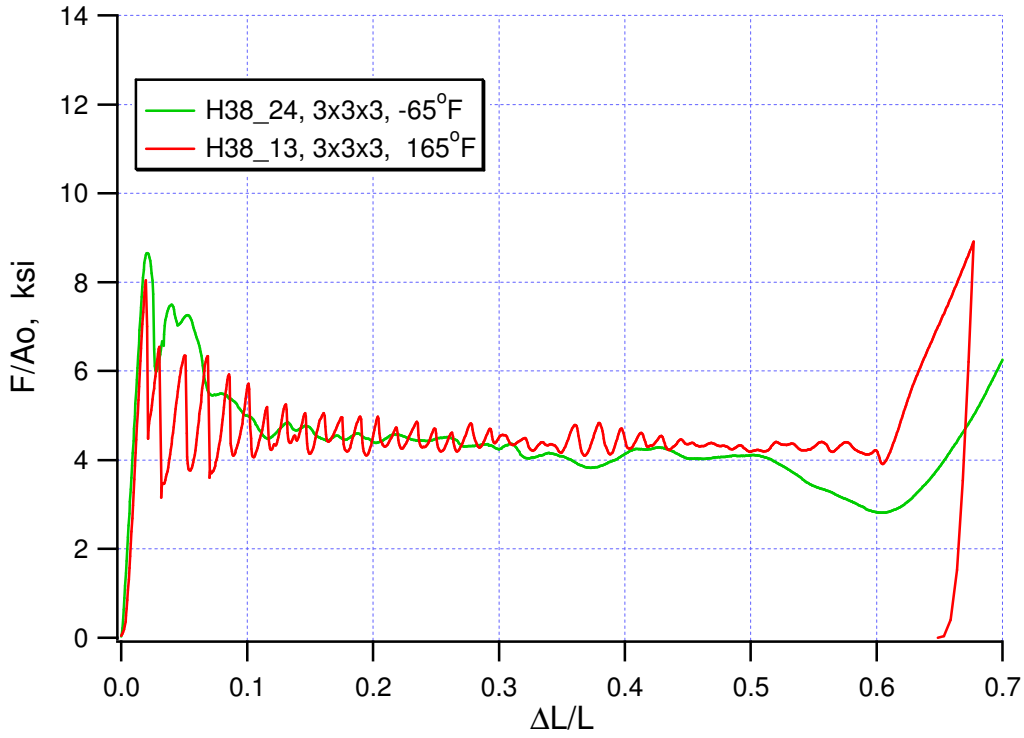

Figure 3-15. Normalized load-displacement curves of Hexcel38 compressed in the T direction at -65°F and 165°F.

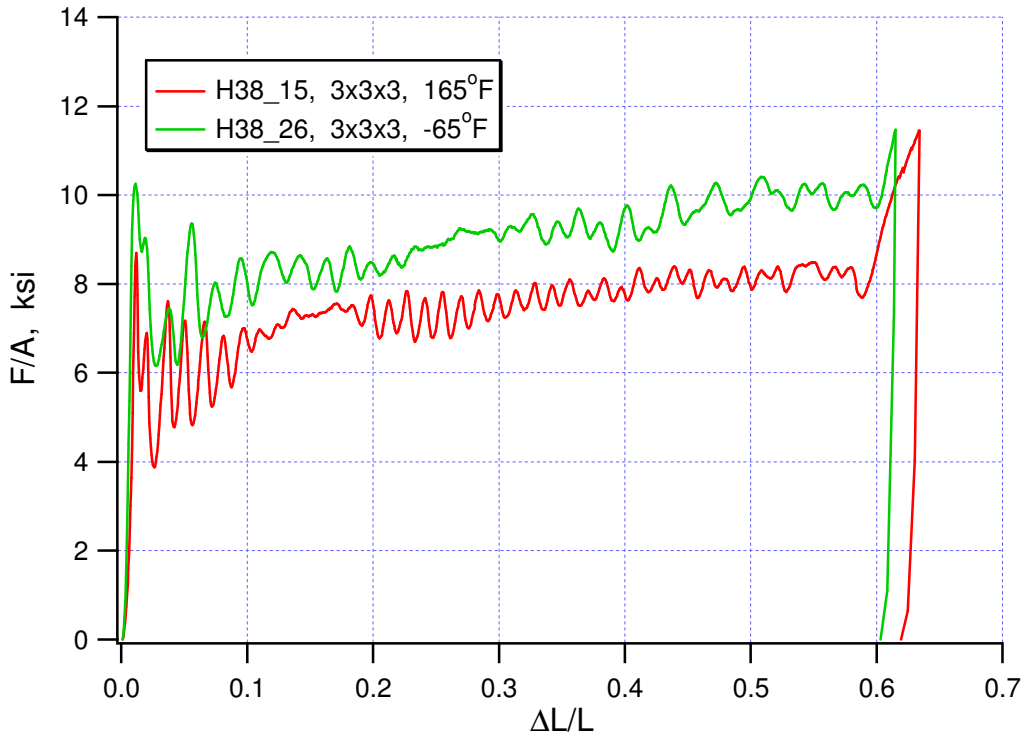

Figure 3-16. Normalized load-displacement curves of Hexcel38 punched in the T direction at -65°F and 165°F.

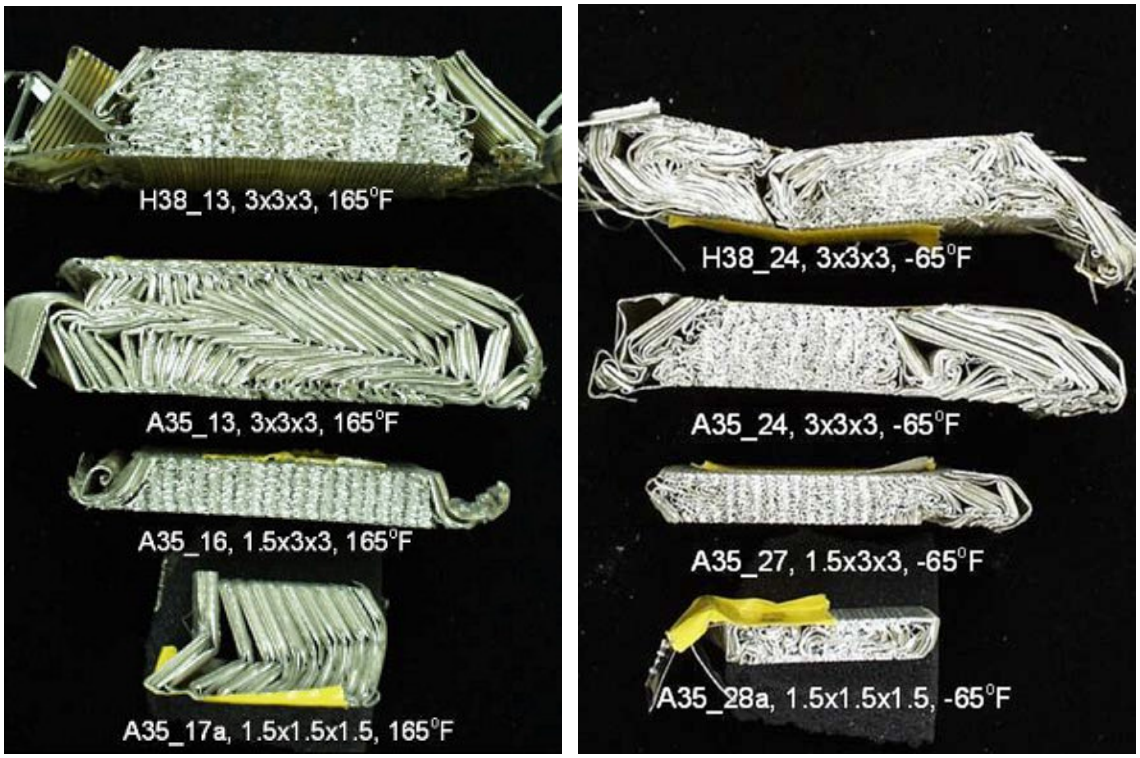

Figure 3-17. Post-experiment specimens crushed at -65°F and 165°F.

3.5 Aspect Ratio of Honeycomb Specimens

The aspect ratio of a specimen is defined as the length of the specimen (the dimension that is parallel to the loading axis) over the width (the dimension that is perpendicular to the loading axis). The honeycomb specimens listed in Table 3-2 and 3-3 all had square cross-sections. This set of specimens involved three geometries: 3 in. × 3 in. × 3 in., 1.5 in. × 1.5 in. × 1.5 in. and 1.5 in. × 3 in. × 3 in.; the aspect ratios were 1.0, 1.0, and 0.5, respectively.

Shown in Figures 3-5, 3-8, and 3-14, specimens of three geometries were included in the same type of test. The specimen with an aspect ratio of 0.5 always had a crush curve of typical normal mode, whereas specimens with an aspect ratio of 1.0 usually turned into an abnormal crush mode.

The result implies that specimens with a lower aspect ratio have a better chance to crush in normal mode during bare compression.

3.6 Size Effect of Honeycomb Specimen

From the results shown in Sections 3.2 and 3.3, the cross-section of a specimen does not appear to affect the crush strength of honeycomb, where the width of the specimen is greater than 1.5 in. For the convenience of experiments, specimens with a smaller cross-section are desired. One practical reason is that the high-rate testing system is needed for characterizing the rate effect of honeycomb. The capacity of the system is limited to 20 kips. In a typical normalized load-displacement curve of A35_27 in Figure 3-8, for example, there is an initial peak (about 8.3 ksi) that precedes relatively constant-load crush (about 5.5 ksi). The initial peak strength could be more than 50 percent higher than the crush strength. It corresponds to a load of 18.7 kips. The initial peak load of this quasi-static experiment already exceeds 90 percent capacity of the system, which poses concerns for the high-rate experiment if the same size specimen is used.

Details of the size effect experiments and the results are included in Appendix I. The results suggest that specimens with a cross-sectional area greater than 0.6 in. × 0.6 in., or approximately 50 or more cells) are acceptable for characterizing high-density (35 – 38 pcf) aluminum honeycombs.

4. INTERMEDIATE RATE ON-AXIS COMPRESSION

4.1 Bare Compression and Punch Test

The ability to absorb energy during impact (i.e., high speed loading) is an important feature of honeycomb. The dynamic crush strength is, in general, higher than the static crush strength, but this dynamic enhancement of honeycomb is not well understood due to its composite constituents, as well as complex geometry and crush mechanism. The dynamic crush strength versus impact velocity could be nonlinear and it always requires tests to quantify [4].

Under quasi-static loading, honeycomb may crush in various modes, as described before. At higher loading rates, it is even harder to crush honeycomb in the normal mode under the bare condition. Attempts were made for intermediate rate bare compression and punch tests, as listed in Table 4-1. The experimental setup was built on a customized MTS high-rate system. Shown in Figure 4-1, the specimen was adhered to the upper platen that was attached to a piezoelectric load washer, and the punch rod was fastened to the lower platen connected to the actuator through a shear pin. For bare compression tests, the punch rod was removed.

The experimental results did not quite resemble the quasi-static data. Bare compression specimens could not sustain a constant load during crush, as shown in Figure 4-2, and the punch load did not show an increase, but decreased, as depicted in Figure 4-3. These different trends indicated multiple crush modes. The major problem was that the specimen usually split into two or three segments during impact and did not display the progressive plastic buckling pattern. For example, a punch specimen split open during test, as shown in Figure 4-4. It was difficult to identify the honeycomb properties (or to extract parameters) from this data consistently and unequivocally. Experimental methods needed to be modified and improved.

Table 4-1. Intermediate bare compression and punch test.

Specimen	Material	Dimension (in.)	Rod diameter (in.)	Velocity (ft./s)
AT_HR1	Alcore35	1.5 x 1.5 x 1.5	-	14.58
ATP_HR2	Alcore35	3 x 3 x 3	1	11.25
HT_HR2	Hexcel38	1.5 x 1.5 x 1.5	-	14.58
HTP_HR3	Hexcel38	3 x 3 x 3	1	11.25

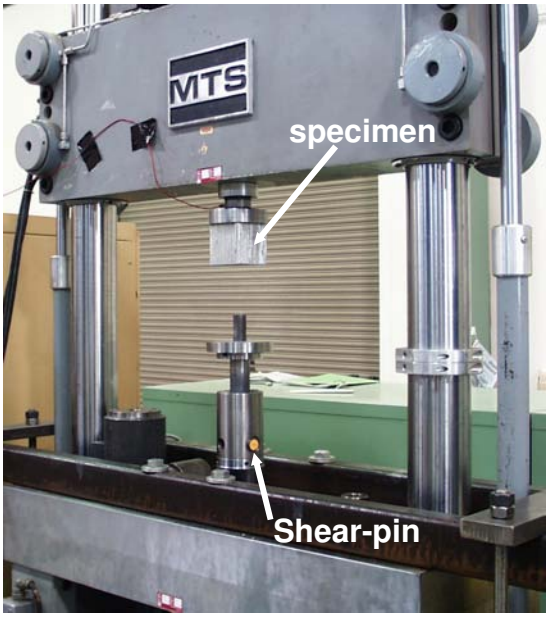

Figure 4-1. The high-rate loading frame and experimental setup for intermediate punch test. Punch rod was removed during intermediate rate bare compression.

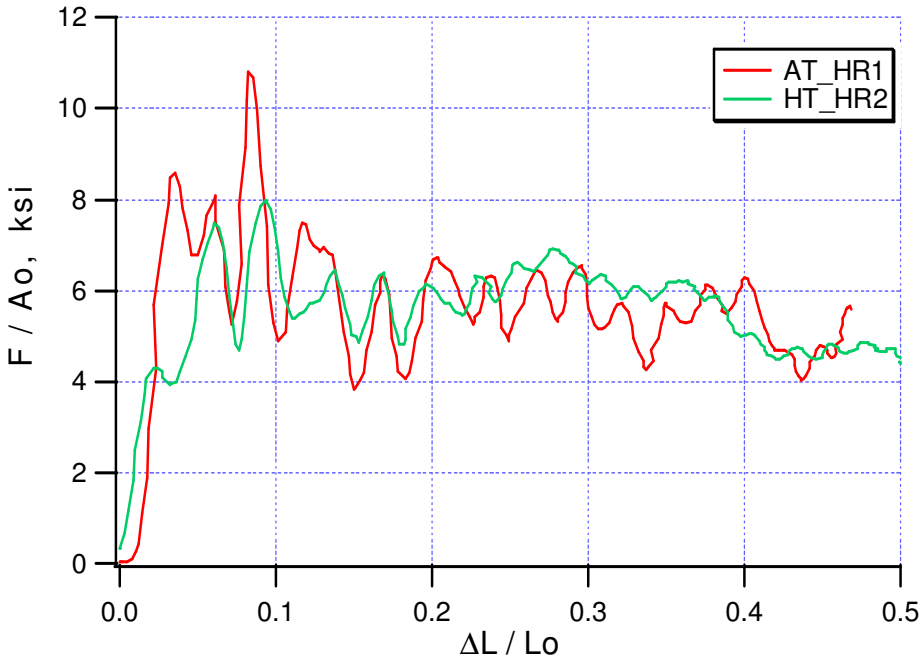

Figure 4-2. Normalized load-displacement curves for bare compression at 15 ft./s.

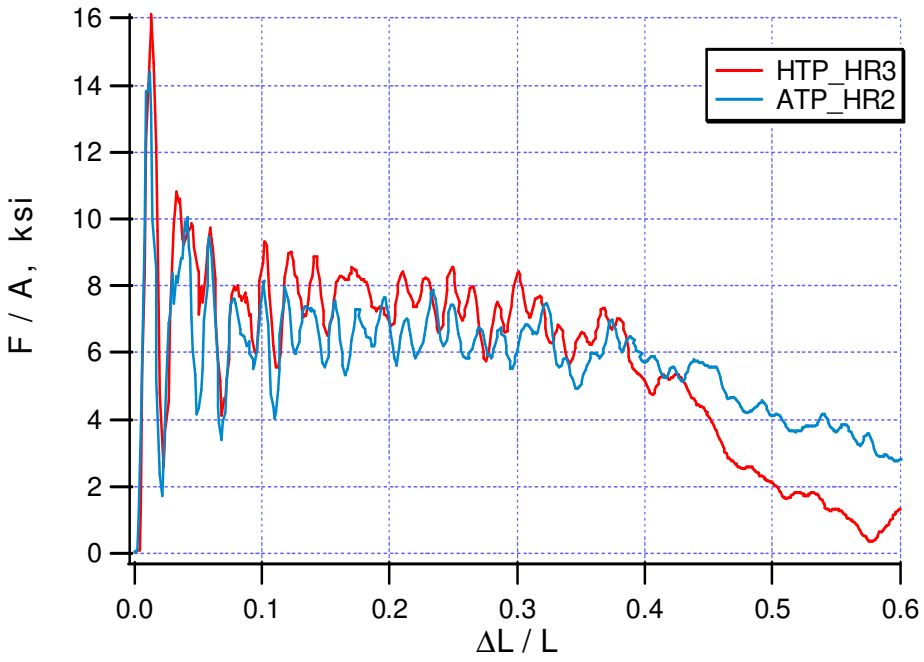

Figure 4-3. Normalized load-displacement curves for bare compression at 11 ft./s.

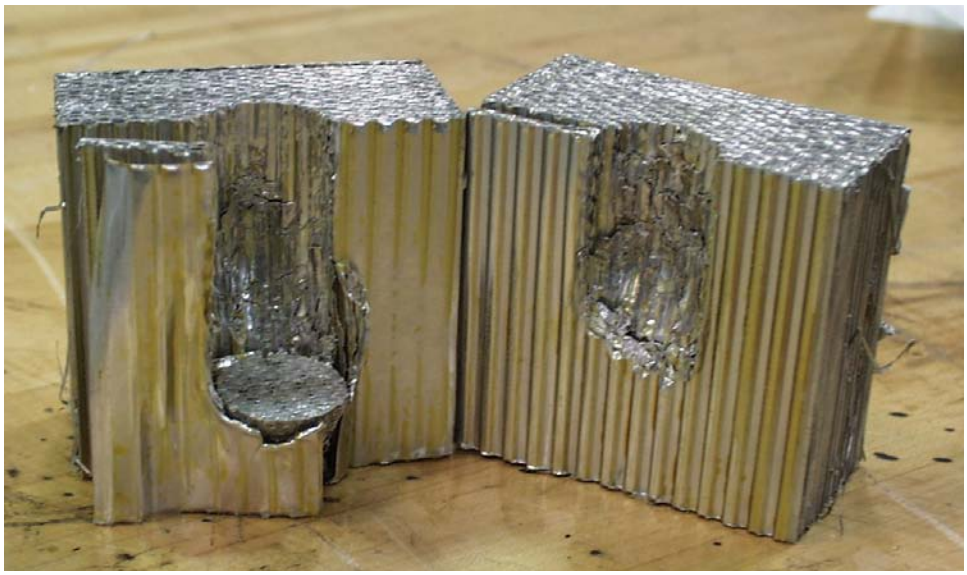

Figure 4-4. Hexcel38 specimen split during intermediate rate punch.

4.2 Confined Compression Test

Since the normal mode was the only mode appropriate for application and modeling, a confined intermediate rate (up to 200 in/s) crush experiment was developed based on the same MTS high-rate system (Figure 4-5). A rigid confined chamber, shown in Figure 4-6, was used to ensure the normal mode crush of honeycomb specimen. To mimic the condition of bare compression where there is no friction, a dimensional tolerance of 0.010 in. between the specimen and chamber was designed, and lubrication was applied to the confining walls. The nominal size of the specimen

for this confined test had a 1.5 in. gage length and cross-section of 1.2 in. square. A comparison of confined and bare tests was made for quasi-static loading. The average crush strengths of three bare compressions and four confined compressions of Alcore38 were 5.51 and 5.48 ksi, respectively, which were practically identical. Details of the experimental setup and results are documented in Appendix I. Since this confined setup worked very well, it became a standard configuration for many characterization experiments, such as intermediate rate, off-axis, etc., in this investigation.

Figure 4-5. Confined compression on the MTS high-rate system.

When conducting the intermediate rate test, about 15 ft./s, the high-rate system was switched to open-loop control. (Due to large inertia of the actuator, the applicable close-loop control was typically limited to less than 1 ft./s for a hydraulic testing system.) The actuator requires approximately the first one inch of travel to ramp to speed and the last half inch to brake and stop; in between, it travels at a constant speed. The initial engagement of compressive rod and the specimen should be during the constant speed range.

In order to protect the load cell and fixtures in the loading train, a shear-pin break-off mechanism was incorporated in the actuator. The shaft of the confined chamber was connected to the actuator through a shear pin. It was then allowed to slide freely in the actuator after the shear pin broke. The double-grooved shear pin was made of brittle cast iron, and the size and shape of the

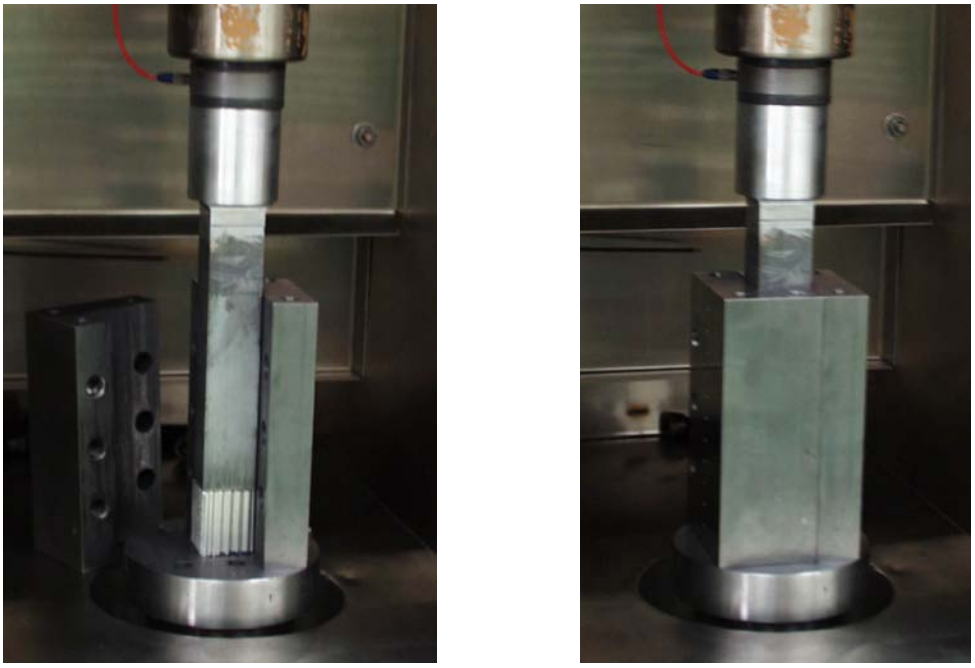

Figure 4-6. Confined fixture in temperature controlled chamber: (a) open to place the specimen, and (b) closed and ready for confined compression.

groove was designed to control the maximum force allowed during a test. Unfortunately, the property of the cast iron varied from batch to batch. The pins used usually broke at 5 to 10 kips higher than the designed value.

Figure 4-7 shows a typical set of load and displacement time data for an intermediate rate test. The dashed displacement curve shows that the acceleration period was from 0 to 1.0 in. and braking was from 4.7 to 5.2 in. The red load curve indicated the engagement of loading rod and specimen, beginning about 1.8 ms, where the displacement was about 2.7 in. The velocity remained nearly constant at 175 in./s and decreased slightly during lock up, when the load increased quickly. When the load reached approximately 25 kips, or at 8.0 ms, the shear pin broke and the load immediately dropped to zero. The actuator continued to move, but it was disengaged from the confined chamber and no longer loading the specimen.

Table 4-2 shows the first set of intermediate rate tests of honeycomb using the confined chamber. Tests were conducted at ambient and 170°F. Their results are plotted in Figure 4-8. Compared to the same honeycomb under quasi-static loading, shown in Figure 2-2, these stress-strain curves have similar crush and densification features, but the intermediate curves display high-frequency contents, which may be due to the ringing in the loading system. Since these high-frequency contents do not affect the calculation of average crush strength or energy absorption rate, they are not filtered out from the signal. The influence of temperature on crush strength is clearly demonstrated: about 7.5 percent decrease at 170°F.

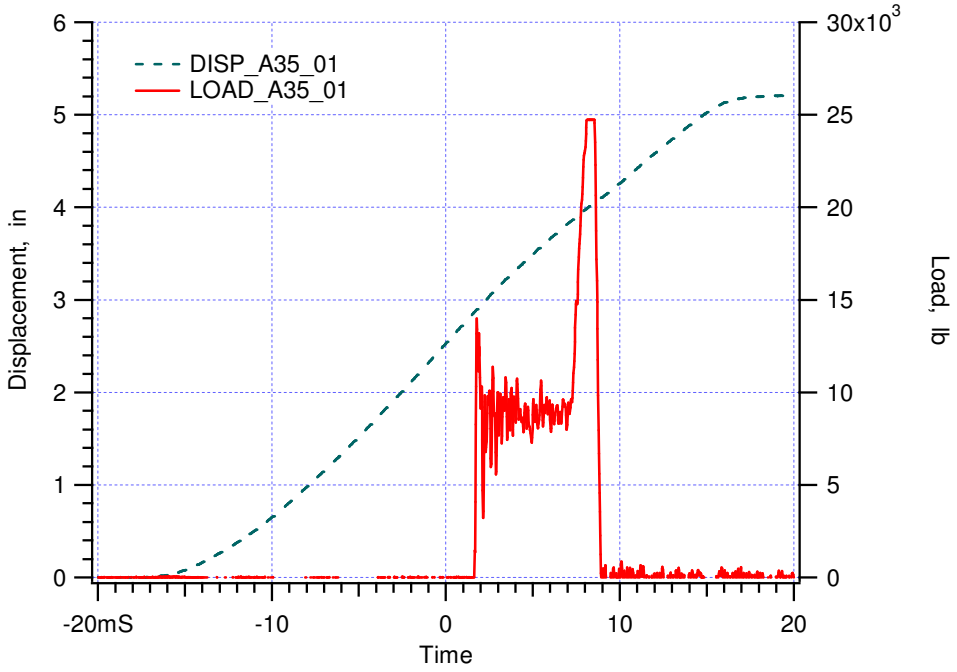

Figure 4-7. Typical load and displacement time data of intermediate rate, 15 ft./s, compression of high density aluminum honeycomb.

Table 4-2. Test matrix of intermediate rate confined compression of Hexcel CR-8-LC-1/8-5-52-0.006-R2 (38 pcf) honeycomb.

Specimen	d_1, in	d_2, in	d_3, in	Density, pcf	Temperature, degree F	Crush Velocity, ft/s	Crush strength, ksi
440	1.499	1.210	1.221	37.26	77	14.17	6.12
441	1.500	1.211	1.233	36.81	77	14.08	5.89
442	1.499	1.211	1.233	36.61	77	14.17	5.93
443	1.501	1.212	1.220	37.85	170	14.42	5.62
444	1.499	1.212	1.211	37.40	170	14.50	5.60
445	1.501	1.194	1.207	37.56	170	14.75	5.39

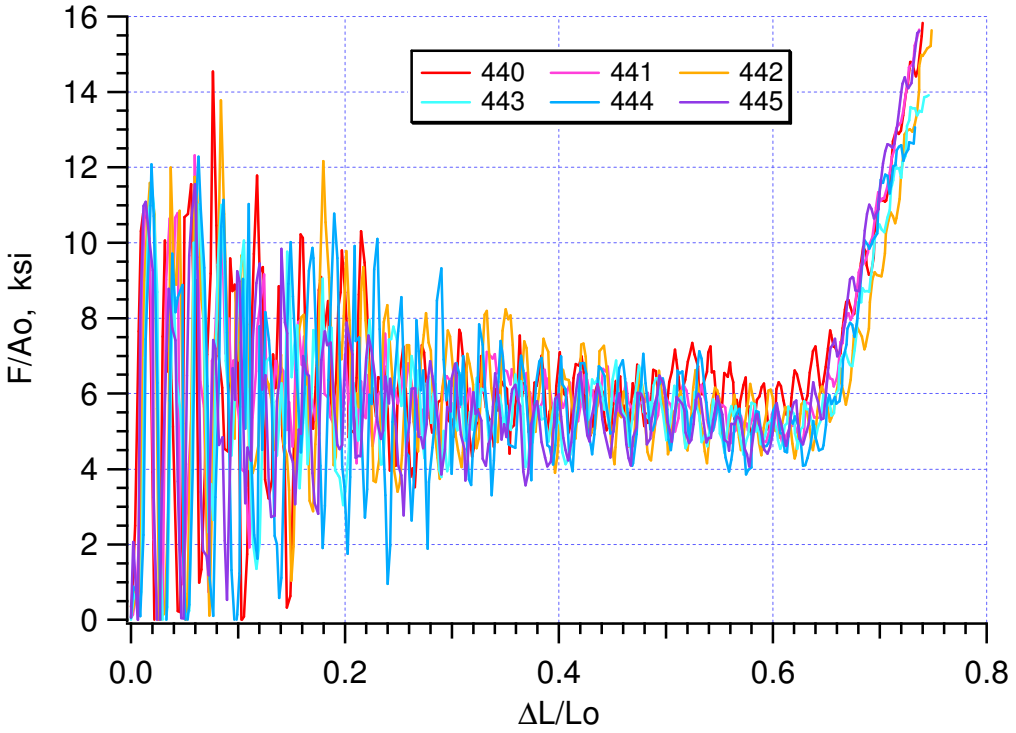

Figure 4-8. Normalized load-displacement curves of Hexcel CR-8-LC-1/8-5-52-0.006-R2 (38 pcf) crushed in the T direction at 14 ft./s.

This page intentionally left blank.

5. QUALIFICATION OF HONEYCOMB CRUSH BEHAVIOR

5.1 Test Plan Description

As the experimental techniques for high-density honeycomb were gradually established, a test plan was designed to quantify the crushing behavior and energy absorber capability of aluminum honeycomb for application to the B61 3/4/7/10 Radar Nose Assembly. There were three objectives: (1) identify a set of quasi-static tests to compare directly with the honeycomb vendor tests required by the honeycomb purchase specification; (2) quantify any increase in crush strength due to dynamic loading; and (3) provide sufficient aluminum honeycomb material response data to validate the Orthotropic Crush Constitutive parameters that will be used in the PRONTO3D B61 Radar Nose Crush model. The scope of the test plan included quasi-static unconfined and confined, dynamic confined, and on-axis and off-axis crush response measurements; ambient and elevated temperature tests; and bond strength effects. Five batches of aluminum honeycomb, listed in Table 3-1, were examined. Please refer to Appendix II for details of the plan, test matrix, and experimental data.

5.2 Summary of Results

A brief summary of results is presented in Tables 5-1 through 5-4.

Table 5-1. Qualification of Alcore38 in the T direction.

Test #	B.C.	Specimen	Size (in.)	Temp (°F)	Rate (ft./s)	Strength (ksi)	Peak (ksi)	Efficiency (Percent)
4	unconfined	normal	1.5 x 3 x 3	70	0.0167	5.59	7.25	60.56
5	unconfined	normal	1.5 x 3 x 3	70	0.0167	5.51	7.34	62.80
6	unconfined	normal	1.5 x 3 x 3	70	0.0167	5.44	6.67	63.73
19	confined	normal	1.5 x 1.2 x 1.2	70	0.0167	5.49	8.18	60.80
20	confined	normal	1.5 x 1.2 x 1.2	70	0.0167	5.24	8.08	61.10
21	confined	normal	1.5 x 1.2 x 1.2	70	0.0167	5.57	8.76	60.70
21b	confined	normal	1.5 x 1.2 x 1.2	70	0.0167	5.62	8.76	60.00
22	confined	normal	1.5 x 1.2 x 1.2	177	0.0167	4.67	7.60	61.20
23	confined	normal	1.5 x 1.2 x 1.2	177	0.0167	4.56	7.34	60.80
25	confined	unbonded	1.5 x 1.2 x 1.2	70	0.0167	1.07	5.75	68.80
26	confined	unbonded	1.5 x 1.2 x 1.2	70	0.0167	0.95	6.04	70.00
27	confined	unbonded	1.5 x 1.2 x 1.2	70	0.0167	1.13	5.04	69.12
28	confined	normal	1.5 x 1.2 x 1.2	70	13.5	7.24	12.49	70.00
28b	confined	normal	1.5 x 1.2 x 1.2	70	13.5	6.30	11.41	70.00
29	confined	normal	1.5 x 1.2 x 1.2	70	13.5	5.55	12.30	67.40
29b	confined	normal	1.5 x 1.2 x 1.2	70	13.5	5.39	11.76	67.40
30	confined	normal	1.5 x 1.2 x 1.2	70	13.5	6.42	12.52	65.40
30b	confined	normal	1.5 x 1.2 x 1.3	70	13.5	5.52	12.99	67.90

Table 5-1. Qualification of Alcore38 in the T direction (continued).

Test #	B.C.	Specimen	Size (in.)	Temp (°F)	Rate (ft./s)	Strength (ksi)	Peak (ksi)	Efficiency (Percent)
45	unconfined	1/2 crushed	1.5 x 3 x 3	70	0.0167	5.90		
46	unconfined	1/2 crushed	1.5 x 3 x 3	70	0.0167	6.00		
47	unconfined	1/2 crushed	1.5 x 3 x 3	70	0.0167	6.04		

Table 5-2. Qualification of Alcore38 in the L direction.

Test #	B.C.	Specimen	Size (in.)	Temp (°F)	Rate (ft./s)	Strength (ksi)	Peak (ksi)	Efficiency (Percent)
16	unconfined	normal	1.5 x 3 x 3	70	0.0167	1.165		54.77
17	unconfined	normal	1.5 x 3 x 3	70	0.0167	1.105		55.01
18	unconfined	normal	1.5 x 3 x 3	70	0.0167	1.151		55.98

Table 5-3. Qualification of Alcore35 in the T direction.

Test #	B.C.	Specimen	Size (in.)	Temp (°)F	Rate (ft./s)	Strength (ksi	Peak (ksi)	Efficiency (Percent)
1	unconfined	normal	1.5 x 3 x 3	70	0.0167	5.32	7.22	61.15
2	unconfined	normal	1.5 x 3 x 3	70	0.0167	5.70	6.98	61.03
3	unconfined	normal	1.5 x 3 x 3	70	0.0167	5.66	6.39	60.67

Table 5-4. Qualification of Hexcel MAVEN 38 pcf in the T direction

Test #	B.C.	Specimen	Size (in.)	Temp (°)F	Rate (ft./s)	Strength (ksi)	Peak (ksi)	Efficiency (Percent)
13	unconfined	normal	1.5 x 3 x 3	70	0.0167	5.24	8.52	66.32
14	unconfined	normal	1.5 x 3 x 3	70	0.0167	5.24	8.70	67.87
15	unconfined	normal	1.5 x 3 x 3	70	0.0167	5.25	8.57	67.61

Most of tests were related to Alcore38. Unconfined (#4 – 6) and confined (#19 – 21) tests yield identical results; the averaged crush strength was 5.51 and 5.48 ksi, respectively. At high temperature (177°F), the crush strength decreased about 15 percent, to 4.62 ksi. Intermediate rate (13.5 ft./s) enhanced the crush strength by ~10 percent (6.07 ksi).

Test #45 – 47 were added to the matrix at a later date. These specimens were crushed in two stages; first by Alcore, and then by Sandia National Laboratories/California (SNL/CA). Figure 5-1 shows an as-received, half-crushed specimen. The experimental data on each specimen were directly compared. The Alcore data, for these specimens were 5.98, 6.02, and 5.97 ksi. Both

sets of data were essentially the same; the difference was within 2 percent. Those specimens were prepared by Alcore, and were not from the same honeycomb block as other specimens.

Test #7 – 12, for Hexcel35 and Hexcel38, were not performed, but these two honeycombs were later included in another qualification test.

The results flexure shear test, #36 – 38, is discussed in Appendix III. The result of a two-layer crush article, Test #42-44, is detailed in Appendix II.

Figure 5-1. Half-crushed honeycomb specimen from Alcore.

5.3 Crush of Unbonded Honeycomb Specimen

Tests #25 – 27 in Table 5-1 called for compressions of unbonded specimens. The purpose was to identify the maximum effect of adhesive bond strength on the crush behavior of honeycomb. Temperature and humidity may affect the strength of the bond.

Alcore38 specimens were first machined to the designed dimension. Each specimen was put in a small container and soaked in solvent paint remover. After several weeks, specimens were removed from the solvent. All adhesive between the aluminum sheets of Alcore 38 was dissolved. Each specimen became a deck of loose aluminum sheets, as shown in Figure 5-2. A typical confined specimen had 19 seragated sheets and 19 flat sheets. The unbonded specimen, or a deck of loose aluminum sheets, was placed in the confined chamber, as demonstrated in Figure 5-3, and loaded quasi-statically in the T direction. The crush curves are plotted in Figure 5-4. The crush strength was significantly reduced (less than 20 percent of its typical value).

Figure 5-2. A honeycomb specimen with adhesive bond removed.

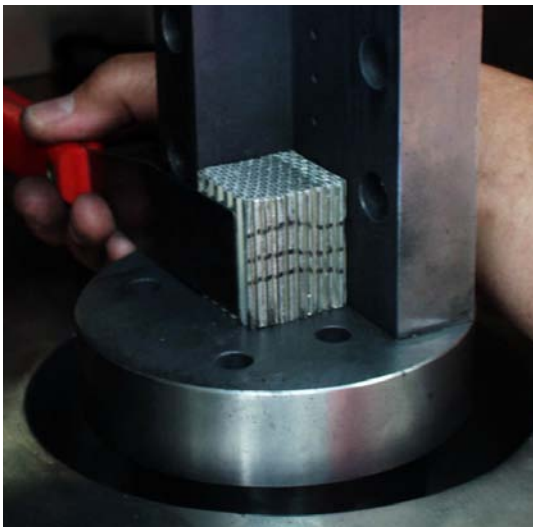

Figure 5-3. A unbonded specimen in the confined chamber.

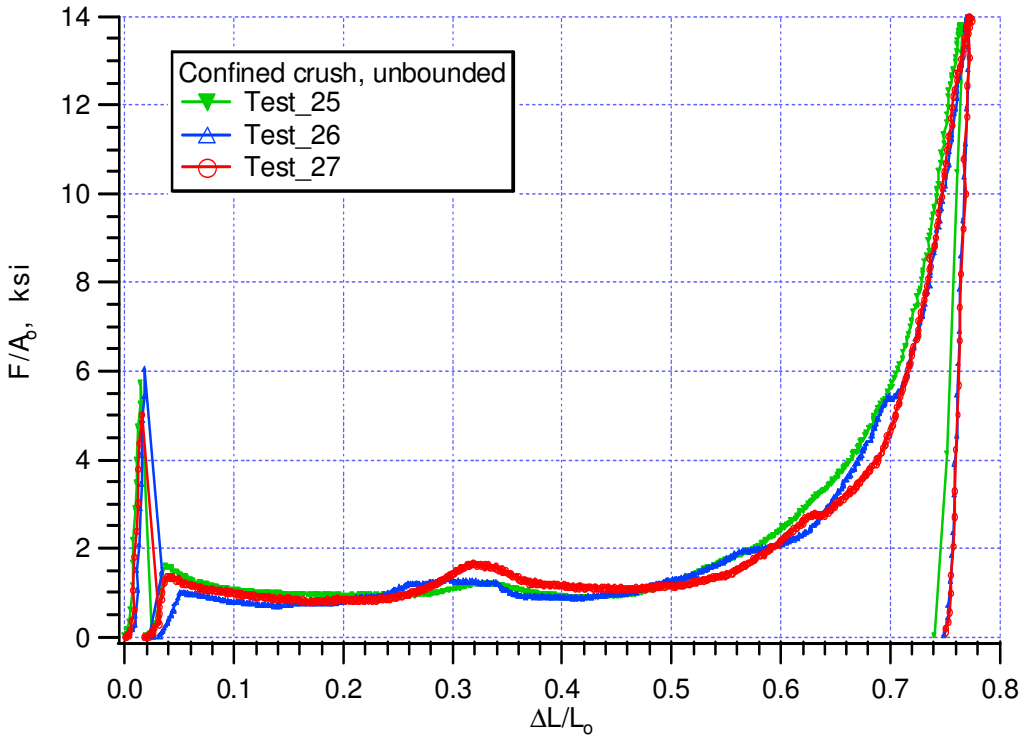

Figure 5-4. Normalized load-displacement curves of unbonded specimens under confined compression.

5.4 Crush of Segmented Honeycomb

The purpose of confined compression is to prevent honeycomb from crushing in the abnormal modes. Some other methods can achieve the same result. One technique is to properly arrange segmented honeycomb. A possible arrangement of a LW disk. Quad specimen is shown in Figure 5-5, where, L axis of a quarter dish is always diametrically aligned. During crush, each

quarter is virtually confined by the adjacent quarters, thus averting the unwanted abnormal modes.

A few more tests were also appended to the qualification matrix. Table 5-5 listed a set of Alcore38 Quad specimens, prepared by Honeywell Federal Manufacturing and Technologies Kansas City Plant, which was available for T axis compression tests. Each specimen consisted of four honeycomb quarters bonded together. Some had a coating on the circumference surface. The nominal size of the specimen was 5 in. diameter and 1.5 in. high.

Quasi-static compressions of these Quad specimens at ambient condition were performed on the MTS two million pound system. The results are given in Table 5-6 and Figure 5-6. All specimens with MA562 bond were stronger than the FM123-5 bonded ones, indicating the influence of bonds on test results. Compression on Quad specimens, in general, exhibited a little higher crush strength than confined compression, which was 5.23 ksi for the same loading and temperature condition. The difference could be contributed from the additional bond lines in the Quad specimen.

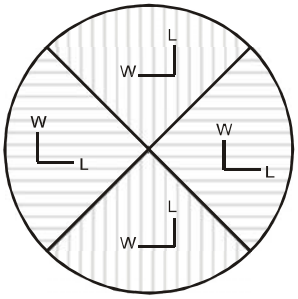

Figure 5-5. Schematic of Quad specimens

Table 5-5. Test matrix of Quad specimens.

SPECIMEN	DESCRIPTION
S1	FM123-5 QUAD BONDS
S2	FM123-5 QUAD BONDS
S3	FM123-5 QUAD BONDS & MA562 COATING
S4	FM123-5 QUAD BONDS & MA562 COATING
S5	FM123-5 QUAD BONDS & MA562 COATING
S6	MA562 QUAD BONDS
S7	MA562 QUAD BONDS
S8	MA562 QUAD BONDS

Table 5-6. Specimen dimensions and experimental results of Quad specimens.

SPECIMEN	INITIAL HEIGHT, in	INITIAL DIAMETER, in	FINAL DIAMETER, in	CRUSH LOAD, kips	CRUSH STRENGTH, ksi
S1	1.5013	5.083	5.218	119.6	5.89
S2	1.503	5.083	5.215	118.6	5.84
S3	1.504	5.088	5.215	126.0	6.20
S4	1.502	5.087	5.21	124.3	6.12
S5	1.532	5.091	5.25	127.7	6.27
S6	1.5	5.082	5.16	127.0	6.26
S7	1.472	5.083	5.19	126.8	6.25
S8	1.474	5.081	5.185	126.5	6.24

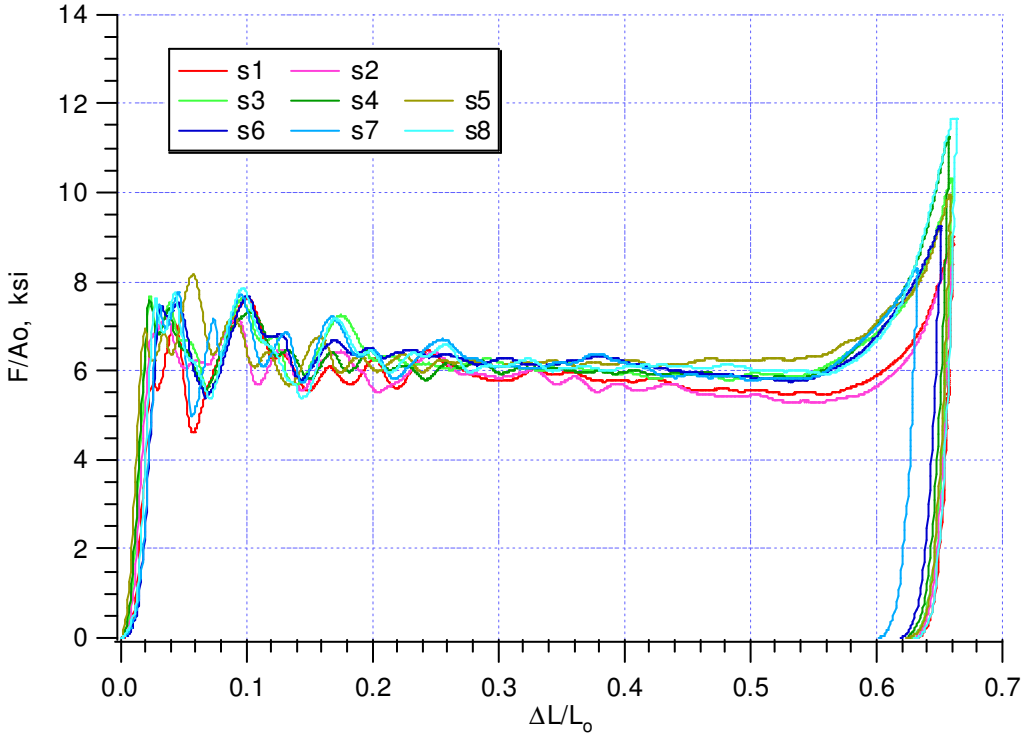

Figure 5-6. Quasi-static crush of Quad samples, quasi-static loading in the T direction at ambient temperature.

6. OFF-AXIS COMPRESSION

6.1 Shear Experiment

In addition to normal loading on the material axes, the shear-coupling phenomenon of high-density aluminum honeycomb needed to be investigated. Available shear experimental techniques, such as two-rail shear test, were mainly for low-density honeycomb (less than 8 pcf). The honeycomb-plate interface was not strong enough for high-density aluminum honeycomb and always failed before shear-coupled crush.

Plate shear test and beam flexure tests were modified to test high-density aluminum honeycomb. By filling cells with polymer at the loading section, the modified plate shear experiment eliminated the problem of interface failure. The initial shear strength can be determined, but tearing of the aluminum sheets prevents the measure of shear strength as a function of volumetric strain for crush applications. A beam flexure test was performed using Hexcel38 and the result was analyzed by finite element method; however, the test could not achieve the peak beam shear strength 4300 psi quoted by the manufacturer apparently due to the onset of localized crushing and/or delamination of the sandwich.

For orthotropic materials, off-axis tension or compression is commonly used to obtain the shear properties. Confined compressions of off-axis specimens were conducted using the same setup as the on-axis compression experiment described in Section 5. Combined with finite element simulations, the inferred model parameters were estimated from the off-axis test data. The friction between honeycomb and the confined wall was difficult to characterize and was an issue in modeling. Off-axis compression might be not an ideal experiment, but it was simple and the best method so far to deal with the shear deformation of high-density aluminum honeycomb. Figure 6-1 shows off-axis specimens in TL plane, and Figure 6-2 illustrates the load-displace response of honeycomb at various off-axis angles. The loading rate was about 180 in./s. The above-motioned work is detailed in Appendix III.

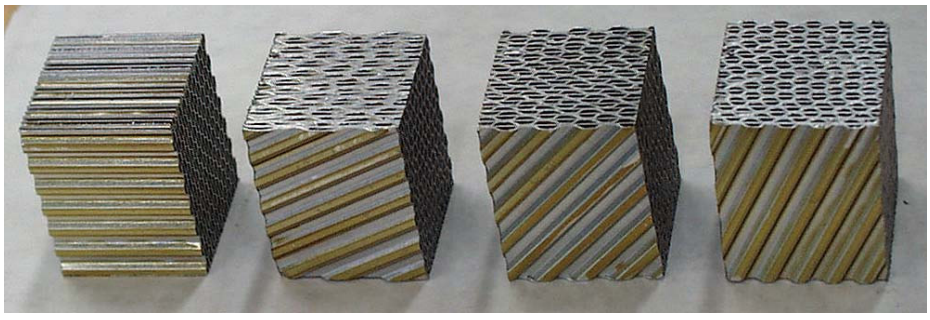

(a) (b) (c) (d)

Figure 6-1. TL off-axis specimens showing various angles between the loading axis and the T axis: (a) 90, (b) 65, (c) 45, and (d) 25 degree.

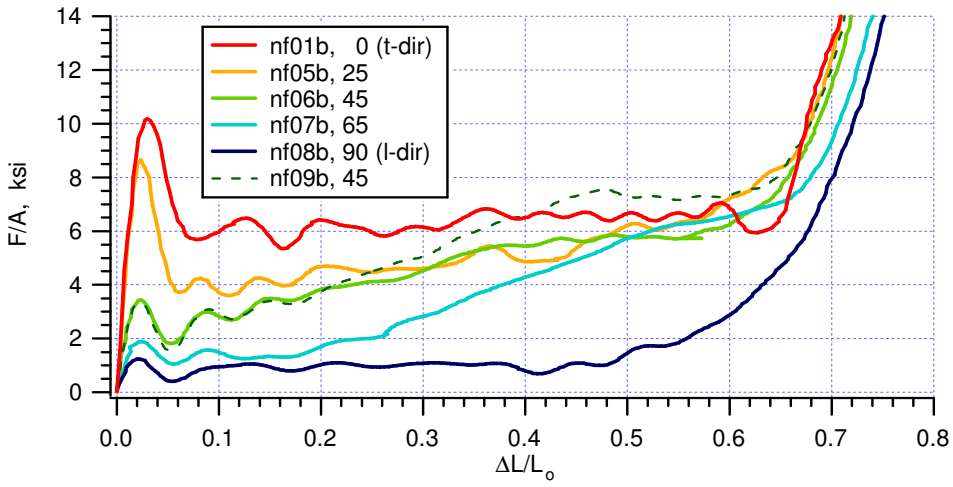

Figure 6-2. Normalized load-displace curves TL off-axis specimens of Hexcel CR-8-LC-1/8-5052-006-R2 honeycomb.

6.2 Off-Axis Experiment

Table 6-1 lists off-axis compressions that are not reported in Appendix III. Experiments included different test conditions. Tests took account of two temperatures, ambient and 165°F, and two loading rates, about 0.1 in./s and 180 in./s. All specimens were Alcore38, but consisted of three different configurations. The loading axis formed an equal angle with respect to each honeycomb axis indicated in the specimen ID, shown in Figure 6-3. TLW specimens, for example (the angle between the loading direction and T, L, or W) were about 55 degrees. How TLW specimens were cut from a honeycomb block is also show in Figure 6-3.

Table 6-1. Additional Off-Axis Experiments.

Specimen	d1 (in.)	d2 (in.)	d3 (in.)	Density (pcf)	T (°F)	Rate (in./s)
A38LW1	1.193	1.211	1.531	38.84	70	180
A38TL1r	1.23	1.235	1.503	39.06	70	180
A38TL3	1.218	1.216	1.503	38.64	70	180
A38TL5	1.23	1.208	1.508	39.12	165	180
A38TL6	1.229	1.216	1.503	39.53	165	180
A38TLW1	1.206	1.205	1.515	39.00	70	0.072
A38TLW2	1.154	1.228	1.514	39.33	70	0.086
A38TLW4	1.204	1.213	1.492	40.09	165	0.057
A38TLW5	1.231	1.217	1.499	39.27	70	180
A38TLW6	1.213	1.22	1.539	39.51	70	180
A38TLW7	1.227	1.225	1.500	38.90	70	180

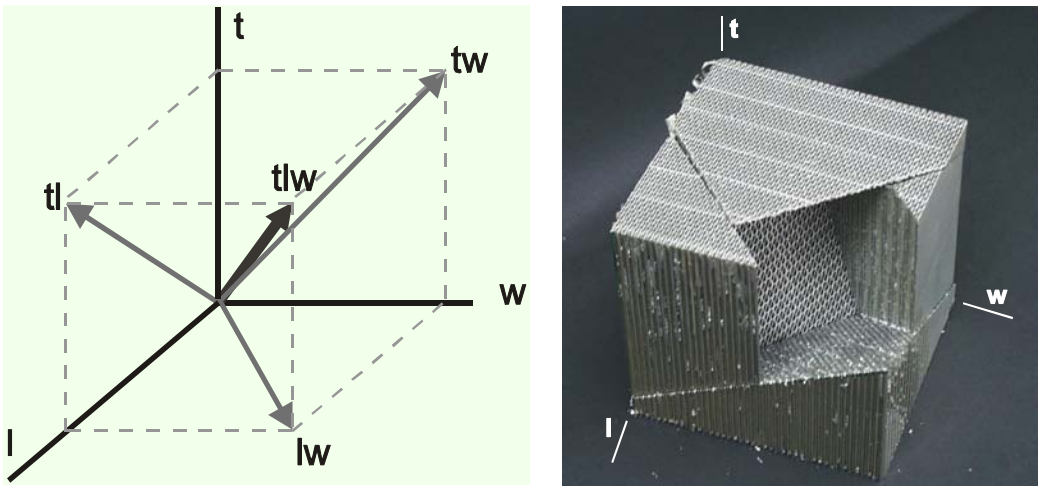

Figure 6-3. Definition of equal-angle off-axis honeycomb specimen.

Experimental results are given in Figures 6-4 through 6-7. The load-displacement curves followed the same trends as the temperature effect of honeycomb, with the lower load corresponding to a higher temperature condition. TLW specimens did not exhibit much rate effect.

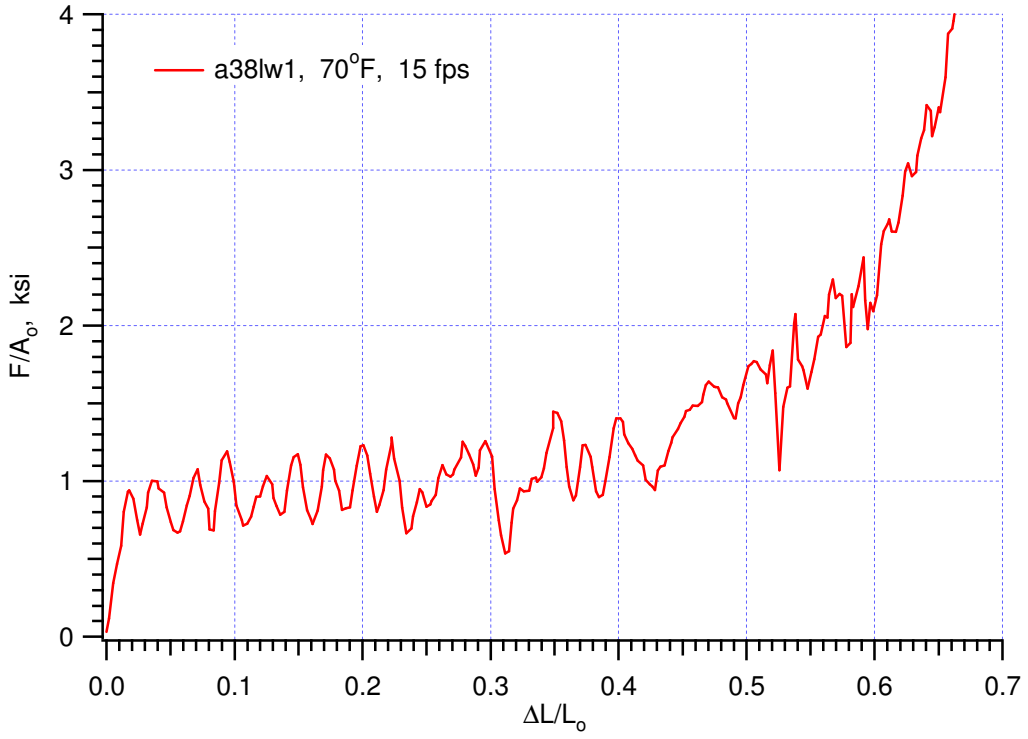

Figure 6-4. Normalized load-displacement curves for the Alcore38 LW45 specimen.

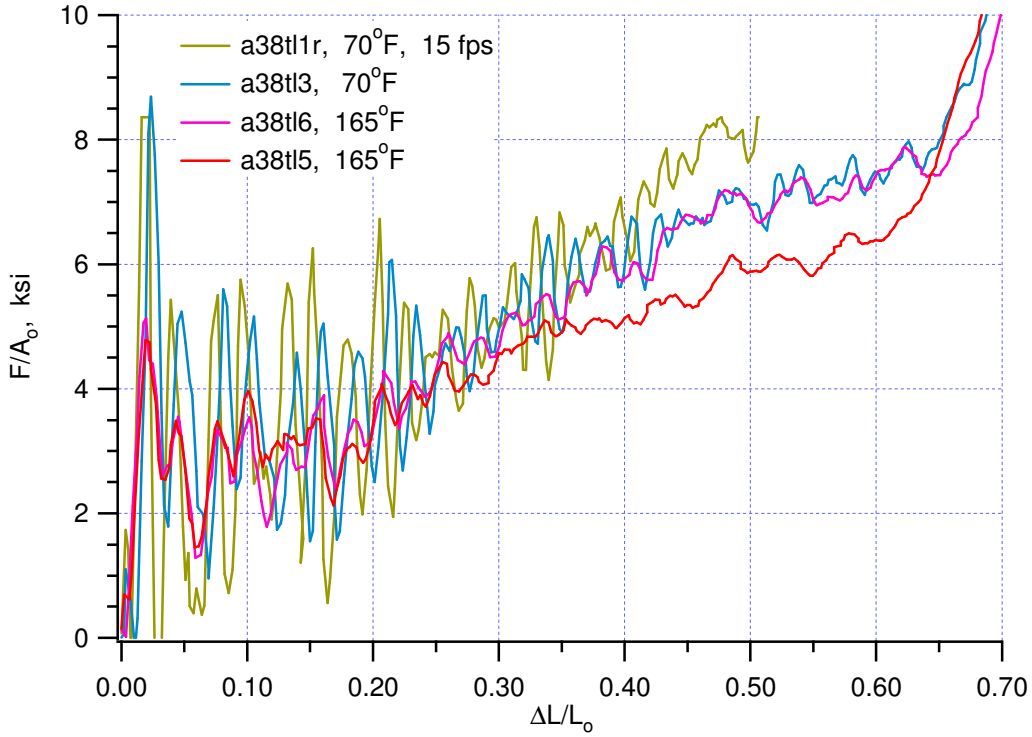

Figure 6-5. Normalized load-displacement curves for Alcore38 TL45 specimens.

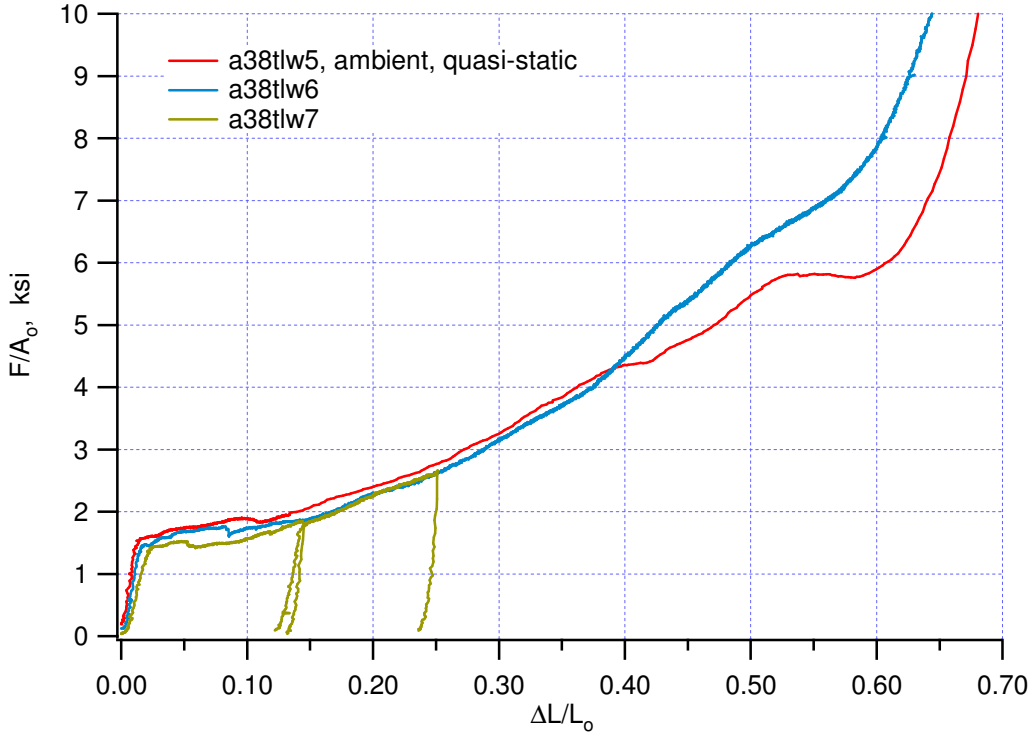

Figure 6-6. Normalized load-displacement curves for Alcore38 TLW off-axis specimens, quasi-static loading.

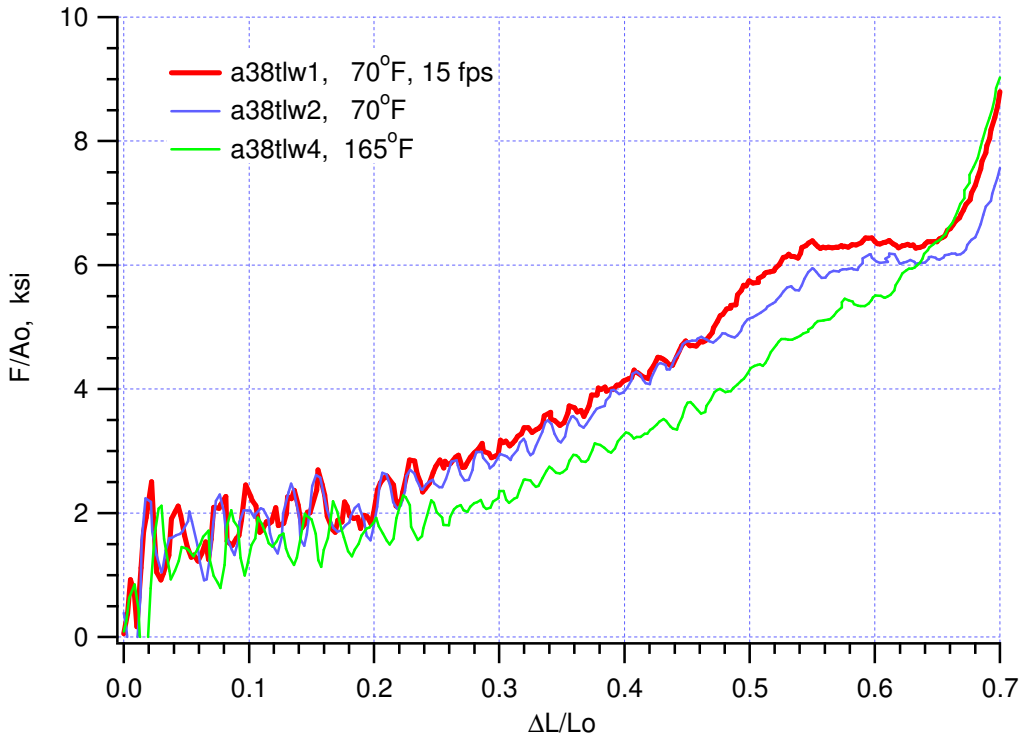

Figure 6-7. Normalized load-displacement curves for Alcore38 TLW off-axis specimens, loading at 15 ft./s.

This page intentionally left blank.

7. AUGMENTED QUALIFICATION TEST

7.1 Objectives

The additional set of qualification tests had the following objectives:

1. To develop a more significant statistical database for ambient/hot/cold crush behavior.
2. To take advantage of moderate rate testing with a confining chamber for a more reliable dynamic testing approach.
3. To investigate off-axis behavior.
4. To measure crush behavior in the W direction.

7.2 Summary of Results

The original test matrix is given in Appendix IV. Extra tests were included later. More than 200 individual tests were included. Experimental results have been distributed in the form of memos, which are attached in this report as Appendices IV to XIV. They are summarized in Tables 7-1 and 7-2. The tests marked in red were not in the original matrix.

Table 7-1. Averaged crush strength of four batches of honeycomb.

Material	Direction	Intermediate rate, 14ft./s			Quasi-static		
		-65°F	ambient	165°F	-65°F	ambient	165°F
Alcore 38	T	**7.34**	**6.35**	**5.49**	6.23	5.23	4.60
	L		**1.25**	1.06			
	W	0.74	**0.54**	0.53	0.68	0.53	0.45
Alcore 35	T	**7.04**	**5.74**	**4.94**			
	L						
	W						
Hexcel 38	T	**8.21**	**7.17**	**6.43**	7.30	5.88	5.55
	L		**1.05**	0.84	1.04	0.98	0.91
	W	0.84	**0.60**	0.56	0.59	0.54	0.54
Hexcel 35	T	**8.05**	**6.67**			5.83	
	L						
	W						

Table 7-2. Summary of augmented qualification test.

B61/MAVEN TEST MATRIX				EXPERIMENTAL RESULTS						MEMO
Test #	**Honeycomb**	**Dir.**	**Temperature (°F)**	**Specimen**	**Density (pcf)**	**Impact Speed (ft./s)**	**Crush Strength (ksi)**	**Std Deviation (ksi)**	**Crush Efficiency (Percent)**	**Date/ Appendix**
1 - 15	Alcore 38	T	ambient	rotated	38.82	14.13	6.35	0.08	63.80	991203/ VI
16 - 30	Hexcel 38	T	ambient	rotated	38.70	13.67	7.17	0.15	63.89	000110/ IX
	Hexcel 38	T	ambient	rotated	38.78	0.001392	5.88		59.20	000110/ IX
31 - 45	Alcore 35	T	ambient	rotated	35.39	14.35	5.74	0.18	64.46	000103/ VIII
46 - 60	Hexcel 35	T	ambient	rotated	37.79	13.83	6.67	0.24	63.91	000110/ IX
	Hexcel 35	T	ambient	rotated	37.89	0.001391	5.83		60.30	000110/ IX
60 - 75	Alcore 38	T	165	rotated	38.96	14.33	5.49	0.10	62.52	000118/ X
76 - 90	Hexcel 38	T	165	rotated	38.65	13.82	6.43	0.15	64.31	000118/ X
	Alcore 35	T	165	rotated	35.62	14.59	4.94	0.23	62.54	
91 - 105	Alcore 38	T	-65	rotated	38.94	13.48	7.34	0.24	62.71	000225/ XII
106 - 120	Hexcel 38	T	-65	rotated	38.65	13.17	8.21	0.17	64.68	000225/ XII
	Alcore 35	T	-65	rotated	35.59	13.77	7.04	0.36	62.89	000307/ XIII
	Hexcel 35	T	-65	rotated	37.92	13.29	8.05	0.09	64.20	000307/ XIII
121 - 125	Alcore 38	L	ambient	rotated	38.88	16.45	1.25	0.13	53.24	000307/ XIII
126 - 130	Hexcel 38	L	ambient	rotated	38.62	16.50	1.05	0.09	46.12	000307/ XIII
131 - 135	**Alcore 38**	**W**	**ambient**	**normal**	**38.94**	**16.56**	**0.54**	**0.06**	**36.80**	**000316/ XIV**
136 - 140	**Hexcel 38**	**W**	**ambient**	**normal**	**38.70**	**16.72**	**0.60**	**0.02**	**37.03**	**000316/ XIV**
159 - 161	Alcore 38	T	ambient	segmented	41.41	0.0014	6.14		52.30	991130/ V
162 - 164	Hexcel 38	T	ambient	segmented	41.29	0.0014	6.85		53.70	991213/ VII

8. IN-PLANE BIAXIAL CRUSH OF HONEYCOMB

Among the possible loading conditions for honeycomb in the intended applications, many are under combined loading and the stress is not uniaxial. Honeycomb models need to predict these cases accurately. Since models were typically developed from the observations of uniaxial experimental data, there were issues when generalizing from uniaxial to multiaxial cases. For example, in the orthotropic crush model, no coupling between stress components was assumed and each stress component was treated independently. This assumption had not been evaluated. During uniaxial crushing of honeycomb, engineering stress and true stress had the same value. Which one should be used in multiaxial conditions? In-plane biaxial compression experiments were conducted to investigate the multiaxial behavior of honeycomb and validate the models.

The experimental setup and the biaxial system calibration are detailed in Appendix XV. The in-plane biaxial system and compression fixtures are shown in Figures 8-1 and 8-2, respectively. There are four hydraulic actuators (North, South, East, and West; two opposing actuators per loading axis) and four control channels allowing independent control of each actuator. A load cell is bolted to the end of each actuator. A biaxial compression fixture (or platen) with a capacity of 40 kips is attached to each load cell through two bearing assemblies that fix the fixture to move with the actuator in the loading direction while accommodating motion perpendicular to the loading direction in the loading plane. A sliding guide mechanism is mounted on each fixture plate to control and adjust relative position and motion between adjacent fixtures.

The maximum friction between loading fixtures was found to be less than 50 lb, and the maximum crosstalk between fixtures was less than 10 lb. The total uncertainty of load measurement was within 100 lb. Considering a specimen with a cross section of 2 in. × 2 in.,

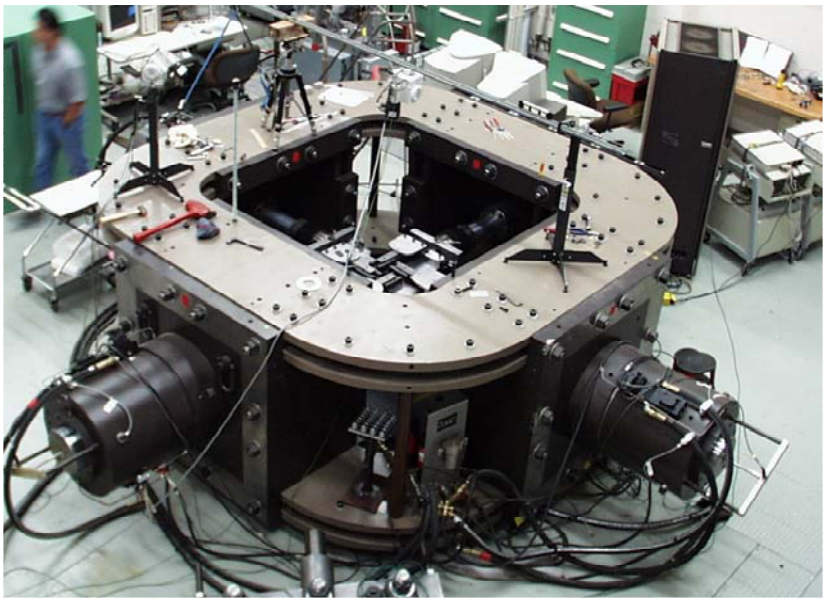

Figure 8-1. The in-plane biaxial system. The South and East actuators are shown in the lower left and right corners, respectively. All four actuators are identical. Each has a half-million pound capacity.

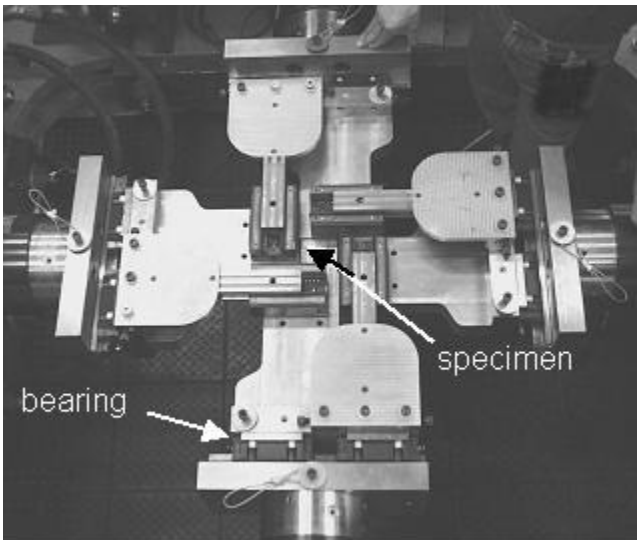

Figure 8-2. The biaxial fixtures. Each one is attached to a load cell, which is connected to an actuator. The bearing allows the fixture to move transversely. The slide guide controls the relative position between adjacent fixtures. The loading capacity of each fixture is 40 kips.

100 lb corresponds to 25 psi. The friction and crosstalk was insignificant compared to the crush strengths of high-density aluminum honeycombs.

8.1 Biaxial Experiment

Three loading paths were designed in this set of experiments: uniaxial, equal biaxial, and nonproportional. In uniaxial compression, the North and South actuators did not move, but confined the specimen. The East (or East and West) actuator(s) moved toward the center and compressed the specimen. The motion of fixtures was demonstrated in Figure 8-3(a). During equal biaxial compression, all four actuators move simultaneously toward the center at the same rate and reached the position shown in Figure 8-3(b) in a single step.

The nonproporational path had two steps. The first was to move the East and West actuators toward the center to a predetermined displacement and the North and South actuators stayed fixed, just like the uniaxial compression shown in Figure 8-4(a). In the second step the East and West actuators stayed fixed and the North and South actuators moved toward each other and to a position like that in Figure 8-4(b).

Biaxial experiments included both on-axis and off-axis compressions. Figure 8-5(a) shows the system for defining the biaxial test sample configurations. They are designated as XYθθ, where X (or Y) represents the principal axis (i.e., T, L, or W) of the honeycomb, the XY plane is parallel to the loading plane, and θ is the angle between the material axis (X or Y) and the loading axis (EW or NS). Figure 8-5(b) and (c) give specific examples using this convention. In Figure 8-5(b), the angle θ is zero for the TL00 configuration, whereas in Figure 8-5(c), θ is 45 degrees for the LW45 configuration.

The biaxial experiment matrix is listed in Table 8-1.

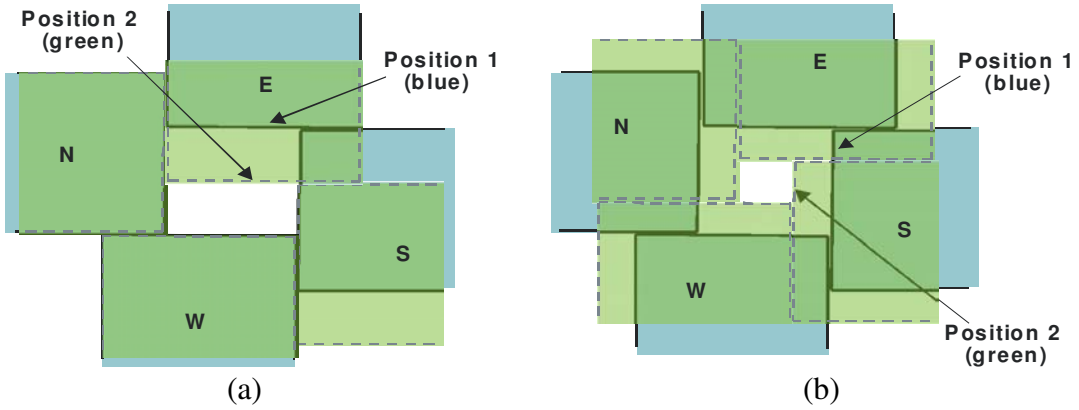

Figure 8-3. Biaxial fixture movements: (a) uniaxial compression, (b) equal biaxial compression.

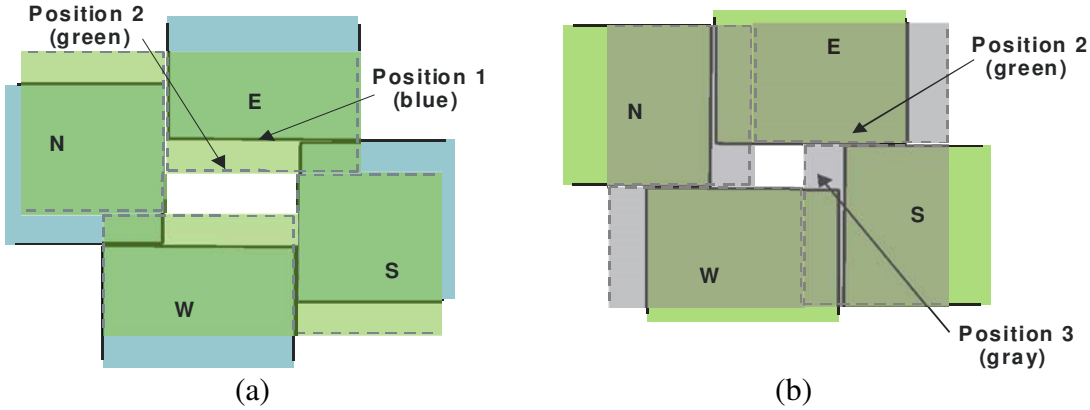

Figure 8-4. Fixture movements for the nonproportional path: (a) first step, E-W compression; (b) second step, N-S compression.

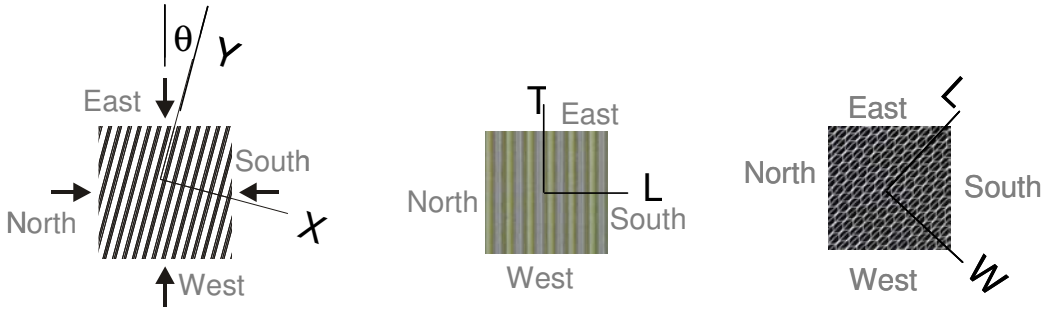

Figure 8-5. Examples of biaxial specimen configurations: (a) definition, (b) TL00, and (c) LW45.

Table 8-1. Test matrix of in-plane biaxial compression.

Specimen		Loading				Temp.	Dimension, in			Density
#	Honeycomb	plane	angle	dir.	path	°F	d1	d2	d3	ρ, pcf
1	Hexcel38	LW	00		axial-L	70	1.500	1.800	1.255	38.09
2	Alcore38	LW	00		equal	70	3.000	1.500	3.000	39.01
3	Alcore38	TW	00		equal	70	3.000	1.500	3.000	38.02

Table 8-1. Test matrix of in-plane biaxial compression (continued).

Specimen		Loading				Temp.	Dimension, in			Density
#	Honeycomb	plane	angle	dir.	path	°F	d1	d2	d3	ρ, pcf
4	Alcore35	TW	00		equal	70	3.015	1.400	3.060	35.53
5	Alcore35	TW	00		equal	70	3.008	1.570	3.040	35.73
6	Alcore35	TW	15		equal	70	3.017	1.885	3.010	35.65
7	Alcore35	TW	15		equal	70	3.019	1.965	3.020	35.70
8	Alcore35	TW	30		equal	70	2.958	1.950	2.932	35.40
9	Alcore35	TW	30	-	equal	70	2.950	1.860	2.926	35.67
10	Alcore35	TW	45		equal	70	3.044	1.938	3.062	35.48
11	Alcore35	TW	45	-	equal	70	3.032	1.922	2.923	35.27
23	Alcore35	TW	00		nonprop.	70	1.997	1.977	1.907	35.72
24	Alcore35	TL	00		axial-T	70	1.982	1.977	1.962	35.93
25	Alcore35	TW	15	-	equal	70	2.189	2.132	1.878	35.26
26	Alcore35	TW	15	+	equal	70	2.059	2.110	1.868	35.70
28	Alcore35	TW	30	-	equal	70	2.026	1.991	1.878	35.89
29	Alcore35	TW	30	+	equal	70	1.962	2.005	1.948	34.49
2b	Alcore35	TW	45	-	equal	70	2.093	2.080	1.781	34.80
2c	Alcore35	TW	45	+	equal	70	2.116	2.090	1.759	35.53
2f	Alcore35	TW	00		nonprop.	70	2.017	2.039	1.925	34.55
2g	Alcore35	TL	00		equal	70	2.025	1.995	1.767	36.03
31	Alcore38	TL	00		equal	70	2.030	1.980	1.634	38.44
32	Alcore38	TL	00		equal	70	1.969	1.975	1.624	38.79
34	Alcore38	TL	15	+	equal	70	1.972	1.967	1.633	38.37
35	Alcore38	TL	15	-	equal	70	2.004	2.045	1.513	38.36
36	Alcore38	TL	30	+	equal	70	1.981	2.010	1.626	38.97
37	Alcore38	TL	30	-	equal	70	2.025	1.937	1.632	37.71
38	Alcore38	TL	45	-	equal	70	2.020	2.026	1.616	38.31
39	Alcore38	TL	45	+	equal	70	1.995	2.037	1.565	39.09
3a	Alcore38	TW	15	-	equal	70	2.064	1.919	1.819	38.86
3b	Alcore38	TW	15	-	equal	70	2.065	1.905	1.844	39.01
3c	Alcore38	TW	30	+	equal	70	1.944	1.836	1.871	39.07
3d	Alcore38	TW	30	-	equal	70	1.930	1.820	1.784	38.96
3e	Alcore38	TW	45	-	equal	70	1.872	1.793	1.868	39.20
3f	Alcore38	TW	45	+	equal	70	1.857	1.778	1.811	38.60
41	Alcore35	TL	45		equal	70	1.982	1.975	1.518	37.08
42	Alcore35	TL	45		equal	70	2.026	1.977	1.499	38.77
43	Alcore35	TL	45		equal	70	2.093	1.991	1.475	35.66
44	Alcore35	TL	45		equal	70	1.969	2.090	1.473	35.73

Table 8-1. Test matrix of in-plane biaxial compression (continued).

Specimen		Loading				Temp.	Dimension, in			Density
#	Honeycomb	plane	angle	dir.	path	°F	d1	d2	d3	ρ, pcf
45	Alcore35	TL	45		equal	70	1.972	1.975	1.497	36.58
46	Alcore35	TW	45		equal	70	1.981	1.981	1.491	38.39
47	Alcore35	TW	45		equal	70	1.995	2.010	1.489	37.52
48	Alcore35	TW	45		equal	70	1.984	1.937	1.514	36.99
49	Alcore35	TW	45		equal	70	1.983	1.919	1.523	38.43
4a	Alcore35	TW	45		equal	70	1.976	1.965	1.498	38.97
51	Hexcel35	TW	00		equal	165	1.977	2.049	1.501	37.70
52	Hexcel35	TW	45		equal	165	1.983	1.995	1.518	35.18
53	Hexcel35	TW	15		equal	165	1.993	1.989	1.492	37.37
54	Hexcel35	TL	00		equal	165	2.004	1.980	1.499	37.05
55	Hexcel35	TL	45		equal	165	1.976	2.043	1.560	36.97
56	Hexcel35	TL	15		equal	165	2.004	2.030	1.538	37.01
61	Alcore35	TL	00		equal	165	1.993	2.007	1.483	36.61
62	Alcore35	TL	00		equal	165	1.998	2.014	1.482	36.32
63	Alcore35	TW	00		equal	165	1.991	1.980	1.540	35.73
64	Alcore35	TW	00		equal	165	1.994	1.988	1.515	34.96
65	Alcore35	TL	45		equal	165	2.003	1.996	1.497	36.19
66	Alcore35	TL	45		equal	165	1.985	2.011	1.552	35.68
67	Alcore35	TW	45		equal	165	1.997	1.988	1.510	35.58
68	Alcore35	TW	45		equal	165	2.000	2.009	1.511	35.07
69	Alcore35	TL	15		equal	165	2.052	2.057	1.491	35.69
6a	Alcore35	TL	15		equal	165	2.052	2.053	1.489	36.06
6c	Alcore35	TW	15		equal	165	2.051	2.049	1.519	35.51
71	Hexcel35	TW	00		equal	70	2.031	1.983	1.494	37.73
72	Hexcel35	TW	45		equal	70	1.990	1.996	1.523	35.21
73	Hexcel35	TW	15		equal	70	2.030	1.973	1.495	37.19
74	Hexcel35	TL	00		equal	70	1.985	2.004	1.498	36.82
75	Hexcel35	TL	45		equal	70	1.977	2.033	1.518	37.15
76	Hexcel35	TL	15		equal	70	2.000	2.037	1.563	36.88

Due to the availability of honeycomb, Alcore35 was the baseline material for the biaxial experiments. Alcore38 and Hexcel35 were also included for a limited number of tests. Most tests were conducted at ambient temperature, but some were at 165°F to obtain temperature effects. In all biaxial tests, the out-of-plane direction was free and unconfined.

The purposes of the first three specimens were to test the loading paths and evaluate the biaxial results with the honeycomb properties obtained previously from other test configurations. From

the results of bare compression discussed in Sections 2 and 3, abnormal crush of honeycomb is often caused by splitting between aluminum sheets. With the W direction confined or under compression, splitting is unlikely to happen. In-plane biaxial loading started with the LW and TW plane.

The results of the first specimen, uniaxial compression of Hexcel38 in the L direction, is plotted in Figure 8-6. The L crush strength is 0.98 ksi, exactly the same value obtained from the qualification test. This confirms that the data obtained from the biaxial experiment are consistent with the results from the prior method. The advantage of performing uniaxial compression on the biaxial system is that the confined force can be measured. During crush of Specimen #1, the normalized force in the confined W direction shows an increase with respect to the compressive strain, which can be described by: σ_W = -0.021 + 0.57 * ε_L ksi.

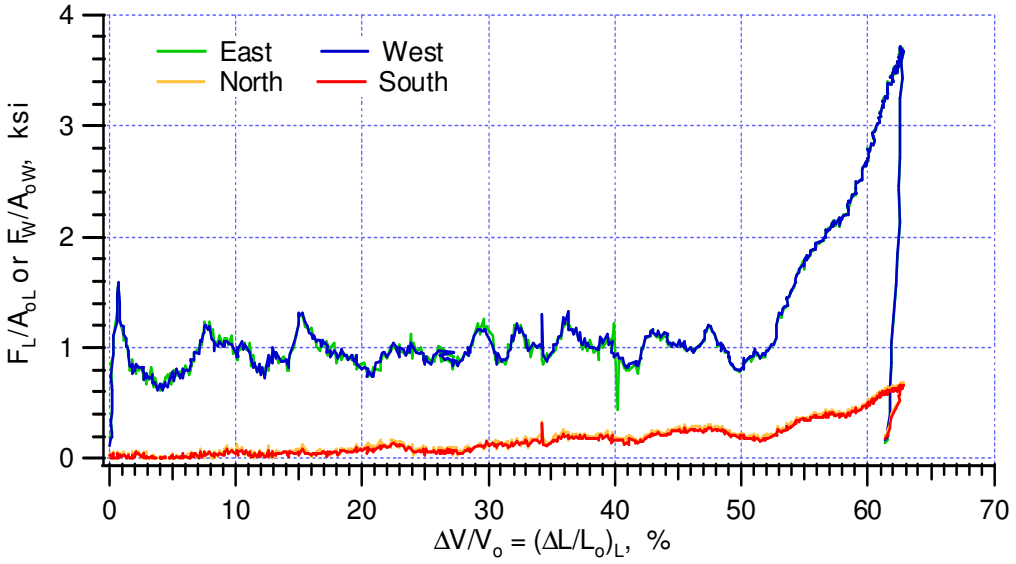

Figure 8-6. Normalized load-displacement curves of biaxial Specimen #1; uniaxial compression of Hexcel38.

Figure 8-7 shows the results of an equal compression of Alcore38 in the LW plane of the second specimen. The crush load in the L direction remained constant even though the cross-sectional area was continuously decreasing during the crush. If the calculation of crush strength is based on the engineering stress definition, the value is 1.01 ksi. Quasi-static crushing of Alcore38 has not been performed before, but is reasonable in value compared with 1.25 ± 0.13 ksi from qualification tests at the intermediate rate. The crush load in the W direction, however, did not remain constant as the L direction and continued to increase during the crush. After the initial peak, the crush load increases continuously, and the amount of increase is greater than the confined stress measured from Specimen #1.

The result of an equal compression of Alcore38 in the TW plane, Specimen #3, is shown in Figure 8-8. The specimen crushed in the normal mode up to about 15 percent. At that point, it turned into an abnormal mode with global buckling and the stress started to drop. Similar to Specimen #2, the crush load in W direction did not stay constant. It showed an increase until the deformation became abnormal.

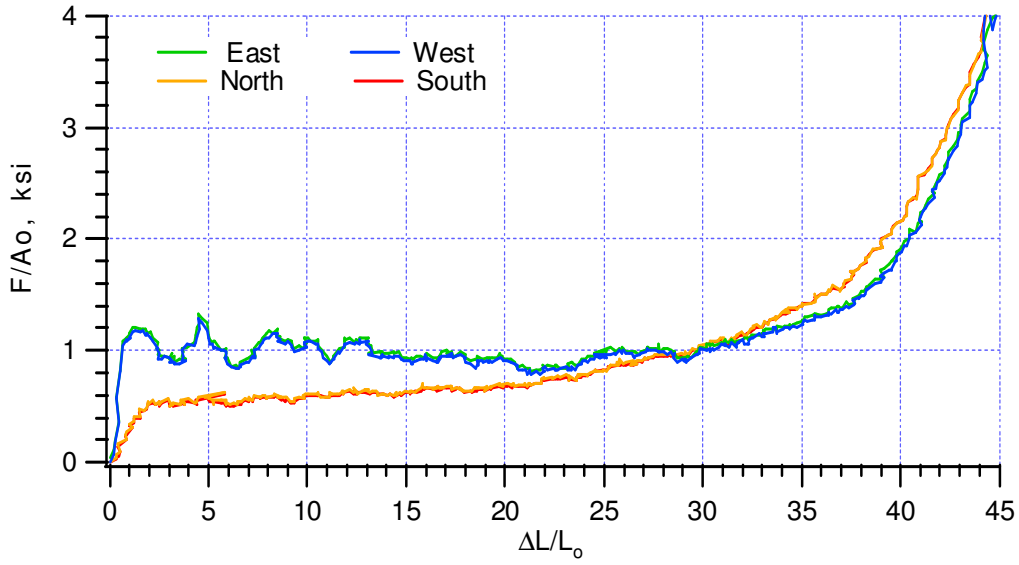

Figure 8-7. Normalized load-displacement curves of biaxial Specimen #2; equal biaxial compression of Alcore38 in the LW plane.

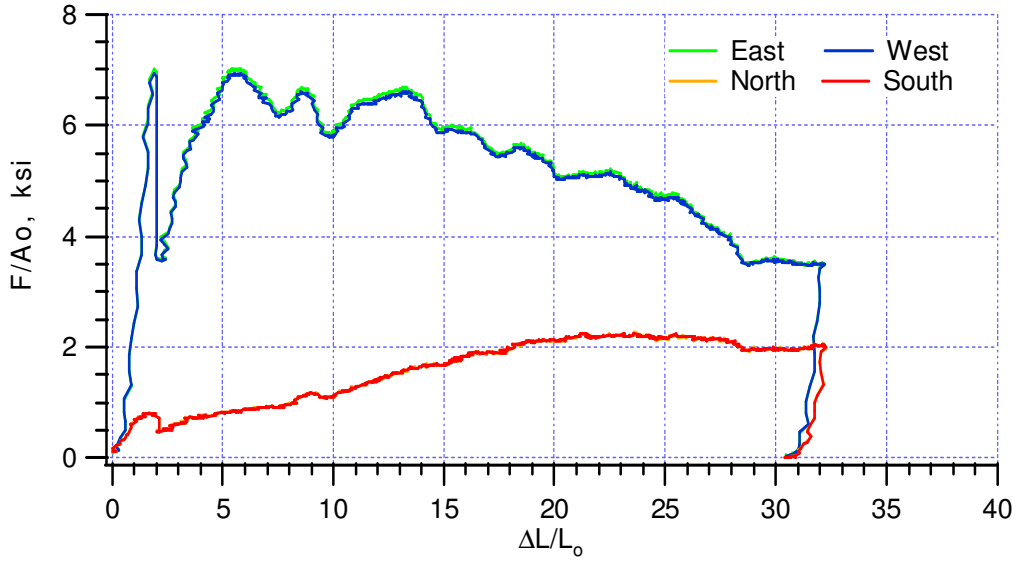

Figure 8-8. Normalized load-displacement curves of biaxial Specimen #3; equal biaxial compression of Alcore38 in the TW plane.

The increase of crush stress in the W direction during equal biaxial compression was not expected from the orthotropic crush model.

8.2 Equal Biaxial Compression of Alcore35 in Ambient Conditions

Specimens #4 - 2g and #41 - 4a were all Alcore35 specimens. Most of these tests were equal biaxial compression and dealt with off-axis specimens along with the TW and TL planes. The angles included $\theta = 0$, 15, 30, and 45 degrees. During equal biaxial compression, the motion of each platen has normal and tangential components with respect to the surface of the specimen.

For the current setup of biaxial fixtures, the tangential force component (i.e., friction) resulted in applying a torque on the specimen in the clockwise direction (Figure 8-9(a)). Except 0 and 45 degrees, the torque would make the loading condition different for the same angle off-axis specimens depending on how they were oriented in the fixture. The off-axis specimens could be put in place with a positive or negative angle, as depicted in Figure 8-9(b). To find the influence of this torque, experiments with both positive and negative orientations were considered in the later set of experiment (Specimen #23 – 2g); the orientations of some specimens in the earlier set, #4 – 11, were not recorded.

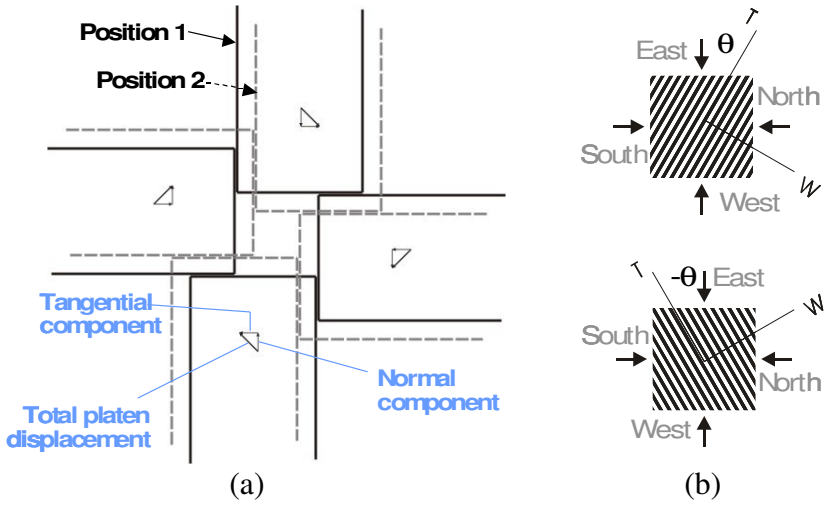

Figure 8-9. The tangential force component (friction) on the specimen surface may cause different responses in θ and -θ off-axis specimens.

Experimental results for equal biaxial compression of TWθθ (θθ = 0, 15, 30, and 45) in ambient conditions are shown in Figures 8-10 through 8-14. The two normalized load-displacement curves North and South (or East and West) of North-South (or East-West) loading axis are from independent measurements, but they are practically identical for all experiments, which is demonstrated in Figure 8-10; therefore, only one curve for each axis will be plotted in all of the following figures.

During the in-plane biaxial experiment, the out-of-plane direction was not confined and the out-of-plane displacement was not measured. In general, there is not enough information to calculate the volumetric strain Expansion of specimens in the out-of-plane direction during crush, i.e., L direction for TWθθ specimens, would delay the densification until a larger strain in comparison with the case that the out-of-plane is confined.

The crushing of TW00 for Alcore35 was similar to that of Alcore38 (#3) in the last section. The crush stress in the T direction remained constant, but the stress in the W direction continued to increase. Specimen #5 remained in the normal mode during the crush, but #4 changed to global buckling after 20 percent deformation.

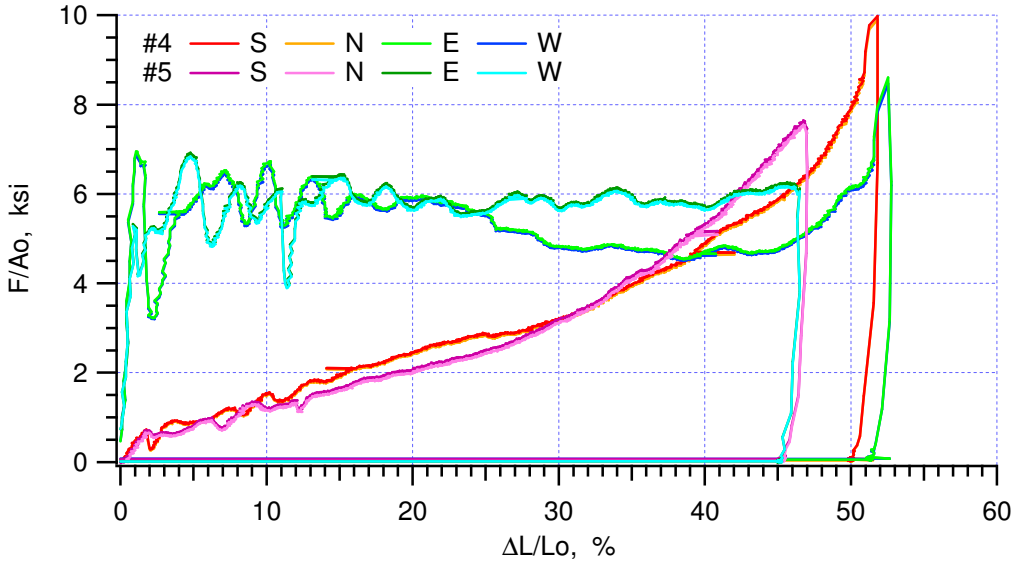

Figure 8-10. Normalized load-displacement curves of Alcore35, TW00; equal biaxial loading at ambient. NS and EW are the T and W direction, respectively.

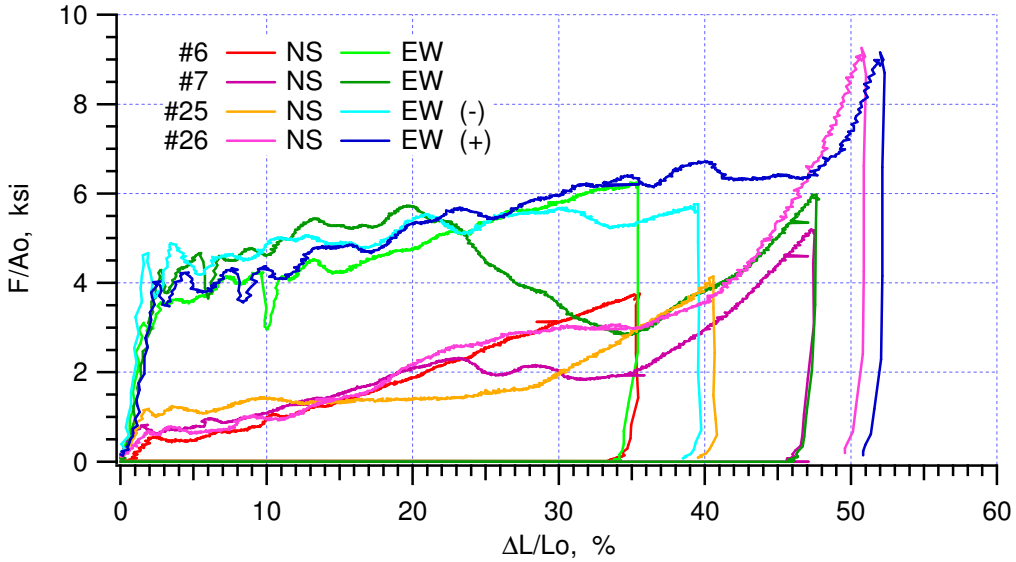

Figure 8-11. Normalized load-displacement curves of Alcore35, TW15; equal biaxial loading at ambient temperature.

For TW15 specimens, Figure 8-11, the crush load of both loading axes increased during the initial crush period; then the slope decreased, signaling the crush mode becaming abnormal. This happened at 20 percent and 40 percent strain for Specimens #7 and #26, respectively. Comparing the load of two specimens, which the orientation clearly recorded, the one with negative orientation (#25) was about 0.4 ksi higher than the positive one (#26) for both axes.

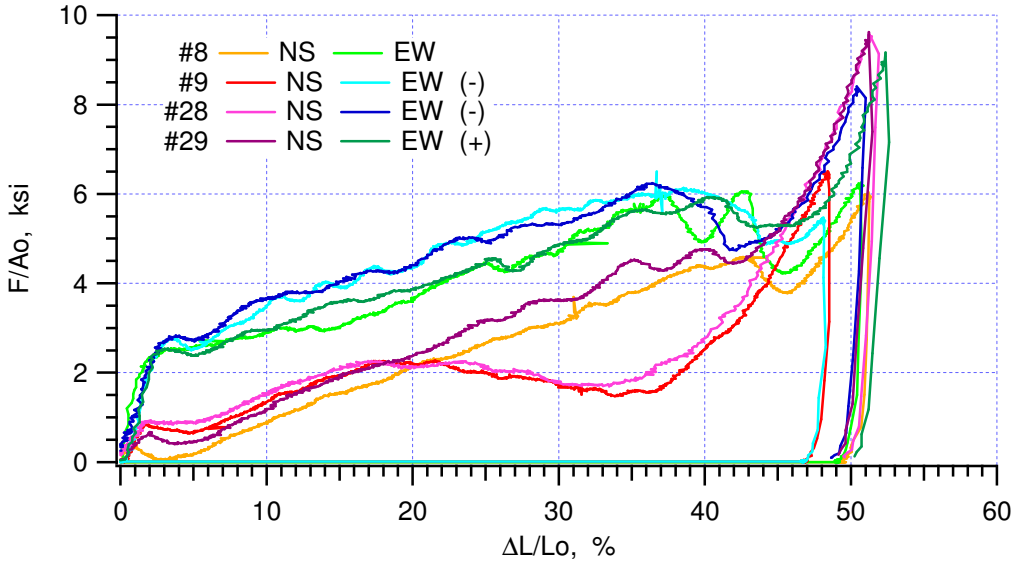

Figure 8-12. Normalized load-displacement curves of Alcore35, TW30; equal biaxial loading at ambient temperature.

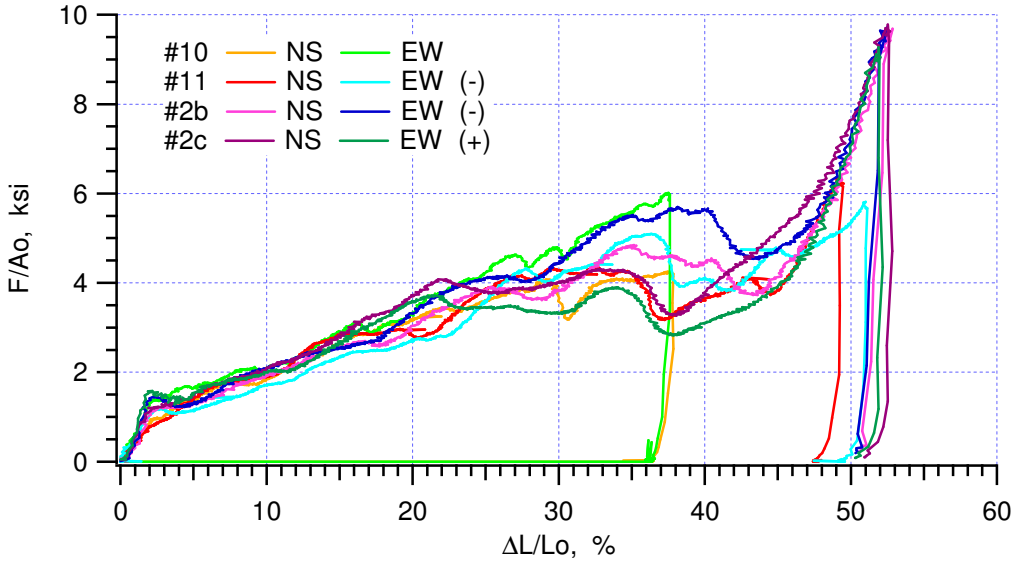

Figure 8-13. Normalized load-displacement curves of Alcore35, TW45; equal biaxial loading at ambient temperature.

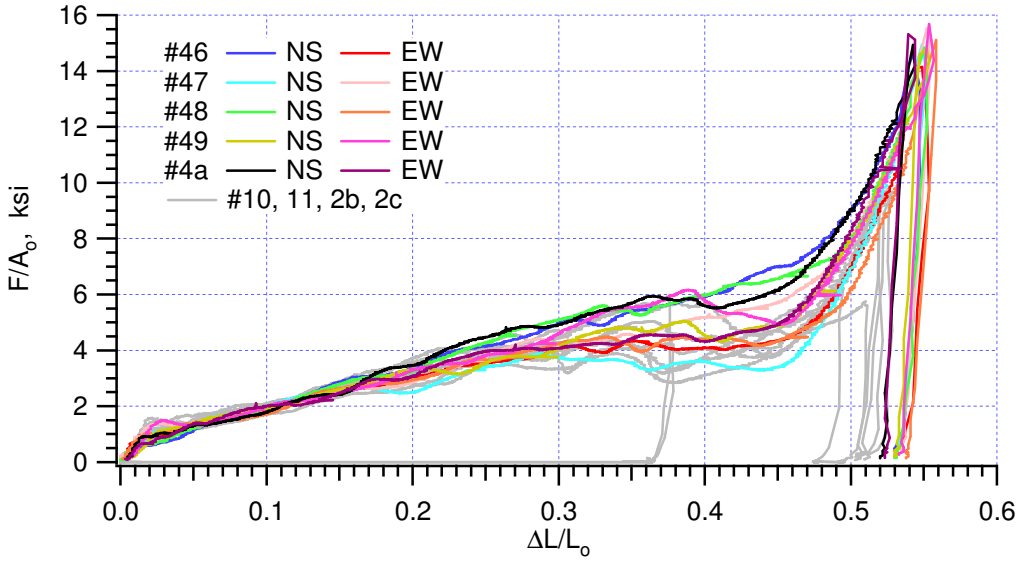

Figure 8-14. Normalized load-displacement curves of equal biaxial compression at ambient temperature for all Alcore35, TW45 specimens.

The results of TW30 specimens show similar trends as TW15. The specimens were initially crushing in a normal mode, and then turned into an abnormal mode. The transition could occur at a strain as small as 17 percent, #9 and #28. Specimens #9 and 28, with negative orientation had the crush stress consistently higher; about 0.5 ksi more than the positive specimen (#29).

With the off-axis angle, $\theta = 45$ degree, the effects of the torque on the positive and negative specimens were the same, and the responses of two loading axes would be about the same. As expected, the load-displacement curves of the NS and EW axes coincide and do not display distinctive differences between positive and negative angles, as shown in Figure 8-12. The curves also reveal that unstable deformations are likely to happen when the strain is greater than 20 percent.

Figure 8-14 shows the results of additional tests of TW45 specimens #46 – 4a with the curves of #10, 11, 2b, and 2c on the background. These two sets of specimens were prepared and tested at different times. All TW45 curves agree well. The scatter of data appears to be a function of strain. The results of data analyses at discrete strains from and 18 curves are summarized in Figure 8-15 and Table 8-2.

8.3 Nonproportional Loading

Regardless of the type of honeycomb (Alcore38 or Alcore35), equal biaxial compressions of TW00 and LW00 consistently show constant crush load in the stronger material axis and increasing crush load in the weaker axis. This means engineering stress, not true stress, should be used in the orthotropic crush model, and that there is a stress coupling effect. If true stress were considered, the stress of the stronger axis would increase, since the cross-section area was reduced, and the model would overestimate the energy absorption capacity of honeycomb. By neglecting stress coupling, the model would somewhat underestimate the amount of energy

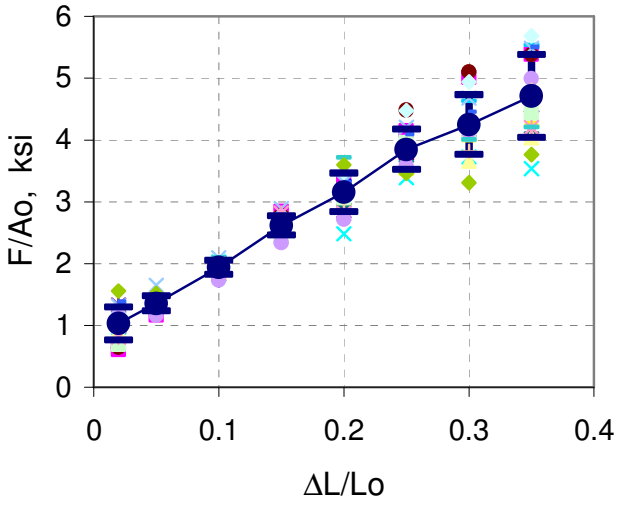

Figure 8-15. Scatter of data of Alcore35, TW45; equal biaxial loading at ambient temperature.

Table 8-2. Standard deviation of Alcore35 data.

ΔL/Lo	F/Ao, ksi	
	mean	std dev
0.02	1.03	0.27
0.05	1.36	0.12
0.10	1.94	0.12
0.15	2.62	0.15
0.20	3.15	0.31
0.25	3.85	0.33
0.30	4.25	0.49
0.35	4.71	0.67

absorption. The purpose of the nonproporational experiments was to confirm that engineering stress is the correct stress to use.

As shown in Figure 8-16, TW00 Specimens #23 and 2f were compressed in the W directions to 25 percent and 10 percent, respectively, while keeping the T direction confined. It was immediately followed by compressing in the T direction and confining in the the W direction. The results are plotted in Figure 8-17, where an equal biaxial compression of TW00 #5 is also plotted for comparison. In the plot, the abscissa is in volumetric strain, which is calculated by $\Delta V/V_o = \Delta L_T/L_To + \Delta L_W/L_Wo$. Since the issue is crush stress, which is more or less constant over a period of strain, and the accuracy of the strain does not affect the stress value, the calculation is a good approximation, even if there are some out-of-plane deformations. Using volumetric strain is strictly for convenience and an easy presentation. Results show that the T crush load of honeycomb is not affected by different amounts of pre-strain in the W direction.

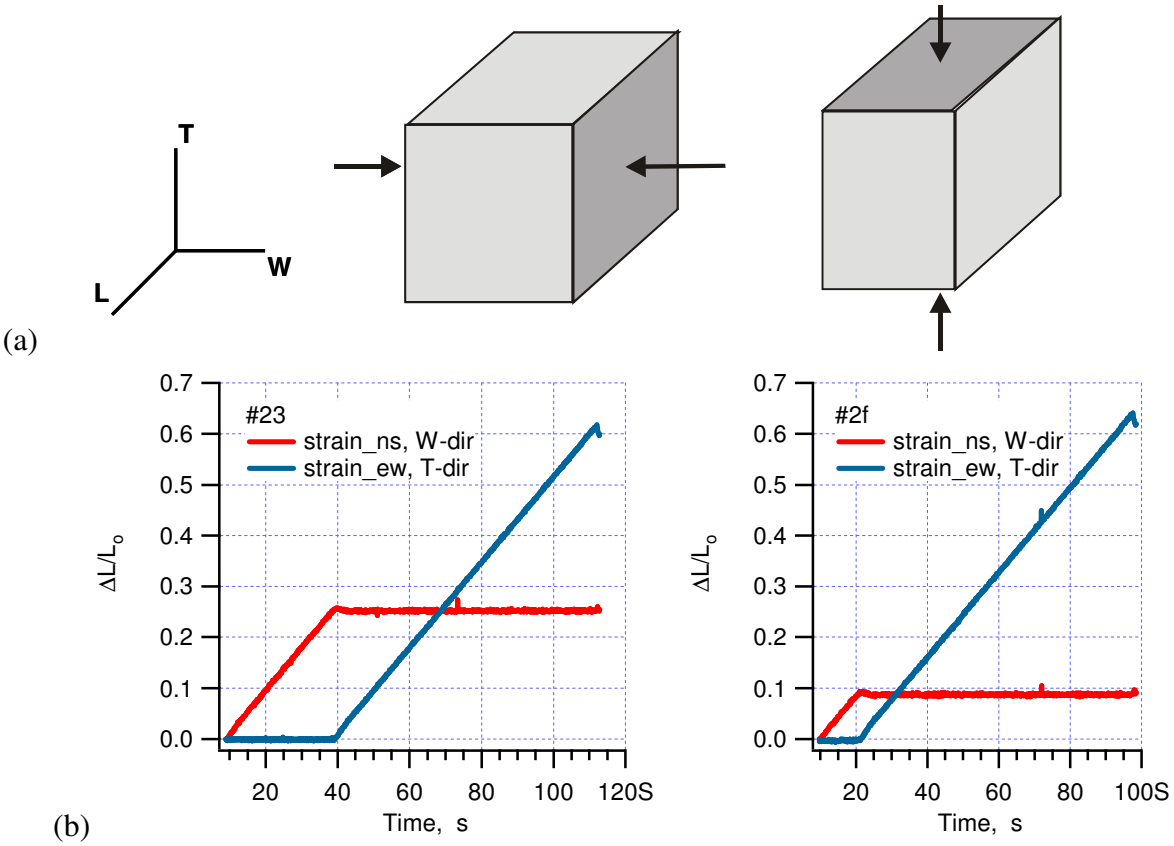

Figure 8-16. Nonproportional loading: (a) schematics, (b) strain histories.

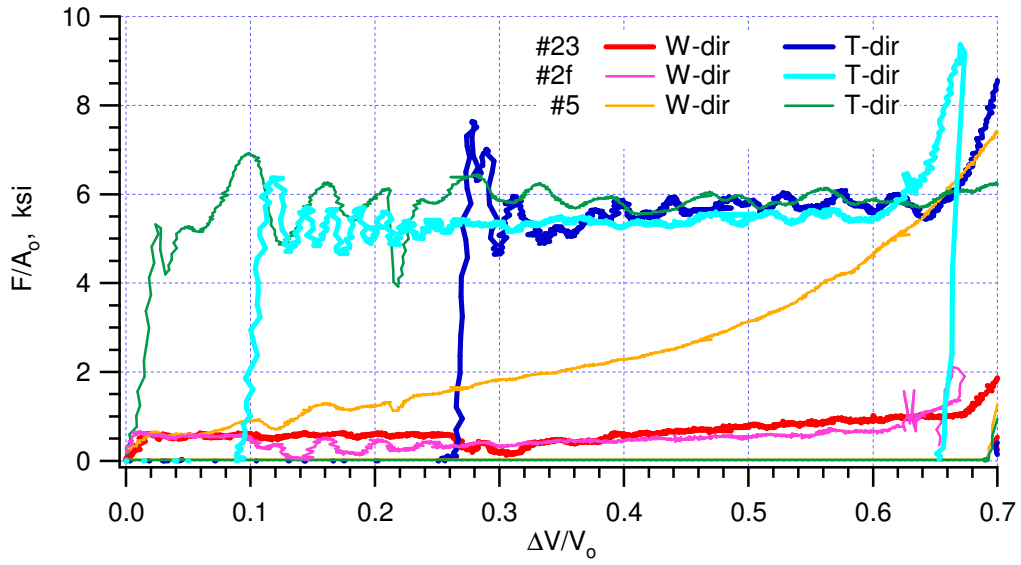

Figure 8-17. Normalized load-displacement curves for nonproportional loading of Alcore35.

The engineering stress definition should be used to match the description that the crush stress is constant for honeycomb.

Experimental results for biaxial experiments of Alcore35 in the TL plane are shown in Figures 8-18 and 8-19. The deformation behaviors in TL plane resemble that of TW plane. The crush strength of the T direction, 5.51 (up to 30 percent) and 5.70 ksi for #24 and #2g, respectively, is consistent with previous quasi-static data in Table 3-2. The loads in the L and TL45 off-axis direction are all slightly higher than the counterpart in the TW experiments, which is reasonable, since the L direction is stronger than the W direction.

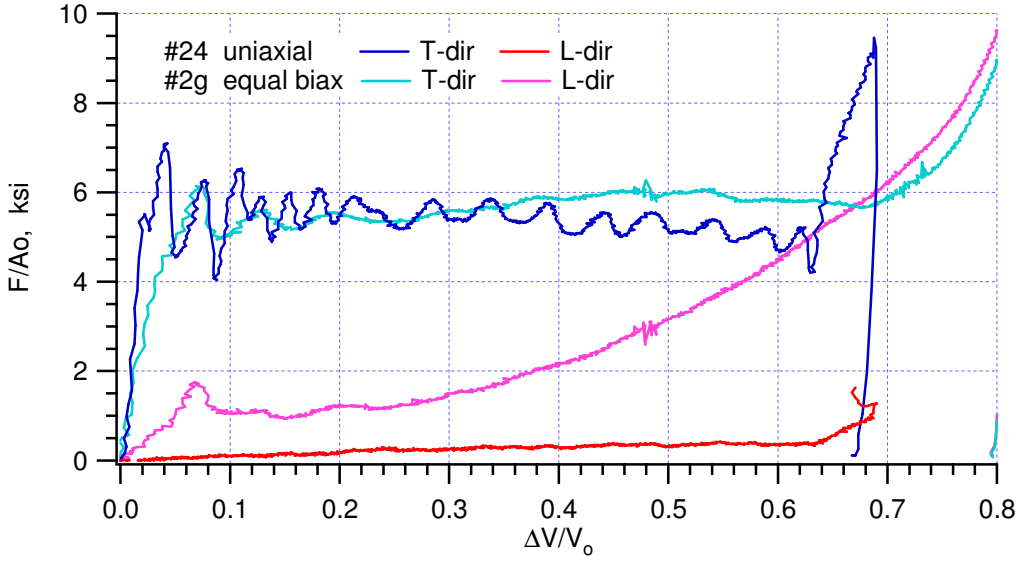

Figure 8-18. Biaxial experiments of Alcore35 TL00 specimens at ambient temperature.

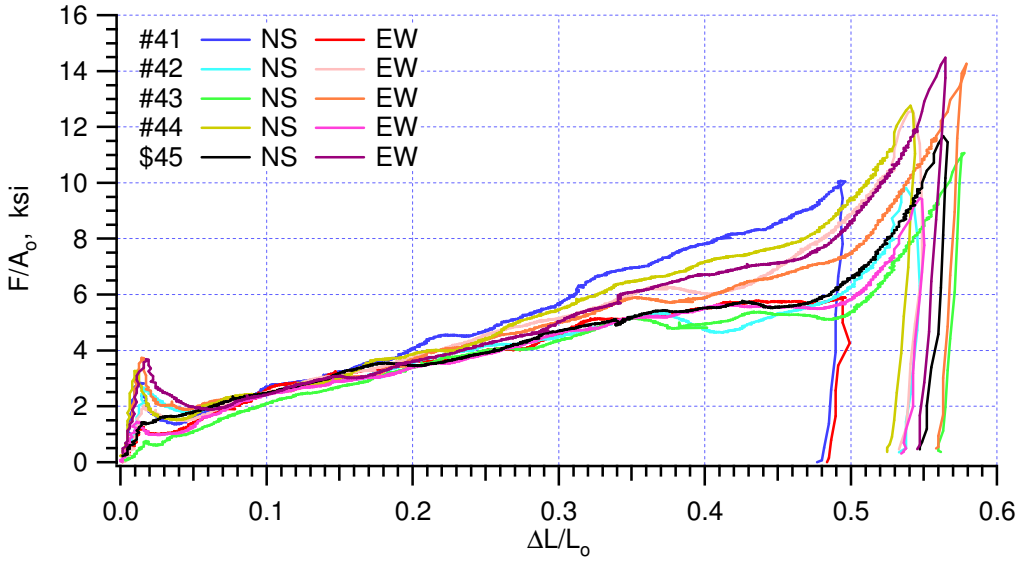

Figure 8-19. Equal biaxial compression of Alcore35 TL45 specimens at ambient temperature.

8.4 Equal Biaxial Compression of Alcore38 at Ambient Temperature

Biaxial experiments of Alcore38 included both the TL and the TW planes. The purpose was to confirm that the observed crush behaviors of Alcore35 could be generalized to the same class of high-density aluminum honeycomb. The experimental results are shown in Figures 8-20 to 8-26. The load-displacement curves of the Alcore38 off-axis specimens indeed have the same trends as Alcore35. As the off-axis angle θ changes from 0 to 45 degrees (when θ = 0, T direction was aligned with the East actuator), the initial crush stress measured from East-West actuators would decrease and the slope of EW load-displacement curve would increase; the response of North-South axis showed an opposite trend. Out-of-plane deformation was much more evident for the TL specimens. The experiments show that the out-of-plane deformation was insignificant when the crush strain was less than 20 percent. The crush strength in the T direction was about 6.5 ksi, which was high comparing with 5.23 ksi in qualification test. The negative angle specimens generally showed a slightly higher load than the positive specimens.

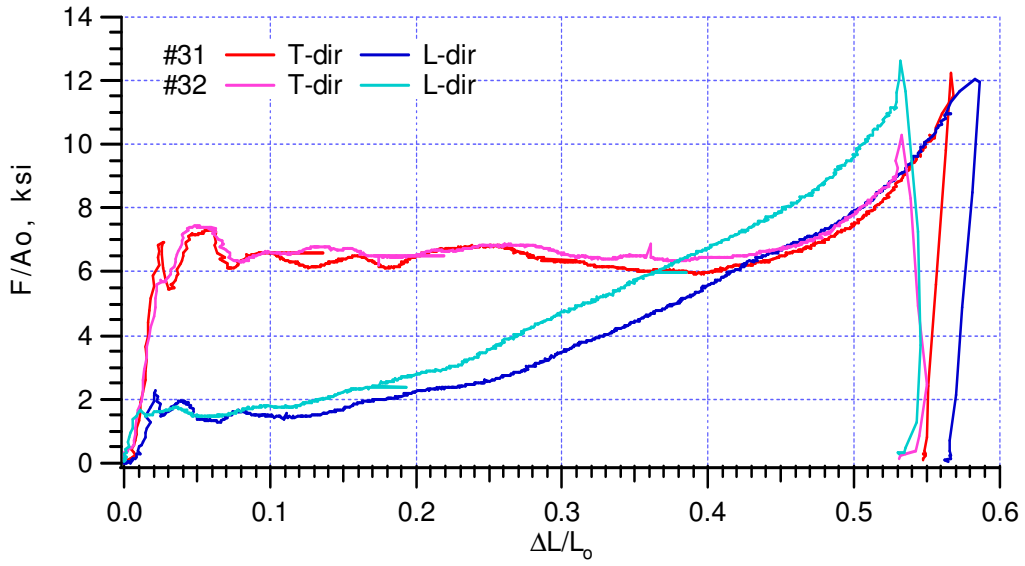

Figure 8-20. Normalized load-displacement curves of Alcore38, TW00; equal biaxial loading at ambient temperature.

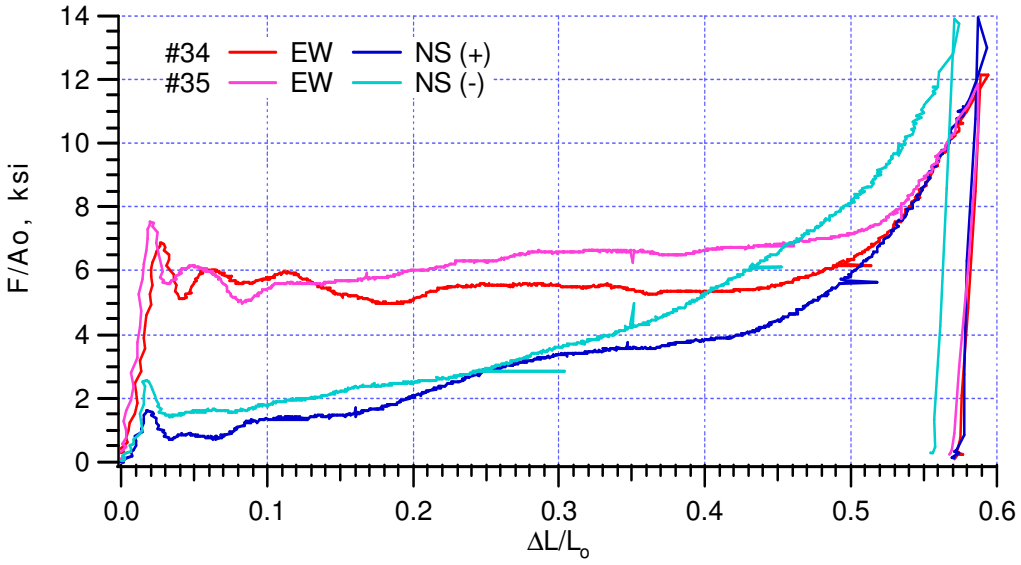

Figure 8-21. Normalized load-displacement curves of Alcore38, TL15; equal biaxial loading at ambient temperature.

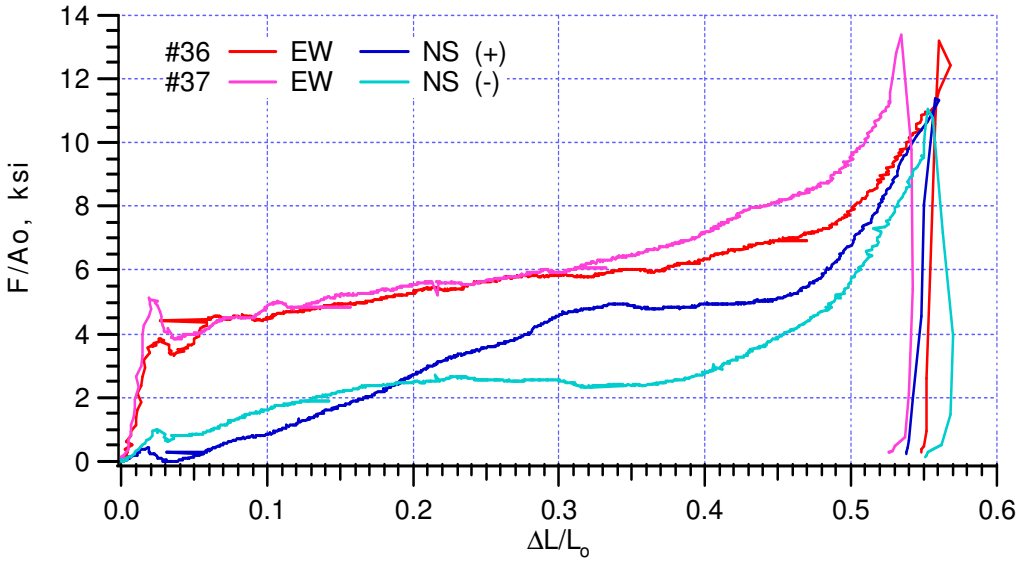

Figure 8-22. Normalized load-displacement curves of Alcore38, TL30; equal biaxial loading at ambient temperature.

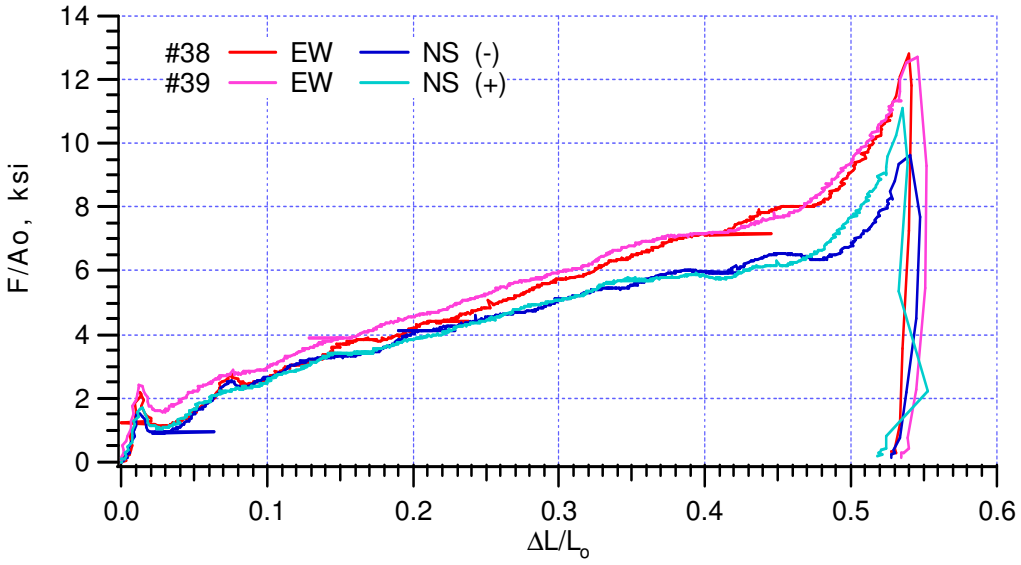

Figure 8-23. Normalized load-displacement curves of Alcore38, TL45; equal biaxial loading at ambient temperature.

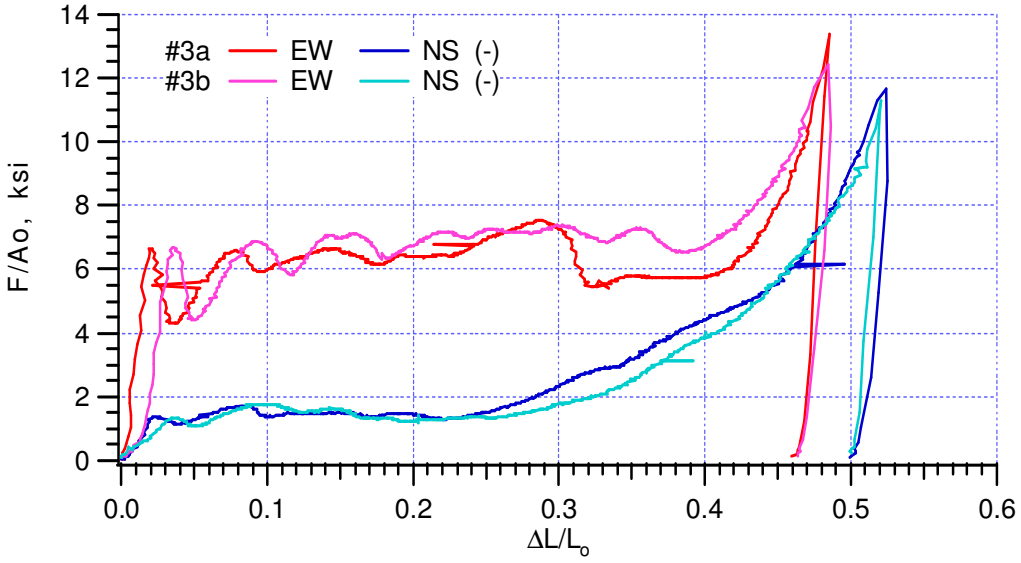

Figure 8-24. Normalized load-displacement curves of Alcore38, TW15; equal biaxial loading at ambient temperature.

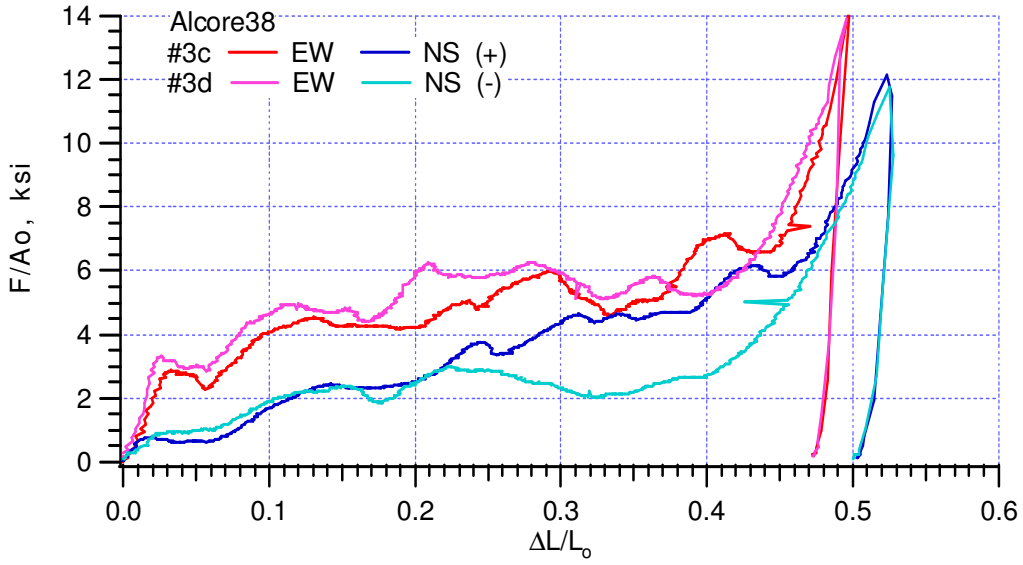

Figure 8-25. Normalized load-displacement curves of Alcore38, TW30; equal biaxial loading at ambient temperature.

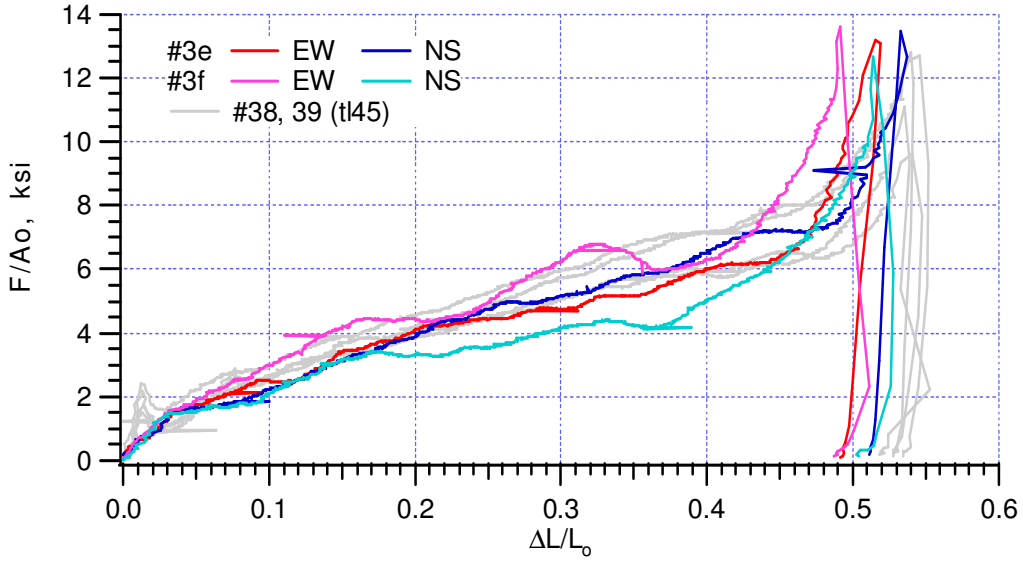

Figure 8-26. Normalized load-displacement curves of Alcore38, TW45; equal biaxial loading at ambient temperature.

8.5 Equal Biaxial Experiment at 165°F

The temperature effect on the uniaxial crush strength of high-density aluminum honeycomb has been demonstrated and characterized in Section 3.3. Higher temperatures lower the crush strength of honeycomb and make it crush in an abnormal mode, if unconfined. Here, the effect of high temperature on biaxial crush of honeycomb is studied.

To generate an elevated temperature environment for the honeycomb specimen, each biaxial fixture was modified by drilling a hole on the side for inserting a heating cartridge, as shown in

Figure 8-27. The fixtures became compression platens, as well as heating walls. Thermal couples (TCs) were welded to the platens and inserted into the specimen to monitor and control the temperature. As shown in Figure 8-28, TC2 and TC3 were located close to the edges of South and West fixtures to monitor platen temperatures. TC1 measured the temperature at the top surface of the specimen and controlled the heating of all four heating cartridges. A piece of insulating foam was placed on the top of the specimen. TC4 monitored the temperature on the bottom side of the specimen and controls the elephant heater, which blew hot air to the specimen from below. The specimen equilibrated at the desired temperature of 165°F for at least 15 minutes before loading started. The variance of temperature was within ± 3°F.

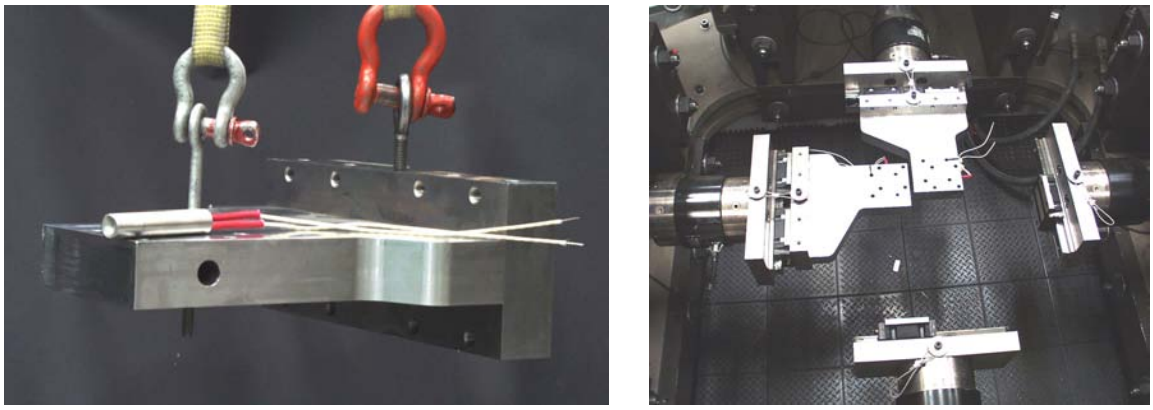

Figure 8-27. Modified biaxial fixtures. A hole was drilled on the side of each fixture and a heating cartridge was inserted in the hole.

The test matrix is listed in Table 8-1, from Specimens #51 to #6C, which includes two honeycombs (Alcore35 and Hexcel35), two loading planes (TL and TW) for each honeycomb, and three offset angles (θ = 0, 15, and 45 degrees) for each loading plane.

Experimental results are shown in Figure 8-29 to 8-40. High-density aluminum honeycombs show the same biaxial crush behaviors at high temperature. Compared with the experiments conducted at ambient temperature, the effect of temperature on biaxial loading is the same as that of uniaxial loading — the crush load at 165°F is lower. The biaxial results show the decrease of crush strength spreading from 5 percent to 20 percent. The temperature effect is confirmed using the data from the qualifying experiments, Table 7-2, which is adequate to describe the temperature effect.

The high temperature does not seem to have a significant effect on the crush mode during biaxial loading. Judging from the normalized load-displacement curves of Alcore35, #67 (TW45 at 165°F) had the shortest period of normal crush: about 17 percent. Specimens #9 and 28, TW30 at ambient temperature, became unstable at the exactly same strain.

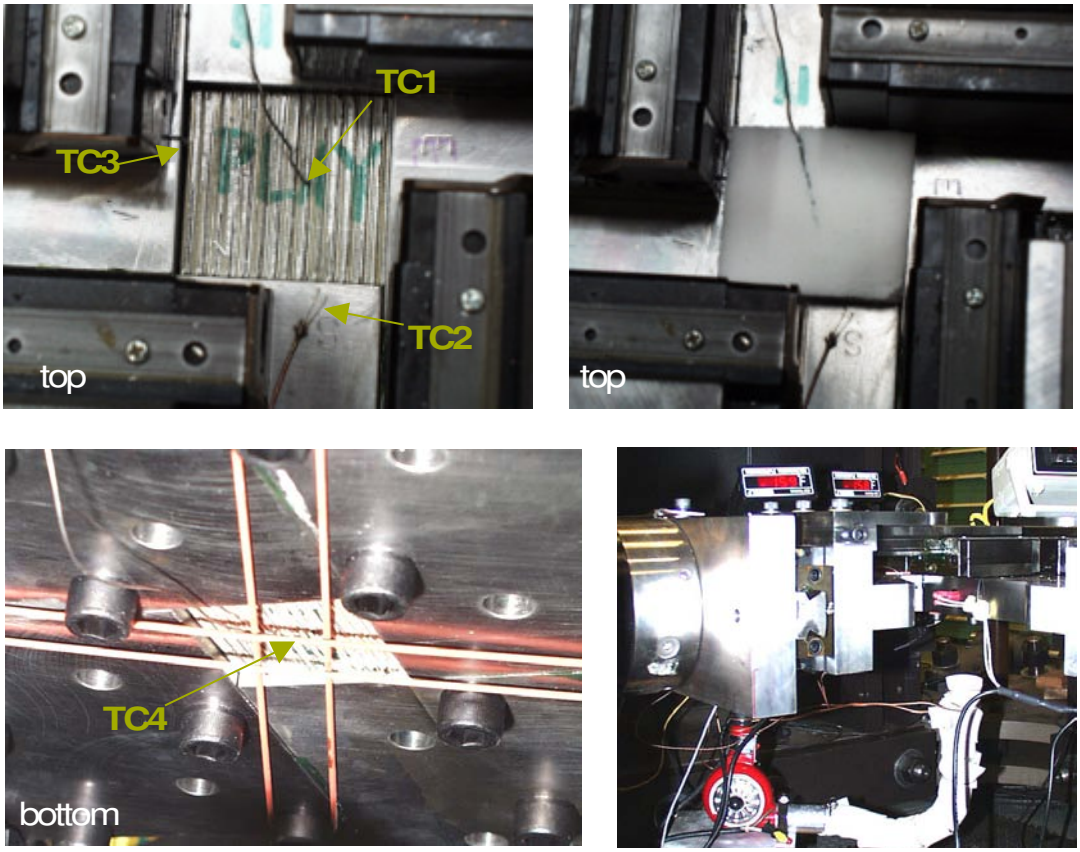

Figure 8-28. The setup of the high-temperature biaxial experiment.

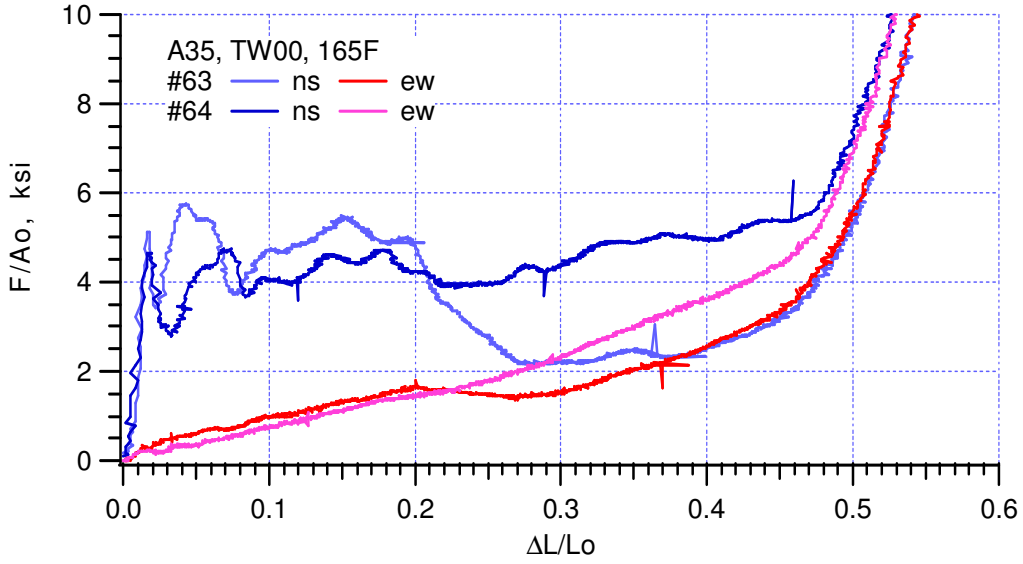

Figure 8-29. Normalized load-displacement curves of Alcore35, TW00; equal biaxial loading at 165°F.

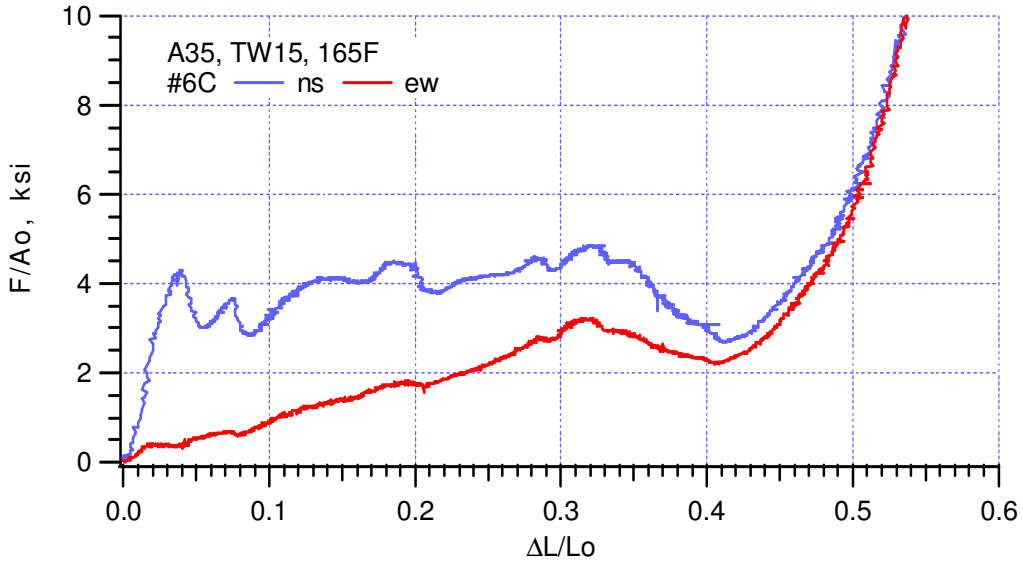

Figure 8-30. Normalized load-displacement curves of Alcore35, TW15; equal biaxial loading at 165°F.

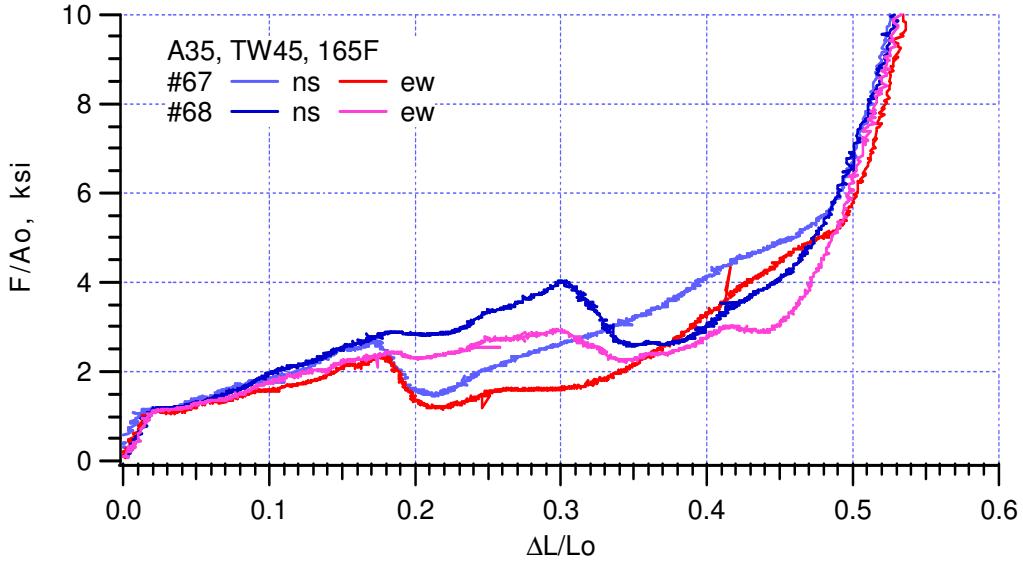

Figure 8-31. Normalized load-displacement curves of Alcore35, TW45; equal biaxial loading at 165°F.

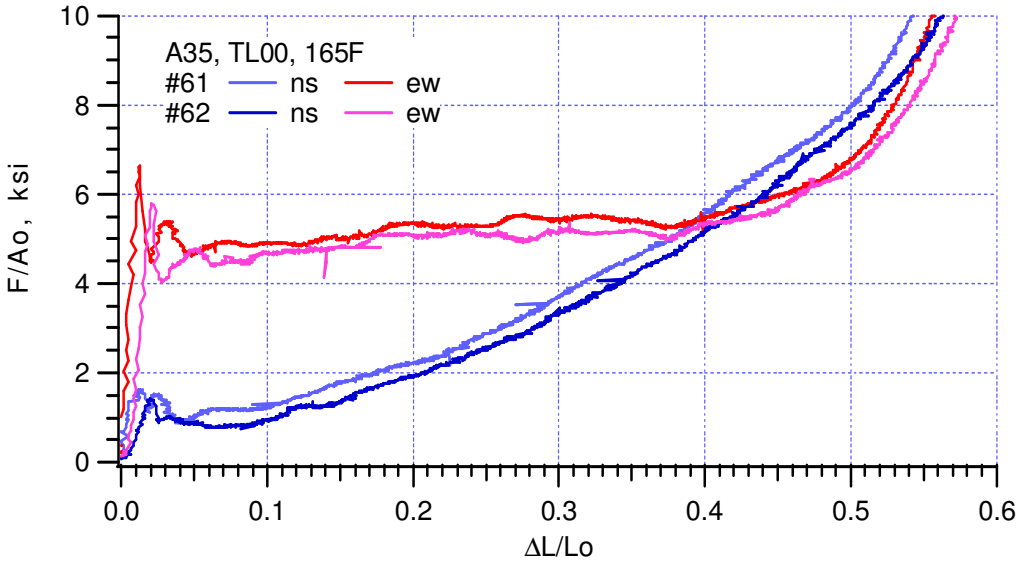

Figure 8-32. Normalized load-displacement curves of Alcore35, TL00; equal biaxial loading at 165°F.

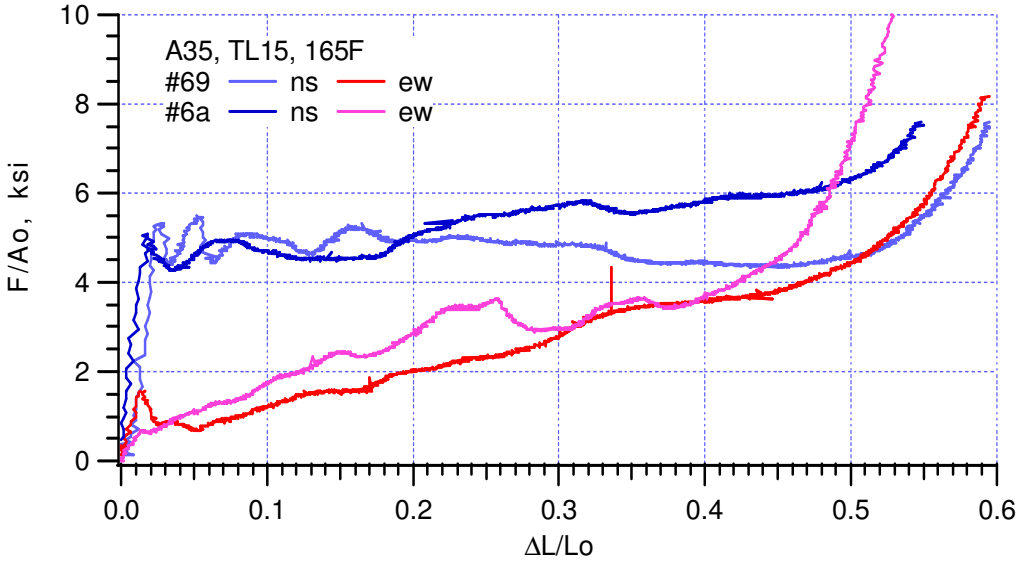

Figure 8-33. Normalized load-displacement curves of Alcore35, TL15; equal biaxial loading at 165°F.

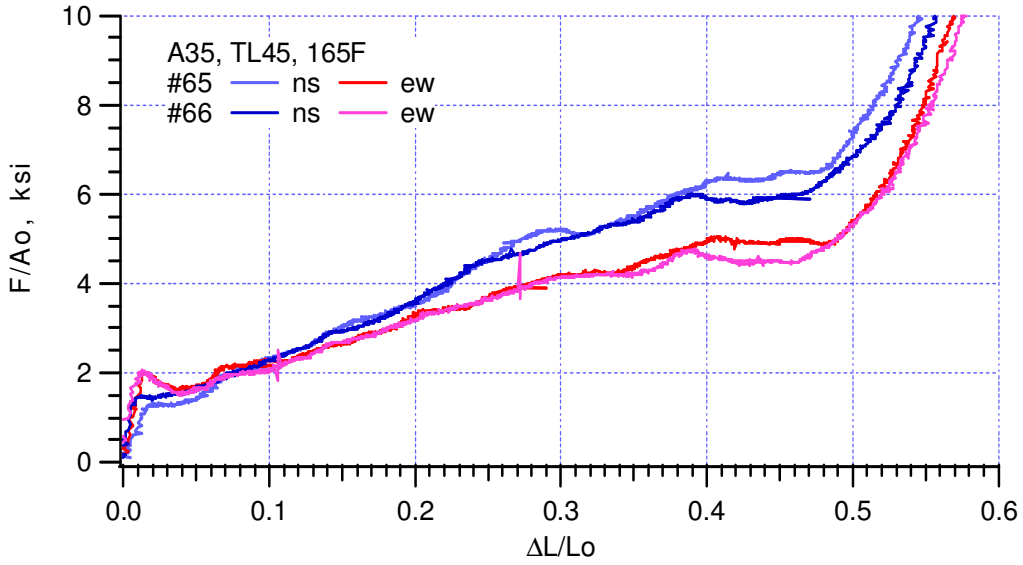

Figure 8-34. Normalized load-displacement curves of Alcore35, TL45; equal biaxial loading at 165°F.

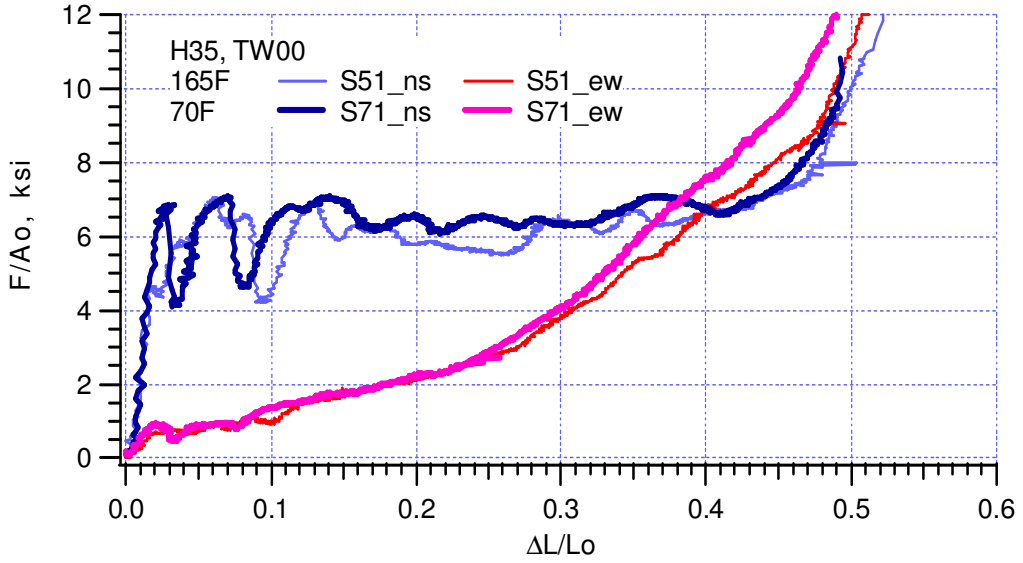

Figure 8-35. Normalized load-displacement curves of Hexcel35, TW00; equal biaxial loading.

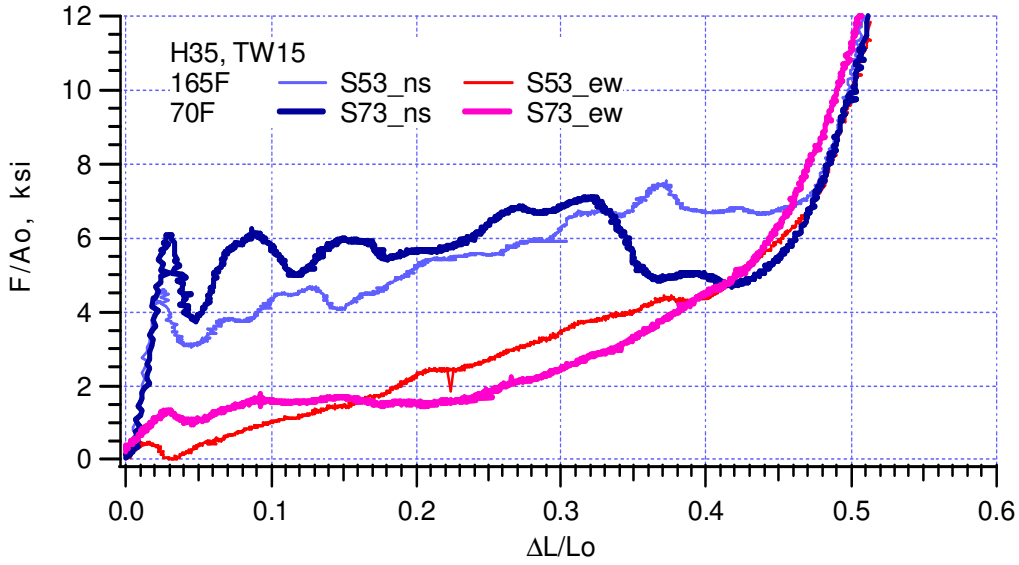

Figure 8-36. Normalized load-displacement curves of HexcelL35, TW15; equal biaxial loading.

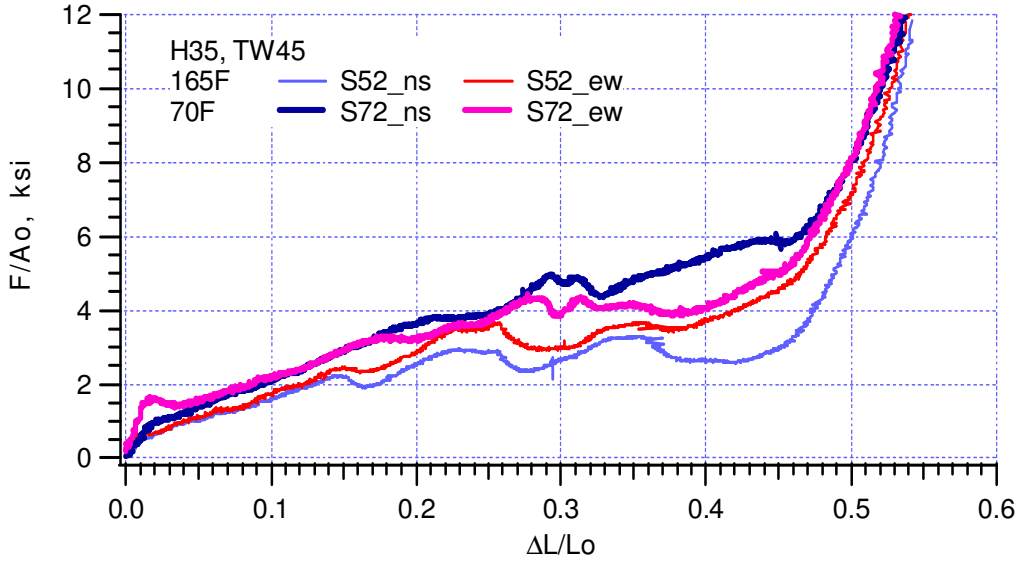

Figure 8-37. Normalized load-displacement curves of Hexcel35, TW45; equal biaxial loading.

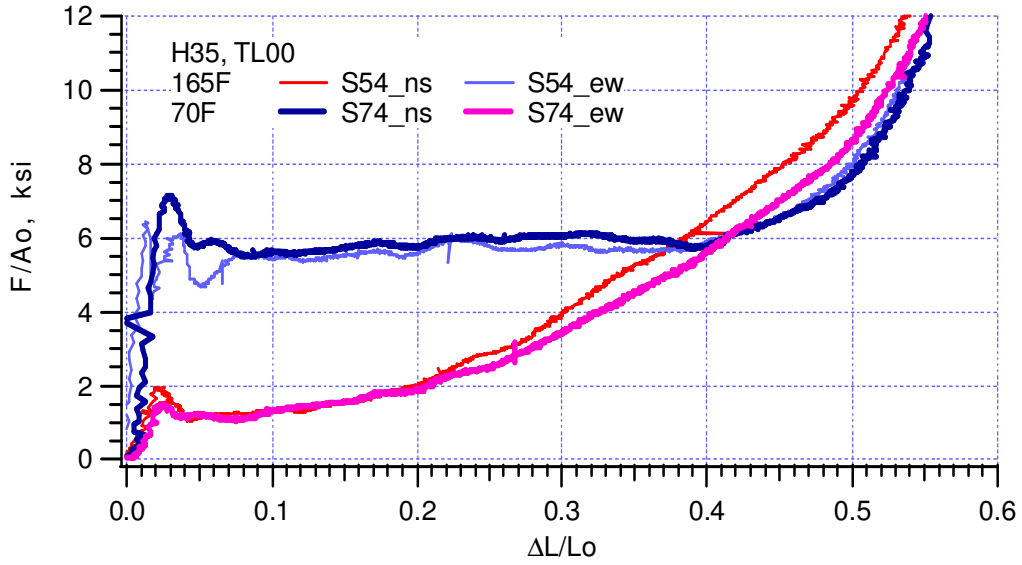

Figure 8-38. Normalized load-displacement curves of Hescel35, TL00; equal biaxial loading.

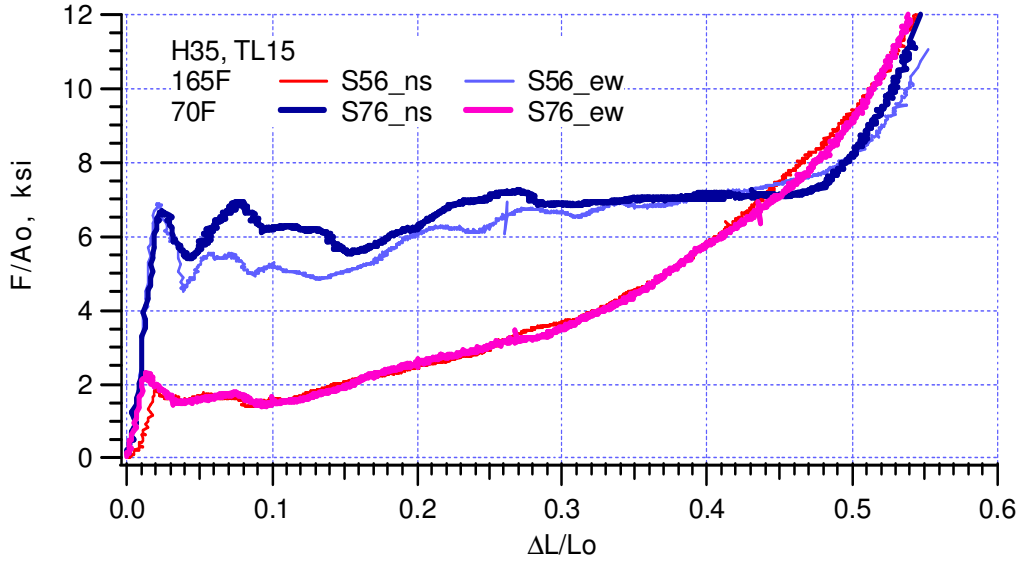

Figure 8-39. Normalized load-displacement curves of Hexcel35, TL15; equal biaxial loading.

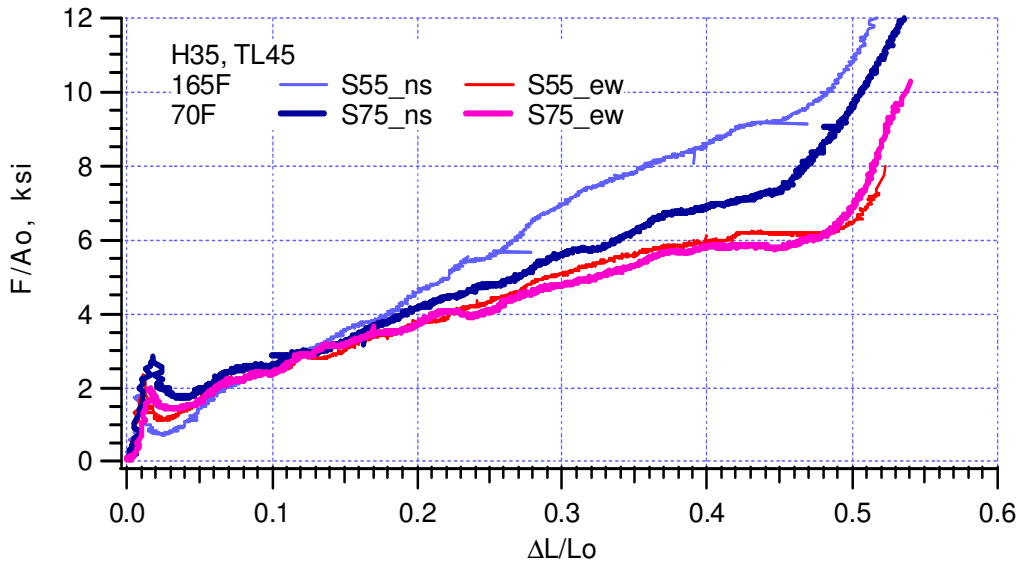

Figure 8-40. Normalized load-displacement curves of Hexcel35, TL45; equal biaxial loading.

9. EFFECT OF HUMIDITY ON THE CRUSH OF HONEYCOMB

The experiment described in Section 5.3 clearly demonstrates that the adhesive bond influences the crush behavior of honeycomb. The crush strength and energy absorbing capacity are severely degraded when the epoxy bond is intentionally removed. The adhesive bond is also affected by temperature and humidity, which is solely responsible for reduction in properties, e.g., crush strength, because the aluminum alloy is unaffected by humidity and this temperature range.

Recently, the adhesive bonds of Hexcel and Alcore honeycombs were involved in an aging study by Reedy [2003, 6]. The adhesive used in Alcore honeycomb is like FM1000 filled with nylon and a glass transition temperature of Tg ~ 45°C (113°F); the Hexcel adhesive appears to be unfilled epoxy Tg ~ 60°C (140°F), but the precise material is unknown. The results show that the node-bond adhesive of Alcore honeycomb can absorb a relatively large amount of moisture, altering Tg and mechanical properties (reversible with drying). The Hexcel adhesive seems relatively insensitive to moisture.

These findings present a need to assess the susceptibility of the honeycomb's aluminum-epoxy bond to moisture to determine the performance degradation of honeycomb in a humid environment. Experiments to evaluate the effect of humidity on the performance of honeycomb are described in the following sections. The focus is on the crush strength in the T direction of Alcore35 honeycomb. Based on how the specimen is prepared, the experiments are grouped into two sets.

9.1 Honeycomb Soaked in Water

Samples were machined from the same Alcore35 block that was the source of all previous Alcore35 specimens. Each specimen was measured and weighed right after machining. As shown in Figure 9-1, the nominal dimension of the specimen was 1.2 in. × 1.2 in. × 1.8 in. (T), with a rotated LW plane to avoid potential jamming between push rod and the confining wall. Half of these specimens, randomly selected, were then stored in sealed plastic bags as dry specimens. The other half were wet specimens. Each wet specimen was placed in a container filled with water. The period of treatment was set at 80 days to make sure water permeated the adhesive bond. Dry and wet specimens were always at room temperature (~ 70°F).

Specimens were removed from the bags and containers a few hours before testing. Wet specimens were blown dry by air and weighed again. The drying process would dry the aluminum surface, but not the adhesive, since that moisture migration would take a long time. In average, a wet specimen had gained 0.3 g. The tests were all confined compressions at intermediate rate and ambient conditions, listed in Table 9-1.

Experimental results of dry and wet specimens are plotted in Figure 9-2(a) and (b), respectively, and the values of crush strength are also listed in Table 9-1. Weighing the wet results against dry, the crush strength of wet specimens is 12 percent lower.

Figure 9-1. Representative specimens for the humidity effect experiment showing a dry specimen stored in bag and a wet specimen soaked in water.

Table 9-1. Test matrix of the first set of humidity experiments.

Specimen		W_1, in	W_2, in	H, in	m(1), g	pcf	m(2), g	Δm, g	%	σ_c, ksi
HA1	Dry	1.215	1.203	1.798	24.379	35.34				6.73
HA2		1.217	1.190	1.786	24.106	35.50				6.75
HA3		1.213	1.201	1.805	24.604	35.64				7.15
HA4		1.218	1.201	1.769	23.972	35.29				6.42
HA5		1.218	1.201	1.785	24.406	35.61				6.80
HA6		1.217	1.203	1.762	23.921	35.33				6.53
Average										6.73
HB1	Wet	1.212	1.197	1.801	24.382	35.55	24.745	0.363	1.49%	6.00
HB2		1.219	1.201	1.792	24.308	35.30	24.583	0.275	1.13%	5.86
HB3		1.216	1.205	1.789	24.395	35.45	24.724	0.329	1.35%	6.01
HB4		1.214	1.205	1.808	24.577	35.40	24.969	0.392	1.60%	5.82
HB5		1.218	1.205	1.814	24.910	35.64	25.185	0.275	1.10%	6.13
HB6		1.210	1.199	1.817	24.573	35.51	24.774	0.200	0.82%	5.86
Average										5.95

m(1) is the mass of a specimen after machining.
m(2) is the mass of a specimen just before test.
$\Delta m = m(2) - m(1)$

The average crush strength is 6.73 ksi for this set of dry specimens. The value appears to be quite high compared to the qualification result 5.74 ksi listed in Table 7-1. The qualification experiments were conducted more than four years before the humidity experiment. It is also possible that the difference is because the qualification specimens and humidity specimens were cut from very different part of the honeycomb block. The degradation in crush strength due to humidity, however, is apparent, since all material and testing parameters of the specimens in the experiment are exactly the same except humidity.

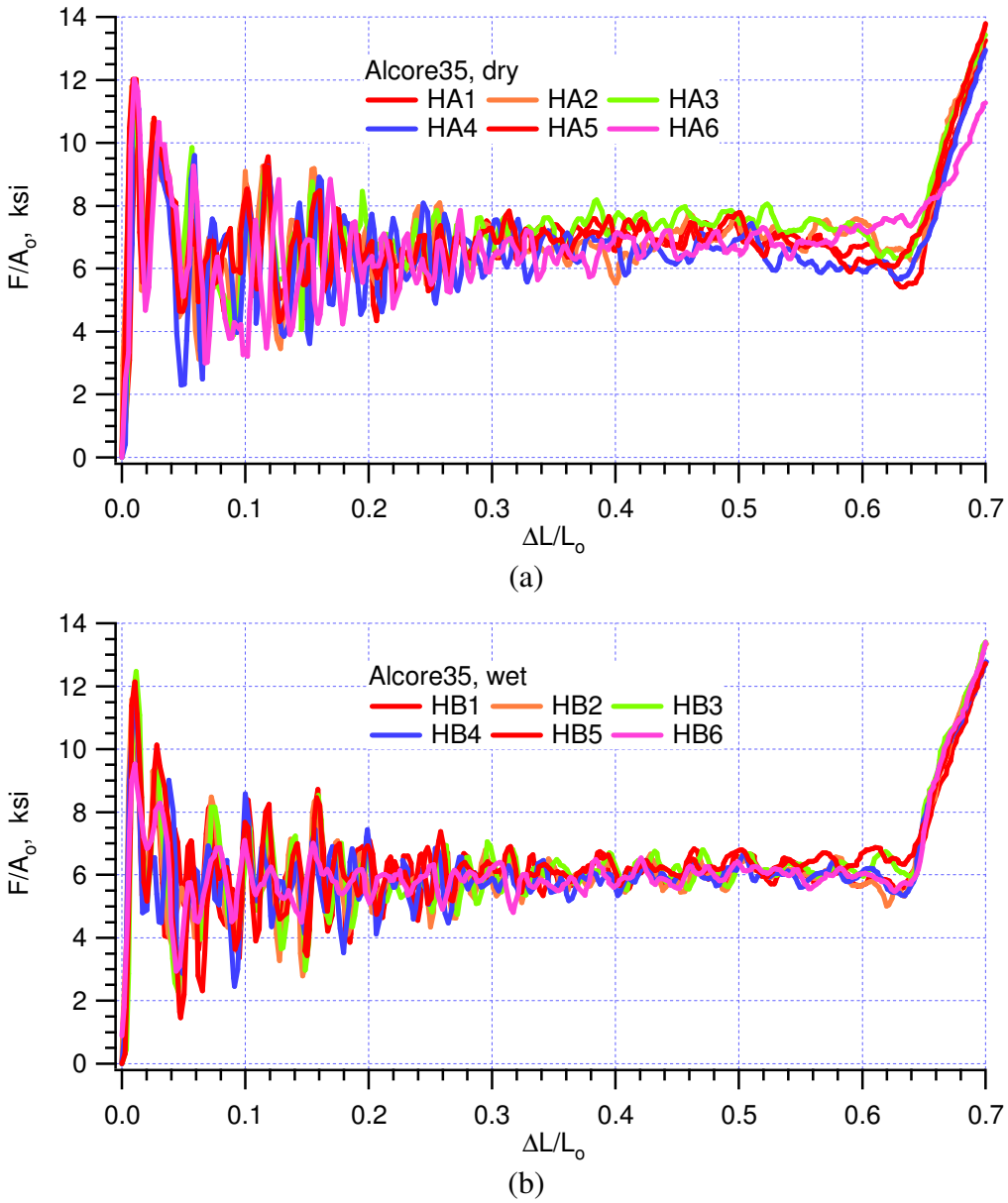

Figure 9-2. Normalized load-displacement curves of Alcore35 (a) dry and (b) wet specimens under intermediate rate confined compression at ambient temperature.

9.2 Honeycomb at 70°C and 100 Percent Relative Humidity

The humidity effect was demonstrated. It also generated two follow-up issues: (1) would honeycomb be further degraded under the condition of high temperature and 100 percent relative humidity (RH) than simply soak in room temperature water, and (2) what is the combined effect of high temperature and high humidity?

A second set of experiments was designed and conducted to investigate these concerns. In Table 9-2, all specimens were cut from the same Alcore35 block and all tests were the standard

intermediate rate confined compression. There were three parameters involved. The first was the conditioning time $\Delta t_{70C,\ 100\%RH}$, i.e., how long the specimen had been conditioned. Three values were considered; approximately 0, 10, and 100 days. The 0-day specimen was never exposed to a high temperature or high humidity environment. The 100-day specimen was assumed to be the worst case, in that the adhesive bond was saturated with humidity. The second parameter was the testing temperature T_{test}. The conditioned specimens were tested at either ambient temperature or 165°F. The third parameter was the drying time Δt_{drying}, which was the time period between when a specimen was removed from the conditioning tank and it being tested. Most were tested within two hours.

Table 9-2. Test matrix for the second set of humidity experiments.

	W_1	W_2	Height	Mass	Density	70°C, 100%	Drying	T_{test}	σ_{crush}
Specimen	in.	in.	in.	g	pcf	hour	hour	°F	ksi
HC_01	1.200	1.209	1.755	23.63	35.36	2,232	<2	70	5.41
HC_02	1.210	1.216	1.747	24.12	35.74	2,232	<2	70	5.73
HC_03	1.218	1.225	1.769	24.66	35.59	2,232	<2	70	5.87
HC_04	1.213	1.215	1.725	23.93	35.86	2,232	144	70	6.08
HC_06	1.212	1.218	1.750	24.05	35.46	2,232	264	70	5.49
HC_09	1.207	1.217	1.737	24.36	36.37	2,496	<2	165	4.91
HC_10	1.205	1.212	1.737	23.75	35.67	2,496	<2	165	4.79
HC_11	1.209	1.211	1.767	24.23	35.68	2,520	<2	70	5.38
HC_12	1.204	1.219	1.755	24.62	36.41	2,520	<2	70	5.37
HD_01	1.201	1.195	1.555	21.04	35.92	0	-	70	6.26
HD_02	1.198	1.201	1.541	20.60	35.39	0	-	70	6.20
HD_03	1.196	1.195	1.551	20.81	35.76	0	-	70	6.28
HD_04	1.195	1.196	1.551	21.08	36.23	240	<2	165	5.07
HD_05	1.194	1.201	1.531	20.77	36.04	240	<2	165	4.95
HD_06	1.200	1.185	1.553	20.90	36.05	264	<2	70	5.58
HD_07	1.184	1.195	1.559	20.94	36.16	0	-	70	6.24
HD_08	1.186	1.230	1.550	20.94	35.28	0	-	165	5.24

As shown in Figure 9-3, a sealed fish tank partially filled with water and a submerged temperature-controlled heater created a simple high-temperature, high-humidity environment. Honeycomb specimens and temperature/humidity sensors were above water.

As usual, the result of dry specimens, $\Delta t_{70C,\ 100\%RH} = 0$, tested at ambient temperature, T_{test} = 70°F, was the baseline for the second set of humidity experiment. Shown in Figure 9-4, the average crush strength of four dry specimens (Alcore35) is 6.35 ksi. The value is about 6 percent lower than the first set of humidity experiments, but is still 10 percent higher than the qualification result.

Figure 9-5 shows the result of the only dry specimen tested at 165°F. The crush strength is 5.24 ksi, which shows 17 percent reduction from tests at ambient conditions. Comparing the data of the same conditions in qualification test, the crush strength of Alcore35 tested at the high

temperature is 14 percent lower than that tested at ambient conditions. The percentage of changing crush strength due to the temperature is in the same order.

For those specimens with 100 days at 70°C and 100 percent RH tested at ambient conditions, the results are plotted in Figure 9-6 to 9-8. The conditioning time of these specimens is not exactly 100 days; there are actually two groups, 93 and 105 days. The drying time ranges from two hours to 11 days. Due to the number of these tests being limited, small variations in these parameters are not clearly apparent. The averaged crush strength of these specimens is 5.62 ksi, which corresponds to an 11 percent decline because of the high humidity/temperature conditioning. This is almost the same as the first set of humidity experiment (12 percent).

Figure 9-3. Honeycomb specimens at 70°C and 100 percent RH.

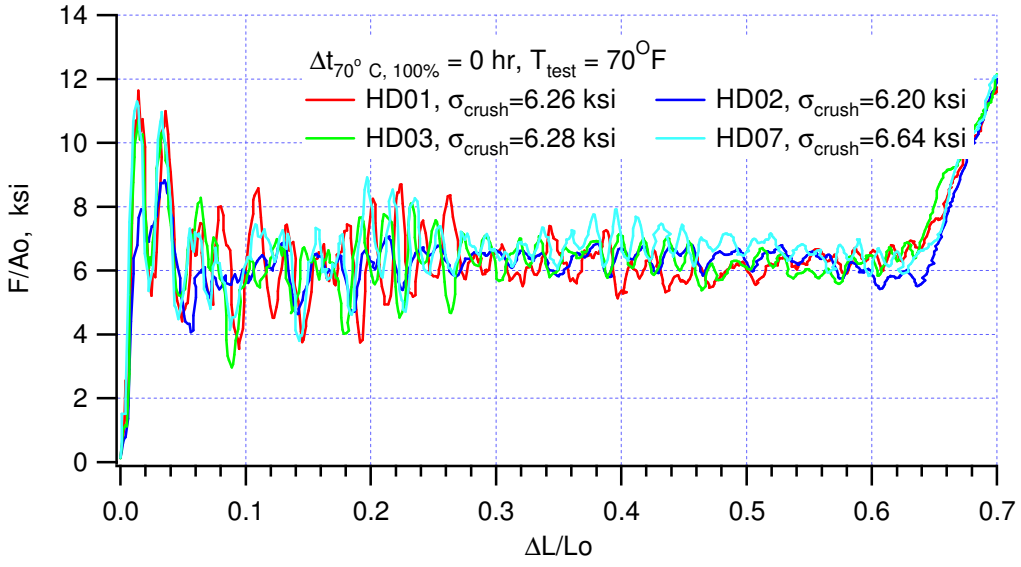

Figure 9-4. Normalized load-displacement curves for dry specimens of the second set of humidity experiment tested at ambient temperature.

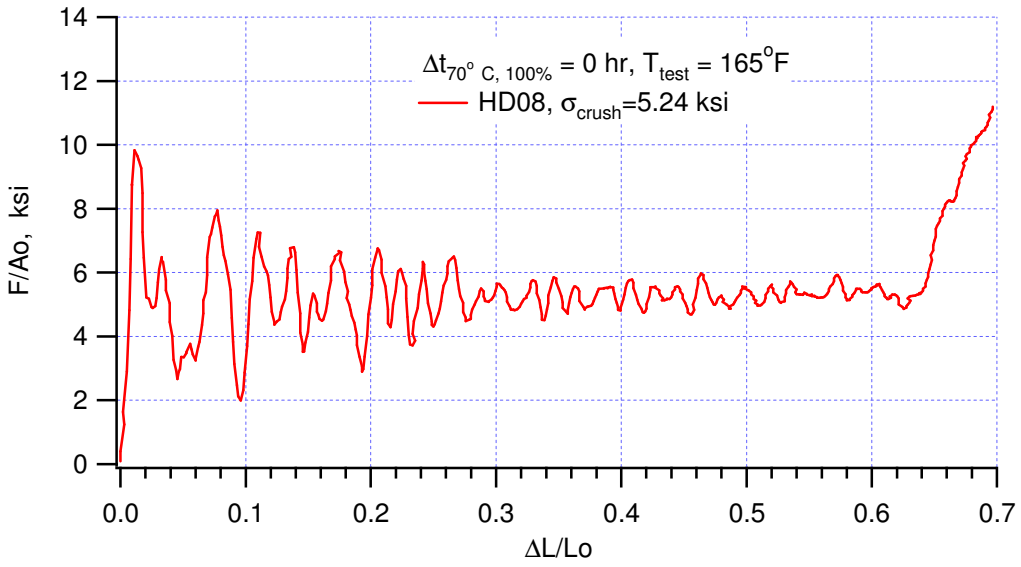

Figure 9-5. Normalized load-displacement curves for dry specimens of the second set of humidity experiment tested at 165°F.

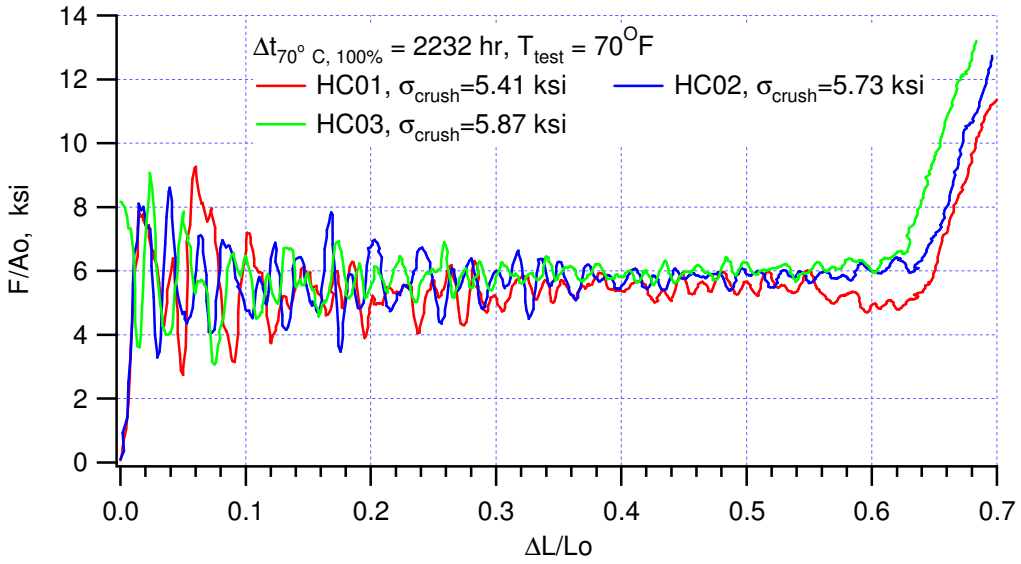

Figure 9-6. Normalized load-displacement curves of $\Delta t_{70C,\ 100\%RH}$ = 93 day specimens tested at ambient temperature.

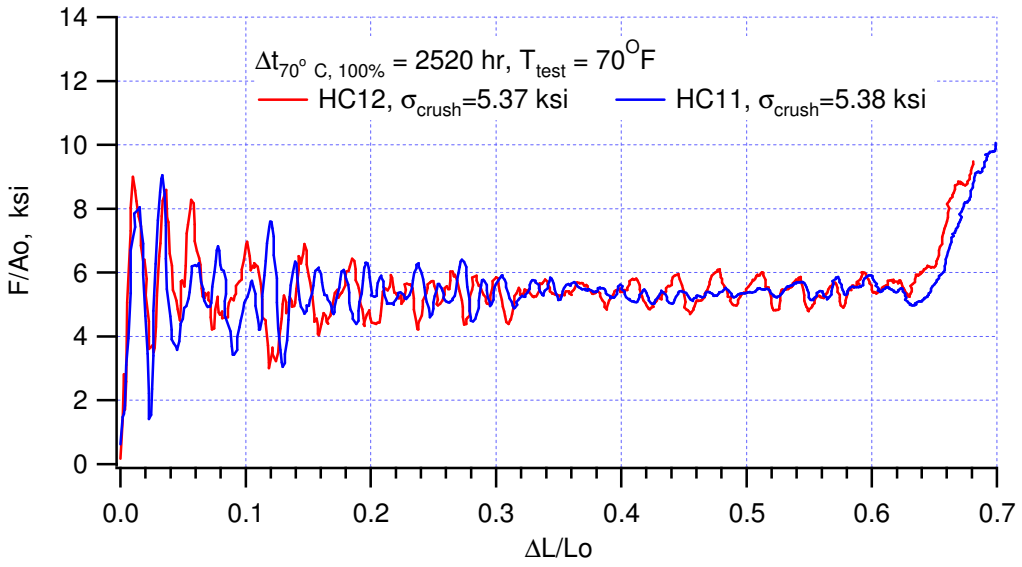

Figure 9-7. Normalized load-displacement curves of $\Delta t_{70C,\ 100\%RH}$ = 105 day specimens tested at ambient temperature.

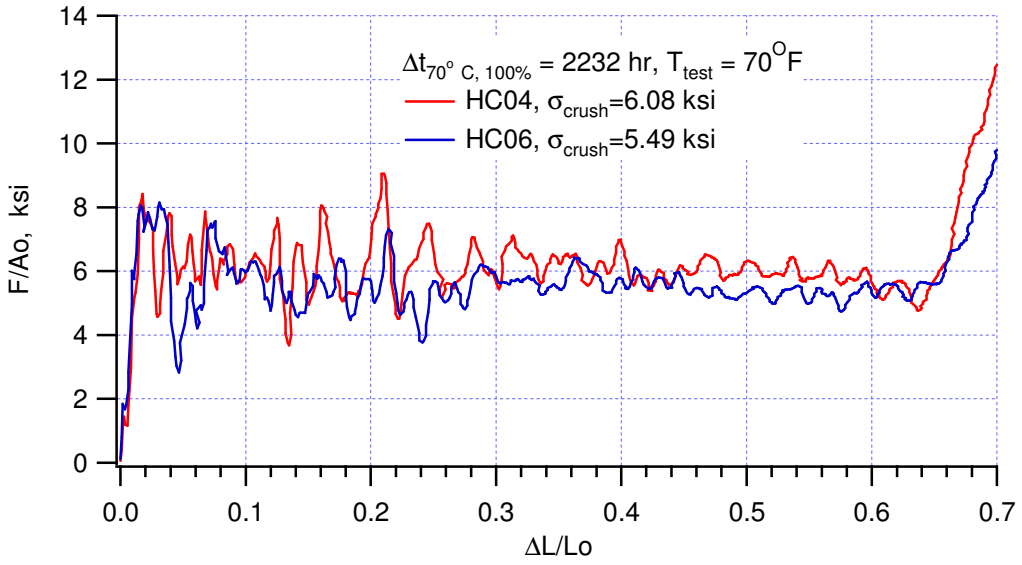

Figure 9-8. Normalized load-displacement curves of $\Delta t_{70C,\ 100\%RH}$ = 93 day specimens tested at ambient temperature. Specimen HC04 and HC06 were tested at 6 and 11 days respectively, after removal from the high temperature/humidity environment.

The combined high temperature and high humidity effect is shown in Figure 9-9. These two specimens had been conditioned at 70°C and 100 percent RH for 104 days and tested at 165°F. The averaged crush strength is 4.85 ksi, which is about 24 percent lower than the dry specimen at ambient temperature. According to the results discussed earlier, the individual effect of temperature and humidity are a 17 percent and 11 percent reduction in crush strength, respectively. The overall effect is almost a linear combination of individual effects.

Three specimens had a much short conditioning time: $\Delta t_{70C,\ 100\%RH}$ = 10 days. Two were tested at 165°F and one was tested at 70°C. The results, plotted in Figure 9-10, are comparable to those of 100-day specimens. The humidity effect is 12 percent, and the combined humidity/ temperature effect is 21 percent. This means that within 10 days the adhesive bond is already saturated with moisture.

The investigation of humidity effects was brief. In some case, only one or two tests were performed. Obviously, more tests are required to confirm the results and quantify the effects more precisely.

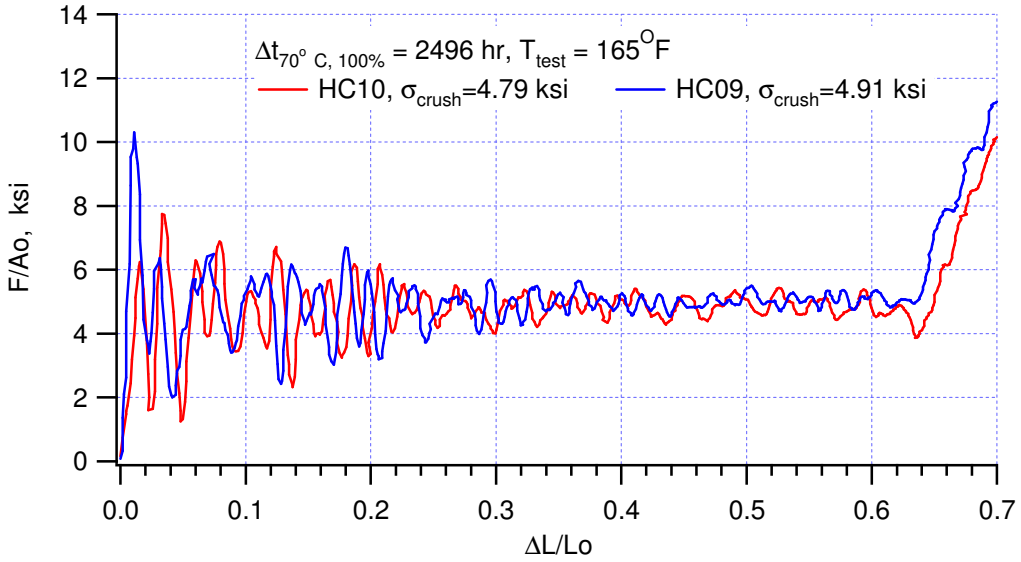

Figure 9-9. Normalized load-displacement curves of $\Delta t_{70C,\ 100\%RH}$ = 104 day specimens tested at 165°F.

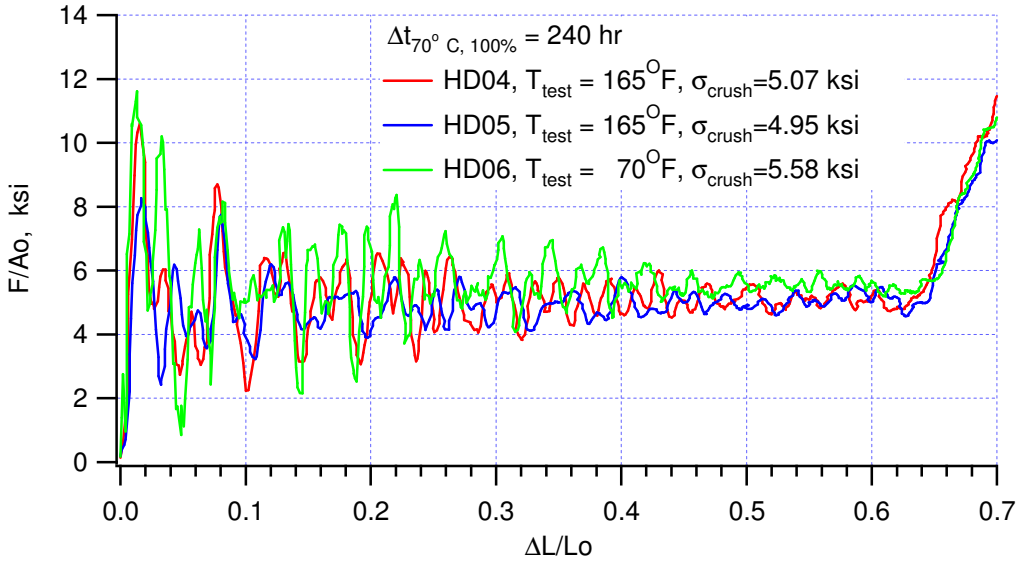

Figure 9-10. Normalized load-displacement curves of $\Delta t_{70C,\ 100\%RH}$ = 10 day specimens.

10. FOAM-FILLED HONEYCOMB

Experiments were conducted to study the crush behavior of foam-filled honeycomb. The specimens were obtained from a returned component. The cone-shape component was first cut open diametrically, as shown in

Figure 10-1. From top to bottom, the cone was further sliced into four sections. Section I and II were unfilled honeycomb, but Sections III and IV were foam-filled honeycomb. Section I was partially crushed as received, but all other sections appeared to be intact. Unfilled honeycomb specimens and foam-filled honeycomb specimens were machined from Section II and III, respectively (displayed in Figure 10-2). The test matrix is listed in Table 10-1. All tests were confined compression on three principal material axes, the T, L, and W directions. Two loading rates, quasi-static (approximately 10^{-2} in/s) and intermediate (about 2×10^{2} in./s), were included.

Sensitive photos removed for publication.

Figure 10-1. A component contains honeycomb (I and II) and foam-filled honeycomb (III and IV).

The pedigree of the honeycomb and foam was unavailable. Some material parameters were determined from the measurement of these specimens. For the unfilled honeycomb, the density was 17.8 pcf, the hexagon cell size was 3/16 in., and the aluminum sheet thickness was 0.006 in. A commercial honeycomb, Hexcel 3/16-5052-.006, had the same structural features, but a lower density (15.7 pcf). Assuming the honeycomb was the same for the unfilled and filled, it could be calculated that the foam occupied about 89 percent of the volume of the foam-honeycomb composite. The composite had a density of 25.24 pcf, so the density of the foam was estimated to be 8.3 pcf. From the micrograph (Figure 10-3), the foam was closed-cell and the cell size was about 200 μm.

Normalized load-displacement curves of quasi-static compressions in the T, L, and W direction of these unfilled and foam-filled honeycombs are plotted in Figures 10-4 and 10-5. Calculated crush strengths are listed in Table 10-1. For the foam-filled honeycomb, the crush strength in T direction improves about 20 percent. The foam has a significant enhancement in the L and W direction; the crush strength becomes five times stronger. Even the crush efficiency is reduced, but the energy absorption rate is higher.

Notice that, ideally, the honeycombs have transversely isotropic symmetry. The responses should be very close. For the foam-filled honeycomb, the difference is within 10 percent; the unfilled is greater than 10 percent. Shown in Figure 10-2, the cell geometry of the unfilled specimens was not a perfect hexagon. The unfilled might have been pre-deformed. This could be the reason for the larger difference between the crush strength of the L and W directions.

Table 10-1. Test matrix of foam-filled honeycomb.

Specimen			W(1)	W(2)	H	ρ	Rate	σ_c
#	Type	Dir	in	in	in	pcf	in/s	ksi
A1	unfilled	T	1.200	1.210	1.220	17.66	8.00E-03	1.96
A2		T	1.200	1.210	1.220	18.00	1.70E+02	2.27
A3		T	1.195	1.215	1.235	17.80	1.70E+02	2.30
A4		T	1.200	1.210	1.220	18.07	1.70E+02	2.26
A5		L	1.200	1.210	1.220	17.93	8.00E-03	0.09
A6		W	1.190	1.230	1.270	17.52	8.00E-03	0.07
B1	filled	T	1.200	1.210	1.220	24.80	8.00E-03	2.41
B2		T	1.195	1.215	1.235	24.89	1.70E+02	3.29
B3		T	1.200	1.215	1.230	24.84	1.70E+02	3.09
B4		T	1.195	1.205	1.215	25.07	1.70E+02	2.98
B5		L	1.215	1.215	1.215	26.16	8.00E-03	0.40
B6		W	1.200	1.215	1.230	25.66	8.00E-03	0.37
Hexcel 3/16-5052-.006		T				15.70		2.40

The intermediate rate results are displayed in Figures 10-6 and 10-7. The quasi-static curve is plotted for comparison. A stronger rate effect is observed in foam-filled honeycomb than the unfilled, a 29 percent increase versus 16 percent.

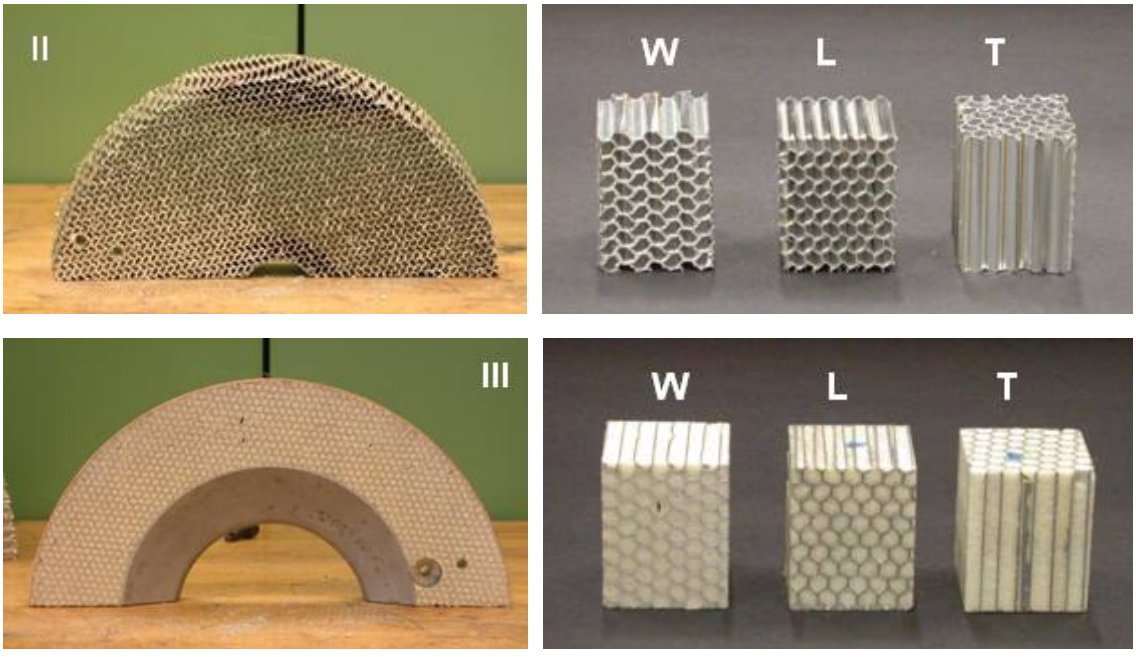

Figure 10-2. Honeycomb specimens machined from the parts shown on the left.

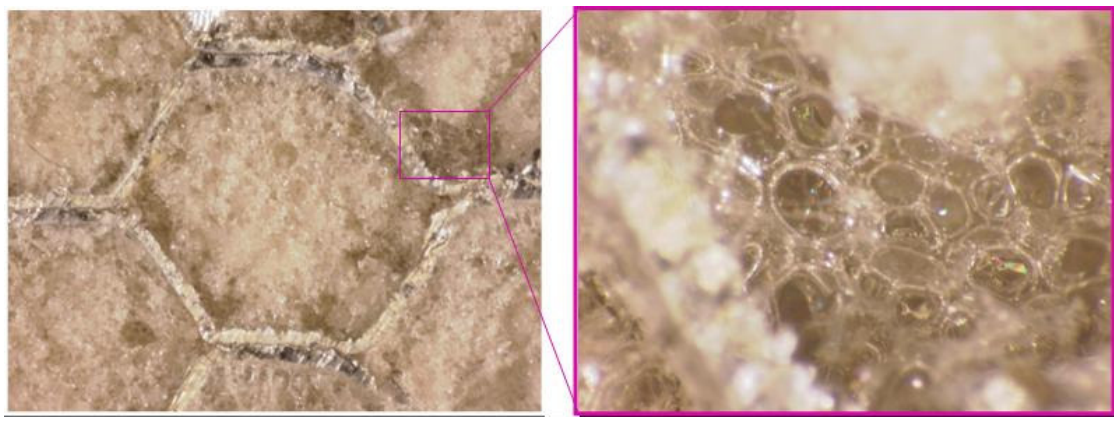

Figure 10-3. Micrographs showing foam-filled honeycomb.

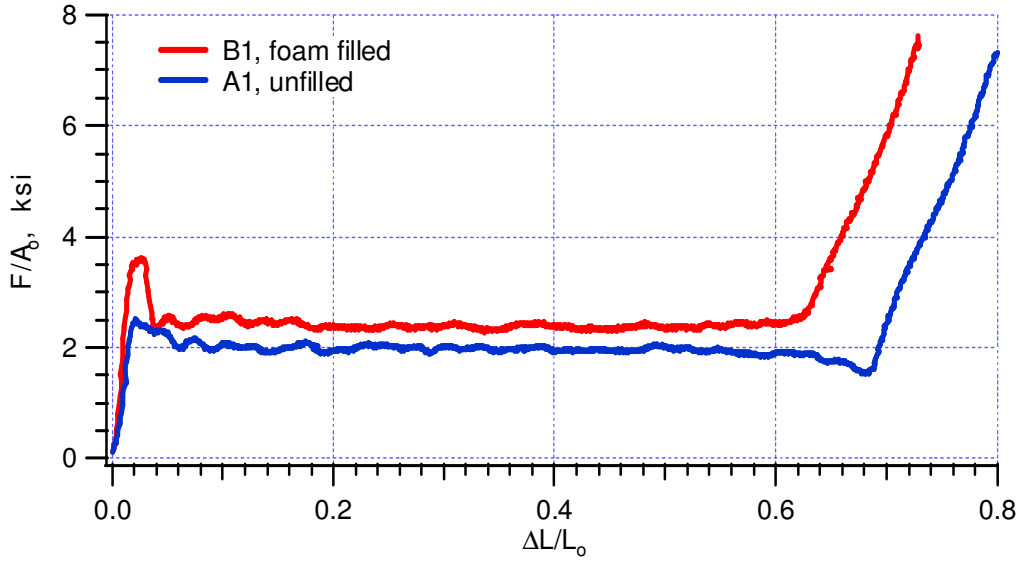

Figure 10-4. Normalized load-displacement curves of confined quasi-static compressions of unfilled and foam filled honeycombs in the T direction at ambient temperature.

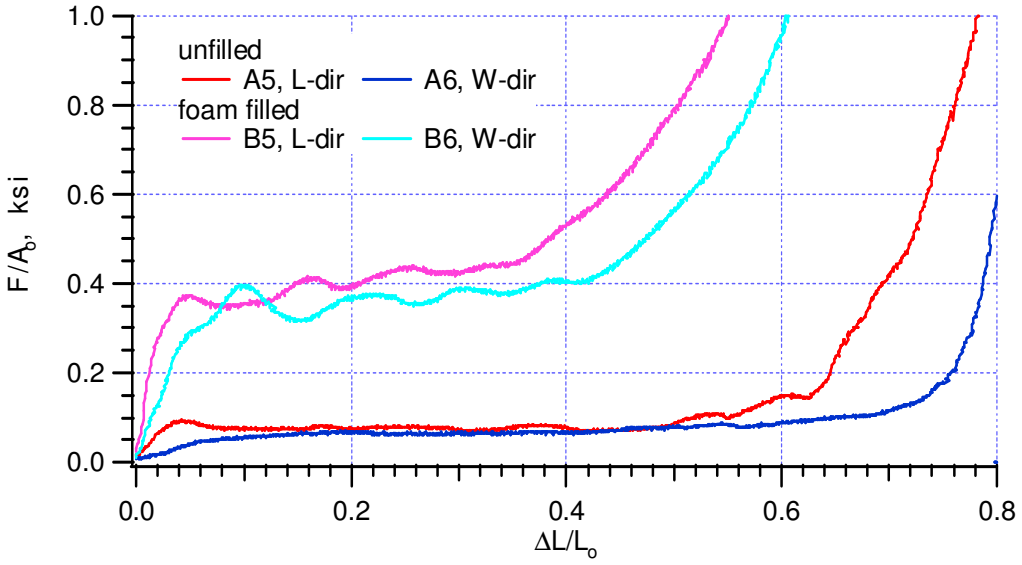

Figure 10-5. Normalized load-displacement curves of confined quasi-static compressions of unfilled and foam-filled honeycombs in the L and W direction at ambient temperature.

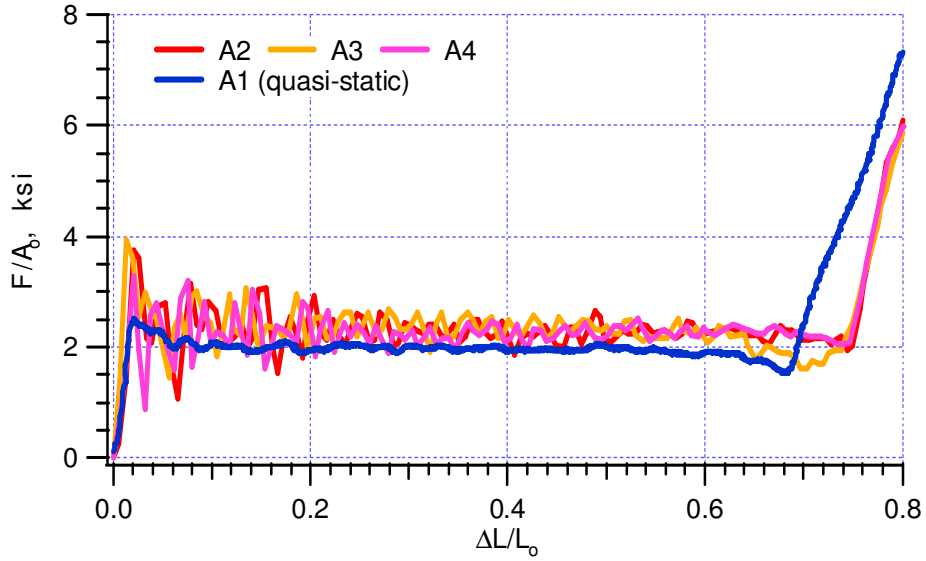

Figure 10-6. Normalized load-displacement curves for confined compressions of unfilled honeycombs in the T direction at intermediate rate and ambient temperature.

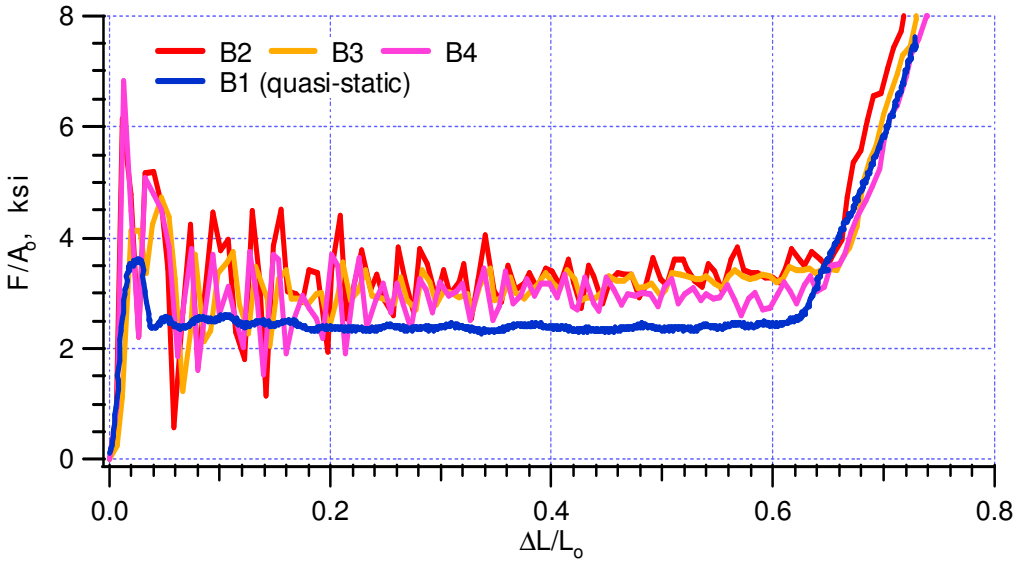

Figure 10-7. Normalized load-displacement curves for confined compressions of foam-filled honeycombs in the T direction at intermediate rate and ambient temperature.

This page intentionally left blank.

11. SUMMARY AND CONCLUDING REMARKS

11.1 General

The crush behaviors of high-density aluminum honeycomb are complex. Depending on the specimen size, aspect ratio, and loading conditions, the honeycomb could crush in normal (local plastic buckling) or abnormal (global buckling/splitting) mode.

The normal crush mode yields the upper bound values of crush strength and energy absorption capacity of honeycomb. These properties are significantly degraded when crushed in abnormal mode.

The material properties provided by vendors are based on the normal crush mode.

The orthotropic crush model of honeycomb describes normal crush mode only. The model does not have the capability to predict the transition from the normal to abnormal crush mode.

11.2 Test Methods

Standard honeycomb test methods do not always yield consistent data within the range of application conditions of interest, which includes parameters such as density, size, aspect ratio, temperature, loading rate, etc.

Using the confined compression technique developed in this study, it has been demonstrated that the experimental results are consistent with the standard method; in addition, honeycomb specimens are always crushed in the normal mode. Confined compression has become a regular test for many characterization and validation experiments.

Biaxial compression of high-density aluminum honeycomb was developed based on an in-plane biaxial system. Uniaxial and biaxial experiments were performed successfully on the system.

Biaxial loading paths were designed to study the stress coupling effects. The results clearly show that the engineering stress definition should be used in describing the orthotropic crush model and the stress coupling effect should be included. Biaxial compression has also become a regular test for characterization and validation experiments.

11.3 Honeycomb Qualification

Four batches of high-density aluminum honeycomb, Hexcel38, Hexcel35, Alcore38, and Alcore35, were included in a series of qualification tests.

The crush strength of honeycomb will increase due to dynamic loading. For example the intermediate rate 13.5 ft./s enhanced the crush strength for the T direction of Alcore38 by ~10 percent.

Higher temperature results in lower crush strength. At 165°F, the crush strength for the T direction of Alcore38 degrades ~14 percent from the room temperature.

Off-axis compression provides data to estimate the shear crush parameter for the model.

A significant statistical database for ambient/hot/cold crush behavior of four batches of honeycomb has been developed.

11.4 Effect of Humidity and Others

Humidity will affect the performance of honeycomb. When the adhesive bond is saturated with moisture, the crush strength degrades ~12 percent for Alcore35.

High humidity at high temperature will further degrade the crush strength of honeycomb. The overall effect is almost a linear combination of individual effects.

A foam-filled honeycomb was tested. The densities of the honeycomb and foam were estimated to be 17.8 and 8.3 pcf, respectively.

For the foam-filled honeycomb, the crush strength in the T direction improves about 20 percent. The foam has a significant enhancement in the L and W direction; the crush strength becomes five times stronger.

11.5 Areas for Future Studies

Perform shear-compression experiments, shown schematically in Figure 11-1. The shear-compression data will provide a clear function of how crush and shear strengths vary with combined shear and volumetric crush strains.

Investigate and establish the criterion for normal mode to abnormal mode transition.

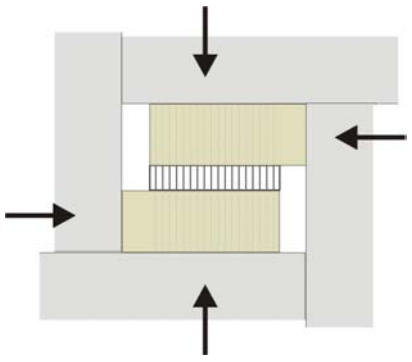

Figure 11-1. Schematics of a shear-compression experiment.

12. REFERENCES

[1] Whirley, R.G., Engelman, B.E., and Hallquist, J.O. 1991. "DYNA3D Users Manual," Lawrence Livermore Laboratory, Livermore, CA.

[2] Hinnerichs, T.D. 2001. *Validation Plan for the B61-3/4/7/10 Radar Nose Assembly Crush Model*, SAND2001-0817. Sandia National Laboratories, Albuquerque, NM.

[3] Lu, W-Y and Hinnerichs, T.D. 2001. "Crush Of High Density Aluminum Honeycombs" (IMECE2001/AMD-25453) *Proceedings of 2001 ASME International Mechanical Engineering Congress and Exposition*, November 11-16, 2001, NY, NY.

[4] Bitzer, T. 1997. *Honeycomb Technology*, Chapman & Hall, London, UK.

[5] Lu, W-Y, Korellis, J. and Hinnerichs, T.D. 2003. "Shear Deformation of High Density Aluminum Honeycombs," (IMCHE2003-44092) *Proceedings of 2003 ASME International Mechanical Engineering Congress and Exposition*, November 15-21, 2003, Washington, DC.

[6] Reedy, D., Stavig, M. and Neilsen, M., 2003, "Adhesive Bond Degradation in Aluminum Honeycomb," Enhanced Surveillance Campaign presentation.

This page intentionally left blank.

APPENDIX I:

"Crush Of High Density Aluminum Honeycombs" (IMECE2001/AMD-25453) Proceedings of 2001 ASME International Mechanical Engineering Congress and Exposition, November 11-16, 2001, NY, NY.

CRUSH OF HIGH DENSITY ALUMINUM HONEYCOMBS

Wei-Yang Lu
Sandia National Laboratories, MS9042
Livermore, CA 94551-0969

Terry Hinnerichs
Sandia National Laboratories, MS0847
Albuquerque, NM 87123

ABSTRACT

The orthotropic crush model has commonly been used to describe the stress-strain behavior of honeycomb. Important model parameters include crush strength and crush efficiency of each principal direction. Experiments were conducted to obtain these model parameters of high-density honeycombs. Various deformation modes were observed during "bare" compression tests. The normal crush mode of honeycomb is progressive plastic buckling. Low energy absorption (or abnormal) modes include transverse splitting and global buckling. To obtain a consistent normal mode of deformation under wide testing conditions, a confined compression test was developed. A series of confined compressions on T-, L-, and W-directions were performed to get crush parameters for the orthotropic crush model. The temperature dependence and loading rate effects on crush parameters were also obtained.

INTRODUCTION

Honeycomb is an efficient energy absorbent material with limited force transmission, which has been widely used as a protective substance for impact loading. In some applications, the weight and the volume of the honeycomb are constrained. Computational analysis is often required to determine the optimal design and to evaluate the performance of such a structure. Validated constitutive models are needed for numerical simulation. The orthotropic crush model [1] has commonly been used to describe the stress-strain behavior of honeycomb.

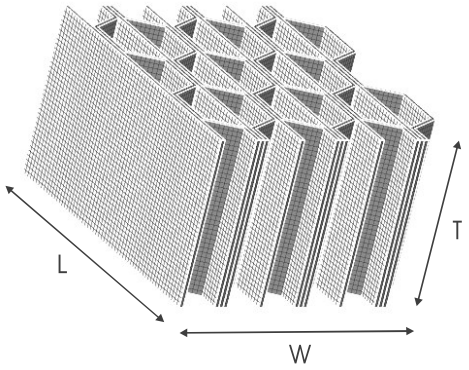

Figure 1. Aluminum honeycomb geometry and principal directions.

Aluminum honeycomb has three principal directions due to its composure of corrugated and flat aluminum sheets. These directions T, the strongest, L, the intermediate strength, and W, the weakest are shown schematically in Figure 1.

The Orthotropic Crush constitutive algorithm [1] in PRONTO3D [2] is an available model to simulate the orthotropic deformation and crush of the aluminum honeycomb. This algorithm is composed of three zones of constitutive behavior as shown in Figure 2. Zone 1

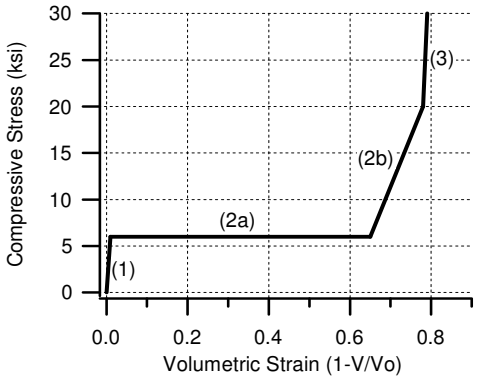

Figure 2. Three zones of orthotropic crush model behavior.

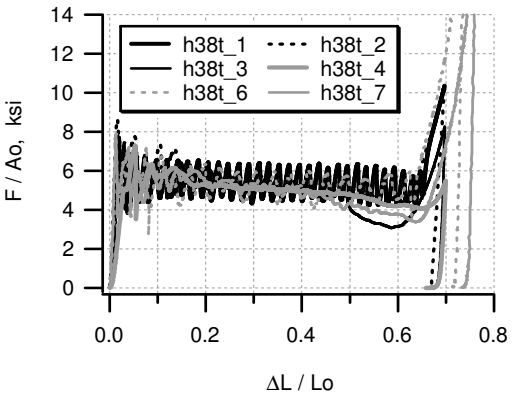

Figure 3. Normalized load-displacement curves of Hexcel 38 pcf compressed in T-direction.

represents an initial linear elastic loading phase. Zone 2 contains all the permanent volumetric crush displayed by the model and begins when the applied stress, in any direction, exceeds the crush strength which must be defined as a function of volumetric strain in each direction. Zone 2a is a typical constant crush value versus volumetric strain region and zone 2b represents a hardening portion of the curve prior to the "Full Compaction" that initiates Zone 3. The theoretical "Full Compaction" volumetric strain for 38 pcf is 0.78. The Zone 3 constitutive model is an isotropic and incompressible elastic-perfectly plastic constitutive model. These three zones of the Orthotropic Crush model provide the flexibility and modeling power to handle large amounts of effectively uncoupled uniaxial strain behavior. The Orthotropic Crush model, however, does not include temperature effects and loading effects of honeycomb.

Almost all energy absorption is done in the crush Zone 2. Three model parameters are required to describe Zone 2 in each direction: crush strength and crush efficiency in Zone 2a and hardening modulus in Zone 2b. Crush efficiency is defined as the volumetric strain that initiates the hardening portion of Zone 2b. In large deformation analyses of structures that involve honeycomb components, the force and displacement results depend strongly on Zone 2 parameters.

This paper describes axial crush experiments to characterize model parameters of high-density aluminum honeycombs, nominal 38 pcf (pound per cubic foot), under various loading speeds and temperatures. Honeycomb materials manufactured by Hexcel (CR-8-LC-1/8-5052-006-R2, etc. [3]) and Alcore (HIGRID DURA-CORE [4]) were used in this study. They are all hexagonal core honeycombs with a cell size of 1/8", made of 5052 aluminum alloy and foil thickness of 0.006". There is a flat aluminum foil between corrugated aluminum ribbons in 38 pcf honeycomb, Figure 1.

QUASI-STATIC COMPRESSION EXPERIMENTS

Compression tests were performed along the principle material directions, that is the T-, W-, and L-directions of hexagonal core materials. Most tests were conducted under the "bare" condition, where cell edges of a compressive specimen were not stabilized [5]. ("Stabilized" specimen has plates bonded on each loading face.) In general, bare tests are faster and easier to perform, and result in slightly conservative properties; moreover, there are "bare" boundary conditions in particular applications of interest.

The standard specimen size suggested by Hexcel is 3"x3"x0.625", or 2"x2"x0.625" by Alcore. However, almost all specimens tested here had larger height to cross section area ratios because they were close to real parts used in applications.

Depending on the maximum compressive force required, three testing systems were used. They were MTS AT, 220K, and 2M systems with capacities of 100 kilo-pounds (kips), 200 kips, and 2 million pounds, respectively. Specimens were placed between steel platens and no special fixture was used initially. The AT system use TestStar for loading control and data acquisition. Systems 220K, 2M and High Rate use MTS448.85 controller for test control and Nicolet 440 for data acquisition. The deformation of honeycomb was measured by the stroke of the loading system. The data acquisition rate was at least 10 Hz. The loading rate was about 10^{-3} in/s.

Compression in T-Direction

Figure 3 shows the compression results of CR-8-LC-1/8-5-52-0.006-R2 (Hexcel 38 pcf). The load-displacement curves are normalized with respect to the cross-sectional area and initial height of the specimen, which may be considered as "stress-strain" curves. All these curves show the three-stage deformation described by the orthotropic crush model, but there are deviations from the model.

When examining the experimental results more closely, the crushing behavior differed from one specimen to another. For specimen h38t_1 and h38t_6, group 1, the stress oscillated with a fairly constant amplitude through the whole crush region, and the mean stress decreased slightly before lock-up. For the other four specimens, the amplitude of stress oscillation decreased rapidly in the crush region. The oscillation was almost negligible for crush strain greater than 20%. The mean stress decreased much faster when the strain was greater than 40%.

It is well known and we have observed repeatedly from experiments that honeycomb specimen does not deform homogeneously during crush. The constitutive aluminum sheets (or ribbons) buckle locally, which create many plastic hinges. The buckling front propagates through a specimen as the displacement increases. The crush of honeycomb in the t-direction is actually a series of instability (local buckling) events. If the buckling is synchronized, the load will repeatedly increase and decrease as the buckling front advances, and an orderly crushed pattern is formed. A local buckling event starts when load is a relative maximum.

The major difference between the stress-strain curves of specimen h38t_1 and h38t_6 is the oscillation period of crush. These two specimens were conducted on different systems, AT and 220K, respectively. Lateral motions of the actuator were noticed for the 220K system but not the AT system. This suggests that the buckling period of honeycomb is dependent on the lateral stiffness of a testing system. More experiments are required to verify this postulation. Fortunately, the buckling period does not appear to affect the crush strength or the energy absorption of honeycomb.

Post-experiment specimens are shown in Figure 4. The picture shows the crushed t-w plane of specimens. Specimen h38t_1 and h38t_6 were almost ideal crushes as described in the last paragraph. An orderly pattern of deformation is displayed; only a limited number of aluminum sheets on both edges of the specimen exhibit delaminating and global buckling. As those edge-layers gradually detached from the specimen and bent globally, the mean stress decreased because fewer ribbons were supporting the load.

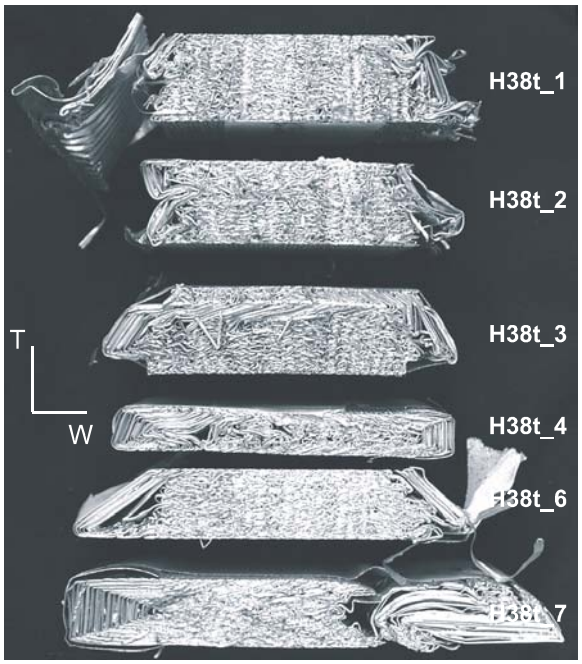

Figure 4. Hexcel 38 post-experiment specimens, compressed in T-direction.

Specimen h38_t2 was crushed nicely in the beginning. As crush progressed, some aluminum sheets wrinkled, rolled, distorted, and did not form the orderly crushed pattern. The synchronization of local buckling soon disappeared, and crushing stress did not oscillate, none the less the specimen remained near normal energy absorption capability throughout the crush region.

The crush of other three specimens was more complicated. In the early stage of crush, delaminating or splitting was observed, which divided a specimen into several pieces with a smaller w-dimension. Some outside pieces started to lose their alignment. When strain was greater than 40%, either the edge layers fell off or the uncrushed part of a specimen buckled globally with only one or two plastic hinges. At this time, the energy absorption capability of the specimen was degraded considerably, which corresponded to the decrease of mean stress before lock-up. The orthotropic crush model does not describe and can not predict such low energy absorption modes.

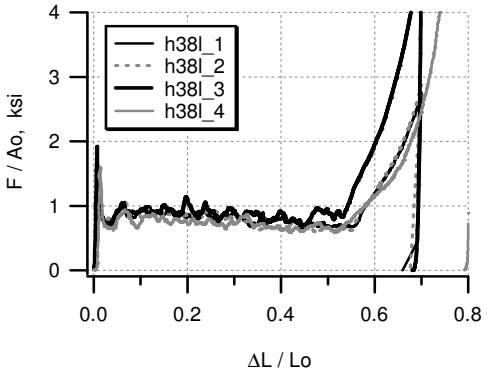

Figure 5. Stress-strain curves of Hexcel 38 compressed in L-direction.

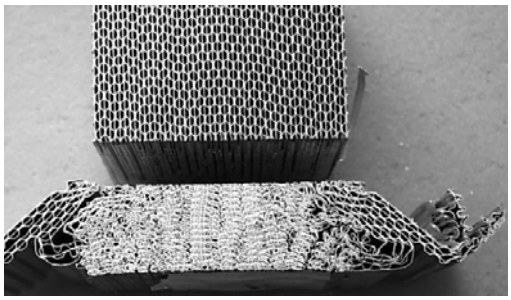

Figure 6. Post-experiment specimen h38l_1, on the top is an undeformed sample.

End caps were used in h38t_3 to constrain the edge displacement and prevent delaminating, which could be considered as "semi-stabilized. It worked fine, but the lateral force generated during local buckling pushed one end of the specimen out of alignment and the specimen did not end with a good crush pattern.

The variation in these stress-strain curves may also be caused by some parameters that we have not accounted for. One is the dimensional accuracy of specimens. The initial imperfection has a significant influence on stability related deformations, which causes misalignment and leads to different deformation modes. The other possible parameter is the bonding between ribbons. The consistency and quality of the bond from the manufacturing process and damages from specimen preparation may contribute to the variations among specimens and, subsequently, their deformations. Both initial imperfection and bonding quality are difficult to measure.

Compression In L-Direction

Figure 5 shows the results of four compression tests. Peak stress was 1.7±0.2 ksi. Crush stress fluctuated between 0.6 to 1.0 ksi. Lock-up started at 53±2 % strain. Figure 6 shows the l-w plane of a typical l-compressed specimen. Similar to compression in t-direction, the deformation was not homogeneous during crush and it was a series of instability processes. Delaminating occurred in every specimen. During crush, the mean stress decreased gradually because edge layers did not deform in the local buckling mode like the central layers. The only exception was h38l_3, where end caps were applied. The mean stress did not decline because end caps limited delaminating. In this test, the end cap was not pushed out of alignment.

Compression in w-direction

The results are shown in Figure 7. There was no peak stress before crush. Crush stress started at 0.5 ksi and increased slightly. The transition from Zone 2a to 2b was gradual and did not have a distinctive change of slope as observed in t- and l-compressions. Also, unlike compressions in t- and l-direction, the deformation could be considered as homogeneous. There was only one consistent deformation mode, which was bending and folding of free walls. The reinforcing flat aluminum sheets confined the motion of corrugated sheets. No delamination was observed.

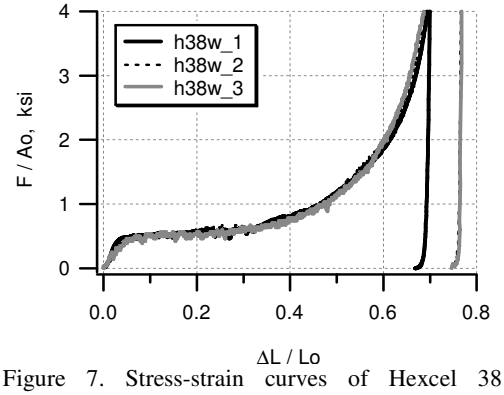

Figure 7. Stress-strain curves of Hexcel 38 compressed in W-direction.

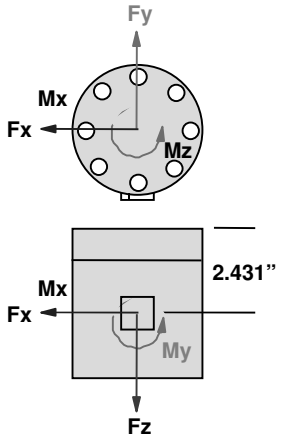

Figure 8. A schematic drawing of a six-component lad cell.

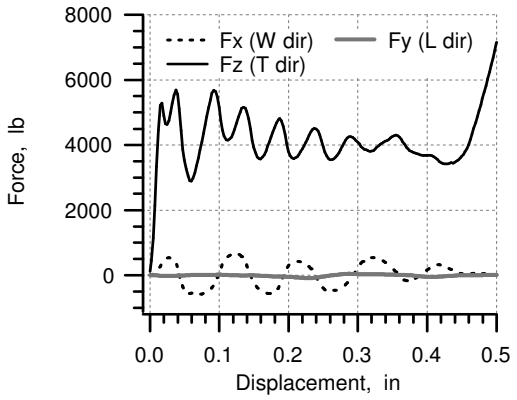

Figure 9. Three components of force versus displacement during compression in the T-direction.

Lateral Force During Compression

It is evident that the force generated during the compression in T-direction has both axial and transverse components. To quantify all force components, a six-component load cell was mounted in series with the existing axial-torsional load cell on the AT system. As shown in Figure 8, the six-component load cell is capable of measuring all force and moment components, while the AT load cell measures Fz and Mz only. Two small size specimens of Hexcel 38, about 0.9”x0.9”x0.7”, were used in the tests to fit the capacity of the six-component load cell, 20 kips in the z-direction. The specimen was placed in the center of the load cell, and the W-, L- and T-directions of honeycomb were aligned with the x-, y- and z-axes of the load cell, respectively. Figure 9 shows the results of a typical experiment. All three components of forces are plotted against the displacement. The Fz component corresponds to the crush force in the T-direction. During constant crush, Zone 2a, the load oscillates with a mean value of 4,500 lb. The lateral force in the W-direction, Fx, cycles between ±600 lb with a period about twice of the Fz component; the lateral force in the L-direction, Fy, is negligible. This result indicates that the peak lateral force is approximately 15% of the crush strength.

The lateral force during compression applies an undesirable side load on the actuator and load cell of the testing system, which may cause misalignment and damage. To isolate the testing system from such side loading, a compression fixture was designed and built for honeycomb compression, Figure 10. A normally crushed Alcore 38 sample using the compressive fixture on the AT system is shown in Figure 11.

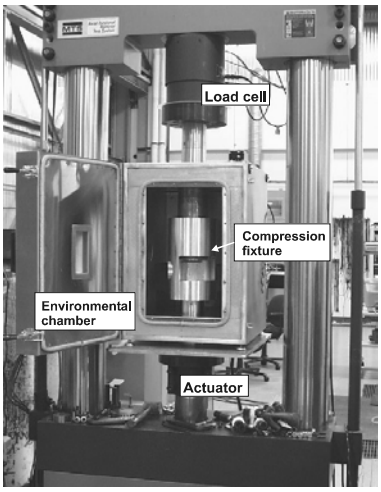

Figure 10. Self-aligned compression fixture and the AT system.

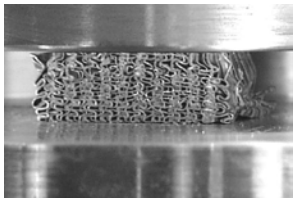

Figure 11. A normally crushed honeycomb (Alcore 38).

Table 1. Dimension and crush strength of small Alcore specimens

Specimen	*T, in.*	*L, in.*	*W, in.*	*Crush strength, ksi*
A01	0.844	0.675	0.572	5.32
A02	0.844	0.461	0.572	5.19
A03	0.716	0.453	0.436	4.88
A04	0.458	0.481	0.430	4.83
A05	0.458	0.485	0.292	4.64
A06	0.718	0.465	0.294	4.35

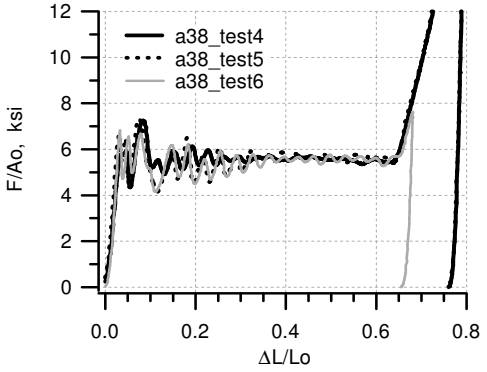

Figure 12. Stress-strain curves of Alcore 38 specimens, 3"x3"x1.5".

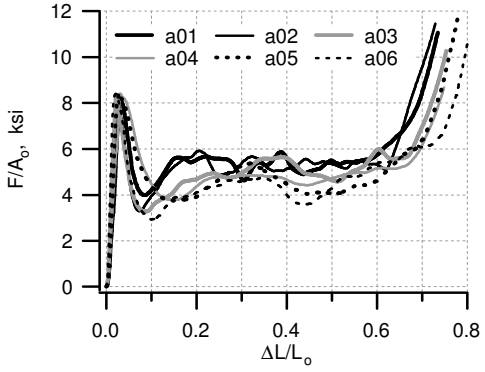

Figure 13. Stress-strain curves of Alcore 38 small specimens.

Size Effect of Honeycomb Specimen

For a standard specimen with 3"x3" cross-sectional area, there are about 50 layers of corrugated sheets and more than 1,350 hexagonal cells. This standard size puts restraints on experiments since it requires systems with large force capacity to deform 38 pcf honeycomb specimens. Smaller sizes are preferable. For example, small samples had to be used in the tests involving the six-component load cell described in the last section. It is important to establish an acceptable specimen size so valid honeycomb experiments can be more conveniently done.

Three Alcore 38 samples with standard cross section were tested using the setup shown in Figure 10. All samples were crushed normally. The stress-strain curves, displayed in Figure 12, match the description of orthotropic crush model very well. The average mean crush strength is 5.51 ksi. Crush strength is constant and does not have the problems described in Figure 3.

Specimens of various sizes of cross section, machined from the same Alcore 38 honeycomb, were tested. Their results are shown in Figure 13. Table 1 is a summary of six non-standard specimens. Based on the number of cells in the W-dimension, these specimens can be separated into three groups, which has four, three and two hexagonal cells in W direction as shown in Figure 14. The results indicate that when the specimen has four cells in the W-direction and crushes normally, its crush strength is within 5% of the standard specimen. Aluminum sheets always buckled in the W-direction, so W is the most critical minimum dimension of the cross section. The results suggest that specimens with a cross sectional area greater than 0.6"x0.6" are acceptable to be used for honeycomb characterization.

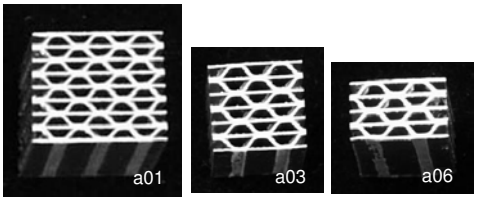

Figure 14. Cross sections of small Alcore 38 specimens.

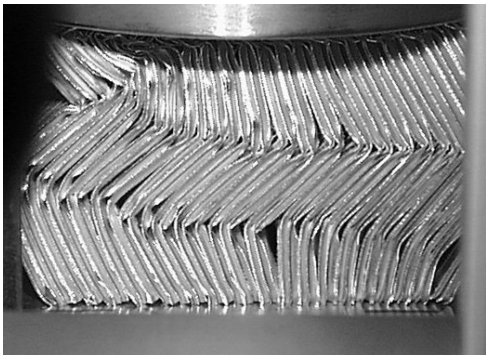

Figure 15. Global buckling of a 3"x3"x3" Alcore 38 specimen compressed in T-direction at 165°F.

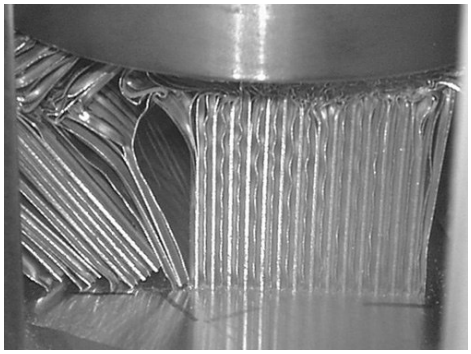

Figure 16. Delamination of a 3"x3"x3" Alcore 38 specimen compressed in T-direction at -65°F.

Compression at High and Low Temperatures

Utilizing the self-align fixture, honeycomb specimens usually exhibited the normal crush mode at ambient. The same setup, shown in Figure 10, was also used for compressions at high and low temperatures, 165 °F and -65 °F, respectively. Unfortunately, honeycomb specimens often resulted in abnormal deformation modes at these temperatures. For Alcore 38, global buckling was commonly observed at 165 °F and delamination was typical at -65 °F as shown in Figures 15 and 16, respectively. These undesired deformation modes significantly degraded the energy absorption capability of honeycomb. The degradation could be more than 50%.

The honeycomb is aluminum ribbons joined together using adhesive bonding. Since the mechanical properties of aluminum alloy 5052 remain fairly constant for the temperature range -65 °F to 165 °F [6], these temperature-dependent deformation modes may be influenced by the properties of the adhesive. Little information is available for the mechanical properties of the adhesive. If its glass transition temperature is within the test temperature range, the elastic modulus of the adhesive could vary over several orders of magnitude.

HIGH RATE CONFINED COMPRESSION

To obtain a normal crush mode was also very difficult in the high rate and bare situation. Splitting was always observed. Confined compression was then developed to ensure honeycomb specimens were deformed normally under various temperature and rate conditions.

Figure 17 illustrates the setup of confined tests. A steel chamber, which confines the lateral deformation of honeycomb, is attached on the actuator. The aluminum punch is in series with the load washer, which is mounted on the loading frame. An environmental chamber encloses the testing area.

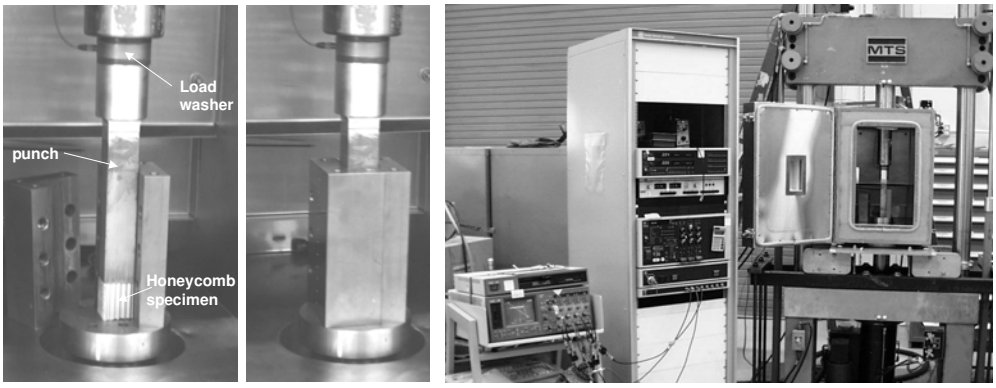

Figure 17. Setup of confined compression of honeycomb on the high rate system.

Table 2. A comparison of bare and confined compressions of Alcore 38 at ambient

Specimen	Condition	Dimension	Crush strength ksi	Peak strength ksi	Efficiency, %
1	Bare	3"x3"x1.5	5.59	7.25	60.56
2	Bare	3"x3"x1.5	5.51	7.34	62.80
3	Bare	3"x3"x1.5	5.44	6.67	63.73
4	confined	1.2"x1.2"x1.5"	5.49	8.18	60.80
5	confined	1.2"x1.2"x1.5"	5.24	8.08	61.10
6	confined	1.2"x1.2"x1.5"	5.57	8.76	60.70
7	confined	1.2"x1.2"x1.5"	5.62	8.76	60.00

Table 3. Summary of crush strength (ksi) / crush efficiency (%) of confined compressions

Material	Direction	High rate, 14ft/s			Quasi-static		
		-65°F	ambient	165°F	-65°F	ambient	165°F
Alcore 38_B2	T	7.34 / 62.7	6.35 / 63.8	5.49 / 62.5	6.23 / 62.0	5.23 / 61.5	4.6 / 61.3
	L		1.25 / 53.2	1.06 / 53.8			
	W	0.74 / 42.7	0.54 / 36.8	0.53 / 37.7	0.68 / 43.9	0.53 / 42.0	0.45 / 41.3
Hexcel 38_B2	T	8.21 / 64.7	7.17 / 63.9	6.43 / 64.3	7.3 / 60.8	5.88 / 59.2	5.55 / 60.0
	L		1.05 / 46.1	0.84 / 46.7	1.04 / 39.3	0.98 / 46.9	
	W	0.84 / 44.0	0.60 / 37.0	0.56 / 38.7	0.59 / 35.4	0.54 / 38.0	0.54 / 39.1

All specimens used for confined compression had a nominal dimension of 1.2"x1.2"x1.5". After the specimen was put in place, the steel chamber was bolted tightly, Figure 17. The inside chamber wall was lubricated. Table 2 compares the results of confined and bare compressions of Alcore 38 at ambient and quasi-static loading condition. The differences in Zone 2 parameters between these two compression methods are negligible, which is within the range of experimental uncertainty.

A matrix of confined compressions is listed in Table 3. Alcore 38_B2 and Hexcel 38_B2, which are new batches of material, were used in this series of test. For tests at 165°F or -65°F there was a thermal couple inserted in each specimen to monitor its temperature. Repeated tests, as many as 15 for each condition, were performed for most of the high rate compressions. Results were consistent and no abnormal deformation was observed. The values of averaged crush strength and efficiency are reported in the table. Typical displacement/load-time and stress-strain curves of confined high rate compressions are shown in Figure 18 for ambient conditions.

The values of the crush strength of the new batches are consistently higher than those of the previous batches. It shows the crush strength of honeycomb depends on both temperature and loading rate. Within the range tested, higher crush strength corresponds to lower temperature and higher loading rate.

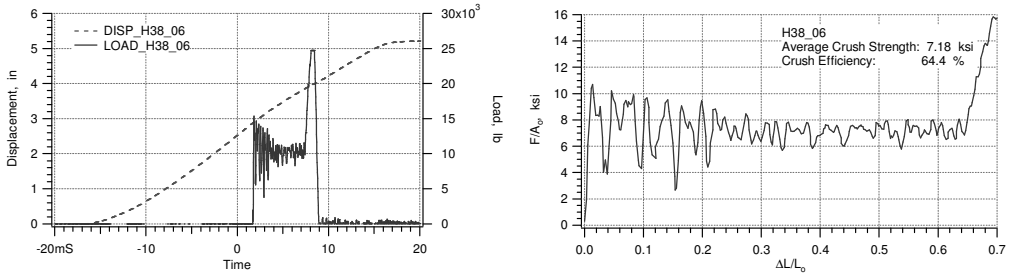

Figure 18. Displacement/load-time and stress-strain curves of a typical confined high rate test of Hexcel 38_B2 at ambient.

The crush efficiencies in three directions are different. Similar to the crush strength, T-direction is the maximum and W-direction is the minimum. In the T-direction it seems that the higher loading rate slightly increases the crush efficiency, but the effect of temperature is not very clear. In the W-direction, it looks like there are noticeable variations; however, it has a large measuring uncertainty since the transitions from Zone 2a to Zone 2b, i.e., from constant crush strength to hardening region, is gradual and not clearly defined as shown in Figures 7. In general, the rate and temperature effects on crush efficiency are small.

SUMMARY

The deformation of honeycomb is complex, depending on both size and boundary conditions of the sample. The orthotropic crush model is commonly used to describe the crush behavior of honeycomb; however, it describes only one normal deformation mode and does not predict the low energy absorption modes and the onset of such conditions. Experimental techniques were developed to deform honeycomb specimens in the normal mode, and tests were performed to obtain the model parameters, i.e., crush strength and efficiency, of Alcore 38 and Hexcel 38 honeycombs. Experimental results also demonstrate the temperature and rate effects of these high density honeycombs. Careful design is needed to ensure normal crush during loading and to fully utilize the energy absorption capability of honeycomb. For example, a thin shell can be used for confinement, or special orientations of honeycomb sheets to mitigate the global splitting. The model tends to over-predict the stand alone strength of honeycomb unless it is adequately confined by one or both of the prior design strategies.

ACKNOWLEDGEMENT

We are most grateful to our colleagues John Korellis, who designed the self-aligned and confined compression fixtures, and Jesse Lim, who performed the lateral force experiment. We also thank Mike Neilsen and Kenneth Gwinn for discussions and suggestions for the experiments. Sandia is a multiprogram laboratory operated by Sandia Corporation, a Lockheed Martin Company, for the United States Department of Energy under contract DE-AC04-94-AL85000.

REFERENCES

1. Whirley, R.G., Engelman, B.E., and Hallquist, J.O., 1991, "DYNA3D Users Manual," Lawrence Livermore Laboratory, Livermore, CA.
2. Attaway, S.W. *et al*., 1998, "PRONTO3D Users' Instructions: A Transient Dynamic code for Nonlinear Structural Analysis," Report SAND98-1361, Sandia National Laboratories, Albuquerque, NM.
3. "Mechanical Properties of Hexcel Honeycomb," TSB-120, Hexcel Corporation, Dublin, CA, 1992.
4. Alcore, Inc., Belcamp, MD.
5. Bitzer, T., 1997, Honeycomb Technology, Chapman & Hall, London, UK.
6. ASM Handbook, v.2, Properties and Selection: Nonferrous Alloys and Special-Purpose Materials, 1990.

APPENDIX II:

B61 Radar Nose Crush Model Validation – Qualification of Aluminum Honeycomb Crush Behavior

B61 Radar Nose Crush Model Validation

Qualification of Aluminum Honeycomb Crush Behavior

Test Plan

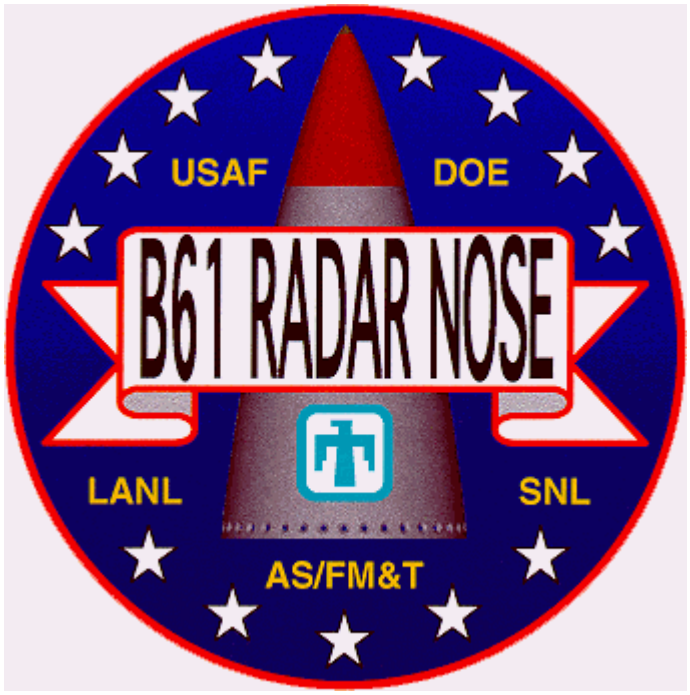

March 23, 1999

Approved By:

D. J. Giersch, SNL/2167	Date
T. D. Hinnerichs, SNL/9234	Date
Wei-Yang Lu, SNL/8746	Date
B. D. Boughton, SNL/9119	Date

1.0 Introduction

This test plan focuses on quantifying the crushing behavior and energy absorber capability of aluminum honeycomb for application to the B61 3/4/7/10 Radar Nose Assembly. Specifically this test plan has three objectives: 1) identify a set of quasi-static tests that can be used to compare directly with the honeycomb vendor tests required by the honeycomb purchase specification, 2) quantify any increase in crush strength due to dynamic loading and 3) provide sufficient aluminum honeycomb material response data to validate the Orthotropic Crush Constitutive parameters that will be used in the PRONTO3D B61 Radar Nose Crush model. The scope of this test plan includes quasi-static unconfined and confined, dynamic confined, and on-axis and off-axis crush response measurement, ambient and elevated temperature tests, and bond strength effects. Five batches of aluminum honeycomb will be examined which are defined in Table 1 based on their nominal density. Two of these batches (35 lb/ft3 density) represent candidate aluminum honeycomb material for the Radar Nose rear energy absorber. The other three batches (38 lb/ft3 density) relate to the forward energy absorber.

Table 1. Aluminum Honeycomb Batches

Vendor	Density (lb/ft^3)	Density (lb/ft^3)
Alcore	35	38
Hexcel	35	38
Hexcel-MAVEN		38

2.0 Responsibilities

The personnel identified in Table 2 are authorized consulting personnel for these Qualification of Aluminum Honeycomb Crush Behavior Tests.

Table 2. Authorized Consulting Personnel

Individual	Org.	Responsibility	Phone
J. M. Montoya	2167	B61 3/4/7/10 Test Engineer	844-3171
T. Hinnerichs	9234	Structural Analyst	844-9257
Wei-Yang Lu	8746	Quasi-Static Test Facility Engineer	294-3181
T. Carne	9119	Dynamic Test Facility Engineer	844-3266

3.0 Description of Tests

3.1 Measure and report the apparent density (weight/volume) for each batch of aluminum honeycomb.

3.2 Quasi-Static Unconfined Crush Tests in the T-direction at Ambient Temperature

3.2.1 The objectives for this test are to:

3.2.1.1 Evaluate the crush behavior of five batches of honeycomb in their strongest or “T” direction,

3.2.1.2 Quantify crush strength,

3.2.1.3 Quantify crush efficiency,

3.2.1.4 Quantify transverse deformation, and

3.2.1.5 Meet all applicable security and environmental, safety, and health requirements.

3.2.2 A listing of the test numbers, their corresponding honeycomb batch and the responsible Test Engineer is given in Table 3.

Table 3. Quasi-Static Unconfined Crush Tests in the T-direction at Ambient Temperature

Test #	Batch Description	Test Engineer
1 - 3	Alcore – 35 lb/ft^3	Wei-Yang Lu
4 - 6	Alcore – 38 lb/ft^3	Wei-Yang Lu
7 - 9	Hexcel – 35 lb/ft^3	Wei-Yang Lu
10 - 12	Hexcel – 38 lb/ft^3	Wei-Yang Lu
13 – 15	Hexcel Maven – 38 lb/ft^3	Wei-Yang Lu

3.2.3 Test Unit Description – Each of these 15 test articles will be cut from larger slabs of aluminum honeycomb and have the dimensions 1.5" x 3" x3" which correspond to the honeycomb's T x L x W directions.

3.2.4 Test Description – The aluminum honeycomb test articles will be compressively loaded in the T-direction at a quasi-static rate (e.g., 1 in/min) between two flat plates using a MTS Servo hydraulic system in the displacement control mode. For two out of the three tests for each batch, the maximum load applied should be 180,000 pounds, which corresponds to an applied stress level of 20,000 psi. For one of the three tests for each batch, the maximum load at lock up should only be equal to the original load spike at the beginning of crush. Measure post-test cross-section dimensions in the L and W direction for each of these tests.

3.2.5 Test Data Requirements

3.2.5.1 Load versus time

3.2.5.2 Crush distance vs. time

3.2.5.3 Post-test L-cross-section dimension

3.2.5.4 Post-test W-cross-section dimension

3.2.5.5 Report average crush strength as per SS706955-000 Aluminum Honeycomb purchase specification

3.2.5.6 Report average crush efficiency as per SS706955-000

3.2.5.7 Integrate area under load versus crush distance curve and report work done on honeycomb versus crush distance.

3.2.6 Photography Requirements – still photography of a deformed post-test article standing next to an undeformed pretest article from each of the five batches of material.

3.2.7 Schedule – These quasi-static unconfined crush tests in the T-direction shall be completed within two weeks after receiving the aluminum honeycomb material.

3.3 Quasi-Static Unconfined Crush Tests in the L-direction at Ambient Temperature

3.3.1 The objectives for this test are to:

3.3.1.1 Evaluate the crush behavior of two batches of honeycomb in their L-direction,

3.3.1.2 Quantify crush strength,

3.3.1.3 Quantify crush efficiency,

3.3.1.4 Quantify transverse deformation, and

3.3.1.5 Meet all applicable security and environmental, safety, and health requirements.

3.3.2 A listing of the test numbers, their corresponding honeycomb batch and the responsible Test Engineer is given in Table 4.

Table 4. Quasi-Static Unconfined Crush Tests in the L-direction at Ambient Temperature

Test #	Batch Description	Test Engineer
16 - 18	Alcore – 38 lb/ft^3	Wei-Yang Lu

3.3.3 Test Unit Description – Each of these 3 test articles will be cut from larger slabs of aluminum honeycomb and have the dimensions 3" x 1.5" x3" which correspond to the honeycomb's T x L x W directions.

3.3.4 Test Description – The aluminum honeycomb test articles will be compressively loaded in the L-direction at a quasi-static rate (e.g., 1 in/min) between two flat plates using a MTS Servo hydraulic system in the displacement control mode. For two out of the three tests for each batch, the maximum load applied should be 27,000 pounds, which corresponds to an applied stress level of 3,000 psi. For one of the three tests for each batch, the maximum load at lock up should only be equal to the original load spike at the beginning of crush. Measure post-test cross-section dimensions in the T and W direction for each of these tests.

3.3.5 Test Data Requirements

3.3.5.1 Load versus time

3.3.5.2 Crush distance versus time

3.3.5.3 Report post-test T-cross-section dimension

3.3.5.4 Report post-test W-cross-section dimension

3.3.5.5 Integrate area under load versus crush distance curve and report work done on honeycomb versus crush distance

3.3.6 Photography Requirements – still photography of a typical deformed post-test article standing next to an undeformed pretest article from each of the five batches of material.

3.3.7 Schedule – These quasi-static unconfined crush tests in the L-direction shall be completed within two weeks of receiving the aluminum honeycomb material.

3.4 MAVEN Quasi-static Confined Crush Tests in the T-direction

3.4.1 The objectives for this test are to:

3.4.1.1 Evaluate the confined crush behavior of honeycomb in its strongest or T-direction at ambient temperature and 172 –182 deg F.

3.4.1.2 Evaluate the confined crush behavior of unbonded (i.e., dissolve out the epoxy bond before testing) honeycomb at ambient temperature.

3.4.1.3 Quantify crush strength,

3.4.1.4 Quantify crush efficiency,

3.4.1.5 Meet all applicable security and environmental, safety, and health requirements.

3.4.2 A listing of the test numbers, their corresponding honeycomb batch and the responsible Test Engineer is given in Table 5.

Table 5. MAVEN Quasi-static Confined Crush Tests in the T-direction

Test #	Batch Description	Temperature	Bond	Test Engineer
19 - 21	Alcore – 38 lb/ft^3	Ambient	Bonded	Wei-Yang Lu
22 - 24	Alcore – 38 lb/ft^3	172-182 deg F	Bonded	Wei-Yang Lu
25 - 27	Alcore – 38 lb/ft^3	Ambient	Unbonded	Wei-Yang Lu

3.4.3 Test Unit Description – Each of these 9 test articles will be cut from larger slabs of aluminum honeycomb and have the dimensions 1.5” x 1.2” x 1.2” which correspond to the honeycomb’s T x L x W directions.

3.4.4 Test Description – The aluminum honeycomb test articles will be compressively loaded at a quasi-static rate (e.g., 1 in/min) using a MTS Servo hydraulic system in the displacement control mode. The hydraulic system will drive a piston into a honeycomb-filled chamber that has rigid walls and prevents any honeycomb expansion in the W-direction. The L-direction may be left open unless there is significant expansion in that direction. The maximum load applied should be 25,000 pounds.

3.4.5 Test Data Requirements

3.4.5.1 Load versus time

3.4.5.2 Crush distance versus time

3.4.5.3 Integrated work done on honeycomb versus crush distance

3.4.6 Photography Requirements – still photography of a typical deformed post-test article standing next to an undeformed pretest article for each of the three test conditions.

3.4.7 Schedule – These quasi-static confined crush tests in the T-direction shall be completed within two weeks of receiving the aluminum honeycomb material.

3.5 MAVEN Dynamic Confined Crush Tests in the T-direction at Ambient Temperature

3.5.1 The objectives for this test are to:

3.5.1.1 Evaluate the dynamic crush behavior of confined aluminum honeycomb in its strongest or T-direction at ambient.

3.5.1.2 Quantify crush strength,

3.5.1.3 Quantify crush efficiency,

3.5.1.4 Meet all applicable security and environmental, safety, and health requirements.

3.5.2 A listing of the test numbers, their corresponding honeycomb batch and the responsible Test Engineer is given in Table 6.

Table 6. MAVEN Dynamic Confined Crush Tests in the T-Direction

Test #	Batch	Impact Speed	Test Engineer
28 - 30	Alcore –38 lb/ft^3	100 in/sec.	Wei-Yang Lu
31 - 33	Hexcel MAVEN 38 lb/ft3	?? In/sec	Tom Carne

3.5.3 Test Unit Description – Test articles 28, 29 and 30 will have the dimensions 1.5" x 1.2" x 1.2". Test articles 31, 32 and 33 will have dimensions 1.5" x 2" x 2". Both sets of dimensions correspond to the honeycomb's T x L x W directions.

3.5.4 Test Description – The aluminum honeycomb test articles will be compressively loaded in the T-direction at the given dynamic rates. Lu will use a high speed Servo hydraulic system in the displacement control mode. The hydraulic system will drive a piston into a honeycomb-filled chamber that has rigid walls and prevents any honeycomb expansion in the W-direction. Carne will use a drop table to apply the high speed impact conditions.

3.5.5 Test Data Requirements

3.5.5.1 Load versus time

3.5.5.2 Crush distance versus time

3.5.5.3 Report average crush strength as per SS706955-000 honeycomb purchase specification

3.5.5.4 Report crush efficiency as per SS706955-000 honeycomb purchase specification

3.5.6 Photography Requirements – still photography of a typical deformed post-test article standing next to an undeformed pretest article for each of the two test conditions.

3.5.7 Schedule – These dynamic confined crush tests in the T-direction shall be completed within two weeks of receiving the aluminum honeycomb material.

3.6 Flexural Shear Tests at Ambient Temperature

3.6.1 The objectives for this test are to:

3.6.1.1 Evaluate the fshear behavior of aluminum honeycomb in the T-L plane at ambient temperature.

3.6.1.2 Quantify the shear modulus,

3.6.1.3 Quantify the shear strength,

3.6.1.4 Meet all applicable security and environmental, safety, and health requirements.

3.6.2 A listing of the test numbers, their corresponding honeycomb batch and the responsible Test Engineer is given in Table 7.

Table 7. MAVEN Flexural Shear Test at Ambient Temperature

Test #	Batch	Orientation	Test Engineer
34 - 36	Alcore –38 lb/ft^3	T-L Shear	Wei-Yang Lu

3.6.3 Test Unit Description – Comply with the test unit description in MIL-C-7438G, paragraph 4.7.7.2. Test articles 34, 35 and 36 will have the dimensions 0.625" x 8"" x 3". These dimensions correspond to the honeycomb's T x L x W directions.

3.6.4 Test Description – Perform test as described in MIL-C-7438G and MIL-STD-401B, paragraph 5.2.4.3. This is a 4-point bend test where the load rate is 0.015 to 0.020 in/min.

3.6.5 Test Data Requirements

3.6.5.1 Load versus time

3.6.5.2 Midspan deflection versus time

3.6.5.3 Report sandwich core shear strength as per MIL-STD-401B, paragraph 5.2.4.4.

3.6.5.4 Report sandwich core shear modulus as per MIL-STD-401B, paragraph 5.2.4.4.

3.6.6 Photography Requirements – still photography of a typical deformed post-test article standing next to an undeformed pretest article for each of the two test conditions.

3.6.7 Schedule – These flexural shear tests shall be completed within four weeks of receiving the aluminum honeycomb material.

3.7 MAVEN Dynamic 2-Layer Crush Tests in the T-direction at Ambient Temperature

3.7.1 The objectives for this test are to:

3.7.1.1 Evaluate the dynamic crush behavior of confined aluminum honeycomb in its strongest or T-direction at ambient temperature.

3.7.1.2 Quantify dynamic crush strength,

3.7.1.3 Quantify dynamic crush efficiency,

3.7.1.4 Meet all applicable security and environmental, safety, and health requirements.

3.7.2 A listing of the test numbers, their corresponding honeycomb batch and the responsible Test Engineer is given in Table 8.

Table 8. MAVEN Dynamic 2-Layer Crush Tests in the T-Direction at Ambient Temperature			
Test #	Batch	Impact Speed	Test Engineer
37 - 39	Hexcel MAVEN 38 lb/ft3	~800. In/sec	Tom Carne

3.7.3 Test Unit Description – The cylindrical cross-section of the MAVEN 2-Layer test article is described in Figure 1.

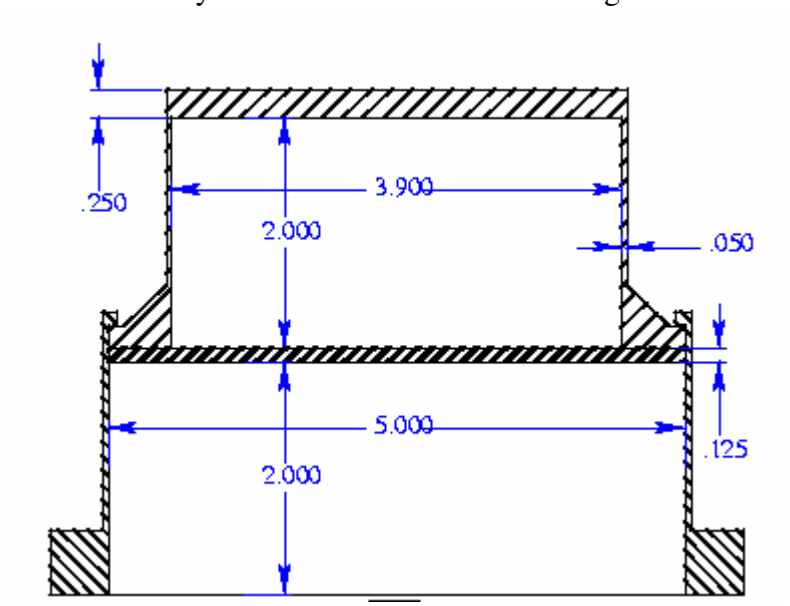

Figure 1. Cylindrical Cross-Section of MAVEN 2-Layer Test Article

These shell structures will be filled with uniform honeycomb from the Hexcel MAVEN 38 lb/ft3 batch of material.

3.7.4 Test Description – 18" actuator facility will drive impact mass into test article with normal incidence.

3.7.5 Test Data Requirements

3.7.5.1 Load versus time

3.7.5.2 Crush distance versus time

3.7.6 Photography Requirements – still photography of the deformed post-test article standing next to an undeformed pretest article.

3.7.7 Schedule – April 1999.

3.8 MAVEN Dynamic 2-Layer Off-Axis Crush Tests at Ambient Temperature

3.8.1 The objectives for this test are to:

3.8.1.1 Evaluate the dynamic crush behavior of confined aluminum honeycomb when impacted at a 20 degree pitch angle from normal at ambient temperature.

3.8.1.2 Quantify dynamic crush strength,
3.8.1.3 Quantify dynamic crush efficiency,
3.8.1.4 Meet all applicable security and environmental, safety, and health requirements.

3.8.2 A listing of the test numbers, their corresponding honeycomb batch, impact velocity, impact orientation and the responsible Test Engineer is given in Table 9.

Table 9. MAVEN Dynamic 2-Layer Off-Axis Crush Tests at Ambient Temperature

Test #	Batch	Impact Velocity	Impact Orientation	Test Engineer
40	Hexcel MAVEN – 38 lb/ft3	??	20 deg Pitch / Roll parallel with L-direction	Tom Carne
41	Hexcel MAVEN – 38 lb/ft3	??	20 deg Pitch / Roll is 45 deg from L-direction	Tom Carne

3.8.3 Test Unit Description – The cylindrical cross-section of the MAVEN 2-Layer test articles is described in Figure 1. These shell structures will be filled with segmented aluminum honeycomb from the Hexcel MAVEN 38 lb/ft3 batch of material.

3.8.4 Test Description – for test #40, the 18" actuator will be used to drive an impact mass with a 20 degree pitch angle (relative to axial) wedge mounted on it into the test article which will be mounted to a reaction mass suspended in the path of the impactor. The roll angle of the wedge will be oriented so that its normal is parallel to the L-direction of the segmented core honeycomb.

Test #41 will be similar to Test #40 except the roll angle for the wedge will oriented such that its normal is parallel to a plane 45 degrees from the L-direction of the segmented core honeycomb.

3.8.5 Test Data Requirements
3.8.5.1 Load versus time
3.8.5.2 Crush distance versus time

3.8.6 Photography Requirements – still photography of the deformed post-test article standing next to an undeformed pretest article.

3.8.7 Schedule – April 1999.

3.9 MAVEN - Quasi-Static Crush Test of 2-Layer Test Article in the T-direction

3.9.1 The objectives for this test are to:

3.9.1.1 Evaluate the crush behavior of confined aluminum honeycomb in its strongest or T-direction at ambient temperature,

3.9.1.2 Evaluate the crush behavior of confined aluminum honeycomb in the T-direction at 172-182 deg F,

3.9.1.3 Evaluate off-axis crush of confined aluminum honeycomb at ambient temperature,

3.9.1.4 Quantify quasi-static confined crush strength,

3.9.1.5 Quantify quasi-static confined crush efficiency,

3.9.1.6 Meet all applicable security and environmental, safety, and health requirements.

3.9.2 A listing of the test numbers, their corresponding honeycomb batch and the responsible Test Engineer is given in Table 10.

Table 10. MAVEN - Quasi-Static Crush of 2-Layer Test Article in the T-direction

Test #	Batch	Test Engineer
42 - 44	Hexcel MAVEN – 38 lb/ft3	Wei-Yang Lu

3.9.3 Test Unit Description – The cylindrical cross-section of the MAVEN 2-Layer test article is described in Figure 1. These shell structures will be filled with uniform honeycomb from the Hexcel MAVEN 38 lb/ft3 batch of material.

3.9.4 Test Description:

3.9.4.1 Perform displacement controlled crush at 1 in/min in the axial direction of the test unit at ambient temperature. Matching crush work done on test article to maximum kinetic energy absorbed in MAVEN actuator tests. This is the most important test out of the three tests described in paragraph 3.9.4.

3.9.4.2 Optional Test - Perform the above test (paragraph 3.7.4.1) at 172-182 degrees F **if the ambient test goes well.**

3.9.4.3 **2nd Optional Test** - Perform the same test as paragraph 3.9.4.1 but include a 20 degree wedge to load the top of the 2-layer test unit **if the above two tests go well**. Orient the plane of the wedge perpendicular to the L-direction of the aluminum honeycomb contents (i.e., the 20 deg angle should be in the L-plane of the honeycomb)

3.9.5 Test Data Requirements

3.9.5.1 Load versus time

3.9.5.2 Crush distance versus time

3.9.5.3 Report final average height of each layer of honeycomb for the axial crush tests.

3.9.6 Photography Requirements – still photography of the deformed post-test article standing next to an undeformed pretest article.

3.9.7 Schedule – April 1999.

4.0 Documentation Requirements

4.1 Quasi-static Test Report – a Sandia Technical Report is required to document the quasi-static testing accomplished. This report would also include the single dynamic test to be performed with the hydraulic testing machine.

4.2 Dynamic Test Report – a Sandia Technical Report is required to document the dynamic drop table testing and the 2-layer MAVEN tests to be conducted in the 18" actuator facility.

4.3 The required information in these reports includes:

4.3.1 Photographs of the test set up,

4.3.2 Photographs of the pretest and post-test honeycomb specimens

4.3.3 Test data from all tests conducted

4.3.4 Quantification of the error and uncertainty associated with the test data presented on the test data plots.

5.0 Directions for Cutting the Honeycomb Slabs into Test Articles

Information for cutting the aluminum honeycomb test articles is given in Table 11.

Table 11. Aluminum Honeycomb Test Article Cutting Information

Batch	Test #	Quantity**	Size (T x L x W)*	Test Engineer
Alcore – 35 lb/ft3	1-3	4	1.5" x 3" x3"	Wei-Yang Lu
Alcore – 38 lb/ft3	4-6	4	1.5" x 3" x 3"	Wei-Yang Lu
Hexcel – 35 lb/ft3	7-9	4	1.5" x 3" x 3"	Wei-Yang Lu
Hexcel – 38 lb/ft3	10-12	4	1.5" x 3" x 3"	Wei-Yang Lu
Hexcel MAVEN – 38 lb/ft3	13-15	4	1.5" x 3" x 3"	Wei-Yang Lu
Alcore – 38 lb/ft3	16-18	4	3" x 1.5" x 3"	Wei-Yang Lu
Alcore – 38 lb/ft3	19-30	16	1.5" x 1.2" x 1.2"	Wei-Yang Lu
Hexcel MAVEN – 38 lb/ft3	31-33	4	1.5" x 2" x 2"	Tom Carne
Alcore – 38 lb/ft3	34-36	6	0.625" x 8" x 3"	Wei-Yang Lu

*Tolerances: Dimensions to within plus or minus 0.015", Sides of Test Articles shall be parallel to within 0.010 of aluminum sheets"

**Quantity is based on one or more extra test articles for each type of test.

Distribution:

MS9042 Wei-Yang Lu, 8746
MS0437 J. Pott, 9117
MS0437 K. Gwinn, 9117
MS0557 T. Carne, 9119
MS0557 B. Boughton, 9119
MS0483 D. Giersch, 2167
MS0481 J. Montoya, 2167
MS0481 V. Willan, 2167

MS0533	R. Woodrum, 2343
MS0437	H. Morgan, 9117
MS0439	D. Martinez, 9234

Experimental Results

2M System

Load Cell calibration

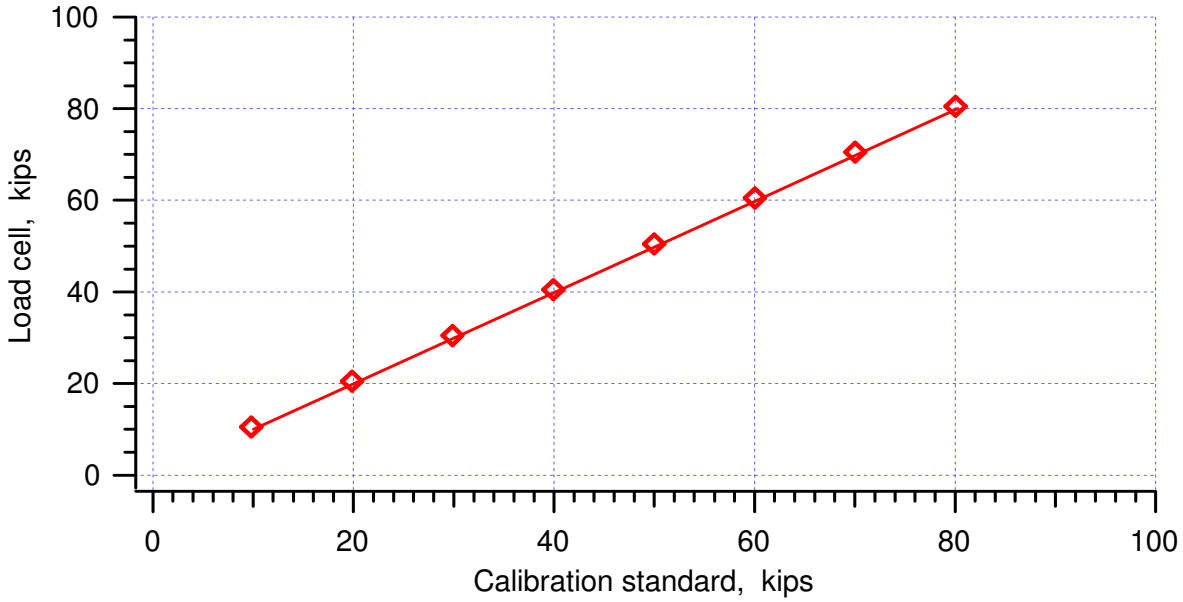
Load cell, kips
100
80
60
40
20
0
0
20
40
60
80
100
Calibration standard, kips

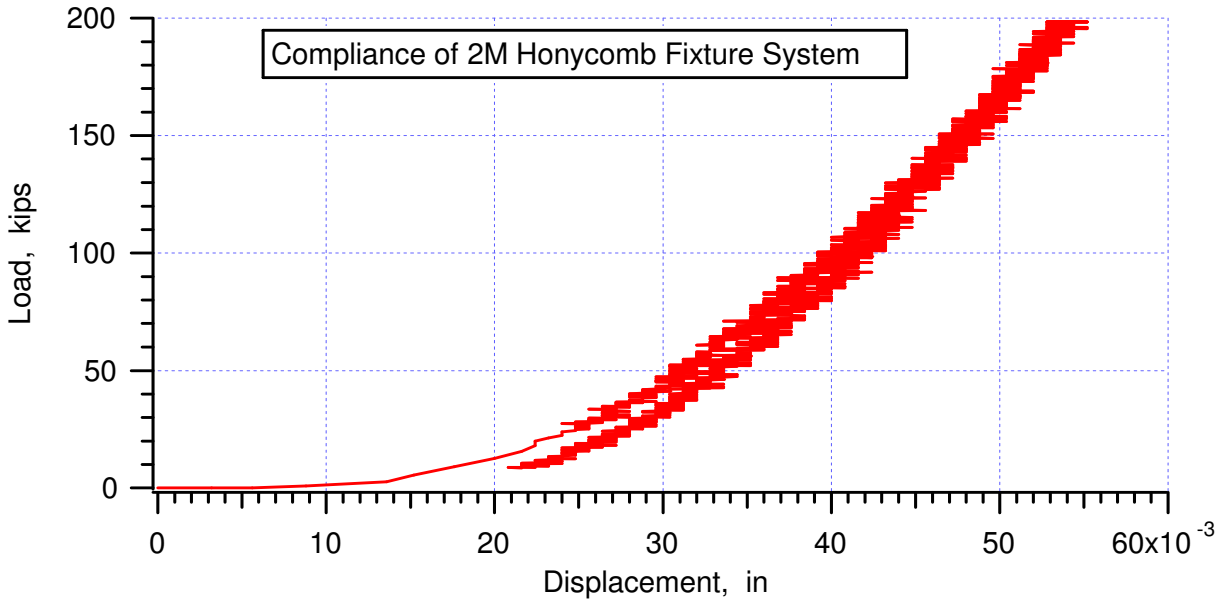
Compliance of 2M Honycomb Fixture System
Load, kips
200
150
100
50
0
0
10
20
30
40
50
60x10 -3
Displacement, in

AT System

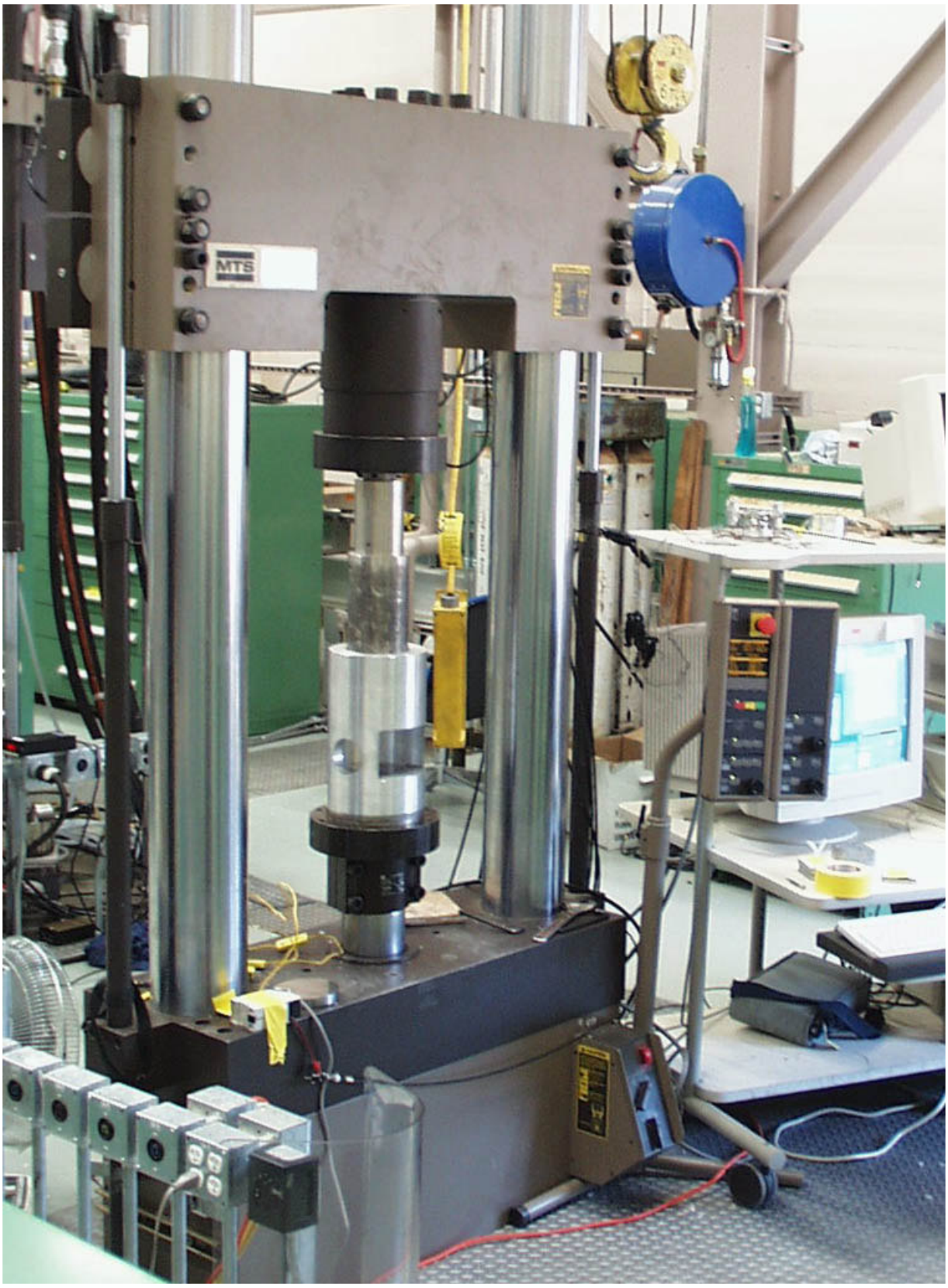

Candy-Jar compression fixture

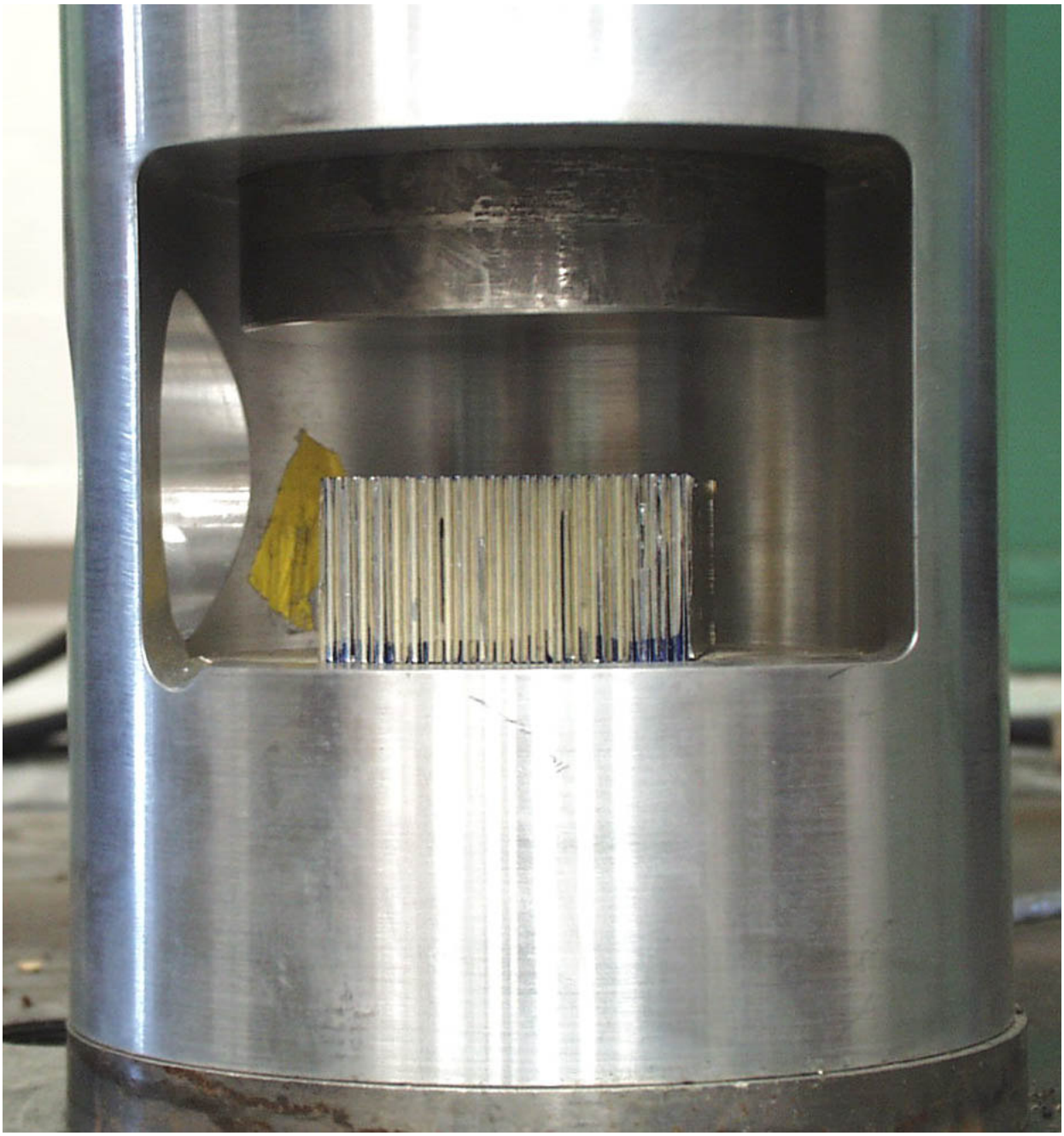

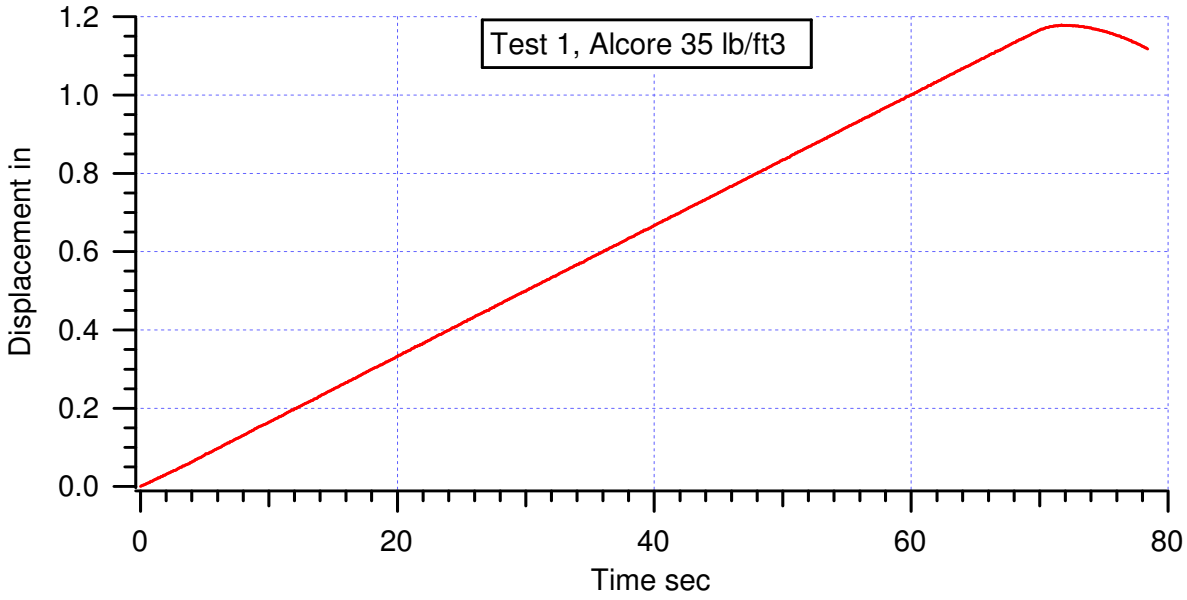
Test 1, Alcore 35 lb/ft3
Displacement in
1.2
1.0
0.8
0.6
0.4
0.2
0.0
0
20
40
60
80
Time sec

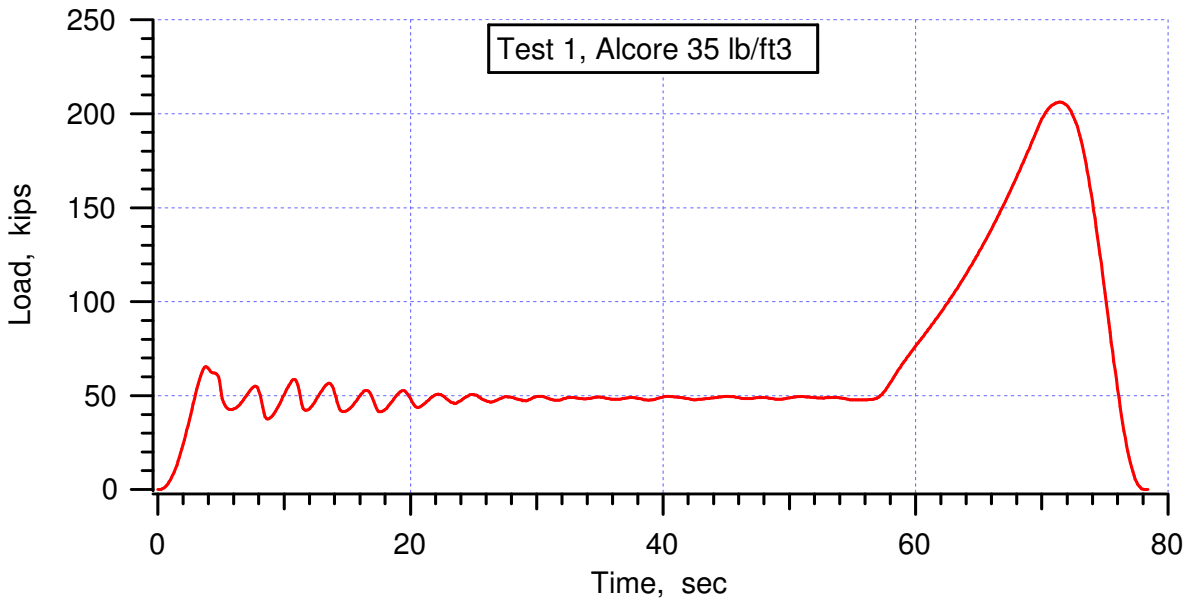
Test 1, Alcore 35 lb/ft3
Load, kips
250
200
150
100
50
0
0
20
40
60
80
Time, sec

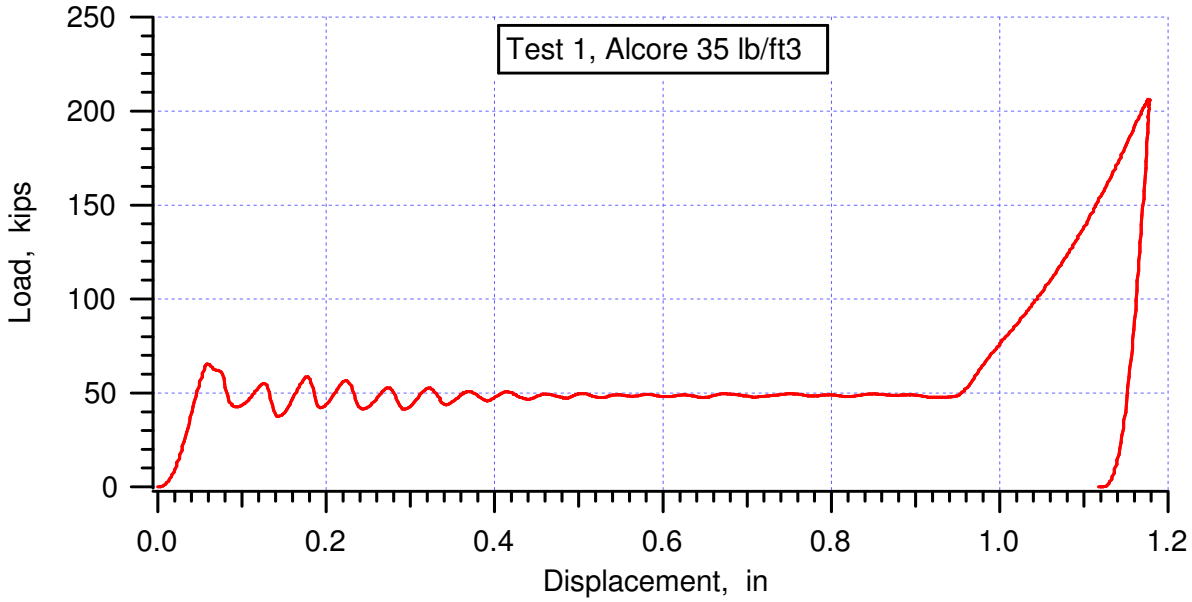
Test 1, Alcore 35 lb/ft3
Load, kips
250
200
150
100
50
0
0.0
0.2
0.4
0.6
0.8
1.0
1.2
Displacement, in


Test 1, Alcore 35 lb/ft3
work, x10^3 in-lb
80
60
40
20
0
0.0
0.2
0.4
0.6
0.8
1.0
1.2
crush distance, in

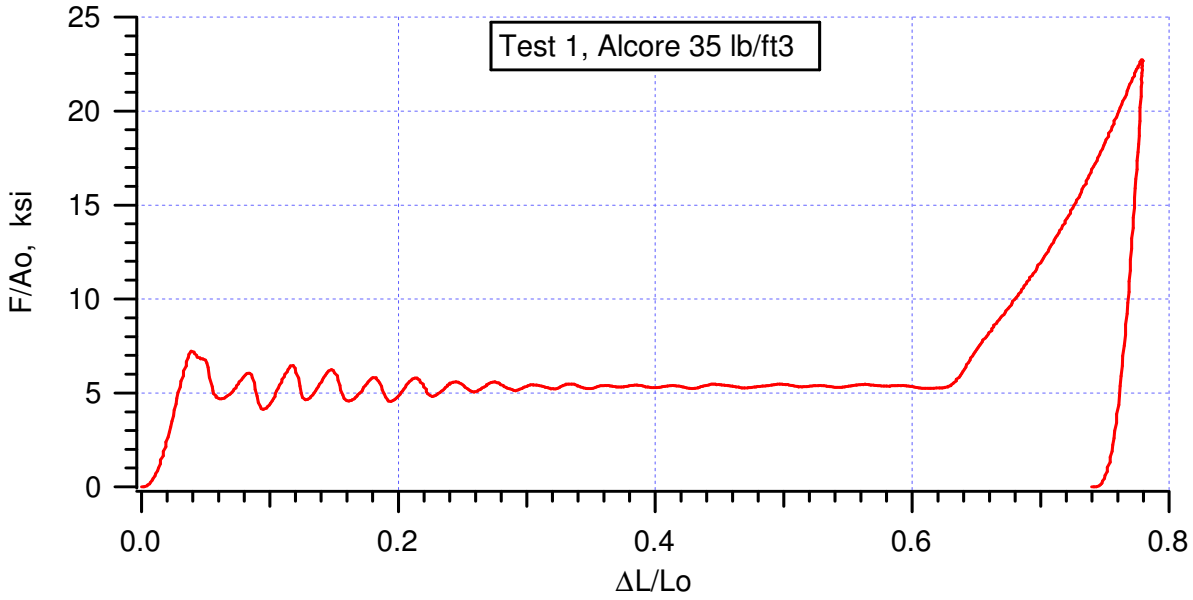

compressive peak = 7.22 ksi at 3.87%

average crush strength = 5.32 ksi averaged from (6.00%, 4.697 ksi) to (62.8%, 5.325 ksi)

crush efficiency = 61.15% from (3.87%, 7.22 ksi) to (65.02%, 7.31 ksi)

Test #1

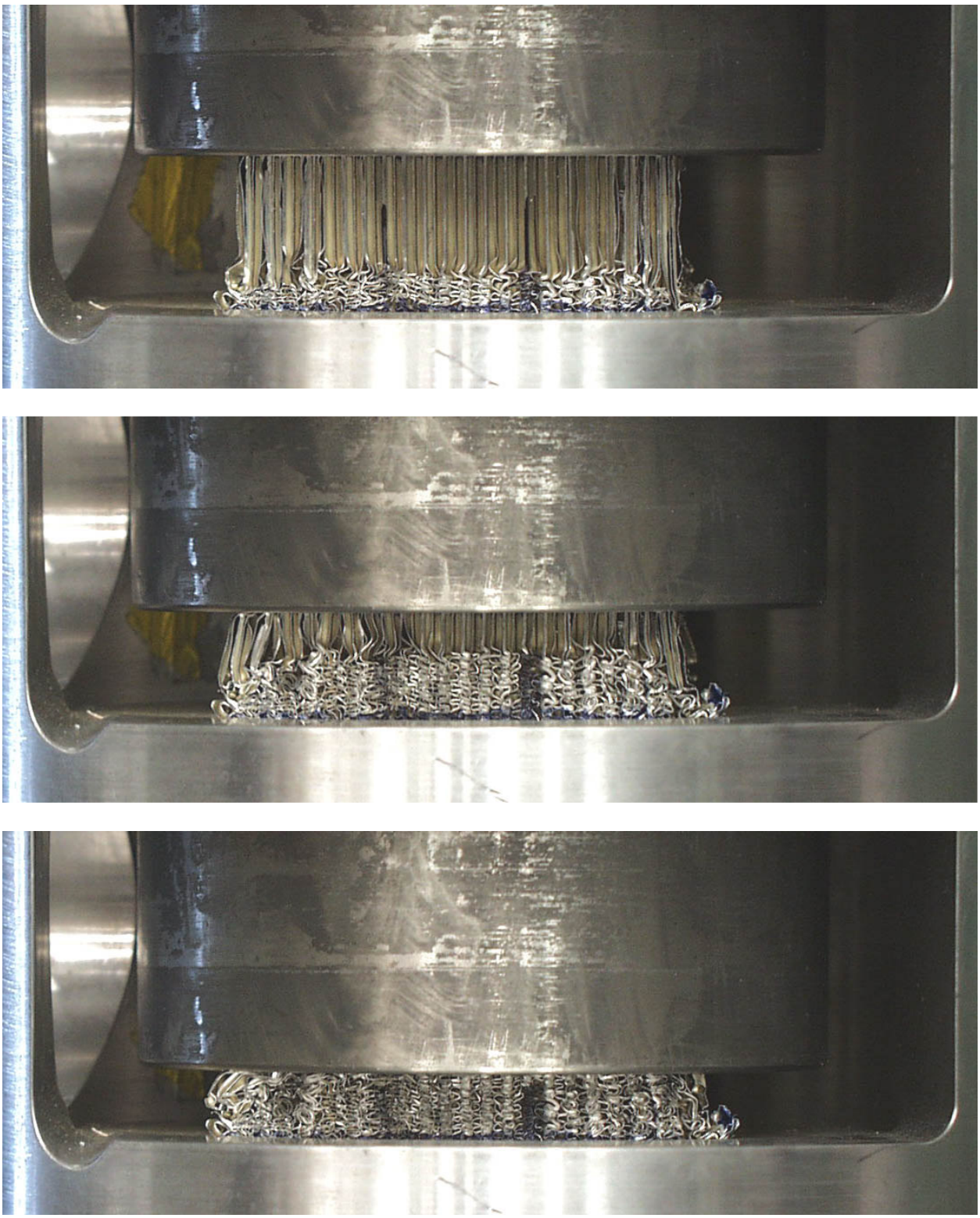

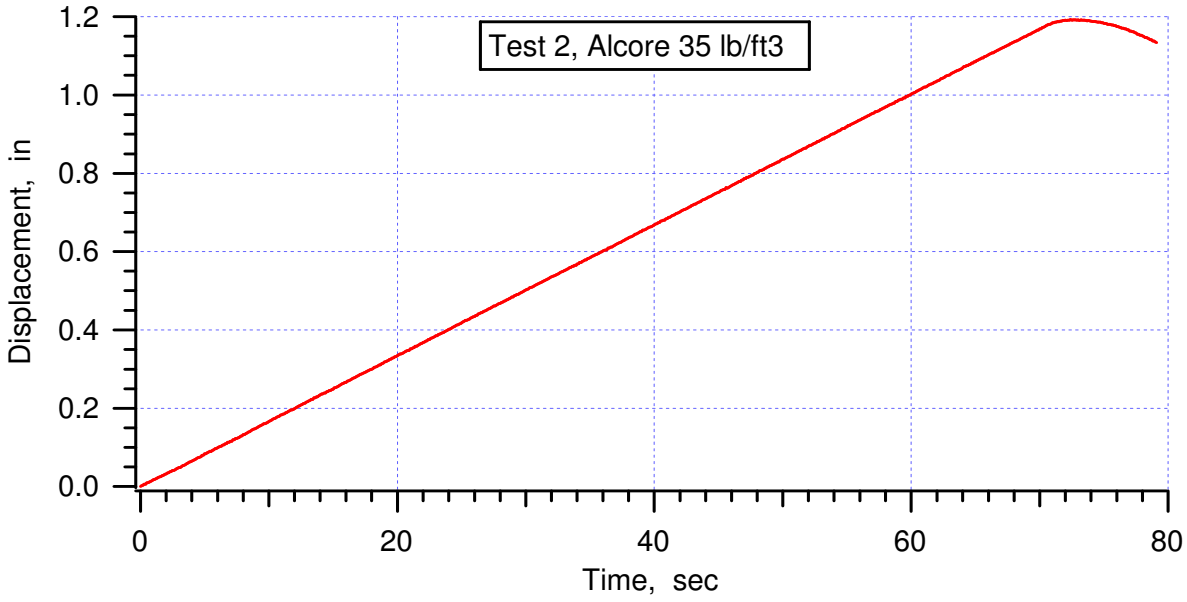
Test 2, Alcore 35 lb/ft3
Displacement, in
1.2
1.0
0.8
0.6
0.4
0.2
0.0
0
20
40
60
80
Time, sec

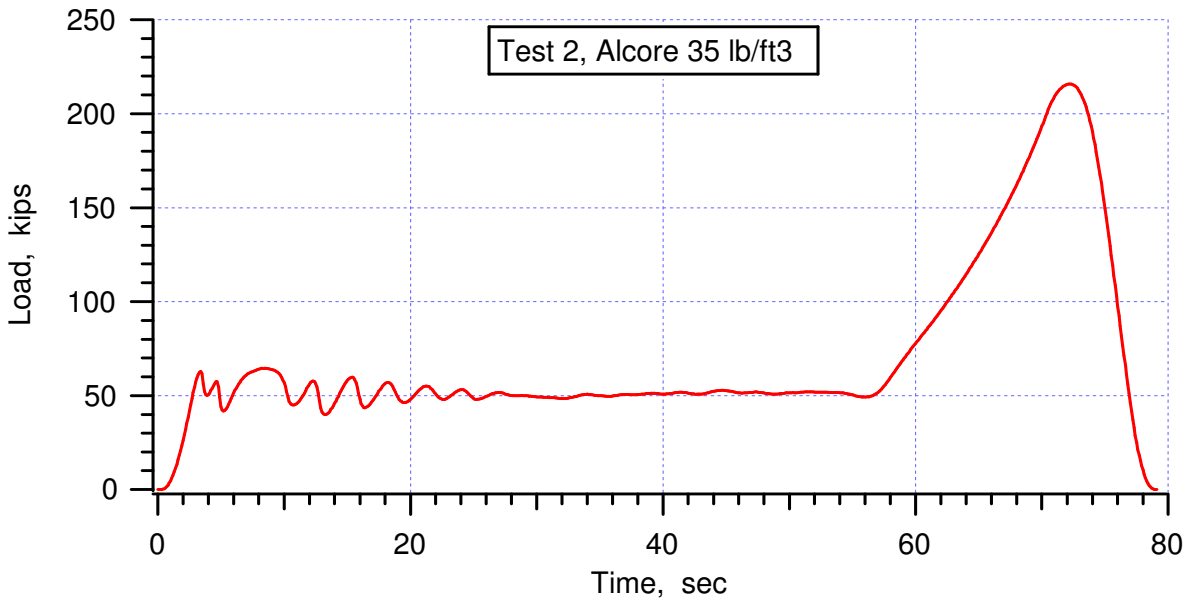
Test 2, Alcore 35 lb/ft3
Load, kips
250
200
150
100
50
0
0
20
40
60
80
Time, sec

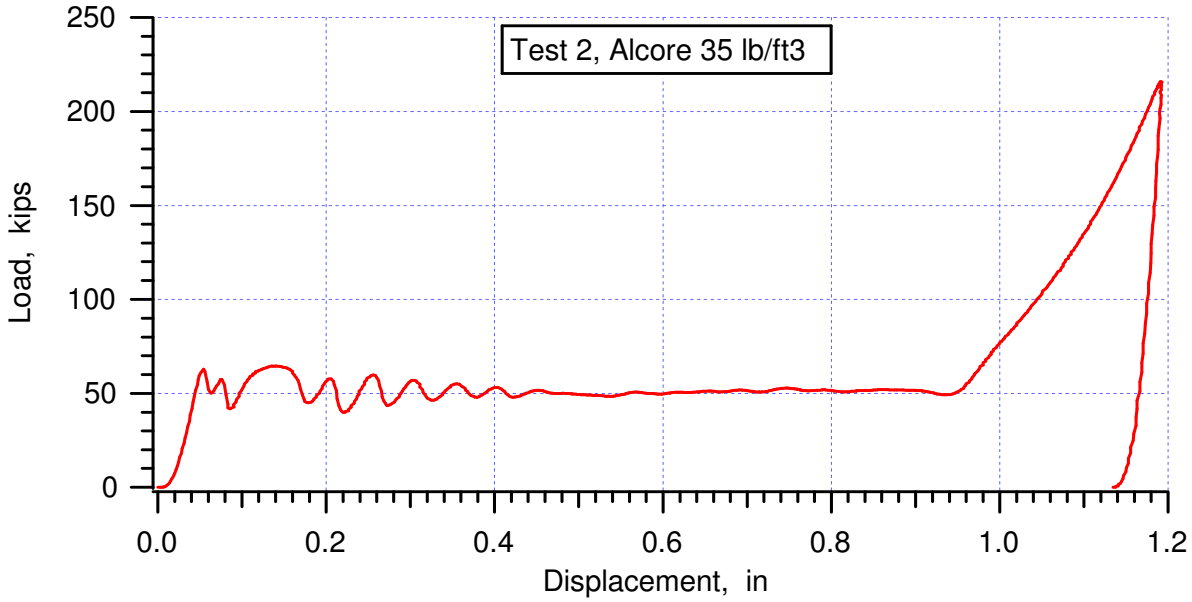
Test 2, Alcore 35 lb/ft3
Load, kips
250
200
150
100
50
0
0.0
0.2
0.4
0.6
0.8
1.0
1.2
Displacement, in


Test 2, Alcore 35 lb/ft3
work, x10^3 in-lb
80
60
40
20
0
0.0
0.2
0.4
0.6
0.8
1.0
1.2
crush distance, in

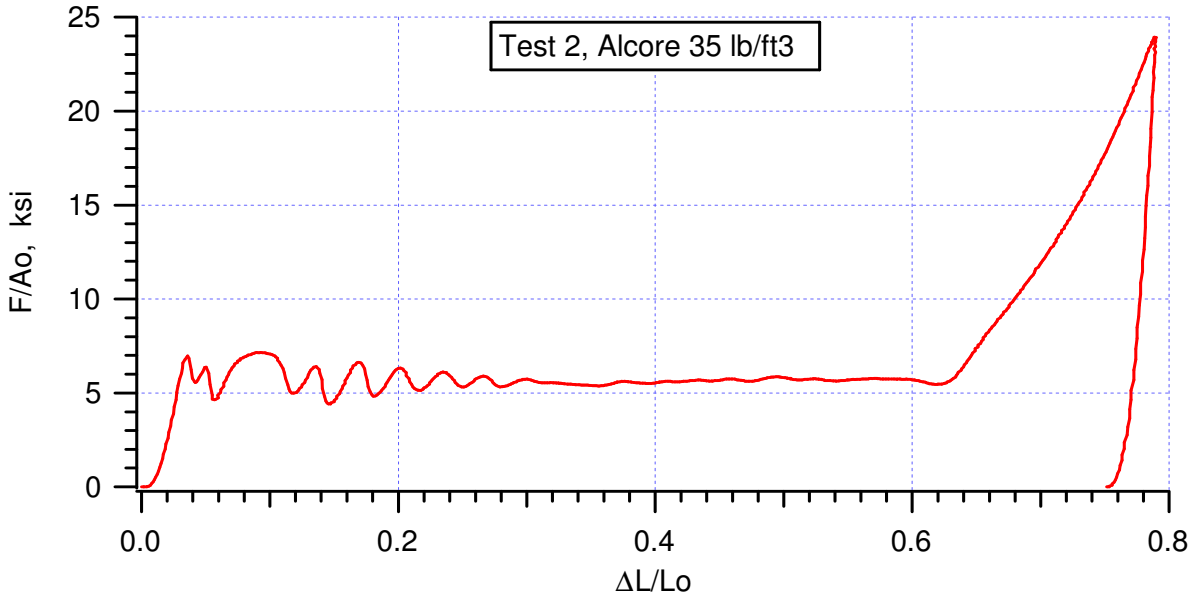

compressive peak = 6.98 ksi at 3.60%

average crush strength = 5.70 ksi averaged from (4.29%, 5.5994 ksi) to (61.9%, 5.4574 ksi)

crush efficiency = 61.03% from (3.60%, 6.98 ksi) to (64.64%, 7.03 ksi)

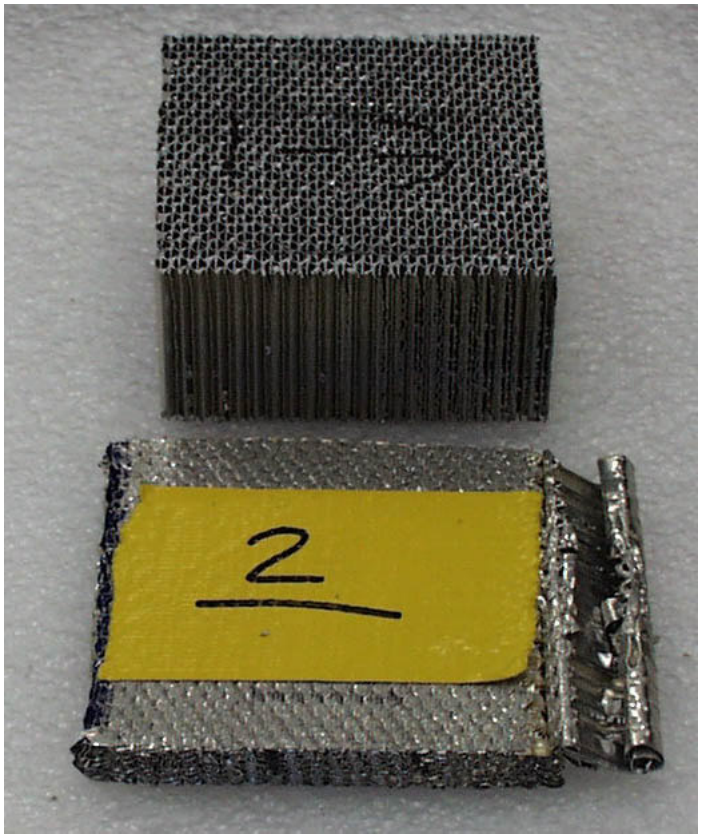

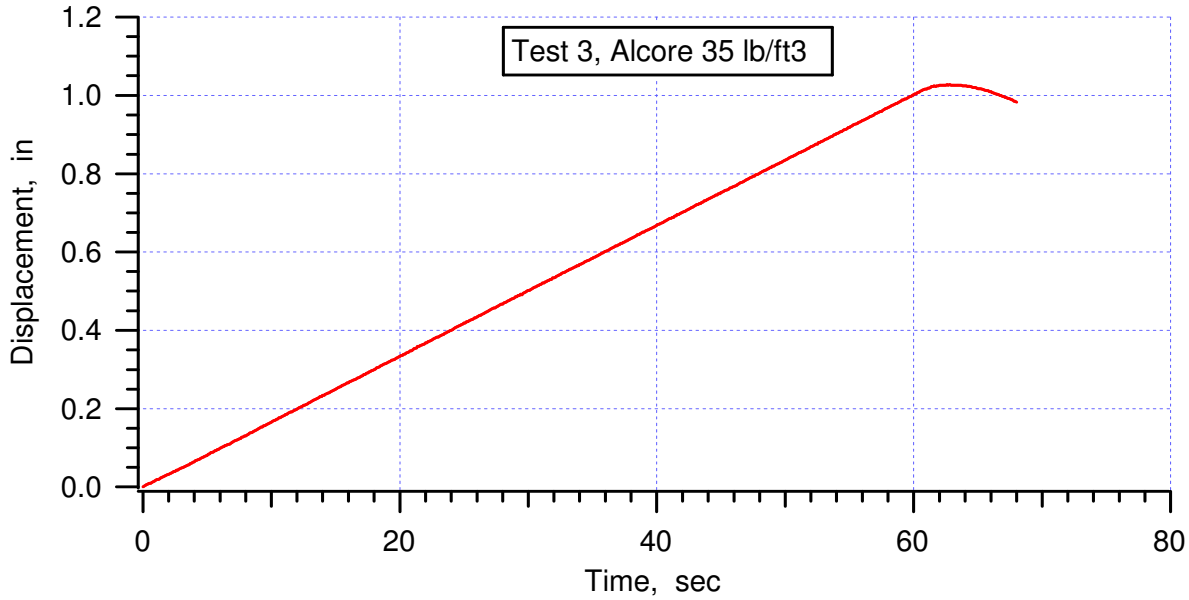
Test 3, Alcore 35 lb/ft3
Displacement, in
Time, sec
0.0
0.2
0.4
0.6
0.8
1.0
1.2
0
20
40
60
80

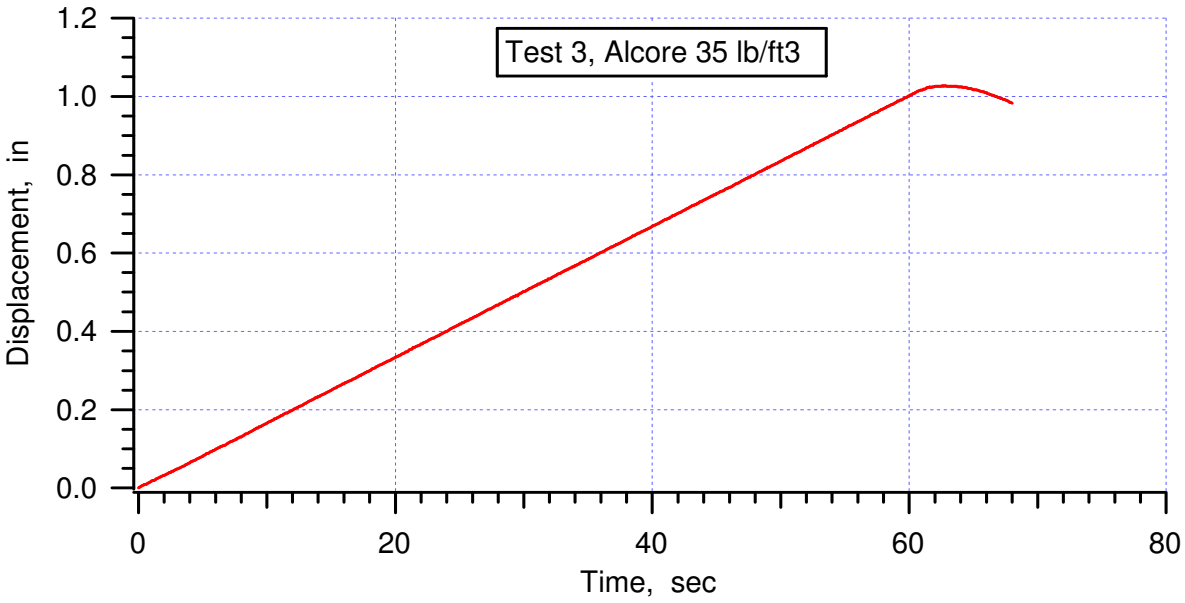
Test 3, Alcore 35 lb/ft3
Displacement, in
Time, sec
0.0
0.2
0.4
0.6
0.8
1.0
1.2
0
20
40
60
80

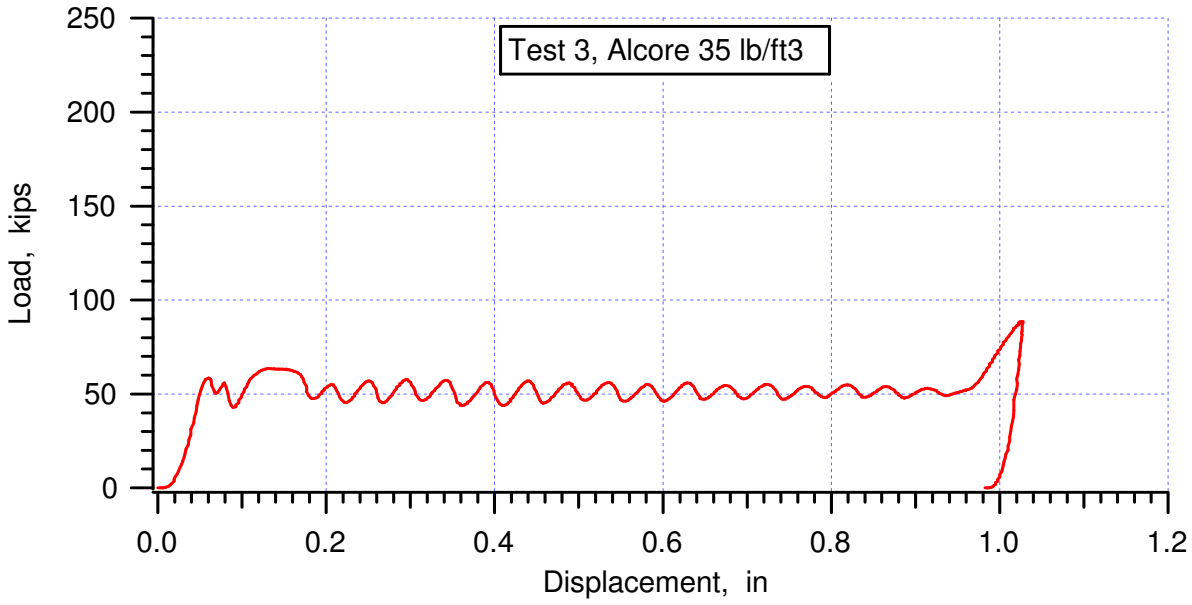
Test 3, Alcore 35 lb/ft3
Load, kips
250
200
150
100
50
0
0.0
0.2
0.4
0.6
0.8
1.0
1.2
Displacement, in

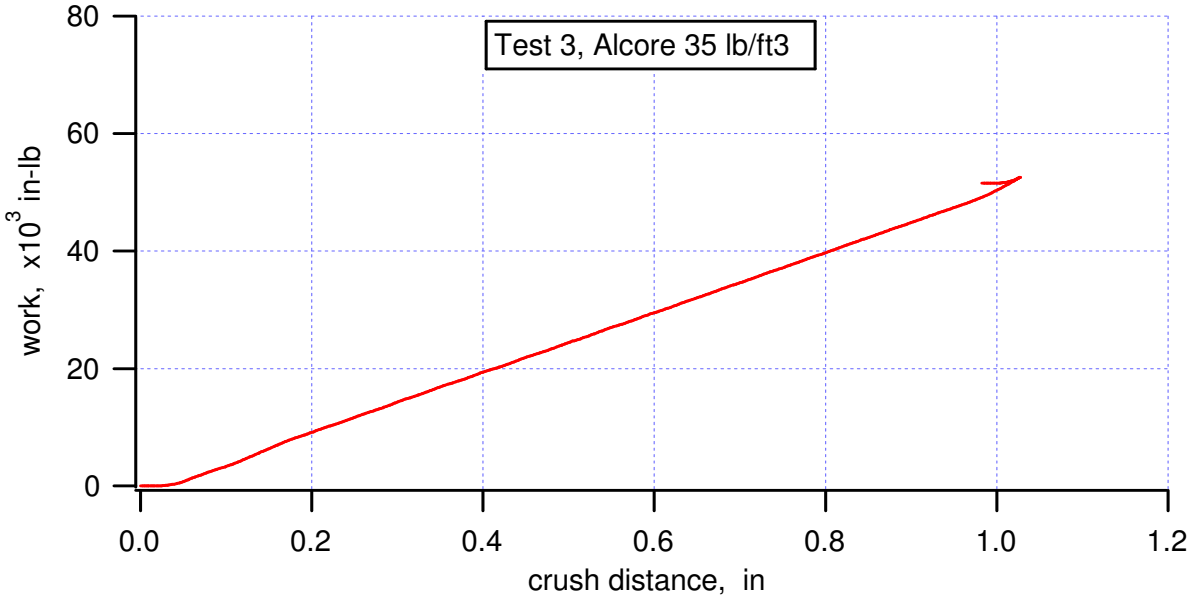
Test 3, Alcore 35 lb/ft3
work, x10^3 in-lb
80
60
40
20
0
0.0
0.2
0.4
0.6
0.8
1.0
1.2
crush distance, in

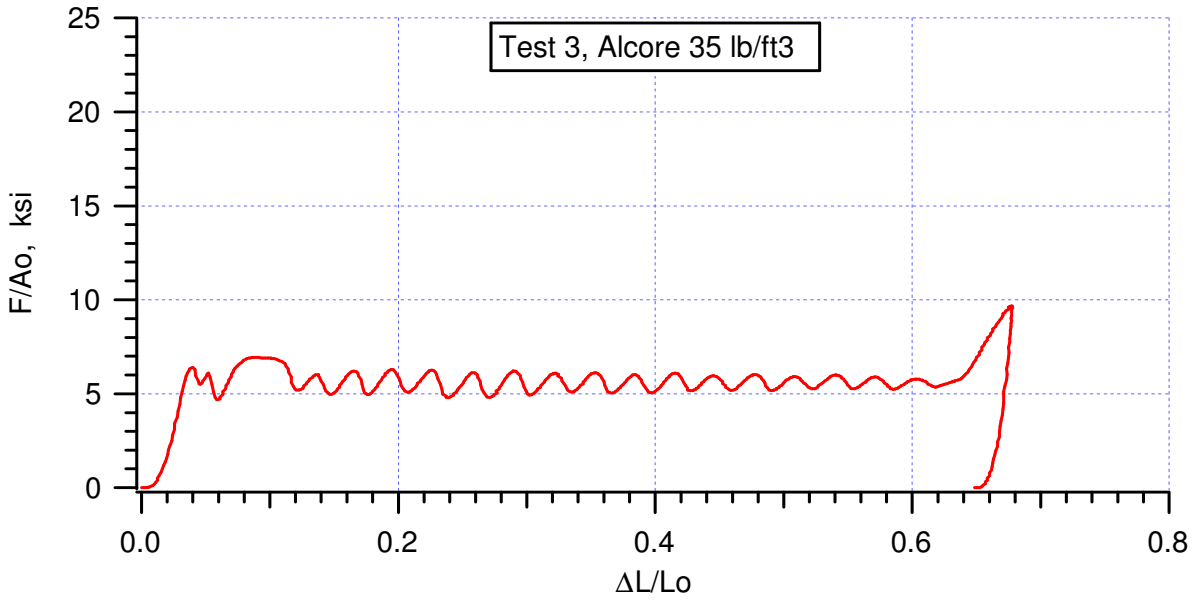

compressive peak = 6.39 ksi at 4.01%

average crush strength = 5.66 ksi averaged from (4.59%, 5.5051 ksi) to (61.8%, 5.3582 ksi)

crush efficiency = 60.67% from (3.96%, 6.38 ksi) to (64.63%, 6.45 ksi)

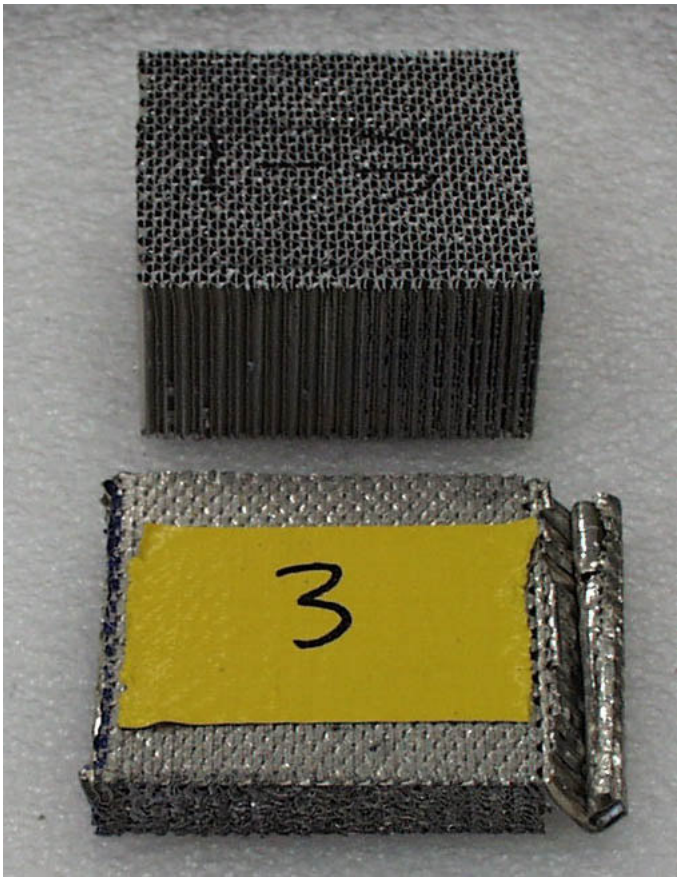

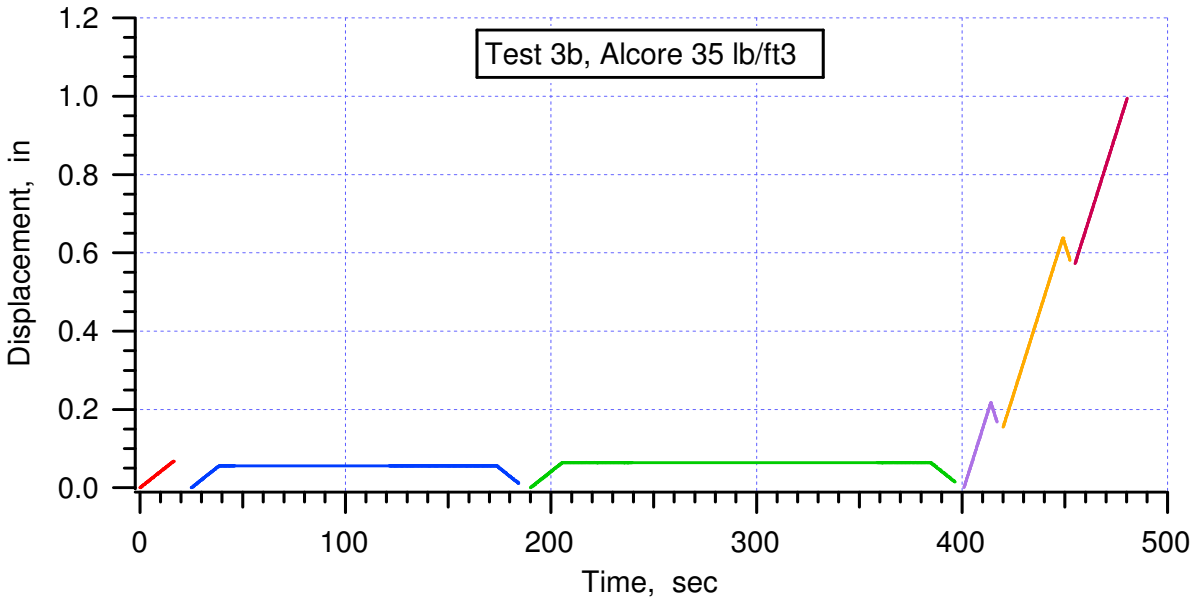
Test 3b, Alcore 35 lb/ft3
Displacement, in
1.2
1.0
0.8
0.6
0.4
0.2
0.0
0
100
200
300
400
500
Time, sec

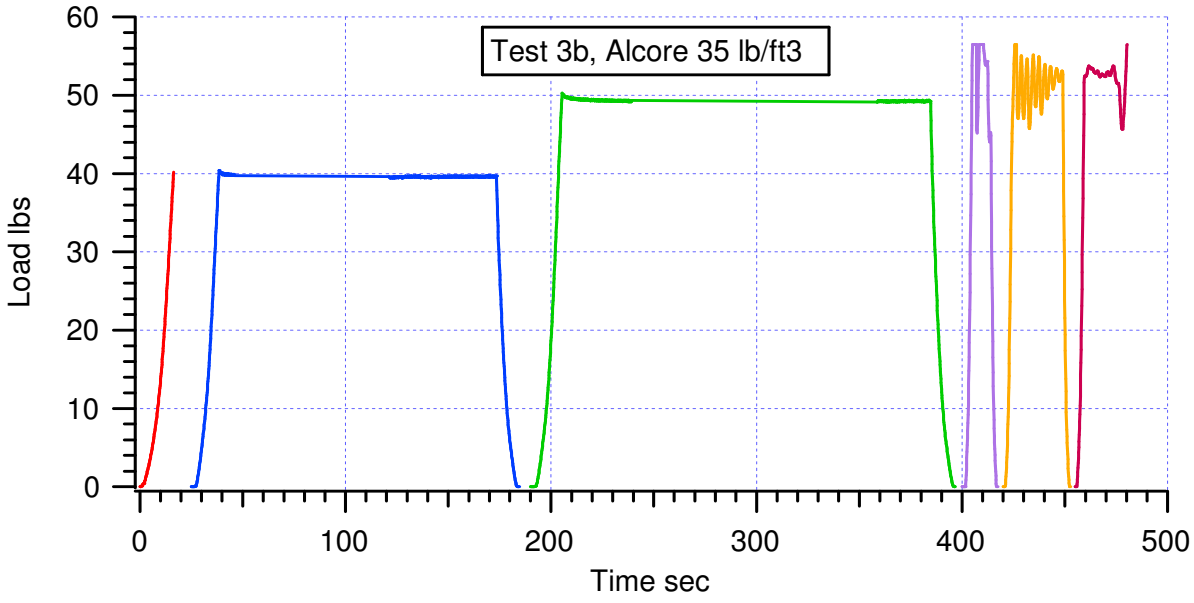
Test 3b, Alcore 35 lb/ft3
Load lbs
60
50
40
30
20
10
0
0
100
200
300
400
500
Time sec

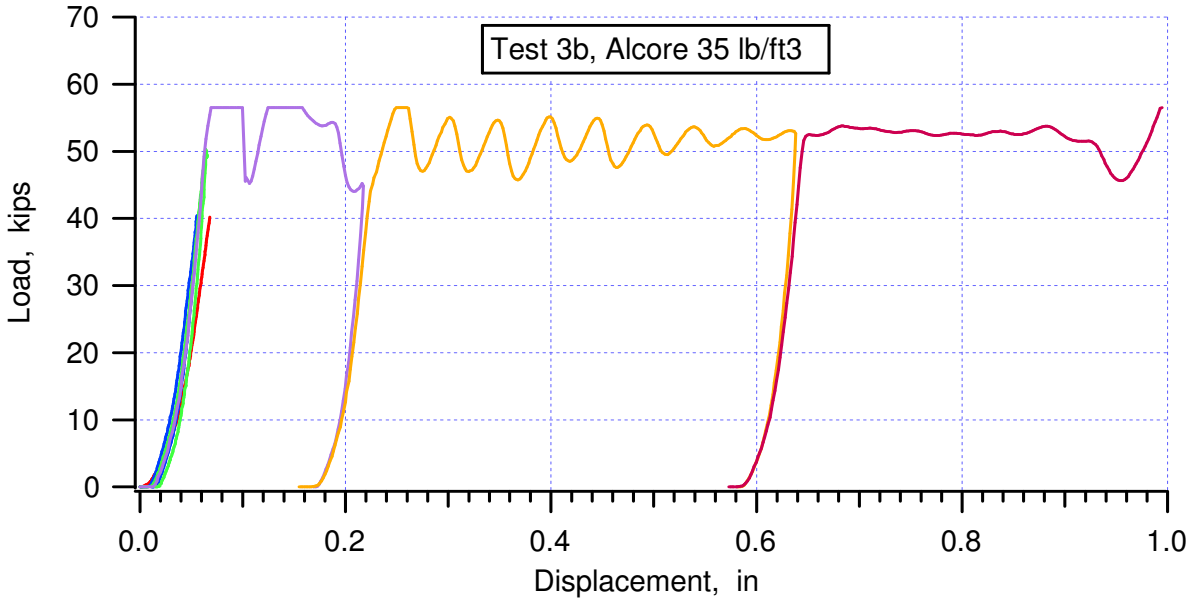
Test 3b, Alcore 35 lb/ft3
Load, kips
Displacement, in
0
10
20
30
40
50
60
70
0.0
0.2
0.4
0.6
0.8
1.0

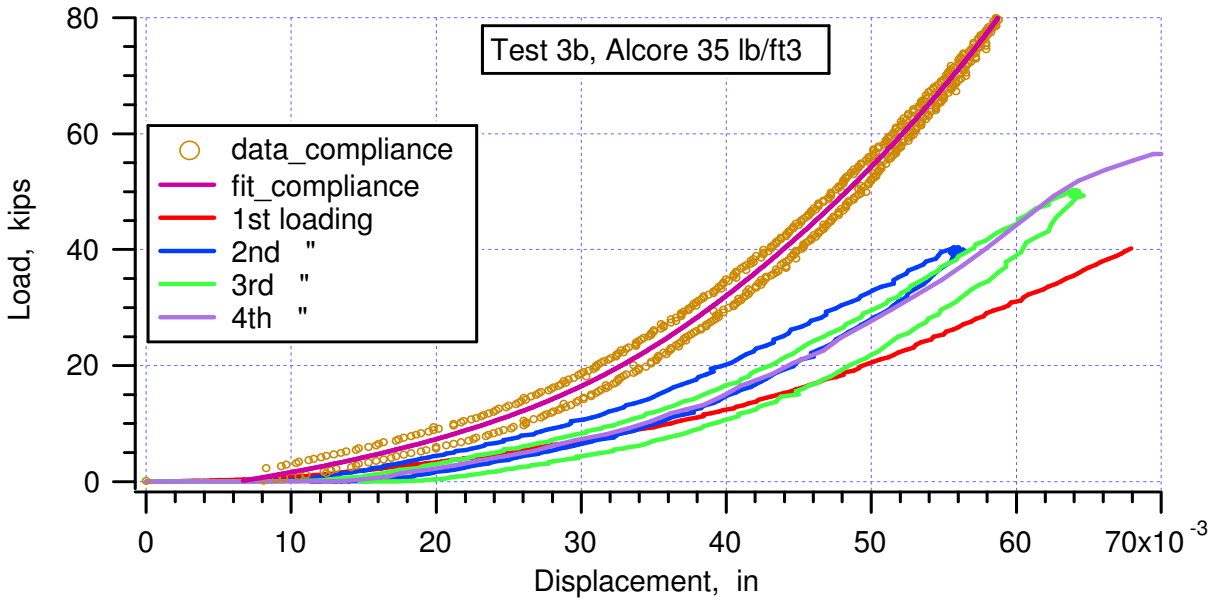
Test 3b, Alcore 35 lb/ft3
data_compliance
fit_compliance
1st loading
2nd "
3rd "
4th "
Load, kips
Displacement, in
0
20
40
60
80
0
10
20
30
40
50
60
70x10 -3

Compliance function:

displacement = - 7.0947860e-013*force^6 + 2.2713945e-010*force^5 - 2.9847316e-008*force^4 + 2.0765803e-006*force^3 - 8.3726978e-005*force^2 + 2.3651631e-003*force + 6.4182527e-003

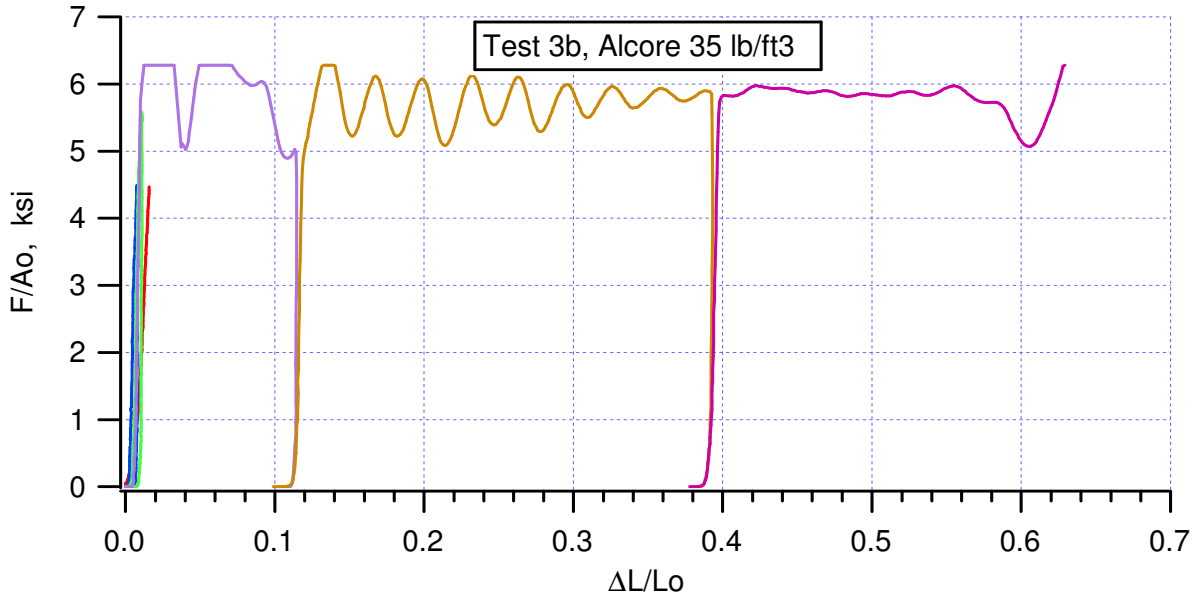

path	Elastic modulus, x10^6 psi	Start (in/in, ksi)	End (in/in, ksi)
1st	0.550	(0.0106, 1.9229)	(0.0143, 3.7413)
2nd	1.165	(0.0037, 1.0221)	(0.0058, 3.1971)
3rd	1.357	(0.0069, 1.0156)	(0.0816, 3.9729)
4th	1.523	(0.0072, 1.0229)	(0.0090, 3.8537)
5th	1.211	(0.1154, 1.5693)	(0.1173, 3.6490)
6th	0.968	(0.3927, 1.1506)	(0.3957, 4.0901)

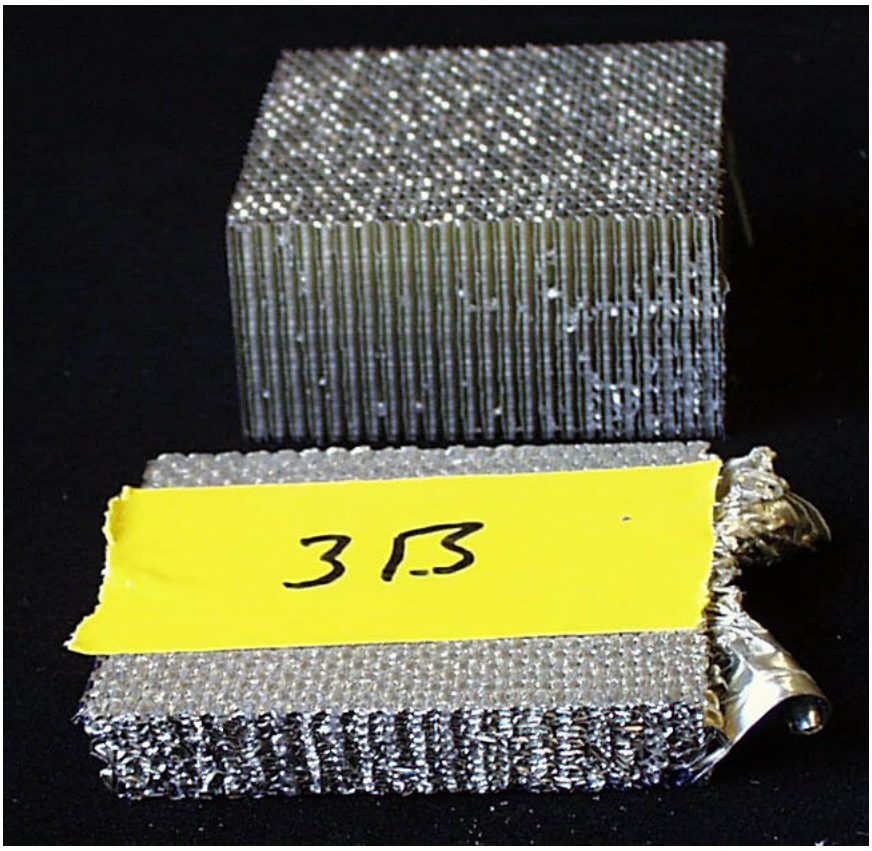
3 B

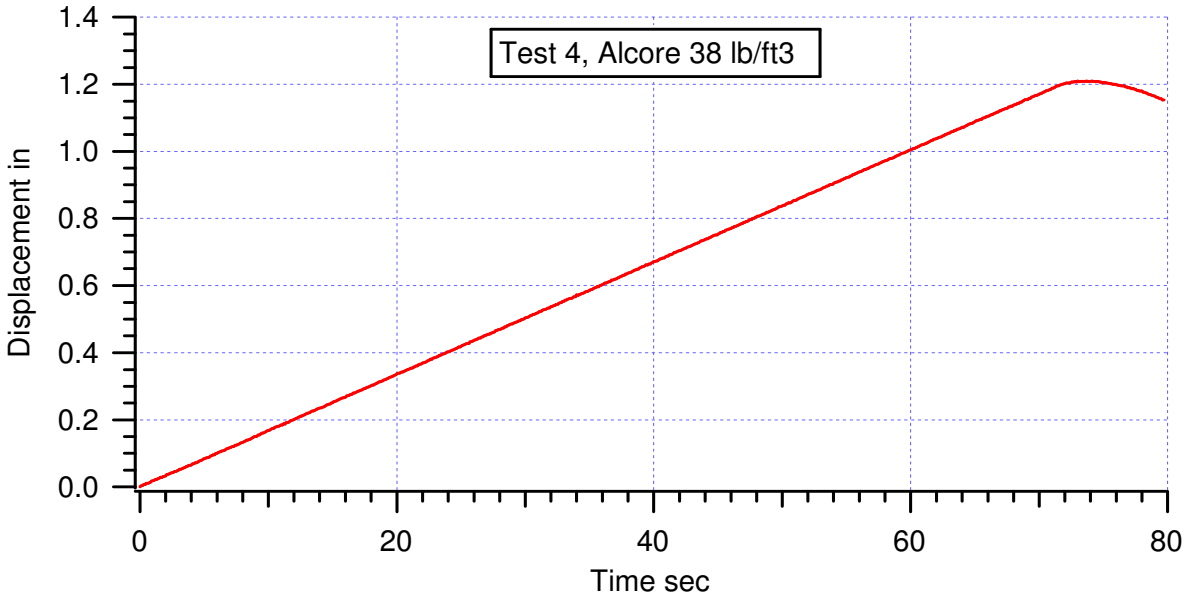
Test 4, Alcore 38 lb/ft3
Displacement in
Time sec
0.0
0.2
0.4
0.6
0.8
1.0
1.2
1.4
0
20
40
60
80

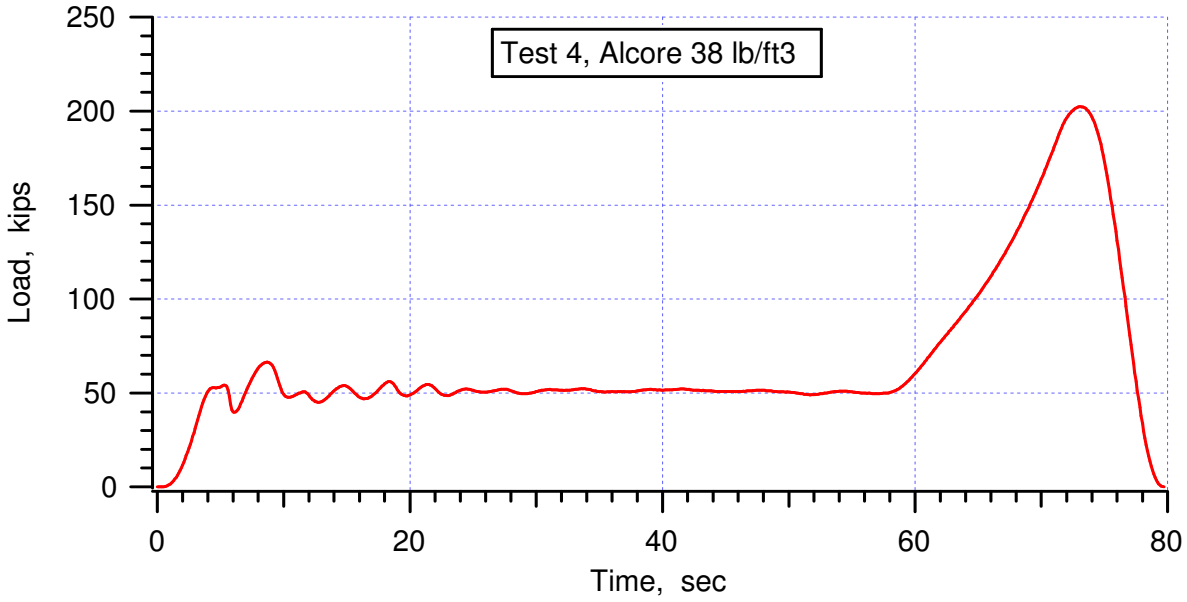
Test 4, Alcore 38 lb/ft3
Load, kips
250
200
150
100
50
0
0
20
40
60
80
Time, sec

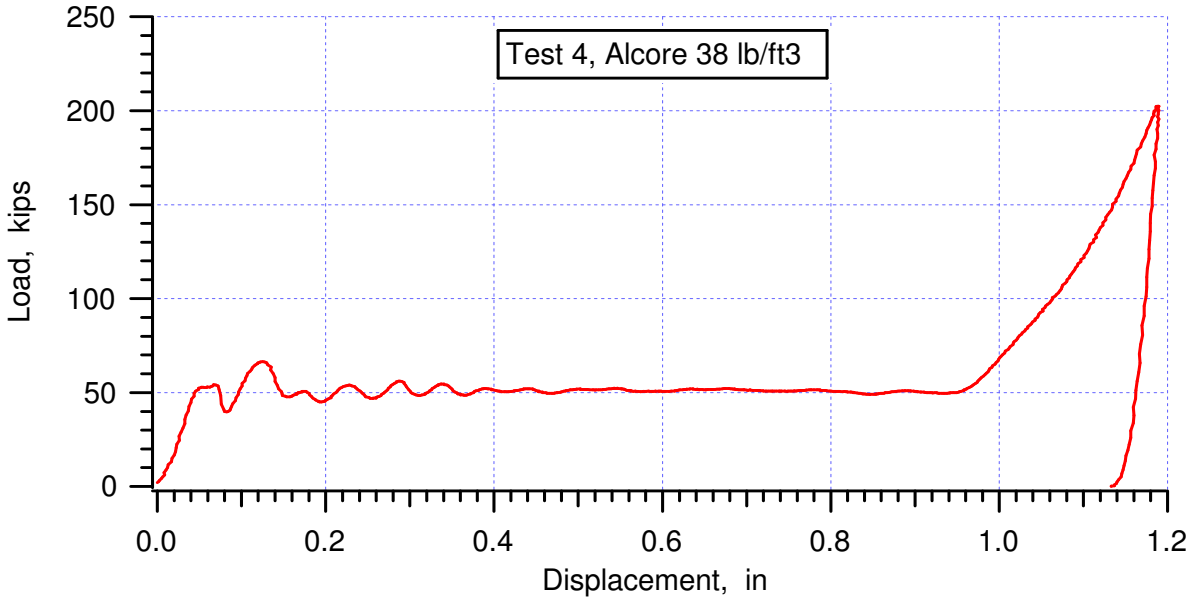
Test 4, Alcore 38 lb/ft3
Load, kips
250
200
150
100
50
0
0.0
0.2
0.4
0.6
0.8
1.0
1.2
Displacement, in

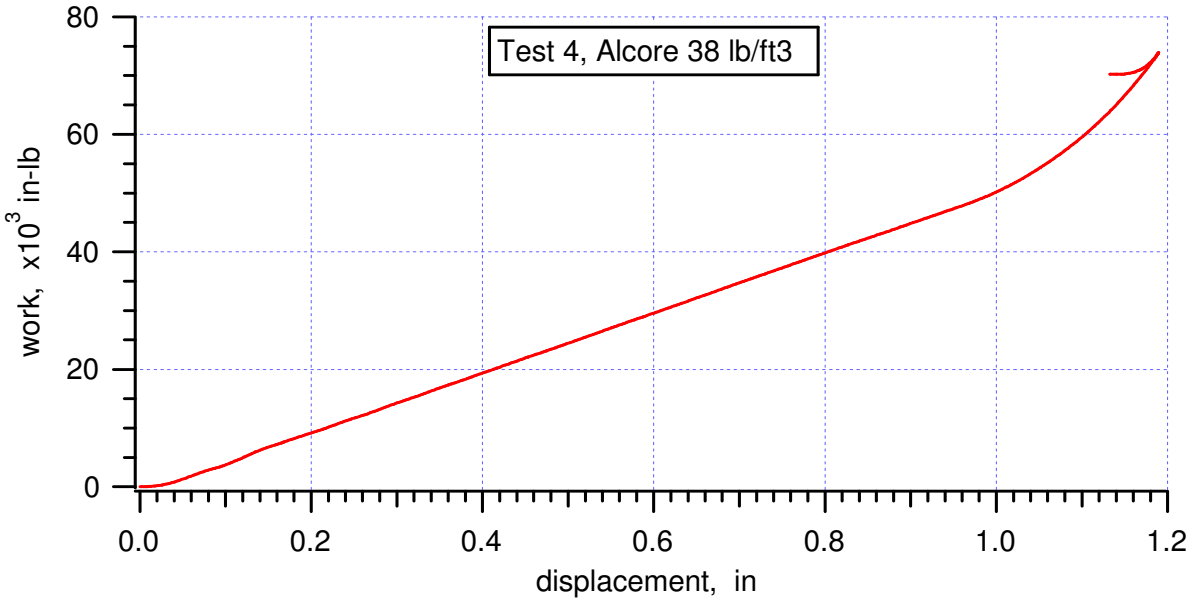
Test 4, Alcore 38 lb/ft3
work, x10^3 in-lb
80
60
40
20
0
0.0
0.2
0.4
0.6
0.8
1.0
1.2
displacement, in

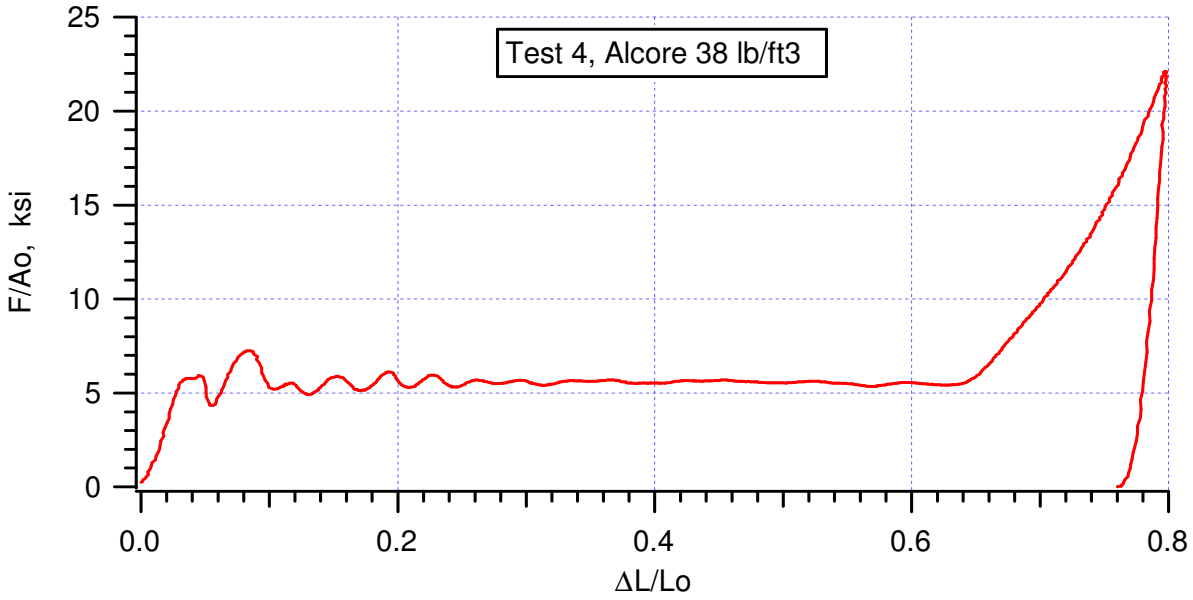

compressive peak = 7.254 ksi at 8.38%

average crush strength = 5.59 ksi averaged from (5.53%, 4.3398 ksi) to (62.8%, 5.423 ksi)

crush efficiency = 60.56% from (4.51%, 5.93 ksi) to (65.07%, 5.93 ksi)

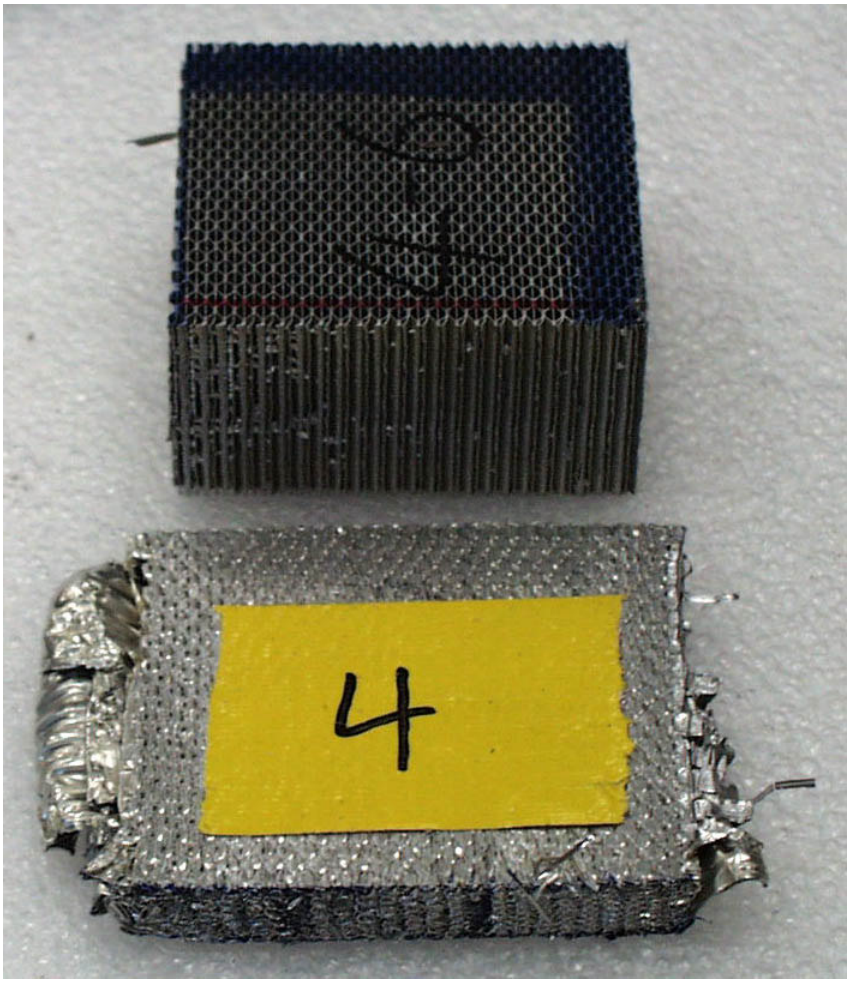
4

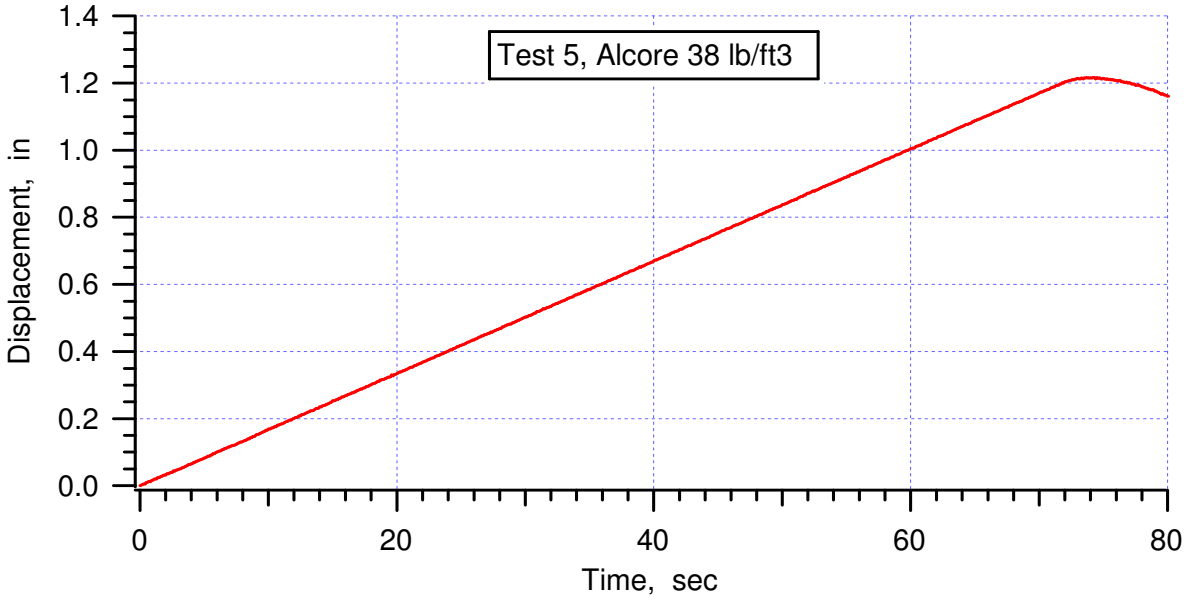
Test 5, Alcore 38 lb/ft3
Displacement, in
1.4
1.2
1.0
0.8
0.6
0.4
0.2
0.0
0
20
40
60
80
Time, sec

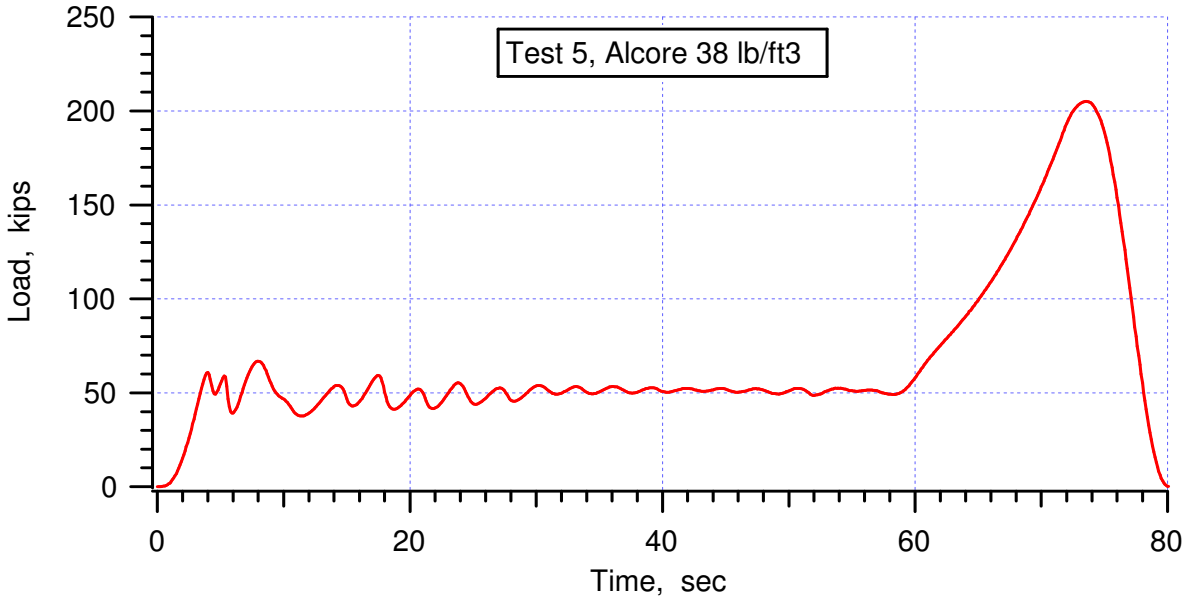
Test 5, Alcore 38 lb/ft3
Load, kips
250
200
150
100
50
0
0
20
40
60
80
Time, sec

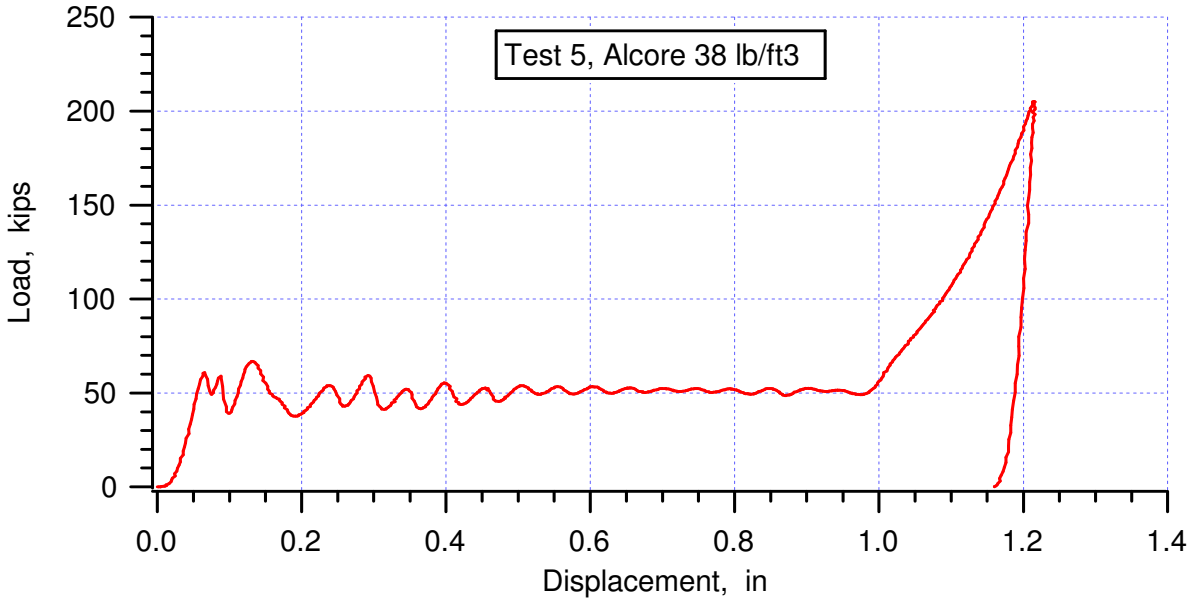
Test 5, Alcore 38 lb/ft3
Load, kips
250
200
150
100
50
0
0.0
0.2
0.4
0.6
0.8
1.0
1.2
1.4
Displacement, in

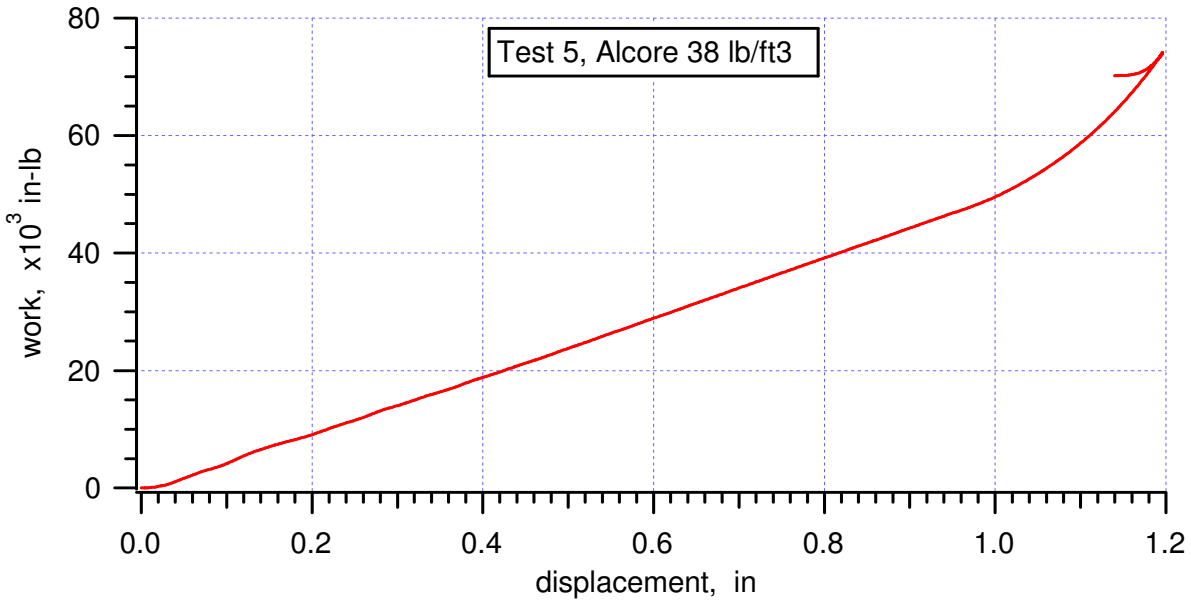
Test 5, Alcore 38 lb/ft3
work, x10^3 in-lb
80
60
40
20
0
0.0
0.2
0.4
0.6
0.8
1.0
1.2
displacement, in

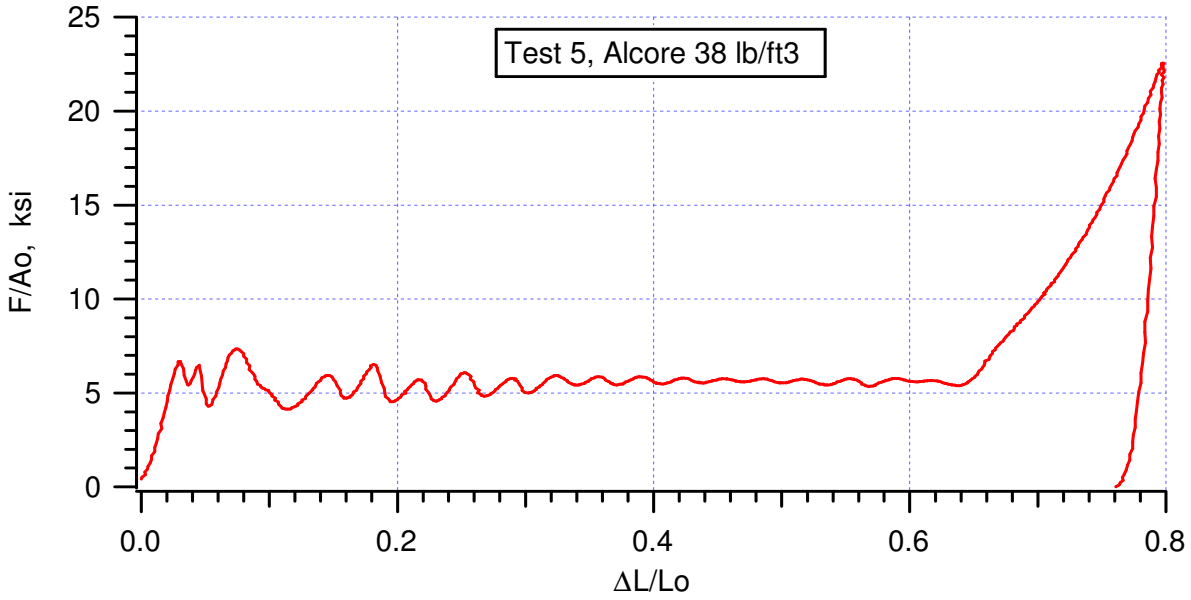

compressive peak = 7.34 ksi at 7.37%

average crush strength = 5.5113 ksi averaged from (3.69%, 5.4237 ksi) to (63.9%, 5.3886 ksi)

crush efficiency = 62.80% from (3.05%, 6.68 ksi) to (65.85%, 6.69 ksi)

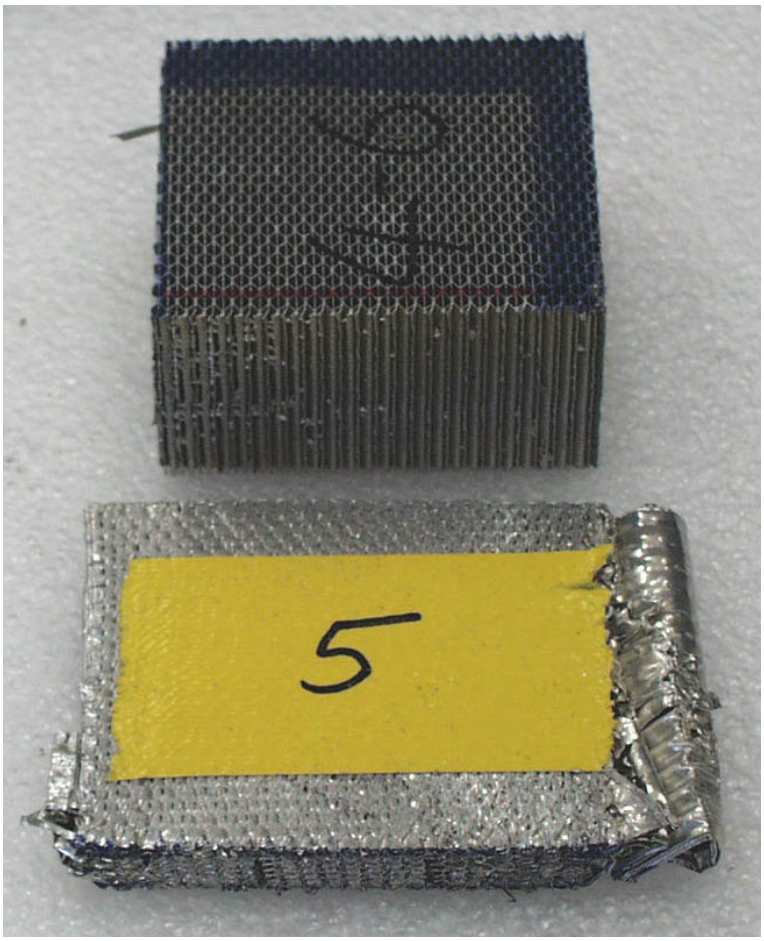

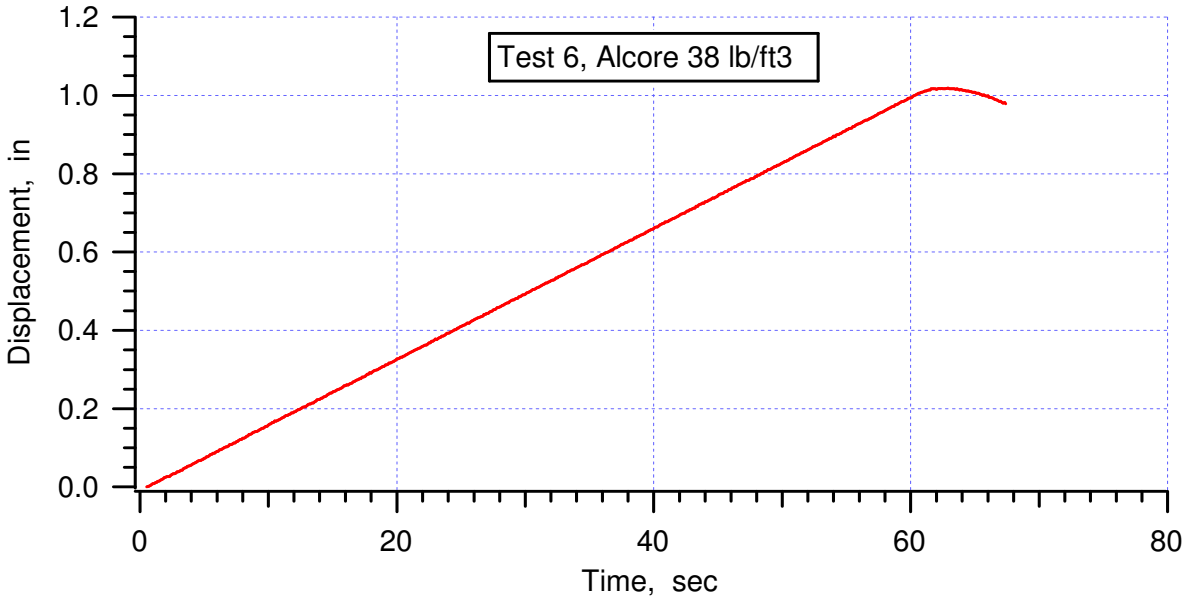
Test 6, Alcore 38 lb/ft3
Displacement, in
1.2
1.0
0.8
0.6
0.4
0.2
0.0
0
20
40
60
80
Time, sec

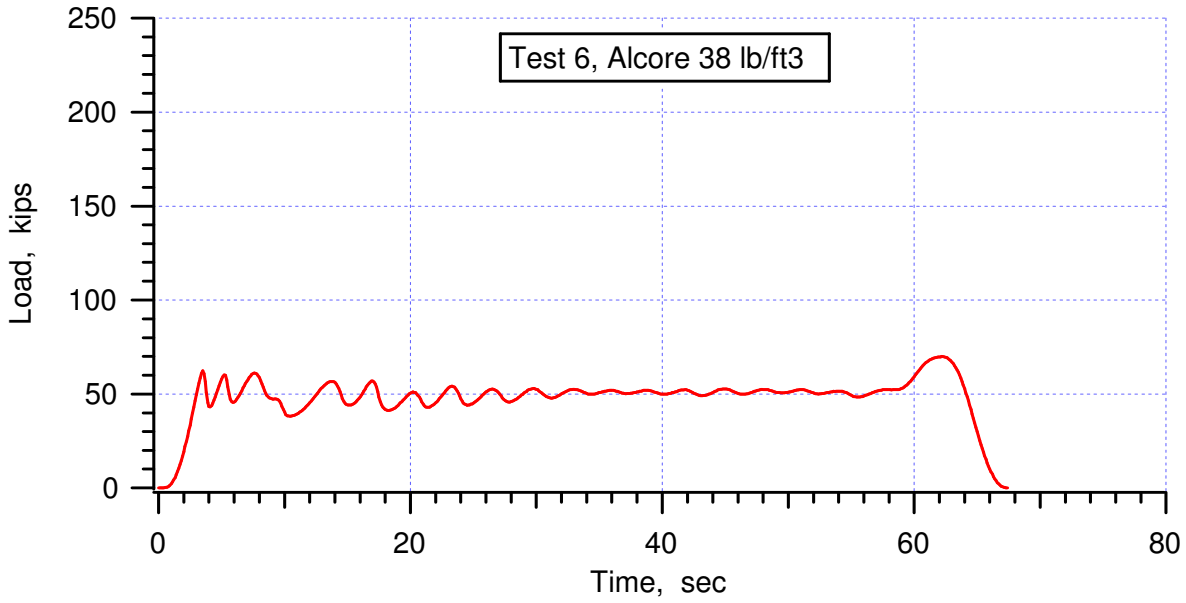
Test 6, Alcore 38 lb/ft3
Load, kips
250
200
150
100
50
0
0
20
40
60
80
Time, sec

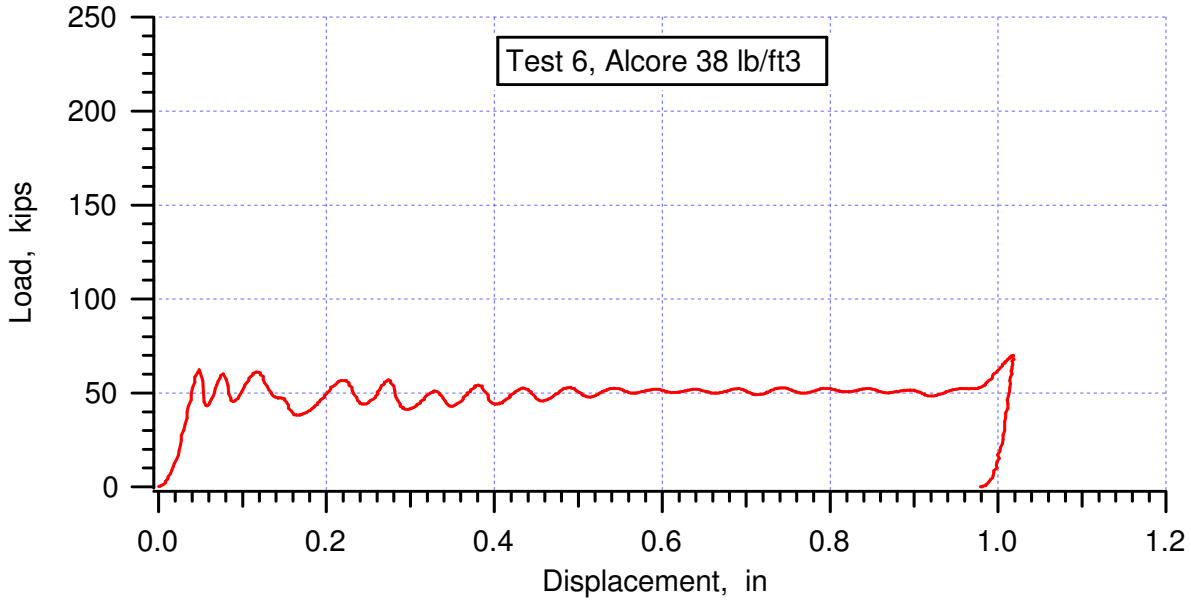
Test 6, Alcore 38 lb/ft3
Load, kips
250
200
150
100
50
0
0.0
0.2
0.4
0.6
0.8
1.0
1.2
Displacement, in

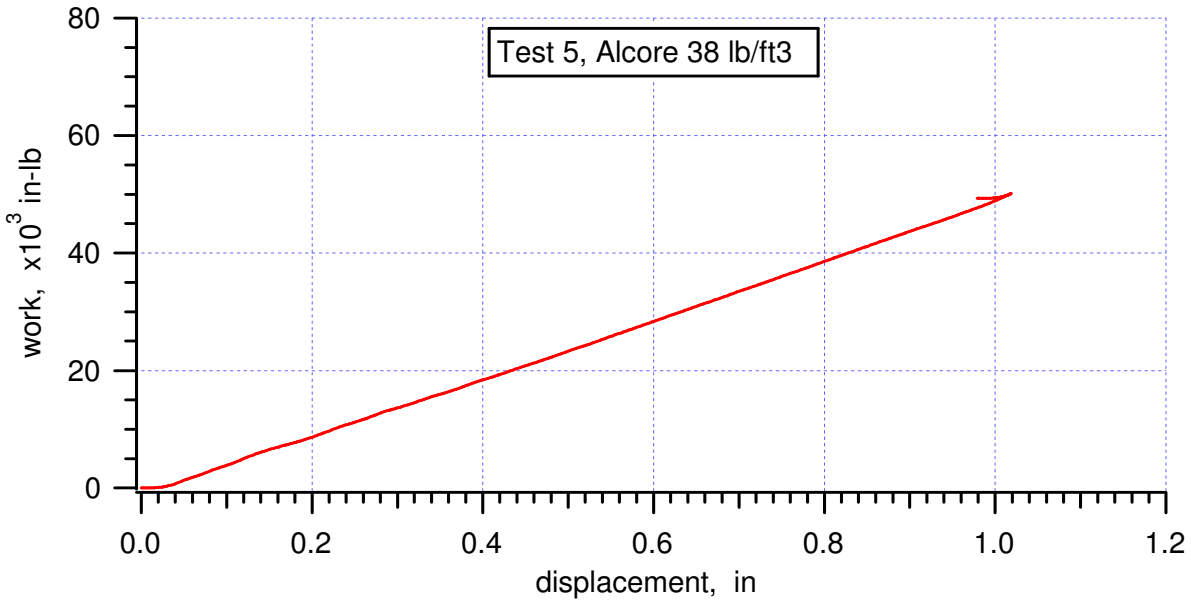
Test 5, Alcore 38 lb/ft3
work, x10^3 in-lb
80
60
40
20
0
0.0
0.2
0.4
0.6
0.8
1.0
1.2
displacement, in

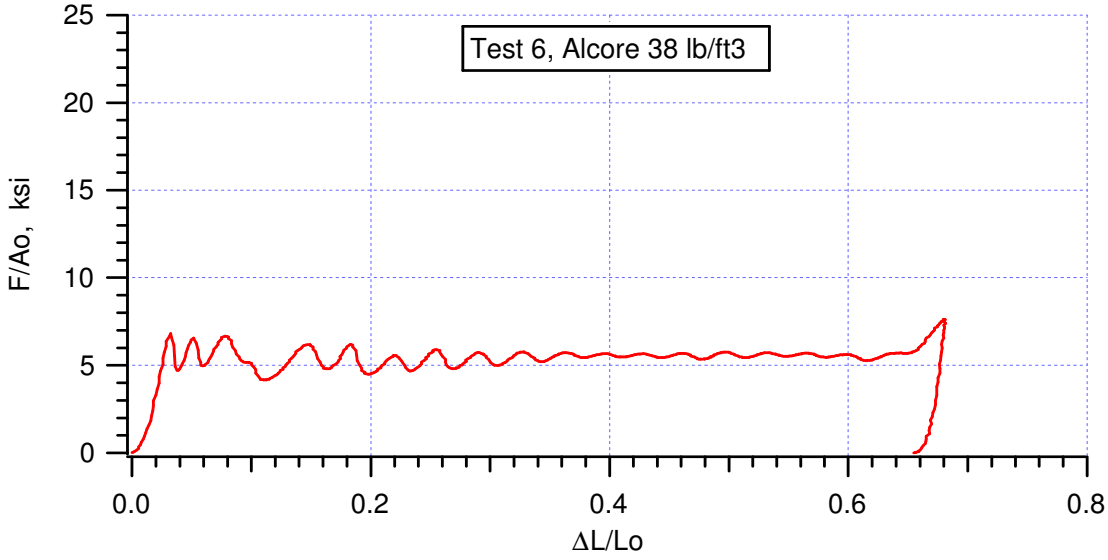

compressive peak = 6.67 ksi at 7.79%

average crush strength = 5.4443 ksi averaged from (3.88%, 4.7091 ksi) to (65.58%, 5.8044 ksi)

crush efficiency = 63.73% from (3.24%, 6.809 ksi) to (66.97%, 6.84 ksi)

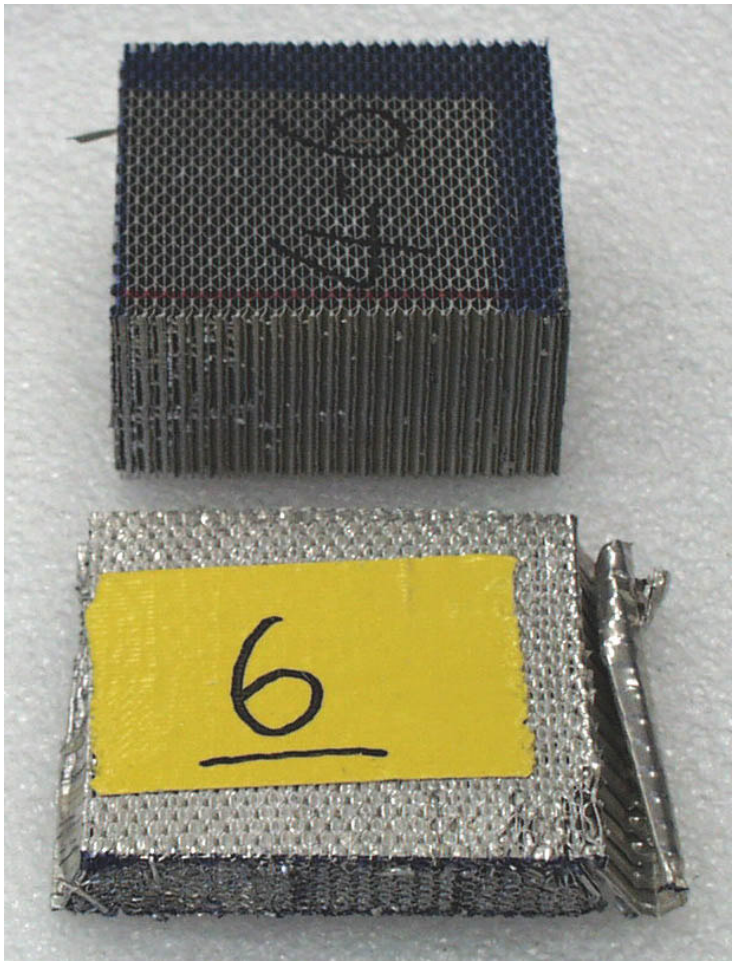

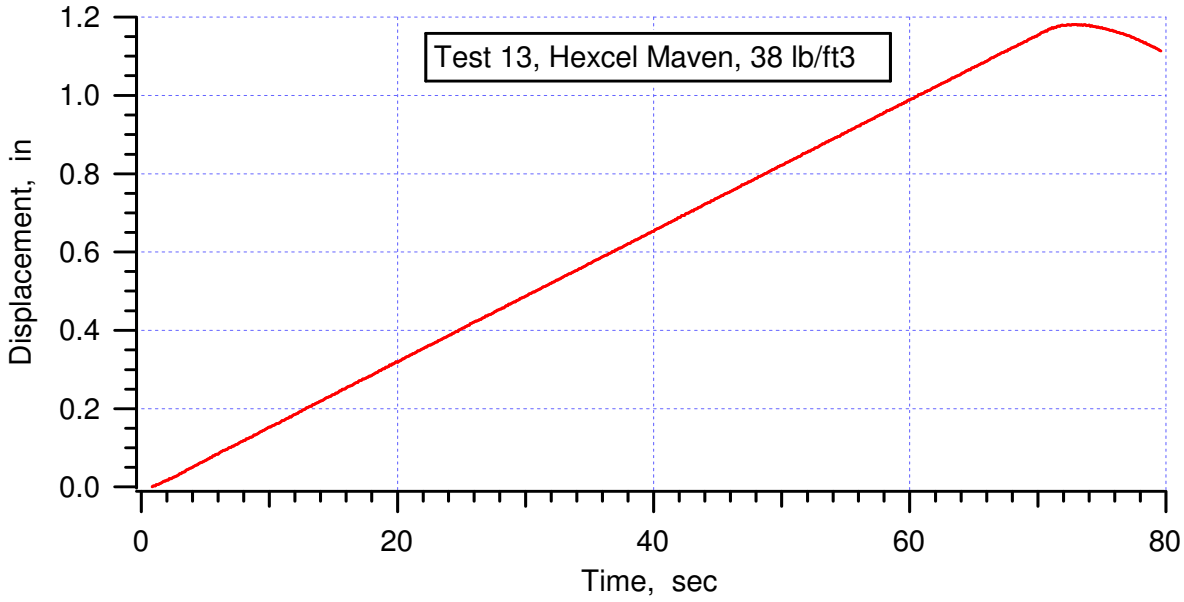
Test 13, Hexcel Maven, 38 lb/ft3
Displacement, in
1.2
1.0
0.8
0.6
0.4
0.2
0.0
0
20
40
60
80
Time, sec

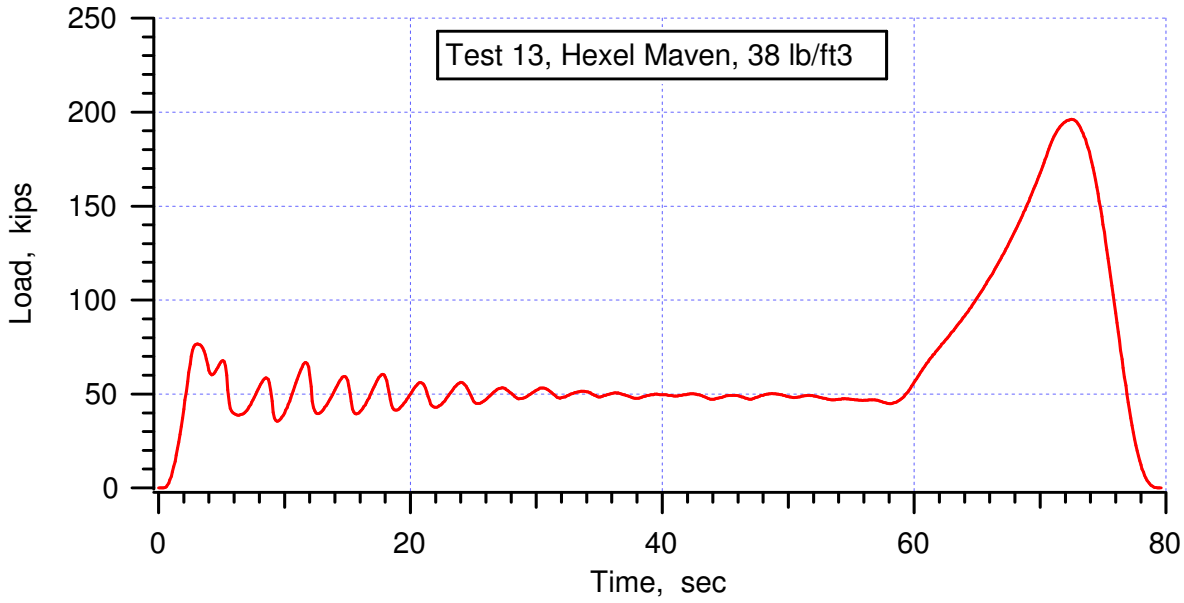
Test 13, Hexel Maven, 38 lb/ft3
Load, kips
250
200
150
100
50
0
0
20
40
60
80
Time, sec

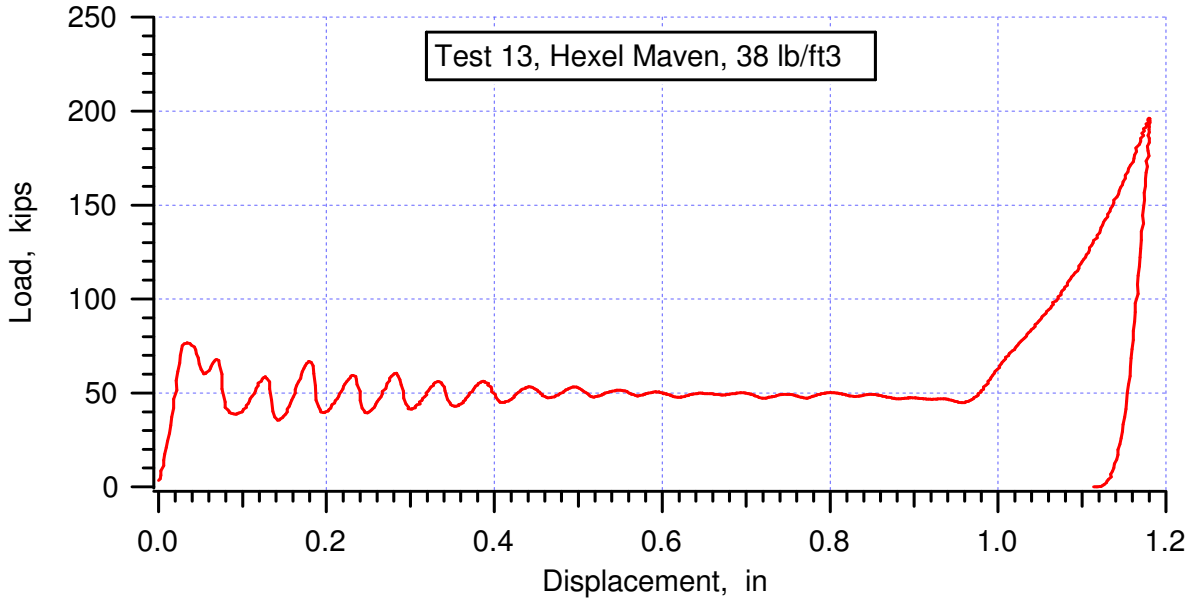
Test 13, Hexel Maven, 38 lb/ft3
Load, kips
250
200
150
100
50
0
0.0
0.2
0.4
0.6
0.8
1.0
1.2
Displacement, in

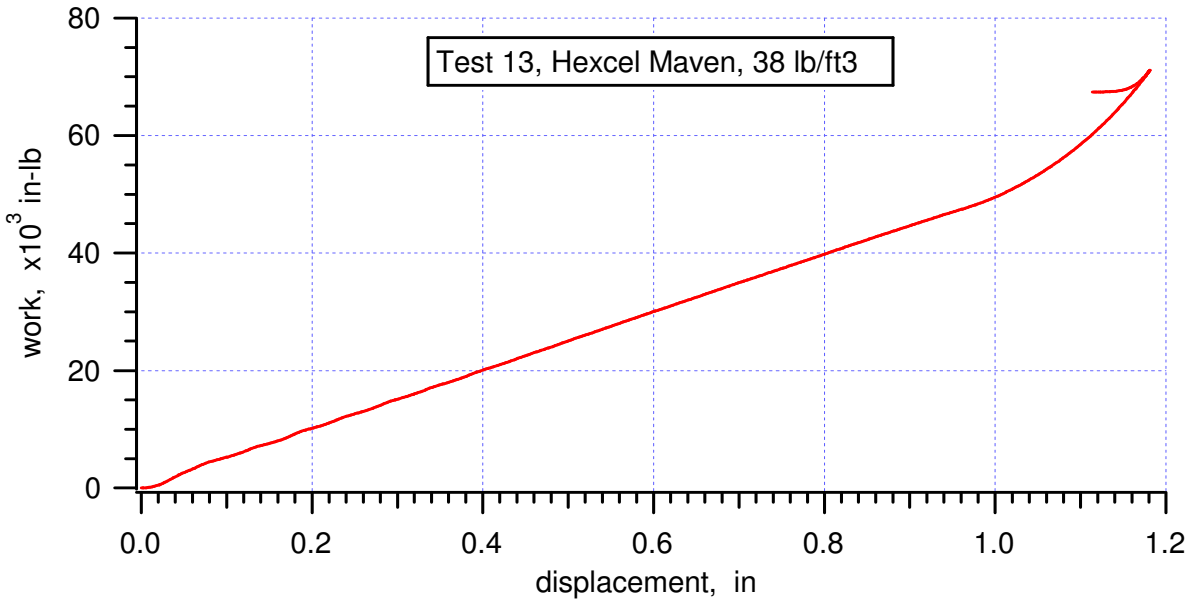
Test 13, Hexcel Maven, 38 lb/ft3
work, x10^3 in-lb
80
60
40
20
0
0.0
0.2
0.4
0.6
0.8
1.0
1.2
displacement, in

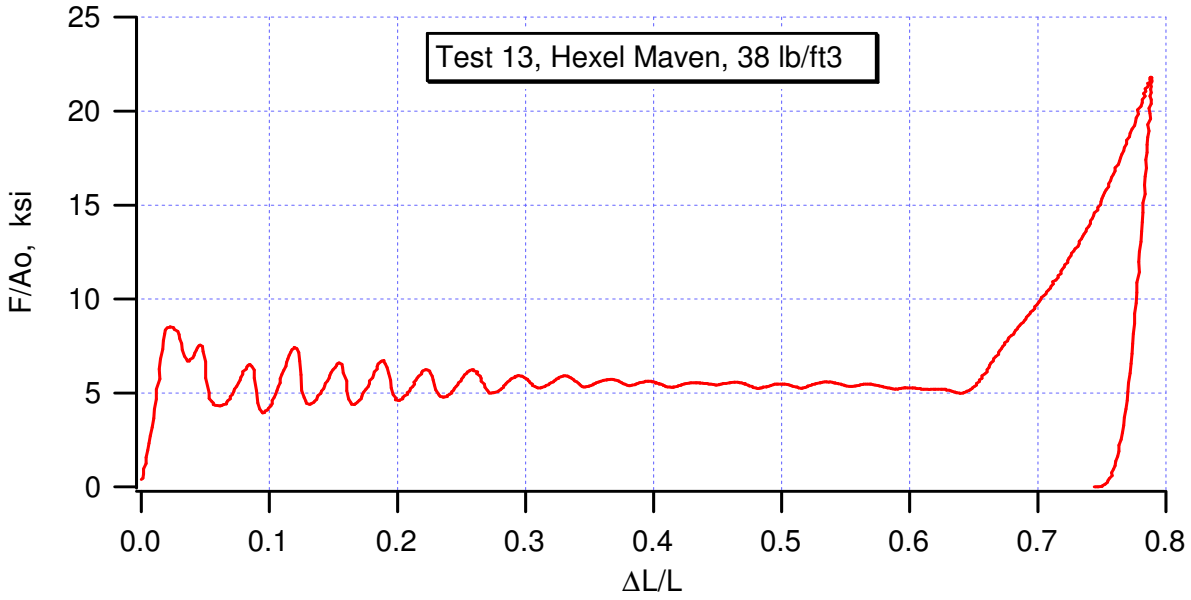

compressive peak = 8.52 ksi at 2.26%

average crush strength = 5.2446 ksi averaged from (3.54%, 6.7814 ksi) to (63.93%, 4.9811 ksi)

crush efficiency = 66.32% from (2.26%, 8.5177 ksi) to (68.58%, 8.59 ksi)

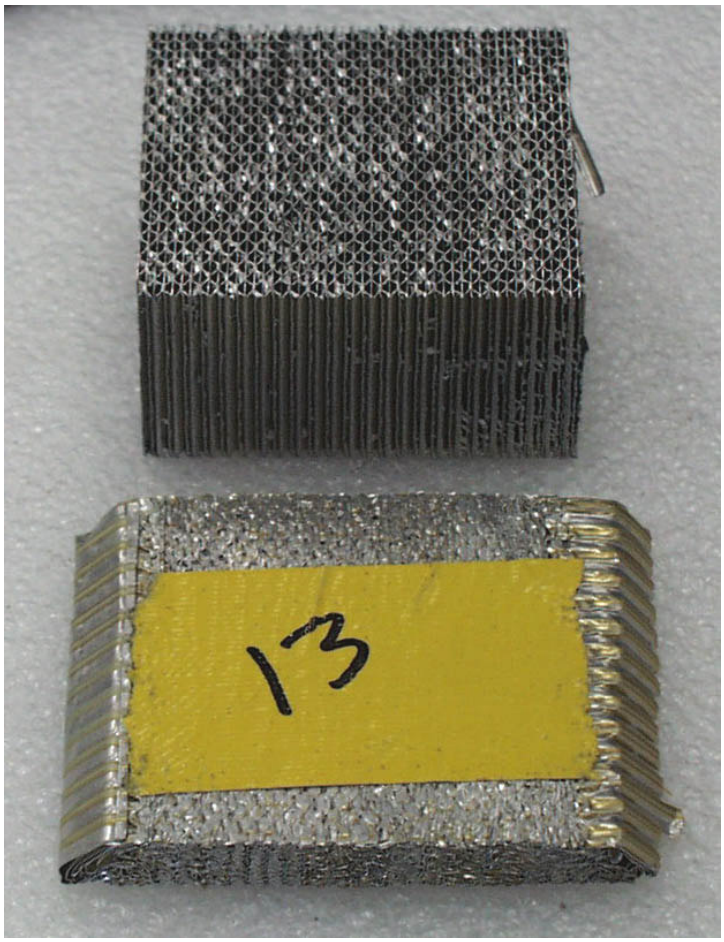

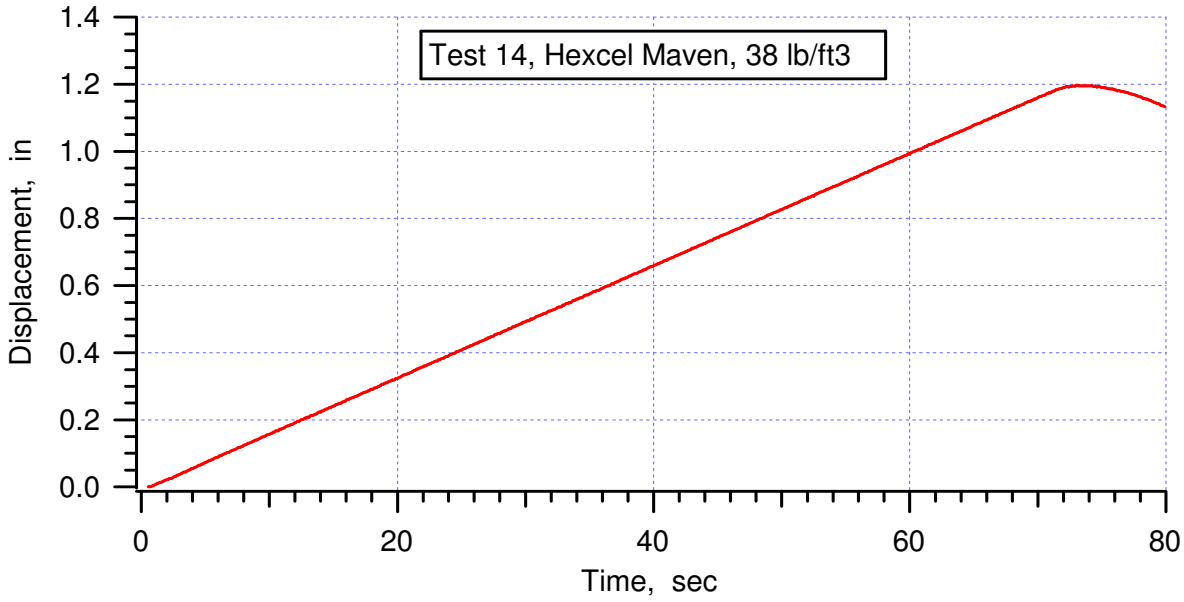
Test 14, Hexcel Maven, 38 lb/ft3
Displacement, in
1.4
1.2
1.0
0.8
0.6
0.4
0.2
0.0
0
20
40
60
80
Time, sec

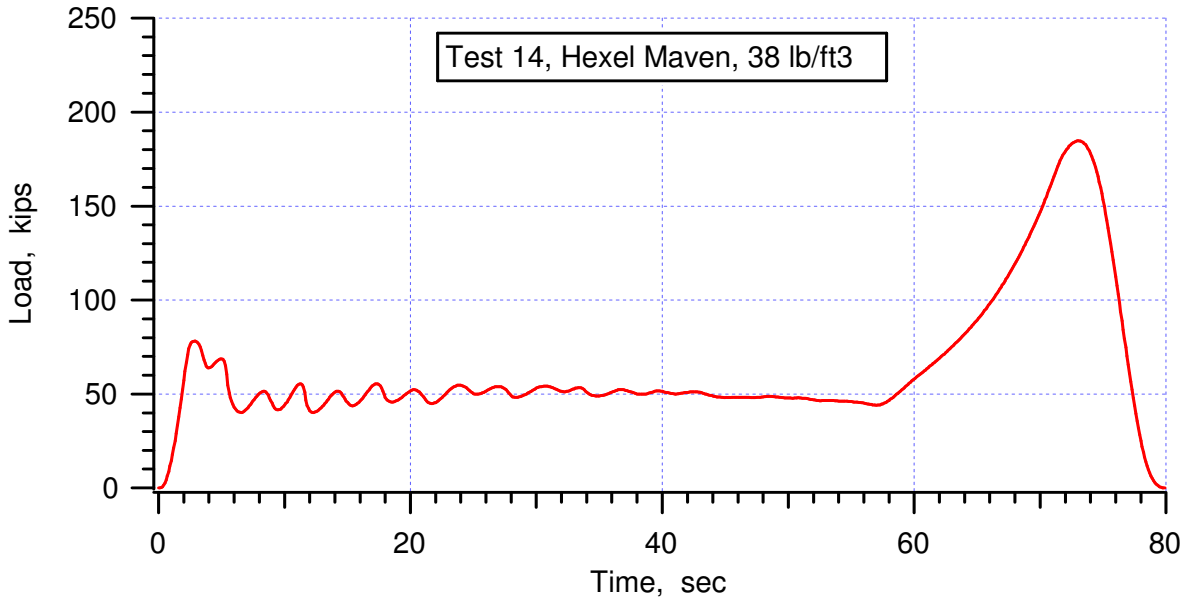
Test 14, Hexel Maven, 38 lb/ft3
Load, kips
250
200
150
100
50
0
0
20
40
60
80
Time, sec

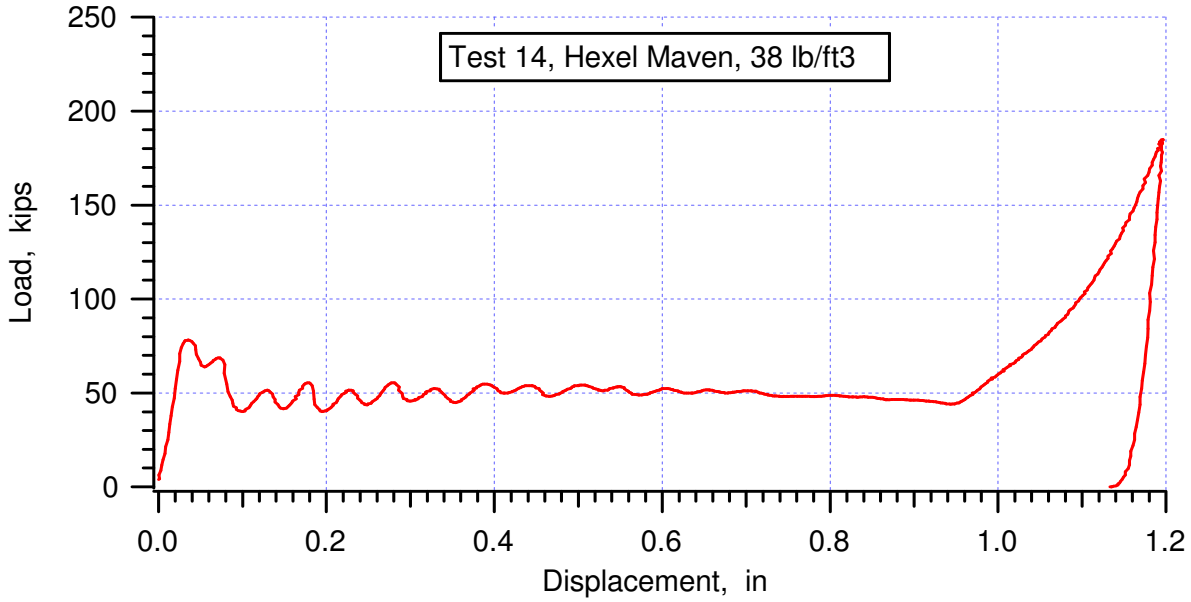
Test 14, Hexel Maven, 38 lb/ft3
Load, kips
250
200
150
100
50
0
0.0
0.2
0.4
0.6
0.8
1.0
1.2
Displacement, in

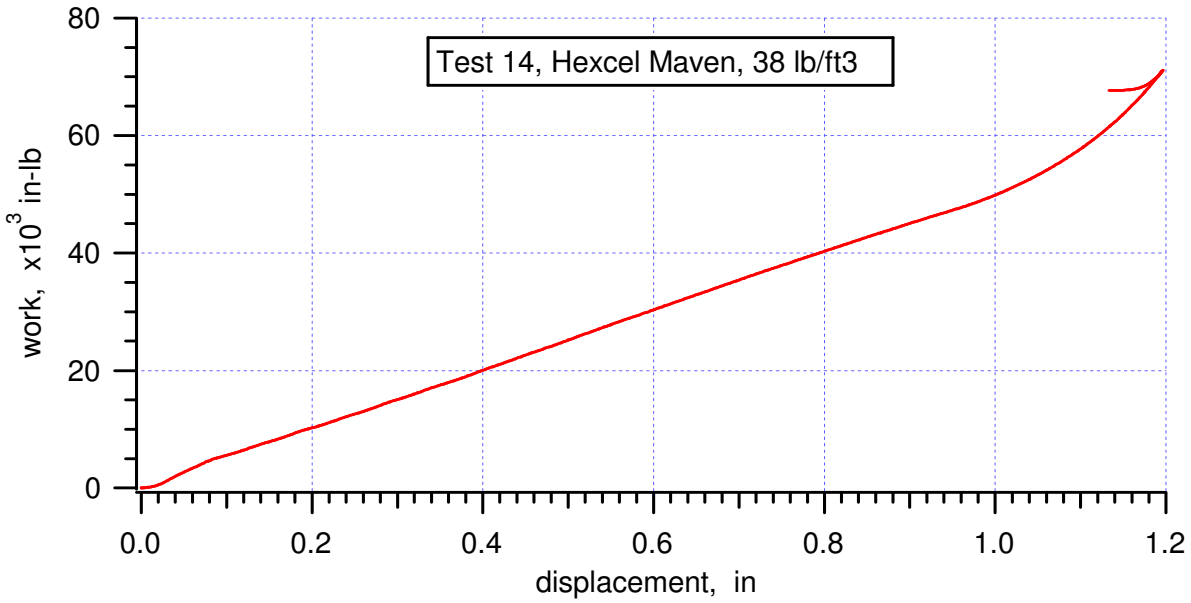
Test 14, Hexcel Maven, 38 lb/ft3
work, x10^3 in-lb
80
60
40
20
0
0.0
0.2
0.4
0.6
0.8
1.0
1.2
displacement, in

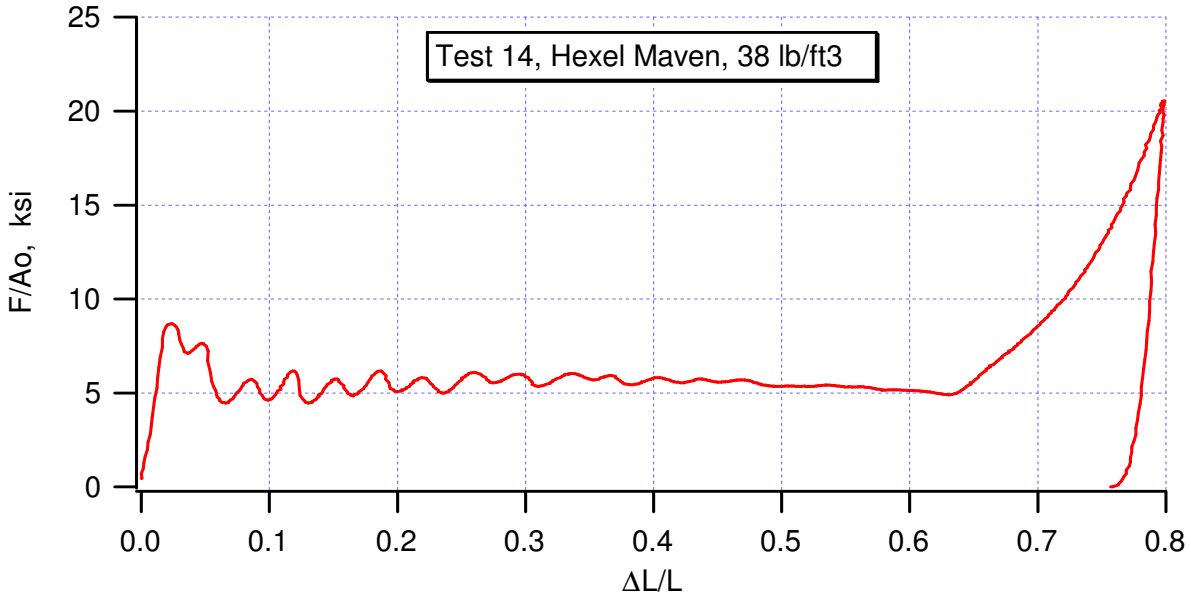

compressive peak = 8.70 ksi at 2.35%

average crush strength = 5.2381 ksi averaged from (3.63%, 7.1016 ksi) to (63.00%, 4.8957 ksi)

crush efficiency = 67.87% from (2.35%, 8.6956 ksi) to (70.22%, 8.7169 ksi)

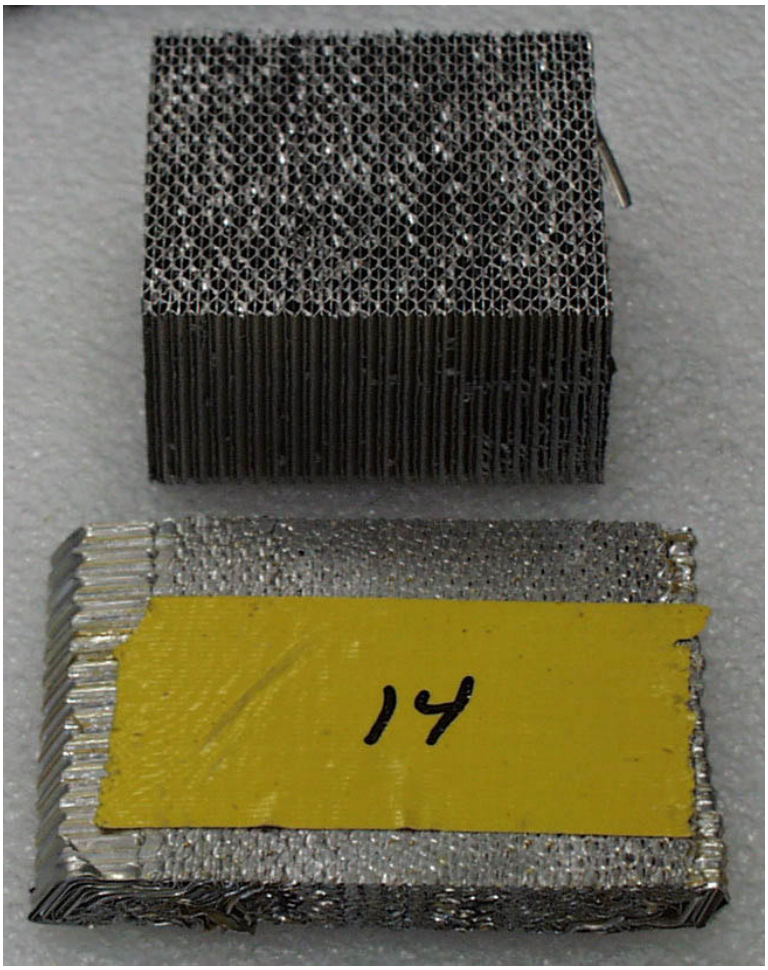

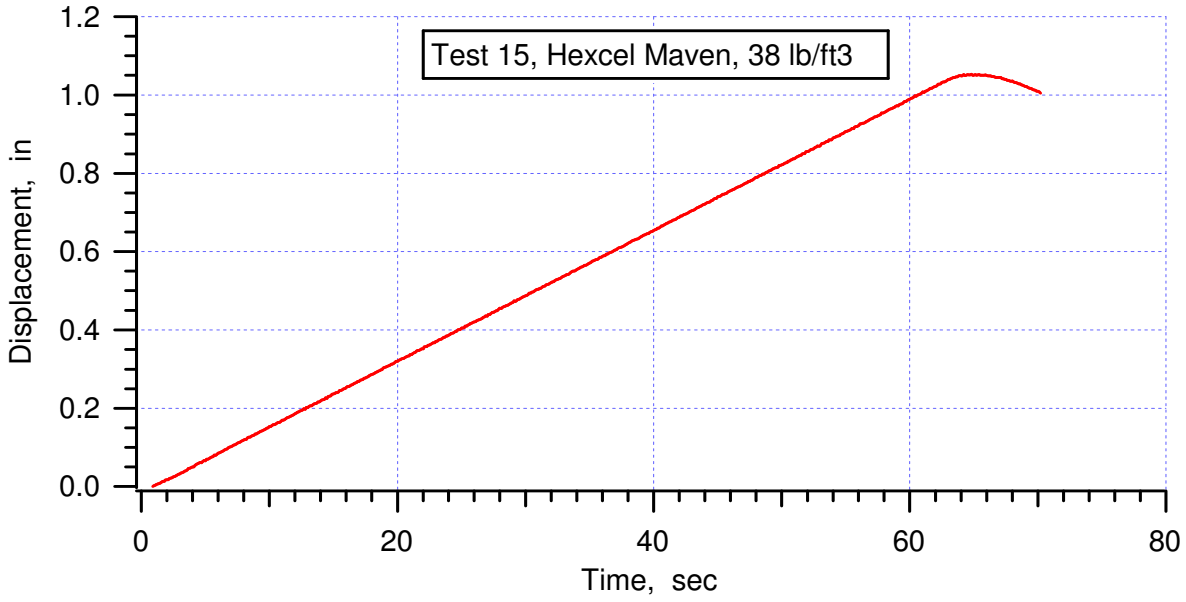
Test 15, Hexcel Maven, 38 lb/ft3
Displacement, in
1.2
1.0
0.8
0.6
0.4
0.2
0.0
0
20
40
60
80
Time, sec

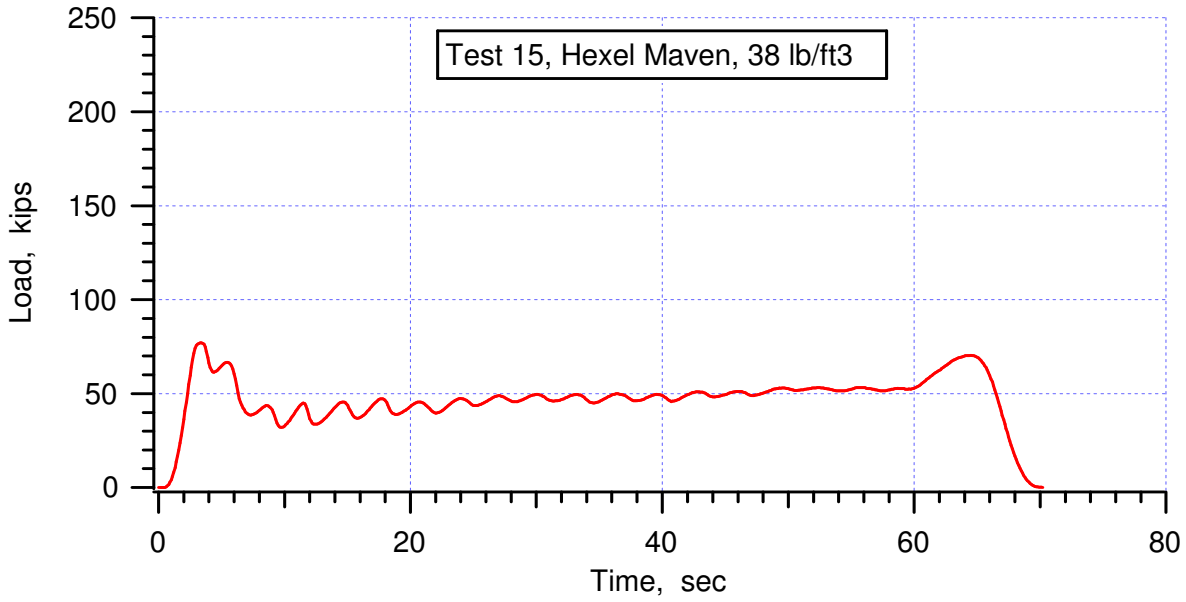
Test 15, Hexcel Maven, 38 lb/ft3
Load, kips
250
200
150
100
50
0
0
20
40
60
80
Time, sec

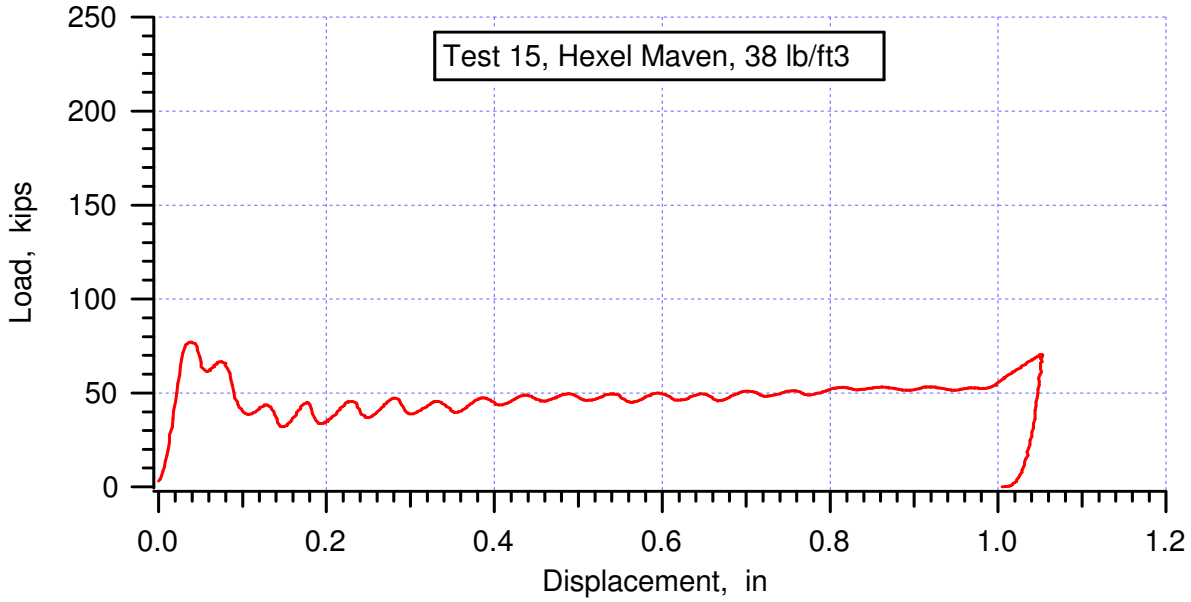
Test 15, Hexel Maven, 38 lb/ft3
Load, kips
250
200
150
100
50
0
0.0
0.2
0.4
0.6
0.8
1.0
1.2
Displacement, in

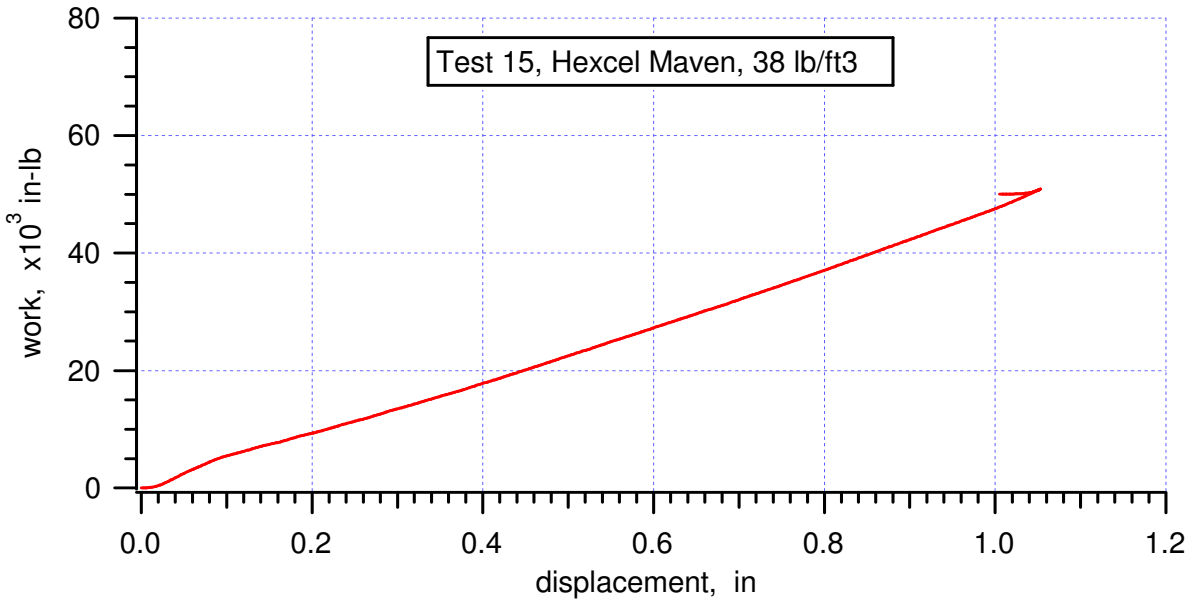
Test 15, Hexcel Maven, 38 lb/ft3
work, x10^3 in-lb
80
60
40
20
0
0.0
0.2
0.4
0.6
0.8
1.0
1.2
displacement, in

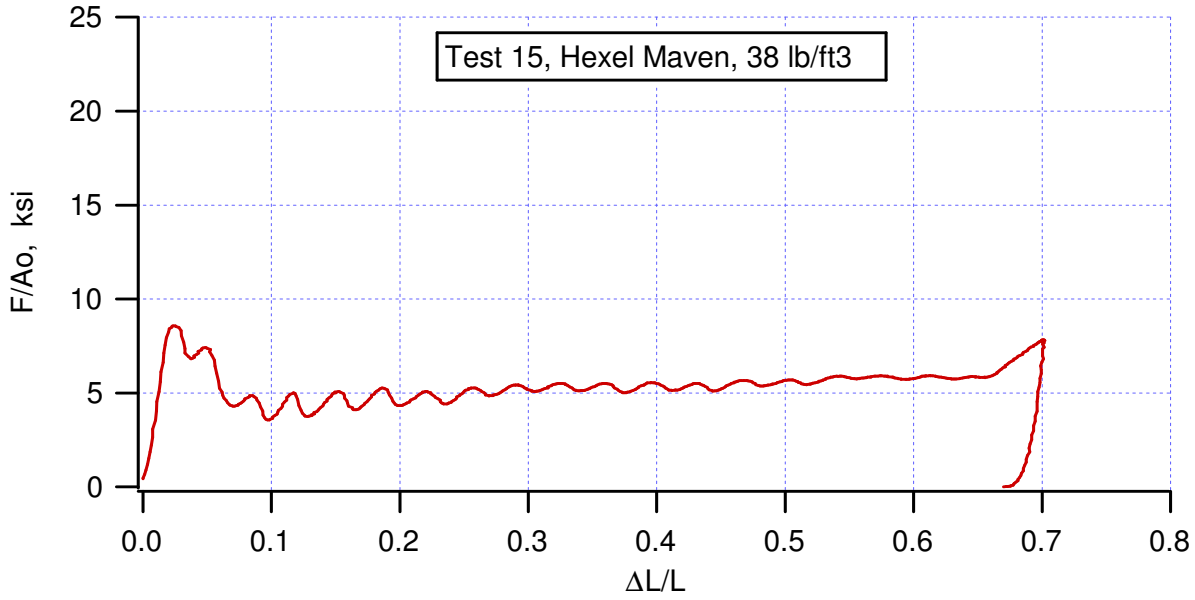

compressive peak = 8.57 ksi at 2.53%

average crush strength = 5.2548 ksi averaged from (3.76%, 6.8287 ksi) to (65.87%, 5.8674 ksi)

crush efficiency = 67.61% from (2.53%, 8.5661 ksi) to (70.14%, 7.8042 ksi)

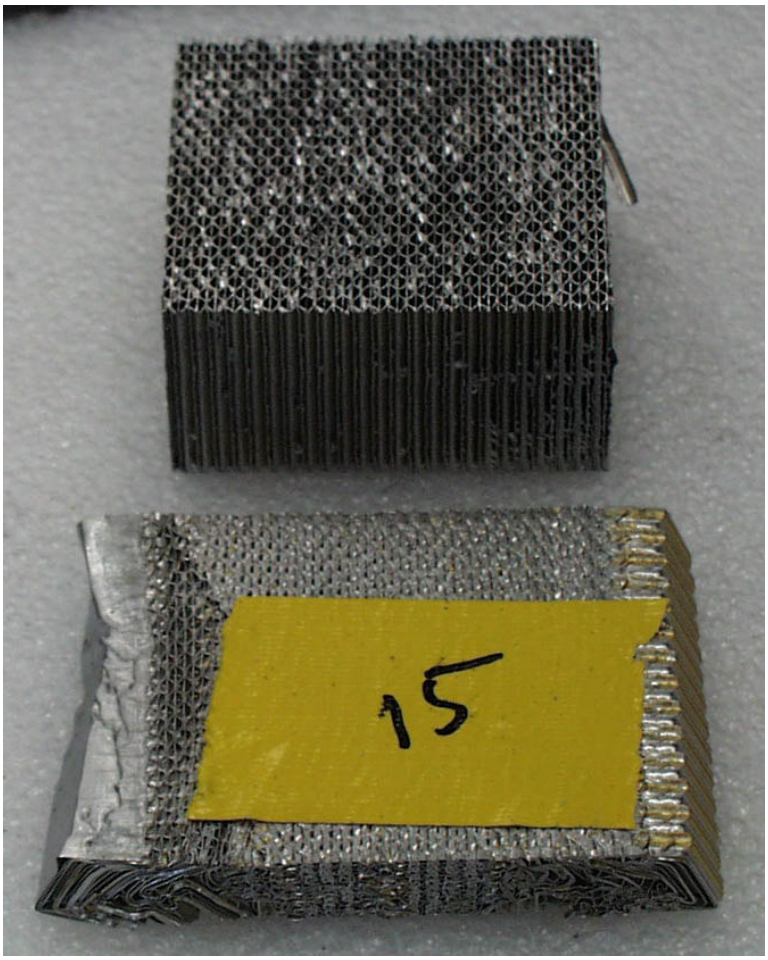

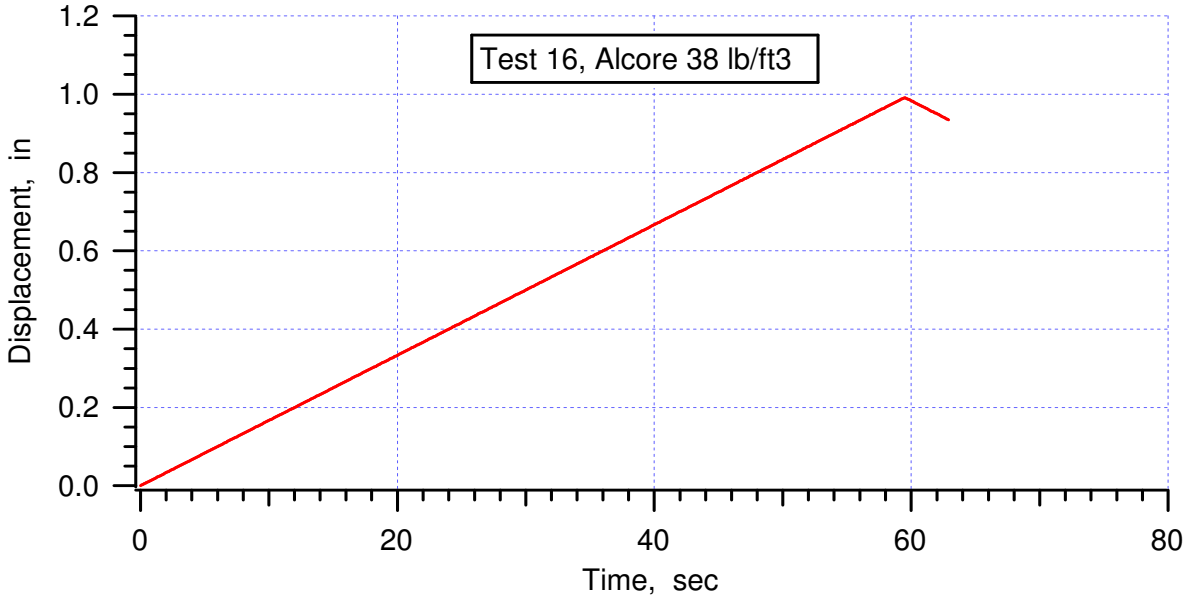
Test 16, Alcore 38 lb/ft3
Displacement, in
1.2
1.0
0.8
0.6
0.4
0.2
0.0
0
20
40
60
80
Time, sec

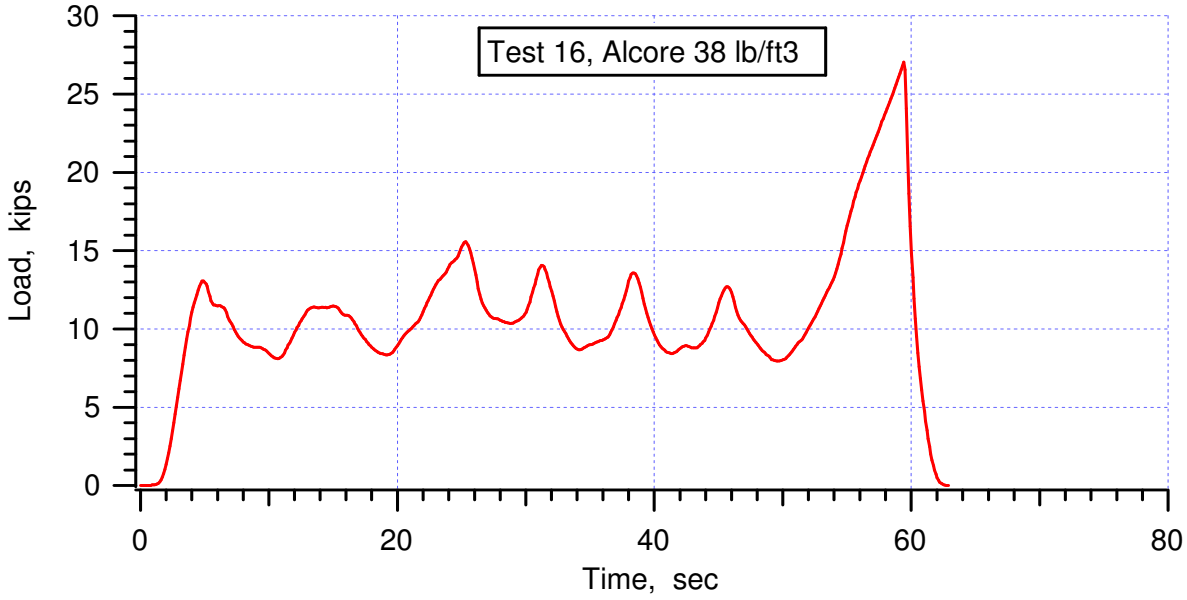
Test 16, Alcore 38 lb/ft3
Load, kips
30
25
20
15
10
5
0
0
20
40
60
80
Time, sec

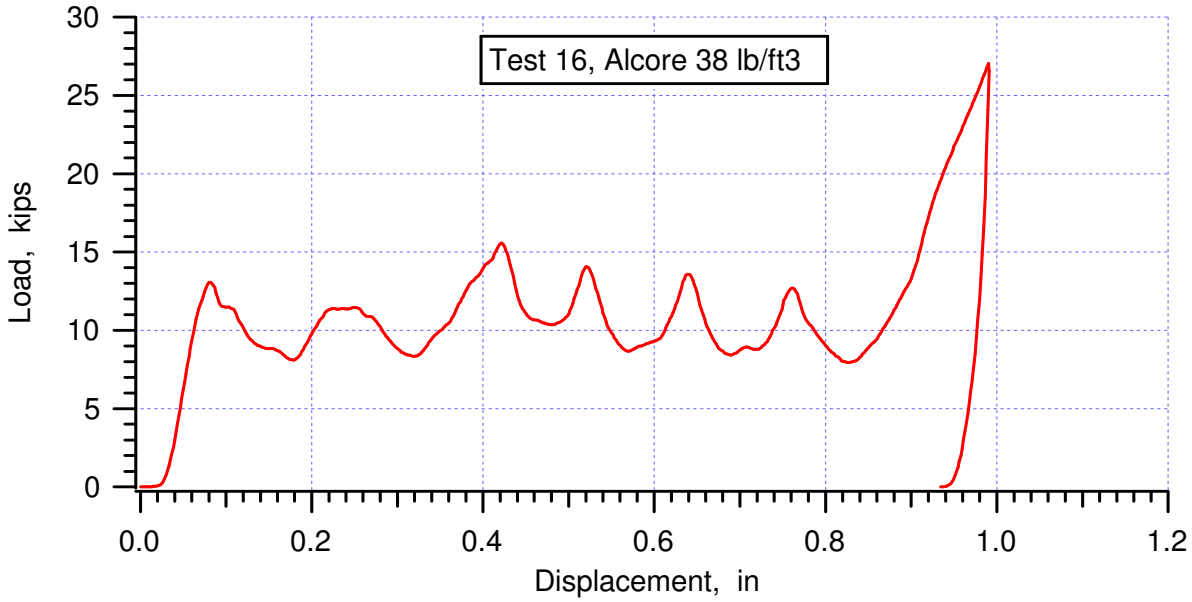
Test 16, Alcore 38 lb/ft3
Load, kips
Displacement, in
0
5
10
15
20
25
30
0.0
0.2
0.4
0.6
0.8
1.0
1.2

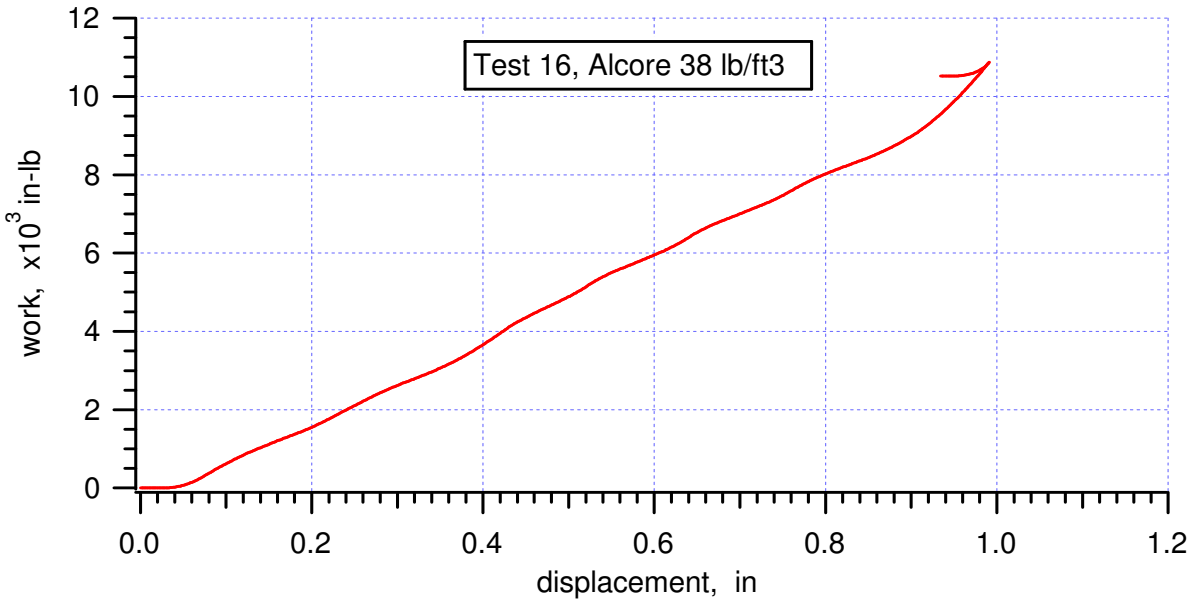
Test 16, Alcore 38 lb/ft3
work, x10^3 in-lb
displacement, in
0
2
4
6
8
10
12
0.0
0.2
0.4
0.6
0.8
1.0
1.2

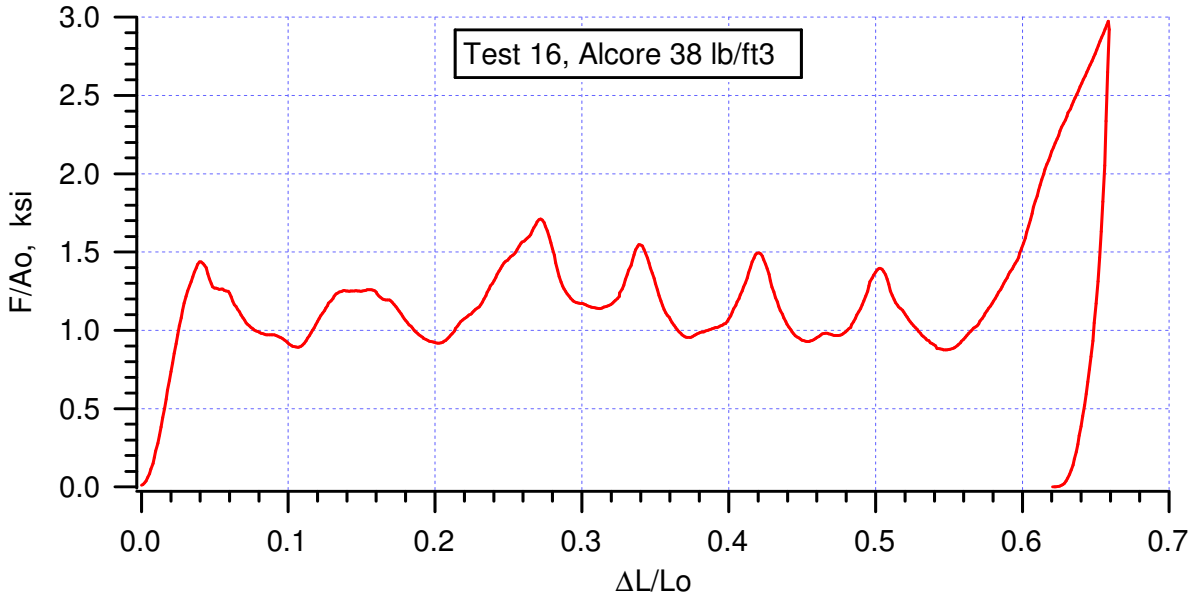

crush strength = 1.165 ksi, averaged from (0.1030, 0.8984) to (0.5477, 0.8749)

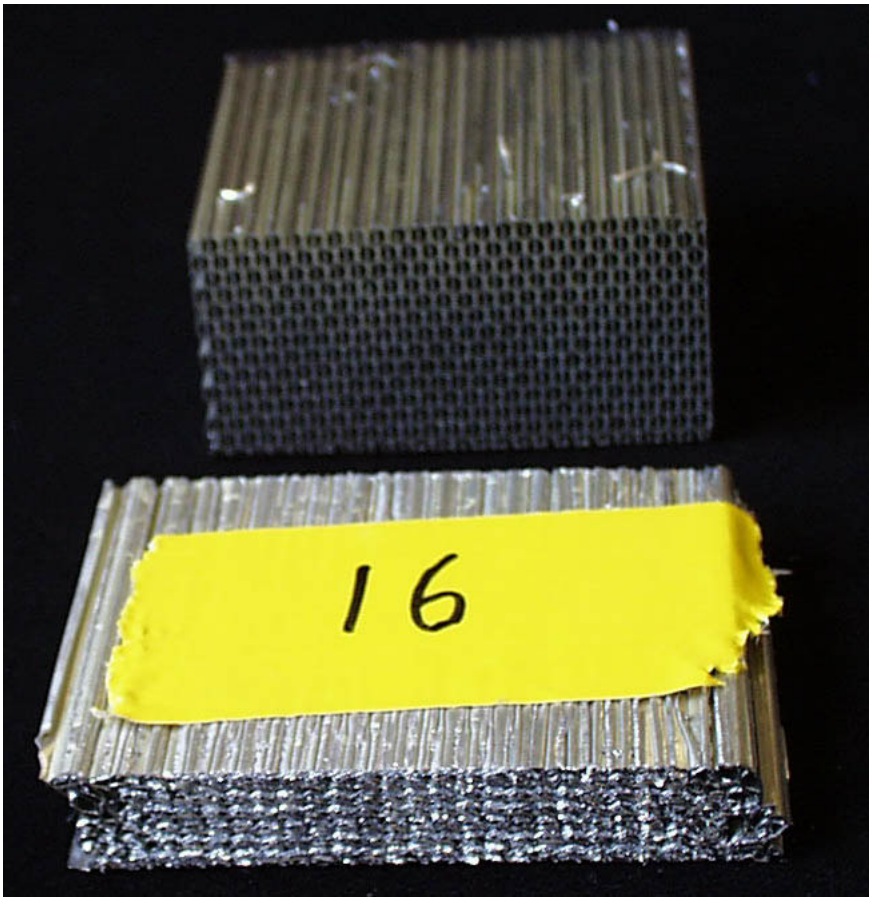

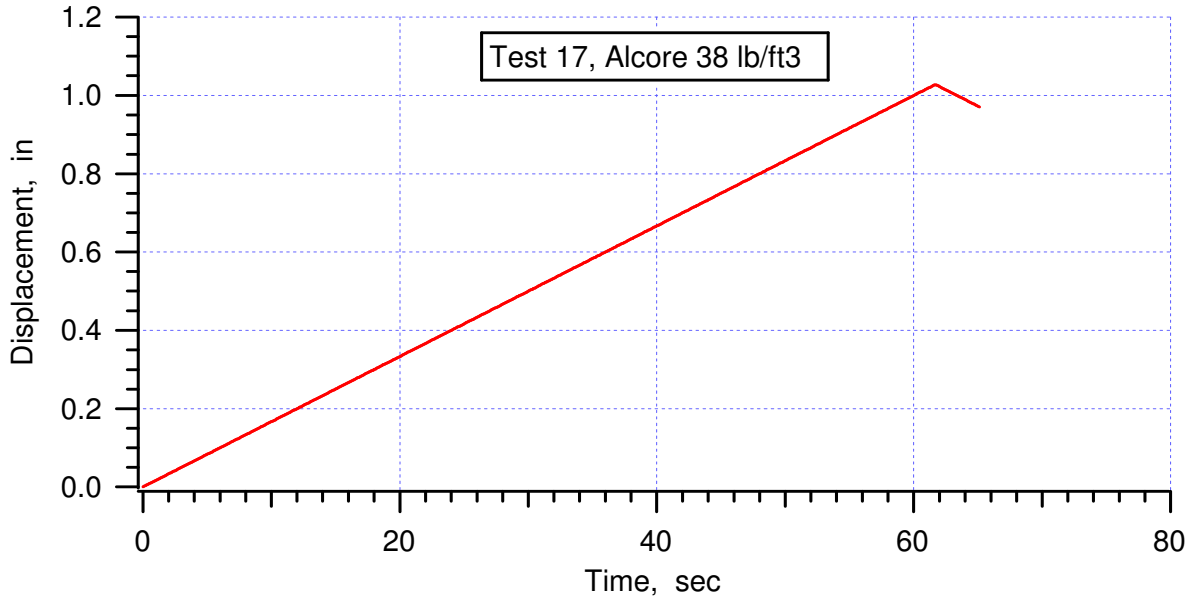
Test 17, Alcore 38 lb/ft3
Displacement, in
1.2
1.0
0.8
0.6
0.4
0.2
0.0
0
20
40
60
80
Time, sec

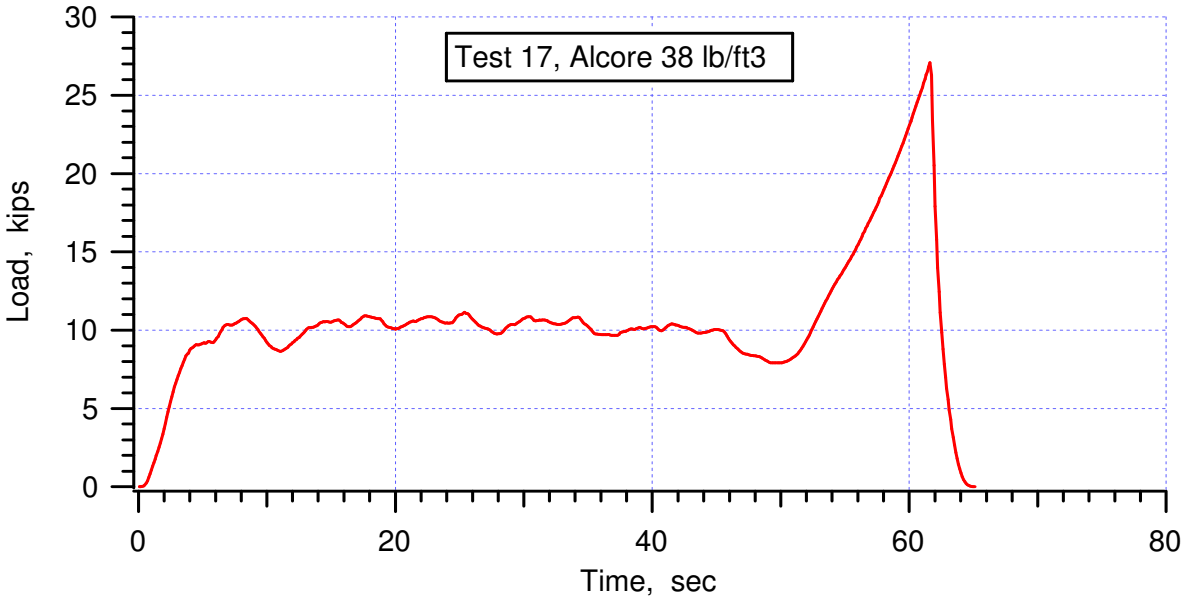
Test 17, Alcore 38 lb/ft3
Load, kips
30
25
20
15
10
5
0
0
20
40
60
80
Time, sec

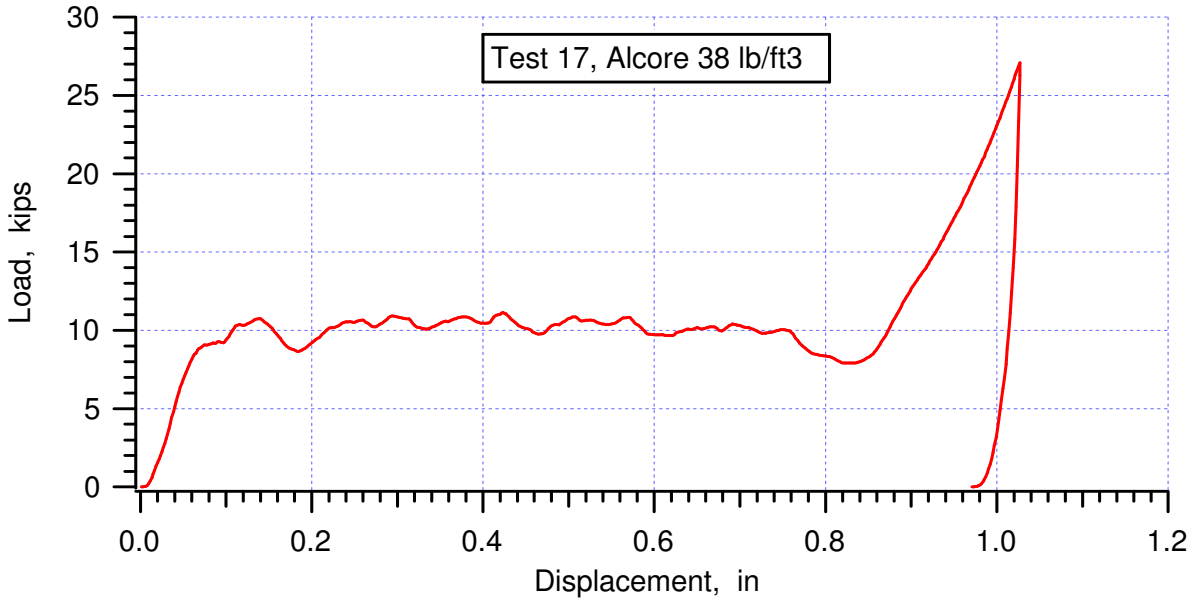
Test 17, Alcore 38 lb/ft3
Load, kips
Displacement, in
0
5
10
15
20
25
30
0.0
0.2
0.4
0.6
0.8
1.0
1.2

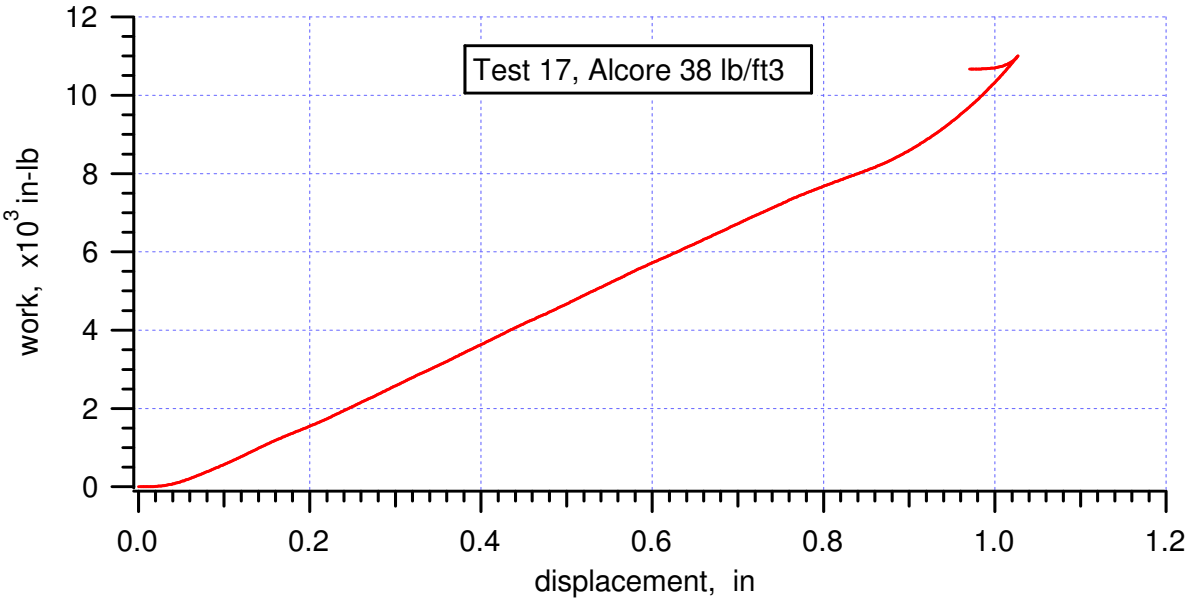
Test 17, Alcore 38 lb/ft3
work, x10^3 in-lb
displacement, in
0
2
4
6
8
10
12
0.0
0.2
0.4
0.6
0.8
1.0
1.2

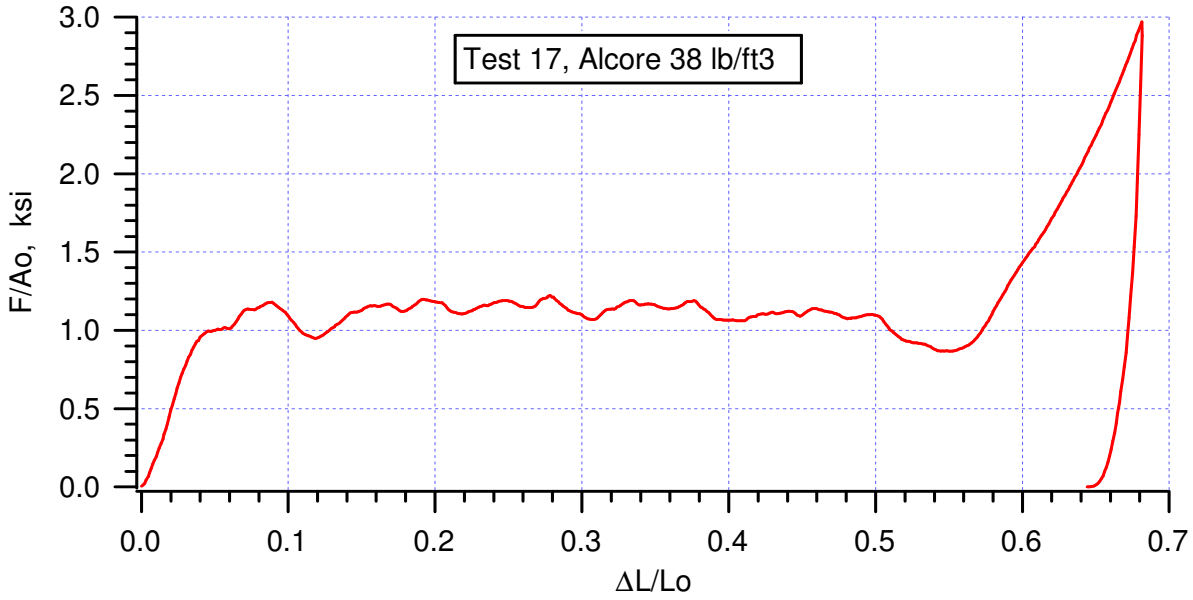

crush strength = 1.105 ksi, averaged from (0.1179, 0.9488) to (0.5501, 0.8668)

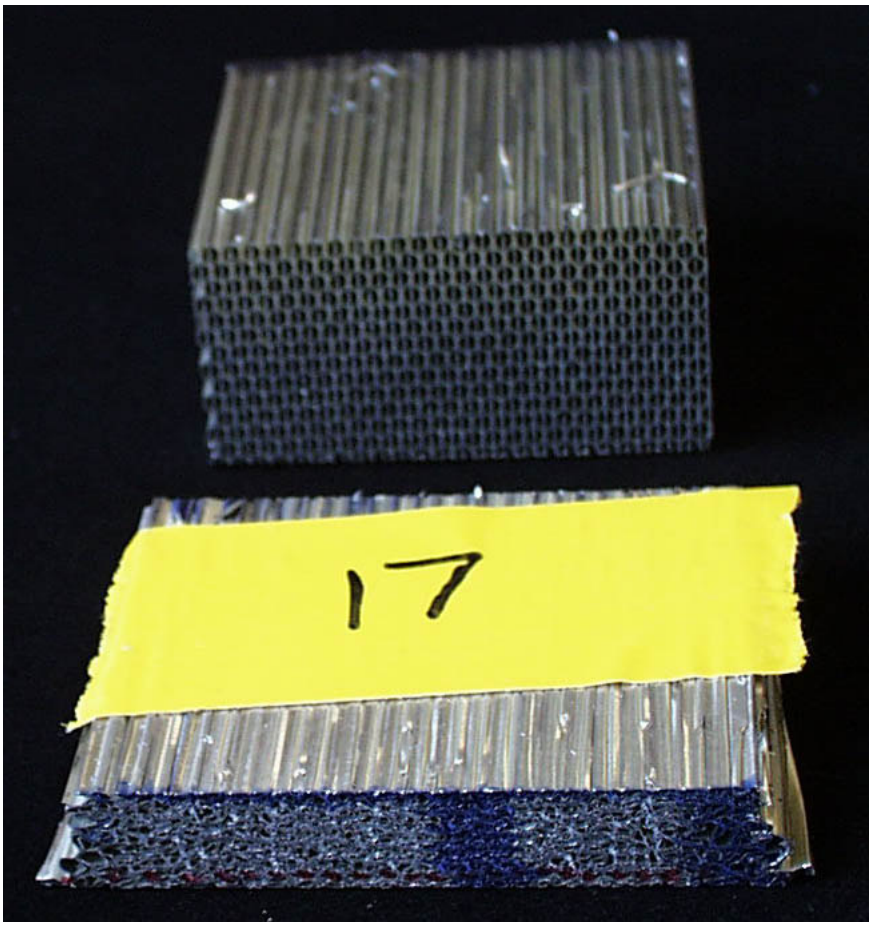

Test #17

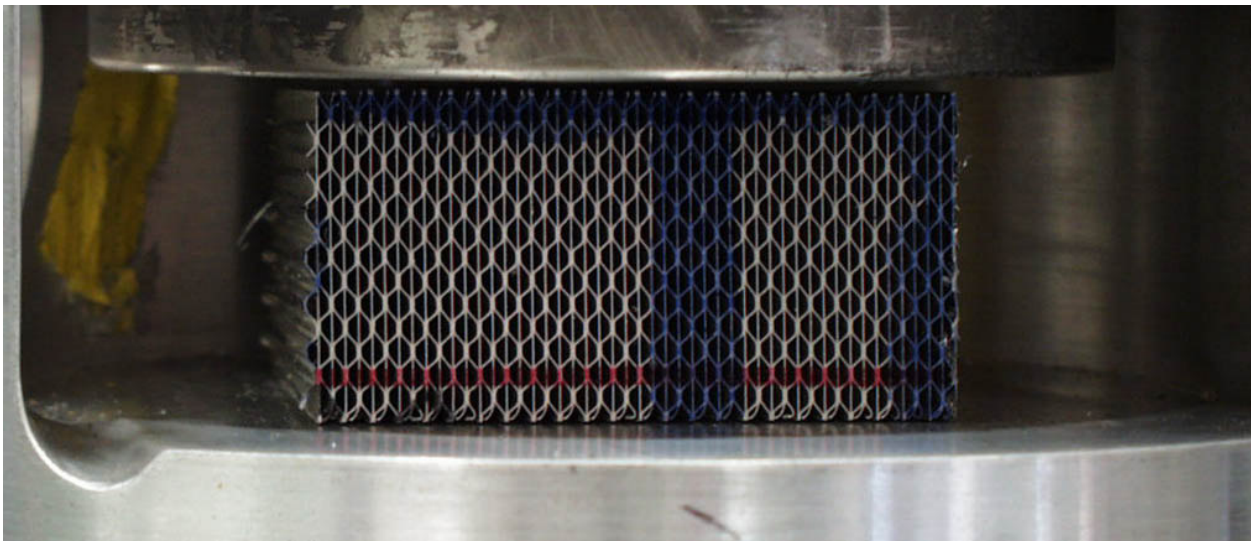

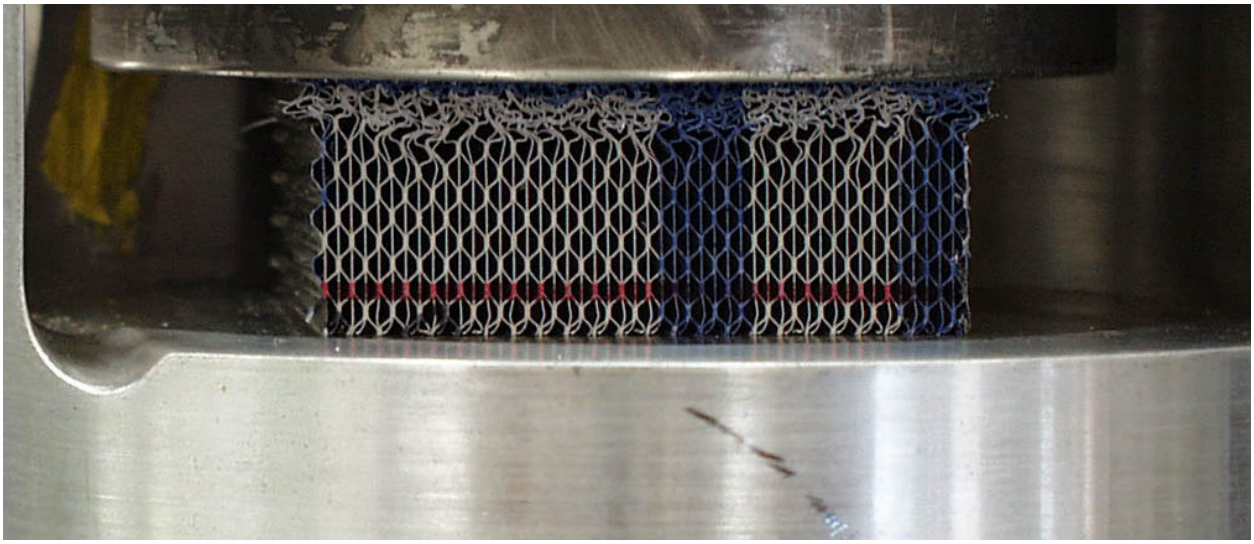

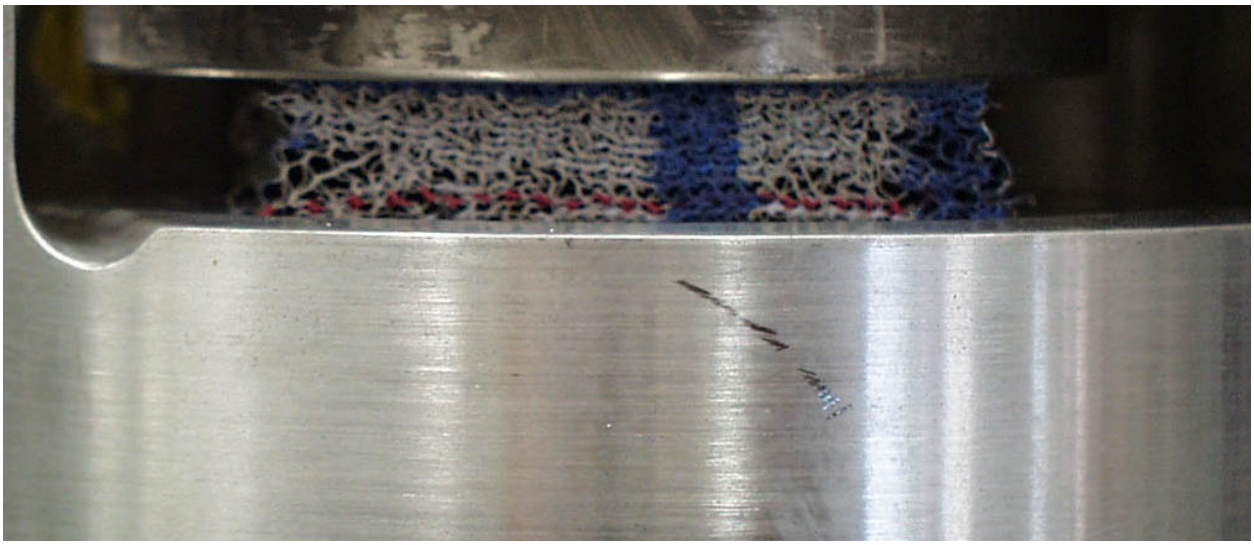

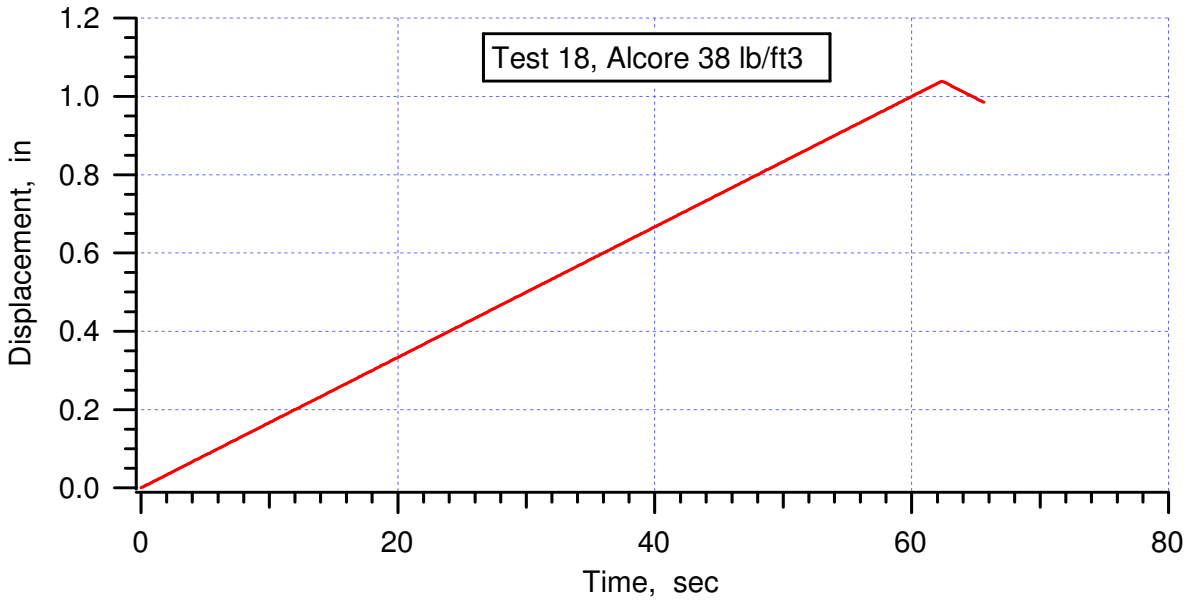
Test 18, Alcore 38 lb/ft3
Displacement, in
1.2
1.0
0.8
0.6
0.4
0.2
0.0
0
20
40
60
80
Time, sec

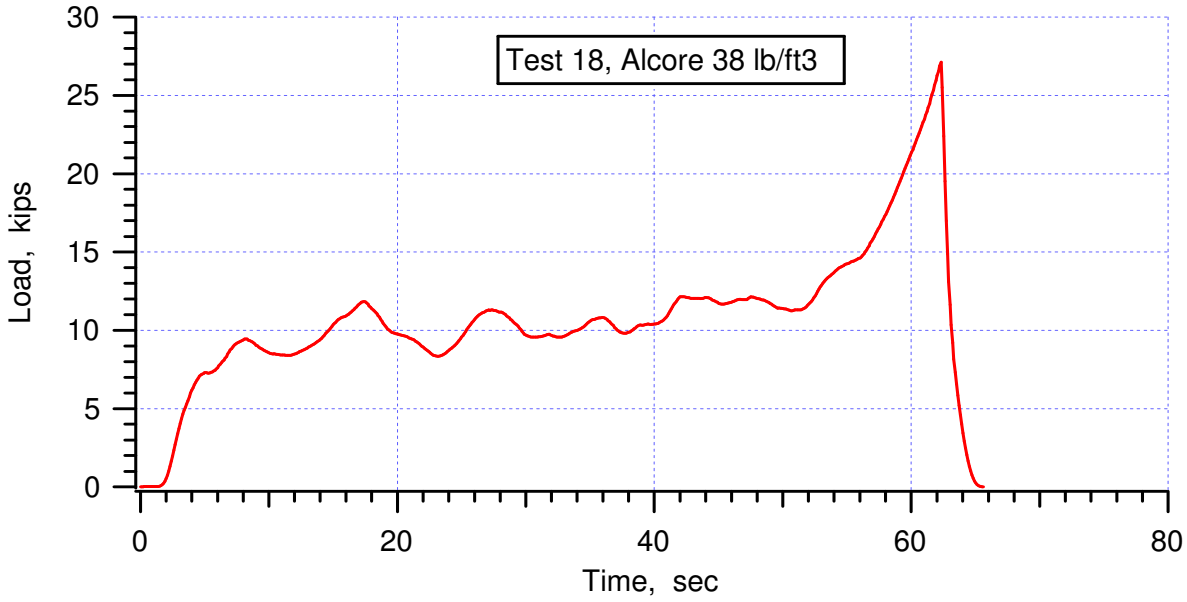
Test 18, Alcore 38 lb/ft3
Load, kips
Time, sec
0
5
10
15
20
25
30
0
20
40
60
80

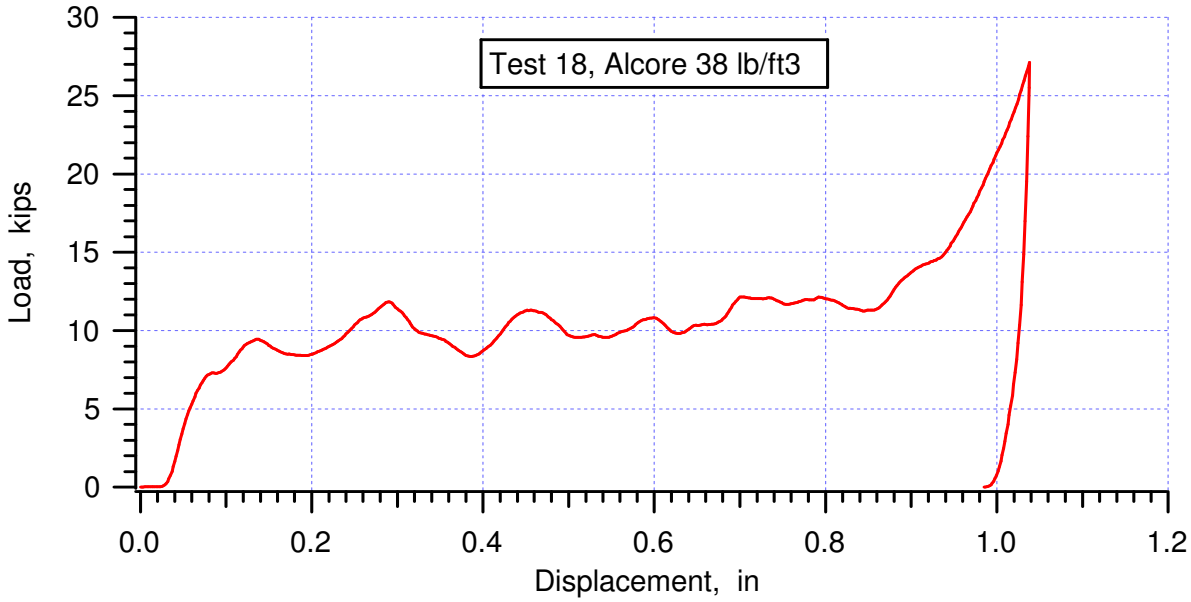
Test 18, Alcore 38 lb/ft3
Load, kips
Displacement, in
0
5
10
15
20
25
30
0.0
0.2
0.4
0.6
0.8
1.0
1.2

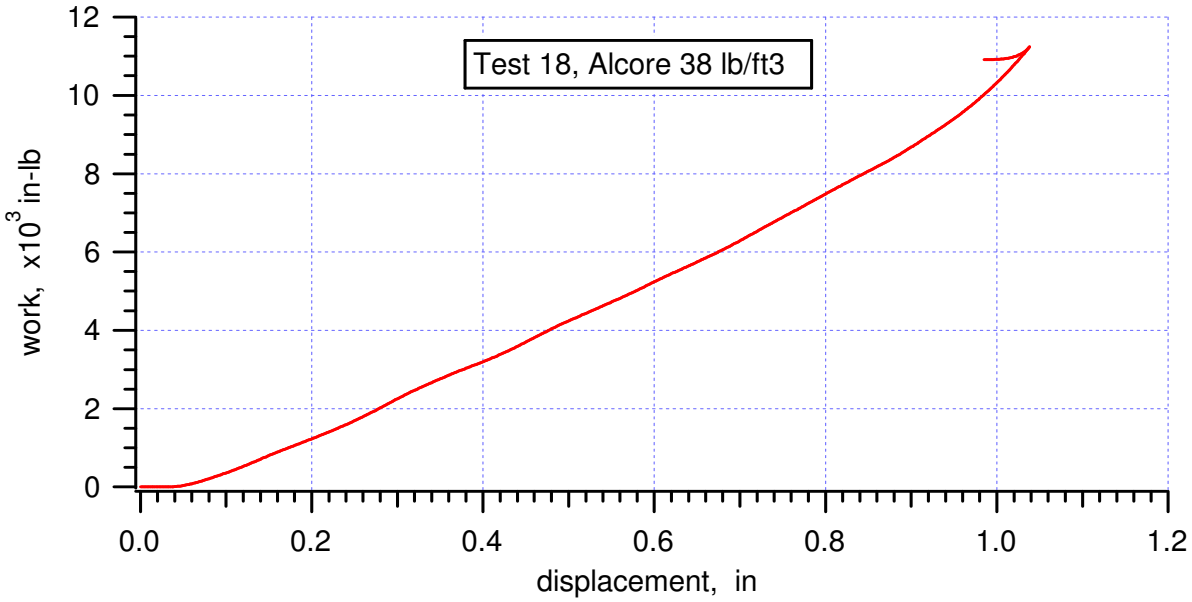

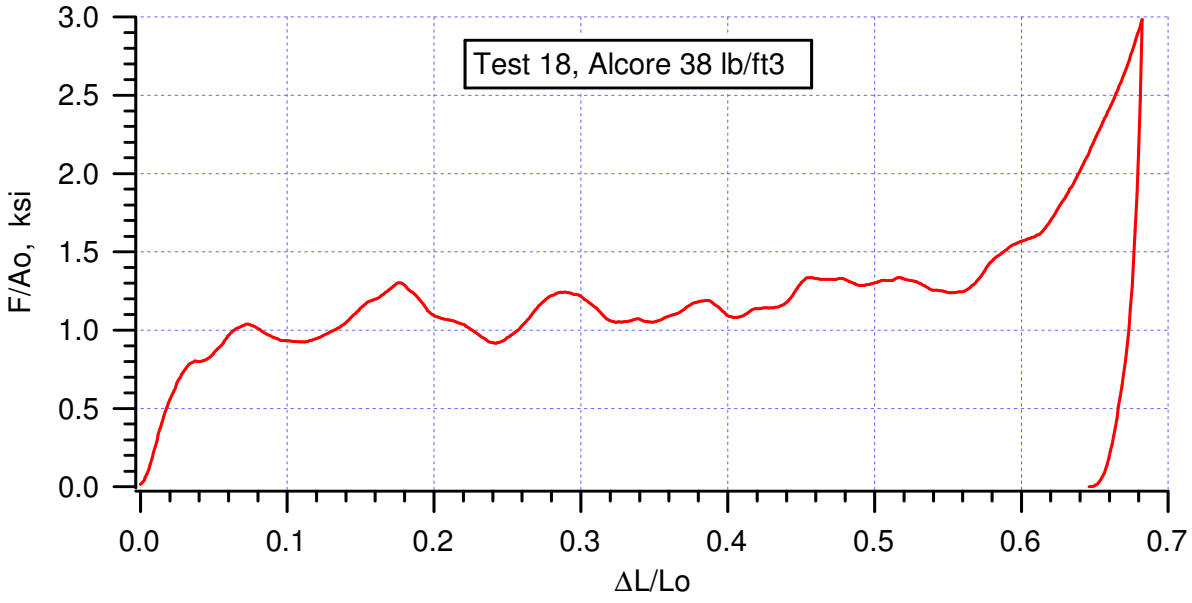

crush strength = 1.151 ksi, averaged from (0.1036, 0.9278) to (0.5598, 1.2449)

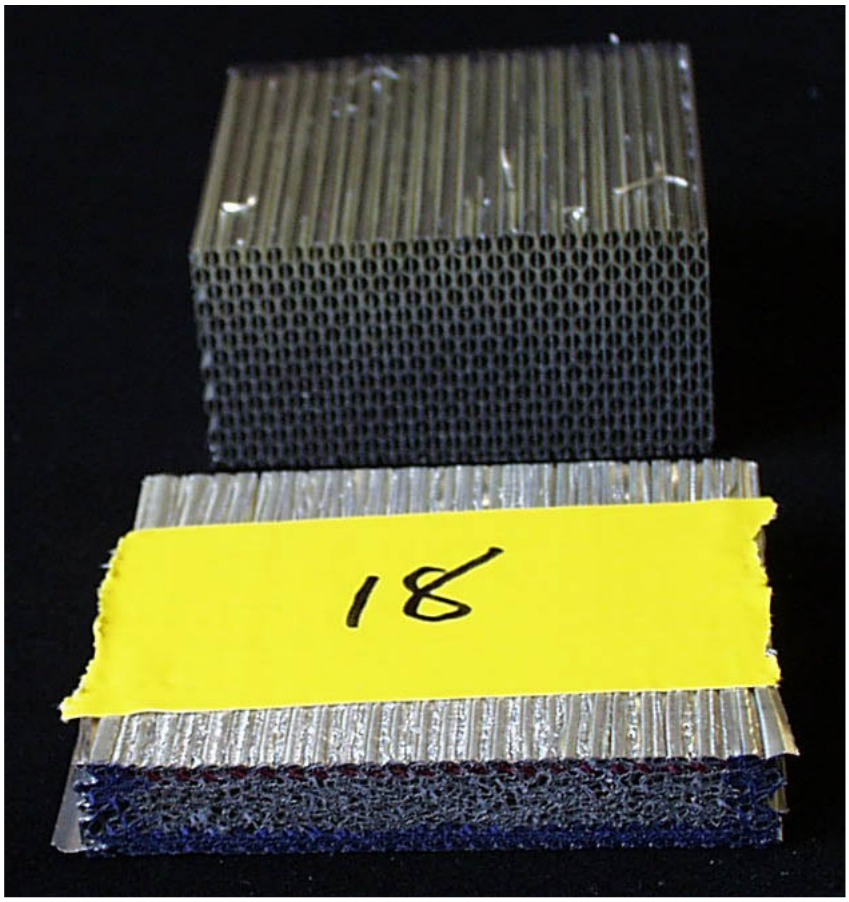
18


MTS

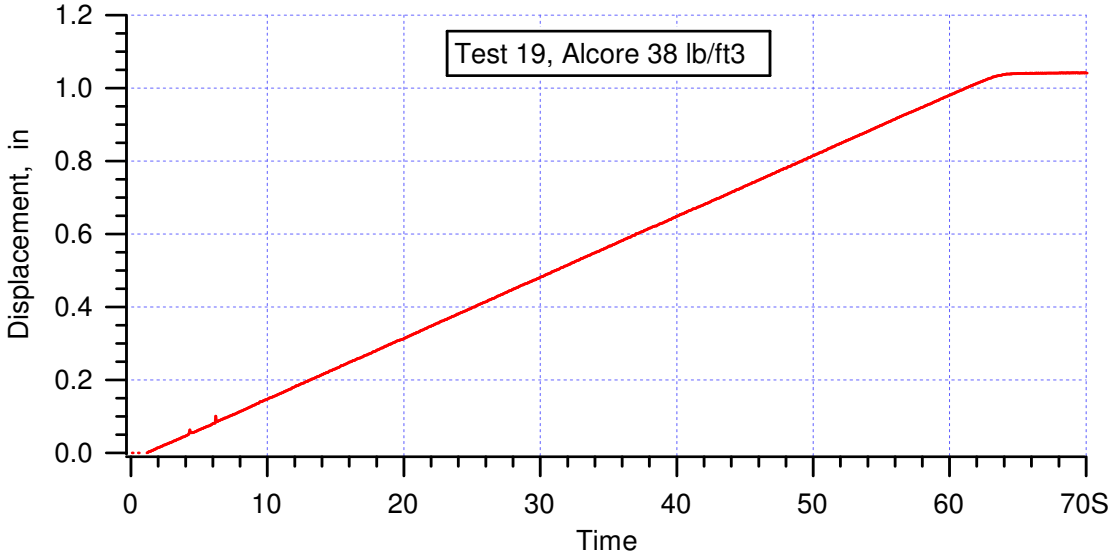
Test 19, Alcore 38 lb/ft3
Displacement, in
1.2
1.0
0.8
0.6
0.4
0.2
0.0
0
10
20
30
40
50
60
70S
Time

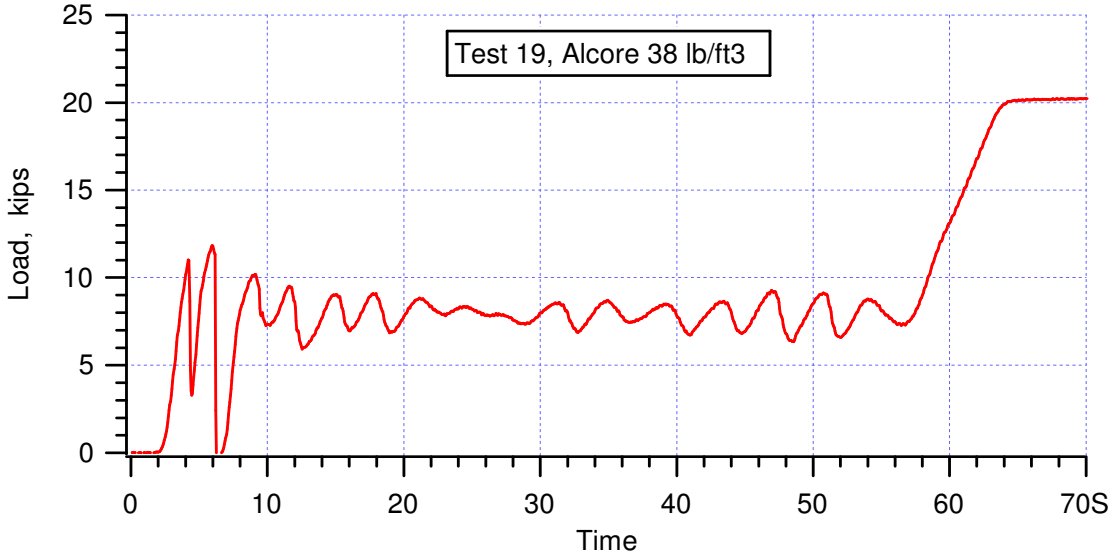
Test 19, Alcore 38 lb/ft3
Load, kips
25
20
15
10
5
0
0
10
20
30
40
50
60
70S
Time

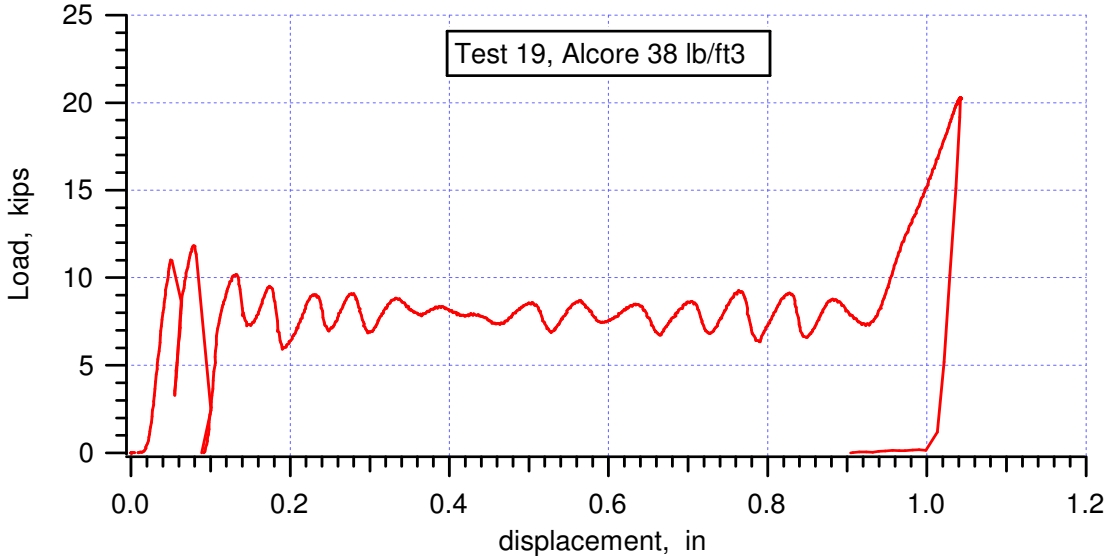
Test 19, Alcore 38 lb/ft3
Load, kips
displacement, in
0
5
10
15
20
25
0.0
0.2
0.4
0.6
0.8
1.0
1.2

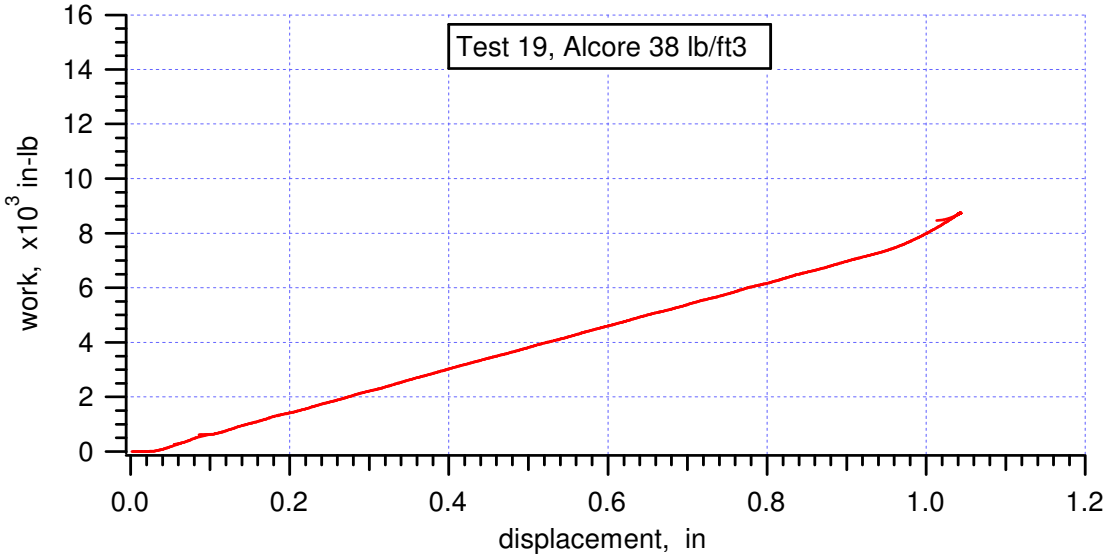
Test 19, Alcore 38 lb/ft3
work, x10^3 in-lb
displacement, in
0
2
4
6
8
10
12
14
16
0.0
0.2
0.4
0.6
0.8
1.0
1.2

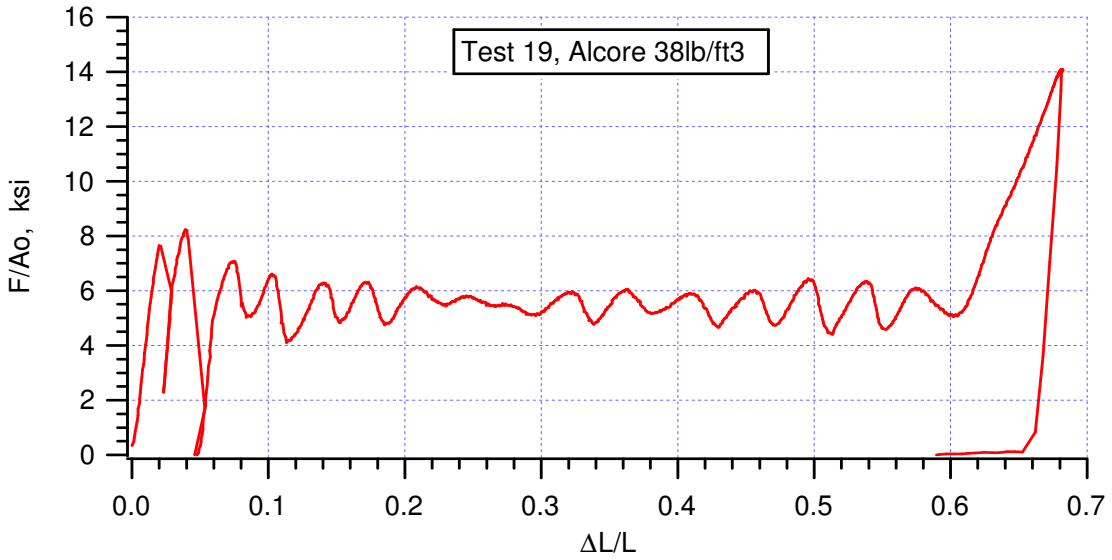

crush strength = 5.49 ksi, averaged from (0.0842, 5.0844) to (0.6021, 5.0533)

peak stress = 8.1778 ksi @ 0.0384

crush efficiency = 60.8%, from (0.02, 7.6533) to (0.628, 7.7022)

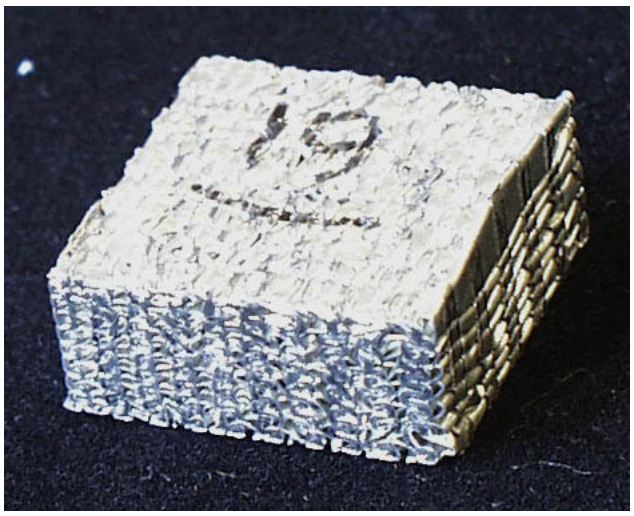

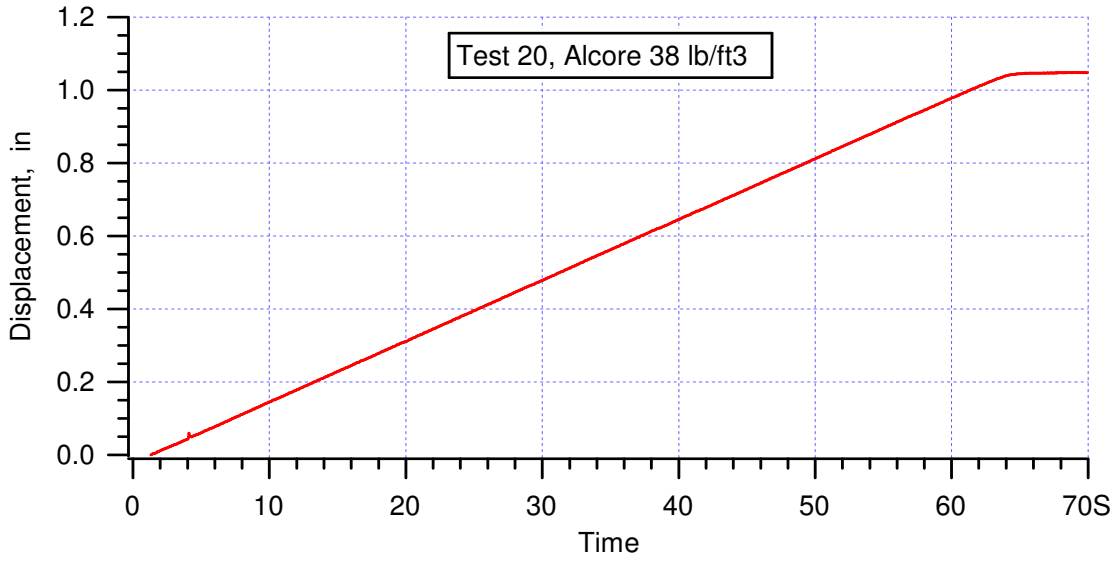
Test 20, Alcore 38 lb/ft3
Displacement, in
1.2
1.0
0.8
0.6
0.4
0.2
0.0
0
10
20
30
40
50
60
70S
Time

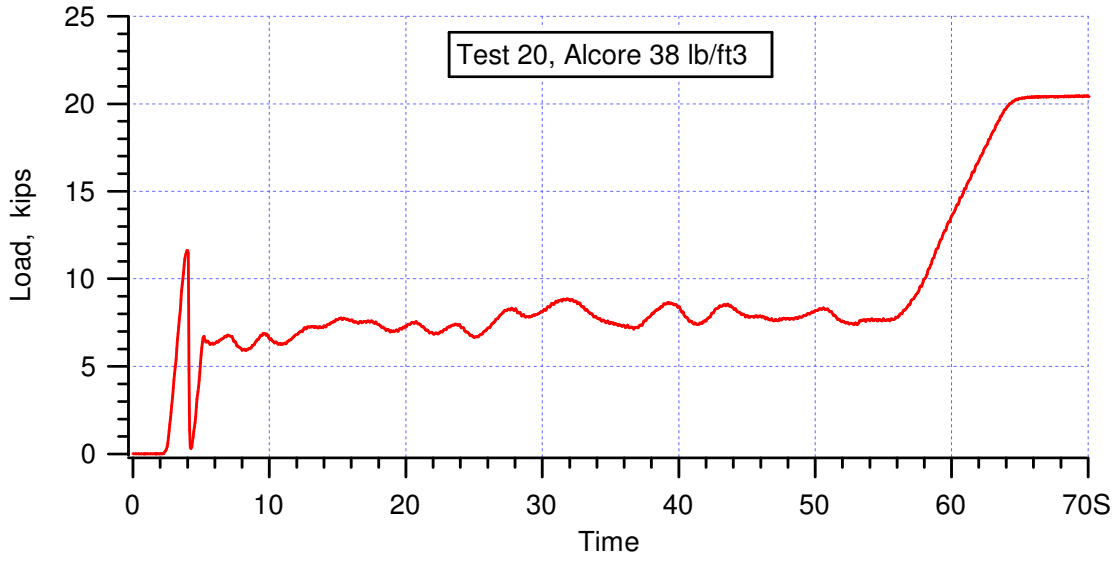
Test 20, Alcore 38 lb/ft3
Load, kips
25
20
15
10
5
0
0
10
20
30
40
50
60
70S
Time

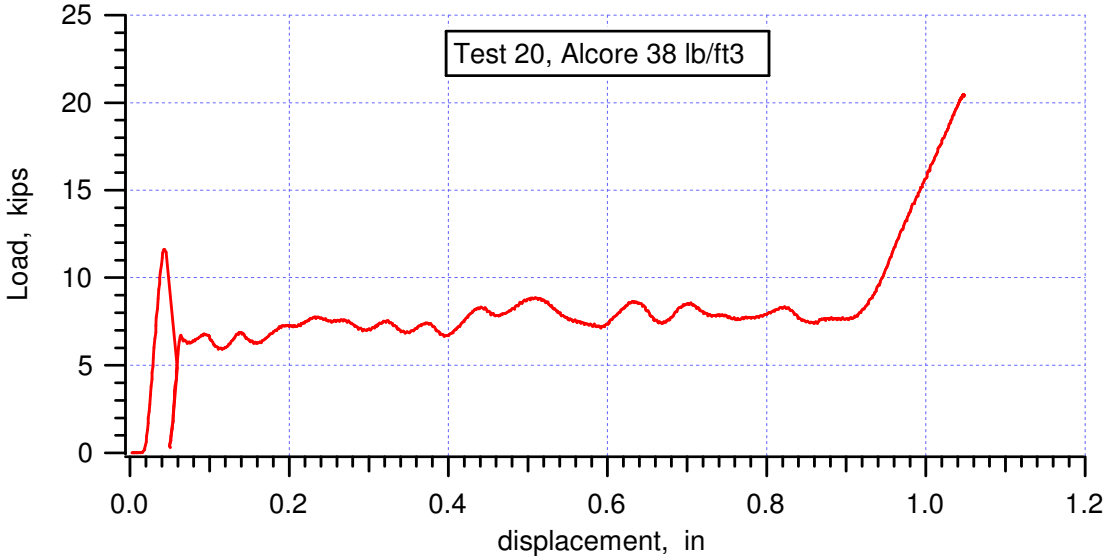
Test 20, Alcore 38 lb/ft3
Load, kips
displacement, in
0
5
10
15
20
25
0.0
0.2
0.4
0.6
0.8
1.0
1.2

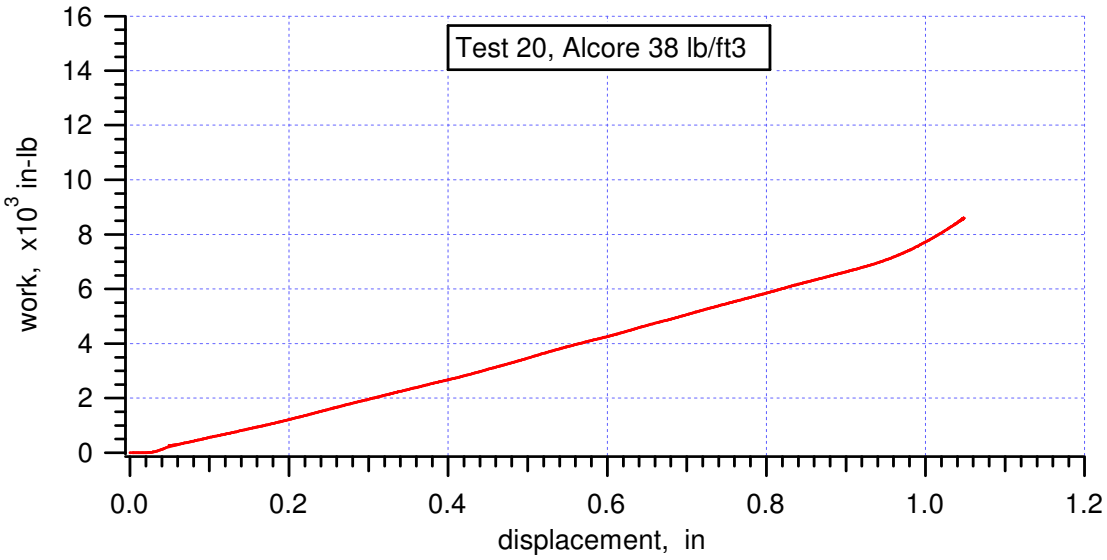
Test 20, Alcore 38 lb/ft3
work, x10^3 in-lb
displacement, in
0
2
4
6
8
10
12
14
16
0.0
0.2
0.4
0.6
0.8
1.0
1.2

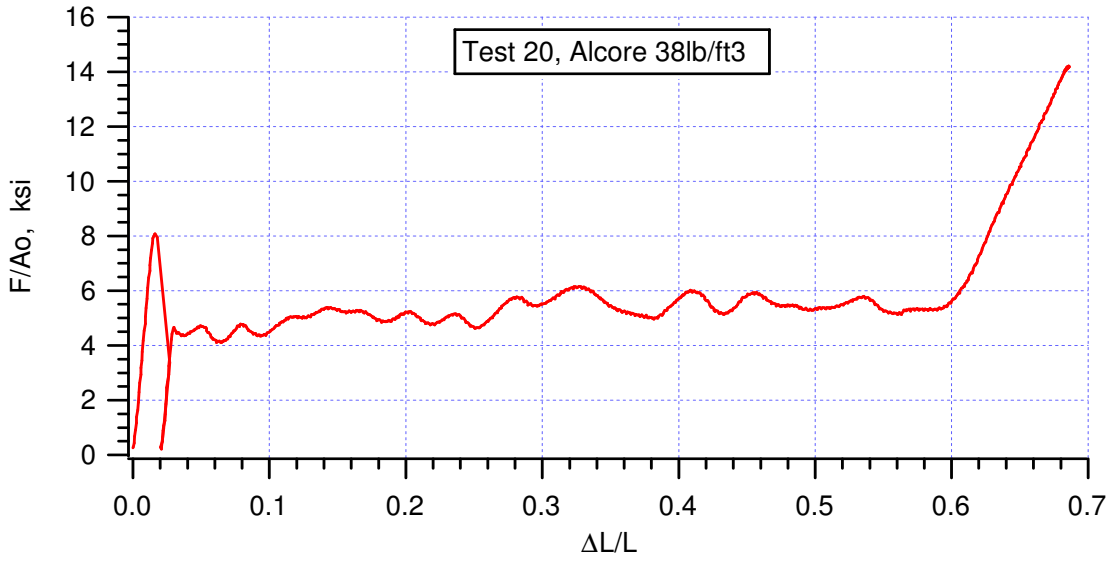

crush strength = 5.24 ksi, averaged from (0.035, 4.4) to (0.5895, 5.3333)

peak stress = 8.0756 ksi @ 0.0161

crush efficiency = 61.1%, from (0.01613, 8.0756) to (0.628, 8.0622)

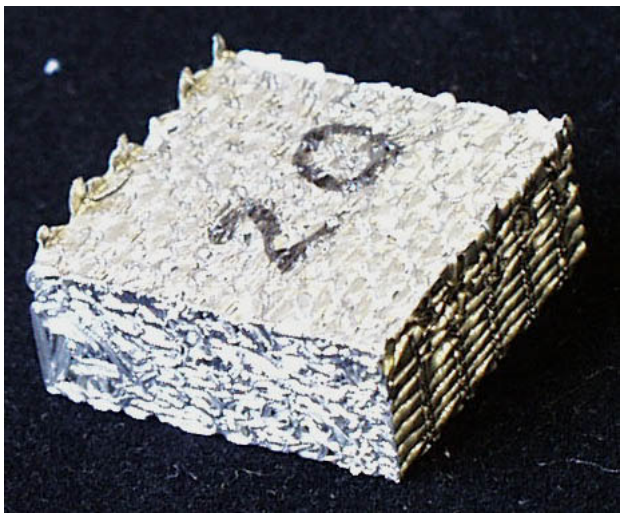

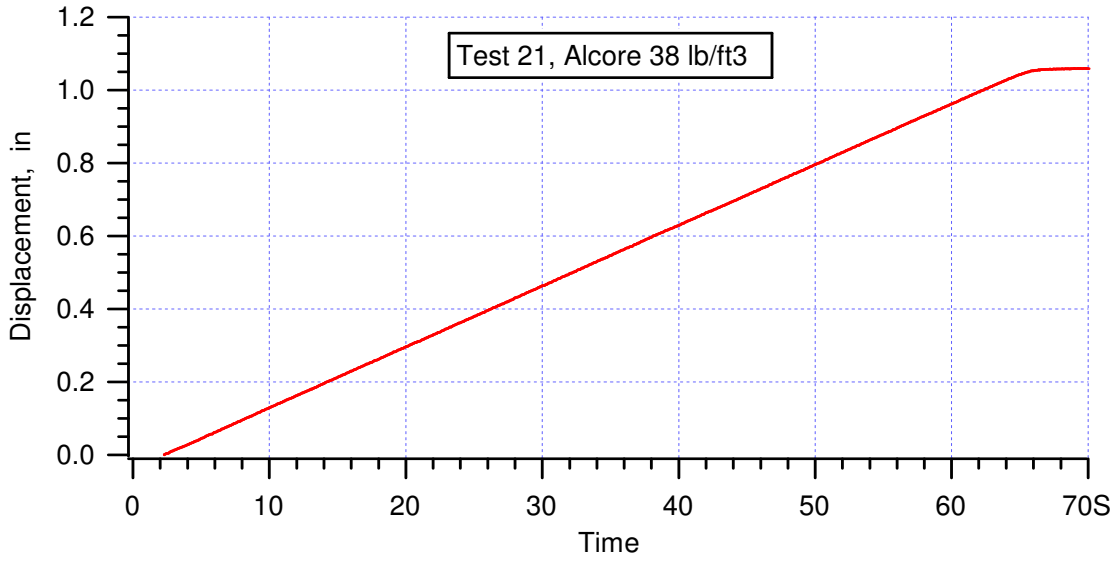
Test 21, Alcore 38 lb/ft3
Displacement, in
1.2
1.0
0.8
0.6
0.4
0.2
0.0
0
10
20
30
40
50
60
70S
Time

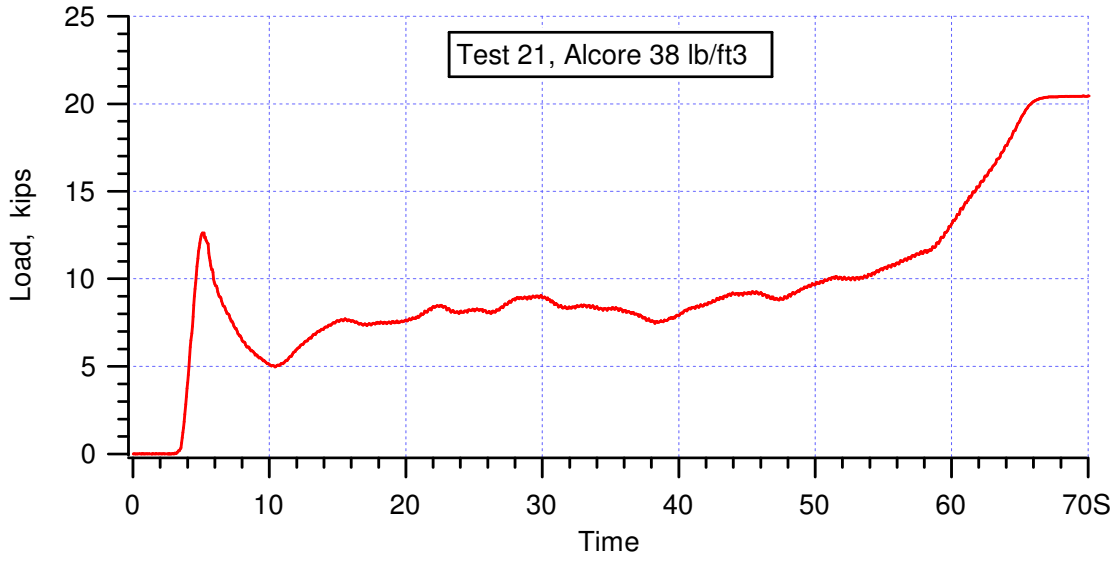
Test 21, Alcore 38 lb/ft3
Load, kips
25
20
15
10
5
0
0
10
20
30
40
50
60
70S
Time

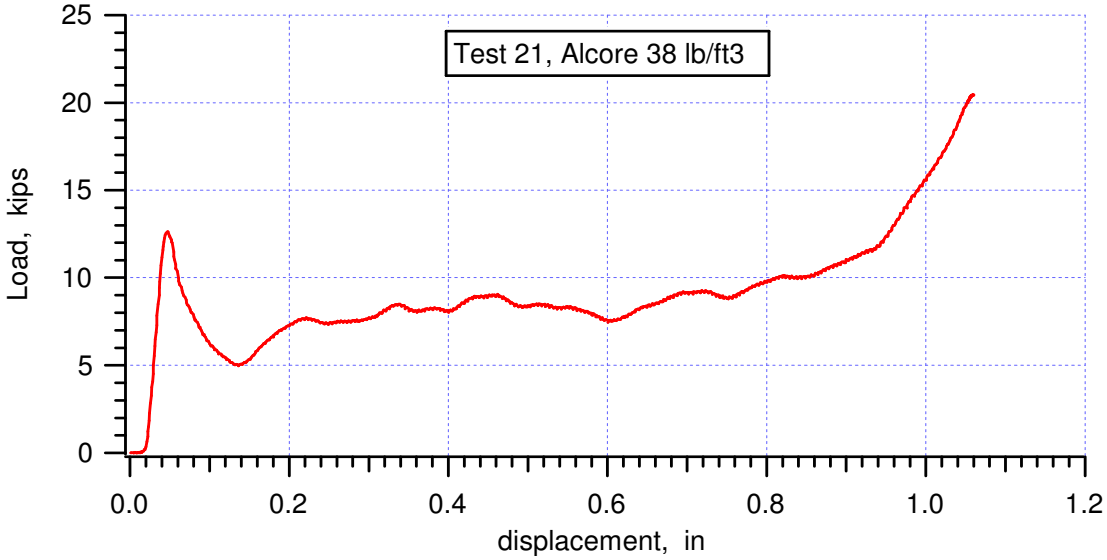
Test 21, Alcore 38 lb/ft3
Load, kips
displacement, in
0
5
10
15
20
25
0.0
0.2
0.4
0.6
0.8
1.0
1.2

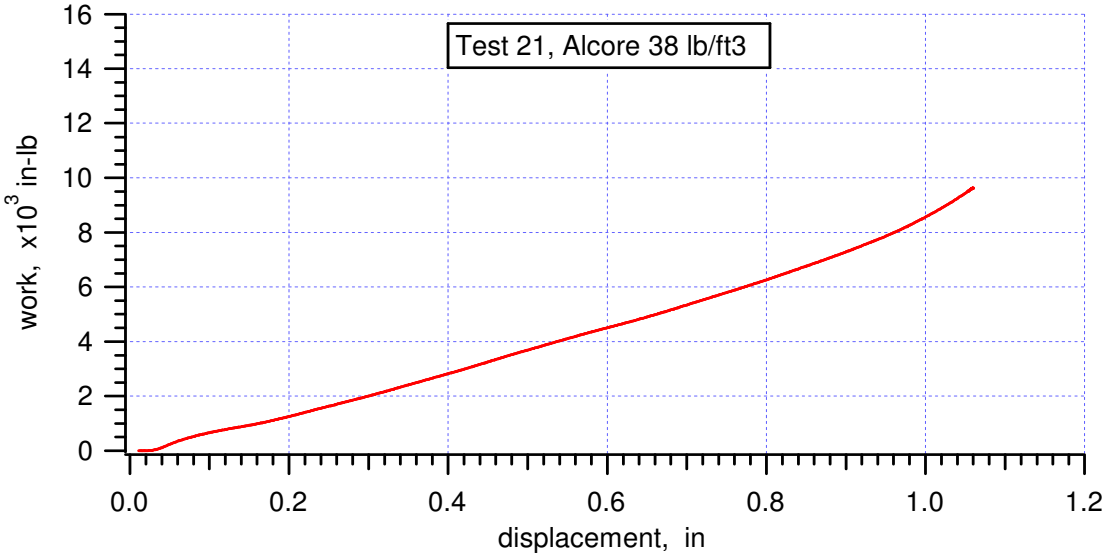
Test 21, Alcore 38 lb/ft3
work, x10^3 in-lb
displacement, in
0
2
4
6
8
10
12
14
16
0.0
0.2
0.4
0.6
0.8
1.0
1.2

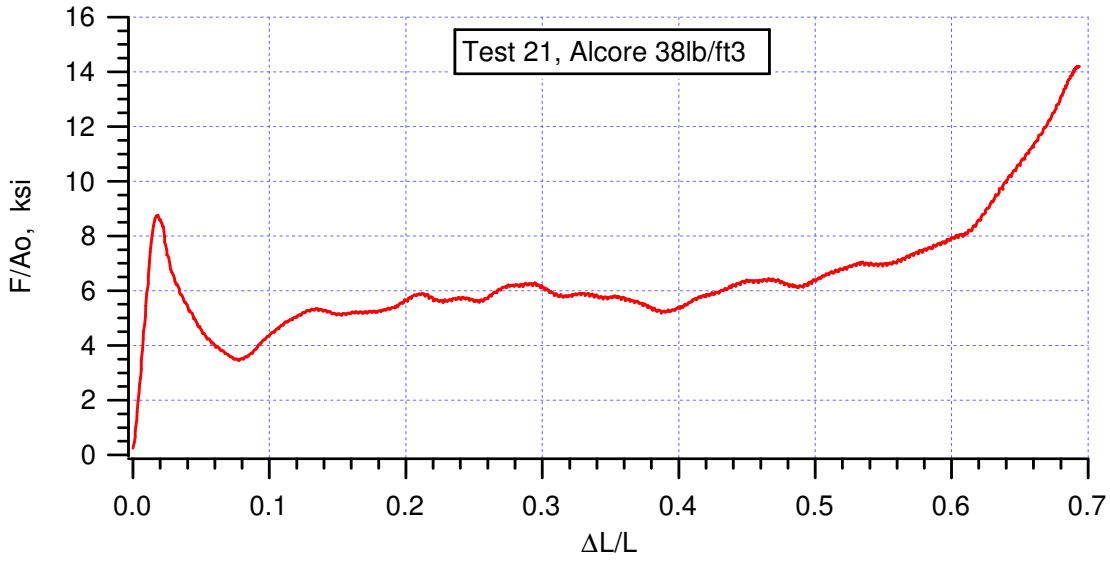

crush strength = 5.57 ksi, averaged from (0.0757, 3.5111) to (0.4.888, 6.1911)

peak stress = 8.7644 ksi @ 0.01786

crush efficiency = 60.7%, from (0.01786, 8.7644) to (0.6248, 8.9289)

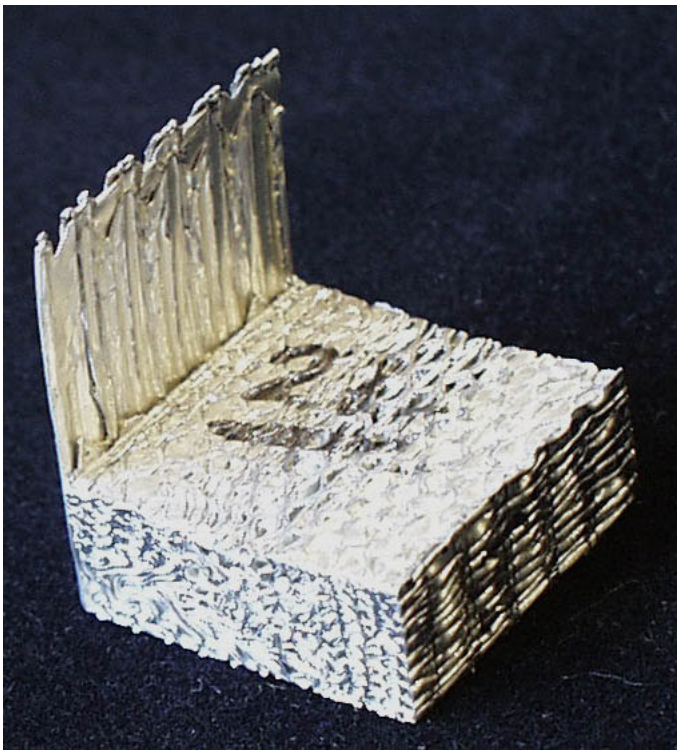

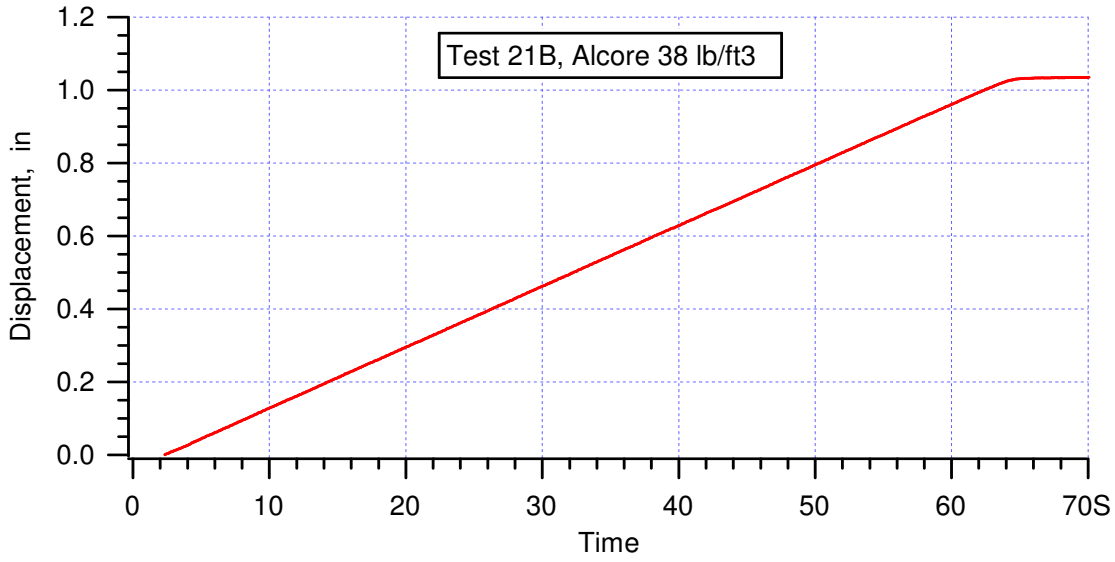
Test 21B, Alcore 38 lb/ft3
Displacement, in
1.2
1.0
0.8
0.6
0.4
0.2
0.0
0
10
20
30
40
50
60
70S
Time

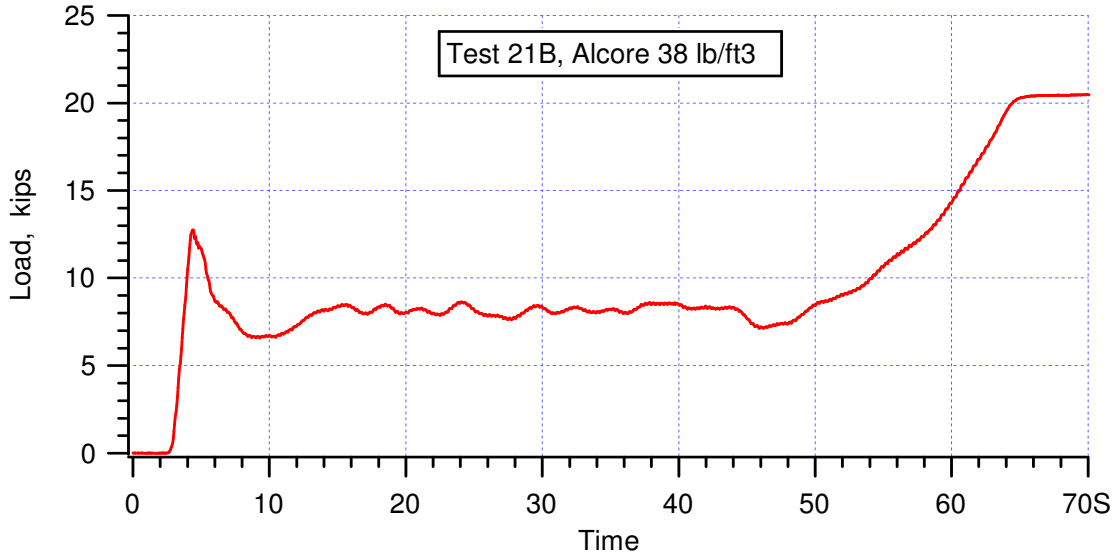
Test 21B, Alcore 38 lb/ft3
Load, kips
25
20
15
10
5
0
0
10
20
30
40
50
60
70S
Time

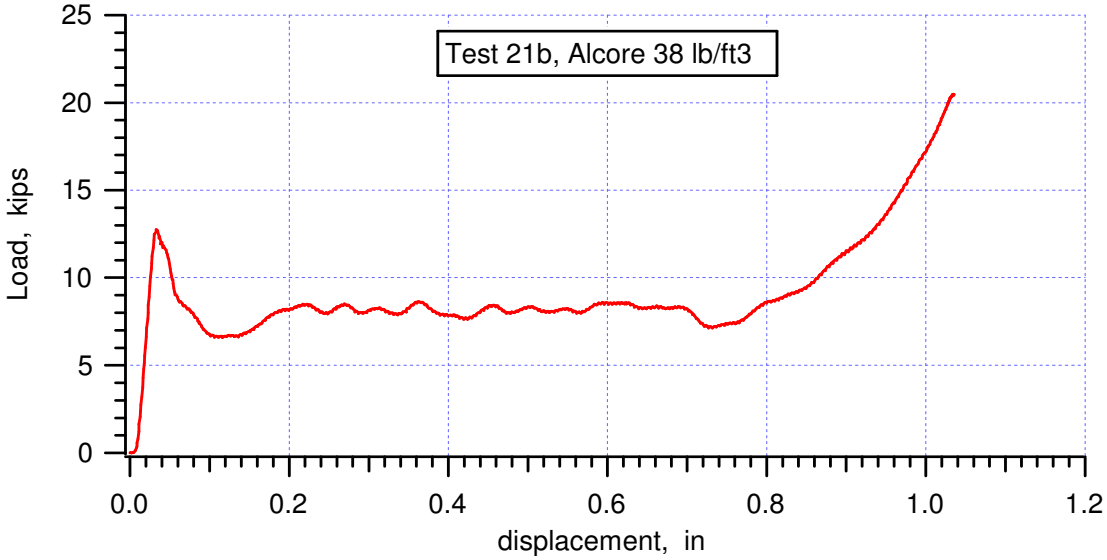
Test 21b, Alcore 38 lb/ft3
Load, kips
displacement, in
0
5
10
15
20
25
0.0
0.2
0.4
0.6
0.8
1.0
1.2

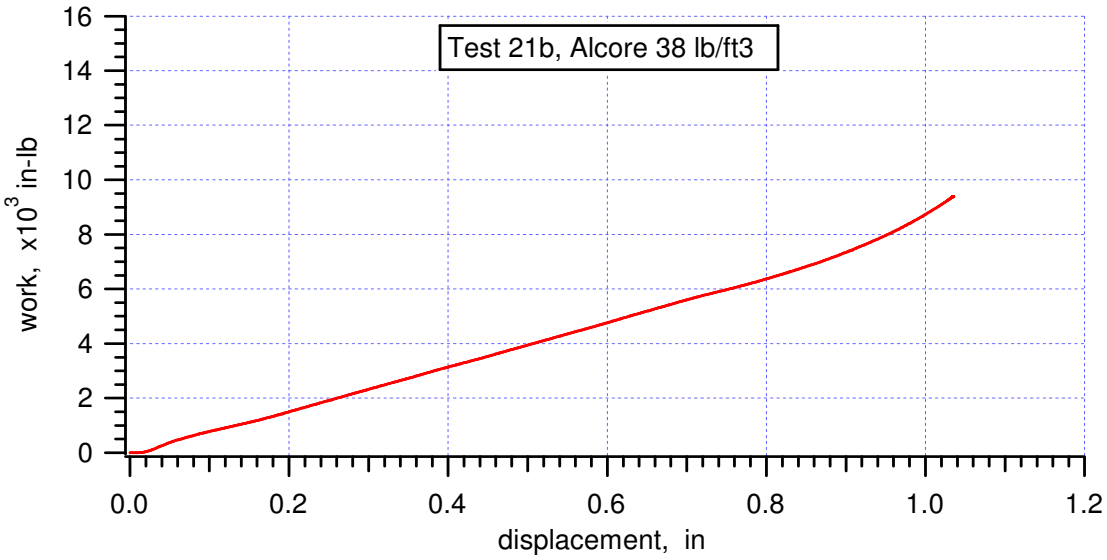
Test 21b, Alcore 38 lb/ft3
work, x10^3 in-lb
displacement, in
0
2
4
6
8
10
12
14
16
0.0
0.2
0.4
0.6
0.8
1.0
1.2

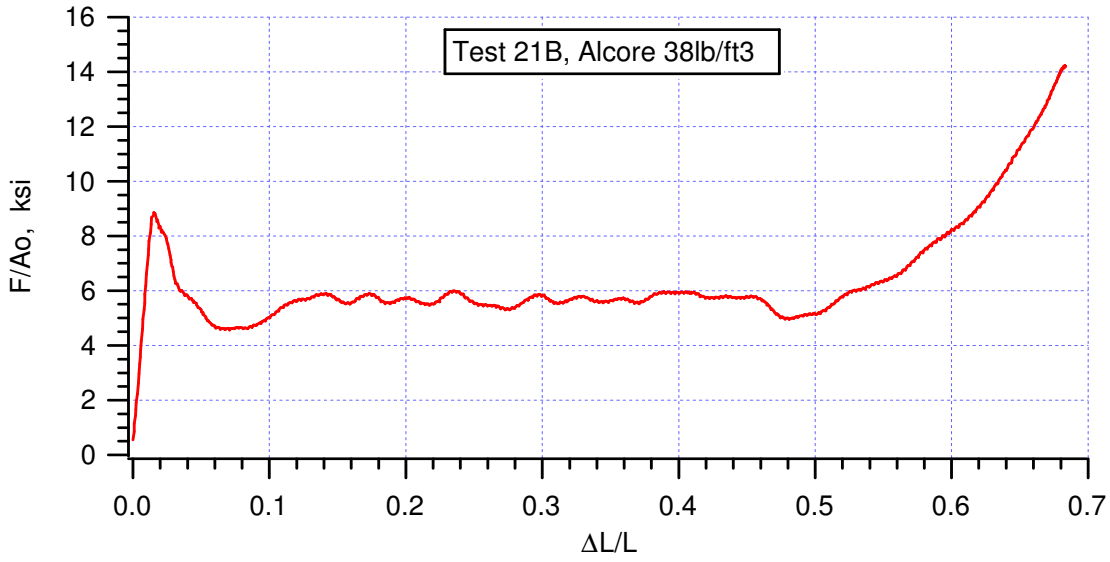

crush strength = 5.62 ksi, averaged from (0.0827, 4.6444) to (0.4.787, 4.9911)

peak stress = 8.76 ksi @ 0.52

crush efficiency = 60.0%, from (0.0152, 8.76) to (0.6149, 8.7644)

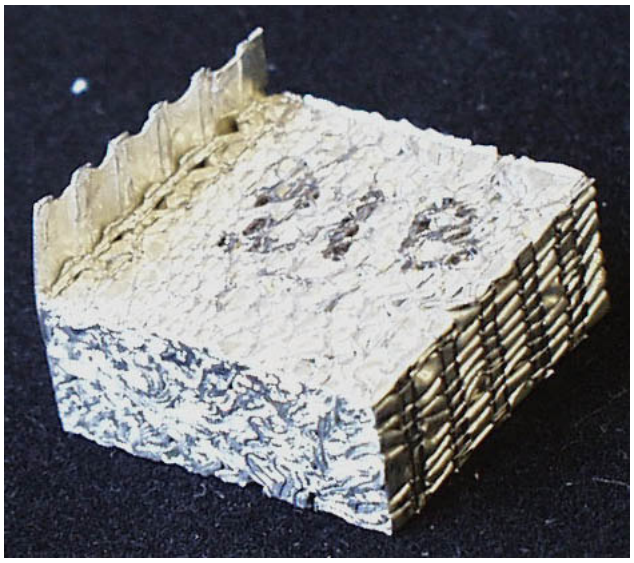

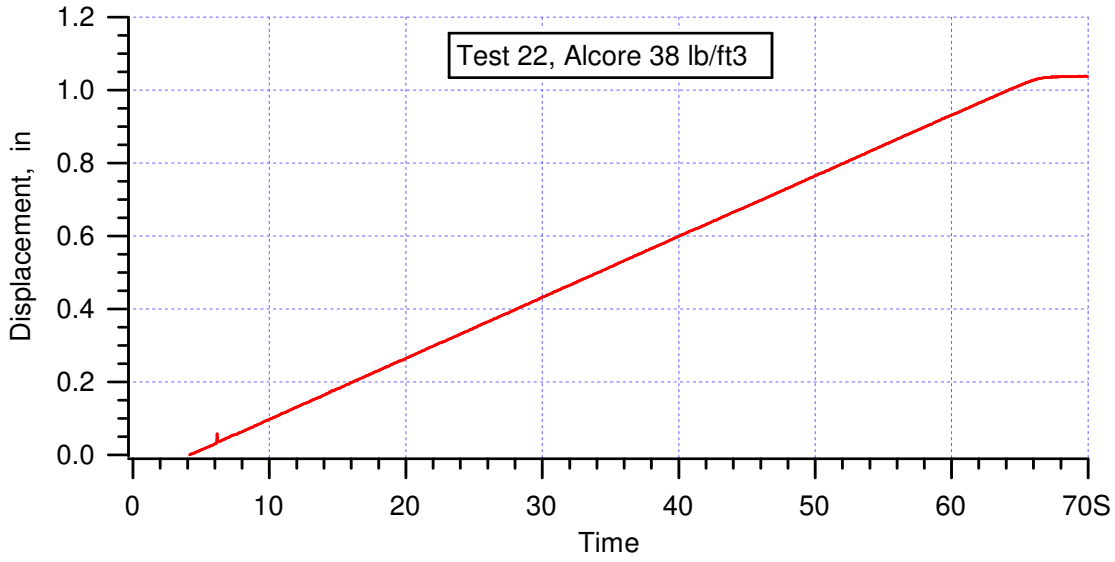
Test 22, Alcore 38 lb/ft3
Displacement, in
1.2
1.0
0.8
0.6
0.4
0.2
0.0
0
10
20
30
40
50
60
70S
Time

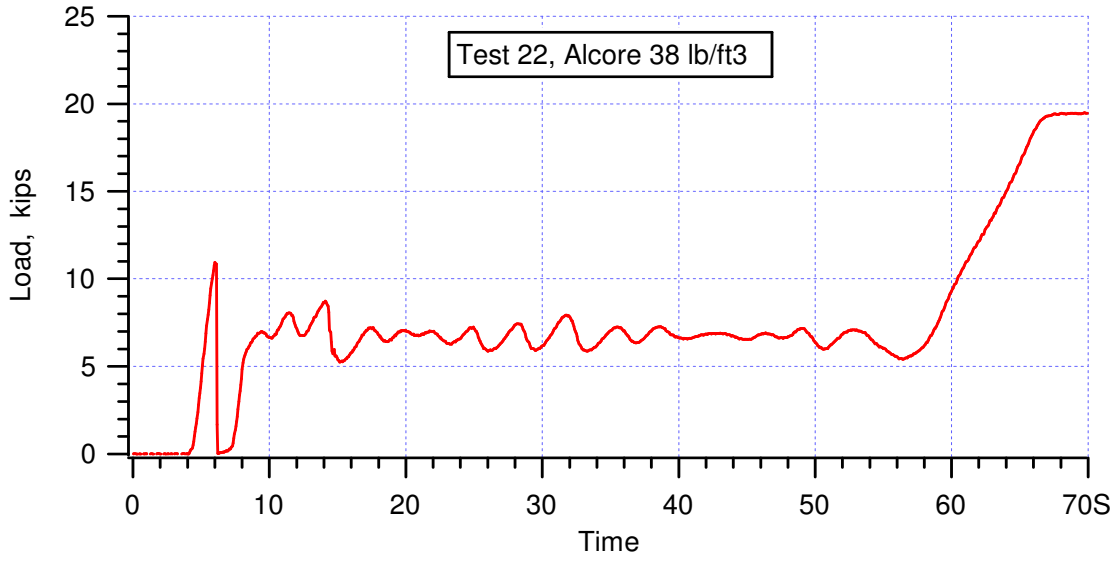
Test 22, Alcore 38 lb/ft3
Load, kips
25
20
15
10
5
0
0
10
20
30
40
50
60
70S
Time

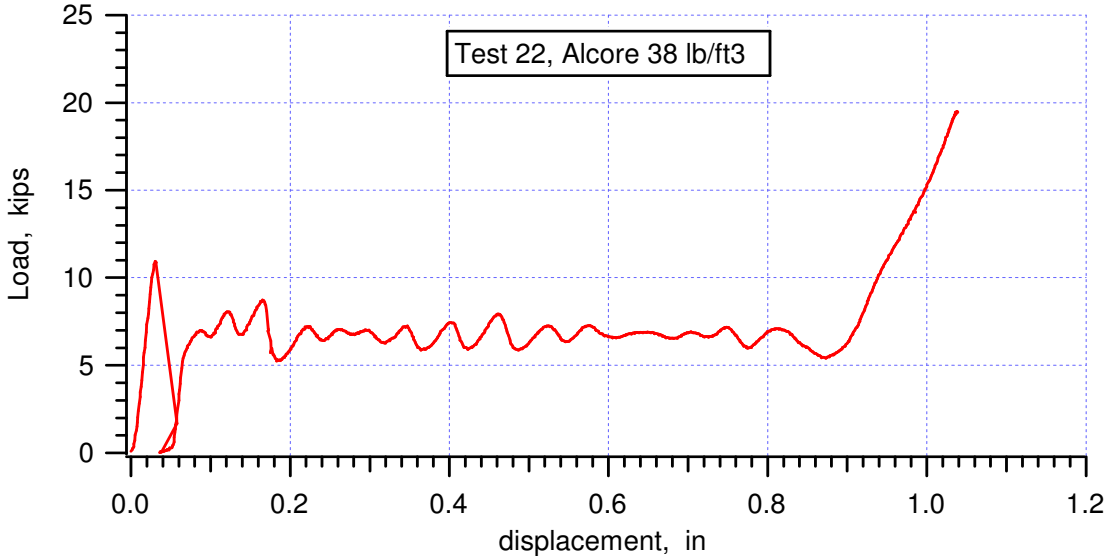
Test 22, Alcore 38 lb/ft3
Load, kips
displacement, in
0
5
10
15
20
25
0.0
0.2
0.4
0.6
0.8
1.0
1.2

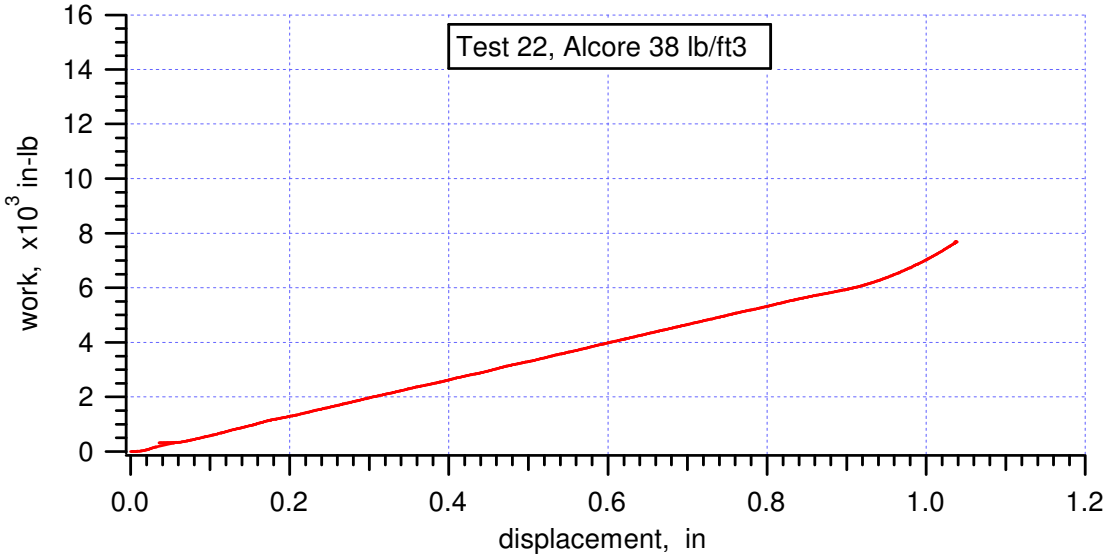
Test 22, Alcore 38 lb/ft3
work, x10^3 in-lb
displacement, in
0
2
4
6
8
10
12
14
16
0.0
0.2
0.4
0.6
0.8
1.0
1.2

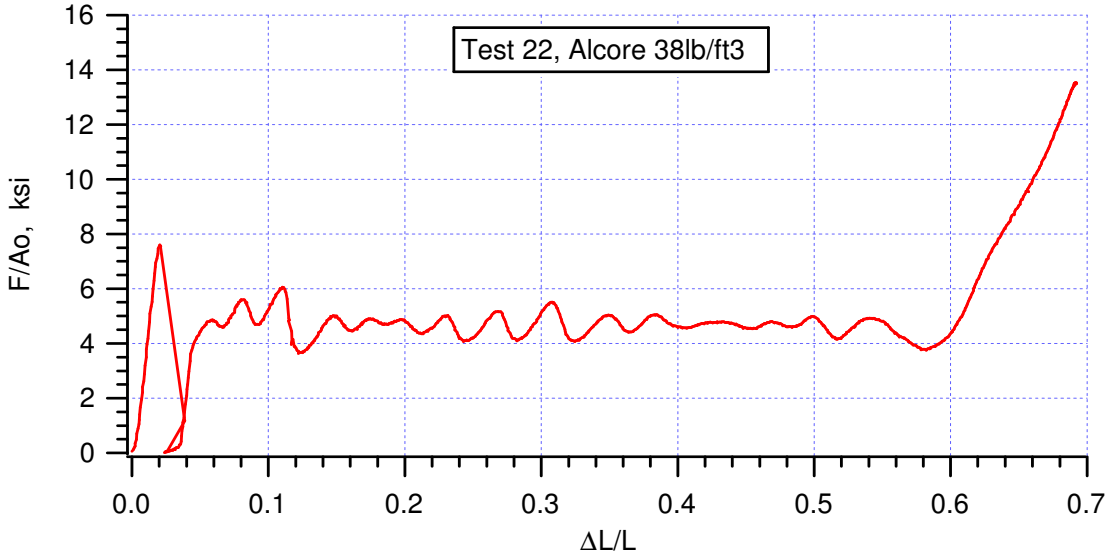

crush strength = 4.67 ksi, averaged from (0.0448, 3.9244) to (0.5819, 3.7644)

peak stress = 7.5956 ksi @ 0.02

crush efficiency = 61.2%, from (0.0203, 7.5659) to (0.632, 7.5644)

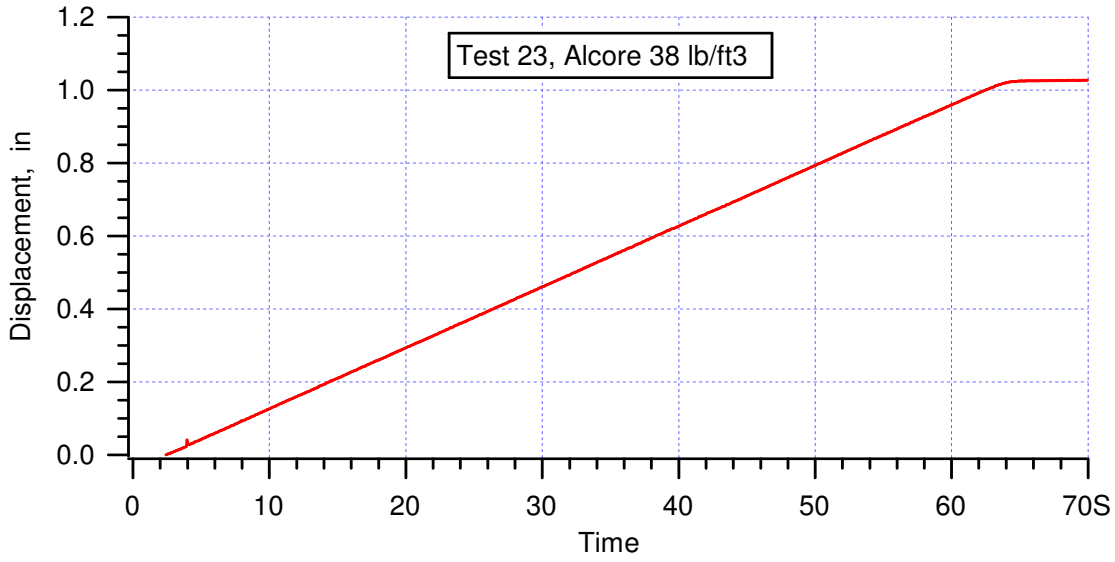
Test 23, Alcore 38 lb/ft3
Displacement, in
1.2
1.0
0.8
0.6
0.4
0.2
0.0
0
10
20
30
40
50
60
70S
Time

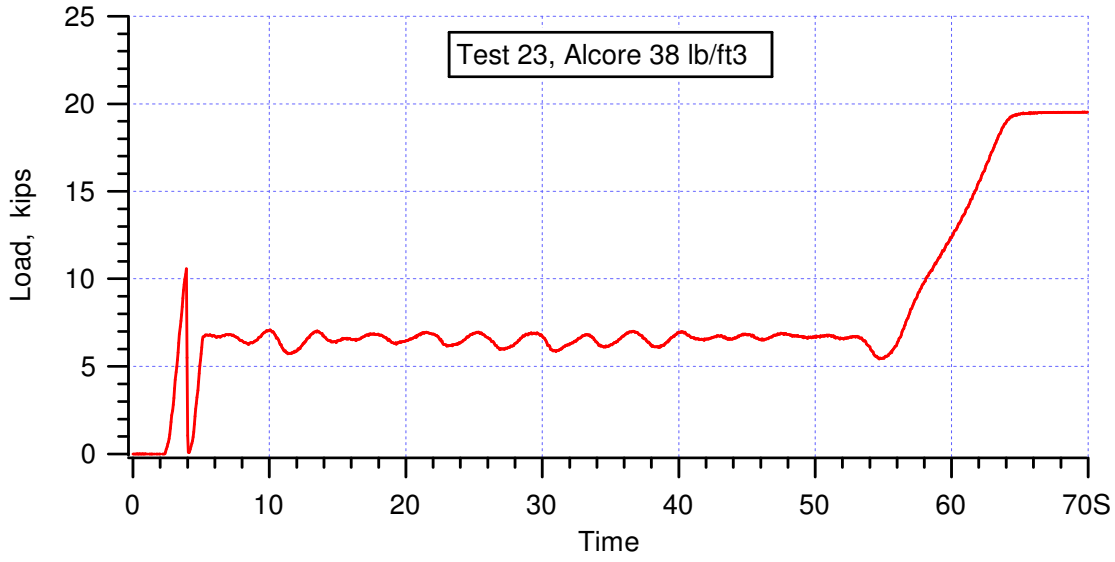
Test 23, Alcore 38 lb/ft3
Load, kips
25
20
15
10
5
0
0
10
20
30
40
50
60
70S
Time

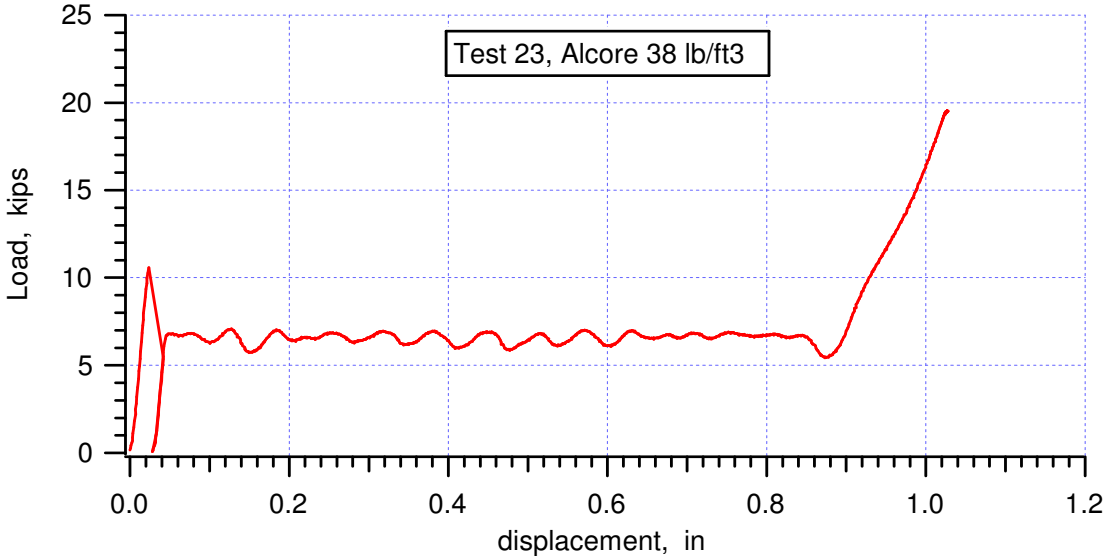
Test 23, Alcore 38 lb/ft3
Load, kips
displacement, in
0
5
10
15
20
25
0.0
0.2
0.4
0.6
0.8
1.0
1.2

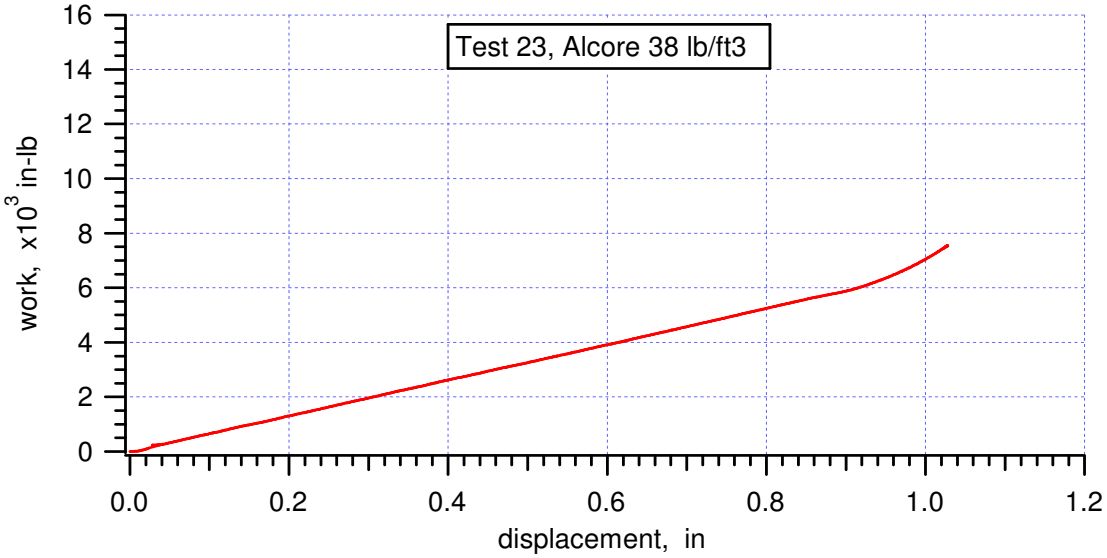
Test 23, Alcore 38 lb/ft3
work, x10^3 in-lb
displacement, in
0
2
4
6
8
10
12
14
16
0.0
0.2
0.4
0.6
0.8
1.0
1.2

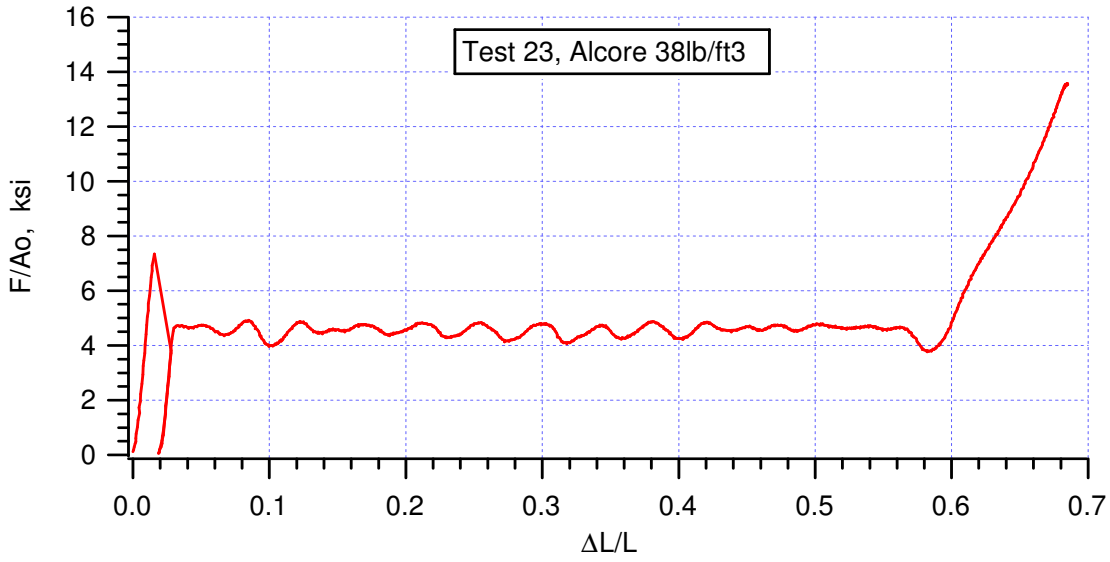

crush strength = 4.56 ksi, averaged from (0.0285, 4.2311) to (0.5811, 3.8044)

peak stress = 7.3422 ksi @ 0.016

crush efficiency = 60.8%, from (0.0157, 7.3422) to (0.623, 7.3022)

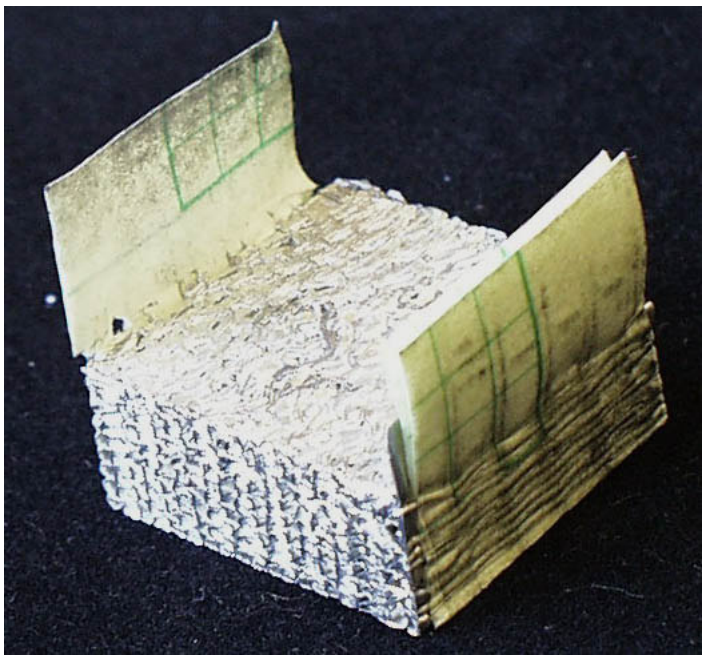

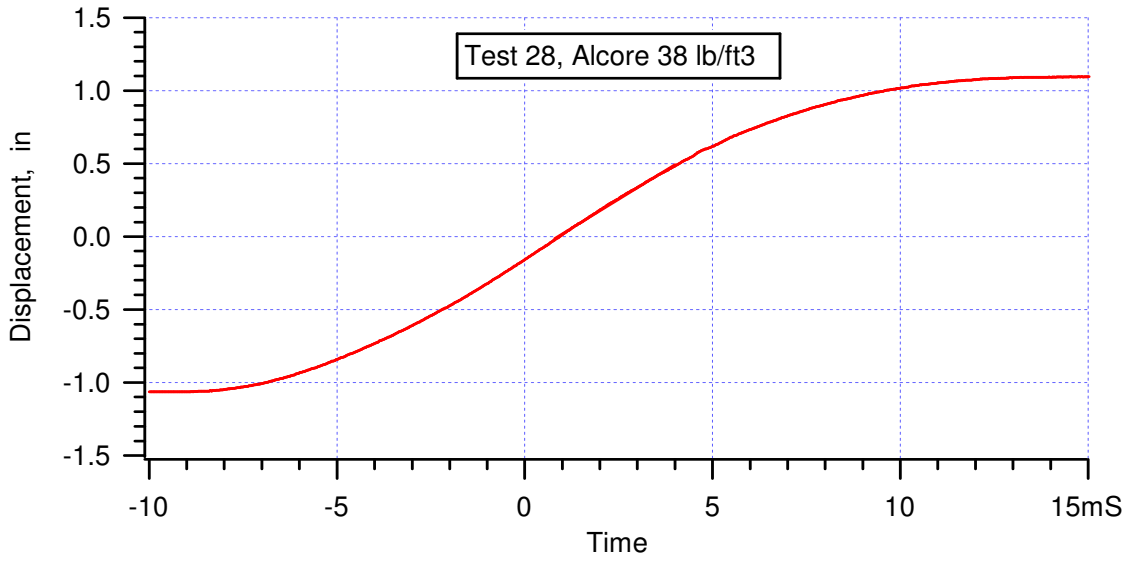

Loading rate = 158 in/s, averaged from (0.0008,-0.0212) to (0.0040, 0.4844)

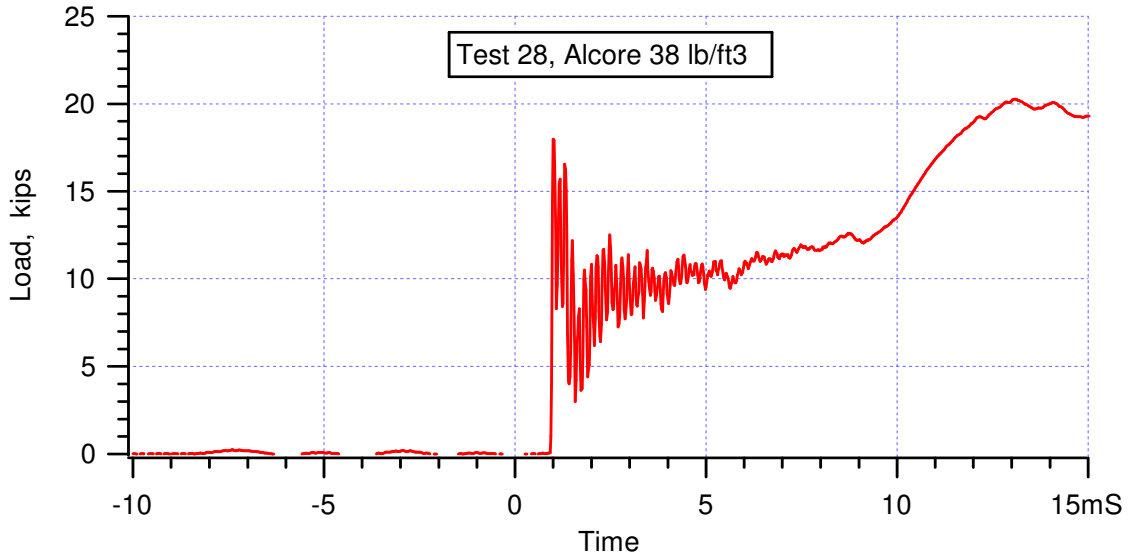

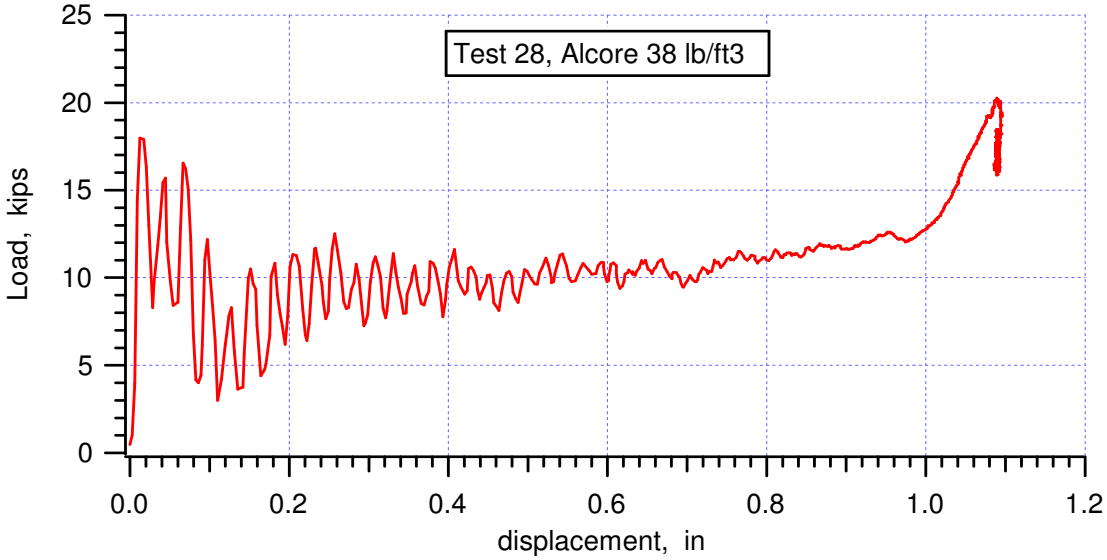
Test 28, Alcore 38 lb/ft3
Load, kips
displacement, in
0
5
10
15
20
25
0.0
0.2
0.4
0.6
0.8
1.0
1.2

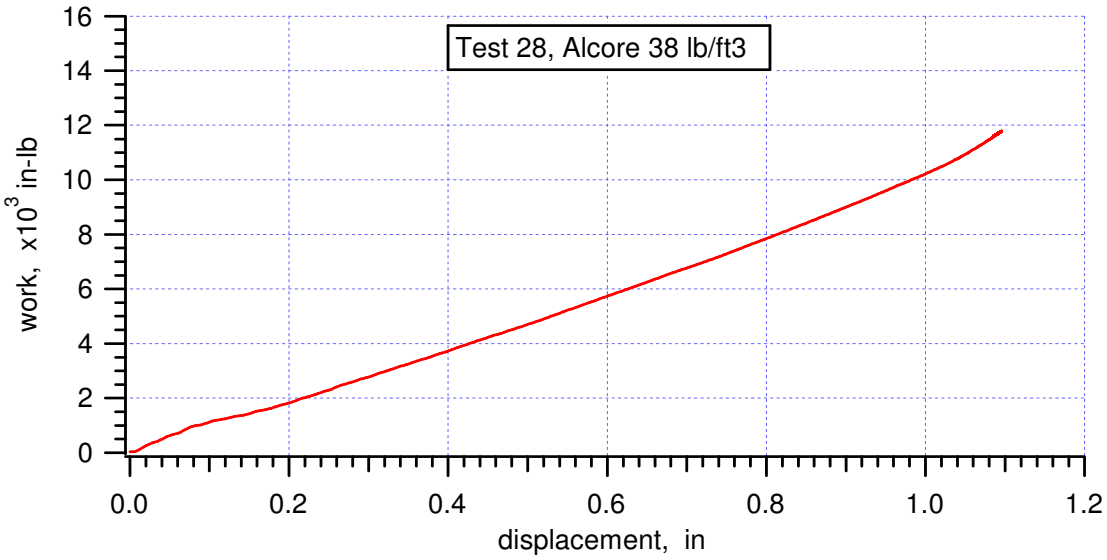
Test 28, Alcore 38 lb/ft3
work, x10^3 in-lb
displacement, in
0
2
4
6
8
10
12
14
16
0.0
0.2
0.4
0.6
0.8
1.0
1.2

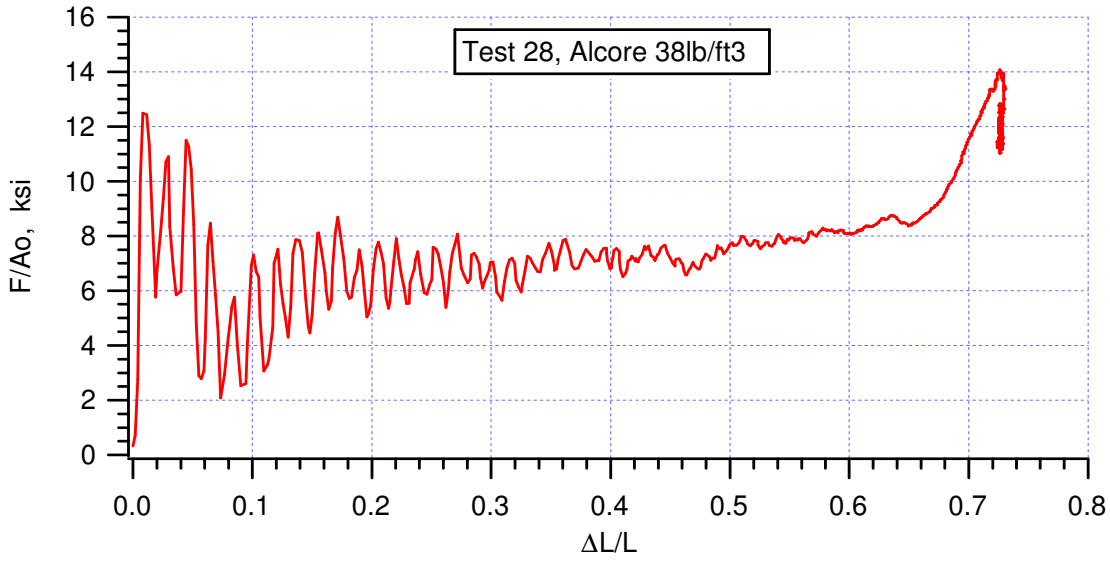

crush strength = 7.24 ksi, averaged from (0.0189, 5.7644) to (0.6494, 8.3956)

peak stress = 12.493 ksi @ 0.0082

crush efficiency =70%, from (0.0082, 12.493) to (0.7112, 12.511)

Note: one ribbon was jammed between die and punch

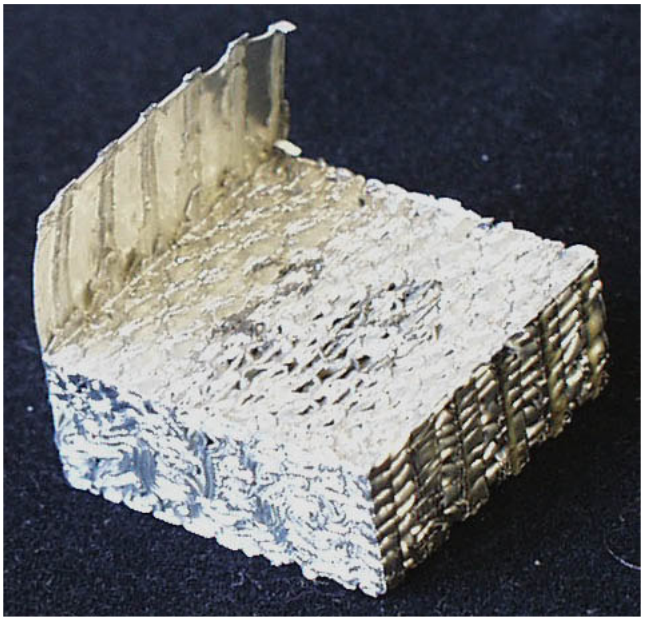

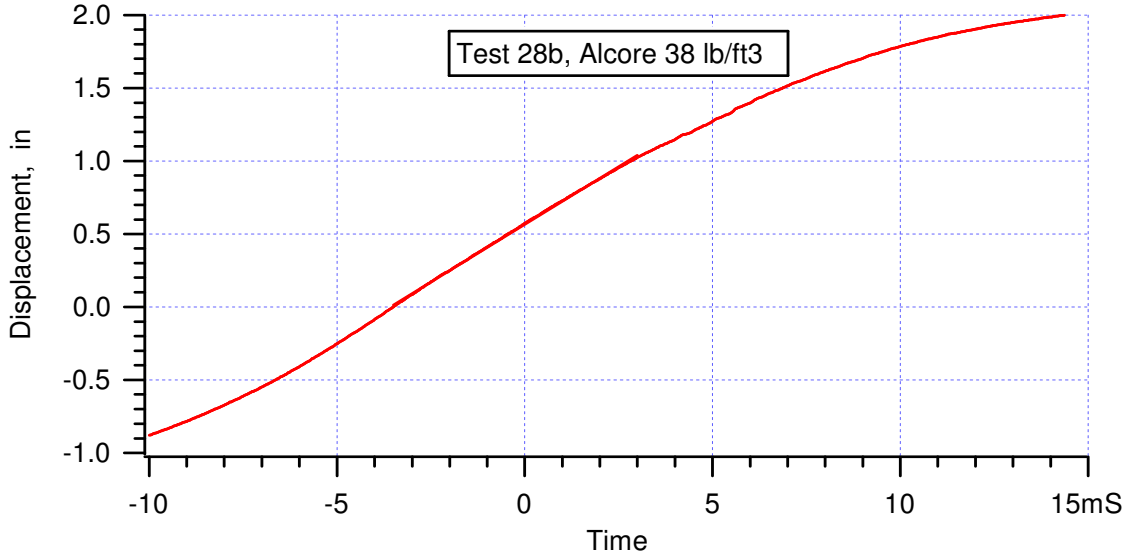

Loading rate = 158 in/s, averaged from (-0.0035, 0.0004) to (0.003, 1.0244)

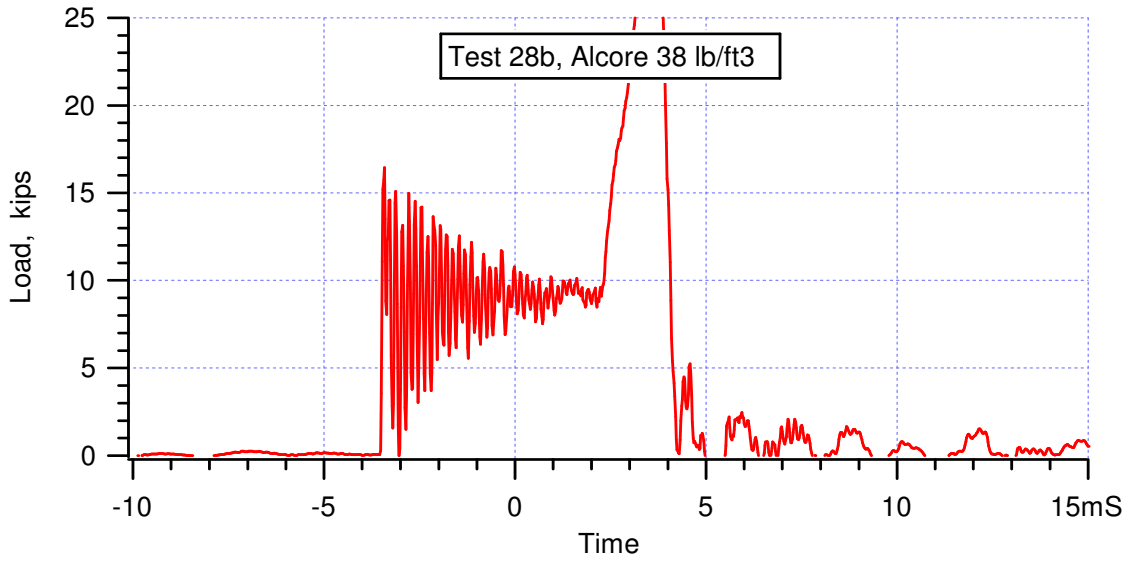

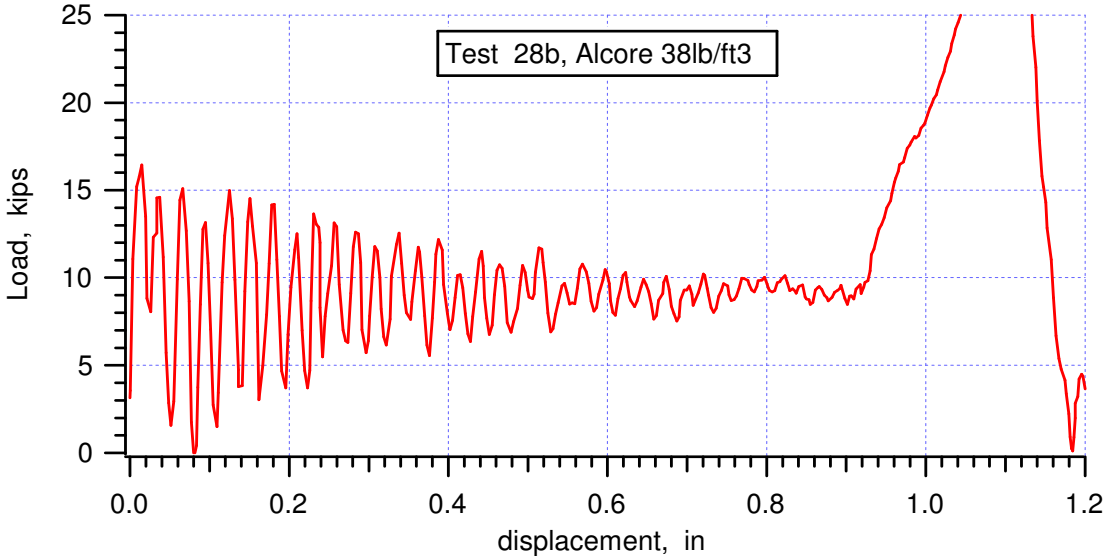
Test 28b, Alcore 38lb/ft3
Load, kips
displacement, in
0
5
10
15
20
25
0.0
0.2
0.4
0.6
0.8
1.0
1.2

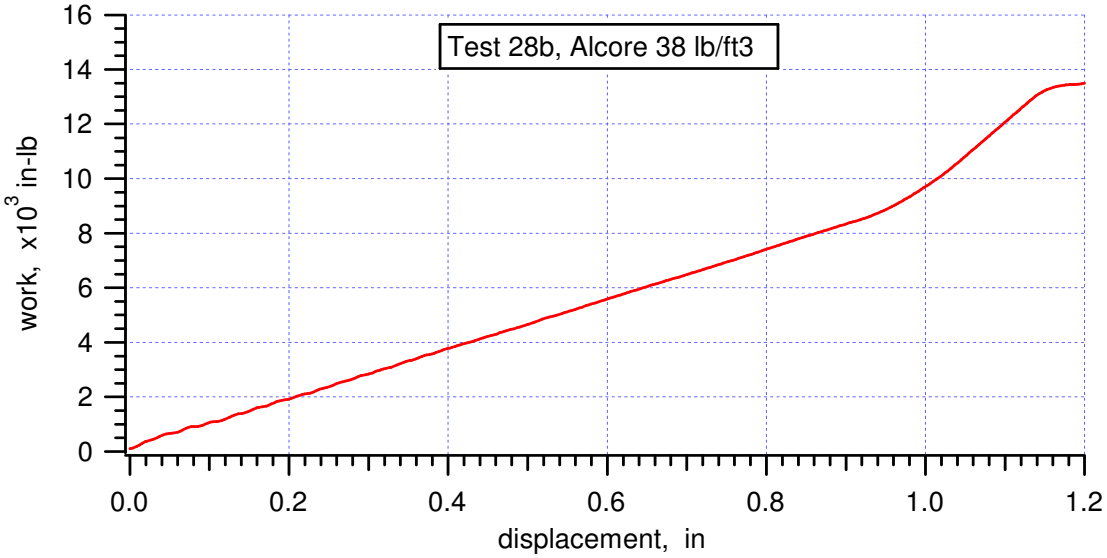
Test 28b, Alcore 38 lb/ft3
work, x10^3 in-lb
displacement, in
0
2
4
6
8
10
12
14
16
0.0
0.2
0.4
0.6
0.8
1.0
1.2

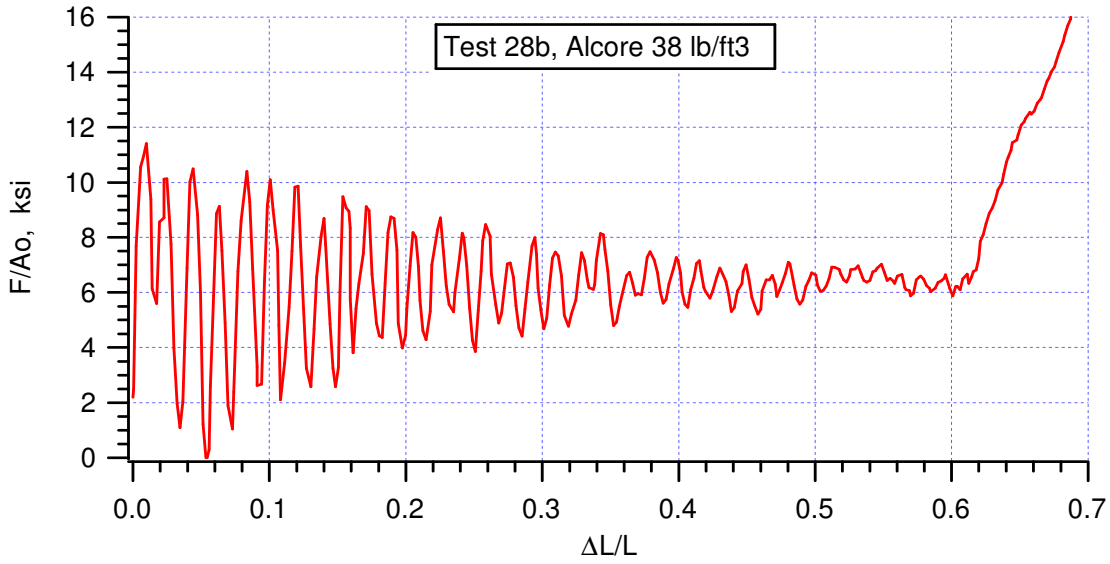

crush strength = 6.30 ksi, averaged from (0.0173, 5.6000) to (0.5987, 6.1289)

peak stress = 11.413 ksi @ 0.0099

crush efficiency =70%, from (0.0099, 11.413) to (0.6477, 11.538)

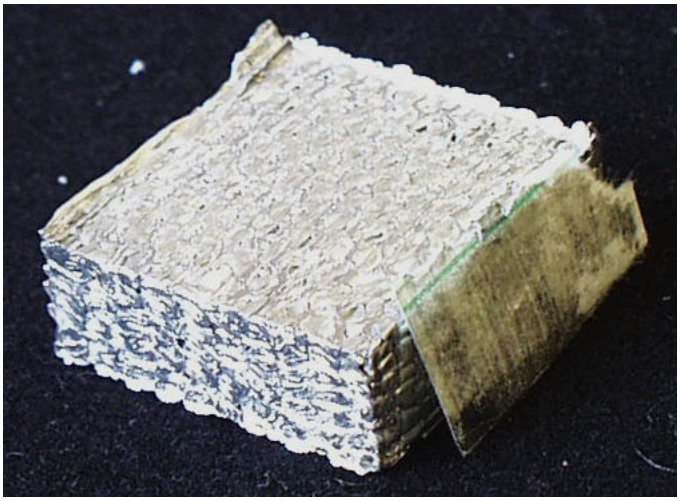

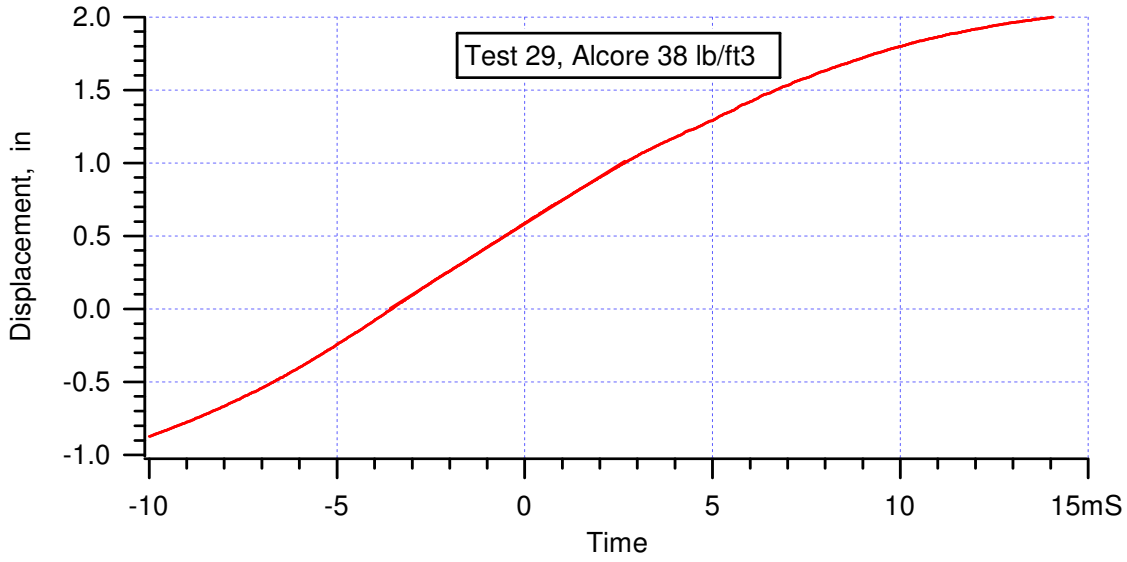

Loading rate = 162 in/s calculated from (-0.00358, -0.0068) to (0.00266, 1.0012)

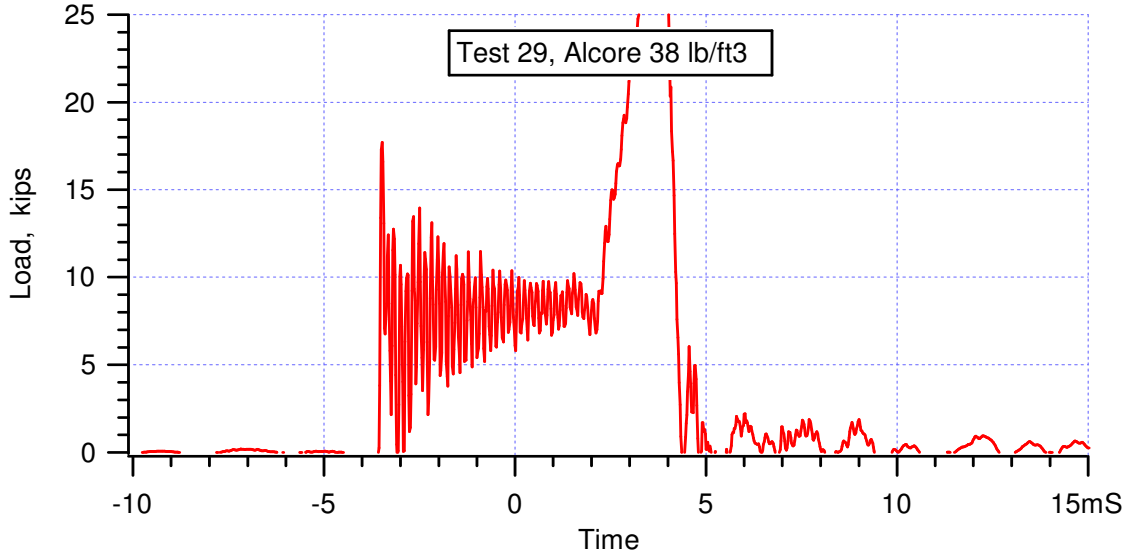

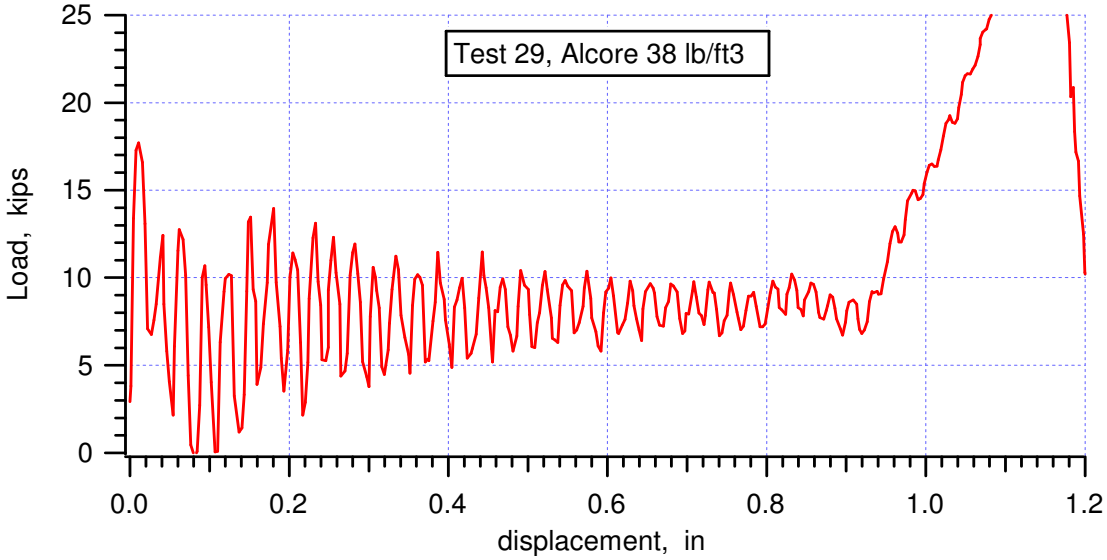
Test 29, Alcore 38 lb/ft3
Load, kips
displacement, in
0
5
10
15
20
25
0.0
0.2
0.4
0.6
0.8
1.0
1.2

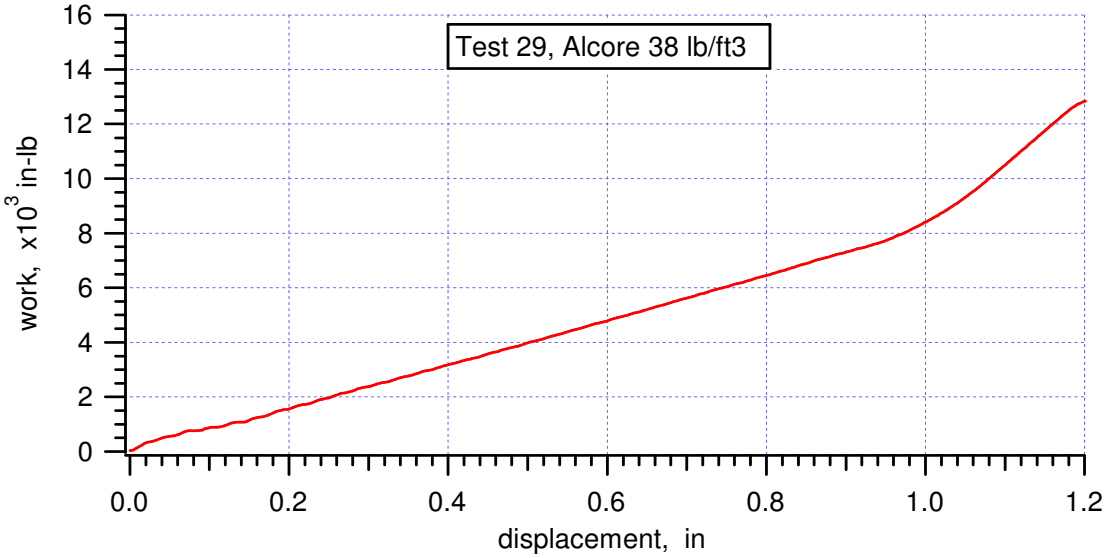
Test 29, Alcore 38 lb/ft3
work, x10^3 in-lb
displacement, in
0
2
4
6
8
10
12
14
16
0.0
0.2
0.4
0.6
0.8
1.0
1.2

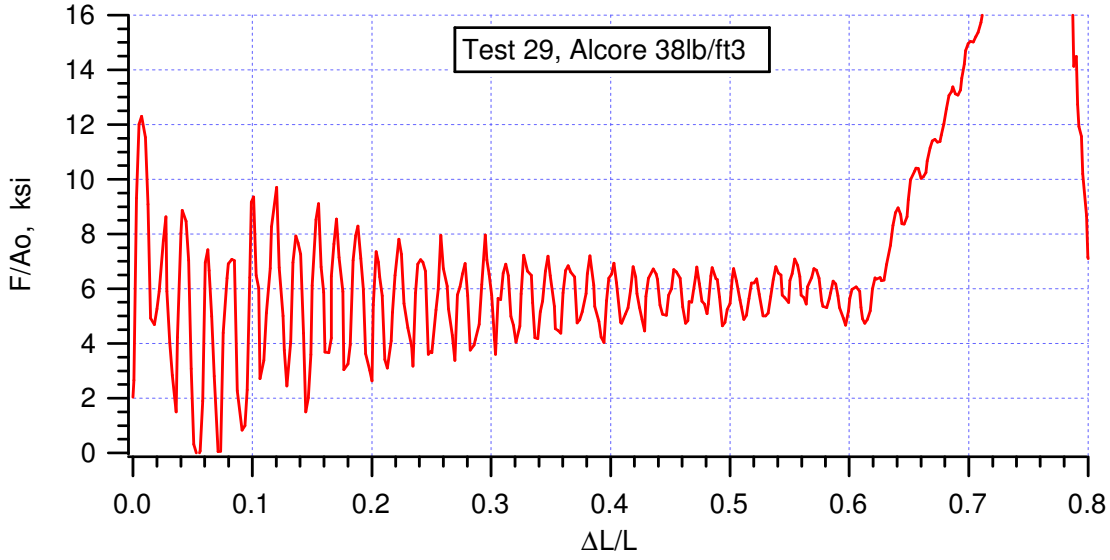

crush strength = 5.55 ksi, averaged from (0.0179, 4.6889) to (0.61307, 4.7289)

peak stress = 12.302 ksi @ 0.0072

crush efficiency =67.4%, from (0.0072, 12.302) to (0.681, 12.569)

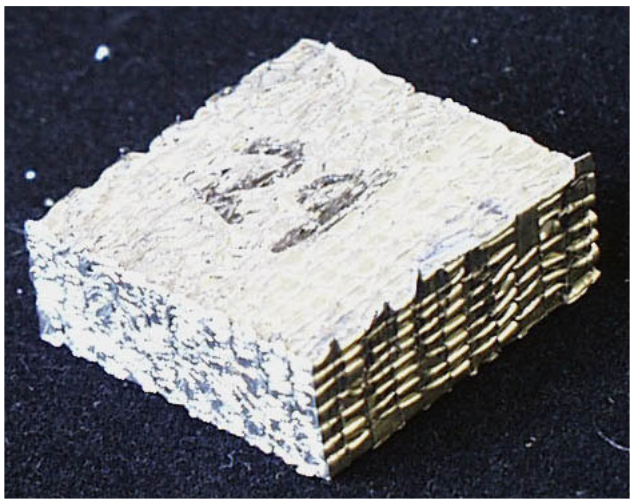

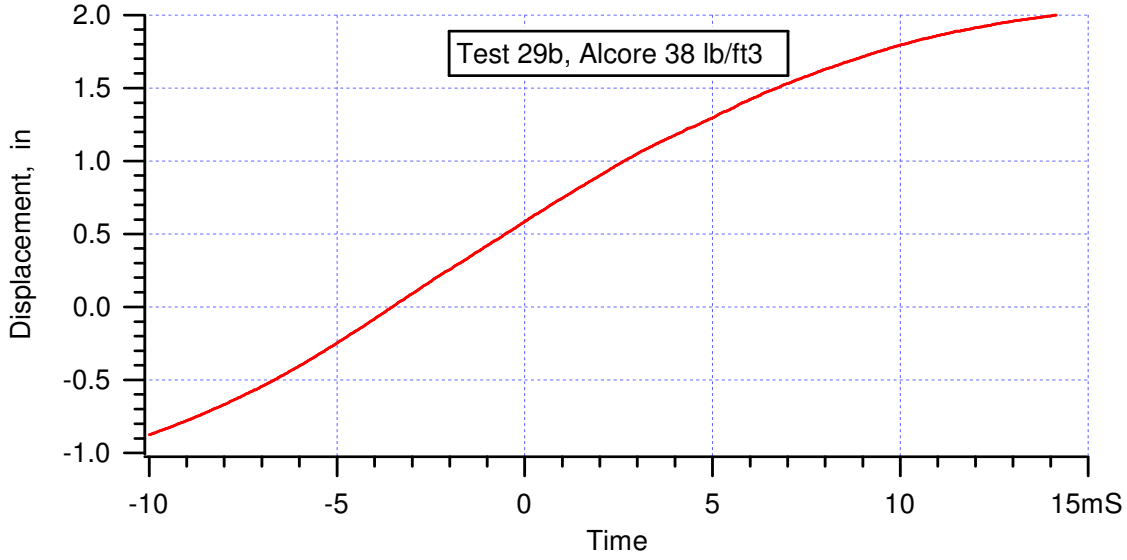
Test 29b, Alcore 38 lb/ft3
Displacement, in
2.0
1.5
1.0
0.5
0.0
-0.5
-1.0
-10
-5
0
5
10
15mS
Time

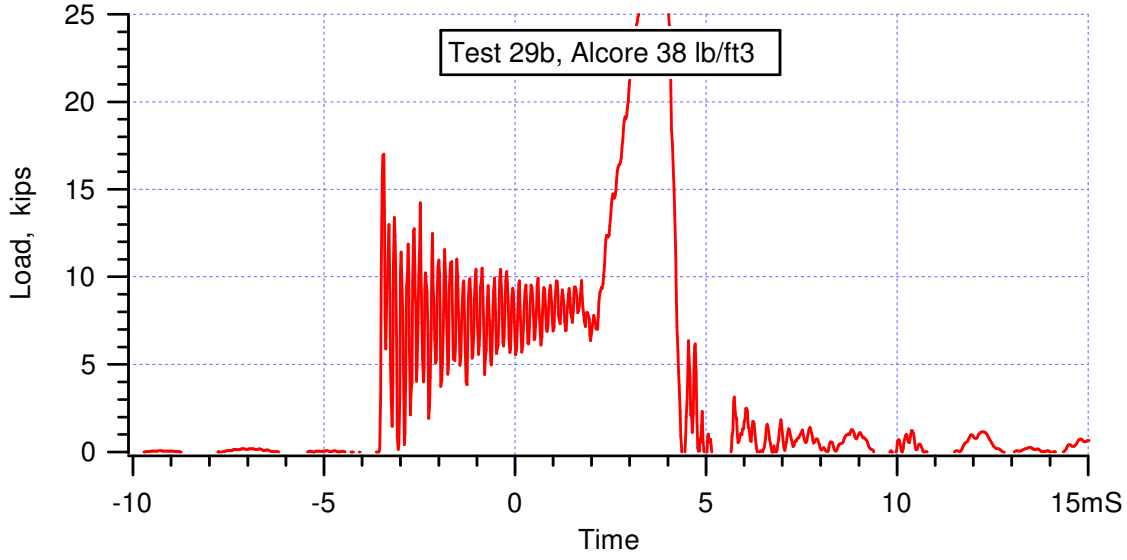
Test 29b, Alcore 38 lb/ft3
Load, kips
25
20
15
10
5
0
-10
-5
0
5
10
15mS
Time

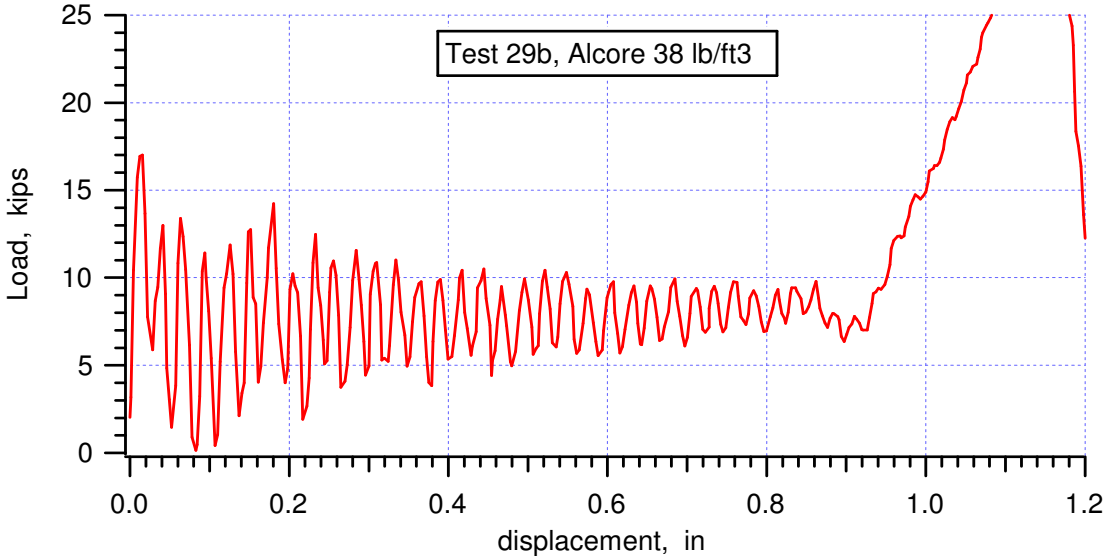
Test 29b, Alcore 38 lb/ft3
Load, kips
displacement, in
0
5
10
15
20
25
0.0
0.2
0.4
0.6
0.8
1.0
1.2

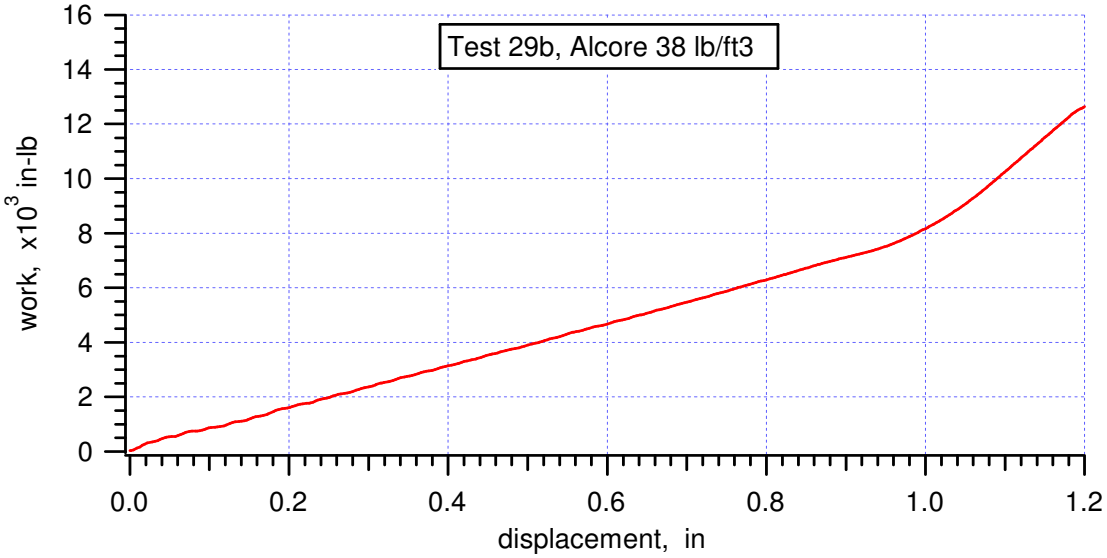
Test 29b, Alcore 38 lb/ft3
work, x10^3 in-lb
displacement, in
0
2
4
6
8
10
12
14
16
0.0
0.2
0.4
0.6
0.8
1.0
1.2

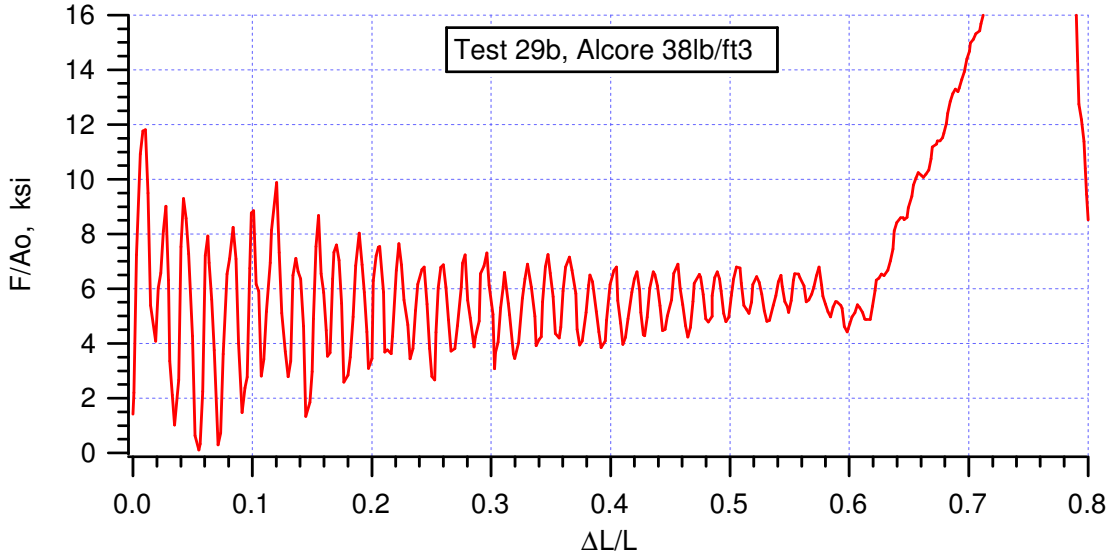

crush strength = 5.39 ksi, averaged from (0.0189, 4.08) to (0.61307, 4.8889)

peak stress = 11.76 ksi @ 0.0083

crush efficiency =67.4%, from (0.0082, 11.76) to (0.681, 12.04)

Note: The responses of #29 & 29b are almost identical.

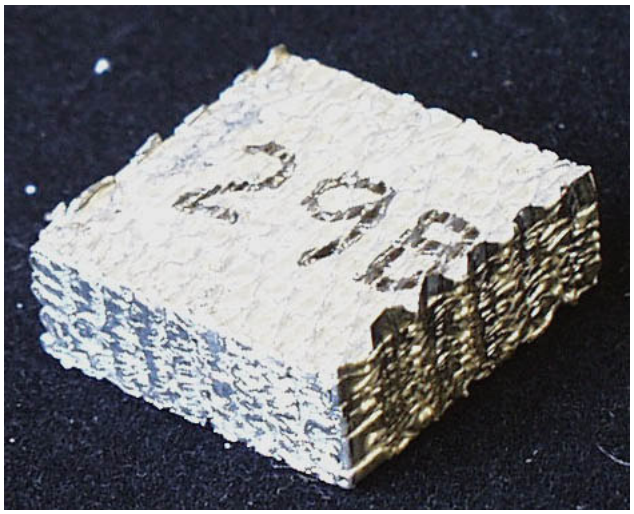

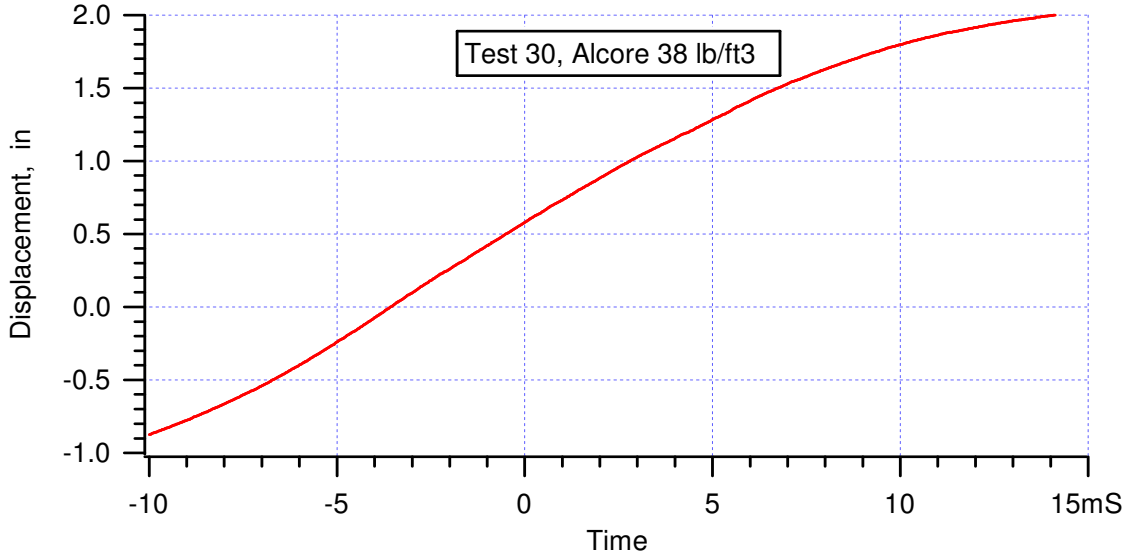
Test 30, Alcore 38 lb/ft3
Displacement, in
2.0
1.5
1.0
0.5
0.0
-0.5
-1.0
-10
-5
0
5
10
15mS
Time

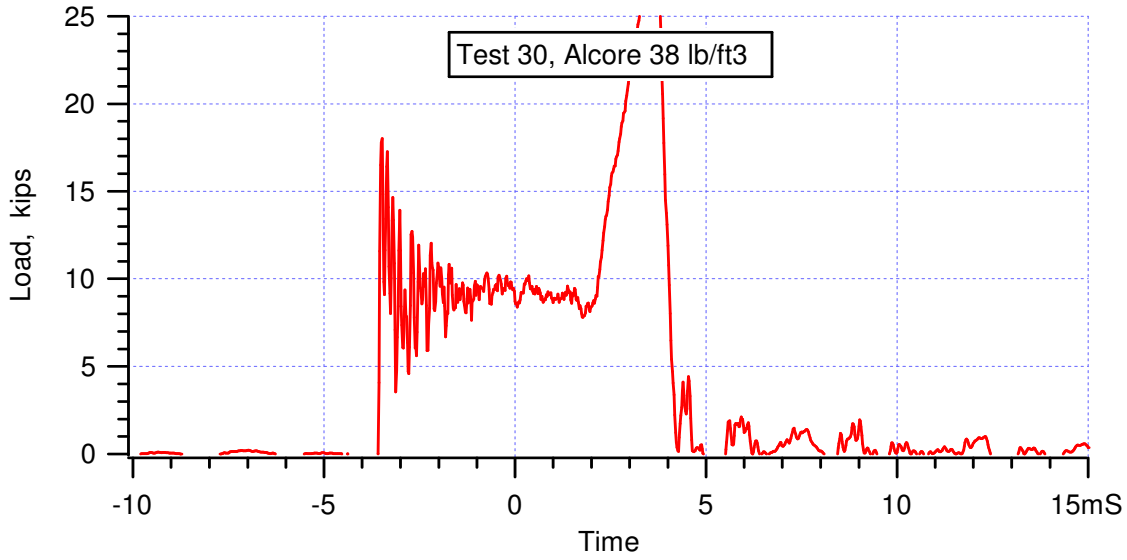
Test 30, Alcore 38 lb/ft3
Load, kips
25
20
15
10
5
0
-10
-5
0
5
10
15mS
Time

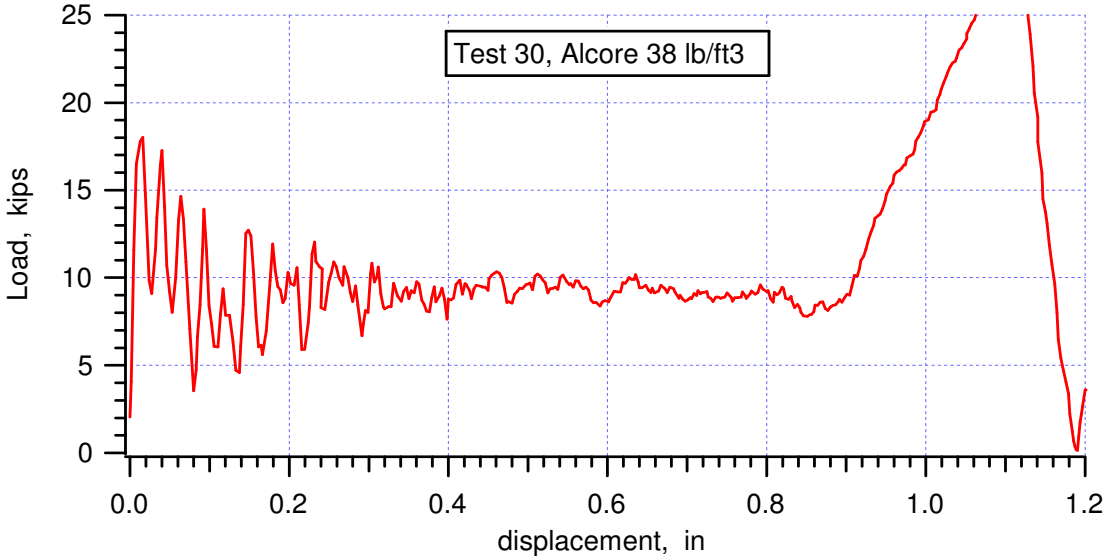
Test 30, Alcore 38 lb/ft3
Load, kips
displacement, in
0
5
10
15
20
25
0.0
0.2
0.4
0.6
0.8
1.0
1.2

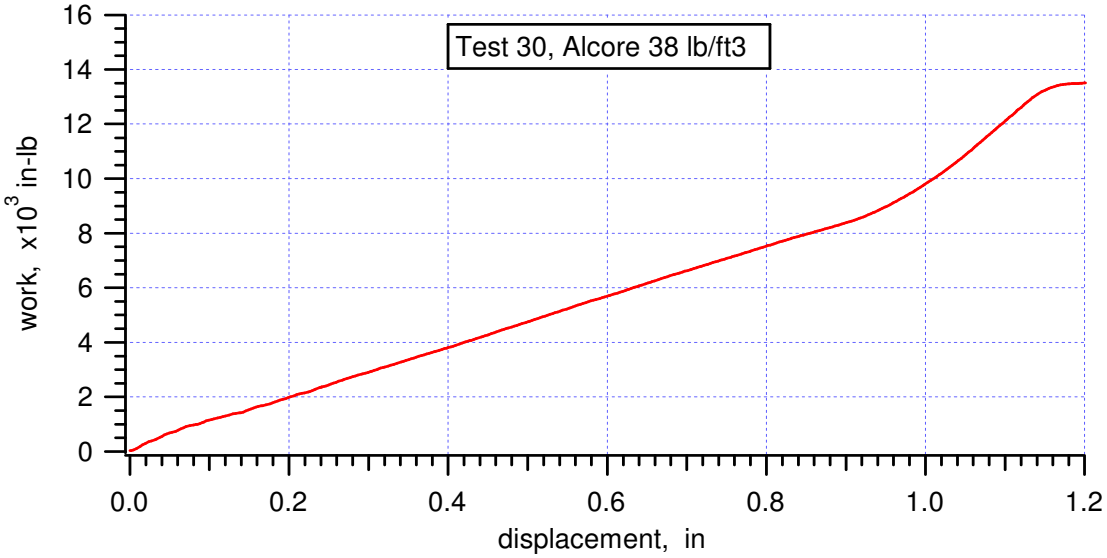
Test 30, Alcore 38 lb/ft3
work, x10^3 in-lb
displacement, in
0
2
4
6
8
10
12
14
16
0.0
0.2
0.4
0.6
0.8
1.0
1.2

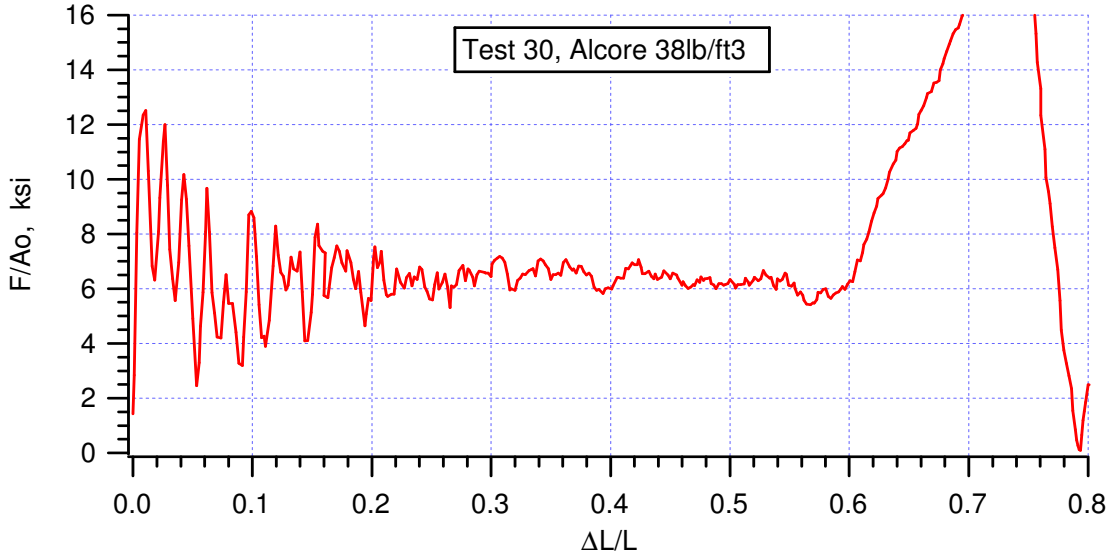

crush strength = 6.4197 ksi, averaged from (0.0181, 6.32) to (0.5675, 5.4133)

peak stress = 12.516 ksi @ 0.0107

crush efficiency =65.4%, from (0.0107, 12.516) to (0.6645, 12.987)

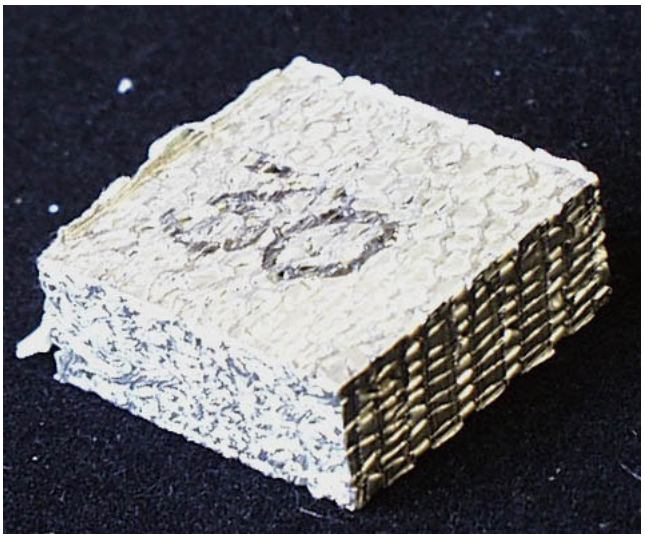

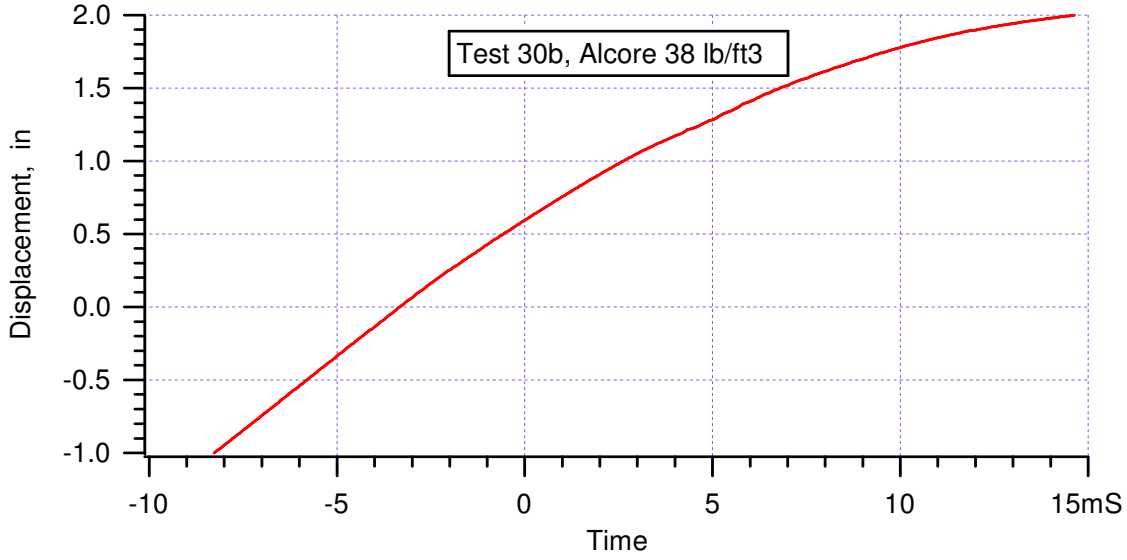
Test 30b, Alcore 38 lb/ft3
Displacement, in
2.0
1.5
1.0
0.5
0.0
-0.5
-1.0
-10
-5
0
5
10
15mS
Time

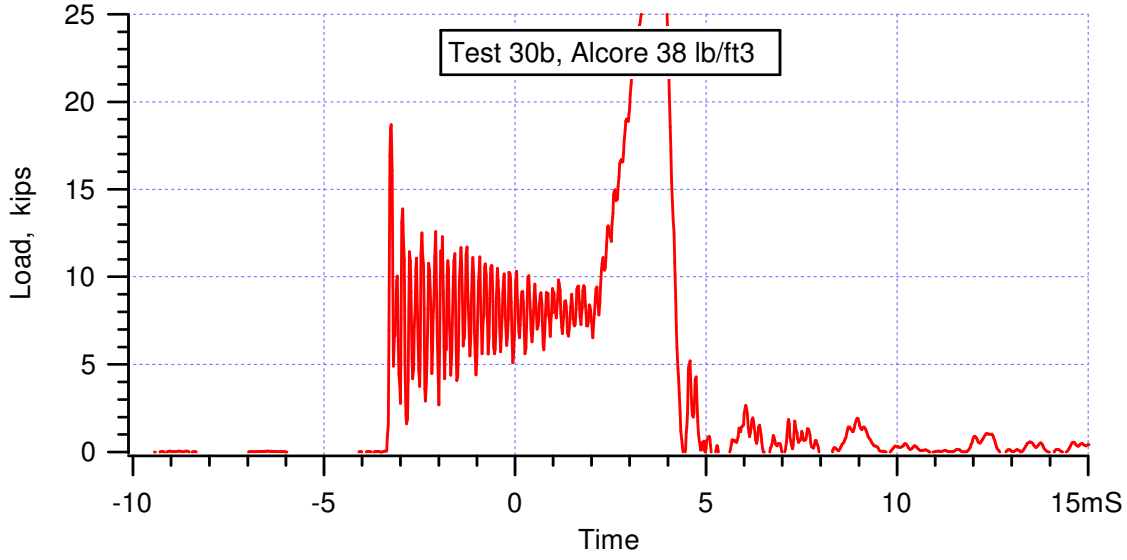
Test 30b, Alcore 38 lb/ft3
Load, kips
25
20
15
10
5
0
-10
-5
0
5
10
15mS
Time

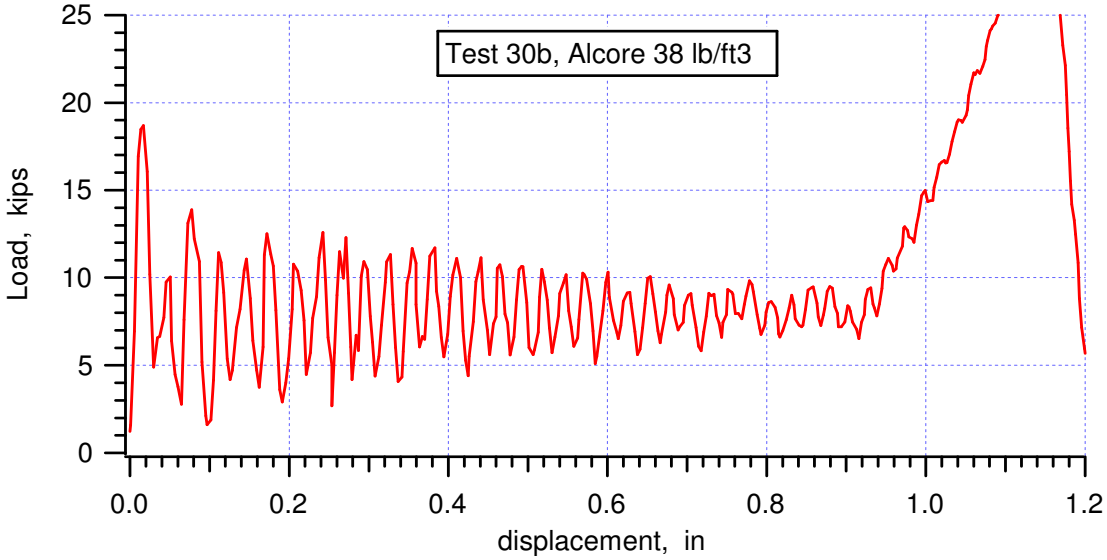
Test 30b, Alcore 38 lb/ft3
Load, kips
displacement, in
0
5
10
15
20
25
0.0
0.2
0.4
0.6
0.8
1.0
1.2

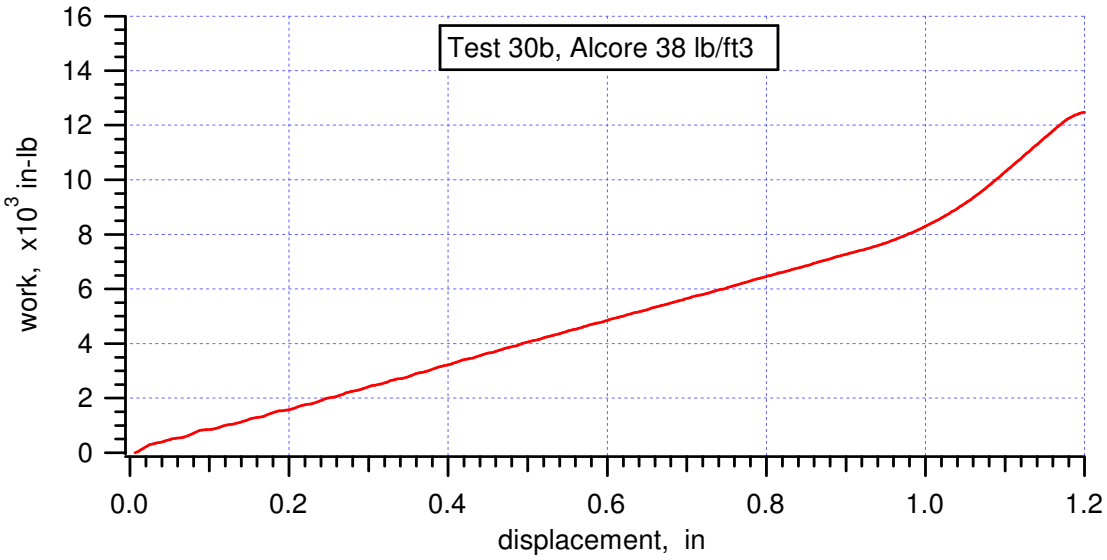
Test 30b, Alcore 38 lb/ft3
work, x10^3 in-lb
displacement, in
0
2
4
6
8
10
12
14
16
0.0
0.2
0.4
0.6
0.8
1.0
1.2

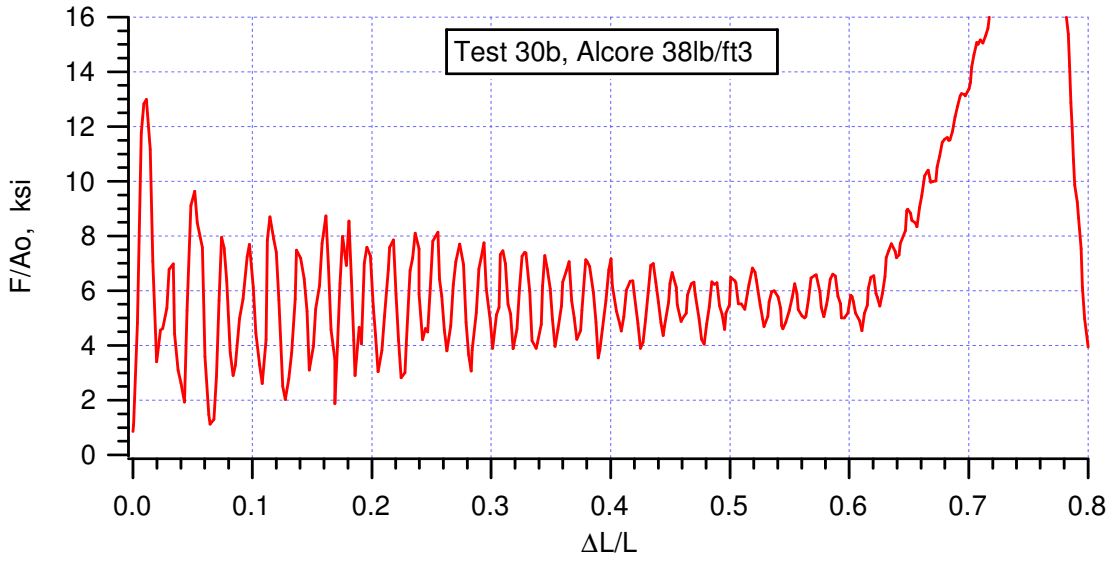

crush strength = 5.52 ksi, averaged from (0.0197, 3.4) to (0.6107, 4.5333)

peak stress = 12.987 ksi @ 0.0112

crush efficiency =67.9%, from (0.0112, 12.987) to (0.6907, 12.747)

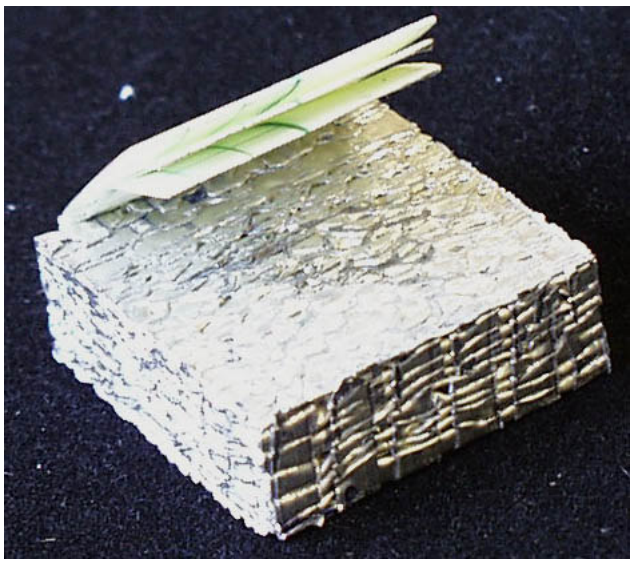

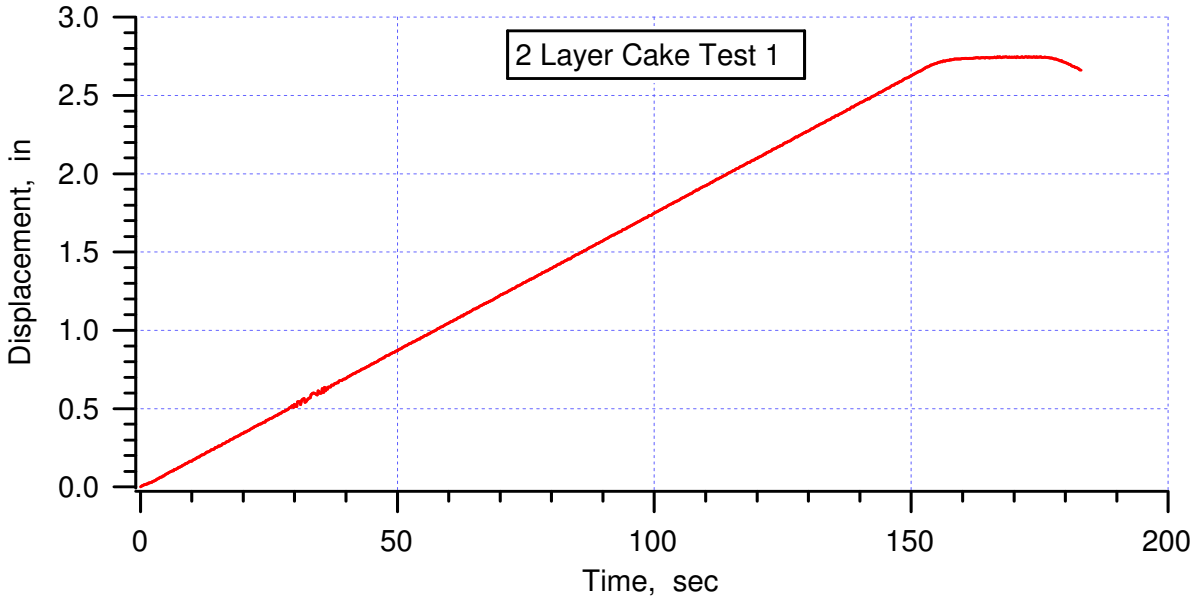
2 Layer Cake Test 1
Displacement, in
3.0
2.5
2.0
1.5
1.0
0.5
0.0
0
50
100
150
200
Time, sec

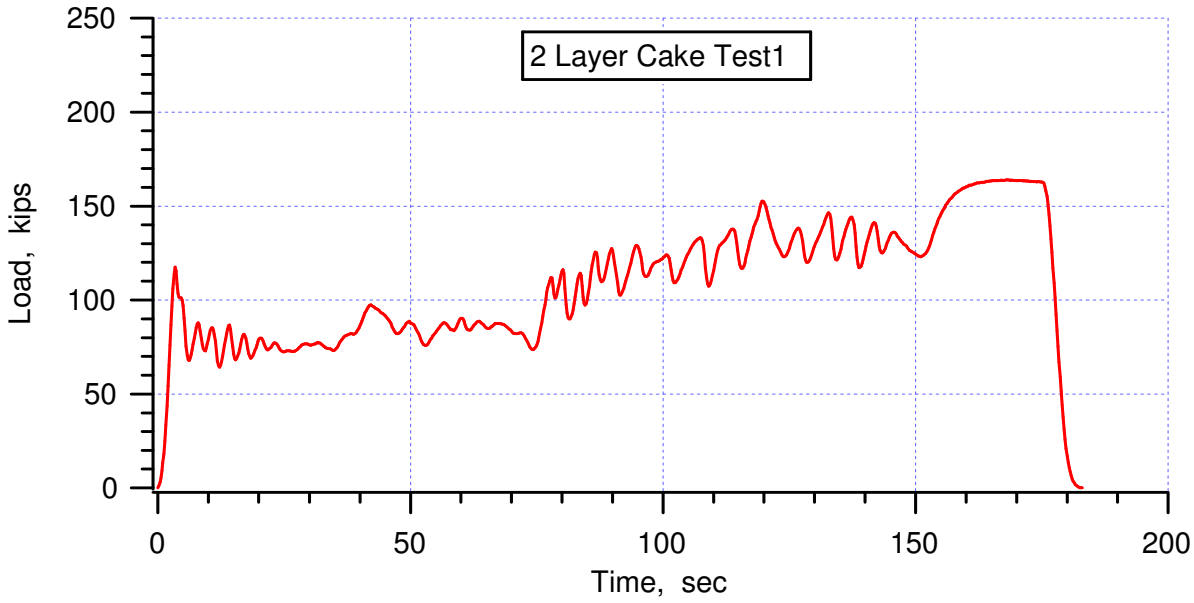
2 Layer Cake Test1
Load, kips
250
200
150
100
50
0
0
50
100
150
200
Time, sec

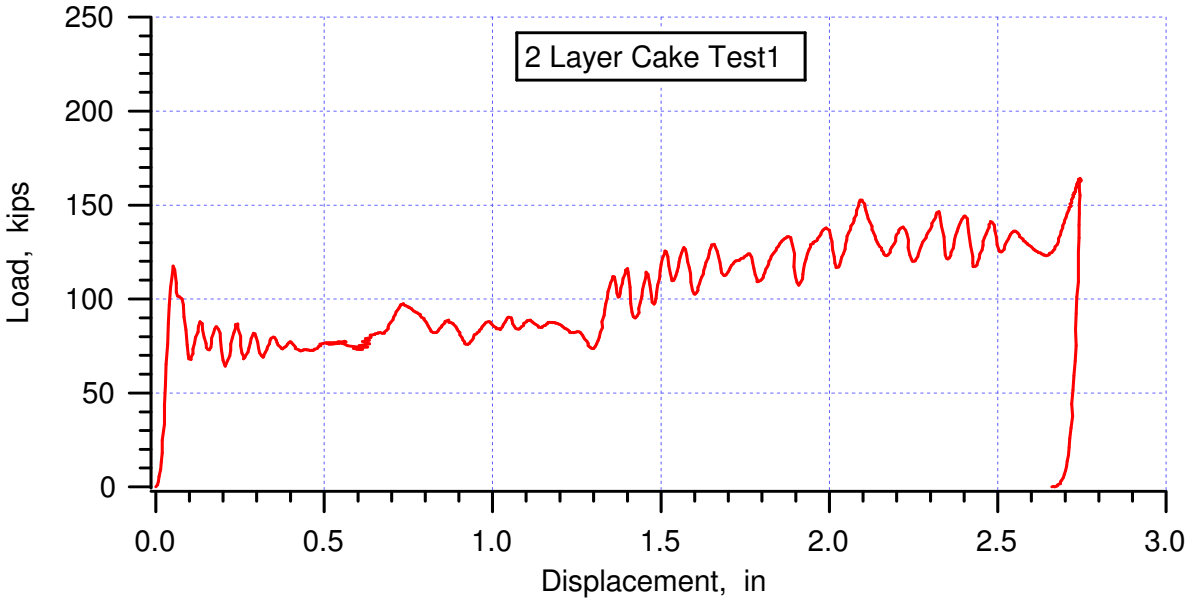
2 Layer Cake Test1
Load, kips
250
200
150
100
50
0
0.0
0.5
1.0
1.5
2.0
2.5
3.0
Displacement, in

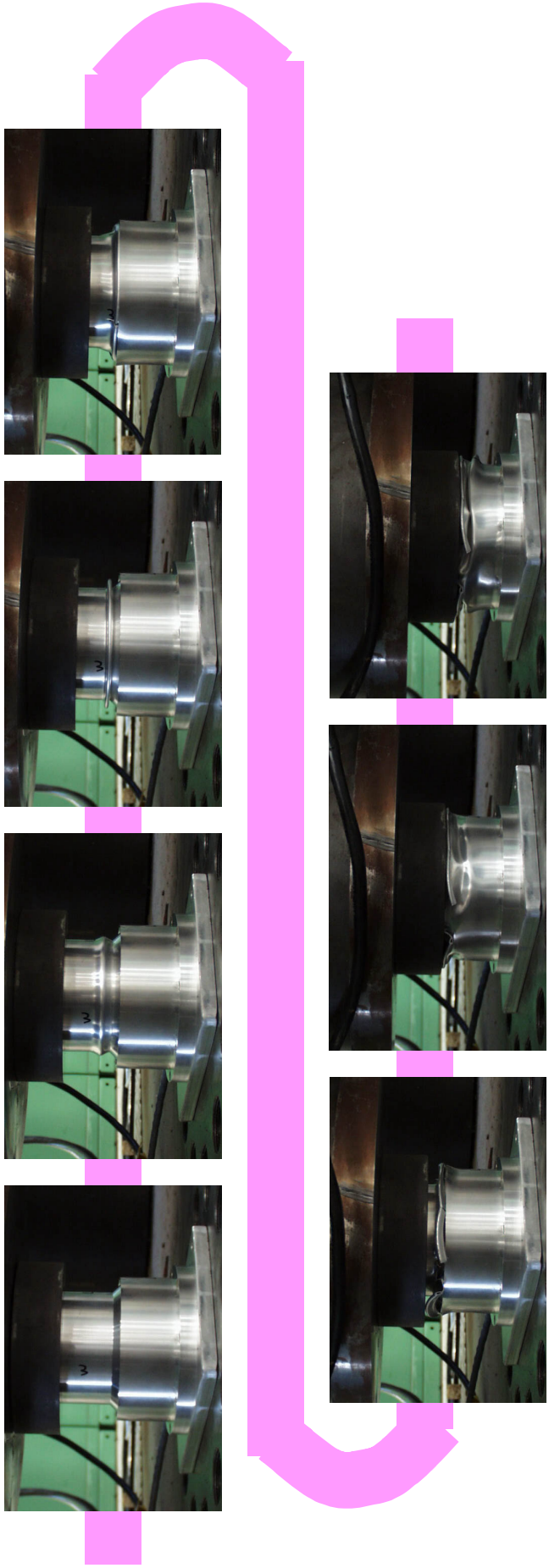

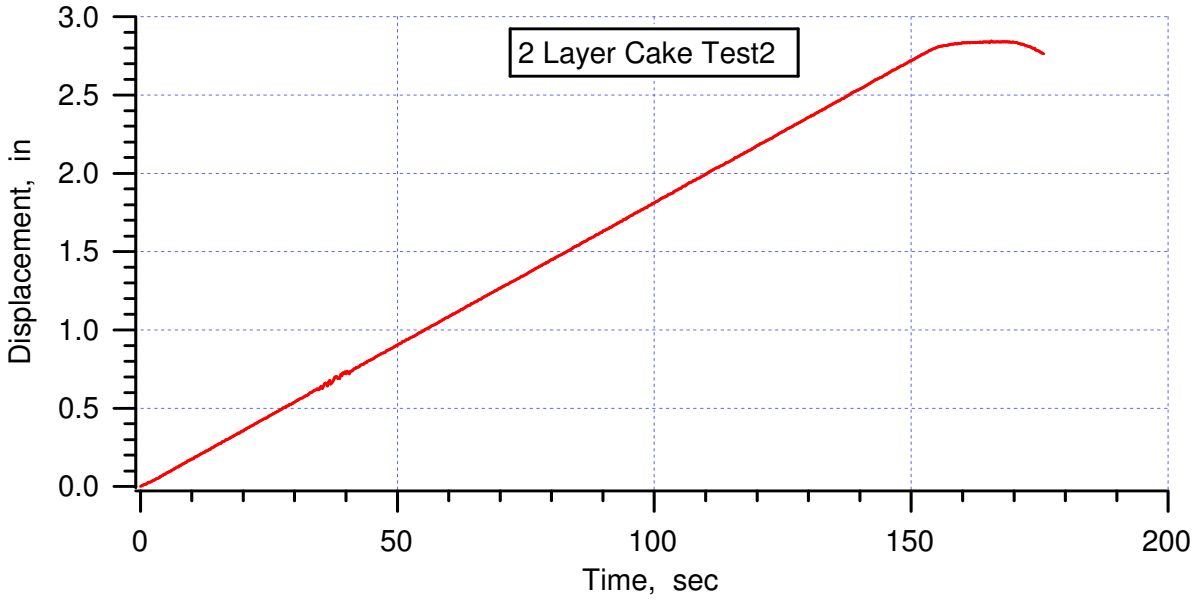
2 Layer Cake Test2
Displacement, in
3.0
2.5
2.0
1.5
1.0
0.5
0.0
0
50
100
150
200
Time, sec

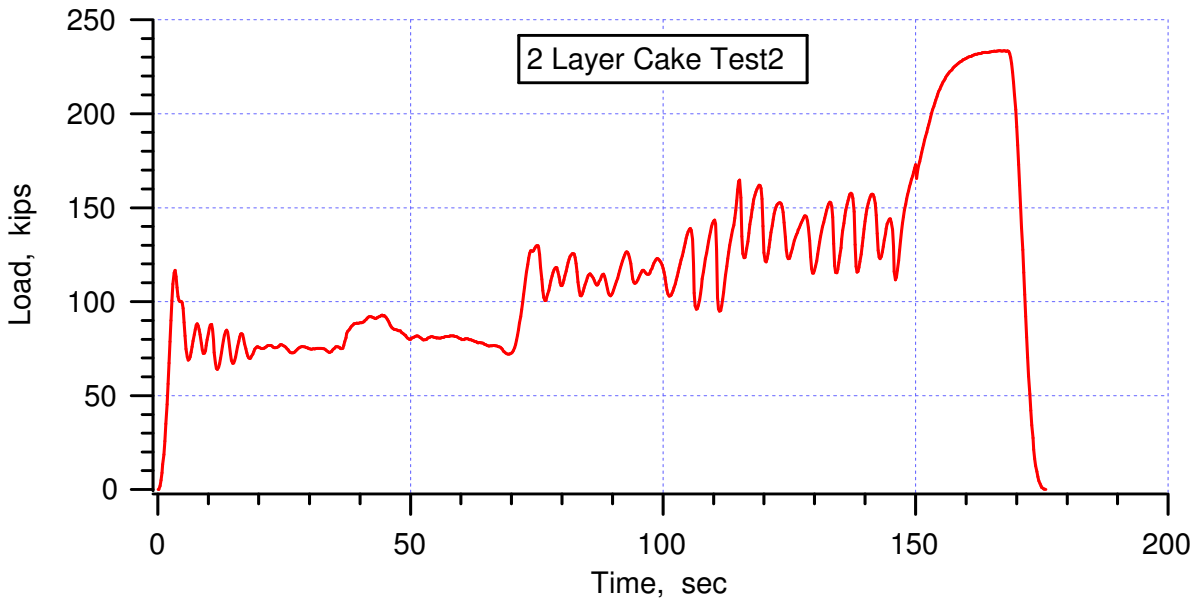
2 Layer Cake Test2
Load, kips
250
200
150
100
50
0
0
50
100
150
200
Time, sec

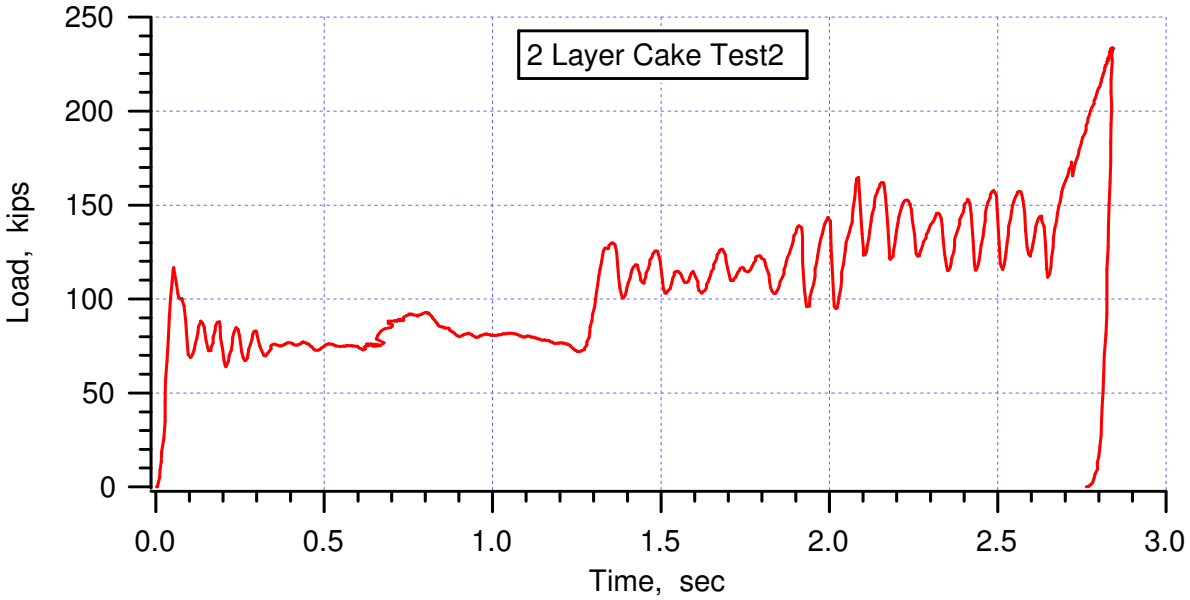
2 Layer Cake Test2
Load, kips
250
200
150
100
50
0
0.0
0.5
1.0
1.5
2.0
2.5
3.0
Time, sec

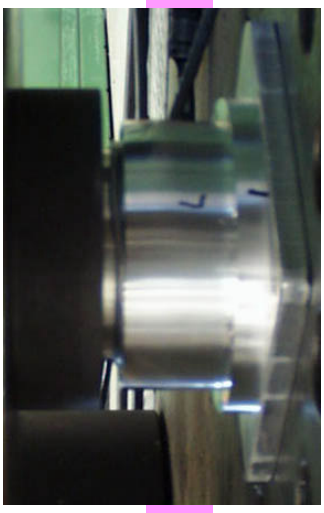

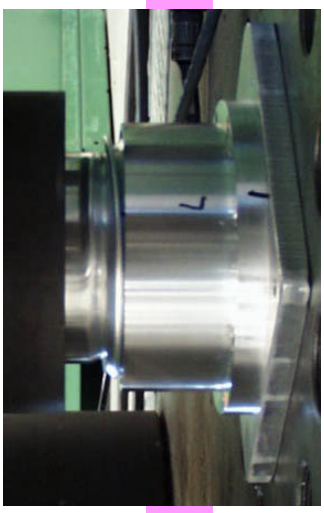

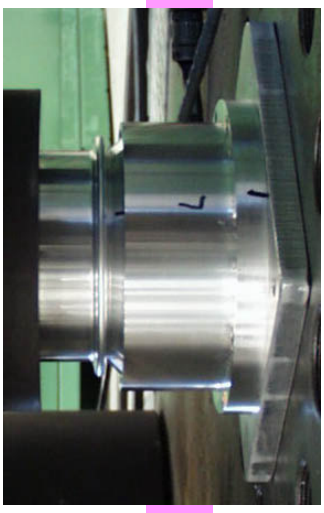

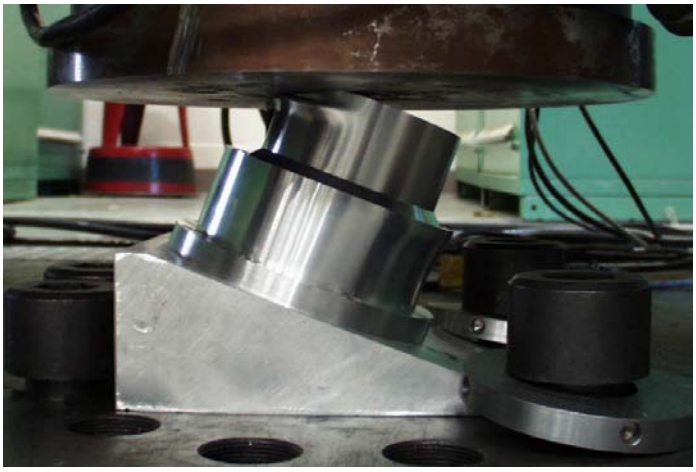

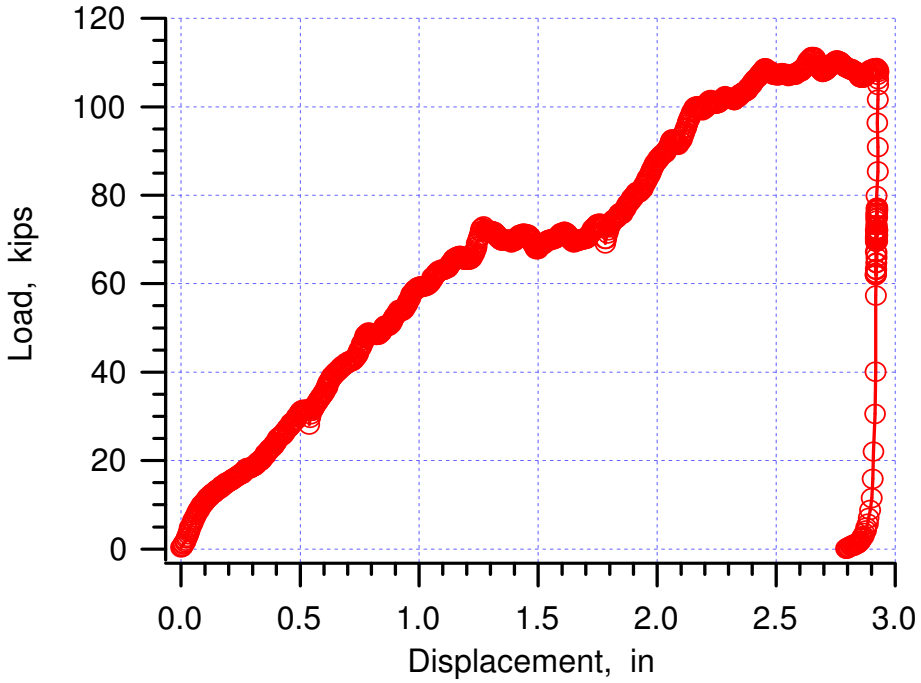
120
100
80
60
40
20
0
Load, kips
0.0
0.5
1.0
1.5
2.0
2.5
3.0
Displacement, in

APPENDIX III:

"Shear Deformation of High Density Aluminum Honeycombs," (IMCHE2003-44092) Proceedings of 2003 ASME International Mechanical Engineering Congress and Exposition, November 15-21, 2003, Washington, DC.

IMECE2003-44092

Shear Deformation of High Density Aluminum Honeycombs

Wei-Yang Lu and John Korellis
Sandia National Laboratories, MS9404
Livermore, CA 94551-0969

Terry Hinnerichs
Sandia National Laboratories, MS0847
Albuquerque, NM 87123

ABSTRACT

The orthotropic crush model has commonly been used to describe the constitutive behavior of honeycomb [1]. To completely define the model parameters of a honeycomb, experimental data of axial crushes in T, L, and W principal directions as well as shear stress-strain curves in TL, TW, and LW planes are required. The axial crushes of high-density aluminum honeycombs, e.g., 38 pcf (pound per cubic foot), under various loading speeds and temperatures have been investigated and reported [2]. This paper describes experiments and model simulations of the shear deformation of the same high-density aluminum honeycomb. Results of plate shear test, beam flexure test, and off-axis compression are presented and discussed.

INTRODUCTION

Aluminum honeycomb has three principal directions due to its composure of corrugated and flat aluminum sheets. These directions T, the strongest, L, the intermediate strength, and W, the weakest are shown schematically in Figure 1 . An earlier paper [2] described the on-axis behavior of high density aluminum honeycomb. This paper describes several shear experiments of a high-density aluminum honeycomb Hexcel (CR-8-LC-1/8-5052-006-R2 [3]), nominal 38 pcf. Also, finite element simulations of these tests are used to study the experimental results and develop validated models for honeycomb crush.

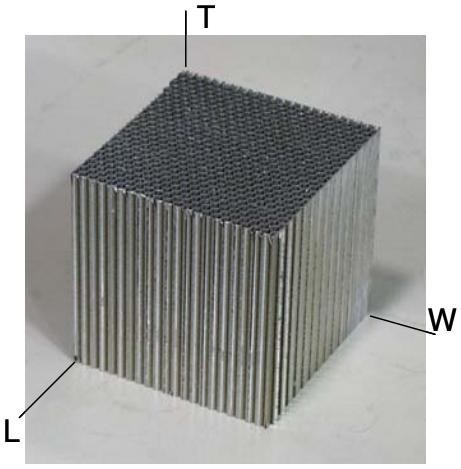

Figure 1. Aluminum honeycomb geometry and principal directions.

The Orthotropic Crush constitutive model [1] in PRONTO3D [4] is an available model to simulate the orthotropic deformation and crush of the aluminum honeycomb. The model requires three axial crush behaviors in T, L and W directions, as well as three shear deformation behaviors in TL, TW, and LW planes. This algorithm is composed of three zones of constitutive behavior as shown in Figure 2. Zone 1 represents an initial linear elastic loading phase. Zone 2 contains all the permanent volumetric crush displayed by the model and begins when the applied stress, in any direction, exceeds the crush strength that must be defined as a function of

volumetric strain in each direction. Zone 2a is a typical constant crush value versus volumetric strain region and zone 2b represents a hardening portion of the curve prior to the "Full Compaction" that initiates Zone 3. The theoretical "Full Compaction" volumetric strain for 38 pcf is 0.78. The Zone 3 constitutive model is an isotropic and incompressible elastic-perfectly plastic constitutive model. These three zones of the Orthotropic Crush model provide the flexibility and modeling capability to handle large amounts of uncoupled uniaxial strain behavior. However, the Orthotropic Crush model does not include loading rate, temperature, and coupling between axes other than what develops with the volumetric strain formulation. Also, it does not include any direct dependence on plastic shear strain.

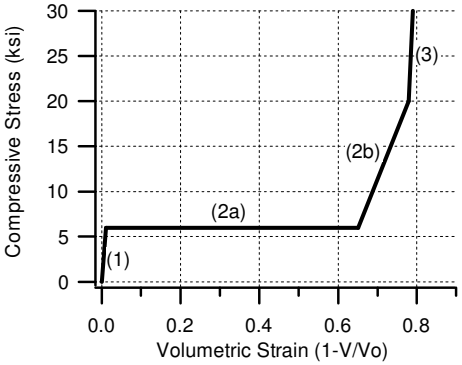

Figure 2. Three zones of Orthotropic Crush Model behavior

Almost all energy absorption is done in the crush Zone 2. Three model parameters are required to describe Zone 2 in each direction: crush strength and crush efficiency in Zone 2a and hardening modulus in Zone 2b. Crush efficiency is defined as the volumetric strain that initiates the hardening portion of Zone 2b. In large deformation analyses of structures that involve honeycomb components, the force and displacement results depend strongly on Zone 2 parameters.

Plate shear test and beam-flexure test are typical methods to obtain shear properties of honeycomb [3, 5]. Plate shear method is preferred in general since the results from beam-flexure method have been found to be influenced by several parameters, such as facing thickness, facing material, core thickness and loading conditions. A comparison of shear strength of low density (2 to 9 pcf) honeycombs obtained from these two methods shows flexure shear strength is consistently higher than plate shear strength. Take 8 pcf honeycomb for example, the beam-flexure method overestimates the TL shear strength by 20%. The data also shows the amount of overestimation increases with density [3]. Even with such a large uncertainty involved, the available shear strength data of 20 pcf and heavier honeycombs are all from beam-flexure testing because of difficulties in plate shear method. For heavier density honeycombs, the adhesive bond between the honeycomb and steel plates of plate shear specimen fails prematurely due to the high shear load.

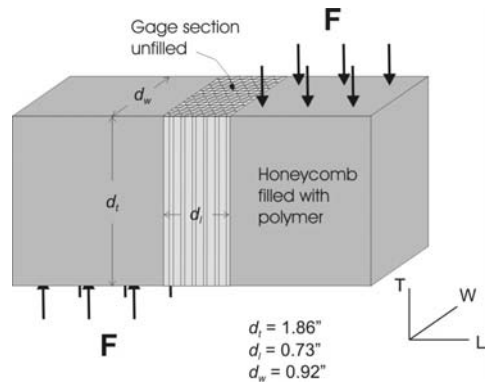

Figure 3. A schematic of modified shear specimen. Loading sections are honeycomb filled with polymer.

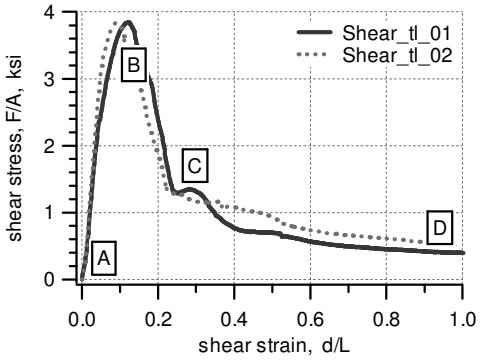

Figure 4. Shear stress-strain curves of 38 pcf honeycomb.

MODIFIED SHEAR EXPERIMENTS

The major difficulty of the plate shear method is the limited adhesive bonding strength between the core and steel plates, which is not strong enough to fail high density honeycombs. Instead of using steel plates for load introduction, the standard specimen was modified and prepared differently so that the desired plate shear test could be achieved. A novel approach was developed by creating loading sections from the same piece of honeycomb and filling cells with polymer, but left the gage section unfilled. A schematic of this modified specimen is shown in Figure 3. First, simple shear tests were

conducted on a MTS system to study the feasibility of this approach. Experimental results of two specimens are plotted in Figure 4; pictures of the simple shear setup and deformed gage sections are shown in Figure 5. Notice that the distance d_L was fixed during the test. Specimen dimensions are listed in Table 1.

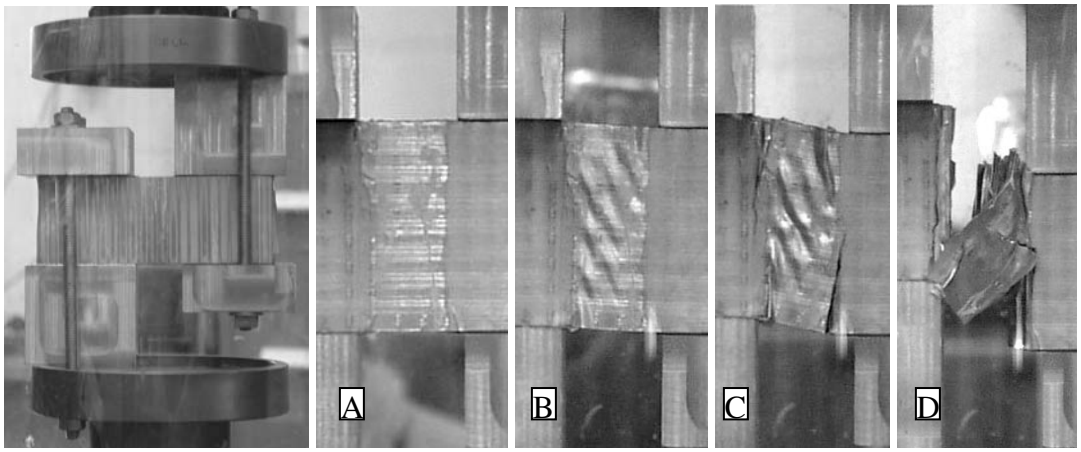

Figure 5. Simple shear experimental setup and deformed gage section. Deformed states A, B, C and D correspond to 0, 0.11, 0.25 and 1.0 engineering shear strains of specimen shear_tl_01.

Table 1. Dimension of shear specimens

Specimen	Test	d_T, in	d_L, in	d_W, in
shear_tl_01	simple shear	1.86	0.73	0.92
shear_tl_02	simple shear	1.86	0.73	0.86
shear_tl_03	plate shear	4.95	1.00	1.15
shear_tl_04	plate shear	5.86	1.00	1.40
Typical	plate shear	7.50	0.63	2.00

The modified specimen worked well. No damage was observed at the polymer-honeycomb interface. Shear deformed honeycomb was evident in state B, which was before reaching the peak stress, 3.85 ksi. After the peak stress, tearing started to occur at upper left and lower right corners and the cracks propagated as load dropped quickly until two cracks reached about the same level, shown as state C; then the load decreased slowly, while honeycomb continued tearing and rotating. Little crush was observed.

Since polymer-filled loading section worked well, two specimens were prepared for plate shear test. The dimensions of the gage sections are also listed in Table 1. These specimens were tested as shown in Figure 6. The loading sections of a specimen were bolted between two 0.25 inch thick aluminum plates, one side was connected to the load cell and the other to the actuator. The first test, tl_03, failed at the bolted area before peak stress was reached. In the second test, specimen tl_04 was modified to have a larger loading section. Results are shown in Figure 7. After peak stress, 3.6 ksi, aluminum sheets started to tear and the averaged stress dropped to about 1.0 ksi. There were crushing and tearing, shown in Figure 8, at that stress level before the final failure. The deformation behavior was similar to simple shear test except crushing occurred during the plate shear test. The simple shear strength is slightly higher than the plate shear strength by 7%. Comparing with the preliminary data of beam shear strength of Hexcel 38, 4.3 ksi [3], the plate shear strength was about 20% lower.

The tear mode of deformation is not observed in applications when honeycomb is subjected to oblique crush. The modified shear test can only provide peak shear properties and to apply such results in a crush condition is still questionable.

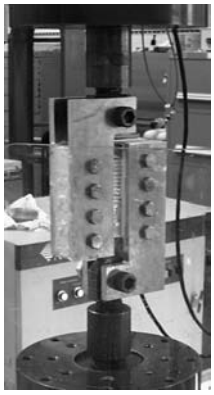

Figure 6. Plate shear setup.

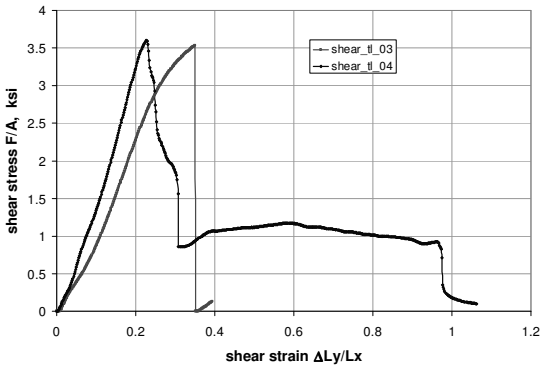

Figure 7. Shear stress-strain curves of Hexcel 38 obtained from plate shear test.

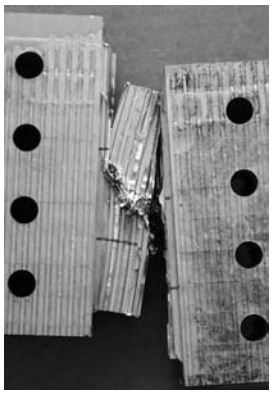

Figure 8. Post-experiment specimen tl_04.

BEAM-FLEXURE TEST

Traditionally, core shear values obtained by flexure tests have large uncertainties because of the complexity of sandwich structure. This uncertainty may be alleviated with finite element simulations of experiments. These simulations provide information about stress and strain distributions generated within the test specimen and help with the interpretation of experimental results. By varying material parameters to match the experiment, inferred shear properties can be obtained.

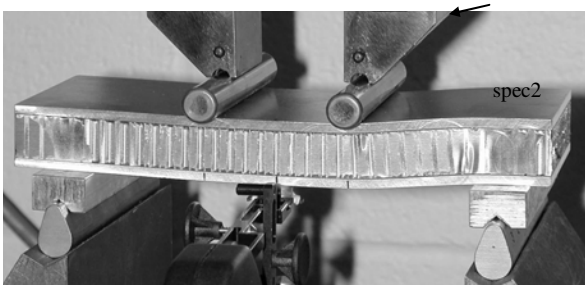

Figure 9. Four-point flexure experiment of a sandwich beam with honeycomb core (Specimen #2).

The beam-flexure tests followed MIL-C-7438 standard. Specimen size was 8x3 inches with honeycomb core thickness of 0.625" and 0.125" thick Al2024-T3 facings. (Specimens were prepared by Honeywell Federal Manufacturing and Technologies Kansas City Plant.) The four-point flexure test was performed on an Instron System as shown in Figure 9. The span between supports was 6" and the distance between two loading rollers was 2". A displacement extensometer was placed at the bottom surface to measure the displacement of the center section of the beam.

The load-displacement curves of three sandwich beams are plotted in Figure 10. Specimen #1 and #3 debonded at top-left and top-right corners after reached the peak load of 11,097 lb and 12,084 lb, respectively. Specimen #2 had the highest peak load 13,017 lb and no debonding.

Post-experiment Specimen #2 is displayed in Figure 9. The right section of the specimen, between loading roller and support, is permanently deformed in shear, but not the center and left sections. Within the right section, the deformation appears to be uniform, but concentrations close to the supporting pad and under the roller are apparent.

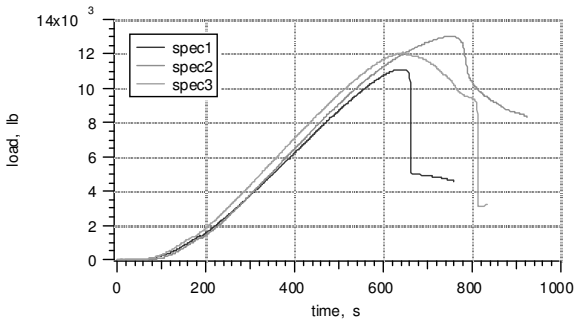

Figure 10. Load-displacement curves of sandwich beams under four-point bending.

A finite element model was built to simulate the 4-point beam flexure test unit as described earlier and shown in Figure 9.

The purpose of this model was to help quantify the apparent shear strength of the honeycomb displayed in this flexure test and to provide some model validation. The simulations were performed using the explicit transient dynamic PRONTO finite element code [4] and the Orthotropic Crush material model [1] for the honeycomb constitutive relationship. The dynamic PRONTO code was used to validate the model for a crash worthiness application. The following mechanical properties of the aluminum honeycomb were chosen based on Lu's crush tests on Hexcel 38 lbs/ft^3 material [2], the material used in the sandwich. The T crush strength is 6000 psi, L crush strength is 1200 psi. The elastic moduli values of 2 and 1 million psi were used respectively, for the T and L directions. The TL shear modulus was set at 0.67 million psi based on a sensitivity study to match the initial slope of the beam flexure test data. The shear strength was left as an open parameter

and the values of 1000 and 3000 psi were used as candidate values. The skin material of the sandwich was 2024-T3 aluminum and modeled with an elastic modulus of 10 million psi, Poisson's ratio of 0.33, yield strength of 50 ksi and a hardening constant of 27 ksi and hardening exponent of 0.42.

Figure 11 shows the load deflection curves predicted by the model along with the test data. The model prediction using 3000 psi shear strength agrees very well with the highest test data curve and peak. Also, the peak test load of 13,017 lbf corresponds to a 3174 psi shear strength using the Mil-STD-401B formula of P/(Hs+Hc)B, where P is the peak load, Hs is the sandwich height, Hc is the core height and B is the width . This value of 3174 psi agrees well with the model's value of 3000 psi shear strength. After the sandwich is loaded up to its peak load it appears to lose much of its shear strength and falls down to around 1000 psi residual shear strength. The manufacturer, Hexcel, quotes peak beam shear strength as 4300 psi for this honeycomb but this value apparently could not be achieved here due to the onset of localized crushing and/or delamination of the sandwich.

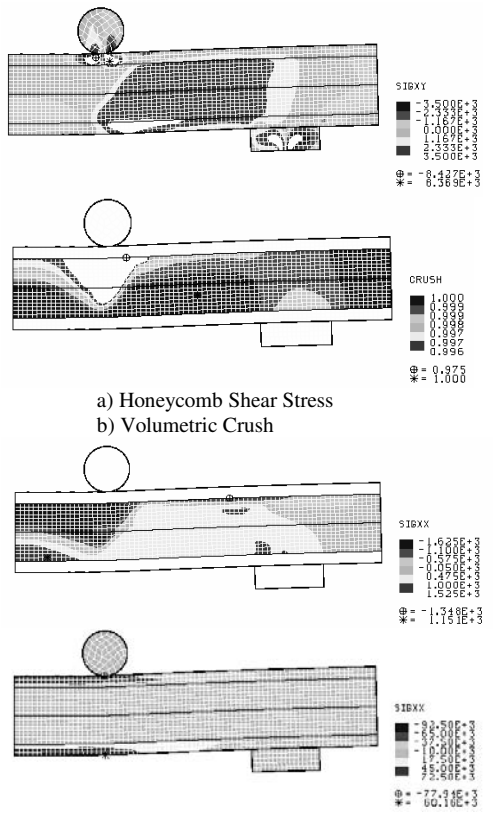

a) Honeycomb Shear Stress
b) Volumetric Crush
c) Honeycomb Bending Stress
d) Outer Skin Bending Stress

Figure 12. Beam Flexure Model Prediction Contours: a) honeycomb shear stress, b) volumetric crush, c) honeycomb bending stress, and outer skin bending stress.

Figure 12a-d shows stress and crush contours predicted by the model around the max load. Figure 12a shows how the honeycomb core supports most of the shear load in the beam by the zone of high shear stress, 3000 psi, between the lower support and the upper loading rod expected from beam theory. Figure 12b shows the onset of crushing under the loading point and the right support similar to the test results. Although, the model did display crushing, it did not directly include shear strength degradation due to crushing in these runs. Also, no failure criterion was enabled to simulate the onset of delamination between the honeycomb and the sandwich skin. Thus the model shows no load drop off similar to the test. Figure 12c shows the typical tension/compression bending stress distribution in the area left of the upper loading rod where a constant moment is expected from beam theory. Finally, Figure 12d shows the high stresses that develop in the skin and support over 90% of the bending moment.

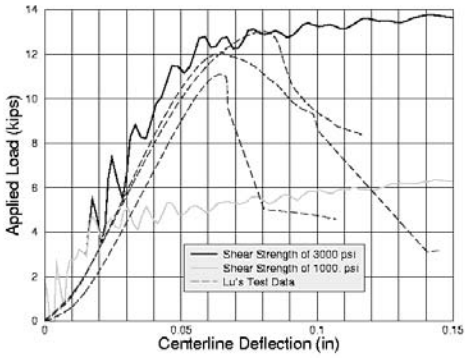

Figure 11. Load-deflection curves from test data and model predictions

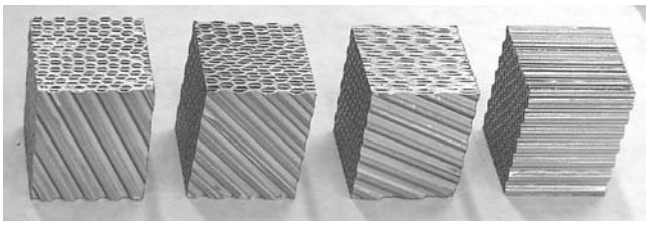

Figure 13. Off-axis specimens, from left to right, 25, 45, 65 and 90 degrees with respect to T-direction in the TL plane.

OFF-AXIS COMPRESSION

For orthotropic materials, off-axis loading is often used to investigate the shear-coupling phenomenon and to validate models in multiaxial stress conditions. In this series of experiments, rectangular honeycomb specimens were machined in five different angles in the TL plane, 0, 25, 45, 65, and 90 degrees with respect to the T-direction. Figure 13 shows specimens of the last four angles. Specimens of 0 and 90 degree are in T and L direction, respectively. Nominal cross-section is 1.2"x1.2", and length is 1.5". These specimens were crushed in an intermediate rate, about 14 ft/s, under confined condition [2]. The crush engineering stress-strain curves are shown in Figure 14.

Examining the post-experiment specimens, the deformed 45-degree specimen, shown in Figure 15, is different from the others. In the TL plane, the material was drawn in from one of the diagonal direction, and the initially sharp corners at upper-right and lower left of the specimen became blunt or disappeared.

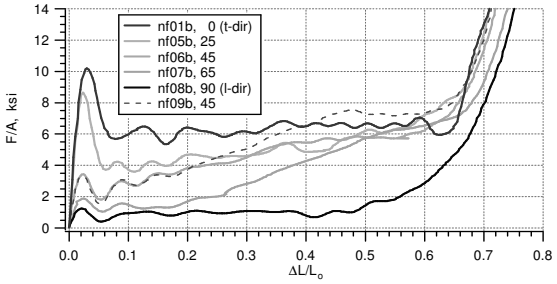

Figure 14. Engineering stress-strain curves of off-axis specimens.

Figure 15. Post-experiment 45-degree off-axis specimen.

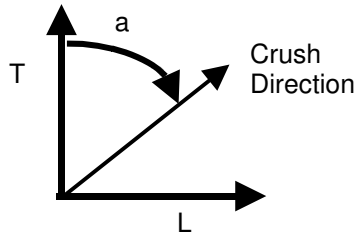

Figure 16. Off-axis crush orientation angle

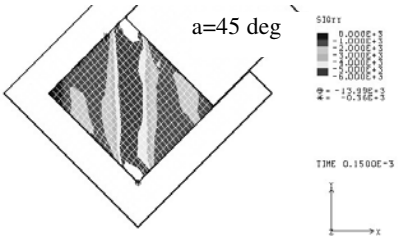

Figure 17. Model predicted y-direction normal stress contours for 45 degree.

The PRONTO finite element code coupled with the Orthotropic Crush model was also used to model and simulate the off-axis crush of 38 lb/ft^3 aluminum honeycomb as part of a calibration and validation process. Figure 16 shows the definition of the crush direction relative to the material T-direction of the honeycomb. Figure 17 shows the model of a uniaxial compression test where the crush direction is 45 degrees from the T-direction. Notice that the highest y-direction normal stress contour is parallel with the T or vertical direction.

The same T and L mechanical properties were used here for the orthotropic crush model as in the prior beam flexure model. These values of 6000 psi and 1200 psi also correlate well with zero angle (T-direction) and 90 degree (L-direction) crush test data curves, respectively, shown in Figure 14. Notice in Figure 14 the T-crush strength has an initial peak of 10,000 psi and then falls back to approximately a constant 6000 psi value. This exact zero degree curve could be used to define the T-direction crush strength function in the Orthotropic Crush Model, however, the strain-softening that occurs on the down slope from the peak causes numerical instabilities in the code and therefore is clipped off to a constant 6000 psi value for these simulations. Also, a shear strength function was used that had an initial value of 4300 psi and then dropped to 1000 psi or 2000 psi after a volumetric strain level of 1%. The high value of 4300 psi shear strength was chosen based on Hexcel's reported shear strength for 38 pcf honeycomb. The test values for peak shear strength of 3000 to 3800 psi reported earlier in this paper were considered limited by other factors such as delamination or tensile failure within their respective test units. The model's shear strength value for low strain levels is important for predicting the peak load on the flexure test as was demonstrated with the 1000 and 3000 psi shear strength values; this occurs at small strain levels. However, for these off-axis crush tests that include large strain levels, the shear strength specified after 1% volumetric strain primarily controls the response. The lower values of 1000 and 2000 psi were based on a sensitivity study that showed more realistic deformation shapes were predicted if the shear strength after 1% was significantly below 3000 psi. Figure 18 shows the predicted deformed shapes for the shear strengths of 1000, 2000 and 3000 psi. All of these simulations used a friction coefficient of 0.2. The mode shape tends to go towards the shape in Figure 18c for higher shear strength or for lower friction. See the deformed shape in Figure 15 for comparison.

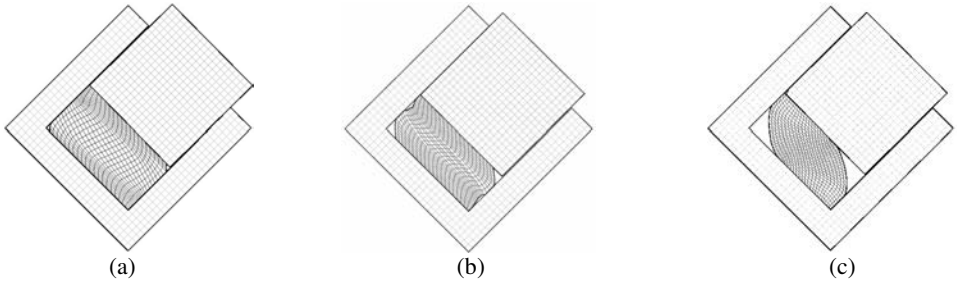

Figure 18. Deformation modes for shear strengths of: a) 1000 psi, b) 2000 psi c) 3000 psi

Figures 19 to 21 show crush stress predicted by the model on the upper surface just below the piston. This location is similar to where the stress is measured in the tests and also includes wall friction forces. Figure 19 shows the test curve and also three predicted curves at the off-axis angle of 25 degrees. The model predictions reflect a sensitivity study for wall friction values of 0.05, 0.2 and 0.5. The lowest friction value appears to agree best with the test data for the given shear strength. The TL shear strength function in the model had 4300 psi out to 1% volumetric strain and then 1000 psi from 1% to the crush efficiency value of 64% for these simulations at the 25 degree angle. The initial peak displayed in the test data is not prevalent in any of the predicted curves. This experimental peak can be simulated better by defining an initial peak in the model for the T-crush strength versus volumetric strain similar to what is displayed in Figure 14 for the zero direction crush. However, as was mentioned earlier, using an initial peak in the crush strength versus volumetric strain function and the subsequent strain softening portion of the curve causes numerical instabilities and therefore was not chosen herein. The predicted crush strength curve, with friction mu=0.05, ranges from 0 to about 25% higher than the test data.

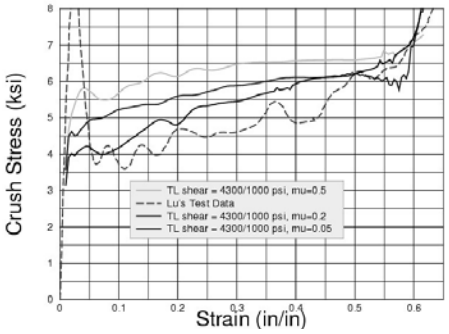

Figure 19. Crush stress predictions for 25 degrees off-axis

Figure 20 shows two test curves and the model's sensitivity to shear strength at the off-axis angle of 45 degrees. The same shear strength values (4300/1000 psi) were used in the model for the blue curve as was used to generate the curves in Figure 19. The dot-dashed black curve is based on a TL shear strength function with 4300 psi out to 1% volumetric strain and then 2000 psi from 1% to the crush efficiency value of 64%. The secondary shear strength of 1000 psi best fits the initial test data whereas the 2000 psi shear strength best fits the large strain region of the test data.

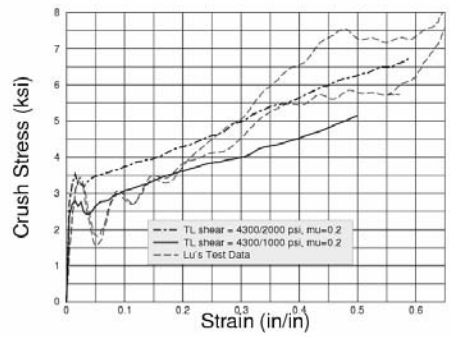

Figure 20. Crush stress predictions for 45 degrees off-axis.

A significant assumption in this model is that the on-axis crush strength for the T and L directions does not degrade during an off-axis crush process. More experiments are necessary to test out this assumption.

Figure 21 shows the test curve and the model's sensitivity to friction at the off-axis angle of 65 degrees. The same shear values were used as for the 25 degree case in Figure 19. The two values used for friction here were 0.2 and 0.5. Friction appears to have little influence here for low strain levels and then significant deviation occurs at the large strain levels.

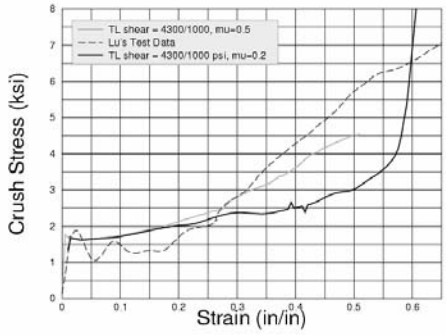

Figure 21. Crush stress predictions for 65 degrees off-axis.

SUMMARY AND CONCLUSIONS

Various types of shear experiments, including beam-flexure, plate shear and off-axis, were performed and reported in the paper. A modified plate shear experiment for heavier density aluminum honeycomb was developed. It works well and eliminates the problem of adhesive bond. The initial shear strength can be determined but tearing of the aluminum sheets prevents the measure of shear strength as a function of volumetric strain for crush applications.

This paper also examined how well the Orthotropic Crush Model handles off-axis and shear deformations by correlating finite element model predictions with off-axis and shear test data. The Orthotropic Crush Model appears to predict the crush strength as a function of angle relative to the T and L material directions reasonably well; similar slopes and magnitudes (within approximately 25%) were predicted subject to uncertainties associated with friction and shear strength. However, to further investigate and more accurately model off-axis crush behavior the Orthotropic Crush model needs to include dependence on plastic shear strains and plastic strain coupling between axes in addition to the current volumetric strain coupling.

Model predictions for the beam flexure test agreed well with the test for a shear strength of 3000 psi. The model also predicted crushing at supports in beam flexure test similar to test results.

The deformation mode in the off-axis crush simulations was found to be sensitive to shear strength and specified friction levels in the PRONTO model. Also, the model showed how crush strength measured at the top of the test sample is sensitive to wall friction.

It remains unclear from the shear tests how shear strength varies with shear strain or volumetric strain. However, the Orthotropic Crush model was shown to predict peak shear loads at low strains by using a representative shear strength based on test values in the beam flexure test. Also, it predicted off-axis crush strengths for larger strains using a lower plateau shear strength based on correlating with posttest deformation shapes. The shear strength was assumed to sharply fall off for volumetric crush strains greater than 1% herein.

The shear tests primarily provided a lower bound estimate of the peak shear strength due delamination in the beam flexure test and tensile failure in the simple shear tests. Additional tests are needed to quantify how on-axis crush and shear strengths vary

with both shear and volumetric crush strains. Further quantifying the effects of friction are also recommended.

ACKNOWLEDGEMENT

We thank Mike Neilsen for discussions and suggestions for experiments and the modeling. Sandia is a multiprogram laboratory operated by Sandia Corporation, a Lockheed Martin Company, for the United States Department of Energy under contract DE-AC04-94-AL85000.

REFERENCES

1. Whirley, R.G., Engelman, B.E., and Hallquist, J.O., 1991, "DYNA3D Users Manual," Lawrence Livermore Laboratory, Livermore, CA.
2. Lu, W.-Y. and Hinnerichs, T., "Crush of High Density Aluminum Honeycombs," IMECE/AMD-25453, 2001.
3. "Mechanical Properties of Hexcel Honeycomb," TSB-120, Hexcel Corporation, Dublin, CA, 1992.
4. Attaway, S.W. *et al*., 1998, "PRONTO3D Users' Instructions: A Transient Dynamic code for Nonlinear Structural Analysis," Report SAND98-1361, Sandia National Laboratories, Albuquerque, NM.
5. Bitzer, T., 1997, Honeycomb Technology, Chapman & Hall, London, UK.

This page intentionally left blank.

APPENDIX IV:

Augmented Qualification Test Matrix, August, 1999

Augmented Qualification Test Matrix for Aluminum Honeycomb
based on the
Aluminum Honeycomb Working Group Meeting, Aug 3, 1999

Augmented Objectives:
Develop a more significant statistical data base for ambient/hot/cold crush behavior.
Take advantage of moderate rate testing with confining chamber for a more reliable dynamic testing approach.
Take advantage of demonstrated quasi-static crush stability of segmented honeycomb for dynamic tests using drop table approach.
Investigate off-axis behavior.
Measure crush behavior in the W-direction.

Scope:
Two batches of aluminum honeycomb.

Table A1. Aluminum Honeycomb Batches		
Vendor	**Density (lb/ft^3)**	**Density (lb/ft^3)**
Alcore	35	38
Hexcel	35	38

Table A2. Moderate Rate Confined Crush Tests in the T-Direction, (1.2" x 1.2" x 1.5") at Ambient Temperature			
Test #	Batch	Impact Speed	Test Engineer
1 - 15	Alcore - 38 lb/ft^3	170 in/sec	Wei-Yang Lu
16 – 30	Hexcel – 38 lb/ft^3	170 in/sec	Wei-Yang Lu
31 - 45	Alcore – 35 lb/ft^3	170 in/sec	Wei-Yang Lu
46 - 60	Hexcel - 35 lb/ft^3	170 in/sec	Wei-Yang Lu

Table A3. Moderate Rate Confined Crush Tests in the T-Direction, (1.2" x 1.2" x 1.5") at Hot (165 deg F) Temperature			
Test #	Batch	Impact Speed	Test Engineer
60 - 75	Alcore - 38 lb/ft^3	170 in/sec	Wei-Yang Lu
76 - 90	Hexcel – 38 lb/ft^3	170 in/sec	Wei-Yang Lu
No Tests*	Alcore – 35 lb/ft^3	170 in/sec	Wei-Yang Lu
No Tests*	Hexcel - 35 lb/ft^3	170 in/sec	Wei-Yang Lu

Table A4. Moderate Rate Confined Crush Tests in the T-Direction, (1.2" x 1.2" x 1.5") at Cold (-65 deg F) Temperature			
Test #	Batch	Impact Speed	Test Engineer
91 - 105	Alcore - 38 lb/ft^3	170 in/sec	Wei-Yang Lu
106 - 120	Hexcel – 38 lb/ft^3	170 in/sec	Wei-Yang Lu
No Tests*	Alcore – 35 lb/ft^3	170 in/sec	Wei-Yang Lu
Not Tests*	Hexcel - 35 lb/ft^3	170 in/sec	Wei-Yang Lu

Table A5. Moderate Rate Confined Crush Tests in the L-Direction, (1.2" x 1.2" x 1.5") at Ambient Temperature			
Test #	Batch	Impact Speed	Test Engineer
121 - 125	Alcore - 38 lb/ft^3	170 in/sec	Wei-Yang Lu
126 – 130	Hexcel – 38 lb/ft^3	170 in/sec	Wei-Yang Lu
No Tests*	Alcore – 35 lb/ft^3	170 in/sec	Wei-Yang Lu
No Tests*	Hexcel - 35 lb/ft^3	170 in/sec	Wei-Yang Lu

Table A6. Moderate Rate Confined Crush Tests in the W-Direction, (1.2" x 1.2" x 1.5") at Ambient Temperature			
Test #	Batch	Impact Speed	Test Engineer
131 - 135	Alcore - 38 lb/ft^3	170 in/sec	Wei-Yang Lu
136 – 140	Hexcel – 38 lb/ft^3	170 in/sec	Wei-Yang Lu
No Tests*	Alcore – 35 lb/ft^3	170 in/sec	Wei-Yang Lu
No Tests*	Hexcel - 35 lb/ft^3	170 in/sec	Wei-Yang Lu

Table A7. Off Axis Crush Test at Ambient Temperature			
Test #	Batch	Orientation	Test Engineer
Computational Simulation	38 lb/ft^3	T-L 45 deg	Mike Neilsen
TBD	TBD	T-L 45 deg	Wei-Yang Lu

Table A8. Drop Table Crush Tests of 5" dia. Segmented Honeycomb, With MA562 adhesive at Ambient Temperature			
Test #	Batch	Impact Speed	Test Engineer
141 – 143	Alcore - 38 lb/ft^3	70 ft/sec	Vesta Bateman
144 – 146	Hexcel – 38 lb/ft^3	70 ft/sec	Vesta Bateman
No Tests*	Alcore – 35 lb/ft^3	70 ft/sec	Vesta Bateman
No Tests*	Hexcel - 35 lb/ft^3	70 ft/sec	Vesta Bateman

Table A9. Drop Table Crush Tests of 5" dia. Segmented Honeycomb, With MA562 adhesive at Hot (165 deg F) Temperature			
Test #	Batch	Impact Speed	Test Engineer
147 - 149	Alcore - 38 lb/ft^3	70 ft/sec	Vesta Bateman
150 – 152	Hexcel – 38 lb/ft^3	70 ft/sec	Vesta Bateman
No Tests*	Alcore – 35 lb/ft^3	70 ft/sec	Vesta Bateman
No Tests*	Hexcel - 35 lb/ft^3	70 ft/sec	Vesta Bateman

Table A10. Drop Table Crush Tests of (5" dia x 1.5") Segmented Honeycomb Disks, With MA562 adhesive at Cold (-65 deg F) Temperature			
Test #	Batch	Impact Speed	Test Engineer
153 - 155	Alcore - 38 lb/ft^3	70 ft/sec	Wei-Yang Lu
156 – 158	Hexcel – 38 lb/ft^3	70 ft/sec	Wei-Yang Lu
No Tests*	Alcore – 35 lb/ft^3	70 ft/sec	Wei-Yang Lu
No Tests*	Hexcel - 35 lb/ft^3	70 ft/sec	Wei-Yang Lu

Table A11. Quasi-Static Crush Tests of (5" dia x 1.5") Segmented Honeycomb Disks, With MA562 adhesive at Ambient Temperature			
Test #	Batch	Impact Speed	Test Engineer
159 - 161	Alcore - 38 lb/ft^3	0.1 in/min	Wei-Yang Lu
162 - 164	Hexcel – 38 lb/ft^3	0.1 in/min	Wei-Yang Lu
No Tests*	Alcore – 35 lb/ft^3	0.1 in/min	Wei-Yang Lu
No Tests*	Hexcel - 35 lb/ft^3	0.1 in/min	Wei-Yang Lu

Issues/Regrets:

1. The confined drop table tests in the T-direction (2" x 2" x 2" cubes) that Tom Carne discussed in the Working Group meeting are already part of the original test matrix and therefore are not shown here in the augmented plan.
2. ***** The behavior for 35 lb/ft3 material for these tests will be inferred based on tests in the T-direction for 35 and 38 lb/ft3 materials, respectively.
3. Wei-Yang Lu will investigate the benefits of machining the cross-section of T-direction test articles at 45 degrees from the L or W directions. This modification is hoped to minimize the tendency for the individual aluminum sheets to squeeze between the confinement chamber wall and the piston during a crush test.
4. Normal and shear stresses (e.g., friction) on the walls are unknowns in these confined tests.
5. Off-axis behavior (e.g., loading in the direction 45 degrees between T and L directions) will be examined initially with Mike Neilsen's "Cell-Level" model and computational simulations. The uncertainty and validity of the "Cell-Level" model must also be examined.
6. Variability of crush behavior throughout a vendor's block of material will not be very accurately quantified due to the limit of 15 test articles and to restrictions on how many locations that test articles can be cut out of the parent block of material.
7. The apparent added crush strength (based on Lu's recent tests) that MA562 provides in segmented honeycomb crush tests will have to be subtracted out to compare with bare honeycomb tests. This added strength will also need to be proportioned for applying to the zones of honeycomb in the nose having different diameters and circumferences.
8. Transverse crush behavior of the segmented honeycomb disks will not be tested so its behavior will have to be estimated based on the L and W crush test data.
9. Dynamic crush behavior will not be measured at full B61 nose impact velocities due to limitations of drop table initial testing velocities. Also, the velocity is not constant during a drop table test; it is continually decreasing.
10. Budget/Schedule constraints.

APPENDIX V:

"Quasi-static Crush Tests of Alcore Segmented Samples at Ambient Temperature," Memo Wei-Yang Lu to Distribution, November 30, 1999.

Sandia National Laboratories
Operated for the U.S. Department of Energy by
Sandia Corporation
MS9042
Livermore, CA 94551-0969

date: November 30, 1999

to: Distribution

from: Wei-yang Lu

subject: Quasi-static Crush Tests of Alcore Segmented Samples at Ambient Temperature

We have completed test # 159 – 161 (Table 2.4. Quasi-Static Crush Test of Segmented Honeycomb Disks, with MA562 adhesive at ambient temperature, ***B61 Radar Nose / MAVEN*** *Test Matrix for Aluminum Honeycomb based on the Aluminum Honeycomb Working Group Meeting, August 3, 1999*, by T.D. Hinnerichs, October 27, 1999). Honeycomb crushed normally, no splitting was observed. The adhesive coating came off during crush. The crush strength is 6.14 ± 0.09 ksi, and the crush efficiency is 52 ± 1 %. Please see Appendix for detail experimental procedures and results.

Distribution:

Darrla Giersch (2167)	MS0481
Darren Hoke (2167)	MS0481
Vernon Willan (2167)	MS0481
Vista Bateman (9126)	MS0553
Tom Carne (9124)	MS0557
Berry Boughten (9132)	MS0557
Jaime Moya (9132)	MS0828
Terry Hinnerichs (9126)	MS0847
Ken Gwinn (9126)	MS0847
John Pott (9126)	MS0847
Rodney May (9126)	MS0847
Mike Neilsen (9123)	MS0847
Bill Scherzinger (9123)	MS0847
Hal Morgan (9123)	MS0847
Wendell Kawahara (8725)	MS9042

Quasi-static Crush Tests of Alcore Segmented Samples at Ambient Temperature

Appendix

SPECIMENS

The undeformed specimens, AS1-1, AS1-2 and AS1-3, shown in Figures 1(a), 2(a) and 3(a), were manufactured by Allied Signal, Kansas City. Their dimensions and weight were measured and recorded in Table 1.

LOADING SYSTEM

Crush tests were performed using the 2M MTS servohydraulic system located at Building 972, SNL/CA. The load cell was calibrated by a MTS service person one week before the tests. Nicolet 400 was used for data acquisition. System compliance test was conducted. The result is shown in Figure 6. A polynomial curve-fit represents the compliance of the system:

$$\Delta Lc = 4.83 + 0.15*F - 0.00027*F^2 \quad (1)$$

where ΔLc ($x10^{-3}$ in) is the displacement, and F (kips) is the load

EXPERIMENT

The setup is shown in Figure 4. Platens were placed on the top and bottom of the specimen. The adhesive coating came off during crush, as shown in Figure 5; in the figure, (a) and (b) indicate 10% and 40% crush of AS1-2, respectively. The crushed honeycombs, Figures 1(b), 2(b) and 3(b), show a neat pattern; no splitting or other abnormal deformation was observed.

RESULTS

Raw experimental data, stroke (or displacement, ΔL) and load (F), of AS1-1, AS1-2 and AS1-3 are plotted in Figures 7, 9 and 11, respectively. "Stress-strain" curves are shown in Figures 8, 10 and 12. Please note that the strain is calculated by

$$\text{Strain} = (\Delta L - \Delta Lc) / L_o \quad (2)$$

That is the contribution due to system compliance has been corrected. (In figures, $\Delta L/ L_o$ is used just for simplicity.)

The values of compressive peak, average crush strength and crush efficiency were obtained according to the definitions described in SS706955 (1/5/99). Elastic modulus is the initial slope, typically from the section between 2 and 5 ksi) of the "stress-strain" curve. These values are summarized in Table 1.

Table 1. Summary of Alcore Segmented Specimens

Specimen	Diameter, in	Height, in	Weight, lb	Density, pcf	Apparent Elastic Modulus, ksi	Compressive Peak, ksi	Average Crush Strength, ksi	Crush Efficiency %
AS1-1	5.082	1.493	0.725	41.385	1200	7.8	6.23	53
AS1-2	5.082	1.508	0.729	41.198	1550	7.6	5.95	53
AS1-3	5.080	1.495	0.730	41.652	842	8.0	6.23	51

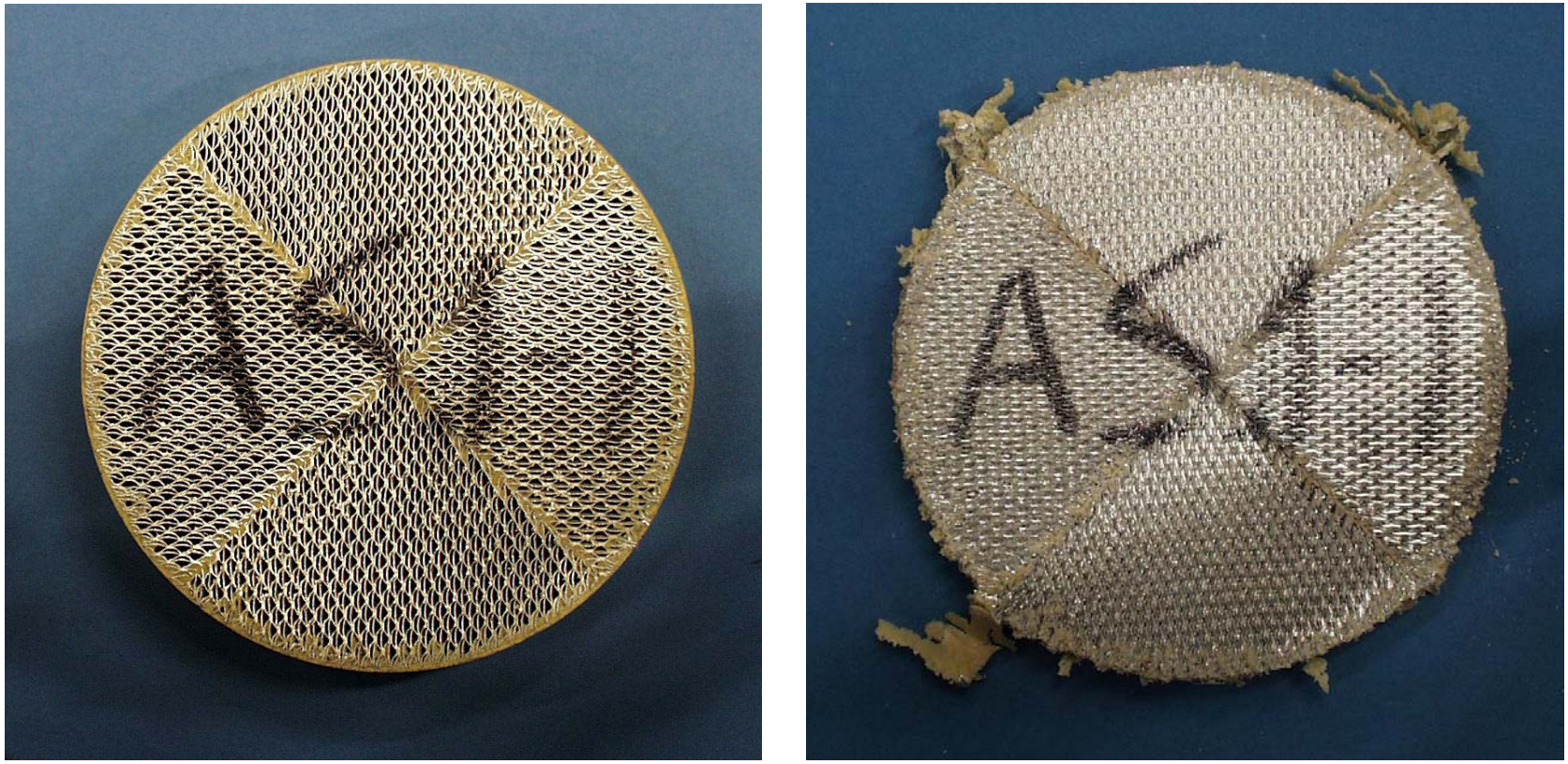

(a) (b)

Figure 1. Sample AS1-1 (a) before and (b) after test.

(b)

(a)

Figure 2. Sample AS1-2 (a) before and (b) after test.

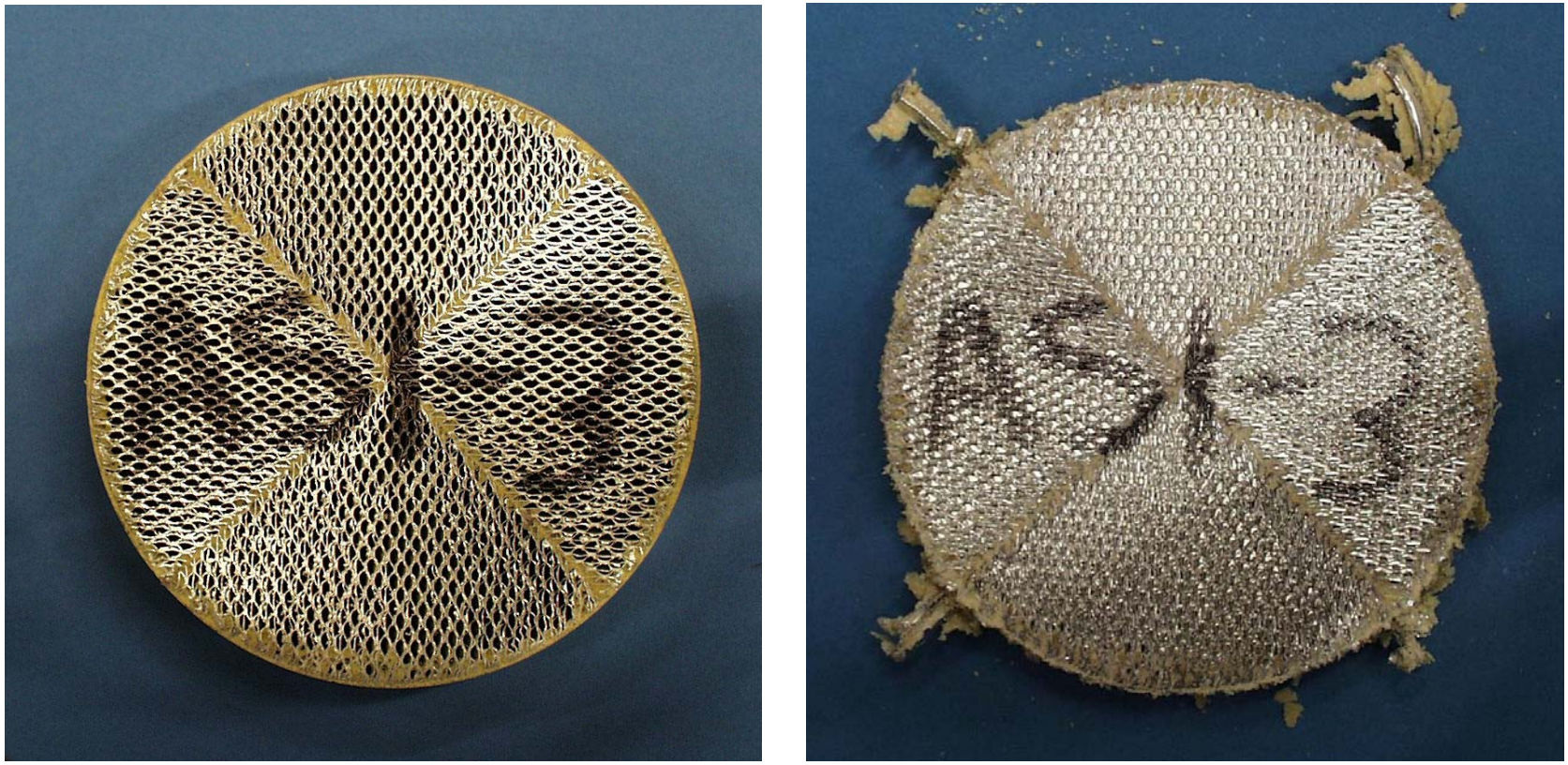

(a) (b)

Figure 3. Sample AS1-3 (a) before and (b) after test.

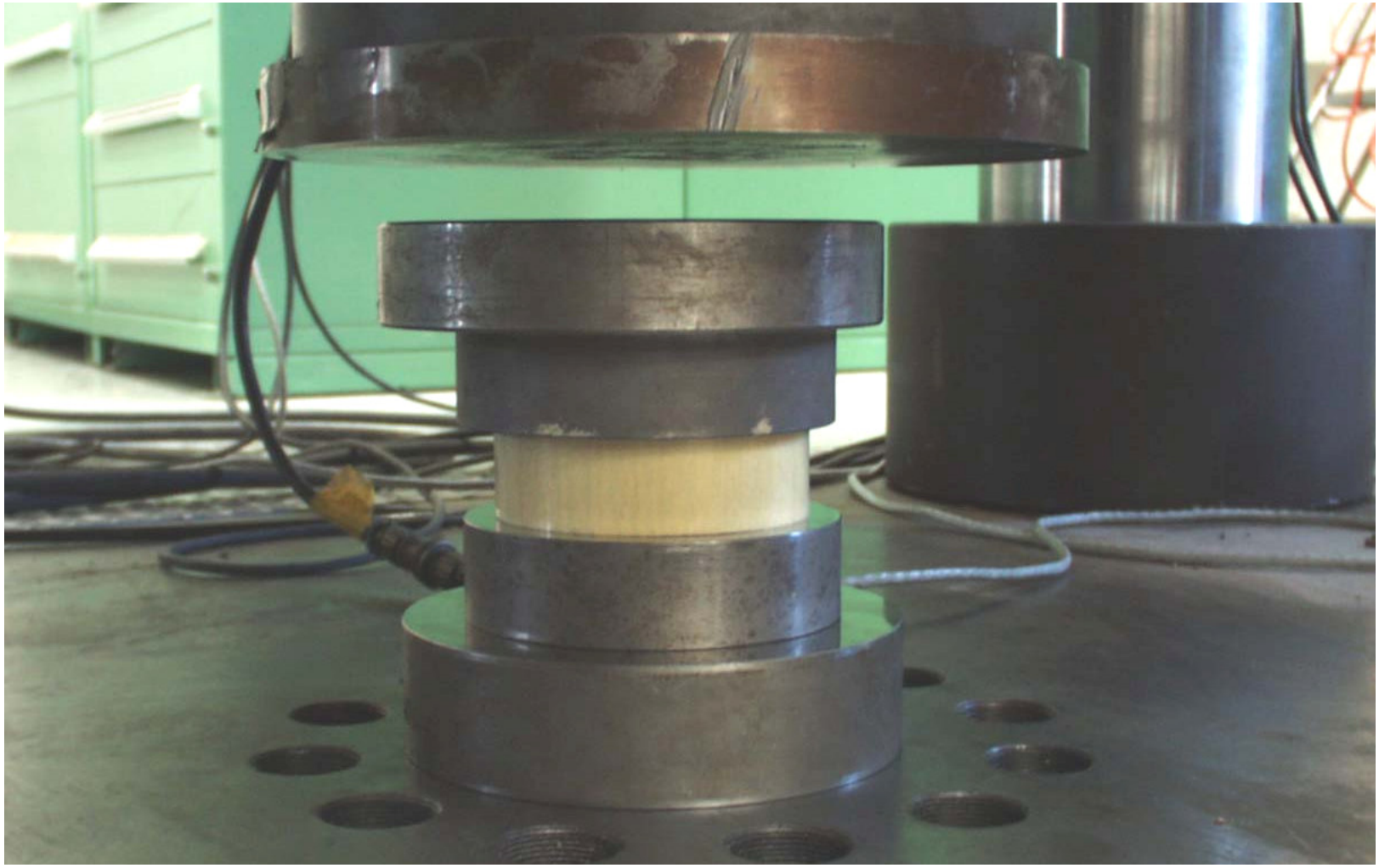

Figure 4. Experimental setup.

(a) (b)

Figure 5. Sample AS1-2 at (a) 10% and (b) 40% crushing.

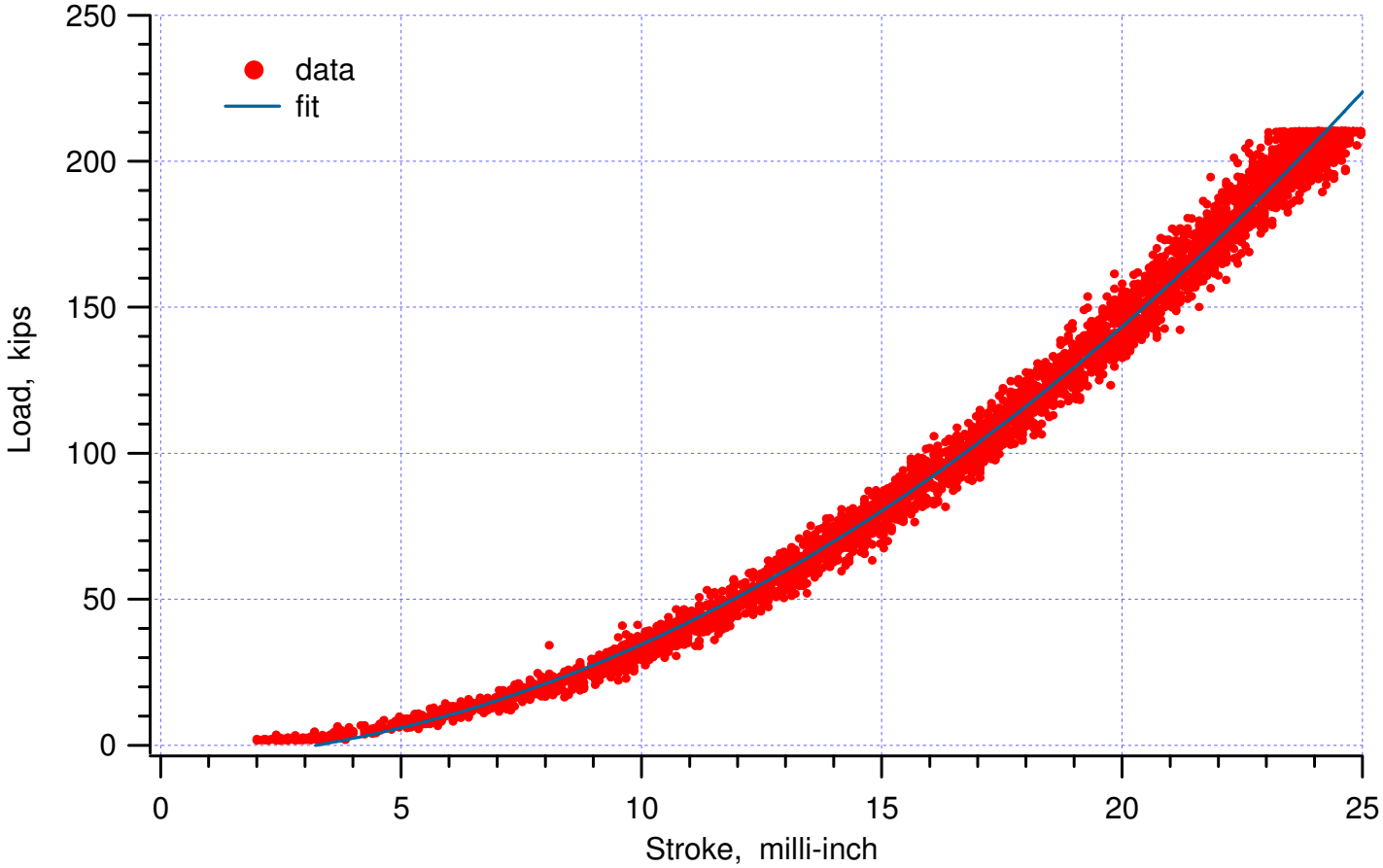

Figure 6. Compliance curve of the loading system.

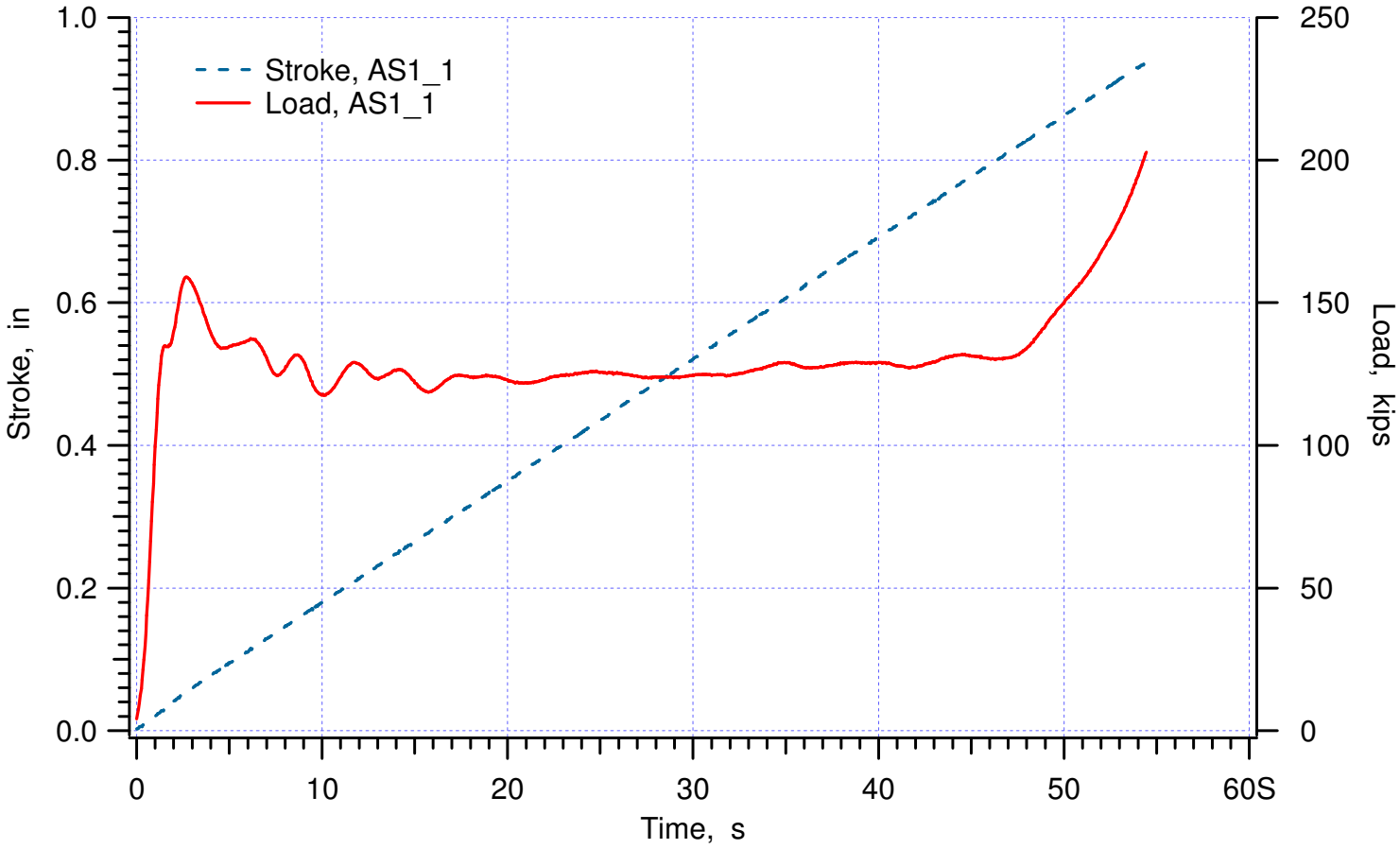

Figure 7. Raw data of AS1-1.

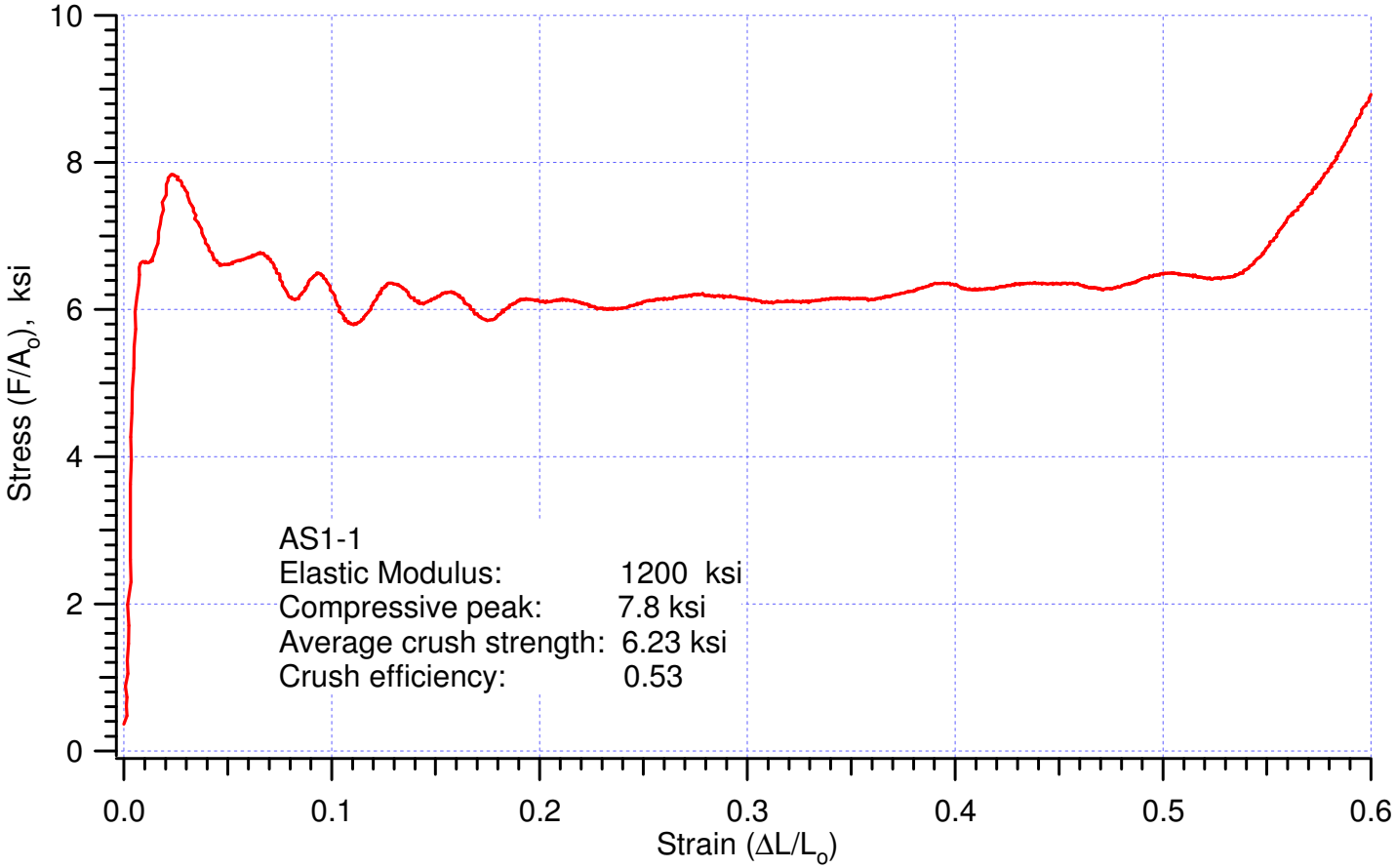

Figure 8. Stress-strain curve of AS1-1.

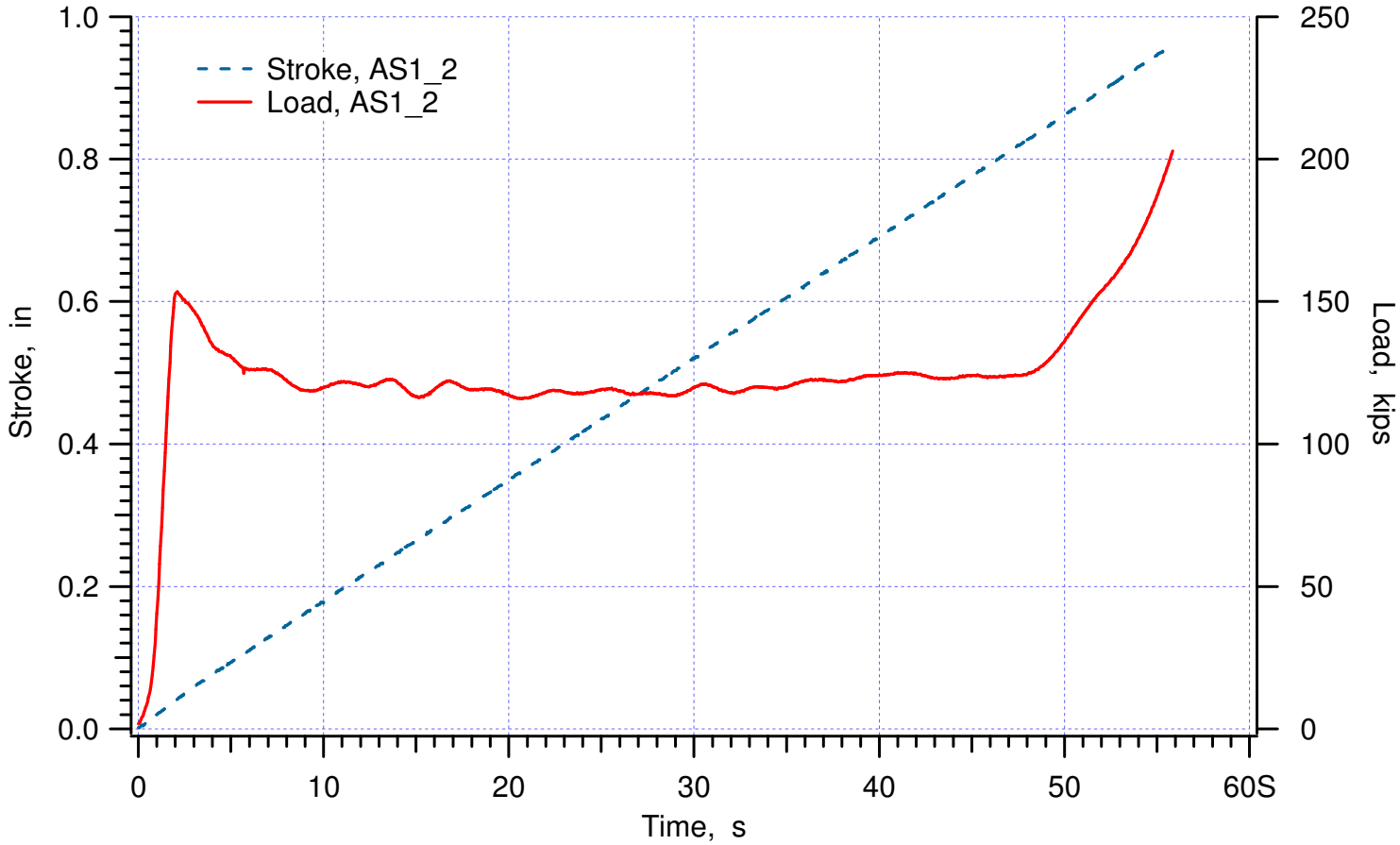

Figure 9. Raw data of AS1-2.

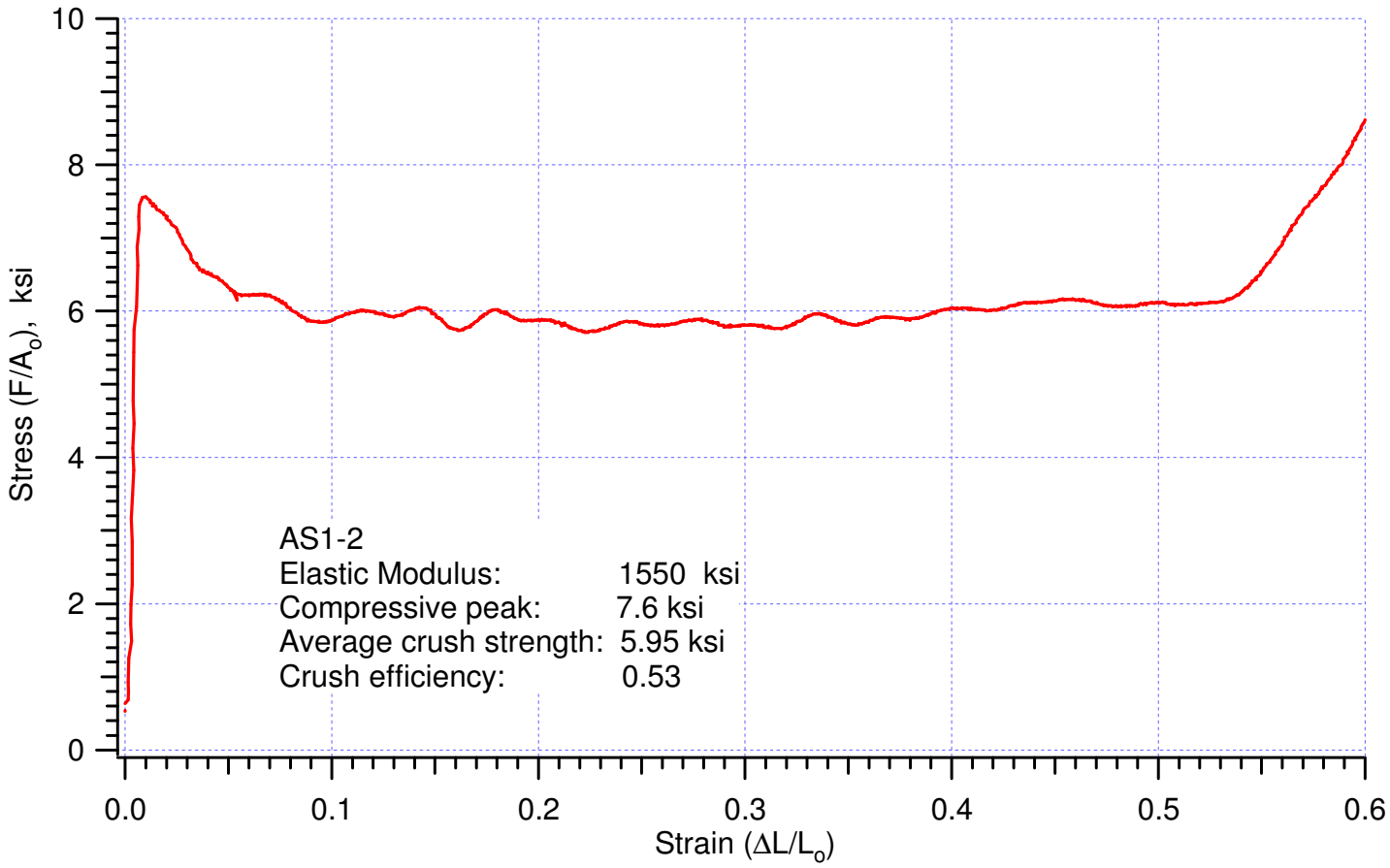

Figure 10. Stress-strain curve of AS1-2.

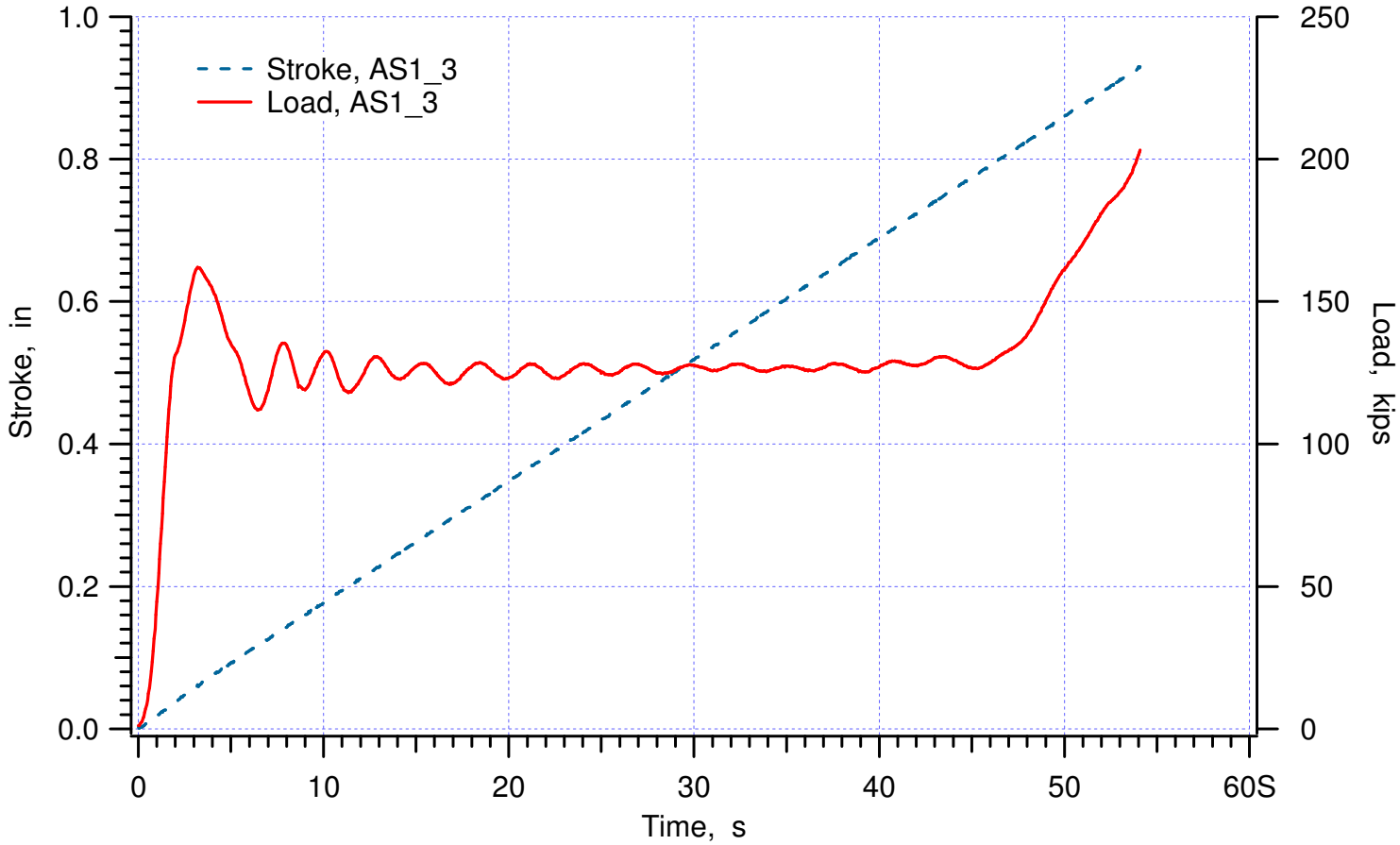

Figure 11. Raw data of AS1-3.

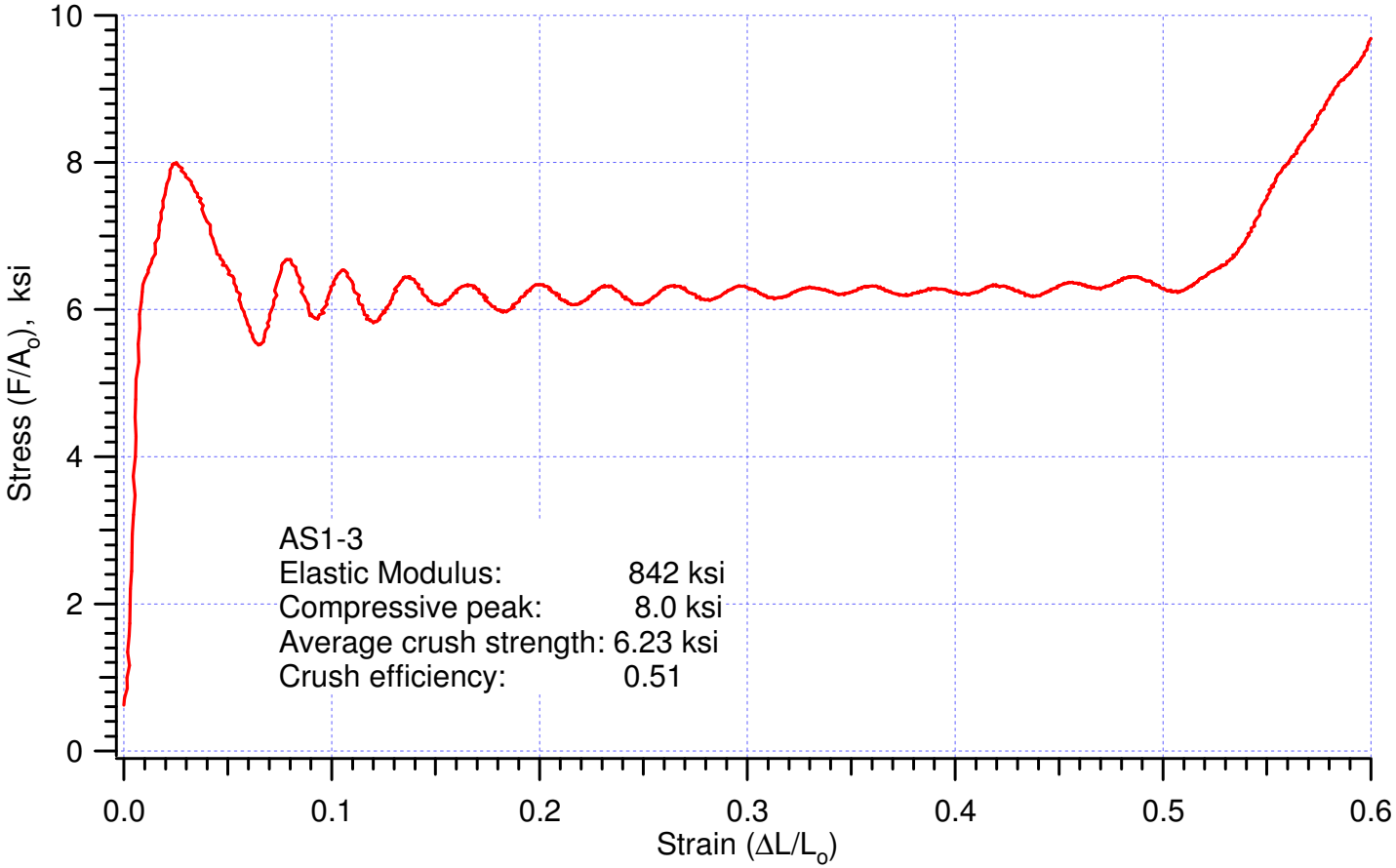

Figure 12. Stress-strain curve of AS1-1.

APPENDIX VI:

"Moderate Rate Confined Crush Tests of Alcore 38 pcf in the t-direction at Ambient Temperature," Memo Wei-Yang Lu to Distribution, December 3, 1999.

Sandia National Laboratories
Operated for the U.S. Department of Energy by
Sandia Corporation
MS9042
Livermore, CA 94551-0969

date: December 3, 1999

to: Distribution

from: Wei-yang Lu

subject: Moderate Rate Confined Crush Tests of Alcore 38 pcf in the t-direction at Ambient Temperature

We have completed Tests # 1 – 15 (Table 1.1., *B61 Radar Nose / MAVEN Test …*, by T.D. Hinnerichs, October 27, 1999). The average density of honeycomb specimen is **38.82 pcf**, the average crush strength is **6.35 ksi**, and the crush efficiency is **63.78 %**. Please see Appendix I for experimental procedures and summary of results, and see Appendix II for detail data and results.

Distribution:

Darrla Giersch (2167)	MS0481
Darren Hoke (2167)	MS0481
Vernon Willan (2167)	MS0481
Vista Bateman (9126)	MS0553
Tom Carne (9124)	MS0557
Berry Boughten (9132)	MS0557
Jaime Moya (9132)	MS0828
Terry Hinnerichs (9126)	MS0847
Ken Gwinn (9126)	MS0847
John Pott (9126)	MS0847
Rodney May (9126)	MS0847
Mike Neilsen (9123)	MS0847
Bill Scherzinger (9123)	MS0847
Hal Morgan (9123)	MS0847
Wendell Kawahara (8725)	MS9042

Moderate Rate Confined Crush Tests of Alcore 38 pcf in the t-direction at Ambient Temperature

Appendix I. Experimental Procedures and Summary of Results

SPECIMENS

The undeformed shape of the crush specimens was rectangular, about 1.2"x1.2"x1.5" in size. The height (1.5") was aligned with the t-direction of honeycomb; however, the other two edges of the rectangular specimen were not parallel to the l- and w- axes but with an angle of 45^{o}. Let us call this the "rotated specimen", Figure 1. In the previous tests of "unrotated specimen", i.e., the edges parallel to l-, w-, and t- directions, one layer of thin aluminum ribbon was often left uncrushed and jammed between the punch and the confined wall, Figure 2, which complicated the interpretation and analysis of test result. The "rotated specimen" should eliminate this problem. Making such specimen, however, is more difficult and time consuming. After experimenting with several techniques, we used the Buehler Abrasimatic Saw to cut specimens since it could produce good specimens with reasonable time. Sample dimensions and weight were measured and recorded in Table 1.

LOADING SYSTEM

Moderate rate confined crush tests were performed on the MTS high rate system, Figure 3(a), located at Building 972, SNL/CA. The load washer (Kistler 9061) was calibrated with respect to a traceable load cell before the tests. Nicolet 400 was used for data acquisition. The shear-pin-break-off mechanism was utilized to allow a constant loading velocity, approximately 14 ft/sec, and to protect the load washer from overloading.

EXPERIMENT

The setup is shown in Figure 3(b) and (c). The specimen is placed in the chamber, then it is closed by tightening the screws. All rotated specimens crushed nicely and negligible ribbon jamming occurred.

RESULTS

The values of crush strength and crush efficiency were obtained according to the definitions described in SS706955 (1/5/99). These values are summarized in Table 1. Table 2 shows the correlation coefficients of each pair of measured data, which are plotted in Figure 4. All parameters are not correlated.

Table 1. Summary of confined crushes of Alcore 38 pcf specimens in t-direction at ambient

Specimen	d_1, in	d_2, in	d_3, in	Weight, lb	Density, pcf	Crush Velocity, ft/s	Crush strenght, ksi	Crush efficiency, %	Remarks
A38_01	1.189	1.193	1.492	0.0476	38.86	-	-	-	R1
A38_02	1.193	1.190	1.498	0.0478	38.80	14.15	6.35	61.80	
A38_03	1.185	1.190	1.501	0.0474	38.70	14.36	6.41	62.00	
A38_04	1.182	1.190	1.520	0.0478	38.67	14.37	6.32	62.40	
A38_05	1.179	1.185	1.497	0.0468	38.67	14.36	6.16	62.30	
A38_06	1.201	1.191	1.492	0.0479	38.79	14.25	6.29	63.60	
A38_07	1.194	1.177	1.490	0.0470	38.81	14.08	6.32	64.40	
A38_08	1.195	1.193	1.494	0.0478	38.76	14.00	6.39	65.20	
A38_09	1.200	1.200	1.493	0.0484	38.91	13.97	6.43	64.40	
A38_10	1.192	1.201	1.499	0.0482	38.82	14.02	6.37	64.00	
A38_11	1.220	1.200	1.493	0.0489	38.62	14.02	6.33	64.00	
A38_12	1.205	1.188	1.498	0.0480	38.66	13.99	6.30	64.70	
A38_13	1.196	1.196	1.499	0.0482	38.84	14.15	6.39	65.10	
A38_14	1.222	1.191	1.506	0.0491	38.74	14.14	6.29	64.60	
A38_15	1.213	1.204	1.487	0.0495	39.38	14.07	6.39	64.30	
A38_16	1.219	1.196	1.507	0.0497	39.12	13.98	6.52	63.90	
				max	39.38	14.37	6.52	65.20	
				min	38.62	13.97	6.16	61.80	
				average	38.82	14.13	6.35	63.78	
				std deviation	0.20	0.15	0.08	1.12	
				median	38.79	14.08	6.35	64.00	
Remarks									
R1	*false trigger, data not recorded*								

Table 2. Correlation coefficients between measured parameters

	Density	Crush velocity	Crush strength	Crush efficiency
Density	1.00	-0.36	0.55	0.24
Crush velocity		1.00	-0.50	-0.72
Crush strength			1.00	0.25
Crush efficiency				1.00

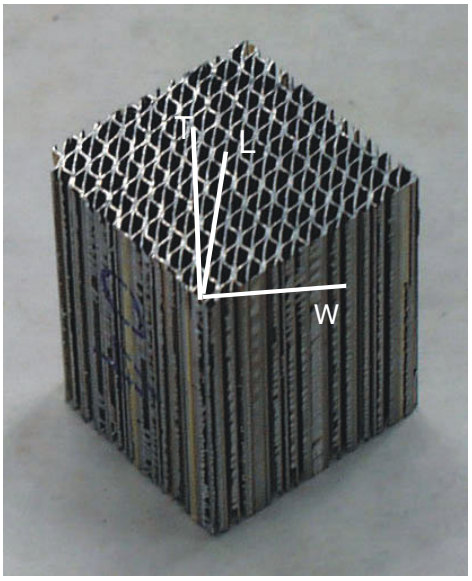

Figure 1. Rotated specimen.

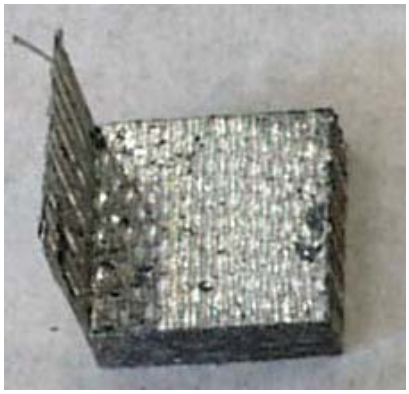

Figure 2. Unrotated specimen may cause a thin ribbon uncrushed.

(a)

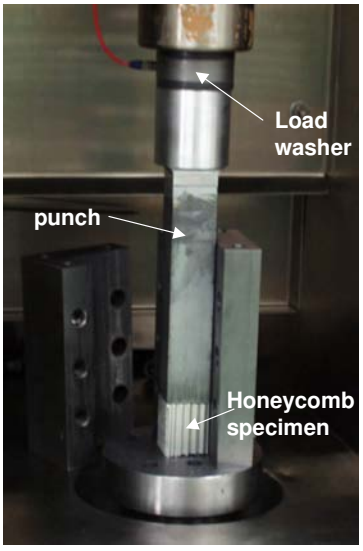

(b)

(c)

Figure 3. Experimental setup for moderate rate confined crush test of honeycomb: (a) MTS high rate system and Nicolet 400 Data Acquisition unit, (b) specimen in the open chamber, and (c) closed chamber.

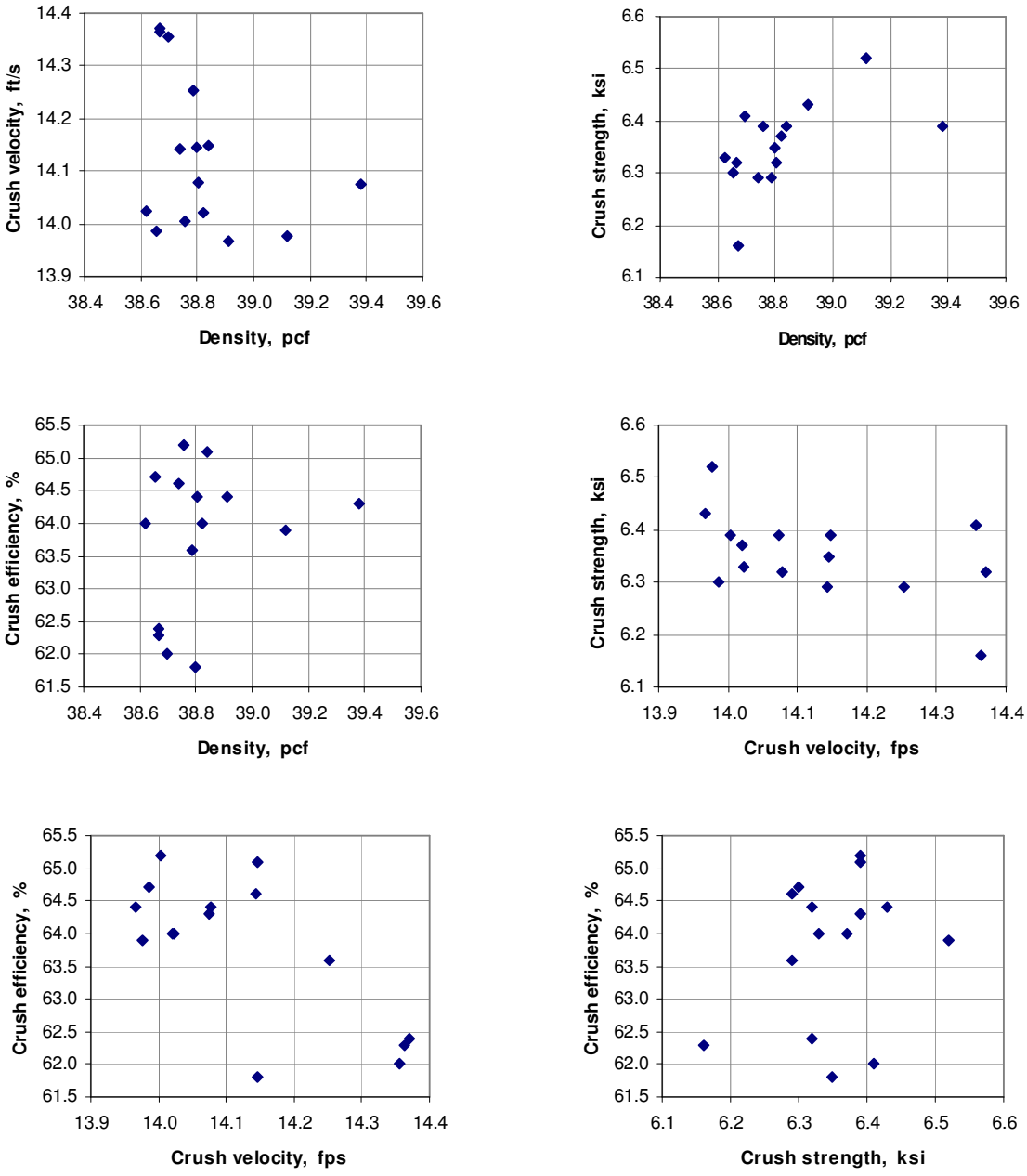

Figure 4. No relation between measured parameters.

Moderate Rate Confined Crush Tests of Alcore 38 pcf in the t-direction at Ambient Temperature

Appendix II. Detail Experimental Data and Results

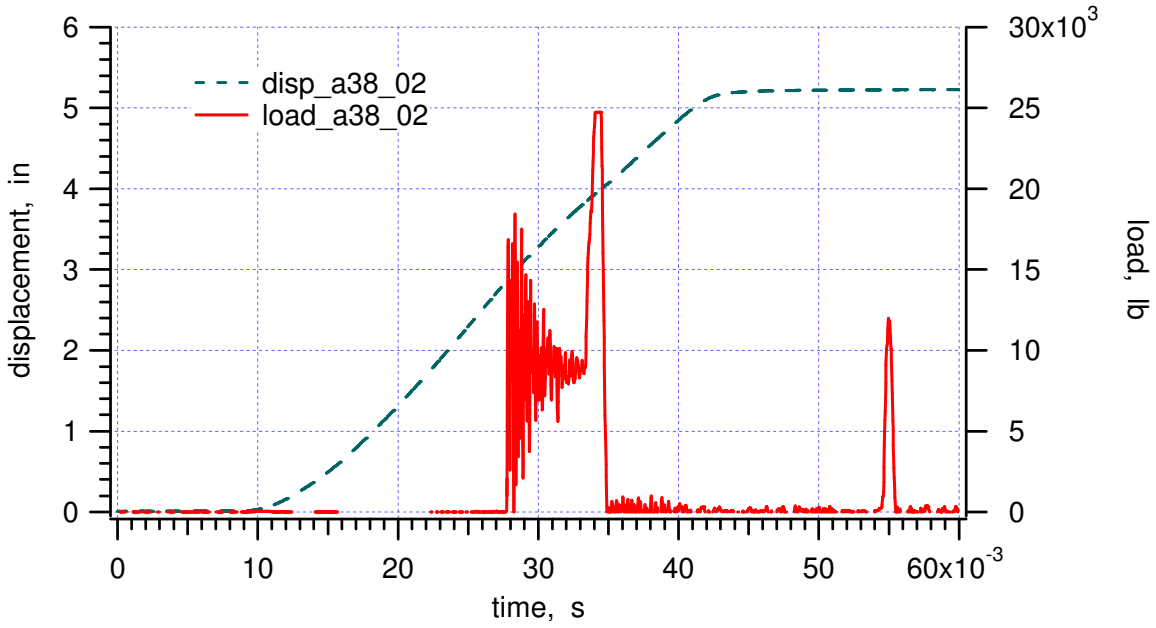

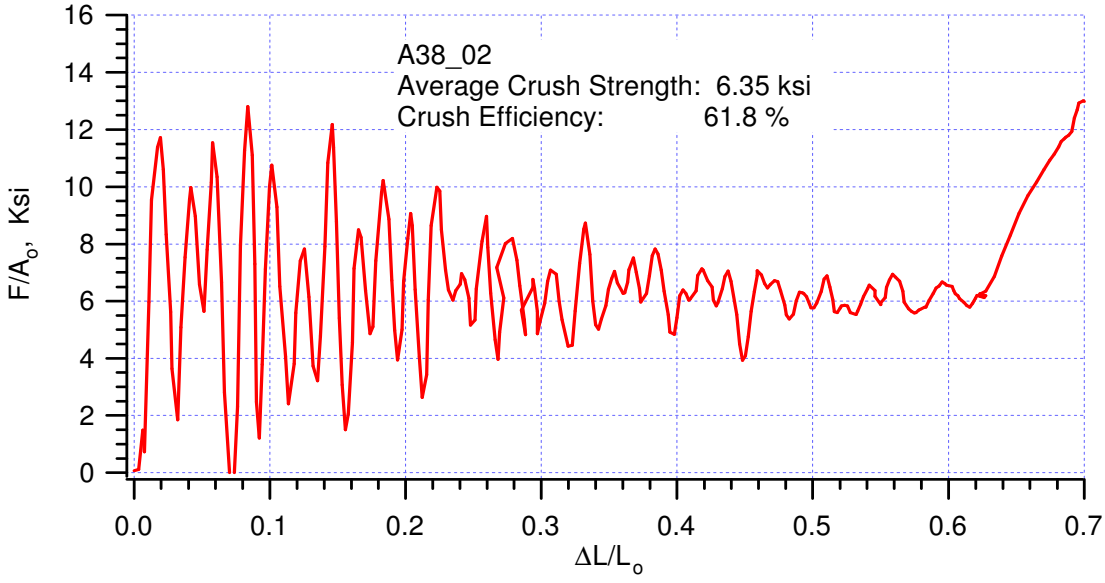

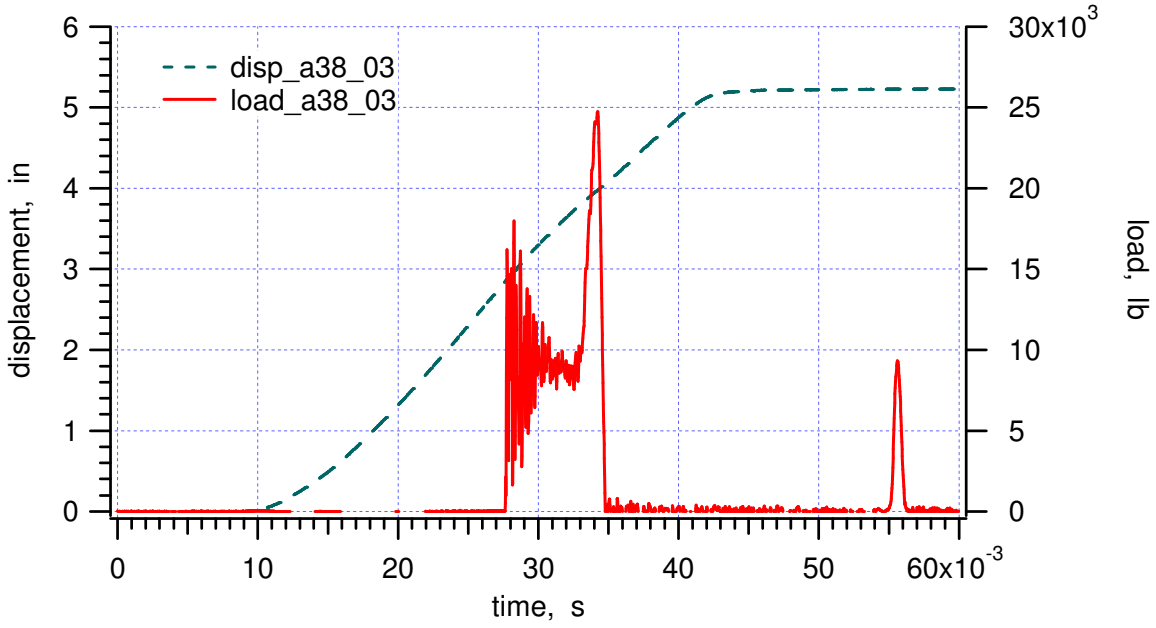
disp_a38_03
load_a38_03
displacement, in
load, lb
time, s
30x10^3
60x10^-3

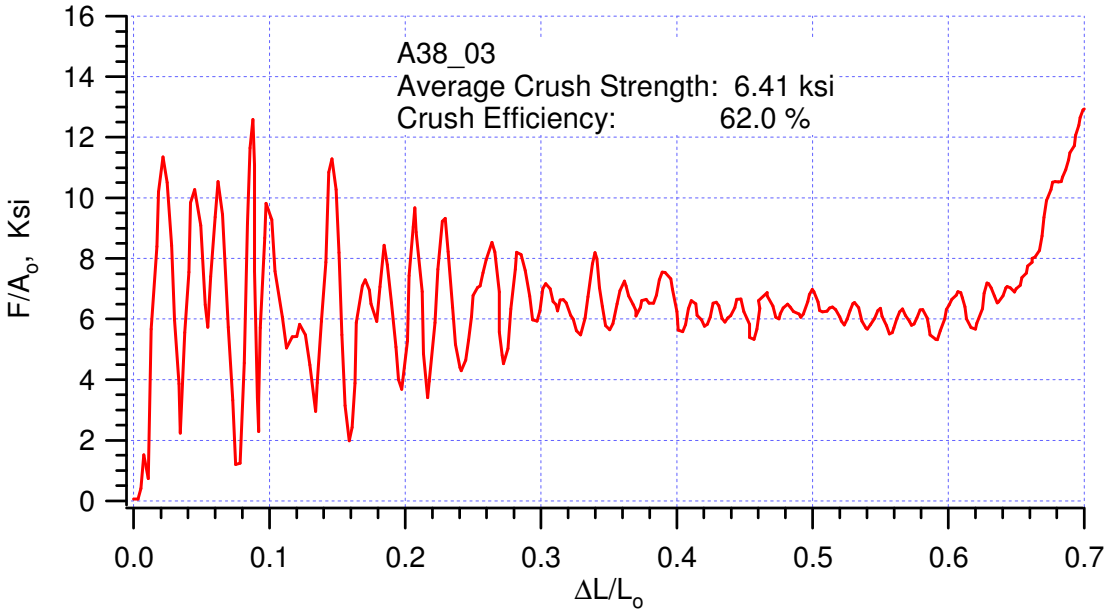
A38_03
Average Crush Strength: 6.41 ksi
Crush Efficiency: 62.0 %
F/A_o, Ksi
ΔL/L_o

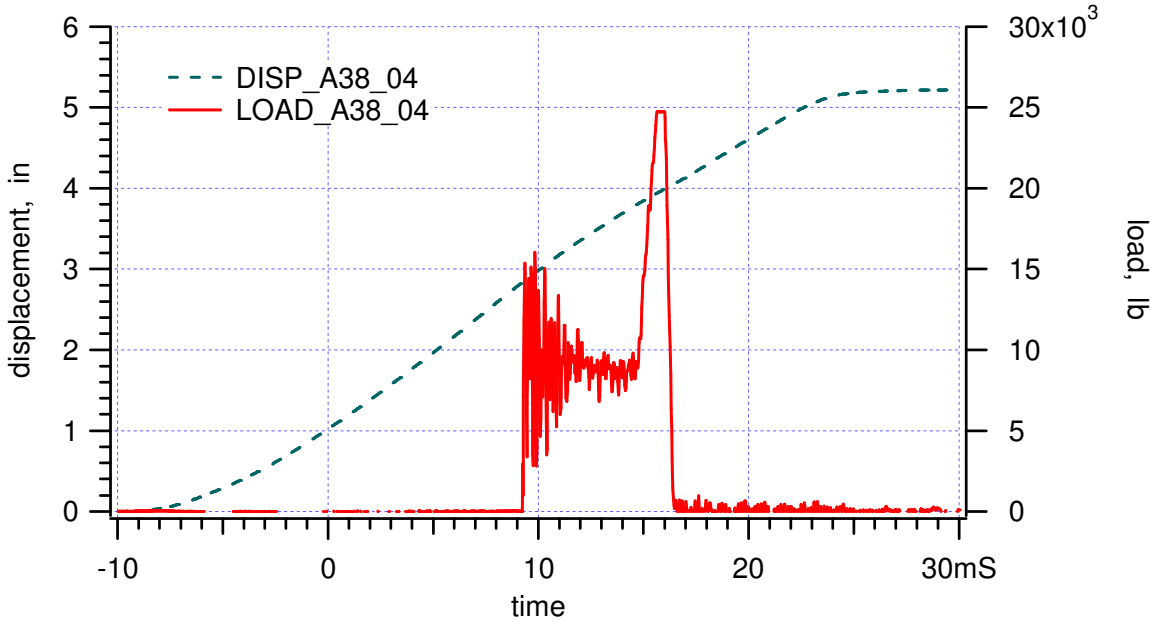
DISP_A38_04
LOAD_A38_04
displacement, in
load, lb
30x10^3
time
-10
0
10
20
30mS

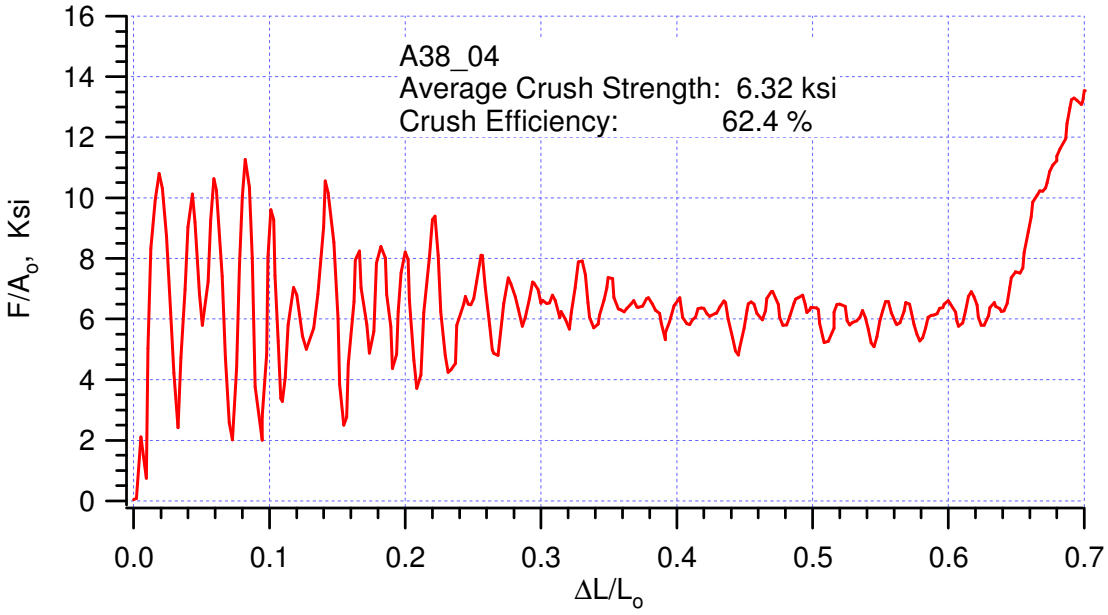
A38_04
Average Crush Strength: 6.32 ksi
Crush Efficiency: 62.4 %
F/A_o, Ksi
ΔL/L_o

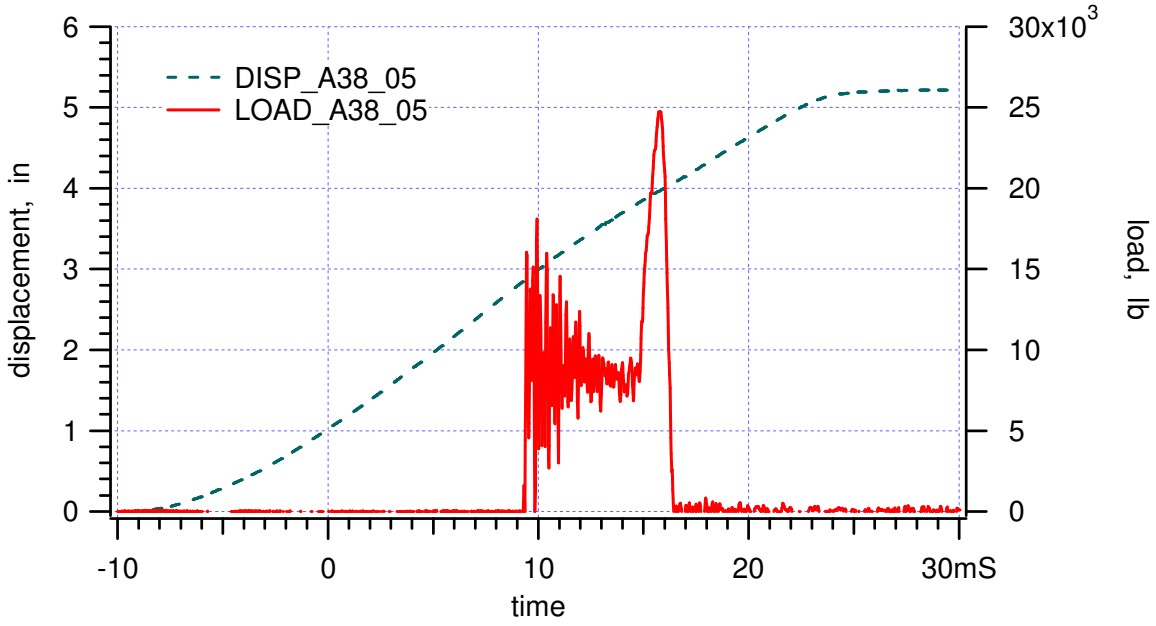
DISP_A38_05
LOAD_A38_05
displacement, in
load, lb
30x10^3
time
-10
0
10
20
30mS

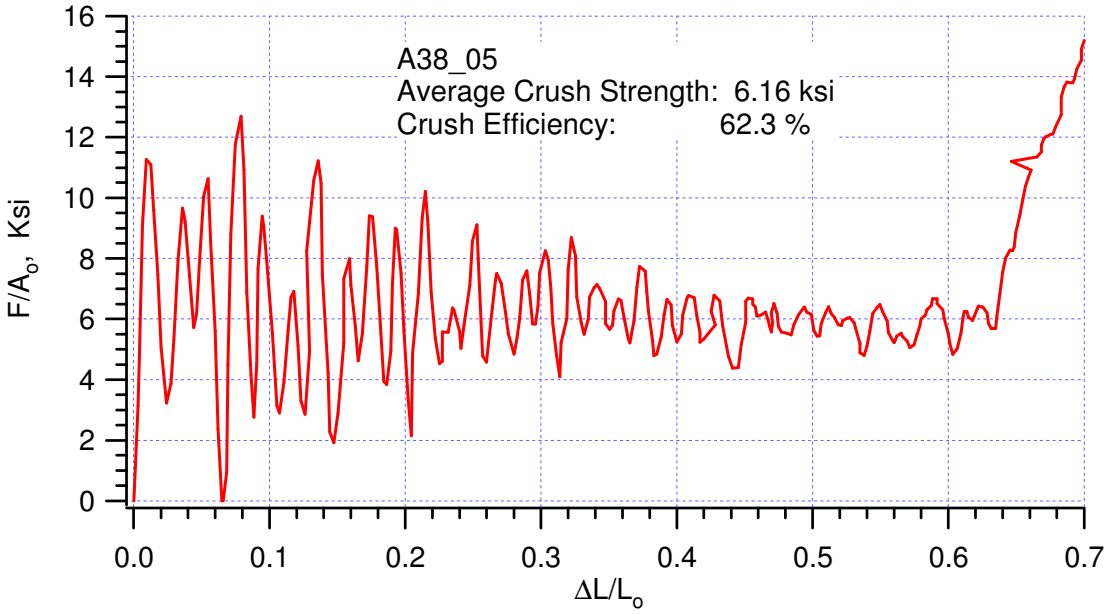
A38_05
Average Crush Strength: 6.16 ksi
Crush Efficiency: 62.3 %
F/A_o, Ksi
ΔL/L_o

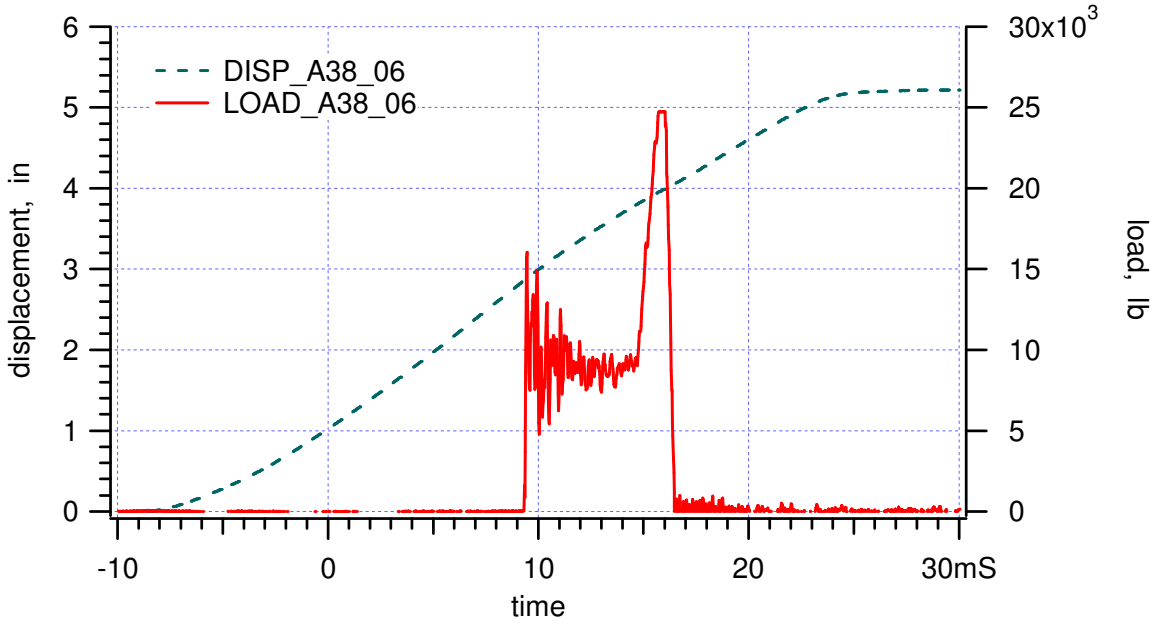
DISP_A38_06
LOAD_A38_06
displacement, in
load, lb
30x10^3
time
-10
0
10
20
30mS

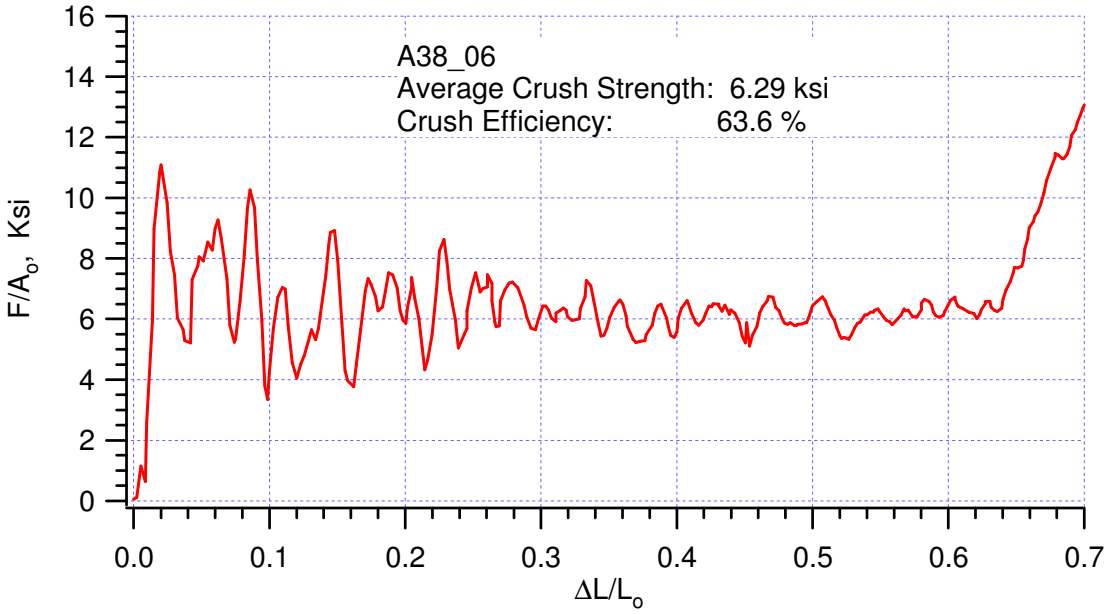
A38_06
Average Crush Strength: 6.29 ksi
Crush Efficiency: 63.6 %
F/A_o, Ksi
ΔL/L_o

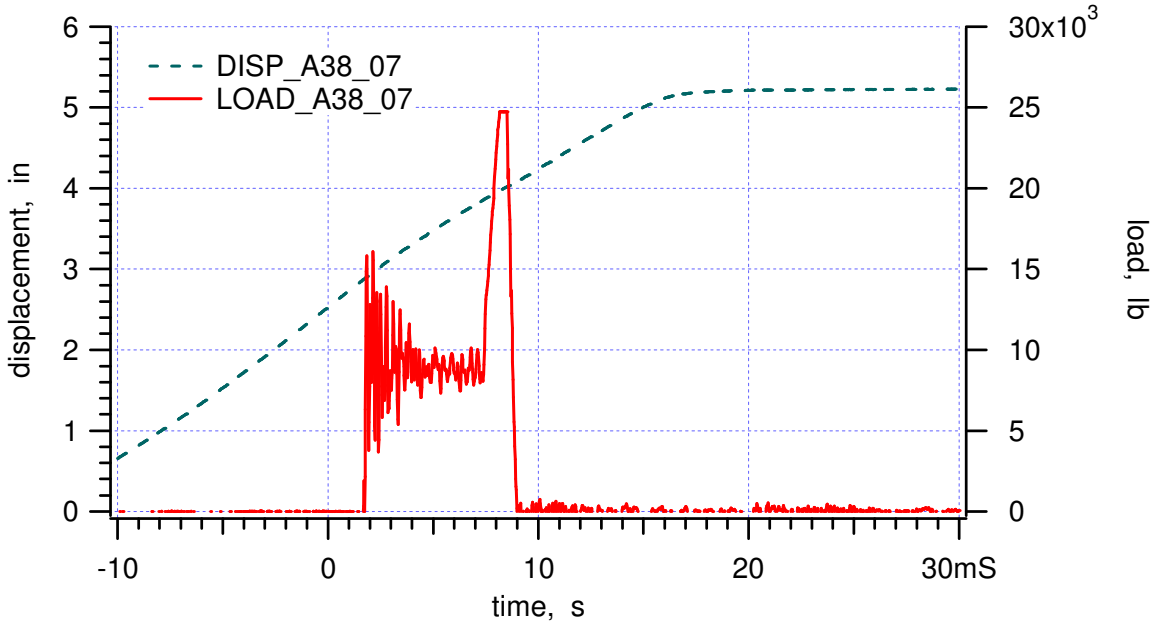
DISP_A38_07
LOAD_A38_07
displacement, in
load, lb
30x10^3
time, s
-10
0
10
20
30mS

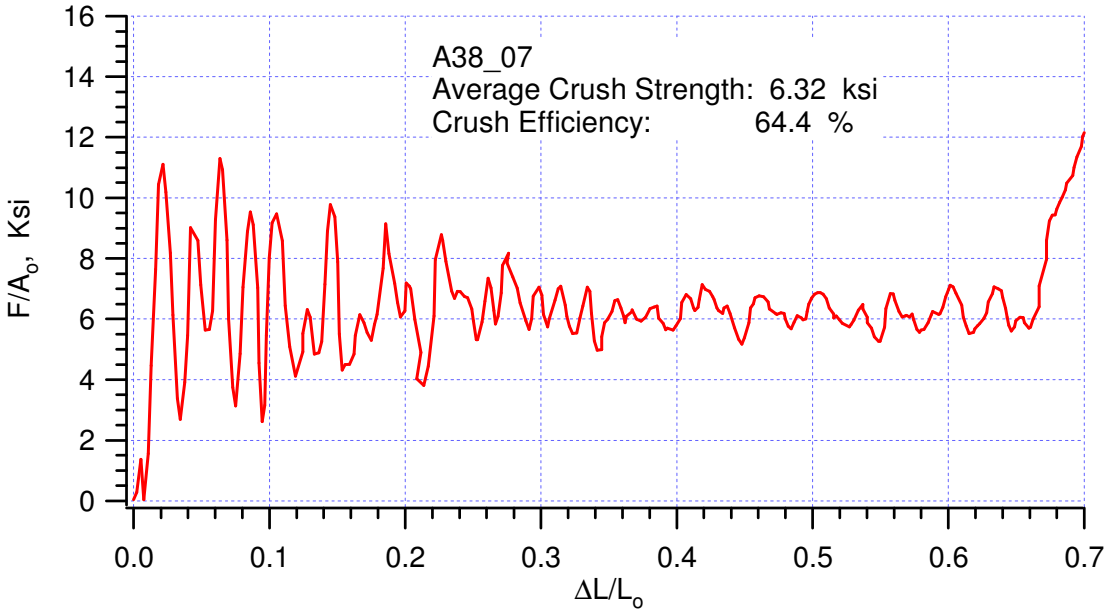
A38_07
Average Crush Strength: 6.32 ksi
Crush Efficiency: 64.4 %
F/A_o, Ksi
ΔL/L_o

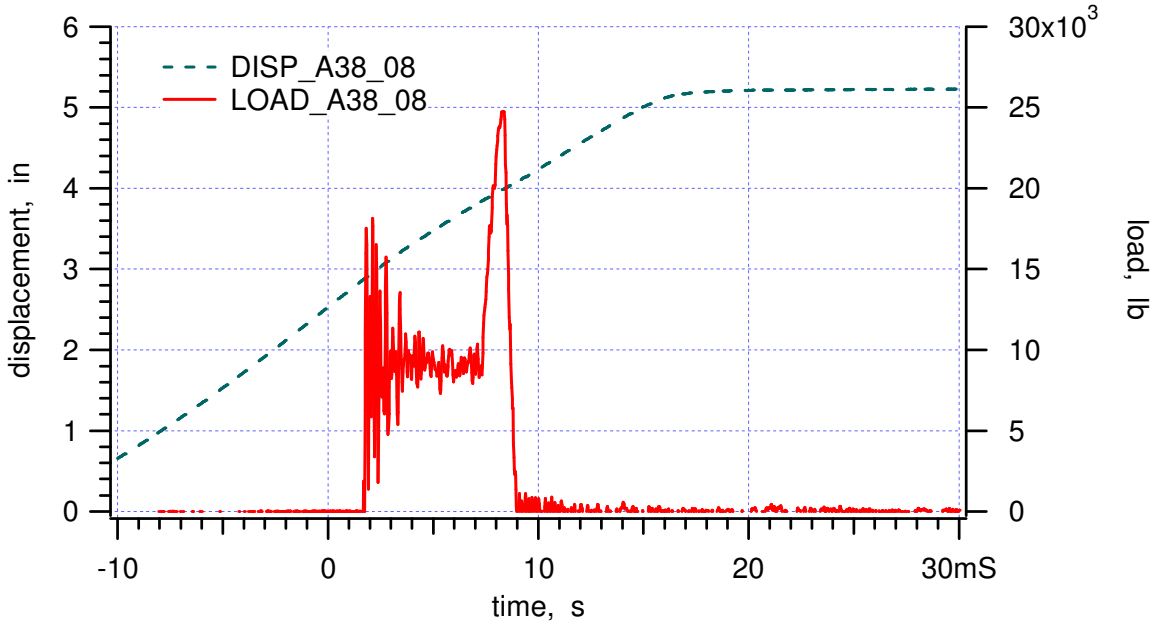
DISP_A38_08
LOAD_A38_08
displacement, in
load, lb
30x10^3
time, s
-10
0
10
20
30mS

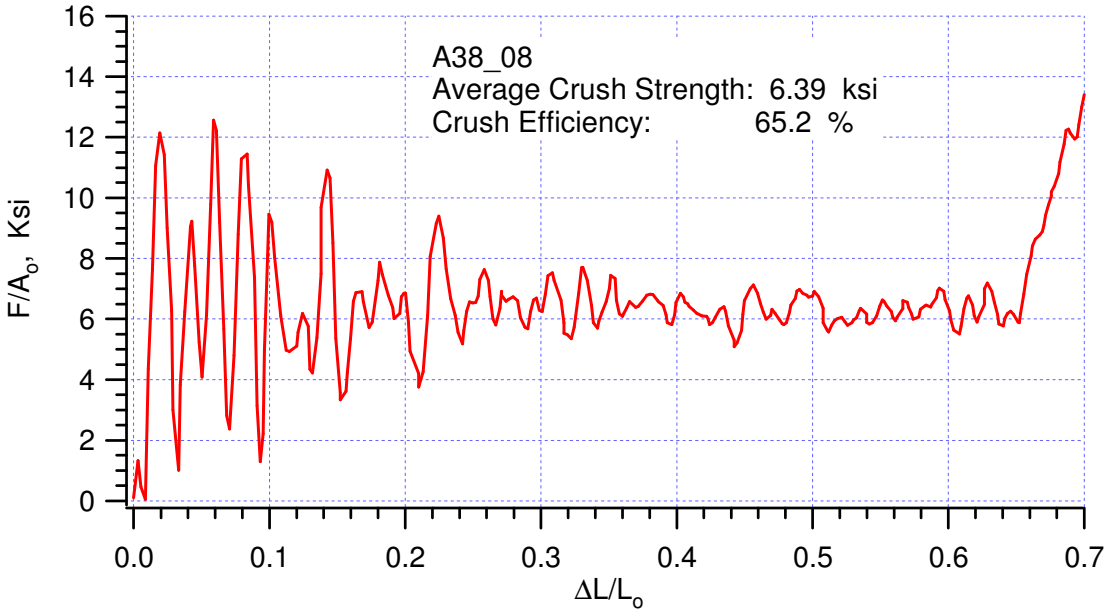
A38_08
Average Crush Strength: 6.39 ksi
Crush Efficiency: 65.2 %
F/A_o, Ksi
ΔL/L_o

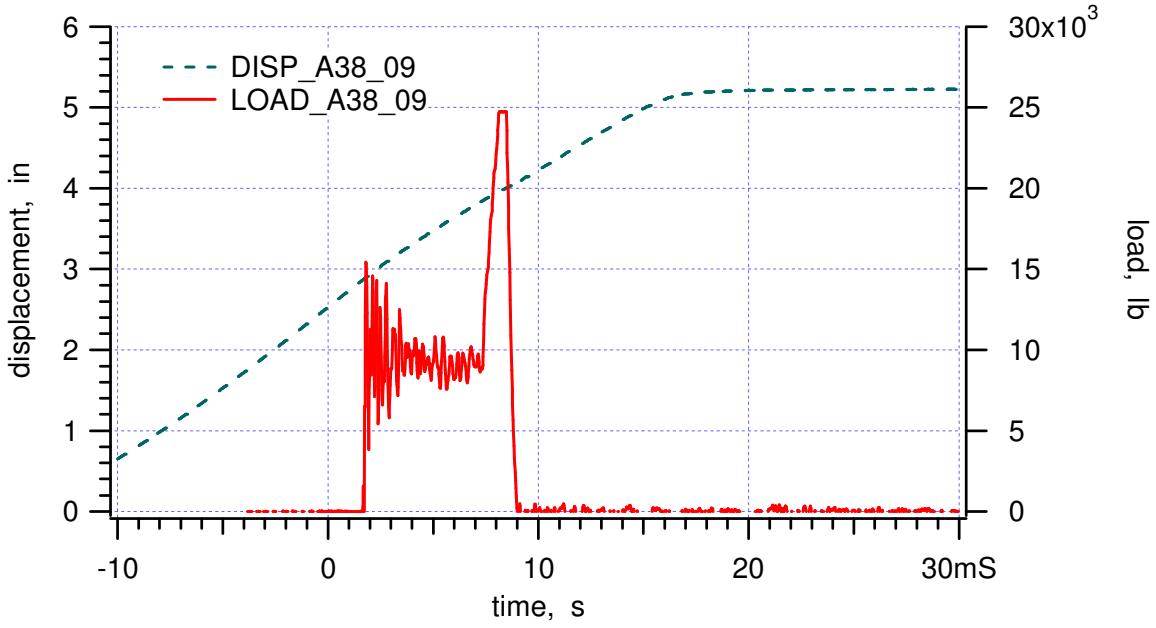
DISP_A38_09
LOAD_A38_09
displacement, in
load, lb
30x10^3
time, s
-10
0
10
20
30mS

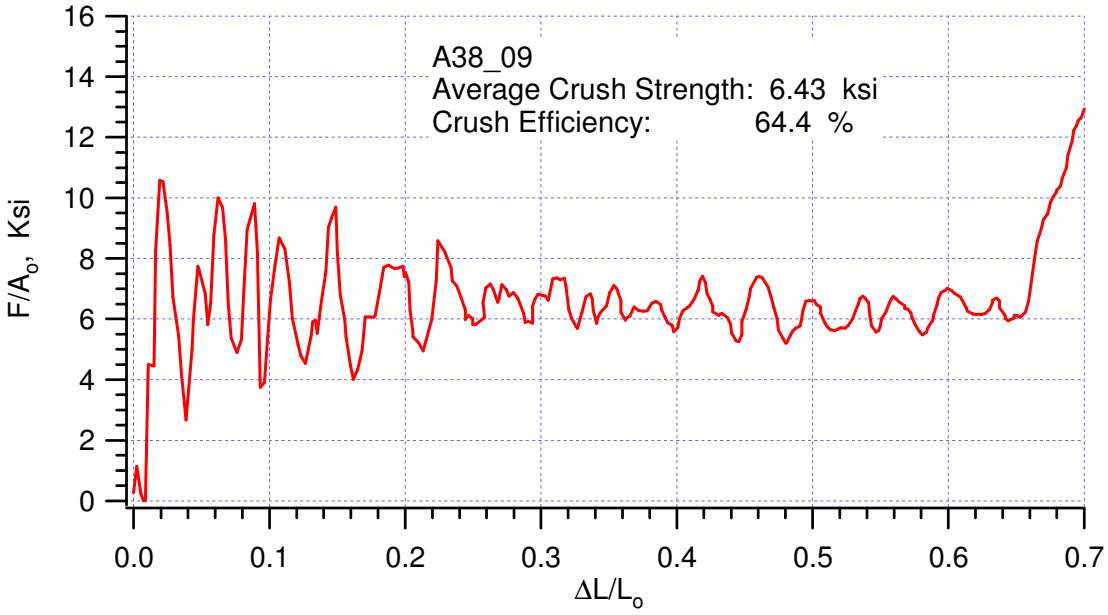
A38_09
Average Crush Strength: 6.43 ksi
Crush Efficiency: 64.4 %
F/A_o, Ksi
ΔL/L_o

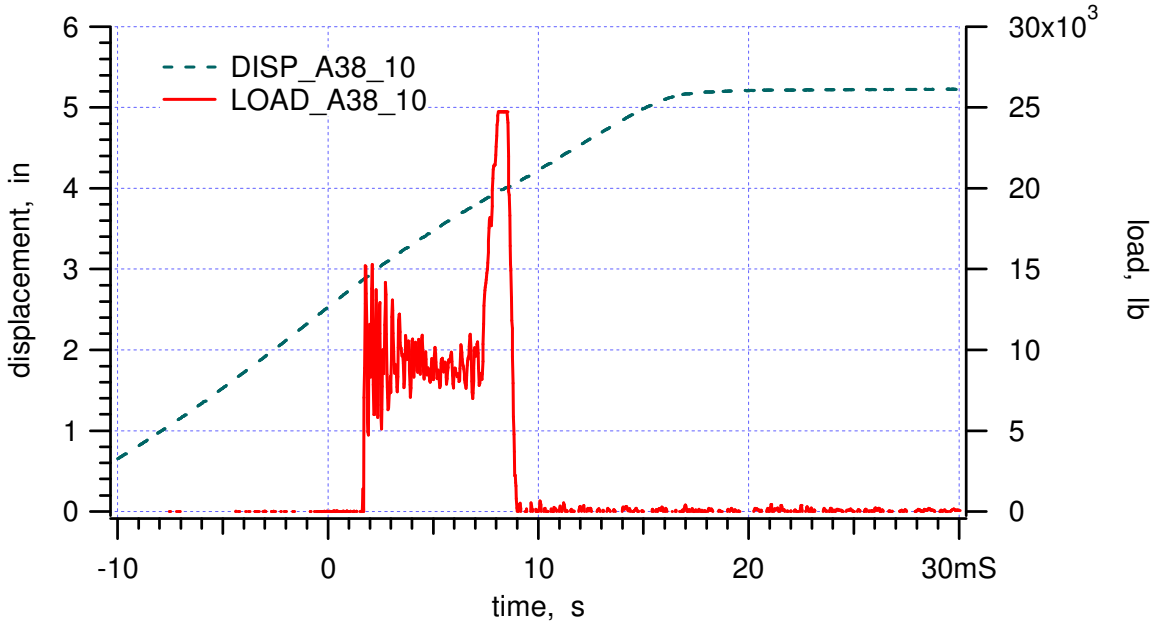
DISP_A38_10
LOAD_A38_10
displacement, in
load, lb
30x10^3
time, s
-10
0
10
20
30mS

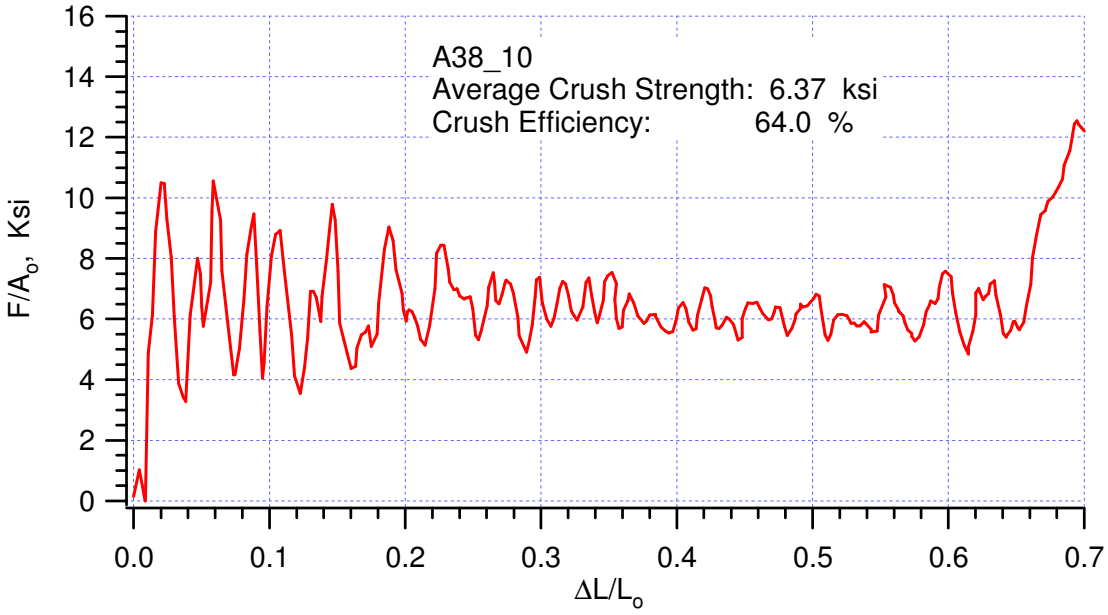
A38_10
Average Crush Strength: 6.37 ksi
Crush Efficiency: 64.0 %
F/A_o, Ksi
ΔL/L_o

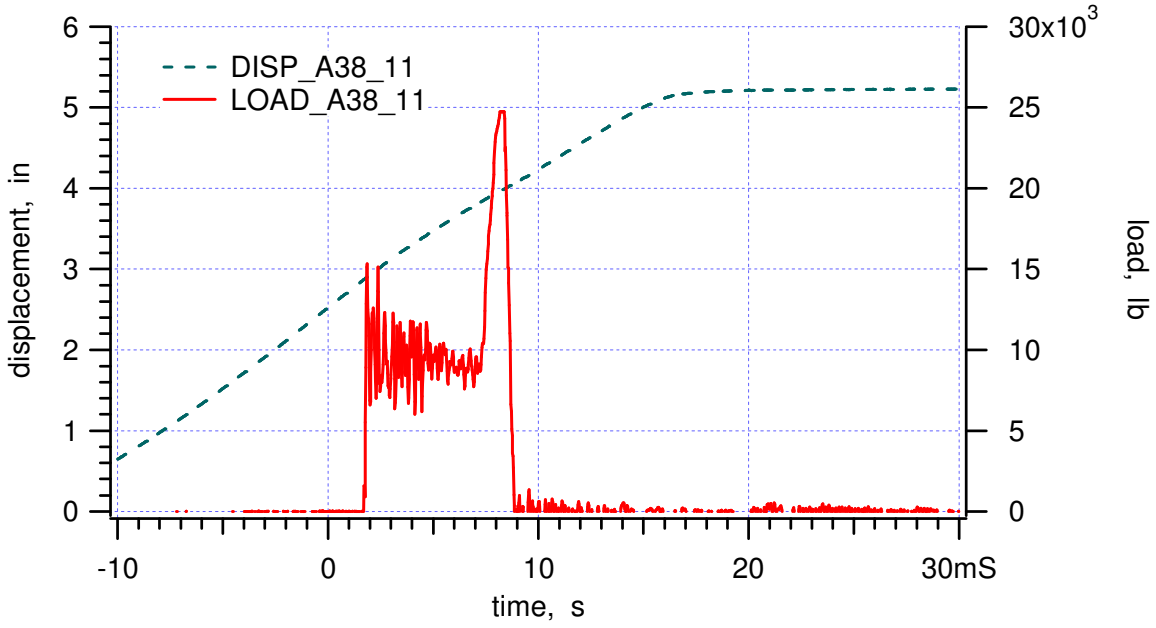
DISP_A38_11
LOAD_A38_11
displacement, in
load, lb
30x10^3
time, s
-10
0
10
20
30mS

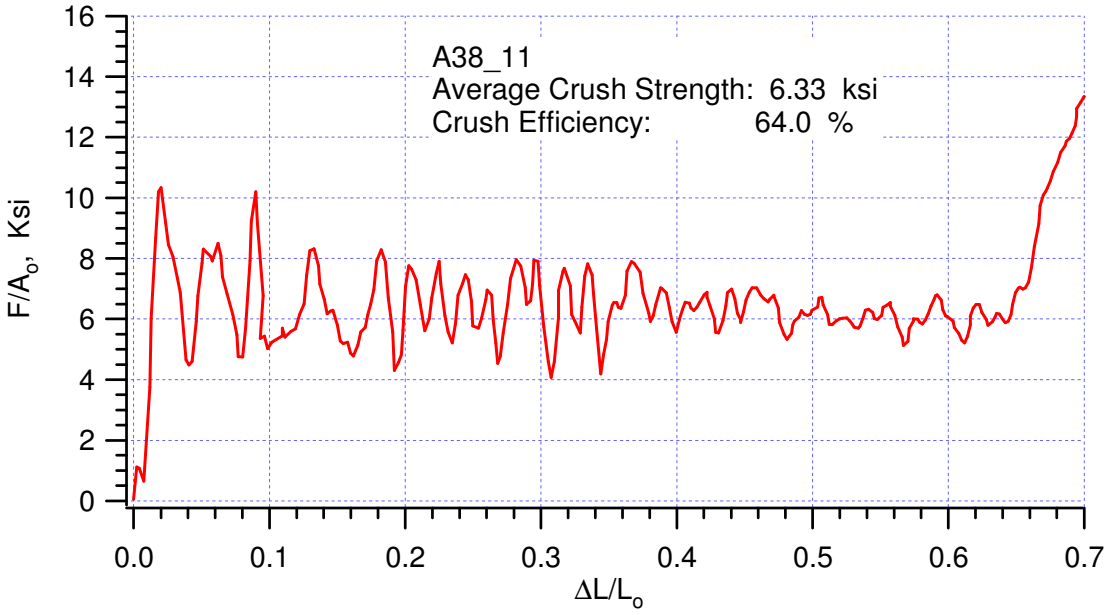
A38_11
Average Crush Strength: 6.33 ksi
Crush Efficiency: 64.0 %
F/A_o, Ksi
ΔL/L_o

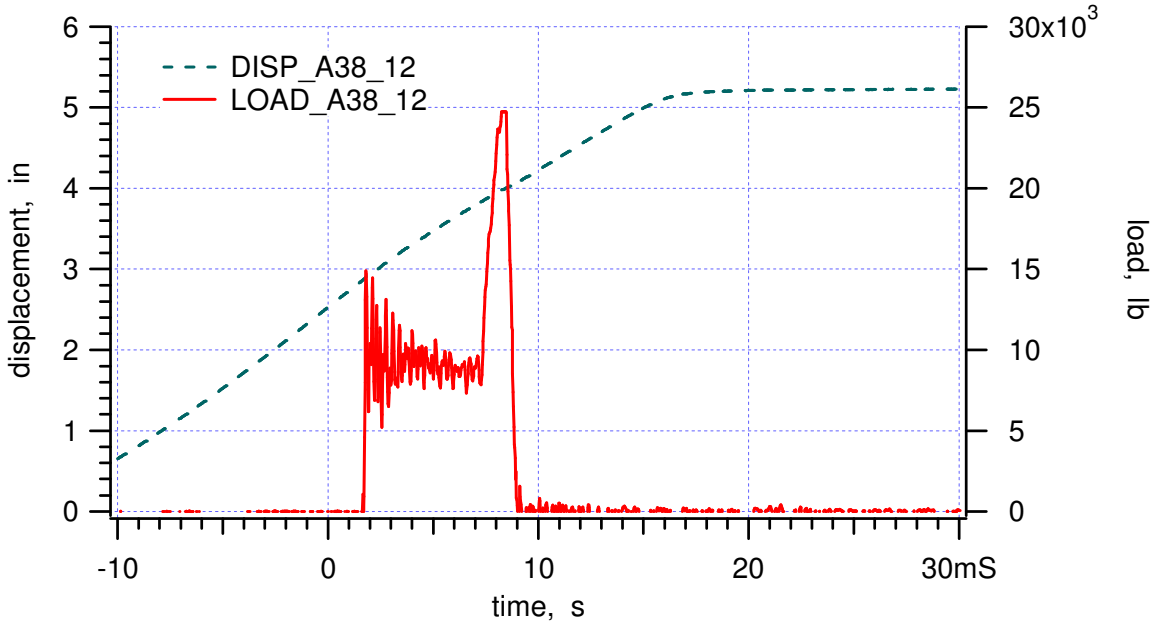
DISP_A38_12
LOAD_A38_12
displacement, in
load, lb
30x10^3
time, s
-10
0
10
20
30mS

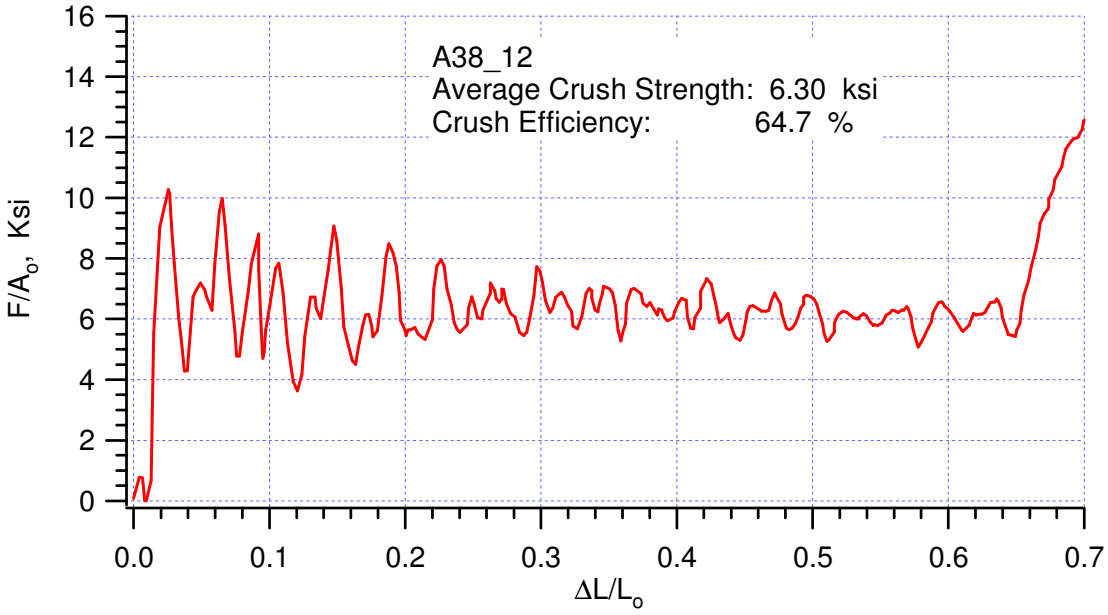
A38_12
Average Crush Strength: 6.30 ksi
Crush Efficiency: 64.7 %
F/A_o, Ksi
ΔL/L_o

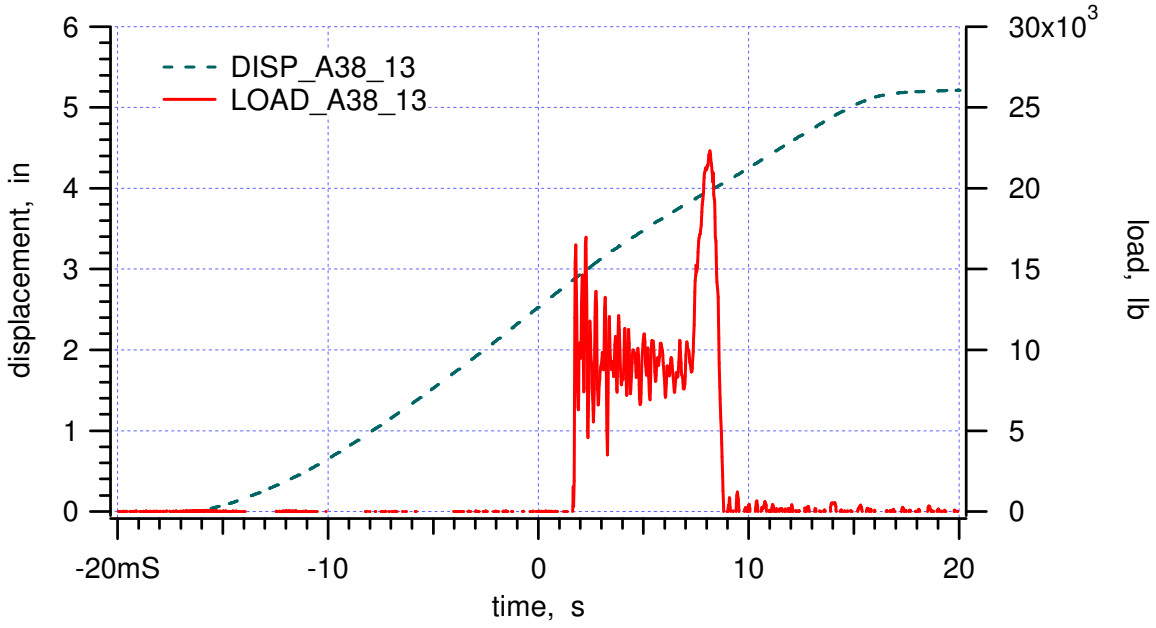
DISP_A38_13
LOAD_A38_13
displacement, in
load, lb
30x10^3
time, s
-20mS
-10
0
10
20

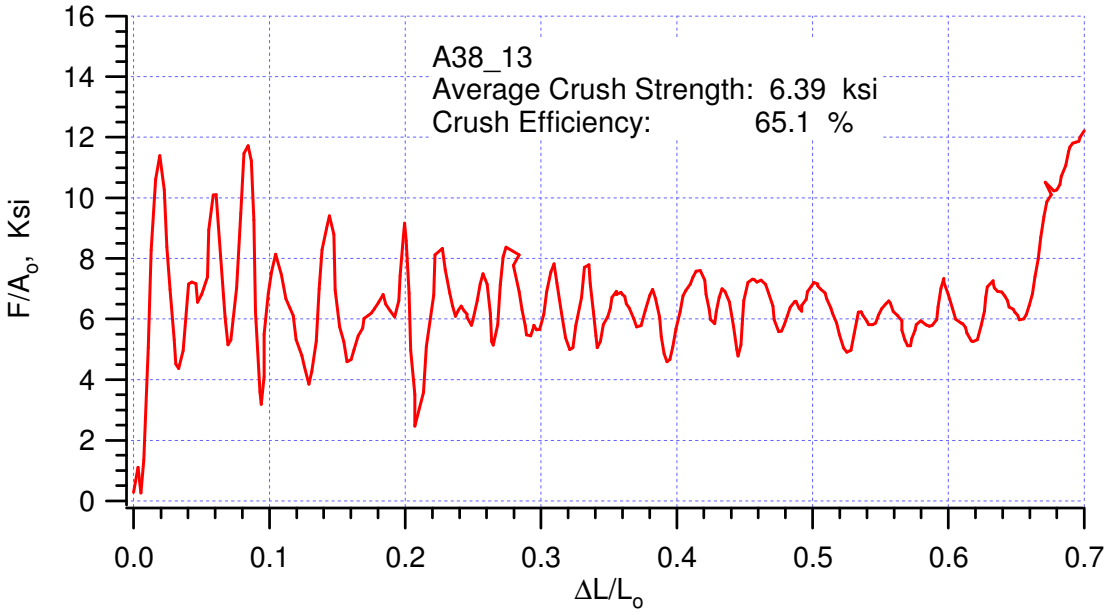
A38_13
Average Crush Strength: 6.39 ksi
Crush Efficiency: 65.1 %
F/A_o, Ksi
ΔL/L_o

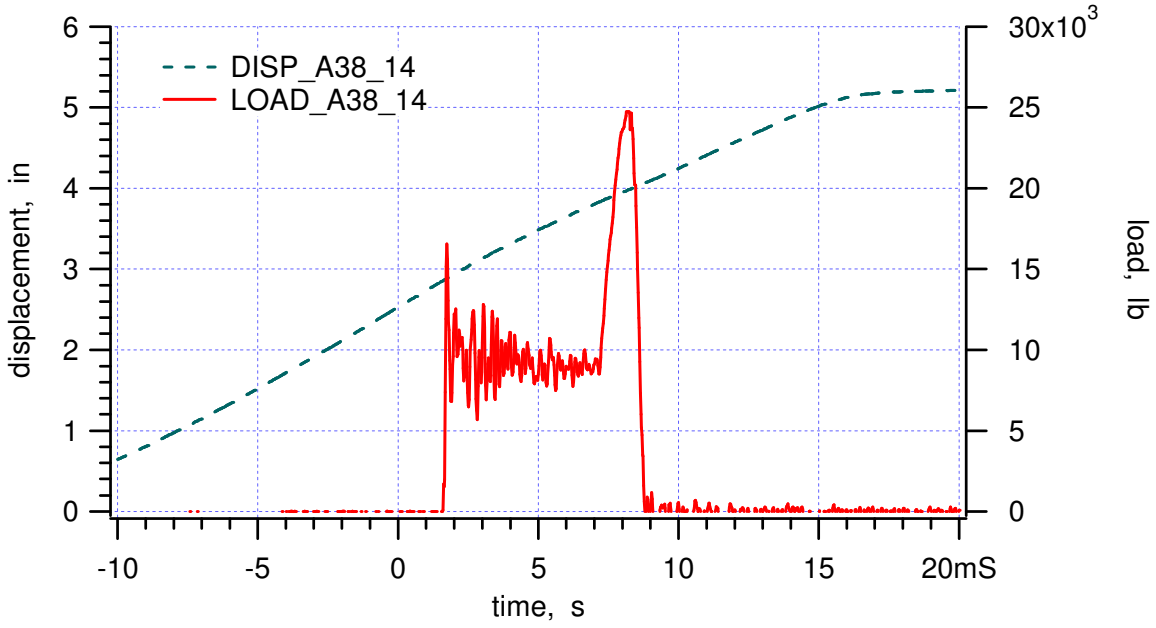
DISP_A38_14
LOAD_A38_14
displacement, in
load, lb
30x10^3
time, s
-10
-5
0
5
10
15
20mS

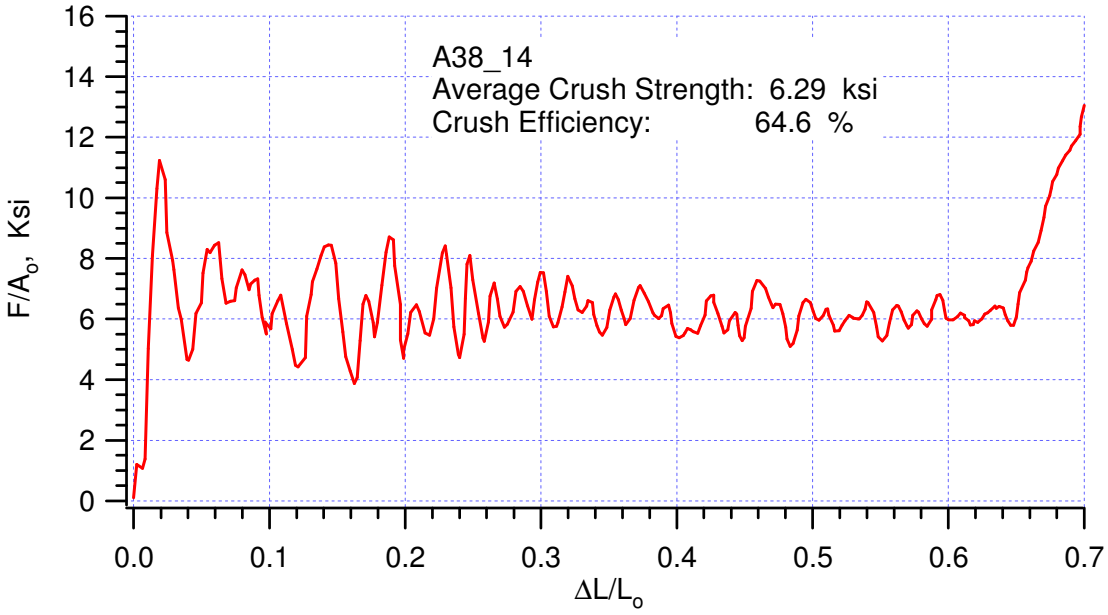
A38_14
Average Crush Strength: 6.29 ksi
Crush Efficiency: 64.6 %
F/A$_o$, Ksi
ΔL/L$_o$

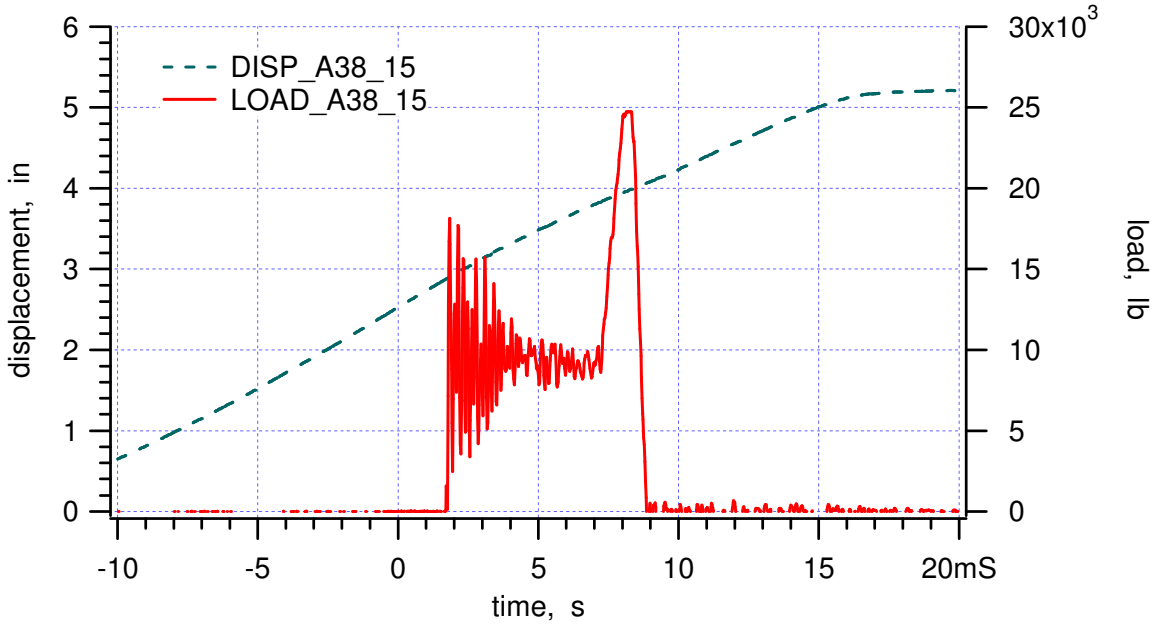
DISP_A38_15
LOAD_A38_15
displacement, in
load, lb
30x10^3
time, s
-10
-5
0
5
10
15
20mS

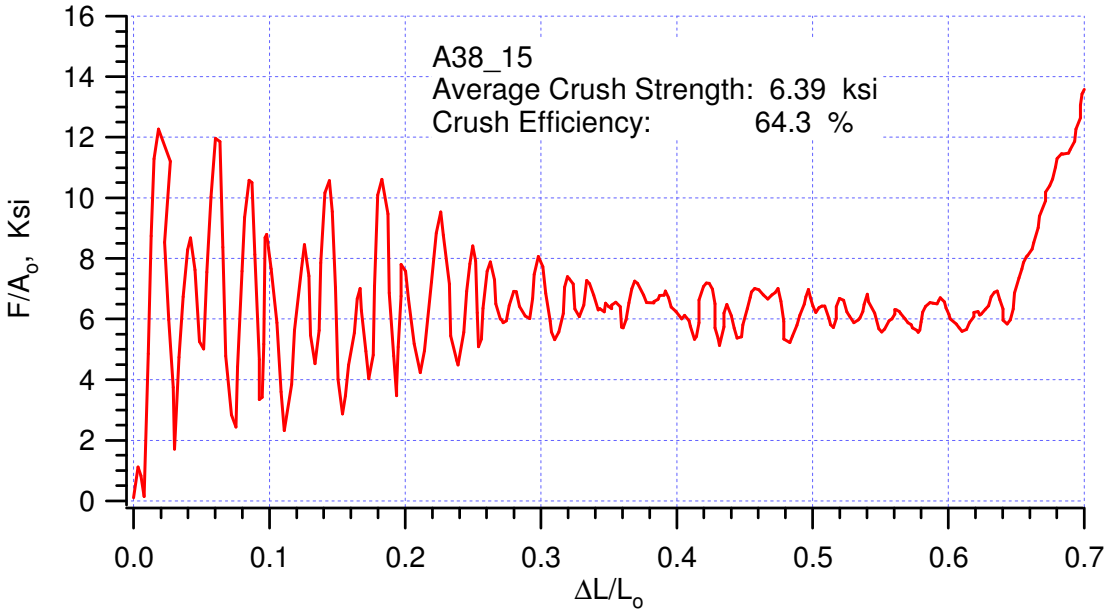
A38_15
Average Crush Strength: 6.39 ksi
Crush Efficiency: 64.3 %
F/A_o, Ksi
ΔL/L_o

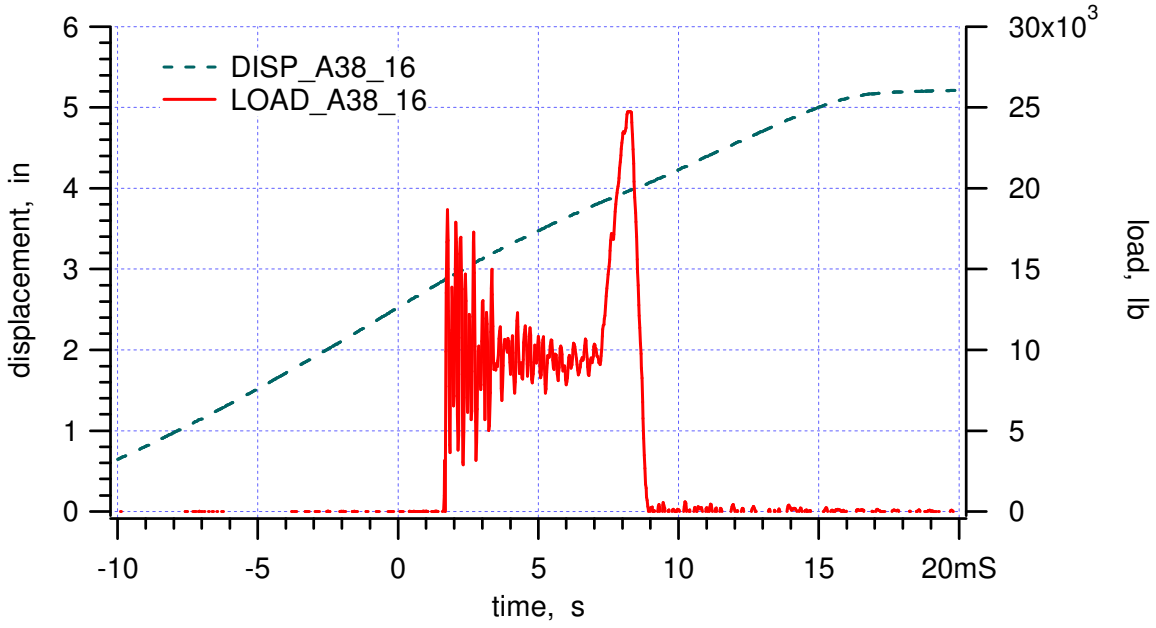
DISP_A38_16
LOAD_A38_16
displacement, in
load, lb
30x10^3
time, s
-10
-5
0
5
10
15
20mS

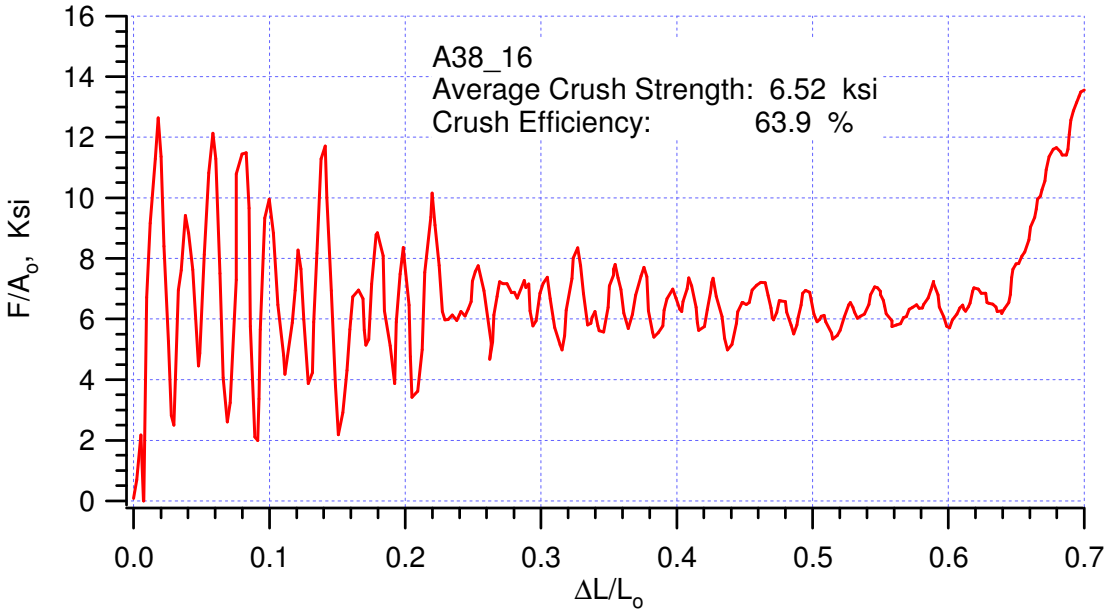
A38_16
Average Crush Strength: 6.52 ksi
Crush Efficiency: 63.9 %
F/A$_o$, Ksi
ΔL/L$_o$

APPENDIX VII:

"Quasi-static Crush Tests of Hexcel Segmented Samples at Ambient Temperature," Memo Wei-Yang Lu to Distribution, December 13, 1999

Sandia National Laboratories
Operated for the U.S. Department of Energy by
Sandia Corporation
MS9042
Livermore, CA 94551-0969

date: December 13, 1999

to: Distribution

from: Wei-yang Lu

subject: Quasi-static Crush Tests of Hexcel Segmented Samples at Ambient Temperature

We have completed test # 162 – 164 (Table 2.4, ***B61 Radar Nose / MAVEN*** *Test Matrix …*, by T.D. Hinnerichs, October 27, 1999). The crush of Hexcel segmented specimen was similar to Alcore specimens, which was reported in the memo of November 30, 1999, from Wei-yang Lu to Distribution; no splitting was observed and the adhesive coating came off during crush. The crush strength is 6.85 ksi, and the crush efficiency is 53.7 %, which are higher than those of Alcore specimens, 6.14 ksi and 52.3 %, respectively. Please see Appendix for detail experimental procedures and results.

Distribution:

Darrla Giersch (2167)	MS0481
Darren Hoke (2167)	MS0481
Vernon Willan (2167)	MS0481
Vista Bateman (9126)	MS0553
Tom Carne (9124)	MS0557
Berry Boughten (9132)	MS0557
Jaime Moya (9132)	MS0828
Terry Hinnerichs (9126)	MS0847
Ken Gwinn (9126)	MS0847
John Pott (9126)	MS0847
Rodney May (9126)	MS0847
Mike Neilsen (9123)	MS0847
Bill Scherzinger (9123)	MS0847
Hal Morgan (9123)	MS0847
Wendell Kawahara (8725)	MS9042

Quasi-static Crush Tests of Hexcel Segmented Samples at Ambient Temperature

Appendix

SPECIMENS

Figures 1, 2 and 3 show the undeformed specimens, HS1-1, HS2-1 AND HS3-1, which were manufactured by Allied Signal, Kansas City. Their dimensions and weight were measured and recorded in Table 1.

We observed some minute differences among these three specimens. In HS1-1, the interface lines (i.e., the adhesive lines between each two segments) and did not meet at the center of the specimen, Figure 1(a), and the edge honeycomb cells at the circumference were pre-crushed in L-direction, Figure 1(b). Specimen HS3-1 was better, the interface lines missed the center just slightly, Figure 3(a), and there was no pre-crush cell at the edge, Figure 3(b). Specimen HS2-1 was ideal.

LOADING SYSTEM

The equipment used was the same as that in the experiment of Alcore segmented specimen. System compliance was measured again. The result is shown in Figure 4. A polynomial curve-fit represents the compliance of the system:

$$\Delta Lc = 1.47 + 0.33 \bullet F - 4.82 \times 10^{-3} \bullet F^2 + 4.43 \times 10^{-5} \bullet F^3 - 1.97 \times 10^{-7} \bullet F^4 + 3.34 \times 10^{-10} \bullet F^5 \quad (1)$$

where ΔLc ($x10^{-3}$ in) is the displacement, and F (kips) is the load

EXPERIMENT

Same as the experiment of Alcore segmented specimen, the adhesive coating came off during crush, and no splitting or other abnormal deformation was observed.

RESULTS

Raw experimental data, stroke (or displacement, ΔL) and load (F), of HS1-1, HS2-1 AND HS3-1 are plotted in Figures 5, 7 and 9, respectively. "Stress-strain" curves are shown in Figures 6, 8 and 10. Please note that contribution due to system compliance has been corrected.

Notice that the crush strength of HS1-1 is about 8% higher than that of HS2-1 and HS3-1, which could be caused by the irregularity of the specimen as described earlier.

Table 1. Summary of Hexcel Segmented Specimens

Specimen	Diameter, in	Height, in	Weight, lb	Density, pcf	Apparent Elastic Modulus, ksi	Compressive Peak, ksi	Average Crush Strength, ksi	Crush Efficiency %
HS1-1	5.079	1.498	0.735	41.866	840	8.4	7.23	54.5
HS2-1	5.081	1.499	0.721	40.992	1067	8.3	6.67	53.4
HS3-1	5.080	1.498	0.720	41.004	1083	8.1	6.65	53.2

(a)

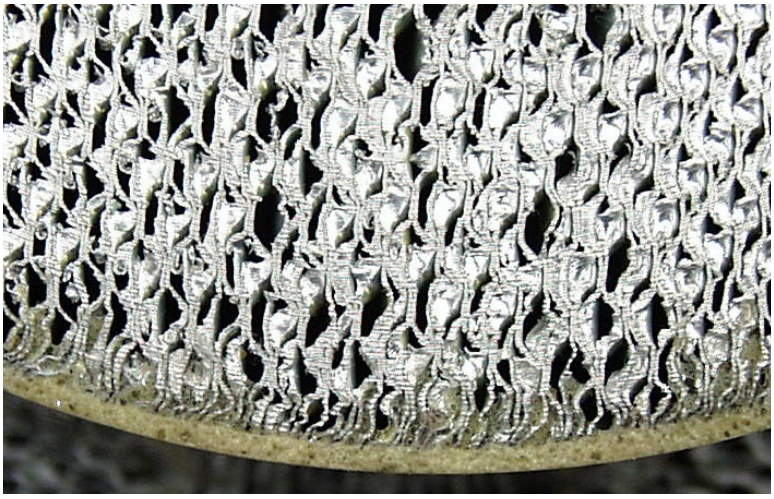

(b)

Figure 1. Sample HS1-1 before deformation. (a) Offsets among four segments can be observed; (b) the honeycomb close to the boundary shows pre-crush.

Figure 2. Sample HS2-1 before deformation. Four segments fit perfectly.

(a)

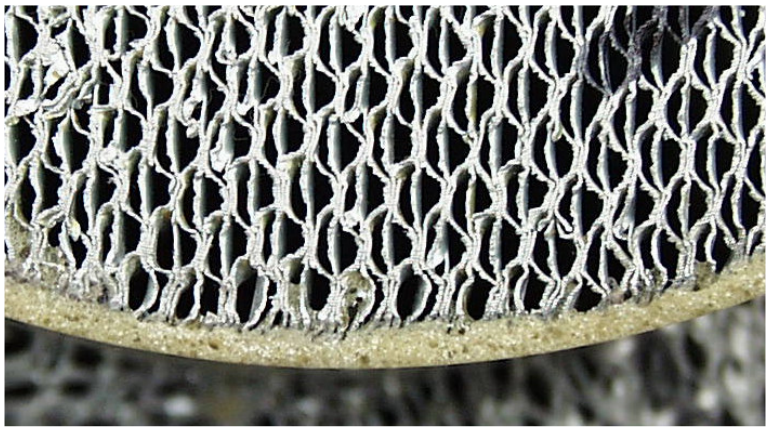

(b)

Figure 3. Sample HS1-3 before deformation. (a) Small amount of offsets can be observed ; (b) the honeycomb close to the boundary does not show pre-crush.

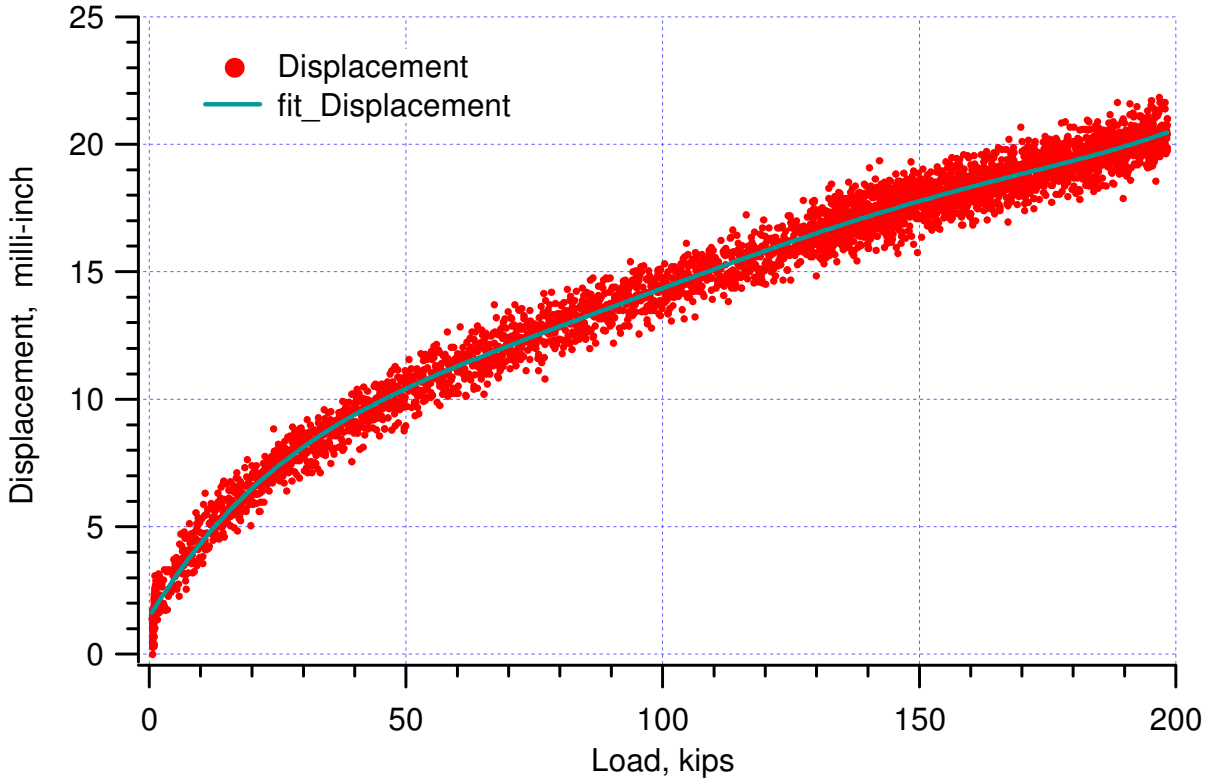

Figure 4. Compliance curve of the loading system.

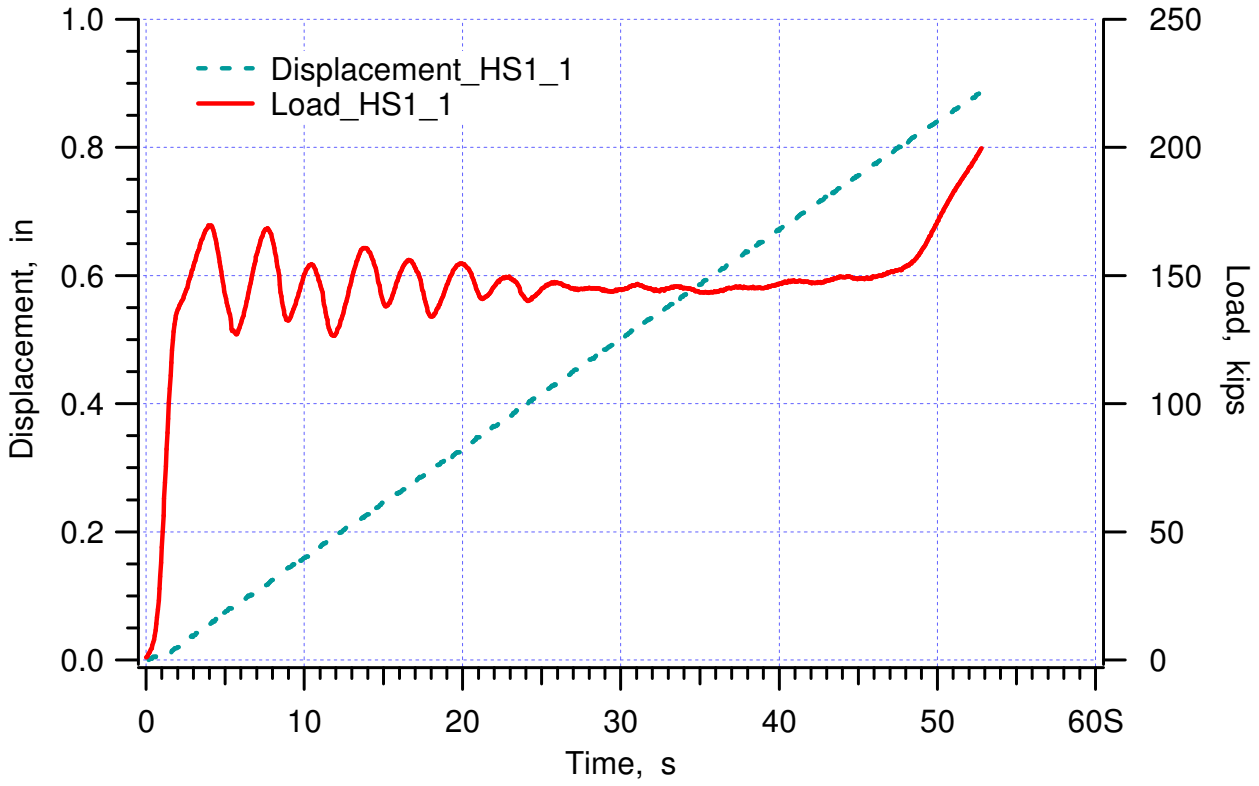

Figure 5. Raw data of HS1-1.

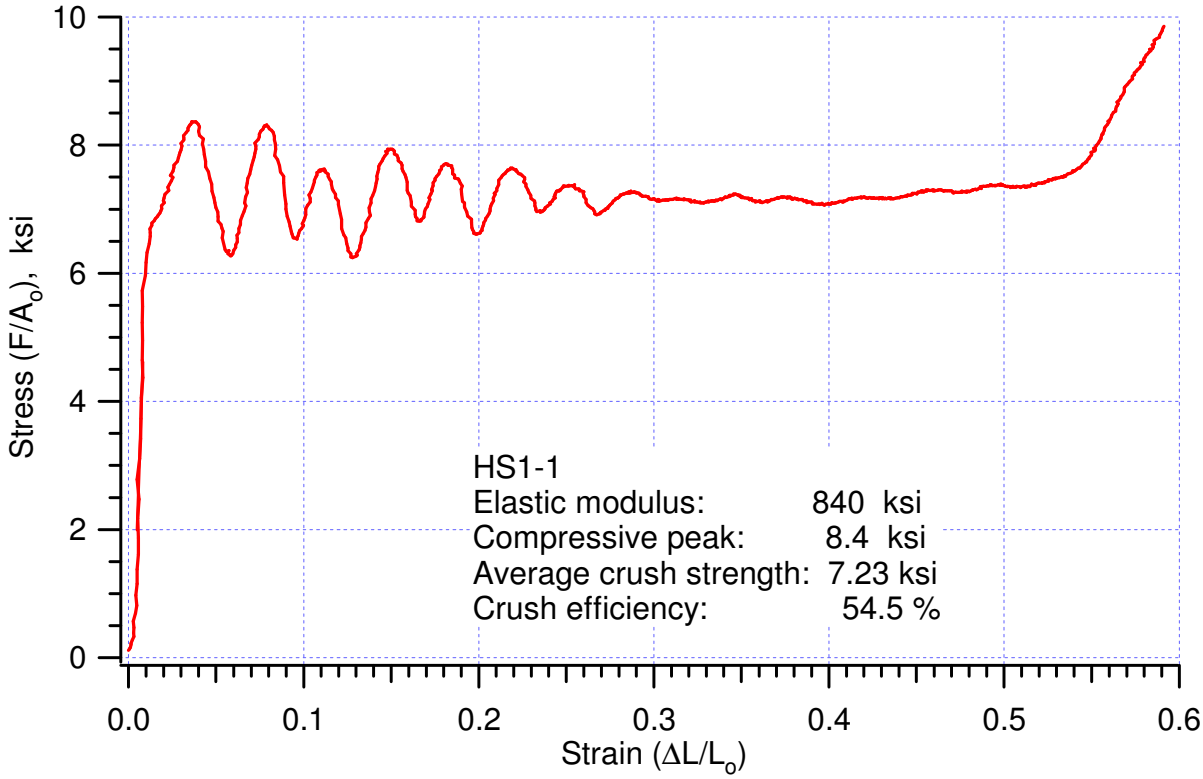

Figure 6. Stress-strain curve of HS1-1.

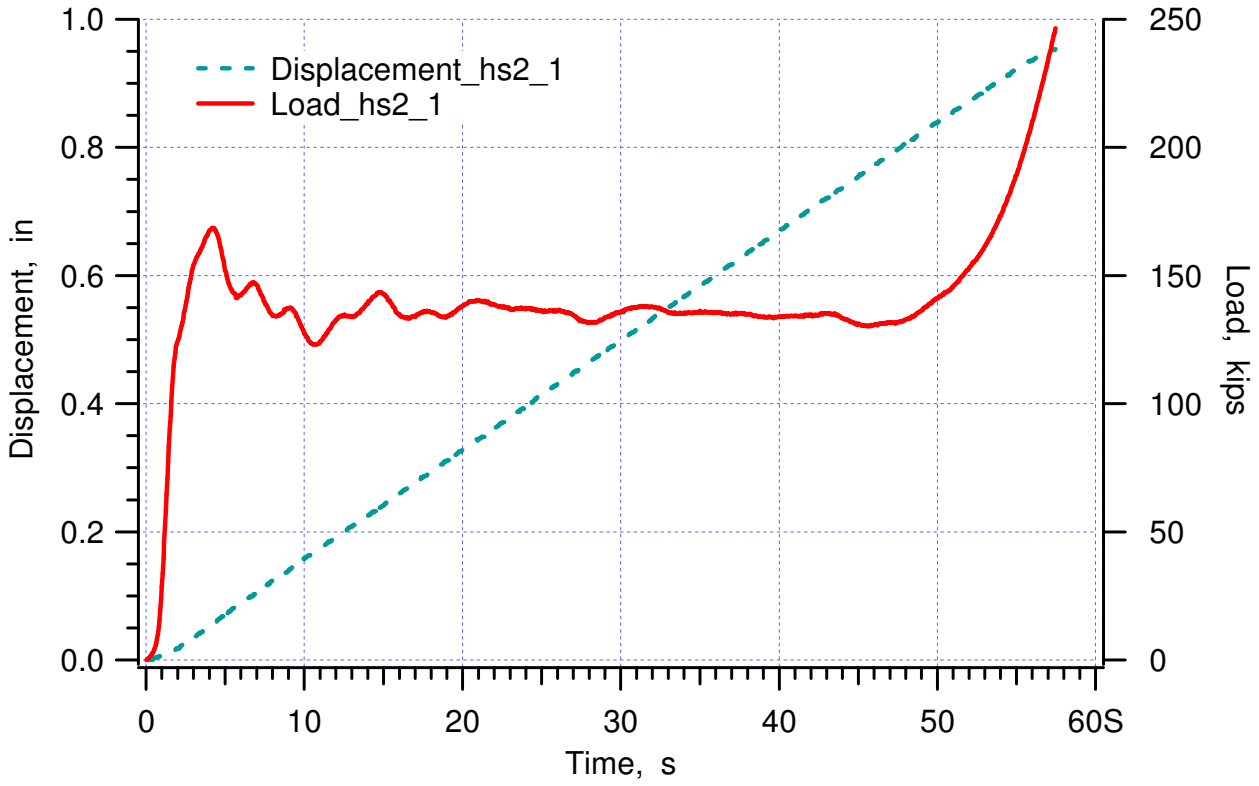

Figure 7. Raw data of HS2-1.

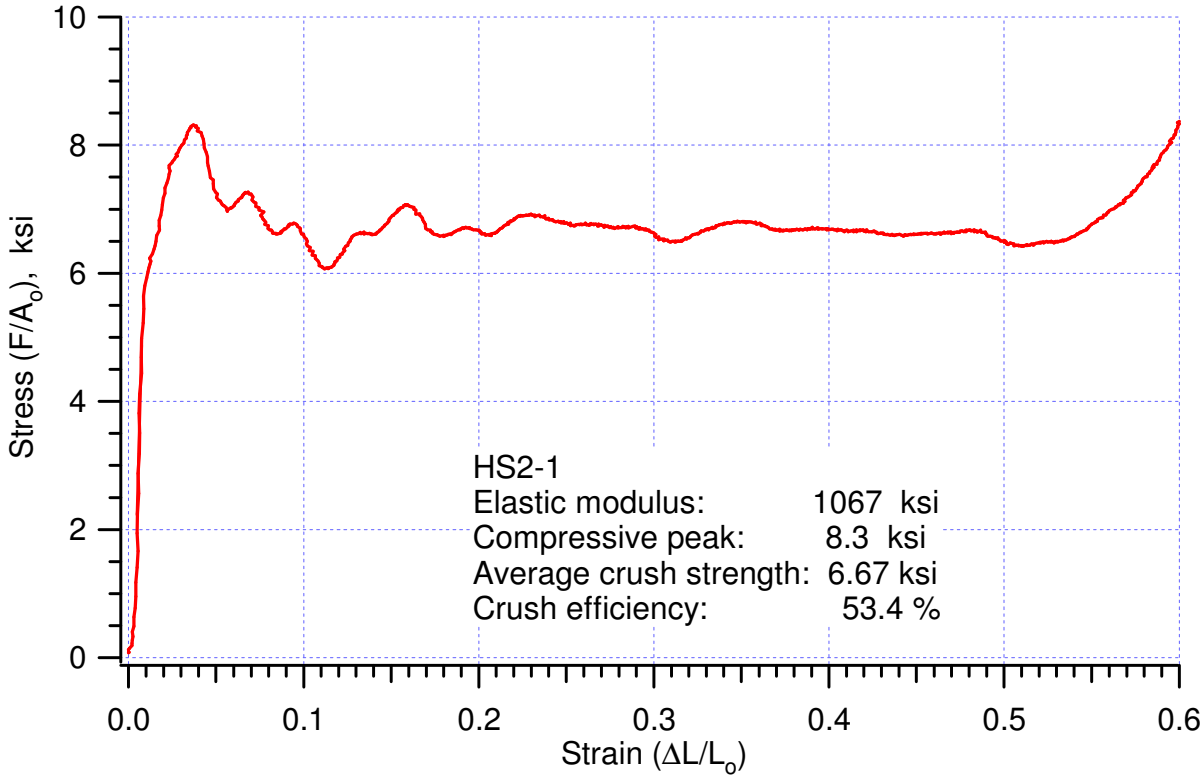

Figure 8. Stress-strain curve of HS2-1.

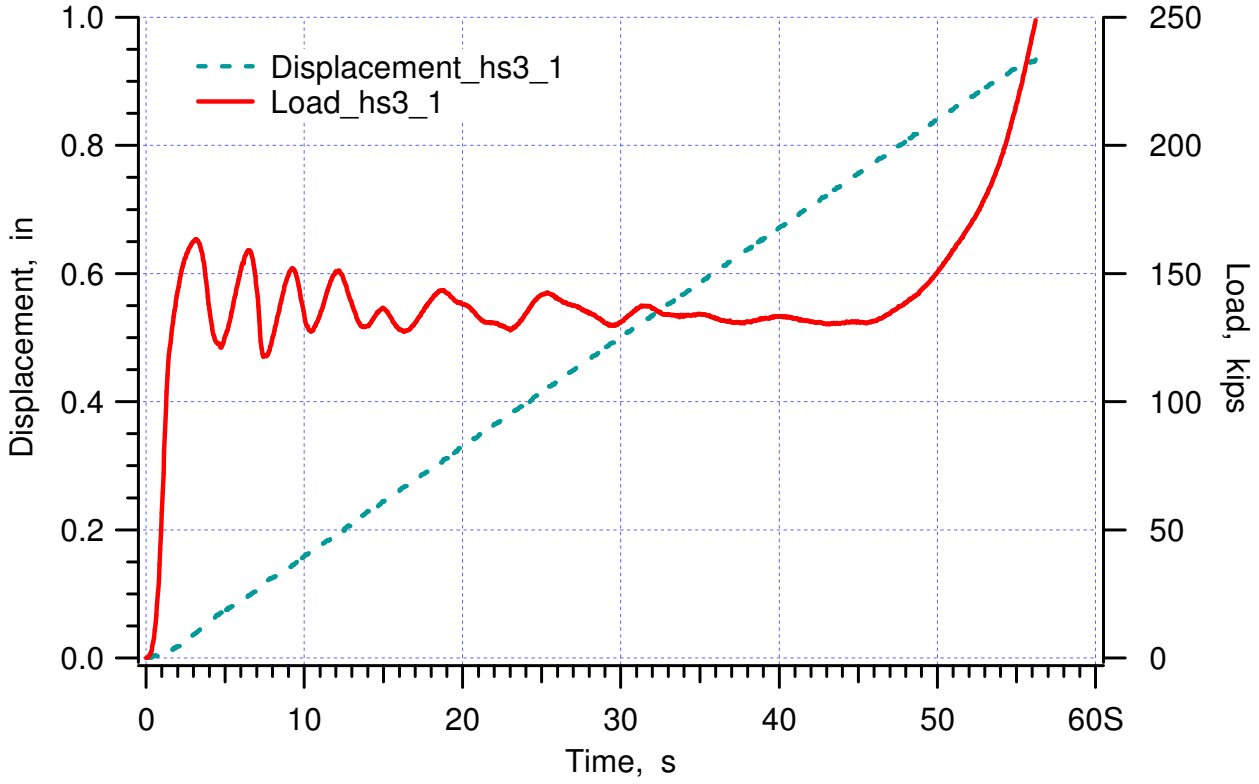

Figure 9. Raw data of HS3-1.

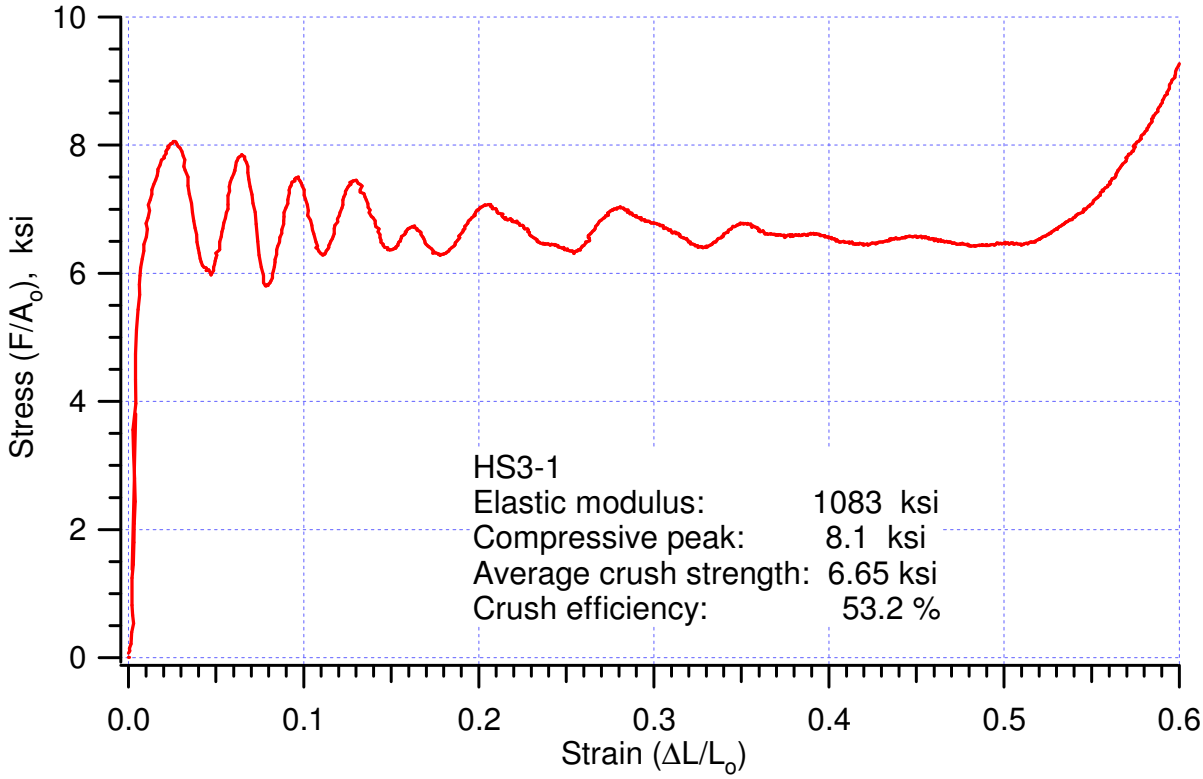

Figure 10. Stress-strain curve of HS3-1.

This page intentionally left blank.

APPENDIX VIII:

"Moderate Rate Confined Crush Tests of Alcore 35 pcf in the t-direction at Ambient Temperature," Memo Wei-Yang Lu to Distribution, January 3, 2000.

Sandia National Laboratories
Operated for the U.S. Department of Energy by
Sandia Corporation
MS9042
Livermore, CA 94551-0969

date: January 3, 2000

to: Distribution

from: Wei-yang Lu

subject: Moderate Rate Confined Crush Tests of Alcore 35 pcf in the t-direction at Ambient Temperature

We have completed Tests # 31 – 45 (Table 1.1, *B61 Radar Nose / MAVEN Test* …, by T.D. Hinnerichs, October 27, 1999). The average density of honeycomb specimen is **35.39 pcf**, the average crush strength is **5.74 ksi**, and the crush efficiency is **64.46 %**. Experimental procedures were the same as that of Alcore 38, Test #1 – 15, which was described in a previous memo (December 3, 1999). Please see Appendix for detail data and results.

Distribution:

Darrla Giersch(2167)	MS0481
Darren Hoke(2167)	MS0481
Vernon Willan(2167)	MS0481
Vista Bateman(9126)	MS0553
Tom Carne(9124)	MS0557
Berry Boughten(9132)	MS0557
Jaime Moya(9132)	MS0828
Terry Hinnerichs(9126)	MS0847
Ken Gwinn(9126)	MS0847
John Pott(9126)	MS0847
Rodney May(9126)	MS0847
Mike Neilsen(9123)	MS0847
Bill Scherzinger(9123)	MS0847
Hal Morgan(9123)	MS0847
Wendell Kawahara (8725)	MS9042

Confined crushes of Alcore 35 pcf specimens in t-direction at ambient

Specimen	d_1, in	d_2, in	d_3, in	Weight, lb	Density, pcf	Crush Velocity, ft/s	Crush strenght, ksi	Crush efficiency, %	Remarks
A35_01	1.191	1.212	1.499	0.0446	35.65	14.42	6.08	65.00	
A35_02	1.199	1.160	1.503	0.0428	35.41	14.65	5.65	65.20	
A35_03	1.183	1.201	1.504	0.0438	35.44	14.43	5.85	63.20	
A35_04	1.194	1.183	1.511	0.0437	35.34	14.24	6.07	66.30	
A35_05	1.195	1.197	1.504	0.0440	35.34	14.34	5.82	63.50	
A35_06	1.201	1.202	1.496	0.0441	35.31	14.49	5.12	64.30	R2
A35_07	1.188	1.198	1.464	0.0427	35.40	14.24	5.72	63.80	
A35_08	1.198	1.200	1.498	0.0441	35.40	14.33	5.67	64.30	
A35_09	1.189	1.200	1.467	0.0427	35.29	14.39	5.69	64.50	
A35_10	1.195	1.208	1.473	0.0435	35.31	14.56	5.54	64.70	
A35_11	1.188	1.205	1.500	0.0440	35.38	14.19	5.52	63.00	
A35_12	1.196	1.196	1.497	0.0439	35.42	14.11	5.89	65.80	
A35_13	1.175	1.215	1.481	0.0429	35.08	14.35	5.47	64.10	
A35_14	1.194	1.197	1.500	0.0440	35.49	14.29	5.76	65.90	
A35_15	1.193	1.208	1.500	0.0444	35.53	14.31	5.60	63.00	
A35_16	1.208	1.201	1.466	0.0437	35.48	14.36	5.80	64.60	
				max	35.65	14.65	6.08	66.30	
				min	35.08	14.11	5.47	63.00	
				average	35.39	14.35	5.74	64.46	
				std deviation	0.12	0.14	0.18	1.05	
				median	35.40	14.34	5.72	64.50	
Remarks									
R2	*shear pin broke early, did not reach lock up*								

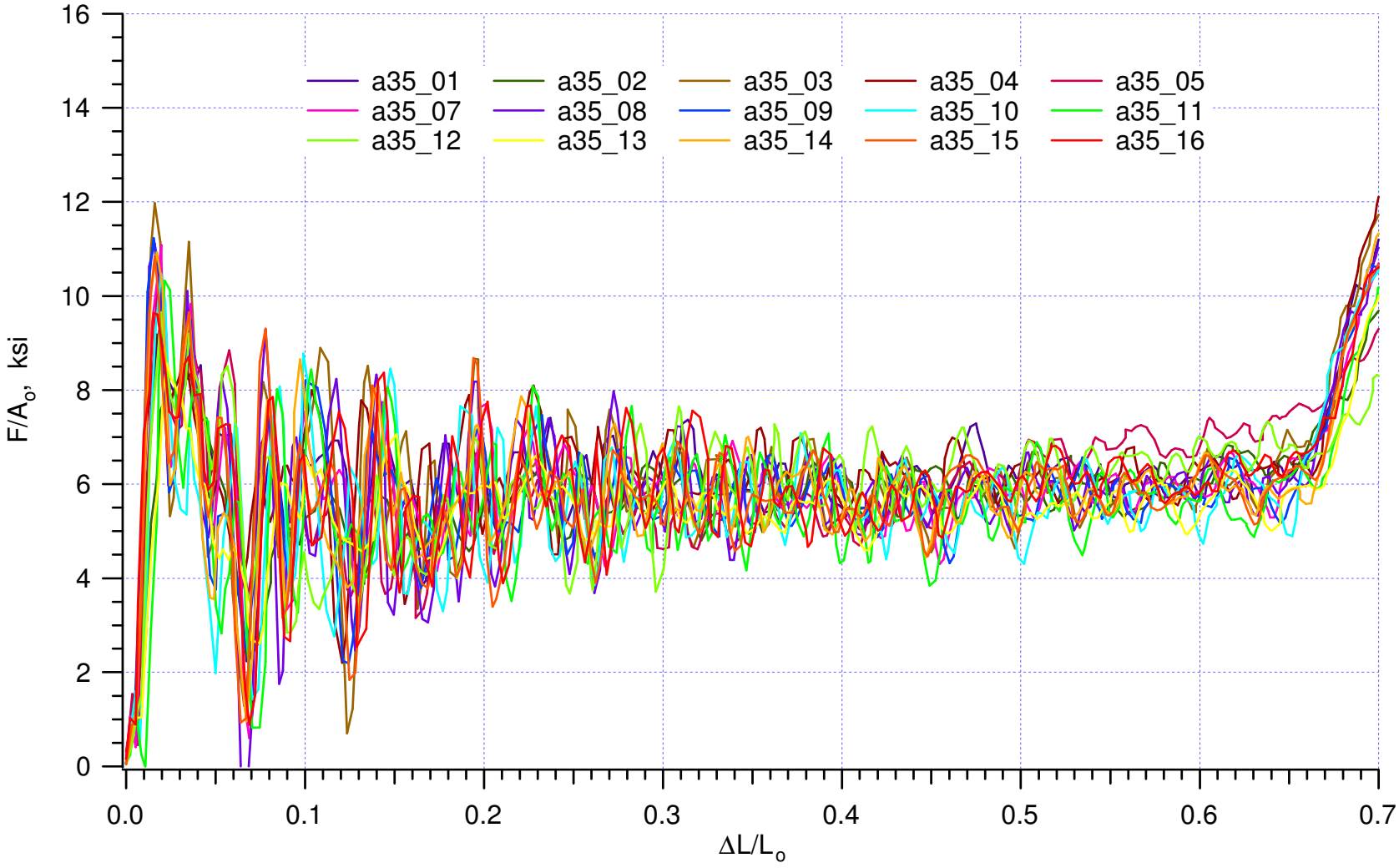
a35_01
a35_02
a35_03
a35_04
a35_05
a35_07
a35_08
a35_09
a35_10
a35_11
a35_12
a35_13
a35_14
a35_15
a35_16
F/A$_o$, ksi
$\Delta L/L_o$
0
2
4
6
8
10
12
14
16
0.0
0.1
0.2
0.3
0.4
0.5
0.6
0.7

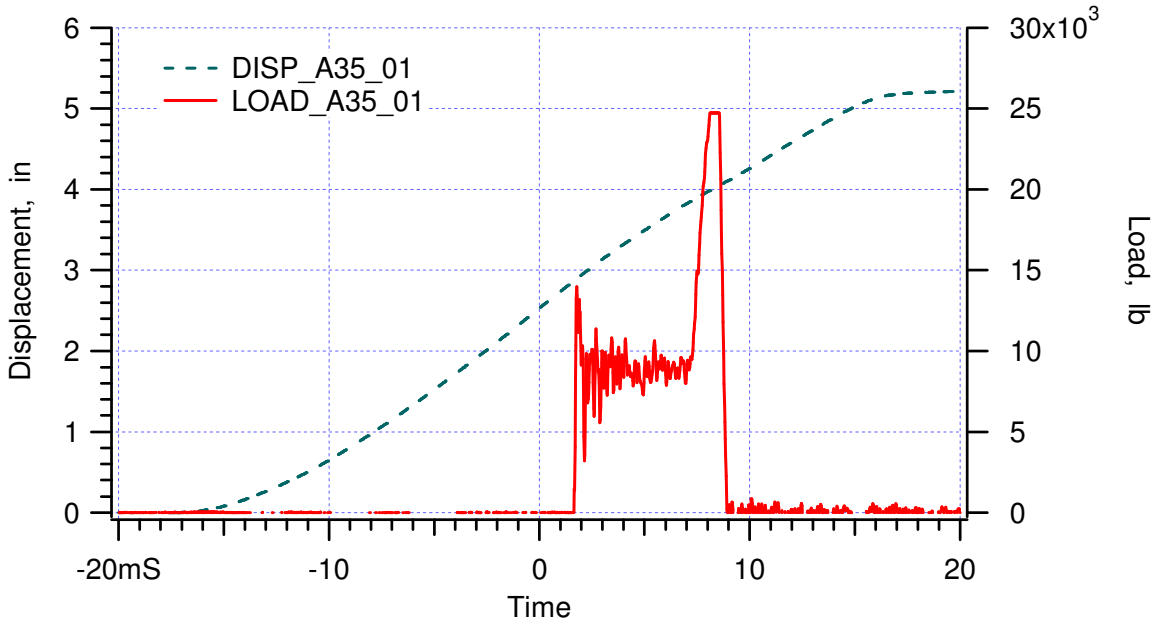
DISP_A35_01
LOAD_A35_01
Displacement, in
Load, lb
30x10^3
Time
-20mS
-10
0
10
20

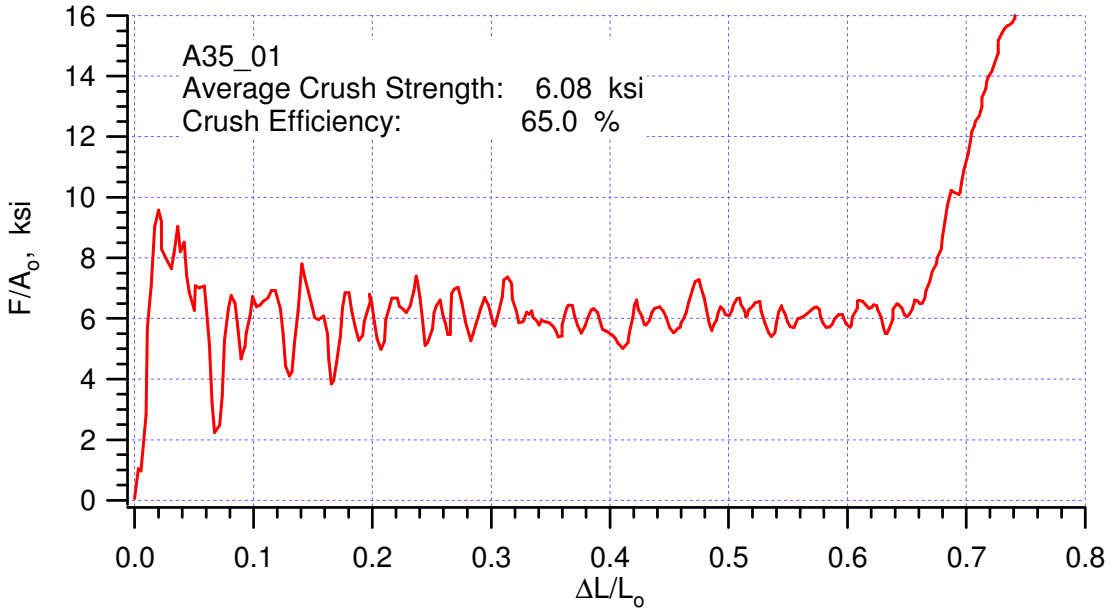
A35_01
Average Crush Strength: 6.08 ksi
Crush Efficiency: 65.0 %
F/A_o, ksi
ΔL/L_o

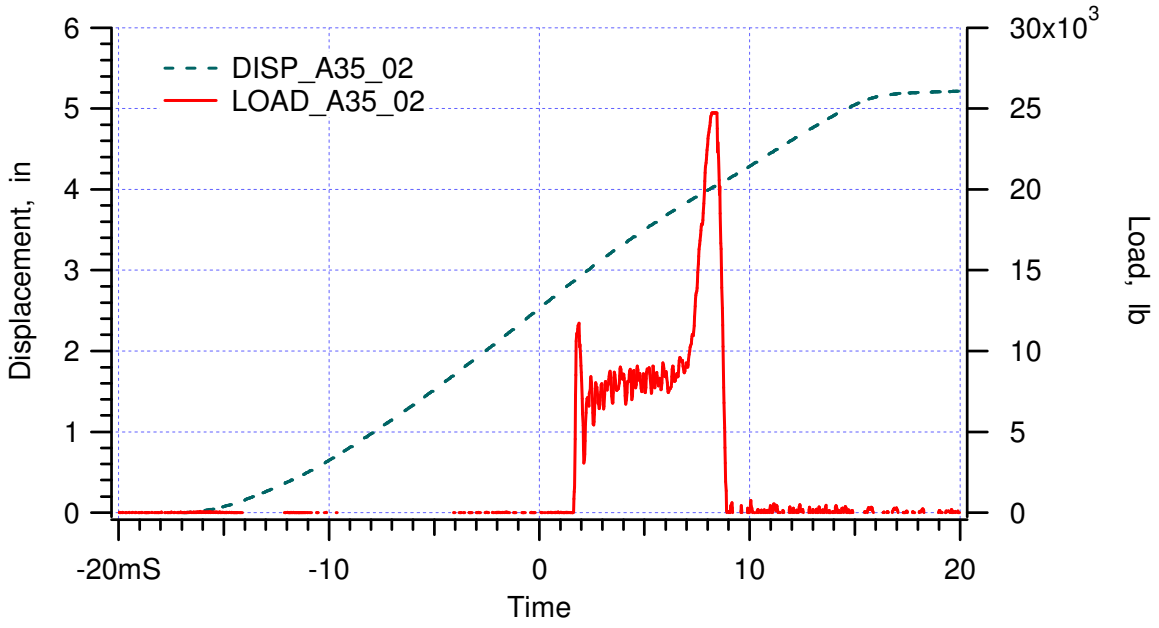
DISP_A35_02
LOAD_A35_02
Displacement, in
Load, lb
30x10^3
Time
-20mS
-10
0
10
20

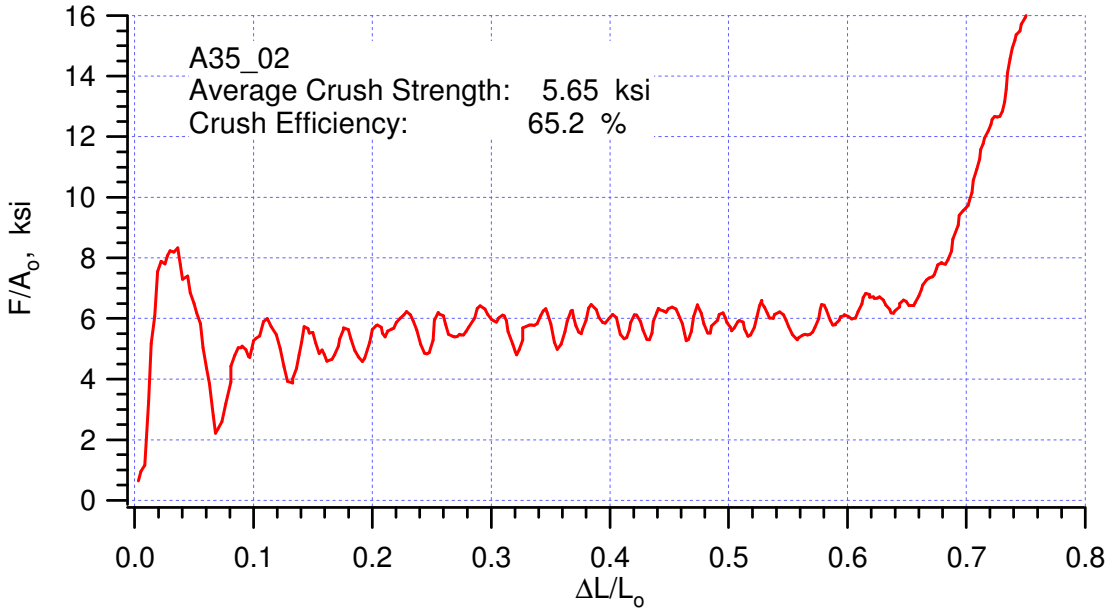
A35_02
Average Crush Strength: 5.65 ksi
Crush Efficiency: 65.2 %
F/A_o, ksi
ΔL/L_o

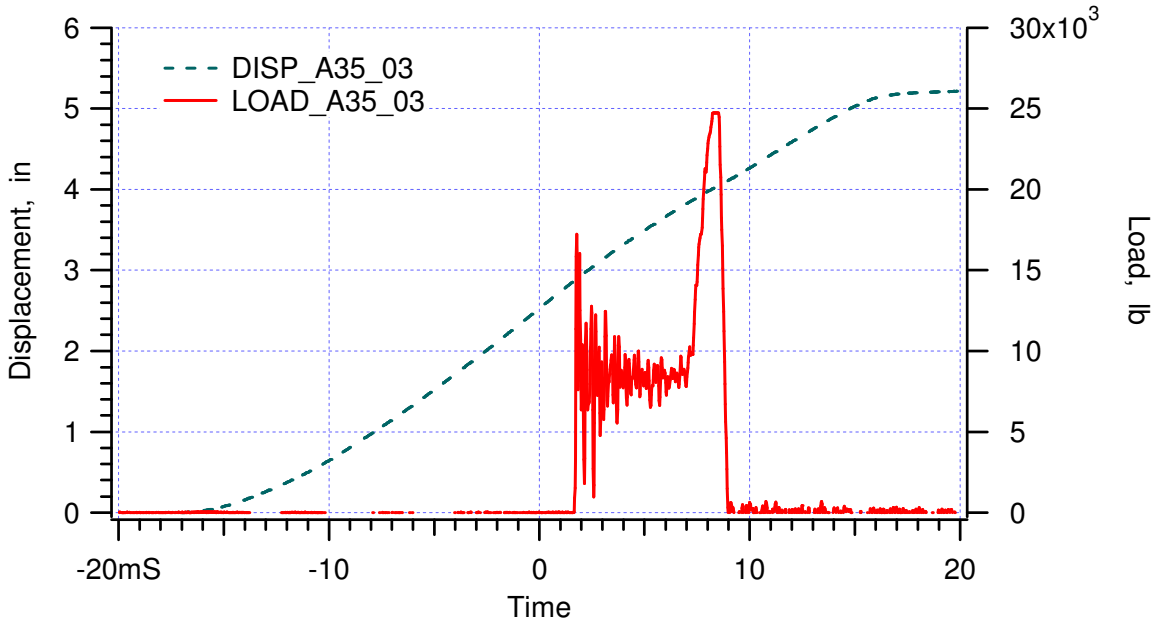
DISP_A35_03
LOAD_A35_03
Displacement, in
Load, lb
30x10^3
Time
-20mS
-10
0
10
20

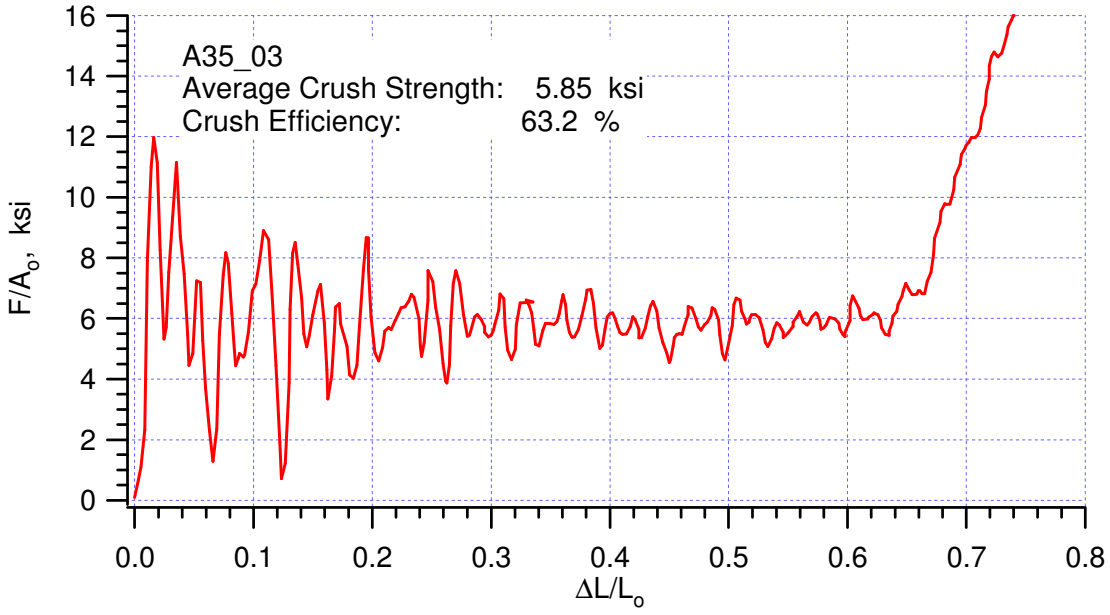
A35_03
Average Crush Strength: 5.85 ksi
Crush Efficiency: 63.2 %
F/A_o, ksi
ΔL/L_o

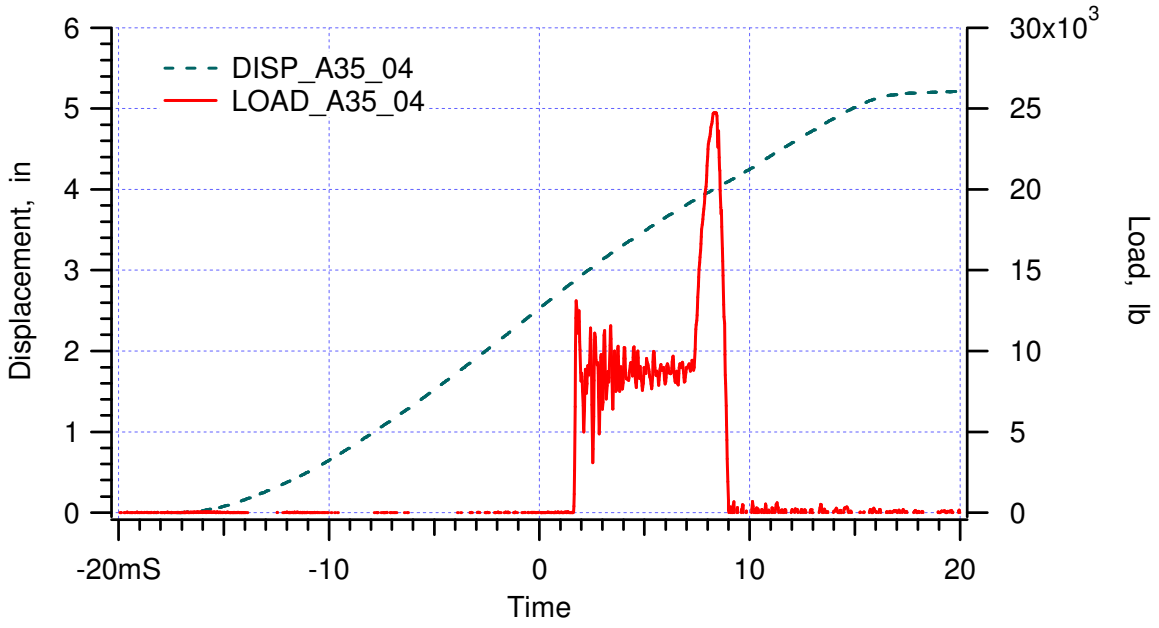
DISP_A35_04
LOAD_A35_04
Displacement, in
Load, lb
30x10^3
Time
-20mS
-10
0
10
20

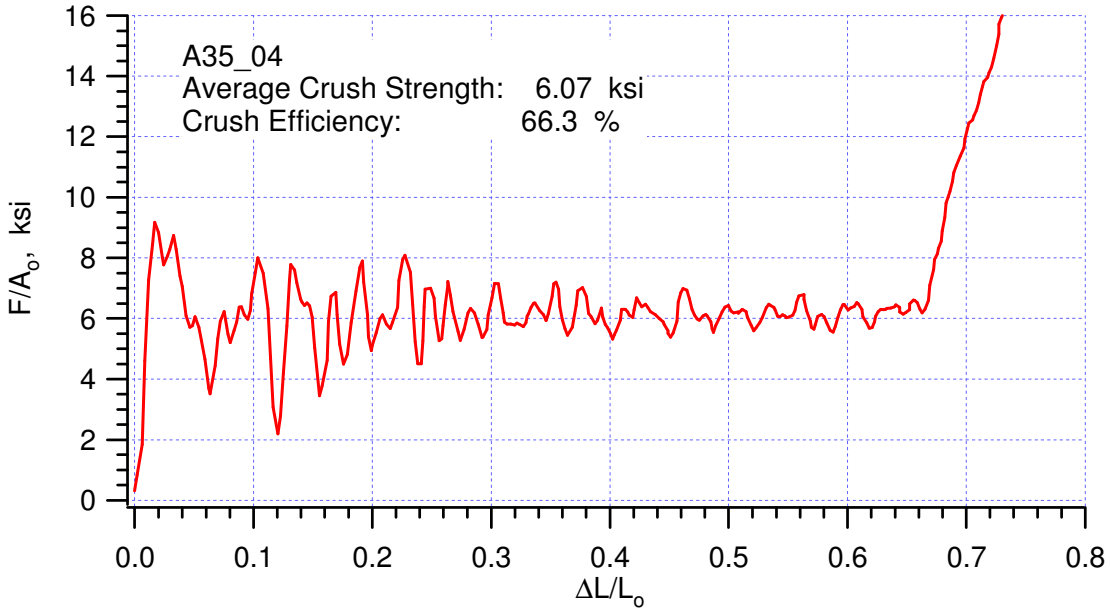
A35_04
Average Crush Strength: 6.07 ksi
Crush Efficiency: 66.3 %
F/A_o, ksi
ΔL/L_o

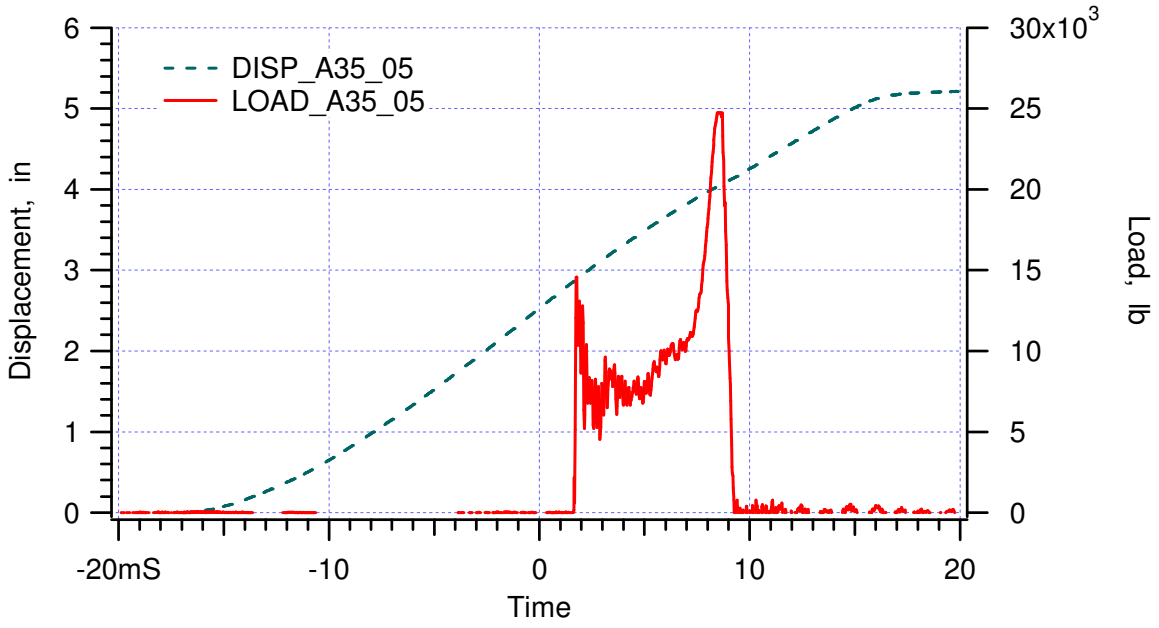
DISP_A35_05
LOAD_A35_05
Displacement, in
Load, lb
30x10^3
Time
-20mS
-10
0
10
20

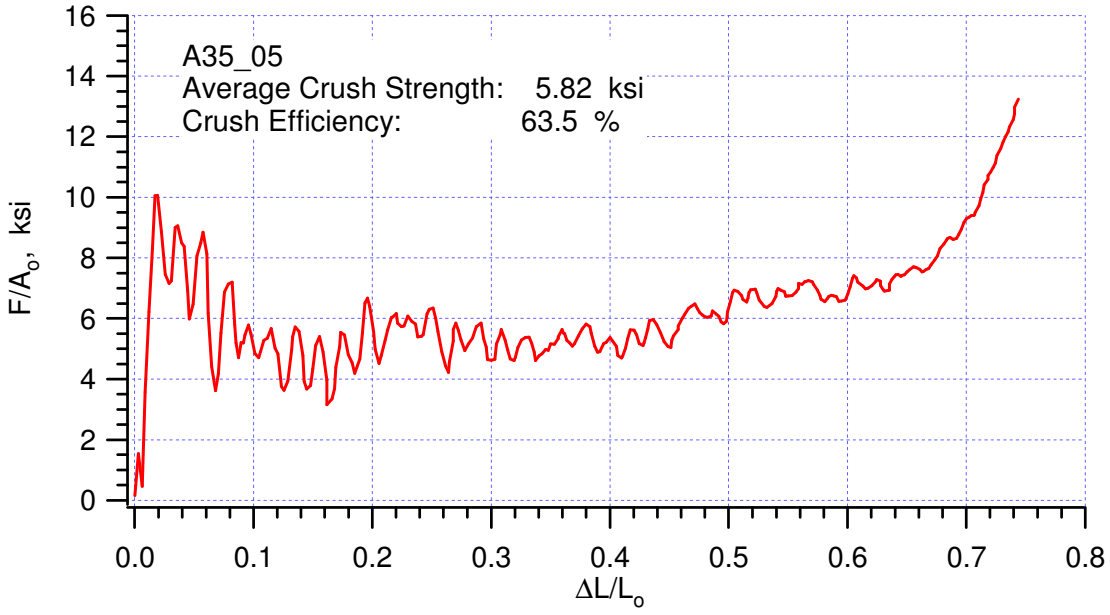
A35_05
Average Crush Strength: 5.82 ksi
Crush Efficiency: 63.5 %
F/A_o, ksi
ΔL/L_o

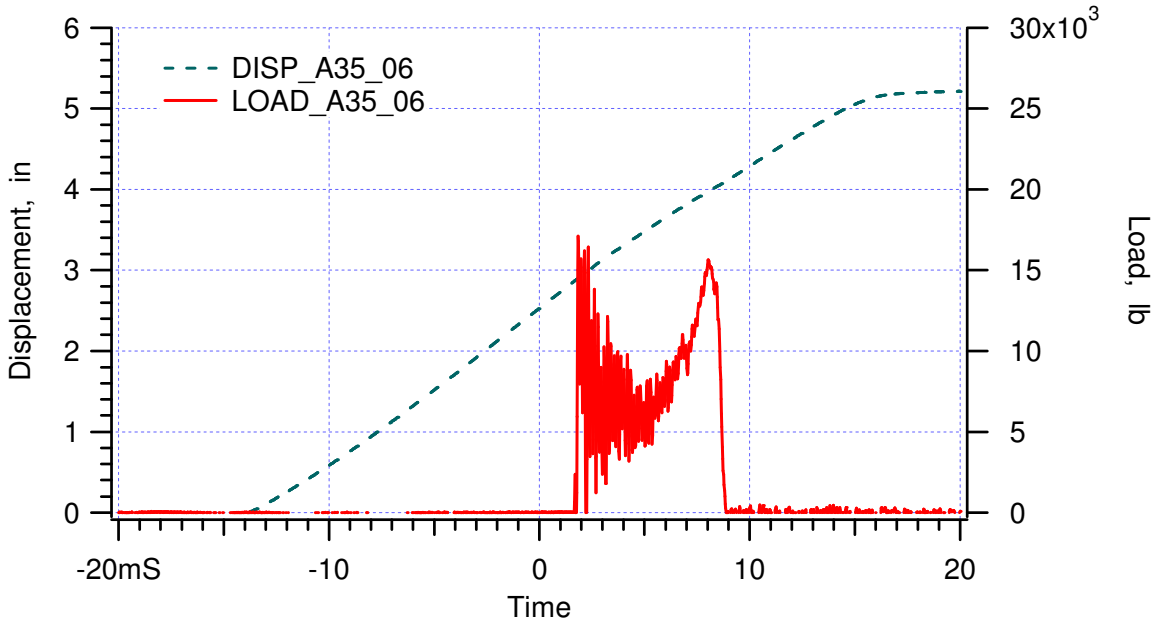
DISP_A35_06
LOAD_A35_06
Displacement, in
Load, lb
30x10^3
Time
-20mS
-10
0
10
20

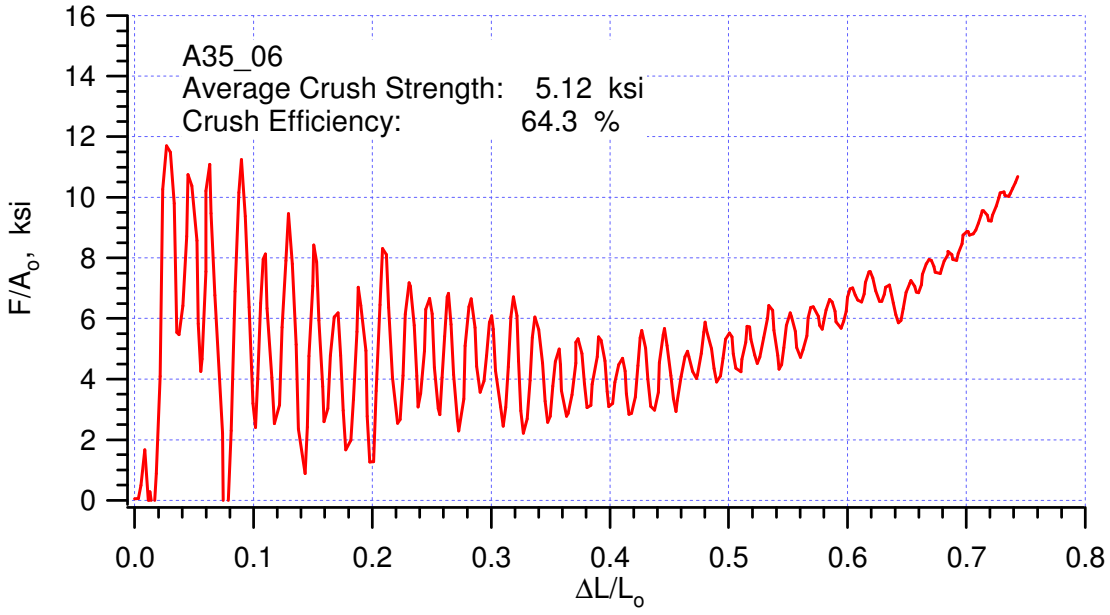
A35_06
Average Crush Strength: 5.12 ksi
Crush Efficiency: 64.3 %
F/A_o, ksi
ΔL/L_o

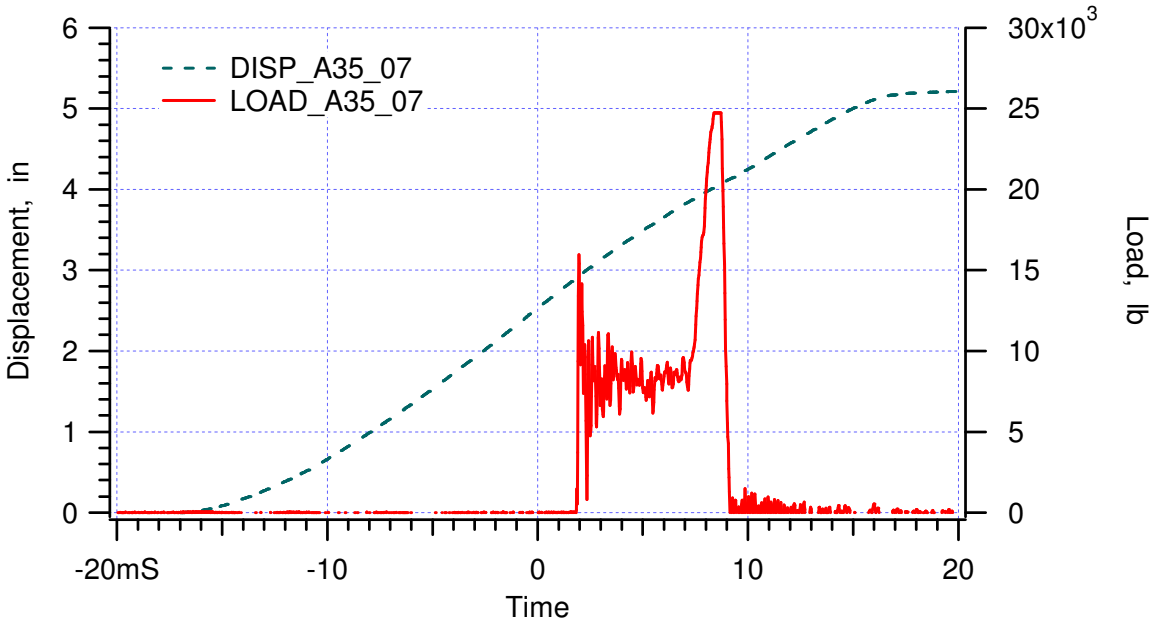
DISP_A35_07
LOAD_A35_07
Displacement, in
Load, lb
30x10^3
Time
-20mS
-10
0
10
20

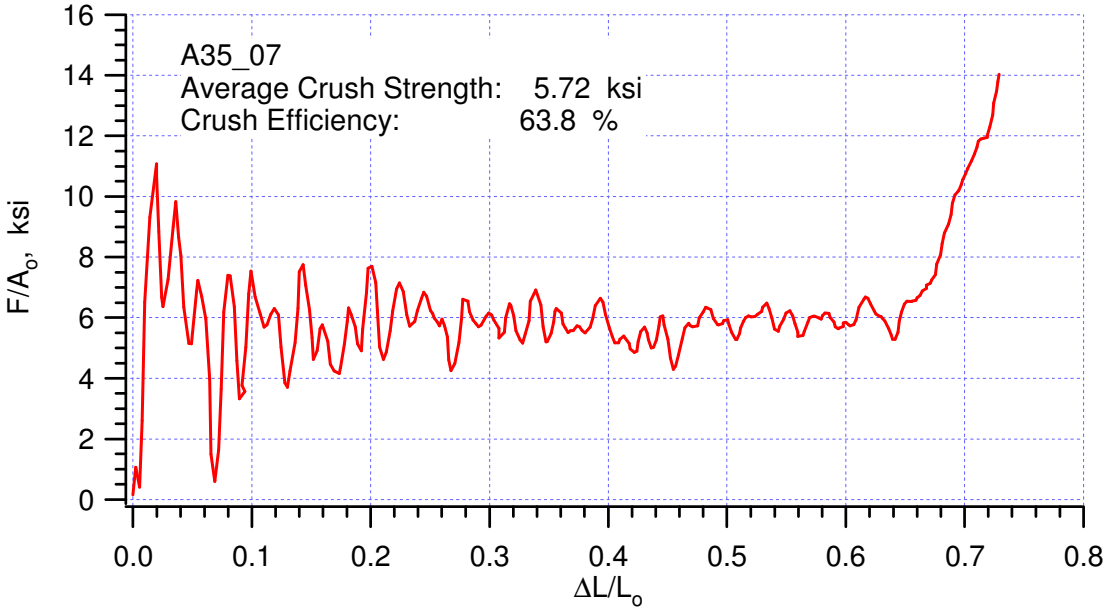
A35_07
Average Crush Strength: 5.72 ksi
Crush Efficiency: 63.8 %
F/A_o, ksi
ΔL/L_o

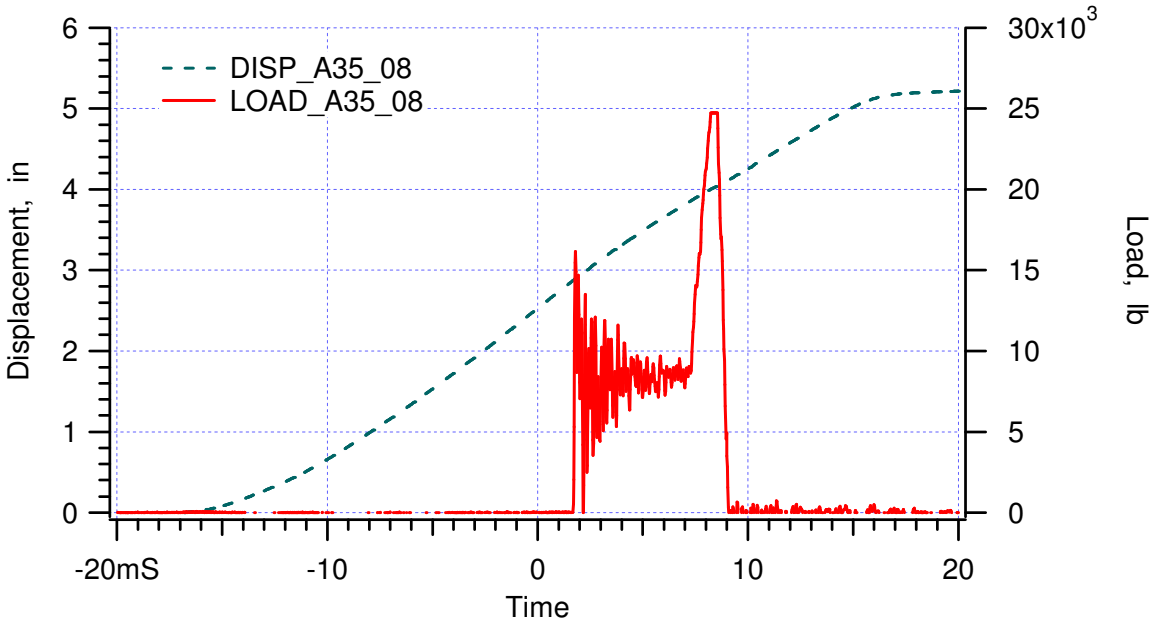
DISP_A35_08
LOAD_A35_08
Displacement, in
Load, lb
30x10^3
Time
-20mS
-10
0
10
20

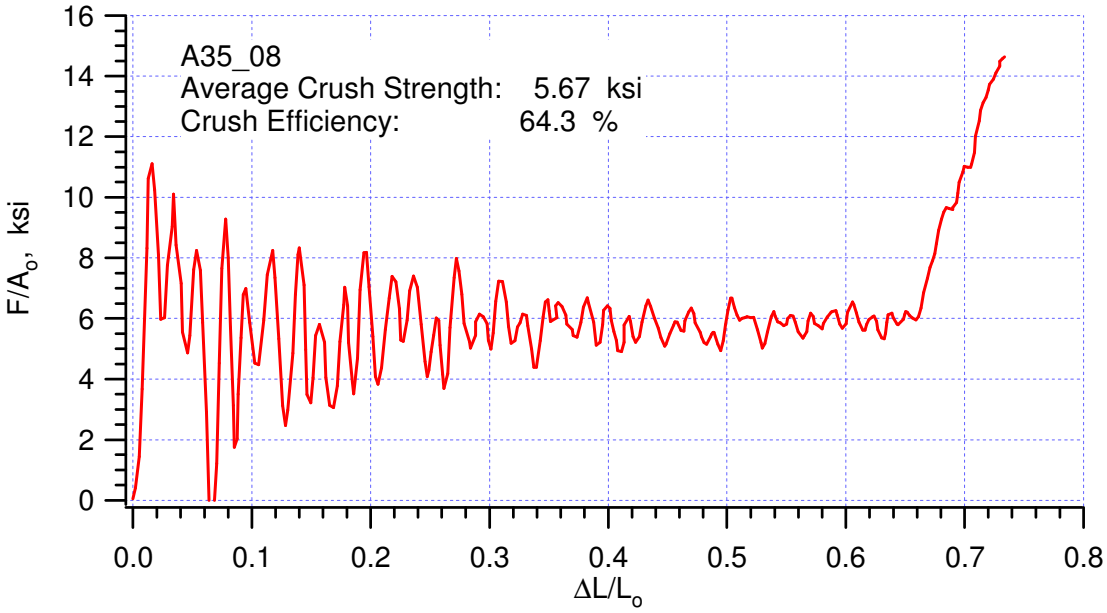
A35_08
Average Crush Strength: 5.67 ksi
Crush Efficiency: 64.3 %
F/A_o, ksi
ΔL/L_o

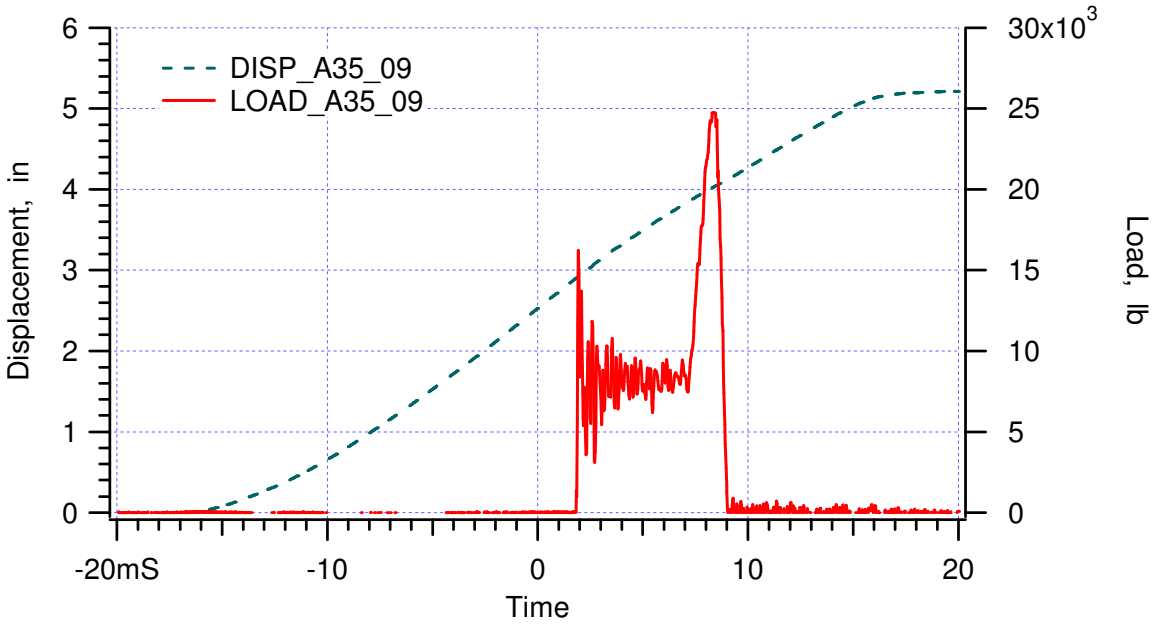
DISP_A35_09
LOAD_A35_09
Displacement, in
Load, lb
30x10^3
Time
-20mS
-10
0
10
20

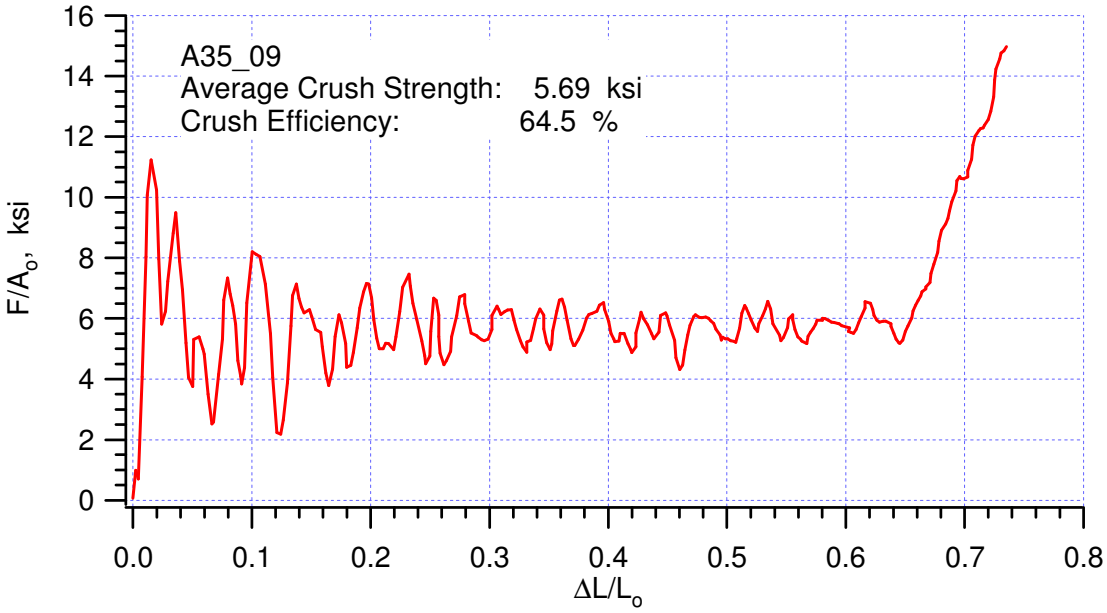
A35_09
Average Crush Strength: 5.69 ksi
Crush Efficiency: 64.5 %
F/A_o, ksi
ΔL/L_o

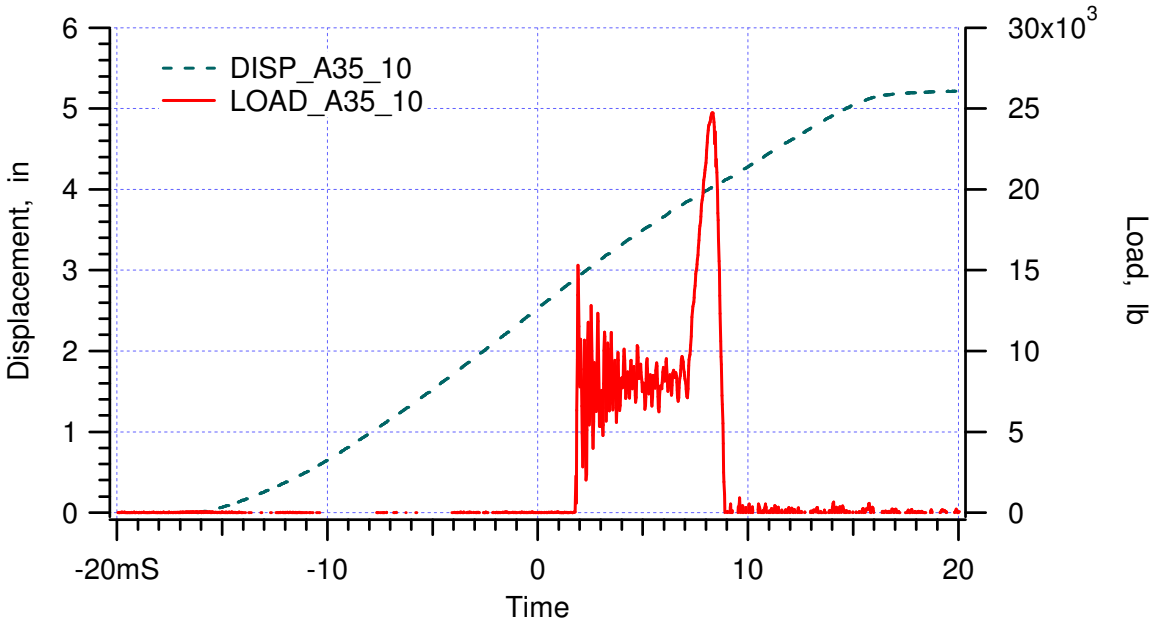
DISP_A35_10
LOAD_A35_10
Displacement, in
Load, lb
30x10^3
Time
-20mS
-10
0
10
20

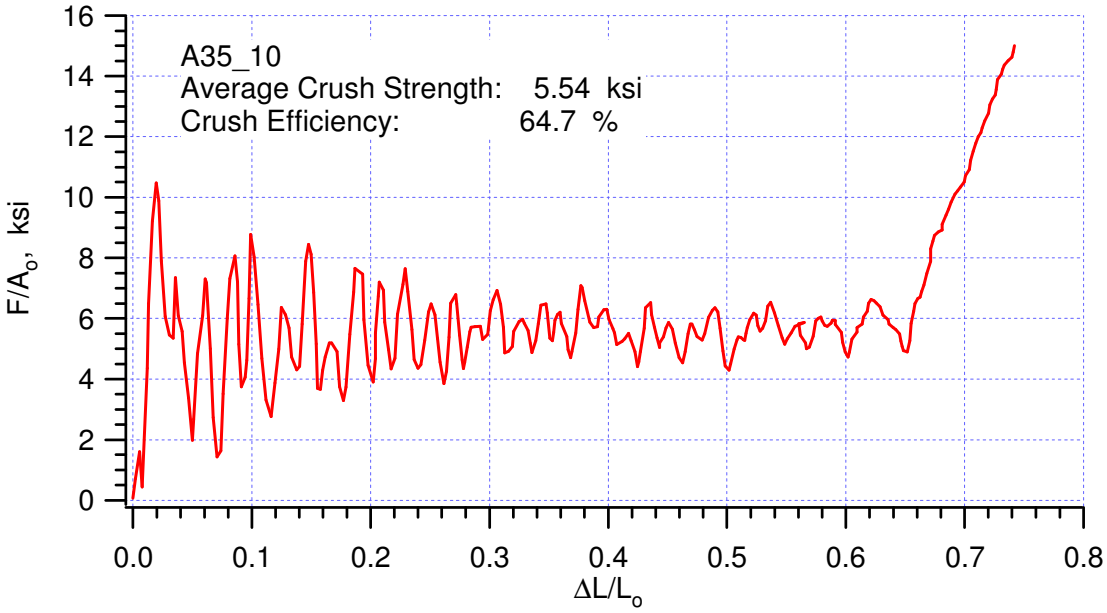
A35_10
Average Crush Strength: 5.54 ksi
Crush Efficiency: 64.7 %
F/A_o, ksi
ΔL/L_o

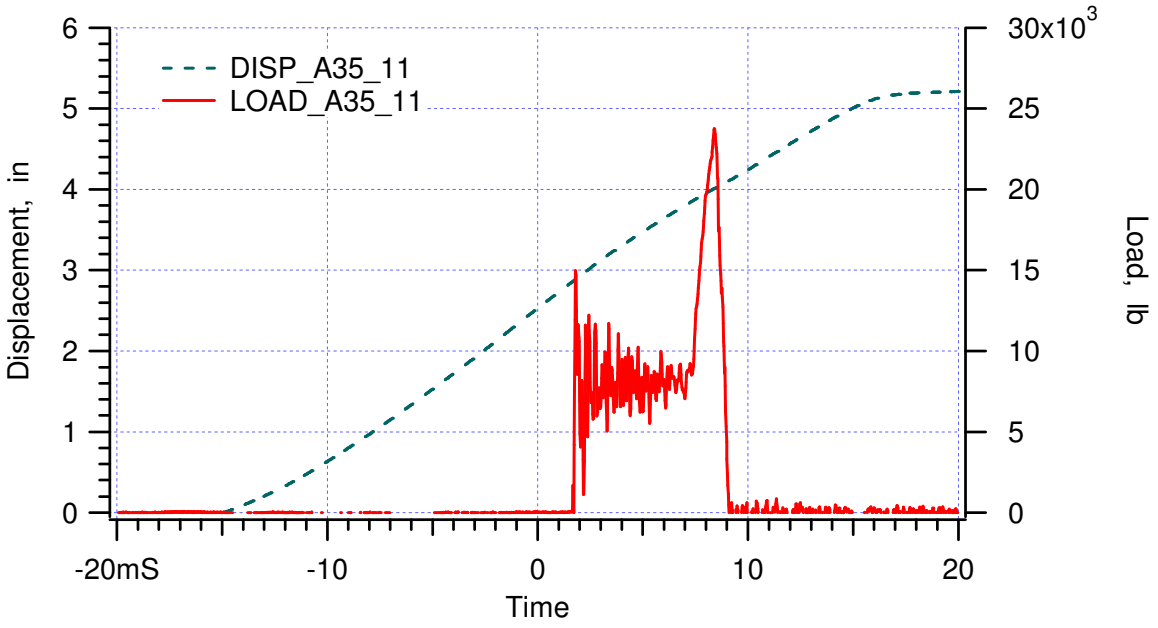
DISP_A35_11
LOAD_A35_11
Displacement, in
Load, lb
30x10^3
Time
-20mS
-10
0
10
20

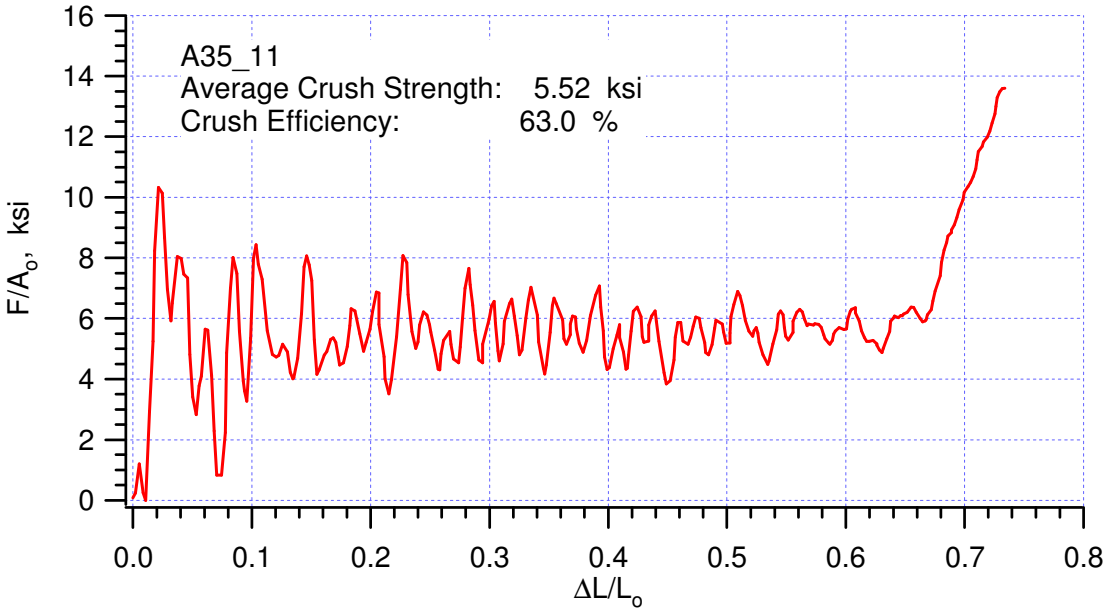
A35_11
Average Crush Strength: 5.52 ksi
Crush Efficiency: 63.0 %
F/A_o, ksi
ΔL/L_o

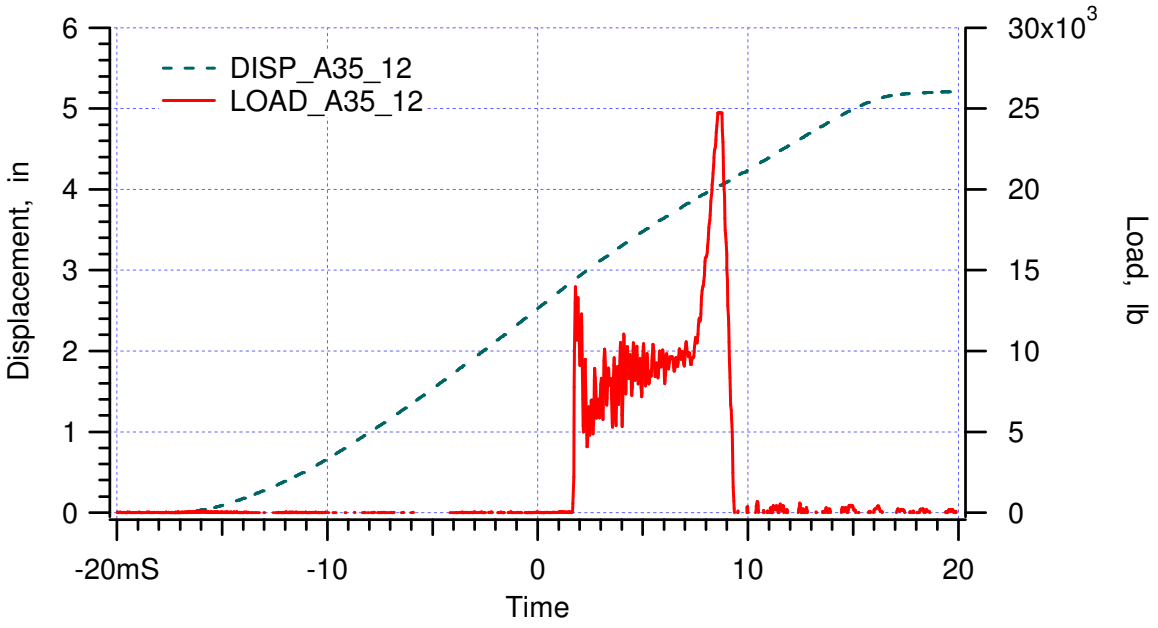
DISP_A35_12
LOAD_A35_12
Displacement, in
Load, lb
30x10^3
Time
-20mS
-10
0
10
20

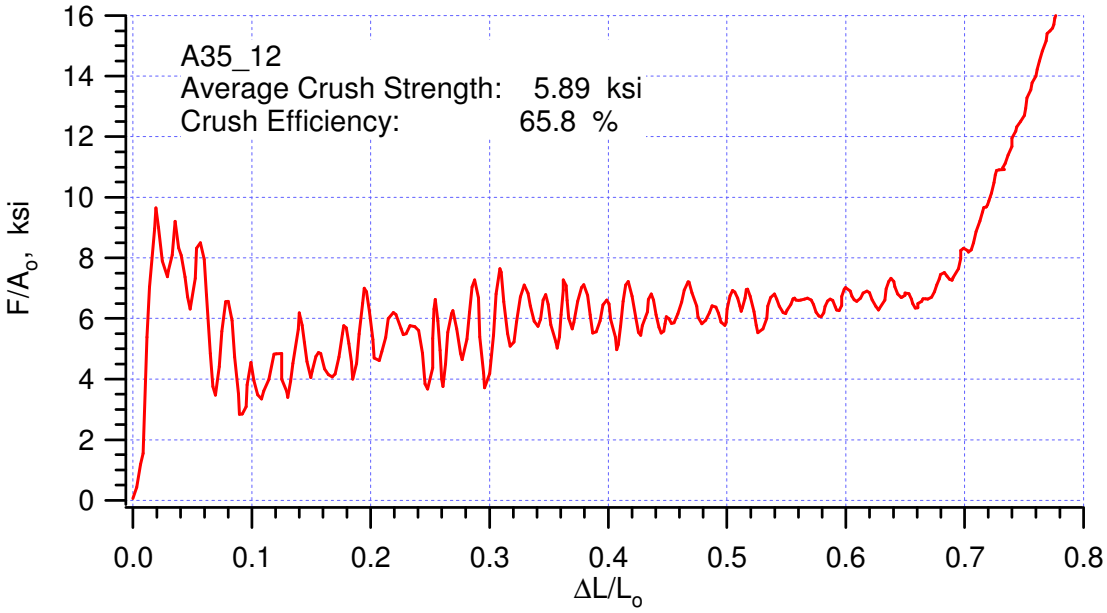
A35_12
Average Crush Strength: 5.89 ksi
Crush Efficiency: 65.8 %
F/A_o, ksi
ΔL/L_o

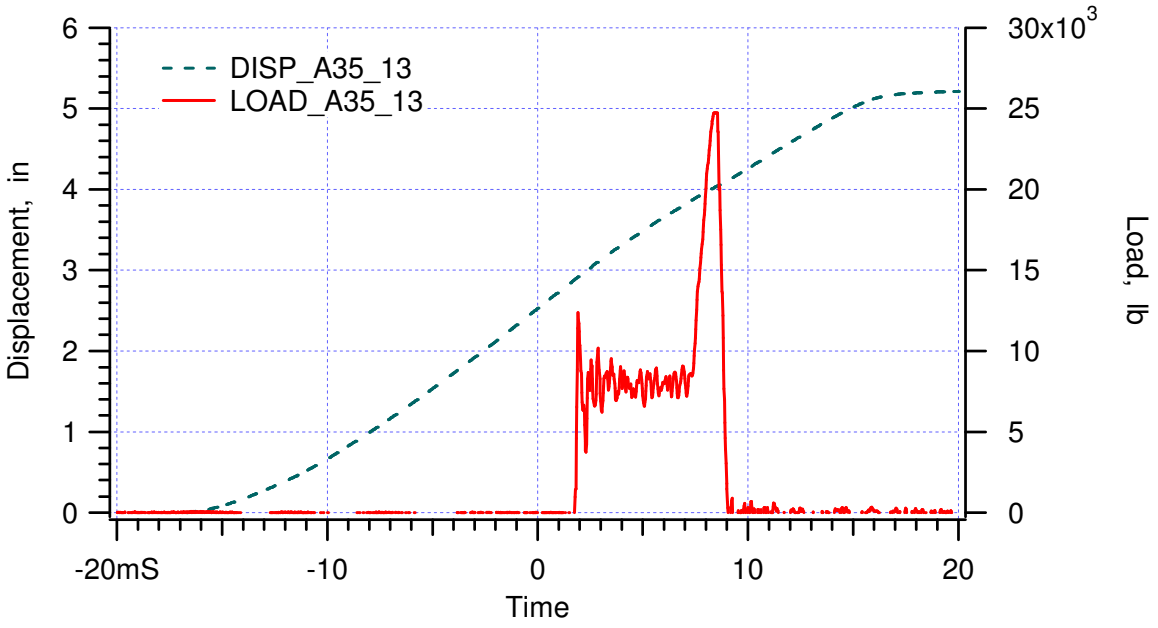
DISP_A35_13
LOAD_A35_13
Displacement, in
Load, lb
30x10^3
Time
-20mS
-10
0
10
20

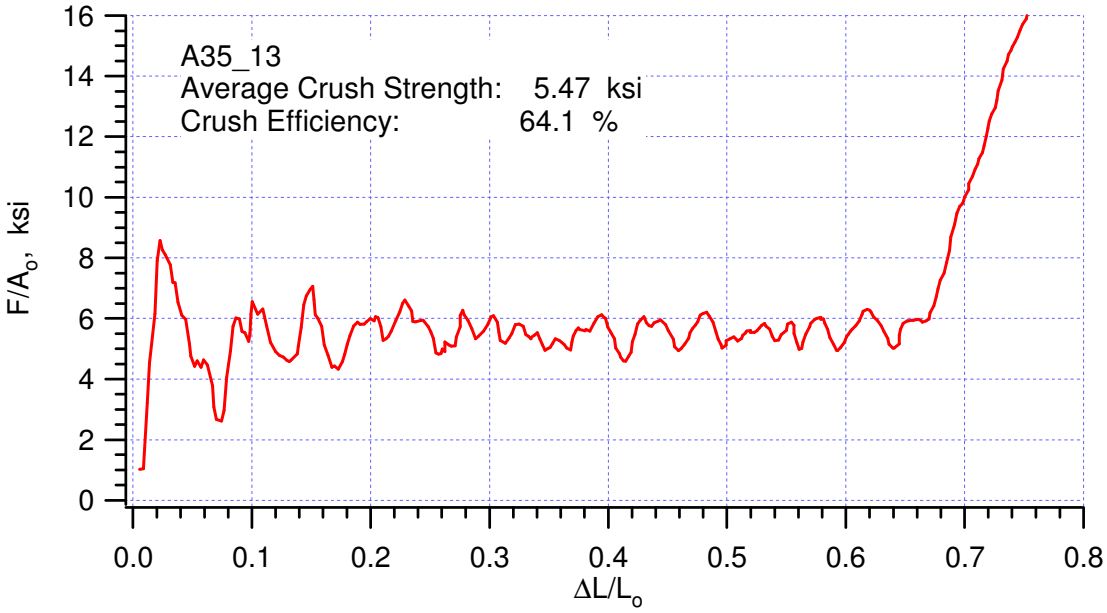
A35_13
Average Crush Strength: 5.47 ksi
Crush Efficiency: 64.1 %
F/A_o, ksi
ΔL/L_o

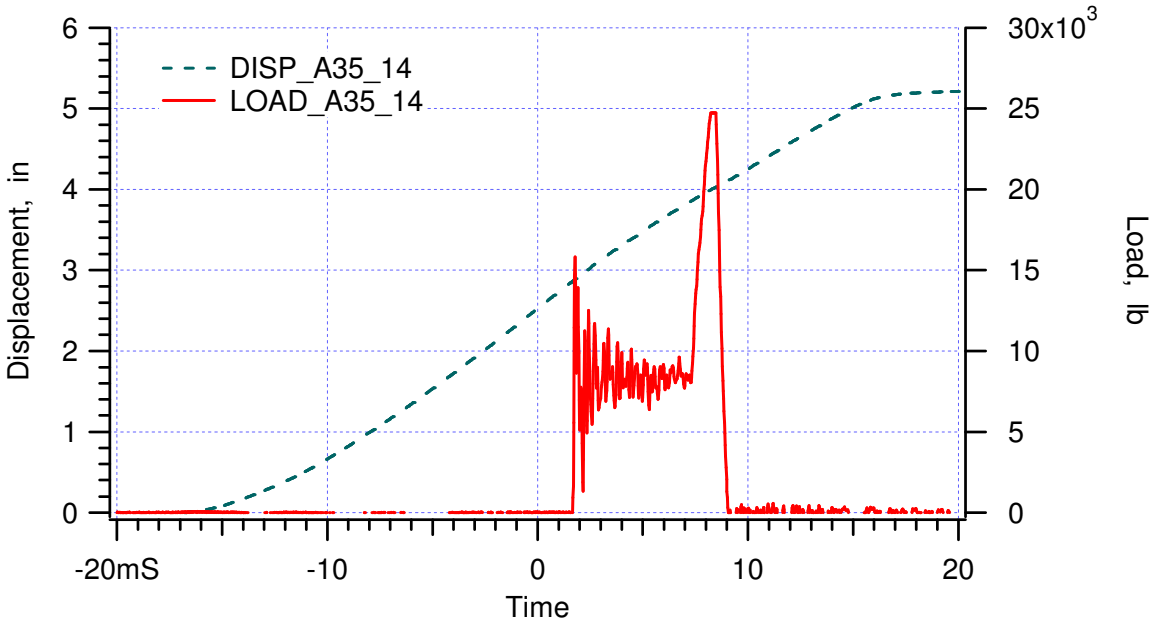
DISP_A35_14
LOAD_A35_14
Displacement, in
Load, lb
30x10^3
Time
-20mS
-10
0
10
20

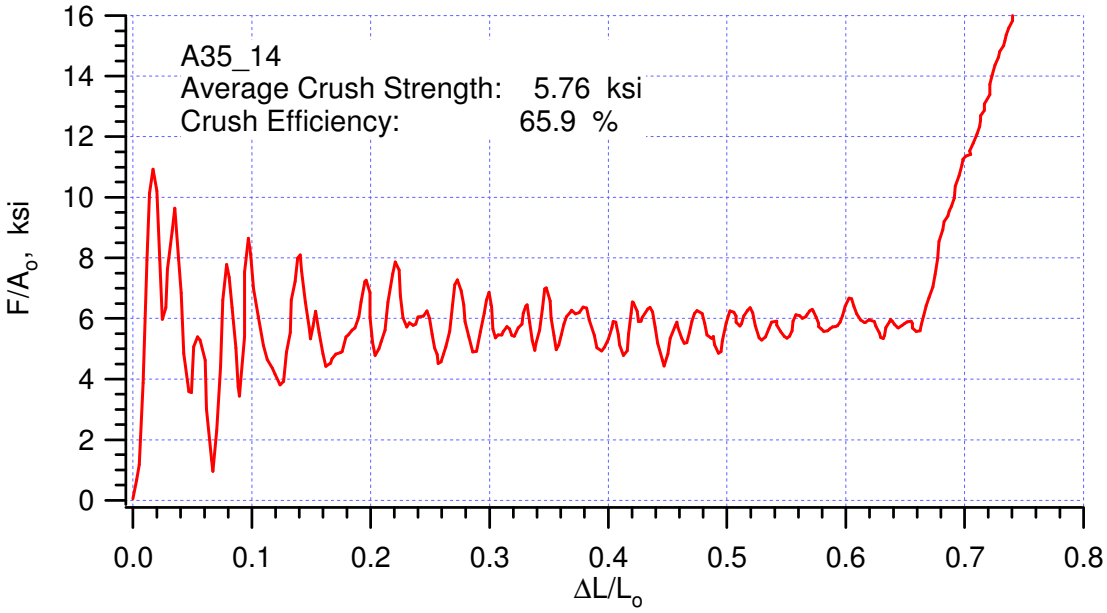
A35_14
Average Crush Strength: 5.76 ksi
Crush Efficiency: 65.9 %
F/A_o, ksi
ΔL/L_o

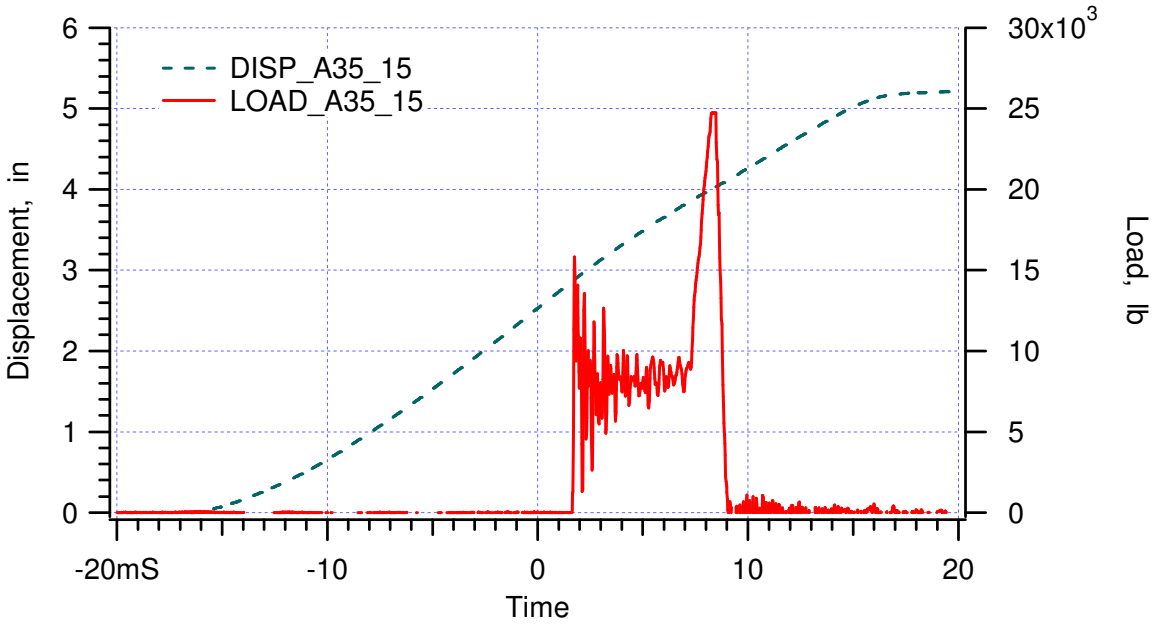
DISP_A35_15
LOAD_A35_15
Displacement, in
Load, lb
30x10^3
Time
-20mS
-10
0
10
20

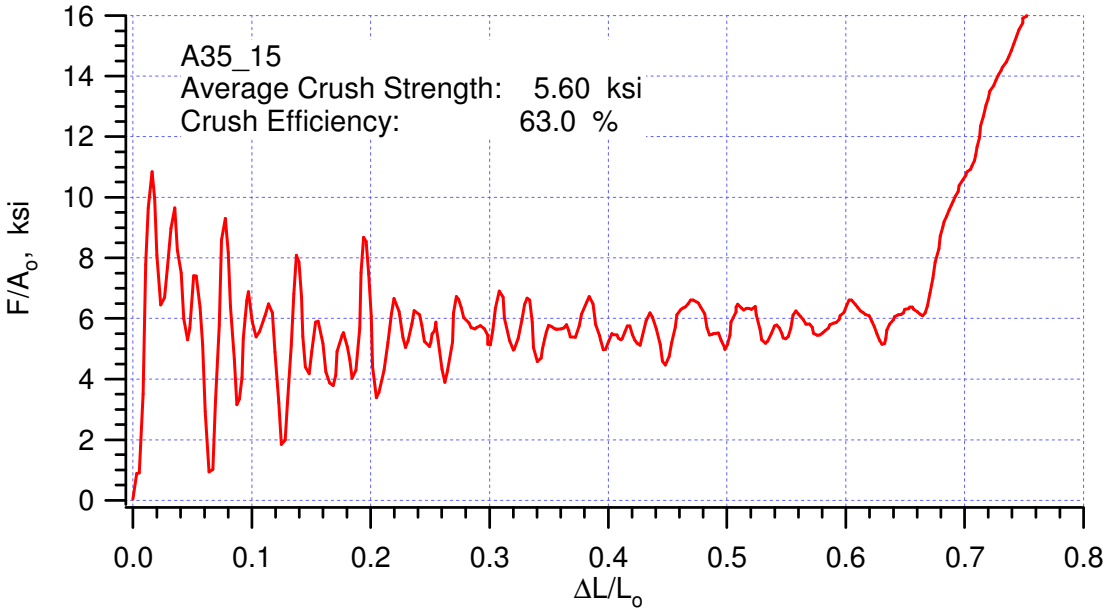
A35_15
Average Crush Strength: 5.60 ksi
Crush Efficiency: 63.0 %
F/A_o, ksi
ΔL/L_o

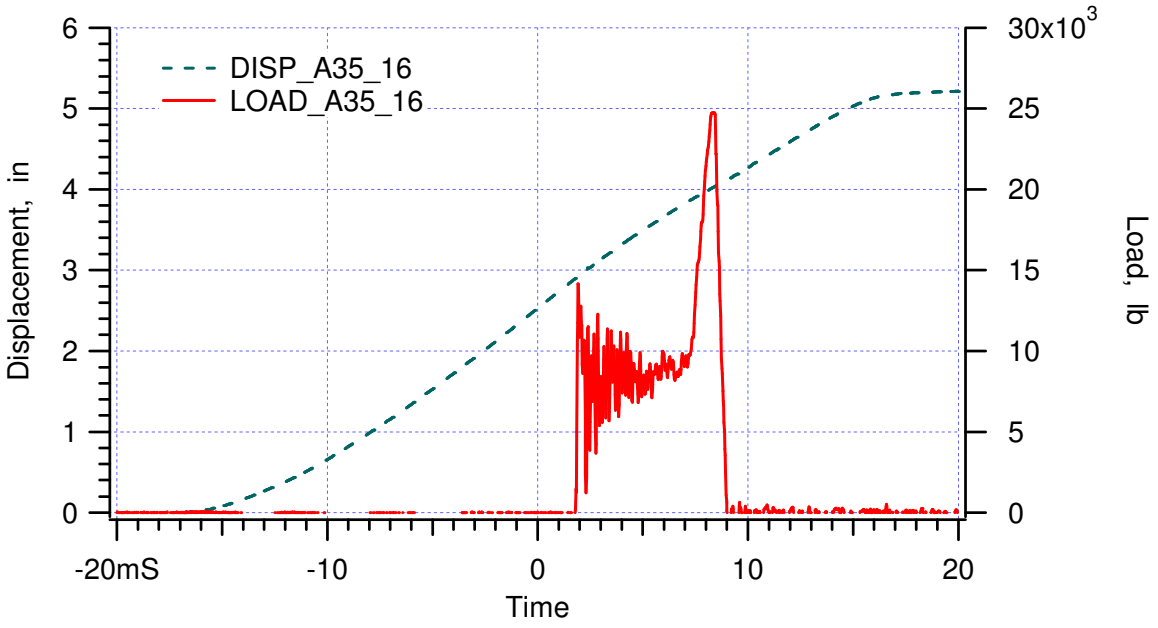
DISP_A35_16
LOAD_A35_16
Displacement, in
Load, lb
30x10^3
Time
-20mS
-10
0
10
20

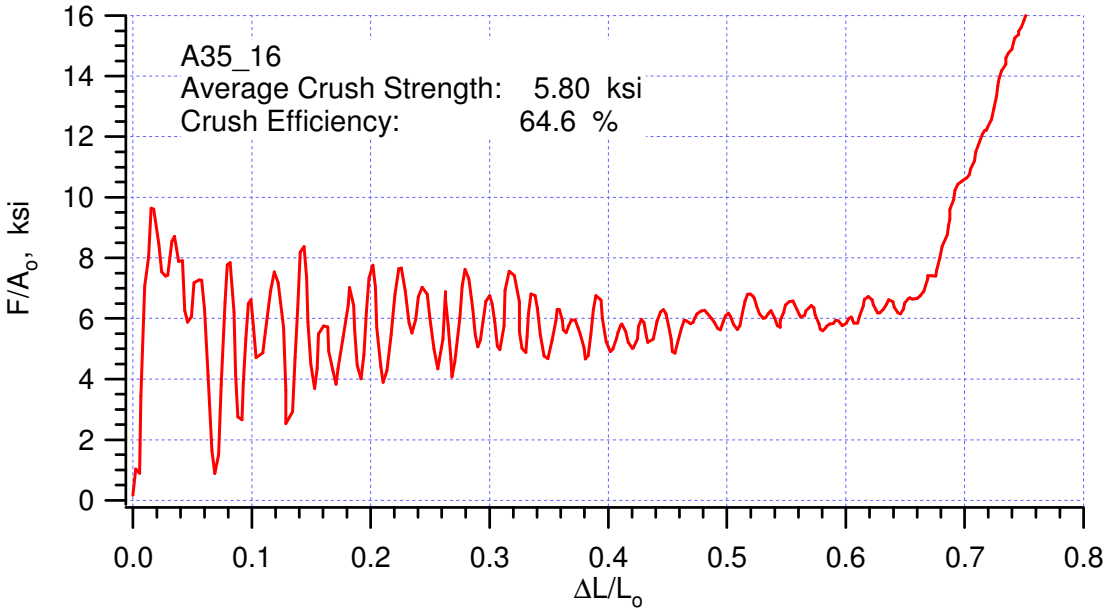
A35_16
Average Crush Strength: 5.80 ksi
Crush Efficiency: 64.6 %
F/A_o, ksi
ΔL/L_o

APPENDIX IX:

"Summary of Moderate Rate Confined Crush Tests of Alcore & Hexcel honeycombs in the t-direction at Ambient Temperature," Memo Wei-Yang Lu to Distribution, January 10, 2000

Sandia National Laboratories
Operated for the U.S. Department of Energy by
Sandia Corporation
MS9042
Livermore, CA 94551-0969

date: January 10, 2000

to: Distribution

from: Wei-yang Lu

subject: Summary of Moderate Rate Confined Crush Tests of Alcore & Hexcel honeycombs in the t-direction at Ambient Temperature

We have completed all the tests in the t-direction at ambient temperature. Test matrix and results are summarized in Table 1. Segmented specimens and Alcore materials have been reported before. The results of Hexcel 38 and 35, shown bold in Table 1, are new; please see Appendix I and II for detail data and results. All stress-strain curves of confined tests of Alcore 38 & 35 and Hexcel 38 & 35 at moderate rate are plotted in Figures 1 – 4, respectively. From these experimental results, we have following observations:

- Except Hexcel 35, the measured densities are within 5% of the nominal values; the measured densities are typically higher. Alcore 38 is slightly heavier than Hexcel 38; however, Hexcel 35 is much heavier than Alcore 35 and can be qualified as 38 pcf material.
- Hexcel materials have higher crush strengths than Alcore materials.
- Lower density materials show larger deviation in crush strength.
- Lower density materials have higher crush efficiency, but the effect is very small.
- Segmented specimens crushed at quasi-static rate show different results as rotated specimens at moderated rate under confinement. Segmented specimens display lower crush strength, 3 – 5 %, and crush efficiency, 15 – 20%.
- Using the same confined experimental setup, one rotated specimen of each Hexcel 38 & 35 was crushed at quasi-static rate, shown red in Table 1. The results show 15 – 20 % dynamic enhancement on crush strength and 6 – 8 % on crush efficiency.

Pictures of Alcore 38 and Hexcel 38 materials are shown in Figures 5 and 6, respectively. Typically, Alcore material has a well-defined cell structure and uniform cell size. Cells are arranged orderly as highlighted by a line, which is fairly straight and perpendicular to the L-direction, Figure 5(a). Close to the edge of the block, however, shift of cells can be seen, Figure 5(b). Some Alcore 38 specimens were cut from the edge region.

For Hexcel 38 material, the arrangement of corrugated sheet is almost random, not as orderly as Alcore materials. As we can see in Figure 6, honeycomb cell does not exist in many regions. The effects of random cell structure can be studied using a cell-level FE model (Neilsen and Scherzinger). Experimental results indicate that random structure increases the crush strength.

Distribution:

Darrla Giersch(2167)	MS0481
Darren Hoke(2167)	MS0481
Vernon Willan(2167)	MS0481
Vista Bateman(9126)	MS0553
Tom Carne(9124)	MS0557
Berry Boughten(9132)	MS0557
Jaime Moya(9132)	MS0828
Terry Hinnerichs(9126)	MS0847
Ken Gwinn(9126)	MS0847
John Pott(9126)	MS0847
Rodney May(9126)	MS0847
Mike Neilsen(9123)	MS0847
Bill Scherzinger(9123)	MS0847
Hal Morgan(9123)	MS0847
Wendell Kawahara (8725)	MS9042

Table 1 Test matrix and experimental results

B61/MAVEN TEST MATRIX				EXPERIMENTAL RESULTS						MEMO
Test #	Honeycomb	Dir.	Temperature, degree F	Specimen	Density, pcf	Impact Speed, ft/s	Crush Strength, ksi	Std Deviation, ksi	Crush Efficiency, %	Date
1 - 15	Alcore 38	T	ambient	rotated	38.82	14.13	6.35	0.08	63.80	991203
16 - 30	**Hexcel 38**	**T**	**ambient**	**rotated**	**38.70**	**13.67**	**7.17**	**0.15**	**63.89**	**000110**
				rotated	38.78	0.00139	5.88		59.20	
31 - 45	Alcore 35	T	ambient	rotated	35.39	14.35	5.74	0.18	64.46	000103
46 - 60	**Hexcel 35**	**T**	**ambient**	**rotated**	**37.79**	**13.83**	**6.67**	**0.24**	**63.91**	**000110**
				rotated	37.89	0.00139	5.83		60.30	
60 - 75	Alcore 38	T	165							
76 - 90	Hexcel 38	T	165							
91 - 105	Alcore 38	T	-65							
106 - 120	Hexcel 38	T	-65							
121 - 125	Alcore 38	L	ambient							
126 - 130	Hexcel 38	L	ambient							
131 - 135	Alcore 38	W	ambient							
136 - 140	Hexcel 38	W	ambient							
159 - 161	Alcore 38	T	ambient	segmented	41.41	0.0014	6.14		52.30	991130
162 - 164	Hexcel 38	T	ambient	segmented	41.29	0.0014	6.85		53.70	991213

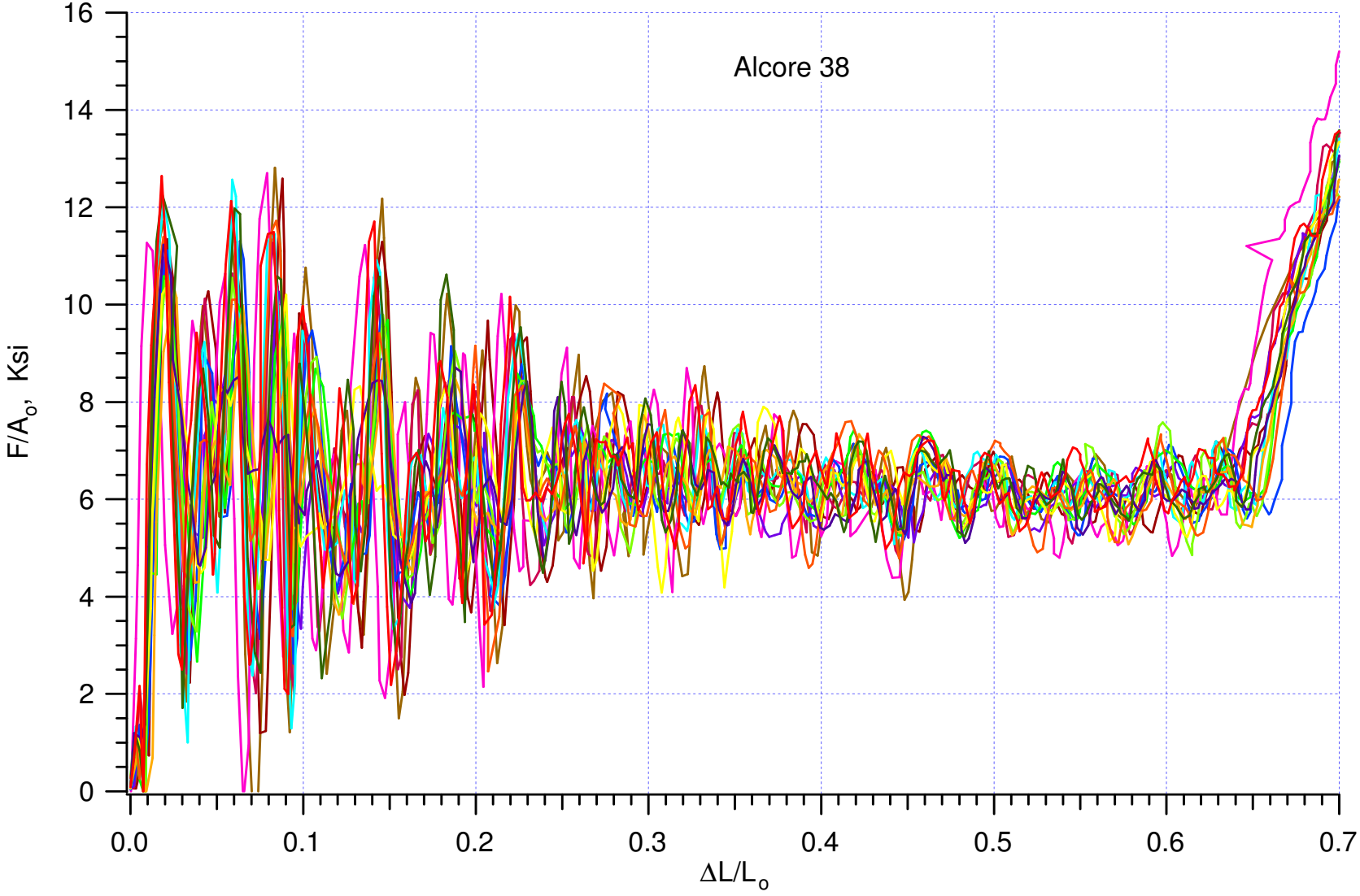

Figure 1 Stress-strain curves of Alcore 38 specimens crushed in t-dir, moderated rate, and confined.

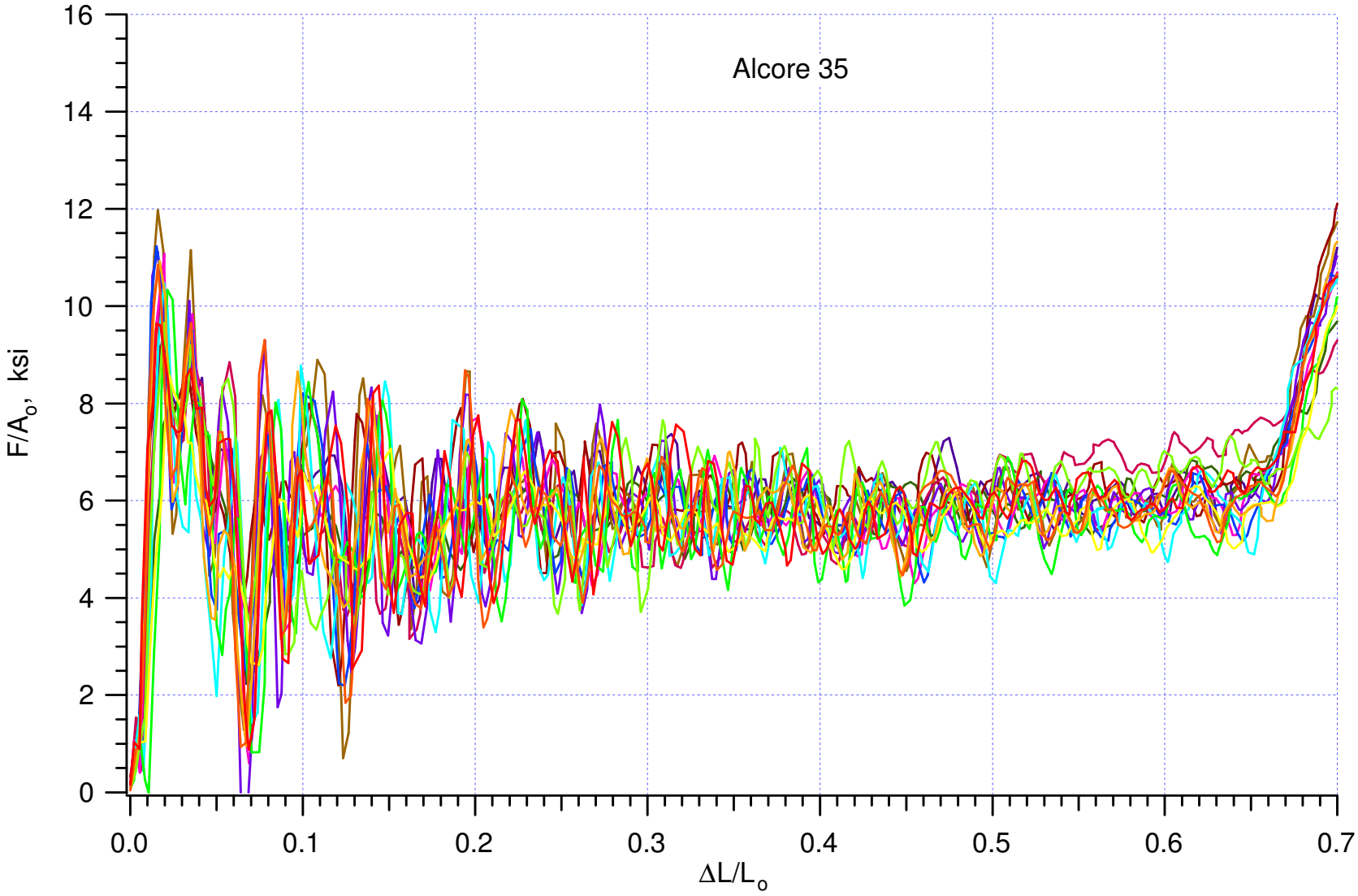

Figure 2 Stress-strain curves of Alcore 35 specimens crushed in t-dir, moderated rate, and confined.

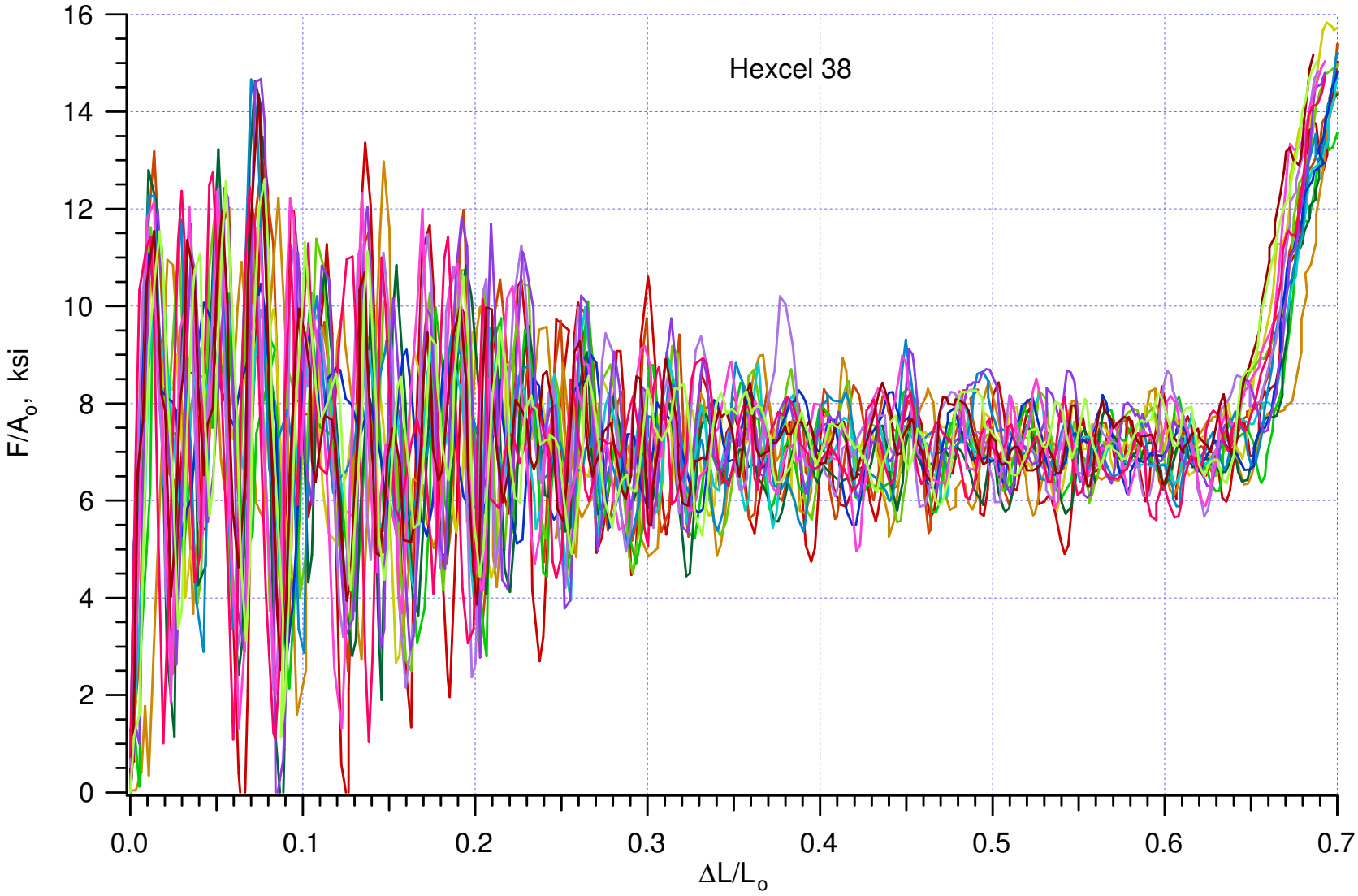

Figure 3 Stress-strain curves of Hexcel 38 specimens crushed in t-dir, moderated rate, and confined.

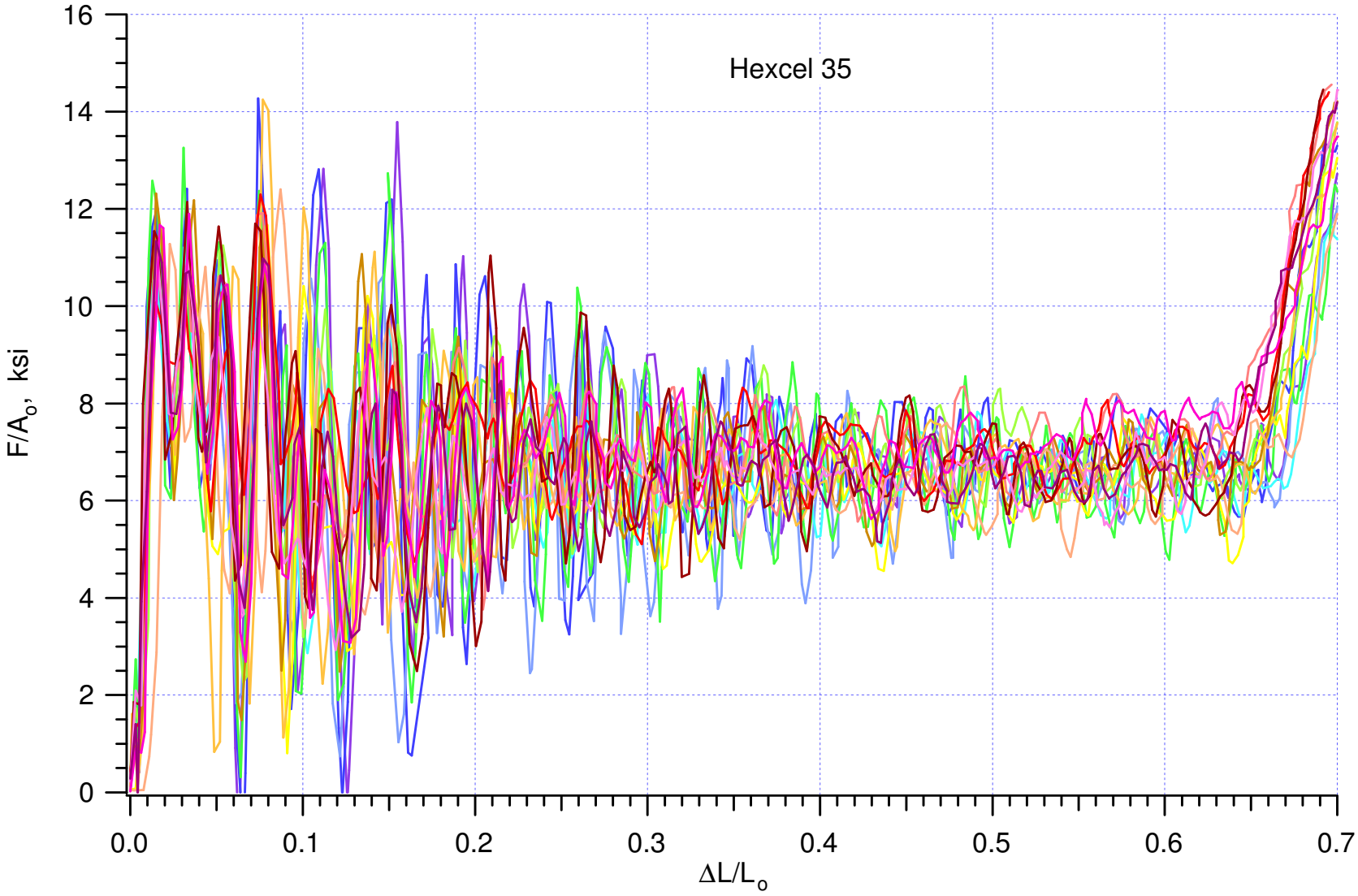

Figure 4 Stress-strain curves of Hexcel 38 specimens crushed in t-dir, moderated rate, and confined.

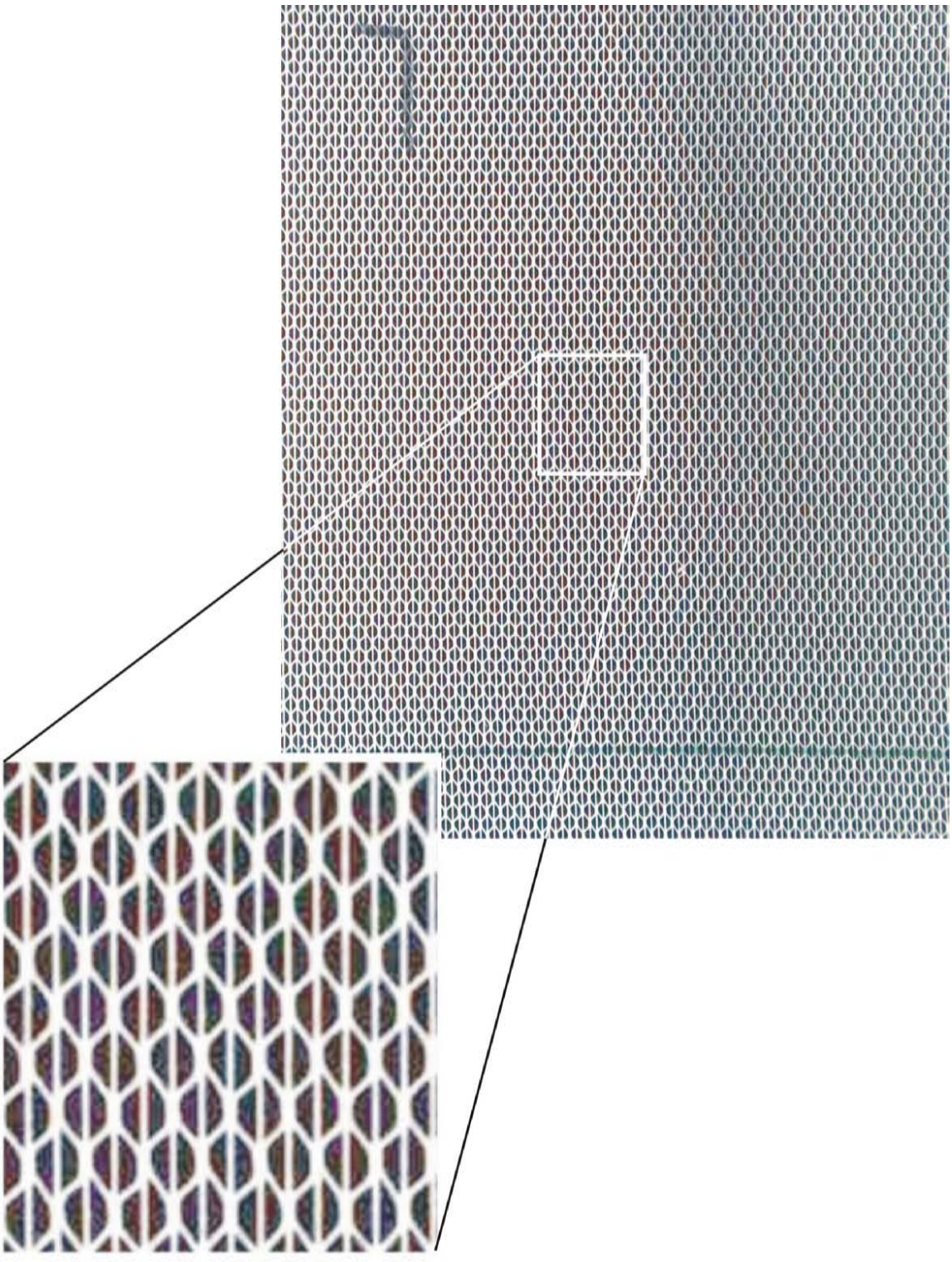

Figure 5(a) Cell structure of Alcore 38 honeycomb.

Figure 5(b) Cell structure of Alcore 38 honeycomb close to the edge of the block.

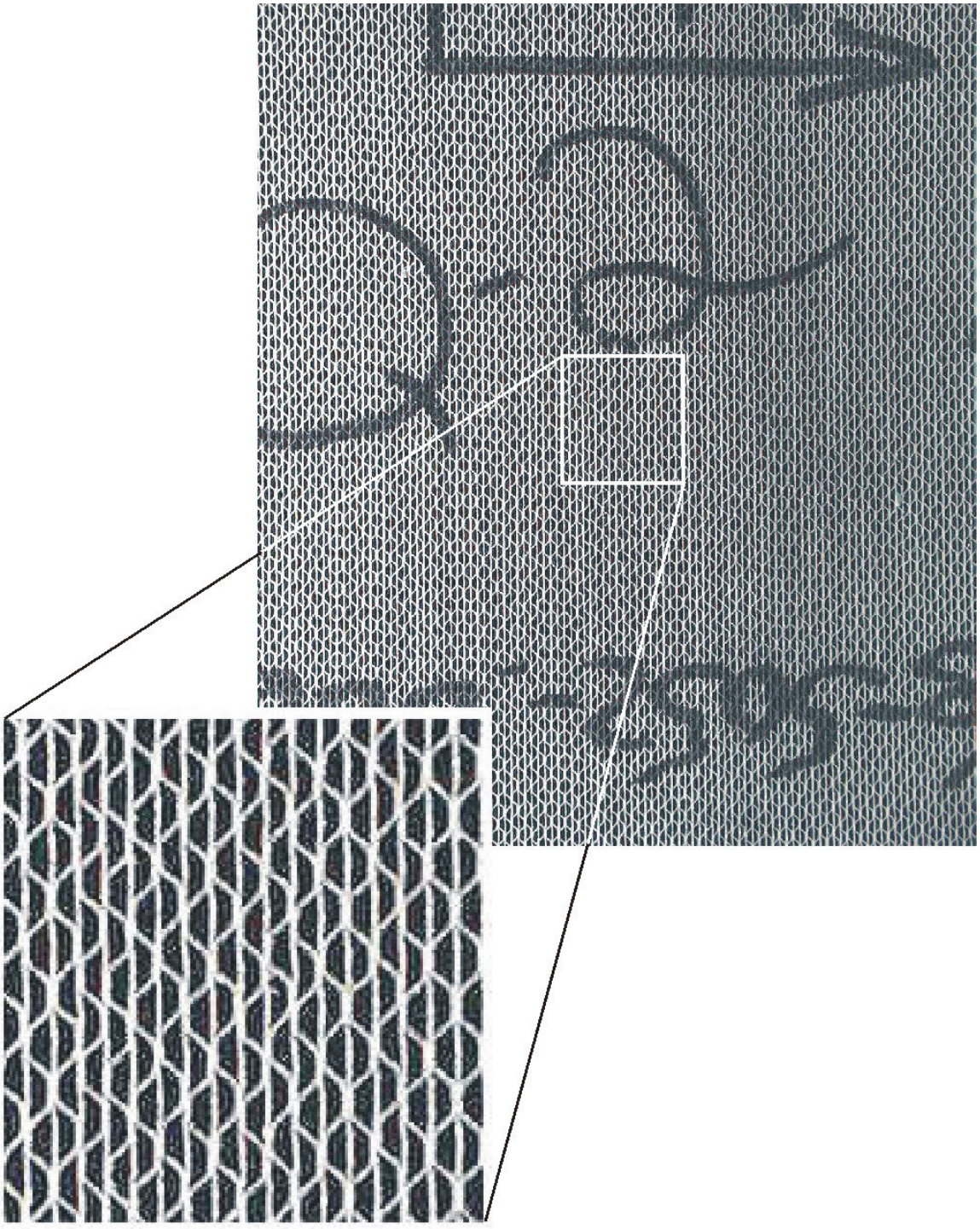

Figure 6 Cell structure of Hexcel 38 honeycomb.

This page intentionally left blank.

APPENDIX X:

"Moderate Rate Confined Crush Tests of Alcore 38 & Hexcel 38 honeycombs in the t-direction at 165°F," Memo Wei-Yang Lu to Distribution, January 18, 2000.

Sandia National Laboratories
Operated for the U.S. Department of Energy by
Sandia Corporation
MS9042
Livermore, CA 94551-0969

date: January 18, 2000

to: Distribution

from: Wei-yang Lu

subject: Moderate Rate Confined Crush Tests of Alcore 38 & Hexcel 38 honeycombs in the t-direction at 165°F

High temperature tests are completed. The up-to-date results are summarized in the following table, in which two boldface lines are high temperature results.

B61/MAVEN TEST MATRIX				EXPERIMENTAL RESULTS						MEMO
Test #	Honeycomb	Dir.	Temperature, degree F	Specimen	Density, pcf	Impact Speed, ft/s	Crush Strength, ksi	Std Deviation, ksi	Crush Efficiency, %	Date
1 - 15	Alcore 38	T	ambient	rotated	38.82	14.13	6.35	0.08	63.80	991203
16 - 30	Hexcel 38	T	ambient	rotated	38.70	13.67	7.17	0.15	63.89	000110
				rotated	38.78	0.00139	5.88		59.20	"
31 - 45	Alcore 35	T	ambient	rotated	35.39	14.35	5.74	0.18	64.46	000103
46 - 60	Hexcel 35	T	ambient	rotated	37.79	13.83	6.67	0.24	63.91	000110
				rotated	37.89	0.00139	5.83		60.30	"
60 - 75	**Alcore 38**	**T**	**165**	**rotated**	**38.96**	**14.33**	**5.49**	**0.10**	**62.52**	**000118**
76 - 90	**Hexcel 38**	**T**	**165**	**rotated**	**38.65**	**13.82**	**6.43**	**0.15**	**64.31**	**000118**
91 - 105	Alcore 38	T	-65							
106 - 120	Hexcel 38	T	-65							
121 - 125	Alcore 38	L	ambient							
126 - 130	Hexcel 38	L	ambient							
131 - 135	Alcore 38	W	ambient							
136 - 140	Hexcel 38	W	ambient							
159 - 161	Alcore 38	T	ambient	segmented	41.41	0.0014	6.14		52.30	991130
162 - 164	Hexcel 38	T	ambient	segmented	41.29	0.0014	6.85		53.70	991213

The crush strength of honeycomb is clearly affected by temperature. At ambient and 165 °F, the corresponding crush strengths are 6.35 ksi and 5.49 ksi for Alcore 38, and 7.17 ksi and 6.43 ksi for Hexcel 38. If we use the ambient values as reference, the decreases of crush strength at 165 °F are about 13% and 10% for Alcore 38 and Hexcel 38, respectively.

Please see Appendix I for detail experimental procedures for high temperature tests and results of Alcore 38, and Appendix II for results of Hexcel 38 at 165 ^{o}F.

Distribution:

Darrla Giersch(2167)	MS0481
Darren Hoke(2167)	MS0481
Vernon Willan(2167)	MS0481
Vista Bateman(9126)	MS0553
Tom Carne(9124)	MS0557
Berry Boughten(9132)	MS0557
Jaime Moya(9132)	MS0828
Terry Hinnerichs(9126)	MS0847
Ken Gwinn(9126)	MS0847
John Pott(9126)	MS0847
Rodney May(9126)	MS0847
Mike Neilsen(9123)	MS0847
Bill Scherzinger(9123)	MS0847
Hal Morgan(9123)	MS0847
Wendell Kawahara (8725)	MS904

Appendix I (memo000118)

Experimental procedures for confined high temperature tests

High temperature experimental setup was the same as that of ambient temperature (reported in memo 991203). A picture of the setup is shown in Figure 1 again to illustrate the procedures of high temperature experiment.

Rotated specimens were used. We stuck a thermal couple in the specimen, where the tip of the wire was approximately at the center of the honeycomb rectangle, Figure 2. A very small groove was made at the bottom of the specimen to accommodate the thermal couple wire so it would not cock the specimen inside the confined testing fixture, Figure 3.

After the specimen was installed, we raised the crosshead of the MTS system so the punch and the load washer were outside the environmental chamber. We then closed the door of the environmental chamber and filled all openings (e.g., actuator, punch, thermal couple, etc.) with insulating foams and started heating. This step had two beneficial results: (1) honeycomb and fixture heated up faster in a closed chamber, and (2) the load washer was not subjected to high temperature.

The temperature of the honeycomb specimen was continuously monitored. When it reached 167 ^{o}F, we stopped heating, opened the chamber door, removed foams, lowered the crosshead assembly, set the actuator and the crosshead at the predetermined positions. These steps took several minutes. Since the specimen was enclosed by fixture, the temperature of the honeycomb cooled very slowly. When the it reached 165 ^{o}F, we fired the actuator and crushed the honeycomb specimen.

Figure 1 Experimental setup. An environmental chamber is bolted on the testing frame.

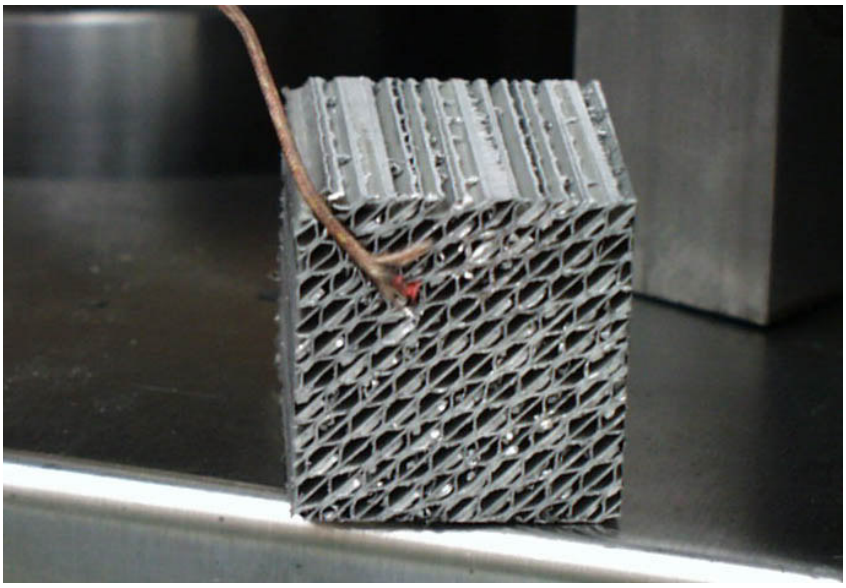

Figure 2 A thermal couple is stuck in from the bottom of the specimen.

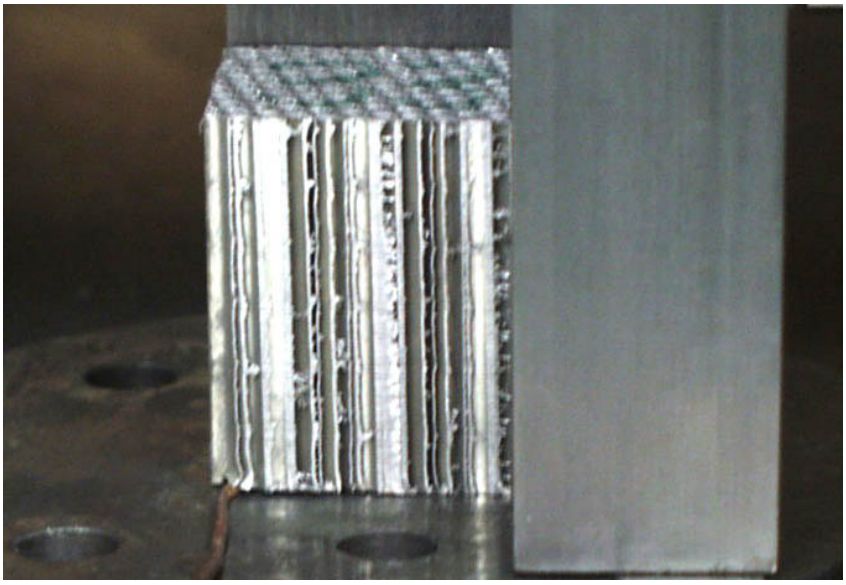

Figure 3. A specimen with a thermal couple in place before closing the confined fixture.

Experimental results of Alcore 38 crushed in t-direction at 165 ^{o}F

Specimen	d_1, in	d_2, in	d_3, in	Weight, lb	Density, pcf	Temperature, degree F	Crush Velocity, ft/s	Crush strenght, ksi	Crush efficiency, %	Remarks
A38_51	1.198	1.191	1.495	0.0480	38.86	184	14.48	5.17	62.61	R5
A38_52	1.198	1.215	1.498	0.0492	38.98	165	14.22	5.40	62.06	
A38_53	1.197	1.219	1.498	0.0493	38.97	165	14.45	5.44	62.80	
A38_54	1.195	1.218	1.498	0.0492	38.96	165	14.27	5.46	62.27	
A38_55	1.215	1.223	1.499	0.0497	38.57	165	14.38	5.31	62.55	
A38_56	1.197	1.204	1.494	0.0491	39.37	165	14.50	5.50	62.76	
A38_57	1.207	1.205	1.493	0.0488	38.86	165	14.62	5.42	63.12	
A38_58	1.198	1.204	1.495	0.0488	39.11	165	-	-	-	R6
A38_59	1.191	1.191	1.493	0.0477	38.94	165	14.48	5.55	62.59	
A38_60	1.202	1.190	1.492	0.0480	38.84	165	14.43	5.45	62.43	
A38_61	1.182	1.202	1.489	0.0474	38.75	165	14.21	5.56	63.13	
A38_62	1.197	1.193	1.492	0.0481	39.03	165	14.32	5.47	62.31	
A38_63	1.198	1.192	1.495	0.0481	38.92	165	14.06	5.65	61.75	
A38_64	1.200	1.187	1.495	0.0482	39.09	165	14.26	5.67	63.57	
A38_65	1.200	1.209	1.495	0.0486	38.71	70	13.63	6.56	62.50	R7
A38_66	1.193	1.207	1.502	0.0489	39.10	165	14.33	5.35	63.28	
A38_67	1.192	1.207	1.502	0.0489	39.06	165	14.29	5.51	61.36	
A38_68	1.201	1.190	1.496	0.0485	39.22	165	14.20	5.56	61.82	
				max	39.37		14.62	5.67	63.57	
				min	38.57		14.06	5.31	61.36	
				average	38.96		14.33	5.49	62.52	
				std deviation	0.19		0.14	0.10	0.62	
				median	38.97		14.32	5.47	62.55	

Remarks	
R5	*temperature too high*
R6	*data not recorded*
R7	*room temperature trial run after the system was moved out of the pit*

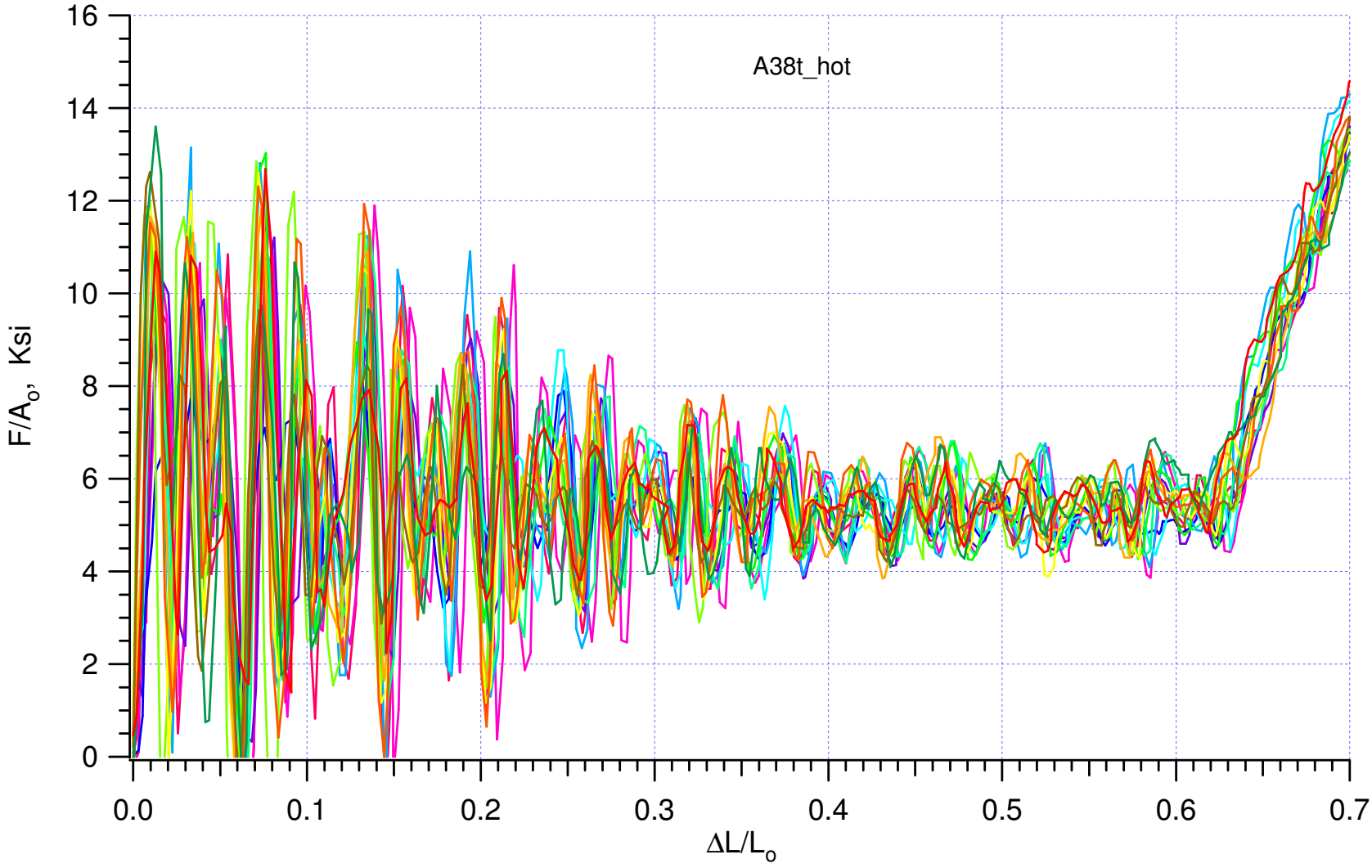
A38t_hot
F/A$_o$, Ksi
$\Delta L/L_o$
0
2
4
6
8
10
12
14
16
0.0
0.1
0.2
0.3
0.4
0.5
0.6
0.7

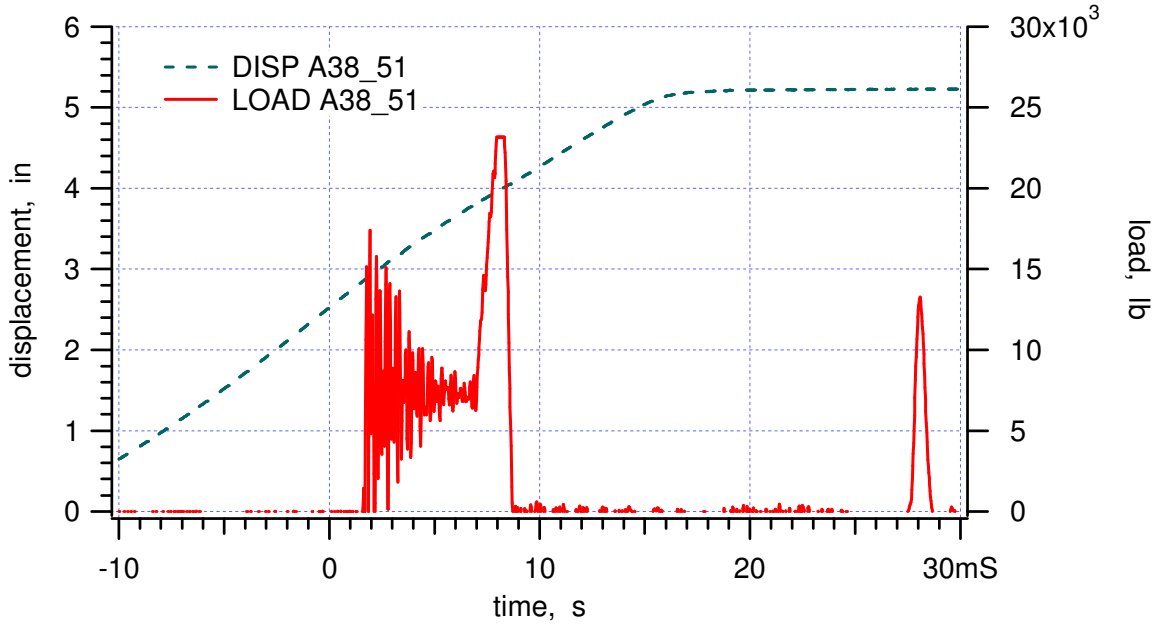
DISP A38_51
LOAD A38_51
displacement, in
load, lb
30x10^3
time, s
-10
0
10
20
30mS

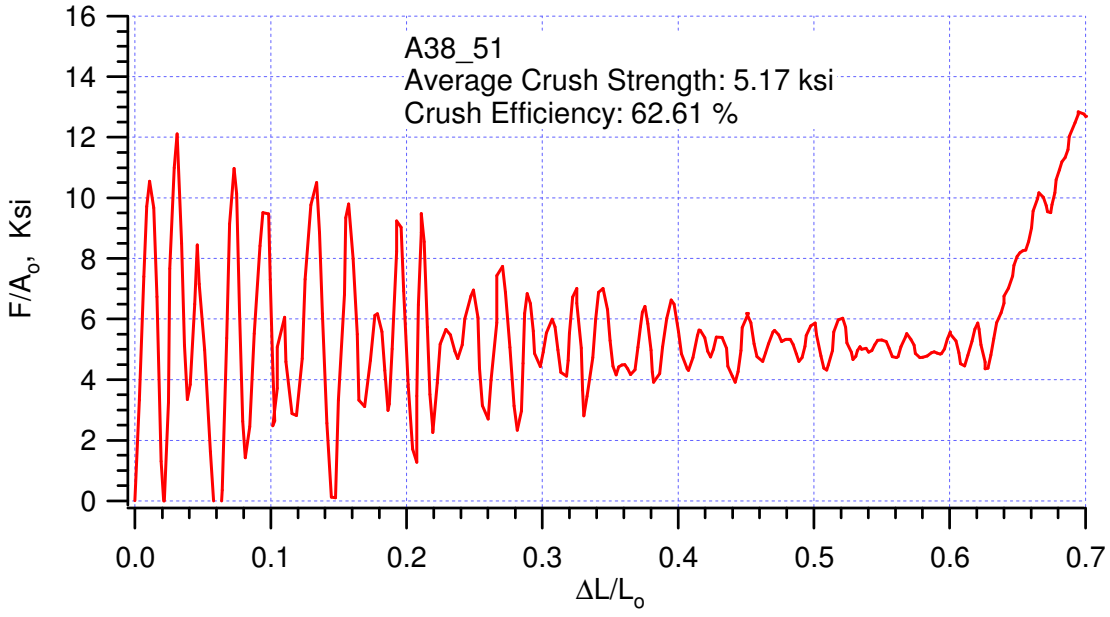
A38_51
Average Crush Strength: 5.17 ksi
Crush Efficiency: 62.61 %
F/A_o, Ksi
ΔL/L_o

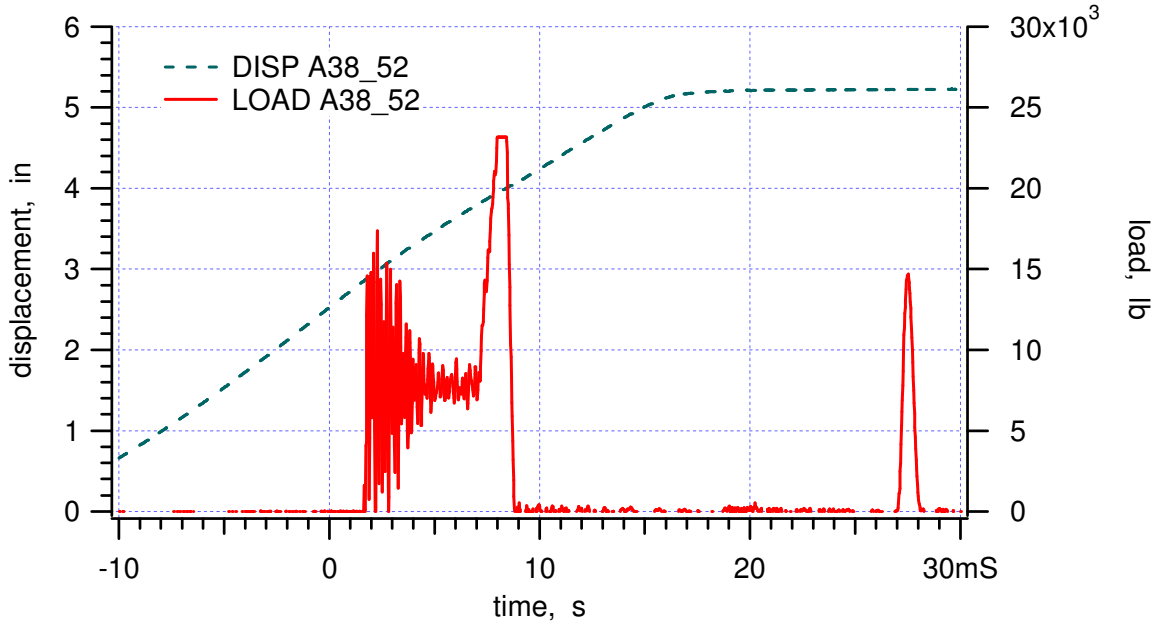
DISP A38_52
LOAD A38_52
displacement, in
load, lb
30x10^3
time, s
-10
0
10
20
30mS

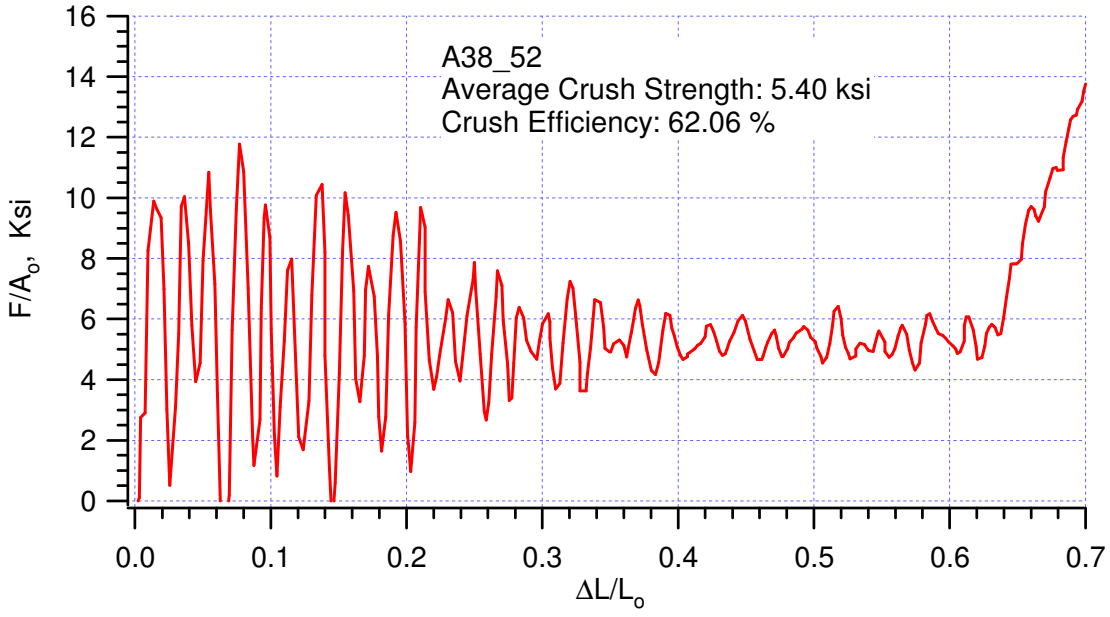
A38_52
Average Crush Strength: 5.40 ksi
Crush Efficiency: 62.06 %
F/A_o, Ksi
ΔL/L_o

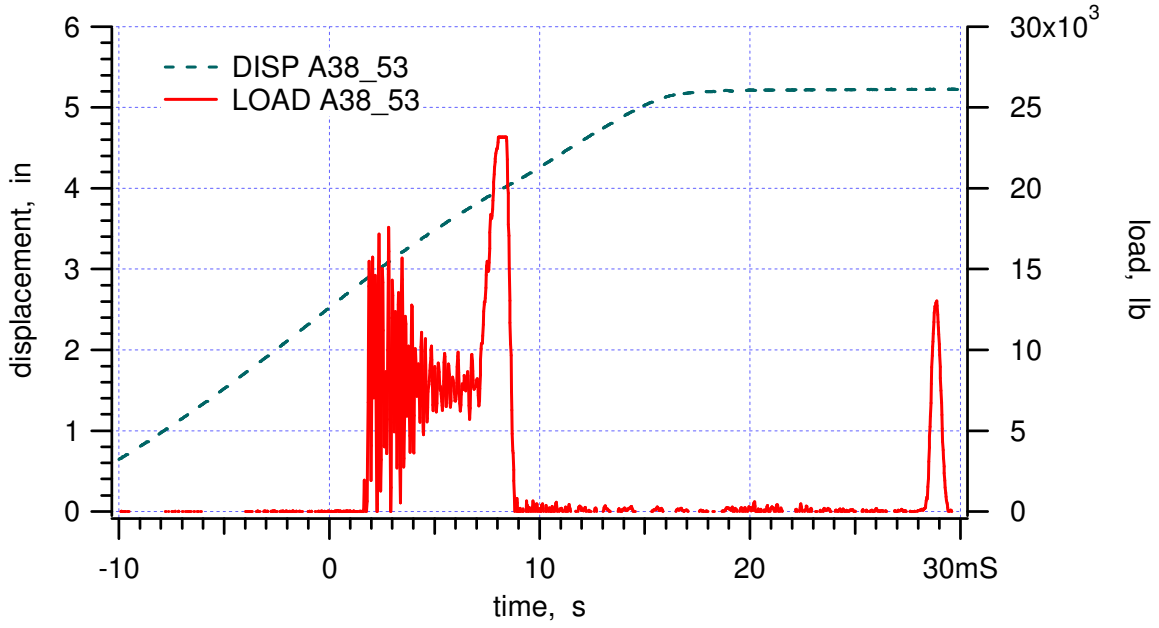
DISP A38_53
LOAD A38_53
displacement, in
load, lb
30x10^3
time, s
-10
0
10
20
30mS

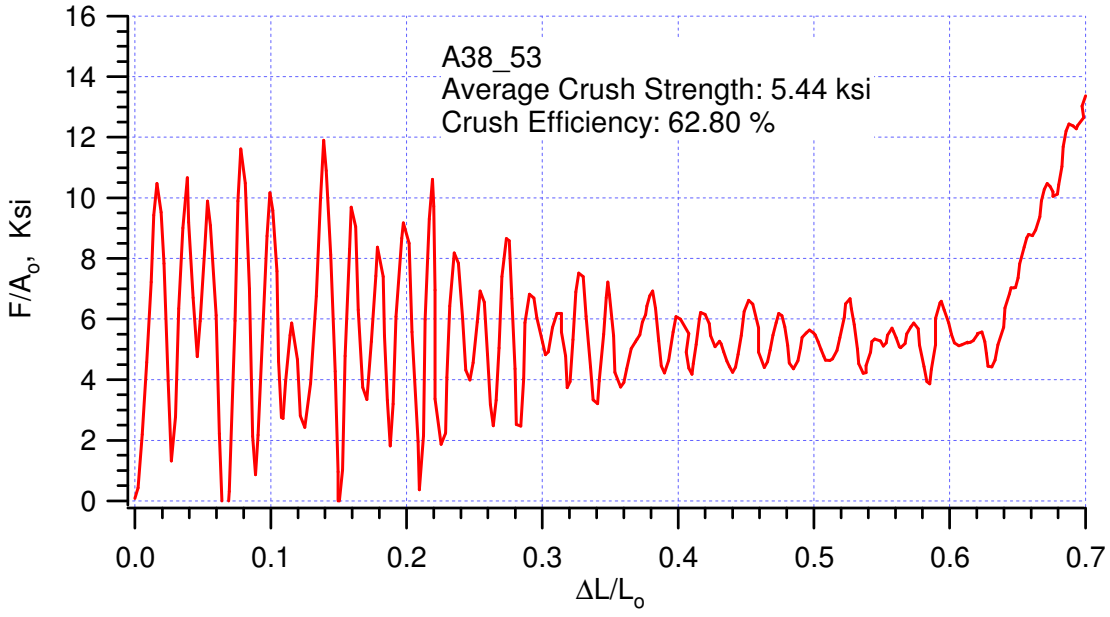
A38_53
Average Crush Strength: 5.44 ksi
Crush Efficiency: 62.80 %
F/A_o, Ksi
ΔL/L_o

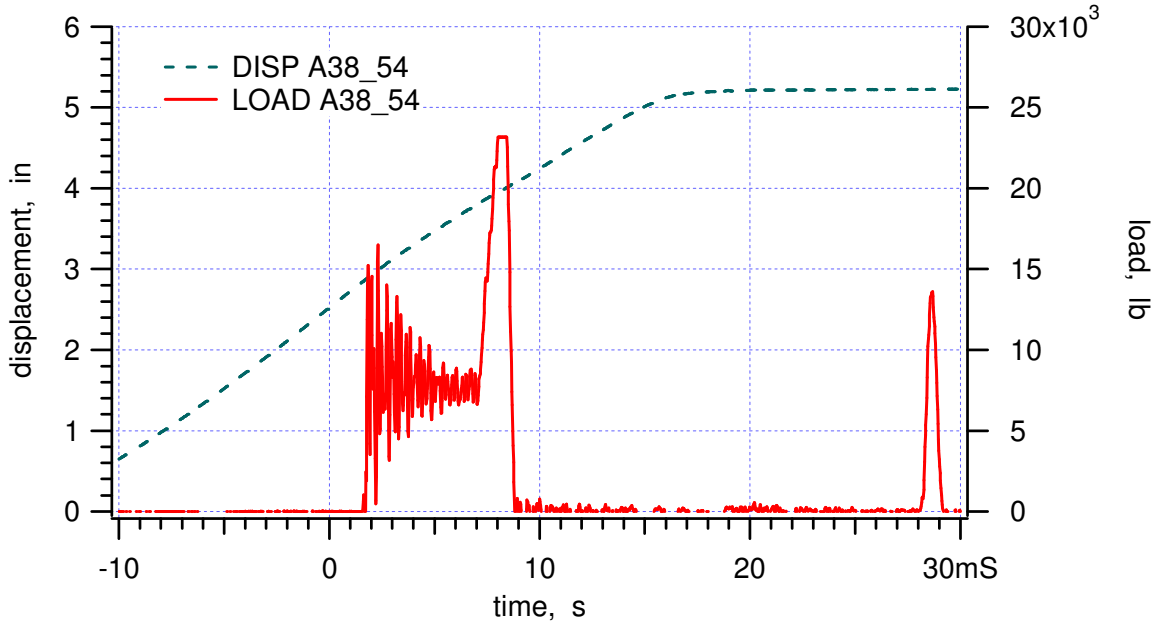
DISP A38_54
LOAD A38_54
displacement, in
load, lb
30x10^3
time, s
-10
0
10
20
30mS

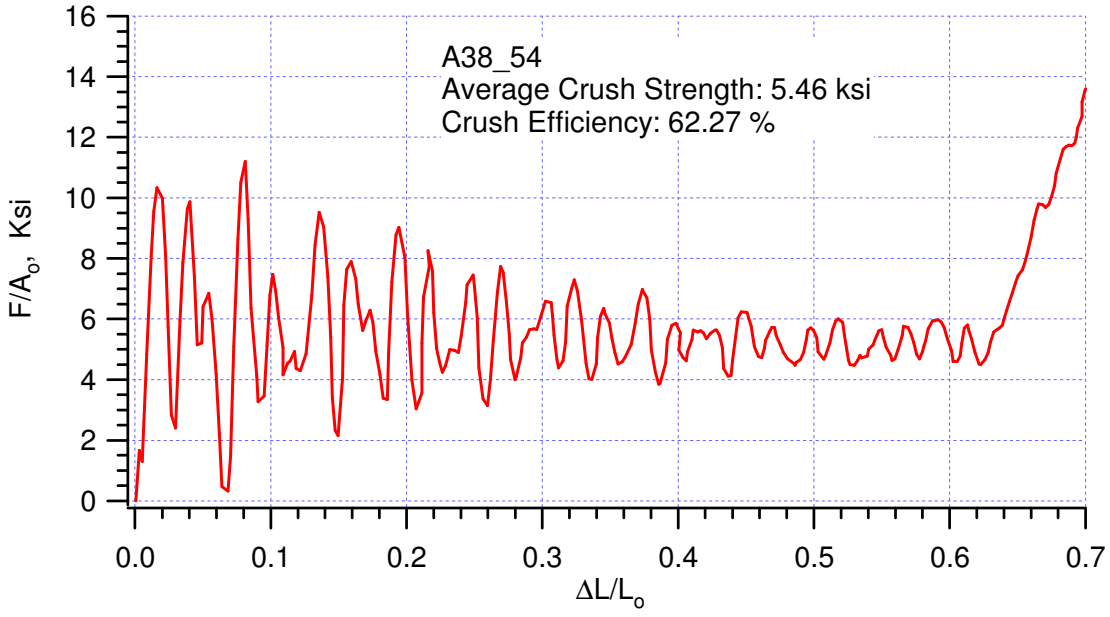
A38_54
Average Crush Strength: 5.46 ksi
Crush Efficiency: 62.27 %
F/A_o, Ksi
ΔL/L_o

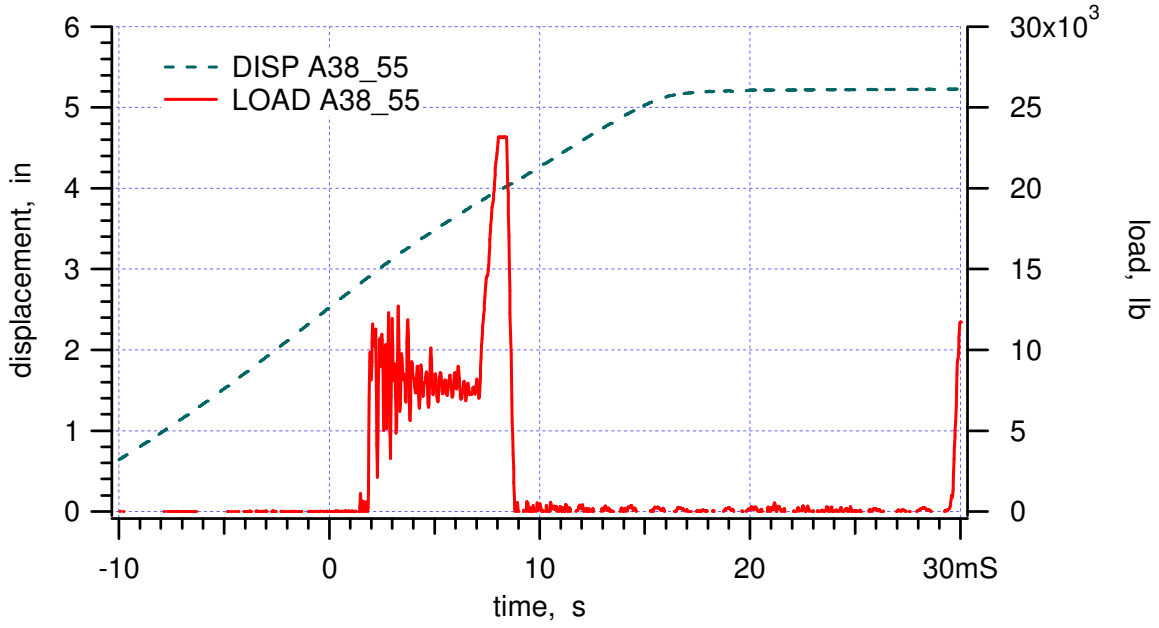
DISP A38_55
LOAD A38_55
displacement, in
load, lb
30x10^3
time, s
-10
0
10
20
30mS

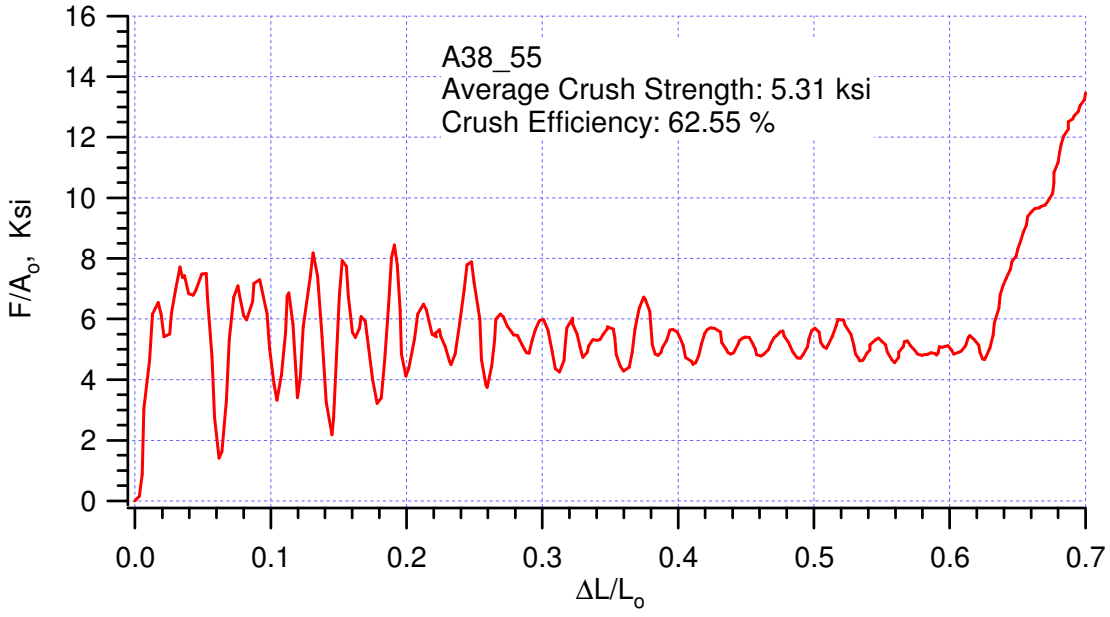
A38_55
Average Crush Strength: 5.31 ksi
Crush Efficiency: 62.55 %
F/A_o, Ksi
ΔL/L_o

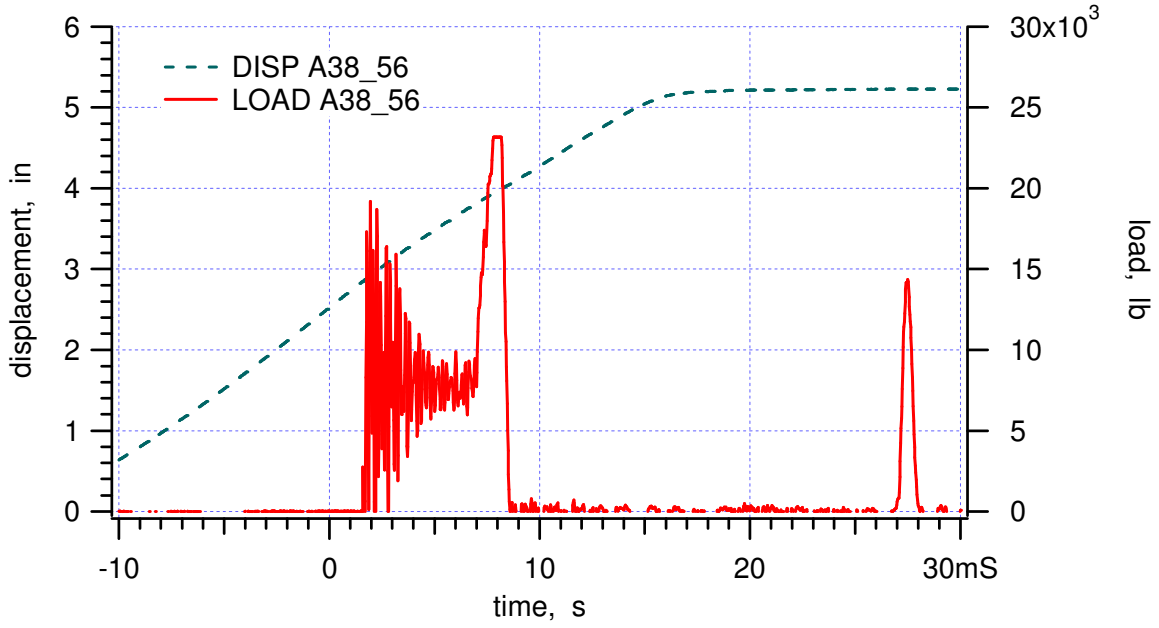
DISP A38_56
LOAD A38_56
displacement, in
load, lb
30x10^3
time, s
-10
0
10
20
30mS

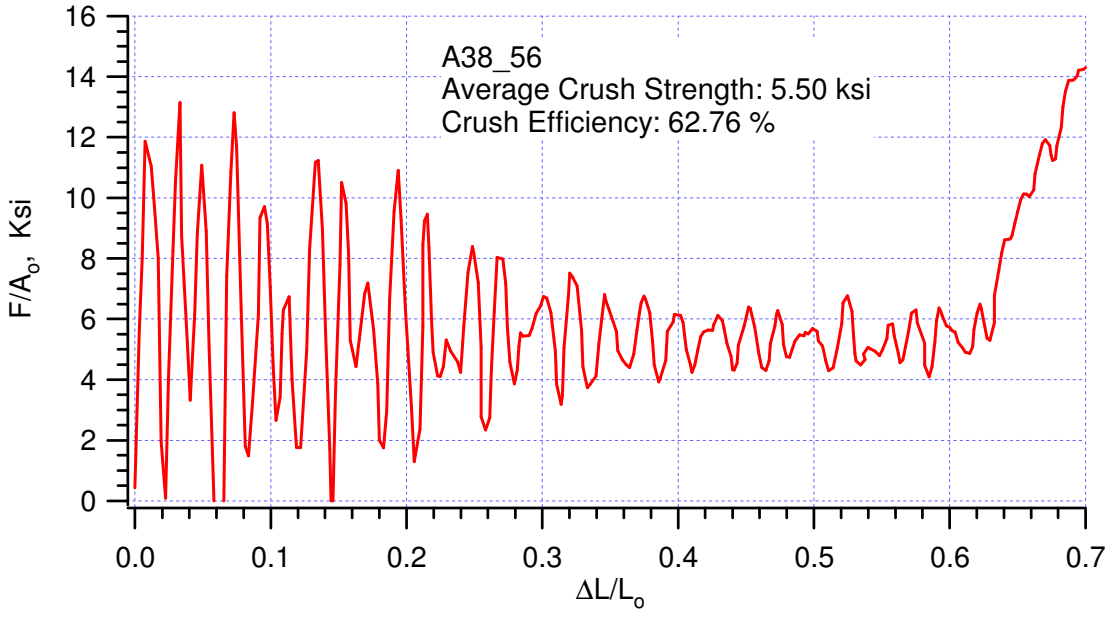
A38_56
Average Crush Strength: 5.50 ksi
Crush Efficiency: 62.76 %
F/A_o, Ksi
ΔL/L_o

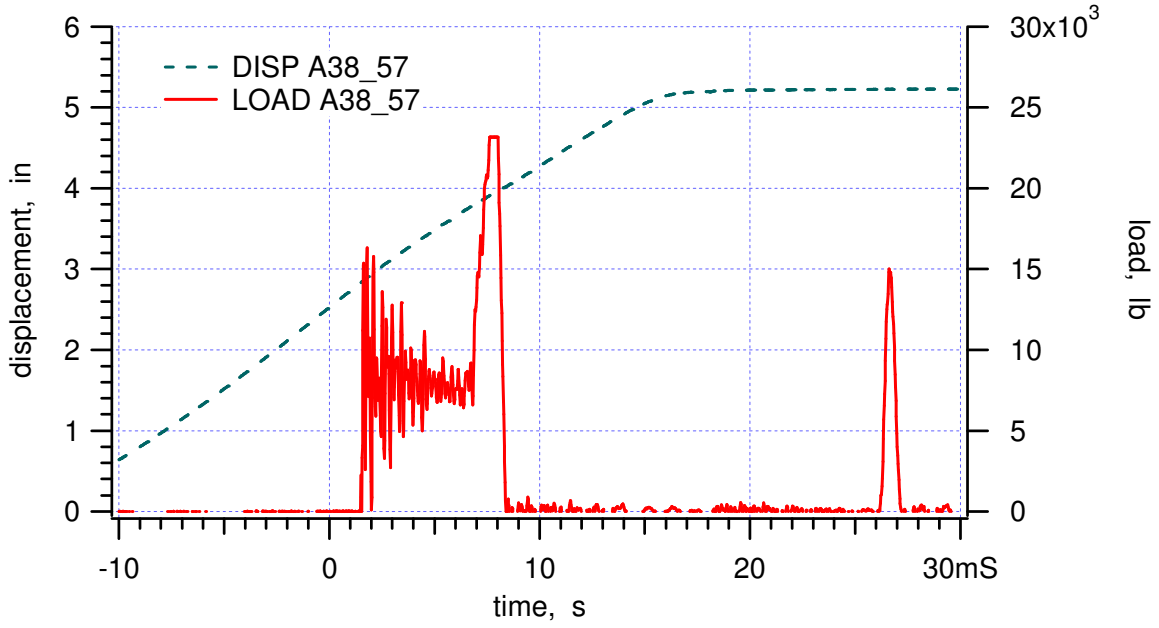
DISP A38_57
LOAD A38_57
displacement, in
load, lb
30x10^3
time, s
-10
0
10
20
30mS

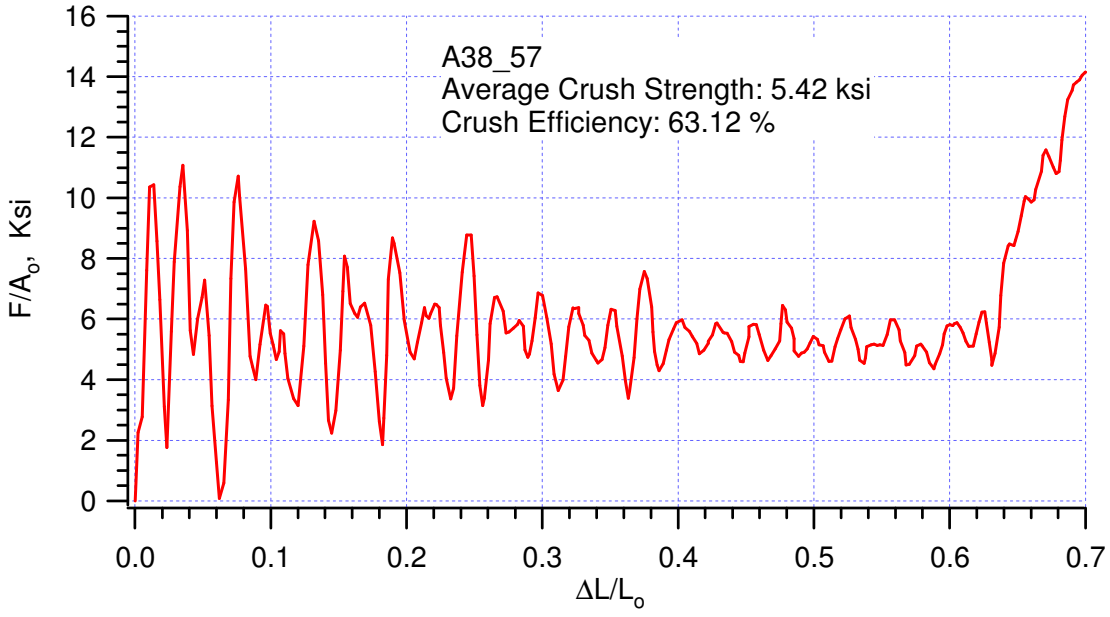
A38_57
Average Crush Strength: 5.42 ksi
Crush Efficiency: 63.12 %
F/A_o, Ksi
ΔL/L_o

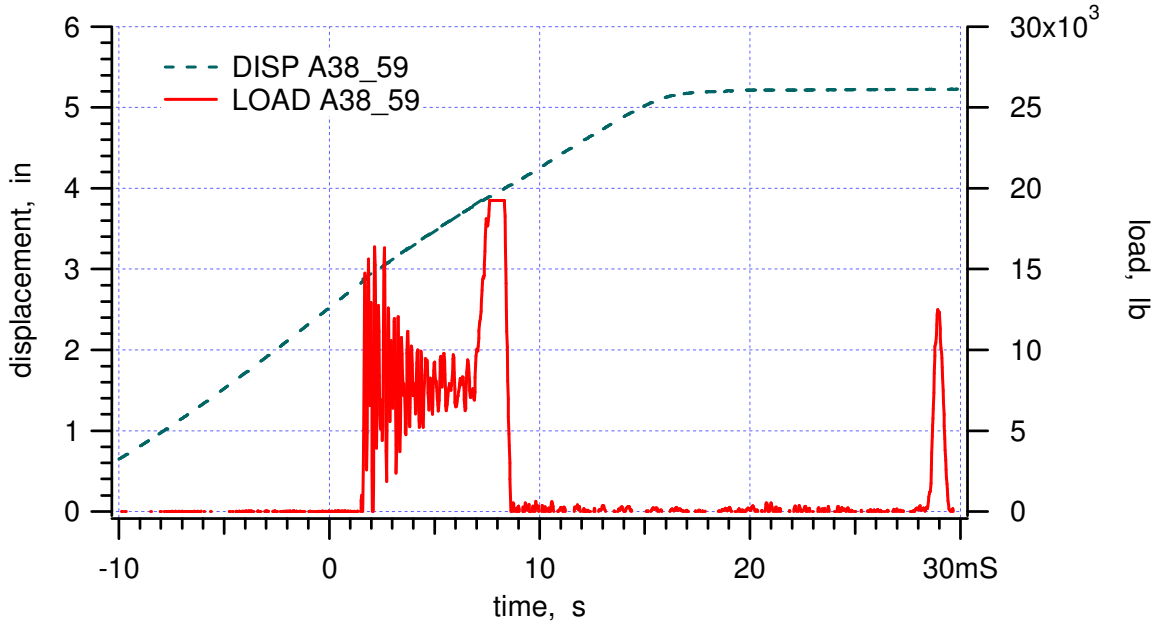
DISP A38_59
LOAD A38_59
displacement, in
load, lb
30x10^3
time, s
-10
0
10
20
30mS

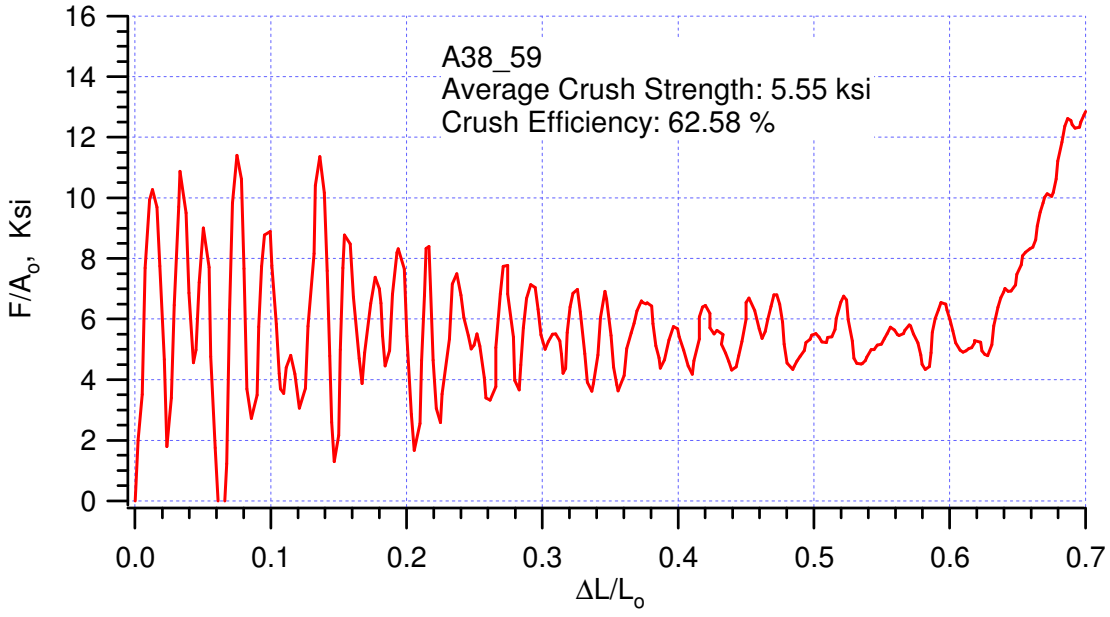
A38_59
Average Crush Strength: 5.55 ksi
Crush Efficiency: 62.58 %
F/A_o, Ksi
ΔL/L_o

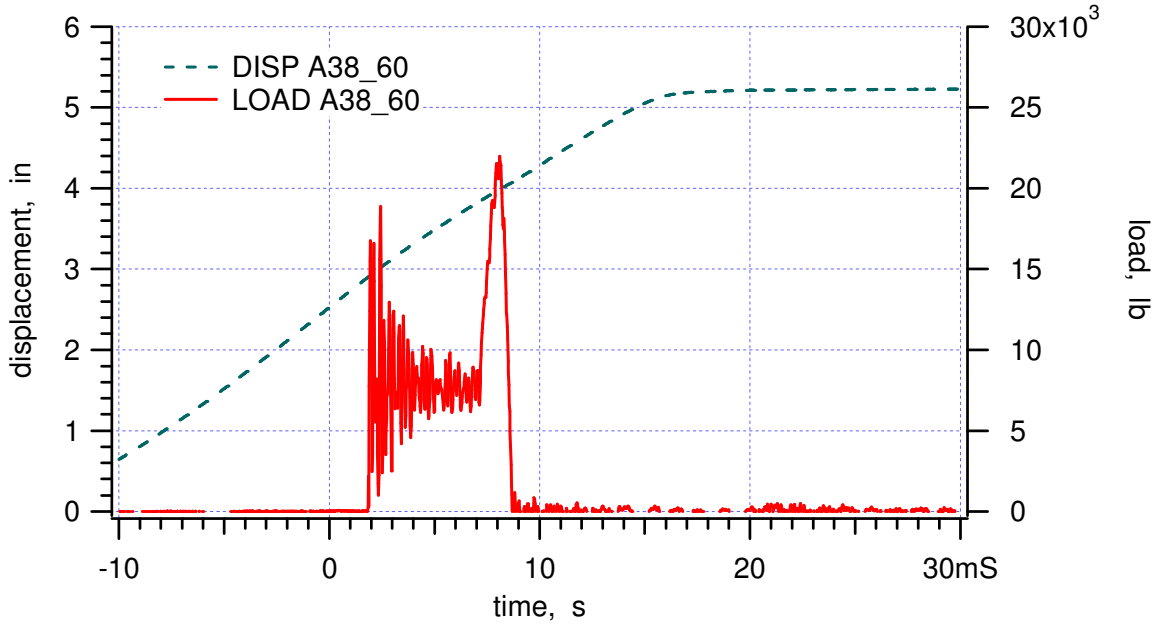
DISP A38_60
LOAD A38_60
displacement, in
load, lb
30x10^3
time, s
-10
0
10
20
30mS

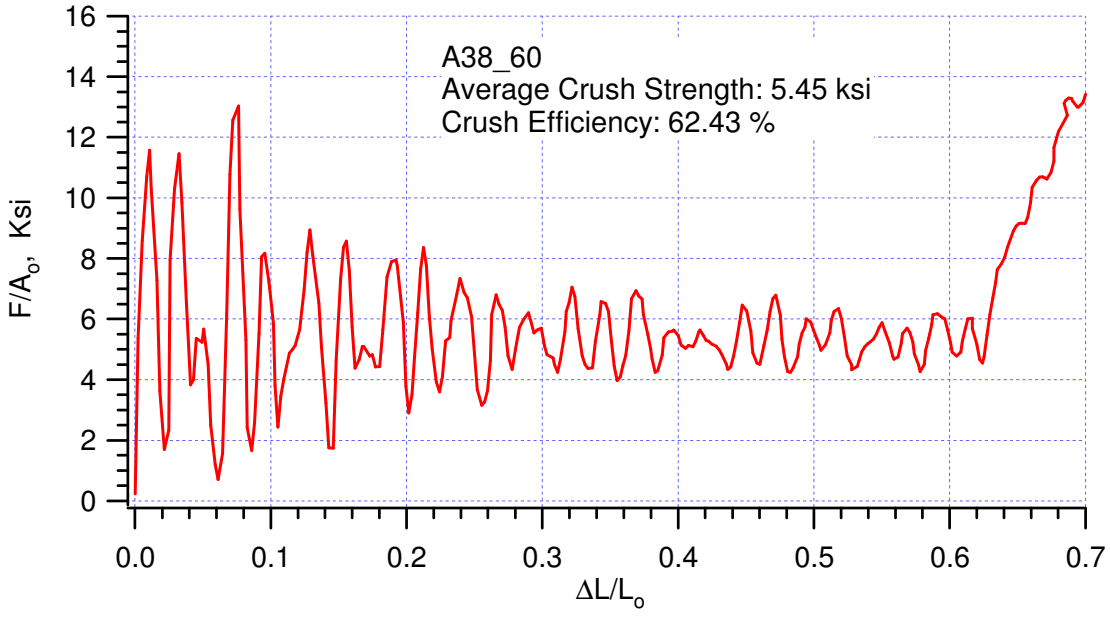
A38_60
Average Crush Strength: 5.45 ksi
Crush Efficiency: 62.43 %
F/A_o, Ksi
ΔL/L_o

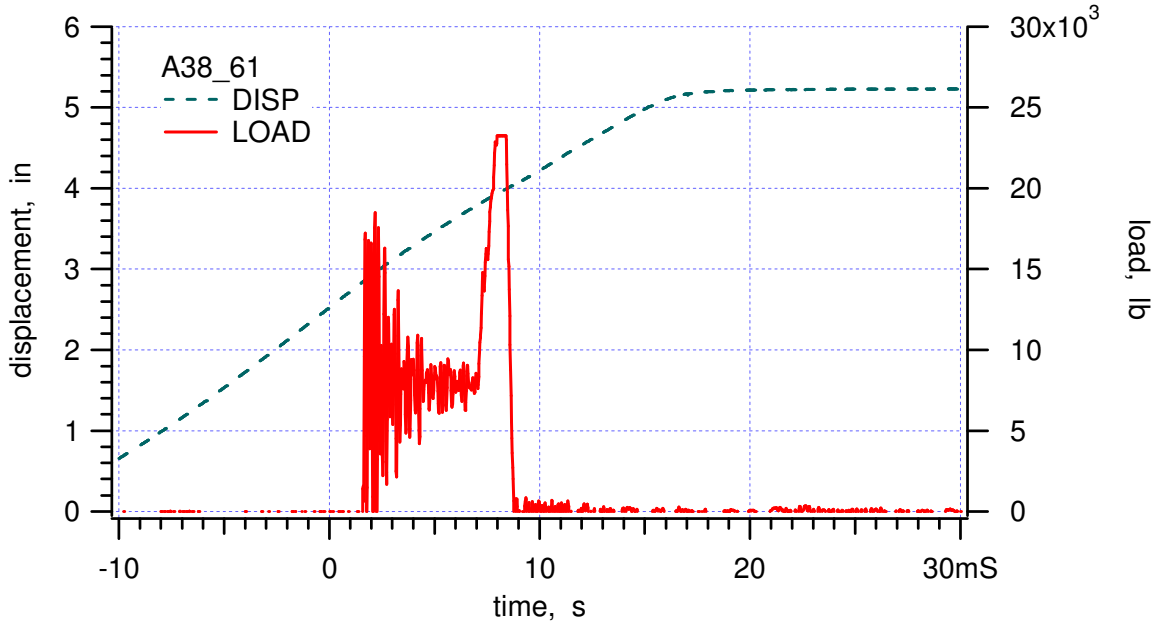
A38_61
DISP
LOAD
displacement, in
load, lb
30x10^3
time, s
-10
0
10
20
30mS

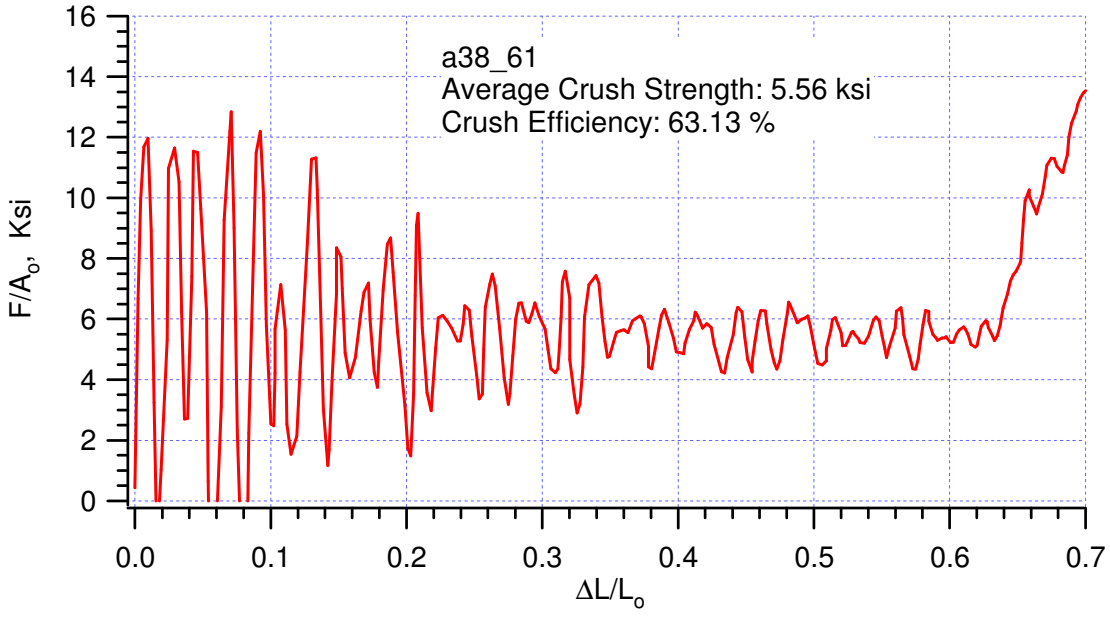
a38_61
Average Crush Strength: 5.56 ksi
Crush Efficiency: 63.13 %
F/A_o, Ksi
ΔL/L_o

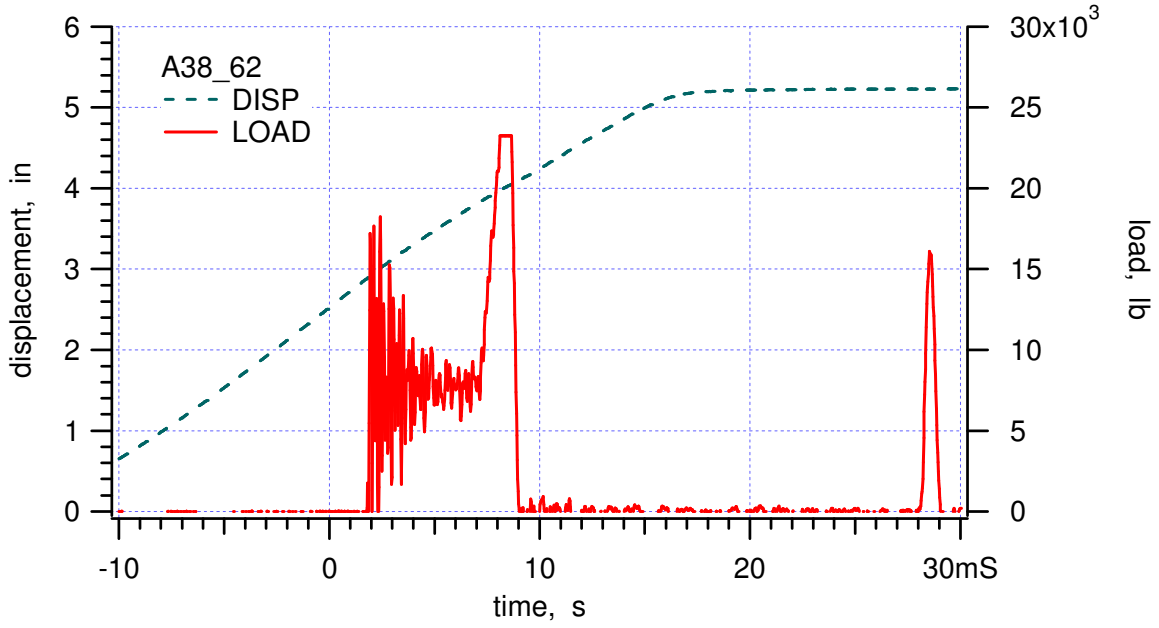
A38_62
DISP
LOAD
displacement, in
load, lb
30x10^3
time, s
-10
0
10
20
30mS

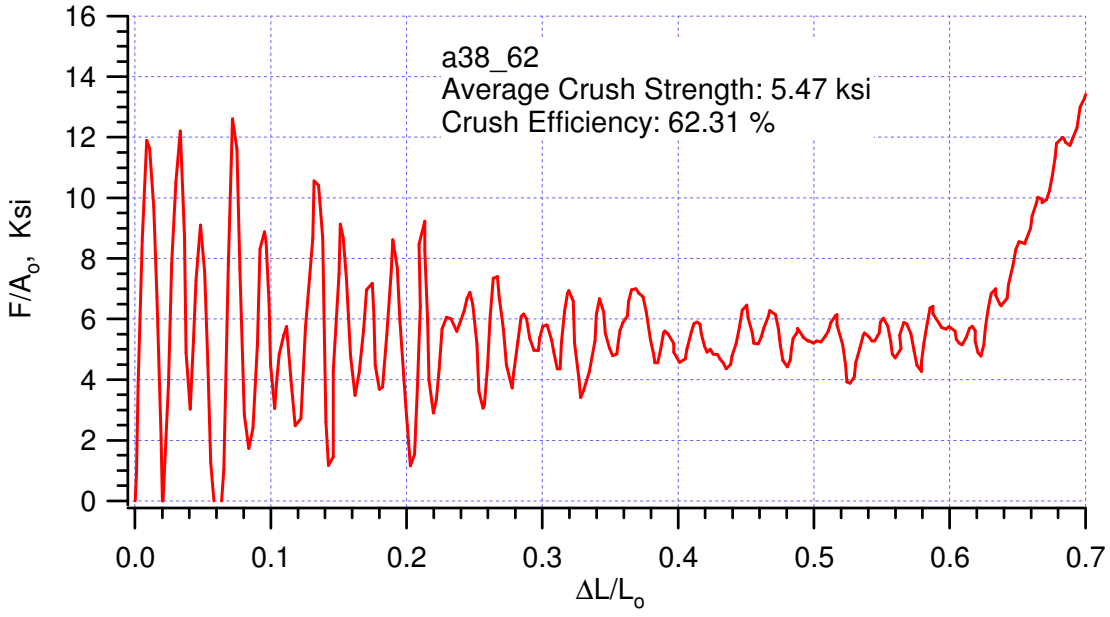
a38_62
Average Crush Strength: 5.47 ksi
Crush Efficiency: 62.31 %
F/A_o, Ksi
ΔL/L_o

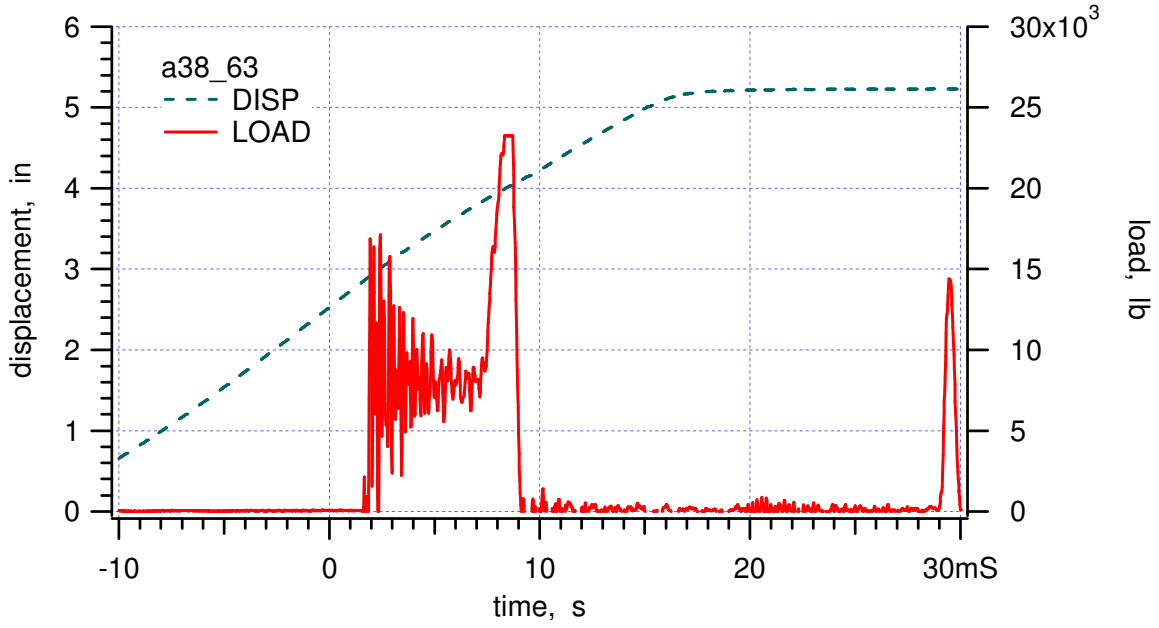
a38_63
DISP
LOAD
displacement, in
load, lb
30x10^3
time, s
-10
0
10
20
30mS

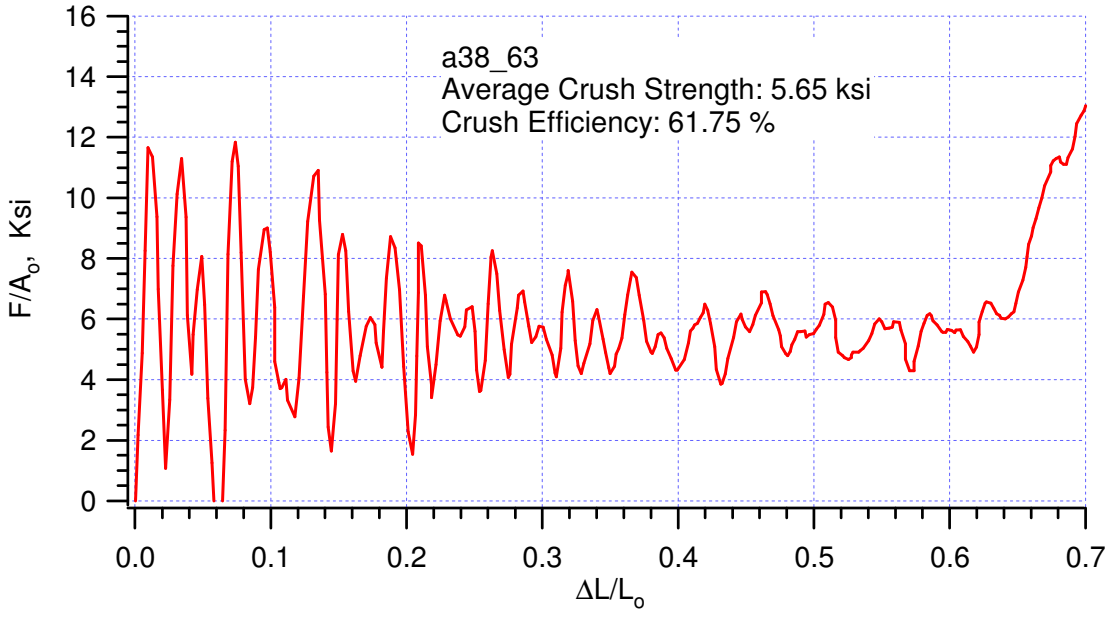
a38_63
Average Crush Strength: 5.65 ksi
Crush Efficiency: 61.75 %
F/A_o, Ksi
ΔL/L_o

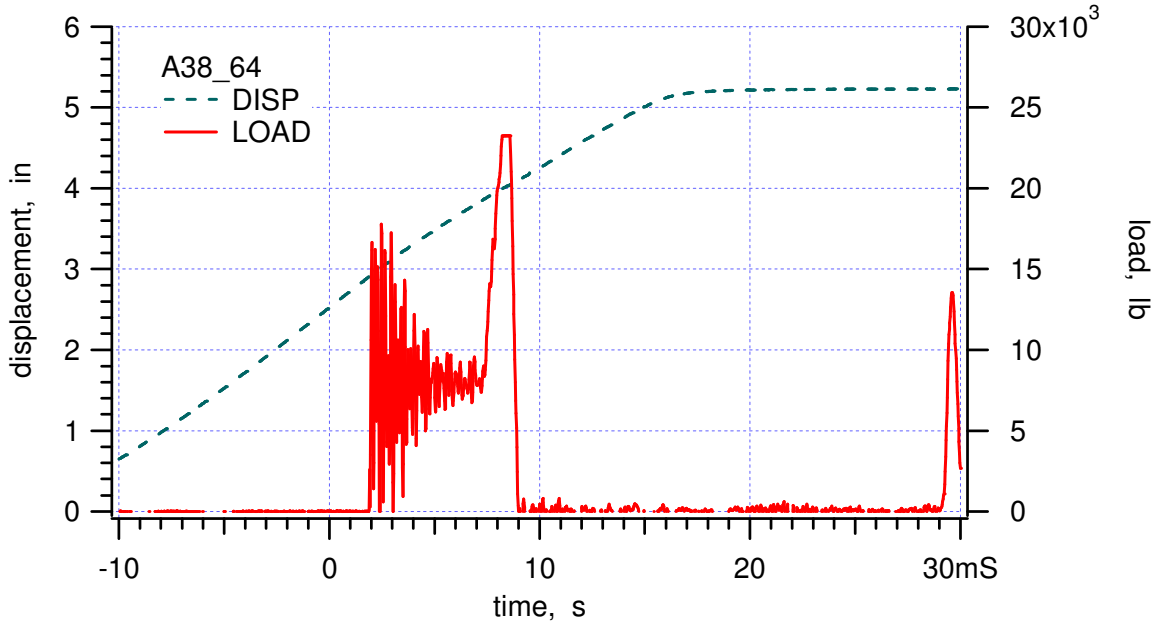
A38_64
DISP
LOAD
displacement, in
load, lb
30x10^3
time, s
-10
0
10
20
30mS

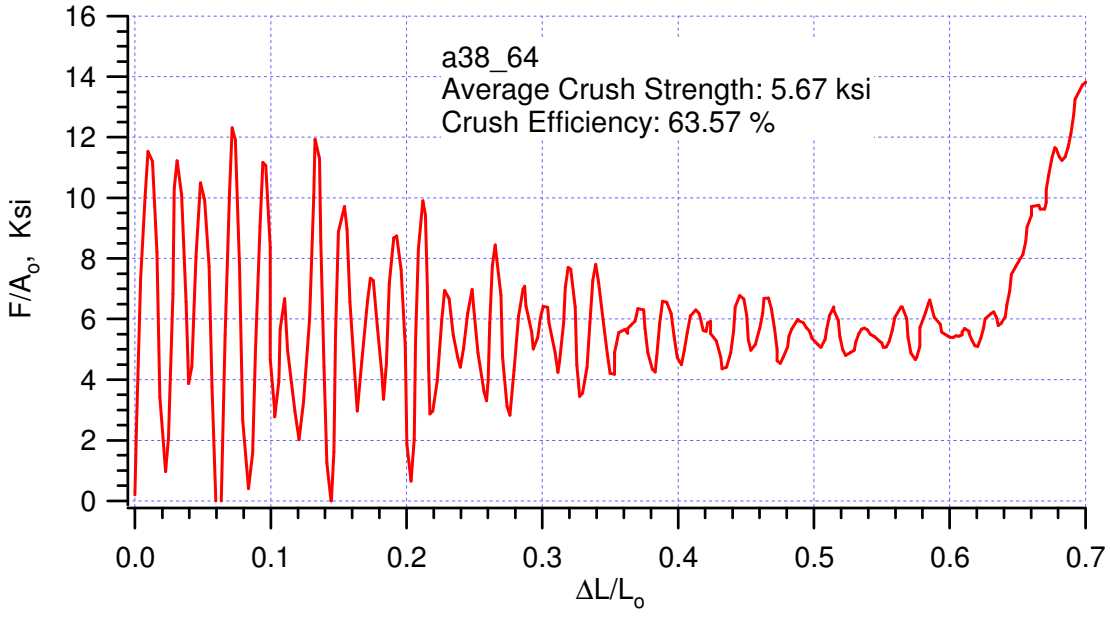
a38_64
Average Crush Strength: 5.67 ksi
Crush Efficiency: 63.57 %
F/A_o, Ksi
ΔL/L_o

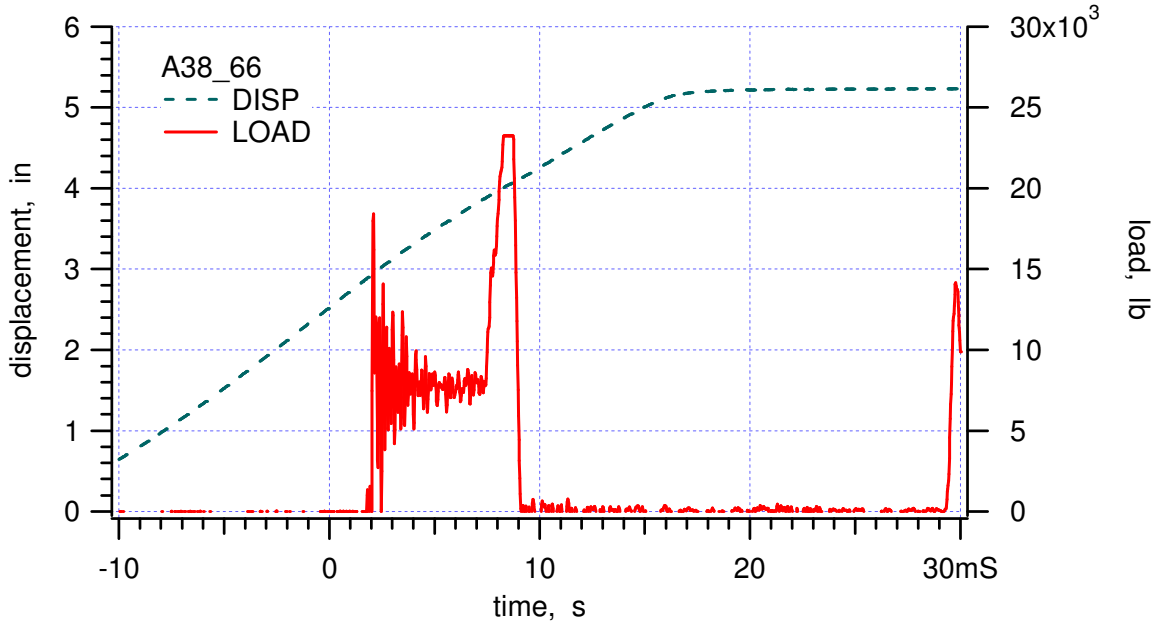
A38_66
DISP
LOAD
displacement, in
load, lb
30x10^3
time, s
-10
0
10
20
30mS

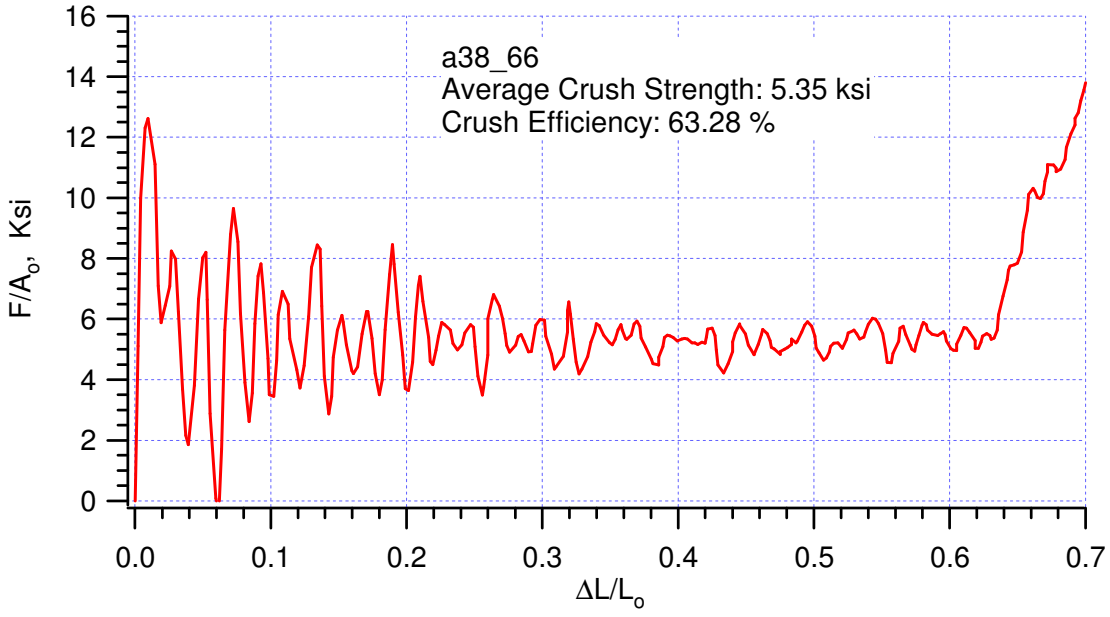
a38_66
Average Crush Strength: 5.35 ksi
Crush Efficiency: 63.28 %
F/A_o, Ksi
ΔL/L_o

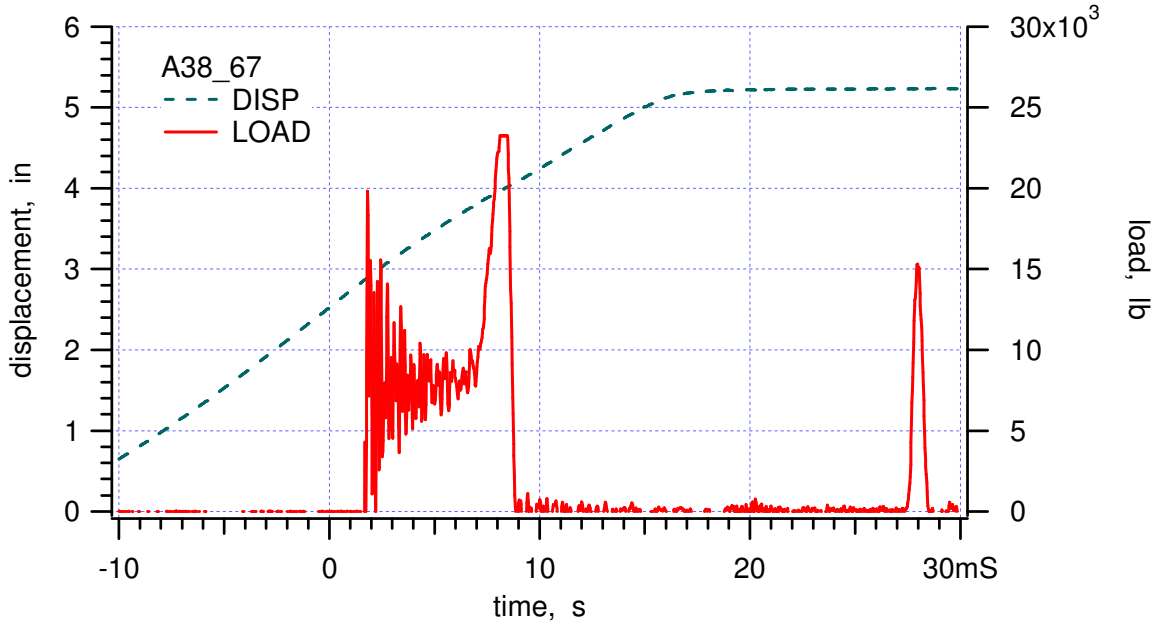
A38_67
DISP
LOAD
displacement, in
load, lb
30x10^3
time, s
-10
0
10
20
30mS

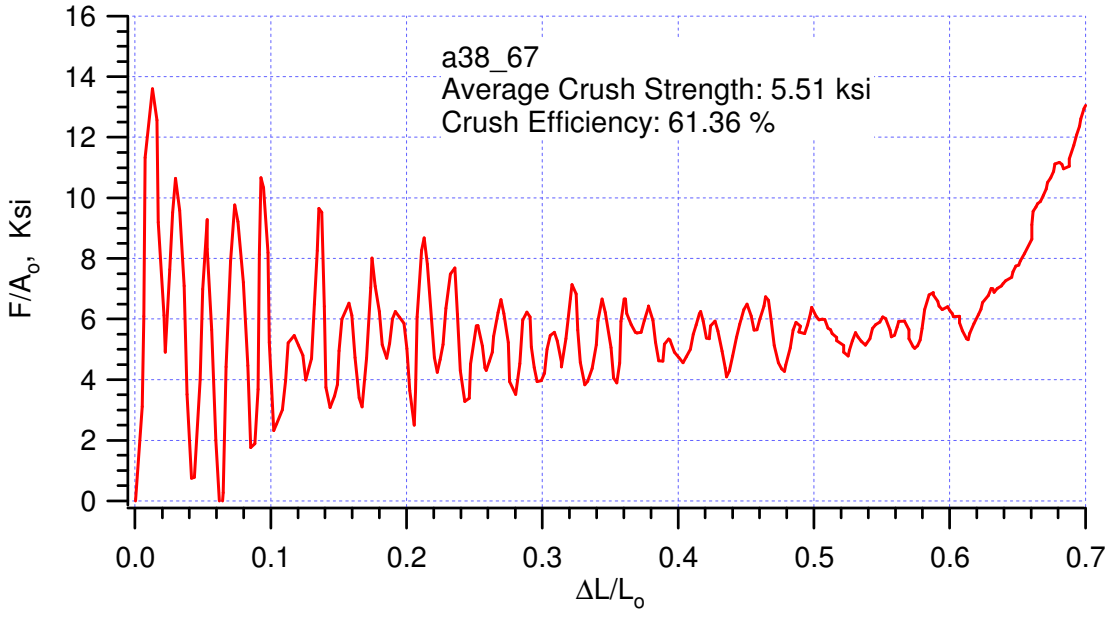
a38_67
Average Crush Strength: 5.51 ksi
Crush Efficiency: 61.36 %
F/A_o, Ksi
ΔL/L_o

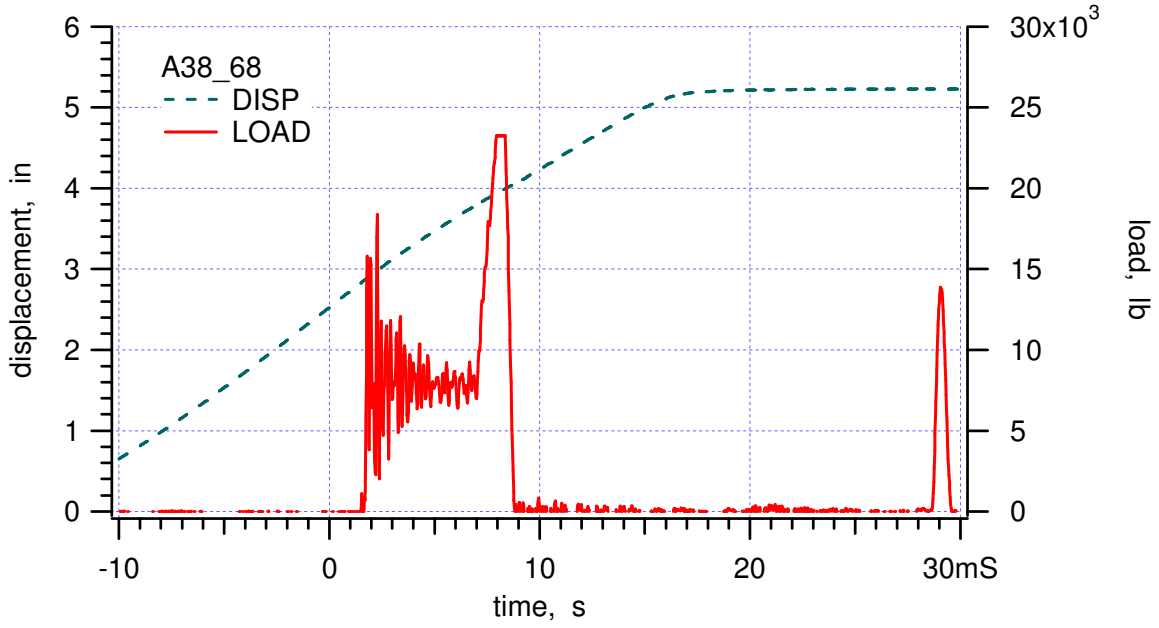
A38_68
DISP
LOAD
displacement, in
load, lb
30x10^3
time, s
-10
0
10
20
30mS

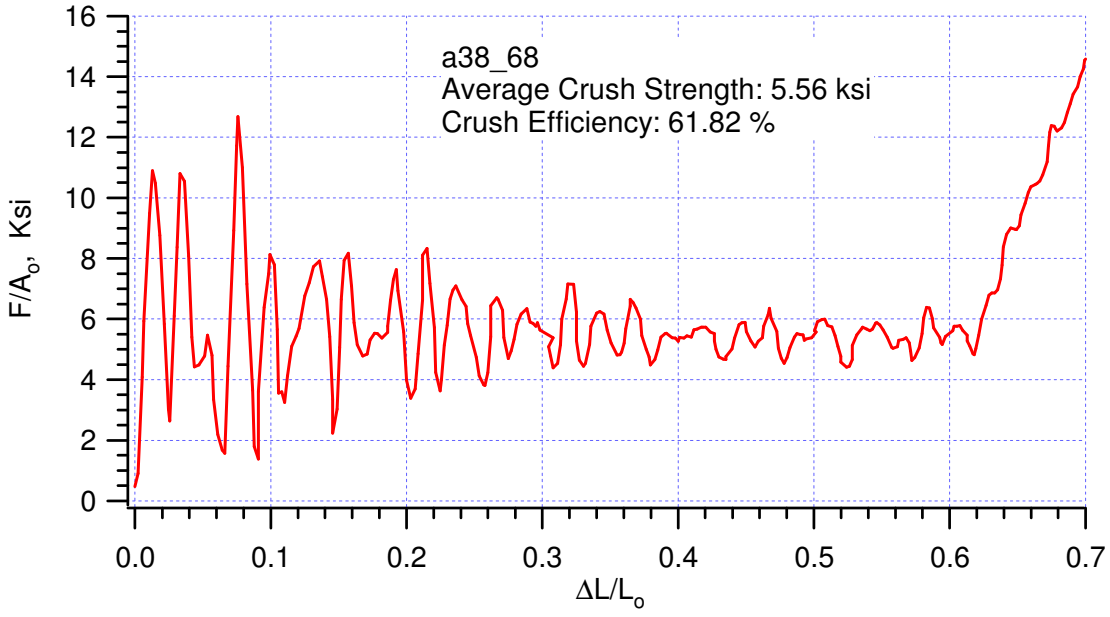
a38_68
Average Crush Strength: 5.56 ksi
Crush Efficiency: 61.82 %
F/A_o, Ksi
ΔL/L_o

Appendix II (memo000118)

Experimental results of Hexcel 38 crushed in t-direction at 165 ^{o}F

Specimen	d_1, in	d_2, in	d_3, in	Weight, lb	Density, pcf	Temperature, degree F	Crush Velocity, ft/s	Crush strenght, ksi	Crush efficiency, %	Remarks
H38_30	1.200	1.199	1.494	0.0484	38.94	165	13.66	6.38	64.15	
H38_31	1.197	1.197	1.507	0.0485	38.78	165	13.73	6.50	65.40	
H38_32	1.201	1.196	1.503	0.0483	38.68	165	13.92	6.28	62.58	
H38_33	1.197	1.200	1.509	0.0482	38.42	165	13.99	6.26	62.24	
H38_34	1.202	1.202	1.499	0.0486	38.77	165	13.91	6.68	64.68	
H38_35	1.196	1.198	1.499	0.0483	38.86	165	14.02	6.47	65.00	
H38_36	1.195	1.200	1.502	0.0484	38.84	165	13.86	6.69	65.09	
H38_37	1.189	1.207	1.510	0.0481	38.34	165	13.62	6.20	64.11	
H38_38	1.205	1.192	1.502	0.0487	39.02	165	13.66	6.51	64.45	
H38_39	1.191	1.196	1.505	0.0475	38.26	165	13.99	6.15	64.53	
H38_40	1.188	1.205	1.500	0.0485	39.07	165				R2
H38_41	1.192	1.202	1.501	0.0481	38.65	165	13.90	6.46	65.56	
H38_42	1.193	1.208	1.504	0.0484	38.58	165	13.75	6.44	64.68	
H38_43	1.197	1.194	1.508	0.0482	38.67	165	13.74	6.43	63.34	
H38_44	1.202	1.195	1.506	0.0479	38.29	165	13.84	6.37	64.81	
H38_45	1.195	1.202	1.502	0.0480	38.48	165	13.85	6.54	63.38	
H38_46	1.207	1.189	1.491	0.0476	38.40	165	13.76	6.55	64.92	
				max	39.07		14.02	6.69	65.56	
				min	38.26		13.62	6.15	62.24	
				average	38.65		13.82	6.43	64.31	
				std deviation	0.25		0.13	0.15	0.96	
				median	38.66		13.84	6.45	64.61	
Remarks										
R2	*shear pin broke early, did not reach lock up*									

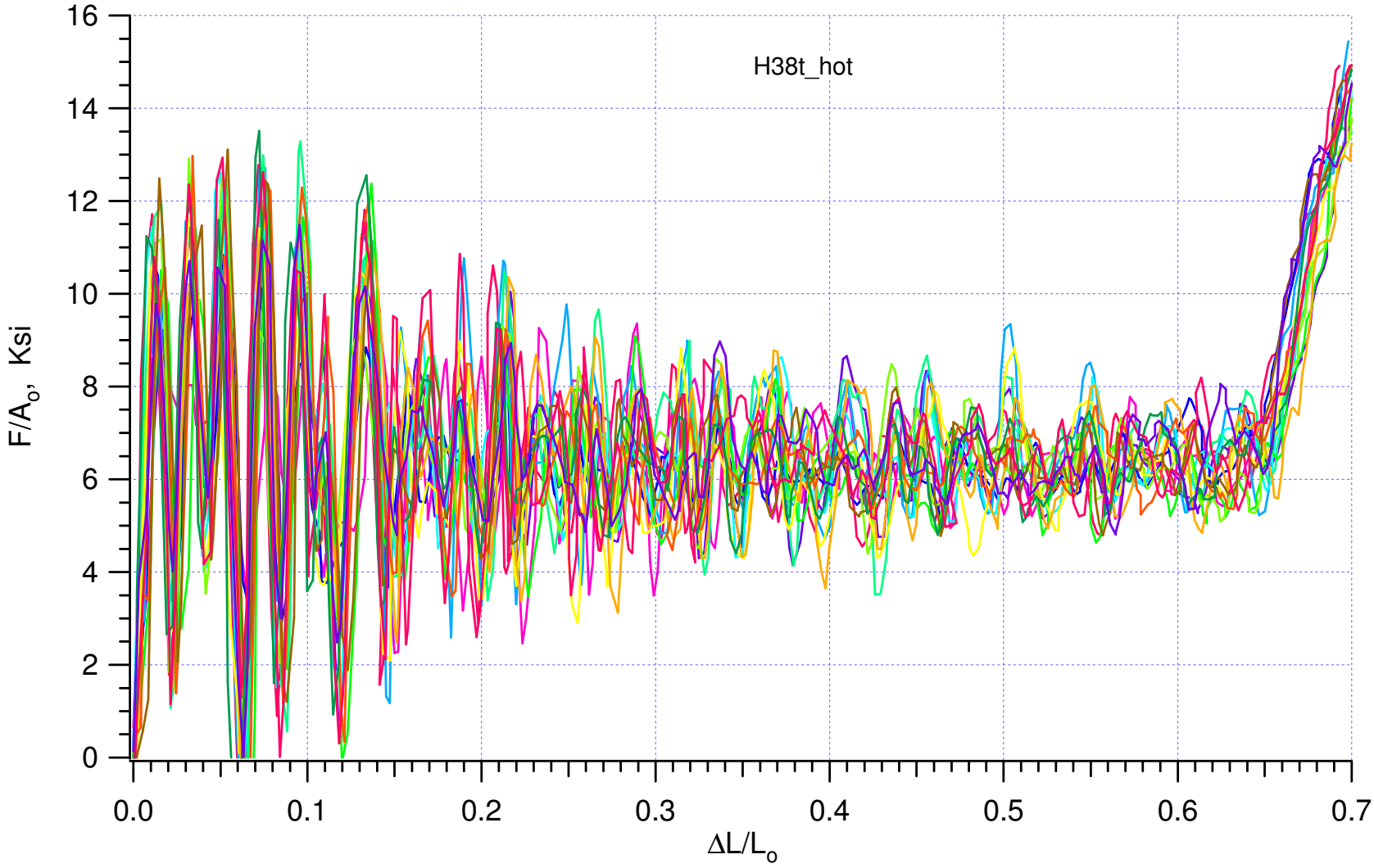
H38t_hot
F/A$_o$, Ksi
$\Delta L/L_o$
0
2
4
6
8
10
12
14
16
0.0
0.1
0.2
0.3
0.4
0.5
0.6
0.7

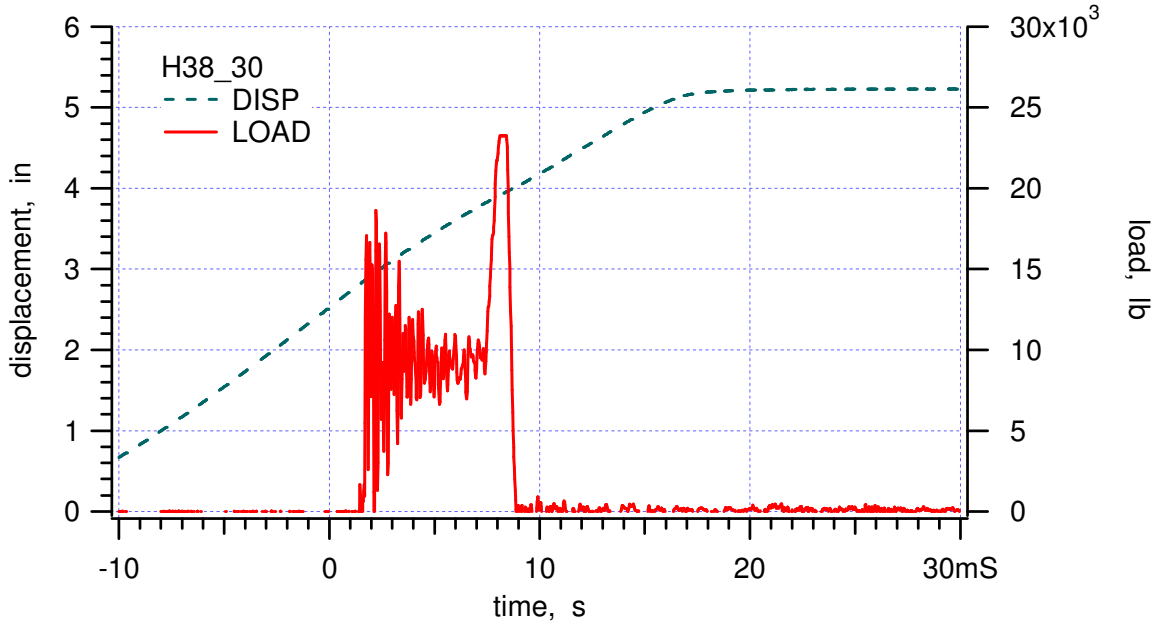
H38_30
DISP
LOAD
displacement, in
load, lb
30x10^3
time, s
-10
0
10
20
30mS

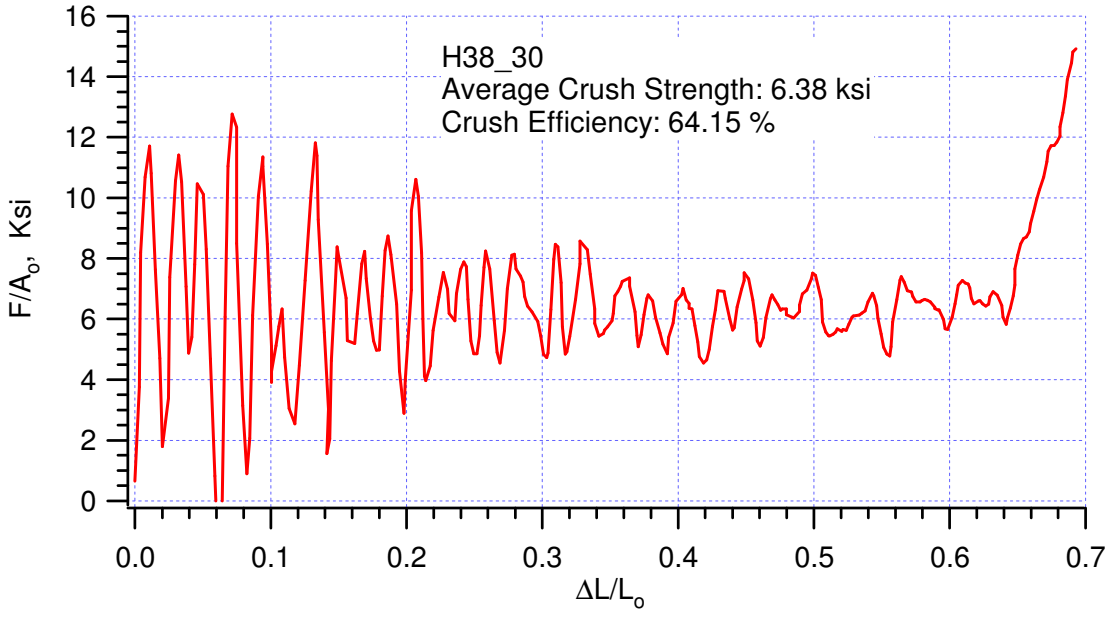
H38_30
Average Crush Strength: 6.38 ksi
Crush Efficiency: 64.15 %
F/A_o, Ksi
ΔL/L_o

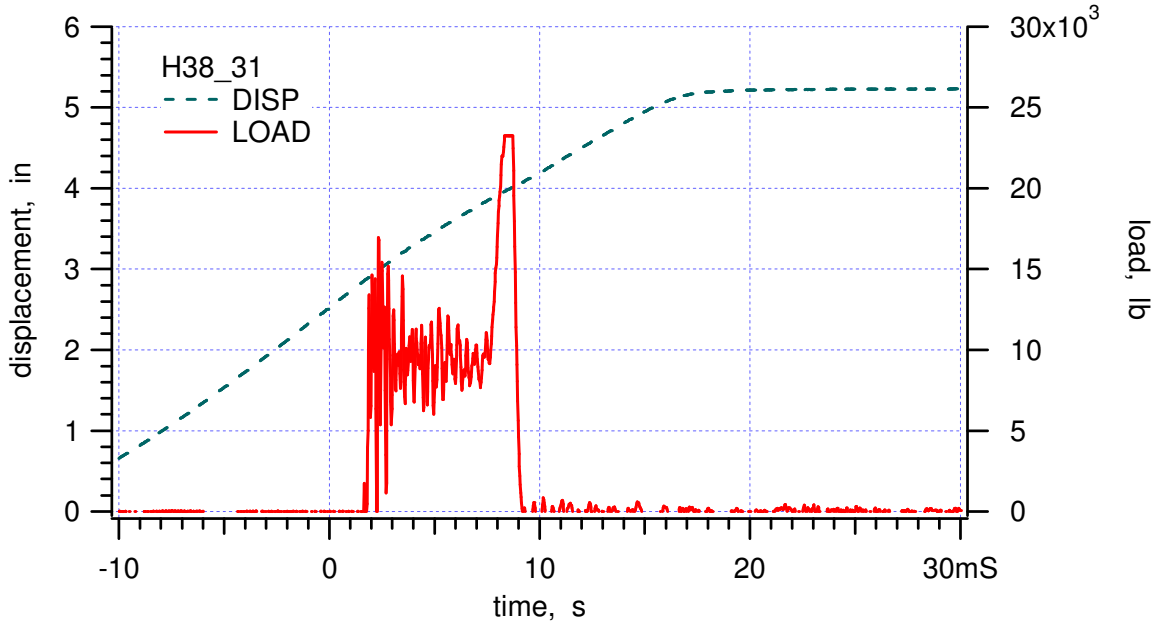
H38_31
DISP
LOAD
displacement, in
load, lb
30x10^3
time, s
-10
0
10
20
30mS

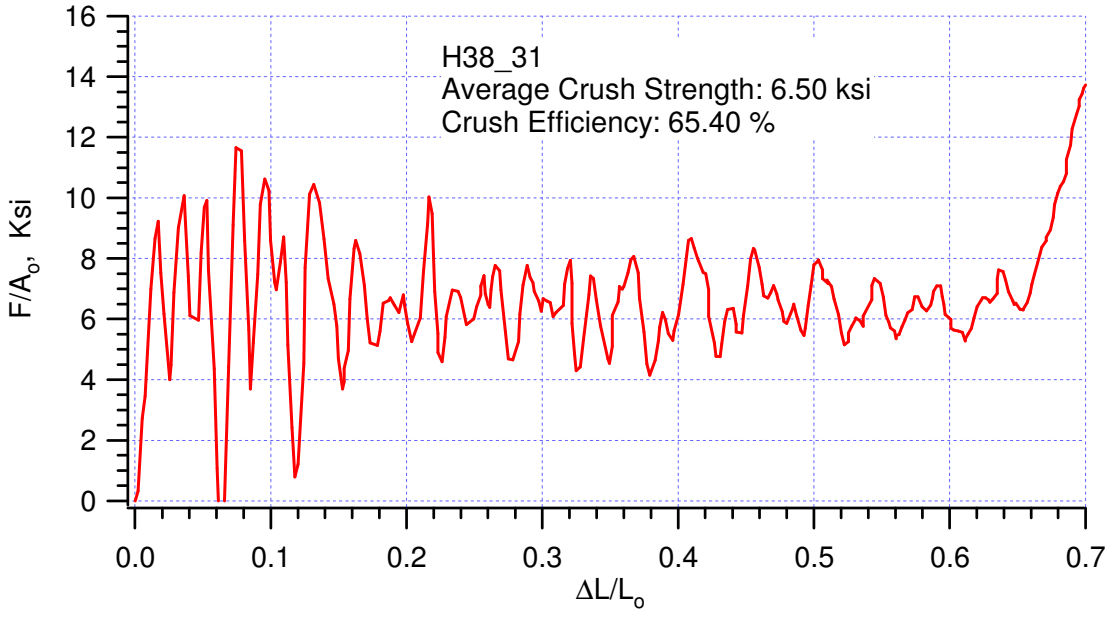
H38_31
Average Crush Strength: 6.50 ksi
Crush Efficiency: 65.40 %
F/A_o, Ksi
ΔL/L_o

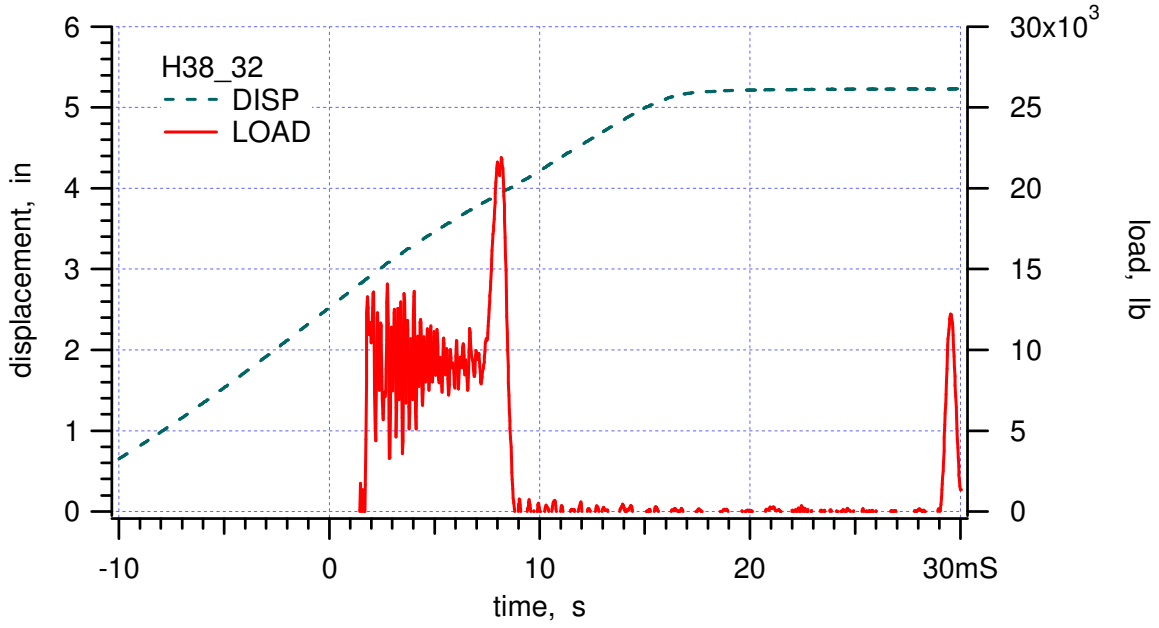
H38_32
DISP
LOAD
displacement, in
load, lb
30x10^3
time, s
-10
0
10
20
30mS

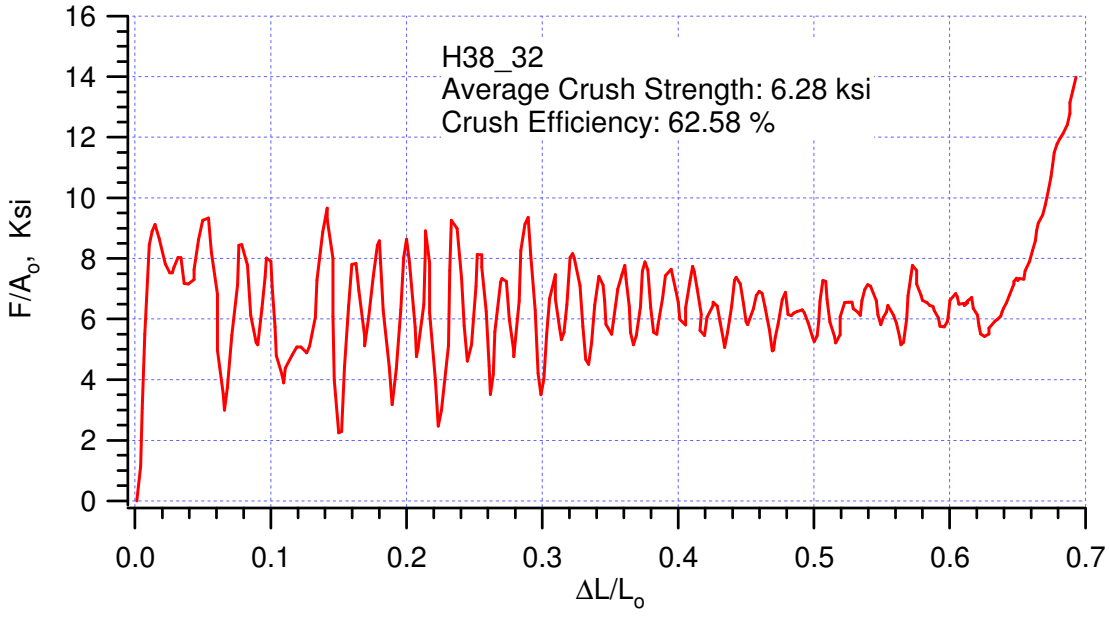
H38_32
Average Crush Strength: 6.28 ksi
Crush Efficiency: 62.58 %
F/A_o, Ksi
ΔL/L_o

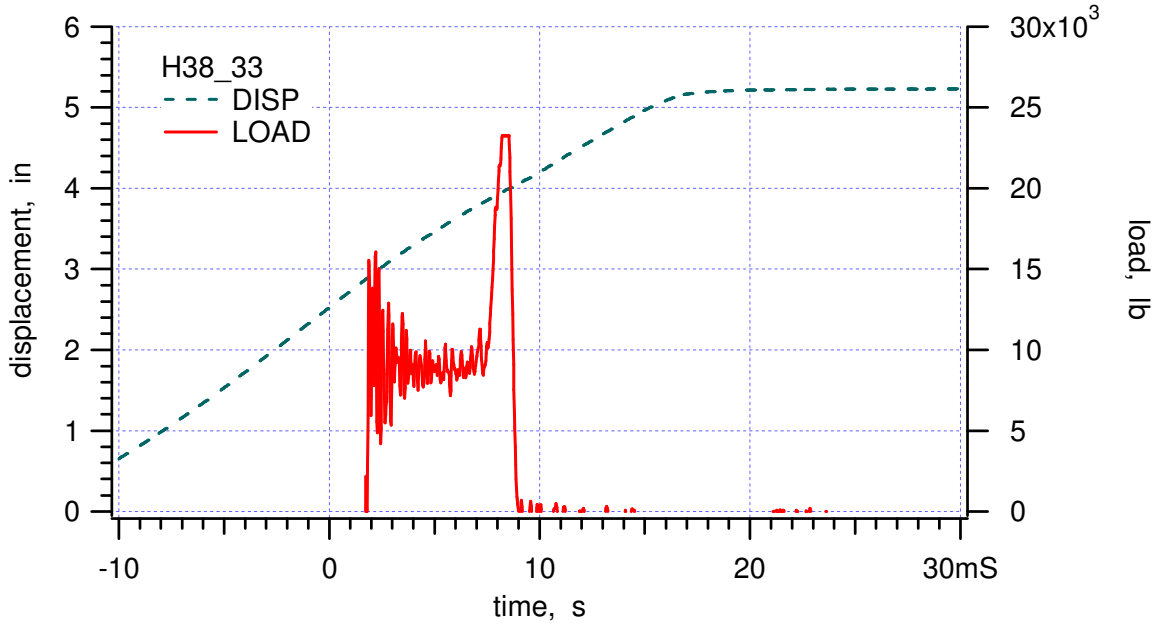
H38_33
DISP
LOAD
displacement, in
load, lb
30x10^3
time, s
-10
0
10
20
30mS

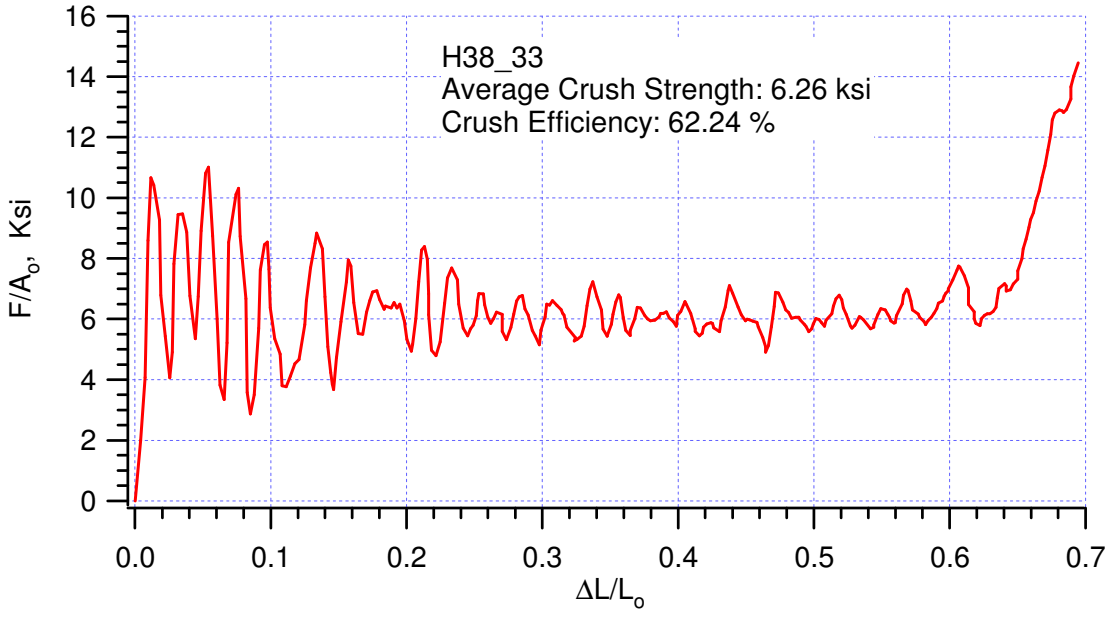
H38_33
Average Crush Strength: 6.26 ksi
Crush Efficiency: 62.24 %
F/A_o, Ksi
ΔL/L_o

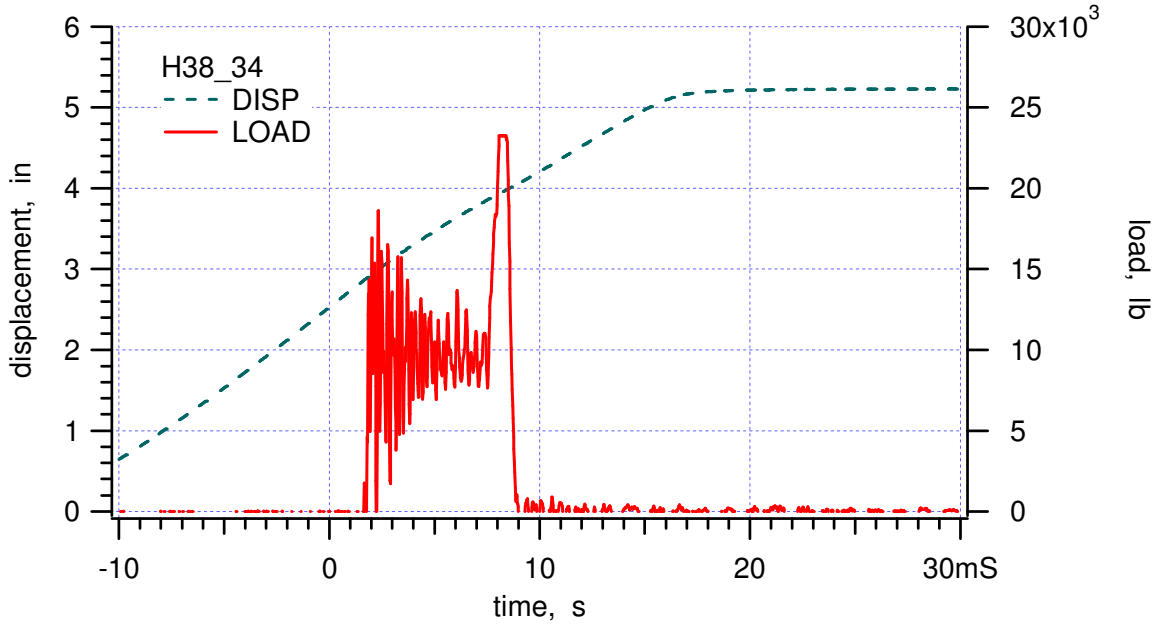
H38_34
DISP
LOAD
displacement, in
load, lb
30x10^3
time, s
-10
0
10
20
30mS

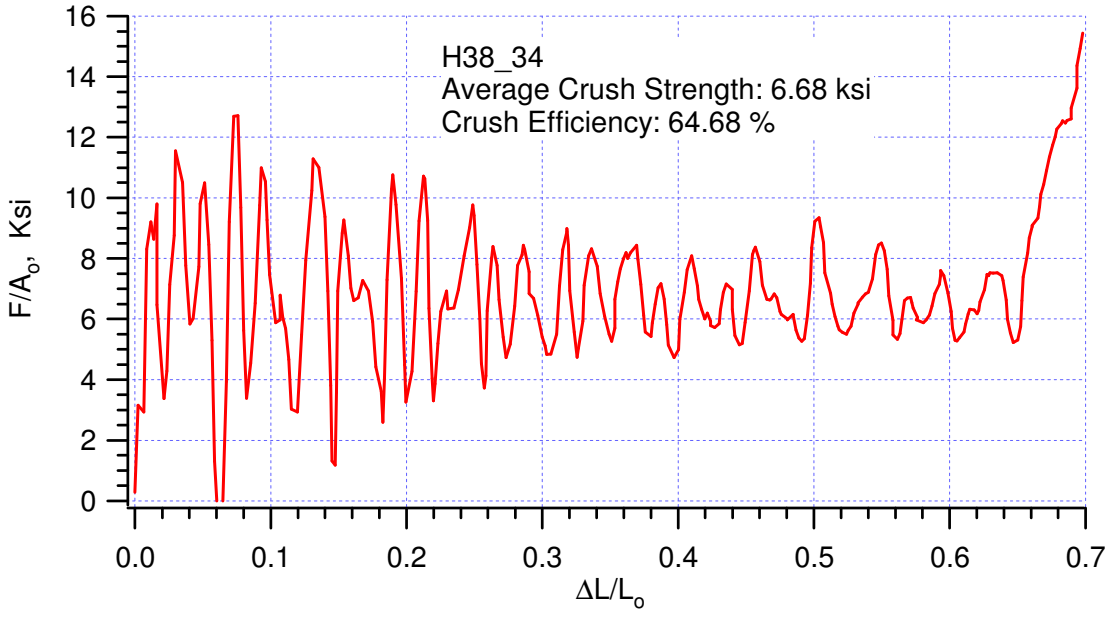
H38_34
Average Crush Strength: 6.68 ksi
Crush Efficiency: 64.68 %
F/A_o, Ksi
ΔL/L_o

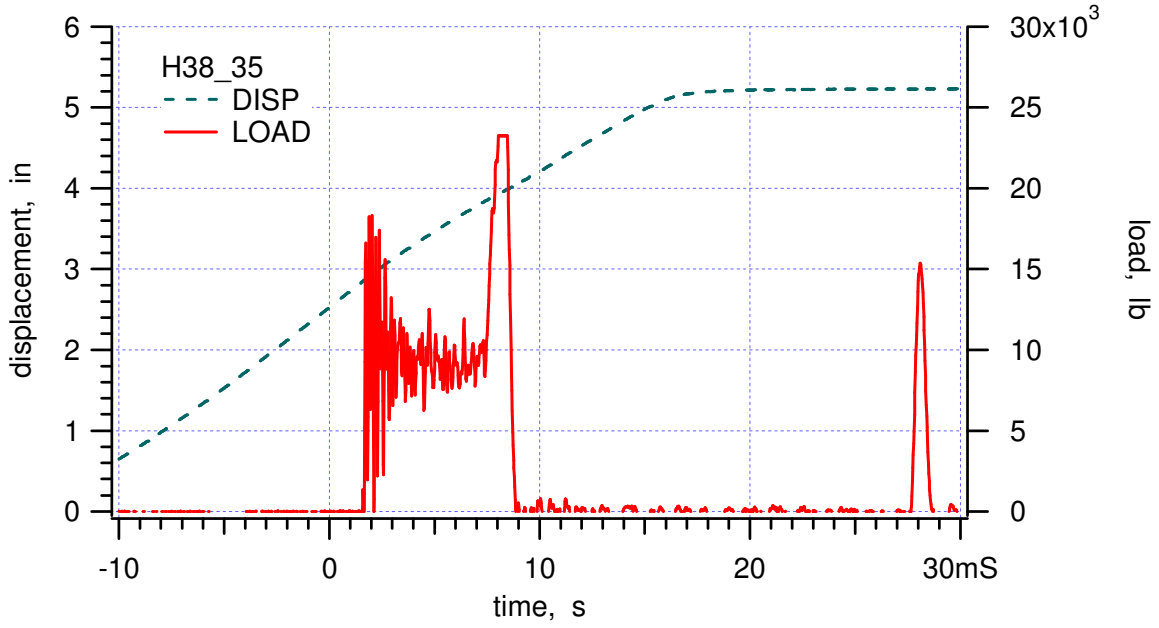
H38_35
DISP
LOAD
displacement, in
load, lb
30x10^3
time, s
-10
0
10
20
30mS

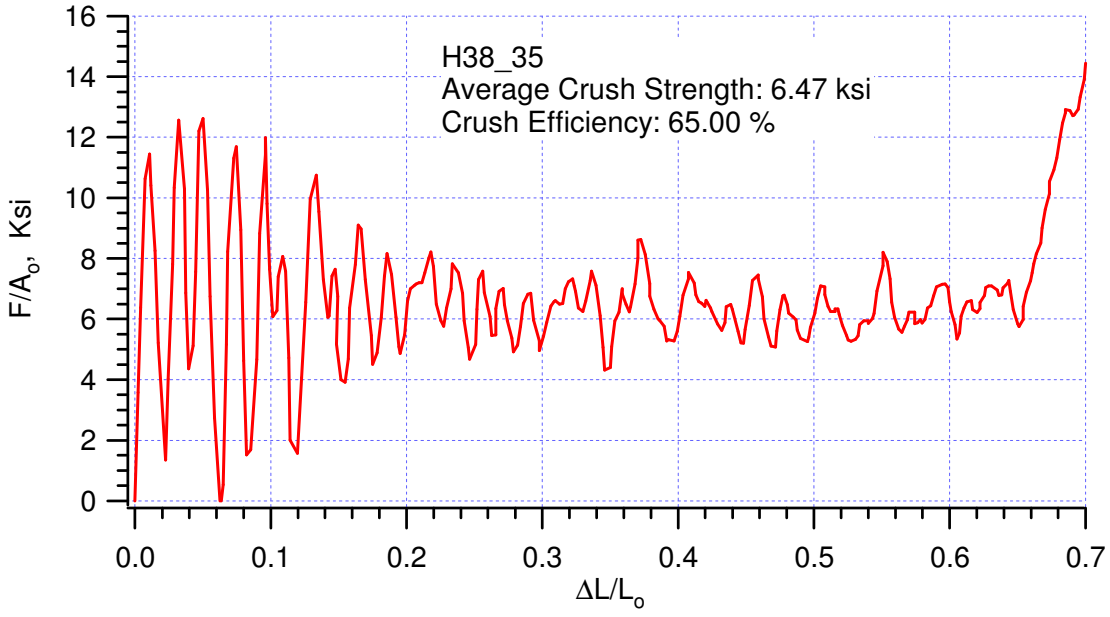
H38_35
Average Crush Strength: 6.47 ksi
Crush Efficiency: 65.00 %
F/A_o, Ksi
ΔL/L_o

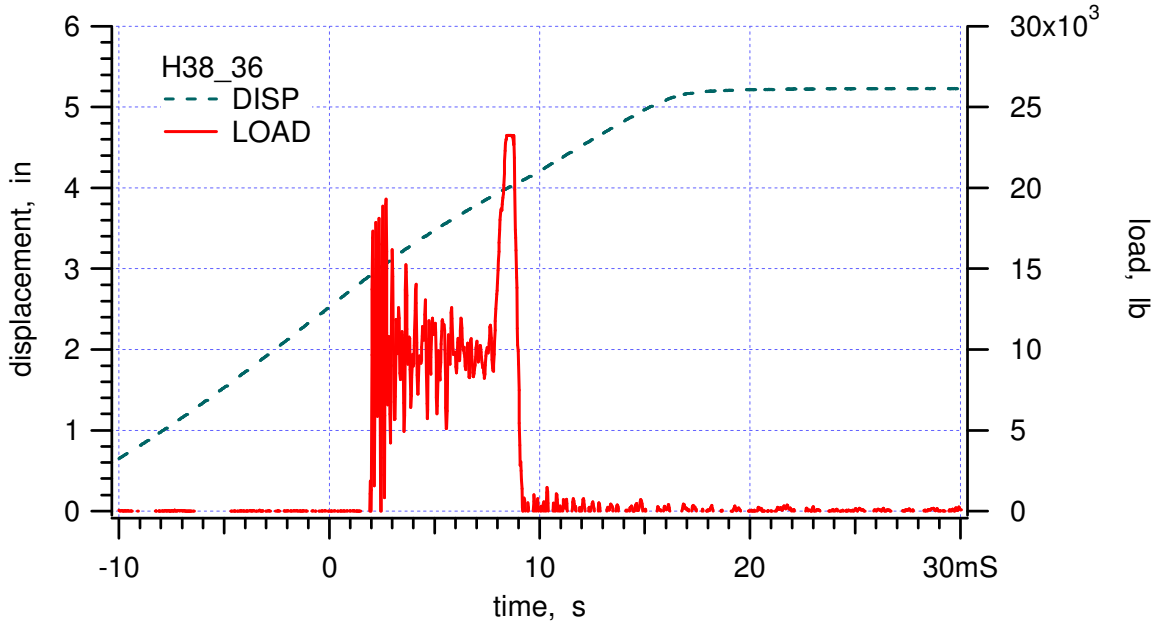
H38_36
DISP
LOAD
displacement, in
load, lb
30x10^3
time, s
-10
0
10
20
30mS

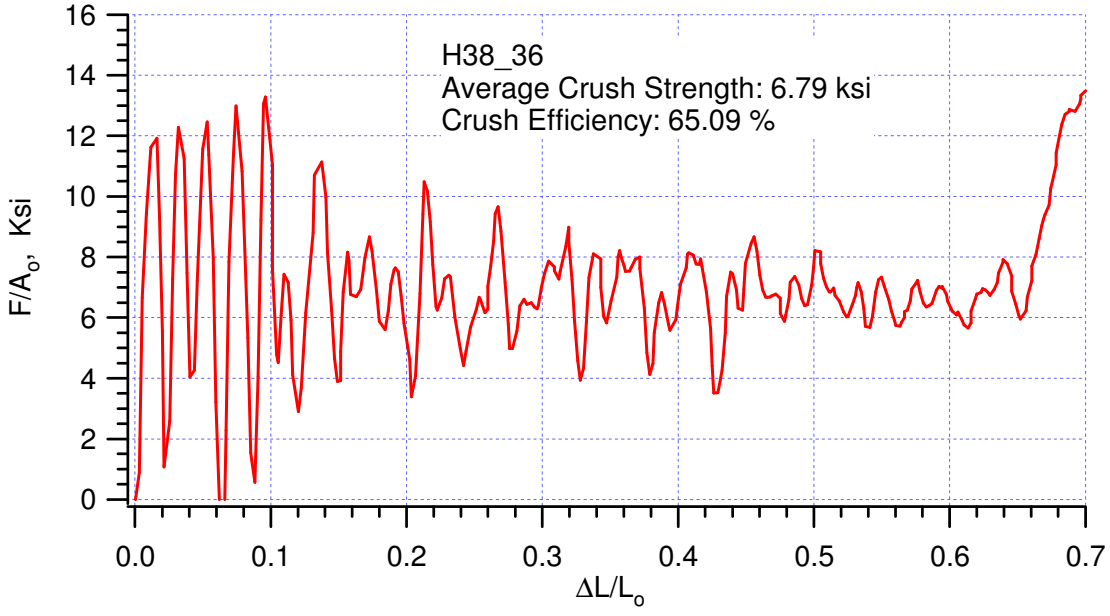
H38_36
Average Crush Strength: 6.79 ksi
Crush Efficiency: 65.09 %
F/A_o, Ksi
ΔL/L_o

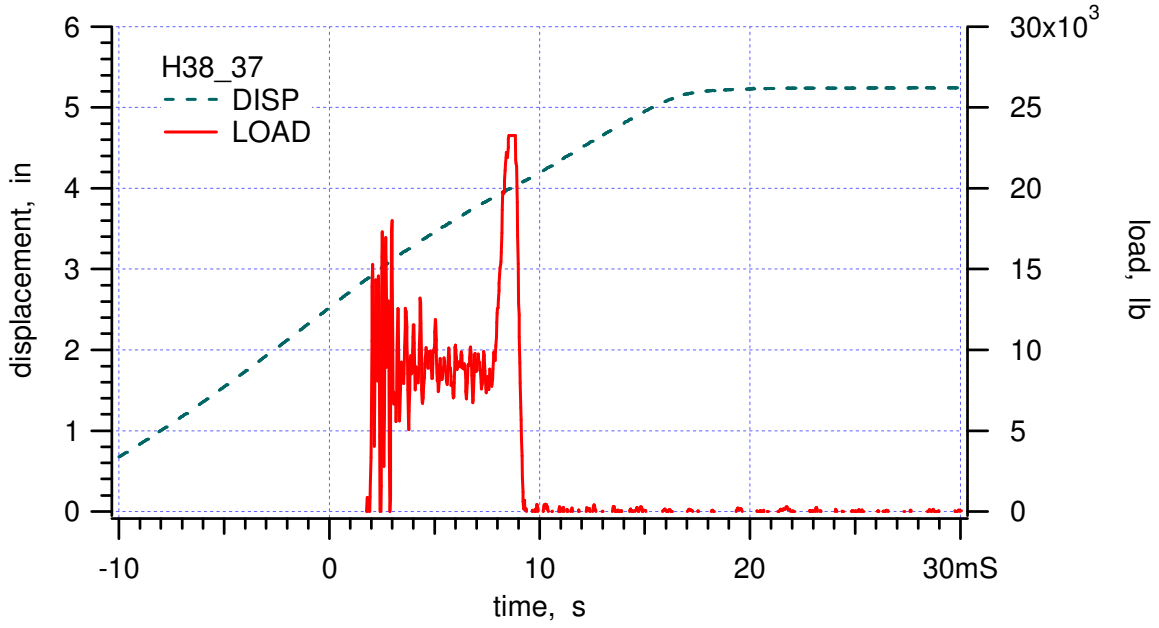
H38_37
DISP
LOAD
displacement, in
load, lb
time, s
30x10^3
-10
0
10
20
30mS

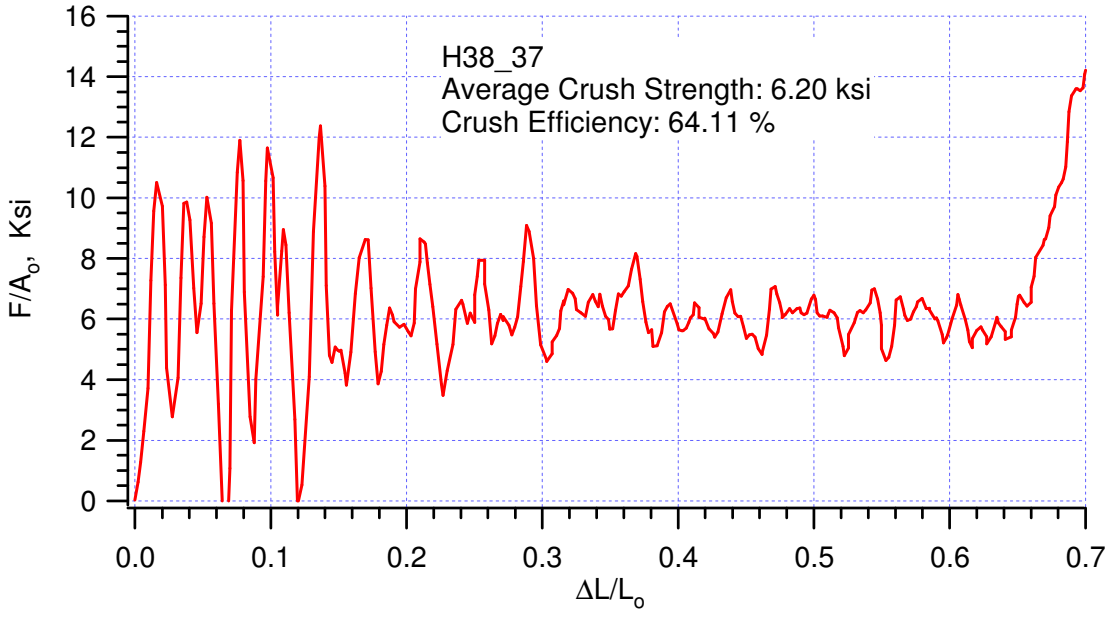
H38_37
Average Crush Strength: 6.20 ksi
Crush Efficiency: 64.11 %
F/A_o, Ksi
ΔL/L_o

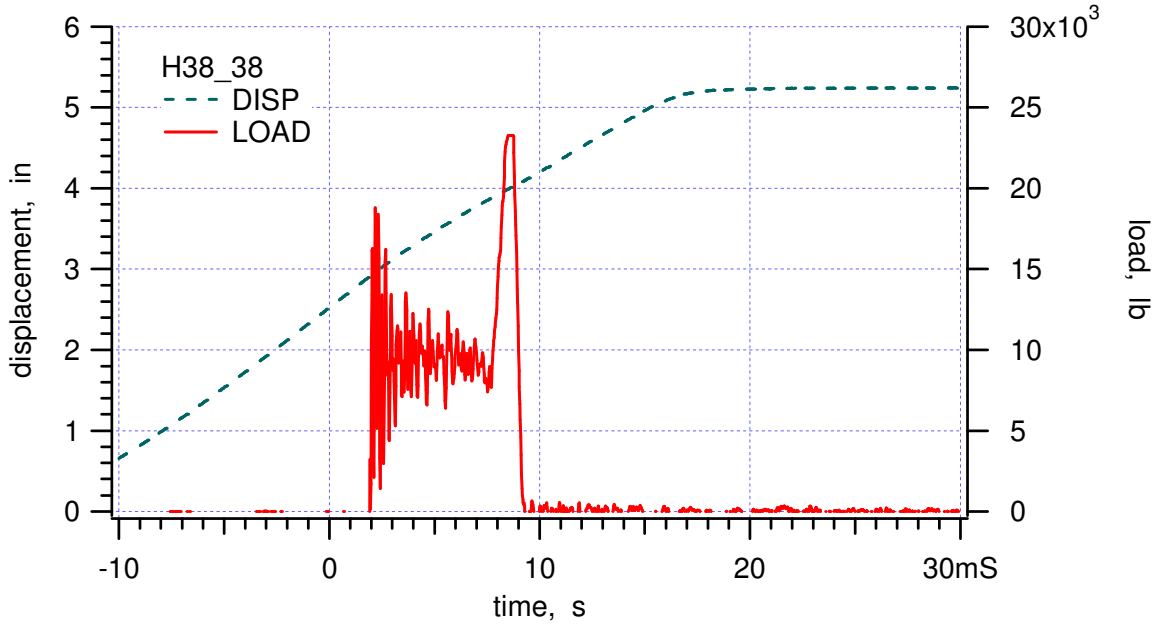
H38_38
DISP
LOAD
displacement, in
load, lb
30x10^3
time, s
-10
0
10
20
30mS

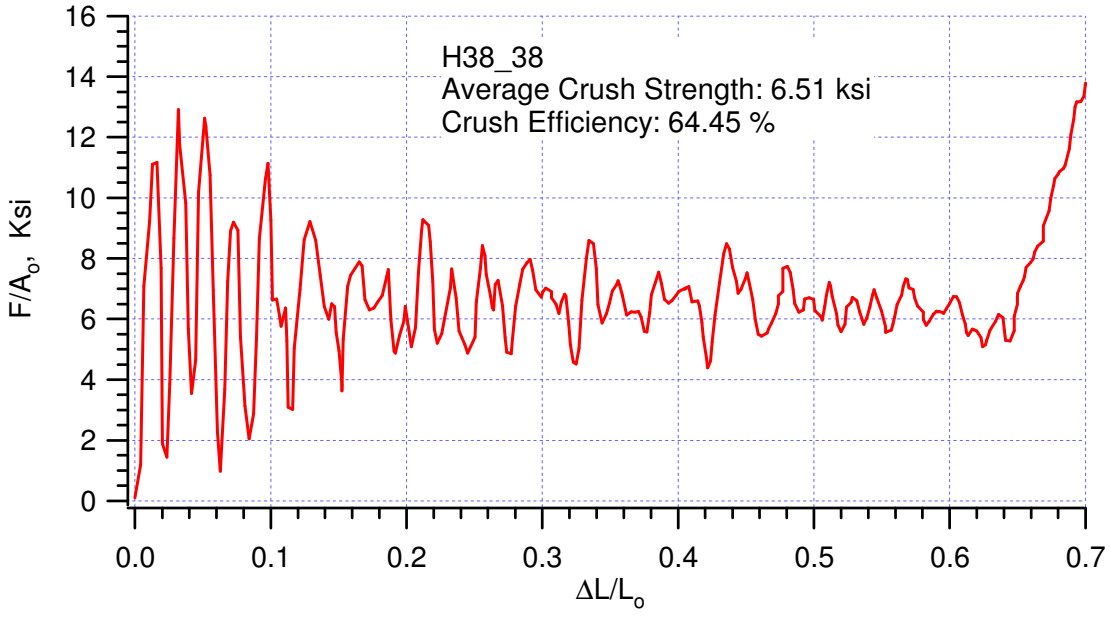
H38_38
Average Crush Strength: 6.51 ksi
Crush Efficiency: 64.45 %
F/A_o, Ksi
ΔL/L_o

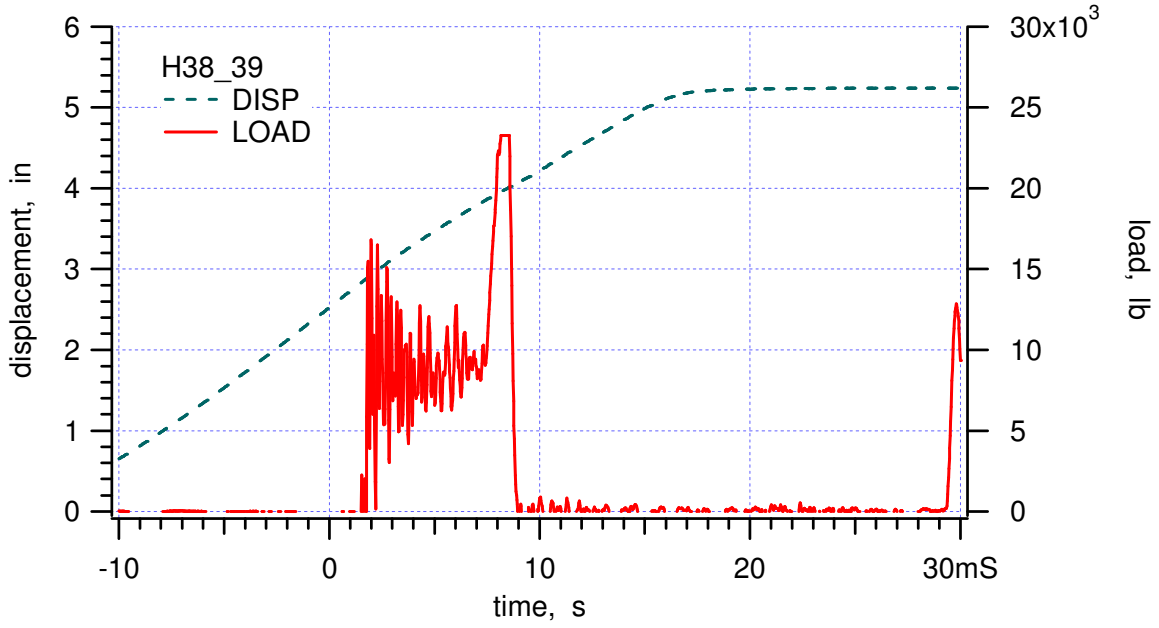
H38_39
DISP
LOAD
displacement, in
load, lb
30x10^3
time, s
-10
0
10
20
30mS

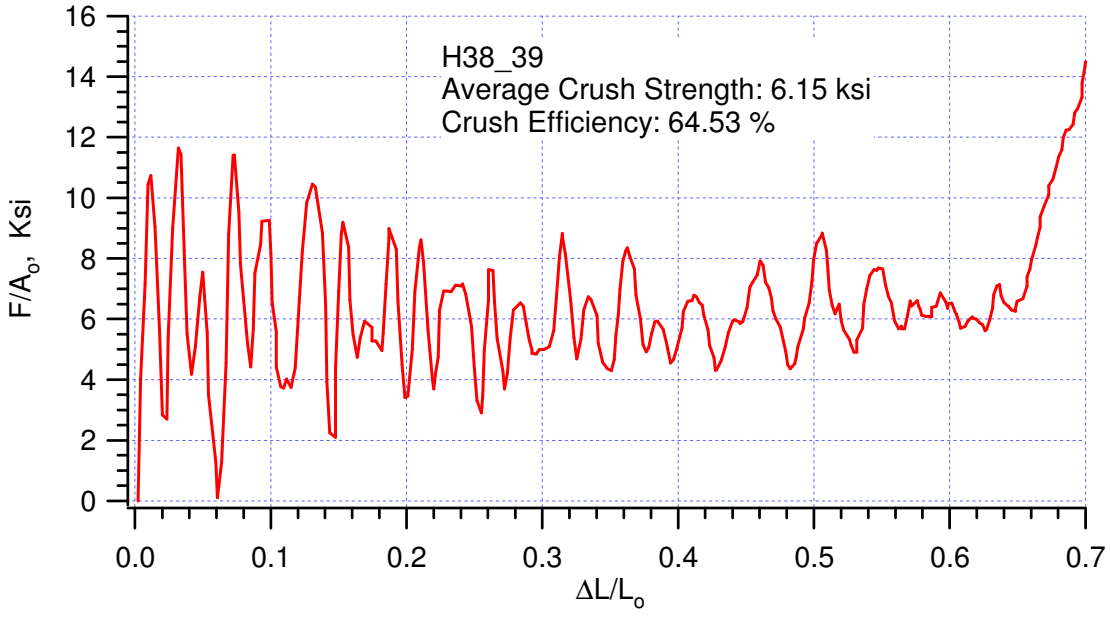
H38_39
Average Crush Strength: 6.15 ksi
Crush Efficiency: 64.53 %
F/A_o, Ksi
ΔL/L_o

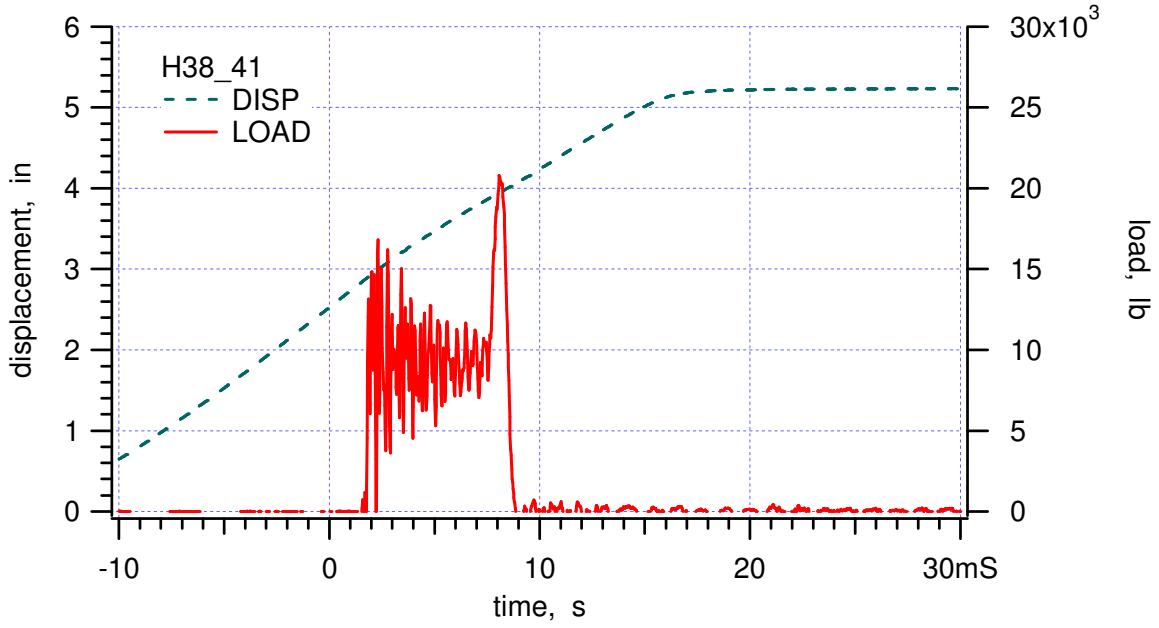
H38_41
DISP
LOAD
displacement, in
load, lb
30x10^3
time, s
-10
0
10
20
30mS

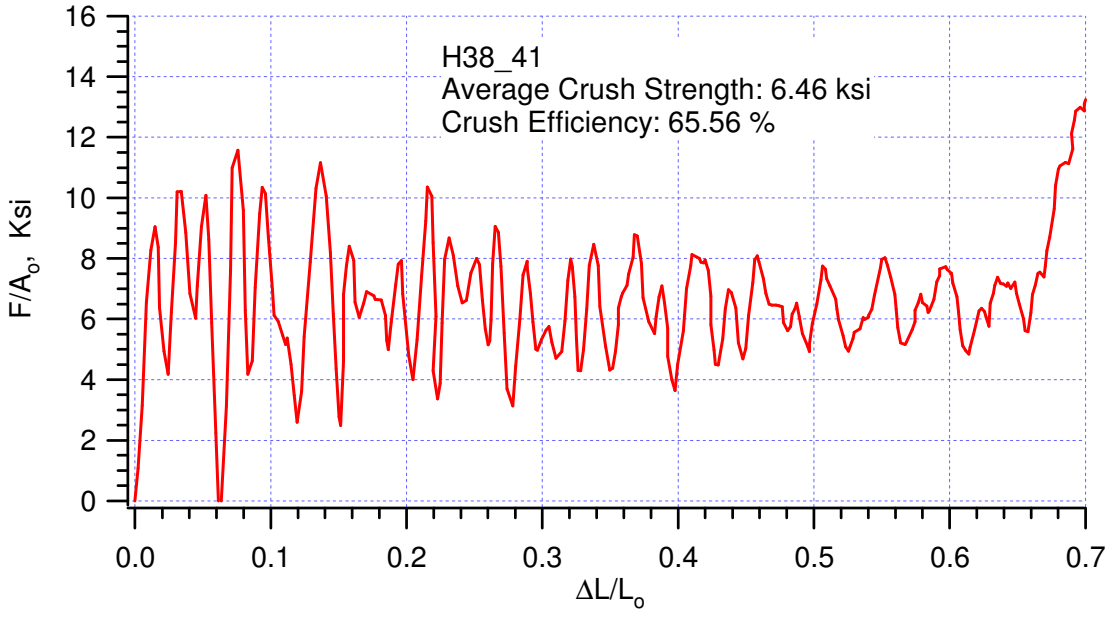
H38_41
Average Crush Strength: 6.46 ksi
Crush Efficiency: 65.56 %
F/A_o, Ksi
ΔL/L_o

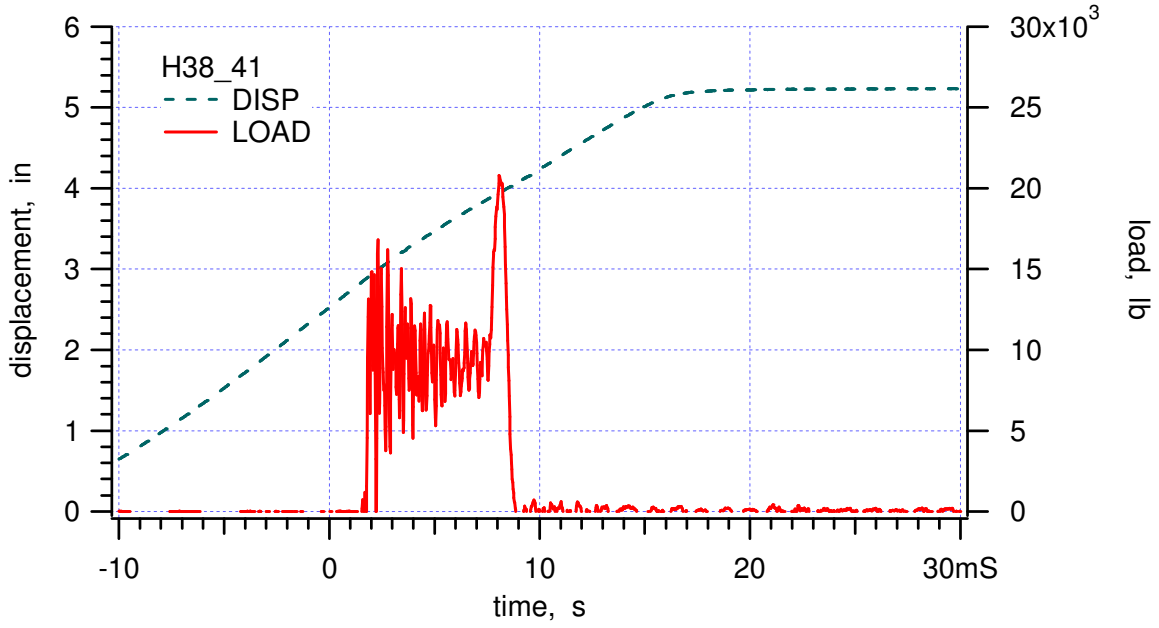
H38_41
DISP
LOAD
displacement, in
load, lb
30x10^3
time, s
-10
0
10
20
30mS

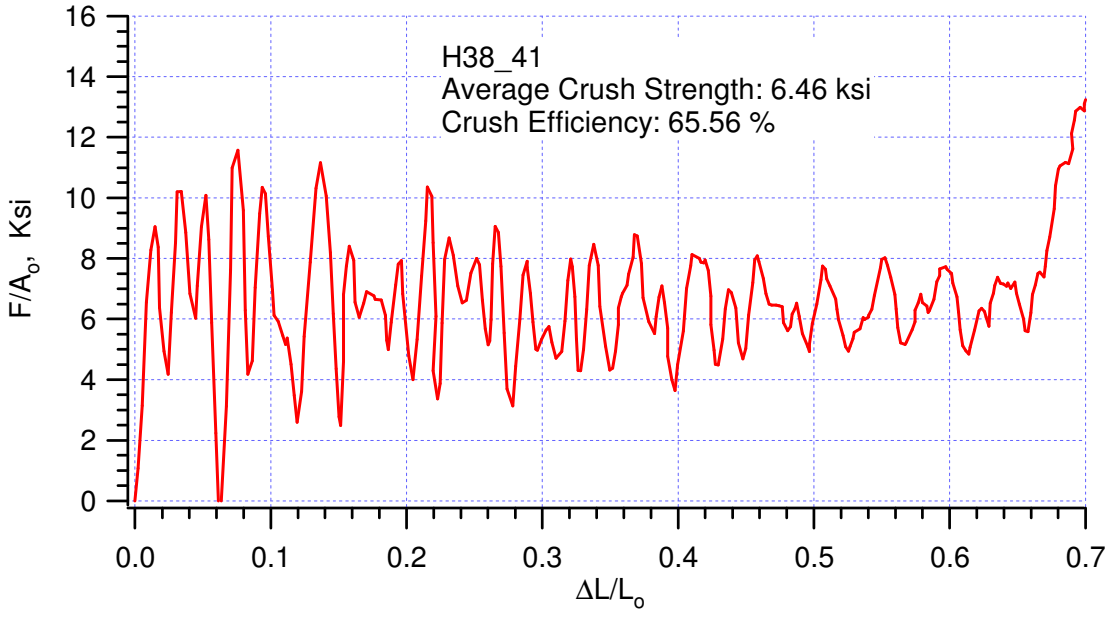
H38_41
Average Crush Strength: 6.46 ksi
Crush Efficiency: 65.56 %
F/A_o, Ksi
ΔL/L_o

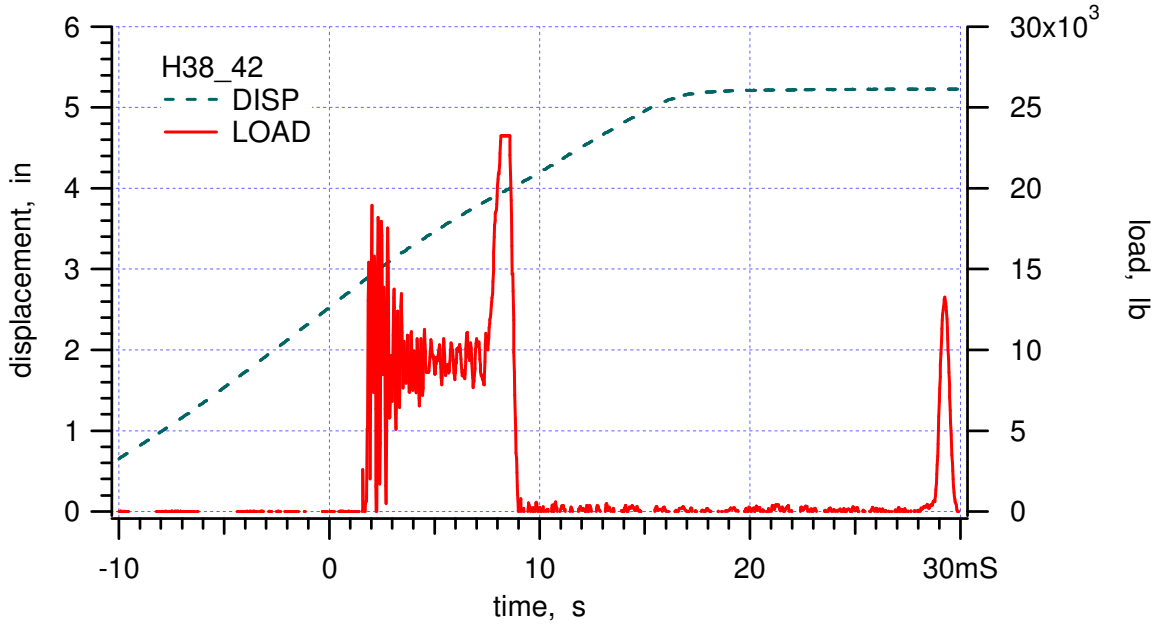
H38_42
DISP
LOAD
displacement, in
load, lb
time, s
30x10^3
25
20
15
10
5
0
-10
0
10
20
30mS
1
2
3
4
5
6

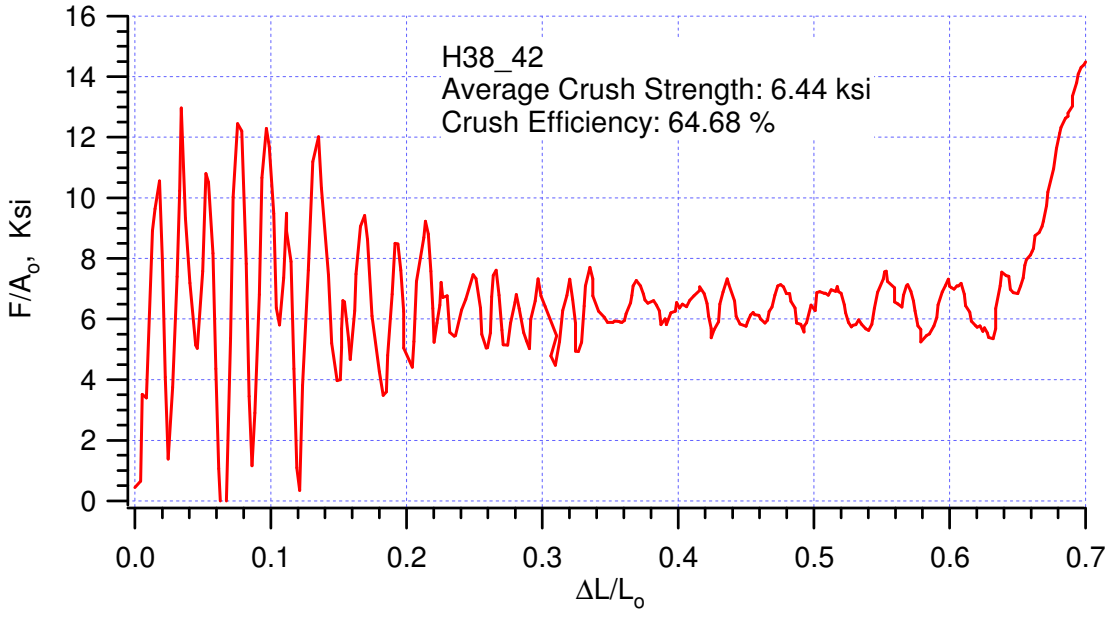
H38_42
Average Crush Strength: 6.44 ksi
Crush Efficiency: 64.68 %
F/A_o, Ksi
ΔL/L_o
0.0
0.1
0.2
0.3
0.4
0.5
0.6
0.7
0
2
4
6
8
10
12
14
16

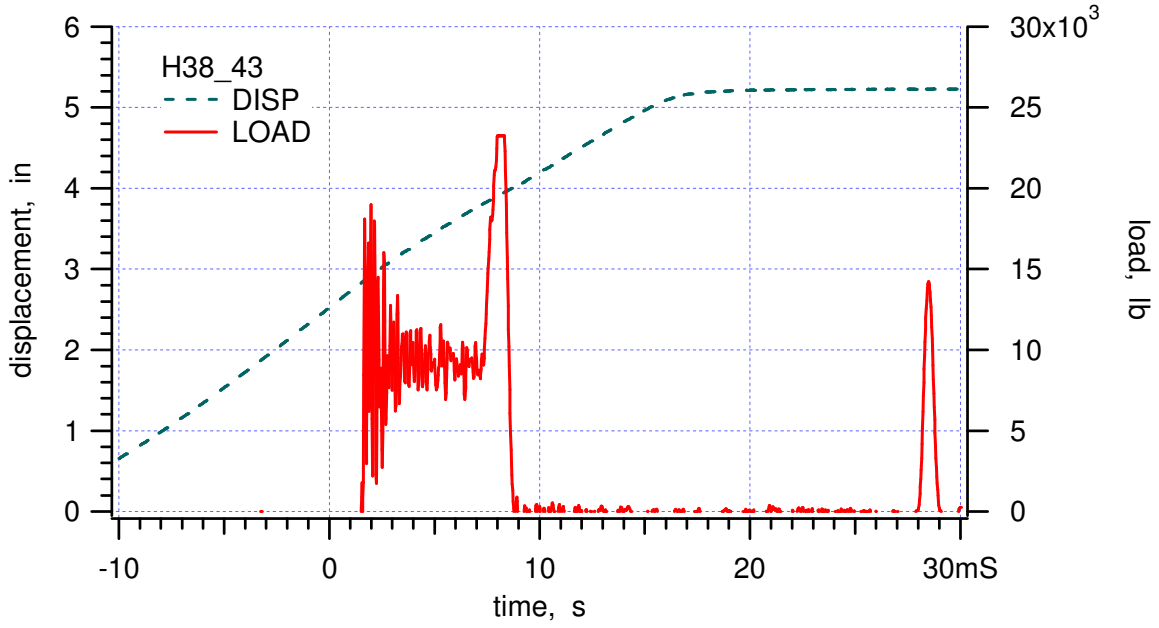
H38_43
DISP
LOAD
displacement, in
load, lb
30x10^3
time, s
-10
0
10
20
30mS

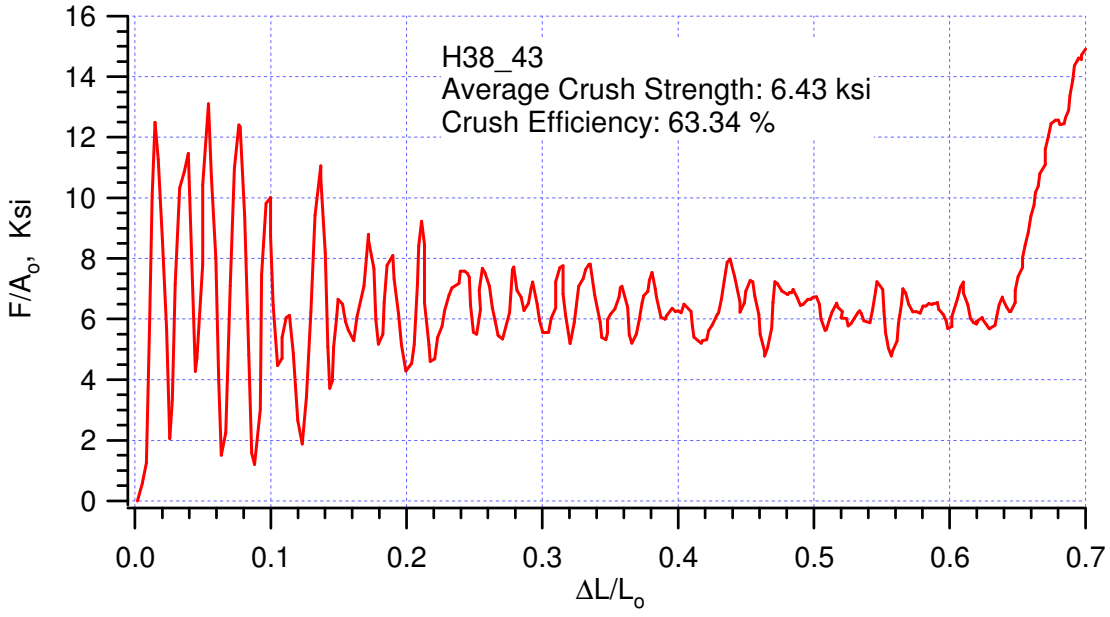
H38_43
Average Crush Strength: 6.43 ksi
Crush Efficiency: 63.34 %
F/A_o, Ksi
ΔL/L_o

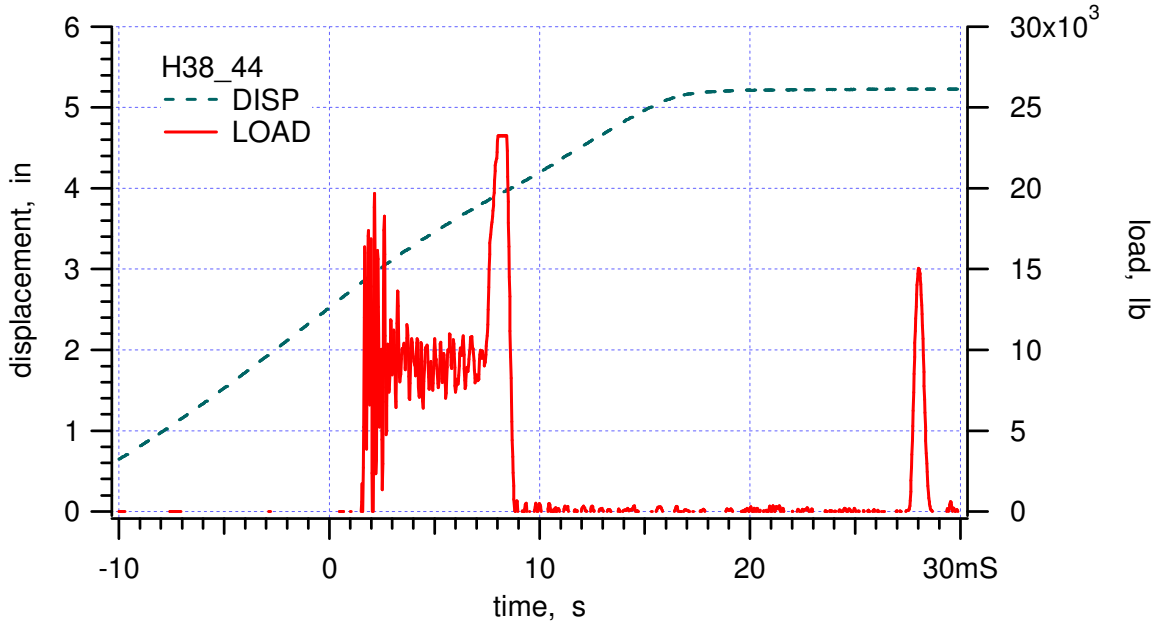
H38_44
DISP
LOAD
displacement, in
load, lb
30x10^3
time, s
-10
0
10
20
30mS

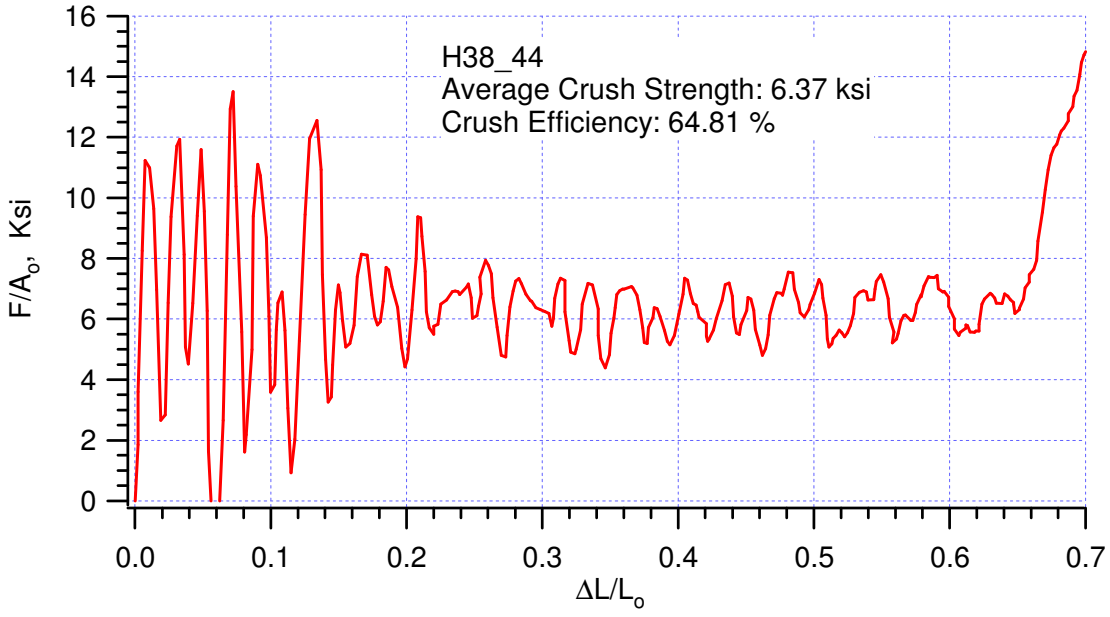
H38_44
Average Crush Strength: 6.37 ksi
Crush Efficiency: 64.81 %
F/A_o, Ksi
ΔL/L_o

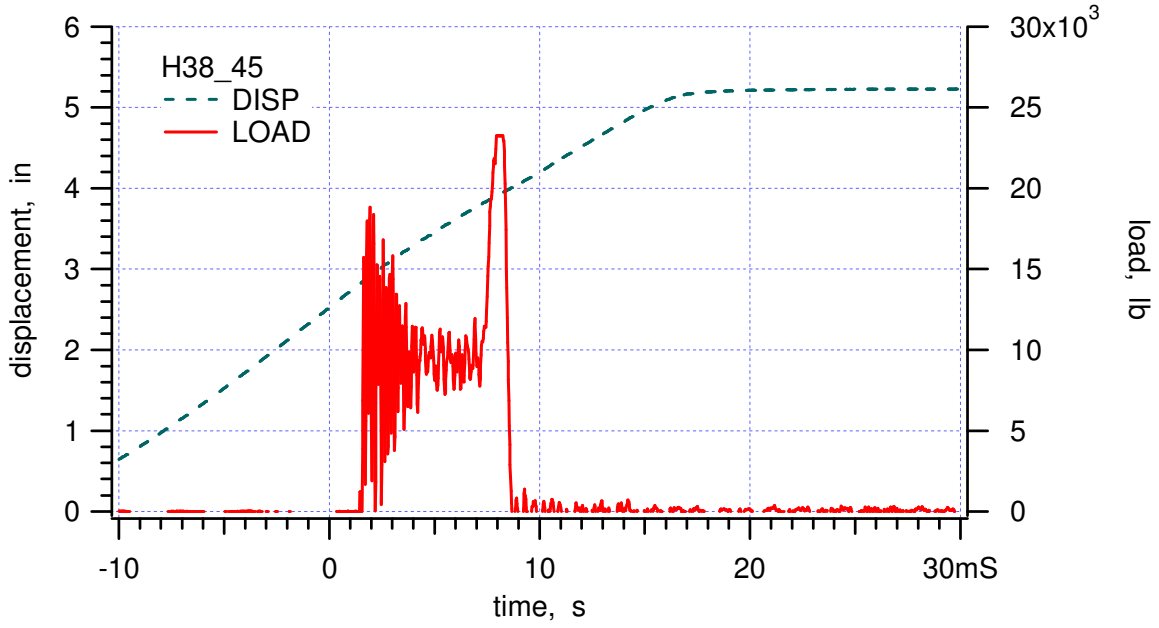
H38_45
DISP
LOAD
displacement, in
load, lb
30x10^3
time, s
-10
0
10
20
30mS

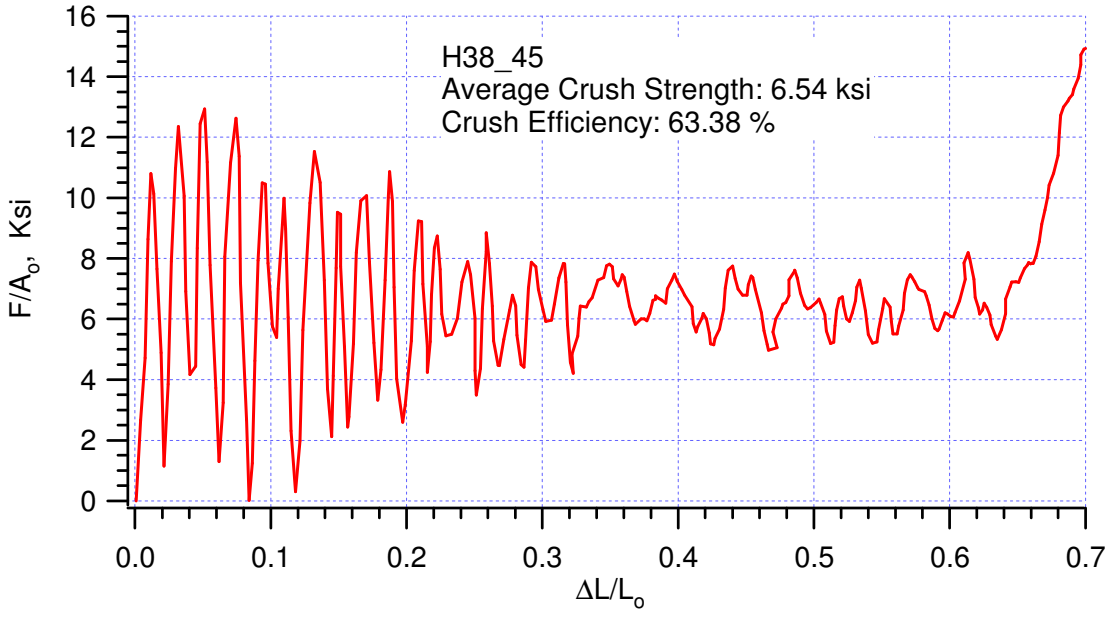
H38_45
Average Crush Strength: 6.54 ksi
Crush Efficiency: 63.38 %
F/A_o, Ksi
ΔL/L_o

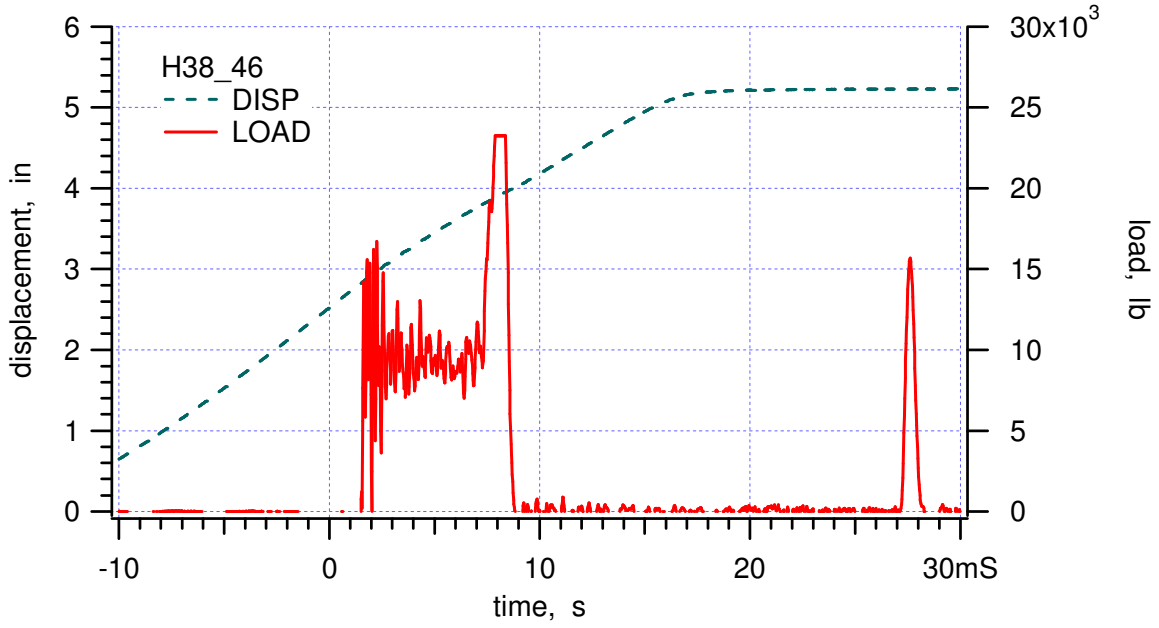
H38_46
DISP
LOAD
displacement, in
load, lb
30x10^3
time, s
-10
0
10
20
30mS

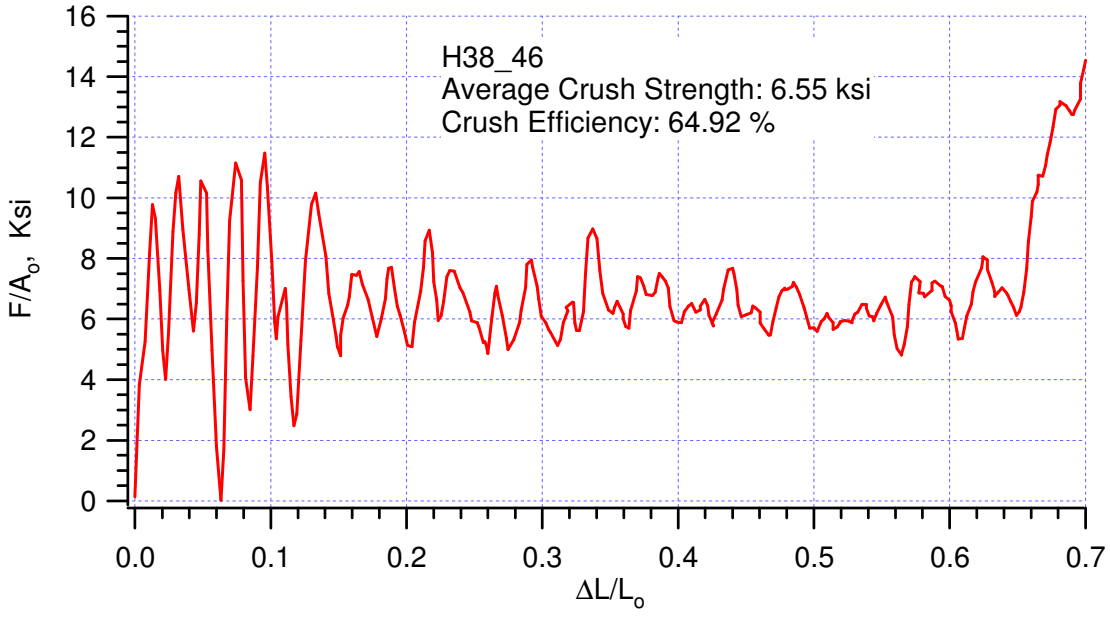
H38_46
Average Crush Strength: 6.55 ksi
Crush Efficiency: 64.92 %
F/A_o, Ksi
ΔL/L_o

APPENDIX XI:

"Moderate Rate Confined Crush Tests of Alcore 35 honeycomb in the t-direction at 165°F," Memo Wei-Yang Lu to Distribution, January 10, 2000

Sandia National Laboratories
Operated for the U.S. Department of Energy by
Sandia Corporation
MS9042
Livermore, CA 94551-0969

date: February 7, 2000

to: Distribution

from: Wei-yang Lu

subject: Moderate Rate Confined Crush Tests of Alcore 35 honeycomb in the t-direction at 165^{o}F

We have completed the experiment of high temperature crush of Alcore 35. These tests, requested by analyst Ken Gwinn, were not on the original matrix. These high temperature data of Alcore 35 are needed for model simulation before the mid-February B61 experiment.

Table 1 summarizes FY00 experimental results, in which the boldface red line is the current high-temperature data of Alcore 35. The results of all Alcore 35 hot tests, a total of 16 specimens, are listed in Table 2. Figure 1 shows all 16 stress-strain curves.

Similar to Alcore 38 and Hexcel 38, the crush strength of Alcore 35 is clearly affected by temperature. Comparing the ambient and 165 ^{o}F, the corresponding crush strengths are 5.74 ksi and 4.94 ksi, respectively, a 16% decrease at the high temperature.

Please see Appendix for detail experimental data.

Distribution:

Darrla Giersch(2167)	MS0481
Darren Hoke(2167)	MS0481
Vernon Willan(2167)	MS0481
Vista Bateman(9126)	MS0553
Tom Carne(9124)	MS0557
Berry Boughten(9132)	MS0557
Jaime Moya(9132)	MS0828
Terry Hinnerichs(9126)	MS0847
Ken Gwinn(9126)	MS0847
John Pott(9126)	MS0847
Rodney May(9126)	MS0847
Mike Neilsen(9123)	MS0847
Bill Scherzinger(9123)	MS0847
Hal Morgan(9123)	MS0847
Wendell Kawahara (8725)	MS904

Table 1. Summary of FY00 experimental results

B61/MAVEN TEST MATRIX				EXPERIMENTAL RESULTS						MEMO
Test #	Honeycomb	Dir.	Temperature, degree F	Specimen	Density, pcf	Impact Speed, ft/s	Crush Strength, ksi	Std Deviation, ksi	Crush Efficiency, %	Date
1 - 15	Alcore 38	T	ambient	rotated	38.82	14.13	6.35	0.08	63.80	991203
16 - 30	Hexcel 38	T	ambient	rotated	38.70	13.67	7.17	0.15	63.89	000110
				rotated	38.78	0.00139	5.88		59.20	"
31 - 45	Alcore 35	T	ambient	rotated	35.39	14.35	5.74	0.18	64.46	000103
46 - 60	Hexcel 35	T	ambient	rotated	37.79	13.83	6.67	0.24	63.91	000110
				rotated	37.89	0.00139	5.83		60.30	"
60 - 75	Alcore 38	T	165	rotated	38.96	14.33	5.49	0.10	62.52	000118
76 - 90	Hexcel 38	T	165	rotated	38.65	13.82	6.43	0.15	64.31	000118
	Alcore 35	**T**	**165**	**rotated**	**35.62**	**14.59**	**4.94**	**0.23**	**62.54**	**000207**
91 - 105	Alcore 38	T	-65							
106 - 120	Hexcel 38	T	-65							
121 - 125	Alcore 38	L	ambient							
126 - 130	Hexcel 38	L	ambient							
131 - 135	Alcore 38	W	ambient							
136 - 140	Hexcel 38	W	ambient							
159 - 161	Alcore 38	T	ambient	segmented	41.41	0.0014	6.14		52.30	991130
162 - 164	Hexcel 38	T	ambient	segmented	41.29	0.0014	6.85		53.70	991213

Table 2. Experimental results of Alcore 35 crushed in t-direction at 165 ^{o}F

Specimen	d_1, in	d_2, in	d_3, in	Weight, lb	Density, pcf	Temperature, degree F	Crush Velocity, ft/s	Crush strenght, ksi	Crush efficiency, %	Remarks
A35_30	1.189	1.196	1.504	0.0444	35.84	165	14.05	4.95	60.96	
A35_31	1.190	1.198	1.503	0.0444	35.77	165	14.25	5.21	62.28	
A35_32	1.190	1.197	1.504	0.0446	35.94	165	14.49	5.19	61.92	
A35_33	1.197	1.196	1.509	0.0446	35.66	165	14.73	5.04	62.03	
A35_34	1.200	1.191	1.502	0.0438	35.28	165	14.88	4.74	63.81	
A35_35	1.202	1.185	1.506	0.0440	35.41	165	14.90	4.84	62.79	
A35_36	1.204	1.197	1.506	0.0448	35.67	165	15.00	4.88	63.11	
A35_37	1.194	1.196	1.505	0.0447	35.93	165	-	-	-	R6
A35_38	1.190	1.197	1.498	0.0444	35.99	165	14.53	5.14	61.52	
A35_39	1.200	1.185	1.500	0.0439	35.58	165	14.63	4.97	62.29	
A35_40	1.203	1.178	1.503	0.0441	35.75	165	14.50	5.07	62.60	
A35_41	1.200	1.210	1.502	0.0451	35.70	165	14.39	4.94	62.53	
A35_42	1.197	1.199	1.505	0.0445	35.61	165	14.40	5.25	62.51	
A35_43	1.205	1.184	1.503	0.0444	35.76	165	14.63	5.01	63.32	
A35_44	1.201	1.184	1.506	0.0436	35.19	165	14.77	4.74	63.43	
A35_45	1.204	1.194	1.502	0.0440	35.18	165	14.67	4.35	62.74	
A35_46	1.204	1.184	1.504	0.0438	35.27	165	14.62	4.79	62.87	
				max	35.99		15.00	5.25	63.81	
				min	35.18		14.05	4.35	60.96	
				average	35.62		14.59	4.94	62.54	
				std deviation	0.26		0.25	0.23	0.72	
				median	35.67		14.63	4.96	62.57	
Remarks										
R6	*data not recorded*									

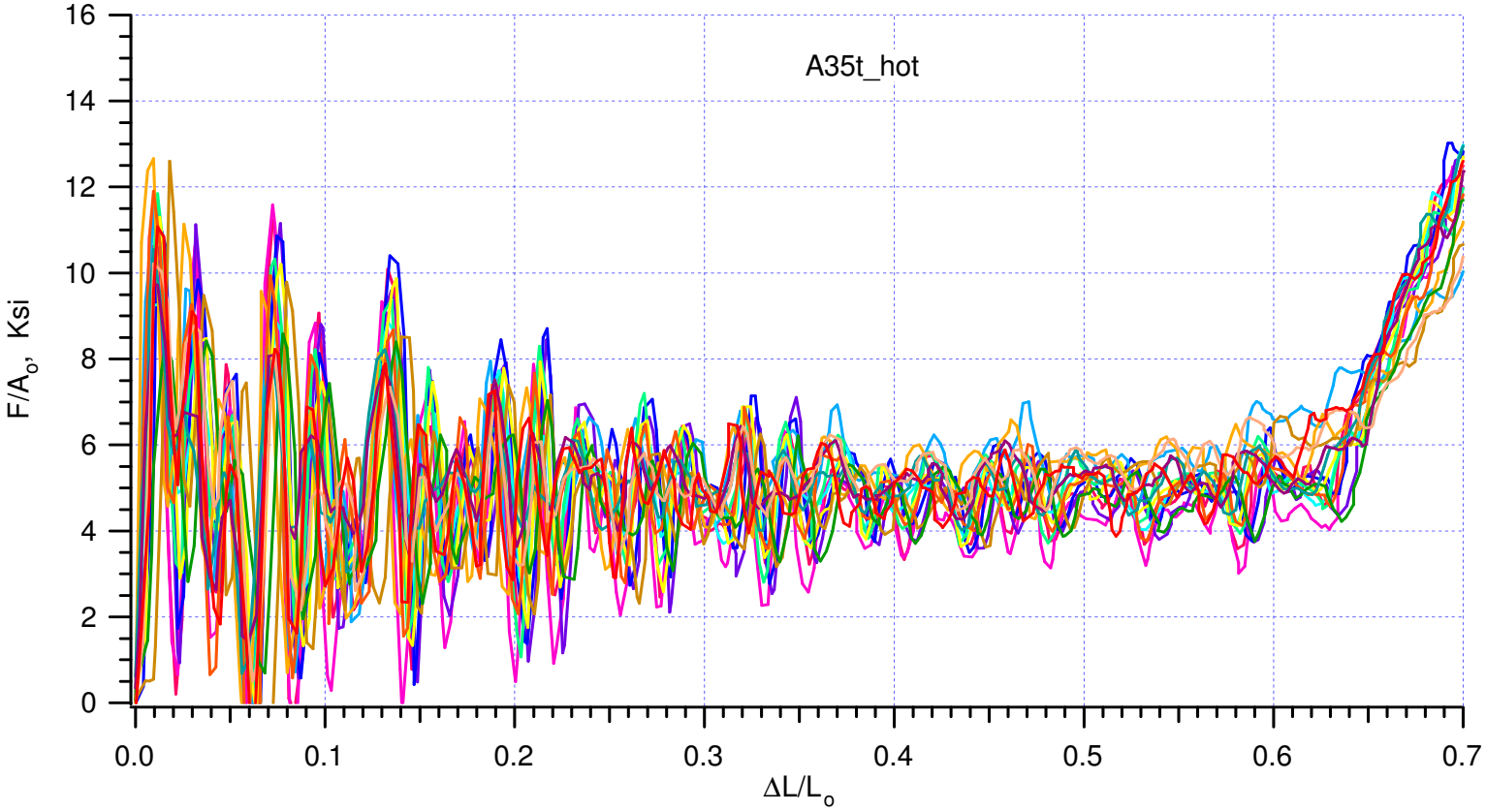

Figure 1. Stress-strain curves of all 16 Alcore 35 specimens crushed in t-direction at 165^{o}F

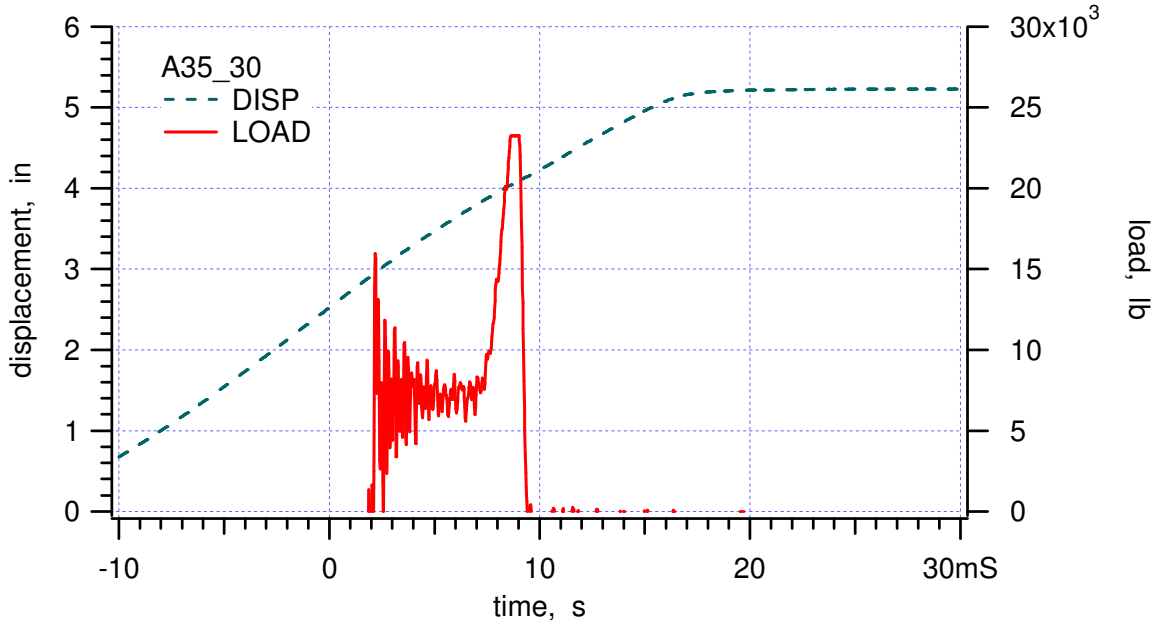
A35_30
DISP
LOAD
displacement, in
load, lb
30x10^3
time, s
-10
0
10
20
30mS

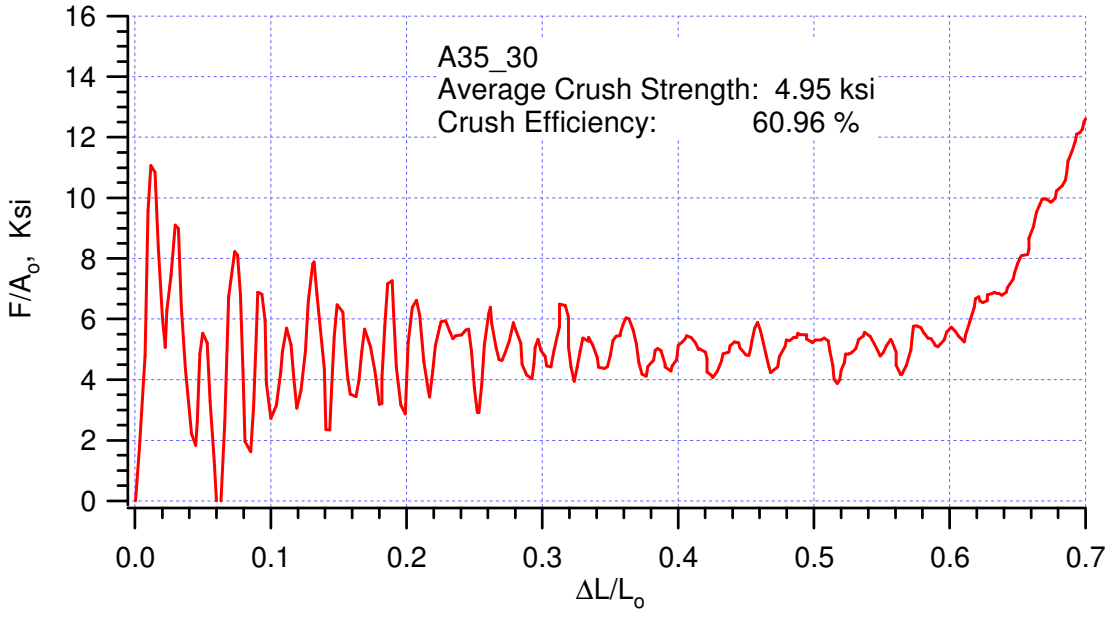
A35_30
Average Crush Strength: 4.95 ksi
Crush Efficiency: 60.96 %
F/A_o, Ksi
ΔL/L_o

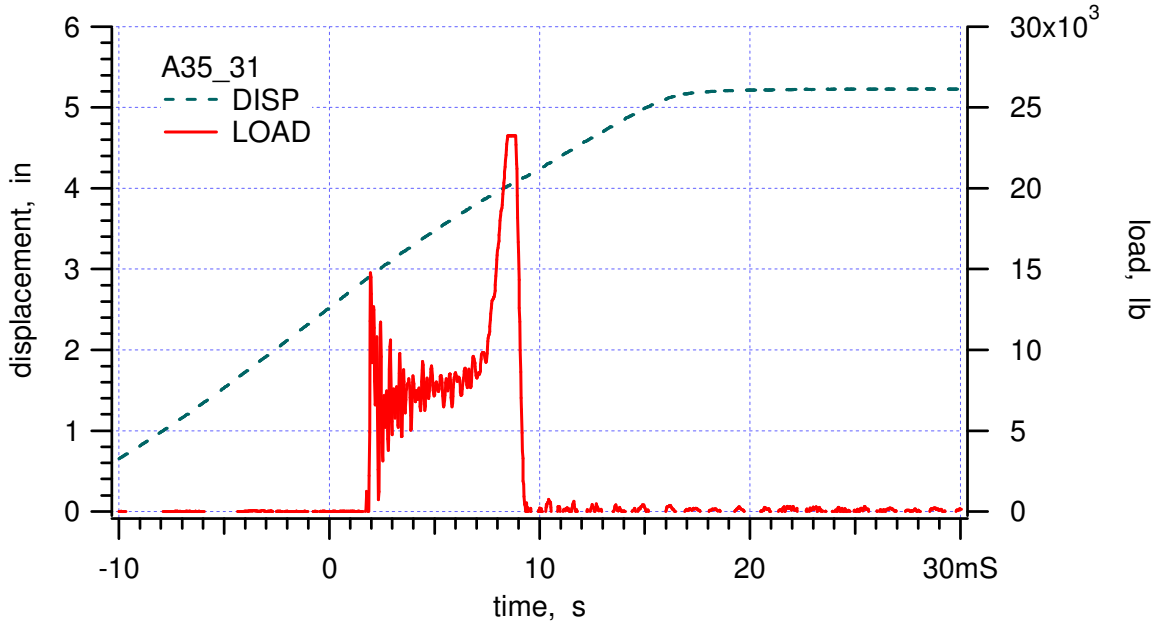
A35_31
DISP
LOAD
displacement, in
load, lb
30x10^3
time, s
-10
0
10
20
30mS

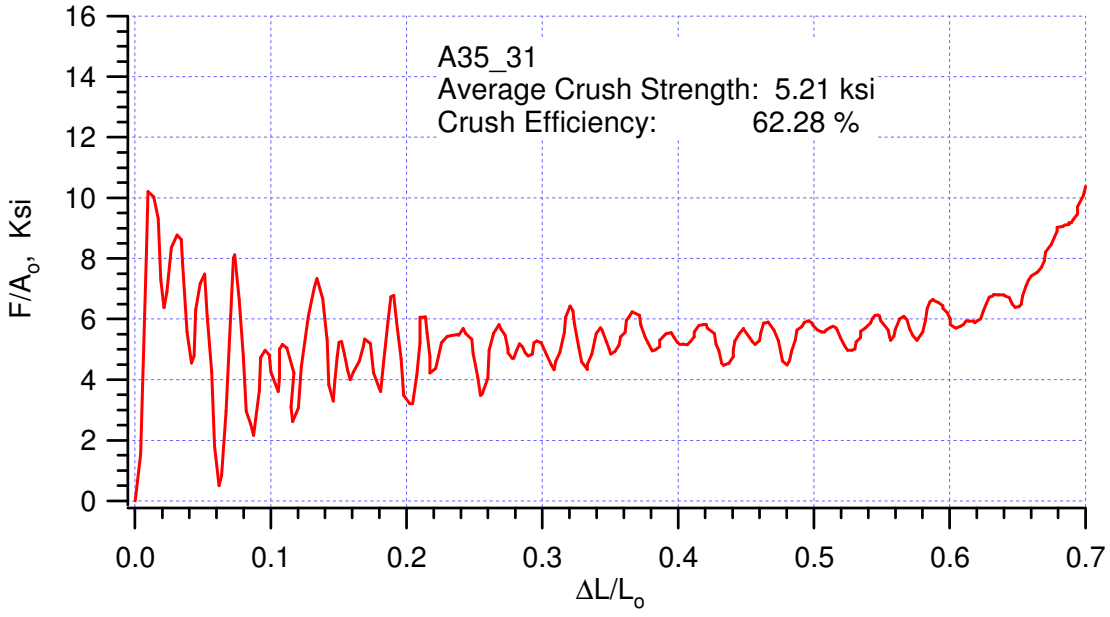
A35_31
Average Crush Strength: 5.21 ksi
Crush Efficiency: 62.28 %
F/A_o, Ksi
ΔL/L_o

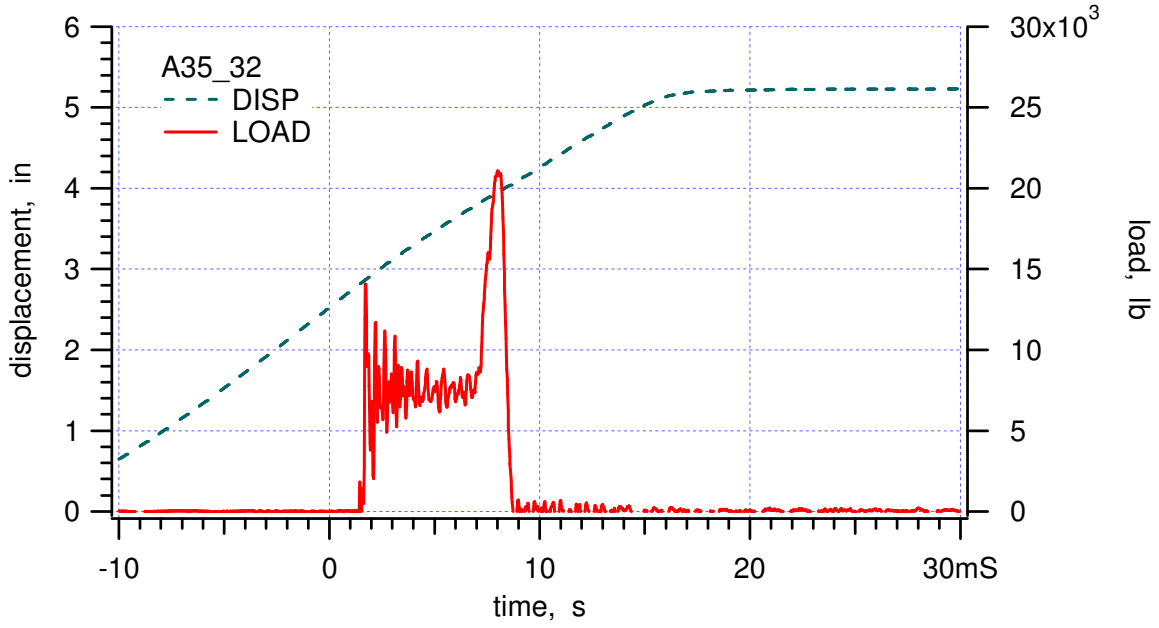
A35_32
DISP
LOAD
displacement, in
load, lb
30x10^3
time, s
-10
0
10
20
30mS

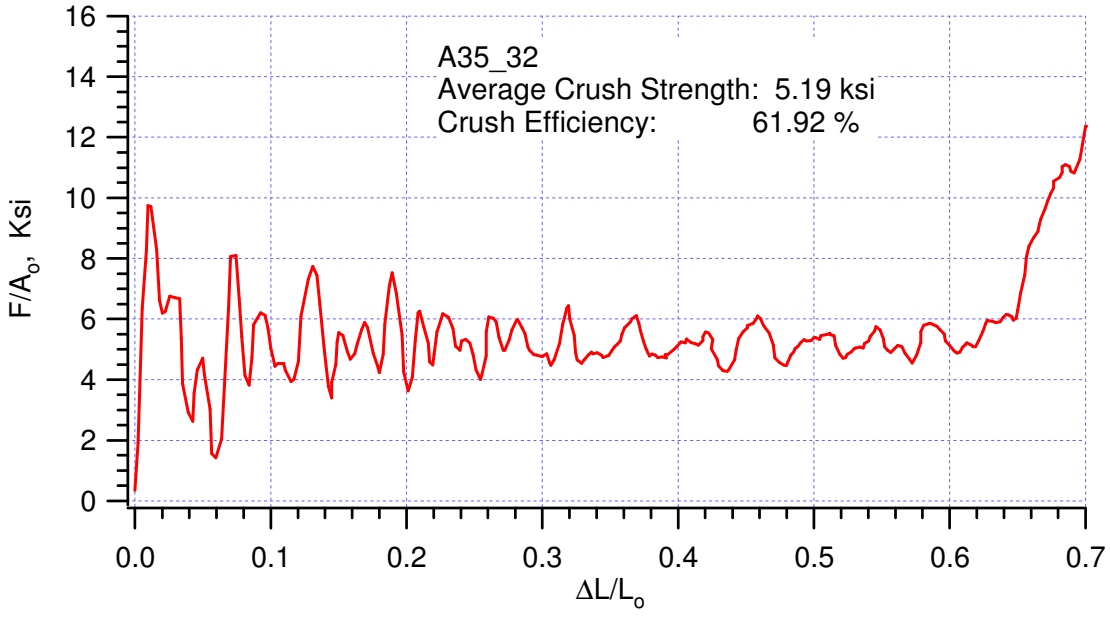
A35_32
Average Crush Strength: 5.19 ksi
Crush Efficiency: 61.92 %
F/A_o, Ksi
ΔL/L_o

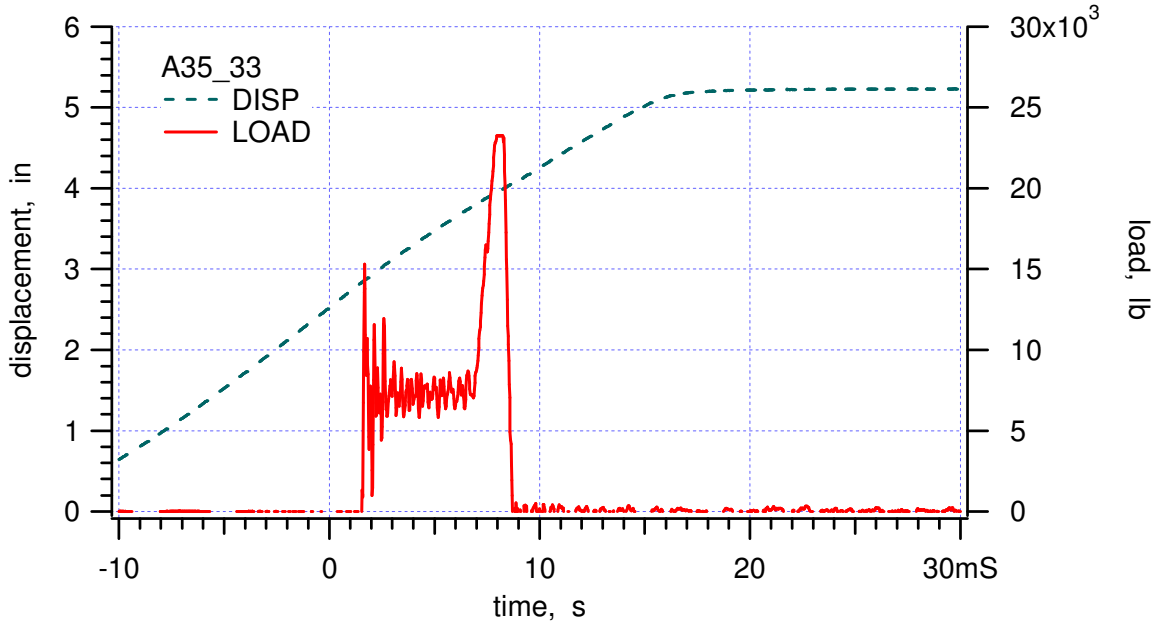
A35_33
DISP
LOAD
displacement, in
load, lb
30x10^3
time, s
-10
0
10
20
30mS

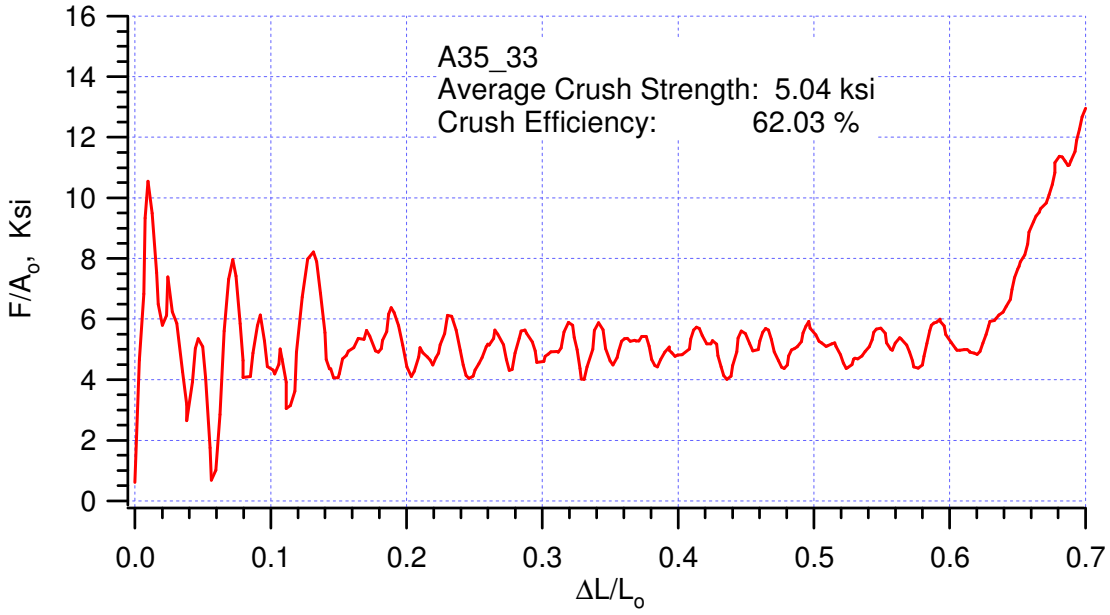
A35_33
Average Crush Strength: 5.04 ksi
Crush Efficiency: 62.03 %
F/A_o, Ksi
ΔL/L_o

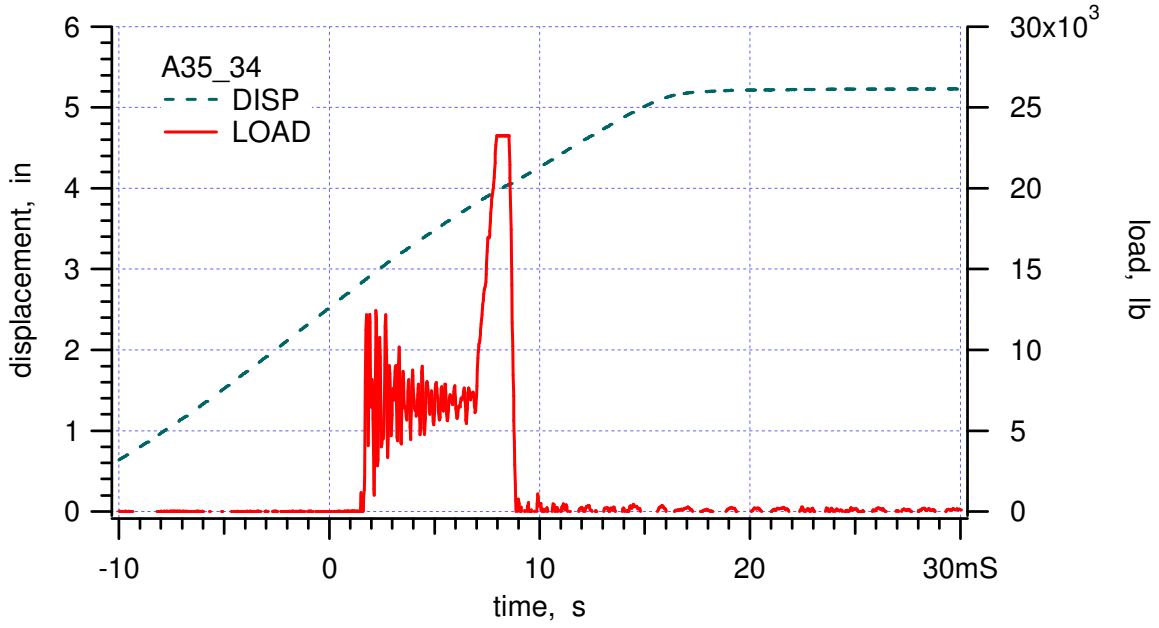
A35_34
DISP
LOAD
displacement, in
load, lb
30x10^3
time, s
-10
0
10
20
30mS

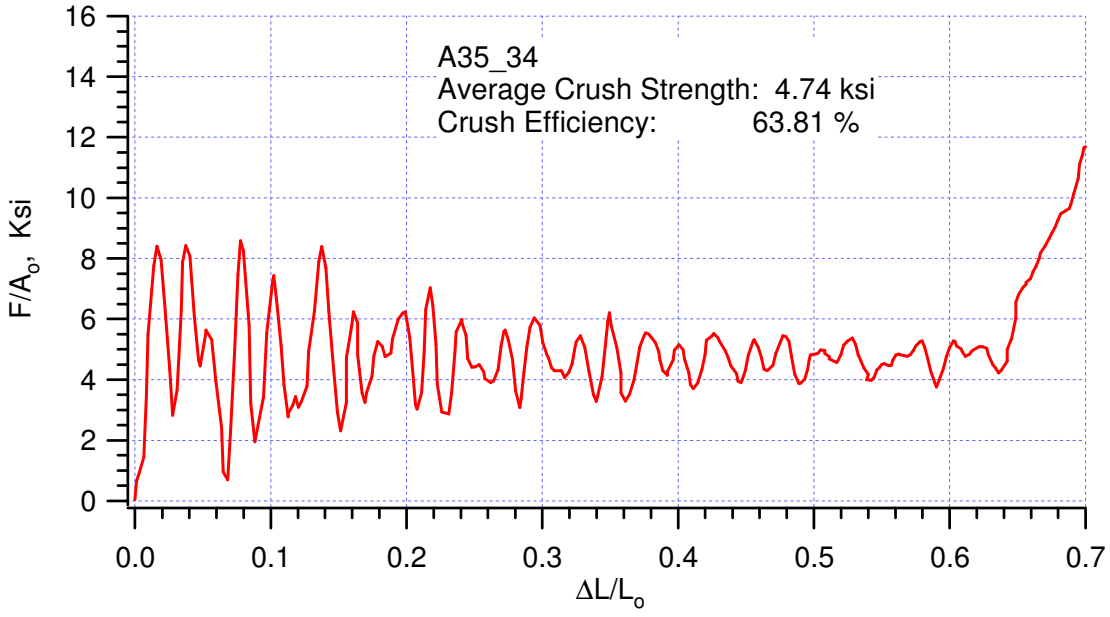
A35_34
Average Crush Strength: 4.74 ksi
Crush Efficiency: 63.81 %
F/A_o, Ksi
ΔL/L_o

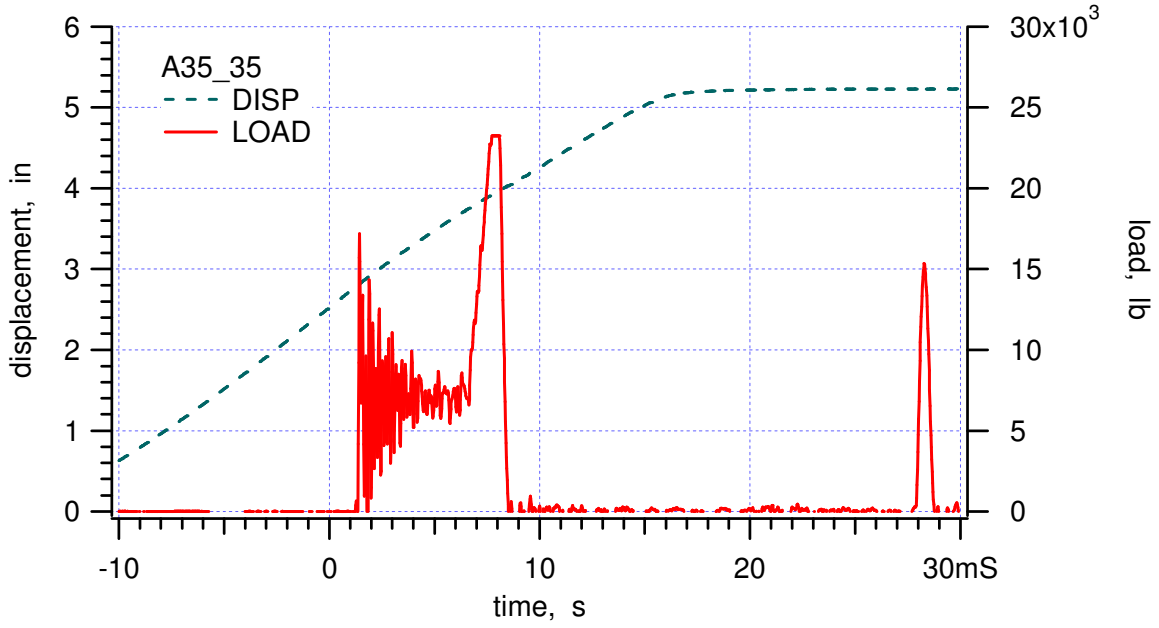
A35_35
DISP
LOAD
displacement, in
load, lb
30x10^3
time, s
-10
0
10
20
30mS

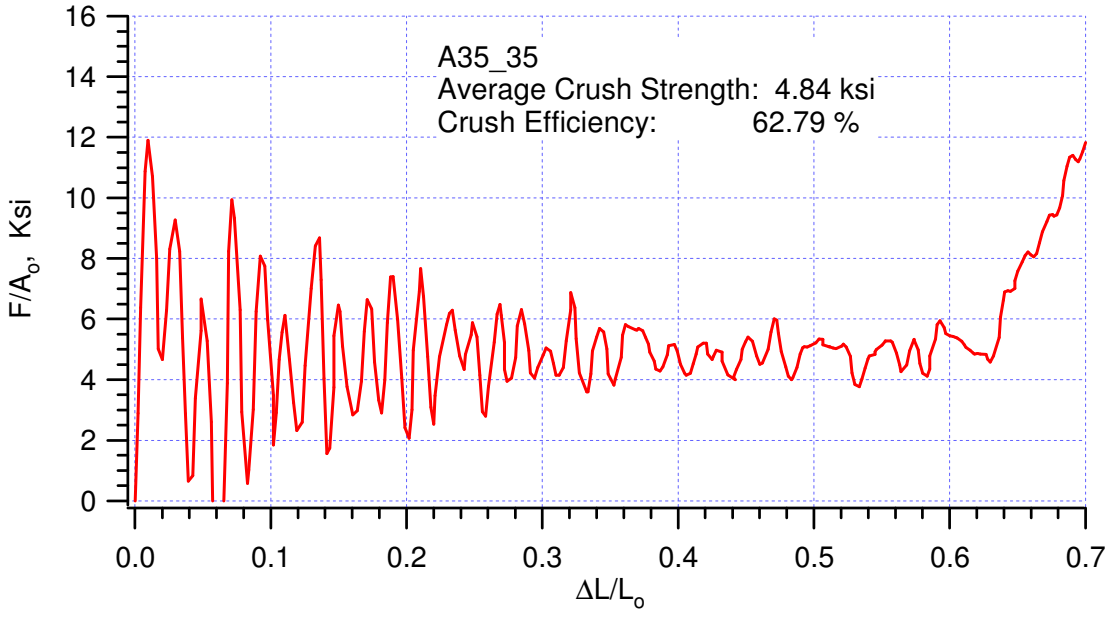
A35_35
Average Crush Strength: 4.84 ksi
Crush Efficiency: 62.79 %
F/A_o, Ksi
ΔL/L_o

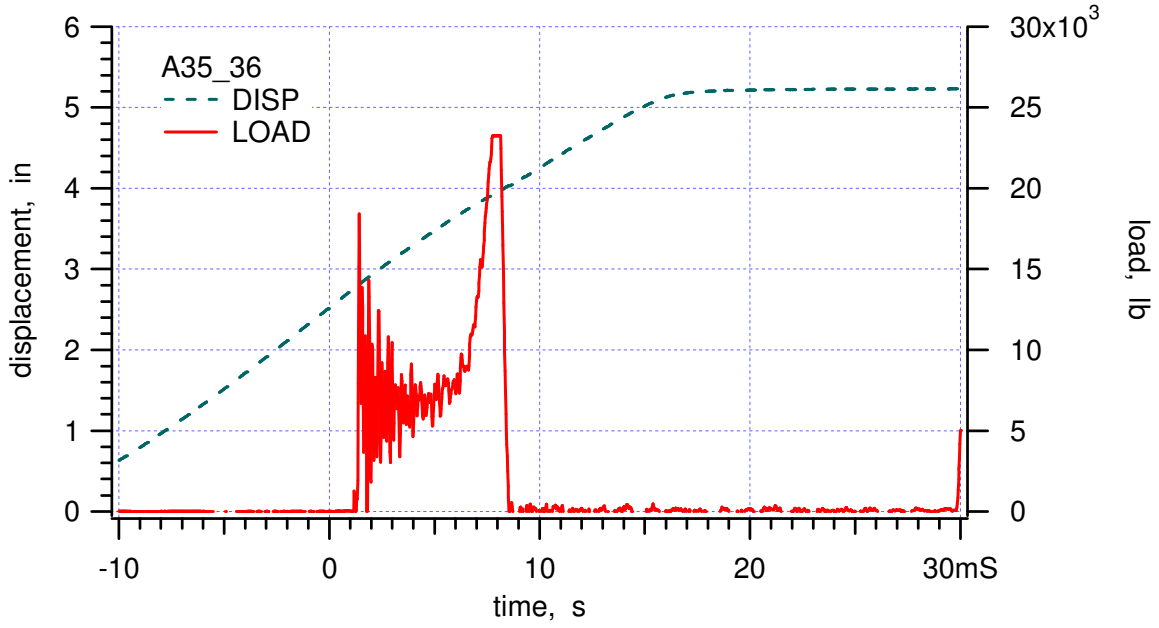
A35_36
DISP
LOAD
displacement, in
load, lb
30x10^3
time, s
-10
0
10
20
30mS

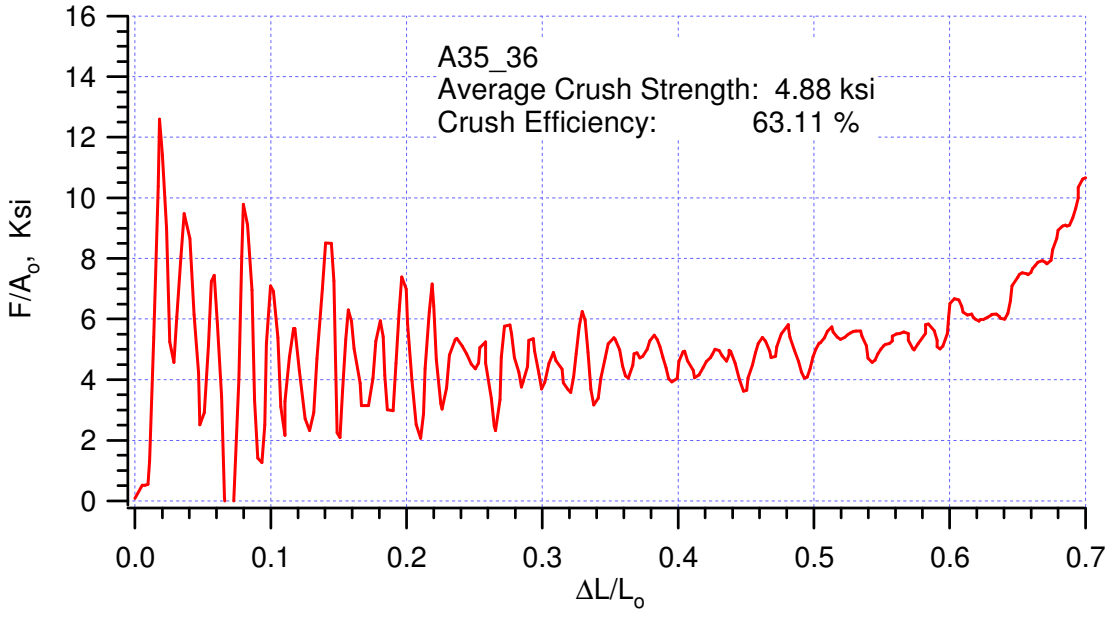
A35_36
Average Crush Strength: 4.88 ksi
Crush Efficiency: 63.11 %
F/A_o, Ksi
ΔL/L_o

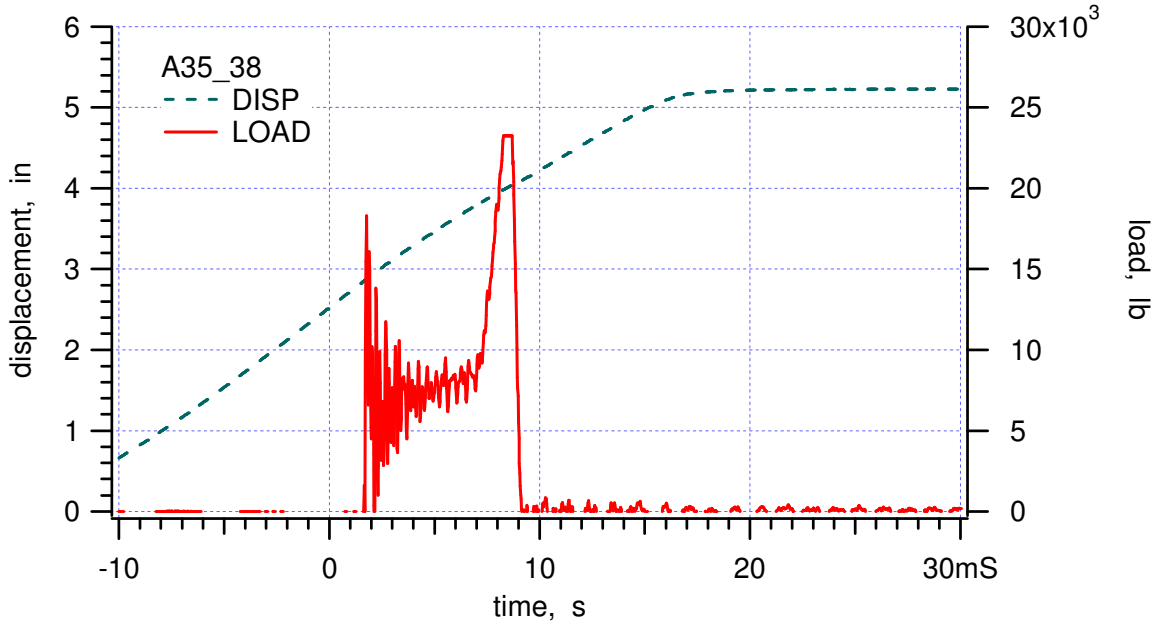
A35_38
DISP
LOAD
displacement, in
load, lb
30x10^3
time, s
-10
0
10
20
30mS

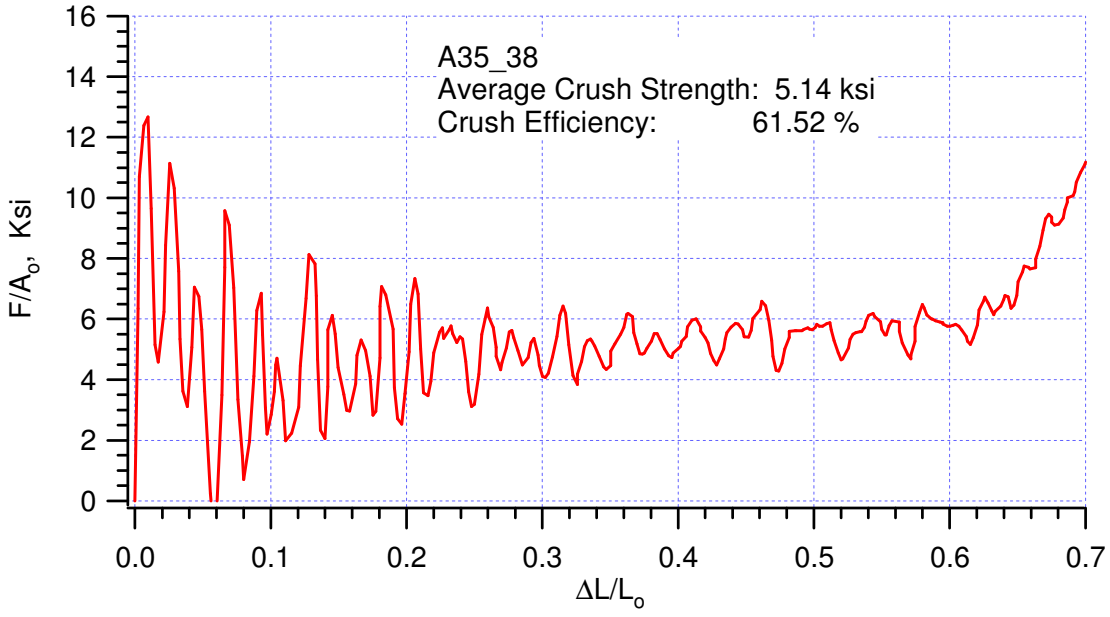
A35_38
Average Crush Strength: 5.14 ksi
Crush Efficiency: 61.52 %
F/A_o, Ksi
ΔL/L_o

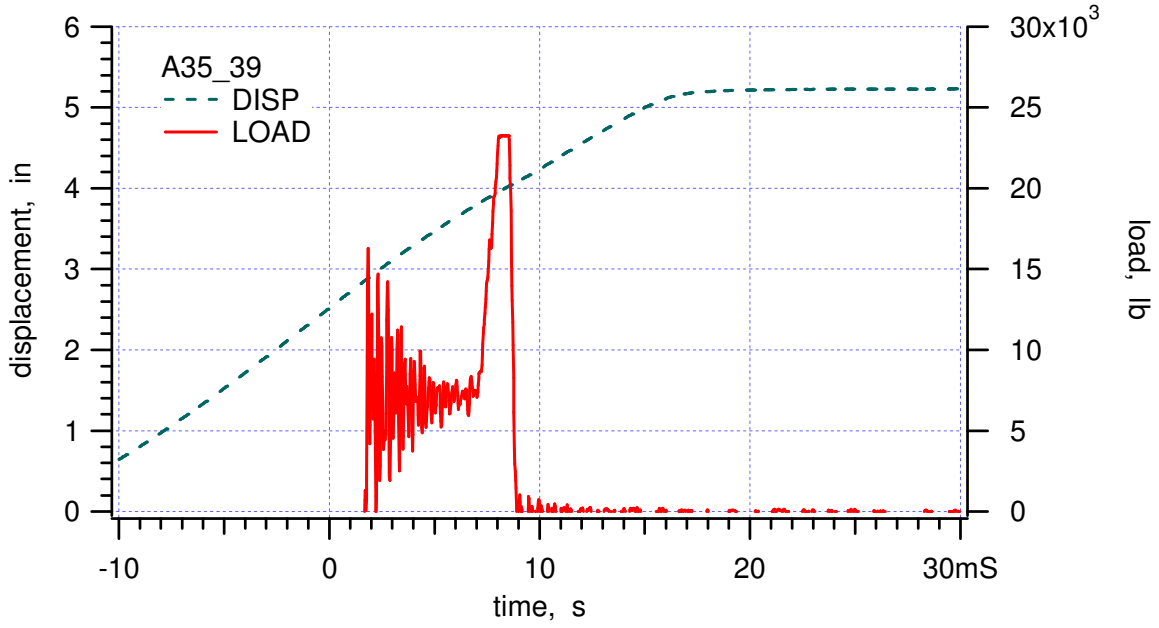
A35_39
DISP
LOAD
displacement, in
load, lb
30x10^3
time, s
-10
0
10
20
30mS

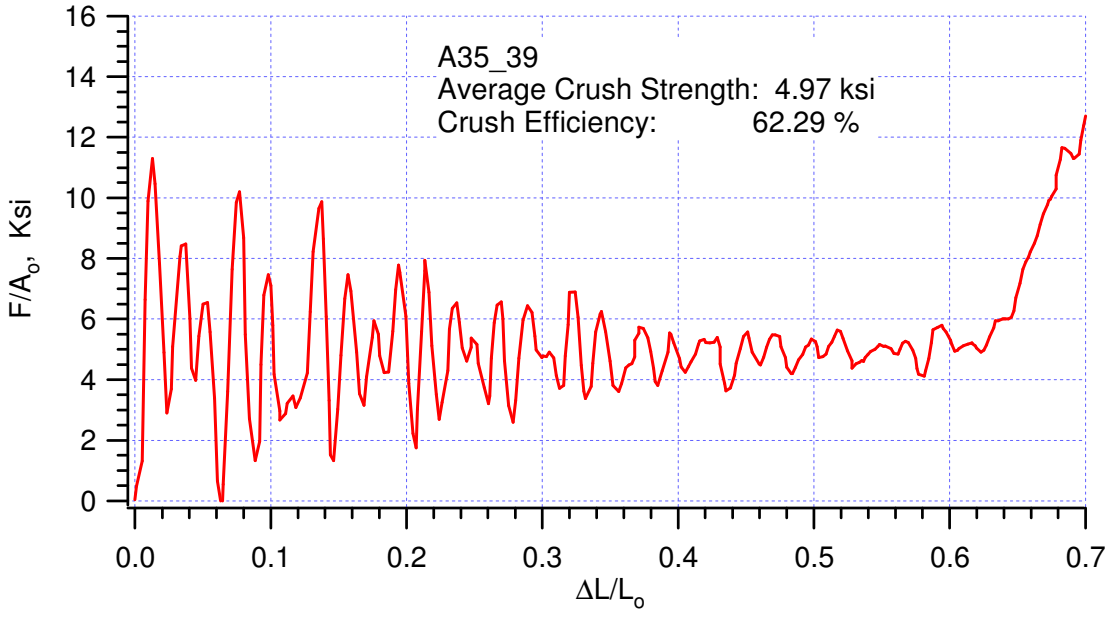
A35_39
Average Crush Strength: 4.97 ksi
Crush Efficiency: 62.29 %
F/A_o, Ksi
ΔL/L_o

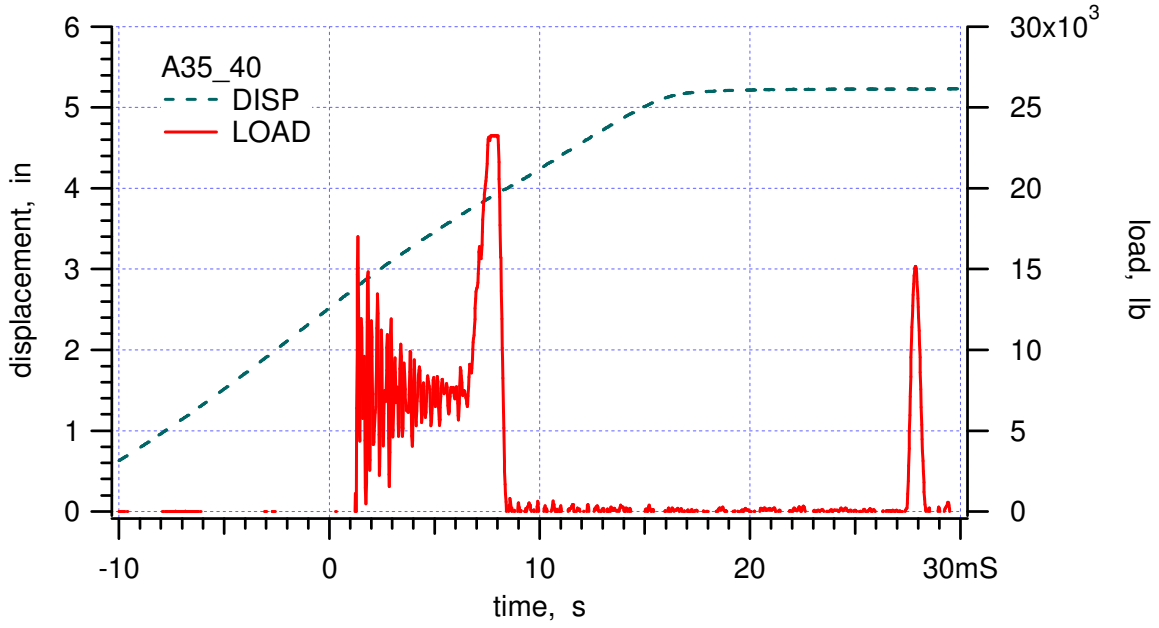
A35_40
DISP
LOAD
displacement, in
load, lb
30x10^3
time, s
-10
0
10
20
30mS

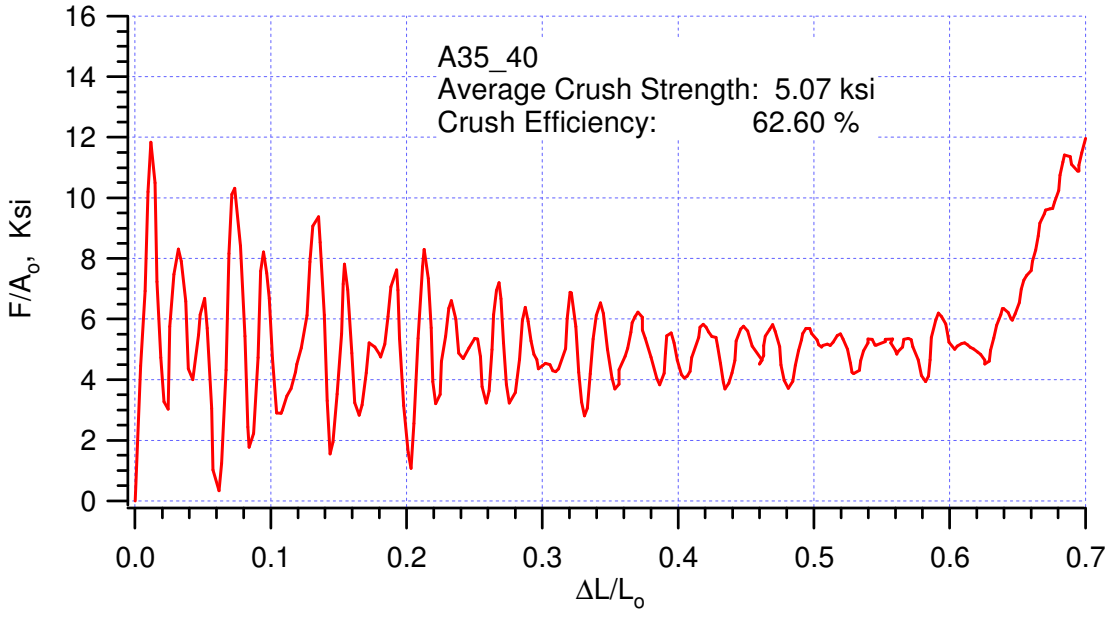
A35_40
Average Crush Strength: 5.07 ksi
Crush Efficiency: 62.60 %
F/A_o, Ksi
ΔL/L_o

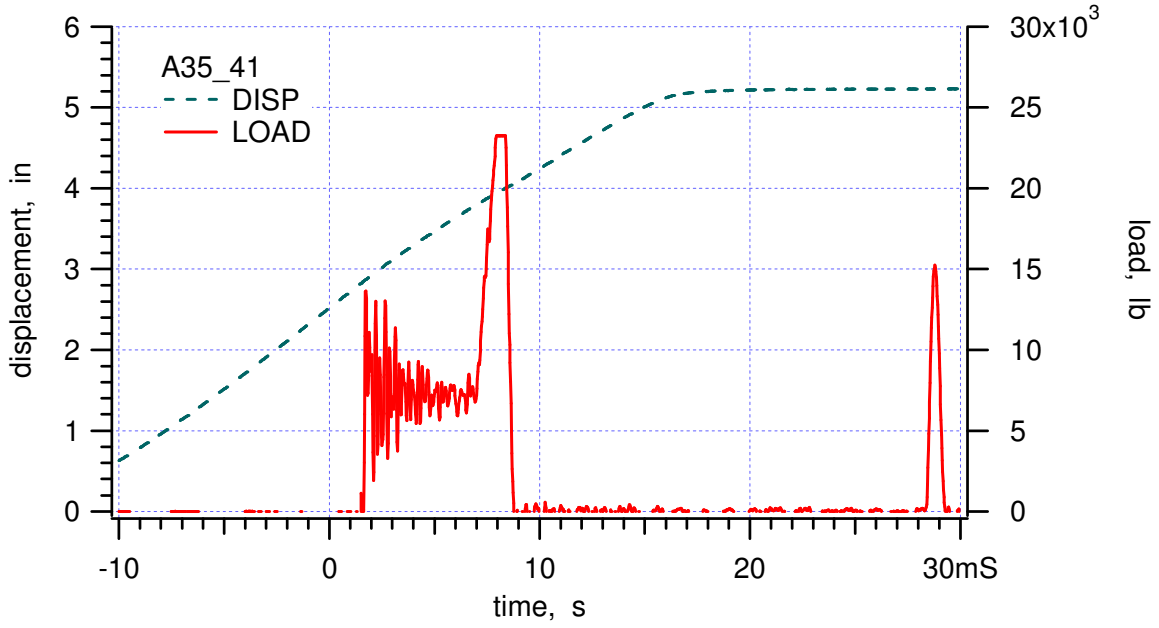
A35_41
DISP
LOAD
displacement, in
load, lb
30x10^3
time, s
-10
0
10
20
30mS

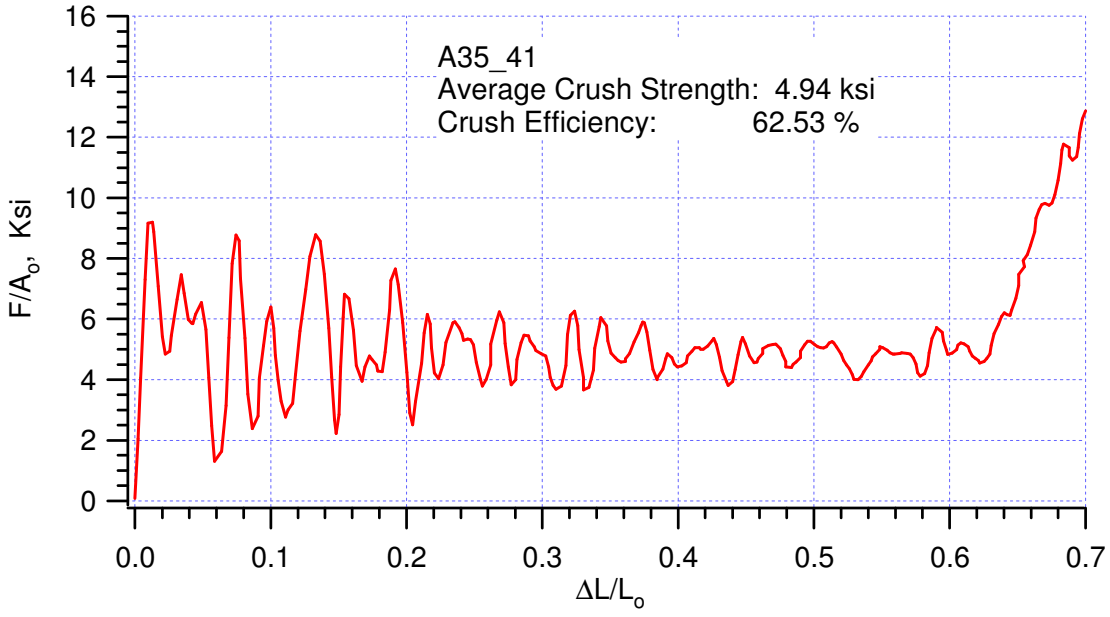
A35_41
Average Crush Strength: 4.94 ksi
Crush Efficiency: 62.53 %
F/A_o, Ksi
ΔL/L_o

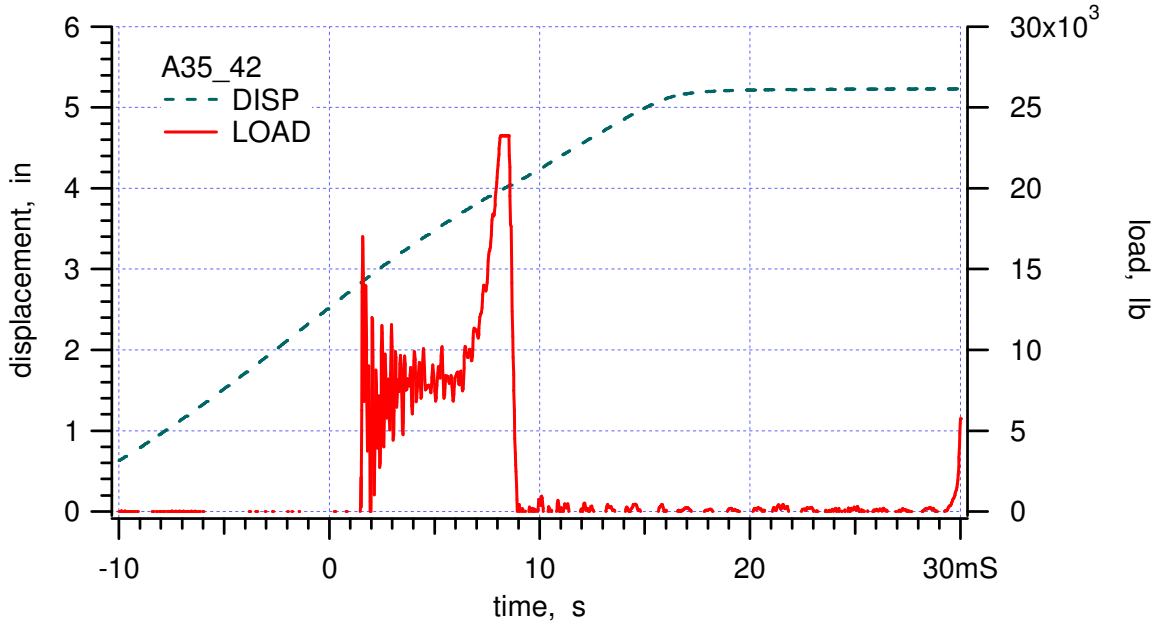
A35_42
DISP
LOAD
displacement, in
load, lb
time, s
30x10^3
-10
0
10
20
30mS

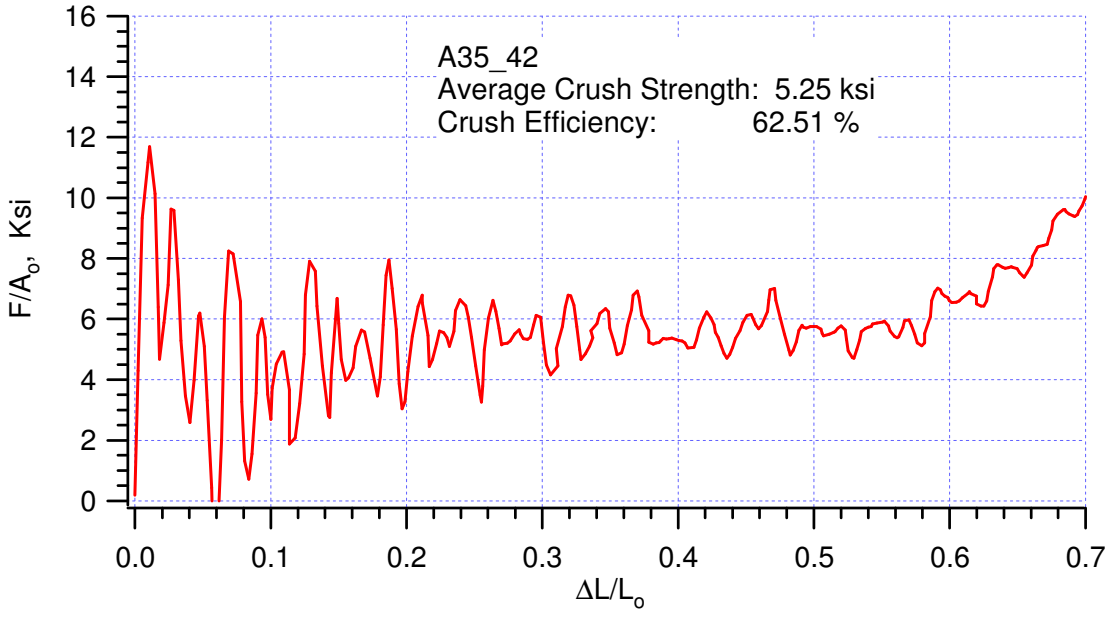
A35_42
Average Crush Strength: 5.25 ksi
Crush Efficiency: 62.51 %
F/A_o, Ksi
ΔL/L_o

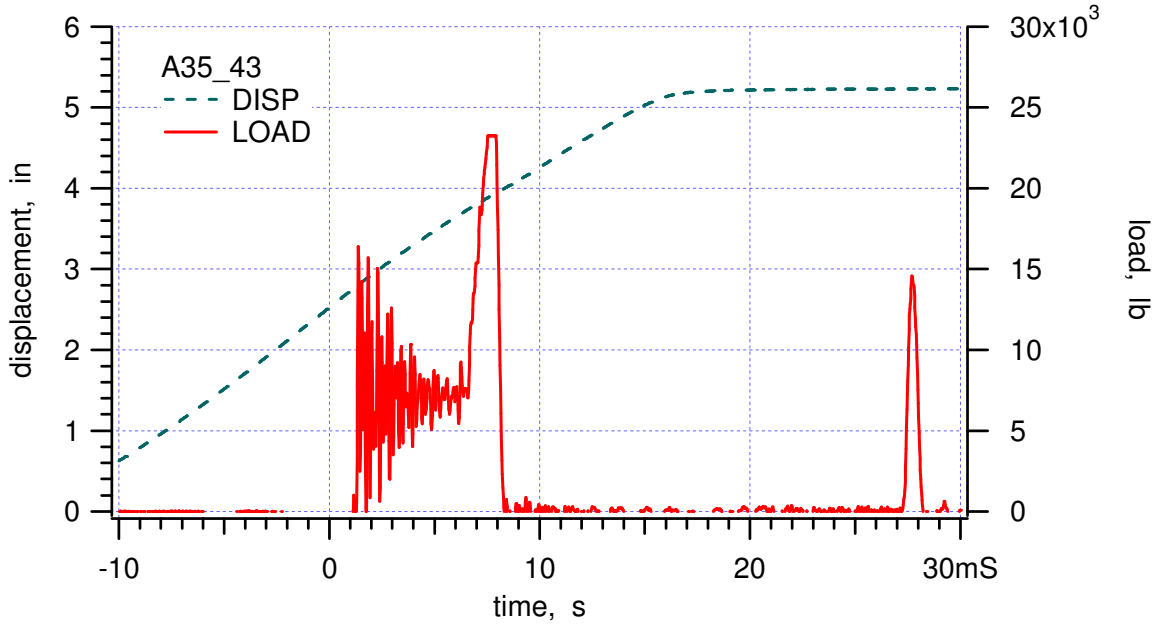
A35_43
DISP
LOAD
displacement, in
load, lb
30x10^3
time, s
-10
0
10
20
30mS


A35_43
Average Crush Strength: 5.01 ksi
Crush Efficiency: 63.32 %
F/A_o, Ksi
ΔL/L_o

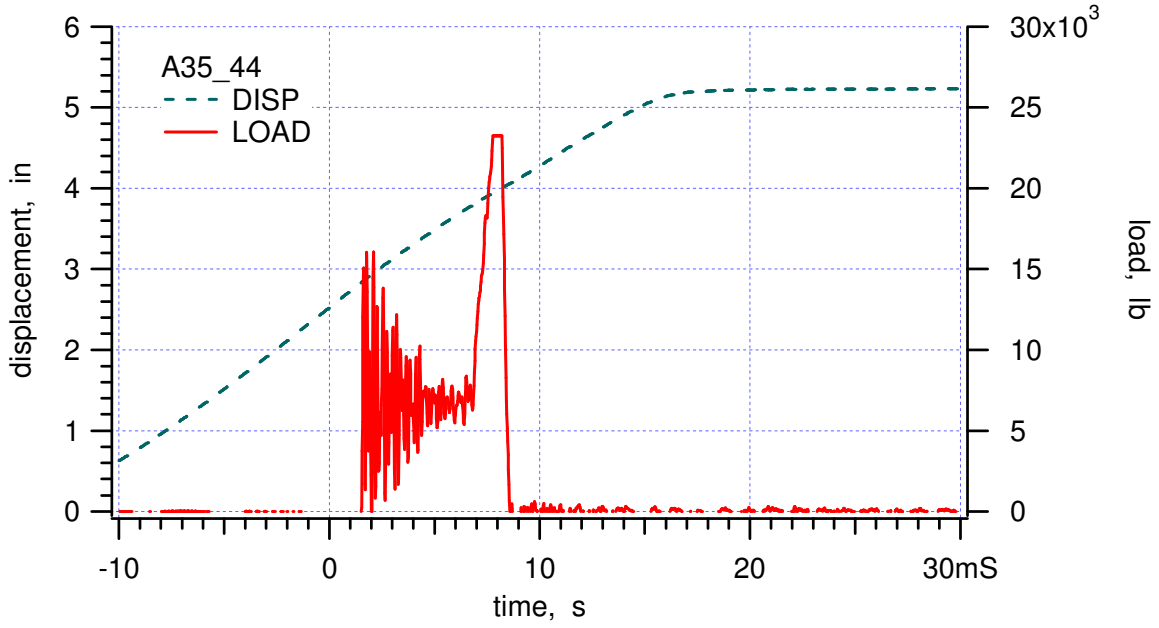
A35_44
DISP
LOAD
displacement, in
load, lb
30x10^3
time, s
-10
0
10
20
30mS

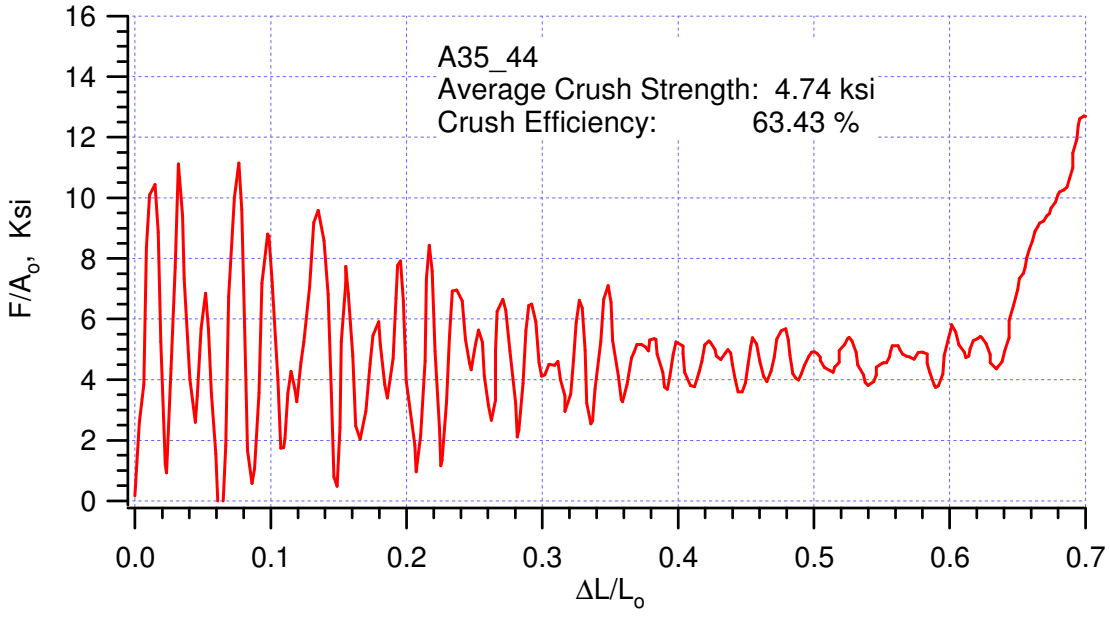
A35_44
Average Crush Strength: 4.74 ksi
Crush Efficiency: 63.43 %
F/A_o, Ksi
ΔL/L_o

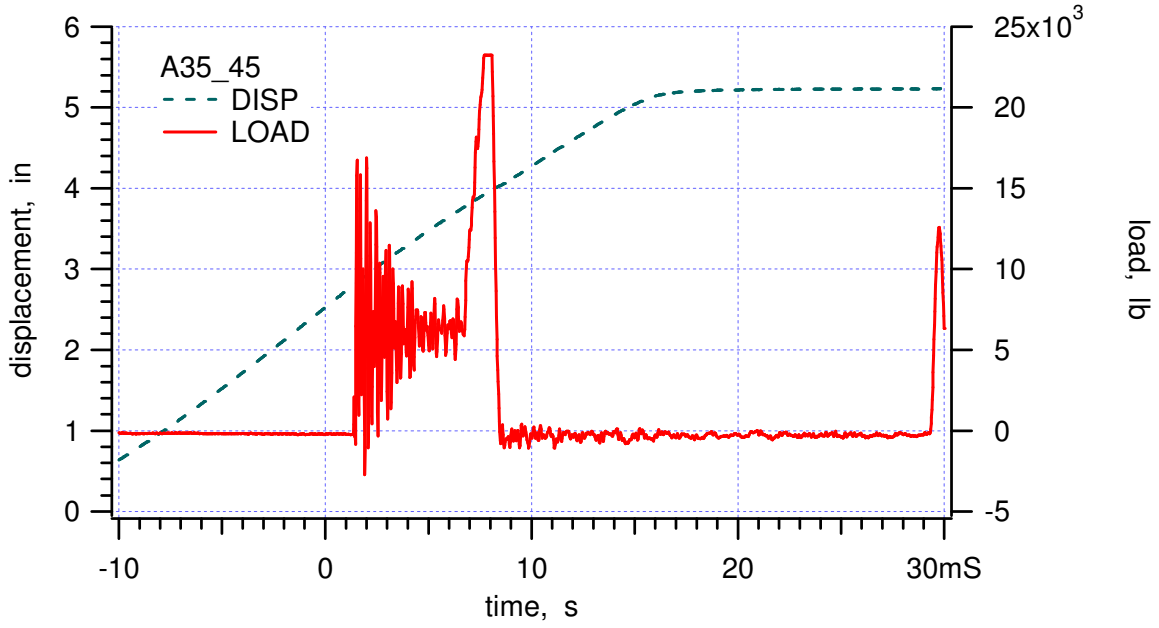
A35_45
DISP
LOAD
displacement, in
load, lb
25x10^3
time, s
-10
0
10
20
30mS

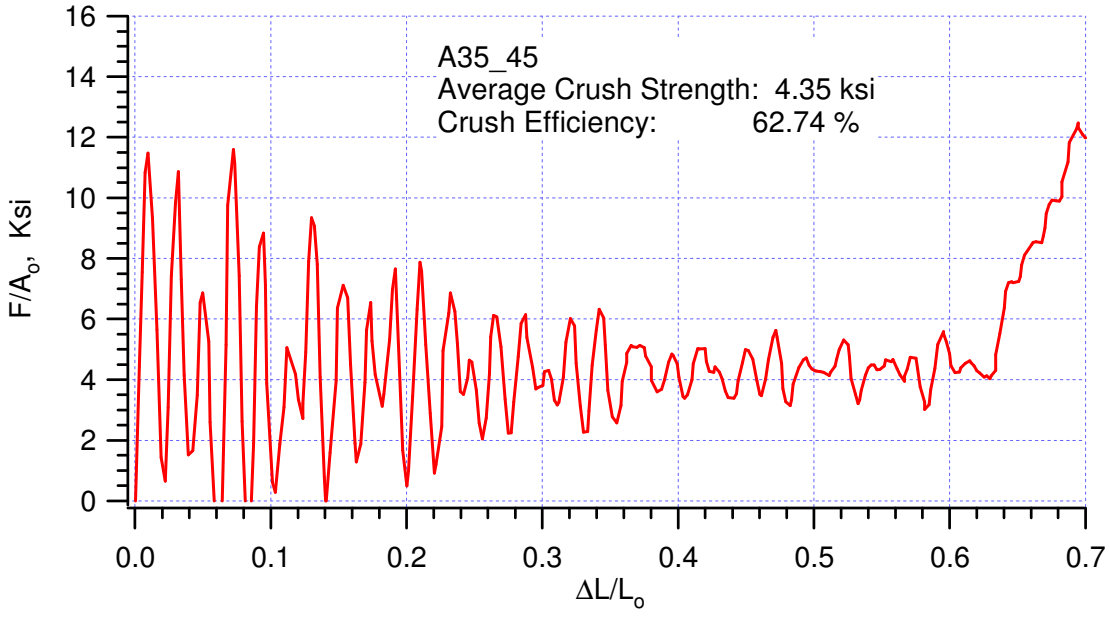
A35_45
Average Crush Strength: 4.35 ksi
Crush Efficiency: 62.74 %
F/A_o, Ksi
ΔL/L_o

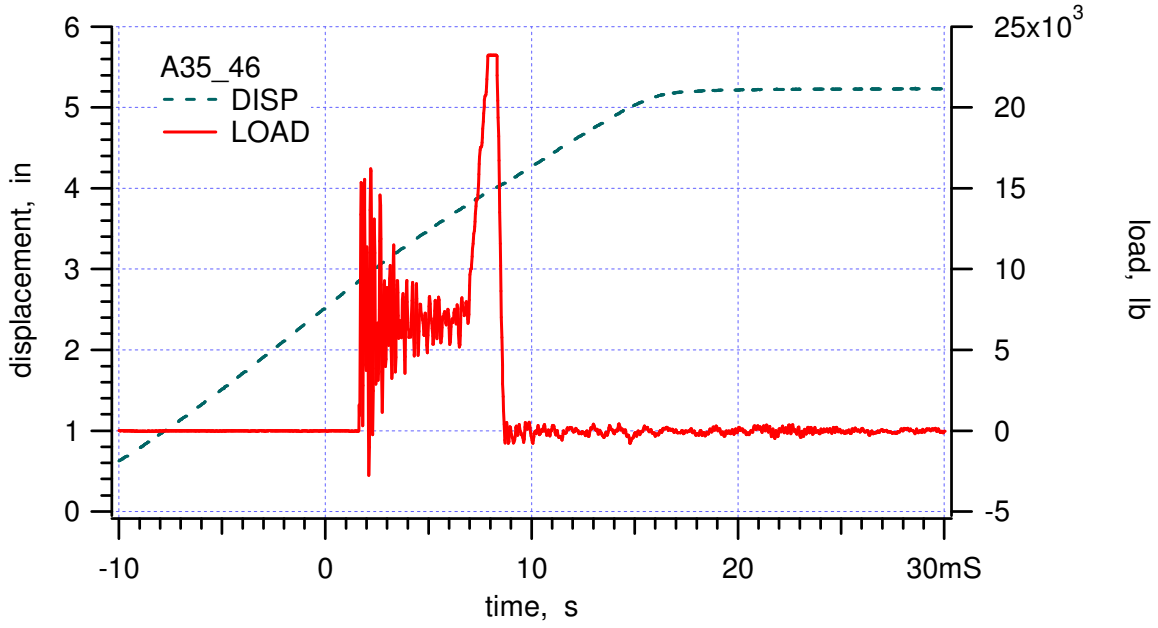
A35_46
DISP
LOAD
displacement, in
load, lb
25x10^3
time, s
-10
0
10
20
30mS

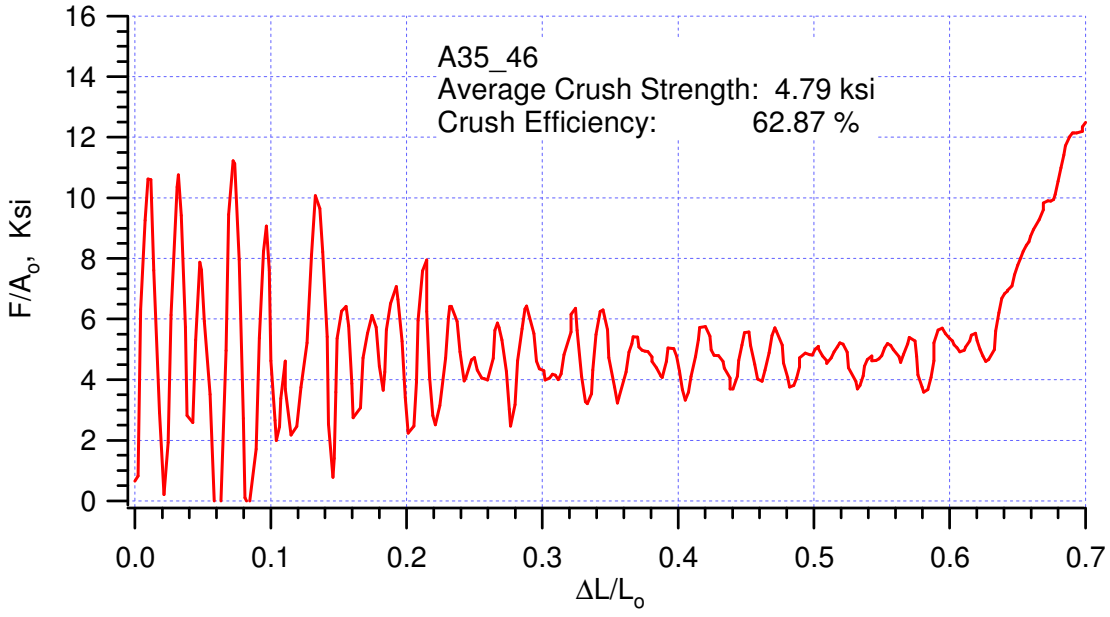
A35_46
Average Crush Strength: 4.79 ksi
Crush Efficiency: 62.87 %
F/A_o, Ksi
ΔL/L_o

This page intentionally left blank.

APPENDIX XII:

"Moderate Rate Confined Crush Tests of 38 pcf honeycombs in the t-direction at -65°F," Memo Wei-Yang Lu to Distribution, February, 2000

Sandia National Laboratories
Operated for the U.S. Department of Energy by
Sandia Corporation
MS9042
Livermore, CA 94551-0969

date: February 25, 2000

to: Distribution

from: Wei-yang Lu

subject: Moderate Rate Confined Crush Tests of 38 pcf honeycombs in the t-direction at **-65°F**

Experimental results of both Alcore 38 and Hexcel 38 are included in this report. The boldface lines in Table 1 summarize the current low-temperature data. Table 2 and 3 list the data of each specimen for Alcore 38 and Hexcel 38, respectively; stress-strain curves are shown in Figure 1 and 2. As expected, the crush strength of honeycomb increases when tested at -65°F, about 15% for both materials.

Following modifications of setup were made, shown in Figure 3, so cold tests could run more efficiently:

1. Cold N_2 line was connected directly into the compression chamber, right above the specimen and below the punch.
2. Vent holes along the confined walls were taped tightly.
3. Shims were placed at the bottom of confined walls, which allowed N_2 to escape from the chamber.

Please see Appendix for detail experimental data.

Distribution:

Darrla Giersch(2167)	MS0481
Darren Hoke(2167)	MS0481
Vernon Willan(2167)	MS0481
Vista Bateman(9126)	MS0553
Tom Carne(9124)	MS0557
Berry Boughten(9132)	MS0557
Jaime Moya(9132)	MS0828
Terry Hinnerichs(9126)	MS0847
Ken Gwinn(9126)	MS0847
John Pott(9126)	MS0847
Rodney May(9126)	MS0847
Mike Neilsen(9123)	MS0847
Bill Scherzinger(9123)	MS0847
Hal Morgan(9123)	MS0847
Wendell Kawahara (8725)	MS904

Table 1. Summary of FY00 experimental results

B61/MAVEN TEST MATRIX				EXPERIMENTAL RESULTS						MEMO
Test #	Honeycomb	Dir.	Temperature, degree F	Specimen	Density, pcf	Impact Speed, ft/s	Crush Strength, ksi	Std Deviation, ksi	Crush Efficiency, %	Date
1 - 15	Alcore 38	T	ambient	rotated	38.82	14.13	6.35	0.08	63.80	991203
16 - 30	Hexcel 38	T	ambient	rotated	38.70	13.67	7.17	0.15	63.89	000110
	Hexcel 39	T	ambient	rotated	38.78	0.00139	5.88		59.20	"
31 - 45	Alcore 35	T	ambient	rotated	35.39	14.35	5.74	0.18	64.46	000103
46 - 60	Hexcel 35	T	ambient	rotated	37.79	13.83	6.67	0.24	63.91	000110
	Hexcel 36	T	ambient	rotated	37.89	0.00139	5.83		60.30	"
60 - 75	Alcore 38	T	165	rotated	38.96	14.33	5.49	0.10	62.52	000118
76 - 90	Hexcel 38	T	165	rotated	38.65	13.82	6.43	0.15	64.31	000118
	Alcore 35	T	165	rotated	35.62	14.59	4.94	0.23	62.54	000207
91 - 105	**Alcore 38**	**T**	**-65**	**rotated**	**38.94**	**13.48**	**7.34**	**0.24**	**62.71**	**000225**
106 - 120	**Hexcel 38**	**T**	**-65**	**rotated**	**38.65**	**13.17**	**8.21**	**0.17**	**64.68**	**000225**
121 - 125	Alcore 38	L	ambient							
126 - 130	Hexcel 38	L	ambient							
131 - 135	Alcore 38	W	ambient							
136 - 140	Hexcel 38	W	ambient							
159 - 161	Alcore 38	T	ambient	segmented	41.41	0.0014	6.14		52.30	991130
162 - 164	Hexcel 38	T	ambient	segmented	41.29	0.0014	6.85		53.70	991213

Table 2. Experimental results of Alcore 38 crushed in t-direction at -65 °F

Specimen	d_1, in	d_2, in	d_3, in	Weight, lb	Density, pcf	Temperature, degree F	Crush Velocity, ft/s	Crush strenght, ksi	Crush efficiency, %	Remarks
A38_21	1.193	1.200	1.498	0.0483	38.90	-60	-	-	-	R3
A38_22	1.205	1.191	1.500	0.0485	38.97	-70	16.26	6.97		R2
A38_23	1.200	1.213	1.505	0.0492	38.78	-65	13.18	7.12	61.77	
A38_24	1.201	1.209	1.509	0.0495	39.02	-75	13.01	7.70	64.04	
A38_25	1.191	1.197	1.500	0.0480	38.82	-70	15.83	7.04		R2
A38_26	1.189	1.212	1.501	0.0491	39.24	-65	13.29	7.67	61.93	
A38_27	1.188	1.206	1.506	0.0491	39.34	-67	13.19	7.66	61.51	
A38_28	1.192	1.201	1.494	0.0484	39.08	-65	13.23	7.59	61.47	
A38_29	1.193	1.210	1.499	0.0489	39.08	-68	15.70	7.36		R2
A38_30	1.196	1.201	1.498	0.0488	39.22	-68	13.27	7.53	61.95	
A38_31	1.200	1.193	1.504	0.0484	38.84	-64	15.80	7.25		R2
A38_32	1.190	1.192	1.499	0.0478	38.88	-63	13.63	7.04	63.83	
A38_36	1.200	1.205	1.505	0.0489	38.86	-65	13.68	7.08	62.72	
A38_37	1.196	1.209	1.506	0.0488	38.75	-65	13.65	7.15	64.38	
A38_38	1.198	1.204	1.505	0.0486	38.71	-65				R2
A38_39	1.200	1.198	1.507	0.0486	38.79	-65	13.33	7.25	62.43	
A38_40	1.200	1.200	1.511	0.0490	38.92	-65	13.73	7.38	61.84	
A38_41	1.200	1.205	1.511	0.0489	38.71	-65				R2
A38_42	1.188	1.189	1.511	0.0480	38.89	-65	13.75	7.12	63.11	
A38_43	1.192	1.195	1.512	0.0485	38.95	-65	13.62	7.44	62.33	
A38_44	1.205	1.205	1.510	0.0493	38.82	-65	13.69	7.32	64.32	
A38_45	1.192	1.198	1.496	0.0484	39.16	-65	13.89	7.11	62.96	
				max	39.34		13.89	7.70	64.38	
				min	38.71		13.01	7.04	61.47	
				average	38.94		13.48	7.34	62.71	
				std deviation	0.18		0.27	0.24	1.02	
				median	38.90		13.62	7.32	62.43	
Remarks										
R2	*shear pin broke early, did not reach lock-up*									

Table 3. Experimental results of Hexcel 38 crushed in t-direction at -65 °F

Specimen	d_1, in	d_2, in	d_3, in	Weight, lb	Density, pcf	Temperature, degree F	Crush Velocity, ft/s	Crush strenght, ksi	Crush efficiency, %	Remarks
H38_51	1.197	1.192	1.504	0.0485	39.02	-65	13.20	8.43	62.55	
H38_52	1.198	1.193	1.499	0.0480	38.73	-65	13.30	8.14	64.90	
H38_53	1.204	1.192	1.500	0.0483	38.81	-65	12.71	8.57	64.21	
H38_54	1.194	1.200	1.508	0.0484	38.68	-65				R2
H38_55	1.199	1.189	1.506	0.0479	38.54	-65	13.17	8.13	65.34	
H38_56	1.197	1.195	1.505	0.0483	38.75	-65	13.08	8.41	63.36	
H38_57	1.191	1.188	1.505	0.0478	38.79	-65	13.34	8.08	65.38	
H38_58	1.193	1.186	1.500	0.0472	38.45	-65	13.39	8.06	65.60	
H38_59	1.190	1.192	1.506	0.0472	38.22	-65	13.51	7.99	65.34	
H38_60	1.198	1.190	1.508	0.0485	38.97	-65	13.24	8.32	65.36	
H38_61	1.193	1.196	1.505	0.0476	38.30	-65	13.33	8.03	65.06	
H38_62	1.197	1.193	1.507	0.0479	38.45	-65	13.10	8.02	65.40	
H38_63	1.197	1.195	1.507	0.0482	38.67	-65	12.78	8.35	62.96	
H38_64	1.195	1.190	1.500	0.0477	38.63	-65	12.88	8.24	64.43	
H38_65	1.196	1.201	1.512	0.0487	38.76	-65	13.19	8.14	66.24	
H38_66	1.194	1.202	1.506	0.0484	38.71	-65				R2
H38_67	1.189	1.168	1.505	0.0467	38.59	-65	13.29	8.18	64.11	
				max	39.02		13.51	8.57	66.24	
				min	38.22		12.71	7.99	62.55	
				average	38.65		13.17	8.21	64.68	
				std deviation	0.21		0.23	0.17	1.06	
				median	38.68		13.20	8.14	65.06	
Remarks										
R2	*shear pin broke early, did not reach lock up*									

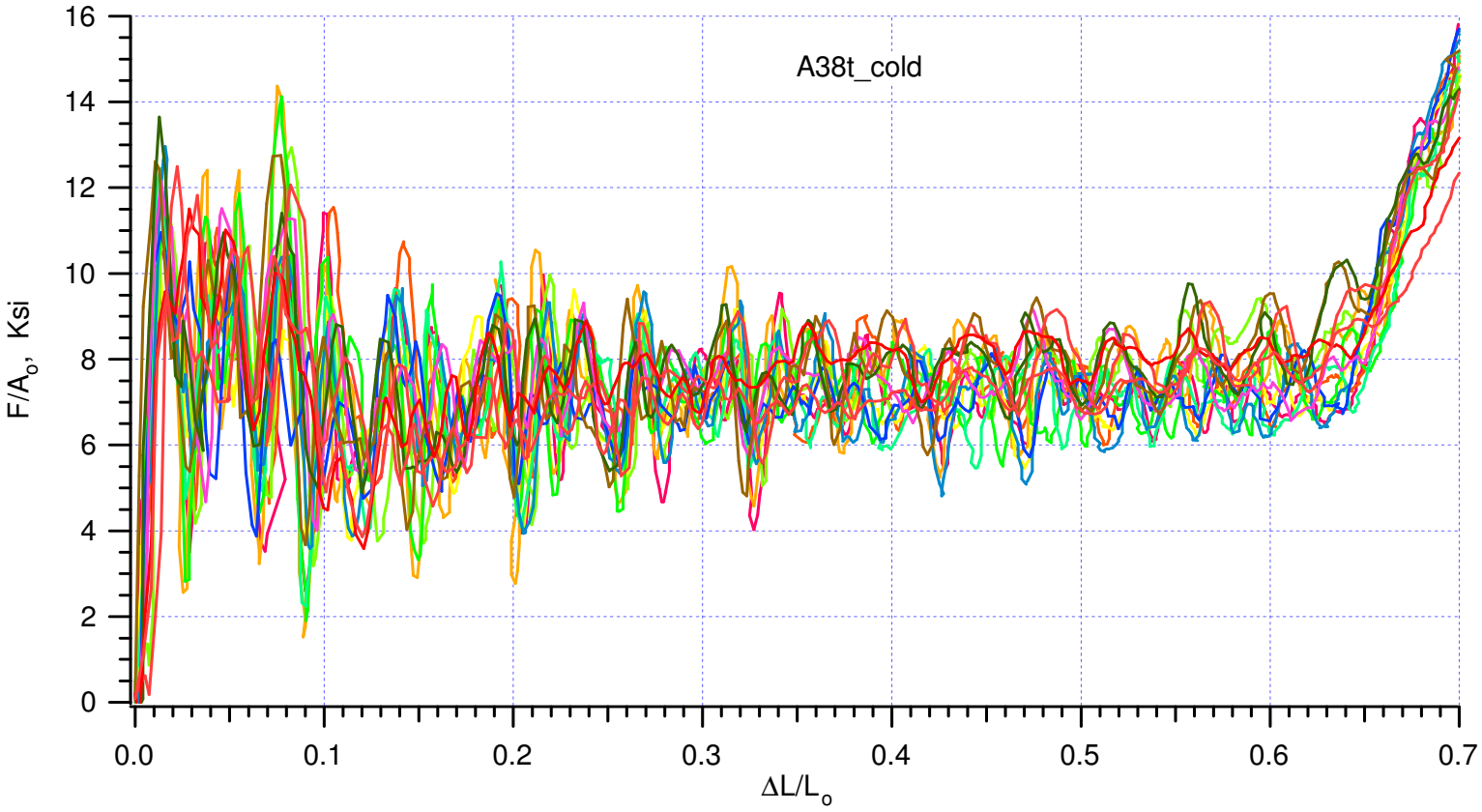

Figure 1. Stress-strain curves of all Alcore 38 specimens crushed in t-direction at -65^{o}F

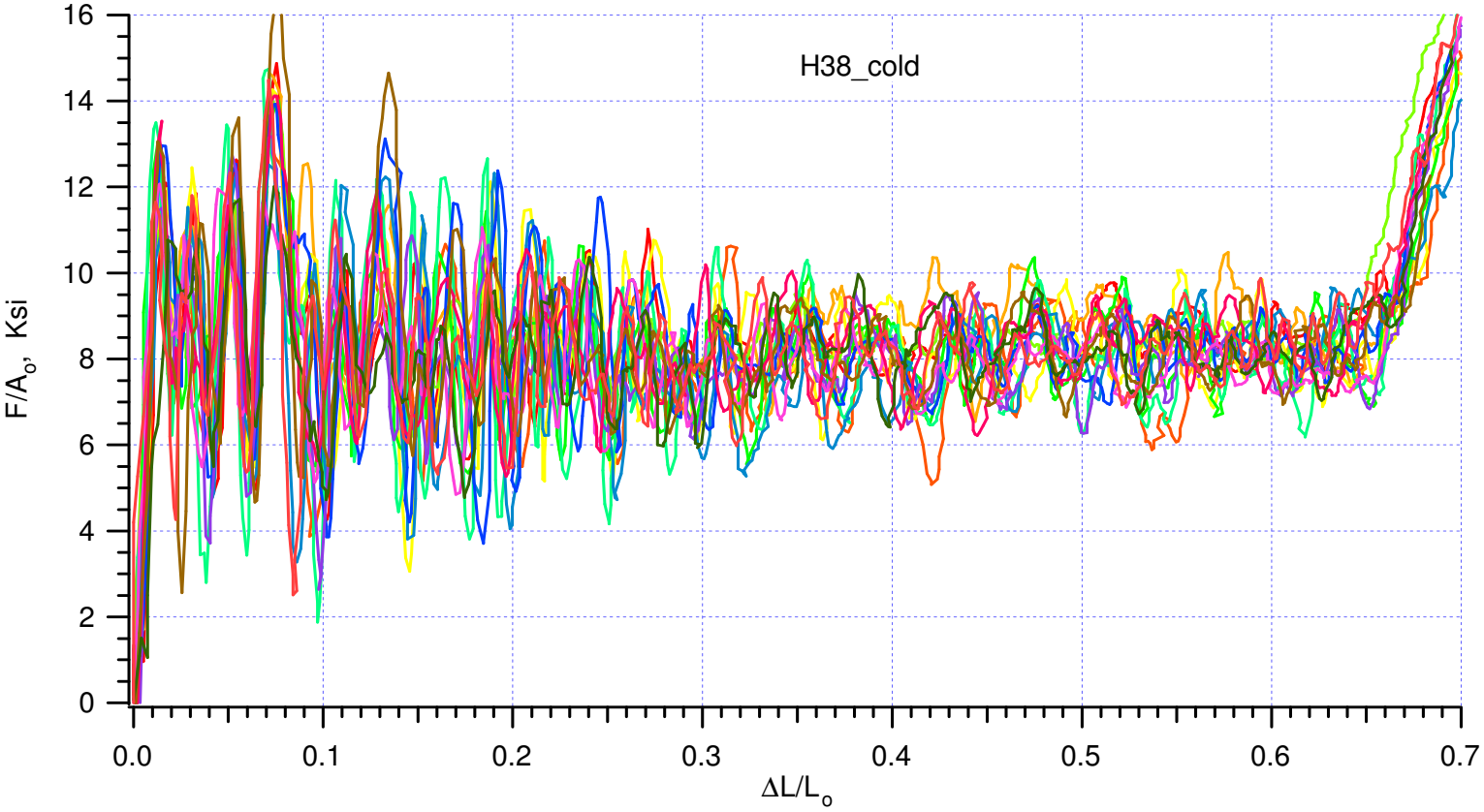

Figure 2. Stress-strain curves of all Hexcel 38 specimens crushed in t-direction at -65°F

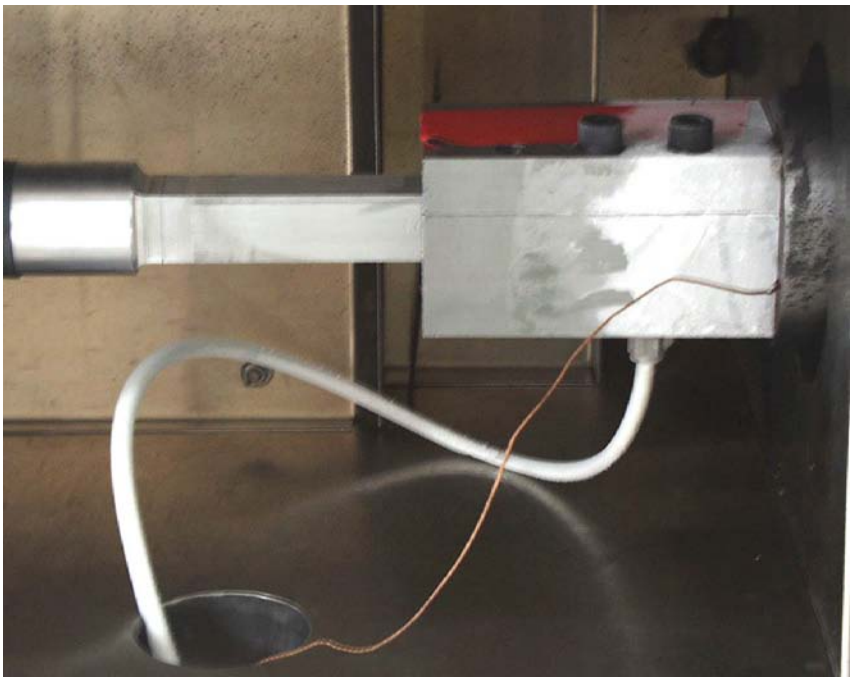

Figure 3. Setup for low temperature experiments.

Appendix A38t_cold

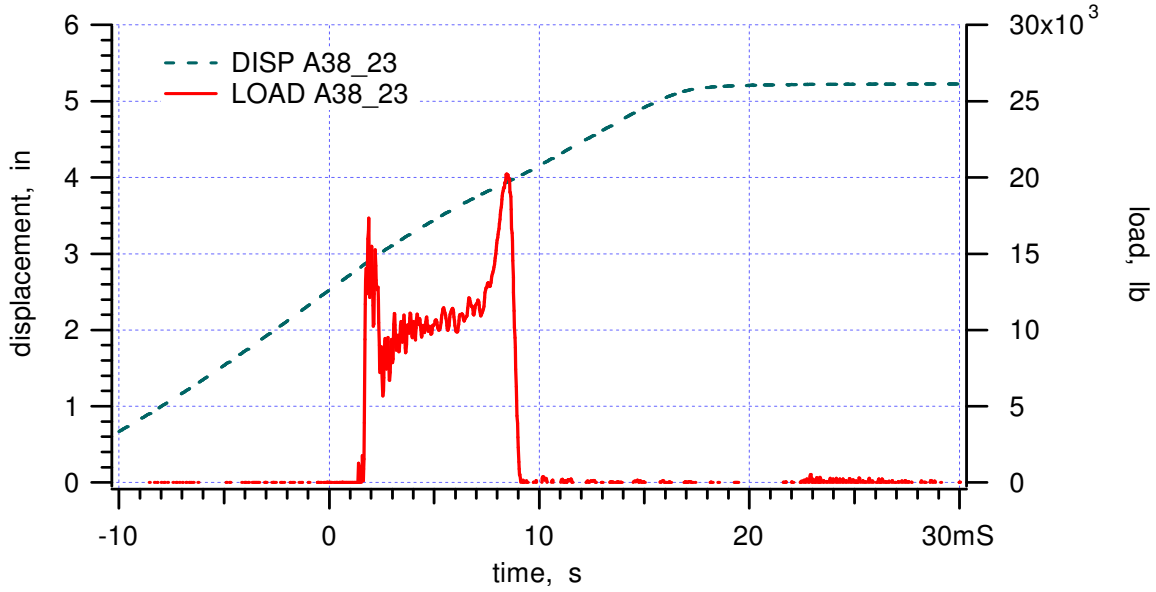

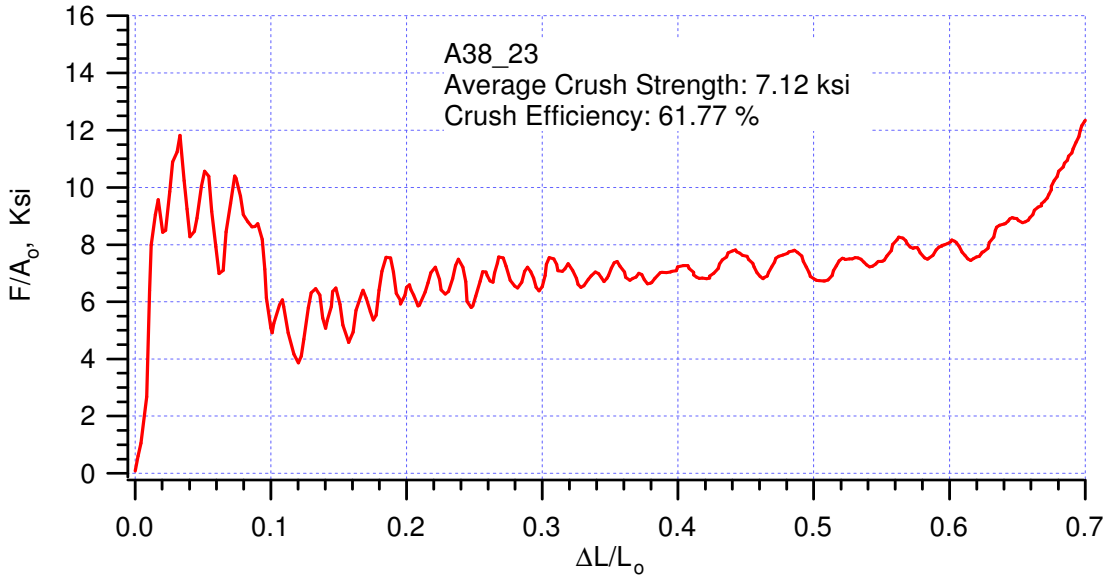

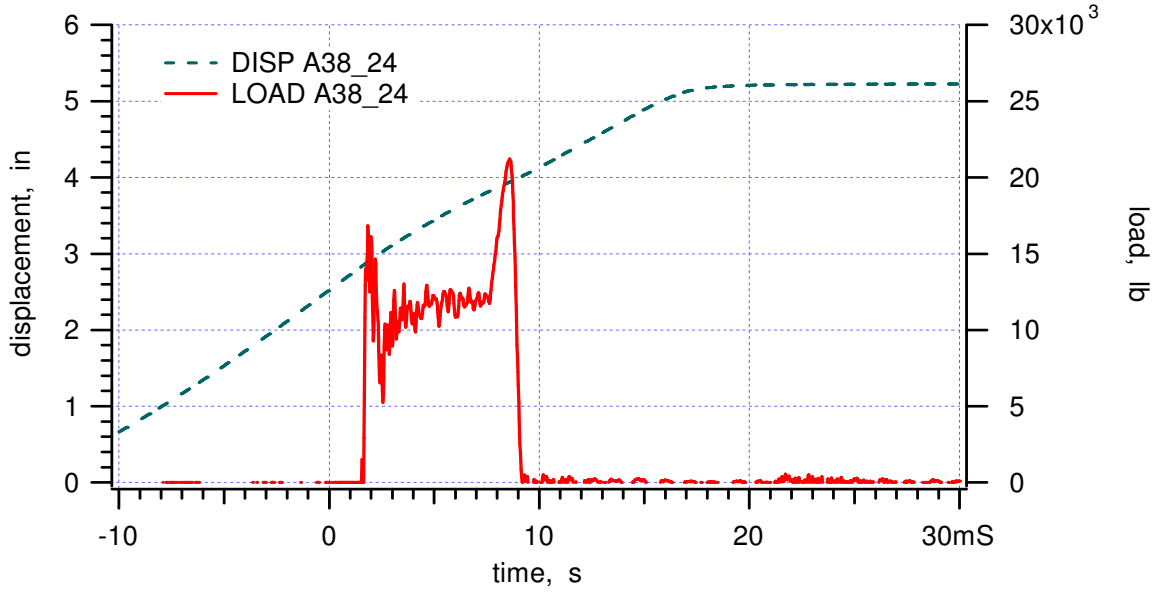
DISP A38_24
LOAD A38_24
displacement, in
load, lb
30x10^3
time, s
-10
0
10
20
30mS

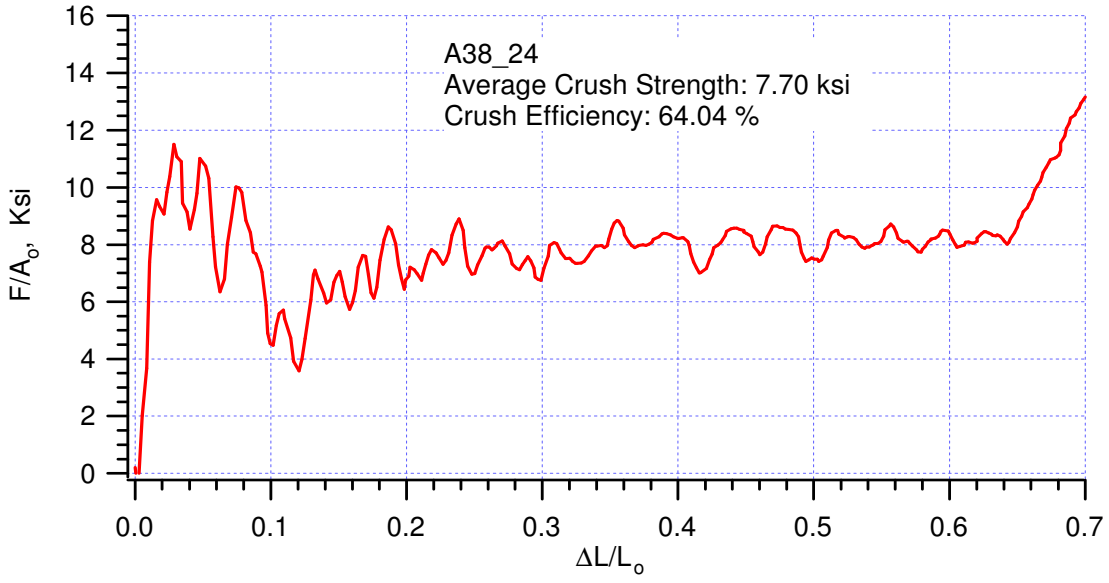
A38_24
Average Crush Strength: 7.70 ksi
Crush Efficiency: 64.04 %
F/A_o, Ksi
ΔL/L_o

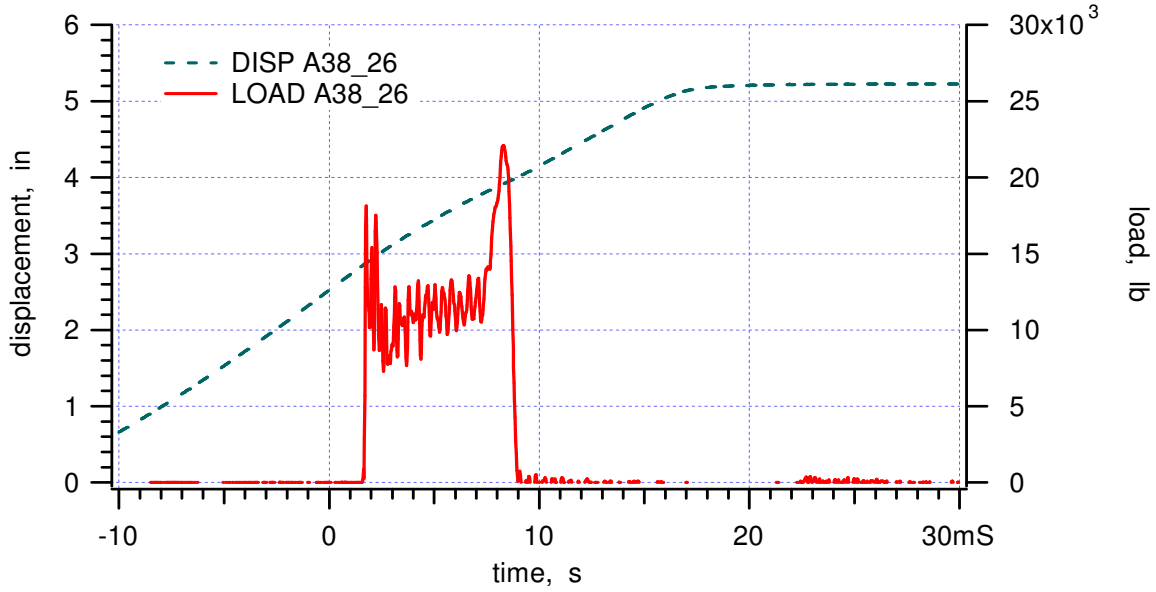
DISP A38_26
LOAD A38_26
displacement, in
load, lb
30x10^3
time, s
-10
0
10
20
30mS

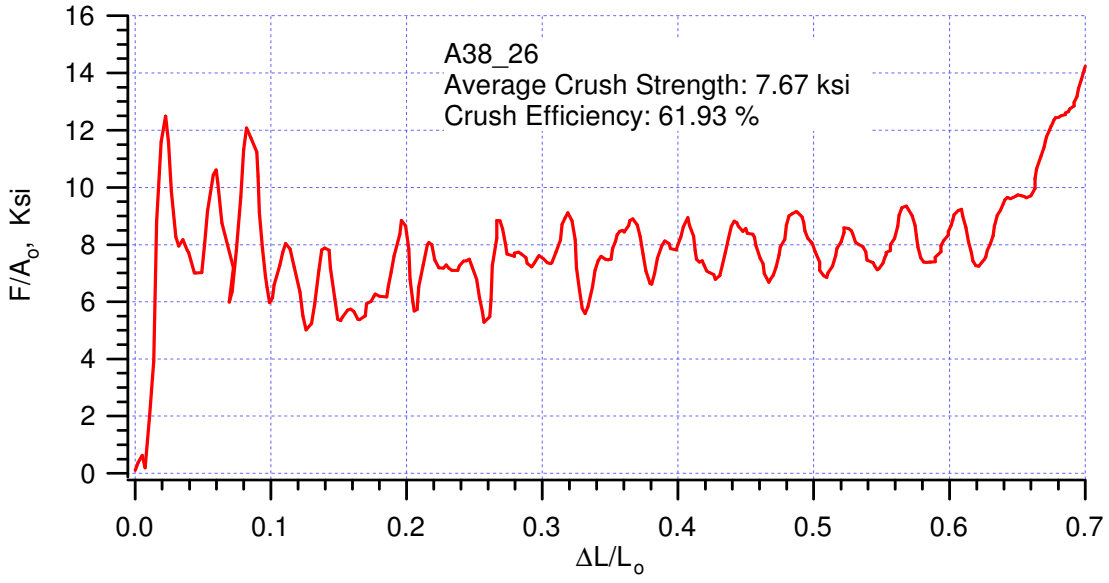
A38_26
Average Crush Strength: 7.67 ksi
Crush Efficiency: 61.93 %
F/A_o, Ksi
ΔL/L_o

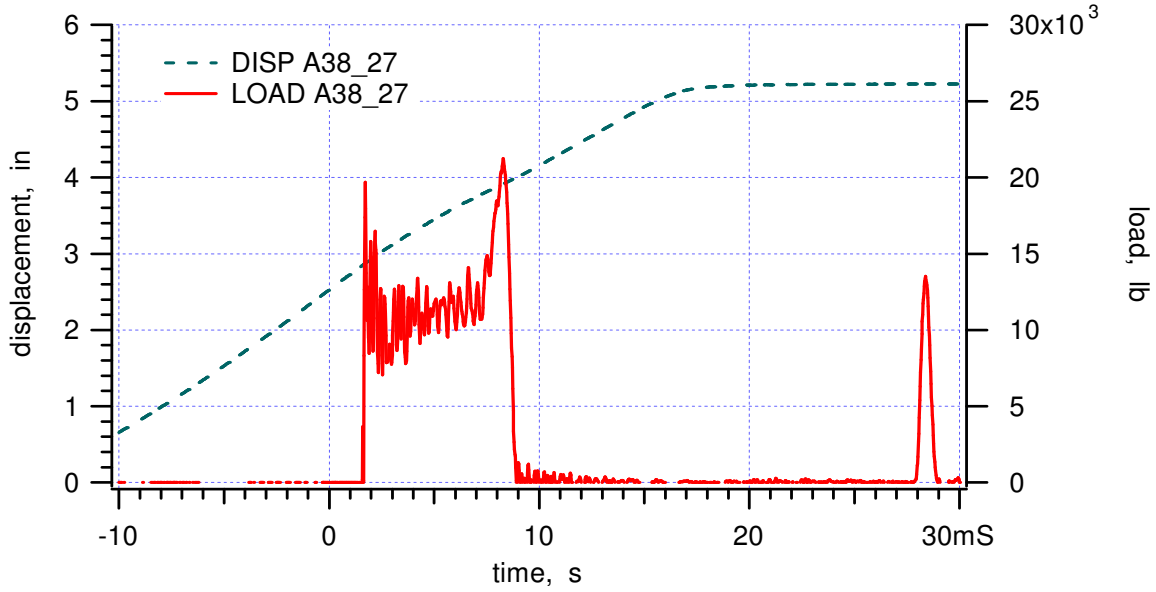
DISP A38_27
LOAD A38_27
displacement, in
load, lb
30x10^3
time, s
-10
0
10
20
30mS

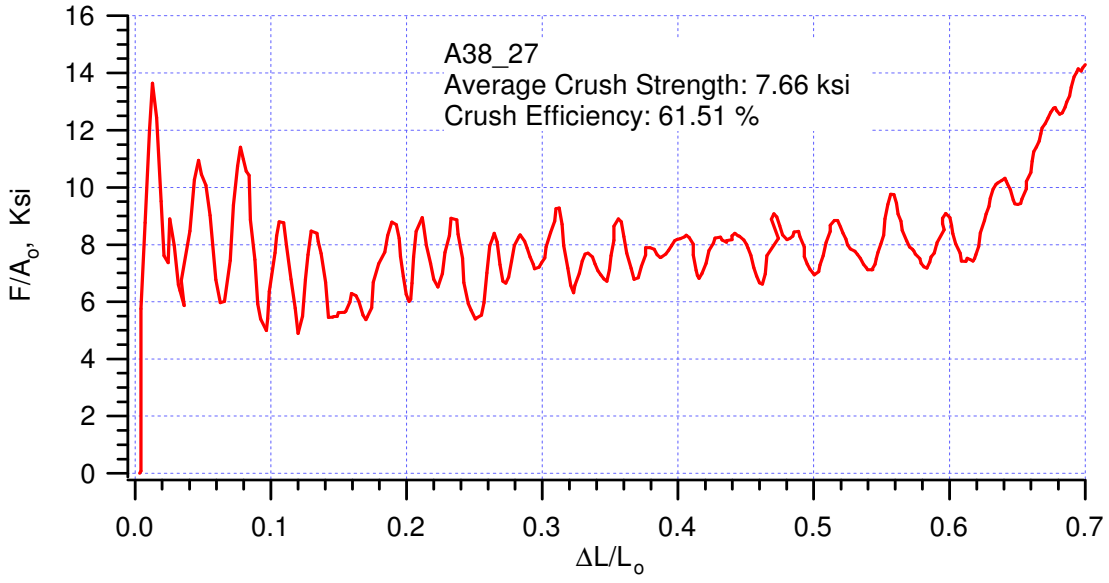
A38_27
Average Crush Strength: 7.66 ksi
Crush Efficiency: 61.51 %
F/A_o, Ksi
ΔL/L_o

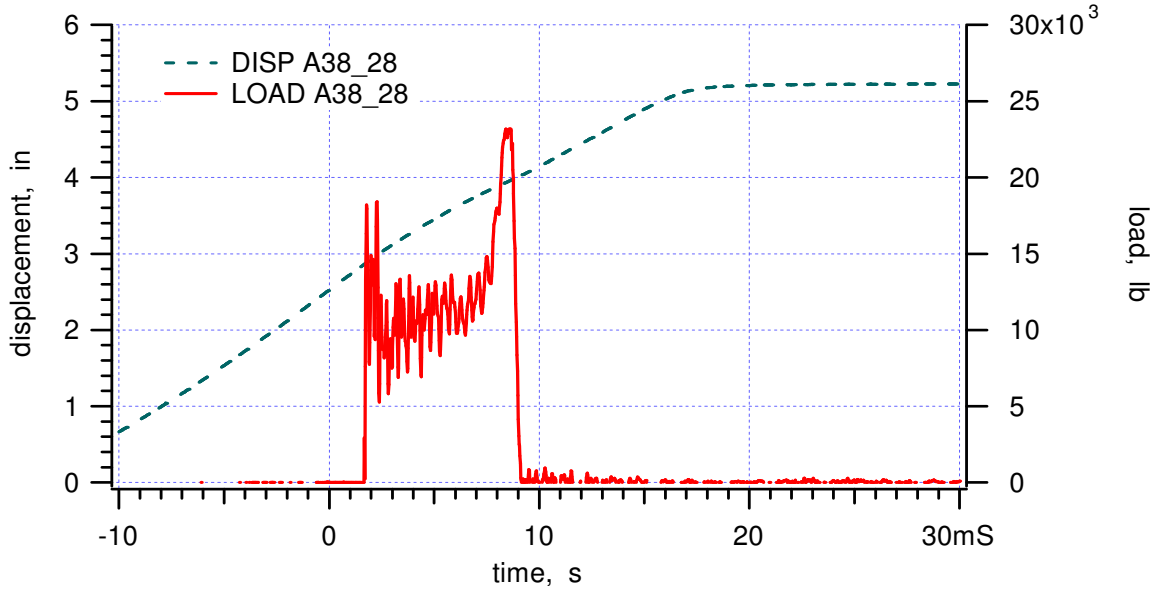
DISP A38_28
LOAD A38_28
displacement, in
load, lb
30x10^3
time, s
-10
0
10
20
30mS

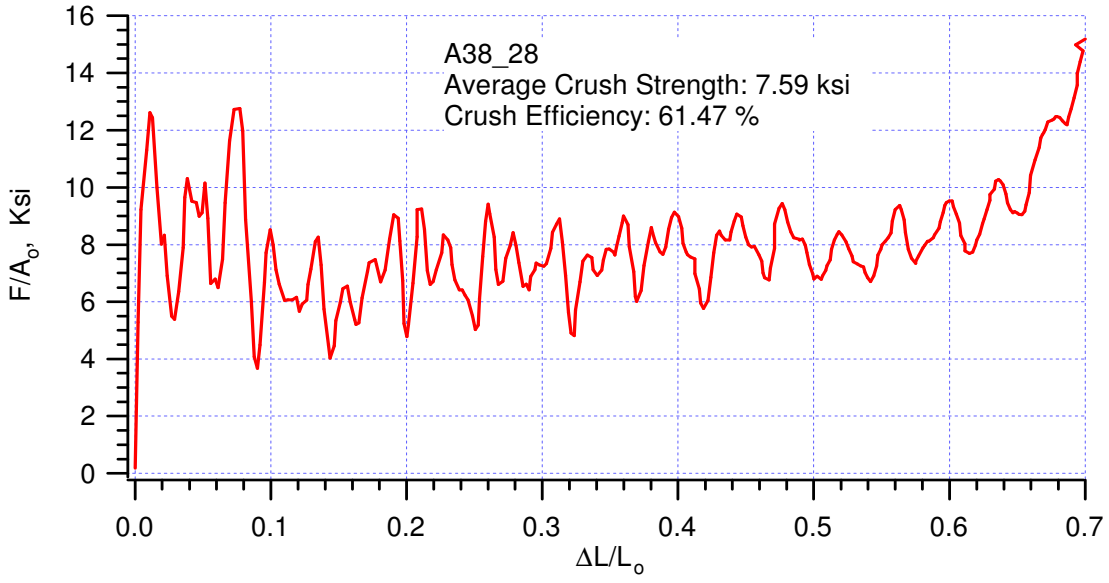
A38_28
Average Crush Strength: 7.59 ksi
Crush Efficiency: 61.47 %
F/A_o, Ksi
ΔL/L_o

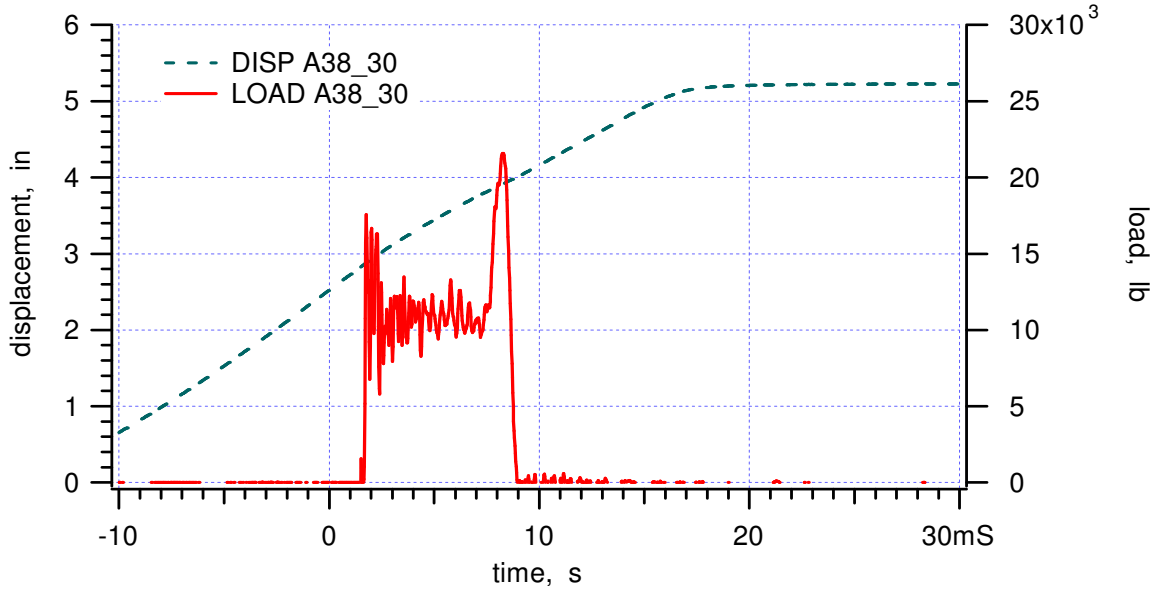
DISP A38_30
LOAD A38_30
displacement, in
load, lb
30x10^3
time, s
-10
0
10
20
30mS

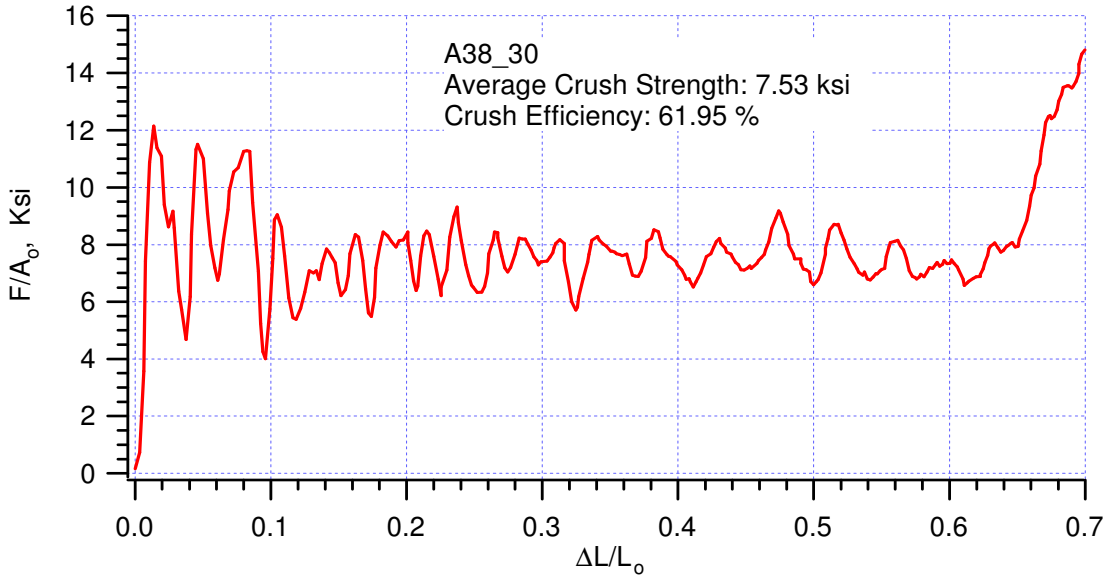
A38_30
Average Crush Strength: 7.53 ksi
Crush Efficiency: 61.95 %
F/A_o, Ksi
ΔL/L_o

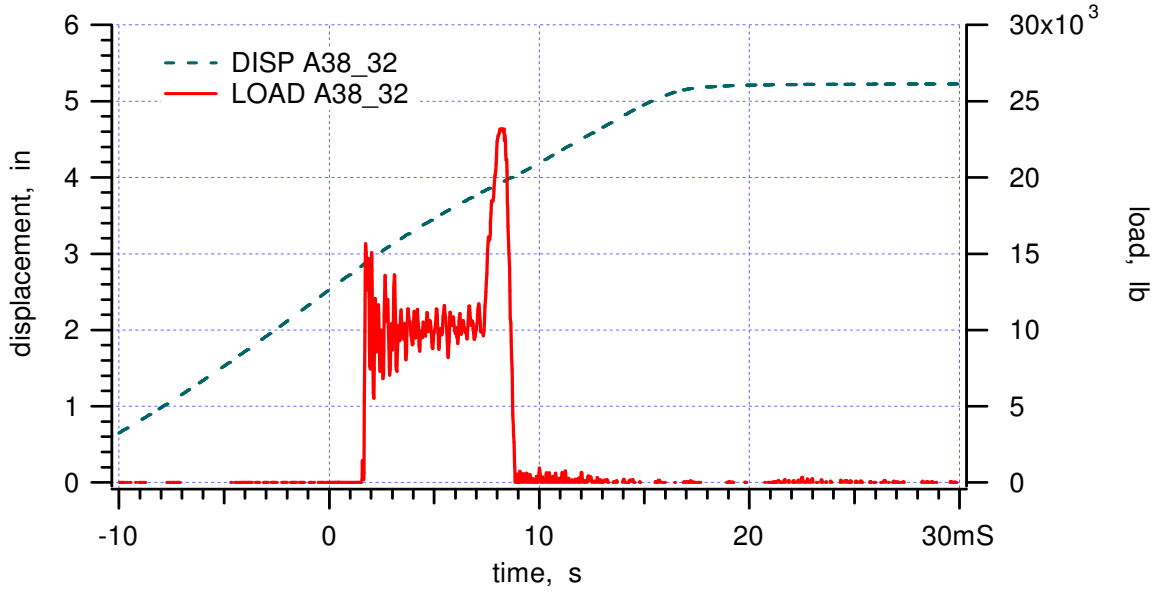
DISP A38_32
LOAD A38_32
displacement, in
load, lb
30x10^3
time, s
-10
0
10
20
30mS

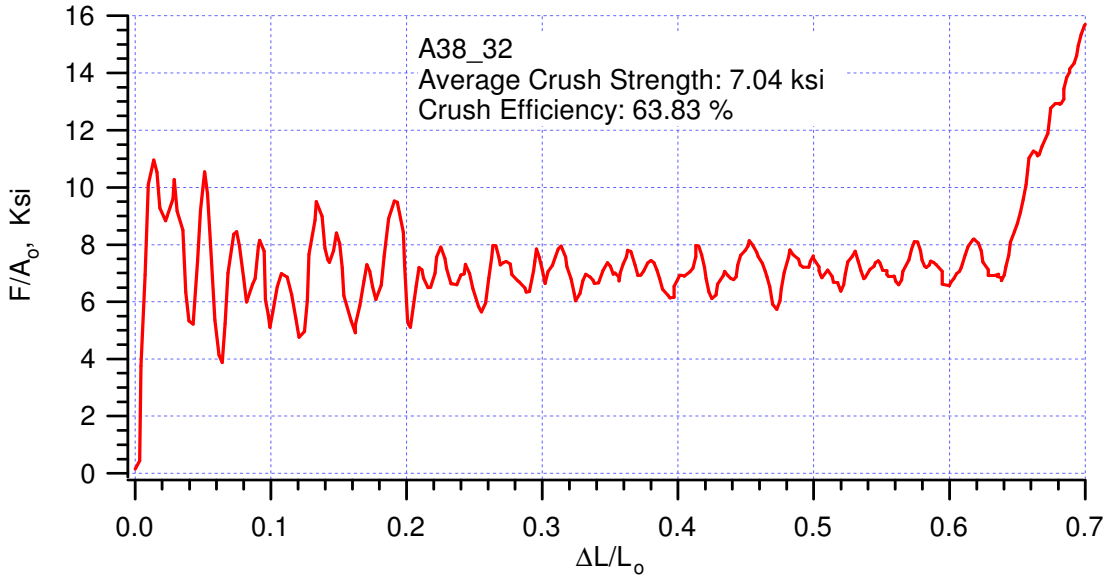
A38_32
Average Crush Strength: 7.04 ksi
Crush Efficiency: 63.83 %
F/A_o, Ksi
ΔL/L_o

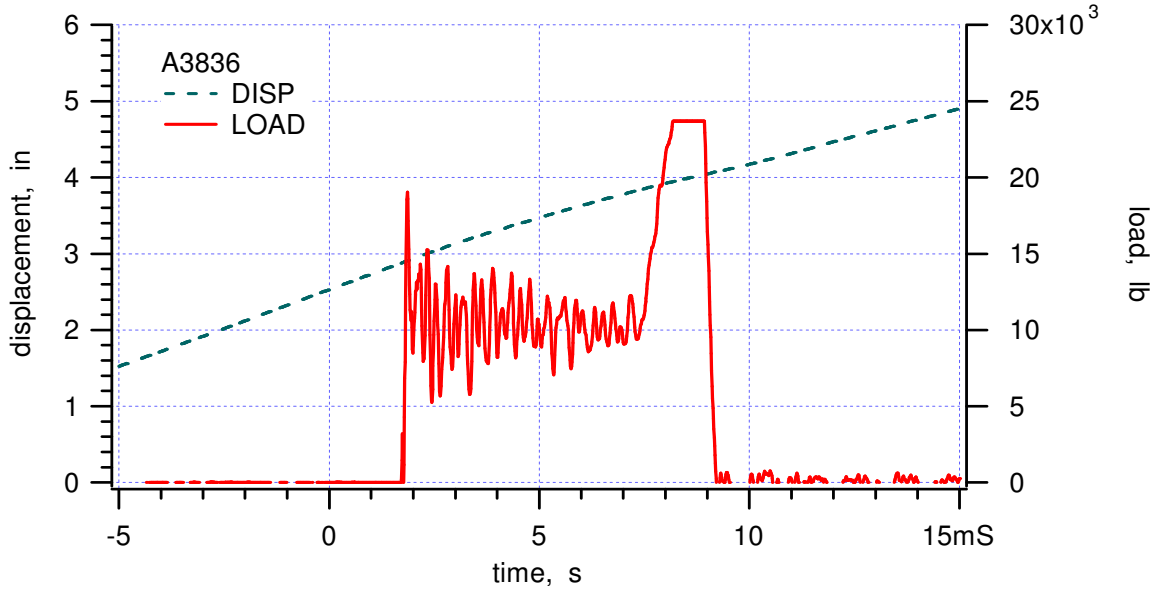
A3836
DISP
LOAD
displacement, in
load, lb
30x10^3
time, s
-5
0
5
10
15mS

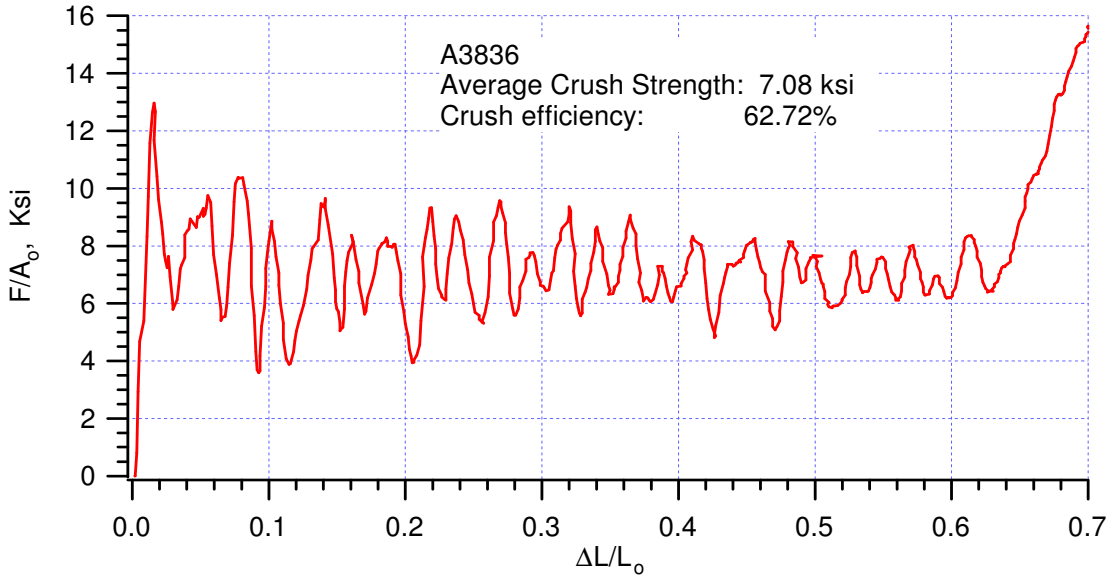
A3836
Average Crush Strength: 7.08 ksi
Crush efficiency: 62.72%
F/A_o, Ksi
ΔL/L_o

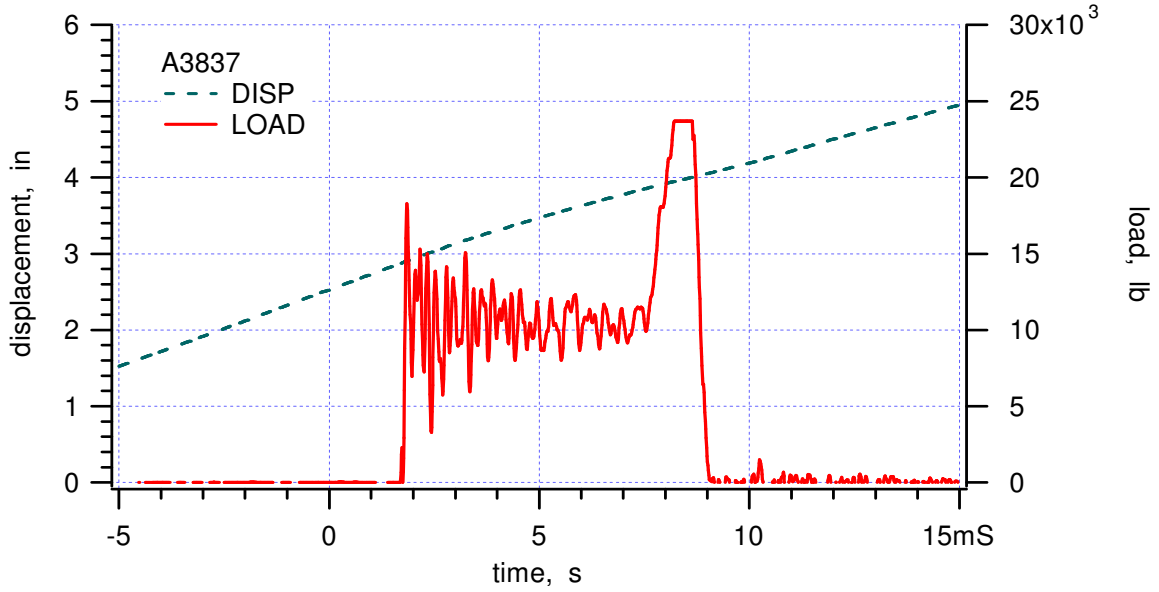
A3837
DISP
LOAD
displacement, in
load, lb
30x10^3
time, s
-5
0
5
10
15mS

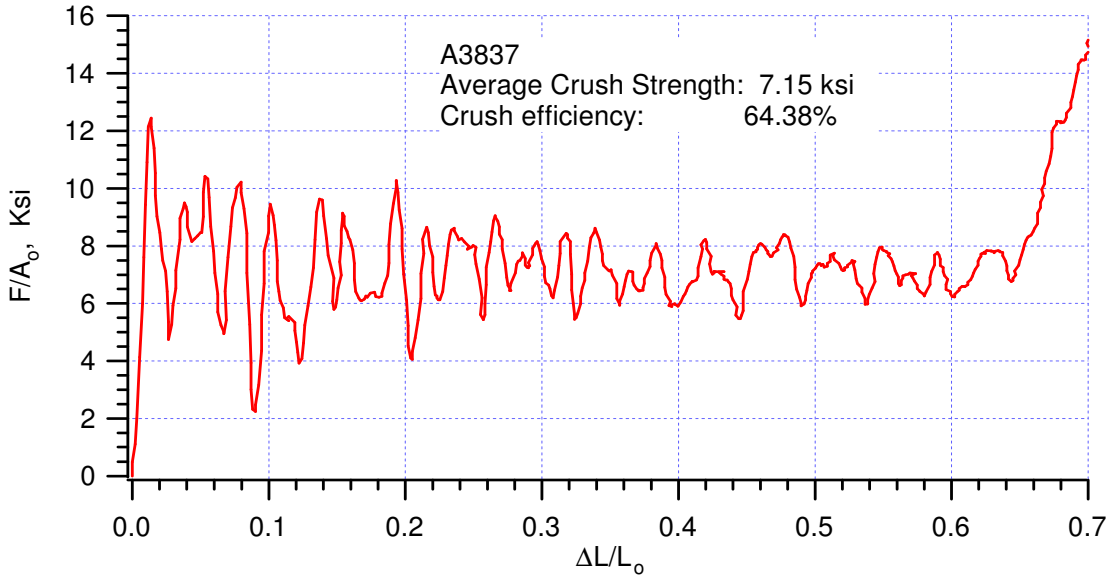
A3837
Average Crush Strength: 7.15 ksi
Crush efficiency: 64.38%
F/A_o, Ksi
ΔL/L_o

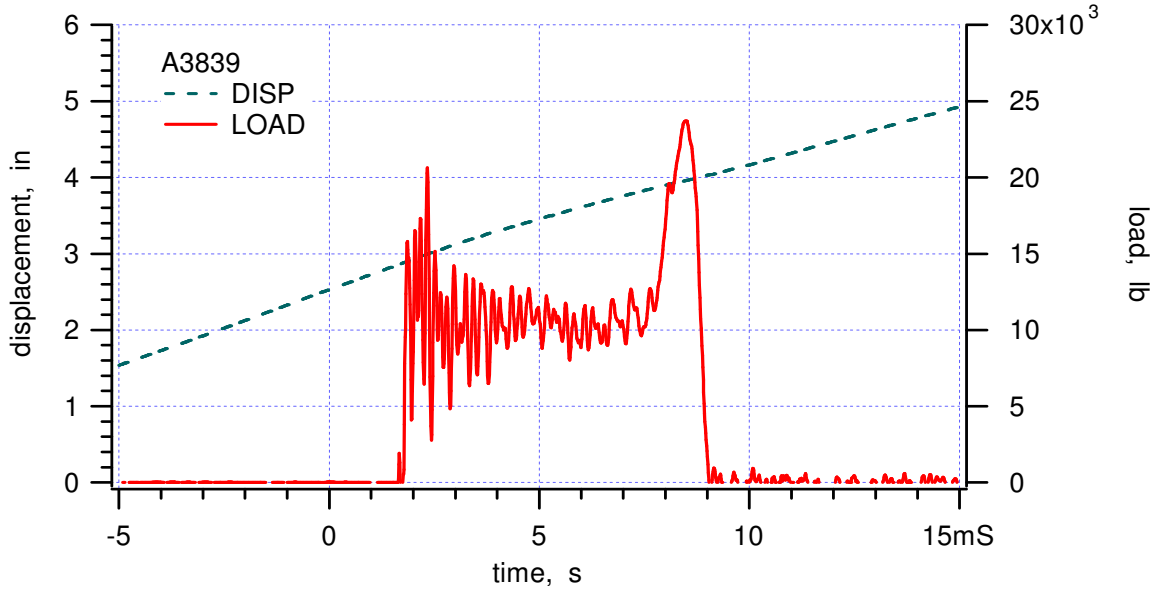
A3839
DISP
LOAD
displacement, in
load, lb
30x10^3
time, s
-5
0
5
10
15mS

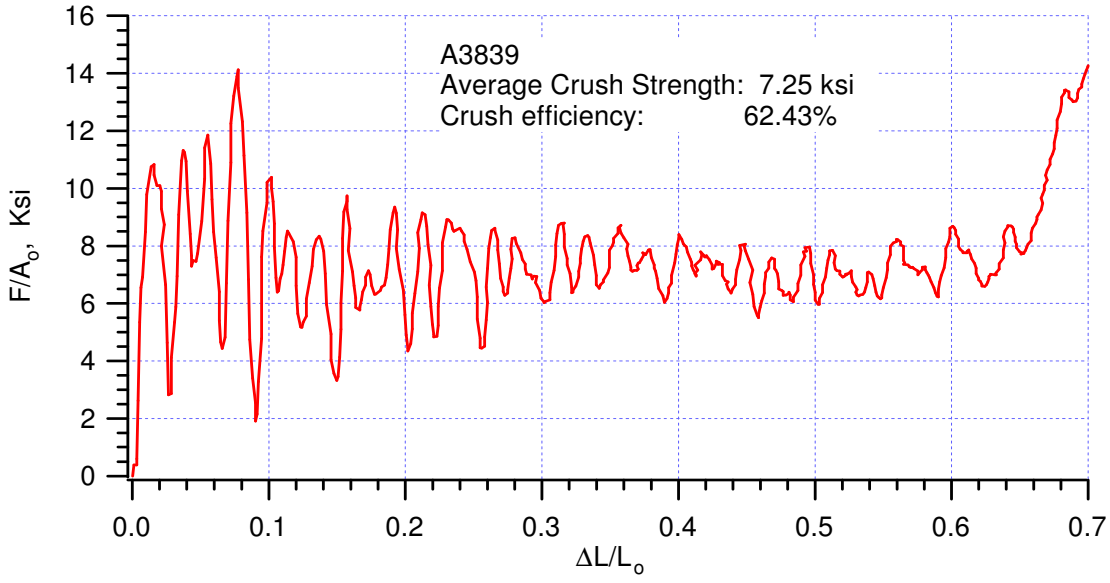
A3839
Average Crush Strength: 7.25 ksi
Crush efficiency: 62.43%
F/A_o, Ksi
ΔL/L_o

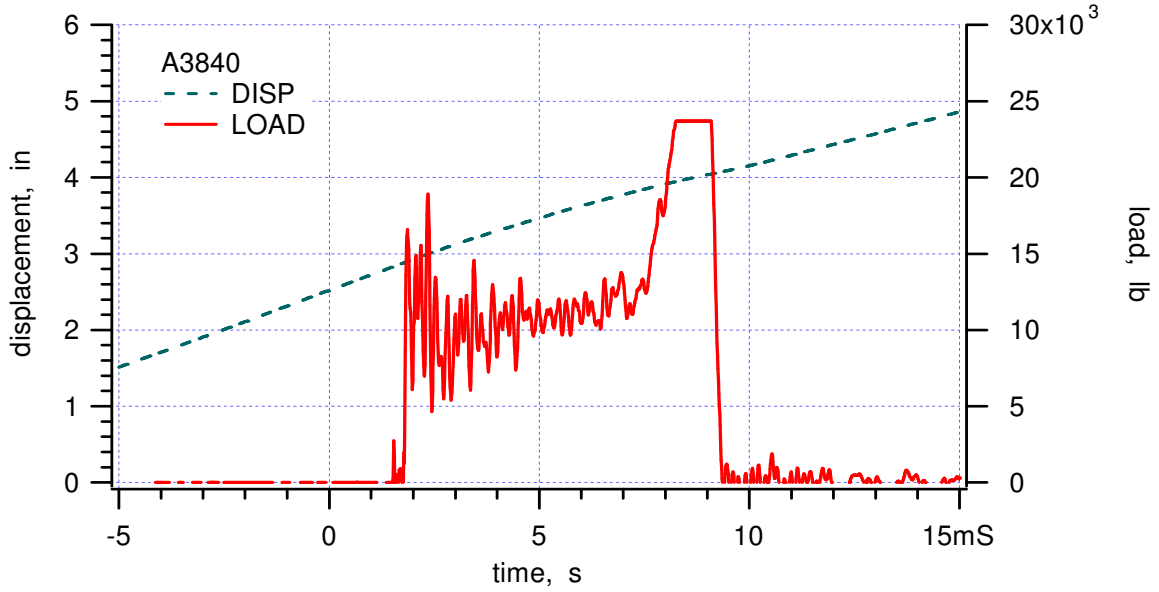
A3840
DISP
LOAD
displacement, in
load, lb
time, s
-5
0
5
10
15mS
30x10^3

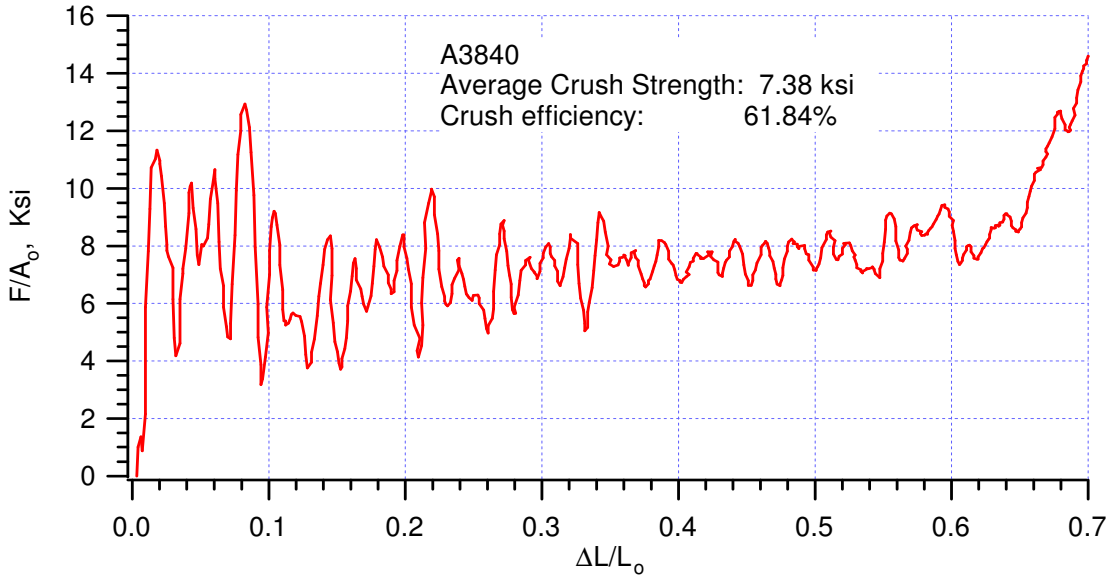
A3840
Average Crush Strength: 7.38 ksi
Crush efficiency: 61.84%
F/A_o, Ksi
ΔL/L_o

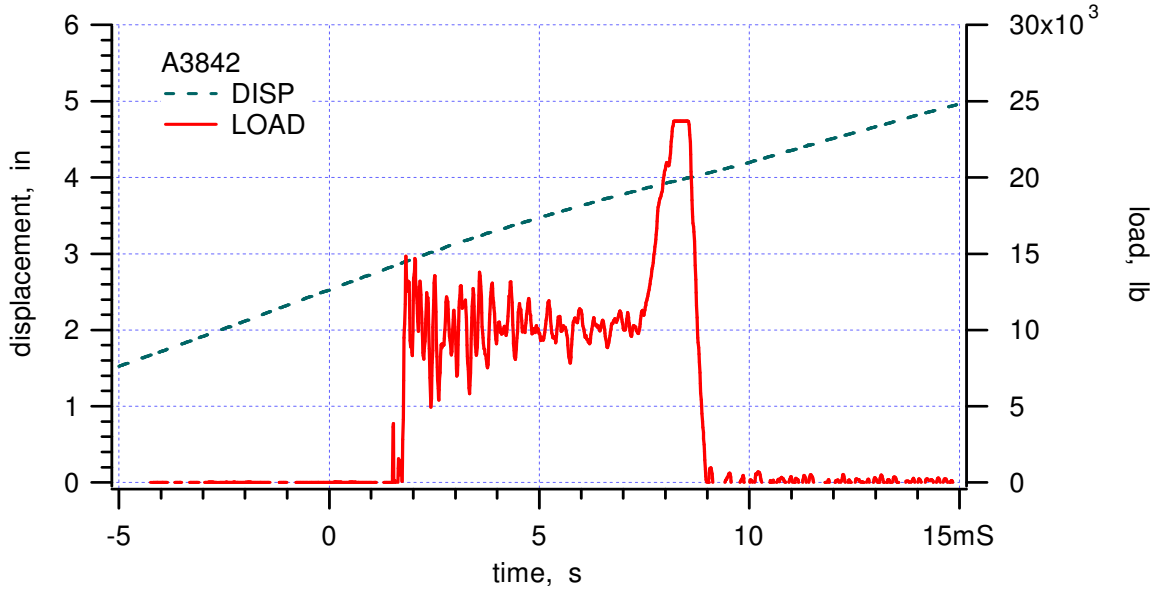
A3842
DISP
LOAD
displacement, in
load, lb
30x10^3
time, s
-5
0
5
10
15mS

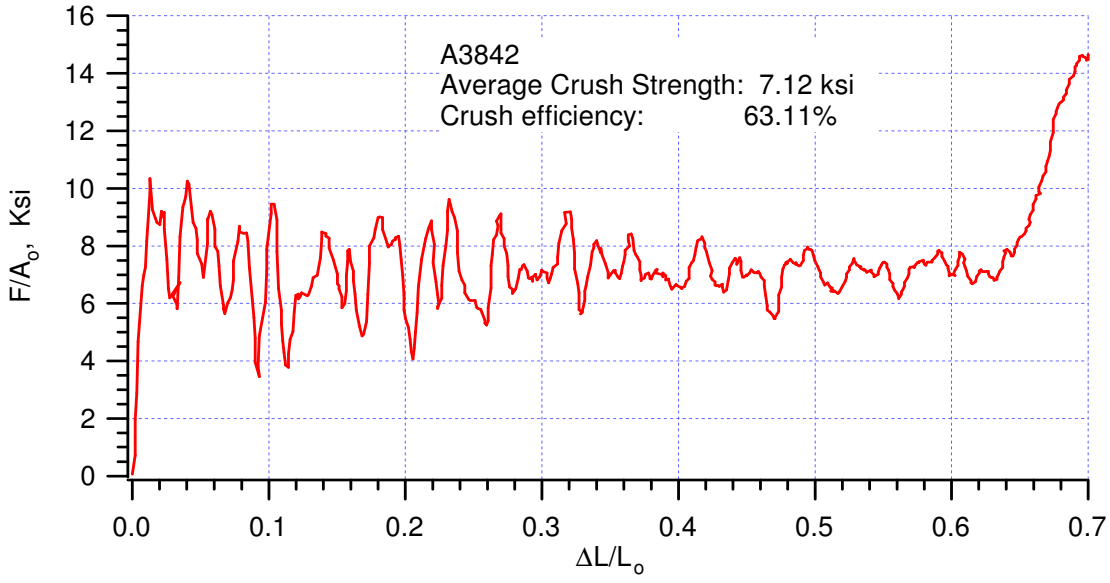
A3842
Average Crush Strength: 7.12 ksi
Crush efficiency: 63.11%
F/A_o, Ksi
ΔL/L_o

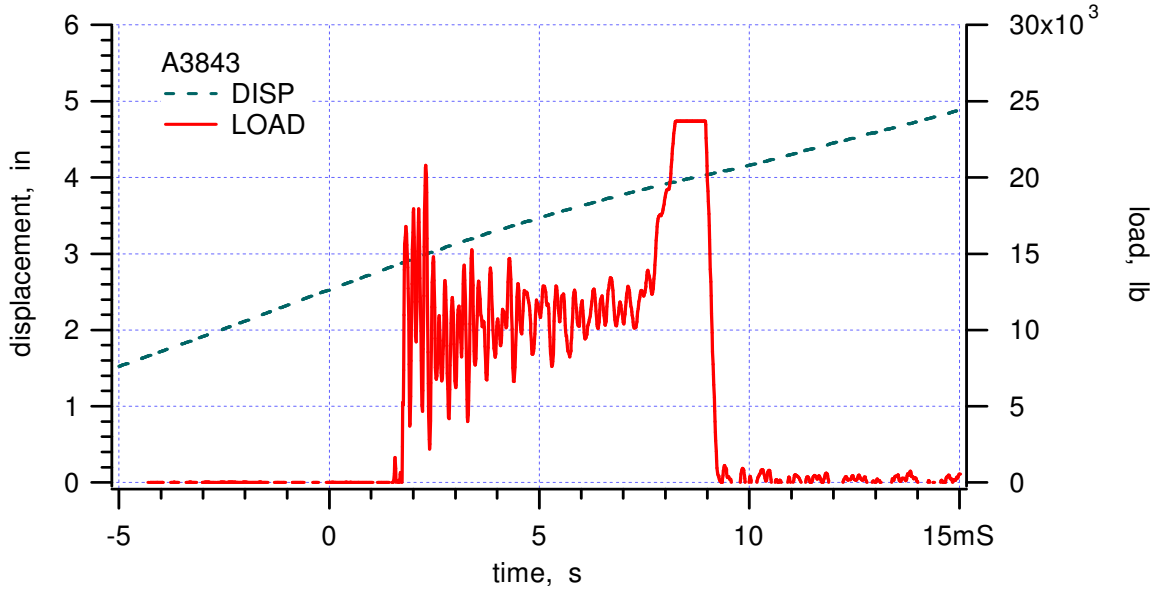
A3843
DISP
LOAD
displacement, in
load, lb
30x10^3
time, s
-5
0
5
10
15mS

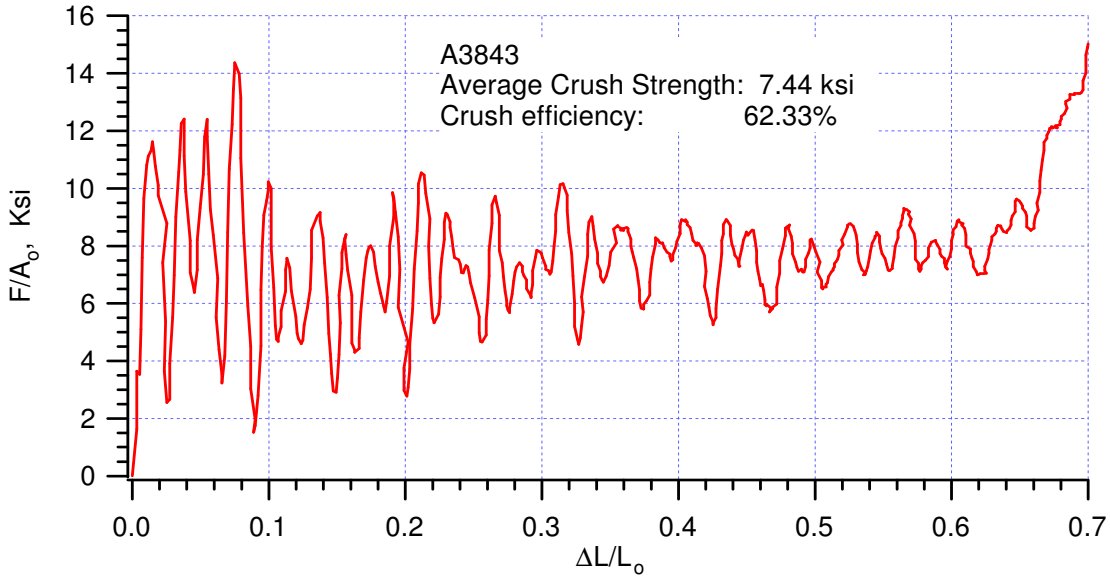
A3843
Average Crush Strength: 7.44 ksi
Crush efficiency: 62.33%
F/A_o, Ksi
ΔL/L_o

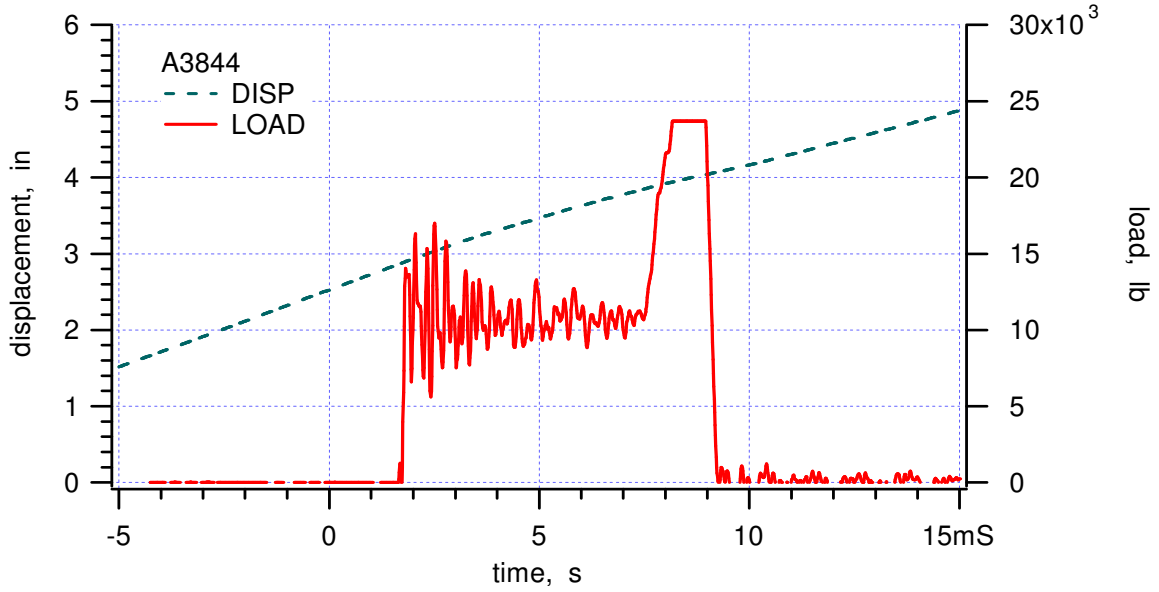
A3844
DISP
LOAD
displacement, in
load, lb
time, s
30x10^3
25
20
15
10
5
0
-5
0
5
10
15mS
1
2
3
4
5
6

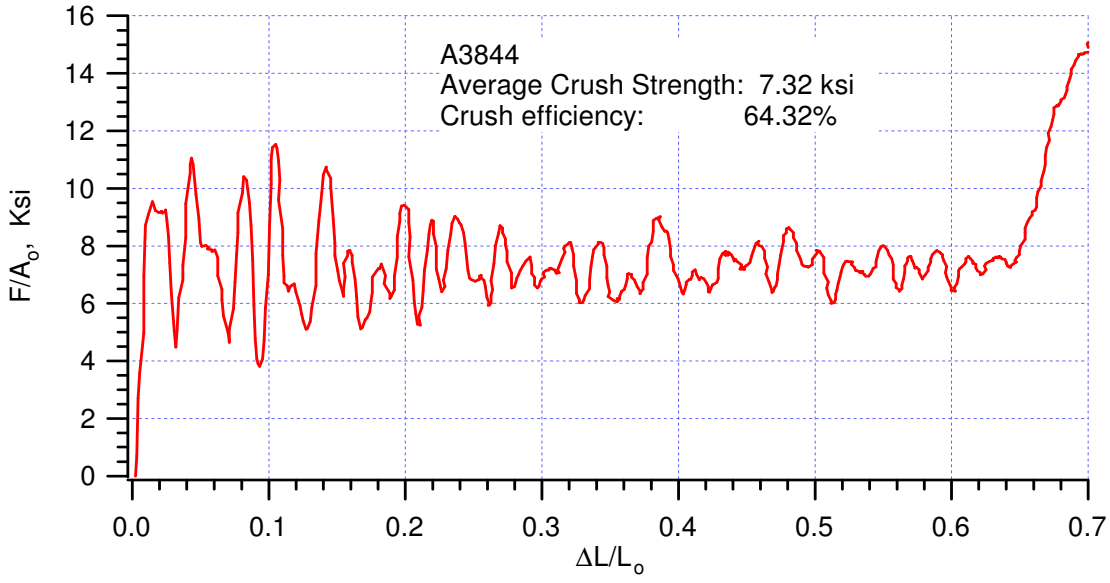
A3844
Average Crush Strength: 7.32 ksi
Crush efficiency: 64.32%
F/A_o, Ksi
ΔL/L_o
0.0
0.1
0.2
0.3
0.4
0.5
0.6
0.7
0
2
4
6
8
10
12
14
16

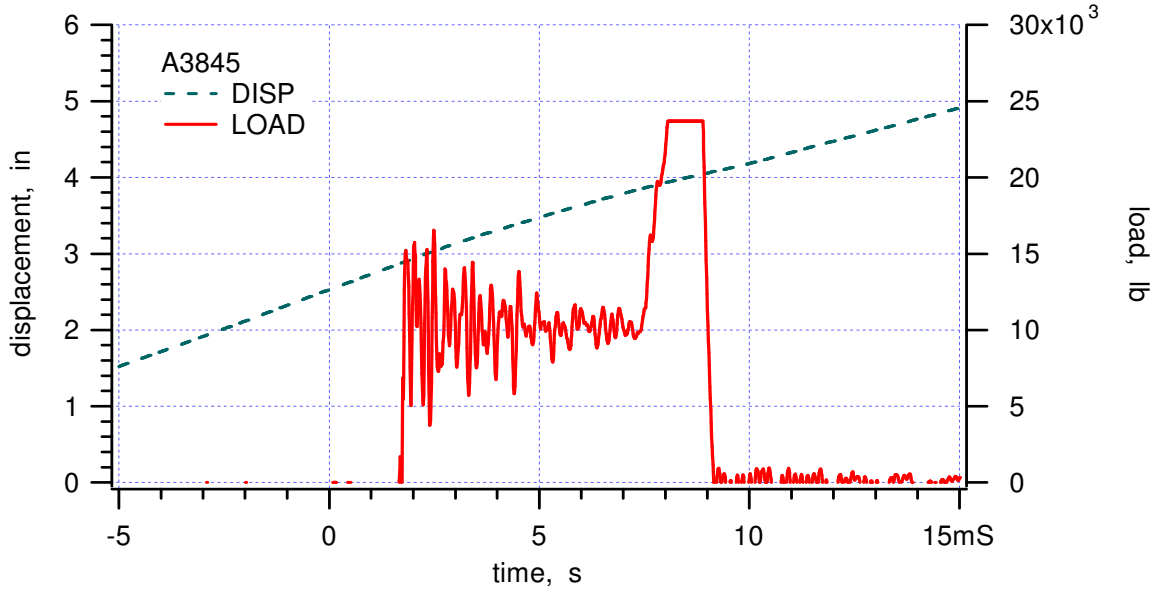
A3845
DISP
LOAD
displacement, in
load, lb
time, s
-5
0
5
10
15mS
30x10^3
25
20
15
10
5
0
1
2
3
4
5
6

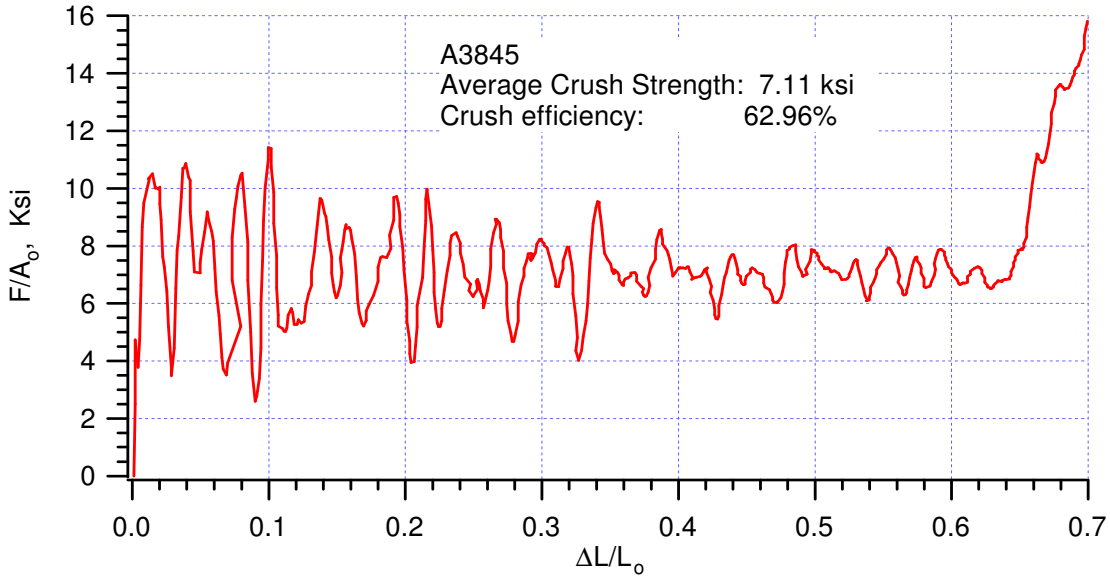
A3845
Average Crush Strength: 7.11 ksi
Crush efficiency: 62.96%
F/A_o, Ksi
ΔL/L_o
0.0
0.1
0.2
0.3
0.4
0.5
0.6
0.7
0
2
4
6
8
10
12
14
16

Appendix H38t_cold

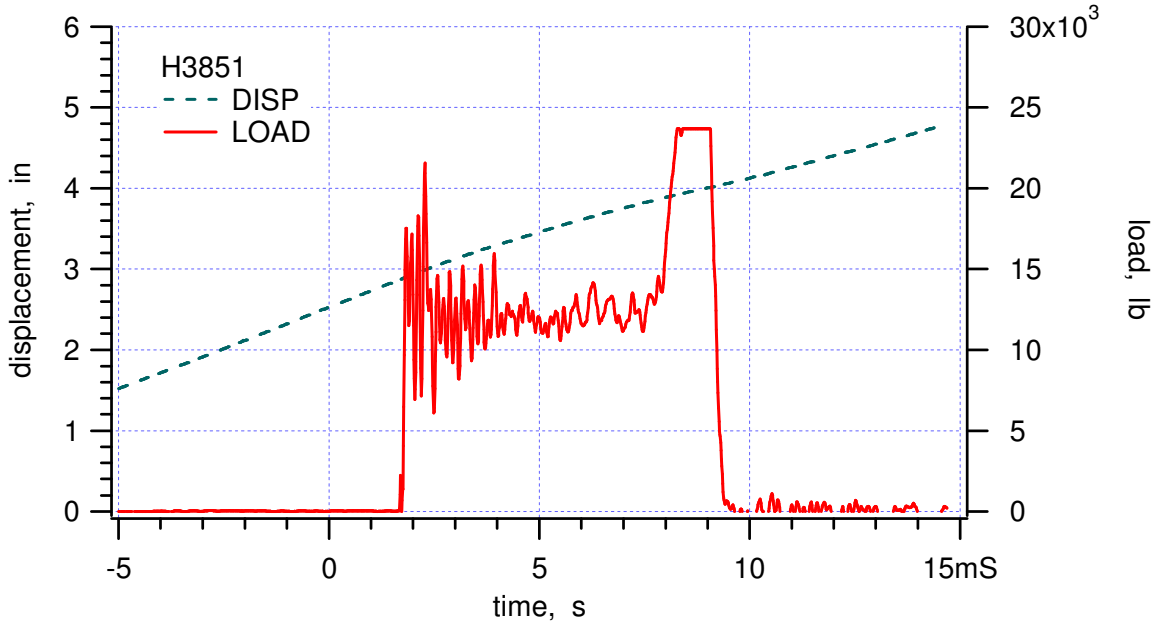

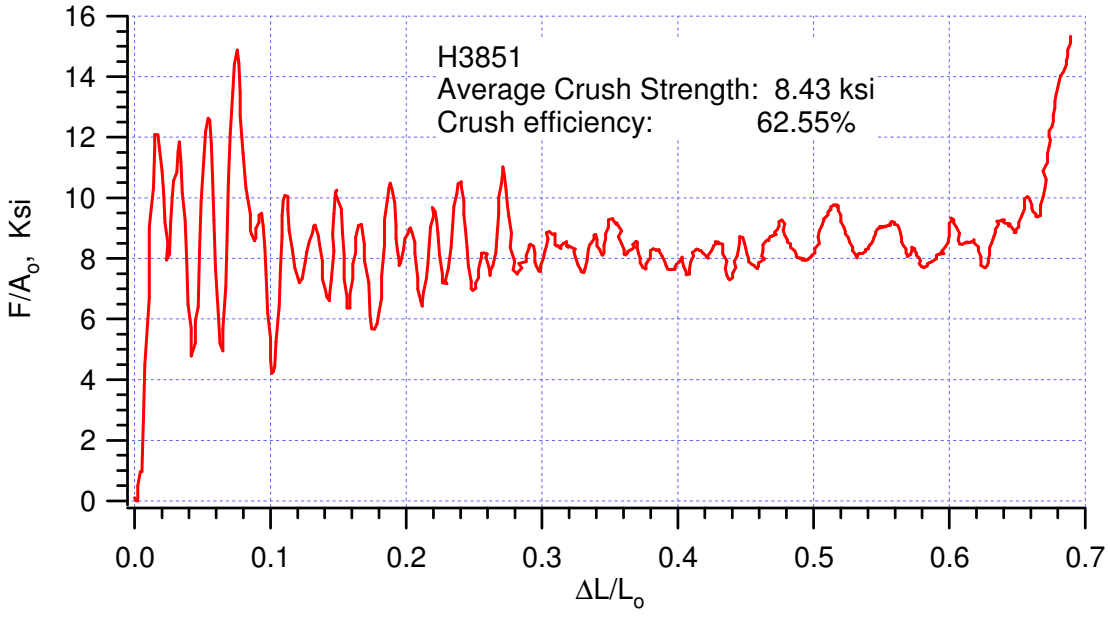

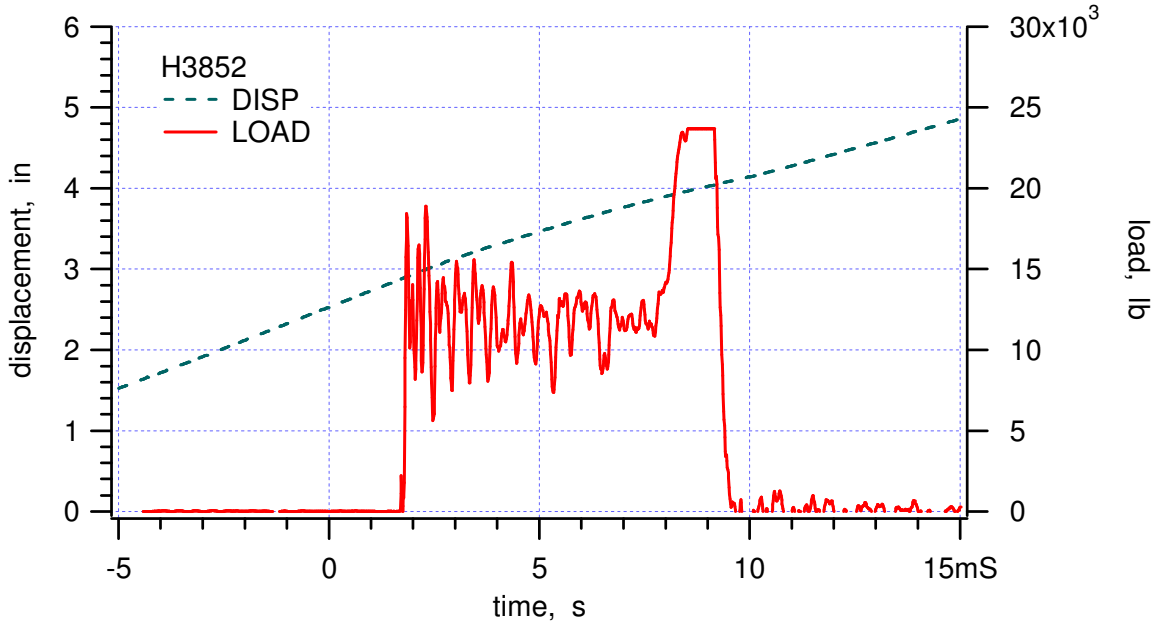
H3852
DISP
LOAD
displacement, in
load, lb
30x10^3
time, s
-5
0
5
10
15mS

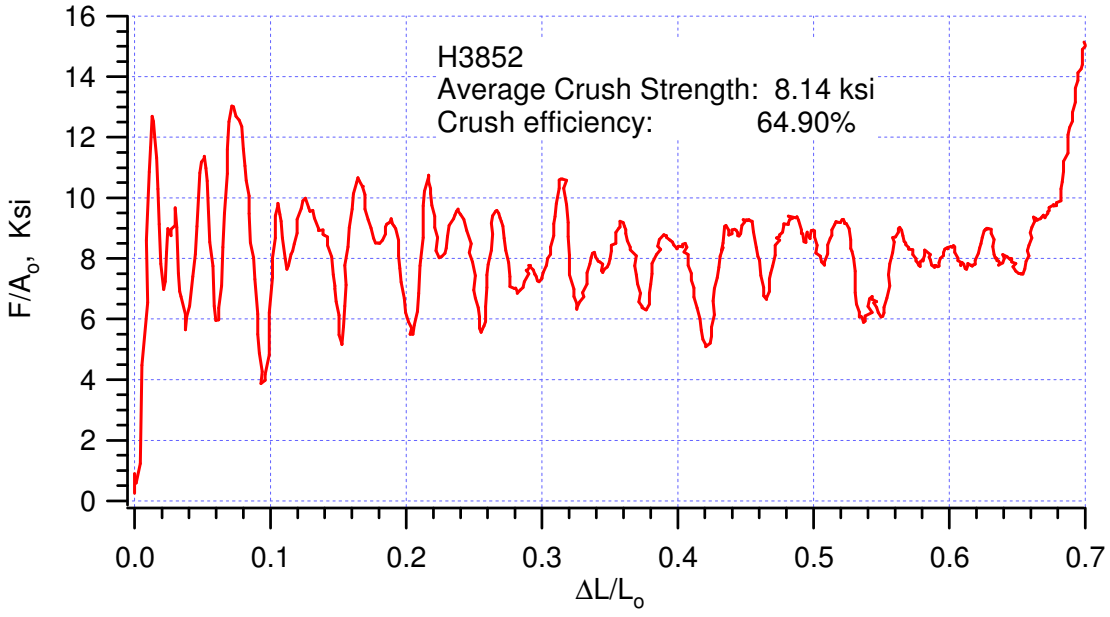
H3852
Average Crush Strength: 8.14 ksi
Crush efficiency: 64.90%
F/A_o, Ksi
ΔL/L_o

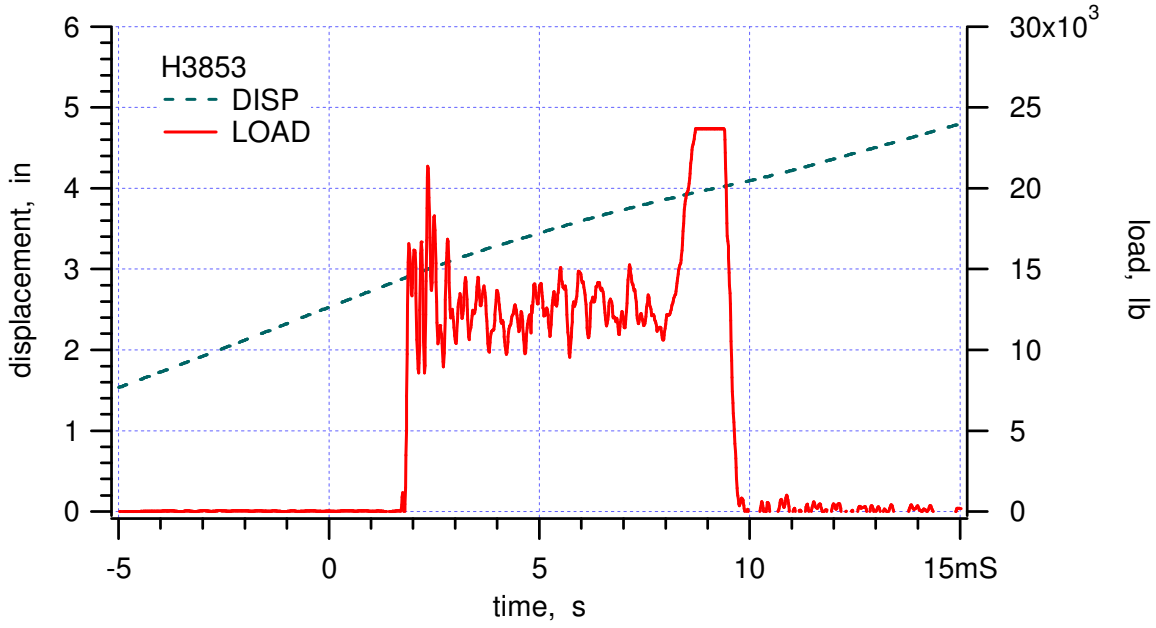
H3853
DISP
LOAD
displacement, in
load, lb
30x10^3
time, s
-5
0
5
10
15mS

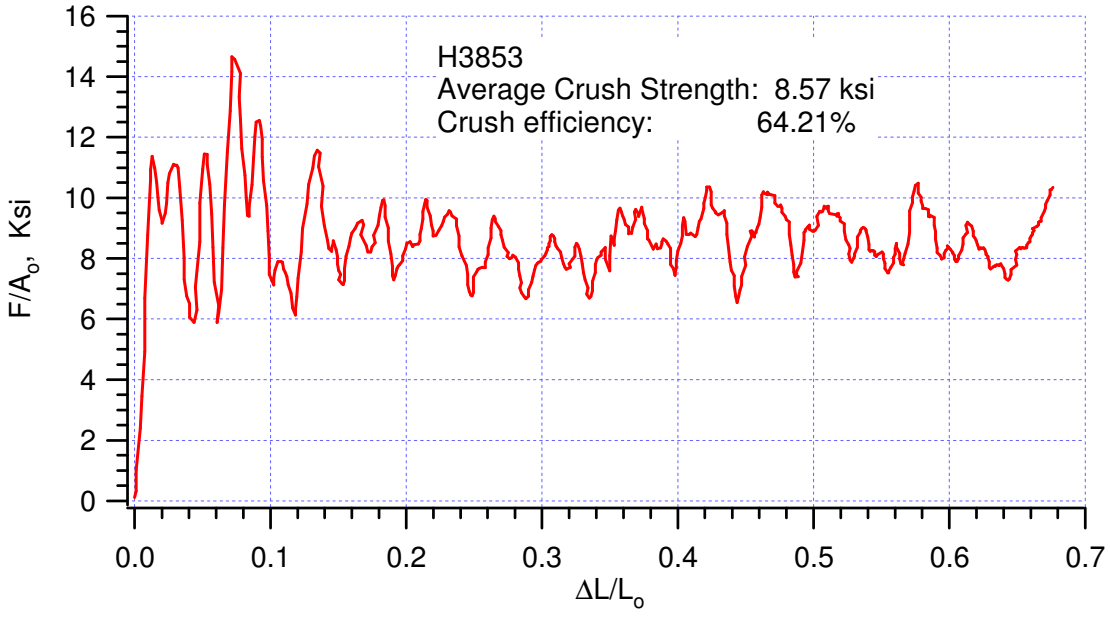
H3853
Average Crush Strength: 8.57 ksi
Crush efficiency: 64.21%
F/A_o, Ksi
ΔL/L_o

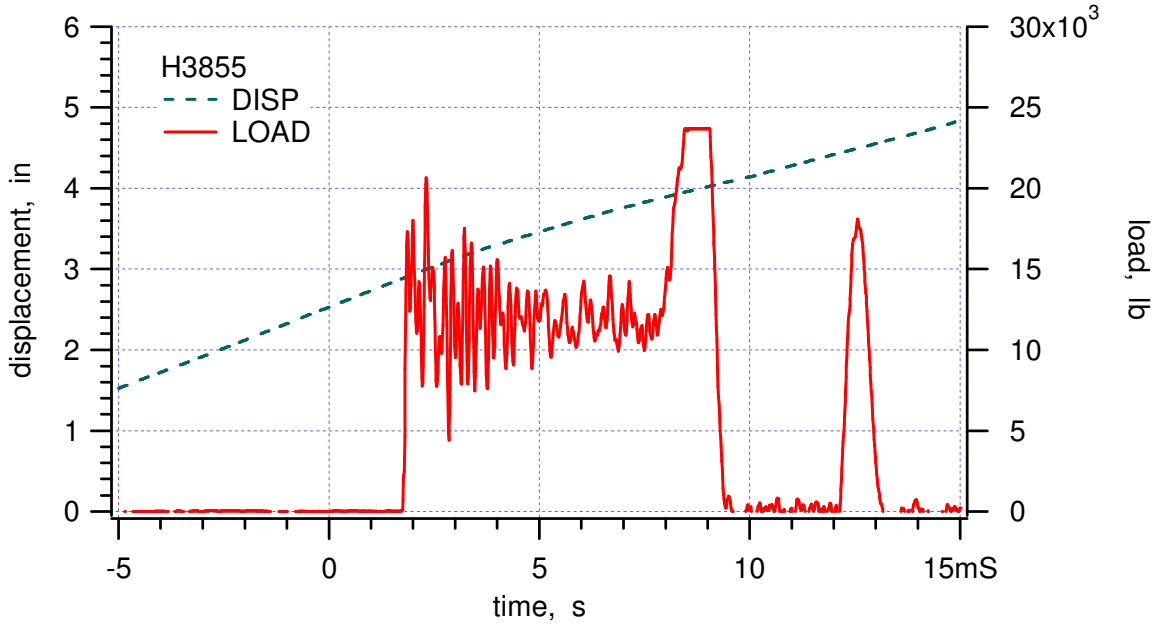
H3855
DISP
LOAD
displacement, in
load, lb
30x10^3
time, s
-5
0
5
10
15mS

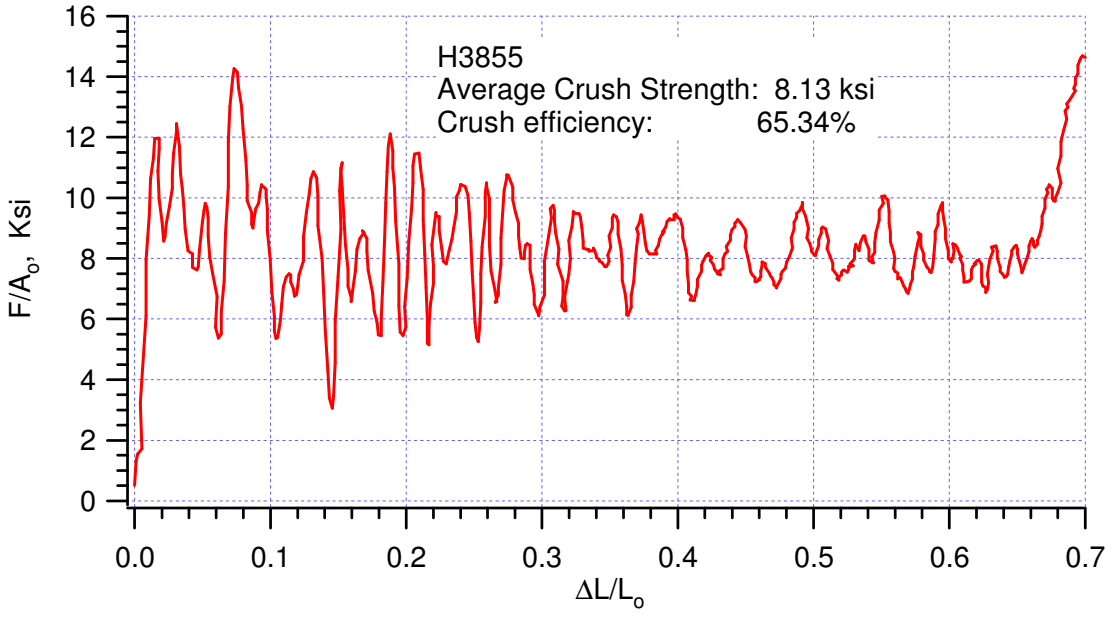
H3855
Average Crush Strength: 8.13 ksi
Crush efficiency: 65.34%
F/A_o, Ksi
ΔL/L_o

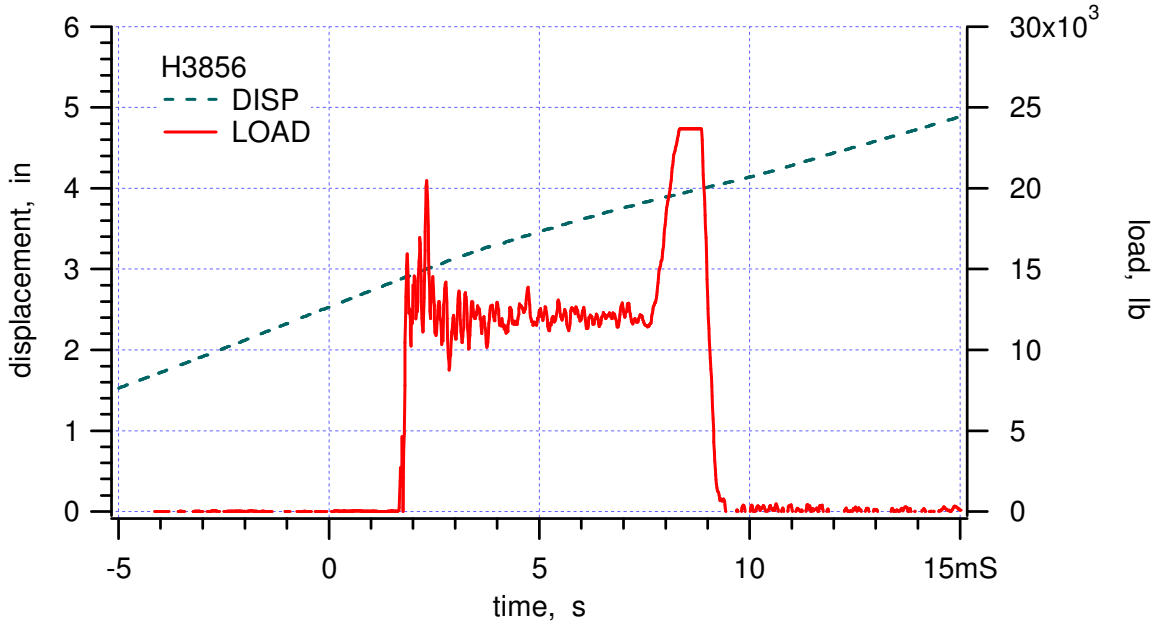
H3856
DISP
LOAD
displacement, in
load, lb
30x10^3
time, s
-5
0
5
10
15mS

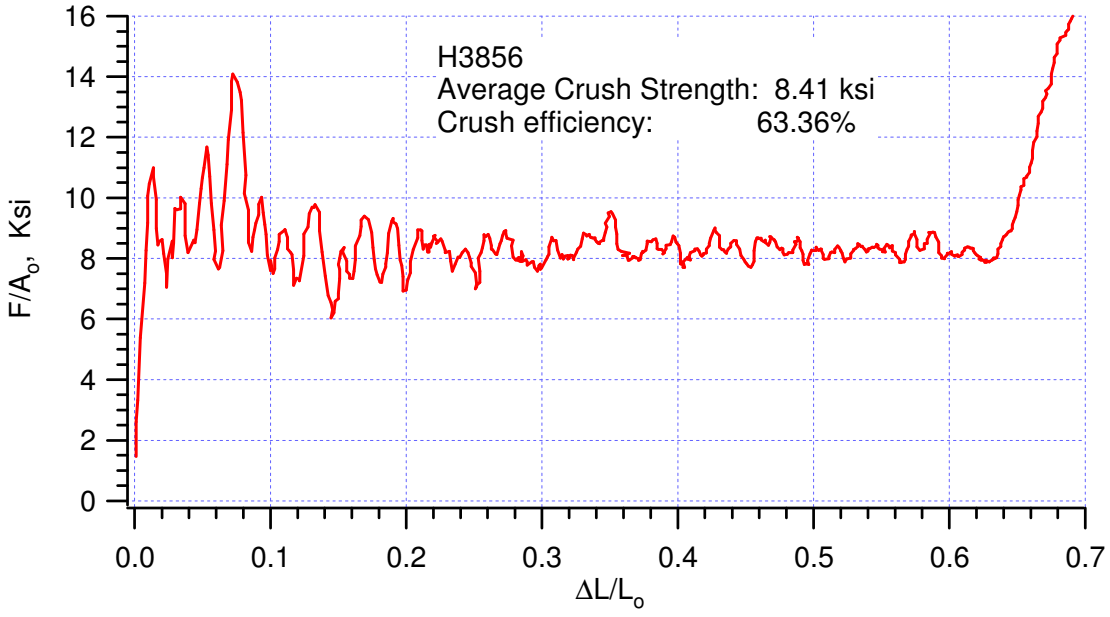
H3856
Average Crush Strength: 8.41 ksi
Crush efficiency: 63.36%
F/A_o, Ksi
ΔL/L_o

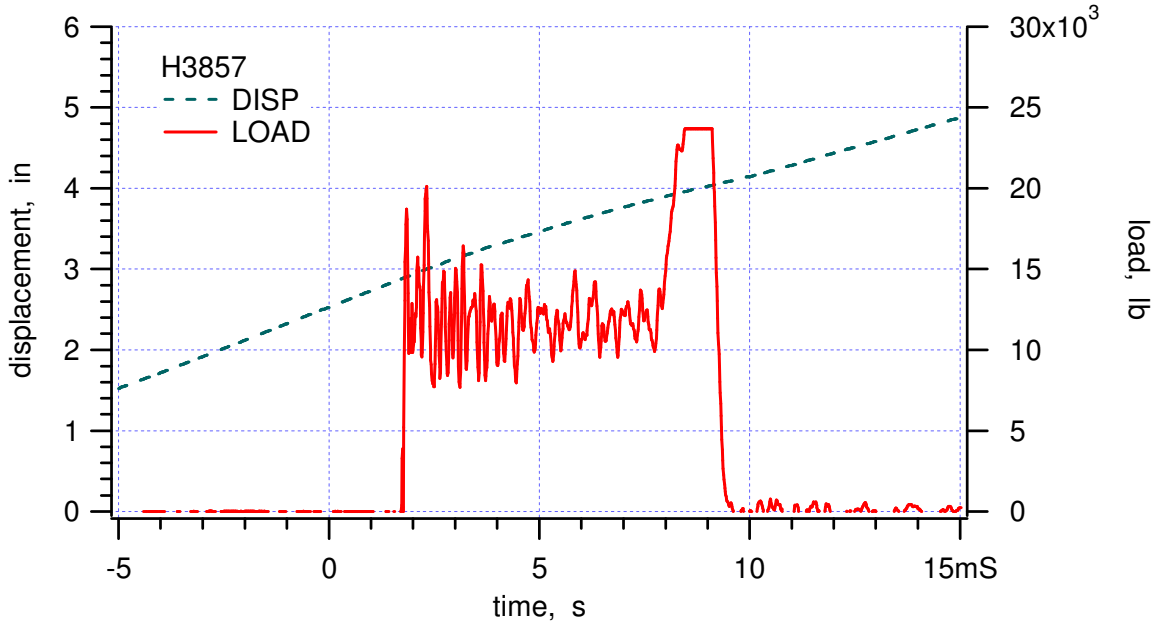
H3857
DISP
LOAD
displacement, in
load, lb
time, s
30x10^3
25
20
15
10
5
0
-5
0
5
10
15mS
1
2
3
4
5
6

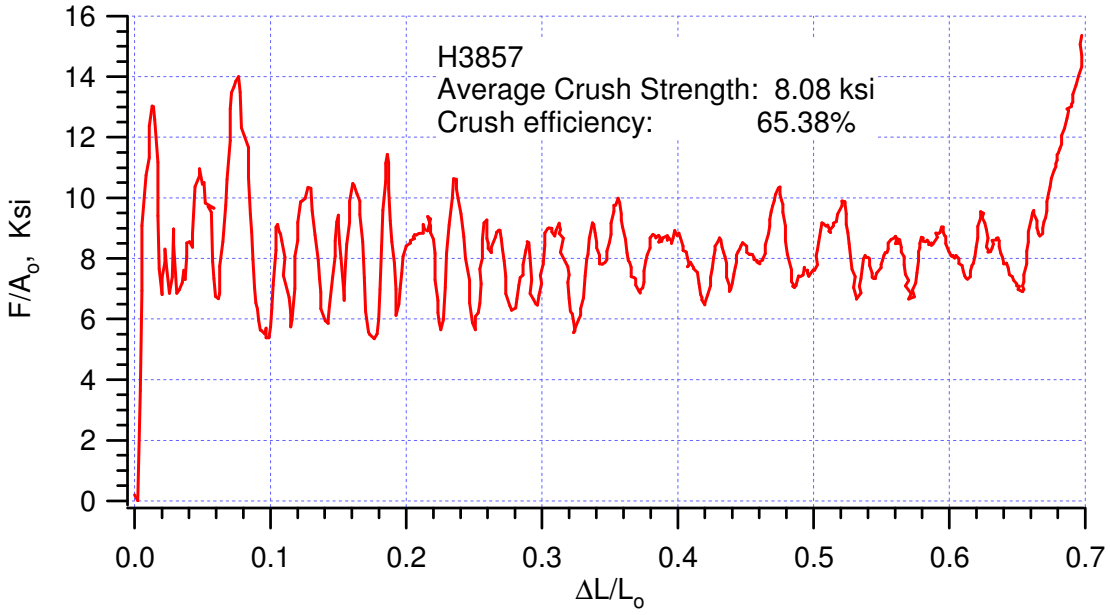
H3857
Average Crush Strength: 8.08 ksi
Crush efficiency: 65.38%
F/A_o, Ksi
ΔL/L_o
0.0
0.1
0.2
0.3
0.4
0.5
0.6
0.7
0
2
4
6
8
10
12
14
16

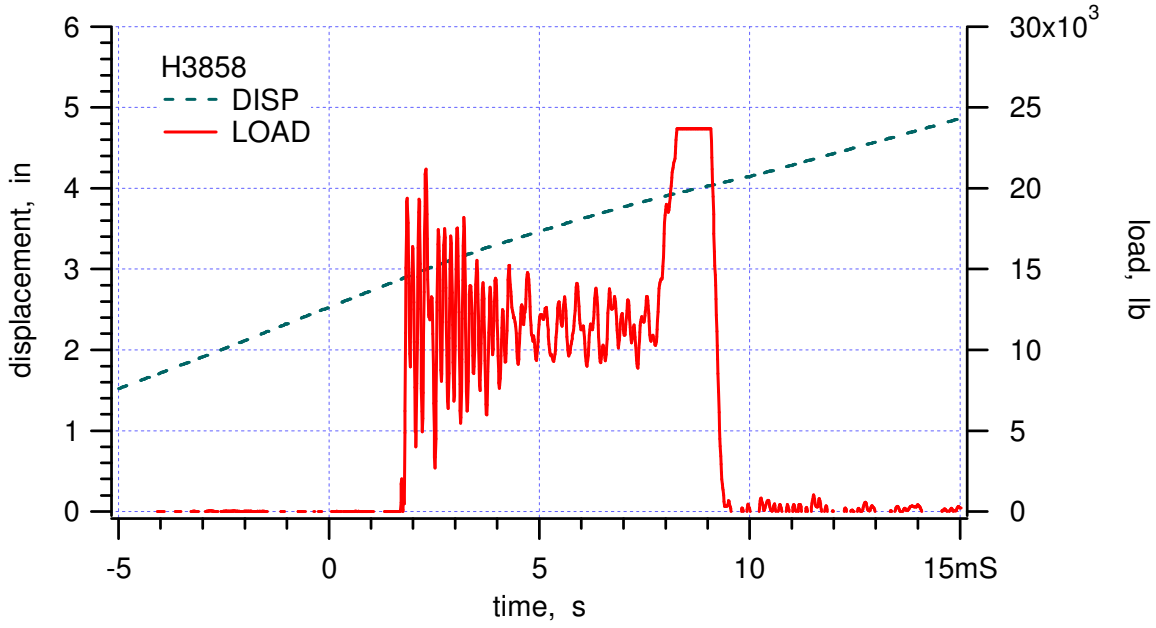
H3858
DISP
LOAD
displacement, in
load, lb
30x10^3
time, s
-5
0
5
10
15mS

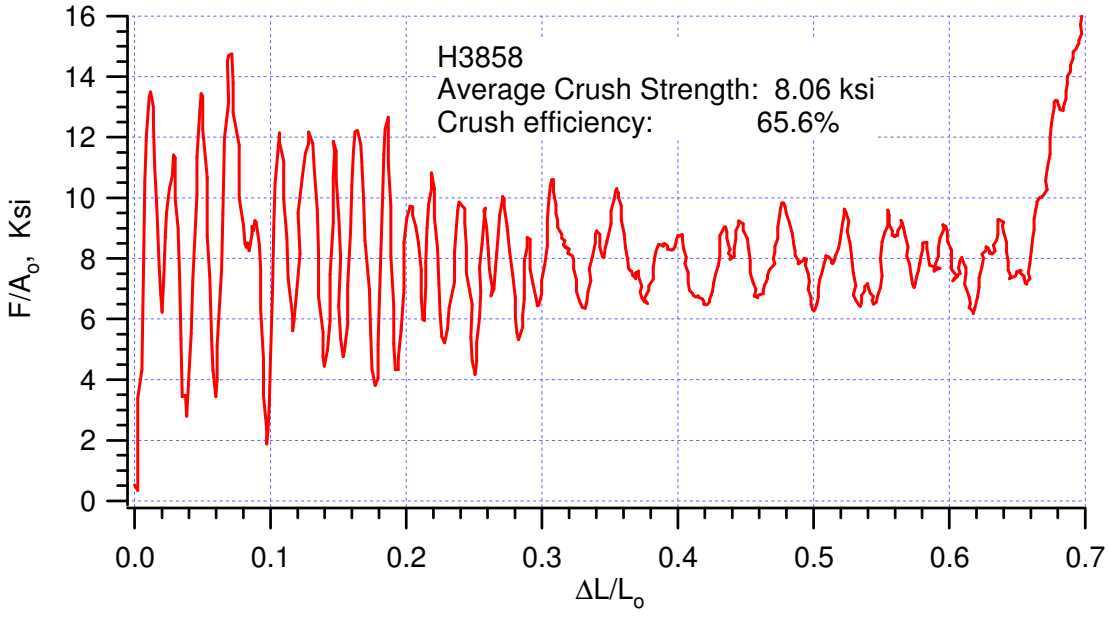
H3858
Average Crush Strength: 8.06 ksi
Crush efficiency: 65.6%
F/A_o, Ksi
ΔL/L_o

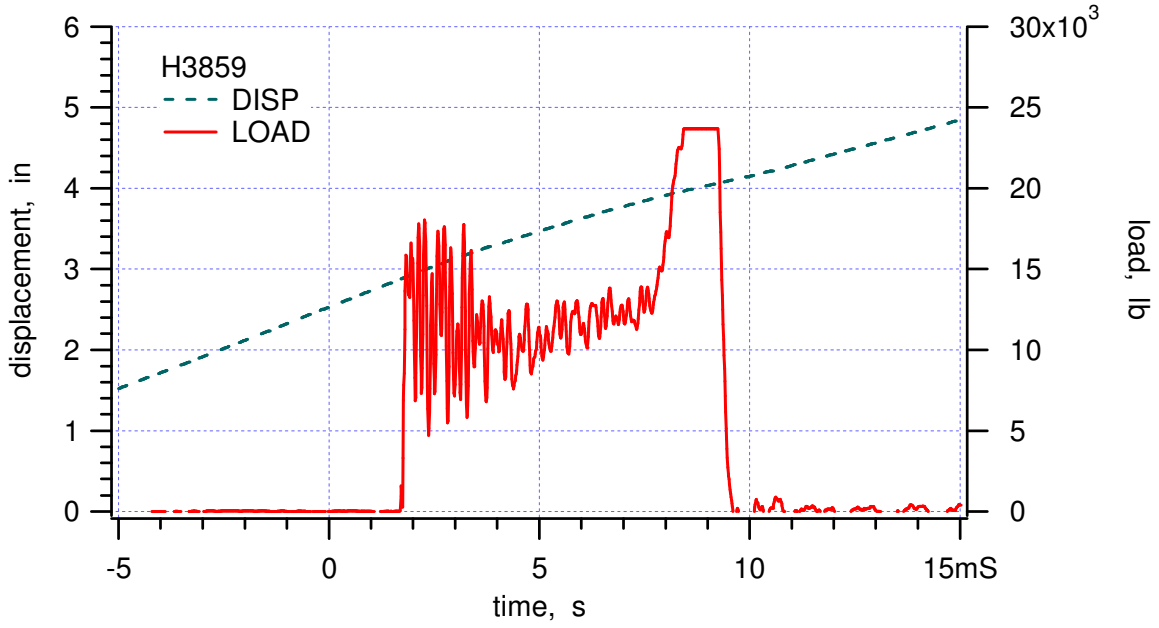
H3859
DISP
LOAD
displacement, in
load, lb
time, s
30x10^3
25
20
15
10
5
0
-5
0
5
10
15mS
1
2
3
4
5
6

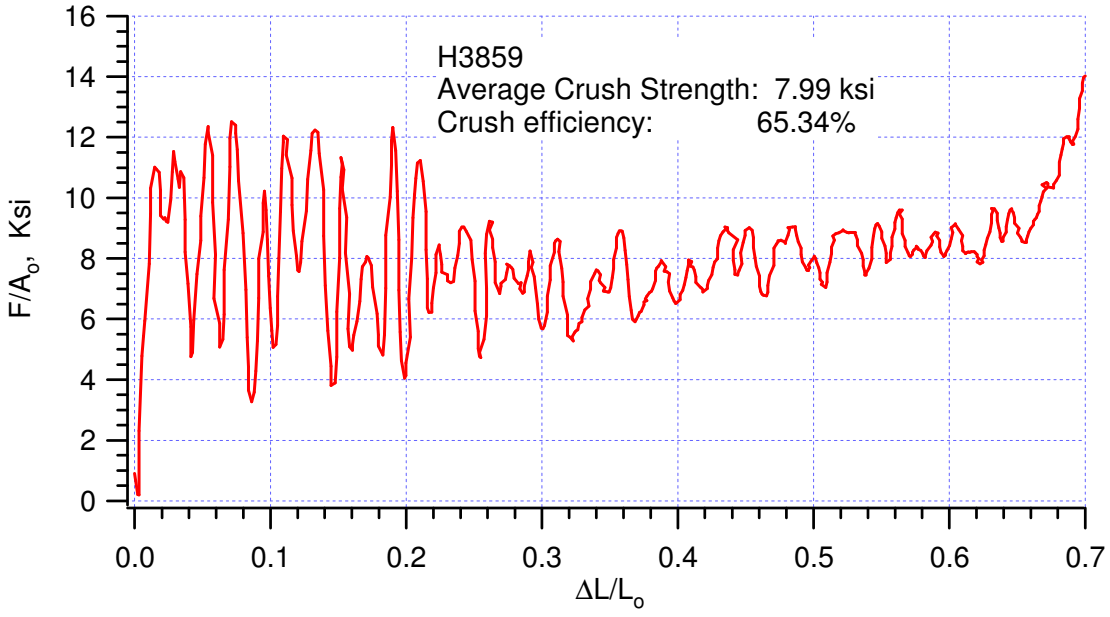
H3859
Average Crush Strength: 7.99 ksi
Crush efficiency: 65.34%
F/A_o, Ksi
ΔL/L_o
0.0
0.1
0.2
0.3
0.4
0.5
0.6
0.7
0
2
4
6
8
10
12
14
16

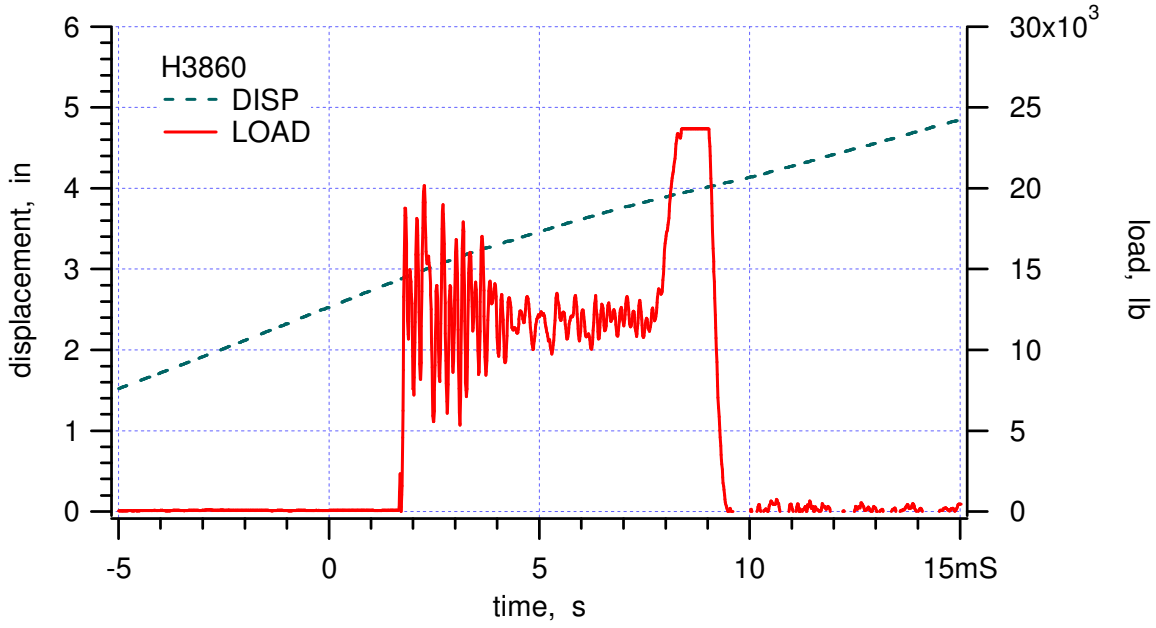
H3860
DISP
LOAD
displacement, in
load, lb
30x10^3
time, s
-5
0
5
10
15mS

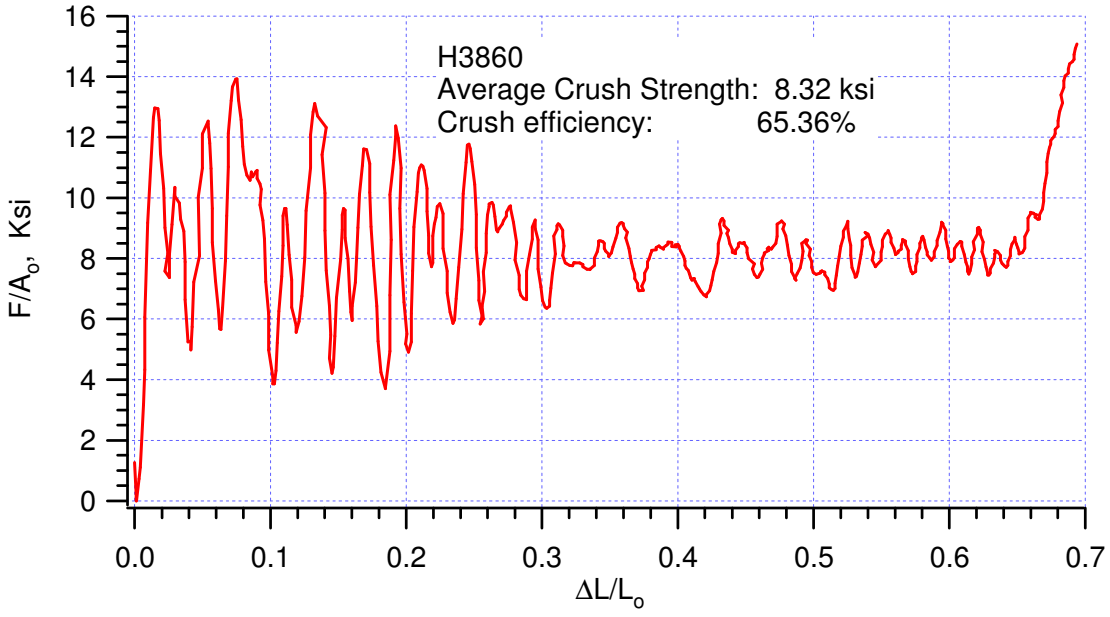
H3860
Average Crush Strength: 8.32 ksi
Crush efficiency: 65.36%
F/A_o, Ksi
ΔL/L_o

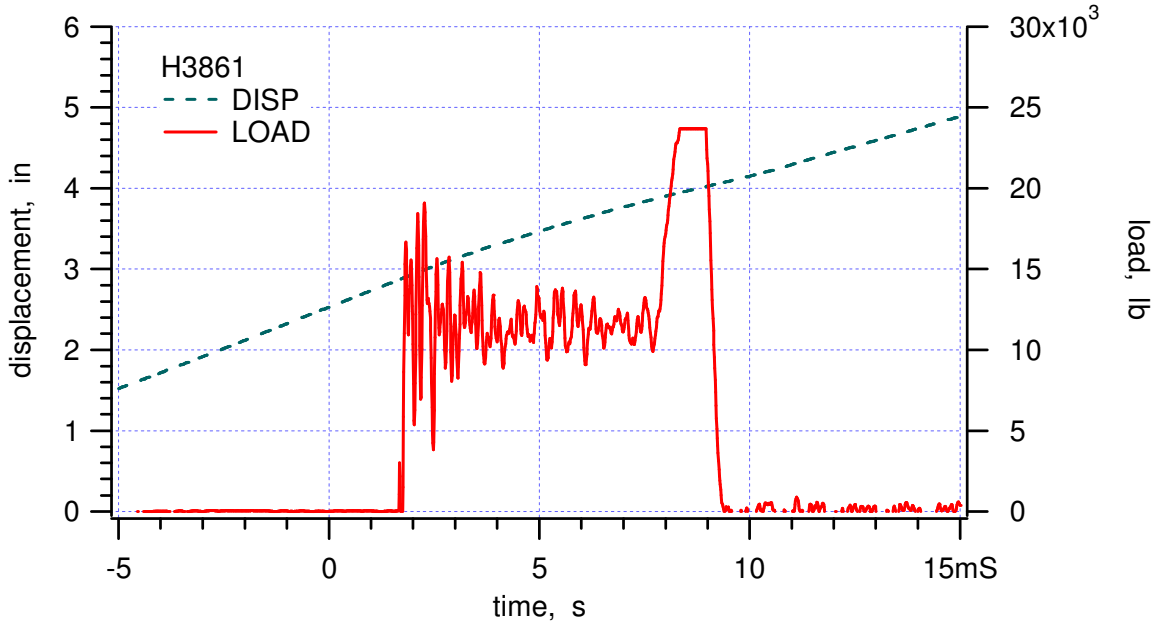
H3861
DISP
LOAD
displacement, in
load, lb
30x10^3
time, s
-5
0
5
10
15mS

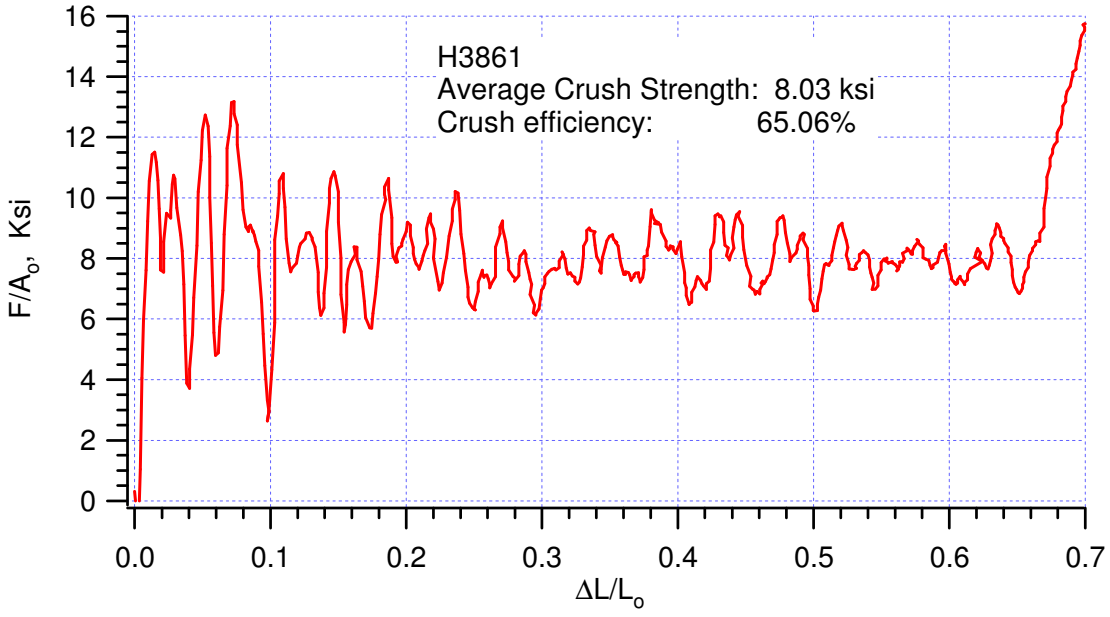
H3861
Average Crush Strength: 8.03 ksi
Crush efficiency: 65.06%
F/A_o, Ksi
ΔL/L_o

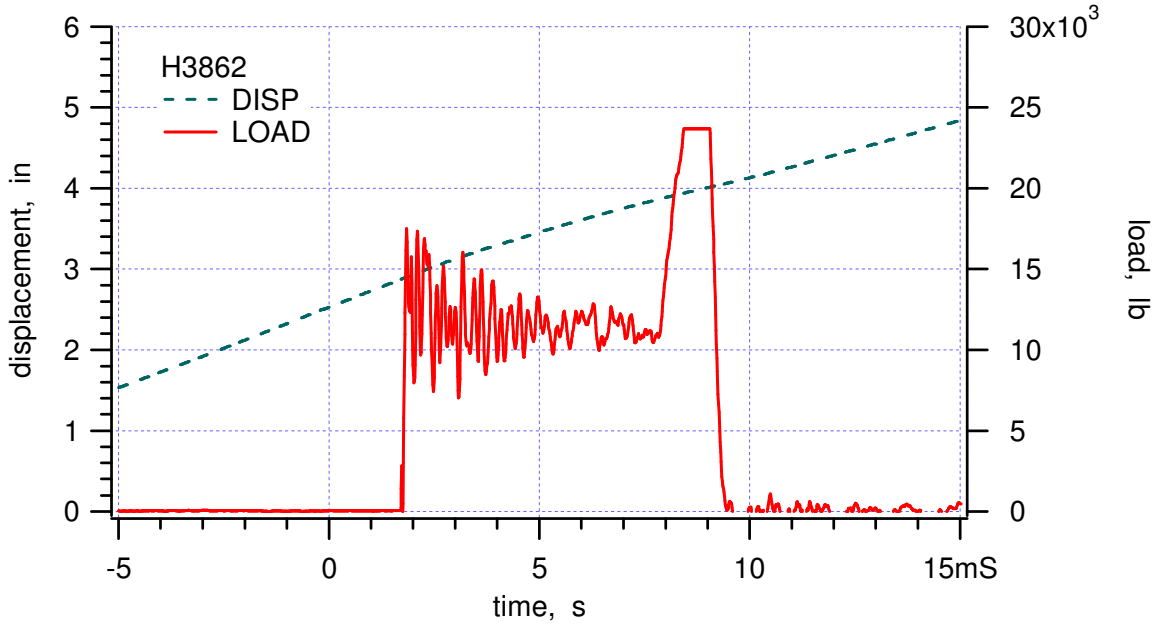
H3862
DISP
LOAD
displacement, in
load, lb
30x10^3
time, s
-5
0
5
10
15mS

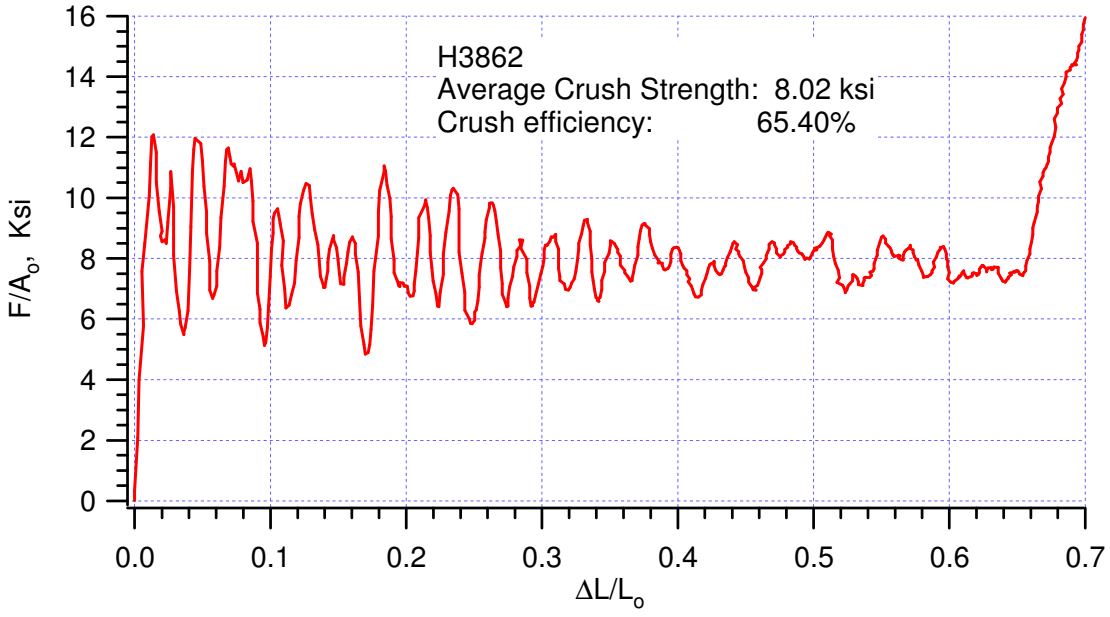
H3862
Average Crush Strength: 8.02 ksi
Crush efficiency: 65.40%
F/A_o, Ksi
ΔL/L_o

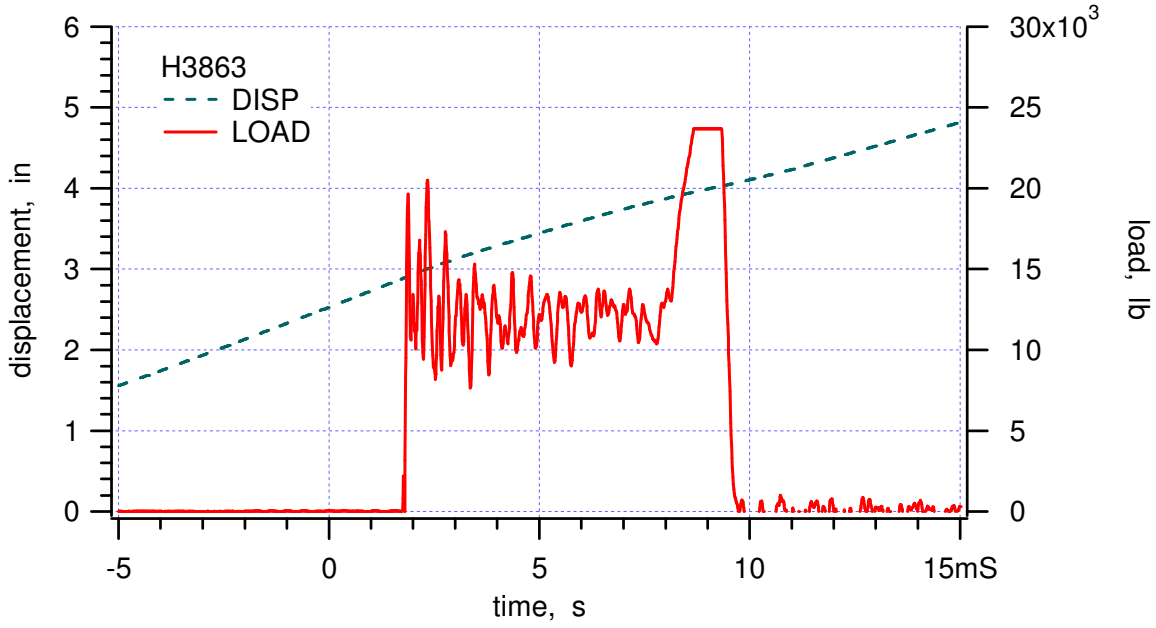
H3863
DISP
LOAD
displacement, in
load, lb
30x10^3
time, s
-5
0
5
10
15mS

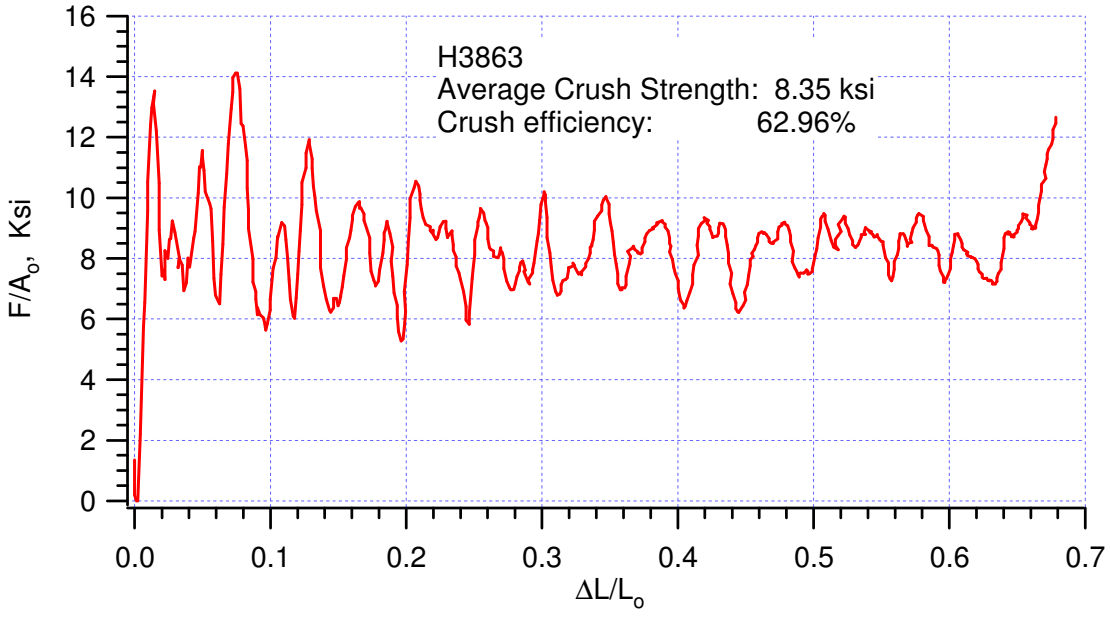
H3863
Average Crush Strength: 8.35 ksi
Crush efficiency: 62.96%
F/A_o, Ksi
ΔL/L_o

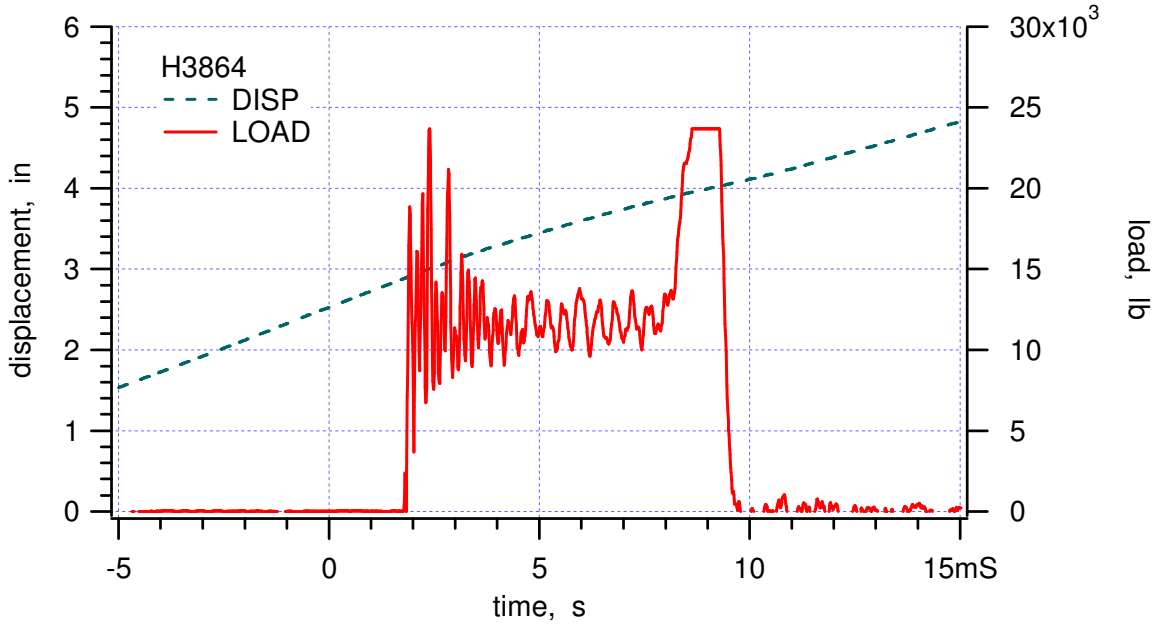
H3864
DISP
LOAD
displacement, in
load, lb
time, s
30x10^3
25
20
15
10
5
0
-5
0
5
10
15mS
1
2
3
4
5
6

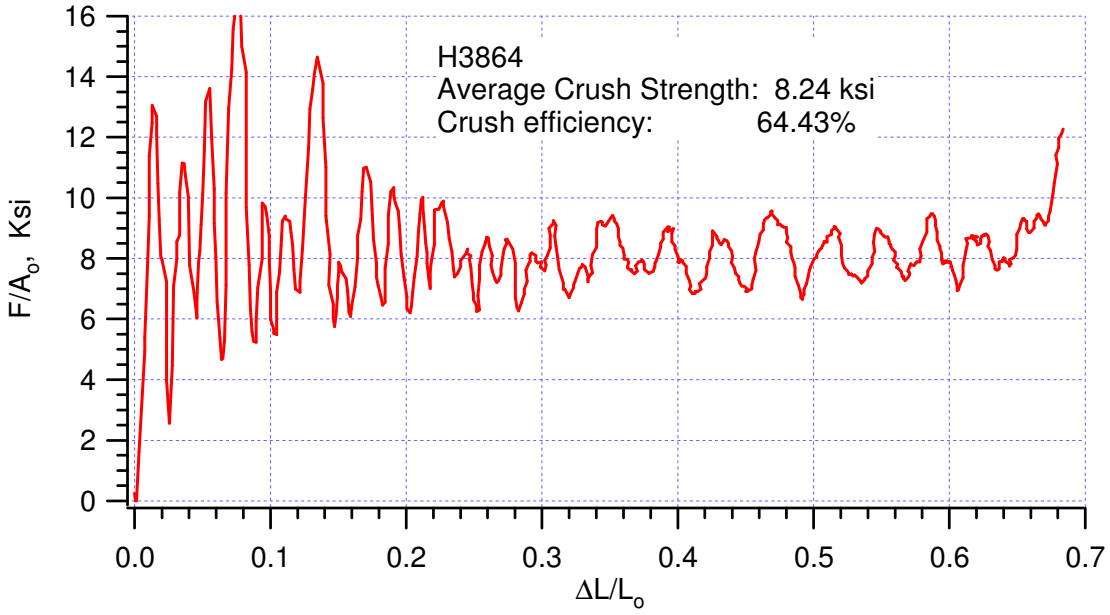
H3864
Average Crush Strength: 8.24 ksi
Crush efficiency: 64.43%
F/A_o, Ksi
ΔL/L_o
0.0
0.1
0.2
0.3
0.4
0.5
0.6
0.7
0
2
4
6
8
10
12
14
16

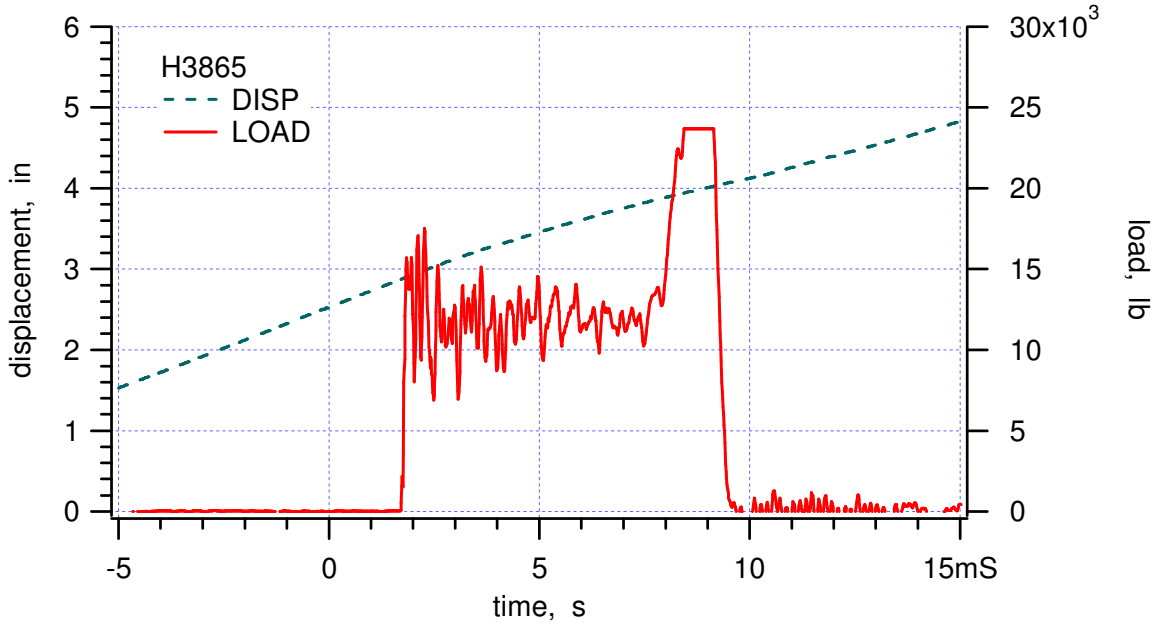
H3865
DISP
LOAD
displacement, in
load, lb
30x10^3
time, s
-5
0
5
10
15mS

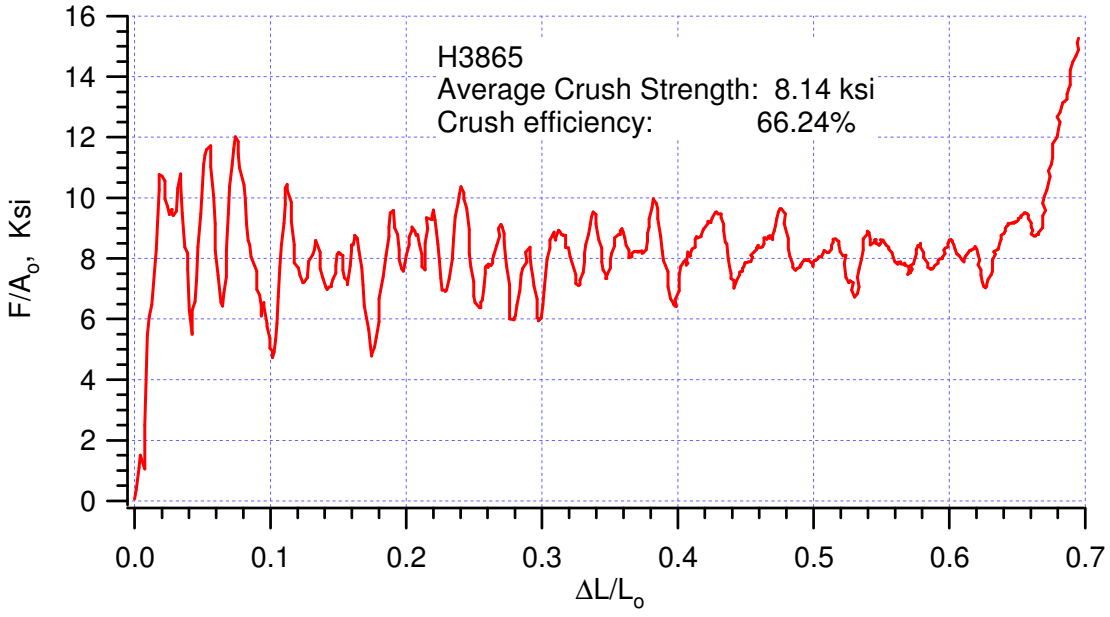
H3865
Average Crush Strength: 8.14 ksi
Crush efficiency: 66.24%
F/A_o, Ksi
ΔL/L_o

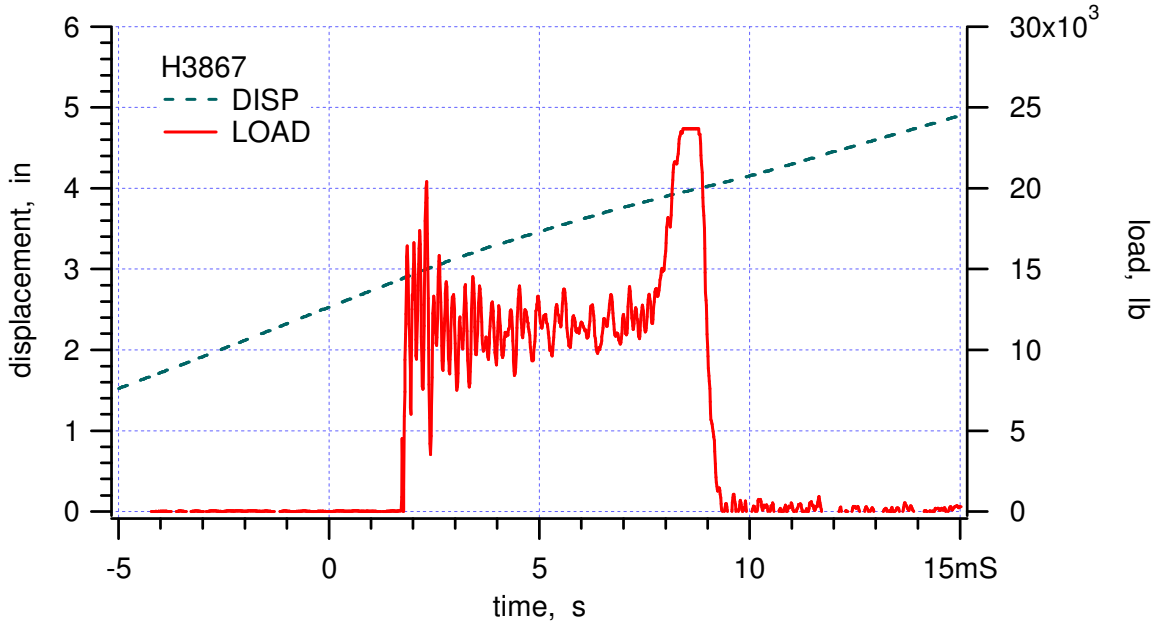
H3867
DISP
LOAD
displacement, in
load, lb
time, s
30x10^3
25
20
15
10
5
0
-5
0
5
10
15mS
1
2
3
4
5
6

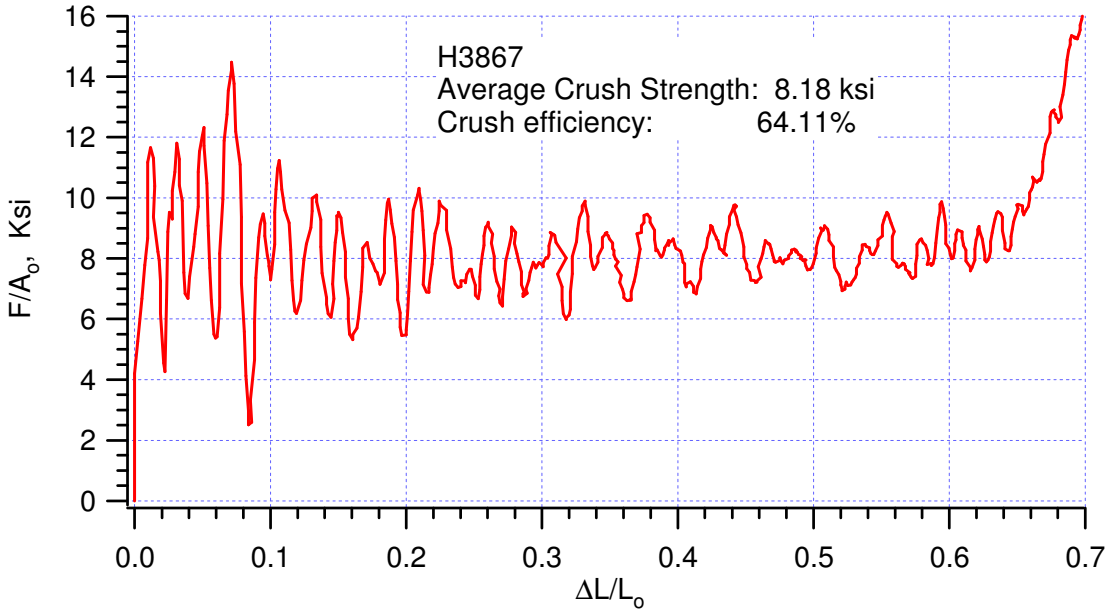
H3867
Average Crush Strength: 8.18 ksi
Crush efficiency: 64.11%
F/A_o, Ksi
ΔL/L_o
0.0
0.1
0.2
0.3
0.4
0.5
0.6
0.7
0
2
4
6
8
10
12
14
16

APPENDIX XIII:

"Moderate Rate Confined Crush Tests of (1)38 pcf honeycombs in the L-direction at ambient, and (2)35 pcf honeycombs in the T-direction at –65°F ," Memo Wei-Yang Lu to Distribution, March 7, 2000

Sandia National Laboratories
Operated for the U.S. Department of Energy by
Sandia Corporation
MS9042
Livermore, CA 94551-0969

date: March 7, 2000

to: Distribution

from: Wei-yang Lu

subject: Moderate Rate Confined Crush Tests of
(1) 38 pcf honeycombs in the L-direction at ambient, and
(2) 35 pcf honeycombs in the T-direction at –65°F

Experimental results of both Alcore and Hexcel materials are included in this report. The boldface lines in Table 1 summarize these new data, item (1) in black and item (2) in red. Item (2) was not in the original test matrix, which were requested to provide timely support for the analysis of certification tests, LDCR1 and 2. A peer review of that program is scheduled in late March.

(1) Crush in L-direction at ambient
Experimental setup and procedures of honeycomb confined crush in L-direction were exactly the same as those in T-direction. Specimens were rotated in T-W plane, as shown in Figure 1.

Data was acquired at 50 KHz. In signal analysis, a low pass filter with a cut-off frequency of 5 KHz was applied to the load signal. Typical "stress-strain" curves are shown in Figure 2, where red and blue are from raw (unfiltered) and filtered data, respectively. The unfiltered signal included dynamic response of the testing system or stress waves that traveled back and forth in the loading train. Due to its relatively low crush strength in comparing to the t-direction, sometime the pre-loaded load washer sensed tensile stress. The filtered data eliminates those high frequency system responses. Both unfiltered and filtered signals were used to calculate the crush strength of the honeycomb specimen. Both results are basically identical. In some tests, there were small portions of the load signal that were beyond the range of recording. We have calculated the crush strength by considering both with and without such saturated data, i.e., using all crush data or a section of good data. The difference is very small and negligible.

It is interesting to point out that Hexcel 38 has a higher crush strength in the t-direction than Alcore 38, 7.17 ksi versus 6.35 ksi, but a lower crush strength in the l-direction, 1.05 ksi versus 1.26 ksi. The l-direction crush efficiency of Hexcel 38 is also noticeably smaller than Alcore 38, 46% vs. 53%. A possible reason for these differences is the not-

so-orderly cell pattern of the Hexcel material (please refer to Figures 5 & 6 of the Memo dated January 10, 2000).

(2) 35 pcf honeycombs in the T-direction at –65°F

Constrained by time and system availability, the sets of test conducted were smaller than the typical 15, seven for Alcore 35 and four for Hexcel 35. The crush strength of honeycomb is clearly higher at low temperature. From ambient to –65°F, it increases about 20% for 35 pcf honeycombs. (For 38 pcf honeycombs, data shows the increase is about 15%.)

Please see Appendix for detail experimental data.

Distribution:

Darrla Giersch(2167)	MS0481
Darren Hoke(2167)	MS0481
Vernon Willan(2167)	MS0481
Vista Bateman(9126)	MS0553
Tom Carne(9124)	MS0557
Berry Boughten(9132)	MS0557
Jaime Moya(9132)	MS0828
Terry Hinnerichs(9126)	MS0847
Ken Gwinn(9126)	MS0847
John Pott(9126)	MS0847
Rodney May(9126)	MS0847
Mike Neilsen(9123)	MS0847
Bill Scherzinger(9123)	MS0847
Hal Morgan(9123)	MS0847
Wendell Kawahara (8725)	MS9042

Table 1. Summary of FY00 experimental results

B61/MAVEN TEST MATRIX				EXPERIMENTAL RESULTS						MEMO
Test #	Honeycomb	Dir.	Temperature, degree F	Specimen	Density, pcf	Impact Speed, ft/s	Crush Strength, ksi	Std Deviation, ksi	Crush Efficiency, %	Date
1 - 15	Alcore 38	T	ambient	rotated	38.82	14.13	6.35	0.08	63.80	991203
16 - 30	Hexcel 38	T	ambient	rotated	38.70	13.67	7.17	0.15	63.89	000110
	Hexcel 39	T	ambient	rotated	38.78	0.00139	5.88		59.20	"
31 - 45	Alcore 35	T	ambient	rotated	35.39	14.35	5.74	0.18	64.46	000103
46 - 60	Hexcel 35	T	ambient	rotated	37.79	13.83	6.67	0.24	63.91	000110
	Hexcel 35	T	ambient	rotated	37.89	0.00139	5.83		60.30	"
60 - 75	Alcore 38	T	165	rotated	38.96	14.33	5.49	0.10	62.52	000118
76 - 90	Hexcel 38	T	165	rotated	38.65	13.82	6.43	0.15	64.31	000118
	Alcore 35	T	165	rotated	35.62	14.59	4.94	0.23	62.54	000207
91 - 105	Alcore 38	T	-65	rotated	38.94	13.48	7.34	0.24	62.71	000225
106 - 120	Hexcel 38	T	-65	rotated	38.65	13.17	8.21	0.17	64.68	000225
	Alcore 35	**T**	**-65**	**rotated**	**35.59**	**13.77**	**7.04**	**0.36**	**62.89**	**000307**
	Hexcel 35	**T**	**-65**	**rotated**	**37.92**	**13.29**	**8.05**	**0.09**	**64.20**	**000307**
121 - 125	**Alcore 38**	**L**	**ambient**	**rotated**	**38.88**	**16.45**	**1.25**	**0.13**	**53.24**	**000307**
126 - 130	**Hexcel 38**	**L**	**ambient**	**rotated**	**38.62**	**16.50**	**1.05**	**0.09**	**46.12**	**000307**
131 - 135	Alcore 38	W	ambient							
136 - 140	Hexcel 38	W	ambient							
159 - 161	Alcore 38	T	ambient	segmented	41.41	0.0014	6.14		52.30	991130
162 - 164	Hexcel 38	T	ambient	segmented	41.29	0.0014	6.85		53.70	991213

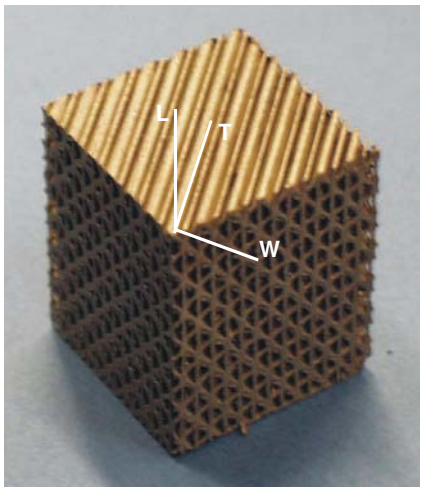

Figure 1. Rotated specimen for crush in L-direction.

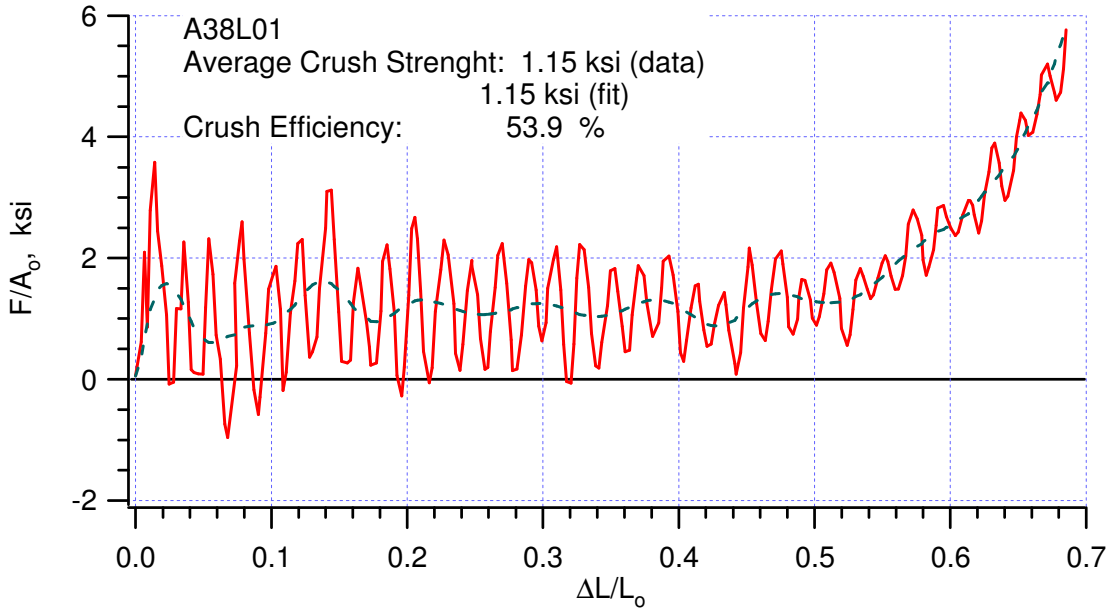

Figure 2. Typical L-direction "stress-strain" curves. The red line is the raw data, which includes high frequency system response; the blue line is the filtered data.

Appendix Hexcel 38L, ambient

Specimen	d_1, in	d_2, in	d_3, in	Weight, lb	Density, pcf	Crush Velocity, ft/s	Crush efficiency, %	Crush strenghth, ksi (fit)	Remarks
H38L01	1.203	1.199	1.503	0.0485	38.62	16.54	45.67	0.98	
H38L02	1.191	1.201	1.506	0.0483	38.71	16.28	44.94	0.98	
H38L03	1.187	1.197	1.510	0.0480	38.69	16.55	46.83	1.13	
H38L04	1.188	1.197	1.501	0.0481	38.91	16.63	45.20	0.97	
H38L05	1.190	1.197	1.509	0.0481	38.69	16.74	47.82	1.03	
H38L06	1.203	1.199	1.509	0.0485	38.54	16.60	41.56	1.01	
H38L07	1.196	1.188	1.510	0.0485	39.06	16.38	45.88	1.06	
H38L08	1.197	1.196	1.508	0.0484	38.72	16.36	46.37	1.00	
H38L09	1.196	1.183	1.502	0.0472	38.42	16.36	46.98	1.04	
H38L10	1.192	1.200	1.507	0.0485	38.88	16.41	46.40	1.01	
H38L11	1.186	1.200	1.508	0.0477	38.39	16.45	47.22	1.12	
H38L12	1.198	1.197	1.500	0.0480	38.56	16.58	46.83	1.00	
H38L13	1.196	1.193	1.505	0.0482	38.76	16.55	47.10	1.18	
H38L14	1.188	1.202	1.513	0.0479	38.35	16.53	44.10	1.04	
H38L15	1.185	1.197	1.495	0.0472	38.43	16.50	47.09	1.28	
H38L16	1.205	1.196	1.507	0.0480	38.19	16.56	47.93	0.96	
				max	39.06	16.74	47.93	1.28	
				min	38.19	16.28	41.56	0.96	
				average	38.62	16.50	46.12	1.05	
				std deviation	0.23	0.12	1.60	0.09	
				median	38.66	16.54	46.61	1.02	

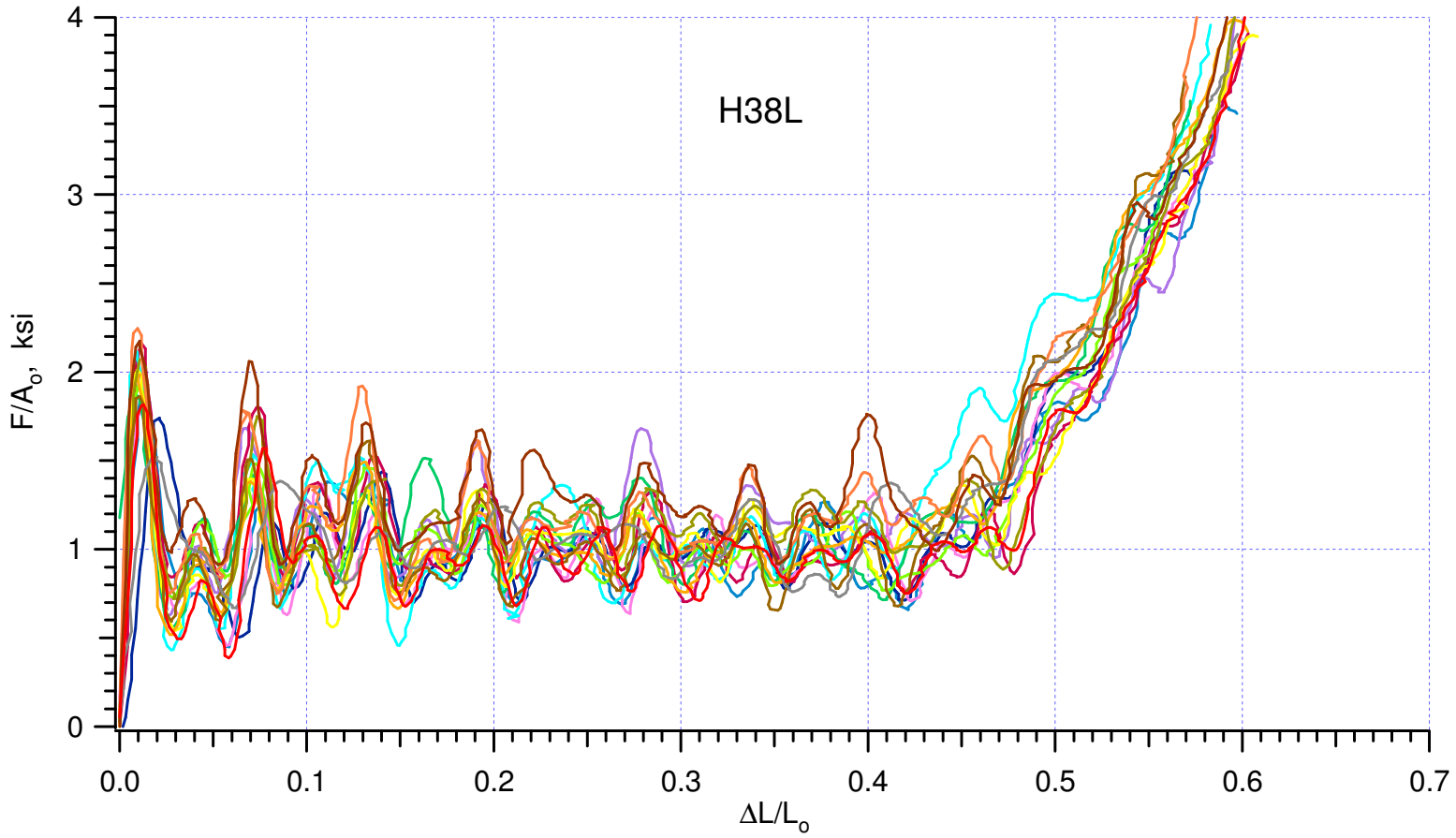
H38L
F/A$_o$, ksi
ΔL/L$_o$
0
1
2
3
4
0.0
0.1
0.2
0.3
0.4
0.5
0.6
0.7

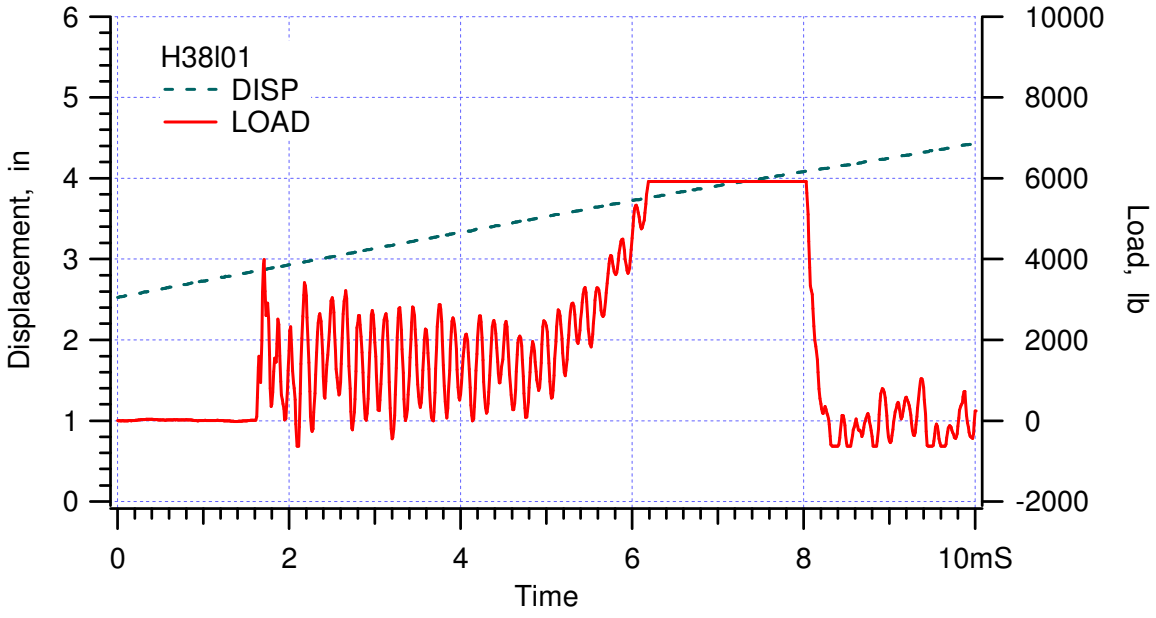
H38I01
DISP
LOAD
Displacement, in
Load, lb
Time
0
2
4
6
8
10mS
10000
8000
6000
4000
2000
0
-2000

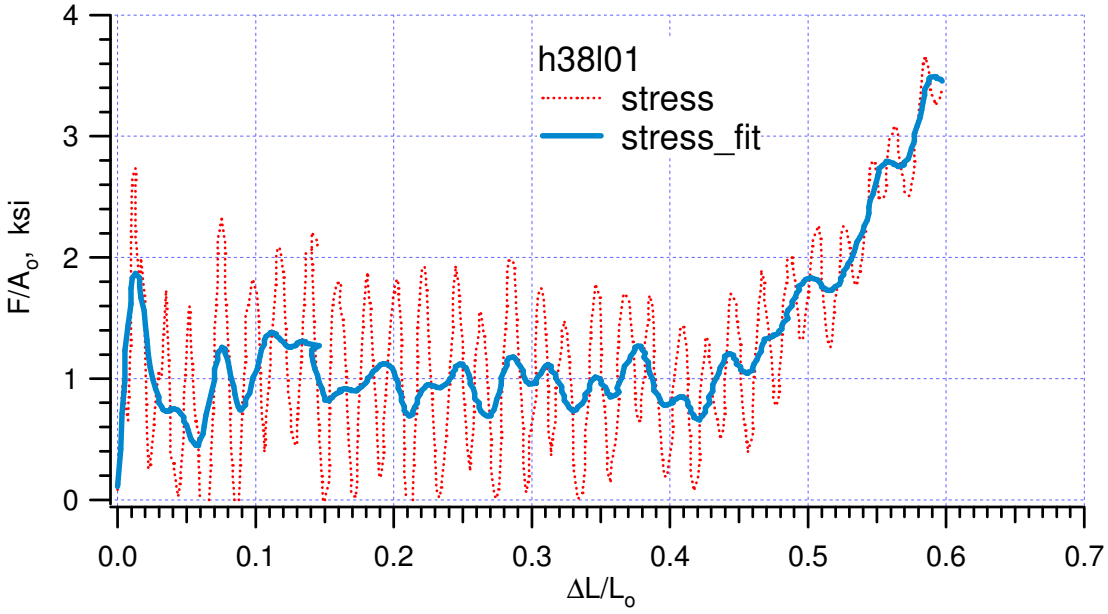
h38l01
stress
stress_fit
F/A$_o$, ksi
ΔL/L$_o$
0.0
0.1
0.2
0.3
0.4
0.5
0.6
0.7

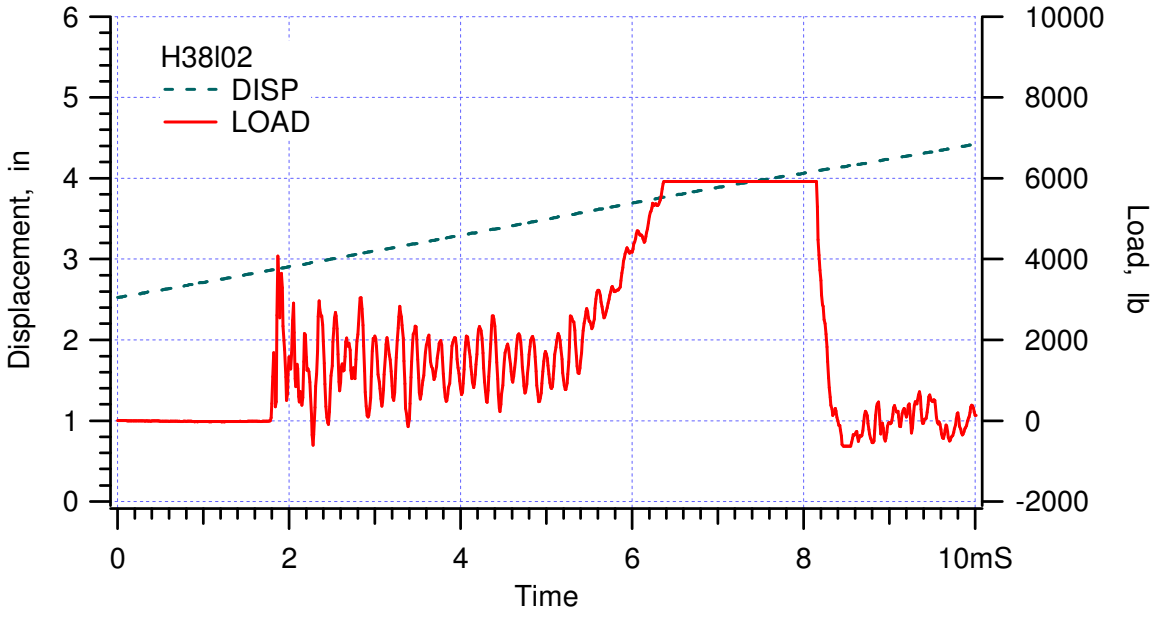
H38I02
DISP
LOAD
Displacement, in
Load, lb
Time
0
2
4
6
8
10mS
10000
8000
6000
4000
2000
0
-2000

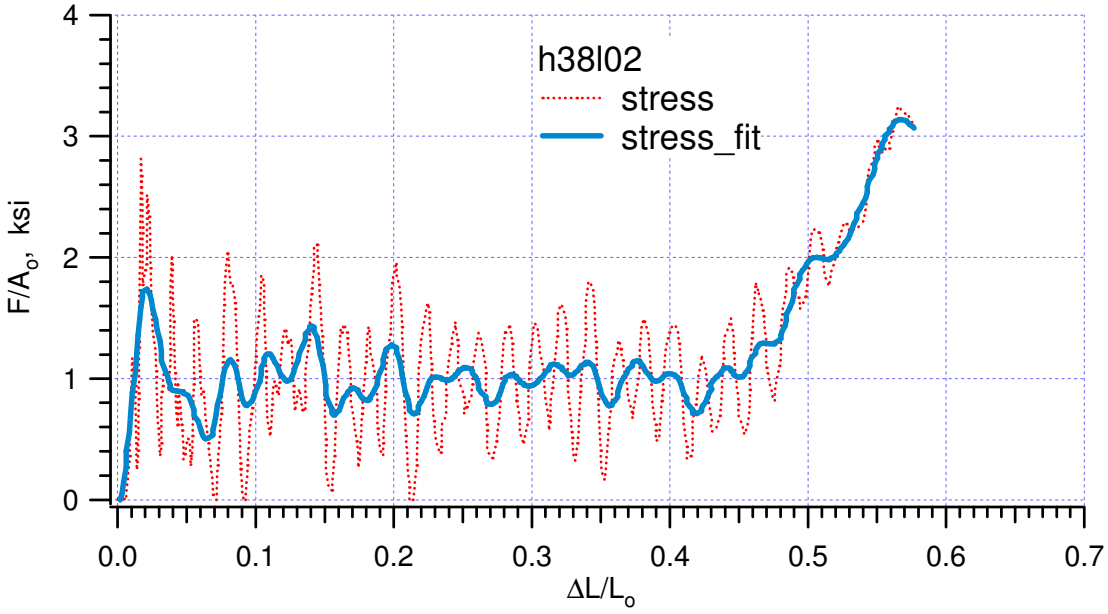
h38I02
stress
stress_fit
F/A$_o$, ksi
ΔL/L$_o$
0.0
0.1
0.2
0.3
0.4
0.5
0.6
0.7

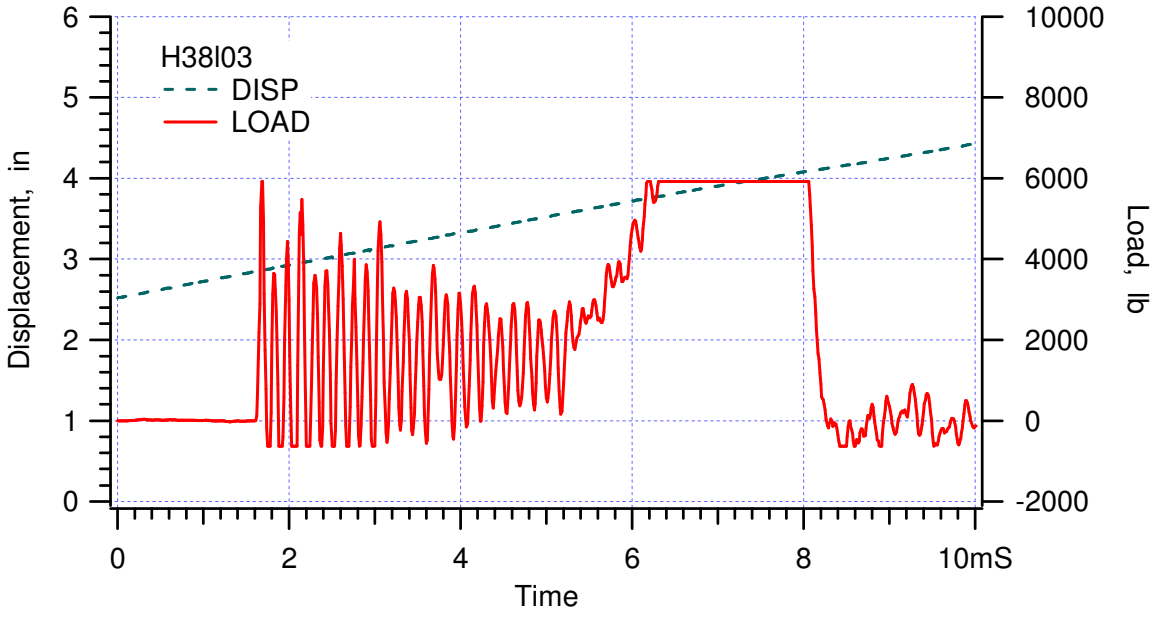
H38I03
DISP
LOAD
Displacement, in
Load, lb
Time
0
2
4
6
8
10mS
10000
8000
6000
4000
2000
0
-2000

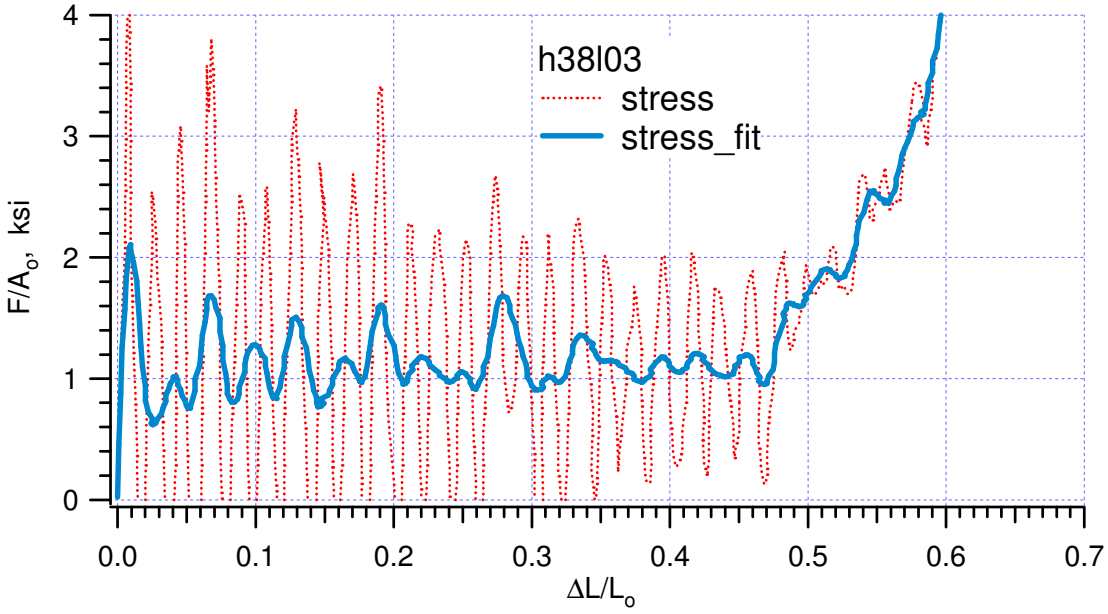
h38l03
stress
stress_fit
F/A$_o$, ksi
ΔL/L$_o$
0.0
0.1
0.2
0.3
0.4
0.5
0.6
0.7

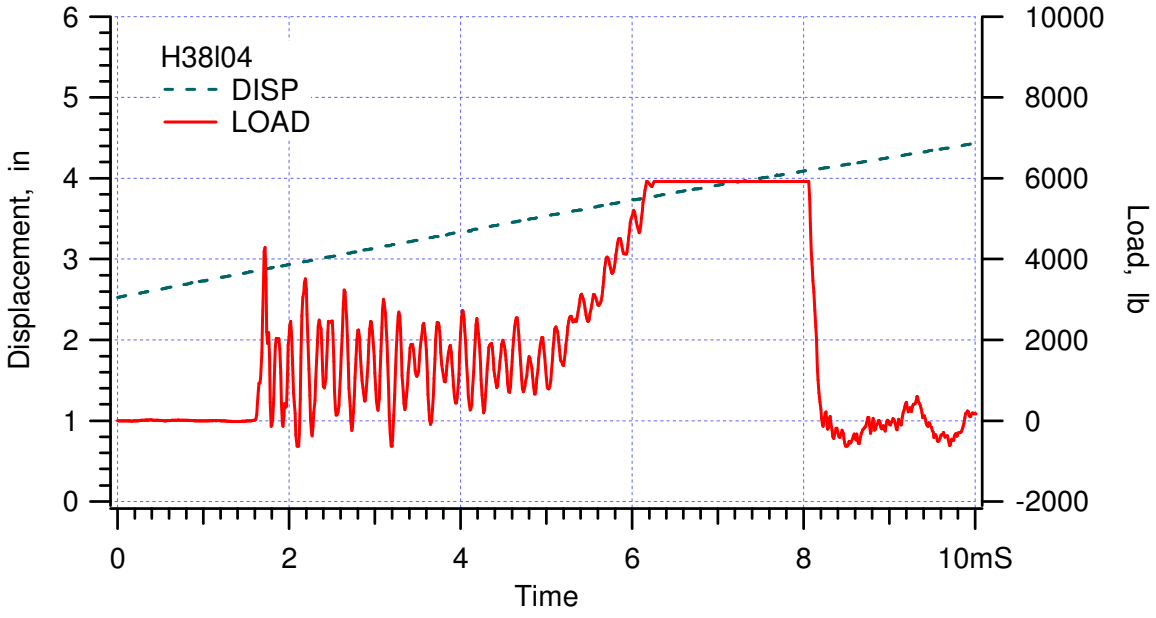
H38I04
DISP
LOAD
Displacement, in
Load, lb
Time
0
2
4
6
8
10mS
10000
8000
6000
4000
2000
0
-2000

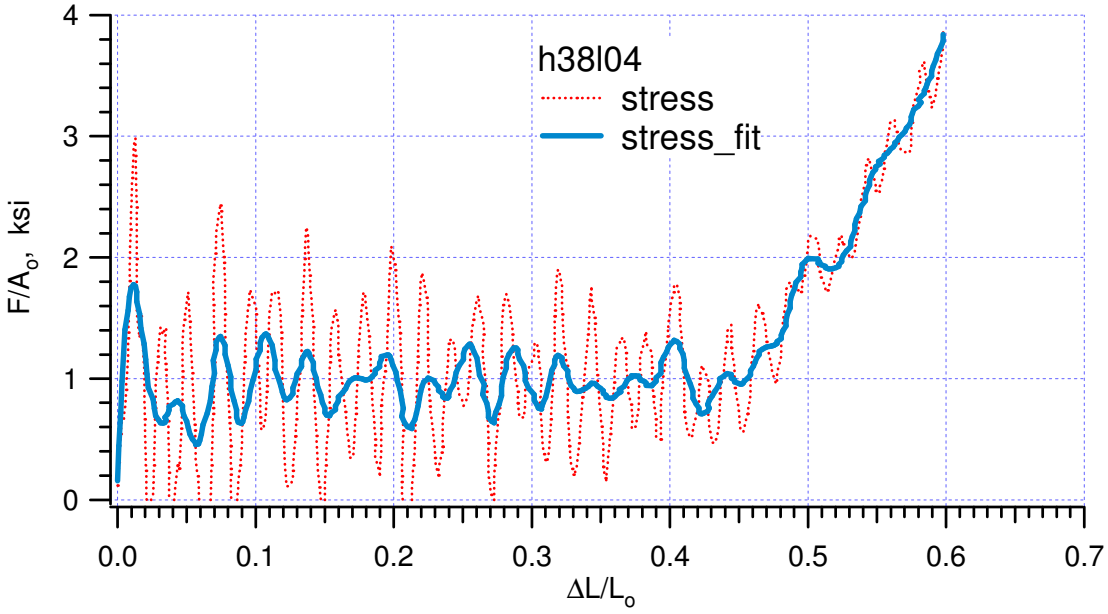
h38l04
stress
stress_fit
F/A$_o$, ksi
ΔL/L$_o$
0.0
0.1
0.2
0.3
0.4
0.5
0.6
0.7

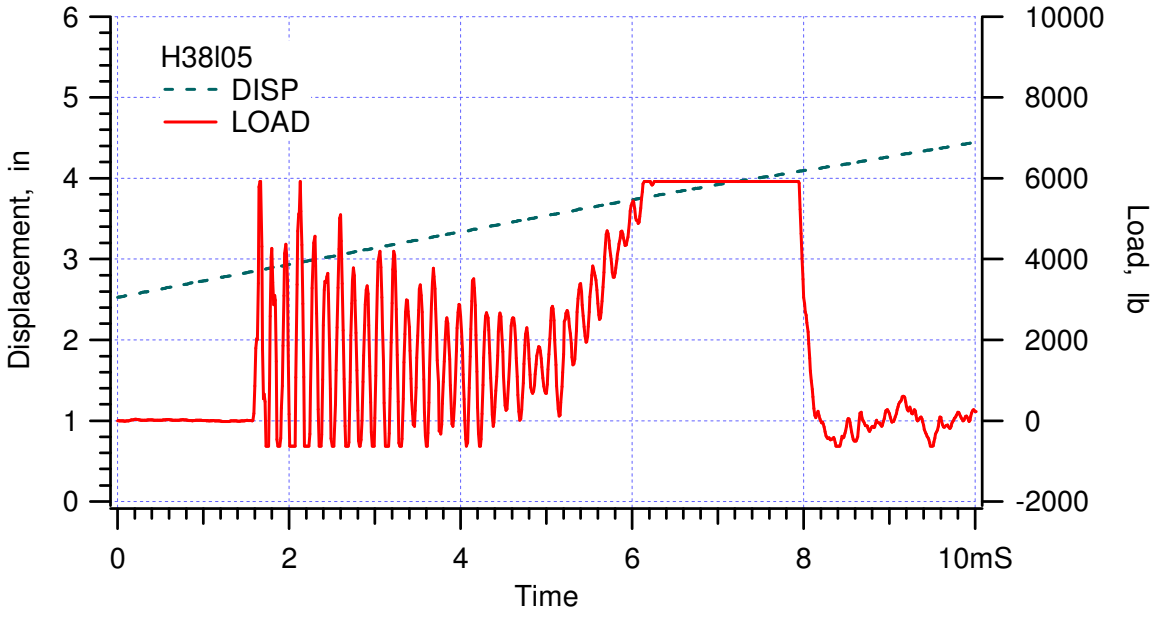
H38I05
DISP
LOAD
Displacement, in
Load, lb
Time
0
2
4
6
8
10mS
0
1
2
3
4
5
6
10000
8000
6000
4000
2000
0
-2000

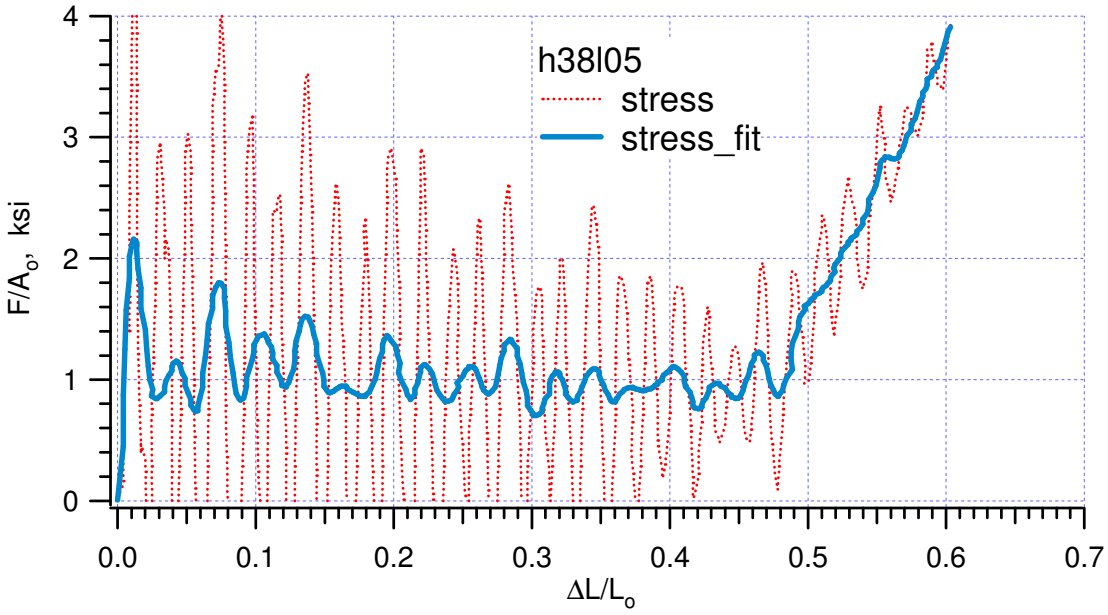
h38l05
stress
stress_fit
F/A$_o$, ksi
ΔL/L$_o$
0.0
0.1
0.2
0.3
0.4
0.5
0.6
0.7
0
1
2
3
4

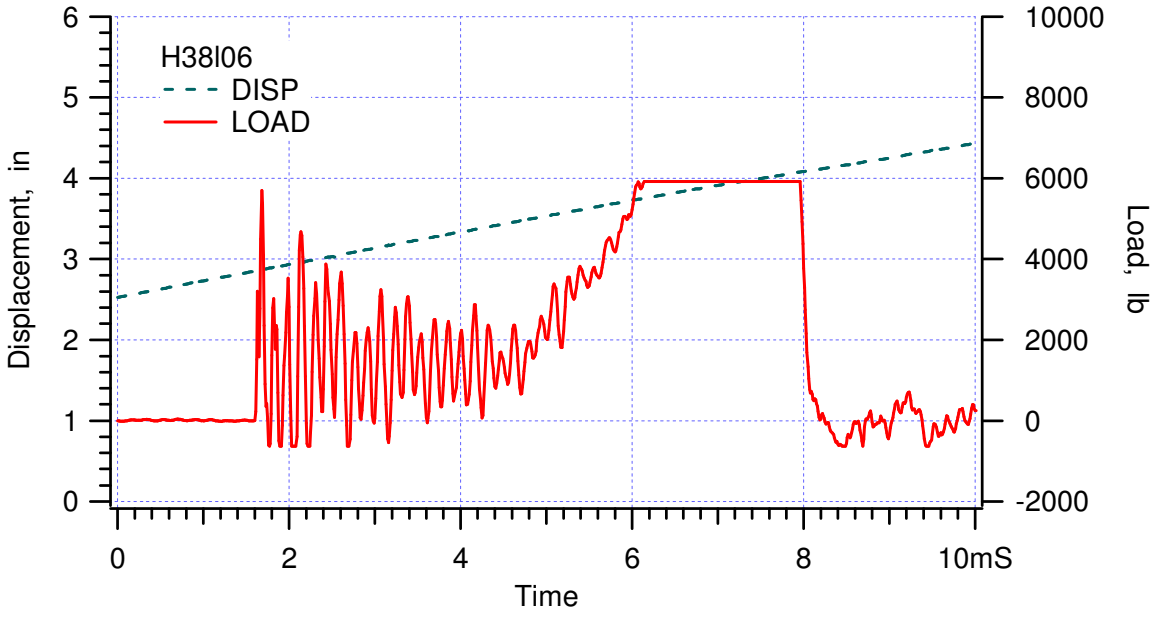
H38I06
DISP
LOAD
Displacement, in
Load, lb
Time
0
2
4
6
8
10mS
10000
8000
6000
4000
2000
0
-2000

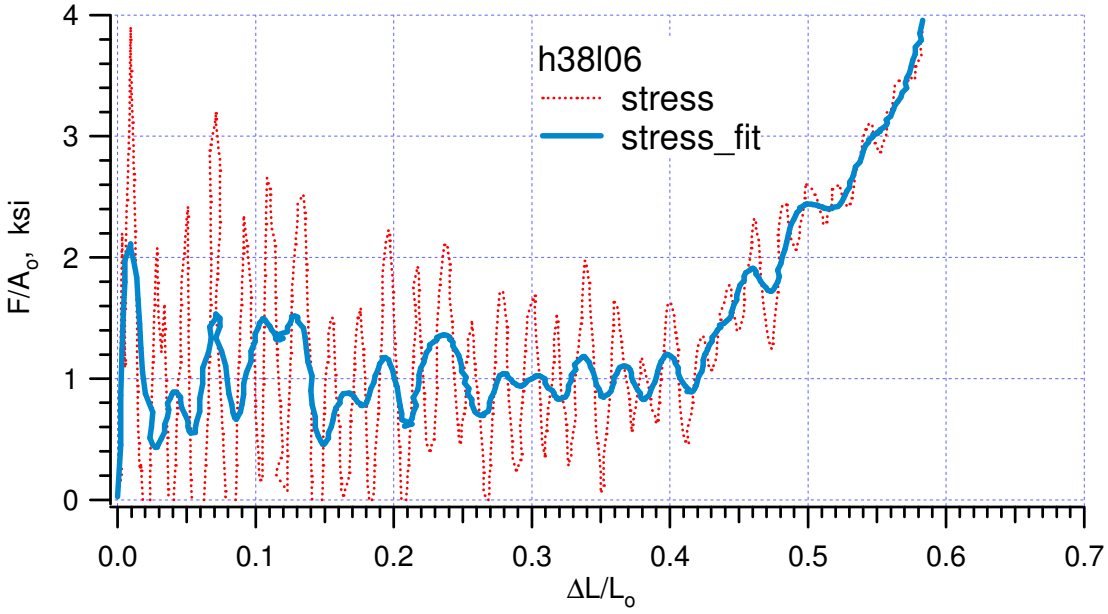
h38l06
stress
stress_fit
F/A$_o$, ksi
ΔL/L$_o$
0.0
0.1
0.2
0.3
0.4
0.5
0.6
0.7

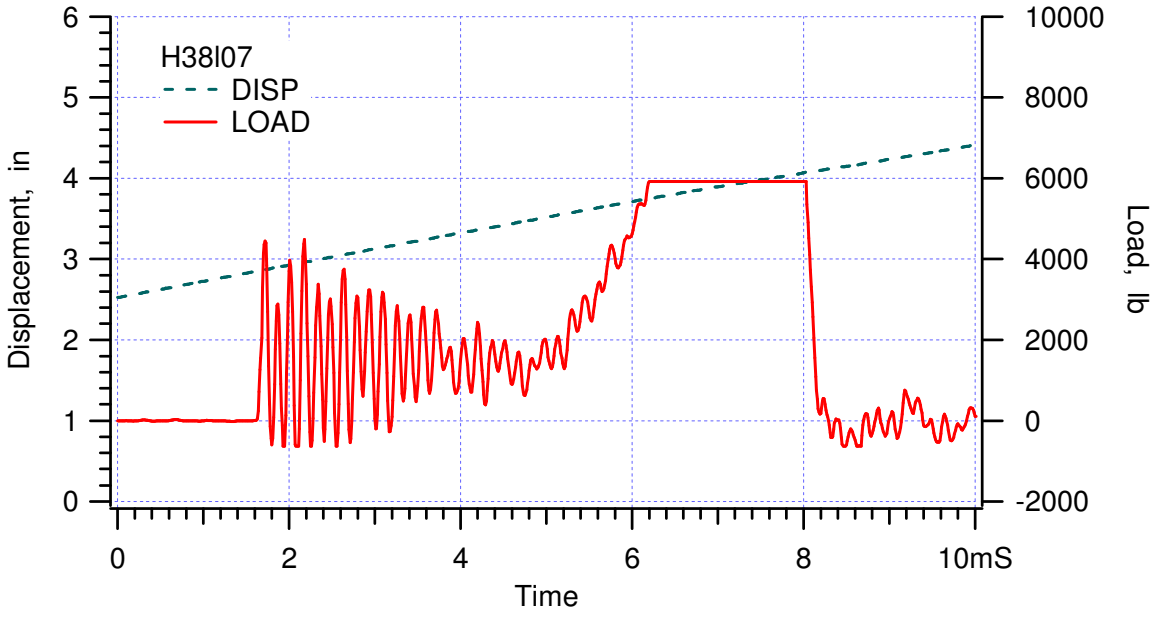
H38I07
DISP
LOAD
Displacement, in
Load, lb
Time
0
2
4
6
8
10mS
10000
8000
6000
4000
2000
0
-2000

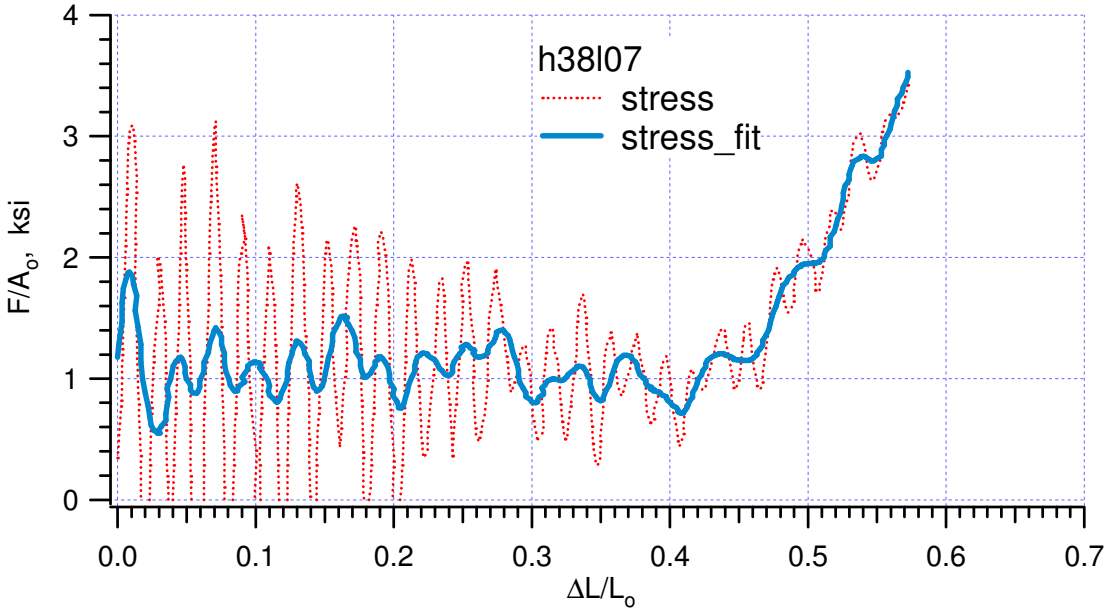
h38l07
stress
stress_fit
F/A$_o$, ksi
ΔL/L$_o$
0.0
0.1
0.2
0.3
0.4
0.5
0.6
0.7

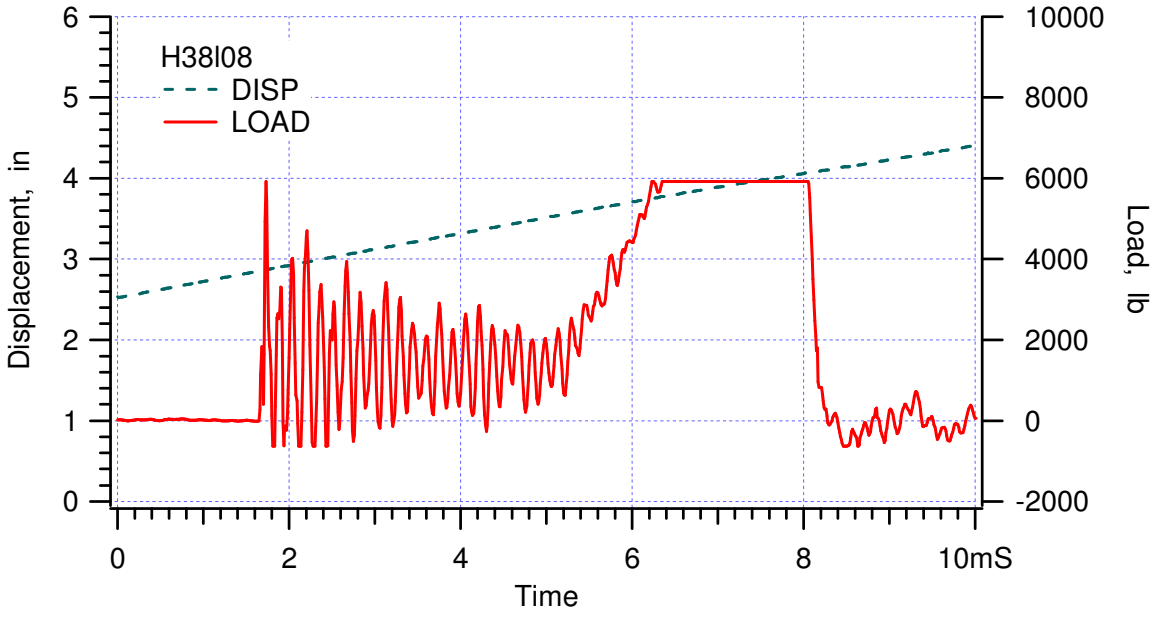
H38I08
DISP
LOAD
Displacement, in
Load, lb
Time
0
2
4
6
8
10mS
10000
8000
6000
4000
2000
0
-2000

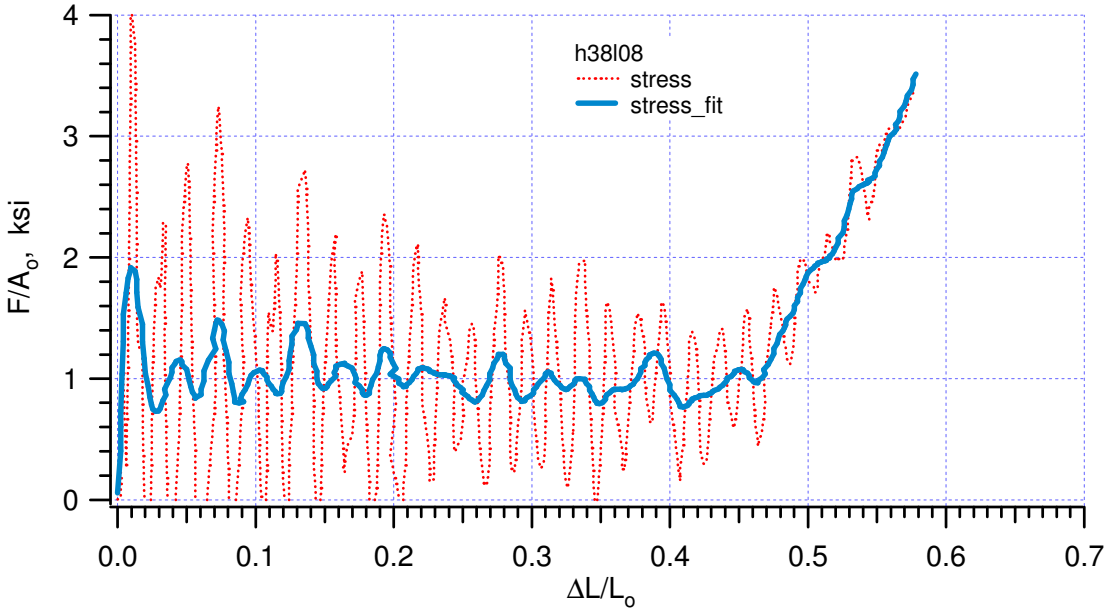
h38l08
stress
stress_fit
F/A$_o$, ksi
ΔL/L$_o$
0.0
0.1
0.2
0.3
0.4
0.5
0.6
0.7

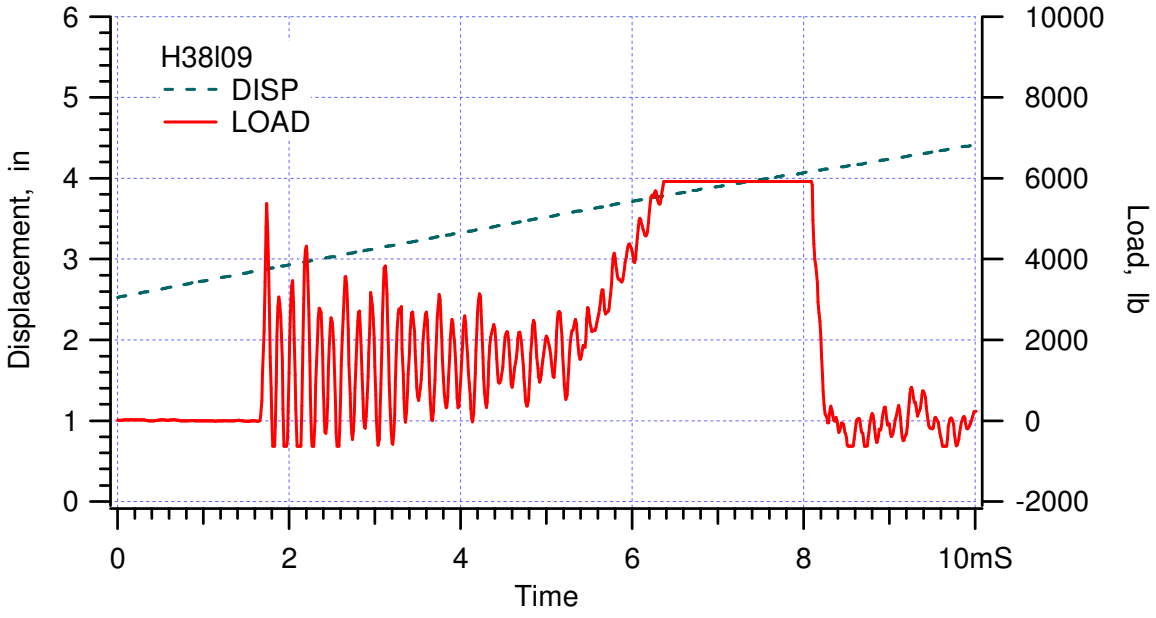
H38I09
DISP
LOAD
Displacement, in
Load, lb
Time
0
2
4
6
8
10mS
10000
8000
6000
4000
2000
0
-2000

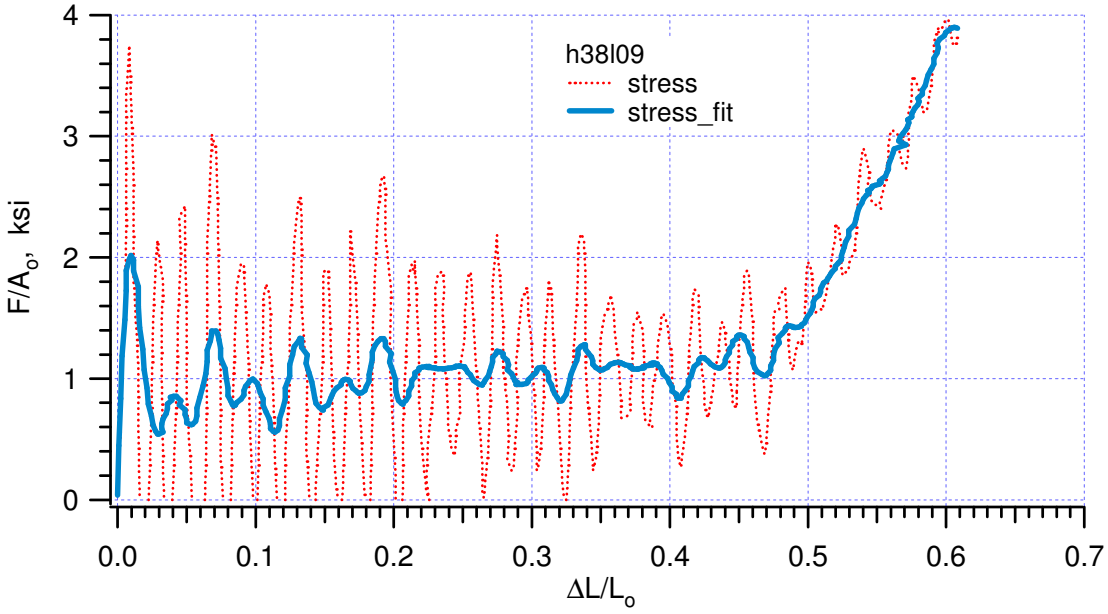
h38I09
stress
stress_fit
F/A$_o$, ksi
ΔL/L$_o$
0.0
0.1
0.2
0.3
0.4
0.5
0.6
0.7

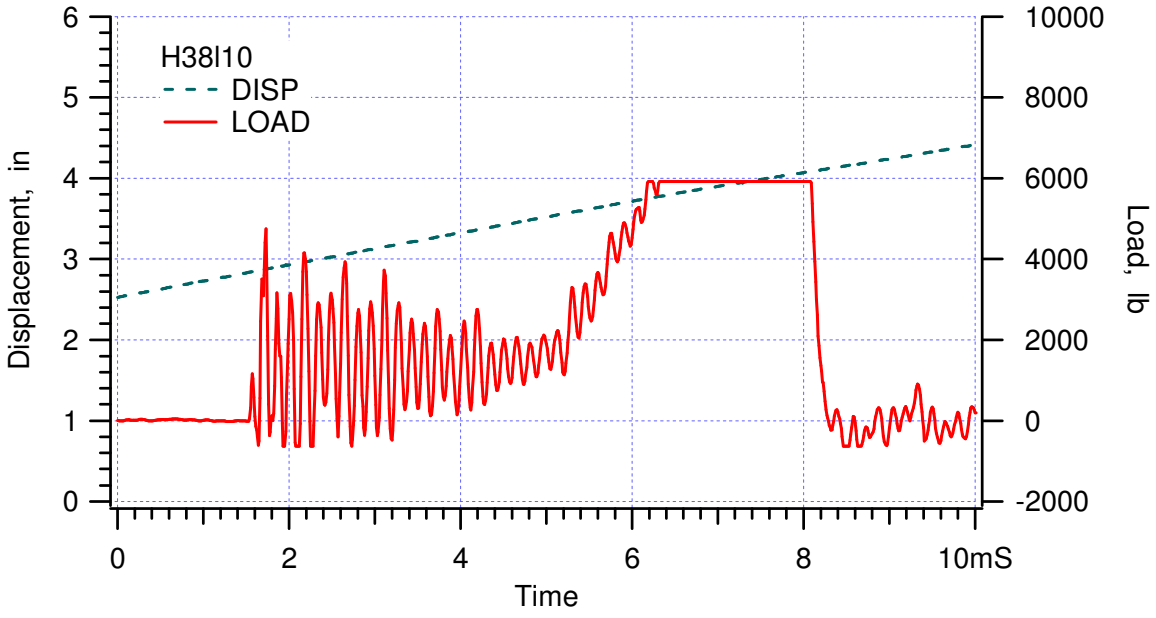
H38I10
DISP
LOAD
Displacement, in
Load, lb
Time
0
2
4
6
8
10mS
10000
8000
6000
4000
2000
0
-2000

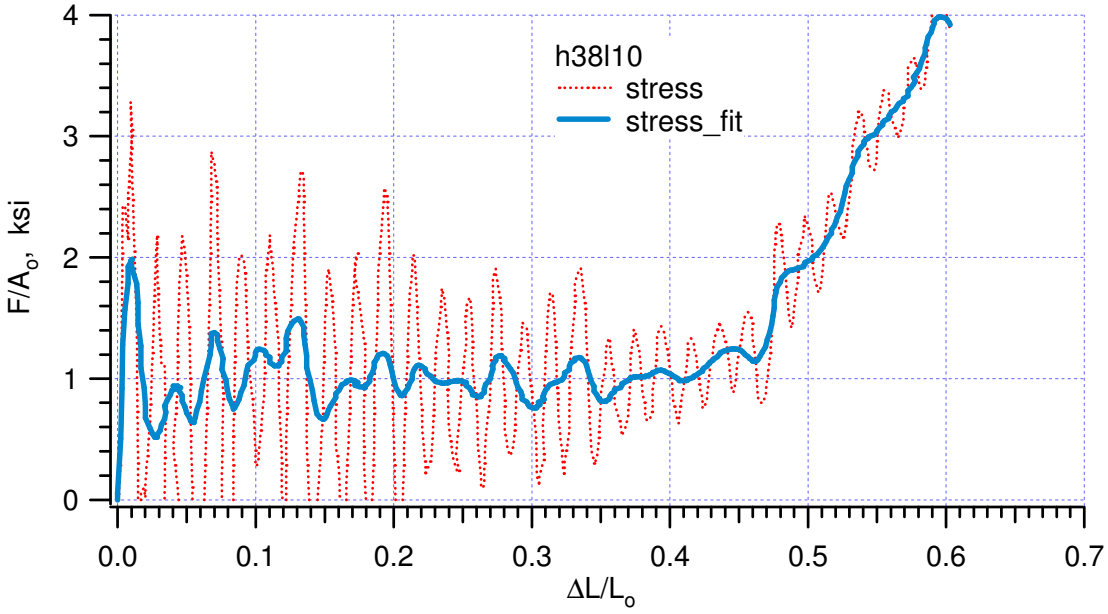
h38I10
stress
stress_fit
F/A$_o$, ksi
ΔL/L$_o$
0.0
0.1
0.2
0.3
0.4
0.5
0.6
0.7

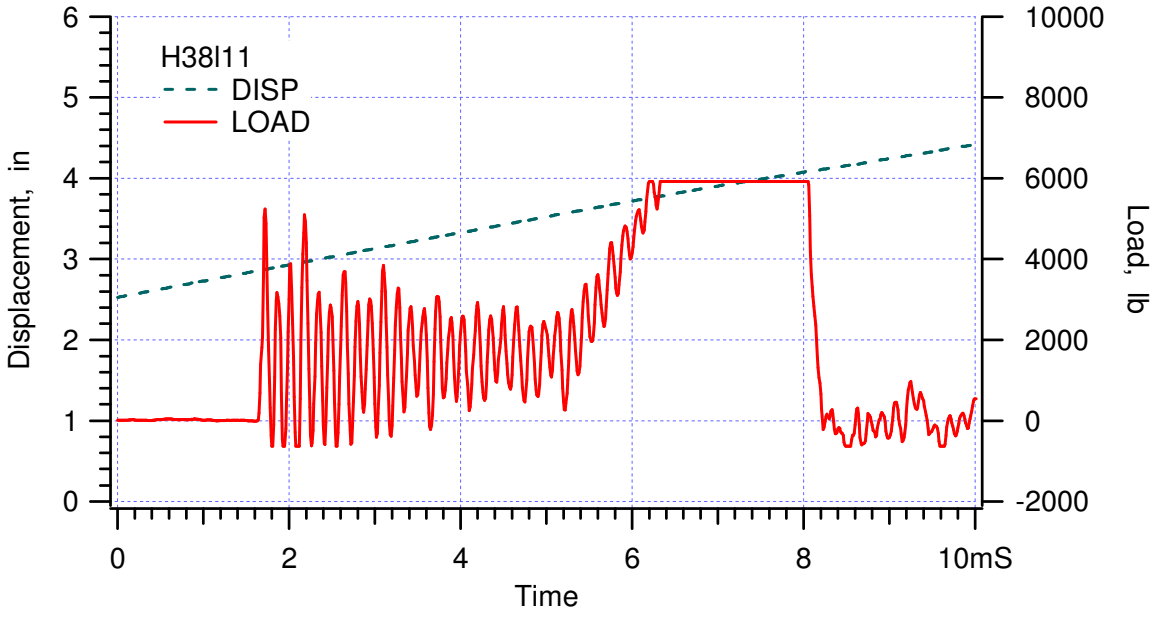
H38I11
DISP
LOAD
Displacement, in
Load, lb
Time
0
2
4
6
8
10mS
10000
8000
6000
4000
2000
0
-2000

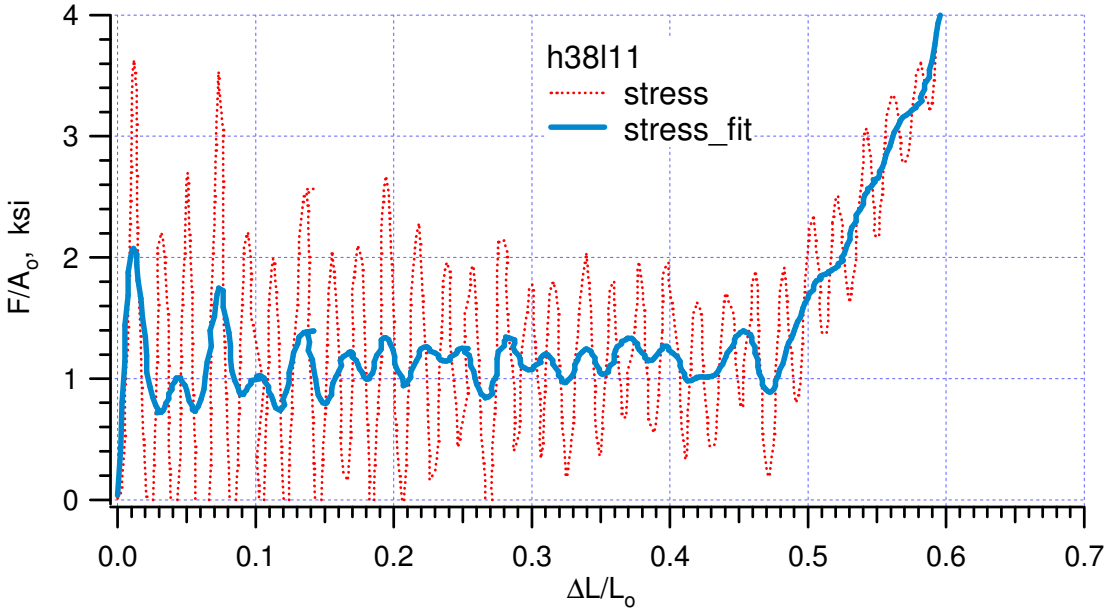
h38l11
stress
stress_fit
F/A$_o$, ksi
ΔL/L$_o$
0.0
0.1
0.2
0.3
0.4
0.5
0.6
0.7

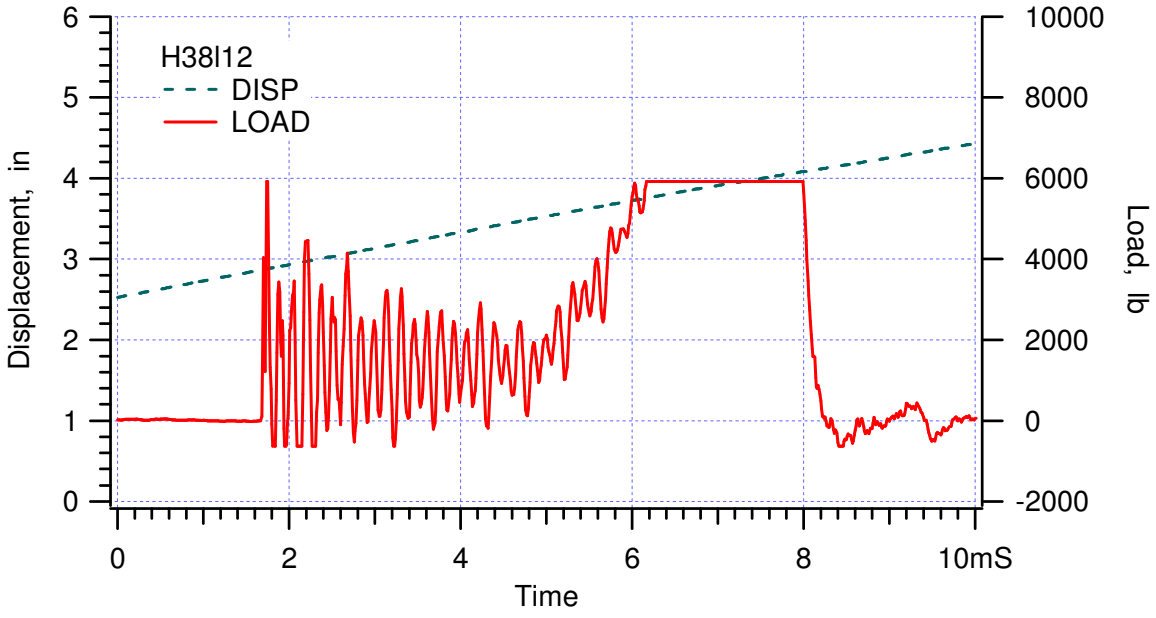
H38I12
DISP
LOAD
Displacement, in
Load, lb
Time
0
2
4
6
8
10mS
10000
8000
6000
4000
2000
0
-2000

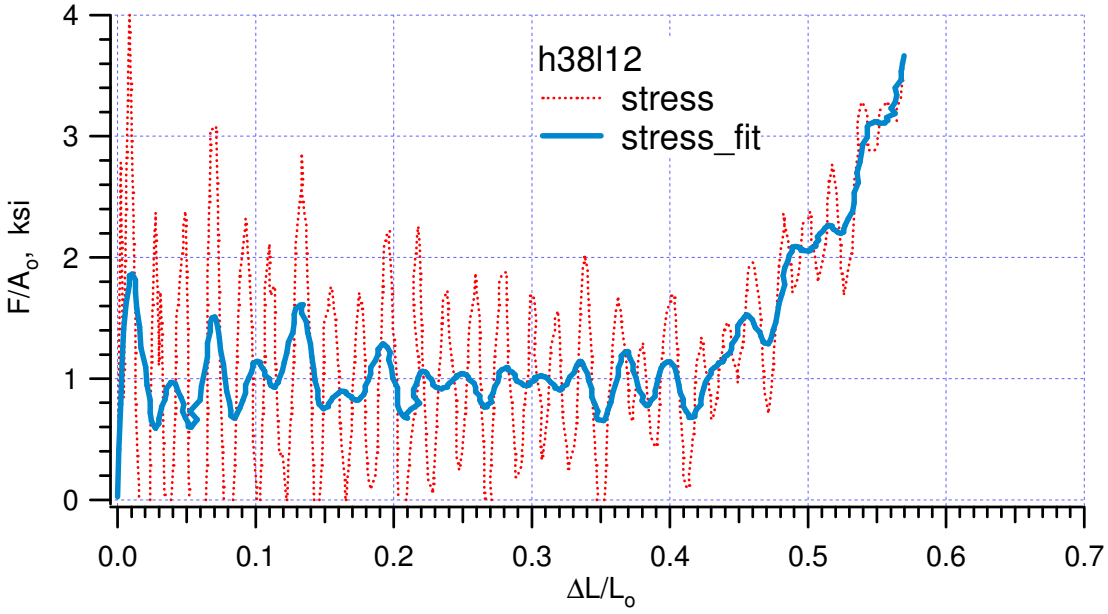
h38l12
stress
stress_fit
F/A$_o$, ksi
ΔL/L$_o$
0.0
0.1
0.2
0.3
0.4
0.5
0.6
0.7

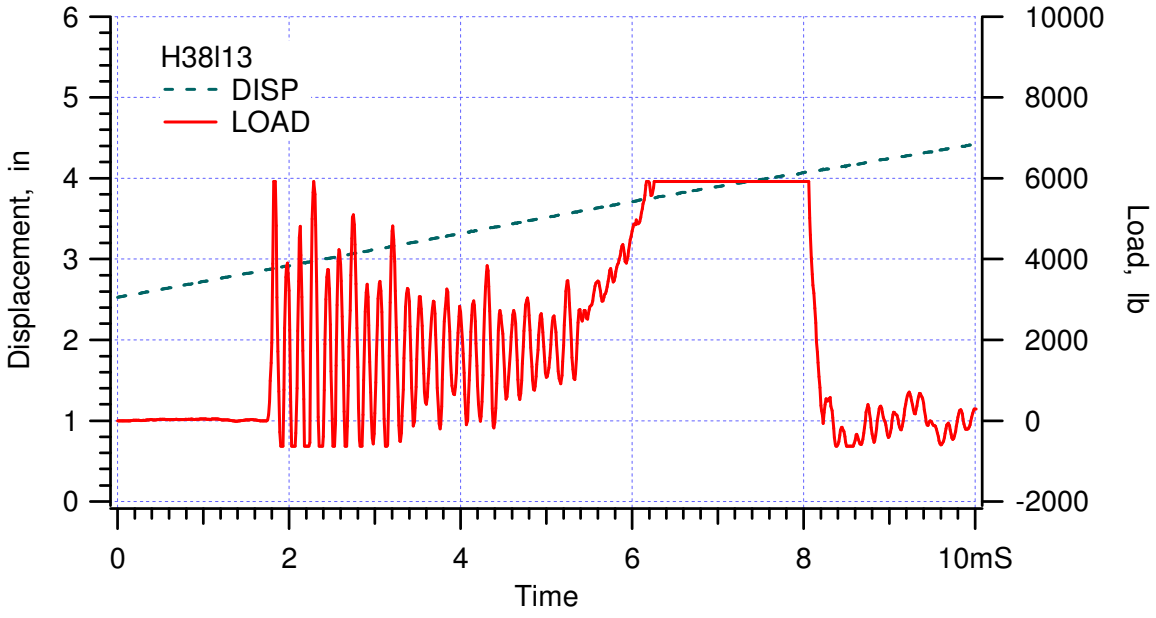
H38I13
DISP
LOAD
Displacement, in
Load, lb
Time
0
2
4
6
8
10mS
10000
8000
6000
4000
2000
0
-2000

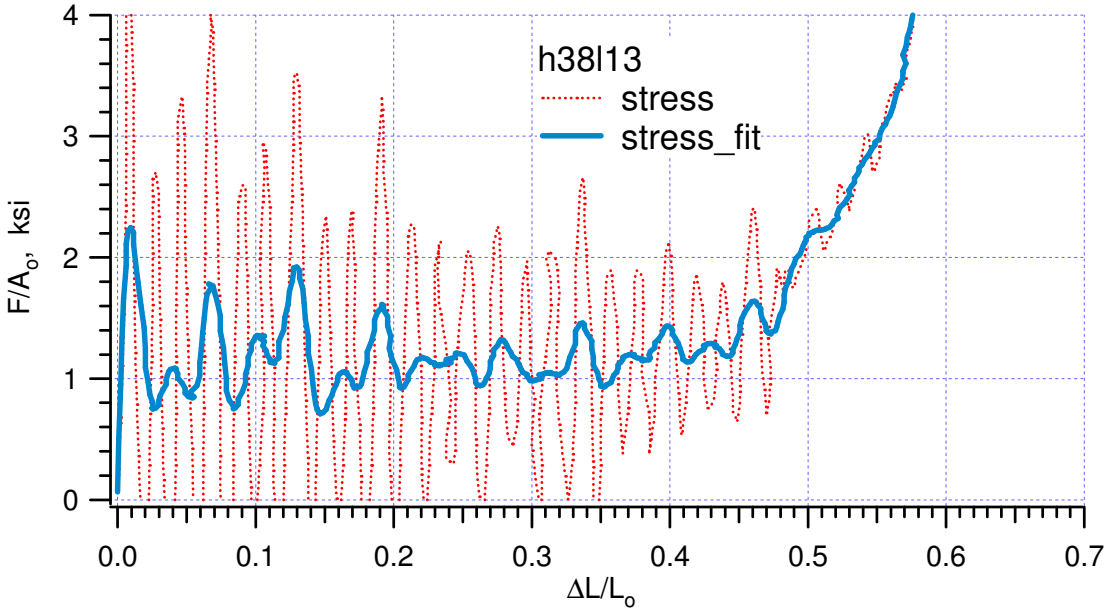
h38l13
stress
stress_fit
F/A$_o$, ksi
ΔL/L$_o$
0.0
0.1
0.2
0.3
0.4
0.5
0.6
0.7

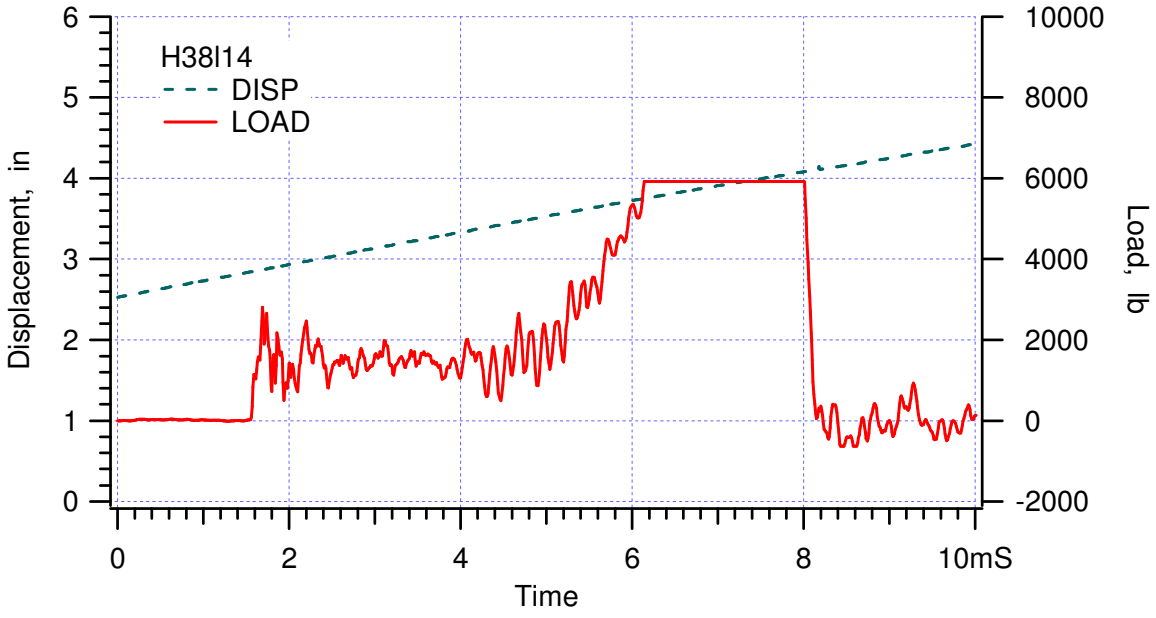
H38I14
DISP
LOAD
Displacement, in
Load, lb
Time
0
2
4
6
8
10mS
10000
8000
6000
4000
2000
0
-2000

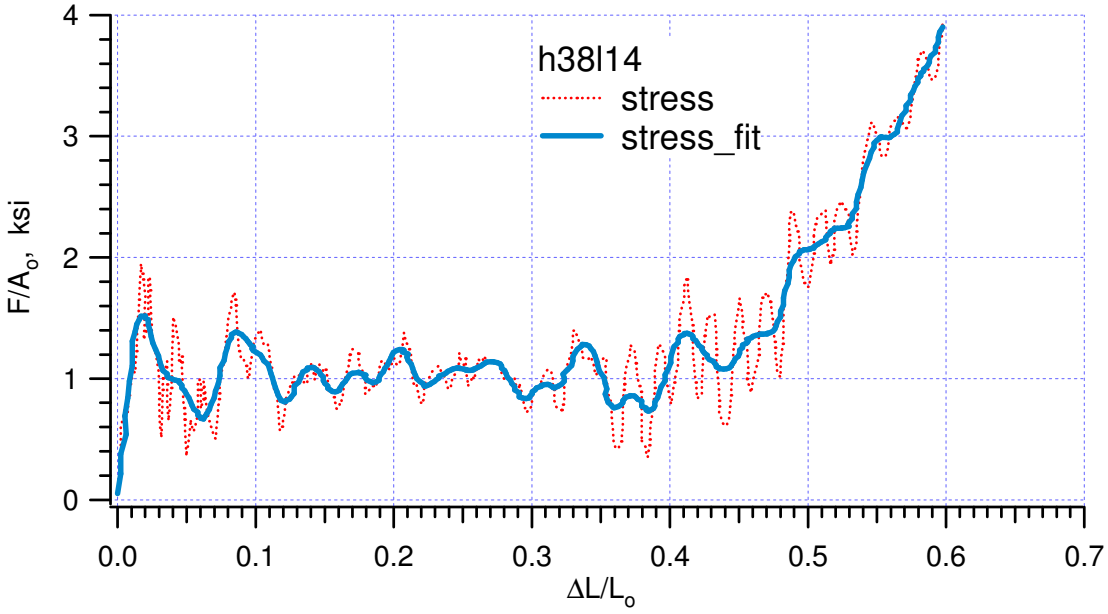
h38I14
stress
stress_fit
F/A$_o$, ksi
ΔL/L$_o$
0.0
0.1
0.2
0.3
0.4
0.5
0.6
0.7

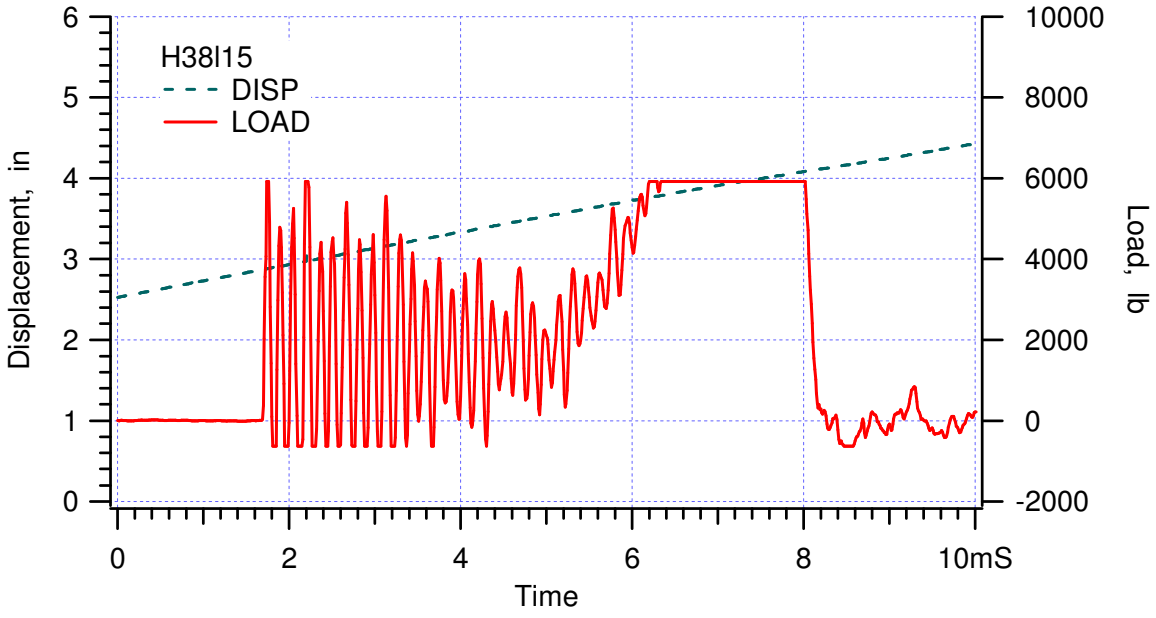
H38I15
DISP
LOAD
Displacement, in
Load, lb
Time
0
2
4
6
8
10mS
10000
8000
6000
4000
2000
0
-2000

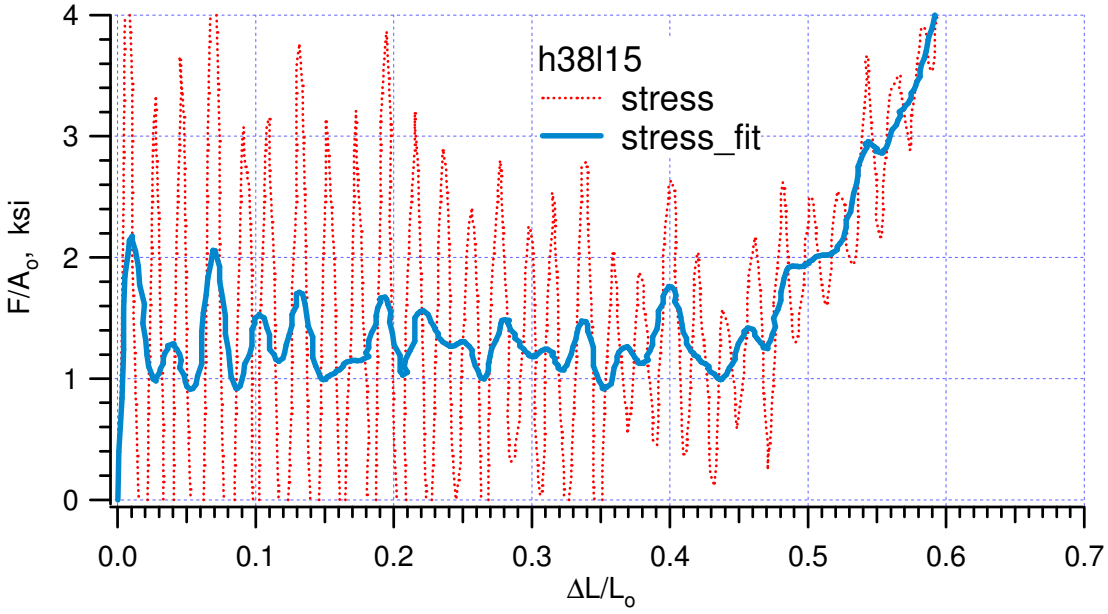
h38I15
stress
stress_fit
F/A$_o$, ksi
ΔL/L$_o$
0.0
0.1
0.2
0.3
0.4
0.5
0.6
0.7

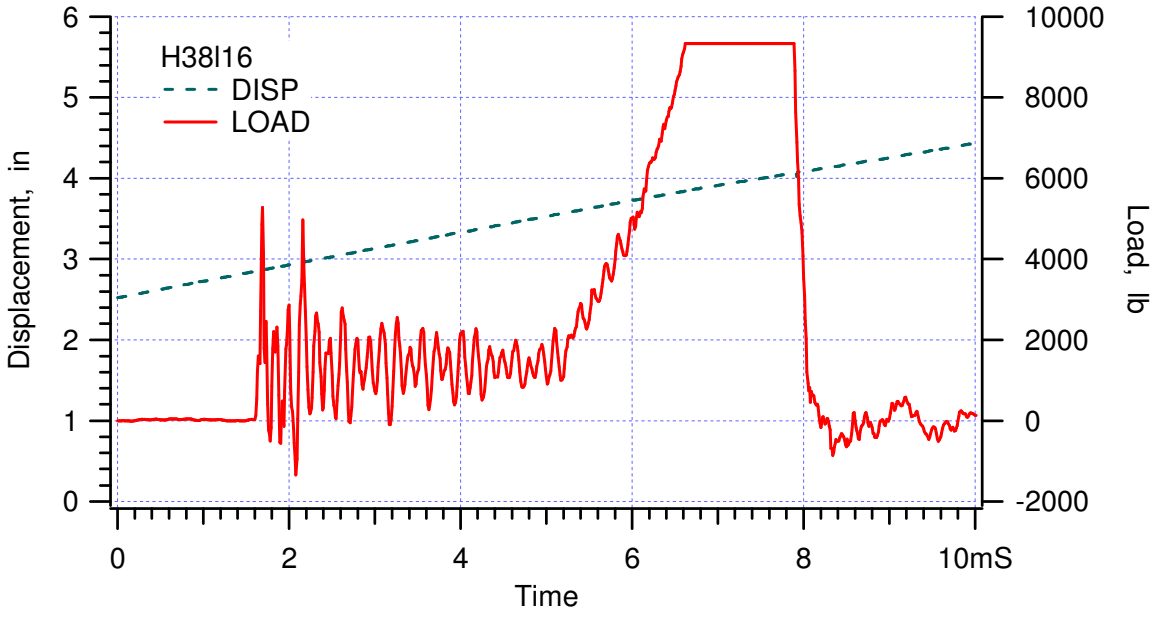
H38I16
DISP
LOAD
Displacement, in
Load, lb
Time
0
2
4
6
8
10mS
10000
8000
6000
4000
2000
0
-2000

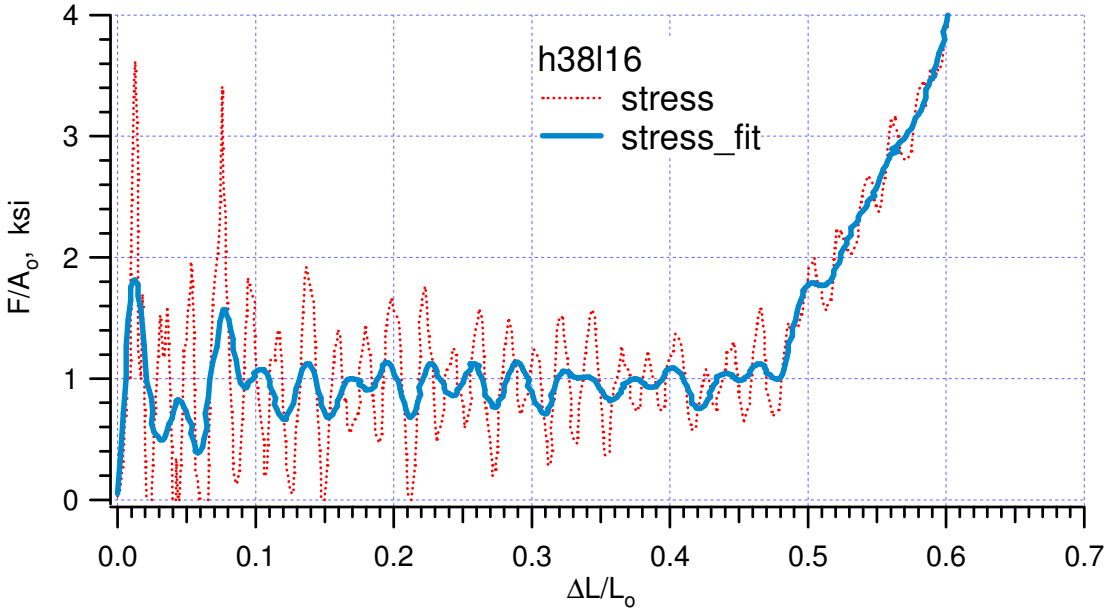
h38l16
stress
stress_fit
F/A$_o$, ksi
ΔL/L$_o$
0.0
0.1
0.2
0.3
0.4
0.5
0.6
0.7

This page intentionally left blank.

APPENDIX XIV:

"Moderate Rate Confined Crush Tests of 38 pcf honeycombs in the W-direction at ambient," Memo Wei-Yang Lu to Distribution, March 16, 2000

Sandia National Laboratories
Operated for the U.S. Department of Energy by
Sandia Corporation
MS9042
Livermore, CA 94551-0969

date: March 16, 2000

to: Distribution

from: Wei-yang Lu

subject: Moderate Rate Confined Crush Tests of 38 pcf honeycombs in the W-direction at ambient

Experimental results of both Alcore and Hexcel materials are included in this report. The boldface lines in Table 1 summarize these new data. Now, we have completed all planned quasi-static and moderate rate qualification tests that were agreed during Aluminum Honeycomb Working Group Meeting, August 3, 1999 (Table 1.1 – 1.5 and 2.4, ***B61 Radar Nose / MAVEN*** *Test Matrix* …, by T.D. Hinnerichs, October 27, 1999).

Specimens used in W-crush were not rotated, shown in Figure 1. Surfaces were parallel to T-, L-, and W-directions.

Data analysis was similar to that used in L-crush. Filtered signals were used to calculate the crush strength of the honeycomb. Crush strengths of Alcore 38 and Hexcel 38 are 0.54 ksi and 0.60 ksi, and crush efficiencies are 36.80% and 37.03%, respectively. Different from T- and L-crush, honeycomb has a relatively short region of constant crush load and locks up slowly during W-crush. A typical stress-strain curve is shown in figure 2. Here, the crush efficiency is the limit of constant crush load.

Please see Appendix for detail experimental data.

Distribution:

Darla Giersch (2167)	MS0481	John Pott (9126)	MS0847
Darren Hoke (2167)	MS0481	Rodney May (9126)	MS0847
Vernon Willan (2167)	MS0481	Mike Neilsen (9123)	MS0847
Vista Bateman (9126)	MS0553	Bill Scherzinger (9123)	MS0847
Tom Carne (9124)	MS0557	Hal Morgan (9123)	MS0847
Berry Boughten (9132)	MS0557	Wendell Kawahara (8725)	MS9042
Jaime Moya (9132)	MS0828		
Terry Hinnerichs (9126)	MS0847		
Ken Gwinn (9126)	MS0847		

Table 1. Summary of FY00 experimental results

B61/MAVEN TEST MATRIX				EXPERIMENTAL RESULTS						MEMO
Test #	Honeycomb	Dir.	Temperature, degree F	Specimen	Density, pcf	Impact Speed, ft/s	Crush Strength, ksi	Std Deviation, ksi	Crush Efficiency, %	Date
1 - 15	Alcore 38	T	ambient	rotated	38.82	14.13	6.35	0.08	63.80	991203
16 - 30	Hexcel 38	T	ambient	rotated	38.70	13.67	7.17	0.15	63.89	000110
	Hexcel 38	T	ambient	rotated	38.78	0.00139	5.88		59.20	000110
31 - 45	Alcore 35	T	ambient	rotated	35.39	14.35	5.74	0.18	64.46	000103
46 - 60	Hexcel 35	T	ambient	rotated	37.79	13.83	6.67	0.24	63.91	000110
	Hexcel 35	T	ambient	rotated	37.89	0.00139	5.83		60.30	000110
60 - 75	Alcore 38	T	165	rotated	38.96	14.33	5.49	0.10	62.52	000118
76 - 90	Hexcel 38	T	165	rotated	38.65	13.82	6.43	0.15	64.31	000118
	Alcore 35	T	165	rotated	35.62	14.59	4.94	0.23	62.54	000207
91 - 105	Alcore 38	T	-65	rotated	38.94	13.48	7.34	0.24	62.71	000225
106 - 120	Hexcel 38	T	-65	rotated	38.65	13.17	8.21	0.17	64.68	000225
	Alcore 35	T	-65	rotated	35.59	13.77	7.04	0.36	62.89	000307
	Hexcel 35	T	-65	rotated	37.92	13.29	8.05	0.09	64.20	000307
121 - 125	Alcore 38	L	ambient	rotated	38.88	16.45	1.25	0.13	53.24	000307
126 - 130	Hexcel 38	L	ambient	rotated	38.62	16.50	1.05	0.09	46.12	000307
131 - 135	**Alcore 38**	**W**	**ambient**	**normal**	**38.94**	**16.56**	**0.54**	**0.06**	**36.80**	**000316**
136 - 140	**Hexcel 38**	**W**	**ambient**	**normal**	**38.70**	**16.72**	**0.60**	**0.02**	**37.03**	**000316**
159 - 161	Alcore 38	T	ambient	segmented	41.41	0.0014	6.14		52.30	991130
162 - 164	Hexcel 38	T	ambient	segmented	41.29	0.0014	6.85		53.70	991213

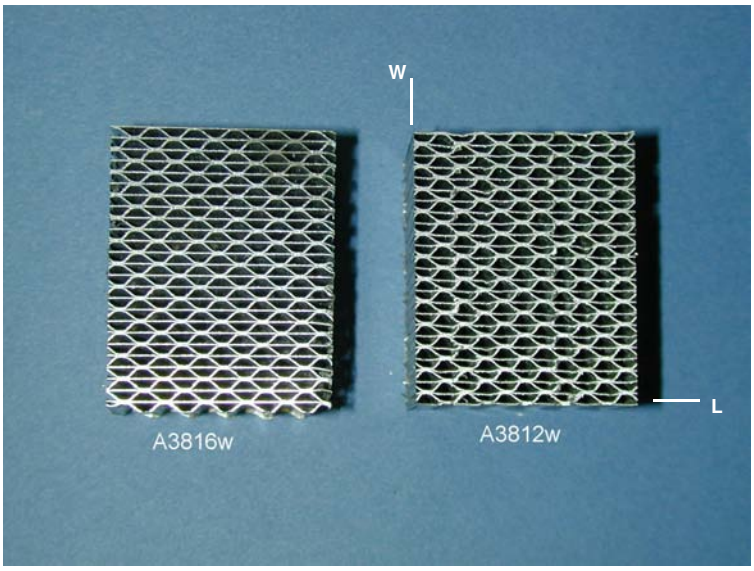

Figure 1. Typical specimens for crush in W-direction.

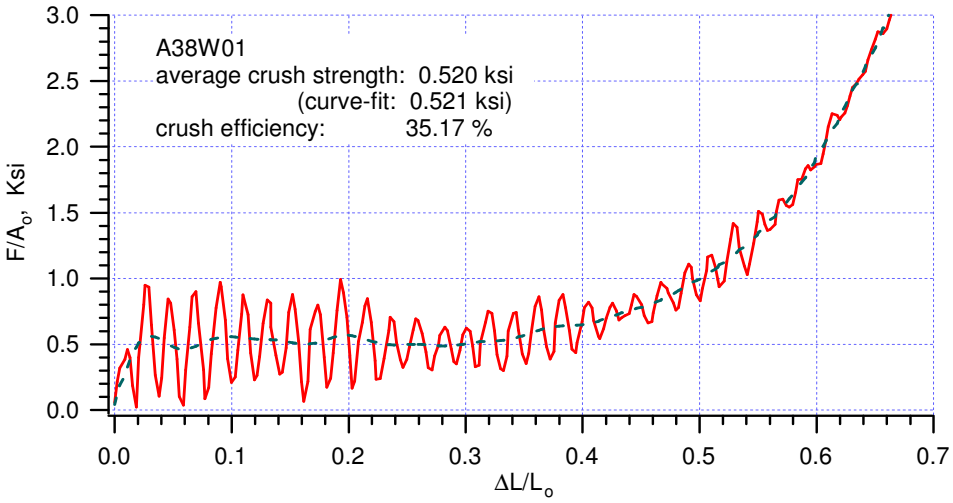

Figure 2. Typical W-direction "stress-strain" curves. The red line is the raw data, which includes high frequency system response; the blue line is the filtered data.

Appendix Alcore 38W

Specimen	d_1, in	d_2, in	d_3, in	Weight, lb	Density, pcf	Crush Velocity, ft/s	Crush strenghth, ksi	Crush efficiency, %	Crush strenghth, ksi (fit)
A38W01	1.195	1.202	1.474	0.0476	38.83	16.37	0.520	35.17	0.521
A38W02	1.208	1.203	1.477	0.0489	39.35	16.49	0.612	38.78	0.616
A38W03	1.202	1.187	1.459	0.0464	38.50	16.48	0.589	39.04	0.588
A38W04	1.187	1.196	1.540	0.0494	39.03	16.60	0.474	35.78	0.478
A38W05	1.193	1.200	1.490	0.0485	39.31	16.44	0.492	34.36	0.495
A38W06	1.209	1.200	1.490	0.0490	39.14	16.61	0.595	41.07	0.605
A38W07	1.209	1.196	1.532	0.0495	38.61	16.76	0.551	40.00	0.553
A38W08	1.192	1.209	1.498	0.0485	38.82	16.76	0.489	33.47	0.492
A38W09	1.212	1.220	1.520	0.0504	38.73	16.58	0.486	34.74	0.488
A38W10	1.198	1.191	1.493	0.0479	38.82	16.50	0.467	34.94	0.469
A38W11	1.210	1.198	1.533	0.0501	38.97	16.57	0.621	38.00	0.626
A38W12	1.191	1.201	1.480	0.0481	39.30	16.63	0.485	35.14	0.486
A38W13	1.178	1.196	1.498	0.0476	38.99	16.60	0.473	34.93	0.475
A38W14	1.209	1.193	1.471	0.0472	38.48	16.61	0.626	36.76	0.631
A38W15	1.204	1.195	1.536	0.0500	39.08	16.61	0.595	36.46	0.599
A38W16	1.201	1.191	1.533	0.0494	38.95				
				max	39.35	16.76	0.626	41.07	0.631
				min	38.48	16.37	0.467	34.36	0.469
				average	38.94	16.56	0.542	36.80	0.545
				std deviation	0.28	0.10	0.062	2.19	0.063
				median	38.97	16.59	0.536	36.12	0.537

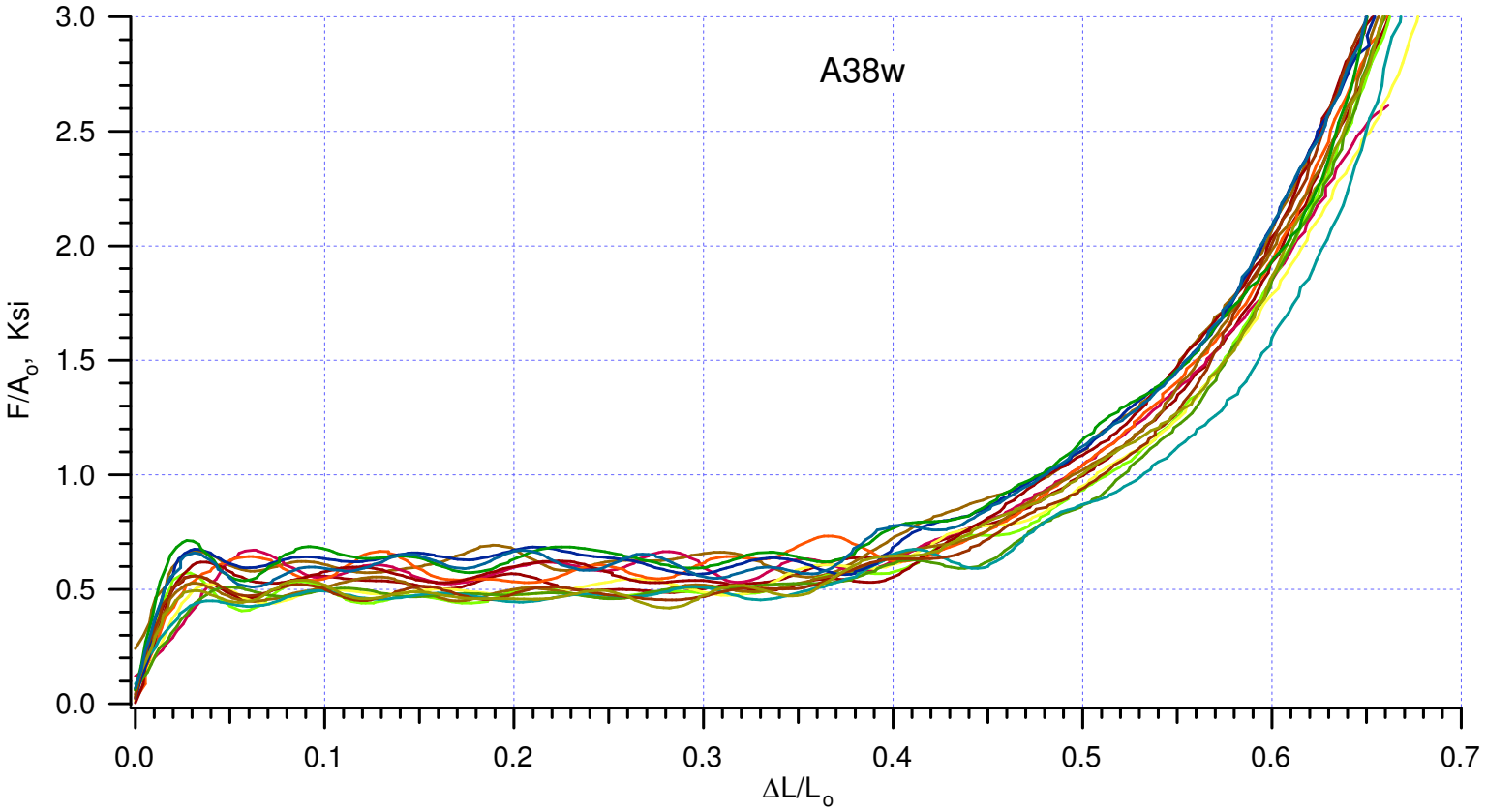
A38w
F/A$_o$, Ksi
3.0
2.5
2.0
1.5
1.0
0.5
0.0
0.0
0.1
0.2
0.3
0.4
0.5
0.6
0.7
ΔL/L$_o$

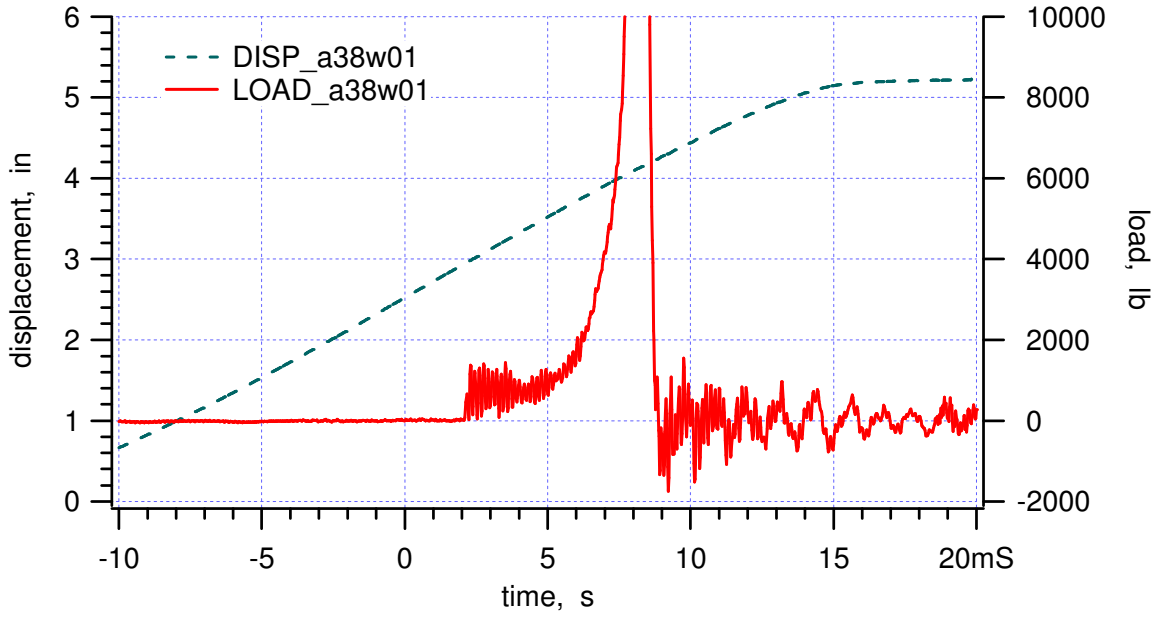
DISP_a38w01
LOAD_a38w01
displacement, in
load, lb
time, s
6
5
4
3
2
1
0
10000
8000
6000
4000
2000
0
-2000
-10
-5
0
5
10
15
20mS

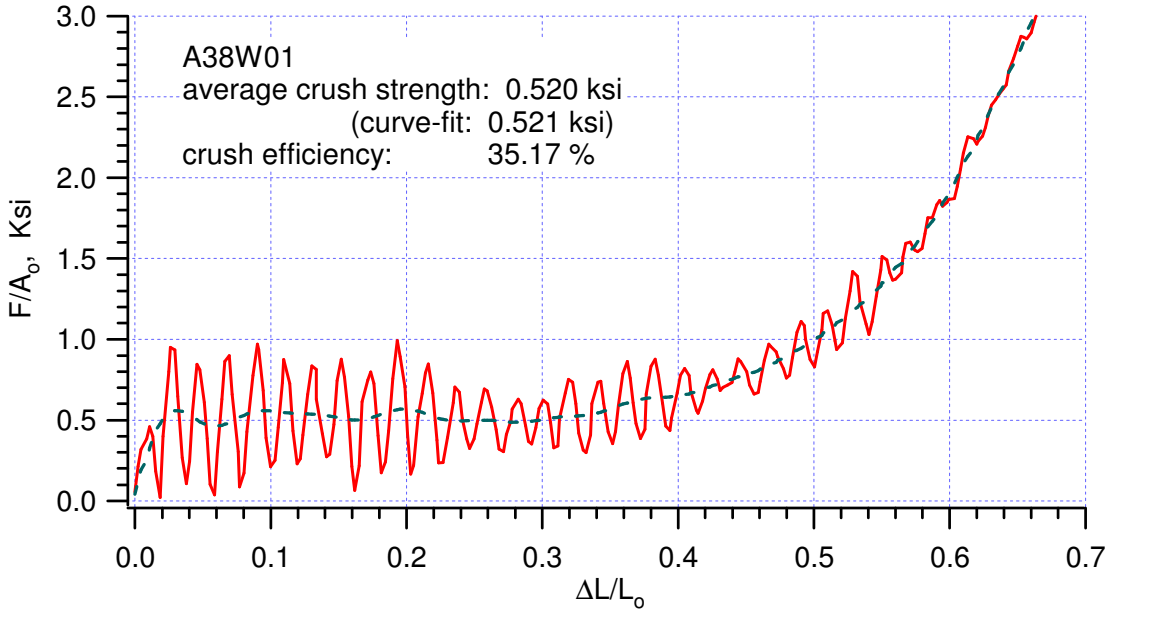
A38W01
average crush strength: 0.520 ksi
(curve-fit: 0.521 ksi)
crush efficiency: 35.17 %
F/A$_o$, Ksi
ΔL/L$_o$
3.0
2.5
2.0
1.5
1.0
0.5
0.0
0.0
0.1
0.2
0.3
0.4
0.5
0.6
0.7

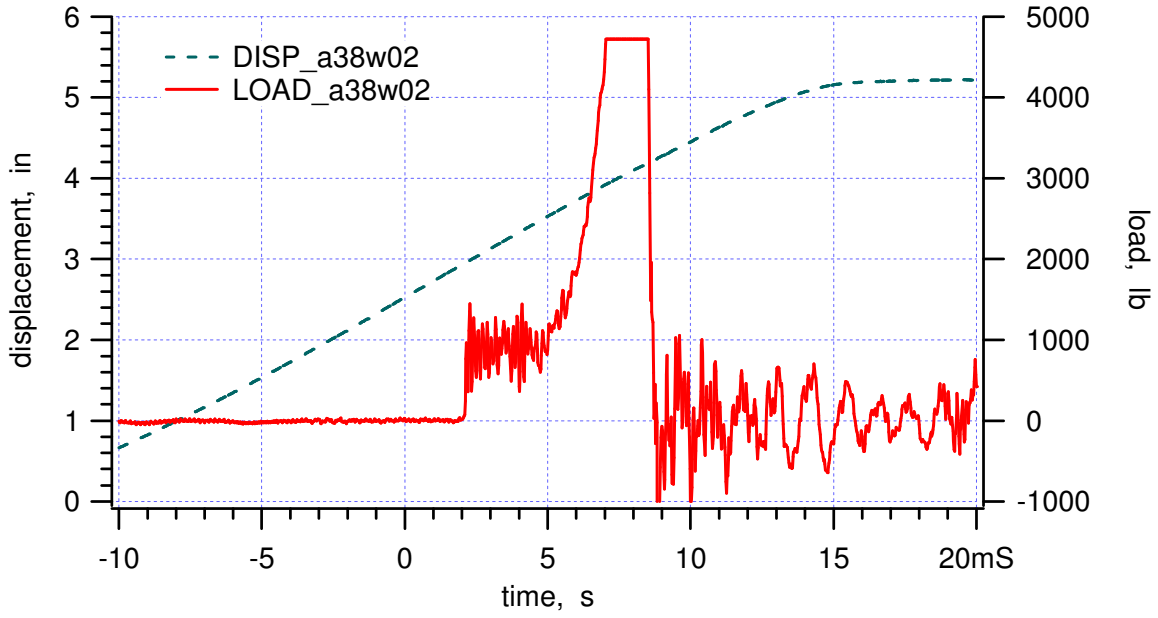
DISP_a38w02
LOAD_a38w02
displacement, in
load, lb
time, s
6
5
4
3
2
1
0
5000
4000
3000
2000
1000
0
-1000
-10
-5
0
5
10
15
20mS

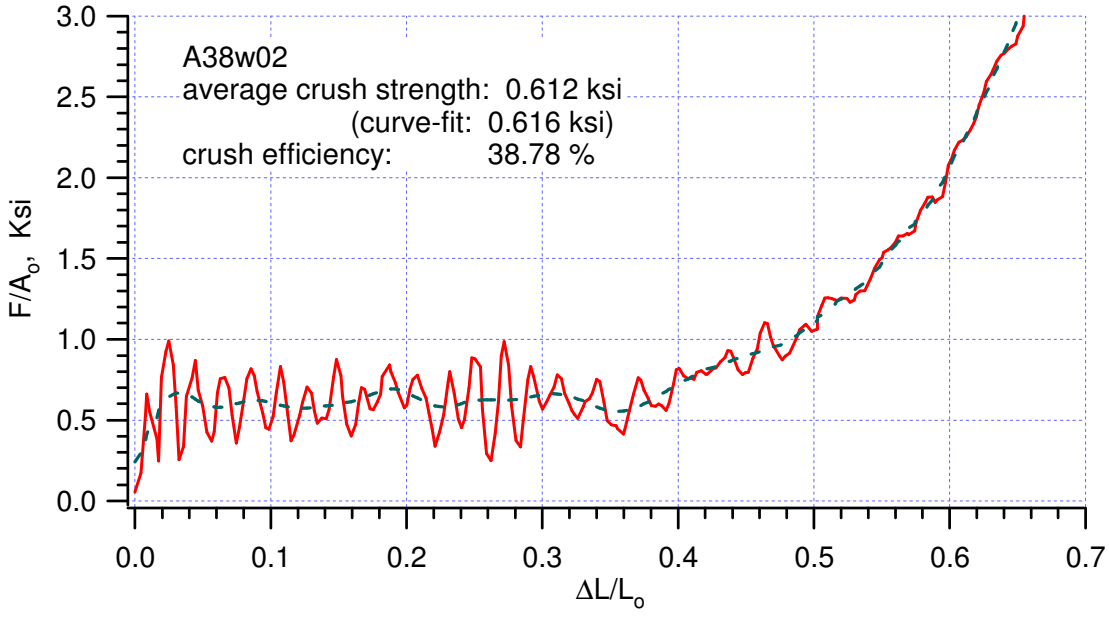
A38w02
average crush strength: 0.612 ksi
(curve-fit: 0.616 ksi)
crush efficiency: 38.78 %
F/A$_o$, Ksi
ΔL/L$_o$
3.0
2.5
2.0
1.5
1.0
0.5
0.0
0.0
0.1
0.2
0.3
0.4
0.5
0.6
0.7

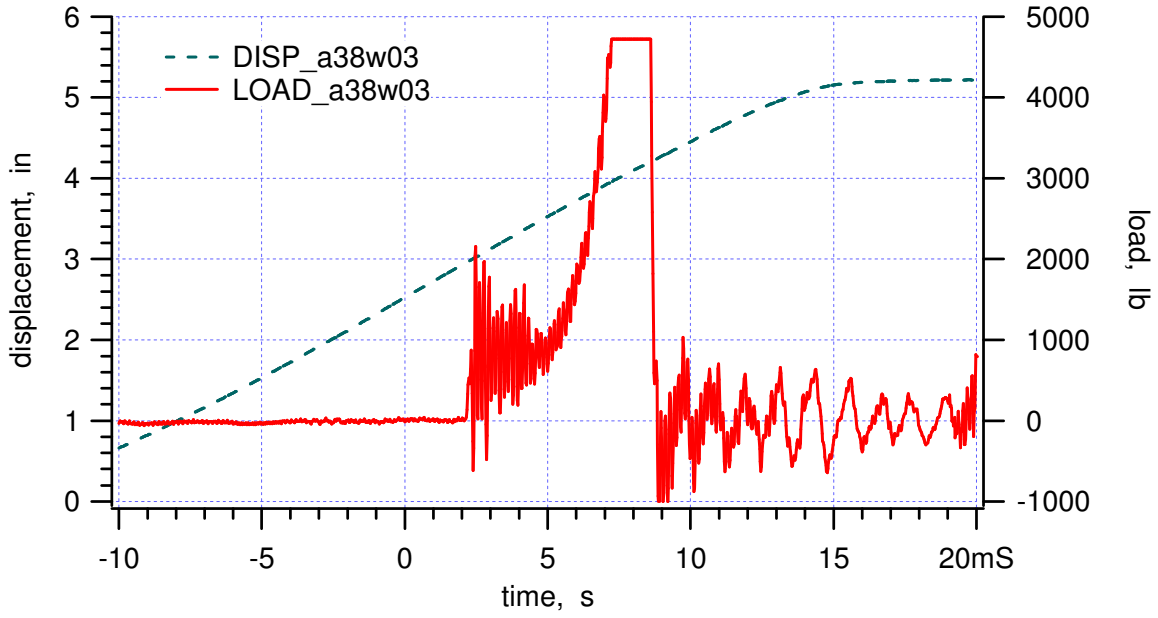
DISP_a38w03
LOAD_a38w03
displacement, in
load, lb
time, s
6
5
4
3
2
1
0
5000
4000
3000
2000
1000
0
-1000
-10
-5
0
5
10
15
20mS

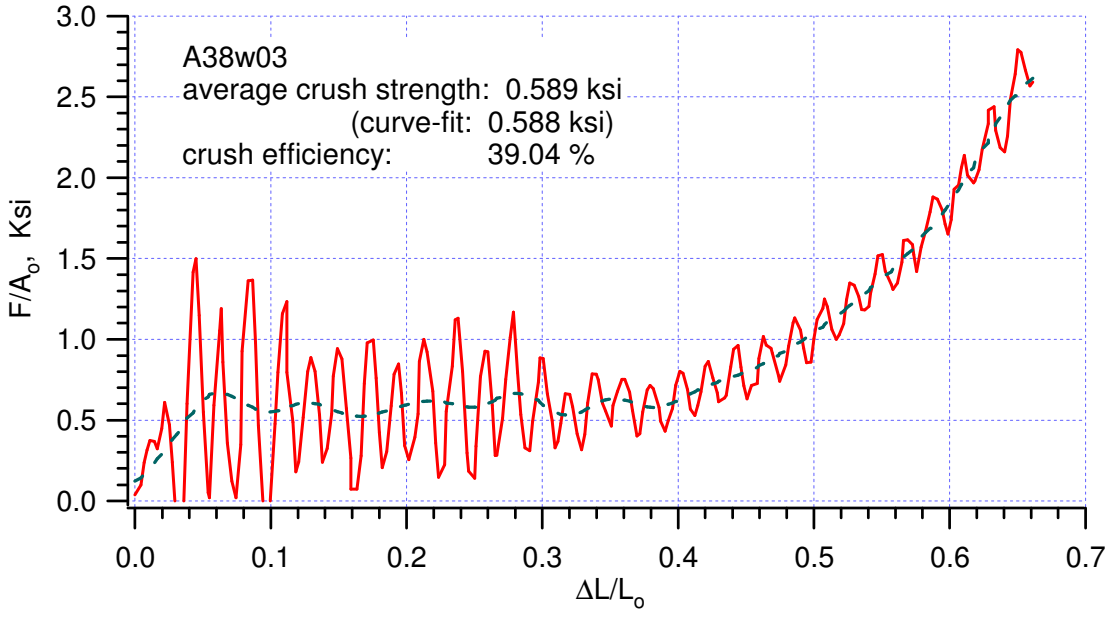
A38w03
average crush strength: 0.589 ksi
(curve-fit: 0.588 ksi)
crush efficiency: 39.04 %
F/A$_o$, Ksi
ΔL/L$_o$
3.0
2.5
2.0
1.5
1.0
0.5
0.0
0.0
0.1
0.2
0.3
0.4
0.5
0.6
0.7

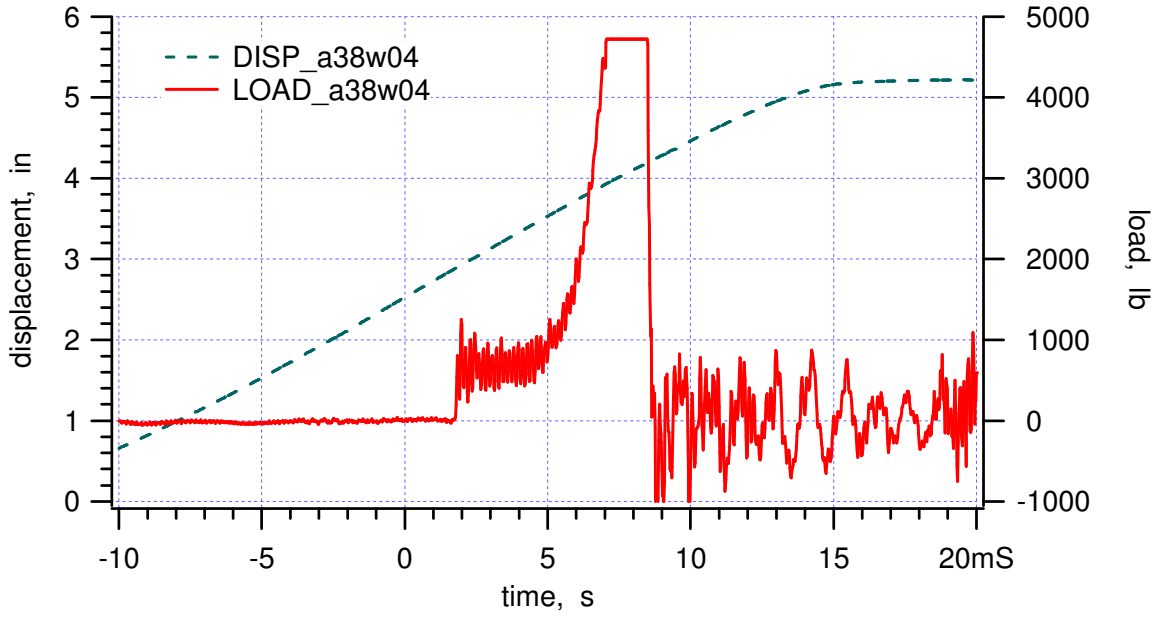
DISP_a38w04
LOAD_a38w04
displacement, in
load, lb
time, s
6
5
4
3
2
1
0
5000
4000
3000
2000
1000
0
-1000
-10
-5
0
5
10
15
20mS

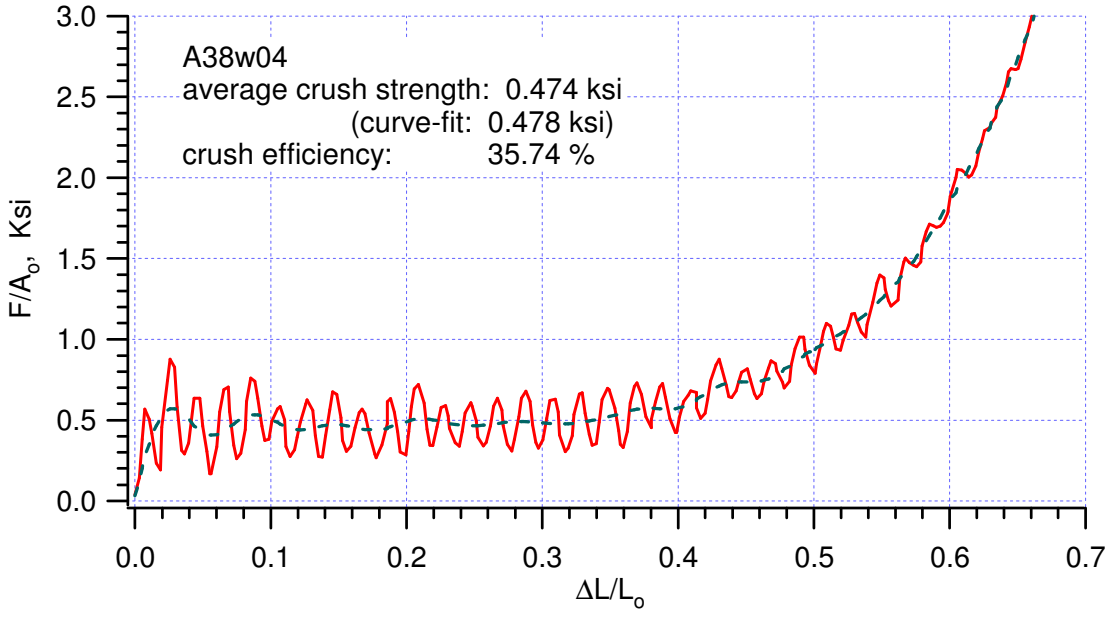
A38w04
average crush strength: 0.474 ksi
(curve-fit: 0.478 ksi)
crush efficiency: 35.74 %
F/A$_o$, Ksi
ΔL/L$_o$
3.0
2.5
2.0
1.5
1.0
0.5
0.0
0.0
0.1
0.2
0.3
0.4
0.5
0.6
0.7

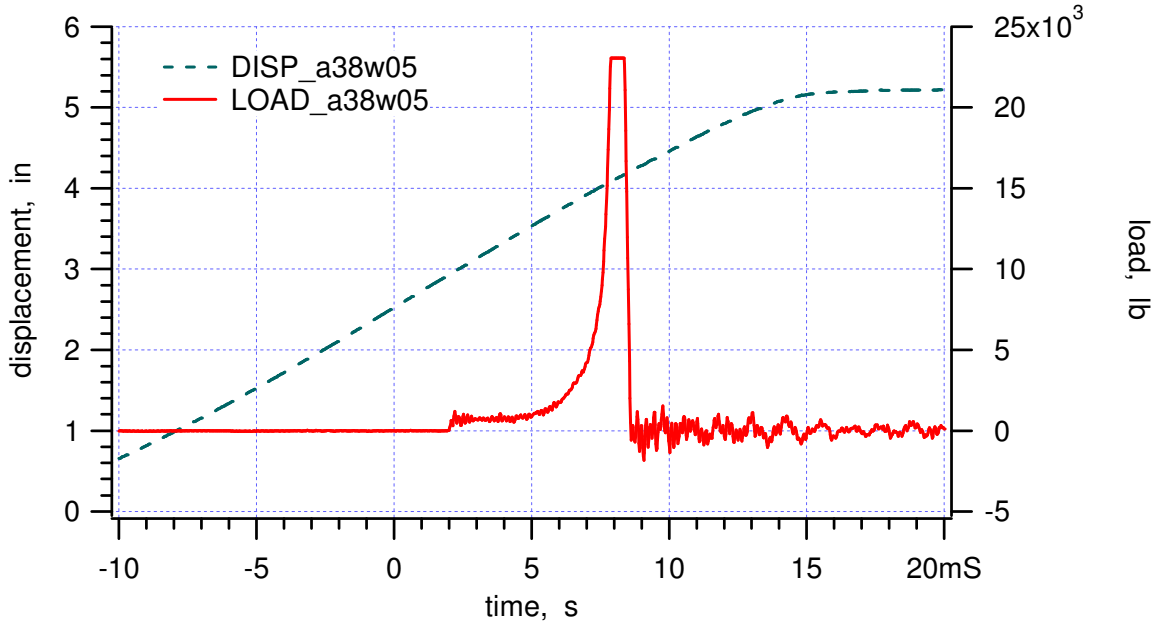
DISP_a38w05
LOAD_a38w05
displacement, in
load, lb
25x10^3
time, s
-10
-5
0
5
10
15
20mS

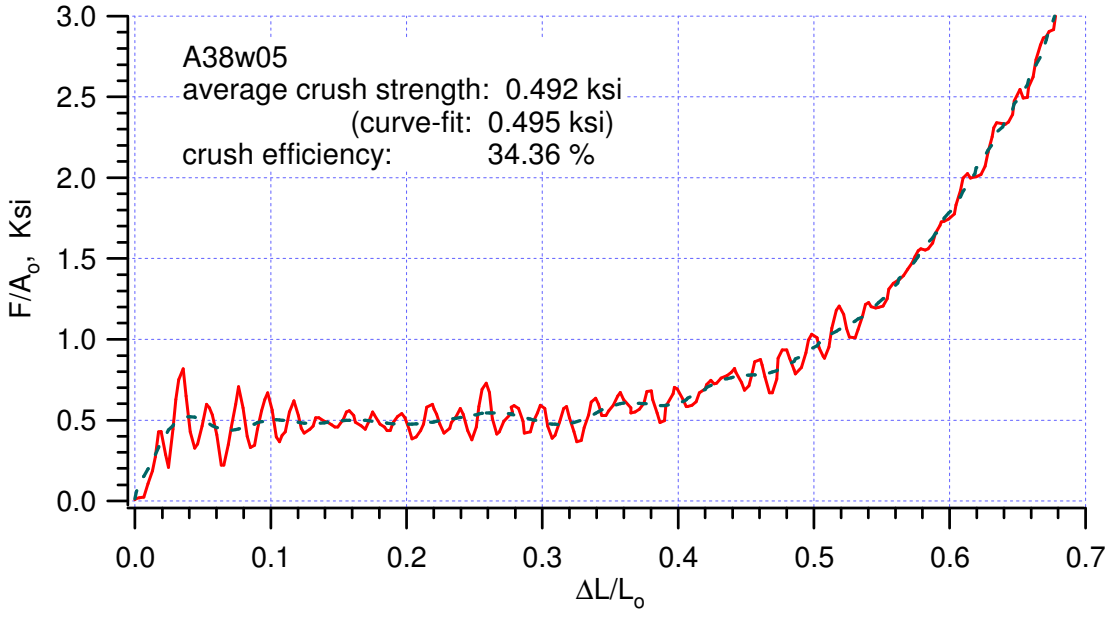
A38w05
average crush strength: 0.492 ksi
(curve-fit: 0.495 ksi)
crush efficiency: 34.36 %
F/A_o, Ksi
ΔL/L_o

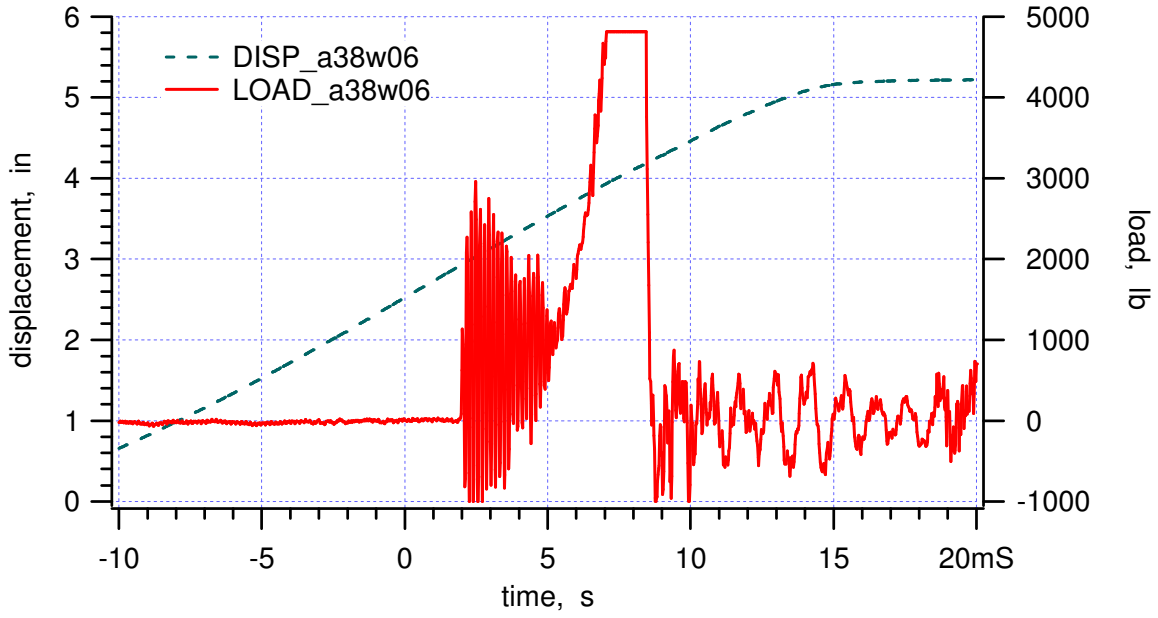
DISP_a38w06
LOAD_a38w06
displacement, in
load, lb
time, s
6
5
4
3
2
1
0
5000
4000
3000
2000
1000
0
-1000
-10
-5
0
5
10
15
20mS

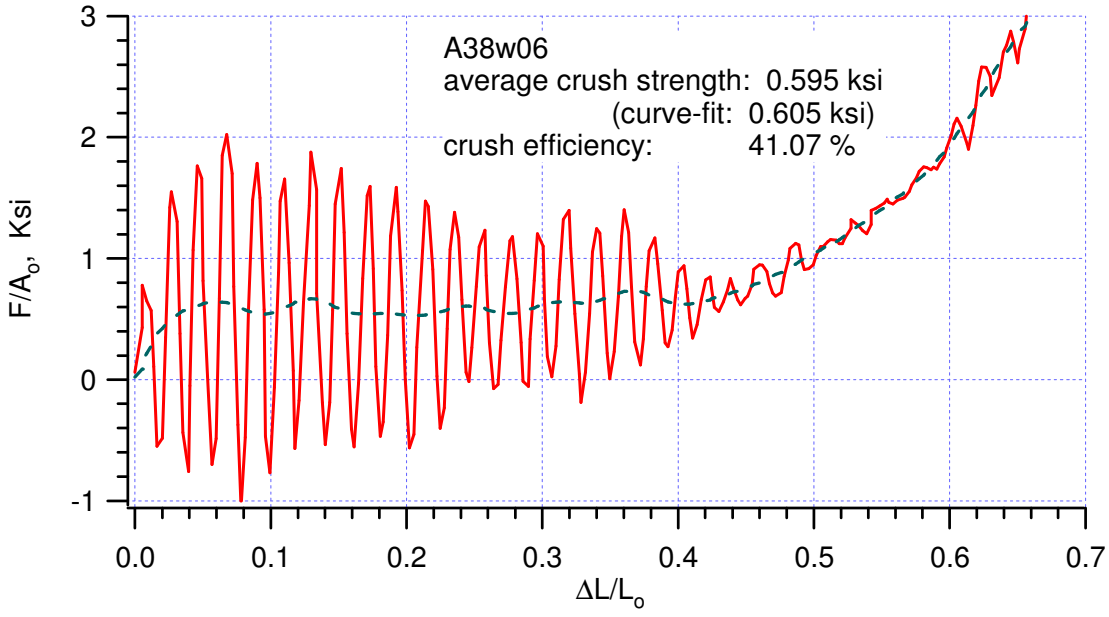
A38w06
average crush strength: 0.595 ksi
(curve-fit: 0.605 ksi)
crush efficiency: 41.07 %
F/A$_o$, Ksi
ΔL/L$_o$
3
2
1
0
-1
0.0
0.1
0.2
0.3
0.4
0.5
0.6
0.7

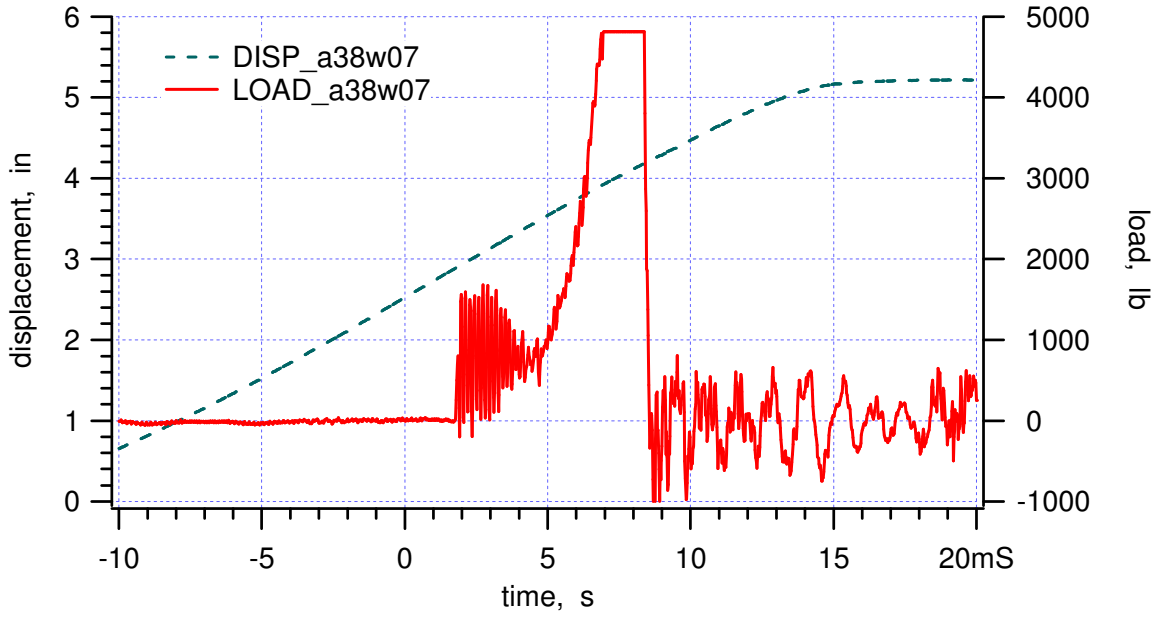
DISP_a38w07
LOAD_a38w07
displacement, in
load, lb
time, s
6
5
4
3
2
1
0
5000
4000
3000
2000
1000
0
-1000
-10
-5
0
5
10
15
20mS

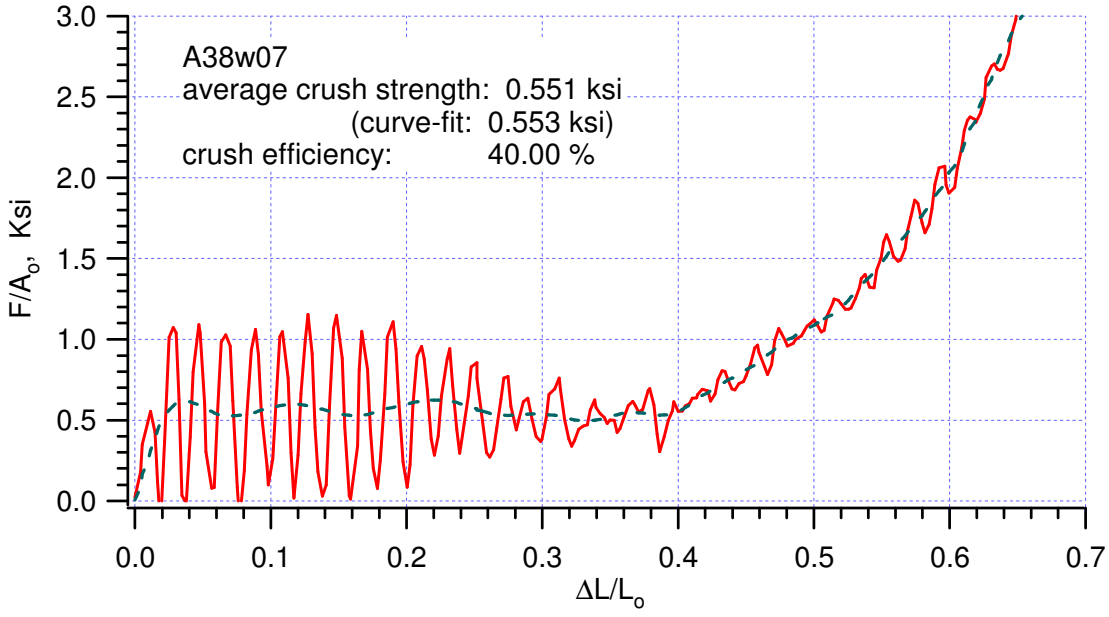
A38w07
average crush strength: 0.551 ksi
(curve-fit: 0.553 ksi)
crush efficiency: 40.00 %
F/A$_o$, Ksi
ΔL/L$_o$
3.0
2.5
2.0
1.5
1.0
0.5
0.0
0.0
0.1
0.2
0.3
0.4
0.5
0.6
0.7

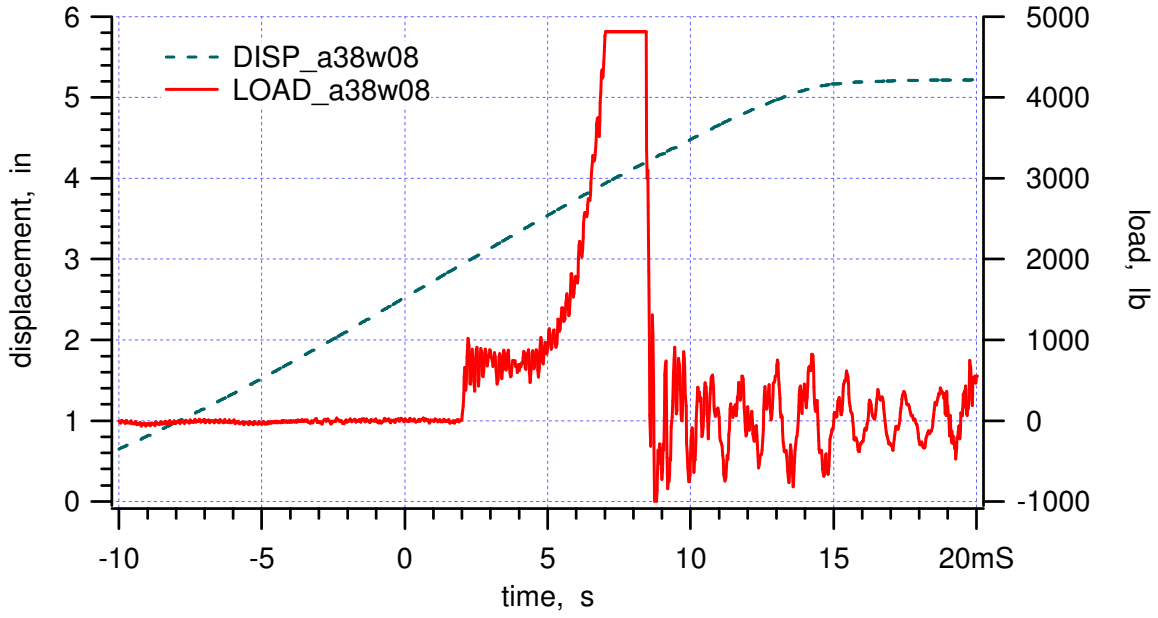
DISP_a38w08
LOAD_a38w08
displacement, in
load, lb
time, s
6
5
4
3
2
1
0
5000
4000
3000
2000
1000
0
-1000
-10
-5
0
5
10
15
20mS

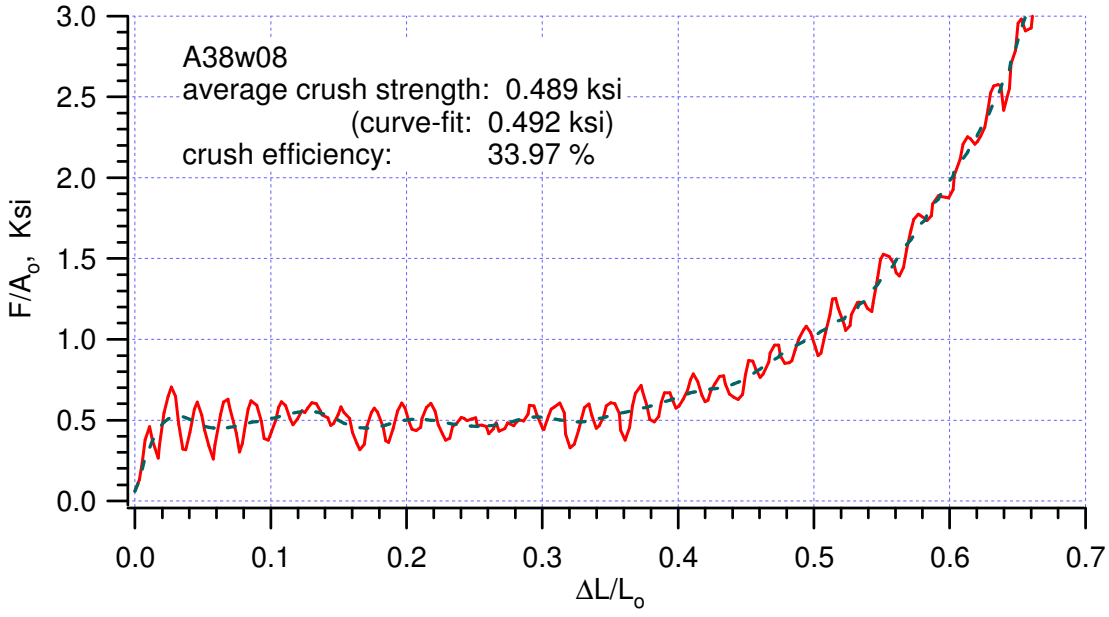
A38w08
average crush strength: 0.489 ksi
(curve-fit: 0.492 ksi)
crush efficiency: 33.97 %
F/A$_o$, Ksi
ΔL/L$_o$
3.0
2.5
2.0
1.5
1.0
0.5
0.0
0.0
0.1
0.2
0.3
0.4
0.5
0.6
0.7

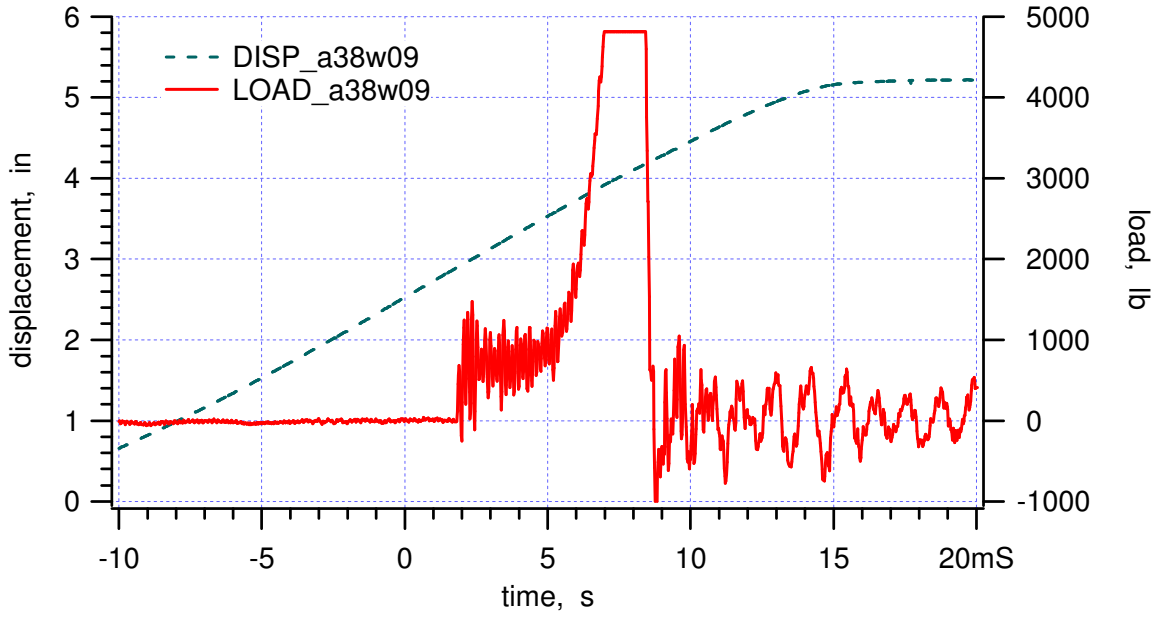
DISP_a38w09
LOAD_a38w09
displacement, in
load, lb
time, s
6
5
4
3
2
1
0
5000
4000
3000
2000
1000
0
-1000
-10
-5
0
5
10
15
20mS

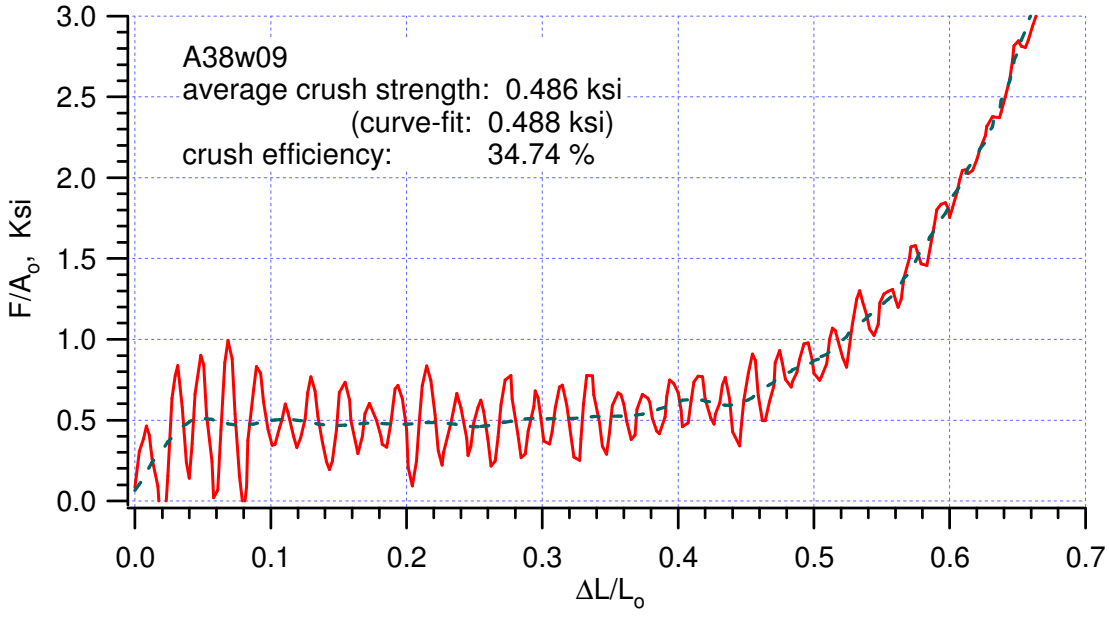
A38w09
average crush strength: 0.486 ksi
(curve-fit: 0.488 ksi)
crush efficiency: 34.74 %
F/A$_o$, Ksi
ΔL/L$_o$
3.0
2.5
2.0
1.5
1.0
0.5
0.0
0.0
0.1
0.2
0.3
0.4
0.5
0.6
0.7

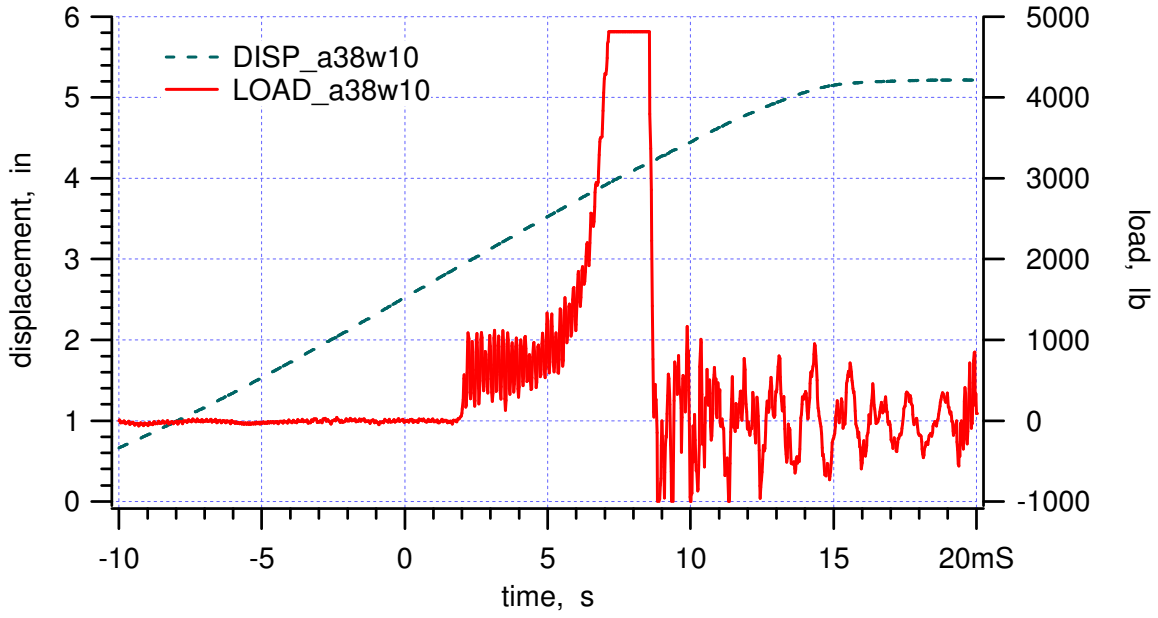
DISP_a38w10
LOAD_a38w10
displacement, in
load, lb
time, s
6
5
4
3
2
1
0
5000
4000
3000
2000
1000
0
-1000
-10
-5
0
5
10
15
20mS

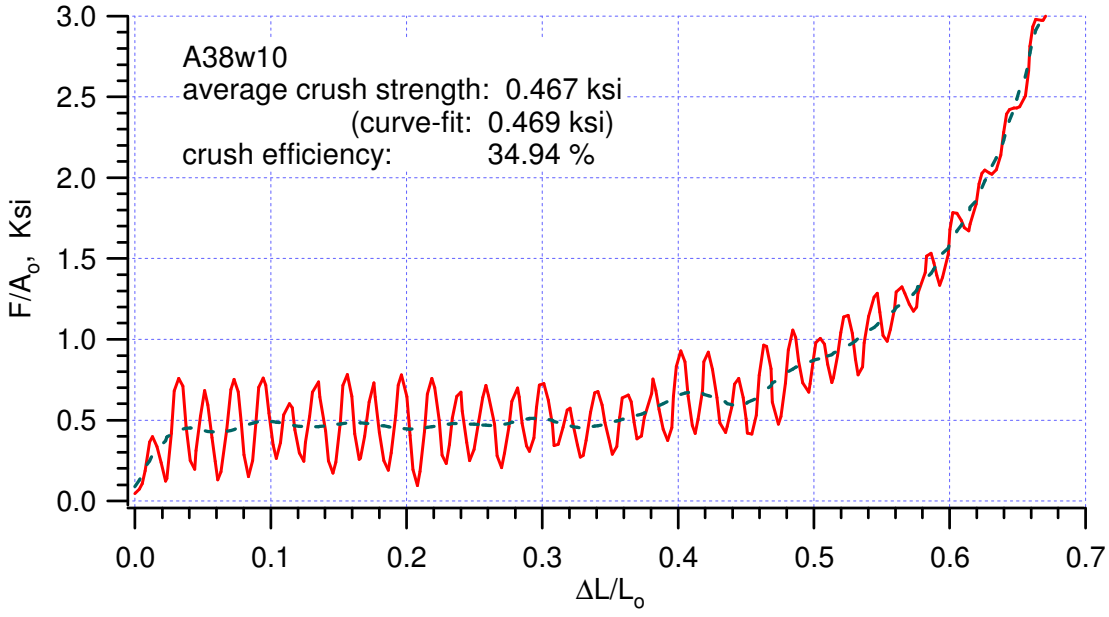
A38w10
average crush strength: 0.467 ksi
(curve-fit: 0.469 ksi)
crush efficiency: 34.94 %
F/A$_o$, Ksi
ΔL/L$_o$
3.0
2.5
2.0
1.5
1.0
0.5
0.0
0.0
0.1
0.2
0.3
0.4
0.5
0.6
0.7

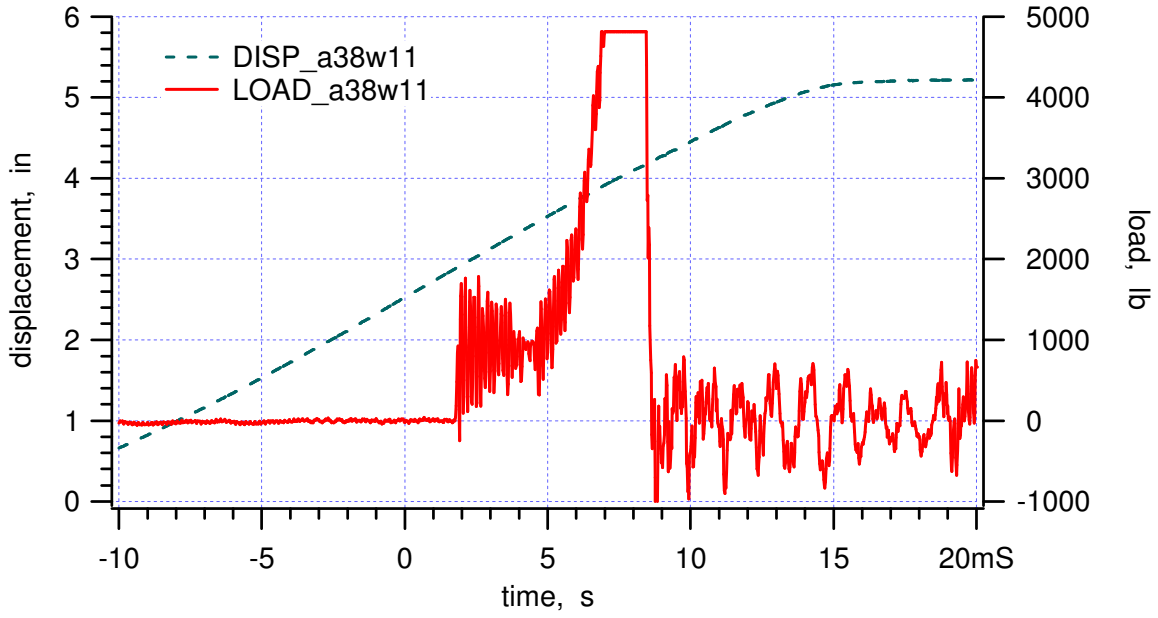
DISP_a38w11
LOAD_a38w11
displacement, in
load, lb
time, s
6
5
4
3
2
1
0
5000
4000
3000
2000
1000
0
-1000
-10
-5
0
5
10
15
20mS

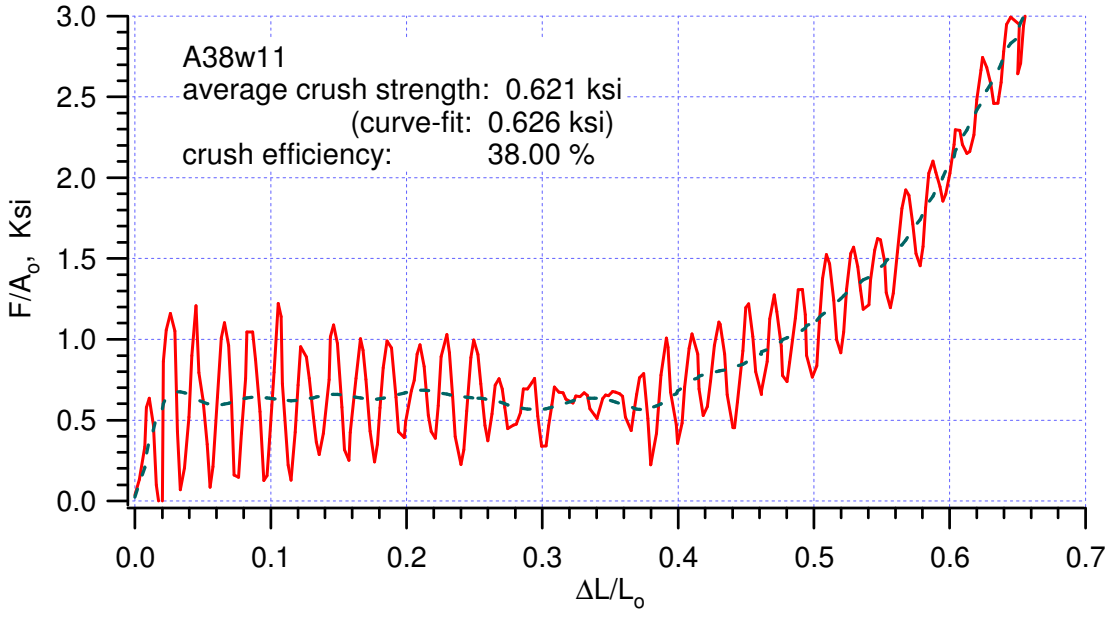
A38w11
average crush strength: 0.621 ksi
(curve-fit: 0.626 ksi)
crush efficiency: 38.00 %
F/A$_o$, Ksi
ΔL/L$_o$
3.0
2.5
2.0
1.5
1.0
0.5
0.0
0.0
0.1
0.2
0.3
0.4
0.5
0.6
0.7

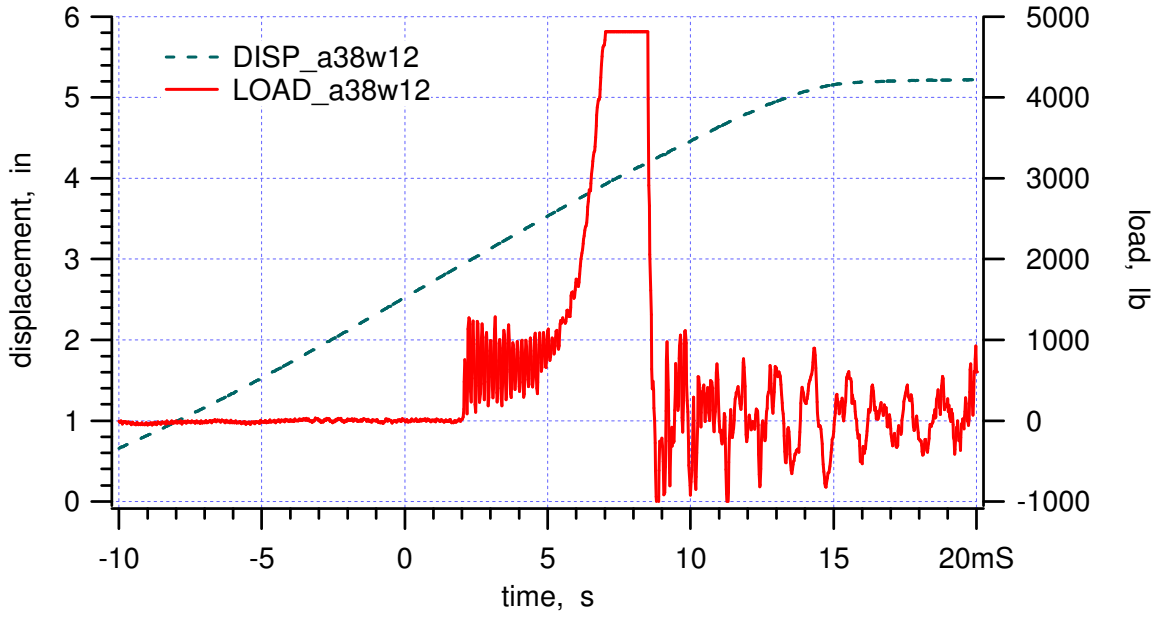
DISP_a38w12
LOAD_a38w12
displacement, in
load, lb
time, s
6
5
4
3
2
1
0
5000
4000
3000
2000
1000
0
-1000
-10
-5
0
5
10
15
20mS

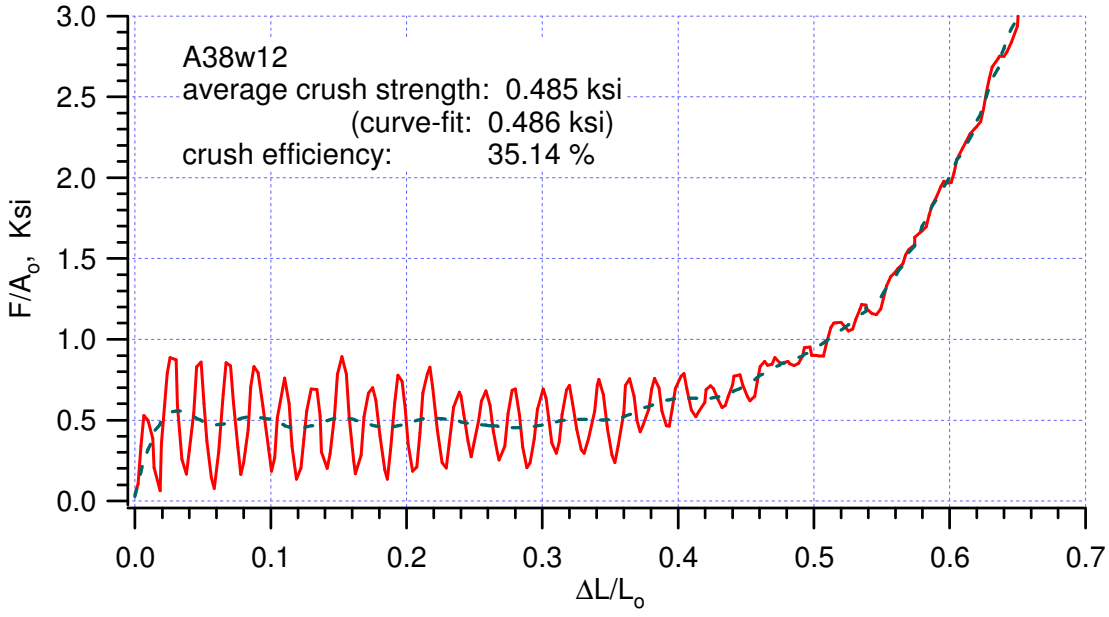
A38w12
average crush strength: 0.485 ksi
(curve-fit: 0.486 ksi)
crush efficiency: 35.14 %
F/A$_o$, Ksi
ΔL/L$_o$
3.0
2.5
2.0
1.5
1.0
0.5
0.0
0.0
0.1
0.2
0.3
0.4
0.5
0.6
0.7

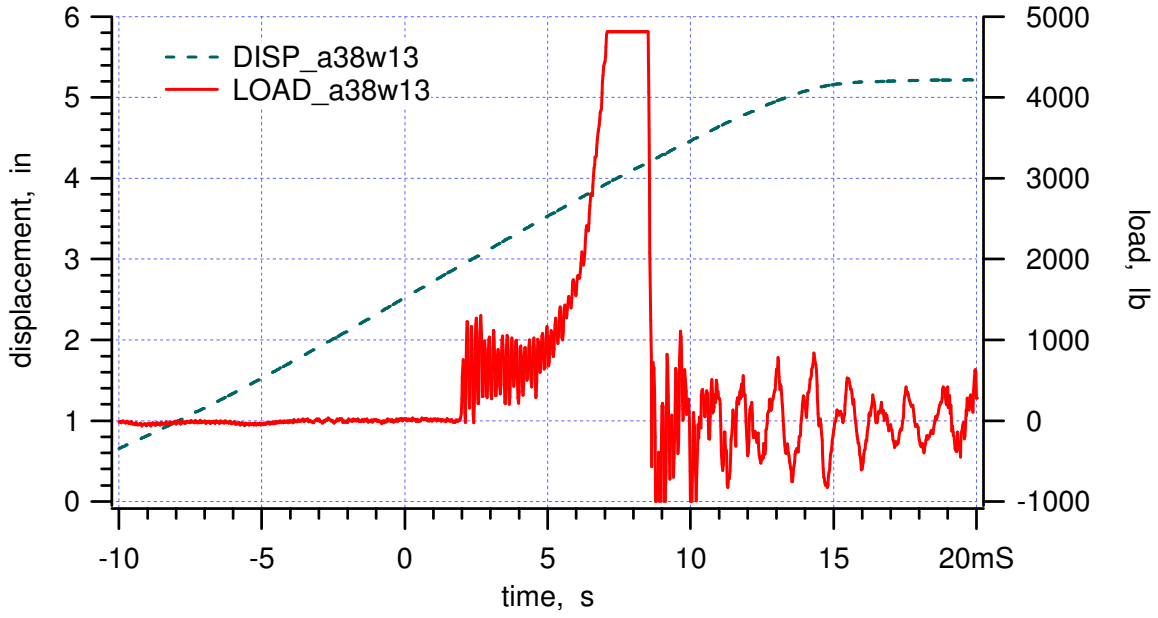
DISP_a38w13
LOAD_a38w13
displacement, in
load, lb
time, s
6
5
4
3
2
1
0
5000
4000
3000
2000
1000
0
-1000
-10
-5
0
5
10
15
20mS

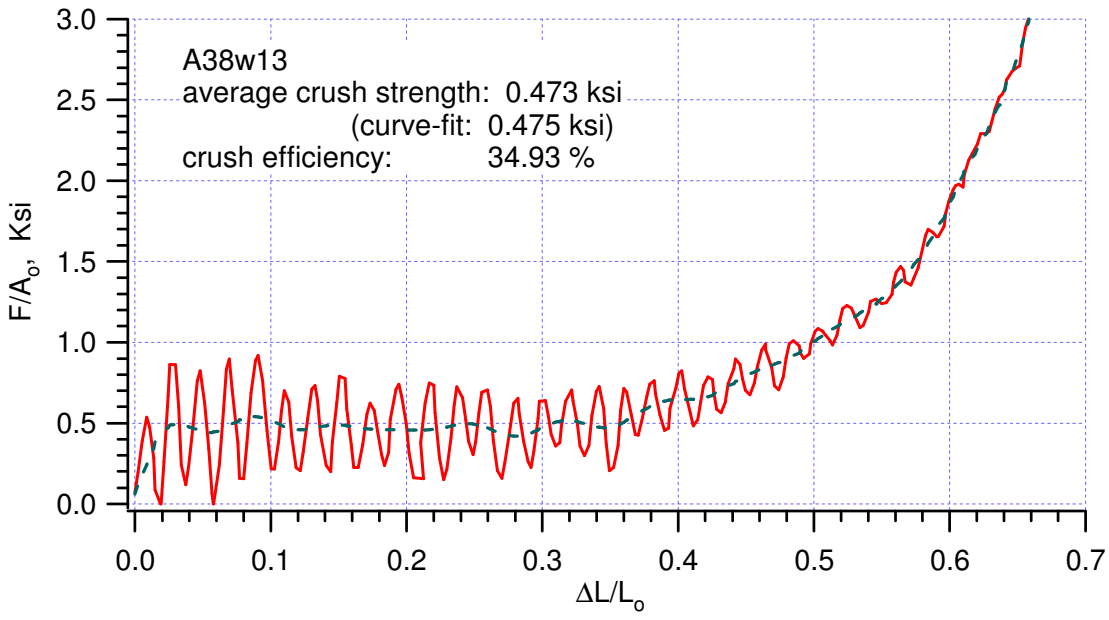
A38w13
average crush strength: 0.473 ksi
(curve-fit: 0.475 ksi)
crush efficiency: 34.93 %
F/A$_o$, Ksi
ΔL/L$_o$
3.0
2.5
2.0
1.5
1.0
0.5
0.0
0.0
0.1
0.2
0.3
0.4
0.5
0.6
0.7

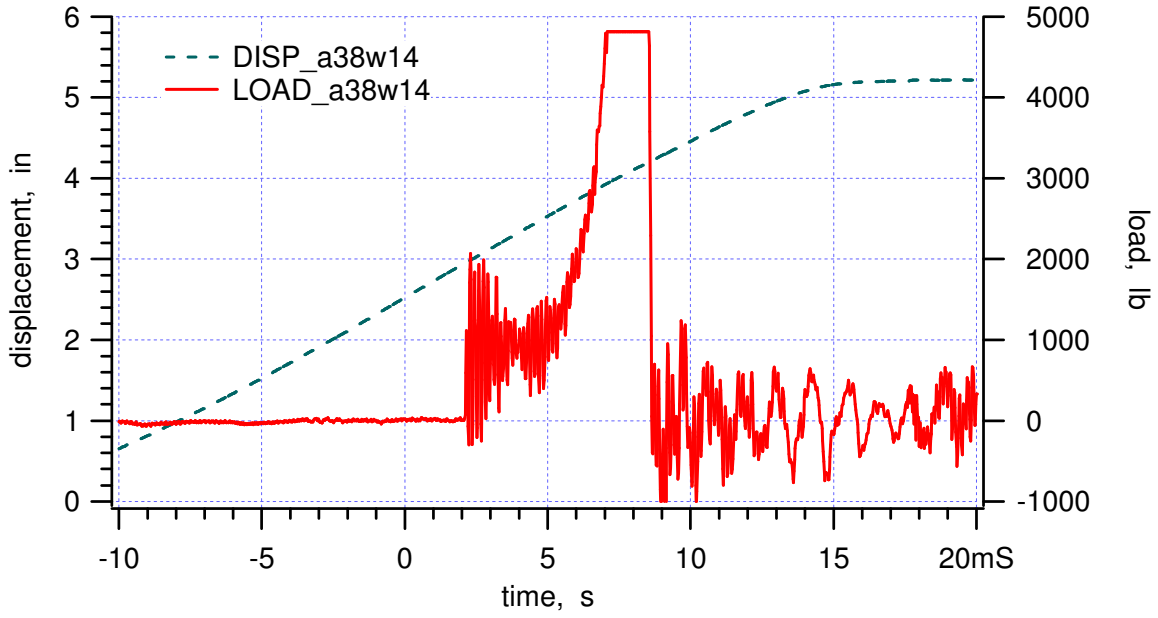
DISP_a38w14
LOAD_a38w14
displacement, in
load, lb
time, s
6
5
4
3
2
1
0
5000
4000
3000
2000
1000
0
-1000
-10
-5
0
5
10
15
20mS

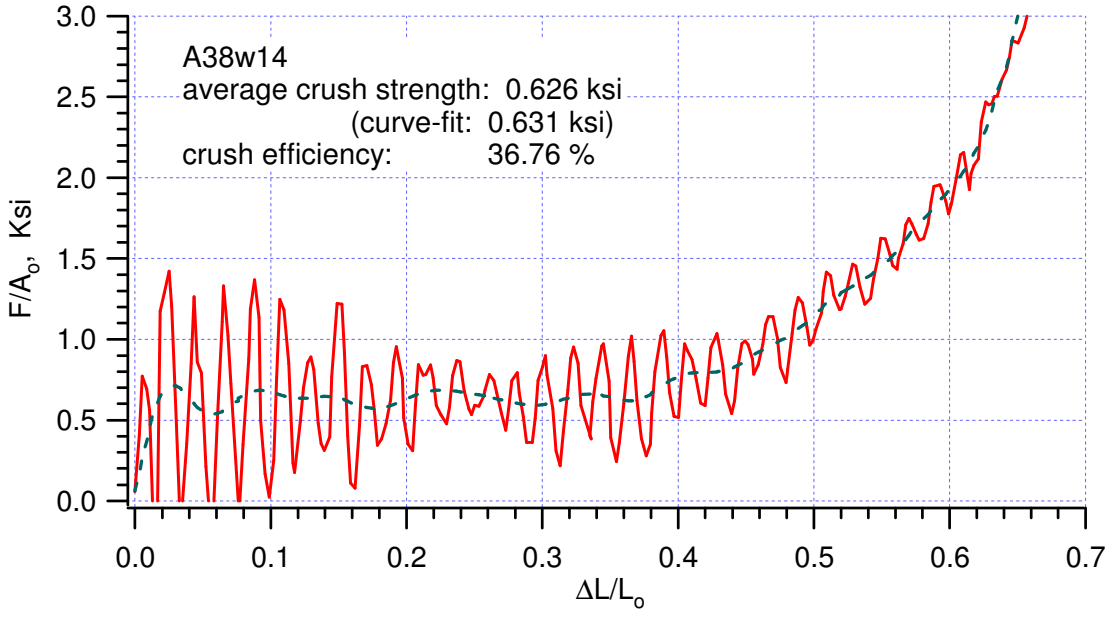
A38w14
average crush strength: 0.626 ksi
(curve-fit: 0.631 ksi)
crush efficiency: 36.76 %
F/A$_o$, Ksi
ΔL/L$_o$
3.0
2.5
2.0
1.5
1.0
0.5
0.0
0.0
0.1
0.2
0.3
0.4
0.5
0.6
0.7

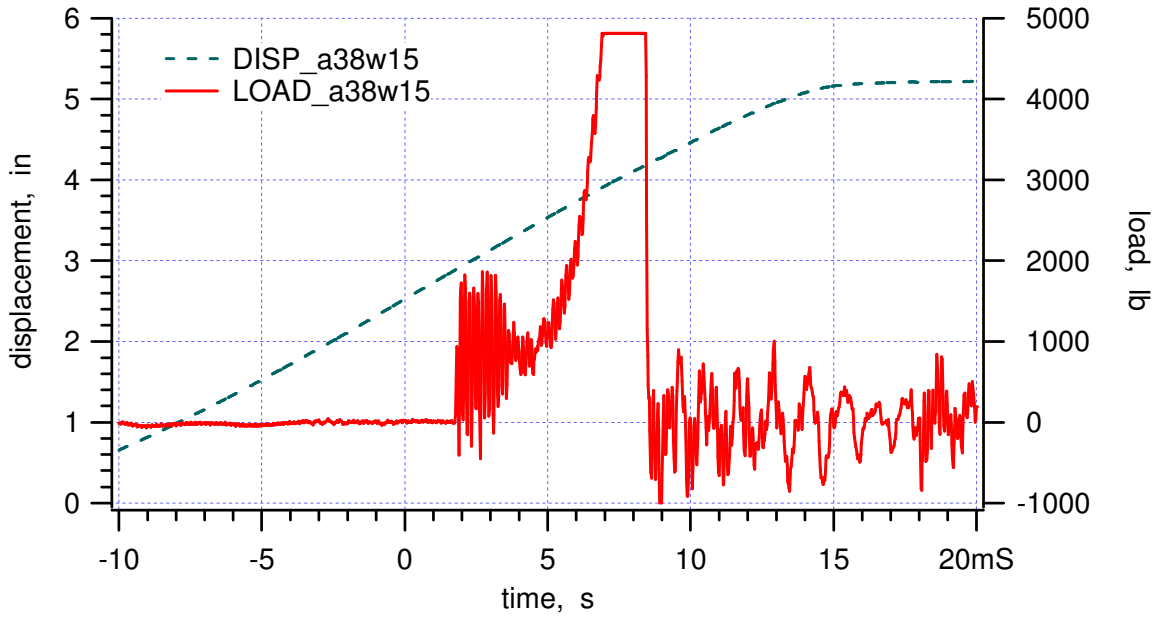
DISP_a38w15
LOAD_a38w15
displacement, in
load, lb
time, s
6
5
4
3
2
1
0
5000
4000
3000
2000
1000
0
-1000
-10
-5
0
5
10
15
20mS

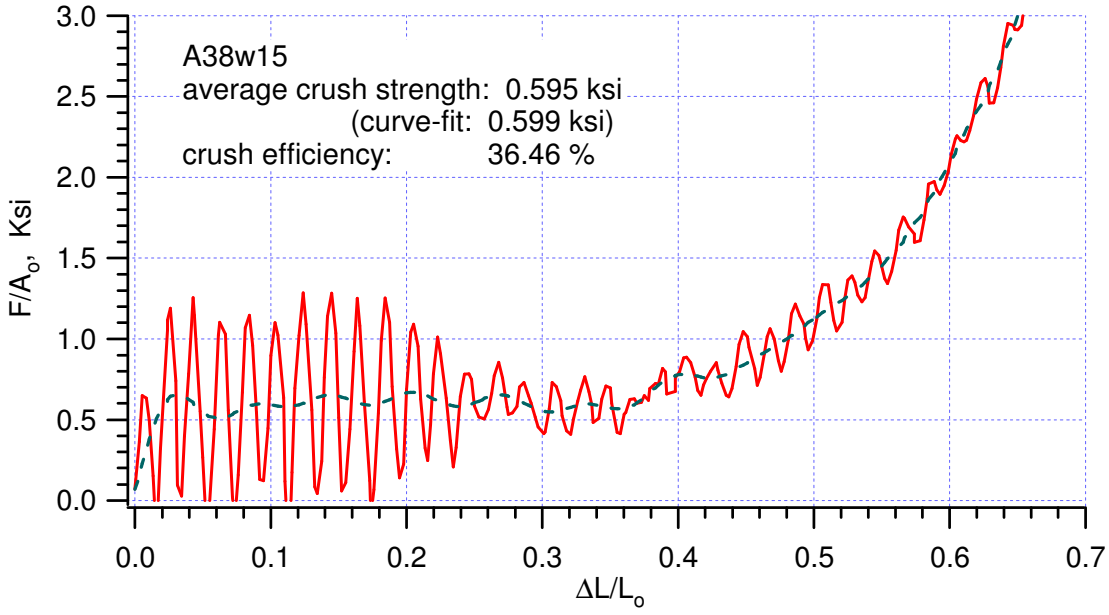
A38w15
average crush strength: 0.595 ksi
(curve-fit: 0.599 ksi)
crush efficiency: 36.46 %
F/A$_o$, Ksi
ΔL/L$_o$
3.0
2.5
2.0
1.5
1.0
0.5
0.0
0.0
0.1
0.2
0.3
0.4
0.5
0.6
0.7

Appendix Hexcel 38W

Specimen	d_1, in	d_2, in	d_3, in	Weight, lb	Density, pcf	Crush Velocity, ft/s	Crush efficiency, %	Crush strenghth, ksi (fit)
H38W01	1.201	1.195	1.514	0.0488	38.83	16.55	38.15	0.602
H38W02	1.189	1.191	1.520	0.0482	38.71	16.58	39.16	0.615
H38W03	1.192	1.190	1.513	0.0480	38.64	16.57	39.44	0.600
H38W04	1.194	1.191	1.512	0.0475	38.20	16.69	35.34	0.623
H38W05	1.191	1.191	1.510	0.0480	38.72	16.65	34.97	0.617
H38W06	1.194	1.192	1.514	0.0486	39.00	16.69	34.87	0.584
H38W07	1.191	1.195	1.506	0.0485	39.07	16.74	37.40	0.621
H38W08	1.201	1.191	1.520	0.0492	39.09	16.67	39.68	0.584
H38W09	1.195	1.195	1.515	0.0484	38.67	16.76	37.18	0.577
H38W10	1.191	1.195	1.507	0.0477	38.45	16.75	36.95	0.608
H38W11	1.195	1.194	1.509	0.0483	38.73	16.77	37.54	0.585
H38W12	1.196	1.194	1.505	0.0478	38.43	16.79	33.91	0.584
H38W13	1.194	1.195	1.509	0.0485	38.91	16.86	37.01	0.607
H38W14	1.200	1.193	1.514	0.0486	38.76	16.83	36.88	0.596
H38W15	1.193	1.195	1.505	0.0476	38.30	16.84	37.00	0.590
				max	39.09	16.86	39.68	0.623
				min	38.20	16.55	33.91	0.577
				average	38.70	16.72	37.03	0.599
				std deviation	0.27	0.10	1.70	0.015
				median	38.72	16.74	37.01	0.600

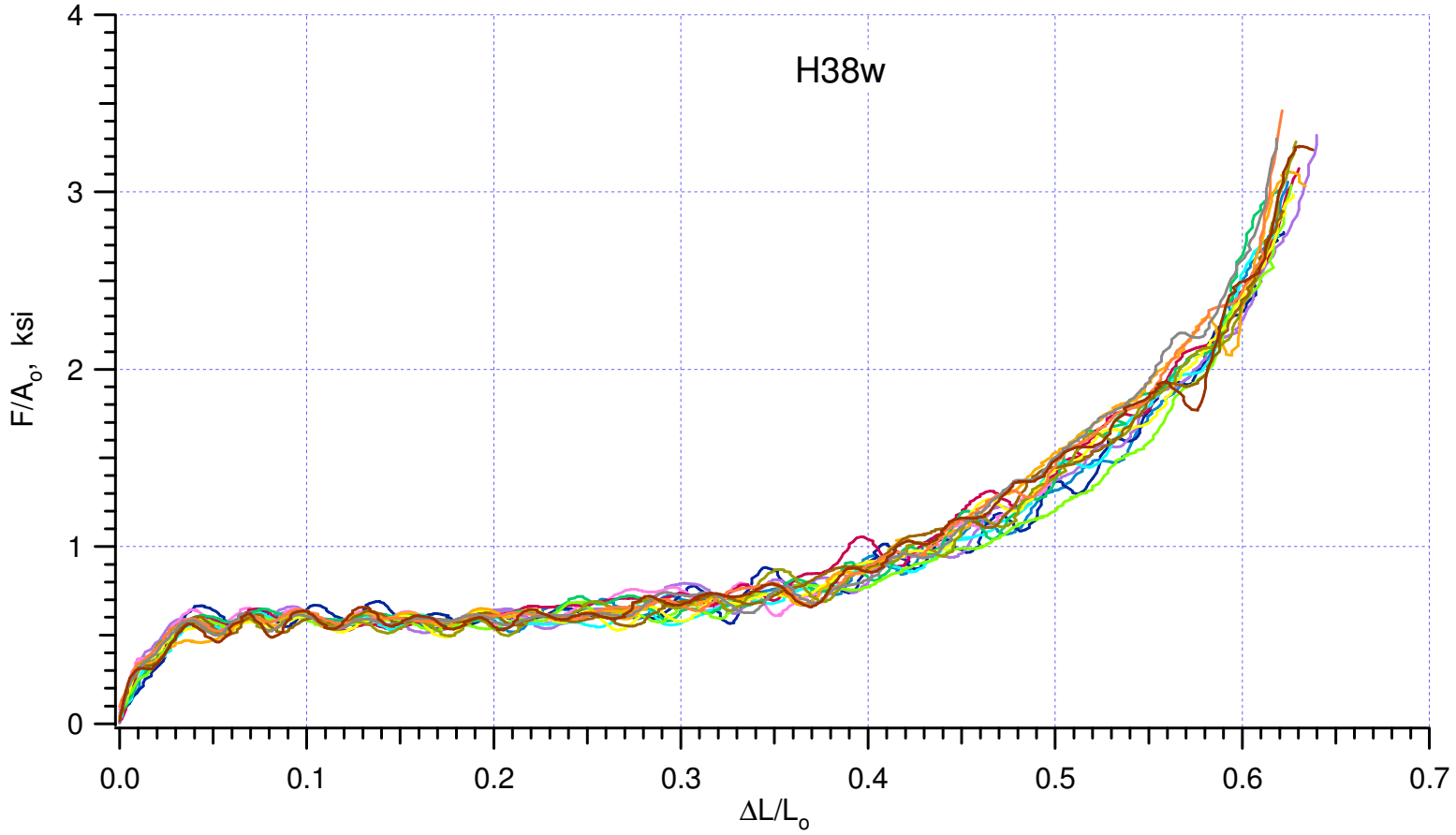
H38w
F/A$_o$, ksi
$\Delta L/L_o$
0
1
2
3
4
0.0
0.1
0.2
0.3
0.4
0.5
0.6
0.7

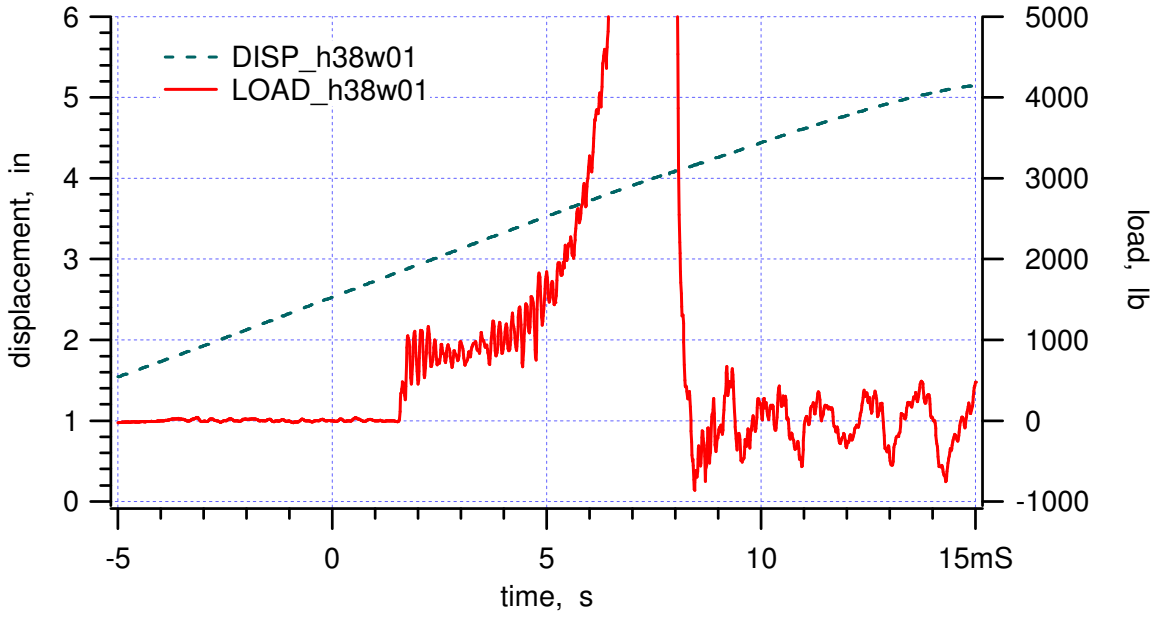
DISP_h38w01
LOAD_h38w01
displacement, in
load, lb
time, s
-5
0
5
10
15mS
6
5
4
3
2
1
0
5000
4000
3000
2000
1000
0
-1000

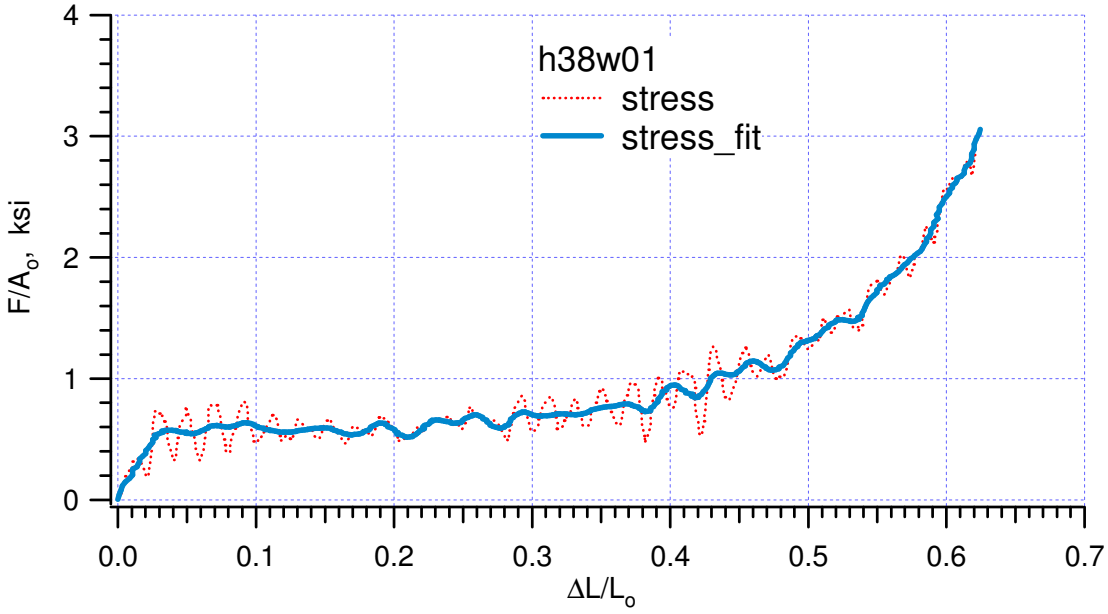
h38w01
stress
stress_fit
F/A$_o$, ksi
ΔL/L$_o$
0.0
0.1
0.2
0.3
0.4
0.5
0.6
0.7
4
3
2
1
0

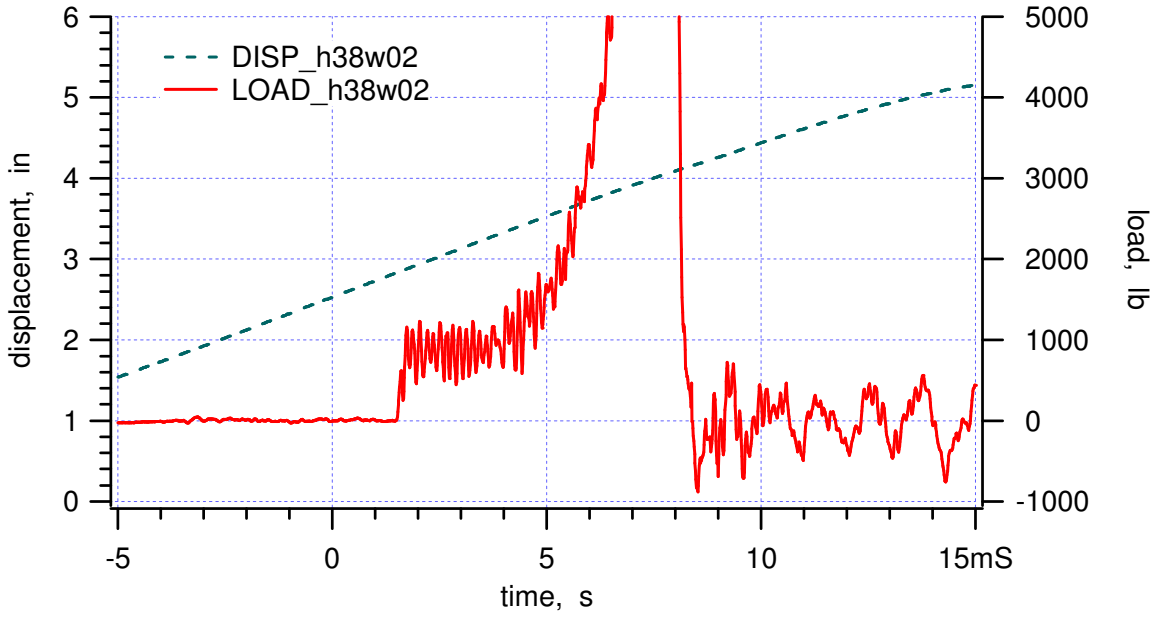
DISP_h38w02
LOAD_h38w02
displacement, in
load, lb
time, s
-5
0
5
10
15mS
6
5
4
3
2
1
0
5000
4000
3000
2000
1000
0
-1000

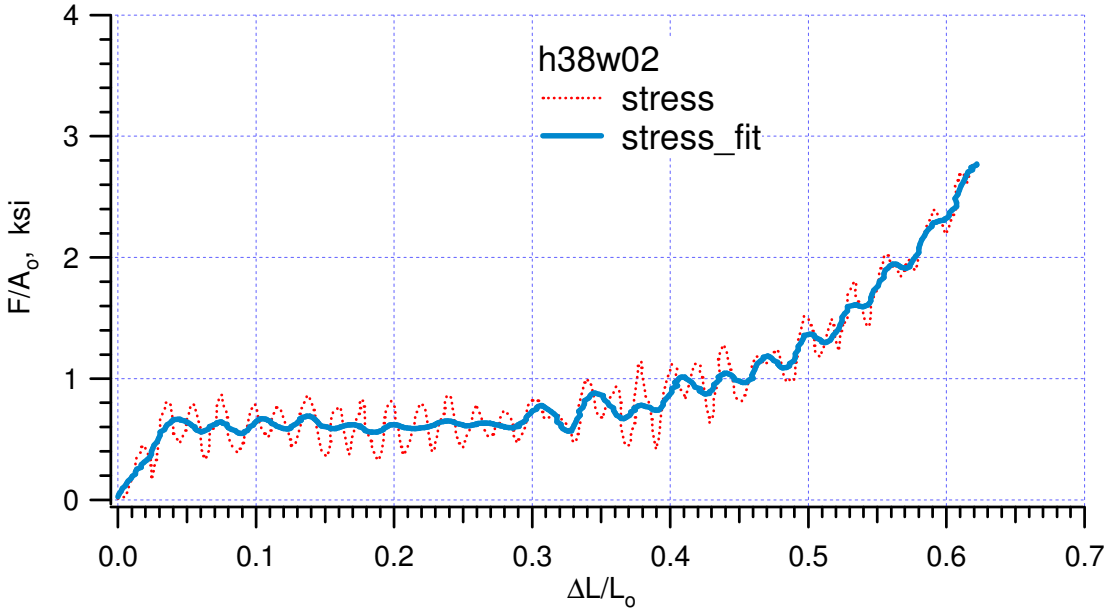
h38w02
stress
stress_fit
F/A$_o$, ksi
ΔL/L$_o$
0.0
0.1
0.2
0.3
0.4
0.5
0.6
0.7
4
3
2
1
0

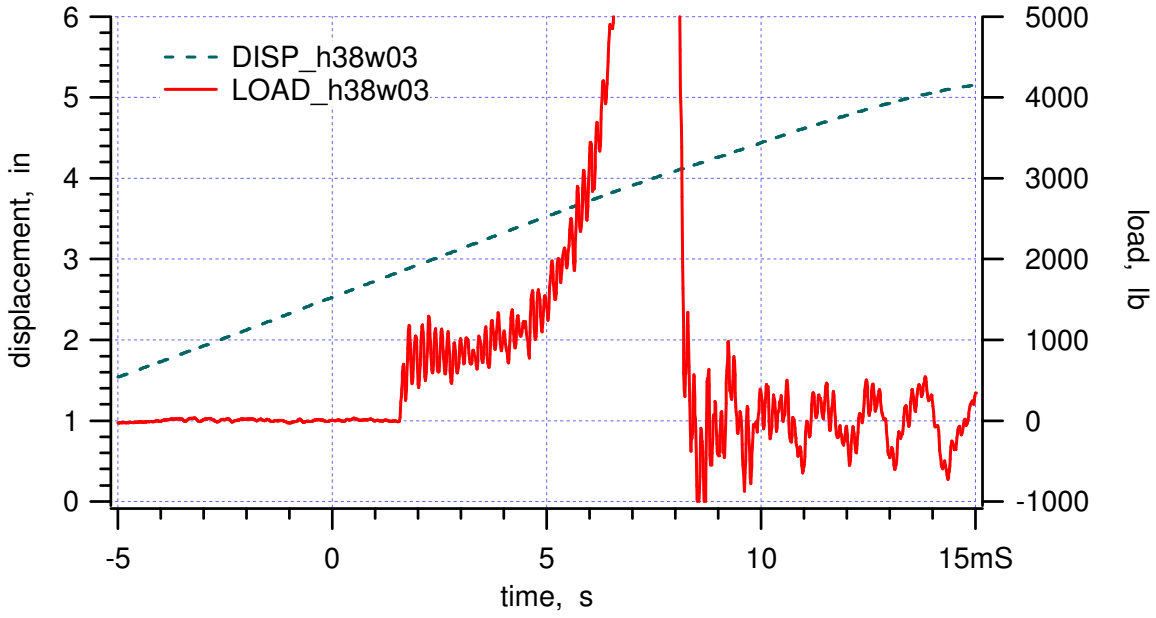
DISP_h38w03
LOAD_h38w03
displacement, in
load, lb
time, s
-5
0
5
10
15mS
0
1
2
3
4
5
6
-1000
0
1000
2000
3000
4000
5000

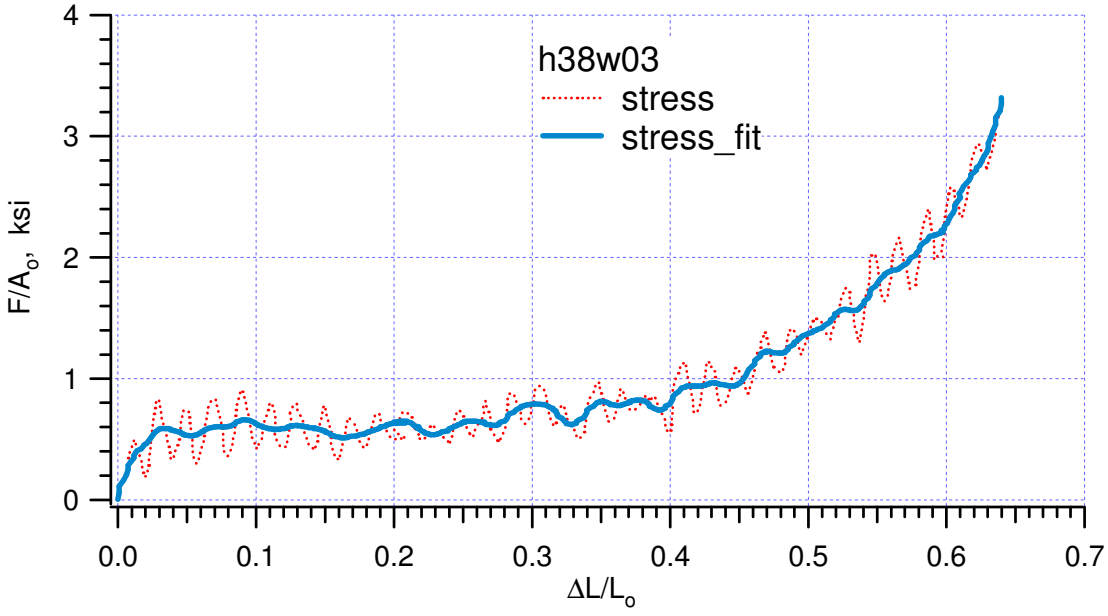
h38w03
stress
stress_fit
F/A$_o$, ksi
ΔL/L$_o$
0.0
0.1
0.2
0.3
0.4
0.5
0.6
0.7
0
1
2
3
4

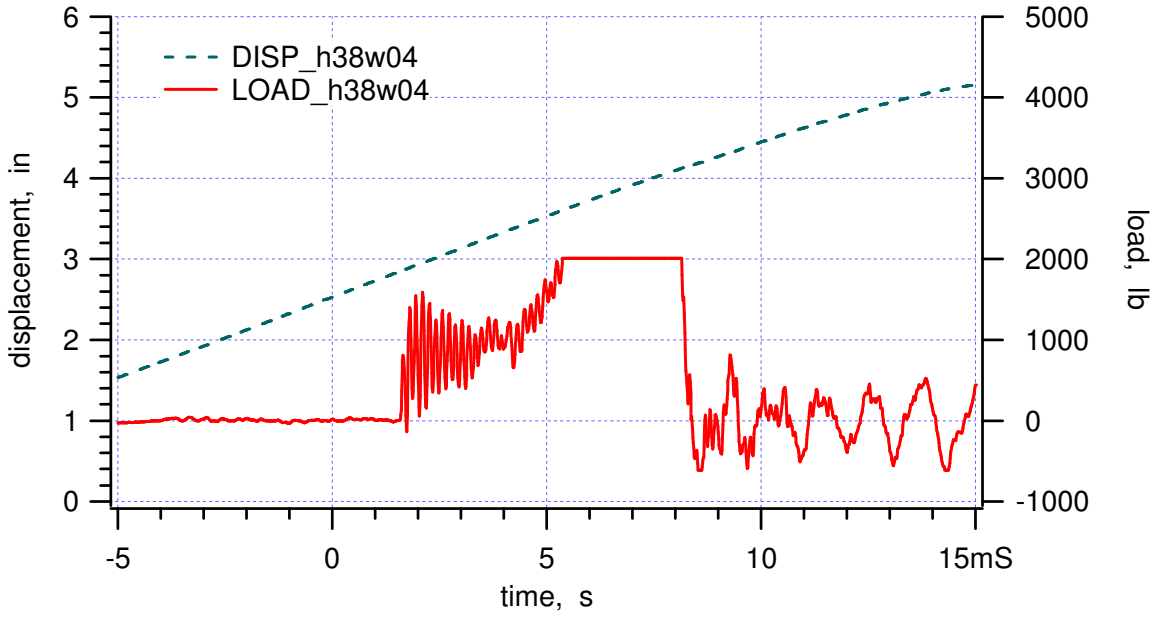
DISP_h38w04
LOAD_h38w04
displacement, in
load, lb
time, s
6
5
4
3
2
1
0
5000
4000
3000
2000
1000
0
-1000
-5
0
5
10
15mS

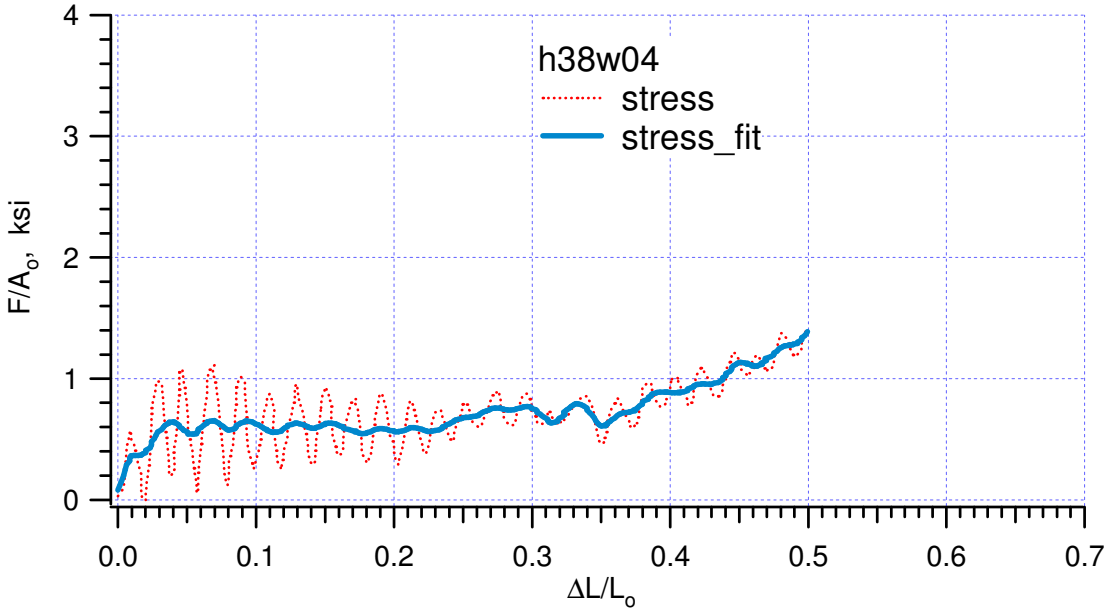
h38w04
stress
stress_fit
F/A$_o$, ksi
ΔL/L$_o$
4
3
2
1
0
0.0
0.1
0.2
0.3
0.4
0.5
0.6
0.7

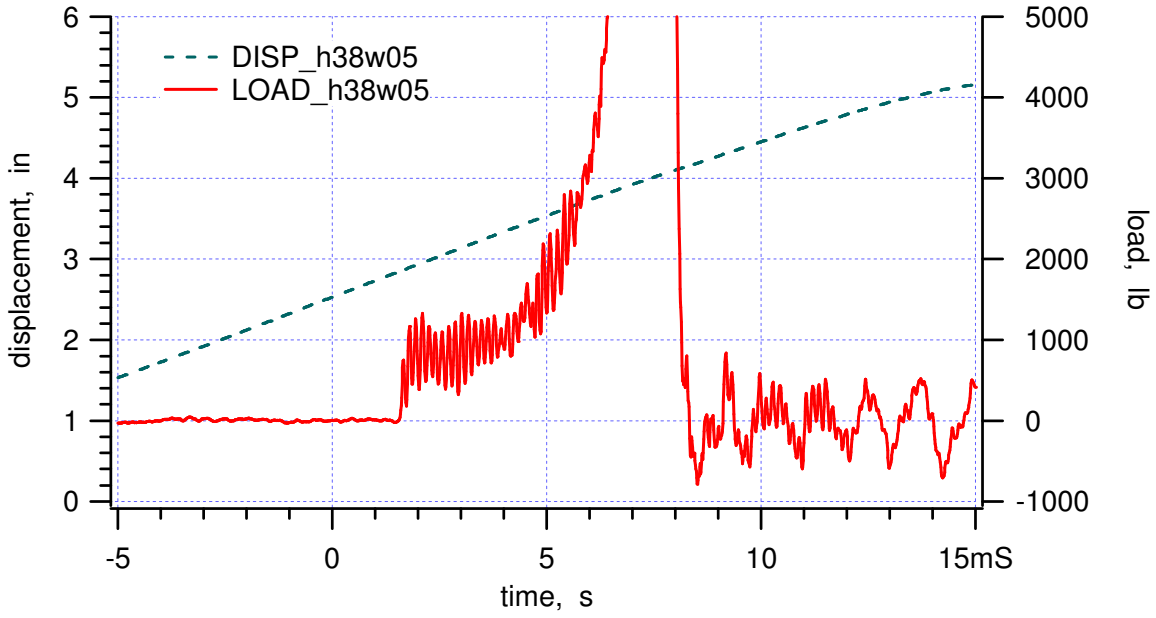
DISP_h38w05
LOAD_h38w05
displacement, in
load, lb
time, s
6
5
4
3
2
1
0
5000
4000
3000
2000
1000
0
-1000
-5
0
5
10
15mS

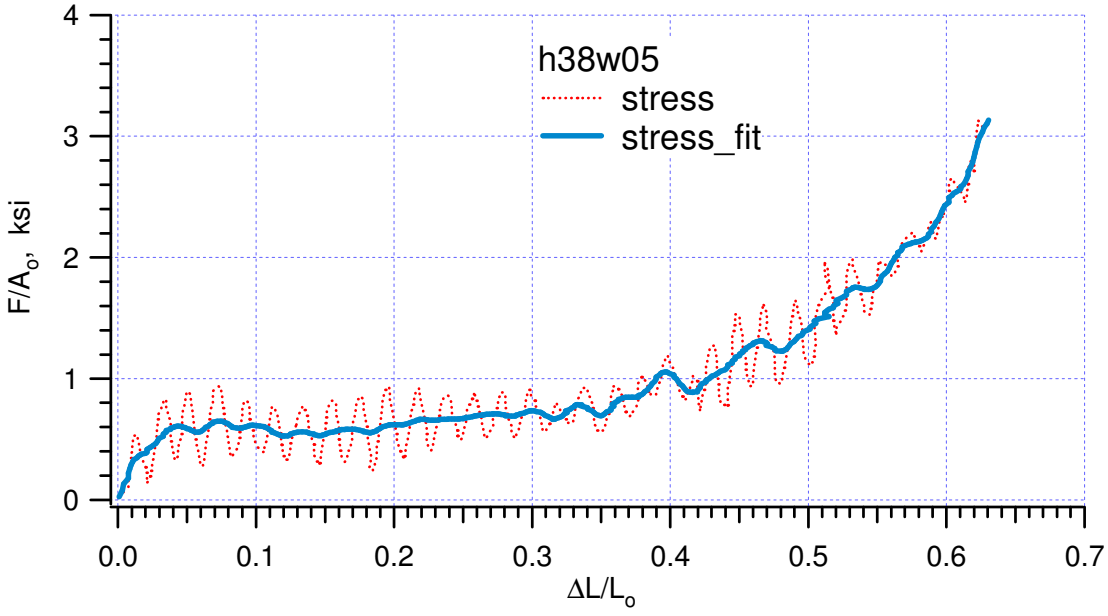
h38w05
stress
stress_fit
F/A$_o$, ksi
ΔL/L$_o$
4
3
2
1
0
0.0
0.1
0.2
0.3
0.4
0.5
0.6
0.7

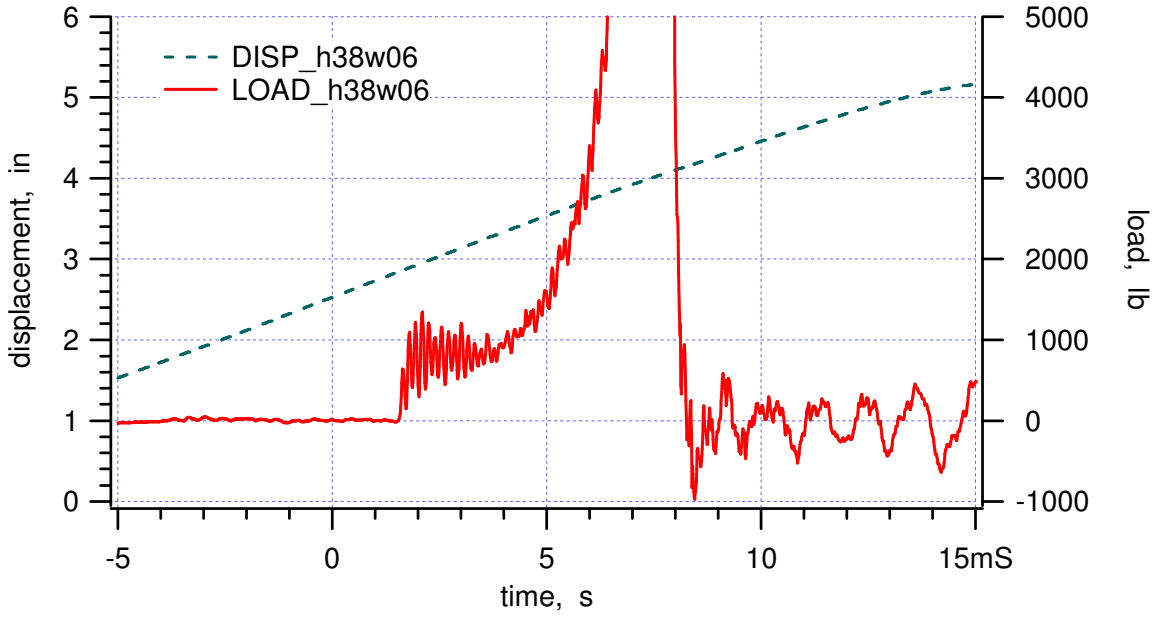
DISP_h38w06
LOAD_h38w06
displacement, in
load, lb
time, s
-5
0
5
10
15mS
0
1
2
3
4
5
6
-1000
0
1000
2000
3000
4000
5000

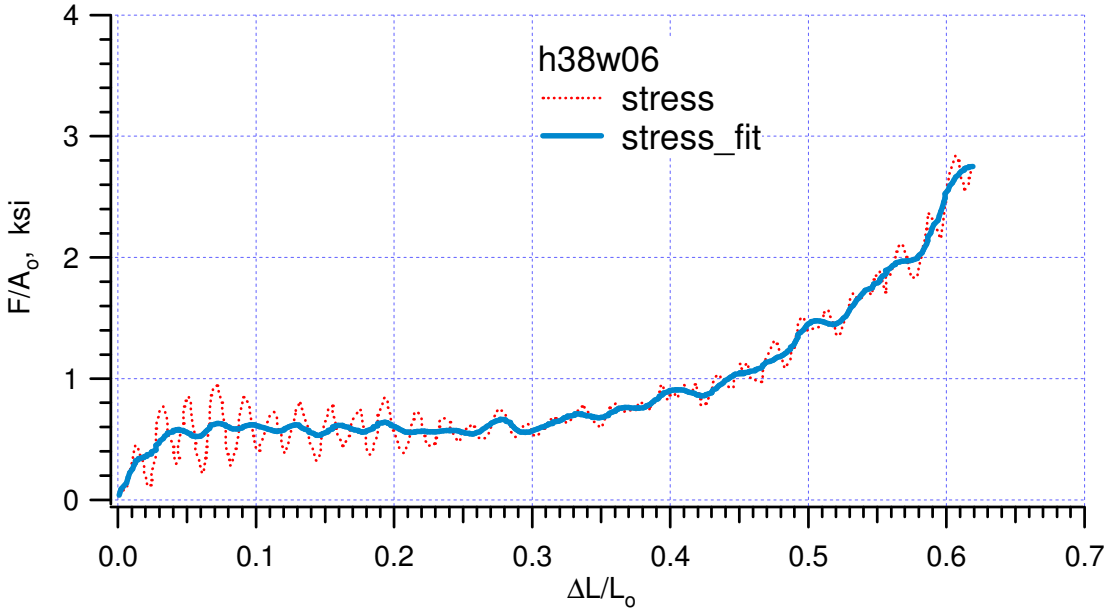
h38w06
stress
stress_fit
F/A$_o$, ksi
ΔL/L$_o$
0.0
0.1
0.2
0.3
0.4
0.5
0.6
0.7
0
1
2
3
4

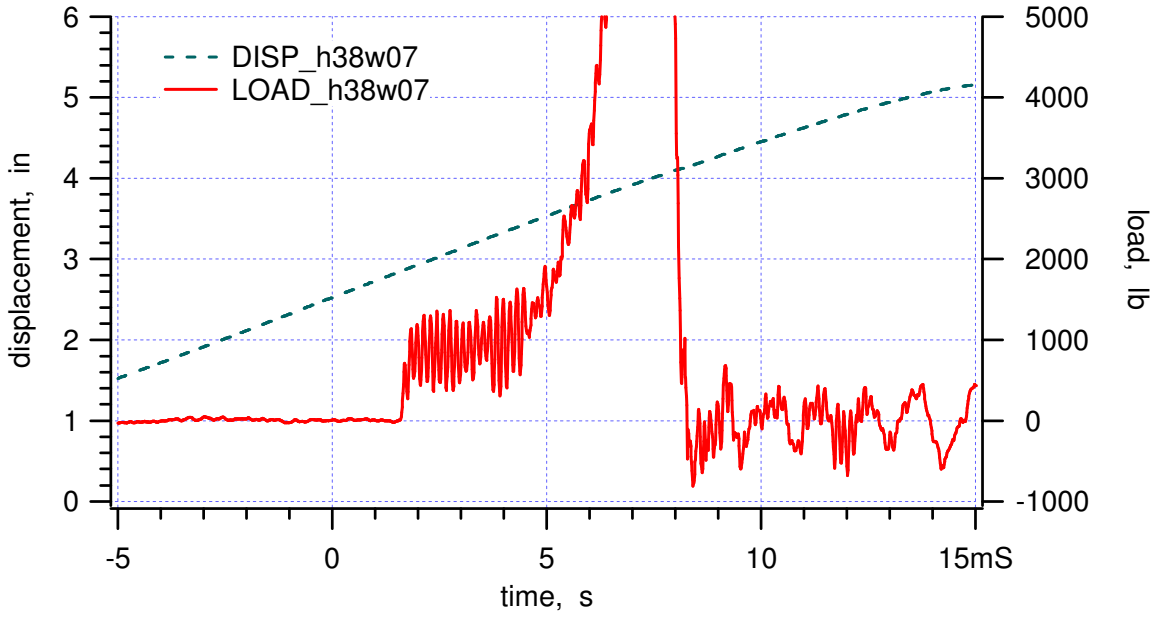
DISP_h38w07
LOAD_h38w07
displacement, in
load, lb
time, s
-5
0
5
10
15mS
0
1
2
3
4
5
6
-1000
0
1000
2000
3000
4000
5000

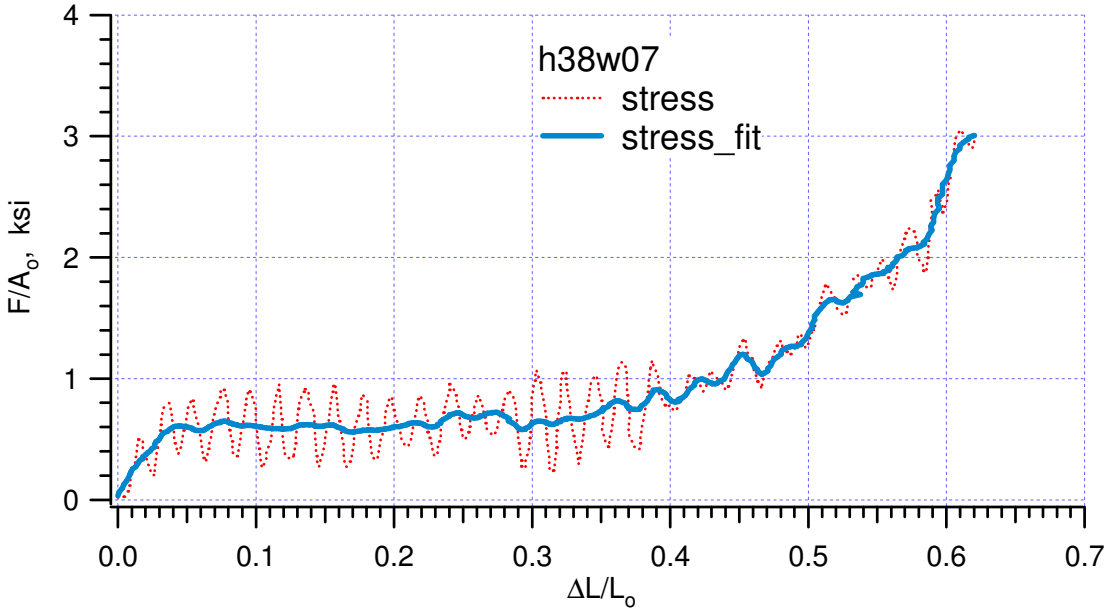
h38w07
stress
stress_fit
F/A$_o$, ksi
ΔL/L$_o$
0.0
0.1
0.2
0.3
0.4
0.5
0.6
0.7
0
1
2
3
4

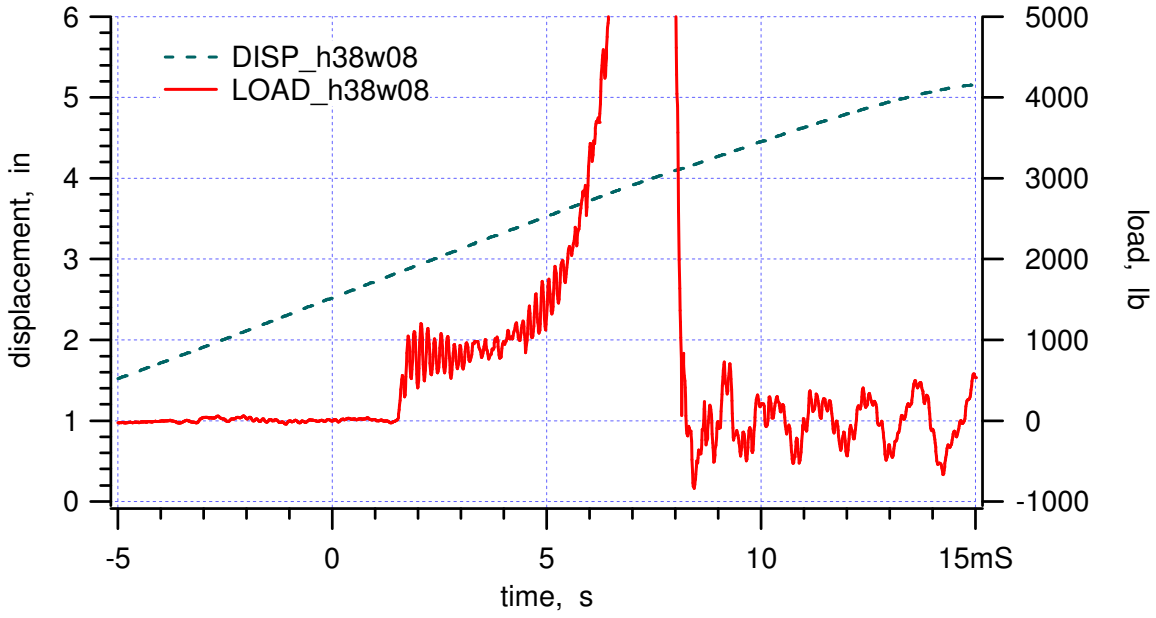
DISP_h38w08
LOAD_h38w08
displacement, in
load, lb
time, s
-5
0
5
10
15mS
6
5
4
3
2
1
0
5000
4000
3000
2000
1000
0
-1000

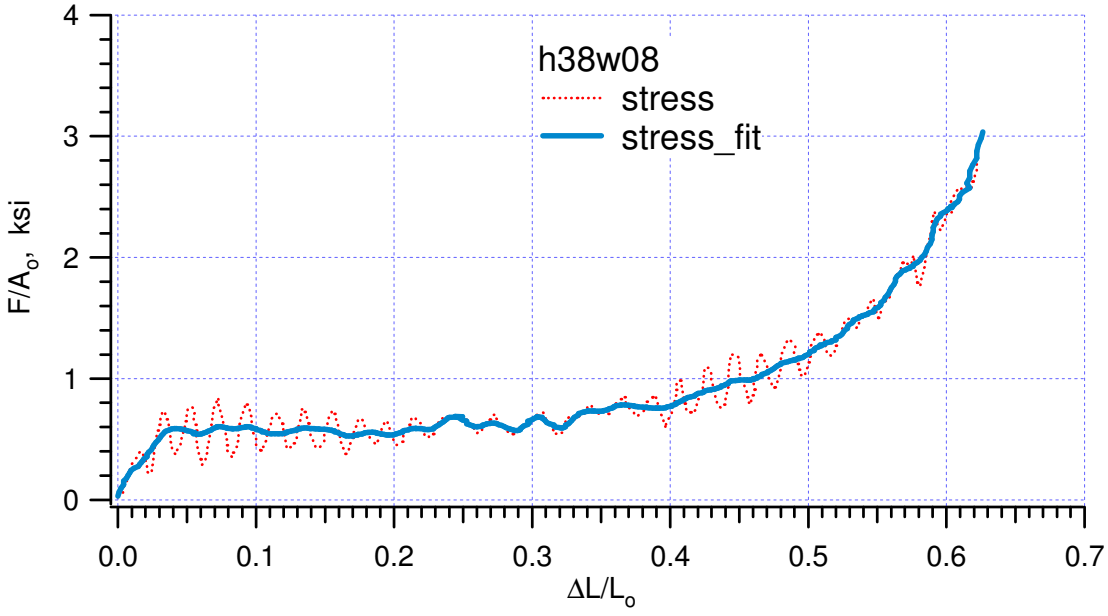
h38w08
stress
stress_fit
F/A$_o$, ksi
ΔL/L$_o$
0.0
0.1
0.2
0.3
0.4
0.5
0.6
0.7
4
3
2
1
0

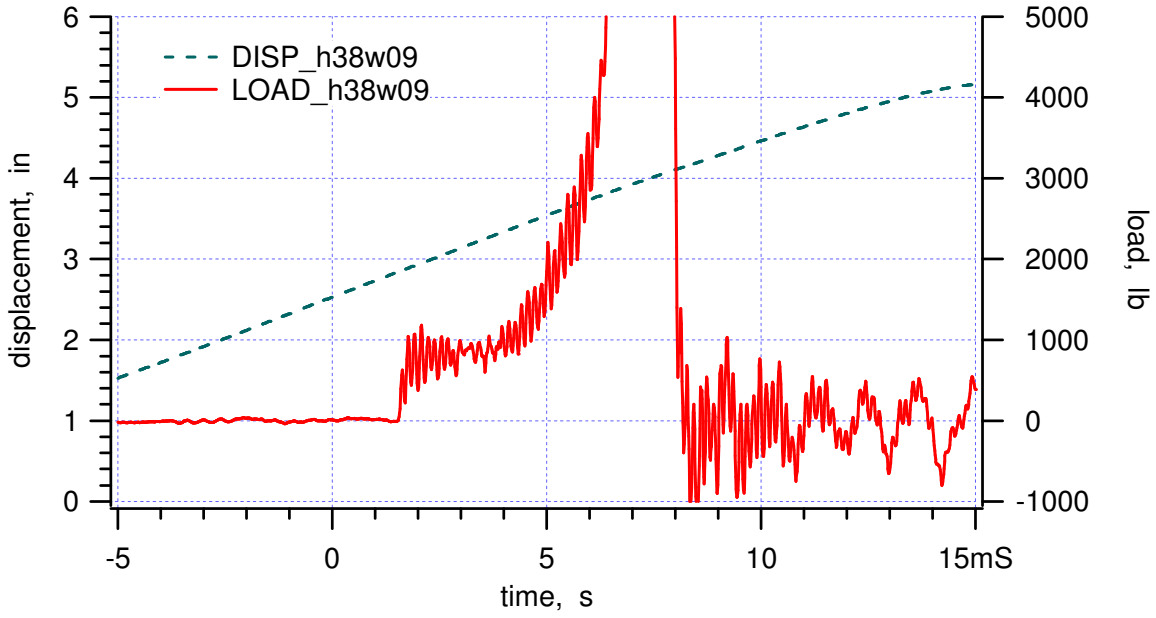
DISP_h38w09
LOAD_h38w09
displacement, in
load, lb
time, s
-5
0
5
10
15mS
0
1
2
3
4
5
6
-1000
0
1000
2000
3000
4000
5000

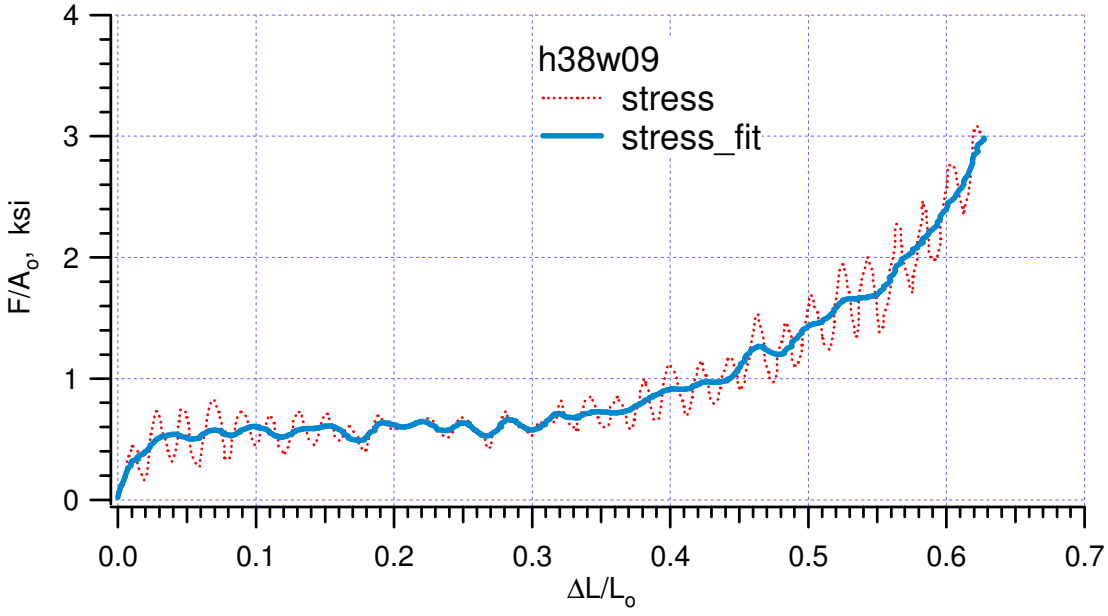
h38w09
stress
stress_fit
F/A$_o$, ksi
ΔL/L$_o$
0.0
0.1
0.2
0.3
0.4
0.5
0.6
0.7
0
1
2
3
4

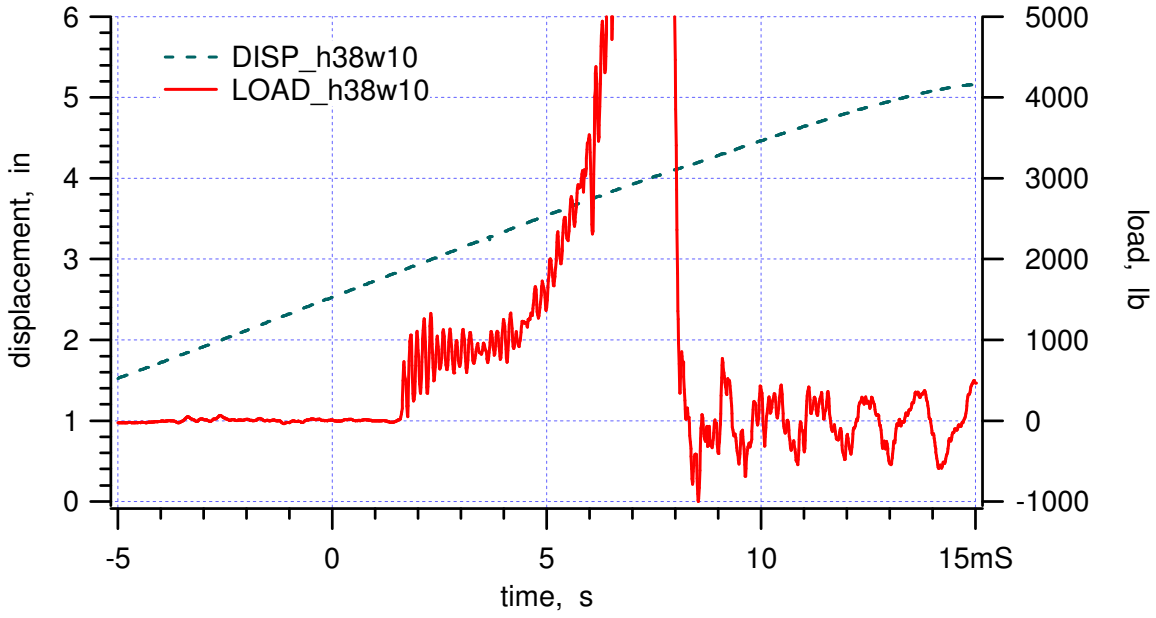
DISP_h38w10
LOAD_h38w10
displacement, in
load, lb
time, s
-5
0
5
10
15mS
0
1
2
3
4
5
6
-1000
0
1000
2000
3000
4000
5000

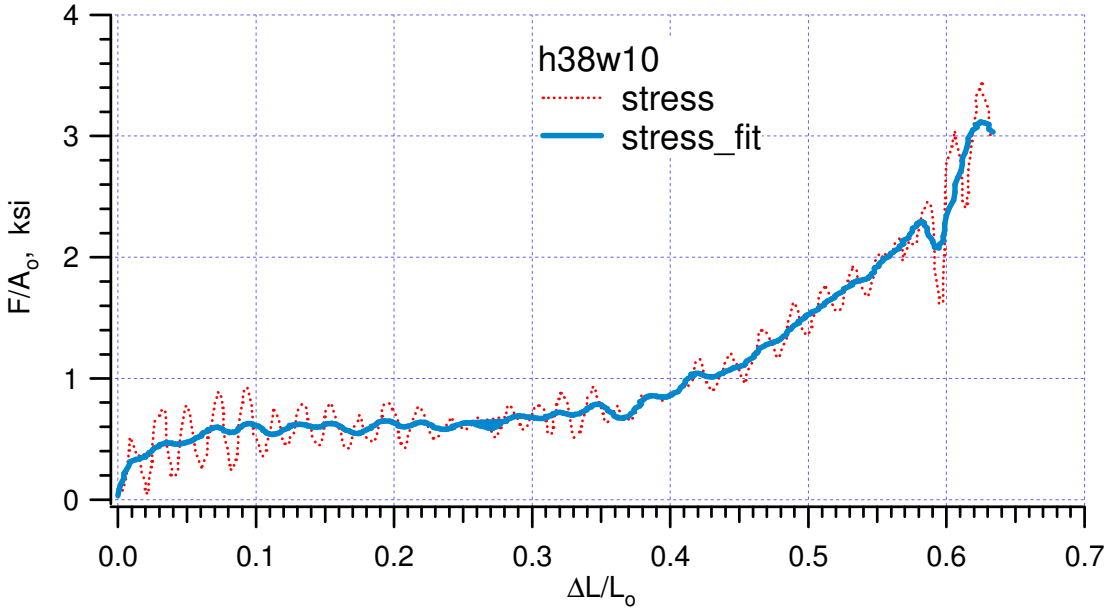
h38w10
stress
stress_fit
F/A$_o$, ksi
ΔL/L$_o$
0.0
0.1
0.2
0.3
0.4
0.5
0.6
0.7
0
1
2
3
4

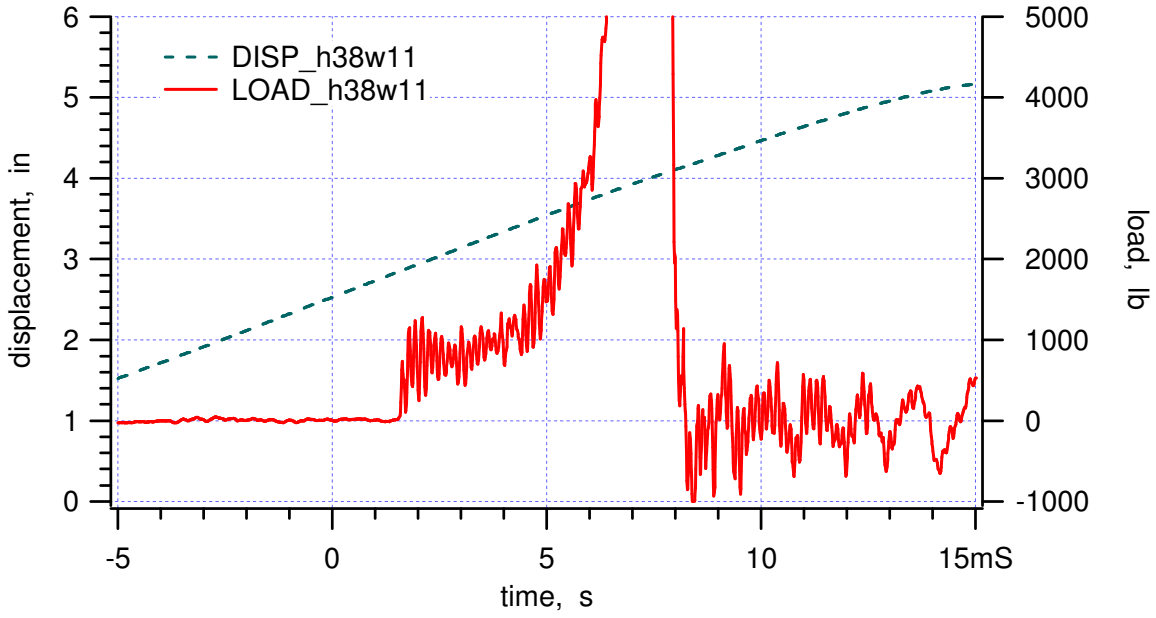
DISP_h38w11
LOAD_h38w11
displacement, in
load, lb
time, s
-5
0
5
10
15mS
6
5
4
3
2
1
0
5000
4000
3000
2000
1000
0
-1000

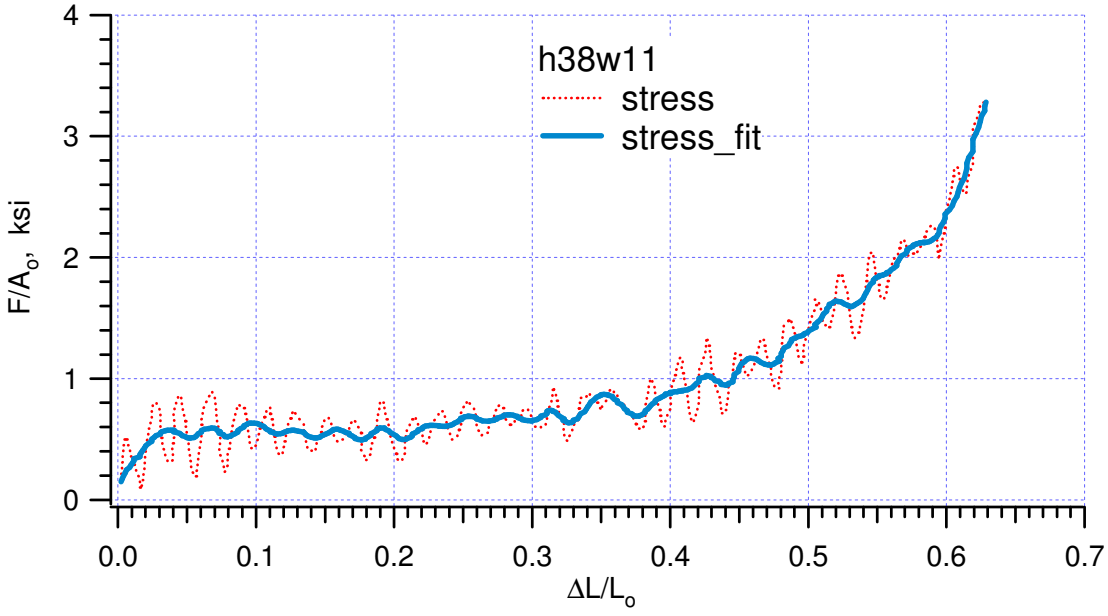
h38w11
stress
stress_fit
F/A$_o$, ksi
ΔL/L$_o$
0.0
0.1
0.2
0.3
0.4
0.5
0.6
0.7
4
3
2
1
0

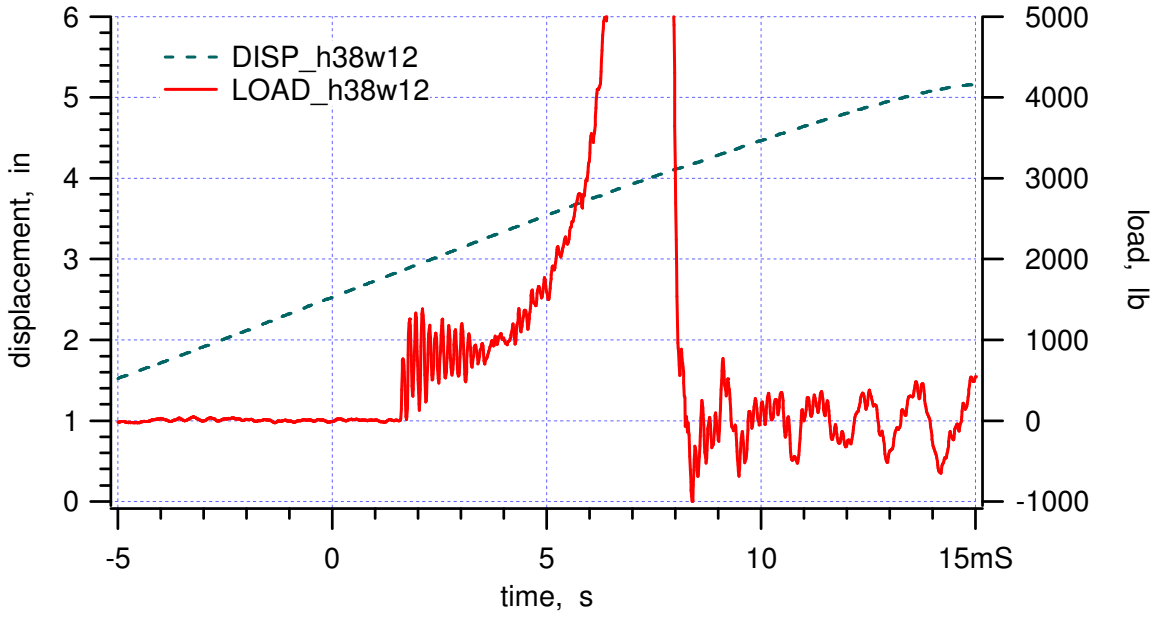
DISP_h38w12
LOAD_h38w12
displacement, in
load, lb
time, s
-5
0
5
10
15mS
6
5
4
3
2
1
0
5000
4000
3000
2000
1000
0
-1000

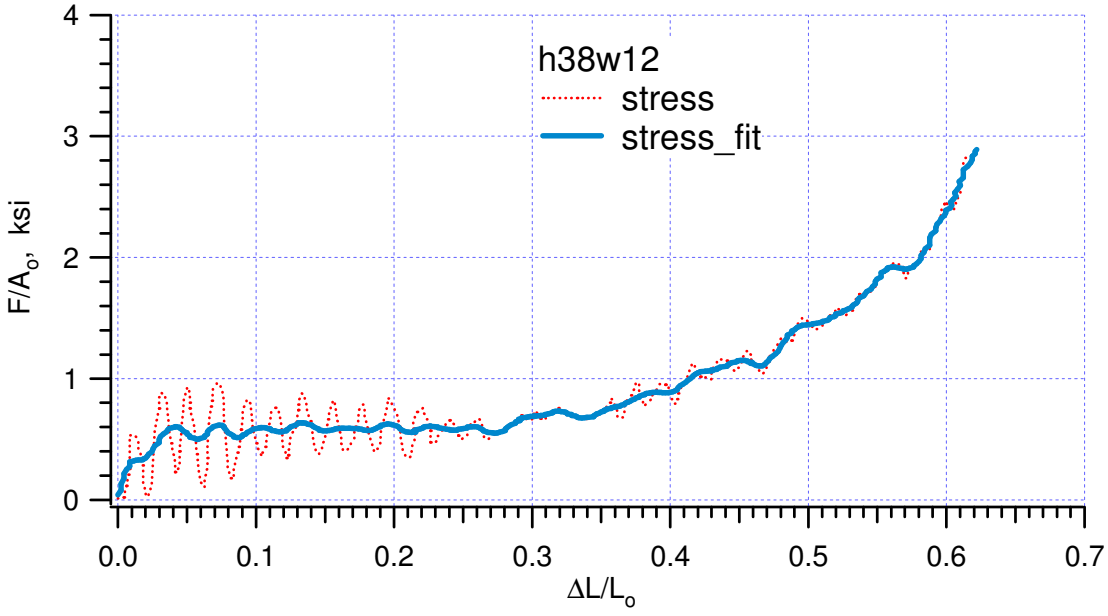
h38w12
stress
stress_fit
F/A$_o$, ksi
ΔL/L$_o$
0.0
0.1
0.2
0.3
0.4
0.5
0.6
0.7
4
3
2
1
0

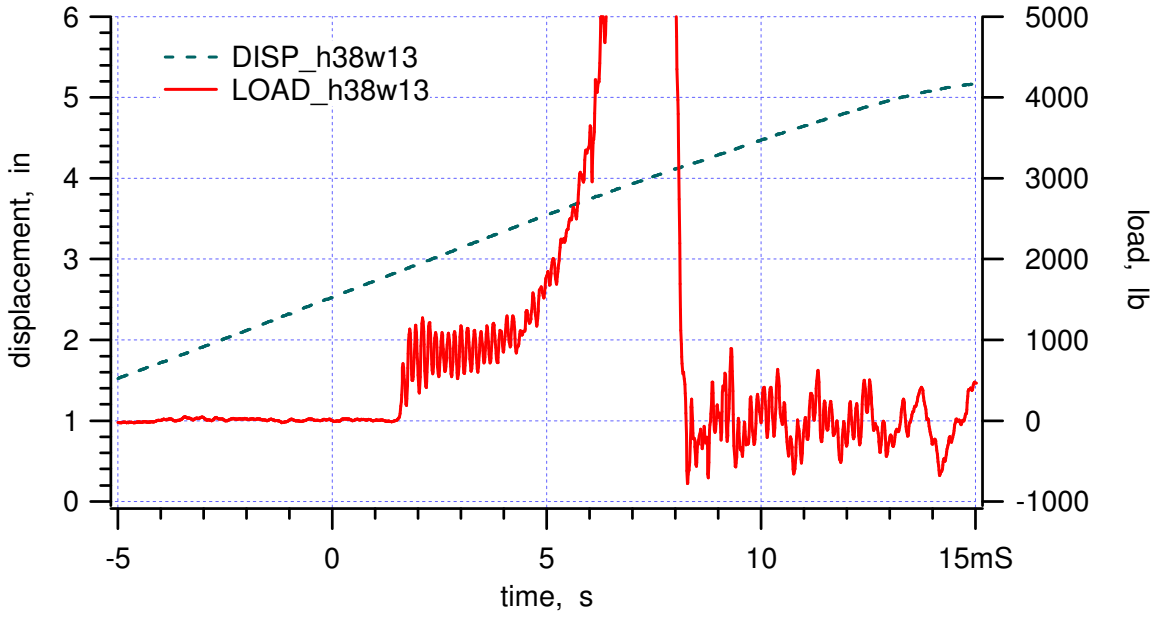
DISP_h38w13
LOAD_h38w13
displacement, in
load, lb
time, s
-5
0
5
10
15mS
0
1
2
3
4
5
6
-1000
0
1000
2000
3000
4000
5000

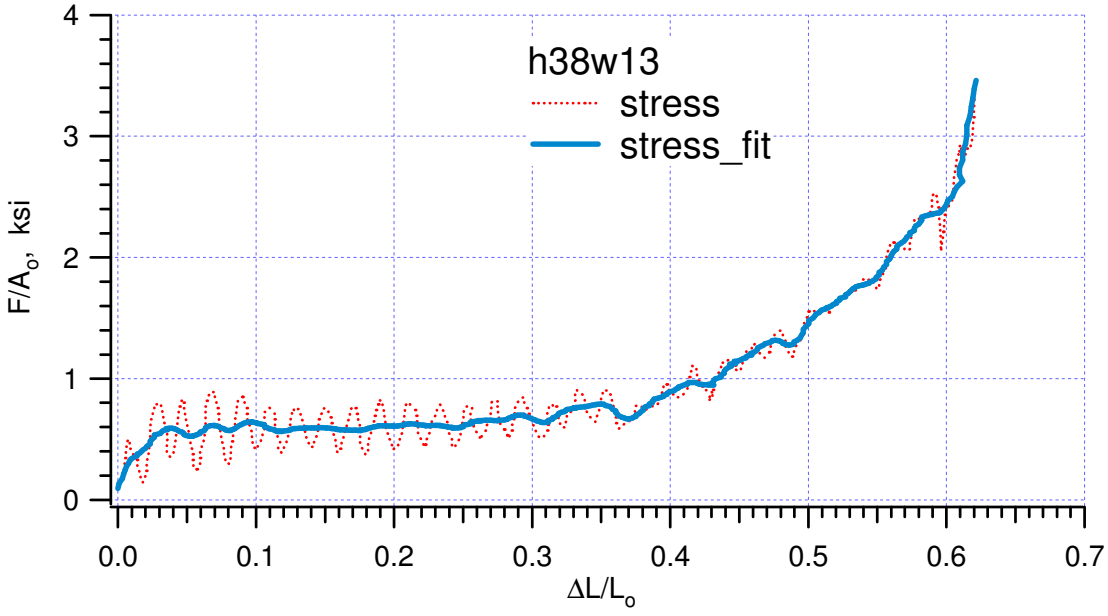
h38w13
stress
stress_fit
F/A$_o$, ksi
ΔL/L$_o$
0.0
0.1
0.2
0.3
0.4
0.5
0.6
0.7
0
1
2
3
4

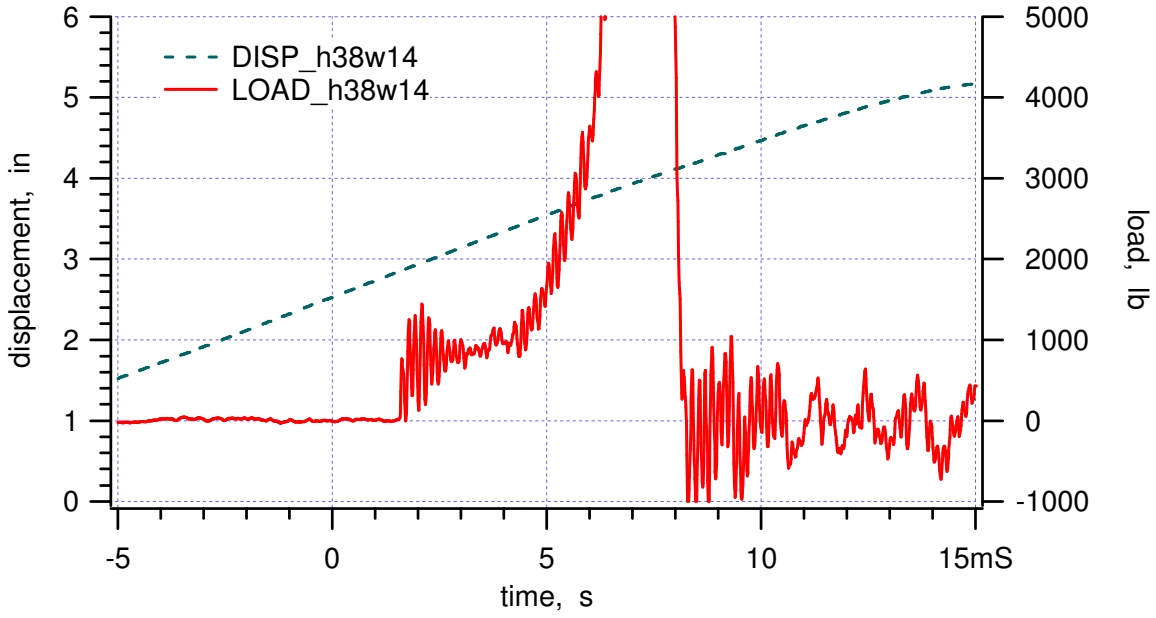
DISP_h38w14
LOAD_h38w14
displacement, in
load, lb
time, s
-5
0
5
10
15mS
6
5
4
3
2
1
0
5000
4000
3000
2000
1000
0
-1000

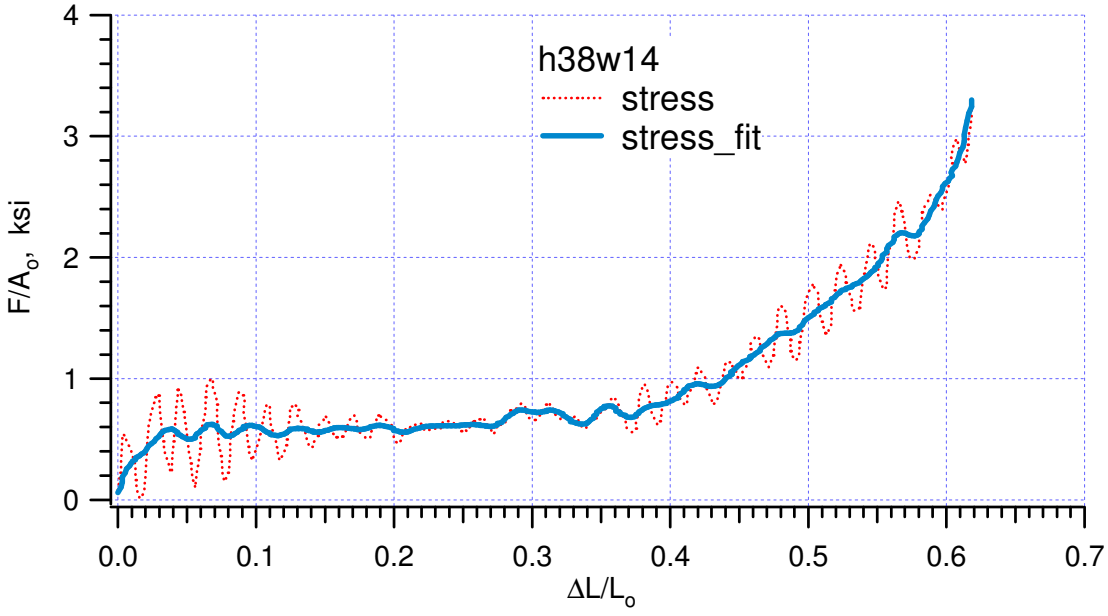
h38w14
stress
stress_fit
F/A$_o$, ksi
ΔL/L$_o$
0.0
0.1
0.2
0.3
0.4
0.5
0.6
0.7
4
3
2
1
0

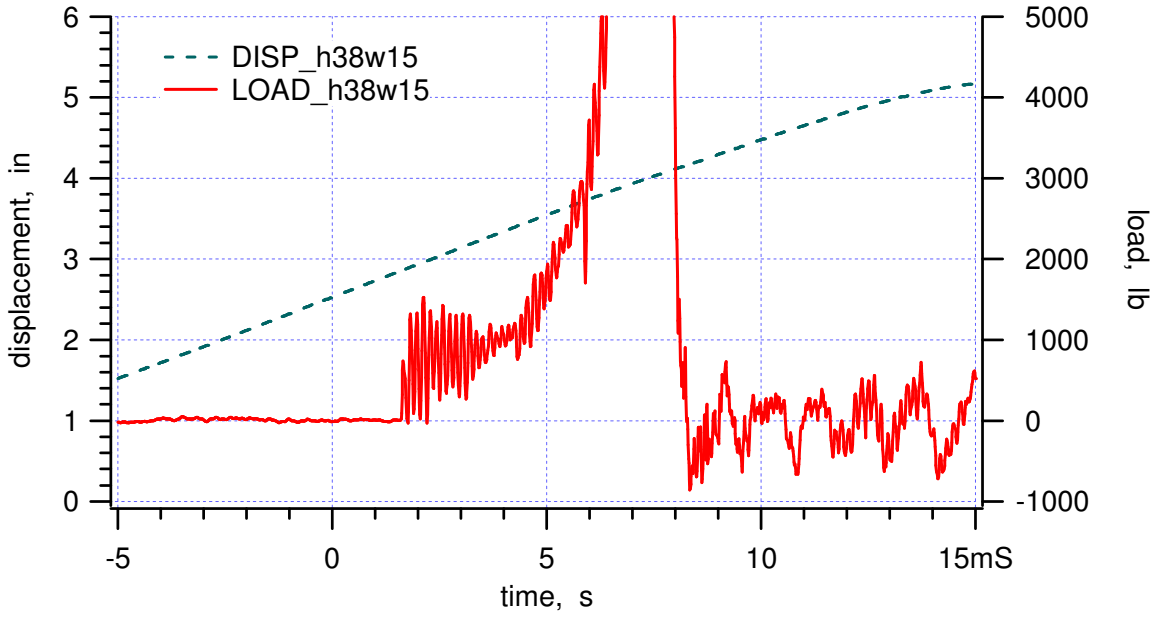
DISP_h38w15
LOAD_h38w15
displacement, in
load, lb
time, s
-5
0
5
10
15mS
0
1
2
3
4
5
6
-1000
0
1000
2000
3000
4000
5000

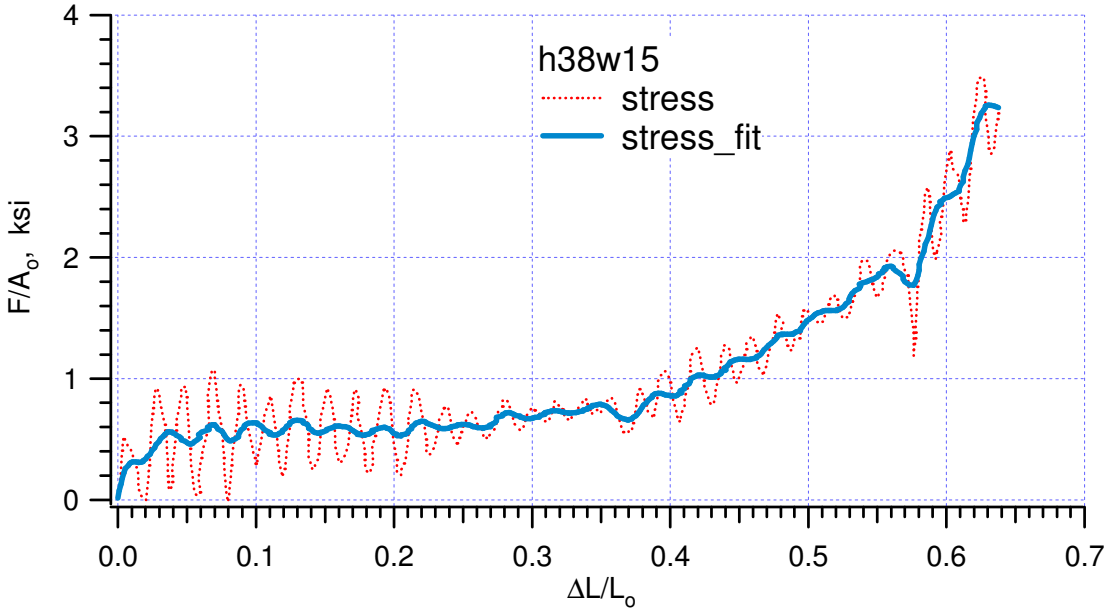
h38w15
stress
stress_fit
F/A$_o$, ksi
ΔL/L$_o$
0.0
0.1
0.2
0.3
0.4
0.5
0.6
0.7
0
1
2
3
4

APPENDIX XV:

"In-Plane Biaxial Compressions of High Density Aluminum Honeycombs," (Paper No. 150) Proceedings of the 2002 SEM Annual Conference & Exposition on Experimental and Applied Mechanics, June 10-12, 2002, Milwaukee, Wisconsin.

IN-PLANE BIAXIAL COMPRESSIONS OF HIGH DENSITY ALUMINUM HONEYCOMBS

Wei-Yang Lu, John Korellis and Ken Lee
Sandia National Laboratories, MS9042
Livermore, CA 94551-0969

ABSTRACT

A custom-designed system and fixture for biaxial compression of high-density aluminum honeycomb is described. Experiments of simple biaxial loading paths have been performed, and results are discussed in terms of the orthotropic crush model.

INTRODUCTION

Honeycomb has been used as an energy absorption component in many structures. These structures may experience any one of an infinite number of impact environments including impact speed, angle of impact, and temperature, making it extremely difficult to evaluate all the possibilities experimentally. A predictive analysis capability, which includes a validated constitutive model of honeycomb, would tremendously increase the confidence level of new and existing systems by enhancing the ability to evaluate structural designs.

As shown in Figure 1, honeycomb has three principal directions due to its composure of corrugated and flat aluminum sheets. T, L, and W are the strongest, intermediate, and the weakest directions, respectively. For 35 or 38 pcf (pound per cubic feet) aluminum, the crush (or yield) strength ratio T/L/W is about 12/2/1.

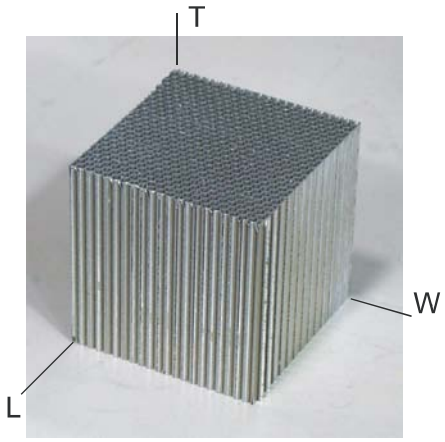

Figure 1. A high-density aluminum honeycomb.

A commonly used constitutive material model of honeycomb, which is implemented in computer codes such as DYNA3D [1] and PRONTO3D [2], is the orthotropic crush model. This simple model, illustrated in Figure 2, considers honeycomb as a continuum. The crush strength, which is constant as shown in Zone 2a, is uncoupled for each stress component in the principal material direction. It also assumes that the load-deformation relation is a function of volumetric strain and is independent of loading rate and temperature. The volumetric strain that initiates the hardening portion of Zone 2b is generally termed as crush efficiency.

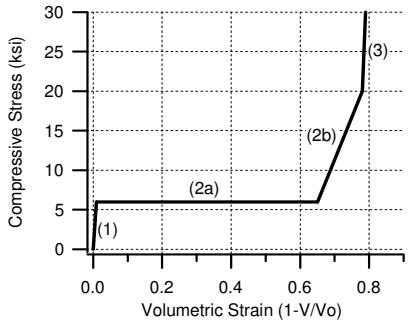

Figure 2. The orthotropic crush model.

Recently, an experimental investigation of the crush behavior of high-density aluminum honeycombs on their principal axes is reported [3] including the effects of temperature and loading rate. For angled impact or significantly off-axis normal impact conditions, the uncertainty and the adequacy of the model have not been studied. Biaxial experiments are required to validate the yield surface and to study the coupling of stress components. The results will also be used for further model improvement.

This paper describes the biaxial experiments of high-density honeycombs at Sandia, which includes design and setup of the biaxial compression system. The investigation pays particular attention to two model parameters, crush strength and crush efficiency. The density of the aluminum honeycomb material under consideration is about 35 pcf. Alcore (HIGRID DURA-CORE [4]) was used in this study.

EXPERIMENTAL SETUP

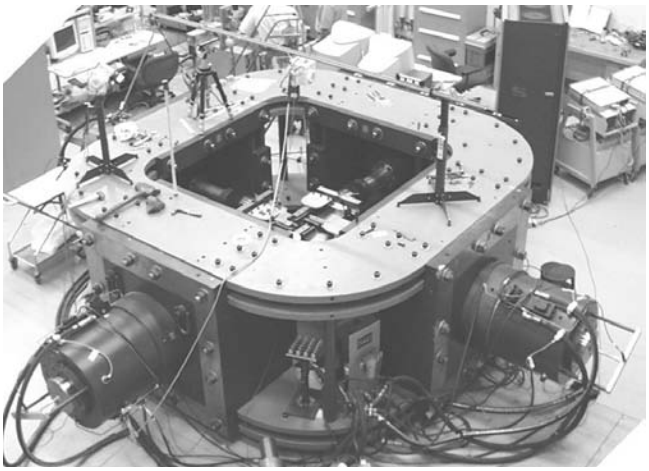

Figure 3. Biaxial loading frame. East and North actuators are on the lower left and right corners, respectively.

The setup is built on a custom designed in-plane biaxial system at Sandia/CA [5], shown in Figure 3. It has four identical servo-hydraulic actuators located on two perpendicular axes, north-south and east-west, in the horizontal plane. Each actuator has a loading capacity of 500,000 pounds and a displacement range of ±5 inches. A load cell is attached to the working end of each actuator. The system uses an MTS Aero90 controller. Like other MTS controllers, either displacement or load can be selected as a control parameter for each channel. Data is acquired using recording Nicolet oscilloscopes.

The suggested cross section of a honeycomb specimen is equal to or larger than 2”x2”. Based on this dimension and the crush strength of the material, the loading capacity of the fixture needs to be greater than 25 kips, which is within the capability of the system.

Figure 4 shows the assembly of the test fixtures. Each loading fixture is attached to a load cell and laterally uncoupled with ball bearings. The four loading fixtures are also inter-connected together with slide-bearing mechanisms. During a biaxial test the displacement of each fixture will have two components: one is in the loading direction that is the same as the actuator, and the other is perpendicular to the actuator in the horizontal plane, which is defined by the adjacent fixture. The East loading fixture for example, the lower one in Figure 4, it can be pushed or pulled in East-West direction, i.e., up-down in the figure, by East actuator. It can also be moved in South-North direction, i.e., left-right way, by North actuator, located on the right side of the figure. The ball bearings allow the fixture to move sideways with negligible resistance, and the slide-bearing mechanism defines the relative position while allowing motion between adjacent fixtures and minimizing loading surface friction. From the geometry of the fixture, the largest specimen that can be fitted in the in-plane compression mechanism is 3”x3”x2”. The compression capacity of the entire system is now reduced to 40 kips per axis, which is the load limit of bearings between load cell and fixture.

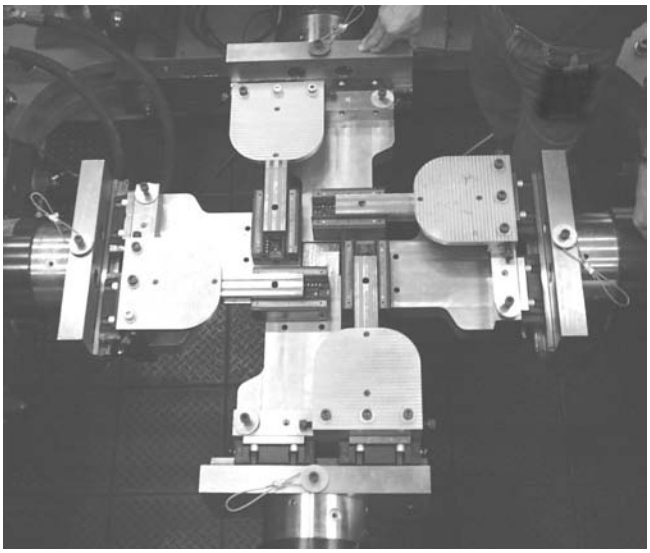

Figure 4. Biaxial compression fixture assembly.

EXPERIMENTS

System Characterization

Before biaxial honeycomb experiments were performed on the system, it was necessary to evaluate friction and cross talk between fixtures to quantify experimental uncertainties. With no specimen in place, each actuator moved in (compressive direction) and out (tensile direction) while the other three actuators were stationary. The displacement-time profile of each actuator was divided into eight segments. As shown in Figure 5, North actuator, for example, was in motion in the first and second segments. It moved in two inches in the first segment then backed out to its initial position at the end of the second segment. In the third to eighth segments, it stayed still. All four loads were monitored during the entire process. A typical waveform of North load cell is displayed in Figure 6. Statistical results of all data are listed in Table 1. A positive number indicates compressive force. If there was no friction and no cross talk, the averaged load in each segment should be zero. When north actuator moved in, North and South load cells read 22 and 10 pounds, respectively, which was due to

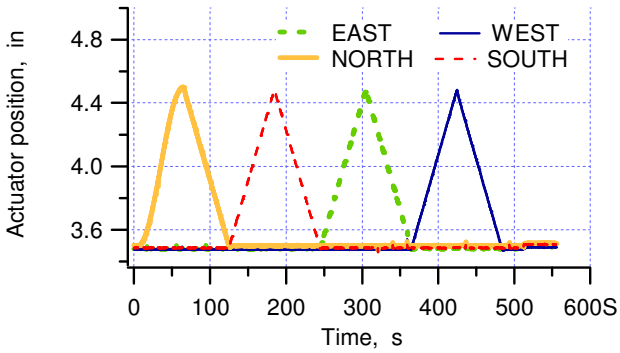

Figure 5. Recorded displacement-time history of system performance experiment.

friction between fixtures. During the same time, East and West load cells read 2 and –7 pounds, which was cross talk or bending due to the friction. The results show the maximum friction for all cases is less than 50 pounds, and the maximum cross talk between fixtures is less than 10 pounds. The uncertainty of load measurement is within 100 pounds. Consider a specimen with a cross section of 2”x2”, 100 pounds corresponds to 25 psi. The friction and cross talk is insignificant compared to the crush strengths of high-density aluminum honeycombs.

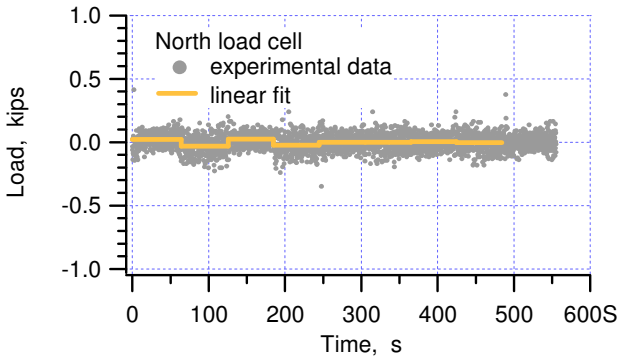

Figure 6. Waveform of North load cell corresponding to motions of actuators without specimen.

Table 1. Results of system characterization.

	loading				mean, lb				standard deviation, lb			
#	N	S	E	W	N	S	E	W	N	S	E	W
1	C	-	-	-	22	10	2	-7	53	48	53	50
2	T	-	-	-	-32	-37	-3	3	74	51	67	63
3	-	C	-	-	24	34	-2	1	50	47	58	52
4	-	T	-	-	-22	-37	3	2	74	61	78	70
5	-	-	C	-	-1	0	47	27	63	56	56	66
6	-	-	T	-	-2	-2	-18	-3	70	57	75	68
7	-	-	-	C	3	-6	29	47	59	49	53	59
8	-	-	-	T	-3	1	0	-8	68	57	72	67

Biaxial Compressions and Results

Biaxial experiments of various specimen orientations and loading paths were performed on the system. Here, on-axis compressions in LW and TL planes are reported. Two simple paths were considered, uniaxial compression and one-to-one proportional compression. The purpose of conducting uniaxial compression on the biaxial system was to compare with the results from typical uniaxial systems for consistency.

In LW on-axis compressions, L and W were aligned with East-West and North-South, respectively. The uniaxial compression in L-direction was conducted by moving East actuator only; the other three were not moving, so W-direction was confined during compression but T-direction was unconfined. The results are displayed in Figure 7. Readings from East and West load cells were identical; similarly, North and South readings were identical. They are engineering stress-strain curves. Since the cross section remained almost constant during the uniaxial compression, the blue (or green) curve is also the true stress – volumetric strain curve for L-direction. The crush strength and efficiency is consistent with those from uniaxial systems [3], which confirms the biaxial fixture functionality. The W confined stress, which is generally not obtainable from a uniaxial system, can be measured in the biaxial system. The stress is shown in red (or gold) in the figure and it is not zero. This indicates some Poisson's effect during crush, which is neglected by the orthotropic crush model.

In LW, one-to-one proportional compression, all actuators moved in at the same speed, about 0.5 inches per minute, simultaneously. Engineering stress-strain curves of L- and W-directions are displayed in Figure 8. The initial crush strengths in L and W were consistent with the uniaxial results.

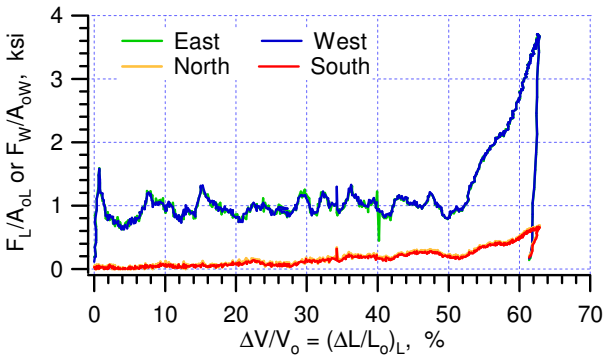

Figure 7. Uniaxial L stress-strain curves obtained from the biaxial system.

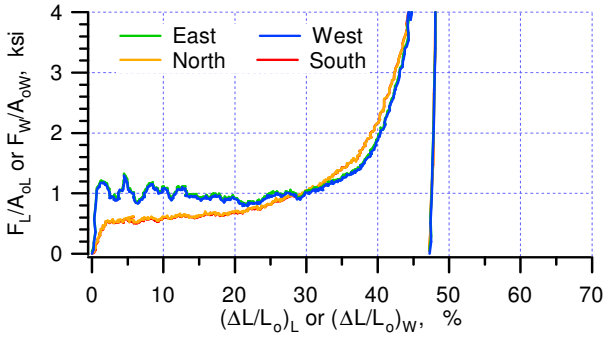

Figure 8. Engineering stress-strain curves of one-to-one proportional compression in LW plane.

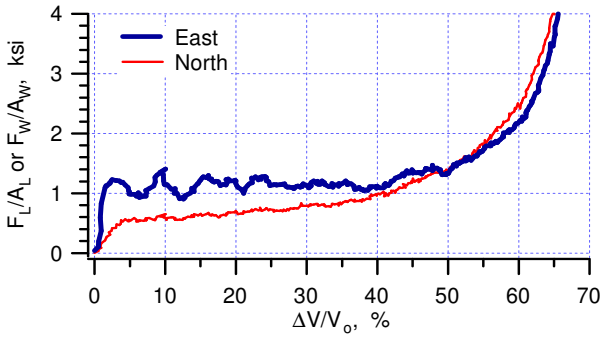

Figure 9. True stress – volumetric strain curves of one-to-one proportional compression in LW plane.

As crush advances, the L crush strength (the stronger one) remains fairly constant, but the W crush strength (the weaker one) increases and gradually reaches the same strength as L. Then both L and W hardened at the same rate and the honeycomb becomes transversely isotropic. Portions of the increase in W crush strength may due to the Poisson's effect shown in Figure 7.

In one-to-one proportional biaxial compression, the cross sectional areas of L- and W- directions are constantly changing. Thus, true stress – volumetric strain curves, shown in Figure 9, are different from engineering stress-strain curves. Comparing this L true stress – volumetric strain curve in Figure 9 with the one from uniaxial compression in Figure 7, the crush strength increases during the crush. The transition from Zone 2a to 2b (ref. Figure 2) is much more gradual than the uniaxial curve. The crush efficiency is hard to define, but the uniaxial data provides a reasonable estimation when volumetric strain is used as a parameter.

Same biaxial experiments in TL plane were conducted. The results, shown in Figures 10 – 12, are quite similar to those of LW experiments: (1) The uniaxial crush strength and crush efficiency of T axis are consistent with those from uniaxial systems, Figure 10. (2) There is a Poisson's effect during crush. (3) The engineering stress-strain curves

show that the crush strength of the stronger axis, T-direction, remains relatively constant. The crush strength of the weaker axis, L-direction, increases rapidly during the crushing, Figure 11. (4) The true stress – volumetric strain curves indicate the crush strengths of T and L are not constant, both are increasing during crushing, Figure 12. (5) The uniaxial data seems to provide a reasonable estimation of crush efficiency when volumetric strain is used as a parameter.

CONCLUSIONS

The custom designed biaxial system and fixture functioned impeccably in high-density aluminum compressions. Initial results of biaxial compression show the orthotropic crush model provides a reasonable estimation of crush efficiency using the parameter of volumetric strain; however, there are deviations in crush strength when true stress is considered. More experiments are needed to further explore the biaxial behavior of honeycomb and to improve and validate the orthotropic crush model.

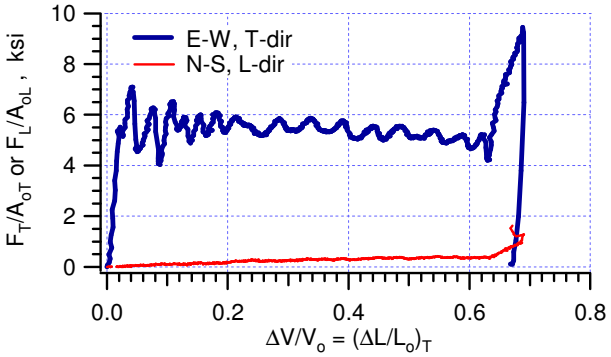

Figure 10. Uniaxial T stress-strain curves obtained from the biaxial system.

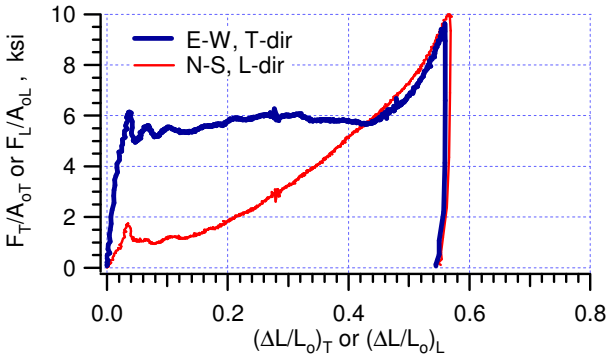

Figure 11. Engineering stress-strain curves of one-to-one proportional compression in TL plane.

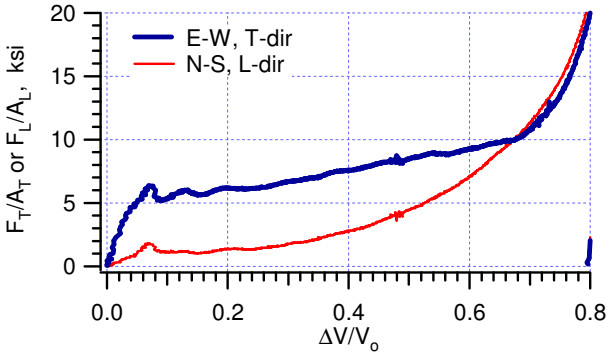

Figure 12. True stress – volumetric strain curves of one-to-one proportional compression in LW plane.

ACKNOWLEDGEMENT

Sandia is a multiprogram laboratory operated by Sandia Corporation, a Lockheed Martin Company, for the United States Department of Energy under contract DE-AC04-94-AL85000.

REFERENCES

2. Whirley, R.G., Engelman, B.E., and Hallquist, J.O., "DYNA3D Users Manual," Lawrence Livermore Laboratory, Livermore, CA, 1991.
3. Attaway, S.W. *et al*., "PRONTO3D Users' Instructions: A Transient Dynamic code for Nonlinear Structural Analysis," Report SAND98-1361, Sandia National Laboratories, Albuquerque, NM, 1998.
4. Lu, W-Y, and Hinnerichs, T., "Crush Of High Density Aluminum Honeycombs," IMECE2001, vol. 1
5. Alcore, Inc., Belcamp, MD.
6. Korellis, J.K., Internal memo, 1995

This page intentionally left blank

DISTRIBUTION

External distribution:

Hexcel Corporation
Attn: Jim Kindinger
11711 Dublin Blvd.
Dublin, CA 94568

Alcore Inc.
Attn: Bernie Nimeth/Bob Woods
1502 Quarry Drive
Edgewood, MD 21040

Dr. Shen Wu
Ford Motor Company
Science Research Laboratory
Department of Safety Research and Development
SRL Ð MD 2115 20000 Rotunda Drive
P.O. Box 2053
Dearborn, MI 48121

Director
US Army Research Laboratory
Attn Rick Bogdan
AMSRD-ARL-CI-OK-T
2800 Powder Mill Rd
Adelphi, MD 20783-1197

Dr. Tomasz Wierzbicki
Impact and Crashworthiness Laboratory, Rm 5-218
Massachusetts Institute of Technology
Cambridge, MA 02139

2 MS9018 Central Technical Files, 8944

Internal distribution:

1	MS-0325	D. A. Hoke	2615
1	MS-0370	T. G. Trucano	1411
1	MS-0372	J. Pott	1524
1	MS-0372	J. D. Gruda	1524
1	MS-0372	K. W. Gwinn	1524
10	MS-0372	T. D. Hinnerichs	1524
1	MS-0372	T. C. Jones	1524
1	MS-0372	C. S. Lo	1524
1	MS-0372	K. E. Metzinger	1524
1	MS-0372	W. M. Scherzinger	1524
1	MS-0372	J. Jung	1525
1	MS-0372	C. M. Stone	1525
1	MS-0372	G. W. Wellman	1525
1	MS-0380	H. S. Morgan	1540
1	MS-0384	A. C. Ratzel	1500
1	MS-0437	R. C. Hartwig	2100
1	MS-0437	J. M. McGlaun	12930
1	MS-0447	J. G. Lewis	2111
1	MS-0447	K. R. Eklund	2111
1	MS-0447	J. A. Rohwer	2111
1	MS-0447	C. Post	2111
1	MS-0447	W. T. Reutzel	2111
1	MS-0447	P. D. Hoover	2111
1	MS-0447	J. D. Mangum	2111
1	MS-0453	M. A. Rosenthal	2130
1	MS-0457	J. S. Rottler	2000
1	MS-0464	T. D. Hernandez	2996
1	MS-0481	J. M. Montoya	2132
1	MS-0481	L. L. Luna	2132
1	MS-0481	D. R. Martinez	2136
1	MS-0521	J. L. Moya	2540
1	MS-0529	G. K. Froehlich	5345
1	MS-0557	D. B. Clauss	1521
1	MS-0557	V. I. Bateman	1521
1	MS-0557	R. A. May	1522
1	MS-0557	E. C. Stasiunas	1521
1	MS-0557	T. G. Carne	1525
1	MS-0632	V. O. Willan	2916
1	MS-0634	D. J. Giersch	2951
1	MS-0718	D. J. Ammerman	6141
1	MS-0774	E. M. Pulling	2991
1	MS-0828	M. Pilch	1533
1	MS-0828	V. J. Romero	1533
1	MS-0836	E. S. Hertel	1516

1	MS-0842	M. K. Neilsen	1526
1	MS-0847	P. J. Wilson	1520
1	MS-0847	T. J. Baca	1523
1	MS-0847	J. M. Redmond	1526
1	MS-0847	L. N. Kmetyk	1523
1	MS-0965	B. D. Boughton	5714
1	MS-1135	N. T. Davie	1535
1	MS-1393	H. J. Abeyta	12120
1	MS-9042	T. Chen	8776
1	MS-9404	D. M. Kwon	8770
10	MS-9409	W. Lu	8725
2	MS-0899	Technical Library Files	4536

This page intentionally left blank